



USMCA 2011

**10th INTERNATIONAL SYMPOSIUM
ON NEW TECHNOLOGIES
FOR URBAN SAFETY
OF MEGA CITIES IN ASIA**

ISBN4-903661-51-2

USMCA 2011



ICUS Report 2011-02 (serial No.56)

*the 10th International Symposium
on New Technologies
for Urban Safety of Mega Cities in Asia*

*October 12-14, 2011
The Empress Hotel Chiang Mai, Thailand*

*Edited by
Akiyuki Kawasaki
&
Eiko Yoshimoto*

*Organized by
International Center for Urban Safety Engineering,
Institute of Industrial Science, The University of Tokyo, Japan
Asian Institute of Technology, Thailand
Chiang Mai University, Thailand
and
Chulalongkorn University, Thailand*

*Sponsored by
Global Center of Excellence for Sustainable Urban Regeneration,
The University of Tokyo, Japan
and
The Foundation for the Promotion of Industrial Science, Japan,*

*Cooperated by
Asian Disaster Preparedness Center, Thailand
Department of Disaster Prevention and Mitigation, Ministry of Interior,
Thailand
Geo-Informatics and Space Technology Development Agency, Thailand
Japan Society for the Promotion of Science, Bangkok Office, Thailand
and
United Nations University Institute for Sustainability and Peace (UNU-ISP)*

SYMPOSIUM ORGANISERS

STEERING COMMITTEE

Boonsom Lerdhirunwong, Chulalongkorn University, Thailand
Ekasit Limsuwan, Chulalongkorn University, Thailand
Jin Young Kim, KDPA, Korea
Katsumi Mushiake, Foundation of River & Watershed Environment Management, Japan
Kazuhiko Takeuchi, United Nations University, Japan
Mahesh C Tandon, ICI, India
Mehedi Ahmed Ansary, BUET, Bangladesh
Pong-in Rakariyatham, Chiang Mai University, Thailand
Rajib Shaw, Kyoto University, Japan
Shunji Murai, Japan Association of Surveyors, Japan
Sudhir Misra, IIT Kanpur, India
Surachai Ratanasermpong, GISTDA, Thailand
Taketo Uomoto, Public Works Research Institute, Japan
Tomonari Yashiro, IIS, The University of Tokyo, Japan
Tran Thuc, VIMHE, Vietnam
Tso-Chien, Pan, Nanyang Technological University, Singapore
Tsuneo Katayama, Tokyo Denki University, Japan
Waon-Ho Yi, NIDP, Korea
Wei Cheng Fan, CPSR, Tsinghua University, China
Worsak Kanok-Nukulchai, AIT, Thailand
Yoshifumi Yasuoka, CRDS, JST, Japan

TECHNICAL COMMITTEE

Chang-Yong Kim, KICT, Korea
Chayanon Hansapinyo, Chiang Mai University, Thailand
Haruo Sawada, ICUS, IIS, The University of Tokyo, Japan
Hiroshi Yokota, Hokkaido University, Japan
Jeffrey C.L. Chiang, Monash University, Malaysia
Kiang Hwee Tan, National University of Singapore, Singapore
Kimiro Meguro, ICUS, IIS, The University of Tokyo, Japan
Lal Samarakoon, AIT, Thailand
Munaz Ahmed Noor, BUET, Bangladesh
Tien Dich, IBST, Vietnam
Nitin Kumar Tripathi, AIT, Thailand
Pennung Warnitchai, AIT, Thailand
Somnuk Tangtermsirikul, Thammasat University, Thailand
Srikantha Herath, United Nations University, Japan
Sucharit Koontanakulvong, Chulalongkorn University, Thailand
Taikan Oki, IIS, The University of Tokyo, Japan
Tai-Ping Chang, NKFUST, Taiwan
Yozo Fujino, G-COE, The University of Tokyo, Japan

ORGANIZING COMMITTEE

Akiyuki Kawasaki, ICUS, IIS, The University of Tokyo, Japan
Anat Ruangrassamee, Chulalongkorn University, Thailand
Arisara Charoenpanyanet, Chiang Mai University, Thailand
Kyung- Ho Park, AIT, Thailand
Michael W. Henry, ICUS, IIS, The University of Tokyo, Japan
Pakawat Sancharoen, Thammasat University, Thailand
Raktipong Sahamitmongkol, Thammasat University, Thailand
Shinya Kondo, ICUS, IIS, The University of Tokyo, Japan

PREFACE

On behalf of the Organizing Institutes of the 10th International Symposium on New Technologies for Urban Safety of Mega Cities in Asia (USMCA2011), I expressed our sincere welcome to all symposium participants and distinguished keynote speakers.

In the Asia and Pacific-Rim regions, rapid economic development and population growth and concentration is fast accelerating the pace of urbanization. Unfortunately, the rapid expansion of infrastructure for urbanization is not adequately balanced with appropriate measures for their maintenance and management, and urban disasters have resulted. During the last few years, there were several big disasters in Asia and the Pacific Rim regions, such as killer cyclones Sidr in Bangladesh (2007), Nargis in Myanmar (2008), and Aila in Bangladesh and India (2009), and Typhoon Ketsna in Philippines (2009), flooding in Mongolia (2009) and Pakistan (2010), the devastating earthquakes in Sichuan, China (2008), Sumatra (2009), Samoa (2009) and Japan (2011), and heat waves in Russia and Japan (2010). The number of fatalities and missing reported due to these disasters was well over 200,000. These unprecedented events show us the importance of urban safety.

The International Center for Urban Safety Engineering (ICUS) was established in 2001 at the Institute of Industrial Science (IIS), the University of Tokyo, with the objectives of carrying out researches on urban safety and implementing them towards the realization of safer cities in the 21st century. ICUS has been actively tackling advanced researches, networking and information collection and dissemination for 10 years. Based on ICUS's past 10-year activities, new ICUS started since April 1, 2011. The purpose of the "new" ICUS is to identify, investigate, and resolve issues towards the realization of sustainable urban systems for the prosperity and safety of society considering challenging socio-economic problems such as depopulation and aging society, shrinking economic resources, advanced technology, environmental awareness and climate change, dense and decentralized urbanization, and so forth. Specifically, three research divisions – "Urban safety and disaster mitigation division," "Environment informatics division," and "Social infrastructure management division" – will form the core of the "new" ICUS, and activities in these fields are intended to fulfill the objectives of "promotion of advanced research," "construction of networks," and "information collection and dissemination" considering the above-mentioned socio-economic problems.

At 14:46:18 (local time) on March 11, 2011, a gigantic earthquake (called "The 2011 Tohoku region Off-Pacific Ocean earthquake") with moment magnitude (Mw) 9.0 occurred in the Tohoku (North-East) region of Japan. This earthquake is historically the largest event ever recorded in Japan. A killer tsunami induced by this earthquake killed approximately 20,000 people and injured 5,700 people. Many buildings and infrastructures, including nuclear power plants, were damaged. Totally collapsed, burnt, and/or washed away structures due to the tsunami, fires, and ground motion was numbered 112 thousand, heavily damaged structures numbered over 140 thousand, and partially damaged structures numbered over 500 thousand. Due to loss of power, including emergency back-up power, at the Fukushima I nuclear power plant, the cooling systems in the nuclear reactor failed, resulting in a severe accident which leaked large amounts of radiation. Due to this accident, people living around the power plant were forced to evacuate and live in refugee camps for long time. The total monetary loss due to the earthquake was officially estimated by the national government at 16.9 trillion yen, but indirect losses and damage due to the nuclear power accident were not included.

Issues with the response, recovery and reconstruction of the affected areas are typical of the purposes of "new" ICUS. In order to fully realize ICUS's vision for safer

cities in Asia and the Pacific Rim regions, ICUS has been annually co-organizing USMCA since 2002 with its partners in the Asian region. In 2011, ICUS jointly organized the 10th USMCA in Chiang Mai, Thailand, with the Asian Institute of Technology, Chiang Mai University, and Chulalongkorn University. The objectives of the symposium was to bring together decision makers, practitioners and researchers involved in the field of urban safety to share their expertise, knowledge and experience in tackling the critical issues for safer cities in Asia and the Pacific Rim regions. It also provided an environment to create and reinforce collaborative networks among experts in the fields relevant to urban safety.

During this two-day symposium, 54 papers in twelve parallel sessions and 23 posters in poster session were presented with five papers by keynote speakers. Total participants were 149 from 13 countries such as Thailand, Australia, Cambodia, China, Costa Rica, Bangladesh, Japan, Korea, Mongolia, India, Indonesia, Singapore and USA. The symposium focused on disaster response and recovery; risk assessment, prediction, and early-warning; decision-making technologies; planning and development of urban infrastructure systems; life-cycle management of infrastructure systems; climate change mitigation and adaptation; development and application of sustainable technologies; and application of geospatial technologies. Also, a specially themed session on “Earthquake and Tsunami in Sumatra and Indian Ocean and Tohoku, Japan” was included.

I would like to thank all the members of the Steering, Technical and Organizing Committees as well as the Symposium Secretariat for their hard work, time and effort in putting this symposium together. I would also like to thank all our sponsors for their generous support and contribution. Thanks are also due to those who have contributed towards making this symposium successful.

Kimiro MEGURO

*Director of ICUS, IIS, The University of Tokyo
(Co-Chairman of Organizing Committee, USMCA2011)*

Copyright and Reprint Permission:

Photocopy of an article is permitted for authors and other researchers for their own reading and research. Abstracting and indexing of the papers are permitted but acknowledgement should be given to “The 10th International Symposium on New Technologies for Urban Safety of Mega Cities in Asia” and the authors of each specific paper. Written permission should be obtained from the publishers prior to any other type of reproduction. Please contact:

*International Center for Urban Safety Engineering (ICUS),
Institute of Industrial Science (IIS),
The University of Tokyo, Japan*

Tel: +81-3-5452-6472

Fax: +81-3-5452-6476

ISBN: 4-903661-51-2

2011 Program Overview

Time	Tuesday, 11 October	
1600-1800	Pre-Registration (Reception Hall of The Empress Hotel)	
Time	Wednesday, 12 October	
0745-0830	Registration (2F Exhibition Area)	
0830-0850	<p>Inauguration Ceremony</p> <p>Mr. Kazuo Shibata, Consul General of the Consulate-General of Japan in Chiang Mai. Prof. Kimiro Meguro, Director of ICUS</p> <p>Moderator: Prof. Sawada</p>	
0850-1020	<p>Keynote Speech (2F Chiangmai 3-5)</p> <p>Dr. Shunichi Koshimura, Tohoku University The 2011 Tohoku Earthquake Tsunami Disaster: Its Impact, lessons of renovation</p> <p>Dr. Ir. Muhammad Dirhamsyah, Syiah Kuala University An Application of Geographic Information System for Aceh Multi-Hazard Disaster</p> <p>Dr. Sidthinat Prabudhanitisarn, Chiang Mai University Environmental Management</p> <p>Moderator: Dr. Kuwano</p>	
1020-1050	Group photo and Tea-break (2F Exhibition Area)	
1050-1200	Special poster session (2F Exhibition Area)	
1200-1330	Lunch (2F Exhibition Area)	
	2F Chiangmai 1	2F Chiangmai 2
1330-1510	<p>Session 1 : Vulnerability and risk assessment for seismic hazard</p> <p>Special Presentation: Prof. Uomoto Session Chairs: Prof. Ansary and Prof. Meguro</p>	<p>Session 2 : Flood risk assessment and management</p> <p>Special Presentation: Dr. Herath Session Chairs: Dr. Dutta and Dr. Kato (T)</p>
1510-1540	Tea-break (2F Exhibition Area)	
1540-1705	<p>Session 3 : Durability of construction materials</p> <p>Special Presentation: Prof. Fan (Prof. Huang) Session Chairs: Prof. Uomoto and Dr. Nagai</p>	<p>Session 4 : Urban Environmental planning and assessment</p> <p>Special Presentation: Dr. Nitin Session Chair: Prof. Rogers and Prof. Sawada</p>
1800-2200	Symposium dinner at Khum Kan Toke Restaurant (Meeting at the reception hall of The Empress Hotel at 1800)	

Time		Thursday, 13 October	
		2F Chiangmai 1	2F Chiangmai 2
0840-1005	Session 5 : Properties and performance of construction materials Special Presentation: <u>Prof. Misra</u> Session Chairs: Dr.Kato(Y) and Dr. Koshihara	Session 6 : Disaster reponse and recovery Special Presentation: <u>Prof. Mansor</u> Session Chairs: Dr. Tanaka and Dr. Dirhamsyah	
1005-1035	Tea-break (2F Exhibition Area)		
1035-1200	Session 7 : Evaluation of infrastructure health and performance Special Presentation: <u>Prof. Tan</u> Session Chairs: Dr. Chayanon and Dr. Nagai	Session 8 : Earthquake and Tsunami in Sumatra and Indian Ocean and Tohoku, Japan Special Presentation: <u>Mr. Ho</u> Session Chairs: Dr. Koshimura and Dr. Herath	
1200-1330	Lunch (2F Exhibition Area)		
1330-1455	Session 9 : Seismic vulnerability and performance of structures Session Chairs: Prof. Msira and Dr.Nishida	Session 10 : Environmental management: air quality, forest, water resources Special Presentation: <u>Dr. Dutta and Mr. Kimkong</u> Session Chairs: Dr. Mansor and Prof. Ichihashi	
1455-1525	Tea-break (2F Exhibition Area)		
1525-1635	Session 11 : Structural vulnerability and safety Special Presentation: <u>Prof. Ansary</u> Session Chairs: Prof. Tan and Dr. Kuwano	Session 12 : Vulnerability and risk assessment for urban safety Special Presentation: <u>Dr. Jargalsaikhan</u> Session Chairs: Dr. Nitin and Dr. Tanaka	
1635-1645	Break		
1645-1745	<p>Keynote Speech (2F Chiangmai 3-5)</p> <p>Prof. Peter Rogers, Harvard University Energy, Food, and Water Security: Implications for Asian Megacities</p> <p>Prof. Haruo Sawada, ICUS, The University of Tokyo Satellite information for large natural hazard</p> <p>Moderator: Dr. Kuwano</p>		
1730-1800	<p>Closing Ceremony (2F Chiangmai 3-5)</p> <p>Dr. Chayanon Hansapinyo (Award presentation and comment to USMCA2011) Dr. Yondonsuren Jargalsaikhan (Announcement of USMCA2012) Prof. Kimiro Meguro (closing speech)</p> <p>Moderator: Dr. Kuwano</p>		

Time		Friday, 14 October	
0850-1530	Short tour		

Contents

Keynote Session

page

- The 2011 Tohoku Earthquake Tsunami Disaster: Its impact, lessons for renovation** 1
Shunichi KOSHIMURA
- Energy, food, and water security: implications for Asian megacities** 11
Peter ROGERS
- Satellite information for large natural hazard** 25
Haruo SAWADA

Poster Session

- Mainstreaming climate change adaptation in urban planning in Africa** 35
Abbadi GIRMAY REDA and Nitin K. TRIPATHI
- Disaster information gathering behavior after the Tohoku earthquake part 1: Results of Japanese respondents** 45
Akiyuki KAWASAKI, Michael HENRY and Kimiro MEGURO
- An experimental study on strengthening lap splice by ferrocement jacket** 57
Amorn PIMANMAS and Rakriangkrai PAOLENG
- Correlation analysis of a reinforced-concrete building under tsunami loads and effect of masonry infill walls in tsunami resistance** 67
Anat RUANGRASSAMEE and Piyawat FOYTONG
- Area suitability modeling for rice cultivation in Saraburi Province of Thailand** 79
Bharambe K. P., Tripathi N. K. and A. R. Phalke
- Bridge deck condition assessment by ground penetrating radar -A case study in Bangladesh** 93
Bushra ISLAM, Raquib AHSAN and Mehedi Ahmed ANSARY
- Urban high speed rail link tunnel projects (GTX) in Korea** 101
Chang-YONG KIM, Seong-WON LEE and Ho-GEUN KIM
- Geospatial technologies in wetland dynamics of Deepor Beel, India** 109
Chitrni MOZUMDER, Taravudh TIPDECHO and Nitin K. TRIPATHI
- Estimation of building stories for HAZUS using light detection and ranging (LiDAR)** 119
Chomchanok LIANGWANNAPHORM and Kiyoshi HONDA
- Long and deep underground road tunnel projects of the mega-city in Korea** 127
Chang-Yong KIM, Seong-Won LEE, Xiu-Mei ZHENG, Ho-Keun KIM and Kyung-Ho PARK

Development of early warning system in Maldives	137
<i>Mahmood RIYAZ, Dugkeun PARK, Chang-Yong KIM, Sung-Wook KIM and Kyung-Ho PARK</i>	
Disaster information gathering behavior after the Tohoku earthquake part 2: Results of foreign respondents	149
<i>Michael HENRY, Akiyuki KAWASAKI and Kimiro MEGURO</i>	
Survey on people's awareness of Earthquake Early Warning before and after the 2011 off the Pacific Coast of Tohoku earthquake	163
<i>Miho OHARA, Kimiro MEGURO and Atsushi TANAKA</i>	
Seismic risk evaluation on existing RC frame buildings for northern part of Sylhet city, Bangladesh	173
<i>Ram Krishna MAZUMDER, Mushtaq AHMED and Mehedi Ahmed ANSARY</i>	
Geospatial analysis of groundwater quality using Geographical Information System: A case study from Maharashtra State of India	187
<i>Parmeshwar UDMALE and Sangam SHRESTHA</i>	
Flood risk modeling in Bangkok Province, Thailand	199
<i>Phalke APARNA, Tripathi NITIN and Bharambe KHAGENDRA</i>	
Geophysical investigation at Meghna Dhonagoda Irrigation Project (MDIP) using ground penetrating radar method	213
<i>Ram Krishna MAZUMDER and Mehedi Ahmed ANSARY</i>	
Review of nuclear energy demand in urban areas of India; VIS-À-VIS seismic disturbances	225
<i>T.Sai Sumanth REDDY and Ramancharla Pradeep KUMAR</i>	
Basic study on restoration capability of bio-cemented sandy soil	235
<i>Reiko KUWANO and Makoto HOSOO</i>	
Transformation of hybrid color space for road extraction using high resolution image	241
<i>Sanit ARUNPOLD</i>	
Future plan for the world longest undersea tunnel projects in Korea	253
<i>Chang-Yong KIM, Seong-Won LEE and Ho-Geun KIM</i>	
Assessment of community fire hazard vulnerability: A case study of ward 65 in Dhaka city	261
<i>Sharmin ARA and Mehedi Ahmed ANSARY</i>	
A study on the preferable urban structure of provincial small town in the depopulation age	271
<i>Shimpei IWAMOTO, Takahiro TANAKA and Daisaku NISHINA</i>	
Microscopic risk analysis of rear-end collisions on Tokyo Metropolitan Expressway	283
<i>Shinji TANAKA and Hisashi MIURA</i>	

Development of Geospatial Disaster Management Information Service (GDMS) as a Social System 293
Takaaki KATO, Mitsuaki KOBAYASHI, Katsuyuki YOSHIDA and Jin NAKAMURA

Comparison of neural network learning algorithms; BR and LM for flood forecasting, upper ping catchment 303
Tawee CHAIPIMONPLIN, Linda SEE and Pauline KNEALE

Building back right learning from Tohoku 313
Tomoko MATSUSHITA and Kimiro MEGURO

Oral Sessions

Session 1:

Vulnerability and risk assessment for seismic hazard

Importance of engineering judgment against unexpected hazards 319
Special Presentation: Taketo UOMOTO

Seismic functional vulnerability of the road network of the metropolitan area of San Jose, Costa Rica 325
Grettel MOLINA, William VARGA and German VALVERDE

Earthquake hazard in Ulaanbaatar city and its surrounding area 335
Ulziibat MUNKHUU, Yasuyoshi ICHIHASHI and Demberel SODNOMSAMBUU

Seismic risk analysis for intercity railway system in the Tokyo metropolitan area 343
Yoshimasa MAEDA, Hisamichi HATTORI, Toshiro SHIZUMA and Hiromichi YOSHIKAWA

SSI effect on seismic response of high-rise building in Jakarta, Indonesia 353
Kullachai TANTAYOPIN, James FRANK, Seong-Won LEE and Kyung-Ho PARK

A fundamental study on social vulnerability for public safety in China 363
Nan ZHANG and Hong HUANG

Session 2:

Flood risk assessment and management

Flood and debris flow disaster management of Mae-Ngon basin Fang District Chiangmai Province 373
Januwat LEARDSILJALEARN and Chatchai PEDUGSORN

Development of 3D viewer of flood disaster risk to enhance evacuation capacity of residents 389
Kohei MAKINODAN, Miho OHARA and Kimiro MEGURO

Sukhothai flood analysis and its response under climate changes 399
*Patinya HANITTINAN, Anurak SRIARIYAWAT
and Sucharit KOONTANAKULVONG*

**Preparing water supply master plan for a newly declared city lacking
land use guidelines and demographic information** 411
Mustafa T. HASAN and Mahmud R. AMIN

Session 3: **Durability of construction materials**

**The major research plan ‘study on unconventional emergency
management’ in China** 421
Special Presentation: Weicheng FAN, Wenguo WENG and Hong HUANG

**Effects of environmental condition on corrosion of structural steel
in marine environment of Thailand** 431
*Prasong PERMSUWAN, Pakawat SANCHAROEN,
Somnuk TANGTERMSIRIKUL, Paiboon SREEARUNATHAI,
Ekkarut VIYANIT and Wanida PONGSAKSAWAD*

Influence of temperature on deterioration process due to chloride attack 443
Takahiro NISHID, Nobuaki OTSUKI and Hiroshi MINAGAWA

**Durability evaluation of marine structure based on continuous
microstructure of concrete** 455
*Hitoshi AKIYAMA, Tomoya SAGAWA, Shafiqul Md. ISLAM
and Toshiharu KISHI*

**Defect detection and crack classification in cementitious materials
by ultrasonic testing with ANN** 465
*Saowanee SAECHAI, Pansaran SARANROM, Raktipong SAHAMITMONGKOL,
Waree KONGPRAWECHNON and Somnuk TANGTERMSIRIKUL*

Session 4: **Urban environmental planning and assessment**

**A study on the proper land use of the hillside urban area in depopulation
tendency-evaluating future scenarios from the view of disaster mitigation
and environmental conservation-** 477
Iyo YONEMASU, Takahiro TANAKA and Daisaku NISHINA

Urban heat island creating a design tool for adaptation 489
Maria B. K. DEWI

**Study on urban air quality risk using spatial technology and public perception:
a case study of Vientiane Capital city, Laos** 499
Southanome KEOLA, Edsel SAJOR and Vivarad PHONEKEO

Potential greenhouse gas reduction in Samui towards becoming carbon neutral island	511
<i>Poon THIENGBURANATHUM, Pongtip THIENGBURANATHUM and Chaya VADDHANAPHUTI</i>	

Session 5:

Properties and performance of construction materials

Using copper slang in cement concrete	519
<i>Special Presentation: Sudhir MISRA and Kunwar Krishna BAJPAI</i>	

Role of coarse aggregate in a cement-based material with strain-hardening subjected to stress-field rotation	527
<i>Kohei NAGAI, Benny SURYANTO and Koichi MAEKAWA</i>	

Effect of bottom ash and mineral admixtures on the curing sensitivity of concrete	537
<i>Kinaanath HUSSAIN, Pongsak CHOKTAWEEKARN, Warangkana SAENGSOY and Somnuk TANGTERMSIRIKUL</i>	

2nd dosage of superplasticizer and slump recovery of concrete using naphthalene based superplasticizer	547
<i>Chalermchai WANICHLAMLERT and Somnuk TANGTERMSIRIKUL</i>	

Evaluation of induced strain in concrete due to ASR expansion by digital image correlation	557
<i>Yuichiro KAWABATA, Hiroki GODA, Ema KATO and Mitsuyasu IWANAMI</i>	

Session 6:

Disaster response and recovery

Development of remote system for supporting building damage assessment during large-scale earthquake disaster	567
<i>Makoto FUJIIU, Miho OHARA and Kimiro MEGURO</i>	

Basin water management under land use and climate changes -Nan Basin as case study-	577
<i>Sucharit KOONTANAKULVONG and Kwanchai PAKOKSUNG</i>	

Relationship among response, recovery and development from the view point of financial resource allocation	589
<i>Yasuhito JIBIKI</i>	

Development and application of triage system (TRACY)	597
<i>Muneyoshi NUMADA, Yasunori HADA, Miho OHARA and Kimiro MEGURO</i>	

Session 7:

Evaluation of infrastructure health and performance

- Alkali-silica reaction in cement mortar with waste glass as fine aggregates** 609
Special Presentation: Kiang Hwee TAN and Hongjian DU
- Health survey of concrete in urban infrastructure by non-contact acoustic imaging method** 619
Noriyuki UTAGAWA, Ryo AKAMATSU and Tsuneyoshi SUGIMOTO
- Service life cycle assessment of chloride attacked concrete structures with silane treatment considering environmental impacts** 629
Aruz PETCHERDCHOO
- Development of probabilistic structural performance evaluation method for port RC structure** 641
Emi KATO, Yuichiro KAWABATA, Mitsuyasu IWANAMI and Hiroshi YOKOTA
- Calibration of roughness prediction for asphalt pavement case study: Thailand's department of highways' roads** 653
Siwarak UNSIWILAI and Boonchai SANGPETNGAM

Session 8:

Earthquake and Tsunami in Sumatra and Indian Ocean and Tohoku, Japan

- Application on spatial information for the reaction of the huge earthquake -supporting recovering activities for the 2011 off the pacific coast of Tohoku earthquake-** 663
Hirotohi KISHI, Ryotaro TAKEDA, Dai YAMAZAKI, Kanya TOKUNAGA, Yoshito SAWADA, Shiro OCHI, Takahiro ENDO and Haruo SAWADA
- Challenges in preparedness, response and relief for people with special needs in times of disasters followings the great East Japan earthquake** 671
Shigeo TATSUKI
- Simple and inexpensive tsunami disaster mitigation system for Indian Ocean Rim Regions by combining multi-purpose ocean observation buoys and properly arranged evacuation centers using religious facilities** 683
Kimiro MEGURO, Shunichi KOSHIMURA and Muneyoshi NUMADA
- Study on recovery curves for housing reconstruction in Sri Lanka, Thailand, and Indonesia after the 2004 Indian Ocean Tsunami Disaster** 691
Osamu MURAO, Kazuya SUGIYASU and Hideaki NAKAZATO
- March 11, 2011, Tsunami Earthquake of Japan –Nine epistles to friends and colleagues** 699
Tsuneo KATAYAMA

Session 9:

Seismic vulnerability and performance of structures

- Seismic vulnerability of low-rise, single long span reinforced concrete buildings** 711
Chayanon HANSAPINYO
- A simple and effective seismic retrofit scheme for masonry-infilled non-ductile reinforced concrete frames** 721
Panitan LUKKUNAPRASIT and Jarun SRECHAI
- Evaluation model of the five story horizontally-mixed hybrid timber structure** 729
Mengting TSAI and Mikio KOSHIHARA
- A study on seismic performance and reinforcement method of rammed earth wall, 'HANCHIKU'** 739
Mikio KOSHIHARA and Akiko TAKADACHI
- A study on the effect of wall stiffness on the vibration characteristics of traditional timber frames including Kumimono** 751
Iuko TSUWA and Mikio KOSHIHARA

Session 10:

Environmental management: air quality, forest, water resources

- A new generation software for regulated river system operations** 761
Special Presentation: Dushmanta DUTTA, Wendy D. WELSH, David NICHOLLS and Shaun KIM
- Environmental management in Cambodia case study: Community forest governance at local context** 771
Special Presentation: Ham KIMKONG
- Potential bioavailability of pops in lake sediment: A case study of Mae Thang reservoir, Northern Thailand** 785
Pannawee MEKWICHAI, Preeda PARKPIAN and Nguyen Thi KIM OANH
- The effect of moisture on the ground surface for LiDAR DEM generation** 797
Takahiro ENDO, Yoshito SAWADA and Haruo SAWADA
- Multi-temporal study on PM10 distribution for urban air quality in upper Northern of Thailand using spatial technology** 803
Nion SIRIMONGKALERKAL, Vivarad PHONEKEO and NGUYEN Luong Bach

Session 11:

Structural vulnerability and safety

- Site characteristics estimation of BUET campus by microtremor H/V technique** 815
Special Presentation: Mehedi Ahmed Ansary and Md. Saidur Rahman

Passporting of buildings, its safety and quality in Ulaanbaatar city, Mongolia 827
*Enebish NINJGARAV, Mendbayar OYUNCHIMEG, Yasuoshi ICHIHASHI
and Danzan DAMIRAN*

**Influence of underground structures on cavity formation due to repetition
of water penetration** 835
Mari SATO and Reiko KUWANO

Application of elastic wave measurement to model tests using bender elements 845
Sho OH and Reiko KUWANO

Session 12:

Vulnerability and risk assessment of urban safety

City development safety and improvement of urban planning of Ulaanbaatar city 855
*Special Presentation: Yondonsuren JARGALSAIKHAN
and Yasuoshi ICHIHASHI*

Evaluation of tsunami strengths of houses subjected to a Tsunami wave load 861
Gaku SHOJI and Hirofumi SHIMIZU

**Integrated climate adaptation and disaster resilience - a landscape
cooperatives paradigm** 873
Alfredo ANCENO, Nitin TRIPATHI and Oleg SHIPIN

**‘Urban environment climate maps (UECM)’ for supporting ‘Urban planning
with urban climate’: trial for mitigating urban heat island in Shanghai, China** 885
Kaoru MATSUO and Takahiro TANAKA

Photographs

Welcome boards



Registration



Inauguration ceremony



Mr. Kazuo Shibata, Consul General of the Consulate-General of Japan in Chiang Mai



Prof. Kimiro Meguro, Director of ICUS



Invited speakers (Keynote)



*Dr. Shunich Koshimura,
Tohoku University, Japan*



*Dr. Ir. Muhammad Dirhamsyah,
Syiah Kuala University, Malaysia*

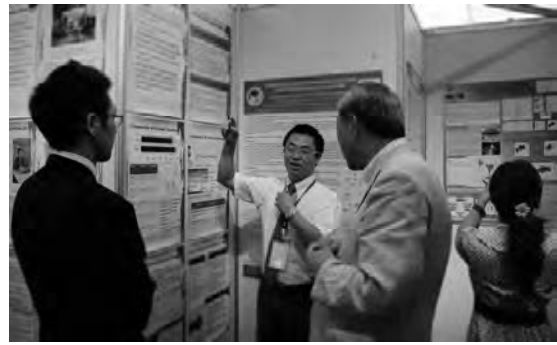
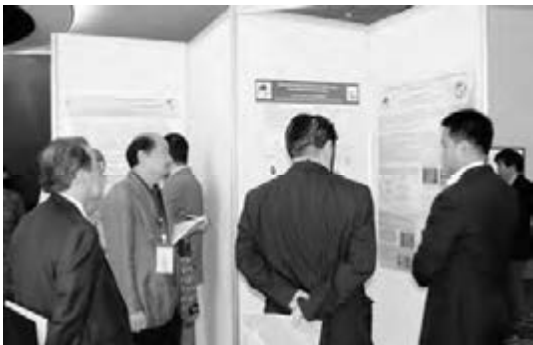


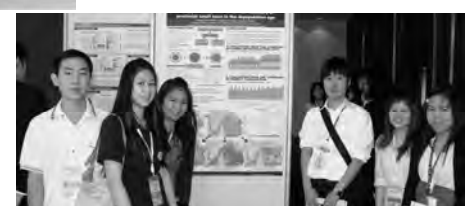
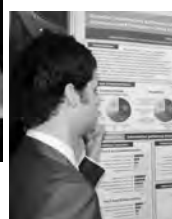
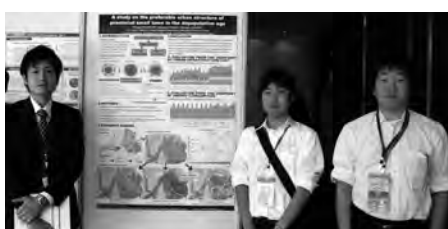
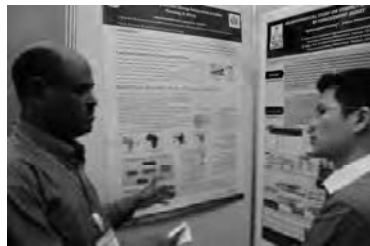
*Dr. Sidthinat Prabudhanitisarn,
Chiang Mai University, Thailand*



*Prof. Peter Rogers,
Harvard University, USA*

Special poster session at Exhibition area





Invited Speakers



*Dr. Taketo Uomoto, Chief Executive,
Public Works Research Institute, Japan*



*Prof. Srikantha Herath,
United Nations University Institute
for Sustainability and Peace, Japan*



*Prof. Hong Huang,
Tsinghua University, Beijing, China*



*Dr. Nitin Kumar Tripathi,
Asian Institute of Technology, Thailand*



*Prof. Sudhir Misra,
Indian Institute of Technology Kanpur,
India*



*Prof. Kiang Hwee Tan,
National University of Singapore, Singapore*



*Mr. Bill Ho,
Asian Disaster Preparedness Center
(ADPC), Thailand*



*Dr. Dushmanta Dutta,
CSIRO Water for a Healthy Country National
Research Flagship, CSIRO Land and Water, Australia*



*Mr. Ham Kimkong,
Royal University of Phnom Penh, Cambodia*



*Prof. Mehedi Ahmed Ansary,
Bangladesh University of Engineering and
Technology, Bangladesh*



*Mr. Yondonsuren Jargalsaikhan,
National Security Council, Mongolia,*



Group photo of participants

Closing Ceremony



Prof. Haruo Sawada, ICUS



Comment of Dr. Chayanon Hansapinyo, Chiang Mai University



Young-researcher-award awardees with Dr. Chayanon Hansapinyo



Thank you to the Thai staffs of conference



Panel presentation awardees: Mr. Mahmood Riyaz, Asian Institute of Technology, Thailand (left) and Ms. Tomoko Matsushita, The Univ. of Tokyo, Japan (right)

Oral presentation awardees: Ms. Sho Oh, The Univ. of Tokyo, Japan (left) and Mr. Hirotoishi Kishi, The Univ. of Tokyo, Japan (right)



Closing speech of Prof. Kimiro Meguro, Director of ICUS

Banquet



Ms. Aphisorn Suwannasuk (MC), RNUS secretary



Dr. Nat Vorayos, Vice president for Research and Academic Services (left) and Prof. Kimiro Meguro, ICUS (right)





Lunch and break time



Tour



Phuping Palace





Suthep Temple



Group photo at Meo Hilltribe Village, Doi Pui with Hmong

Keynote Session

The 2011 Tohoku Earthquake Tsunami Disaster : Its impact, lessons for renovation

Shunichi KOSHIMURA

Associate Professor, Disaster Control Research Center, Tohoku University, Japan
koshimura@tsunami2.civil.tohoku.ac.jp

ABSTRACT

The author reports a comprehensive study to identify the impact of the 2011 Tohoku tsunami disaster and to understand the lessons towards renovation of Tohoku coastal communities. Our team conducted an integrated investigation by field measurement of tsunami heights (flow depths, inundation and run-up heights), optical satellite image analysis, aerial photo inspection based on spatial information sciences. The preliminary findings, combined with numerical modeling technologies, lead to a new understanding of structural vulnerability against tsunami and a guide for land use management and relocation planning to reconstruct resilient coastal communities.

Keywords: The 2011 Tohoku earthquake tsunami disaster, remote sensing, field survey, tsunami fragility curve, GIS

1. INTRODUCTION

On 11 March, 2011, a devastating tsunami accompanied with M9.0 earthquake attacked the northern Pacific coast of Japan, and the coastal communities especially in Iwate, Miyagi, and Fukushima prefectures were totally swept away. The total affected area by the tsunami was estimated as 561 km² along the Pacific coast of Japan (Geospatial Information Authority of Japan, 2011). The tsunami run-up height reached up to 40 m (The 2011 Tohoku Earthquake Tsunami Joint Survey Group, 2011). As of 10 September, six months after the event occurred, National Police Agency reported 15,781 dead (4,656 in Iwate, 9,456 in Miyagi, and 1,603 in Fukushima, 66 in other prefectures) and 4,086 still missing, 115,151 buildings/houses were collapsed or washed-away. The economic impacts were estimated as 16 to 25 trillion yen (Cabinet Office, 24 June, 2011), while FY2010 national budget of Japan was 92 trillion yen (Ministry of Finance, February, 2010).

Having passed six months since the event occurred, the devastated areas have started moving forward to recover and reconstruct, or in other words, renovate their communities. Approximately 82,000 residents who lost houses moved from shelters to temporary houses (supplied 52000 units) and rental housing (Ministry of Land, Infrastructure, Transport and Tourism, 2011), 89 % of 23 million tons of tsunami debris have been removed (Ministry of Environment, 2011). Though the recovery process is still underway, local governments completed the draft of reconstruction plan including infrastructure design, transportation, land use management, urban design, relocation, and economic and industrial outlooks.

Every decision has been made quite fast compared to this wide extent of devastation.

This paper aims to comprehend the impact of the Tohoku tsunami disaster, to understand the lessons for renovation of Tohoku coastal communities. To identify the tsunami impact, our team conducted an integrated investigation by field measurement of tsunami heights (flow depths, inundation and run-up heights), optical satellite image analysis, aerial photo inspection with approach of spatial information sciences. The preliminary findings are combined with numerical modeling technologies to find out structural vulnerability against tsunami and to provide a guidance for land use management and relocation planning to reconstruct resilient coastal communities.

2. MAPPING TSUNAMI INUNDATION ZONE

2.1 Field survey

Mapping tsunami inundation extent was conducted through the analysis of optical satellite image with the ground truth calibration from the field survey. The significant feature of the 2011 tsunami was the wide extent of inundation zone. In fact, on the Sendai plain, the tsunami inundated more than 5 km inland. Since the event occurred, many Japanese groups have conducted emergency field surveys to measure the tsunami inundation and run-up heights, flow depths. Our group focused on mapping the inundation limit of the coast of Tohoku region. We conducted high-resolution surveys of the inundation limit and height in the few-centimeter accuracy by using GPS measurement system (Promark3) in Miyagi, Iwate, and Aomori prefectures. The horizontal measurement interval is ranging from approximately 500 m to several kilometers and we measured nearly 300 sites until the end of April. To draw the inundation line, we applied a remote sensing technology using satellite and aerial photographs acquired after the tsunami.

2.2 Satellite image analysis

Here, the author introduces the analysis of ALOS AVNIR2 image acquired on 14 March, 2011. Figure 1 shows the ALOS AVNIR-2 image with the plot of the field measurement of tsunami inundation limit. To evaluate the inland limit of tsunami inundation, a threshold using normalized difference water index (NDWI) is determined. NDWI is calculated by following formula,

$$NDWI = \frac{DN_{BLUE} - DN_{NIR}}{DN_{BLUE} + DN_{NIR}} \quad (1)$$

where DN_{BLUE} and DN_{NIR} indicate the digital number of blue band and near infrared band, respectively. We preliminarily confirmed that the inundation limit estimated from the satellite image is well consistent with the field measurement results at most places, when threshold value of NDWI is 0.4, although there are some exceptions that might have not been interpreted from the satellite images.

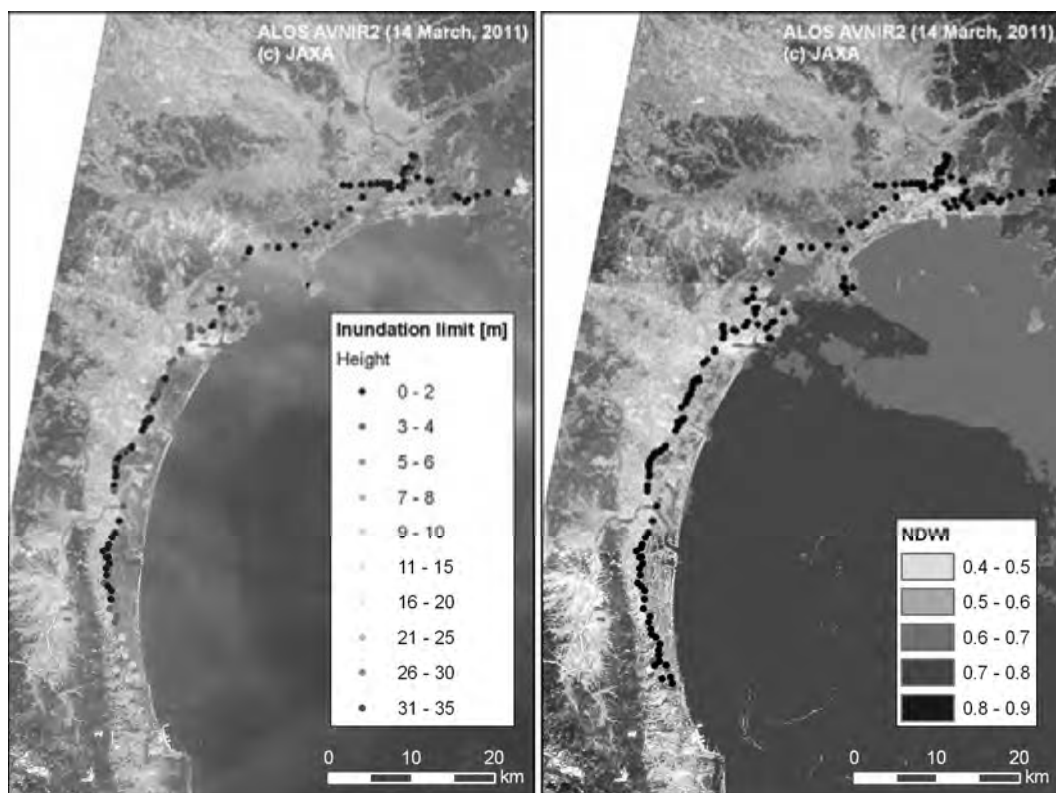


Figure 1 : (a) ALOS AVNIR-2 image acquired on 14 March 2011 with the point of measurement of tsunami inundation limit. (b) NDWI for mapping tsunami inundation extent. Black dots are the survey points used for thresholding.

3. MAPPING STRUCTURAL DAMAGE AND VULNERABILITY

3.1 Visual inspection of aerial photos

Mapping structural damage was conducted through visual interpretation of aerial photos to identify the structural vulnerability against the 2011 tsunami. For visual inspection, we used the aerial photo archives of Geospatial Information Authority of Japan acquired in the devastated area. The ortho photos of 80 cm/pixel resolution were composited with mosaic image processing. Combined with the ZENRIN building data (building shape files), the inspection was conducted for each building, by comparing pre and post tsunami aerial photos focusing on the existence of houses' roofs to add an attribution of classification "washed-away" or "surviving" as the damage status. Figure 2 shows an example of the classification in Ishinomaki city that suffered 3273 fatalities. By mapping the structural damage and overlooking its spatial distribution, not only the impact of tsunami, but the effect of coastal protection and vegetation can be seen. Complete mapping of structural damage in Miyagi Prefecture is on our web site <www.tsunami.civil.tohoku.ac.jp> to be used for field survey, land use management to understand vulnerable areas and reconstruction planning.

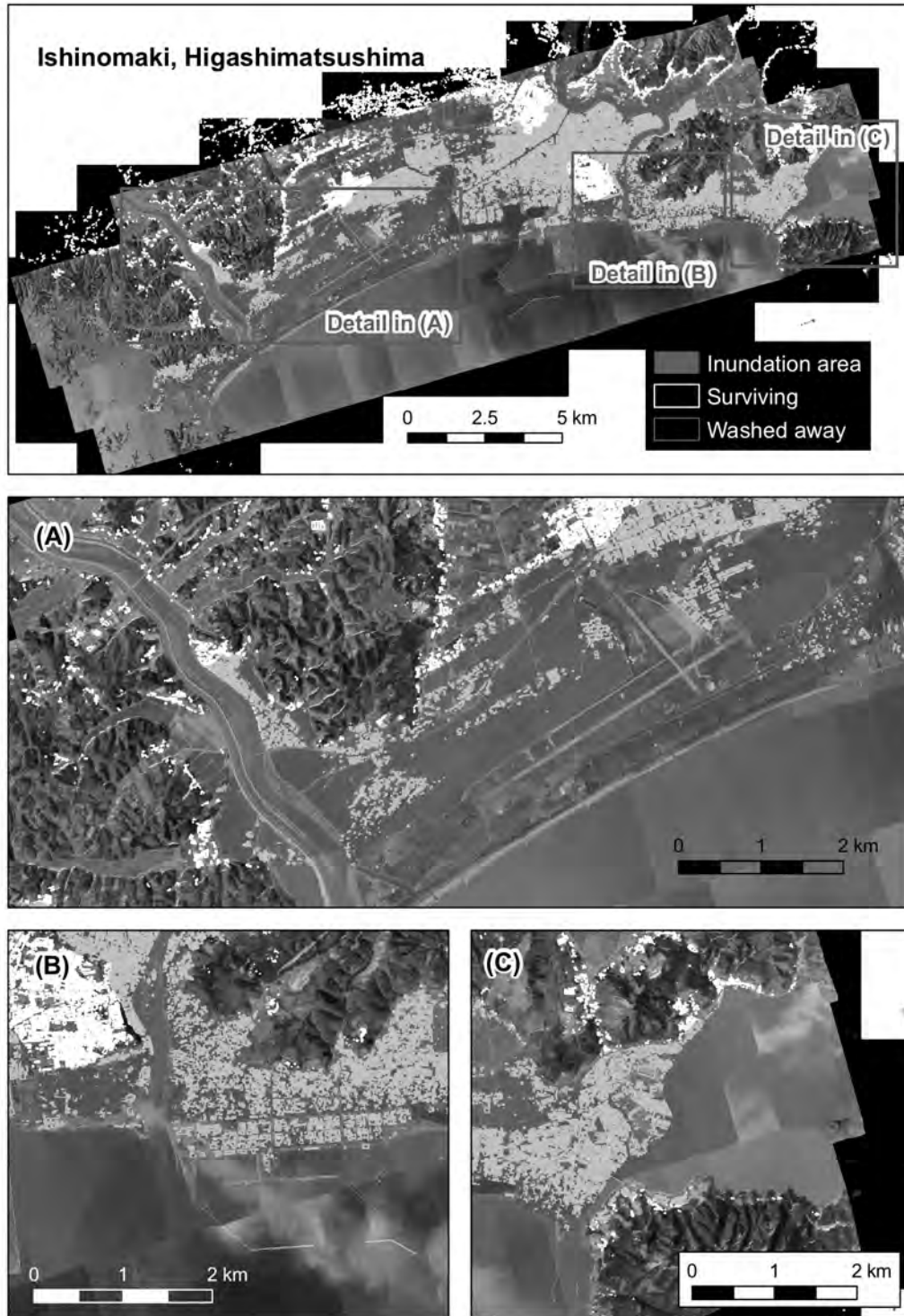


Figure 2 : Mapping structural damage by inspection of post-event aerial photos.

3.2 Structural vulnerability and tsunami fragility curves

Integrating structural damage mapping with field survey data, such as flow depths, lead to a new measure of identifying structural vulnerability against tsunami, as a form of tsunami fragility curve or tsunami fragility function. Tsunami fragility curve is defined as the structural damage probability or fatality ratio with

particular regard to the hydrodynamic features of tsunami inundation flow, such as flow depth, current velocity and hydrodynamic force.

Figure 3 shows a spatial distribution of flow depths measured in tsunami inundation zone. Spatial interpolation of measurement data (point data) to obtain raster data is combined with the structural damage mapping (e.g. Figure 2). The procedure of developing tsunami fragility curves is as follows.

1. Damage data acquisition: obtaining damage data from aerial photo interpretation (e.g. Figure 2).
2. Tsunami hazard estimation: estimating the hydrodynamic features of tsunami by field measurement (e.g. Figure 3).
3. Data integration between the damage data and tsunami hazard information: correlating the damage data and the hydrodynamic features of tsunami through the GIS analysis.
4. Calculating damage probability: determining the damage probabilities by counting the number of damaged or survived structures, for each range of flow depths.
5. Regression analysis: developing the fragility curves by regression analysis of discrete sets of damage probability and hydrodynamic features of tsunami.

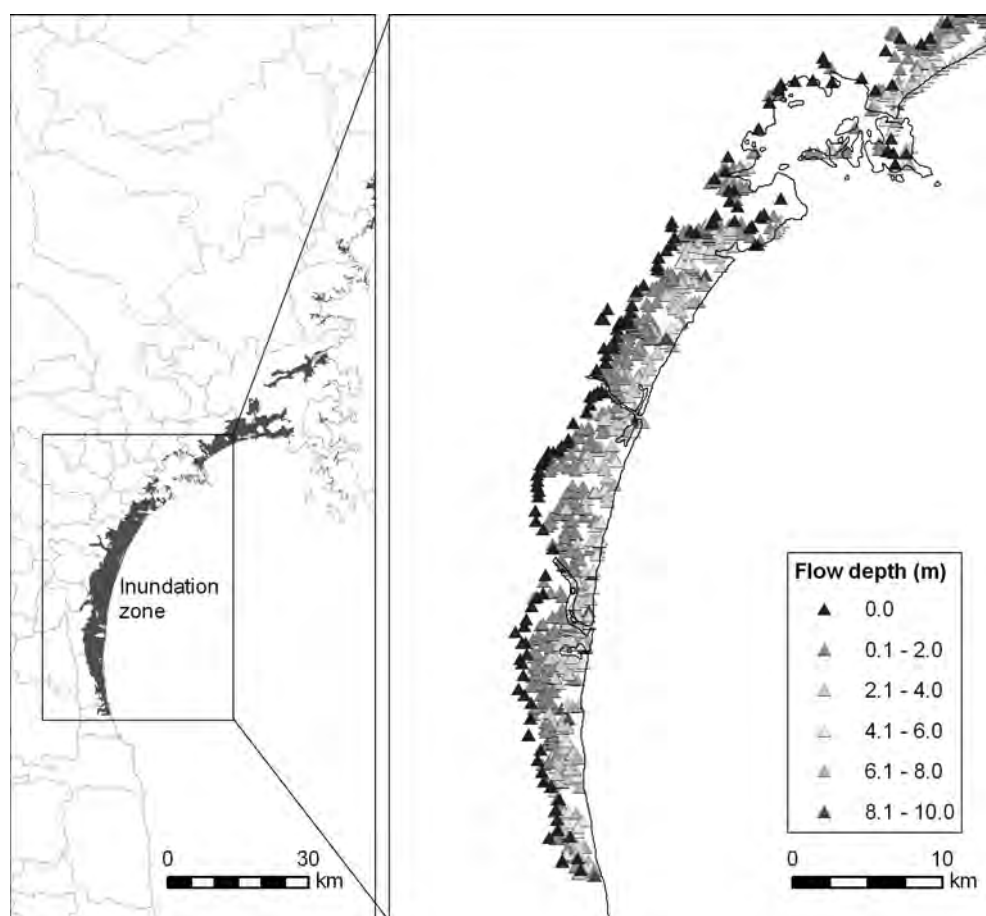


Figure 3 : Mapping the tsunami flow depth measured by Miyagi Prefecture and our survey team.

Taking above procedure, the tsunami fragility curve is preliminary obtained as shown in Figure 4. Fragility curve shown in the figure indicates the damage probabilities of structural destruction equivalent to the flow depth. Structures in Miyagi Prefecture were especially vulnerable when the local flow depth exceeded 2 m, and 6 m flow depth would totally cause washed away. This fact leads to a lesson to determine the land use plan (zoning) which considers the effect of coastal protection.

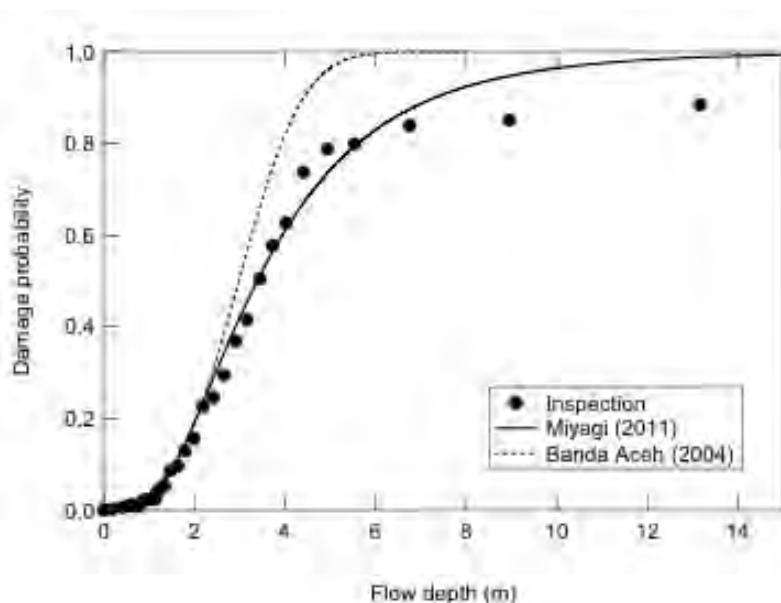


Figure 4 : Tsunami fragility curve for structural destruction (washed-away). The solid line is obtained from Miyagi Prefecture (2011 event) and the dashed one is from Banda Aceh, Indonesia (2004 Indian Ocean tsunami).

4. TSUNAMI FLOW VELOCITY AND HYDRODYNAMIC FORCE ON BUILDINGS INTERPRETED FROM THE SURVIVOR VIDEO

When a tsunami reaches the coast, its characteristics change significantly from water wave to strong water flow. And this strong inundation flow causes damage on infrastructures, buildings and humans. Measuring flow velocities of tsunami inundation on land was quite rare and it was difficult to understand what really happened in the devastated area and to identify the cause and mechanisms of structural destruction by tsunami inundation flow. But in recent years, owing to the handy video cameras and mobile phones, many of tsunami survivors attempted to capture the moment of tsunami attack to their communities and uploaded to the Internet. Applying a video analysis technique, the tsunami flow velocity can be determined.

Here, the author represents one example from Onagawa town, Miyagi Prefecture (10,014 population before the earthquake), which is one of the devastated towns by the 2011 Tohoku earthquake tsunami. The tsunami attacked to the town of Onagawa (Figure 5) at 15:20 (35 minutes after the earthquake occurred) and caused 816 fatalities and 125 still missing. As the author investigated, at least 6 reinforced concrete or steel construction buildings were found overturned or washed away. The video was taken by a resident from the top of the reinforced concrete building in Onagawa harbor (see Figure 5). Figure 6

indicates a snapshot from the video capturing the moment of the houses being washed away. Using this video, the author analyzed the time series of flow depth by measuring the height of the water level on withstanding buildings in the video. Also focusing on the movement of drifting objects, the flow velocity was estimated at the moment when the houses were washed away. As a result, flow velocity of the tsunami inundation was estimated as 6.3 m/s at the flow depth of approximately 5 m. Using this hydrodynamic features, the tsunami force was roughly estimated as 100 kN/m, which is the drag force acting on a house's wall per unit width.

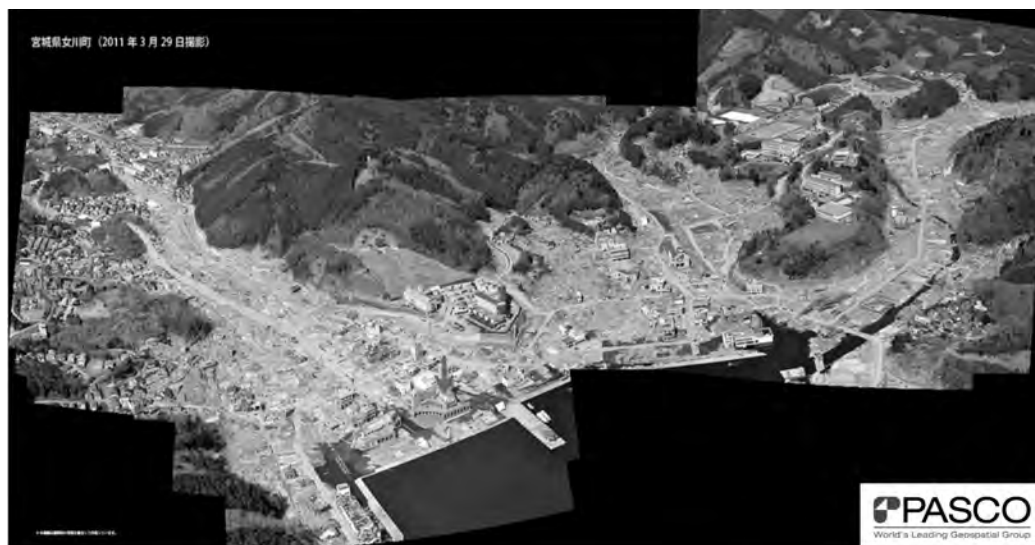


Figure 5 : An overview of Onagawa town, Miyagi Prefecture. Photo taken by PASCO Corporation. The red arrow indicates the point where the survivor video was taken.

5. TOWARDS RESILIENT COASTAL COMMUNITIES

In April 2011, one month after the event occurred, the central government established the reconstruction policy council to develop a national recovery and reconstruction outlook for tsunami-resilient community. Besides, the central government decided the policy of coastal protection such as seawall and break water, which would be designed to ensure their performance to potential tsunami level of 150 year recurrence interval. In this sense, the government policy of designing coastal protection is for 150-year tsunami level (this is called “Prevention Level”) which ensures to protect lives and properties. And for the tsunami level more than 150-year recurrence interval, so-called extreme event, the government calls “Preparedness/Mitigation Level” to reduce the losses and damage by all of the efforts of coastal protection, urban planning, evacuation, and public education.

Under the limitations and uncertain conditions of funding, prefectural and local governments have developed their own recovery and reconstruction plans, which assume 10 years to be completed. These plans consist of the combination of structural prevention/mitigation, urban planning, preparedness, and suggest their land use management, relocation, housing reconstruction and tsunami disaster

mitigation plans. The key role of academia, in engineering point of view, is to verify and evaluate if these plans really work for future disaster reduction.

When the proposed reconstruction plan should be verified, numerical modeling is a powerful tool. Figure 7 shows an example of evaluating Sendai city's reconstruction plan that includes 6.2 m levee and 6 m elevated road. As shown in the figure, through the comparison of the 2011 tsunami simulated under the pre-tsunami condition in coastal protection and land use, potential reconstruction plans can be evaluated with regard to tsunami inundation area and flow depth, exposed population and buildings, and reducing risks.

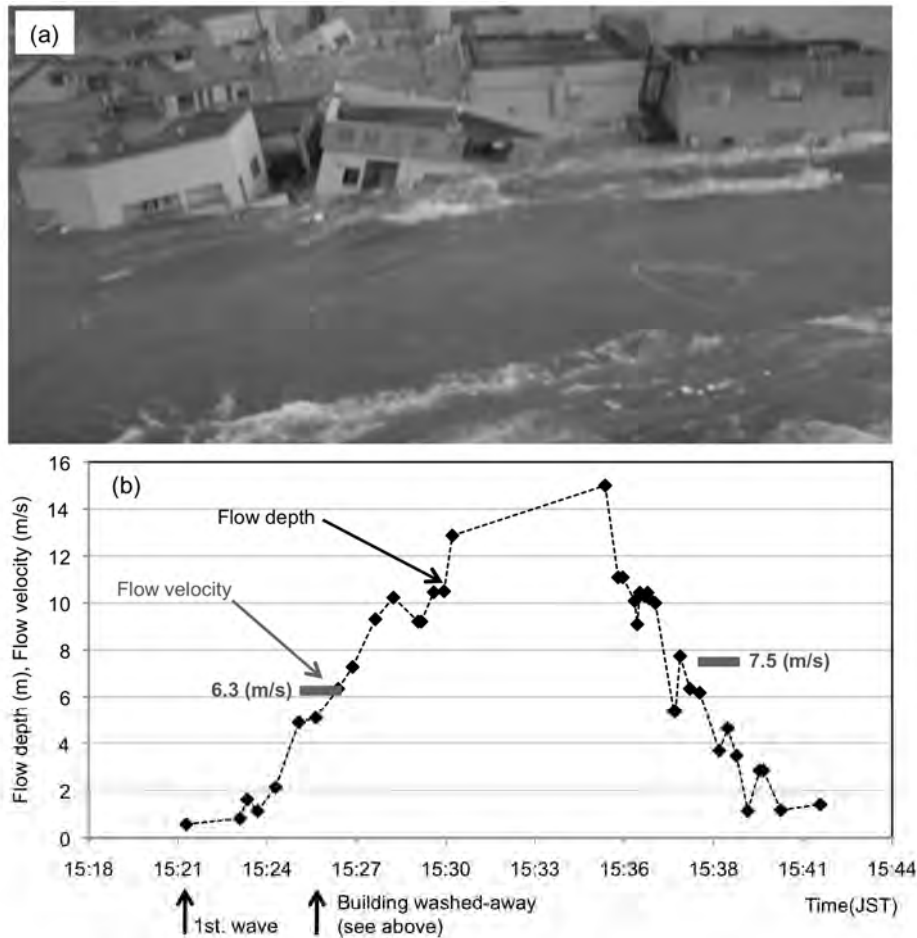


Figure 6 : (a) A snapshot of the survivor video (Yomiuri Shinbun, 2011) capturing the moment that the houses were washed away. (b) Time series of tsunami flow depth and current velocities interpreted by the video.

ACKNOWLEDGEMENTS

The post tsunami field survey was conducted by a group of 20 scientists and engineers. All the data of our measurements can be viewed on the web page <<http://www.tohoku-tsunami.jp/>>. This research was funded Ministry of Education, Culture, Sports, Science & Technology (MEXT), New Energy and Industrial Technology Development Organization (NEDO), and Japan Society for Promotion of Science (JSPS).

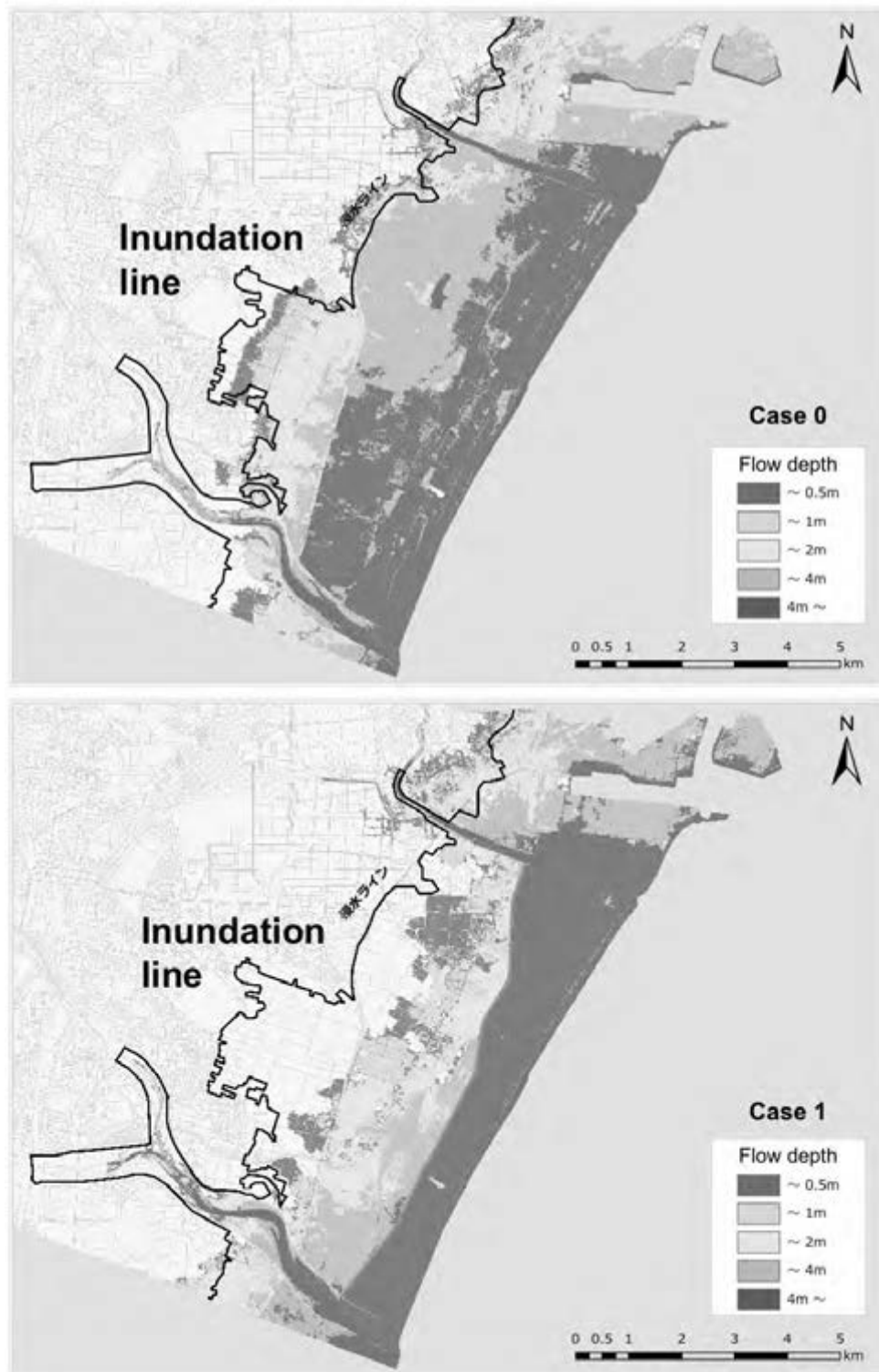


Figure 7 : Preliminary results of tsunami numerical modeling to evaluate the effect of proposed reconstruction plan in Sendai city. Sendai city is now planning coastal levees and elevated roads to minimize tsunami risks. Upper panel: The 2011 tsunami flow depth in Sendai simulated under the pre-tsunami condition in coastal protection and land use. Lower panel: Evaluation of reconstruction plan with 6.2 m levee and 6 m elevated road.

REFERENCES

- Geospatial Information Authority of Japan (GSI), 2011, aerial photo archives, <http://portal.cyberjapan.jp/denshi/index3_tohoku.html>
- Geospatial Information Authority of Japan (GSI), 2011, oblique aerial photo archives, <<http://zgate.gsi.go.jp/SaigaiShuyaku/20110525/index2.htm>>
- National Police Agency, 2011, <<http://www.npa.go.jp/archive/keibi/biki/index.htm>>
- The 2011 Tohoku Earthquake Tsunami Joint Survey Group, 2011, <<http://www.coastal.jp/tsunami2011/>>
- Cabinet Office, <<http://www.bousai.go.jp/oshirase/h23/110624-1kisyu.pdf>>
- Ministry of Land, Infrastructure, Transport and Tourism, 2011, <<http://www.mlit.go.jp/common/000140307.pdf>>
- Ministry of Environment, 2011, <<http://www.env.go.jp/jishin/shori111004.pdf>>
- Gokon, H. and S. Koshimura, 2011, *Mapping of building damage of the 2011 Tohoku earthquake tsunami*, Proceedings of the 9th International Workshop on Remote Sensing for Disaster Management.
- Koshimura, S., Y. Namegaya and H. Yanagisawa, 2009, *Tsunami Fragility, A new measure to assess tsunami damage*, Journal of Disaster Research, Vol. 4, No. 6, pp.479-488.

Energy, food, and water security: implications for Asian megacities

Peter Rogers
Harvard University

ABSTRACT

With the rapid rise in incomes and alarming rates of urbanization, Asia is already experiencing major crises in its fundamental urban resource bases: land and water. The demands for energy and food have skyrocketed as has the water needed to keep expanding the resource base and keep cities functioning. The rate of increase in urban populations is large because of the already high population densities in the rural areas and the increasing population has no place to go but to the cities. Conflict over access to water is increasing in the urban areas, and also in the rural areas as the pressure on food supplies intensifies.

Many of the cities are already badly served with unsafe drinking water and inadequate sanitation. Not only do the cities typically suffer inadequate supplies of potable water but they will have to find rapidly expanding supplies for their future growth. Not an easy task given the industrial and agricultural demands already being placed on the same resource base. Generally there is a poor understanding of the relationship between urban water and wastewater treatment and their impact on the amounts of energy and types of energy infrastructure needed to meet these growing demands. Moreover, megacities exert broad spatial geographical impacts on their regions and hinterlands, often taking the best available water and agricultural lands out of food production.

Urban water has high embedded energy content. Meeting new water demands could increase the total urban energy demands considerably. In the US, for example, as much as one-quarter to one-half of the electricity used in many cities is consumed at municipal water and wastewater treatment facilities. Unfortunately many of the modern ways of increasing water availability greatly increase the embedded energy demanded. This paper analyses technical options for resolving the urban water-food-energy nexus and explores how they could fit into the resource policy and management of these increasingly large urban agglomerations

1. INTRODUCTION

The theme of this symposium is “Urban Safety” and this usually is applied to the mitigation of intermittent shock disasters such as earthquakes, floods, and terrorism. This paper attempts to identify and cope with potential “Silent Disasters” which happen slowly and gather their strength over many

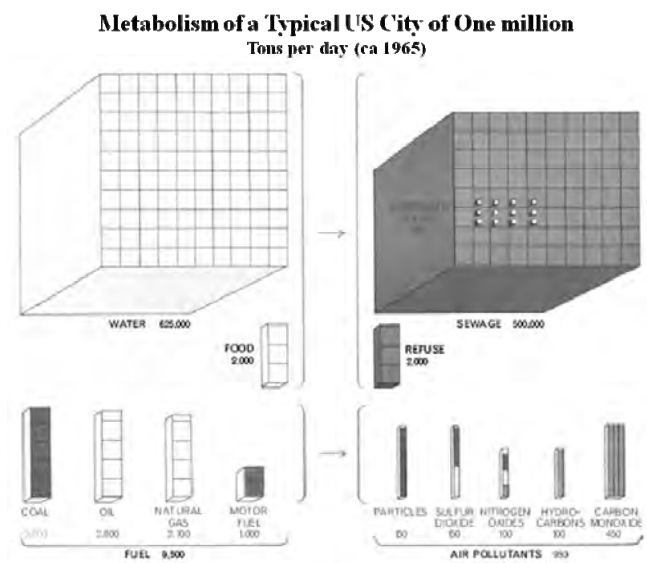
years. Examples of such disasters are the growing demands placed on the urban infrastructure. For example, the need to provide the urban population access to food for nourishment and water for sanitation and commercial use is well understood. On the other hand, the interaction of both the need for food and for water—which directly connect to energy for the system to function—is not well understood. In the literature this is increasingly called the urban “food, water, and energy nexus.” Often the word “sustainability” is applied to studies of resource use in cities; however, there is nothing that is inherently self-sustaining in modern cities. The word “viability” is a better description of what can be achieved in the long-run. Of course there is a long list of desirable properties associated with the concepts of sustainability and viability when applied to cities; however, the concept of efficient resource use is the fundamental property.

Currently of the 20 cities in the world with more than 10 million¹ people, nine are in Asia, and based on UN projections (UN|DESA, World Urbanization Prospects: The 2009 Revision, 2009) by 2050, seven of the 10 largest cities in the world will be in Asia. Over the same period the percentage of urban population in Asia will rise from 42% to 65%. These numbers are unprecedented, but for one country, China, its urban population is predicted to rise to one billion by 2030 (McKinsey, 2009). The UN report forecasts that by 2025 the following Asian cities will be megacities (see Fig.1): Tokyo (37 million), Delhi (29), Mumbai (26), Dhaka (21), Kolkata (20), Shanghai (20), Karachi (19), Beijing (15), Manila (15), Osaka-Kobe (11), Shenzhen (11), Chongqing (11), Guangzhou, Guangdong (11), Jakarta (11), and Lahore (10). London which was the 30th largest city in 2010 with 8.6 million does not make it onto the list of top 30 cities by 2025.

2. HOW PERCEPTIONS OF URBAN METABOLISM HAVE CHANGED OVER TIME

Urban sustainability and viability are strongly related to, and have their roots in, urban metabolism and urban ecology. For most people the era of “urban metabolism” was ushered in by Abel Wolman’s 1965 *Scientific American* article entitled “The Metabolism of Cities.” Wolman’s emphasis on water and wastewater may be understandable because as a leading sanitary engineer he had worked on these issues for his whole career. Nevertheless, Wolman spotted an anomaly in the metabolism of the city when he compared the city to biological organisms which metabolize food, water, and energy to survive and in turn produce waste products which must be excreted. Using a simple materials balance he demonstrated that in terms of materials, water and wastewater were the overwhelming input and outputs to cities in terms of their sheer magnitudes. Wolman’s figure (1965)

¹ It is only recently that the UN (2002) was referring to megacities as those cities of 5 million or more people. Currently the UN (2011) uses 10 million and above. This change is an indication of just how rapidly urbanization has been occurring.



Abel Wolman, *the Metabolism of Cities*, Scientific American, Sept. 1965, pp. 179-190

Figure 1

shown here in Fig. 1, shows the material inputs of water, food, and energy for a typical US city of the mid 1950s. Water at 625,000 tons per day dwarfs the food and energy inputs by 2 orders of magnitude. And on the output side sewage at 500,000 tons predominates, again by two orders of magnitude, over the metabolized food and energy outputs.

Given the clarity of Wolman's exegesis, it is surprising to move the clock forward to 2002 when London was the subject of a comprehensive study on its resources flow and the urban footprint (City Limits, 2002). Despite Wolman's clear signal, the study on the ecological footprint of Greater London ignored the 866,000,000 tons of water input into Greater London and concludes that water with 866,000,000 tons of consumption accounts for only 0.3% of its footprint, while food with only 6,900 tons of input accounts for 14% of the footprint. Part of the problem here is methodology of converting tons of material flow to equivalent global hectares of space on the planet. Nevertheless, the London study is a mine of useful comparative data and methodology for assessing the footprint of many other cities which have not benefited from the meticulous data generation and analysis that London has through this study. As mentioned above the one major problem of the London study is its handling of water as an input and output of urban metabolism, some of which may be due to the possible double counting of water and land for food production in any footprint study.

For the year 2000, with a population of 7.4 million, Londoners consumed 154,400 gwh of energy (13.26 million tons of oil equivalent and 85,494 gwh as actual electricity use), 49 million tons of materials (of which 27.8 million tons were used in the construction sector), generated 27.8 million tons of waste, consumed 6.9 million tons of food, and 876 million cubic meters of water. Figure 2 (City Limits, 2002, p. 17) shows the inputs and outputs graphically. These physical flows were translated into an ecological footprint of 49 million global hectares (the equivalent size of Spain) comprised of 44% for materials and waste, 41% for food, 10% for energy, and only 0.3% for water.

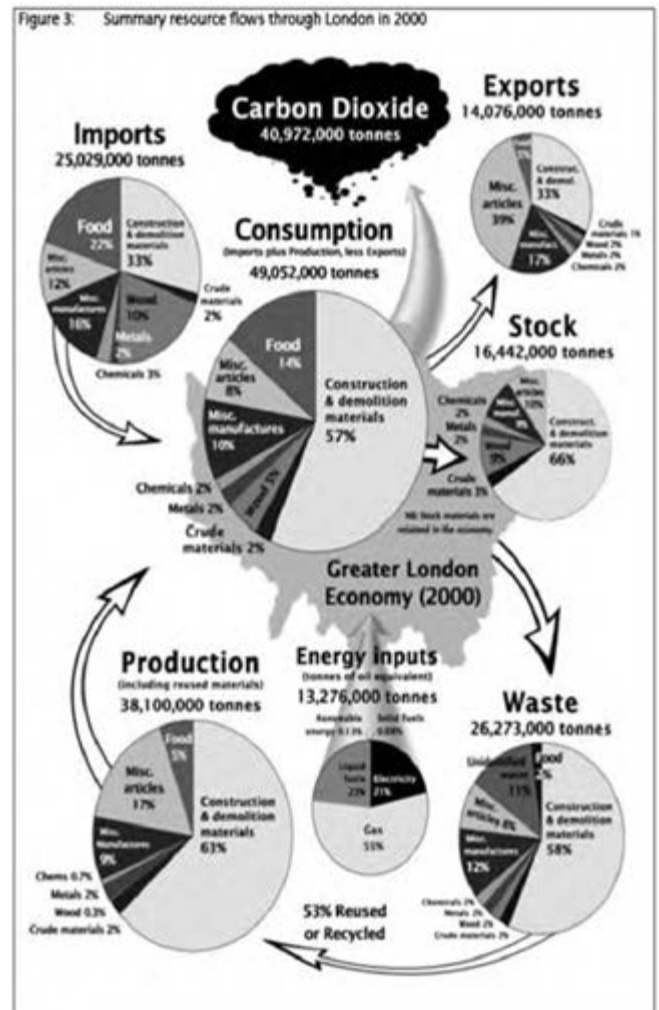
Comparing the development of urban metabolism between the Scientific American's 1965 issue on "Cities," and the 2011 issue of the

Scientific American devoted to “Cities: Smarter, Greener, Better,” we can see the early arc of shock and disbelief that the massive urbanization was actually happening and how unprepared for it we were then, evolving to the current positive embracing of the city as engines of innovation for economic and social life. In the recent issue there is little technical pessimism: we can solve all of the resource and environmental problems that cities create with existing and emerging technologies for wealthy cities in the developed world.

3. URBAN WATER, FOOD, AND ENERGY

In the US of the total 123.45 thousand gwh of electricity used in 2000, fully 3.4% were used by water supply and wastewater treatment (EPRI, 2009). This places the water sector in third place below the chemical and the primary metals industries in energy use. Of this amount more than 50% was used in public and private wastewater treatment and 25% in public water supply and a further 19% were used for supplying irrigation water. The average energy intensity for public water supply was 1,900 kwh/mg (0.5 kwh/cm). Based on Wolman (1965), Decker et al. (2000) delineated the historical energy and material flows through urban ecosystems (Fig. 3) from an estimated 6 tons per year for a human in Neolithic times, through rural individuals ca 1800 mobilizing 25 tons per person per year, up to modern urban individuals ca 1990 mobilizing 100 tons per year, such as in Sydney and London.

The prospects of water shortages in Asia, alone, would be a serious resource-allocation problem, but it will be confounded by climate change and its attendant effects on the hydrology of continents, regions, and nations. Water and energy issues have traditionally been researched as single issues, not as an integrated web of opportunities and limitations, particularly in urban regions. The uncertainties of climate change complicate the resource-management challenges. Studies need to go beyond traditional views of a stationary world in which not only is climate known, but also the future economic and social developments are viewed in similarly narrow terms.



City Limits, p. 17, tons per year

Figure 2

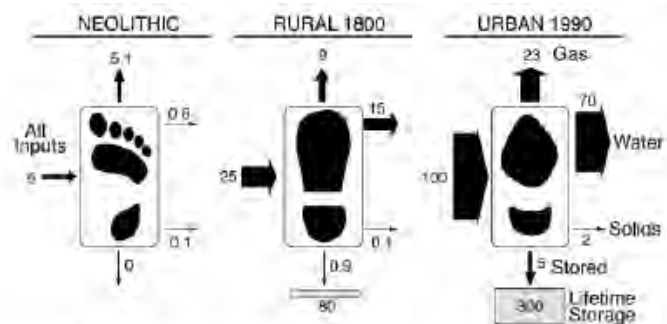


Figure 3 Material budget (tons per year) for an individual human from the Neolithic to present. Lifetime storage includes built structures and artifacts. Adapted from References 46 and 233.

Decker et al., Energy and Material Flow through the Urban Ecosystem, Ann. Rev. Energy Environ., 2000, 25:685-740

Becoming aware of these complex interactions, many countries have spent huge amounts of financial resources to improve their water security. Modern examples of such concerns include Israel's National Water Carrier, the Central Valley Project in California, the PRC's current work on the South-North Water Diversions, and India's attempts to interlink some river basins to bring water to water-scarce regions.

Less well known is the competition for water that exists between the demands for food and energy. For example in the PRC, 76% of the water withdrawn for industrial use was used in the generation of electricity; coal-powered generation is the number one consumer of water in the PRC's industrial sector. Thus, as rapid economic growth leads to large increases in the demand for energy and increased food consumption, countries like the PRC and India find themselves in a serious bind: already their existing water resources are almost fully committed to agriculture and food production, leaving little available for meeting increasing urban and industrial demands. The case of the PRC is particularly severe and the Government is taking it very seriously, not only with massive water diversions (over \$60 billion) but also by beginning to implement water-saving technologies in both the water sector and the energy sector.

According to Goklany (2007) and Brown (2011), access to water and energy will be the major constraints on moving toward a sustainable planet by 2050. The big consumer of water is agriculture and its ability to feed the global populations is in doubt without major improvement in water-use efficiency in agriculture. This paper focuses more on water access in urban areas and its energy implications than on the conflicts over water for agricultural uses. Many of the destination cities of rural-urban migrants, however, are already badly served, having unsafe drinking water and inadequate sanitation. Not only do the cities typically suffer inadequate supplies of potable water but also they will have to find rapidly expanding supplies for their future growth—not an easy task given the industrial and agricultural demands being placed on the same resource base.

Generally, the relationships among urban water and wastewater treatment and their impact on the amounts of energy and types of energy infrastructure needed to meet these growing demands are poorly understood. Urban water uses as much as 1.65 kilowatt-hours per cubic meter supplied (NRDC, 2004). Depending on the nature of the water supply options and the location of the resources, meeting the new water demands could increase the total urban energy demands by 10%–15% and electrical energy by as much as 30%. Unfortunately, many of the modern ways of increasing water availability to relieve urban water stress, such as by recycling and desalination, greatly increase the embedded energy demanded. It is commonly accepted that 40% of the cost of desalination and water recovery using reverse osmosis are due to energy. This paper assesses the current energy demanded by urban water, predicts how large the future demands could be, and reviews technical options for resolving the urban water-energy-food nexus for Asian megacities.

4. ENERGY USE FOR WATER AND WASTEWATER MANAGEMENT

The amounts and types of energy used in the provision of urban water supply and wastewater disposal depend to a large extent on the current water-use behavior of the populations and the nature of the technologies for supply and disposal. For low-income areas, the per capita water use could be as low as 50 liters per day (lpcd), with only 70% of the population being covered by the water systems and as low as 20% with access to sanitation systems. Working toward attaining the Millennium Development Goals (MDGs) could increase the urban coverage into the 90% range and increase the demand to 100 lpcd or above. Thus, even without any population increase, the total water demands placed on the megacities' systems could increase greatly. Rapid population growth will greatly exacerbate the problem.

The most recent summary of progress toward meeting the MDG goals, UN-ESCAP (2010) reported on data from 2008 and projected these forward to the 2015 deadline. Of the major countries with megacities the Philippines and China appear to be on target to meet the 2015 goals, Bangladesh may be on the way, but Pakistan and India lag far behind.

5. FUTURE URBAN WATER-BASED DEMANDS FOR ENERGY AND FOOD

Table 1 reports the 15 Asian megacities projected by the UN Population Division (2011) to be individually at least 10 million in population by 2025. The 15 cities had a combined population in 2010 of 218 million, or 12.39% of the total Asian urban population and the population in these megacities only rose to 267 million by 2025. The total Asian urban population over the same period is projected to grow by over 35%. This indicates a belief that the bulk of the future urbanization will occur in cities smaller than the 10 million plus megacities, probably in the 1 to 5 million-sized cities as the UN predicts. This should give some solace to the mayors and city government of the megacities that their rates of growth will slow down over the next 15 years.

	CITY	Pop in 2010	Pop in 2025
1	Tokyo*+	36.67	37
2	Delhi+	22.16	29
3	Mumbai*+	20.04	26
4	Dhaka*	14.65	21
5	Kolkata+	15.55	20
6	Shanghai*+	16.58	20
7	Karachi*+	13.12	19
8	Beijing+	12.39	15
9	Manila+	11.63	15
10	Osaka-Kobe+	11.34	11
11	Shenzhen	9.01	11
12	Chongqing	9.4	11
13	Guangzhou*+	8.8	11
14	Jakarta*+	9.21	11
15	Lahore	7.13	10
	TOTAL	217.68	267
	TOTAL ASIA	1757.31	2383.27
	% in Megacities	12.39	11.20
* = on World Bank ESMAP study list			
+ = on Green Cities Index			

6. MODELING THE FUTURE URBAN WATER-FOOD-ENERGY NEXUS

In order to assess the magnitudes of potential conflict among urban water use, urban energy use and the urban food supply, I constructed a simple simulation for the food, water and energy resources needed by 2025 for the projected 15 Asian megacities. Results are given in Table 2. The projections of potential urban water and wastewater supply and treatment by country are made from a 2010 base year until 2025. The table reflects the increasing population sizes based on the UN World Urbanization Prospects, 2010, and on estimates of current water consumption, and on estimates of percentage coverage of the population by municipal water supply and sewerage, and on estimates of water footprints of the food imports to the cities. For future dates, I assumed that the megacities are on a path toward meeting the MDGs in terms of coverage and increasing per capita use. Table 2 shows the joint effect of increasing urban populations, increasing coverage by water systems, increasing water for food demands, and increasing per capita water use for each of the megacities. For all of the megacities taken together over the 15-year interval there is a 22% increase in the demand for water services for an 11% increase in population. In the cases of Dhaka and Karachi the increased water demand would be more than 50%, whereas in Tokyo the incremental effects are negligible due to the fact that its water and food intakes are so high that they probably not increase, and of course the population is expected to increase very slightly over the 15 year period.

Table 3 simulates the incremental demand for electricity just for the water and wastewater sectors of the cities. While the cities of Delhi and Dhaka will expect around 10% incremental growth in demand for the WSS sector, the overall energy demand of the WSS sector will remain at a modest 3-5% of total urban electricity use—which is what we experience in the developed countries.

	CITY	Domestic Water lpcd	Food# Water lpcd	food increment		WSS increment		Total water increment	
				2010-25 mcm	%	2010-25 mcm	%	2010-25 mcm	%
1	Tokyo*+	330	5500	665.47	0.90	39.93	0.9	705.39	0.90
2	Delhi+	250	4000	9991.06	30.89	1471.24	72.8	11462.30	33.35
3	Mumbai**	250	4000	8701.60	29.74	1303.05	71.3	10004.65	32.18
4	Dhaka*	115	4000	9271.00	43.34	1914.52	311.3	11185.52	50.83
5	Kolkata+	138	4000	6497.00	28.62	1625.75	207.6	8122.75	34.59
6	Shanghai*+	411	4500	5617.35	20.63	-78.25	-3.1	5539.10	18.64
7	Karachi*+	164	4000	8584.80	44.82	1503.19	191.4	10087.99	50.59
8	Beijing+	218	4500	4286.93	21.07	820.88	83.3	5107.80	23.94
9	Manila+	155	4000	4920.20	28.98	1148.78	174.6	6068.98	34.41
10	Osaka-Kobe+	418	5500	-682.55	-3.00	-405.19	-23.4	-1087.74	-4.44
11	Shenzhen	350	4500	3268.58	22.09	173.92	15.1	3442.50	21.58
12	Chongqing	350	4500	2628.00	17.02	124.10	10.3	2752.10	16.54
13	Guangzhou**	527	4500	3613.50	25.00	-367.77	-21.7	3245.73	20.10
14	Jakarta*+	77	4000	2613.40	19.44	1066.10	411.9	3679.50	26.85
15	Lahore	350	4000	4190.20	40.25	293.64	32.2	4483.84	39.61
	TOTAL			74166.52		10633.88		84800.40	22.56

* = on World Bank ESMAP study list
+ = on Green Cities Index

Hunger Free World, Special issue, No. 26, Jan 24, 2011. Cites Japanese government sources that average Japanese consumes 3 cm of water per day for drinking and food.

Olli Varis, WRD, vol 22, no. 2, pp. 199-225, June 2006, gives figures that high or high-middle income countries consume 5.5 cm per person per day, and lower-middle, or low income countries' city dwellers may consume 4.0 to 4.5 cm per day.

TABLE 3
ASIAN MEGACITIES IN 2025 (UN World Urbanization Prospects, 2010)
ENERGY FOR WSS

CITY	Current	Assumed	Gwh/yr#	Gwh/yr	Gwh/yr	% of 2025	
	Energy kwhe/c	2025 kwhe/c	WSS 2010	WSS 2025	2010-25 increment	%	total city use
1 Tokyo**	6638	6000	73.6	74.3	0.7	0.9	3.3
2 Delhi+	5000	5000	32.3	42.3	10.0	30.9	2.9
3 Mumbai**	5000	5000	29.3	38.0	8.7	29.7	2.9
4 Dhaka*	144	3000	21.4	30.7	9.3	43.3	4.9
5 Kolkata+	5000	4000	22.7	29.2	6.5	28.6	3.7
6 Shanghai**	6666	6000	27.2	32.9	5.6	20.6	2.7
7 Karachi**	475	4000	19.2	27.7	8.6	44.8	3.7
8 Beijing+	6000	5000	20.4	24.6	4.3	21.1	3.3
9 Manila+	5000	5000	17.0	21.9	4.9	29.0	2.9
10 Osaka-Kobe+	6638	6000	22.8	22.1	-0.7	-3.0	3.2
11 Shenzhen	6000	6000	14.8	18.1	3.3	22.1	2.7
12 Chongqing	5000	5000	15.4	18.1	2.6	17.0	3.3
13 Guangzhou**	6000	5000	14.5	18.1	3.6	25.0	3.3
14 Jakarta**	564	5000	13.4	16.1	2.6	19.4	2.9
15 Lahore	3000	5000	10.4	14.6	4.2	40.3	2.9

* = on World Bank ESMAP study list
+ = on Green Cities Index
= assumes 1 kWh per cubic meter processed

7. IMPROVING THE EFFICIENCY OF URBAN WATER AND ENERGY AND FOOD SUPPLIES

When dealing with the approaches to solving the problems of sustainable water resources for urban areas, the type of problem addressed and the scale of the potential solutions must be defined clearly. There is a large and growing literature and databases on the concepts of sustainable cities. Much of the literature (Hao et al., 2010), however, focuses on smart buildings rather than entire cities. Moreover, the discussion tends to focus on new buildings rather than retrofit of the existing building stock of old traditional infrastructure. The literature also bifurcates into those specializing in actual here-and-now cases and those promoting future potential developments.

Unfortunately, many of the cases reported are still largely hypothetical. Hard data on actual cases are difficult to find. For example, hypothetical cases like Qingdao and Dongtan, near Shanghai, are widely discussed (Hao et al., 2010) and promoted because of their widespread integrated energy-water-transport systems approaches, but cases like The Solaire in Battery Park City, New York, or Dockside Green in Victoria, Canada, which have successfully integrated buildings, or multiple buildings with new construction and the rehabilitation of existing cities, receive little attention.

The examples of Solaire and Qingdao are illustrative of the wide discrepancy between the empirically based data and the hypothetical data used in future-oriented studies. The Solaire has consistently achieved a 48% water-consumption reduction in comparison with comparable residential buildings in New York City and a 56% reduction in wastewater discharge. This water and wastewater reduction is achieved by a combination of wastewater reuse and water conservation where non-potable water is distributed in closed-loop systems for uses that include toilet flushing,

cooling tower make-up, laundry, and irrigation. Each building in The Solaire development is unique and the exact components vary somewhat, but the overall program of wastewater and rainwater reuse remains the same. The Qingdao Eco-city is repeatedly cited as an excellent approach to making cities more sustainable with 85% water savings and 100% energy savings. Unfortunately, like most of the future-oriented cases, the basis for the calculations is often optimistic or unrealistic. Wherever possible, I recommend that actual performance of integrated water and waste-recycling data be used instead of the hypothetical data.

Hao et al. (2010) provide a critical review of city-scale developments aimed at improving the actual water and energy nexus. Hammarby Sjöstad (Sweden) actually has been developed; Dongtan, planned near Shanghai (PRC), is apparently one of the first comprehensive conceptual eco-city developments. The final population was planned to be 500,000 around 2050. However, its construction is currently on hold. For Qingdao (PRC), eco-blocks are the foundational units in Fraker's (2008) concept of the eco-city. A super block is a typical high-rise residential development in the PRC, usually 100–200 ha with 2,000–10,000 residential units housing 6,000–30,000 people. The PRC is now building 10–15 super blocks per day with conventional infrastructure, but the innovative Qingdao project is on hold. Two well-funded projects underway are in Tianjin (PRC) with \$9.7 billion invested and Masdar (United Arab Emirates), with an expected funding of \$22 billion. Two projects already developed in the United States are Treasure Island and Sonoma Mountain Village, both in California.

Table 4, from Hao et al. (2010), pulls together some of the salient facts about water and energy conservation in these projects. Note the huge differences between the water savings claimed for the three projects actually developed (Hammarby, Treasure Island, and Sonoma Valley) and those in planning stages. The energy savings reported for the developed projects are remarkably close to those predicted for the remaining projects, implying that energy conservation is inherently easier to accomplish than water conservation at the household and project level. The last column reports the costs or the expected costs for typical units in the projects. The costs for the completed or underway projects are much higher than the predicted costs for the not yet constructed projects. This reveals a bias in favor of lower costs by the planners rather than what the project developers actually see. There is almost a factor of 10 underestimate on the not yet constructed projects.

CONCLUSIONS

The simple simulation models used in this paper do not show unexpected results. First despite the relatively low rates of total population growth in the region, urban populations are likely to increase substantially by 2025 (from 1.75 billion in 2010 to 2.38 billion, a 35% increase), but the large megacities in the region will experience a more modest increase of less than 25%. This implies that there will be large population increases in the smaller cities and towns in the region.

For the current large cities in Asia, the electricity demands for the urban water sector would likely stay well within the 3%-5% range of total city use—well within the range in the industrialized countries. Moreover, each city and country is currently embarked on extensive expansion of their electricity supply capacity, such that electricity capacity will grow along with the demands and does not foresee major crises as long as fossil fuels will be readily available. Unfortunately, this is not the case with water supply. There are some serious limits on water availability, hence the need to conserve water in this sector. This may be quite difficult given the pressures to expand the actual quantities of water supplied and broaden the coverage of the systems and meet the increasing demands for food.

The analysis presented in this paper has two major problems. First and foremost is the absence of reliable comparative data on urban water, food, and electricity use. Secondly, we only consider the water-food-energy nexus for urban water supply and wastewater treatment, the energy and water to produce the food for the cities, and the energy required to keep this integrated system thriving. Third, other important water uses related to flooding and urban drainage are not incorporated. Finally, and equally important, is that the model does not really reflect the dynamic economic behavior of the consumers who ultimately drive the systems. Nevertheless, this simple model does provide some confidence that there can be a sustainable urban future in the megacities without resort to the fancy integrated water and energy solutions promoted in Hao et al. (2010), provided that careful attention is paid to the water management in the cities. One major concern, however, is the potential reduction in water available for agriculture in all the countries of Asia and its repercussions on food, sanitation, health and urban energy use; this needs careful study

Notes

¹ A discussion of the unreliability of the generally available data bases is worth including here. Kallidaikurichi and Rao (2010) review the data on the adequacy of drinking water in 23 Asian countries. They spent a great deal of effort on developing the best available database for the region, but were critical of the quality of available national and local data for serious policy analysis. Their book developed an index of drinking water adequacy, which could be used for ranking countries from the point of view of access to safe drinking water; they did not include the associated food and energy inputs. McIntosh (1993) and McIntosh and Yñiguez (1997) assessed water management in 50 utilities in Asia for the Asian Development Bank (ADB). Their compilation of economic data reveals that the majority of the utilities were unable to cover their operational costs from tariffs alone. Ten of our projected megacities were on the 1993 list of 38 cities surveyed and 10 of 49 in the 1997 list. Later ADB (2004) surveyed 18 Asian cities of which 6 were in our set of future megacities. These data were from 2001 or earlier, and showed only marginal improvement over the situation in 1997. Two sources of energy data for Asian cities are The World Bank's ESMAP Study

(2010) and the Asian Green City Index (2011) which provide some spotty data for 7 and 11 of our cities and 11 respectively. Obvious sources, such as AQUASTAT of the United Nations Food and Agriculture Organization (FAO), the World Bank's rapid assessment framework (ESMAP, 2010), ADB-UNEP (2004), the International Energy Association's energy data (IEA, 2008), and the Pacific Institute's global water data (Gleick, 2009) were all utilized to assemble a workable database for initial estimations. The Southeast Asian Water Utilities Network's (SEAWUN, 2005, 2007) databases on energy use in water and wastewater utilities in Southeast Asia were a very helpful, but outdated, source. It should be understood, however, that the combination of data from different sources and slightly different dates can be misleading. In the end the simulation model is really a "thought model" based on the variety of collected data bolstered by what appear to be reasonable assumptions where the data coverage fails.

Tonnes are metric tons, or 1000 kg.

Gha global hectare is a measure of biocapacity.

Cheng (2011) calculates on p. 19 the electrical energy requirement for providing 35 mgd of 0.22 kWh/m^3 for water supply alone.

The World Bank (ESMAP, 2010) gives a range of $0.1\text{--}0.59 \text{ kwhe/m}^3$ for potable water and $0.21\text{--}0.59 \text{ kwhe/m}^3$ for wastewater.

The Pacific Institute (Gleick, 2009) reports 0.77 kwhe/m^3 for potable and waste treatment, and distribution.

The New York State Energy and Research Development Authority (2008) reports a national average of 0.36 kwhe/m^3 for potable water supply, and 1.25 kwhe/m^3 for secondary treatment and 1.78 kwhe/m^3 for tertiary.

For simplicity we have chosen to use 1.0 kwhe/m^3 for combined water and waste supply and treatment.

REFERENCE

Asian Development Bank. 2004. *Water in Asian Cities: Utilities' Performance and Civil Society Views*. Manila: Asian Development Bank.

Asian Development Bank and United Nations Environment Programme (ADB|UNEP). 2004. *Greater Mekong Subregion Atlas of the Environment*. Manila: Asian Development Bank.

Asian Green City Index: Assessing the Environmental Performance of Asia's Major Cities. 2011. Economist Intelligence Unit. Munich: Siemens AG.

Brown, Lester R. 2011. *World on the Edge: How to Prevent Environmental and Economic Collapse*. Washington, DC: Earth Policy Institute.

Cheng, Likwan. 2011. *Energy and Emission in Water from Great Lake Sources: Life-Cycle Study of Water Production in*

Evanston, mimeo, Harvard University Extension School, 82 pages, August 2011.

City Limits: A Resource Flow and Ecological Footprint Analysis of Greater London. 2002. Chartered Institution of Wastes Management Environmental Body. <http://www.citylimitslondon.com/>.

Decker, Ethan H., et al. 2000. Energy and Material Flow Through the Urban Ecosystem, *Ann. Rev. Energy Environ.* 25:685-740.

Energy Sector Management Assistance Program (ESMAP). 2010. *Rapid Assessment Framework: An innovative Decision Support Tool for Evaluating Energy Efficiency Opportunities in Cities*, ESMAP Report No. 57685. Washington, DC: World Bank.

EPRI, 2009. *Program on Technology Innovation: Electric Efficiency Through Water Supply Technologies-A Roadmap*, Electric Power Research Institute, Technical Report, No.1019360, June 2009.

Fraker, Harrison. 2008. *Made-in-China "Eco-Blocks": A Replicable Model for Sustainable Neighborhoods*. PowerPoint slide show. Lawrence Livermore National Laboratory. April 1, 2008. <http://www.slideshare.net/geoff848/harrison-fraker-ecoblocks>.

Gleick, Peter H. 2009. *The World's Water 2008–2009: The Biennial Report on Freshwater Resources*. Washington, DC.: Island Press.

Goklany, Indur M. 2007. *The Improving State of the World: Why We're Living Longer, Healthier, More Comfortable Lives, on a Cleaner Planet*, Washington, DC: Cato Institute.

Hao, Xiaodi, Vladimir Novotny, and Valerie I. Nelson. 2010. *Water Infrastructure for Sustainable Communities: China and the World*. London: IWA Publishing. <http://www.fishpond.com.au/Books/Water-Infrastructure-for-Sustainable-Communities-Xiaodi-Hao-Vladimir-Novotny/9781843393283>.

International Energy Agency (IEA). 2008. Statistics on electricity/heat available online. <http://www.iea.org/stats/index.asp>.

Kallidaikurichi, Seetharam E., and Bhanoji Rao, eds. 2010. *Index of Drinking Water Adequacy (IDWA): International and Intra-National Explorations*. National University of Singapore Press.

McIntosh, Arthur. 1993. *Water Utilities Data Book*. Manila: Asian Development Bank.

McIntosh, Arthur, and C. E. Yñiguez, eds. 1997. *Second Water Utilities Data Book: Asian and Pacific Region*. Manila: Asian Development Bank.

McKinsey Global Institute. 2009. *Preparing for China's Urban Billion*, McKinsey and Company.

Natural Resources Defense Council (NRDC). 2004. *Energy Down the Drain: The Hidden Costs of California's Water Supply*. Washington, DC: NRDC and the Pacific Institute.

New York State Energy and Research Development Authority (NYSERDA). 2008. *Statewide Assessment of Energy Use by*

Municipal Water and Wastewater Sector.
<http://www.nyserda.org/programs/Environment/muniwwtReports.asp>

ScientificAmerican.com. 2011. Cities: Smarter, Greener, Better. pp. 38–41. September 2011.
<http://www.nature.com/scientificamerican/journal/v305/n3/full/scientificamerican0911-38.html>

Southeast Asian Water Utilities Network (SEAWUN). 2005. *SEAWUN Benchmarking Survey for 2003: Data Book of Data and Results*. Manila: SEAWUN and Asian Development Bank.

———. 2007. *Data Book of Southeast Asian Water Utilities 2005*. Manila: SEAWUN and Asian Development Bank.

United Nations Department of Economic and Social Affairs (UN|DESA). 2011. *World Population Prospects: The 2010 Revision*. <http://www.un.org/esa/population/>.

———. 2009. *World Urbanization Prospects: The 2009 Revision*. <http://esa.un.org/unpd/wup/index.htm>.

United Nations Economic and Social Commission for Asia and the Pacific (UN-ESCAP). 2010. *Paths to 2015 MDG Priorities in Asia and the Pacific. Asia-Pacific MDG Report 2010/11*. Bangkok: UNESCAP, Asian Development Bank, and United Nations Development Programme.

Wolman, Abel. 1965. The Metabolism of Cities. *Scientific American*, Vol. 213, pp. 178-190

Satellite information for large natural hazard

Haruo SAWADA
Professor, ICUS, IIS, The University of Tokyo, Japan
sawada@iis.u-tokyo.ac.jp

ABSTRACT

Remote sensing images are used as an important information source at preparedness, response and recovery stages in hazard and disaster management. Aerial photos are commonly used for many disaster events in Japan because of their high resolution and quick acquisition. A normal aerial photo, however, covers only about 4 km² in average and a large number of aerial photos are required for a large hazard. Although it is not easy to control observation modes of satellite systems, there are many ongoing earth observation satellites and we have chances to get these data. This paper focuses on showing ways to use earth observation satellite systems for a large hazard and to mitigate disasters caused by earthquake including tsunami, flooding, and wildfire. Although manual interpretation technique is useful to identify land covers and land uses on satellite images, speedy reproduction by automatic classification is better solution for large event. As for earthquake, high resolution images are requested to identify conditions of housing and infrastructure. SAR is used to identify geological movement of the surface because the movement of one-fourth of SAR wavelength can be detected. Remote sensing image is the only tool to identify heavily damaged area by tsunami because it destroys all the infrastructures including communication systems and no information comes out from the damaged area. As for flooding, high frequent observation system is useful for monitoring and SAR easily allows us distinguish water coverage and inundated areas. Wildfire issue also requires a large observation area for warning and detecting fires. The International Disaster Charter (IDC) was started in 2000 for mitigating these disasters in the world. Many satellite observation systems have been involved in the IDC through the ten space agencies in the world and the charter was activated more than 300 times. The IDC is a passive action for affected developing countries and more active action might be effective even in developed countries.

Keywords: *remote sensing, image collection, International Disaster Charter*

1. INTRODUCTION

Number of large hazard and disaster has been reported in the world and the impact to human beings is very high in Asia because of their occurrences and dens populations. For large natural hazards and disasters, collecting up-

to-date information safely and efficiently is quite important not only for administrative persons but also for citizens. Satellite remote sensing as well as airborne survey systems are introduced and progressed for that purpose. However, few systems are in operation for large hazards and disasters in the world. Because advanced technologies related to remote sensing and GIS are required for that purpose in affected countries, international collaborations, such as the Disaster Charter and the Sentinel Asia, have been strengthened in the world.

2. CURRENT REMOTE SENSING

With the rapid development of space platform and sensors, remote sensing data have been broadly utilized to natural hazard investigation and management.

Remote sensing data are classified in several ways: ex. airborne vs. satellite, passive vs. active, optical vs. microwave, high-resolution vs. low resolution from the platform and sensor systems. At the data interpretation stage, the technologies are divided into visual (manual) interpretation and automatic classification.

Satellite remote sensing has become an advanced tool for the natural disaster management because of the increasing availability of satellite images with high resolution and decreasing costs. Satellite images show a synoptic overview and provide useful environmental information related to the natural hazard.

Each sensor system is characterized its capabilities mostly on spectral bands, ground resolution, observation width and observation cycle. Although MODIS on Terra and Aqua satellite shows the whole damaged area two times every day, high-spatial resolution satellite images (ex. GeoEye, FORMSAT, IKONOS) could be an efficient and useful resource for decision-makers to prepare rescue and recovery operation, especially for some disaster areas where damage distribution and levels are uneven and hard to reach in time (Table 1).

Imaging RADAR (Radio Detection and Ranging) provides us all-weather, day and night imaging capability. As the microwave energy strikes ground features, the radar antenna receives and measures the strength of the energy that is scattered back towards the system. Therefore worldwide comparison is meaningful for RADAR data, although optical sensors are affected by sun altitude and cloud and have no meaningful data for direct comparison. Remote sensing techniques are summarized in Table 2

There are kinds of LiDAR (Light Detection and Ranging) systems currently. The primary differences among them involve laser wavelength, pulse duration and repetition rate, beam size and divergence angle (which in combination with altitude dictates the ground footprint size), the model of

scanning mechanism and the echoes recorded for each laser pulse. LiDAR provides the highest resolution DEM available for fault interpretation.

Table 1: Characteristics of main remote sensing sensors

Satellite	Sensor	Swath(km)	Nadir spatial resolution	Revisit capability
Airborne sensors	LiDAR	variable		Mobilized to order
	CASI	variable	1–2	
	Hymap	100–225	2–10	
Worldview	Panchromatic	16.4	0.46	1.1 days
	Multispectral	16.4	1.85	
Quickbird	Panchromatic	16.5	0.6	1.5–3 days
	Multispectral	16.5	2.4	
Ikonos	Panchromatic	11	1	1.5–3 days
	Multispectral	11	4	
RapidEye	Multispectral	77 x 1500	6.5	1 day
EO-1	ALI	60	30	Every 16 days
	Hyperion	7.5	30	
Terra	ASTER	60	15,30,90	4–16 days
Terra / Aqua	MODIS	2300	250, 500, 1000	At least twice daily for each
ALOS	PRISM	35	4	Several times per year as per JAXA acquisition plan
	AVNIR	70	10	
	PALSAR (Fine)	40–70	10	
	PALSAR (ScanSAR)	250–350	100	
SPOT-5	Panchromatic	60–80	5	11 times every 26 days
	Multispectra	60–80	10	
Landsat-7	ETM+ Panchromatic	185	15	Every 16 days
	ETM+Multispectral	185	30	
	ETM+Thermal	185	60	
NOAA	AVHRR	2399	1100	Several times per day
Envisat	MERIS	575	300	2-3 days
Radarsat-2	Ultra-fine	20	3	Every few days
TerraSAR-X	Spotlight	10	1	11-day repeat cycle 2.5-day revisit capability
	Stripmap	30	3	
	ScanSAR	100	18	

Table 2: Comparison of remote sensing techniques

Data Type	Technique	Advantages
Multispectral high to moderate resolution:	Manual interpretation	Benefits from analyst’s knowledge of the area in addition to other interpretation cues such as context, site, association, shape, size;
	Spectral classification	Relatively rapid to apply over a large area
Ikonos, Quickbird, SPOT, ASTER, ALOS	Image thresholding (including band ratios)	Simple and rapid to apply, band ratios reduce illumination variability, can be applied with panchromatic data
	Postclassification change detection	Does not require radiometric calibration between multiple images

3. NATURAL HAZARDS AND DISASTER

Every year, disasters related to meteorological, hydrological and climate hazards cause significant loss of life, and set back economic and social development. Between 1980 and 2005, nearly 7500 natural disasters worldwide took the lives of over 2 million people and produced economic losses estimated at over 1.2 trillion US dollars (WMO, 2011). Of this, 90 per cent of the natural disasters, 72.5 per cent of casualties and 75 per cent of economic losses were caused by weather-, climate- water-related hazards such as droughts, floods, windstorms, tropical cyclones, storm surges, extreme temperatures, landslides and wildfires, or by health epidemics and insect infestations directly linked to meteorological and hydrological conditions.

Natural disasters could be classified into 3 groups;

- (1)Hydro-meteorological disasters: flooding, typhoon, hurricane and drought, including wildfire and landslide caused by heavy rain
- (2)Geophysical disasters: earthquake, tsunami and volcanic eruptions
- (3)Biological disasters: epidemics and insect infestations

Here, we consider the first two types of disasters, Hydro-meteorological disasters and Geophysical disasters. Disaster management of an event like cyclone, flood or earthquake etc. requires some ingredients, such as, detection, response, mapping, establishing priorities, developing action plans and implementing the plan to protect human lives, property and the environment. Early detection of large disaster is one of the most important roles of remote sensing. Remote sensing provides cost effective and safe methodology to collect information of a large disaster.

The impacts of natural hazards are increasing as a result of social changes like urbanization and population increase. And there are four stages in disaster management; Reduction (mitigation), Readiness (Preparedness), Response, and Recovery.

3.1 Heavy rain

Weather satellite observes the entire movement of meteorological hazard sources with a short time cycle, 30 minutes to 1 hour, and another satellite observes the affected areas with higher ground resolution but lower repeat cycle. GIS in combination with remote sensing, can be used very effectively to identify hazards and risk for cyclone (Rana et al., 2010).

For meteorological hazard, prediction is the most important for mitigating disaster. The TRMM has very interesting capability to monitor the rainfall in 3D while the cyclones are yet on the sea. The information for predicting the severity is useful for early evacuation. Integrating local knowledge with GIS and remote sensing techniques to develop map and

assess the hazard prone areas is an excellent tool for cyclone disaster management and regional planning development (Rana et al 2010).

SAR (Synthetic Aperture Radar) data would be most useful in the event of storm-induced hazard. For example, SAR has good capability to detect flooding even under heavy cloud. By combining SAR with DEMs, it is also possible to estimate the depth of water in flooded regions. One of the unique features of SAR is the ability to detect flooding under closed-canopy vegetation by the corner-reflector effect formed from the vegetation and water, which is well observed in Amazon.

Information management is the key to make effective the remote sensing data. For example, there is a flood control system to save Bangkok at the sacrifice of agricultural land in northern Thailand to reserve water. In this case, administrative persons decide to control the flood gates according to the meteorological information observed by meteorological satellite and national network of authorities.

3.2 Drought and wildfire

Drought, extreme opposite to the heavy rain, is the most common natural disaster in the world, and the soil moisture content is one of the main indicators of drought monitoring. Remote sensing quantitative retrieval of soil moisture content was scientifically available in semi-arid regions (Yichang, 2010).

Present technology and knowledge is limited to prevent such natural disasters and such events still continue to make an increasing threat to human life and urban development. Avoidance or mitigation of the impact of the disaster could be achieved with effective disaster management strategies along with proper utilization of remote sensing technology (Liou et al., 2010).

Although wildfire is a normal event of dry season in some area, abnormal drought causes severe forest fires. Because many country use fire for agriculture, prediction of drought, especially the abnormality of the drought, must be informed to fire managers as well as farmers for keeping away of using fire. Even though the El Nino influences forest fire in Indonesia and Asian countries, most of the fire ignitions are responsible to people who use fire in severe dry weather. TERRA and AQUA-MODIS and NOAA-AVHRR are commonly used for fire management to predict drought and detect fires because of their capabilities in frequent monitoring and large area coverage.

Early warning and early detection are the keys to mitigate forest fire. Together with these early detections, other meteorological parameter, such as wind speed and dry index, should be monitored in short interval. Geosynchronous satellite is considered the most important satellite to mitigate wildfire because of its high repeated time of observation.

There are many factors which influence wildfire, such as fuels on the ground (types, amount and dryness), meteorological factors (wind direction, wind speed, humidity and sunshine), and terrain condition. It must be necessary to introduce these factors into the system to enhance accuracies.

Fires occur in a large area and a nationwide observation and reporting system is required to mitigate wildfire and the system should be appropriate to the situations for fire management in each country. Our experience for 5 years showed that it is difficult to detect forest fire before human eye in Japan and early warning is effective for forest management to prevent fire uses by introducing the prediction map derived from the dryness index.

3.3 Earthquake

Earthquake causes various damages to buildings, roads, bridges, fuel tanks (gas), dams, traffic systems and other infrastructures in urban cities. Liquefaction, ground sinkage, land slide are also caused by earthquake.

The damage and disaster monitoring require high resolution remote sensing data which covers a large area and requires huge amount of data processing facilities as well as remote sensing data. The International Disaster Charter well supports these demands for earthquake and other disasters.

Manual interpretation technique on optical remote sensing image has been used to detect fault lines. High resolution SAR (Synthetic Aperture Radar) data is also used for mapping changes and damages by analyzing difference between multi-temporal images. ALOS-PALSAR, TerraSAR-X and Radarsat-2 provide polarization data. It is possible to achieve accuracy better than one quarter of SAR wavelength. Phase shift and intensity difference between images of polarizations depend on land cover and are thus used for its classification.

Airborne LiDAR is also useful for mapping fault lines because of its high vertical and horizontal resolution. However, this technique is not suitable for providing information in an emergency situation due to the time for processing the data.

3.4 Tsunami

Earthquakes commonly occur along the plate boundaries. The earthquake that triggered the tsunami occurred at a convergent plate boundary. The 2011 Tohoku-Pacific Earthquake caused tsunami across a very wide area, along the Pacific coastline from Hokkaido to Kanto area. Tsunami, whose wave heights were more than 1m, were observed not only in Tohoku but also Hokkaido and Kanto regions, even in Tokai and Kyushu. Especially in Iwate prefecture and the northern area of Miyagi prefecture, the inundation height and the run-up height of tsunami exceeded 10m.



Figure 1: Tsunami inundation line on the orthophoto map (1/10,000)

The Tsunami caused various huge damages along the Tohoku coastal line. A large number of people were washed away to the ocean with floating matters.

4. RAPID RESPONSE SYSTEMS

A number of different satellite systems are currently providing information on hazards and disasters. Some of these systems are operational and some are experimental, some of the data processing methods are well developed and some are in the research and development phase. The integration is one of the most important matters to develop operational system for disaster management using remote sensing and GIS.

4.1 International Disaster Charter

The International Charter started their activities in 2000 and aims at providing a unified system of space data acquisition and delivery to those affected by natural or man-made disasters through Authorized Users. 20 member agency has committed resources to support the provisions of the Charter and thus is helping to mitigate the effects of disasters on human life and property.

4.2 Sentinel Asia

“Sentinel Asia” is a voluntary basis initiative led by the APRSAF (Asia-Pacific Regional Space Agency Forum) to support disaster

management activity in the Asia-Pacific region by applying the WEB-GIS technology and space based technology, such as earth observation satellites data.

Sentinel Asia was originally proposed in November 2004 when it was realized that maximum benefit from rapid technological advances in the region would occur, and this data could be delivered more quickly via the internet as easy-to-interpret disaster-related information. Sentinel Asia aims to expand efforts of each country and make such data available to all countries and many more people in the region, particularly in countries that do not have their own satellite reception facilities. Through such a backbone, information about disasters could begin to be delivered more efficiently through the 'world-wide-web', even outside national borders, in 'real-time' or 'near real-time', and used as early-warning, or as post-disaster information by various countries and relevant end-user agencies (Sentinel Asia, 2011).

4.3 International activity for forest fire:

Information on fire danger, active fires, burned area, fire emissions and post-fire recovery are required for wildfire management. Although a number of countries are collecting ground-based information, the information that is needed on fire is often missing and a system for monitoring effectively the long-term trends in global fire distributions and characteristics has yet to be supported (GOFC, 2000).

GOFC/GOLD (Global Observations of Forest and Land Cover Dynamics) is a project of the Global Terrestrial Observing System (GTOS) program, which is sponsored by the Integrated Global Observing Strategy (IGOS). The main goal of GOFC/GOLD is to provide a forum for international information exchange, observation and data coordination, and a framework for establishing the necessary long-term monitoring systems.

The GOFC/GOLD-Fire Mapping and Monitoring Theme was established in 2000 aiming at refining the international observation requirements and making the best possible use of fire products from the existing and future satellite observing systems, for fire management, policy decision-making and global change research.

5. CONCLUSIONS

Remote sensing is the only source for severely damaged area because no information comes out from such an area, although the first priority of rescue activities should be considered to that area. The detection of floating materials is also an important to save lives in the sea. Unfortunately, we have to conclude that information integration is not sufficiently operational for a large hazard and disasters. We need to proceed to integrate the observation systems, information technologies, related officers, policy makers, and local people's knowledge and behavior.

REFERENCE

GOFC, 2000, <http://gofc-fire.umd.edu/>

Joyce, K. E., Belliss, S. E., Samsonov, S. V., McNeill, S. J., & Glassey, P. J. (2009) A review of the status of satellite remote sensing and image processing techniques for mapping natural hazards and disasters. *Progress in Physical Geography*, 33(2), 183-207.

Liou, Y.-A., Kar, S. K., & Chang, L. (2010) Use of high-resolution FORMOSAT-2 satellite images for post-earthquake disaster assessment: a study following the 12 May 2008 Wenchuan Earthquake. *International Journal of Remote Sensing*, 31(13), 3355-3368.

Rana, M. S., Gunasekara, K., Hazarika, M. K., Samarakoon, L., & Siddiquee, M. (2010) Application of remote sensing and GIS for cyclone disaster management in coastal area?: A case study at Barguna district. *International Archives of the Photogrammetry Remote Sensing and Spatial Information Science*, XXXVIII(8), 122-126.

Sentinel Asia, 2011, <http://dmss.tksc.jaxa.jp/>

Van Westen, C. J., & Westen, C. J. V. (2002) Remote sensing and geographic information systems for natural disaster management. In A. K. Skidmore (Ed.), *Information Systems Journal* (pp. 1-27). DSIR.

WMO, 2011, WMO Disaster Risk Reduction Programme
<http://www.wmo.int/pages/prog/drr/>

Yichang, W., Fang, Z., Liping, Z., Lingling, K., & Xiaoqiang, L. (2010) Estimating Soil Moisture in Semi-arid Region by Remote Sensing Based on TM Data. *International Conference on Multimedia Technology ICMT 2010* (pp. 1-5). IEEE

Poster Session

Mainstreaming climate change adaptation in urban planning in Africa

Abbadu GIRMAY REDA¹ and Nitin K. TRIPATHI²

¹ Tigray Agri. Research Institute, NRM Research Directorate, Ethiopia and RS and GIS Field of Study, AIT, Thailand (Abbadigirmayreda@gmail.com)

² Asian Institute of Technology (AIT), Remote Sensing and Geographic Info. Systems Field of Study, Thailand

ABSTRACT

Climate change, coupled with unprecedented rates of rapid urbanization, makes the potential impacts of disasters much worse. The frequency and intensity of climate-related disasters has quadrupled in the past two decades. Small and medium-sized cities are currently rapidly emerging with high economic and political importance. Vector-borne diseases such as malaria are expanding to new habitats of higher altitudes where these habitats had been formerly unsuitable and urban adaptation is crucial. Persistent poverty, lack of governance and high rate of population growth have left African countries with scant capacity to manage. Africa will have to combat adverse effects of climate change. The impacts of climate change will fall disproportionately on the urban poor. Vulnerability to climate change can be exacerbated by other stresses, especially in developing country cities. Climate change impacts on urbanization has negative implications on urban infrastructure, health, water availability, economy and high risk of natural disasters such as flooding. International, national and local governments should have to raise the challenges of climate change on urbanization to save millions of urban residents to have a livable continent with better urbanization prospect in the era of globalization. Given the rapid rates of urbanization in Africa, particular attention must be paid to city-level policies and actions. Cities can reduce climate and disaster risks through breaking the nexus between urban poverty, informal settlements and disaster risk reduction through community driven development programs; promoting sound land-use supported by robust local risk assessments; investing in Early Warning Systems and making risk information widely available so communities and businesses can prepare for disasters. Responding to this challenge starts with improving our disaster risk reduction capacity. This will require new models of cooperation and coordinated policy responses across multiple sectors, agencies and ministries; mainstreaming and institutionalizing climate change in sustainable urban planning and a new set of policy instruments for decision-making under deep uncertainty. Neither adaptation nor mitigation alone can avoid all climate change impacts; however, they can complement each other and together can significantly reduce the risks of climate change.

Keywords: climate change, urbanization, urban adaptation, mainstreaming, Africa

1. INTRODUCTION

Africa has a population of 1 billion million people and a land area of 30.3 million km². It is bounded in the north by the Mediterranean Sea, the Atlantic Ocean to the west, and Indian Ocean towards the central and south east of the continent, and the Red Sea to the northeast, Connecting to the Mediterranean via the Suez Canal. The impacts of climate change are already evident. According to the latest Intergovernmental Panel on Climate Change (IPCC) report, the average global temperature has increased by 0.76°C and sea level has risen by 17 cm since the 19th century (IPCC 2007). Climate change is a major threat to sustainable growth and development in Africa, and the achievement of the Millennium Development Goals. Africa is particularly vulnerable to climate change because of its overdependence on rain-fed agriculture, compounded by factors such as widespread poverty and weak capacity. The main longer-term impacts include: changing rainfall patterns affecting agriculture and reducing food security; worsening water security; decreasing fish resources in large lakes due to rising temperature; shifting vector-borne diseases; rising sea level affecting low-lying coastal areas with large populations; and rising water stress. The United Nations Framework Convention on Climate Change (UNFCCC) provides that all Parties must formulate and implement national or regional programmes containing measures to facilitate adequate adaptation to climate change (Art.4.1.b). The developing world already contends with chronic food problems. Climate change presents yet another significant challenge to be met. While overall food production may not be threatened, those least able to cope will likely bear additional adverse impacts (WRI, 2000). Climate change and variability are among the most important challenges facing Least Developed Countries because of their strong economic reliance on natural resources and rain-fed agriculture. These can significantly reverse the progress towards poverty reduction and food security in Africa. Climate change will affect poorer African countries disproportionately. The poorest people in those countries will suffer the greatest consequences. Those least able to cope will be hit the hardest. Hence, climate adaptation strategies should reflect such circumstances in terms of the speed of the response and the choice of options (Easterling, 1996 and FAO, 2010).

Urban population in Africa is growing at an alarming rate. African society is rapidly changing from rural to urban, with cities and towns expanding, not only in terms of population growth, but also spatially. They are taking up more space and encroaching on rural and agriculturally productive land. Rural-urban migration results from landlessness resulting from privatization of property, commercialization and mechanization of agriculture, failing agricultural productivity and increase rural population. One-third of the African population lives in drought-prone areas. Six of the ten largest cities in Africa are located on the coast. Many large population centres are built in coastal zones, which are vulnerable to the loss of land from sea-level rises and to increased storm occurrence. Cities, particularly in developing countries, are especially vulnerable to climate change due to the large concentration of populations and their role as national economic

hubs. In addition, many urban areas are located on the coast, making them susceptible to rising sea levels. Within cities, the urban poor are among the most vulnerable. On the other hand, the concentration of resources in urban areas means cities can be key players in adapting to climate change and mitigating its impact (E.O. Akrofi, 2006).

While the majority (62.1 per cent) of the African population is still rural, urban growth rates at nearly 4 per cent a year are the most rapid in the world, and nearly twice the global average (United Nations Population Division 2001). Growth rates are predicted to average 3.5 per cent per year over the next 15 years, meaning that Africa's share of the world's urban population will increase from 10 to 17 per cent between 2000 and 2015 (United Nations Population Division 2001). North Africa is the most urbanized sub-region with an average urban population of 54 per cent, followed by West Africa (40 per cent), Southern Africa (39 per cent). There are now 43 cities in Africa with populations of more than one million inhabitants, a figure which is expected to increase to almost 70 by 2015 (United Nations Population Division 2001).

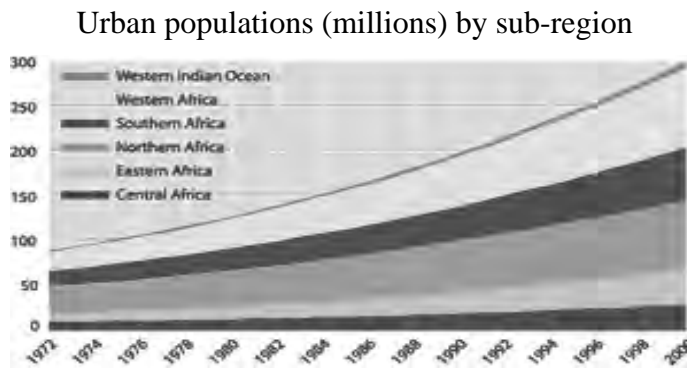
Rates of urbanization in Africa are the highest in the world. By 2025, more than half of the African population will be urban, and during the next quarter century the urban population will be growing almost twice as fast as the general population, increasing by more than half a billion from 1990 levels. Over a third of Africa's 1 billion inhabitants currently live in urban areas, but by 2030 that proportion will have risen to a half. According to a recent report from UN-HABITAT, the United Nations agency for human settlements, the population of some cities is set to swell by up to 85% in the next 15 years. Despite the negative attributes of urbanization, these new and growing areas, which are located in coastal areas and the hinterland, have also become vibrant centers of education, culture, commerce and industry and technological innovation, providing opportunities for various manufacturing and service industries (UNEP, 2008).

Table 1: Sub-Saharan Urban Population Growth to 2025 (millions)

Year	1990	2010	2025	%Growth ('90-'25)
Sub-Saharan Africa	527	937	1362	258
Urban Population	149	387	705	473
Urban % of Total	28	41	52	

Source: J.L. Venard, *Urban Planning and Environment in Sub-Saharan Africa*, UNCED, 1995

Rapid growth in urban populations necessarily entails rapid growth both in the size and number of urban places. By 2020, Africa will have 11 mega-cities (5 million inhabitants or more) and almost 3000 cities with populations of more than 20,000, an increase of almost 300% from 1990 (UNCED, 1995)



Urbanization level (%):

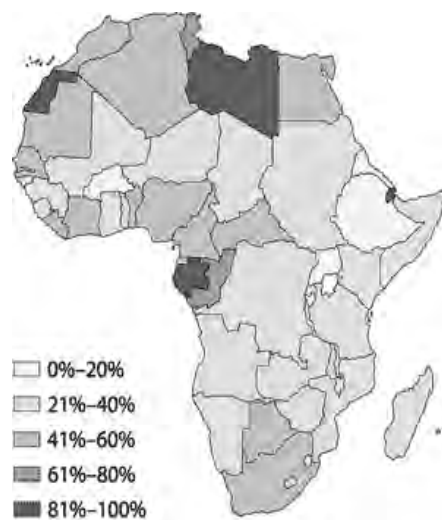


Figure 1: African urban population and urbanization level (United Nations Population Division)

3. CLIMATE CHANGE VULNERABILITY AND IMPACTS IN URBAN AFRICA

Climate change is a major threat to sustainable growth and development in Africa, and the achievement of the Millennium Development Goals. Africa is particularly vulnerable to climate change because of its overdependence on rain-fed agriculture, compounded by factors such as widespread poverty and weak capacity. The main longer-term impacts include: changing rainfall patterns affecting agriculture and reducing food security; worsening water security; decreasing fish resources in large lakes due to rising temperature; shifting vector-borne diseases; rising sea level affecting low-lying coastal areas with large populations; and rising water stress. Climate change, coupled with unprecedented rates of rapid urbanization, makes the potential impacts of disasters much worse. The frequency and intensity of climate-related disasters has quadrupled in the past two decades. Small and medium-sized cities are currently rapidly emerging with high economic and political importance. Vector-borne diseases such as malaria are expanding to new

habitats of higher altitudes where these habitats had been formerly unsuitable. Malaria not only remains a leading cause of morbidity and mortality, but it also impedes socioeconomic development, particularly in sub-Saharan Africa. Rapid and unprecedented urbanization, going hand-in-hand with often declining economies, might have profound implications for the epidemiology and control of malaria, as the relative disease burden increases among urban dwellers. A study by The American Society of Tropical Medicine and Hygiene using a modeling approach found out that entomologic inoculation rates in cities range from 0 to 54 per year, depending on the degree of urbanization, the spatial location within a city, and overall living conditions. The study further indicated that 200 million people (24.6% of the total African population) currently live in urban settings are at risk of contracting the disease. Considering different plausible scenarios, it was estimated that an annual incidence of 24.8-103.2 million cases of clinical malaria attacks occurred among urban dwellers in Africa. As cities in the developing world grow, unmanaged urbanization can outpace infrastructure and environmental safeguards, leading to high pollution and carbon dioxide emissions and to increasing vulnerability for residents (Jennifer Kaiser, 2004). Climate change has implications in physical infrastructure, economy, and social welfare and exposes society to disease epidemics and poverty (WHO, 2010).

Sea Level Rise (SLR) in Coastal Zones of Africa

Africa has a large and growing coastal population, including a number of important coastal cities. With sea-level rise, flooding and inundation of coastal areas would be expected creating problems for infrastructure, transportation, agriculture and water resources within the coastal zone. While risks are not well understood, with 320 coastal cities (with more than 100,000 people) and nearly 56 million people (2005 estimate) living in low elevation (<10-m) coastal zones, indicating the potential magnitude of impacts and identifies to countries which have a high absolute risk. It is also important to note that sea-level rise will not be the only factor shaping Africa's coast in the 21st Century. Other climate change impacts such as increased storminess, higher temperatures and reduced precipitation also have immediate or secondary impacts of the coast. Sea-level rise as an impact of human-induced climate change has significant implications to low-lying coastal areas and beyond. The coastal zone contains valuable ecosystems and typically has higher population densities than inland areas (B. Sally et'al, 2011). Studies indicate that most African coastal countries are highly vulnerable to climate change and sea-level rise, leading to increased rates of coastal erosion and flooding of low-lying coasts (Ibe and Awosika, 1991). A study was undertaken by B. Sally et'al (2011) to assess sea level rise in African coastal zones to predict changes for the period 2000 to 2100 based on DIVA model. The DIVA (Dynamic Interactive Vulnerability Assessment) model is an integrated model of coastal systems that assesses biophysical and socio-economic impacts of sea-level rise and socio-economic. DIVA downscales the sea-level rise scenarios by combining global sea-level rise scenarios due to global warming with local vertical land movement. In this study, four sea-level scenarios (A1FI, A1B,

B1 and Rahmstorf) have been analysed coupled with three socio-economic scenarios describing population density and GDP (A1FI, A1B, and B1). Results of these scenario analysis showed that without adaptation, the physical and economic impacts of sea-level rise tend to increase with time under all sea-level rise scenarios (although in the A1 and B1 socio-economic scenarios used here the population declines after 2050 (Arnell *et al.*, 2004).

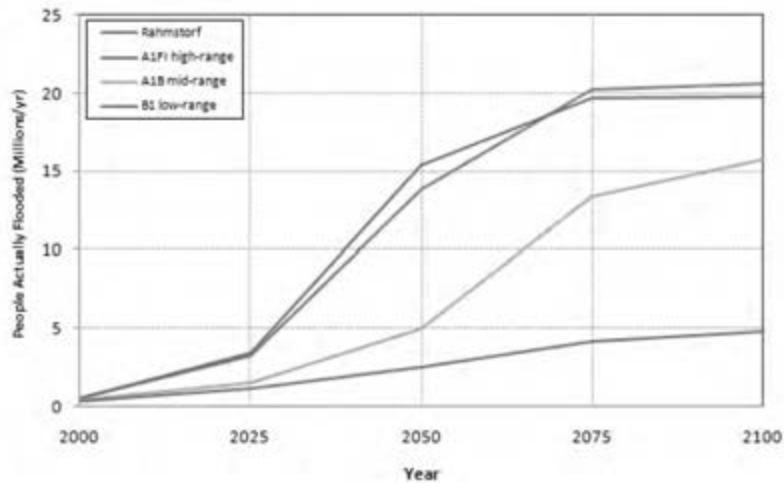


Figure 2: People affected by flooding with no adaptation

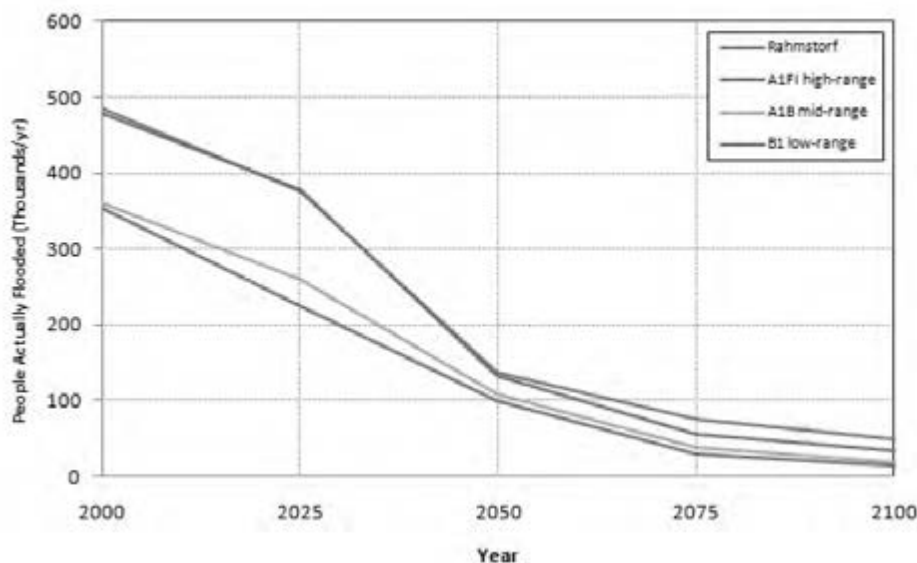


Figure 3: People affected by flooding with adaptation measures (2000- 2100).

CLIMATE CHANGE IMPACTS

The Impacts of Climate Change on African cities include:

- Extreme weather events damage buildings and urban infrastructure
- Coastal cities and small island states affected by sea level rise; Coastal erosion
- Water resources stress: floods and droughts
- Human Health – malaria; waterborne diseases; polluted water

- Food Security – Livelihoods – Tourism
- Climate refugees move to urban slums

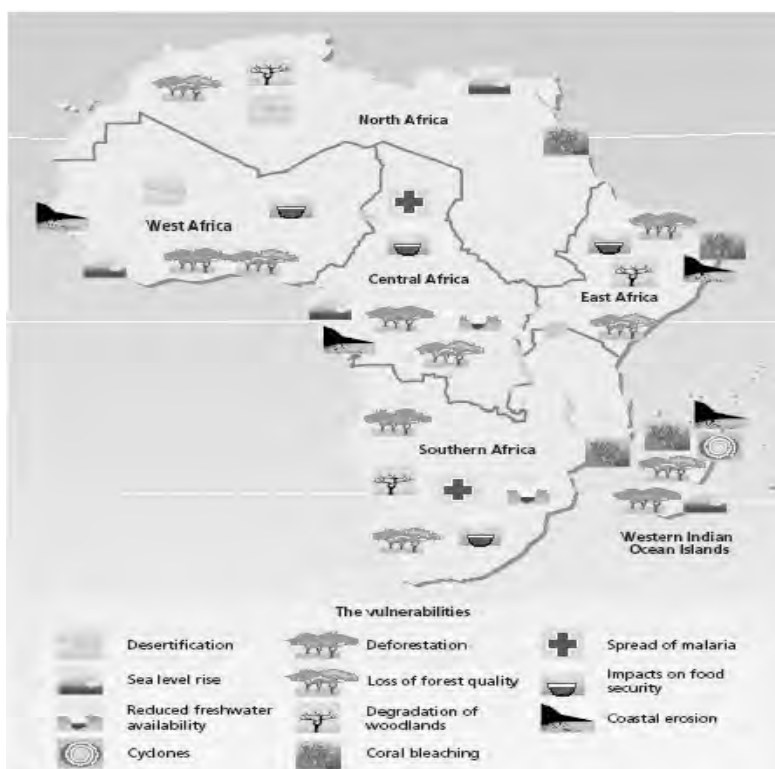


Figure 4: Climate Change Vulnerability in Africa (UN- HABITAT, 2011)

4. MAINSTREAMING CLIMATE CHANGE ADAPTATION IN URBAN DEVELOPMENT

Building cities that are green, inclusive and sustainable should be the foundation of any local and national climate change agenda. This requires better management of cities, mobilization of a global array of stakeholders, additional financing, and strengthened partnerships, as well as specific sector policy reforms such as urban transport policies, sustainable city planning, and enhancing city resilience and energy efficiency. The focus is on approaches and issues on African cities coping with climate change and an integrated perspective on cities and climate change, focusing on mitigation, adaptation and sustainable development. Climate change impacts upon particular social groups and locations differently, both within and beyond urban areas. Building resilience in a city requires a systems, or integrated approach. Cities need an integrated approach that considers mitigation, adaptation and urban development. The improvement of city services is related to the ability of cities to adapt to climate change and reduce their greenhouse gas emissions. Cities with excellent services are generally resilient cities (WRD, 2010). The focus should be on mainstreaming and formulating urban planning and land use strategies in response to current and future climate risks and vulnerability - building on an understanding of underlying socio-economic and environmental trends. Important adaptation potentials for cities are connected to improved land

use and the localisation and standards of urban structures and critical infrastructure (Wilbanks et. al 2007). Urban planning and land management are essential (but obviously not the only) tools for policymakers to develop urban structures resilient towards climate change and build capacity at local level for sustainable city development, linking adaptation and mitigation measures and improving livelihoods and quality of life for the urban population. Attention should shift to integrated development planning, and housing policies that support environmentally sustainable housing. Key environmental issues in urban areas in Africa are related to the provision of services for waste, water and sanitation, and urban air pollution. In the long term, climate change adaptation needs to be supported by an integrated, cross-cutting policy approach. Local action plans (amended every three to five years) are important entry points for change in local governance to accommodate policies that would increase resilience to climate change. Local and international institutions have a great role to play in strengthening local responses to climate change

Responding to this challenge starts with improving our disaster risk reduction capacity. This will require new models of cooperation and coordinated policy responses across multiple sectors, agencies and ministries; and a new set of policy instruments for decision-making under deep uncertainty. Given the rapid rates of urbanization in Africa, particular attention must be paid to city-level policies and actions. Cities can reduce climate and disaster risks by:

- Breaking the nexus between urban poverty, informal settlements and disaster risk reduction through community driven development programs
- Promoting sound land-use supported by robust local risk assessments
- Investing in Early Warning Systems
- Making risk information widely available so communities and businesses can prepare for disasters

From a local government perspective, the extent to which an issue such as climate change becomes successfully institutionalized in day-to-day operations, planning and decision making can be evaluated by using institutional markers similar to the ones outlined below:

- Emergence of an identifiable political/administrative champion(s) for climate change issues;
- Appearance of climate change as a significant issue in mainstream municipal plans;
- Allocation of dedicated resources (human and financial) to climate change issues; and
- Incorporation of climate change considerations into political and administrative decision making.

5. KEY ADAPTATION AND MITIGATION STRATEGIES FOR AFRICAN CITIES

Africa contributes only about 4% to global emissions but will suffer increasingly severe impacts of climate change. Local action plans are important entry points for change in local governance to accommodate policies that would increase resilience to climate change. Local and international institutions have a great role to play in strengthening local responses to climate change. Africa has the lowest GHG emissions, yet is hit hardest by climate change. Adaptation to the unavoidable impacts of climate change will need strong support by the international community and involve all stakeholders (World Bank, 2010). It is necessary to have access to a diverse array of adaptation technologies and practices that are appropriate and affordable in various contexts. Hence, urban adaptation is crucial in Africa. Adaptation and mitigation are interconnected and closely related to the overall development and poverty alleviation agenda. Key adaptation and mitigation strategies include the following options (Elliot et'al, 2011).

Adaptation Options

- Climate proofing of urban infrastructure, e.g. seawalls and storm surge barriers
- Investing in storm water drainage
- Early warning systems
- Enhance community resilience
- Upgrading of slums; Relocation of extremely vulnerable settlements and infrastructure
- Access financing mechanisms such as the UNFCCC Adaptation Fund

Mitigation Options

- Energy efficiency in local government facilities, e.g. street lighting and water pumps
- Foresighted transport and infrastructure planning
- Compact and dense urban patterns to reduce travel distances and infrastructure networks
- Promote energy efficient building materials
- Landfill methane recovery
- Finance: Clean Development Mechanism (CDM)

6. CONCLUSION

Africa is subject to the interaction of 'multiple stresses', occurring at various levels, leading to a reduced adaptive capacity. This vulnerability is exacerbated by existing developmental challenges such as poverty, complex governance issues, weak institutions, limited access to capital and markets, infrastructure and technology, ecosystem degradation, disasters, and conflicts. Africa's weak adaptive capacity increases the continent's vulnerability to projections of climate change. Africa has the lowest GHG

emissions, yet is hit hardest by climate change. Adaptation to the unavoidable impacts of climate change will need strong support by the international community and involve all stakeholders. Urban adaptation is crucial. Urbanization affects climate change, resulting in severe impacts to African cities and livelihoods. The severest burden will be borne by the urban poor in African slums. Climate change actions by African cities need to be expanded and capacities strengthened. City initiatives need to be integrated in national action plans and global reporting. Key environmental issues in urban areas in Africa are related to the provision of services for waste, water and sanitation, and urban air pollution. Climate change impacts on urbanization have negative implications on urban infrastructure, health, water availability, economy and high risk of natural disasters such as flooding. International, national and local governments should have to raise the challenges of climate change on urbanization to save millions of urban residents to have a livable continent with better urbanization prospect in the era of globalization. This deserves cooperation and coordinated policy responses across multiple sectors, agencies and ministries; mainstreaming and institutionalizing climate change in sustainable urban planning and a new set of policy instruments for decision-making under deep uncertainty. Neither adaptation nor mitigation alone can avoid all climate change impacts; however, they can complement each other and together can significantly reduce the risks of climate change.

REFERENCES

- Arnell et al. 2004. *Climate and socioeconomic scenarios for climate change impacts assessment. Global Environmental Change, 14 (1): 3-20.*
- B. Sally et al. 2011. Sea level Rise (SLR) and impacts in Africa 2000-2100.
- E.O. Akrofi. 2006. Urbanization and the urban poor in Africa.
- Elliot. M. et al. 2011. *Technologies for climate change adaptation.* ISBN: 978-87-550-3902-5. New Delhi.
- FAO. 2010. Climate change threat to Africa: Adaptation a priority.
- L.A. Farrell. 2010. Mainstreaming climate change adaptation in urban development in South Africa. MSc Thesis, MIT, USA.
- Rahmstorf, S. 2007. *A semi-empirical approach to projecting future sea level rise. Science, 315: 368-370.*
- UN- HABITAT. 2008. Climate change resilience in urbanizing West Africa.
- UNCED. 1995. Urban planning and environment in Sub-Saharan Africa (SSA). Paper No. 5.
- UNEP. 2008. Urbanization in Africa.
- WHO. 2010. Essential public health package to enhance climate change resilience in developing countries.
- World Bank. 2010. Cities and climate change. Volume 10.
- WRI, UNDP, UNEP and World Bank, 2000. *World Resources 2000-2001: People and Ecosystems - the Fraying Web of Life.* World Resources Institute, Washington D.C

Disaster information gathering behavior after the Tohoku earthquake part 1: Results of Japanese respondents

Akiyuki KAWASAKI¹, Michael HENRY², and Kimiro MEGURO³

¹Project associate professor,
International Center for Urban Safety Engineering,
Institute of Industrial Science, the University of Tokyo, Japan
akiyuki@iis.u-tokyo.ac.jp

²Project researcher, International Center for Urban Safety Engineering,
Institute of Industrial Science, the University of Tokyo, Japan

³Professor and Director, International Center for Urban Safety Engineering,
Institute of Industrial Science, the University of Tokyo, Japan

ABSTRACT

The magnitude 9.0 Tohoku Earthquake, subsequent tsunami along the Pacific seaboard of Japan, and ensuing crisis related to the nuclear reactors at the Fukushima Daiichi power plant have reinforced the importance of clear and timely communication of disaster-related information for mitigating long-term negative impacts and working towards recovery. For people living in Japan, however, this disaster has been one of confusing and conflicting messages from differing information sources, and the atmosphere of uncertainty in the immediate wake of the earthquake led many people, Japanese and foreigners alike, to relocate to western Japan or leave the country entirely. In order to improve the dissemination of information after future disasters, a survey investigation was conducted to understand how people in the Kanto region – the most populous area of Japan and bordering the Tohoku region – received their disaster-related information and how it affected their decisions in the aftermath of the disaster. This paper presents an overview of the responses of Japanese nationals to the survey and discusses some initial impressions of their disaster information gathering behavior.

Keywords: *Tohoku earthquake, disaster information, Japanese, social media, traditional media*

1. INTRODUCTION

At 14:46 Japan Standard Time (05:46 UTC) on March 11, 2011, a magnitude 9.0 earthquake occurred off the Pacific coast of the Sanriku area in the Tohoku region of Japan. This earthquake, the largest ever recorded in Japanese history, not only caused strong ground motion which lasted for minutes but also triggered a massive tsunami which inundated the eastern seaboard of Japan and caused widespread destruction. The earthquake and

tsunami also knocked out the cooling systems at the Fukushima Daiichi nuclear power plant in Fukushima Prefecture, sparking a nuclear-related crisis which culminated with the confirmation of nuclear meltdown in three of the reactors.

In the wake of this triple disaster, people living in Japan began to seek disaster-related information in order to make decisions regarding their post-disaster actions. The primary source of information after environmental or man-made disasters is generally the mass media (Greenberg et al., 2002), and although this information was traditionally accessed via television, radio or printed media, Internet-based media are becoming the predominant means for people to access and communicate disaster-related information (Boyle et al., 2004). After a disaster, during the “response” and “recovery” phases, the information transmitted by the mass media is generally focused on affected areas in order to assist with recovery, but in the long-term “mitigation” phase the mass media help provide information to raise awareness and improve preparation (Quarantelli, 1996).

After the Tohoku Earthquake and during the unfolding of the nuclear crisis in Fukushima, however, there emerged a growing disparity between the information given by domestic Japanese sources and overseas sources (Sanchanta, 2011). Conflicting information and differing approaches between domestic and overseas sources may have contributed to the widely different responses between Japanese and foreigners in Japan; while Japanese people in general continued life as usual, foreign communities reacted much differently, with a large number of people relocating to other parts of the country or leaving Japan entirely – thus spawning the term “fly-jin,” a play on “gaijin,” the Japanese word for foreigner. In order to improve disaster response and recovery, it is necessary to understand what effect these information-related issues may have had on people’s post-disaster actions and how to improve information dissemination in the future.

The objective of this investigation is therefore to examine and clarify people’s information gathering behavior after the Tohoku Earthquake, to understand the relationship between information and people’s actions, and contribute to improving information dissemination in the future, particularly for reducing miscommunication and misunderstanding for foreign nationals residing in Japan. This paper – part one of two – presents the results of a survey developed for this investigation and focuses on the responses of Japanese people. As domestic media sources and information are almost wholly in the Japanese language, the responses of Japanese people can serve as a control sample for comparison to the responses of foreigners, which will be discussed in the second part.

2. SURVEY METHODOLOGY

This study focused just on the behavior of people living in the Kanto region of Japan. The Kanto region lies to the south of the Tohoku region and includes Tokyo – the capitol and political, financial, and entertainment

center of Japan – along with seven surrounding prefectures with a population of approximately 42 million Japanese and 1 million foreigners as of 2009. Tokyo itself lies roughly 370 kilometers southwest of the epicenter of the Tohoku Earthquake and 250 kilometers southwest of the Fukushima Daiichi nuclear power plant.

Data on disaster information gathering behavior were collected using an online survey. This survey was provided in nine different languages (Japanese, English, Chinese, Korean, Portuguese, Nepalese, French, Thai, Vietnamese), and the contents were separated into three sections as shown in Table 1. The first section asked respondents about their information gathering activities, the second section asked respondents about their post-disaster actions and the effect of information, and the third section collected demographic information.

Table 1: Survey contents

Section	Questions
1: Information gathering activities	What information sources did you trust the most / the least during the two weeks following the earthquake?
	During the two weeks following the earthquake, which media did you use to acquire information and in what language?
	In the case of this earthquake and tsunami disaster, by which media would you have preferred to receive disaster-related information?
	What types of information were most important for you during the first day, first week, and second week after the earthquake?
	What types of information were unavailable, unclear, or difficult for you to understand during the first day, first week, and second week after the earthquake?
	In general, what were the reasons why the above information was unclear or difficult to understand?
	When faced with unclear or difficult to understand information, what media did you utilize in order to clarify or better understand that information?
	At the time of the disaster were you familiar with the Japanese Earthquake Early Warning System? ¹
	Were you able to properly receive information regarding the rotating blackouts?*
2: Post-disaster action and effect of information	Within the first two weeks after the earthquake, did you choose to remain in the Kanto area, relocate to another area of Japan, or leave Japan? ¹
	What was the reason for your choice?
	At that time when you made your choice, how useful, if at all, was disaster-related information in making that choice? ¹
	If you chose to relocate to another area of Japan or leave Japan, within which time period after the earthquake did you make your choice? ¹
3: Demographic information	What is your nationality? ¹
	Which prefecture were you residing in at the time of the earthquake? ¹
	What is your occupation? ^{1,2}
	How old are you? ^{1,2}
	What is your yearly income level? ^{1,2}

¹ Questions were restricted to a single response; other questions allowed multiple responses

² Response was optional

The online survey was distributed via two methods: first, through the social and professional contacts of the authors; and second, through direct requests for cooperation with various entities such as business communities, universities, embassies, and so forth. People who were contacted to participate in the survey were also asked to distribute it to their social and professional networks.

3. SAMPLE CHARACTERISTICS

The survey received 497 responses from Japanese people, making up 36% of the total number of responses. The distribution of Japanese respondents by their location and occupation is shown in Figure 1. The majority were from Tokyo, followed by Kanagawa, Chiba, and Saitama Prefectures. Japanese company employees, Japanese educational institution employees, and students were the top occupations and made up more than three-quarters of the Japanese respondents.

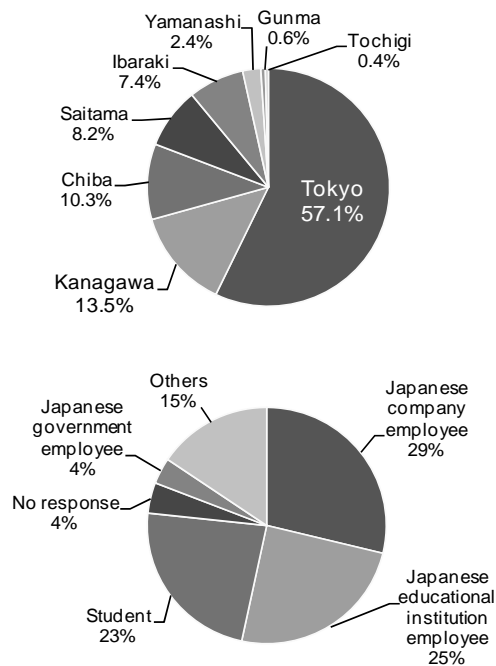


Figure 1: Distribution of respondents by location (left) and top occupations (right)

The age and income distribution of respondents are shown in Figure 2. The most responses were received from people in the 20-29 and 30-39 years old range, with the number of responses decreasing as age increases. The annual income of respondents fell mostly in the less than 1.95 million yen (approx. US\$24,900) range or in the 3.3 to 6.95 million yen (approx. US\$42,130 to US\$88,730) ranges.

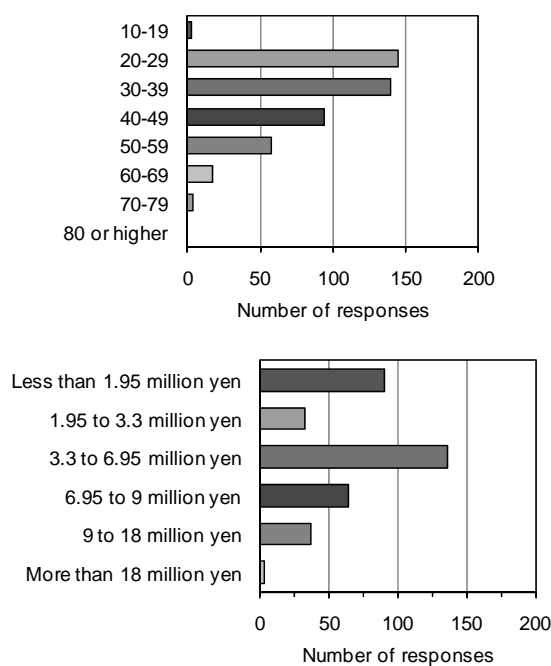


Figure 2: Distribution of respondents by age (left) and annual income (right)

4. SURVEY RESULTS

4.1 Information sources

Figures 3 and 4 show the top five most-trusted and least-trusted information sources, respectively, for Japanese respondents. It can be seen that Japanese news sources were rated as the most trusted, followed by Japanese research and academic institutions; the national Japanese government; family, friends colleagues, etc.; and overseas news sources. However, it can also be seen that the national Japanese government, Japanese news sources, and overseas news sources were also ranked among the top-five least trusted sources of information. Tokyo Electric Power Company was the least-trusted of any information source.

4.2 Media & language for information acquisition

Figure 5 shows the media and language which people used for acquiring disaster information. Japanese television was the most-used means, followed by Japanese traditional internet media (as in websites, information portals, and so forth). As may be expected, Japanese respondents did not utilize media in other languages very much, except for English traditional internet media.

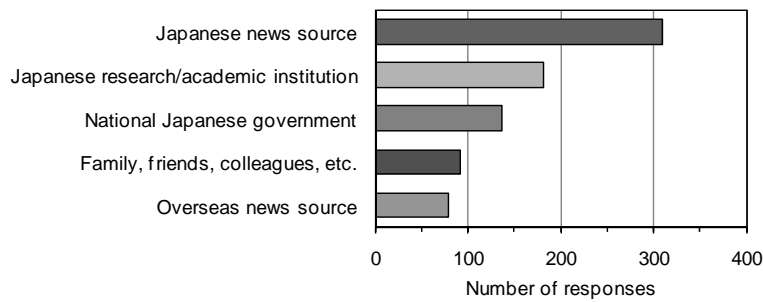


Figure 3: Top five most-trusted information sources

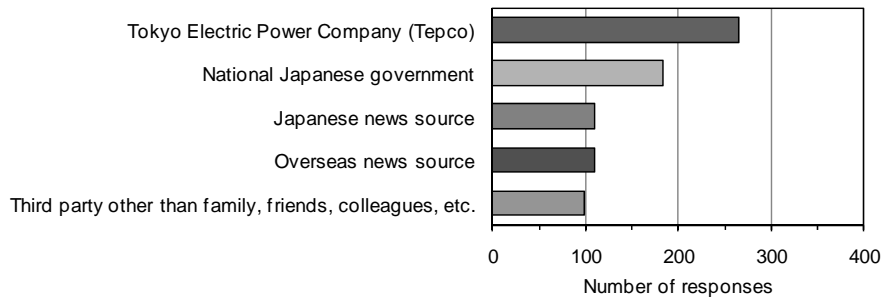


Figure 4: Top five least-trusted information sources

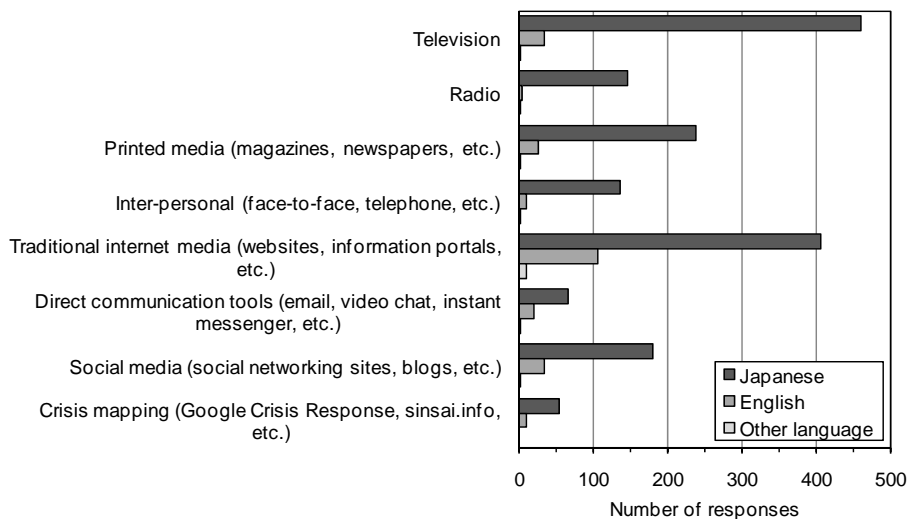


Figure 5: Utilized media and language for disaster information acquisition

Figure 6 shows by what media and language people would prefer to receive the disaster information. Japanese television and traditional internet media are again the highest-rated. The preference for radio can also be seen to be higher relative to other media than it was actually utilized. Understandably, non-Japanese language media were not preferred by the Japanese respondents.

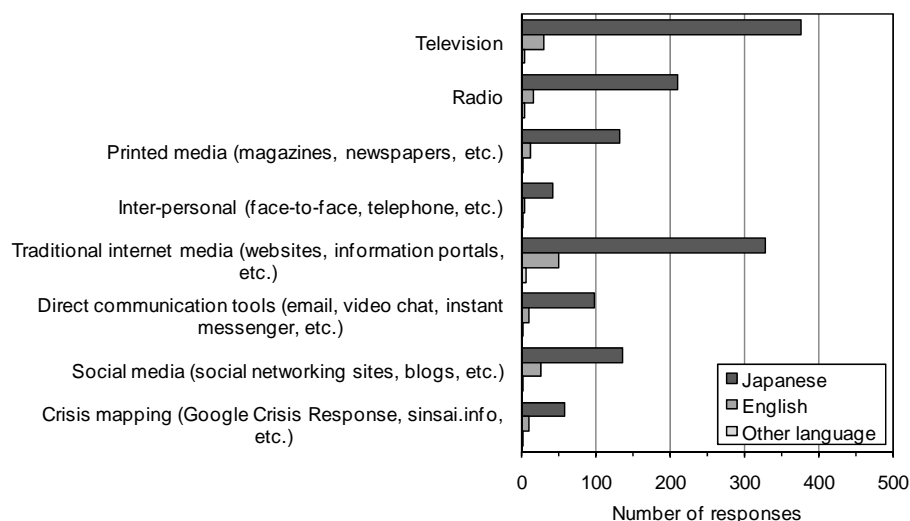


Figure 6: Preferred media and language for disaster information acquisition

4.3 Importance of information

Figure 7 shows the importance of information types as it changed over time from the first day to the first and second weeks. On the first day, the safety of family and friends was by far the most important information, followed by concerns about the transportation systems and earthquake and tsunami damage. By the first week, however, radiation level and risk was the most important type of information, followed by continuing concerns about transportation systems and earthquake and tsunami damage. By the second week, the importance of most information continued to decrease except for radiation level and risk, which actually increased slightly. Also, government response became the second-most important information type.

4.4 Problems related to information

The importance of information needs to be considered in terms of whether that information can actually be obtained or understood. Figure 8 shows what information people found to be unavailable, unclear, or hard to understand over the same two-week period.

For the first day, information related to the safety of family and friends, radiation level and risk, and transportation systems, and earthquake and tsunami damage were the hardest to find or understand. By the first week, these had decreased except for radiation level and risk and government response, which increased. By the second week, the unavailable or difficult to understand information decreased slightly, but radiation level and risk and government response were still highly viewed as unavailable, unclear, or hard to understand.

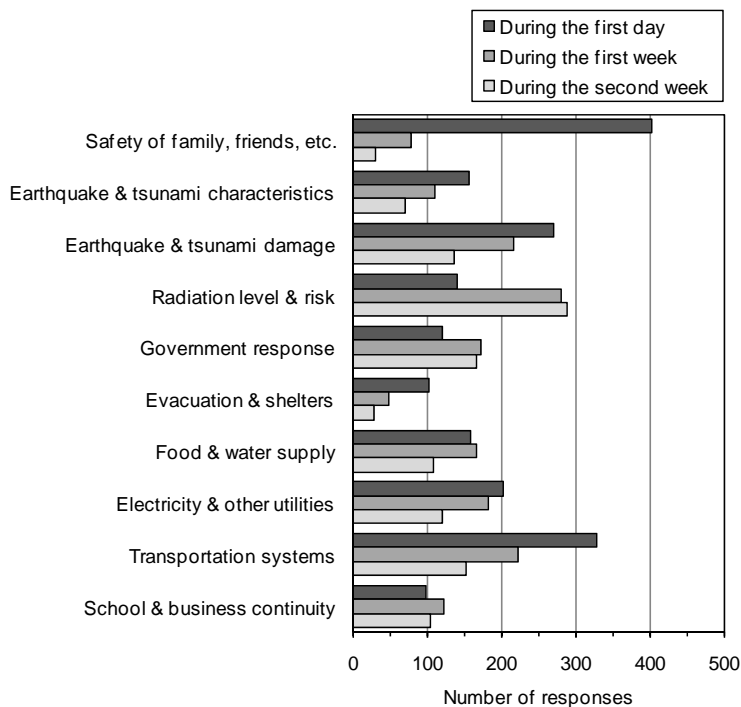


Figure 7: Importance of information types over time

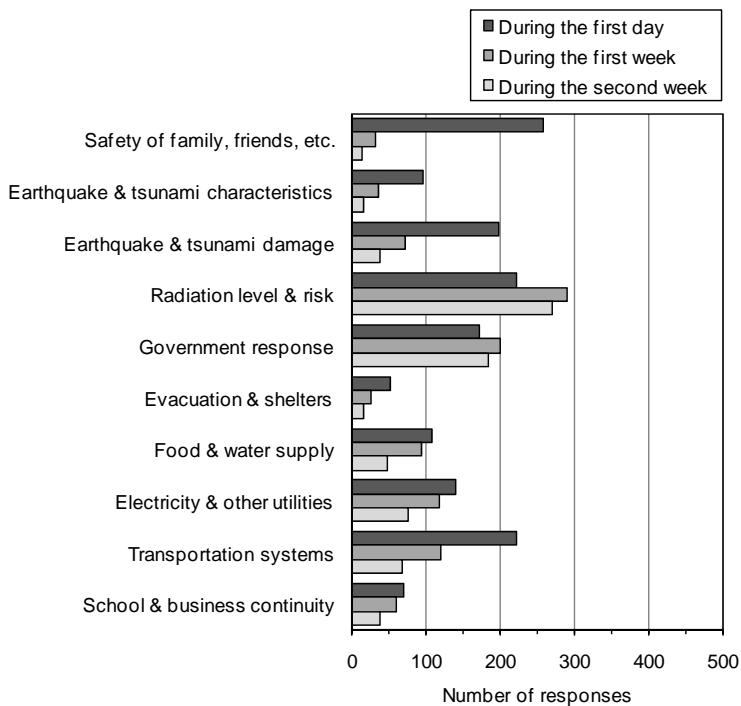


Figure 8: Unavailable, unclear, or hard to understand information over time

The reasons why the previously-discussed information was unclear or hard to understand are shown in Figure 9. The biggest reason appeared to be that people were confused by conflicting or differing information, followed closely by being unable to access information due to problems such as

mobile congestion or power outages. The other reasons were ranked much lower.

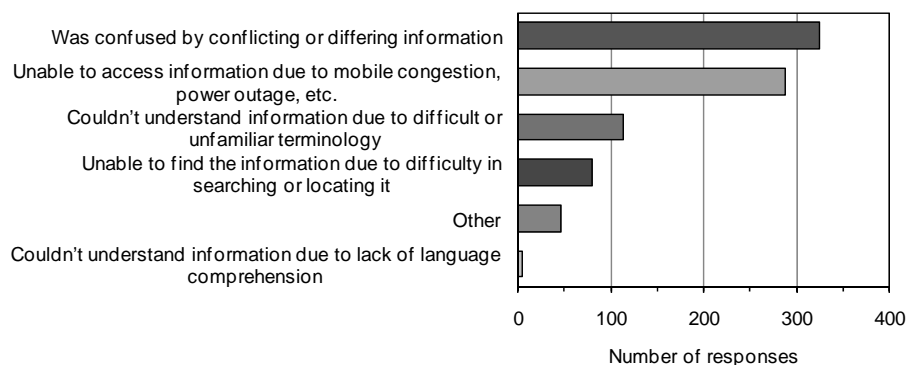


Figure 9: Reasons information was unclear or hard to understand

Figure 10 shows what media and language people turned to in order to clarify problems they had with information. Traditional Japanese internet media was the most-used means, followed by Japanese television. Among non-Japanese language media, traditional English internet media was the highest rated.

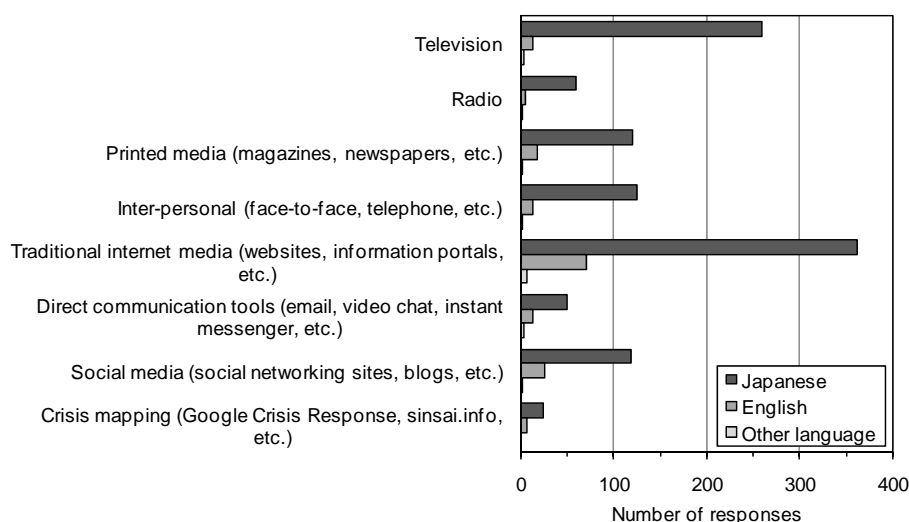


Figure 10: Media and language for clarifying information problems

4.5 Early warning system and rotating blackouts

Figure 11 shows the distribution of respondents who were familiar with the Japanese Earthquake Early Warning System and whether respondents could properly receive information regarding the rotating blackouts. It can be seen that a large majority of Japanese respondents were already familiar with the warning system. Only slightly more than half of the respondents, however, said that they could receive information on the rotating blackouts, with one-third responding that they were unable to receive blackout information. Being unable to access information due to mobile congestion, power outage, etc. was cited as one reason why

information was unclear or hard to understand, which may have contributed to difficulties in accessing rotating blackout information.

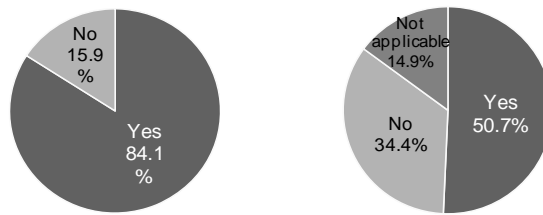


Figure 11: Distributions of whether respondents were familiar with the early warning system before the earthquake (left) and whether they could receive information on the rotating blackouts (right)

4.6 Post-disaster relocation & usefulness of information

The survey also asked people whether they remained in the Kanto area, relocated to another area of Japan, or left Japan within two weeks after the earthquake. As shown in Figure 12, an overwhelming majority of the survey respondents did not relocate – they remained in the Kanto area. Among the very few number of people who relocated or left, it can be seen in Figure 13 that the number increased from within one day up to within one week, and then decreased again.

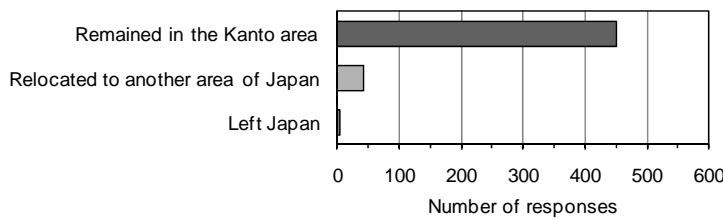


Figure 12: Distribution of whether respondents stayed, relocated, or left

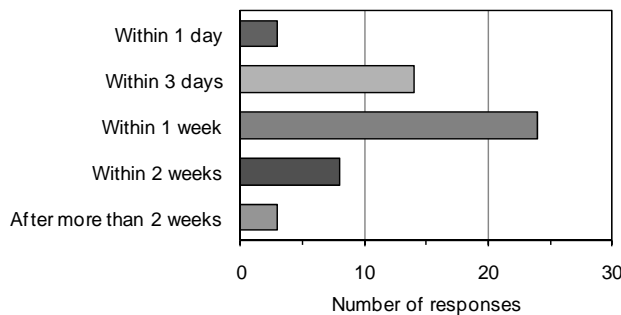


Figure 13: Timing of relocation or leaving

The primary reason people cited for whether they stayed, relocated or left was that it was a personal decision, as shown in Figure 14. This reason by far outranks other reasons such as unable to leave, job obligation, or others. Overall, it appeared that disaster-related information was somewhat useful for people’s decision making, as shown in Figure 15. These results, however, are going to require more analysis to look at which reasons corresponded to which actions.

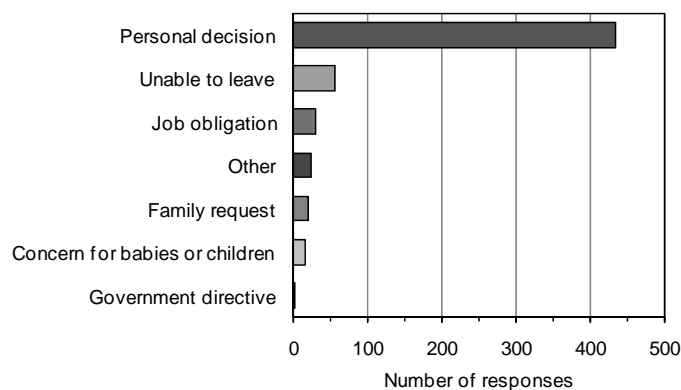


Figure 14: Reasons for staying in Kanto, relocating, or leaving Japan

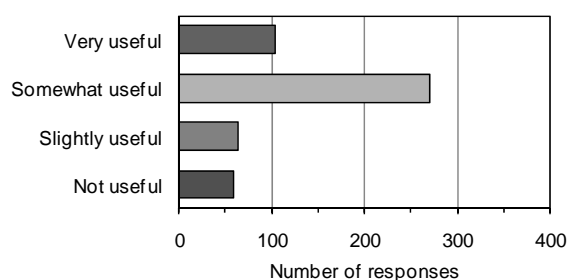


Figure 15: Usefulness of disaster-related information for decision making

5. INITIAL IMPRESSIONS

When considering the information gathering behavior of Japanese respondents, it could be seen that several of the information sources which were among the top five most-trusted sources were also among the top five least-trusted sources. This illustrates one of the difficulties in disseminating disaster information, in that what may be a highly trusted source for one person may be another person's highly distrusted source. Japanese research/academic institutions were the highest trusted source which did not fall within the top five least-trusted sources, indicating that these institutions may be a good, neutral source for disseminating information in the future. To collect their disaster information, Japanese respondents primarily utilized television and traditional internet; as the situation after the disaster was constantly in flux, these media were very useful as they can provide frequent updates with accompanying visual and discussions. The results of this survey, however, may be biased towards people who regularly utilize the internet, as the survey was distributed online.

The importance of and unavailability or difficulty in understanding information was also seen to change over time, which reflects the constantly changing situation as concern shifted from the earthquake to the tsunami and the nuclear situation. These two followed a similar trend, suggesting that as people became more concerned with a certain type of information

they wanted to know it in more detail, thus highlighting issues related to finding or understanding that information.

The majority of the Japanese respondents did not relocate or leave Japan, citing personal decision as their reasoning. It is difficult at this level of analysis to clarify what effect disaster information may have had on this decision, if any.

The results and discussion in this paper (part one of two), however, only represent some initial impressions focusing on the Japanese respondents. Part two continues introducing the survey results by focusing on the responses of foreign nationals and comparing them to those of Japanese respondents.

REFERENCES

Boyle, M., Schierbach, M., Armstrong, C.L., Mcleod, D.M., Shah, D.V., Pan, Z., 2004. Information seeking and emotional reactions to the September 11 terrorist attacks. *Journalism and Mass Communication Quarterly* 181, 155-167.

Greenberg, B.S., Hofschire, L., Lachlan, K., 2002. Diffusion, media use and interpersonal communication behaviors. *Communication and terrorism: public and media responses to 9/11*, Hampton Press, Cresskill, 3-16.

Quarantelli, E.L., 1996. The future is not the past repeated: projecting disasters in the 21st century from current trends. *Journal of Contingencies and Crisis Management* 4(4), 220-240.

Sanchanta, M., 2011. Japanese, foreign media diverge. *The Wall Street Journal*. Available from:

<http://online.wsj.com/article/SB10001424052748703512404576209043550725356.html> (27 September 2011)

An experimental study on strengthening lap splice by ferrocement jacket

Ratkriangkrai PAOLENG

Sirindhorn International Institute of Technology,

Thammasat University, Pathumthani, Thailand

joe.kriangkrai_civil@hotmail.com

Amorn PIMANMAS

Associate Professor, Sirindhorn International Institute of Technology,

Thammasat University, Pathumthani, Thailand

amorn@siit.tu.ac.th

ABSTRACT

This paper presents the experimental program on strengthening sub-standard lap splice of reinforcement using ferrocement jacket. The strengthening technique employed the skeleton steel of 9 mm diameter for confining the lap splice zone. The test program consisted of 7 specimens. One is the control specimen with continuous bar (no lap splice). The other 6 specimens contained lap splice of longitudinal bars. Two of them were un-strengthened and the remaining 4 specimens were strengthened by ferrocement jacket. The main study variables were lap splice length, the ratio of concrete cover to bar diameter, concrete compressive strength and the volume of confining skeleton steel. The ferrocement was made with 50 MPa mortar and reinforced by two layers of hexagonal wire meshes. The thickness of ferrocement jacket was 20 mm. Based on experimental results, the un-strengthened specimens showed a substantial drop in load bearing capacity. The failure was characterized by a horizontal splitting crack along the lap splice. Strengthening by ferrocement jacket could significantly increase the strength by as high as 50% and could develop the yield strength of the bars. The ferrocement jacket could also increase the ductility of the strengthened specimens.

Keywords: *strengthening, lap splice, ferrocement, bond strength*

1. INTRODUCTION

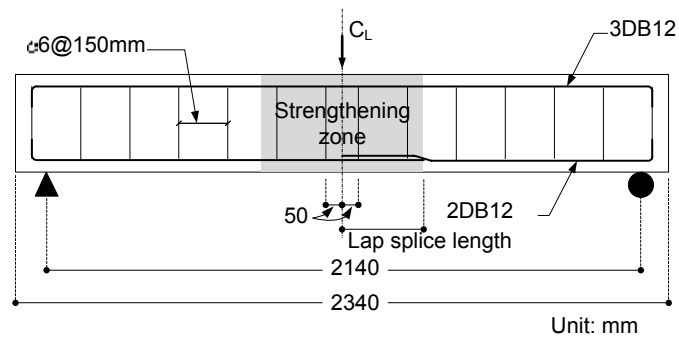
In reinforced concrete construction, lap splice of reinforcing bars is common in many locations of the structures, for example, the lap splice of column longitudinal bars and beam longitudinal bars. If the splice length is inadequate for the bond development, the strength and ductility of the bars can be degraded (Thai, 2010). The premature failure of lap splice is normally caused by the splitting of longitudinal bars leading to the loss of bond and sudden drop in load carrying capacity.

The main factors that affect the bond between concrete and steel bars are (1) lap splice length, concrete compressive strength and the concrete cover-to-bar diameter ratio (Thai, 2010; Harajli, 2006; Harajli, 2009). In existing structures, there is an urgent need to retrofit the substandard lap splice to meet the new requirements (Bournas and Triantafillou, 2010; Jumaat and Alam). There are several methods to retrofit inadequate lap splice such as fiber-reinforced polymer (FRP) wrapping (Thai, 2010; Harajli, 2006; Harajli, 2009), concrete jacketing (Bournas, and Triantafillou, 2010; Jumaat and Alam; Joyklad et al.; Bousias et al., 2006), steel plate jacketing (Lin et al., 2010), ferrocement jacketing (Kumar et al., 2007; Al-Kubaisy and Jumaat, 2000). When considering the cost of retrofitting old structures, ferrocement is a competitive method (Juntanalikit et al., 2009; Bansal et al.). Ferrocement is a thin reinforced material with thickness not more than 25 mm. It is made from closely spaced wire mesh and plastered with high cement mortar (Joyklad et al.; Juntanalikit et al., 2009; ACI549R-97, 2009). The strength can be enhanced by adding skeleton steels made from ordinary plain steel bars. In this research, the authors apply ferrocement to strengthen lap splice zone.

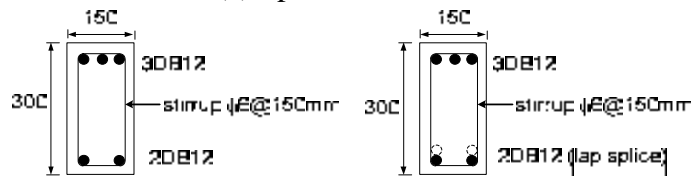
2. EXPERIMENTAL PROGRAM

2.1 Specimen details

The experiment aims to study the effect of strengthening lap splice by ferrocement. The factors to be considered are lap splice length, concrete compressive strength, technique of ferrocement reinforcement and the ratio of concrete cover-to-bar diameter. The experiment consisted of 7 specimens. One of them employed continuous bars without lap splice and served as the control specimen. The rest of specimens were divided into two groups, 25db group with 300 mm splice length and 20db group with 250 mm splice length as shown in Table 1. The specimens are beam type with cross section size 150x300 mm and the span length of 2140 mm. They are tested under a static point load applied at the center of the beam. The reinforcements in the specimens are 3-DB12 (diameter = 12 mm) top bars and 2-DB12 bottom bars. The nominal yield strength of the bar is 400 MPa. The specimens also contain stirrup of 6 mm diameter spaced at 150 mm throughout the length of the specimen. The nominal yield strength of stirrup is 240 MPa. The detail of specimen with lap splice is shown in Fig. 1.



(a) Specimen's detail



(b) control specimen (continuous bar) (c) specimen with lap splice
 Figure 1: Detail of specimens and lap splice

2.2 Strengthened specimens

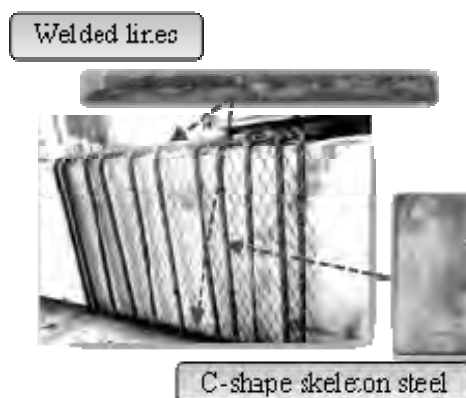


(a) Strengthening of specimen by ferrocement



(b) plastering step

Figure 2: Application of ferrocement



(a) Skeleton steel



(b) Hexagonal Wire mesh

Figure 3: Skeleton steel and hexagonal wire mesh

The 20 mm thick ferrocement is jacketed around the specimen in the lap splice zone. The mortar plaster was high cement content. It is reinforced with 2 layers of hexagonal wire mesh as shown in Figure 2 (a). The skeleton steel are plain round bar RB9 (9 mm diameter) with the spacing of 20 mm as shown in (Figure 2 (b)). The skeleton steels are fabricated in 2 C-shaped pieces and assembled to form a loop by welding as shown in Figure 3.

2.3 Specimen designations

Table 1: Specimens

Series	Beam	Lap splice length (L_{sp} , mm)	f'c member (Mpa)	cover/bar diameter (c/d _b)	Skeletal steel	
					Diameter (mm)	Spacing (mm)
25db	25F0	300	41	1.7	-	-
	25FP	300	41	1.7	-	-
	25F5	300	41	1.7	9	50
20db	20F0	250	41	1.7	-	-
	20FP	250	41	1.7	-	-
	20F5	250	41	1.7	9	50
without lap splice	00C1	-	41	1.7	-	-

From Table 1, the specimens with lap splice are divided into 2 groups, 25db and 20db. The number in the group's name indicates the length of lap splice (L_{sp}) which is equal to the multiple of bar diameter ($d_b=12$ mm) for example, 25db will have the splice length equal to 300 mm. The splice length is indicated in column 3 of Table 1. The specimen designation is composed of three parts. The number indicates the series (20db or 25db). The letter F indicates specimens with lap splice. The last letter or number indicates the type of retrofit, i.e., "0" indicates no retrofit, "P" indicates the retrofit by hexagonal wire mesh only and "5" indicates the retrofit by 9 mm skeleton steel spaced at 50 mm. The control specimen with continuous bar is designated by "00C1".

2.4 Material properties



(a) specimens covered by wet burlaps



(b) Lap splice zone

Figure 4: Curing of specimen

2.4.1 Concrete

The specimens were cast by ready mixed concrete. They were left 24 hours before curing by wet burlaps as shown in Figure 4 (a). The tested compressive strength of standard cylindrical specimen at 28 days is 41 MPa.

2.4.2 Reinforcement

The tested yield strength of main bars (DB12) is 474 MPa and the tensile strength is 782 MPa. The tested yield strength of stirrups (RB6) is 380 MPa and the tensile strength is 457 MPa. The tested yield strength of skeleton steel (RB9) is 346 MPa and the tensile strength is 427 MPa.

2.4.3 Ferrocement

The plastering mortar was mixed at the water:cement:sand ratio = 1:2:4. The target compressive strength at 7 days is 50 MPa. After plastering mortar to the lap splice area, it is left 24 hours and then covered by wet burlaps as shown in Figure 4 (b).

2.5 Instrumentations

The deflection of specimens is measured by 7 transducers as shown in Figure 5. The transducers at position 1 and 2 are to measure support vertical movement. The transducers at position 3 and 4 are to measure vertical deflection at $\frac{1}{4}$ span length. The midspan deflection is measured by transducer 6.

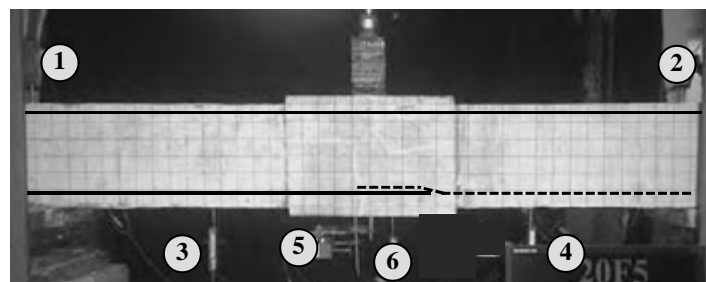


Figure 5: Position of transducers

2.6 Applied load

The point load is statically applied at midspan through hydraulic actuator. The load cell with 100 kN capacity is used to measure the load. The load is applied incrementally at 2.5 kN. At each load increment, the deflection and the cracks are recorded.

3. THE RESULTS

3.1 Load-Displacement

The deflection at mid-span (Δ) is obtained by subtracting measured support deflections (position 1 and 2) from measured mid-span deflection (position 6) as shown in equation (1).

$$\Delta = (6) - \frac{(1) + (2)}{2}$$

(1)

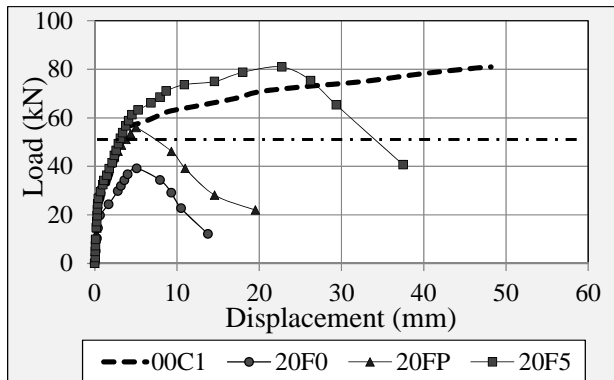


Figure 6: load versus displacement of series 20DB and 00C2

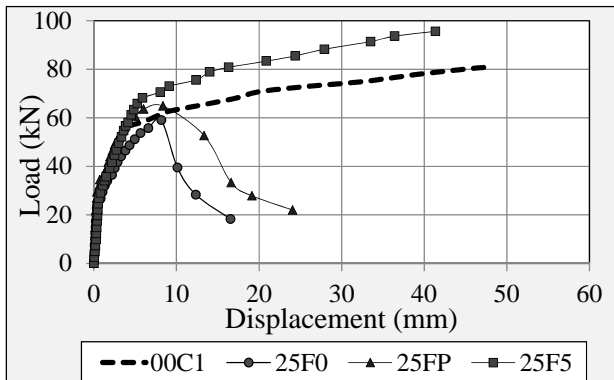


Figure 7: load versus displacement of series 25DB and 00C2

The test results are shown in Figure 6 and 7. In each figure, the control specimen 00C1 is shown as dash line. From Figure 6, when comparing specimen 20F0 with 00C1, it can be seen that specimen 20F0 can resist the maximum load of 40 kN at deflection of 5.1 mm. After that, the graph drops suddenly. As for specimen 20FP, the maximum load is 56 kN at 5.10 mm deflection. The load drops suddenly after reaching the peak load. It can be seen that the use of ferrocement without skeleton steel cannot develop the yield strength of steel bar. As for specimen 20F5, the maximum load is 80.93 kN at 22.75 mm deflection. It can be seen that this specimen can develop yield strength of steel bar. The strengthening by ferrocement jacket with skeleton steel is shown to increase both load and deformation capacity. The strength increase is higher than that of 00C1.

Figure 7 shows the comparison between specimens in series 25db with the lap length of 300 mm. In this figure, specimen 25F0 without any retrofit can resist the maximum load of 59.06 kN at 6.02 mm deflection. The load drops sudden after reaching the peak. The tendency is similar to series 20db. For retrofitted specimens 25FP and 25F5, both of them can reach yield load, but the strength of specimen 25FP drops suddenly when reaching the peak. The highest load that specimen 25FP can reach is 64.89 kN. However, specimen 25F5 can reach the highest load up to 95.65 kN and can deform as

much as 41.4 mm. When compared with specimen 25F0, it can be seen that strengthening by ferrocement jacket with skeleton steel is very effective to increase both strength and deformation capacity of the specimen.

3.2 Crack pattern

The crack patterns are recorded during the tests. The photos of the specimens after the test are shown in Figure 8-12. Figure 8 shows the crack pattern of specimen 00C1. Most of vertical cracks occur in the midspan region of the beam. On the other hand, the failure of specimen 20F0 without retrofitting shows less vertical cracks than observed in 00C1. A large horizontal crack along the lap splice can be clearly observed. It is observed that once this horizontal crack forms, the load drops suddenly. This horizontal crack is thought to be caused by bond splitting failure.



Figure 8: Crack pattern of specimen 00C1 at failure



Figure 9: Crack pattern of specimen 20F0 at failure

The crack pattern of specimens 25F5 retrofitted by ferrocement jacket with skeleton steels is shown in Figure 10. When ferrocement jacket is removed from the main beam, the cracks are revealed as shown in Figure 11-12. Figure 11 shows the crack pattern of specimen retrofitted by ferrocement jacket without skeleton steels. A large horizontal splitting crack can be clearly observed. However, when skeleton steels are added to ferrocement jacket, it can be seen that the crack pattern at failure is similar to specimen 00C1 with continuous bars (Figure 8). From this observation, it can be clearly seen that ferrocement jacket with skeleton steel are effective to retrofit the lap splice in reinforced concrete beam.



Figure 10: Crack pattern of specimens retrofitted by ferrocement jacket

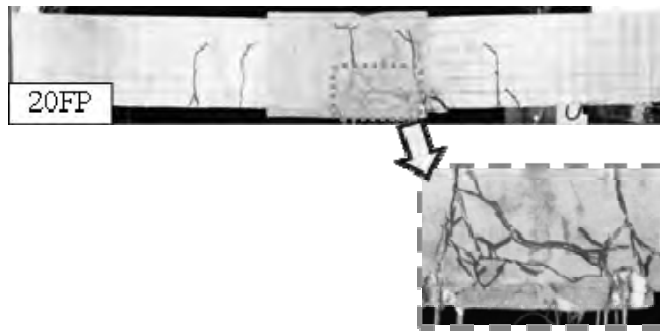


Figure 11: Crack pattern of specimens retrofitted by ferrocement jacket without skeleton steel (observed on main beam)

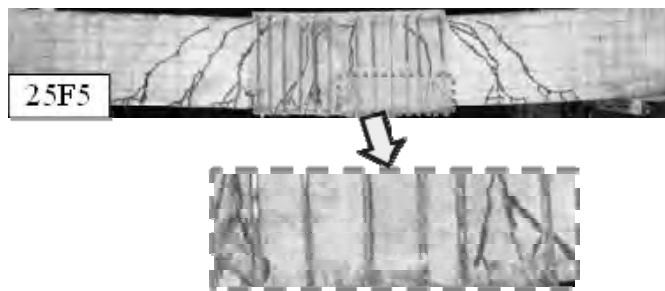


Figure 12: Crack pattern of specimen retrofitted by ferrocement jacket with skeleton steel (observed on main beams)

4. CONCLUSIONS

From the experimental study of retrofitting lap splice by ferrocement jacket. Two experimental series are performed, that is 20db (splice length = 250 mm) and 25 db series (splice length = 300 mm). A total of 7 specimens have been tested under static load applied at the midspan of the beam. From the test results, the following conclusions can be drawn.

- The specimens with lap splice length of 20 and 25 times bar diameter cannot develop yield strength of steel bars. The failure is brittle and caused by the horizontal splitting crack occurring the lap splice zone.
- Retrofitting specimens by ferrocement jacket without skeleton steel can increase the strength of the specimens a little but does not enhance the deformation capacity.
- Retrofitting specimens by ferrocement jacket with skeleton steel can substantially increase both the strength and deformation capacity of the specimens. This retrofit method is also effective to develop the yield strength of steel bars.

ACKNOWLEDGEMENT

The authors are grateful to Thailand Research Fund for providing the research grant RSA 5280034.

REFERENCES

- ACI549R-97, 2009. *Report on Ferrocement*, ACI committee report, ACI committee 549.
- Al-Kubaisy, M.A., Jumaat, M.Z., 2000. *Flexural behaviour of reinforced concrete slabs with ferrocement tension zone cover*, Construction and Building Materials 14, 245-252.
- Bansal, P.P., Kumar, M., and Kaushik, S.K., *Effect of Wire Mesh Orientation on Strength of Beams Retrofitted using Ferrocement Jackets*, International Journal of Engineering, Vol.2 , issue 1, 8-19.
- Bournas, D.A., and Triantafillou, T.C., 2010. *Bond strength of Lap Spliced Bars in Concrete Confined with Composite Jackets*, ASCE Journal of Composites for Construction, 40pp.
- Bousias, S., Spathis, A.L., and Fardis, M.N., 2006. *Concrete or FRP Jacketing of Column with Lap Splices for Seismic Rehabilitation*, Journal of Advanced Concrete Technology, Japan, Vol.4, No.3, 431-444.
- Harajli, M.H., 2006. *Effect of confinement using steel, FRC, or FRP on the bond stress-slip response of steel bars under cyclic loading*, Materials and Structures, 39, 621-634.
- Harajli, M.H., 2009. *Bond Stress–Slip Model for Steel Bars in Unconfined or Steel, FRC, or FRP Confined Concrete under Cyclic Loading*, Journal of Structural Engineering, 509-518.
- Joyklad, P., Jantanalilit, P., and Pimanmas, A., *Shear Strengthening of RC beams using web steel and Ferrocement cover*, Annual Concrete Conference 5, Thailand, STR.41-46.
- Jumaat, M.Z., and Alam, M.A., *Strengthening of reinforced concrete structures” Department of Civil Engineering, University of Malaya, Kuala Lumpur.*
- Juntanalikit, P., Joyklad, P., and Pimanmas, P., 2009. *Shear Strengthening of Reinforced Concrete Beams using Ferrocement*, New Technologies for Urban Safety of Mega Cities in Asia, 301-312.
- Kumar, P.R., Oshima, T., Mikami S., and Yamazaki, T., 2007. *Studies on RC and Ferrocement Jacketed Columns Subjected to Simulated Seismic Loading*, Asian journal of civil engineering (Building and Housing), VOL 8, No.2, 215-225.
- Lin, M.L., Chen, P.C., Tsai, K.C., Yu, Y.J., and Lui, J.G., 2010. *Seismic steel jacketing of rectangular RC bridge columns for the mitigation of lap-splice failures*, Earthquake engineering and structural dynamics.
- Thai, D.X., 2010. *Strengthening Lap Splice in Sub-standard Reinforced Concrete Column by Frp Wrapping*, M.sc. Thesis, Sirindorn International Institute of Technology, Thammasat University, Thailand

Correlation analysis of a reinforced-concrete building under tsunami loads and effect of masonry infill walls in tsunami resistance

Anat RUANGRASSAMEE¹ and Piyawat FOYTONG²

¹Assistant Professor, Department of Civil Engineering,
Chulalongkorn University, Thailand
anat.r@chula.ac.th

²Ph.D. Candidate, Department of Civil Engineering,
Chulalongkorn University, Thailand
piyawat_pwf@yahoo.com

ABSTRACT

The December 26th, 2004 Indian Ocean tsunami caused damage to many buildings in the southern provinces of Thailand. Reinforced-concrete buildings in the area are mainly designed for gravity loads. One-story building which was the former office of Thai Meteorological Department located in Phang-Nga province was tested under tsunami load patterns. In this research, the reinforced-concrete building model is investigated by 3-dimensional non-linear static pushover analysis. In the building model, masonry infill walls are considered and idealized as the diagonal stud. The results of the building model agree well with the test results. To analyze the effect of masonry infill walls, the patterns of the wall are rearranged. The masonry infill walls with the appropriate arrangement can significantly improve the load resisting capacity of the building.

Keywords: *tsunami, tsunami load, reinforced concrete, building, nonlinear analysis*

1. INTRODUCTION

The December 26th, 2004 Indian Ocean tsunami caused damage to several buildings in southern provinces of Thailand. Reinforced-concrete buildings in the area are mainly designed for gravity loads. One-story building which is the former office of Thai Meteorological Department located in Phang-Nga province was tested under tsunami load patterns. This research focuses on correlation analysis of the reinforced-concrete building with in-filled masonry walls under tsunami loading by using 3-dimensional nonlinear pushover analysis. Then the model is used to study the effect of masonry infill walls in a tsunami load resisting capacity.

2. DAMAGE OF BUILDING DUE TO 2004 INDIAN OCEAN TSUNAMI

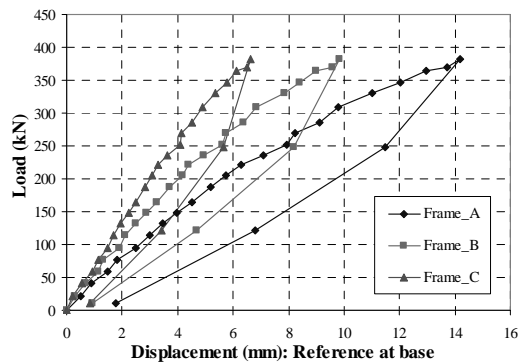
The December 26th, 2004 Indian Ocean tsunami caused damage to buildings in Indian Ocean countries. The damage of buildings were reported and analyzed by several researchers (Ruangrassmee et al., 2006). Damage to reinforced-concrete buildings ranged from no damage to collapse. To understand behavior of a reinforced-concrete building, the former office of Thai Meteorological Department located in Phang-Nga province was tested by Lukkunaprasit et al. (2010). As shown in Figure 1, this building was exposed to the tsunami inundation height of 4.4 m and damaged in non-structural members. In the test, the lateral pushover force was applied to represent the hydrodynamic force due to the tsunami. Figure 2(a) depicts the pushover test setup and Figure 2(b) shows the relationship of lateral force and displacement of each frame.



Figure 1: The former office of Thai Meteorological Department in Phang-Nga (Lukkunaprasit et al., 2008)



(a) Test setup



(b) lateral force vs displacement relation

Figure 2: Pushover test setup and results (Lukkunaprasit et al., 2008)

3. ANALYTICAL MODEL

In this study, the building is analyzed using a non-linear static pushover analysis by the TDAPIII program. The reinforced-concrete frames and masonry infill walls are the main structural components that need to validation with existing results from tests of structural components.

3.1 Reinforced-concrete frames

3.1.1 Analytical model

A 3-dimensional fiber model is used in the plastic region at the end of beams and columns to predict the behavior of reinforced-concrete frames. The plastic lengths of beams and columns are evaluated by using the equation proposed by Pauley and Priestley (1992). The fiber model consists of the unconfined concrete model, confined concrete model, longitudinal reinforcement model. The stress-strain relationship of unconfined concrete is modeled using the equation proposed by Kent and Park (1971). The stress-strain relationship of confined concrete is modeled using the equation proposed by Hoshikuma et al. (1997). The stress-strain relationship by Menegotto-Pinto (1973) is used for longitudinal reinforcement. The shear failure is considered using a non-linear spring as proposed by Sezen and Mohele (2004).

3.1.2 Comparison with test results

To validate the structural model, the experimental results by Wehbe (1999) and Anil and Altin (2007) are considered. From the study by Wehbe (1999), the rectangular reinforced-concrete column with 308 mm x 610 mm section was tested under cyclic loading and subjected to the axial force of 615 kN. The column height was 2.050 m. The analytical column model consists of the zero length shear spring, the fiber section element, and the elastic element. The calculated plastic length of the column is 0.352 m. The comparison between analytical result and experimental result of this column is shown in Figure 3.

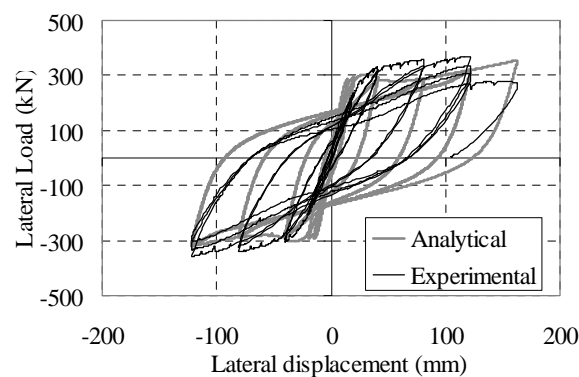


Figure 3: Comparison of experimental results by Wehbe (1999) and analytical results

From the study by Anil and Altin (2007), the reinforced-concrete frame with the 100 mm x 150 mm column section and 150 mm x 300 mm beam section was tested under cyclic loading without axial force. The frame

had columns with a height of 750 mm and a 1,500 mm long beam. The analytical model of the frame consists of the zero length shear springs at the end of columns, the fiber section elements at the end of the columns and the beam, and elastic elements as shown in Figure 4. The plastic lengths are 0.174 m and 0.150 m for the columns and beam, respectively. The comparison between analytical result and experimental result of this column are shown in Figure 5. From Figures 3 and 5, it is found that the reinforced concrete models can capture the actual behaviors satisfactorily.

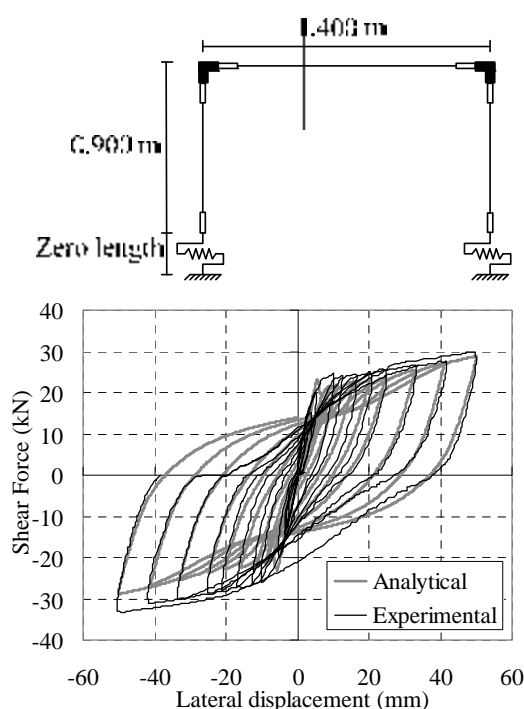


Figure 4: Analytical model of bare frame Figure 5: Comparison of experimental results by Anil and Altin (2007) and analytical results

3.2 Masonry infill wall

3.2.1 Analytical model

There are several models to idealize masonry infill walls. The diagonal stud was used in this research. For the lateral resisting force capacity of infill wall, the formulas proposed by FEMA 306 (1998) and Mostafaei and Kabeyasawa (2004) are considered. The experimental results of Mehrabi et al. (1996) are used to validate the masonry infill wall model. Four specimens were tested under monotonic loadings with the same RC frames, but they were different in the masonry types and the distribution of axial loads. The frame consisted of columns with a height of 1.537 m and a 2.312 m long beam. Table 1 shows the comparison of the lateral resisting forces with calculated forces by equations by FEMA 306 (1998) and Mostafaei and Kabeyasawa (2004). The resisting forces calculated from equations by Mostafaei and Kabeyasawa (2004) agree well with the experimental results, thus the equation by Mostafaei and Kabeyasawa (2004) was used to calculate the wall resisting force.

Table 1: Comparison of lateral resisting forces

Specimen No.	Experiment (1)	Mostafaei and Kabeyasawa (2)	FEMA 306 (3)	(2)/(1)	(3)(1)
2	14515.1	14215.1	8884.4	0.98	0.61
3	28304.5	23845.1	14017.8	0.84	0.50
8	19368.6	14975.9	9178.3	0.77	0.47
9	29846.7	21898.6	13059.8	0.73	0.44

3.2.2 Comparison with test results

The masonry infill wall and frame was modeled as shown in Figure 6. The masonry infill wall is modeled as a diagonal stud. The fiber sections are used in the plastic region at the end of beams and columns. The plastic lengths are 0.174 m for columns and 0.237 m for a beam. Shear springs are used to capture shear behaviors of columns and beam-column joints are assumed to be rigid. The comparison of the lateral load and lateral displacement relationship between the experimental results and analytical results for all four specimens are shown in Figure 7. It is found that the model can capture the maximum load satisfactorily.

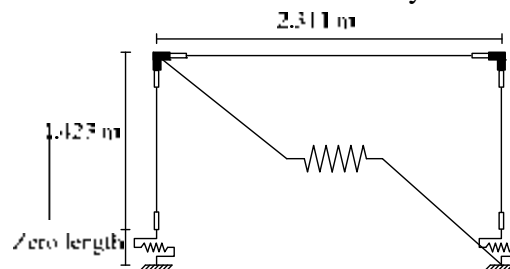
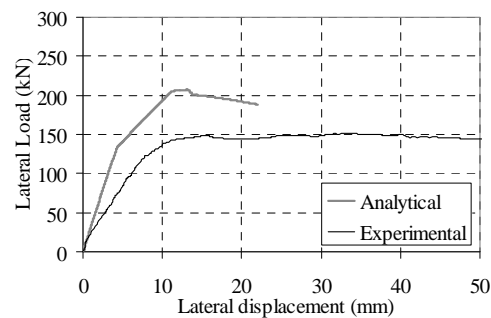
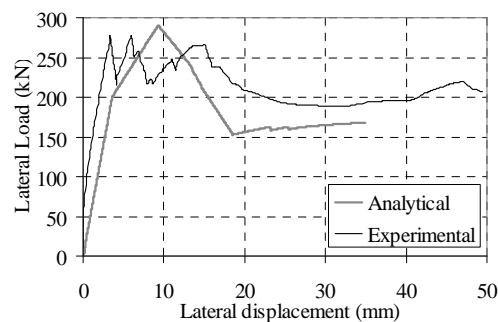


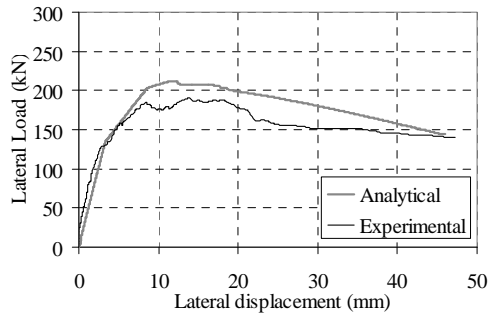
Figure 6: The analytical model of bare frame with masonry infill wall model



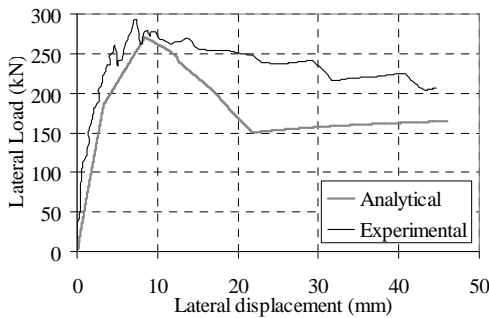
(a) Specimen No.2



(b) Specimen No.3



(c) Specimen No.8



(d) Specimen No.9

Figure 7: Comparison of experimental and analytical results

4. CORRELATION ANALYSIS OF RC BUILDING SUBJECTED TO TSUNAMI LOADS

The reinforced-concrete building which was the former office of Thai Meteorological Department in Phang-Nga Province was tested as mentioned in the previous section. The correlation analysis is conducted to understand the behavior of the building and investigate the effect of masonry infill wall. This building is a one-story reinforced-concrete building. The building plan is illustrated in Figure 8. Figure 9 shows the positions of the masonry infill walls. There is no masonry infill wall in the frame A. For the frame B, there is the masonry in filled wall at the front span. For the frame C, there are walls under window panels. The percentage of masonry infill walls is 21.8% in the plane parallel to direction of tsunami flows. The compressive strength of concrete obtained from in-situ coring was 12 MPa, and the yield strength of reinforcement was 240 MPa. The span to depth ratio of the column is 7.625. The axial load ratio is 0.128. The longitudinal reinforcement ratio and volumetric ratio of transverse reinforcement are 0.0113 and 0.0038, respectively. Due to the large shear span ratio, the column is governed by the flexural failure. The analytical models validated in the previous section are used in the correlation study. The building model is analyzed by using 3-dimensional non-linear pushover analysis under force control as shown in Figure 10. Six point loads consisting of three point loads at the roof level and another three point load at the floor level are applied to the building at the same locations as the field load test. These point loads represents hydrodynamic forces acting on tributary areas. The fiber sections are used in the plastic region at the end of beams and columns. The masonry wall is

modeled as a diagonal springs. The ground and roof slabs are modeled as rigid diaphragms.

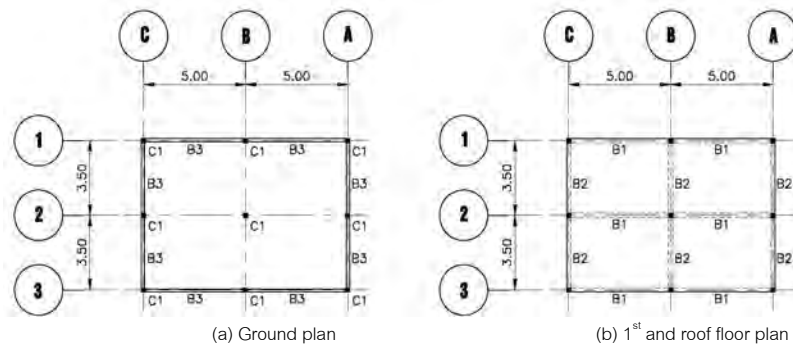


Figure 8: Plan of the former office of Thai Meteorological Department

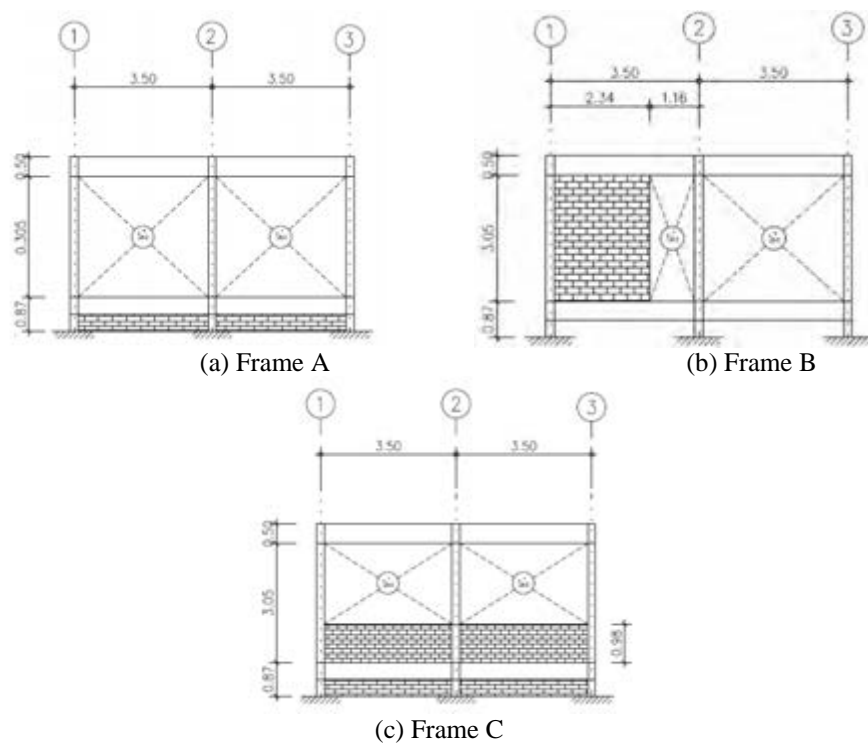


Figure 9: The location of masonry infill wall of each frame

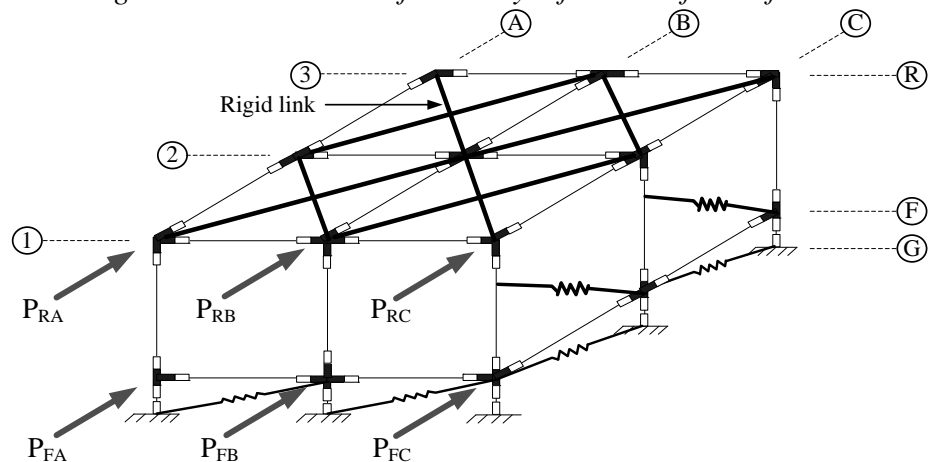


Figure 10: 3-dimensional model of the building

The lateral load and displacement relationships from the experiment and analysis are compared in Figure 11. The load is applied until the total load reaches that in the experiment. It is seen that the analytical model can capture the initial stiffness well however the lateral displacement from the analysis is slightly larger. The masonry infill wall in the frame B reaches the maximum resisting capacity. This result agreed well with the field load test that cracks on the masonry infill wall in the frame B significantly widened at the end of the test.

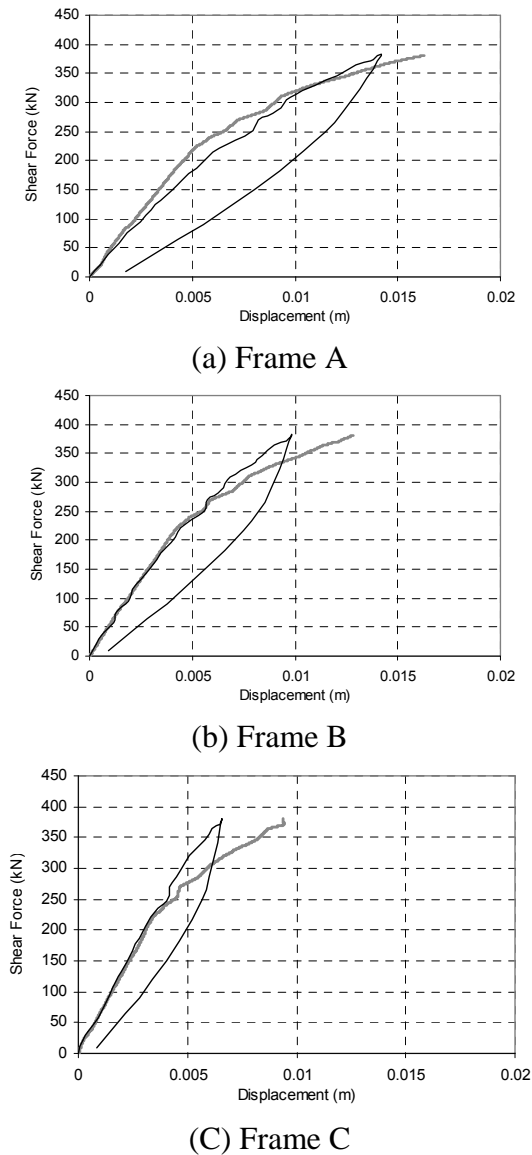


Figure 11: The force and displacement relationship of building model

5. EFFECT OF MASONRY INFILL WALL ON TSUNAMI RESISTING CAPACITY

The effect of masonry infill wall is investigated by arranging patterns of walls. The building model is analyzed with the same load pattern as the field load test. The names of each masonry infill wall are denoted as in

Figure 12. A, B, and C denotes the infill wall in both front and back spans in the frames A, B, and C, respectively.

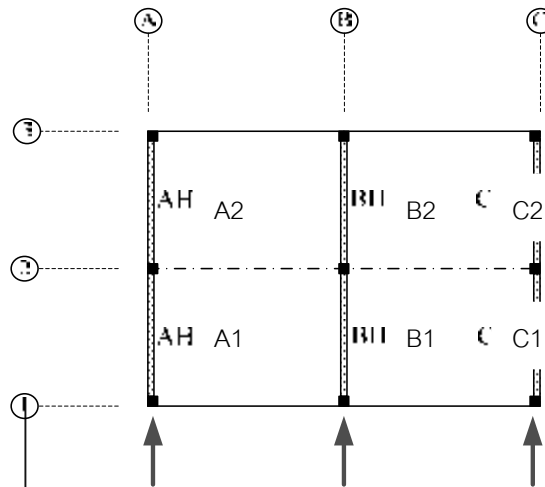


Figure 12: Definition of masonry infill walls

Table 2: Results of rearranged masonry infill wall

No	Description	Percentage of Infill Wall	Max Load (kN)	Failure
1	Without wall	0.0	138.8	All Columns
2	A	33.3	162.1	Columns in Frame C
3	B	33.3	694.1	Shear in Short Columns
4	A-C	66.7	704.6	Shear in Short Columns
5	A-B-C	100.0	706.2	Shear in Short Columns
6	A1-B1-C1	50.0	685.4	Shear in Short Columns

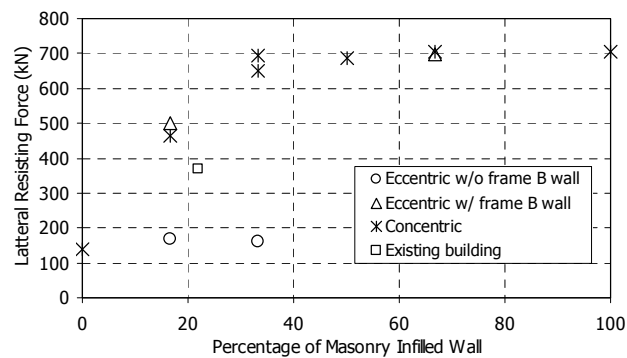


Figure 13: Relationship of lateral resisting force and percentage of infill wall

Table 2 summarizes the cases and results from the analysis. Several arrangement patterns of walls are considered and it is found that if there is no wall in the building the load resistance of the building is limited to only 138 kN which is governed by flexural failure of columns. If walls are provided in the frame A, torsional effect will result in the flexural failure of columns in the frame C. The wall in the frame B will significantly increase the lateral load capacity of the building to about 700 kN. If walls are

provided in all frames, the load resistance is about 700 kN which is limited by shear failure of short columns. Figure 13 illustrates the relation of lateral load resisting capacity vs percentage of walls. It is obvious that providing the wall in the frame B (33% of walls) is the most effective pattern to get a large tsunami resisting capacity. The building is subjected to shear failure of short columns under the floor slab.

6. CONCLUSIONS

This research focuses on correlation analysis of a reinforced-concrete building with in-filled masonry walls under tsunami loading and the effect of masonry infill walls in a tsunami load resisting capacity. The study can be concluded as follows:

- 1) The former office of Thai Meteorological Department located in Phang-Nga province is used for the 3-dimensional nonlinear pushover analysis. Material models are selected and compared with test results before applying to the building. Then the 3-dimensional models are developed and subjected to the load pattern similar to the field test. The good agreement is obtained between the test and analysis.
- 2) It is found that masonry infill walls play a major role in the tsunami load resisting capacity of the building. Hence the effect of infill walls is investigated by varying the arrangement pattern to find the effective pattern of walls. If there is no wall in the building the load resistance of the building is limited to only 138 kN which is governed by flexural failure of columns. The wall in the middle frame significantly increases the lateral load capacity of the building to about 700 kN. If walls are provided in all frames, the load resistance is about 700 kN which is limited by shear failure of short columns. It is obvious that providing the wall in the middle frame is the most effective pattern to get a large lateral load resisting capacity. However, the building is subjected to shear failure of short columns under the floor slab. Enhancement of the shear capacity of the short columns will improve the performance of this building.

REFERENCES

- Anil, O., and Altin, S., 2007. An experimental study on reinforced concrete partially infilled frames. *Engineering Structures*, 29, 449-460.
- FEMA 306., 1998. *Evaluation of earthquake damaged concrete and masonry wall buildings - Basic procedures manual*. Federal Emergency Management Agency, Washington, DC.
- Hoshikuma, J., Kawashima, K., Nagaya, K., and Taylor, A. W., 1997. Stress-strain model for confined reinforced concrete in bridge piers. *Journal of the Structural Engineering, ASCE*, 123(5), 624-633.
- Kent, D. C., and Park, R., 1971. Flexural members with confined concrete. *Journal of Structural Engineering, ASCE*, 97(7), 1969-1990.

Lukkunaprasit, P., Ruanrassamee, A., Stitmannathum, B., Chintanapakdee, C., and Thanasisathit, N., 2010. Calibration of tsunami loading on a damaged building, *Journal of Earthquake and Tsunami*, 4(2), 105-114.

Mehrabi, A. B., Shing, P. B., Schuller, M. P., and Noland, J.L., 1996. Experimental evaluation of masonry-infilled RC frames. *Journal of Structural Engineering*, 122, 228-237.

Mostafaei, H., and Kabeyasawa, T., 2004. Effect of infill masonry walls on the seismic response of reinforced concrete buildings subjected to the 2003 Bam Earthquake strong motion: A case study of Bam telephone center. *Bulletin Earthquake Research Institute Univ. Tokyo*, 79, 133-156.

Paulay, T., and Priestley, M. J. N., 1992. *Seismic design of reinforced concrete and masonry structures*. John Wiley and Sons, Inc.

Ruangrassamee, A., Yanagisawa, H., Foytong, P., Lukkunaprasit, P., Koshimura, S., and Imamura, F., 2006. Investigation of tsunami-induced damage and fragility of buildings in Thailand after the December 2004 Indian Ocean tsunami. *Earthquake Spectra*, 22, S377–S401.

Sezen, H., and Moehle, J. P., 2004. Shear strength model for lightly reinforced concrete columns. *Journal of Structural Engineering, ASCE*. 130, 1692-1703.

Wehbe, N. I., Saiidi, M. S., and Sanders, D. H., 1999. Seismic performance of rectangular bridge columns with moderate confinement. *ACI Structural Journal*, 96(S27), 248-259

Area suitability modeling for rice cultivation in Saraburi Province of Thailand

Bharambe K. P¹., Tripathi N. K² and A. R. Phalke³

¹Research Associate, RSGIS FoS, Asian Institute of Technology, Thailand
khagendra007@gmail.com

²Coordinator, RSGIS FoS, Asian Institute of Technology, Thailand

³Master Student School of Eng., RSGIS FoS, Asian Institute of Technology, Thailand

ABSTRACT

Thailand is the rice bowl of rice in the world. It has the fifth-largest amount of land under rice cultivation in the world and is largest exporter of rice. The world population is increasing at a higher rate which is affecting environment and putting hard stress on available agricultural land for human settlement and food security.

Agricultural land is the most crucial factor that can enhance the possibility for development of rice production. It is necessary first to assess the land suitability for rice growing areas in order to develop a good land management system. This study examines the area suitability classification for rice production in Saraburi Province of Thailand. Relevant data in the form of different layers such as land use, soil pH, annual rainfall, stream network, and slope at 1:250000 scale physical database formats were used and analyzed. Suitability maps were generated applying the suitability criteria for all the respective parameters. Final suitability map was obtained by multi-criteria analysis using Analytical Hierarchy Process (AHP).

The outcomes of the study showed that only 21.21 percent land had been found to be highly suitable for rice cultivation under all suitability criteria. Around 21 percent land from remaining land obtained was found to be moderately suitable where further possibility of conversion exist by adopting some irrigation and management practices. Rest of the areas has under gone in marginally suitable land and least or not suitable land for rice cultivation in Saraburi Province of Thailand.

Keywords: *Agricultural land, Land suitability, Rice cultivation, AHP, Saraburi*

1. INTRODUCTION

Rice is one of the most important crops of Thailand as Thailand is the major exporter of rice in the world. To meet the increasing demand for domestic consumption and to maintain the position in export it is required to bring the

more suitable areas under rice cultivation. Rice is a high water consuming crop. Rice production varies from area to area due to different topographic conditions, soil conditions, weather conditions and agricultural practices within a target-area. Generally in plain region rice production is higher because of high probability of getting more water than hilly region.

Rice is the economic crop and the significant export product of Thailand. Farmer can grow rice in every region, particularly the cultivation are in the central plain. The rice cultivation areas and the rice product have been changed and declined regarding the development and changes of land use from paddy fields to the industrial areas, urban areas, mines and others. From the statistical report of agriculture of Thailand found that the rice cultivation areas of the country have been declined from past to the present. The agricultural areas and rice cultivation are limited in some areas, which lead to the increasing of the invasion for cultivated areas in the forest. Furthermore, there are non suited land use, regarding the rice cultivation, for other forms, which cause the extravagant expensed for land development in some areas and lead to the high demand of chemical fertilizer for the increasing productivity.

Four seasons were recognized in Thailand: the southwest monsoon from May to September; a transition period from the southwest to the northeast monsoon during October; the cool, dry northeast monsoon from November to February; and a pre-monsoon hot, dry season from March to April.

Table 1.1: Rice production seasons in Thailand

Production seasons	Planting	Harvesting
North and Central, Major season	May-July	Nov-Dec
North and Central, Minor season	Dec-Jan	May-Jun
South, major season	Sep-Nov	Mar-May
South, minor season	Apr-May	Aug-Sep

(Source:-IRRI, 2009)

During the wet season, rice was planted nearly everywhere across the central region which covered 21% of the country's total cultivated rice land and produced 30% of the total rice. About 450,000 ha of land in the central region were planted to irrigate dry-season rice.

The various climatic events such as more intense and more frequent droughts, cyclones, flood and heat waves caused incalculable threats on crop production. Crop yield is a function of numerous factors. Most important factors for rice production are favorable temperature, a constant supply of water for irrigation and suitable soils. Apart from the management and cultural practices yield determination factors could be broadly categorized in to three types, as crop factors, climatic factors and soil factors

(Stansel, 1980) and he revealed that crop growth and the yield are highly sensitive to climatic changes. Temperature changes modify growing season constraints and influence the rate of plant development. A difference of one centigrade in mean temperature could result in a change of 117 to 25 days in effective growing season. And finally he had estimated that rice production could be decreased 19% by the combination of a 2 Celsius temperature reduction and 15% precipitation reduction (Stansel, 1980).

As mentioned above several climatic events are affecting ultimately on crop production which caused only due to changes in land use and climatic variables.

Several studies had done of area (or land) suitability for crop production under different variable natural conditions which is affecting mainly different natural hazards mentioned above. Factors which are suitable for rice cultivation vary from place to place. Tyagi (2003) categorized suitability of physical factors for rice cultivation in Southern Goa, India and Ratanakhom *et al*, categorized suitability for rice cultivation in Chinagmai Province, Thailand into four categories as follows

Table 1.2: Criteria and rating of land qualities for paddy in southern Goa, India

Land Quality	Suitability Class			
	Highly Suitable	Moderately Suitable	Marginally Suitable	Not Suitable
Texture	Clay, Silty clay, Silty clay loam.	Sandy clay, silty loam, sandy clay loam	Loamy sand	Sandy and fragmental loam
Drainage	Imperfectly and moderately well drained	Well drained	Excessively drained	Excessively and very poorly drained
Soil depth	Deepy to very deep	Moderately deep	Shallow	Very shallow
Gravelliness/Stoniness	Low	Moderate	High	Very high
Inherent fertility	High	Medium	Low	Very low
Relief	Normal	Subnormal	Concave	Excessive
Slope	Nearly level to very gently sloping	Gently slopping	Undulating	Moderate to very steep
Erosion hazards	None to slight	Moderate	Severe	Very severe
Risk of flooding	Low	Moderate	High	Very high

Table 1.3: Criteria and rating of land qualities for paddy in Chiangmai, Thailand

Crop Requirement		Factor Rating			
Land Quality	Unit	Highly Suitable	Moderately Suitable	Marginally Suitable	Not Suitable
Average Rainfall	mm	>1500	1100-1500	500-1000	500
Nutrient Availability Index(NAI)					
-N	%	>0.2	0.1-0.2	<0.1	-
-P	ppm	>25	10-25	<10	-
-K	ppm	>60	30-60	<30	-
-pH	-	5.6-7.3	7.4-7.8	7.9-8.4	>8.4
			5.1-5.5	4.0-5.0	<4.0
Soil Depth	-	>50	25-50	15-25	<15
Drainage	-	1,2,3	4	5	6
Slope	-		0-2	2-5	>5

This project has studied the land evaluation of rice cultivation in Saraburi province in order to plan for the uses the use of rice cultivation in Saraburi province to be suitable. The use of Geographic Information System (GIS) can be managed and analyzed with the data based in the form of map, all of which are the basic information for planning. The ability of data access and improving descriptions can be studied for the suitability for the physical characteristics and the general uses at present so that there can be planning for the sustainable rice cultivation. The results of the study will be useful for planning the rice planting area in Saraburi province.

The main objective of this exercise is to develop a GIS based model for land suitability assessment for rice production in Saraburi province. However, specific objectives are to classify the area in terms of land suitability for rice cultivation and to prepare the model for favorable land for good yield of rice for Saraburi Province of Thailand.

1.2 Study Area

Geographically Thailand has four regions: Central Thailand (Including Bangkok), Southern Thailand, Northern Thailand, Northeastern Thailand. Saraburi is located in central part of the Thailand east side of the Chao Phraya river valley. The co-ordinates of the study area isN latitude andE toE longitude. Saraburi Province is covering approximately 357650 ha Administratively Saraburi is divided into 13 districts (*amphoe*), 111 communes (*tambon*) and 965 villages (*muban*).

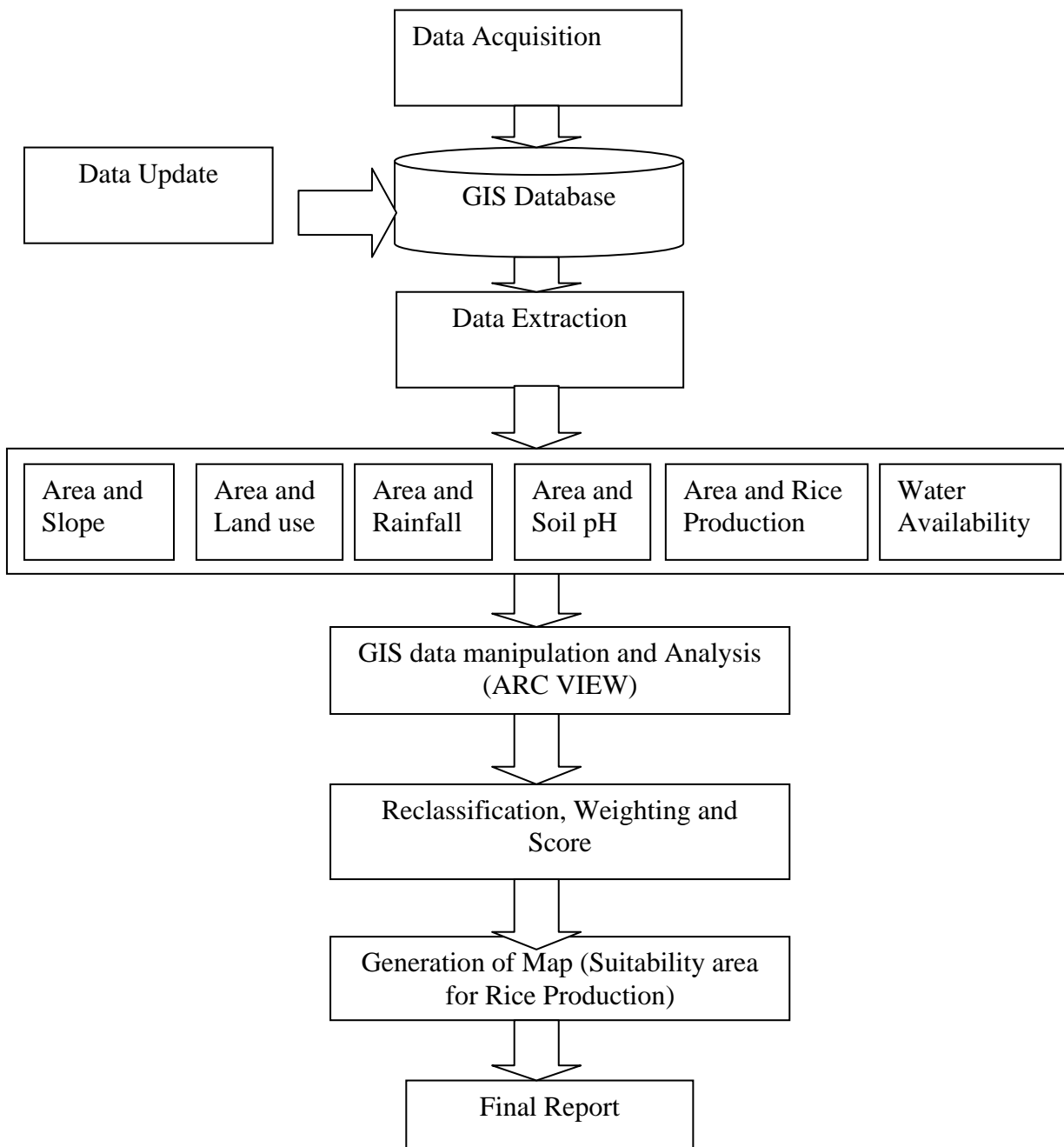


Figure 2.1: Flowchart for Area Suitability Modeling for Rice Cultivation

Relevant data was obtained from Thailand GIS database provided by Remote Sensing and Geographic Information System Department of Asian Institute of Technology which was in 1:250,000 scale physical database format. Required process was done by using GIS software Arc View v. 3.2a. The area of Saraburi province was separated from the map of the central region of Thailand as shown in figure 1. Various processes like table joining, extracting required features from data layers has been done with the help of different tools in arc view.

Similarly the land use, soil pH, stream network, annual rainfall and rice production themes were clipped and stored for Saraburi in a separate database created for this project. These shape files were then converted to

grid for classification as per the required parameter out of all the information given for that class in the database. Then these grid files were reclassified into four categories defining the following suitability criteria as mentioned in the table.

Table 2.1: Ranking criteria and weighing criteria for various suitability factors

Factors	Weight	Suitability			
		Highly Suitable (S1=6)	Moderately Suitable (S2=3)	Marginally Suitable (S3=1)	Not suitable (N=0)
Land use	1	Paddy Fields	Agriculture land	Forest and grass cover	Urban and Industrial
Distance from Stream (m)	1	0-500	501-1000	1001-1500	>1500
Annual rainfall (mm)	1	>1800	1200-1800	900-1200	<900
Soil pH	1	6.0-8.0	5.5-7.0	4.5-5.5	4.0-5.0
Slope	1	0 – 7%	8 – 15%	16 – 24%	>25%
Rice production (kg/household)	1	>3000	2000-3000	1000-2000	<1000

After giving the suitability criteria as per the level three in AHP, following suitability maps of each factor were obtained.

3. RESULTS AND DISCUSSIONS

Existing data layers of Saraburi province was categorized into many categories which were reclassified into four main categories. These categories were then ranked and weigh, as per their suitability rice cultivation assigned to them are presented in table 2.1

Paddy field was assumed to be most suitable for rice cultivation with all requirements needs for growing whereas water body and urban considered as not suitable for rice cultivation as shown in the table 3.1

Table 3.1: Suitability criteria for Land use

Suitability Class	Suitability Criteria	Weight	Suitability
Highly Suitable	[Plu_e] = “Paddy Field”	6	S1
Moderately Suitable	[Plu_e] = “Agriculture Field”	3	S2
Marginally Suitable	[Plu_e] = “Forest”	1	S3
Not Suitable	[Plu_e] = “Miscellaneous” [Plu_e] = “Urban area”	0	N

The Soil pH theme had been grouped in to different range starting from 4.0–8.0 which was then reclassified into four groups as shown in figure 3.2. The suitability criteria and weights assigned to them are presented in table 3.2. The areas with pH in the range of 6.0-8.0 were considered as most suitable and the areas with pH 4.0-5.5 were considered as unsuitable.

Table 3.2: Suitability criteria for soil pH

Suitability Class	Suitability Criteria	Weight	Suitability
Highly Suitable	[pH_upper] = "6.0-8.0"	6	S1
Moderately Suitable	[pH_upper] = "5.5-7.0"	3	S2
Marginally Suitable	[pH_upper] = "4.5-5.5"	1	S3
Not Suitable	[pH_upper] = "4.0-5.0"	0	N

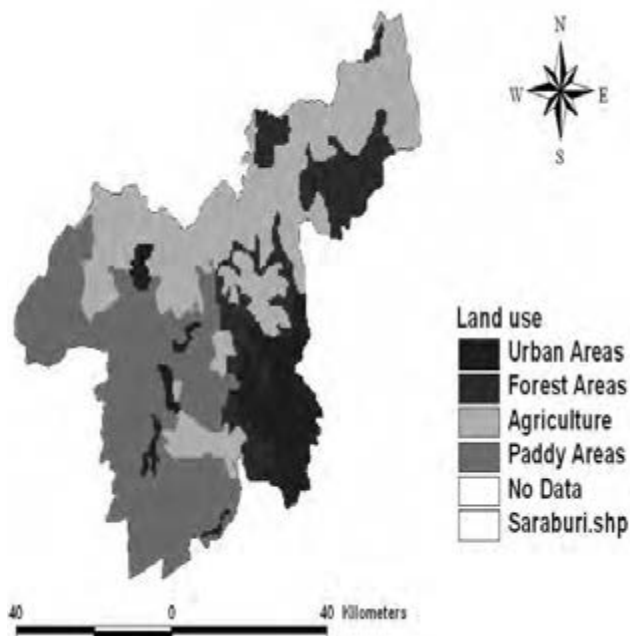


Figure 3.2: Soil pH of Saraburi Province

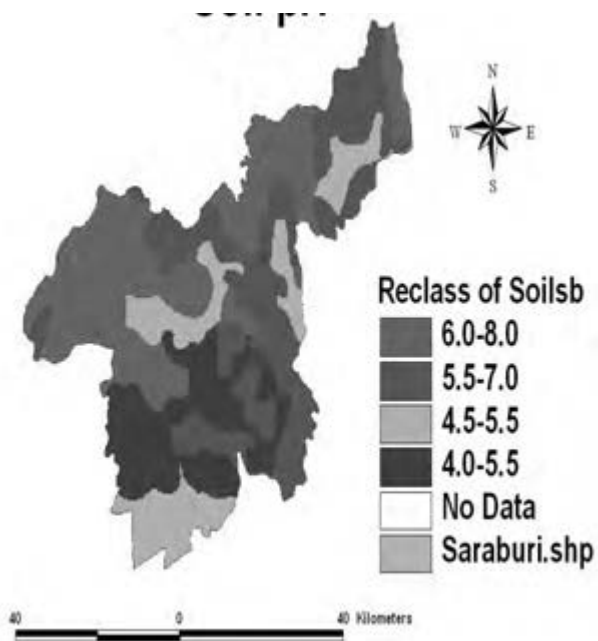


Figure 3.1: Land Use map of Saraburi

The land slope was provided in to four groups starting from <7% to >24% which was then analyzed as shown in figure 3.3. The suitability criteria and weights assigned to them are presented in table 3.3. The areas with slope less than 7% were considered as most suitable and the areas with slope more than 24% were considered as unsuitable.

Table 3.3: Suitability criteria for land slope

Suitability Class	Suitability Criteria	Weight	Suitability
Highly Suitable	[Slope] < 7%	6	S1
Moderately Suitable	[Slope] > 7 and <=16%	3	S2
Marginally Suitable	[Slope] >16 and <=24%	1	S3
Not Suitable	[Slope] >24%	0	N

The information about various types of streams located in Saraburi was provided. To analyze the suitability the buffer distance around the streams created using “Create Buffer” feature of Arc View. The area within the range of 500 m around the stream was considered as most suitable while the area which is farther than 1500 m was considered as unsuitable. The suitability assessment of the area is as presented in table 3.4.

Table 3.4: Suitability criteria on Stream

Suitability Class	Suitability Criteria	Weight	Suitability
Highly Suitable	[BuffDis] <= 500	6	S1
Moderately Suitable	[BuffDis] > 500 and <=1000	3	S2
Marginally Suitable	[BuffDis] > 1000 and <=1500	1	S3
Not Suitable	[BuffDis] > 1500	0	N

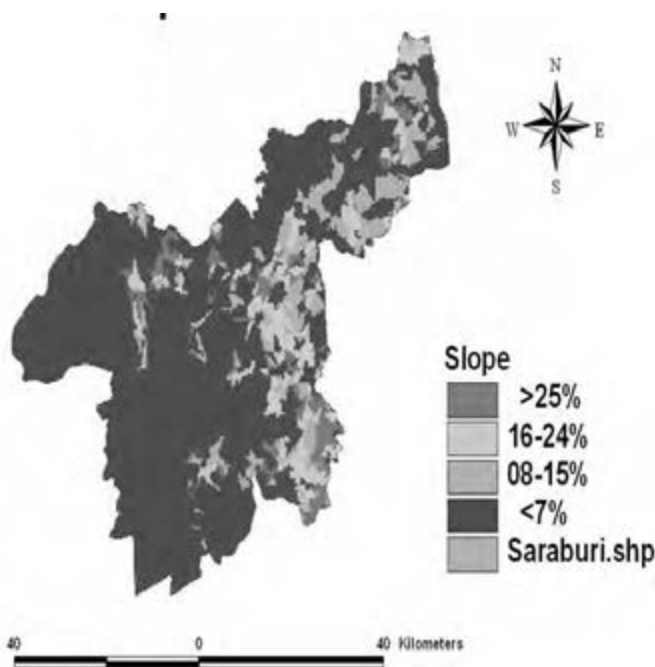


Figure 3.3: Land slope in Saraburi

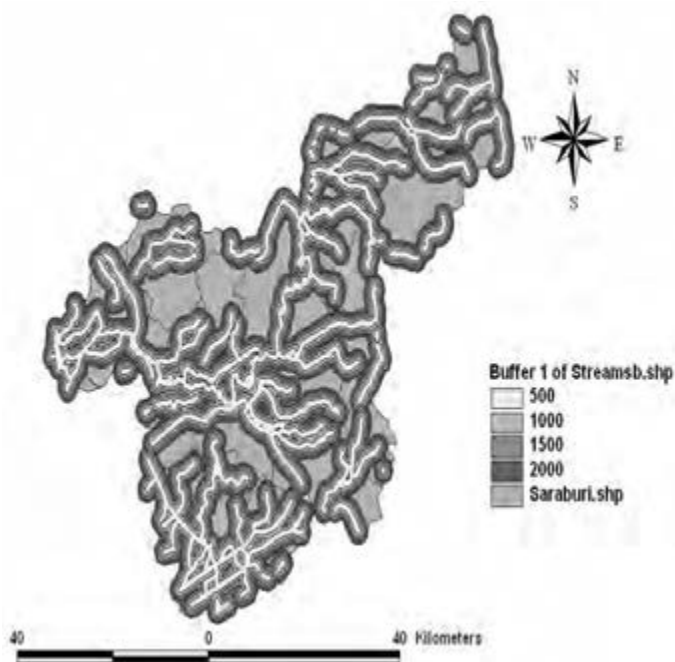


Figure 3.4: Streams of Saraburi with buffers

Annual rainfall data of Saraburi was re-categorized into four levels as shown in Figure 3.5. Since rice crop consumes a lot of water, so the areas having high rainfall i.e. more than 1800 mm per annum were considered as most suitable, while the areas receiving less than 900 mm were considered unsuitable for rice production. The suitability assessment is as presented in table 3.5.

Table 3.5: Suitability criteria for Rainfall

Suitability Class	Suitability Criteria	Weight	Suitability
Highly Suitable	[Annual] > 1800	6	S1
Moderately Suitable	[Annual] > 1200 and <=1800	3	S2
Marginally Suitable	[Annual] >900 and <=1200	1	S3
Not Suitable	[Annual] < 900	0	N

The rice production data was provided in terms of kg per household. It was reclassified into four groups as shown in figure 3.6. The areas producing more than 3000 kg per household were considered as most suitable, and the areas producing less than 1000 kg per household were considered as unsuitable. The suitability assessment is as present in table 3.6.

Table 3.6: Suitability criteria on Rice Production

Suitability Class	Suitability Criteria	Weight	Suitability
Highly Suitable	[Rice_production] > 3000	6	S1
Moderately Suitable	[Rice_production] > 2000 and <= 3000	3	S2
Marginally Suitable	[Rice_production] > 1000 and <= 2000	1	S3
Not Suitable	[Rice_production] < 1000	0	N

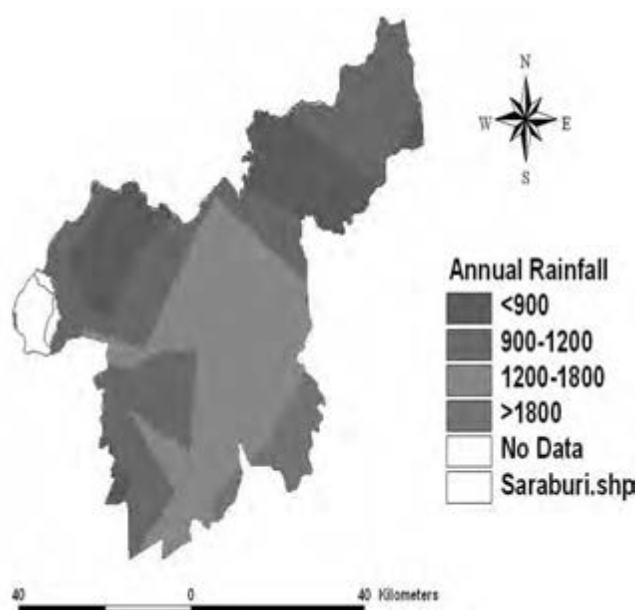


Figure 3.5: Rainfall of Saraburi Province

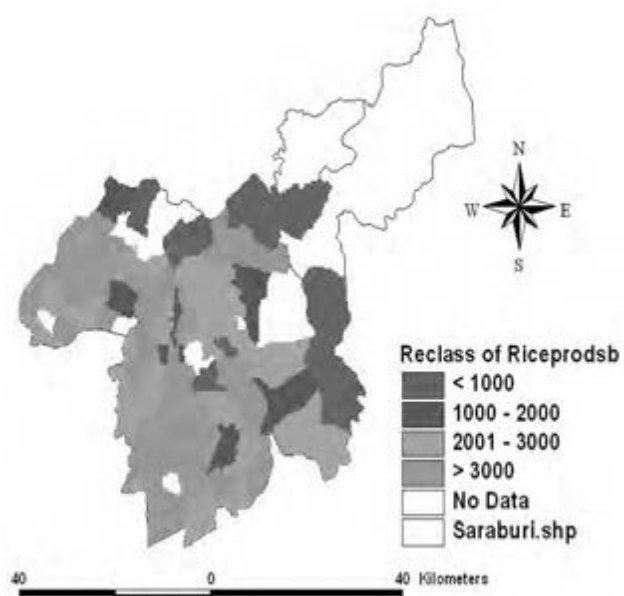


Figure 3.6: Rice production of Saraburi

The following criteria were used to carry out the final land suitability assessment for rice production with considering all the parameters mentioned above

Land suitability = land use + slope + soil pH + stream buffer + rainfall + rice production

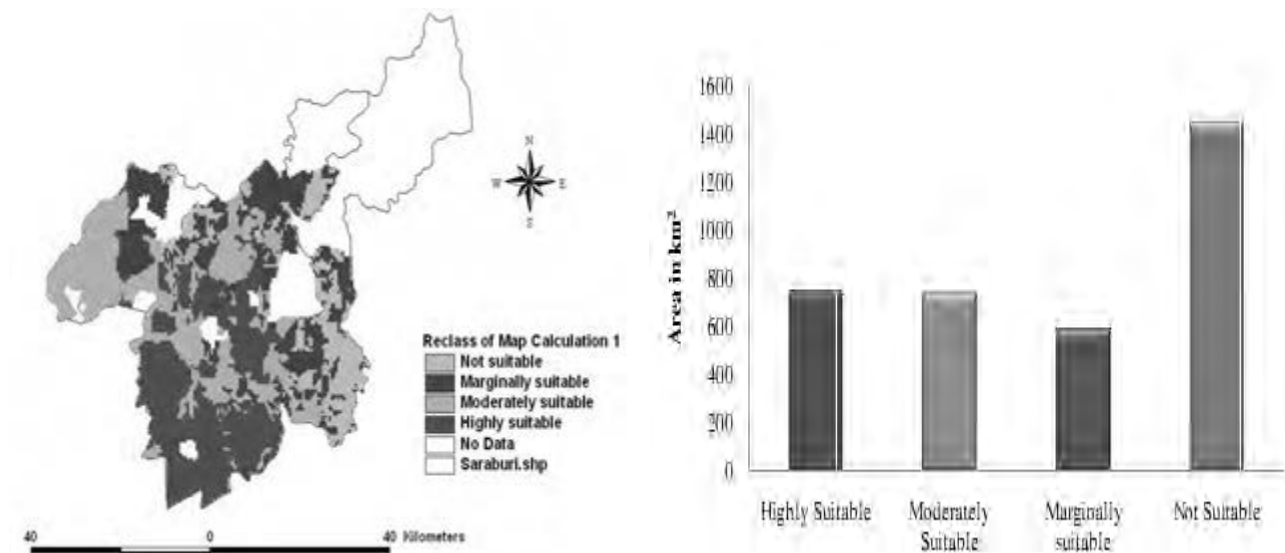


Figure 3.7: Final Land Suitability map and area in KM² as per their suitability for rice cultivation

It was found that the area under highly suitable, moderately suitable, marginally suitable and not suitable derived as about 747 km² (21%), 738 km² (20%), 589 km² (17%) and 1448 km² (41%) respectively.

CONCLUSIONS

Land suitability map showed that southern and western parts of the province are suitable for rice cultivation because the geography of these areas and high fertile soil suited for rice cultivation. On the other hand, north east part of the province is cover by high plains, high slope and national parks, thus this area is classified as not suitable for rice cultivation because rice cannot grow on high plains.

Management practices such as irrigation development, fertilizer application are the crucial parameters which can change marginally suitable area to moderately suitable and moderately suitable to highly suitable area. However, irrigation development is an important issue to rice cultivation in the future due to huge requirement of water for rice cultivation.

REFERENCES

- De Datta, S. K. (1981). In J. W. Sons, Principles and practices of rice production. Canada.
- Mikkelsen *et al.* (1980).,"Rice Culture". In Rice-Production and Utilization. pp. 103-186. Edited by Bor. S. Luh. U.S.A.: Van Nostrand Reinhold.
- Perera, L.K., Kajiwarra, K. and Tateishi, K. (2007). Land Suitability Assessment by GIS for Paddy Cultivation in Sri Lanka. With a concern on environmental conservation. Remote Sensing and Image Research Center, Chiba University, Yayoi-Cho, 1-33. Inage-Ku, Chiba Ciyy 263, JAPAN.

Ratanakhom, Ravi, Ruamkaew, Siriwan, Nongbundit and Sarawut (2008). Land Evaluation for rice in Chiangmai Province. <http://geoinformatics.sut.ac.th/sut> Retrieved on 10 November 2010.

Saaty, T. L. (1980). The Analytic Hierarchy Process. New York: McGraw-Hill.

Saraburi Province. http://en.wikipedia.org/wiki/Saraburi_Province. Retrieved on 18 November 2010.

Stansel, J. (1980). Impact of world weather changes on rice production, Proceeding of a symposium on the agrometeorology of the rice crop. International Rice Research Institute.

Thus-songchun, Akarawuth (1983)., Rice Story. Kasetsart University.

Tyagi, S. (2003). Agricultural land use planning using remote sensing techniques in part of south Goa (India)

Bridge deck condition assessment by ground penetrating radar -A case study in Bangladesh

Bushra ISLAM¹, Raquib AHSAN² and Mehedi Ahmed ANSARY²

¹Research Assistant, JMBSIP, BUET

²Professor, Department of Civil Engg., BUET, Dhaka, Bangladesh

ansary@ce.buet.ac.bd

ABSTRACT

Bridge condition assessment is necessary to evaluate the serviceability and safety of the existing bridge structures. At present a significant number of bridges are functioning in Bangladesh at poor state and require proper maintenance. The bridges which are functioning properly also need regular monitoring. In this study the current condition of an existing bridge deck was evaluated by non-destructive test method using Ground Penetrating Radar (GPR) with high frequency (1.6 GHz) ground coupled antenna. Bridge deterioration mapping and reinforcement layout of bridge deck were produced from the collected data. This information will facilitate effective decision making regarding future maintenance of the bridge.

Keywords: *Ground Penetrating Radar, bridge deck assessment, deterioration mapping, reinforcement corrosion, concrete degradation*

1. INTRODUCTION

In Bangladesh both roads and waterways provides support as major means of travel due to its location on an alluvial plain formed by large rivers. In case of roadways, one of the factors that have essentially influenced the existing transportation system is the presence of large rivers in this country. As a result of the numerous rivers and regular flooding in rural areas most roads are built on embankments with a large number of bridges, culverts and ferries. Approximately over ten thousand bridges and culverts are present in this country. Regular assessment of these bridges is necessary to take appropriate measures for maintenance work and keep them functioning properly for a smooth traffic flow.

The conventional bridge deck evaluation requires time and destructive operations like removal of asphalt layers to acquire feedback regarding the bridge deck condition and accuracy of the collected data mostly depends on the performance and experience of the operator. On the other hand Ground Penetrating Radar (GPR) provides an easier operation and reliable data acquisition resulting into an accurate assessment of the deck condition. It is an established electromagnetic evaluation technique used in diverse area of

applications including concrete structure inspection, utility detection, road quality assessment or quality control, bridge deck evaluation, geological and archeological investigation, forensic research and military applications. A recognized application of GPR is the accurate condition assessment of bridge decks as well as other reinforced concrete structures (Parrillo et. al, 2005; Romero et. al, 2000; Romero, 2003; Schongar, 2004). The condition of a bridge deck can be assessed with higher degree of accuracy with high frequency (1.6 GHz) ground-coupled antenna. It is effective in indentifying rebar location by using reflections from reinforcement. From this reflection it is also possible to produce deterioration maps presenting the condition of bridge deck. The GSSI's instrument setup for Bridgescan consists of a SIR-3000 portable GPR data collection system with 1.6 GHz ground-coupled antenna which allows maximum 18 inches depth of penetration in concrete. A 3 wheeled curt and a small hand cart is available to carry the antenna for application.

In this study, the second Buriganga Bridge was inspected using the BridgeScan GPR system on April 28th, 2011 to evaluate the condition of the existing bridge deck. The bridge is located in Dhaka and also known as Babubajar Bridge. It is a Reinforce Concrete Deck Girder bridge with total 11 girders, constructed in early 1980. The bridge deck is asphalt overlaid. Current condition of bridge deck and the location of bridge are shown in Figure 1 and Figure 2 respectively.



Figure 1: Location of bridge



Figure 2: Bridge Deck

2. DATA ACQUISITION AND PROCESSING

2.1 Data Collection

In the present study GPR data was collected to attain rebar layout and bridge deck condition assessment. At first to identify the orientation of top layer reinforcement sample GPR data was collected in both directions and then the arrival time of rebar reflection was compared. It was found that the rebar in transverse direction reflect wave in less time than in longitudinal direction. So it was confirmed that the top layer reinforcement is in transverse direction. Thus the data for deterioration assessment was collected in the perpendicular direction which is along the longitudinal direction or along the traffic movement.

Since the overall condition of the location was not in favor of collecting data of the whole bridge, only data was collected along two profile lines each 50 ft long, in the mid span of bridge deck. Also the data was collected by preparing a 10ft X 10ft grid near the curb of bridge with grid spacing of 1 ft. Data collection using GPR is shown in Figure 3.



Figure 3: GPR data collection

Reinforcements are observed in GPR as form of hyperbolas. The theory of detecting reinforcement is related to its energy transmission and receiving principle. The reflection pattern will vary in case of deterioration. Weak reflection is an indication of bridge deck deterioration. This attenuation of wave signal may occur due to concrete degradation, reinforcement corrosion or other reasons. Unprocessed GPR data is shown in Figure 4. From this data weaker signal reflection can be observed which is indicating the presence of deterioration. Also the bottom of asphalt layer can be identified from the observation of the reflection pattern. The asphalt bottom and rebar reflections have been shown in Figure 4.

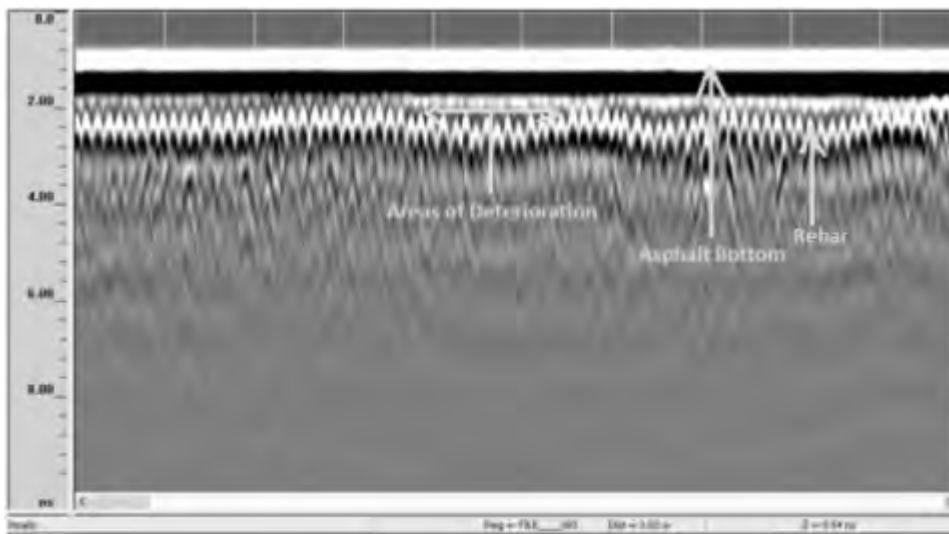


Figure 4: Unprocessed GPR data

2.2 Data Processing

After the data collection all the unprocessed data files were transferred from SIR-3000 to computer and processing operations were performed using Bridge Assessment Module of RADAN. The processing steps include time-zero correction, migration, rebar reflection mapping and interactive interpretation. Finally from this processed data, using a plotting software contour map presenting deterioration can be produced.

2.2.1 Time-Zero correction

At first time-zero correction was applied to the unprocessed data to shift all data scans so that the offset is removed and the top of the scans start from the beginning of the deck surface.

2.2.2 Migration

During data collection process hyperbolic diffraction occurs for specific rebar location. Migration which is a hyperbolic summation process is performed to collapse these diffractions in the point of rebar location. The processed GPR data and 3D view of reinforcement layout is shown in Figure 5 and Figure 6 respectively.

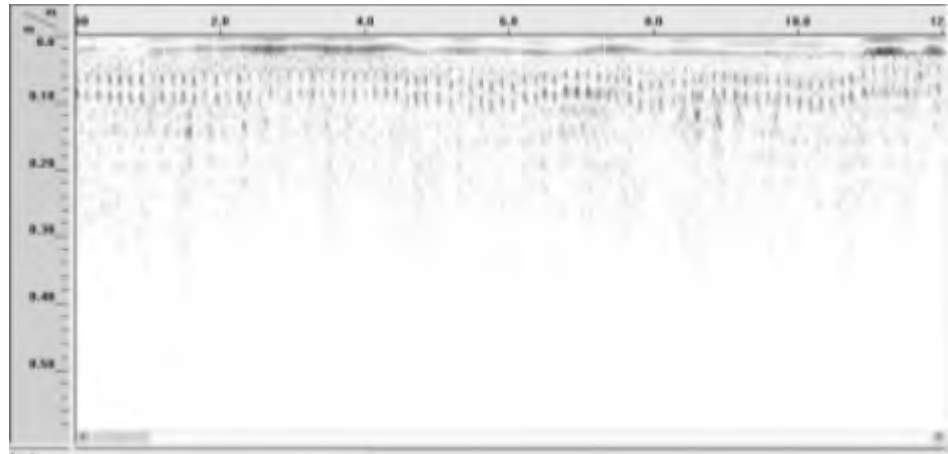


Figure 5: Processed GPR data

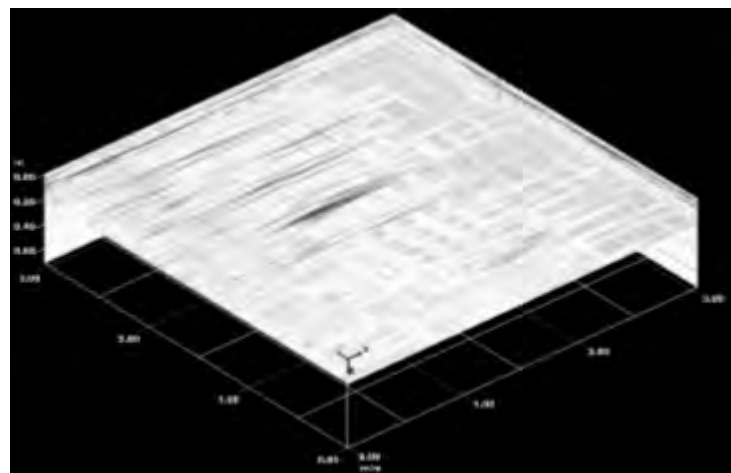


Figure 6: 3D view of Reinforcement Layout

2.2.3 Rebar Reflection Mapping

The option available in Bridge Assessment Module for deterioration mapping locates all rebar reflections and amplitudes and save these data into an ASCII comma-separated value (CSV) file.

2.2.4 Interactive Interpretation

If the bridge is deteriorated and reflections are weak then the rebar reflection peaks in that locations need to be edited. In Figure 7 the rebar reflections located in interactive interpretation process are shown by yellow circles on the top data pane. In the bottom data pane the rebar locations can be seen with varying slab thickness. It can be seen that the top layer reinforcement is located approximately at 40 to 60 mm depth.

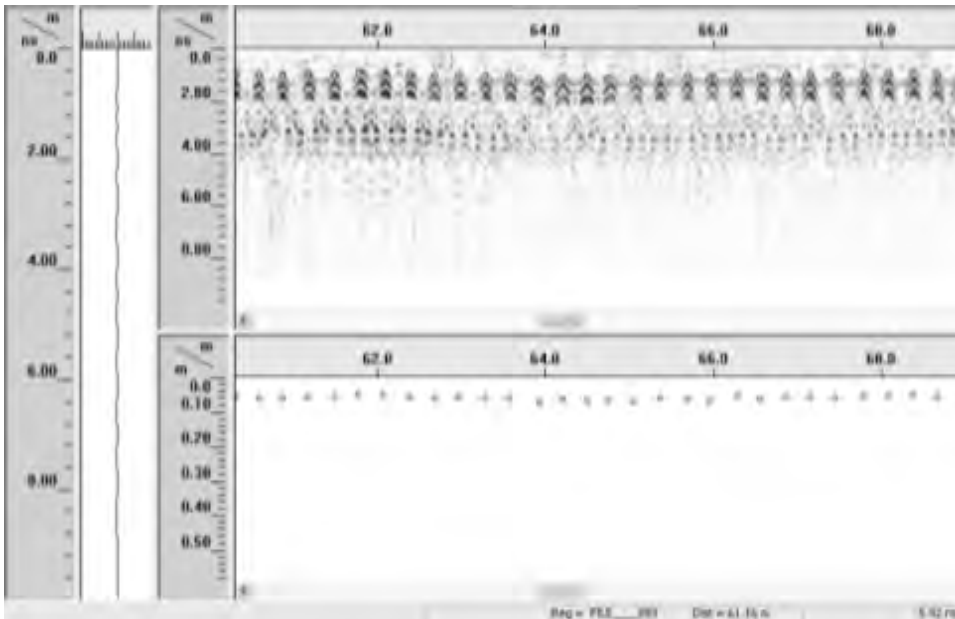


Figure 7: Interactive interpretation process

2.3 Deterioration Mapping

To prepare the deterioration mapping, rebar location X, Y, and reflection amplitude data were imported from the saved ASCII file. Then using a contour mapping tool DPLLOT, a color-coded contour map of the bridge deck deterioration was produced. Lower amplitude value representing weaker rebar reflections were presented with reddish colors to indicate the areas of the bridge deck suspected to be more deteriorated. The deterioration map prepared for the inspected part of bridge deck is presented in Figure 8.

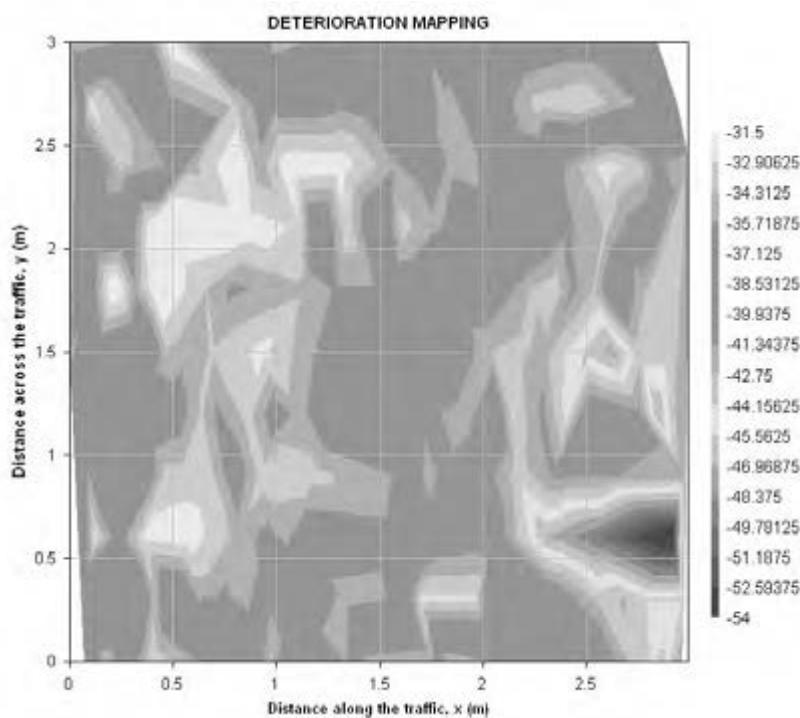


Figure 8: Deterioration map

3. CONCLUSION

In the deterioration map a higher deterioration compared to other places of deck can be observed from the weaker rebar reflections indicated by the reddish colors in Figure 8, which is in a portion near the curb. Different reasons may lie behind this deterioration. Some of these factors might be concrete degradation, corrosion of the reinforcement due to penetration of water, which will attenuate the radar signal. One important factor in case of interpretation is to understand that it is not possible to identify the amount of deterioration quantitatively only by observing color contour. It is a qualitative measure only.

The whole process of bridge quality assessment using Ground Penetrating Radar (GPR) is performed in a non-destructive manner with considerable accuracy which is the most important advantage of the evaluation process. The aim of the present study was to evaluate present deck condition of the Second Buriganga Bridge by Ground Penetrating Radar (GPR). No destructive phenomena were required during the entire performance and the whole data collection and processing steps were done approximately within two hours with a savings of huge amount of time. Moreover due to the benefits of getting deterioration information without any opening up of the deck, this GPR data can be used to locate the places which require repair and maintenance in an economical and effective manner. It is also possible to determine the appropriate repair methodology by observing the deterioration condition. So deterioration map developed in this study using GPR data can be used to locate deteriorated places in the existing deck and proper measures can be taken for condition improvement accordingly.

REFERENCES

- Parrillo, R., Roberts, R.L., and Haggan, A., 2005, Bridge Deck Condition Assessment Using Ground Penetrating Radar, *International Bridge Conference*, June 13-15, 2005, Pittsburgh, PA.
- Romero, F.A., Roberts, G.E., and Roberts, R.L., 2000, Evaluation of GPR bridge deck survey results used for delineation of removal/maintenance quantity boundaries on asphalt-overlaid, reinforced concrete deck, *Structural Material Technology IV*, February 28-March 3, 2000, Technomic Publishing Co, p. 23-30.
- Romero, F.A., 2003, New York State Department of Transportation Ground Penetrating Radar Demonstration on Route 378 Bridge over D&H Railroad and Route 66 Bridge over Kinderhook Creek.
- Schongar, G., 2004, GPR Demonstration Project on Two Steel Reinforced Concrete Bridge Decks, Client Report 87, *Transportation Research and Development Bureau, NYSDOT*, 27 p

Urban high speed rail link tunnel projects (GTX) in Korea

Chang-Yong Kim¹, Seong-Won Lee¹, Ho-Geun Kim¹
¹Korea Institute of Construction Technology,
Daehwa-dong 283, Goyangdae-ro, Ilsanseo-gu, Goyang-si,
Gyeonggi-do, 411-712, Korea
cykim@kict.re.kr

ABSTRACT

Urban high speed rail link tunnel projects, namely GTX(Great Train Express), is suggested by Gyeonggi-province and Ministry of Construction, Transportation and Marine Affairs by this year and start the design by several consortium in Korea. Basically, this project has four lanes with almost 150km long. West-Center line and South-Center line and North-Center line and Southwest-Centerline are planned. And almost below 40m, the tunnel is located, so deep construction will be needed. Average speed of the rail is designed by 100 km/h, and the maximum speed reach 200km/h. Normally, Seoul Subway average speed is about 30km/h. The GTX has very fast connections in between Seoul and other satellite cities, namely Great Mega City. Basically, this kind of mega project has a precedent project such as Seoul Metropolitan Subway projects, but, Seoul metro experiences very shallow tunnel and low speed rail. So there need new approaches for the high speed rail link and deep tunnel conditions.

This kind of project is for the first time in the world, but we have the experiences in Subway construction.

In this paper, the concept of underground transportation infrastructures specially in high speed rail link tunnels that is suitable for Korean circumstances was established and the core base technologies to construct economical and safe underground space was deduced to consider practical use in the future.

In this paper, we emphasis on the needs of consideration of the technical requirements of this kind of projects in high speed rail link and deep urban tunnel conditions

In this paper, we will present the detailed plan of this project and the technical weakness and challenging factors are also discussed.

Keywords: *High speed rail link tunnel, GTX (Great Train Express), Great depth tunnel*

1. INTRODUCTION

Urban high speed rail link tunnel projects, namely GTX(Great Train Express), is suggested by Gyeonggi-province and Ministry of Construction, Transportation and Marine Affairs by this year and start the design by several consortium in Korea. Basically, this project has four lanes with almost 150km long. West-Center line and South-Center line and North-Center line and Southwest-Centerline are planned. And almost below 40m, the tunnel is located, so deep construction will be needed. Average speed of the rail is designed by 100 km/h, and the maximum speed reach 200km/h. Normally, Seoul Subway average speed is about 30km/h. The GTX has very fast connections in between Seoul and other satellite cities, namely Great Mega City. Basically, this kind of mega project has a precedent project such as Seoul Metropolitan Subway projects, but, Seoul metro experiences very shallow tunnel and low speed rail. So there need new approaches for the high speed rail link and deep tunnel conditions.

'G' in GTX, the acronym of 'Great Train eXpress', ambiguously refers to the meanings of 'Great, Green, Global and Governance', so the metropolitan train express contains a meaning of Gyeonggi-do's traffic alternative to solve the Seoul area's traffic problems, to minimize the environment pollution and to enhance the Seoul area's competitiveness.

The land owners can straighten the lines and build the rail infrastructure to make the running time reduced through using the space of 40m underground which is not usually used. It makes reach the Seoul downtown at 2-3 times quickly compared to any road traffic, so it can build the network of 30-minute living zone from Seoul area to Seoul downtown.

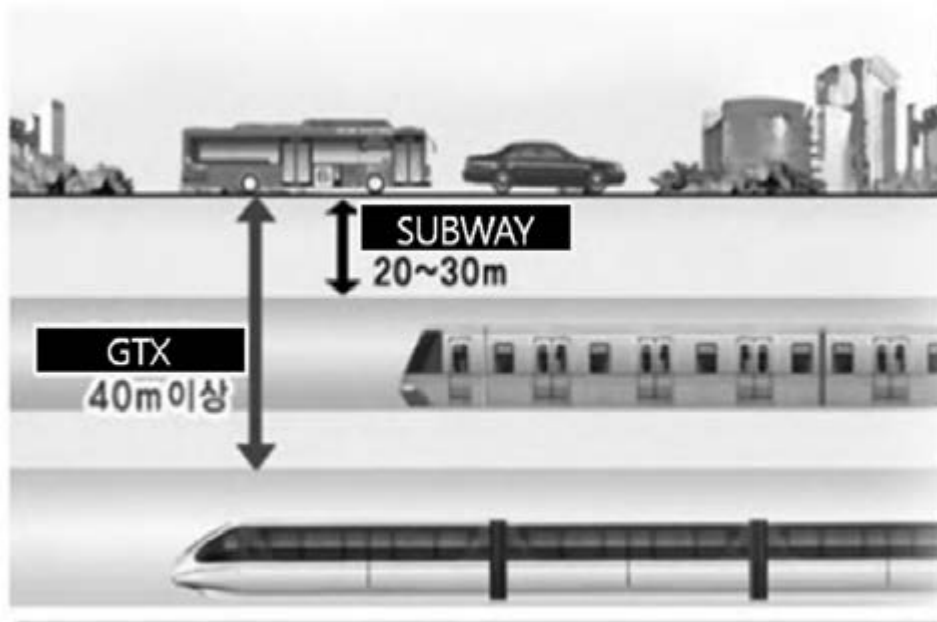


Figure 1. Usage of GTX at the underground of 40m or more

Its scheduled speed, the average passage speed considering stoppage time, was designed as over 100km/h. The scheduled speed of the existing metropolitan rails was about 30-50km/h, but it's expected to be improved through minimizing the number of stations (the required maintenance of interval among stations), arranging the time of getting quickly on and off and building the high-speed rails (Table 1).

Table 1. Characteristics of the GTX

Section	Characteristics
Hierarchical characteristics	Absorption of long-distance wide area traffic The influential area and running speed remaining at middle level of the existing metropolitan rails and general/high-speed rail
Operation characteristics	Reduced passage time up to 30 minutes among key points The scheduled speed over 100km/h at least Running time interval less than 10 minutes Quick getting on and off, sufficient capacity secured
Route characteristics	The maintenance of the distance between stations of at least 10km at Seoul's neighbored areas Selection of station at the points available for the use/construction of linkage traffic modes

2. NECESSITY

While the living zones are expanded and the metropolitan traffic zones are extended thanks to the quick growth of Seoul area and the development of new towns, the total passengers and long-distance passage at the Seoul areas are gradually increasing. As a result, the traffic at the major roads in Seoul areas and the flow-in and -out roads at the Seoul boundary is continuously increasing, but because of deficient traffic infrastructure, the traffic congestion is emerging as one of the key social problems in Seoul areas (Korea Traffic Academy, 2009).

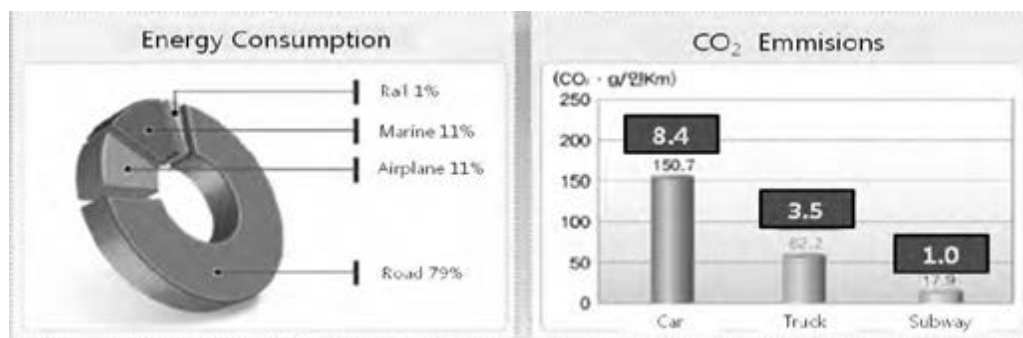
The traffic between Gyeonggi-do and Seoul is continuously increasing; mostly the over-30km long-distance flow-in and -out passage at Seoul boundary. The commuting traffic into Seoul increased by 14%; especially, increased by 37% in 2006 from 2002. Accordingly, the traffic speed among Seoul areas has been reduced. The average commuting time is around 43 minutes; longer compared to the other developed nations.

The facility investment has been continuously conducted through establishing the measures to improve the metropolitan traffic in order to mitigate the increased traffic and travel time caused by the expansion of metropolitan traffic zones, but the measures promoted based on road traffic is resulting in new traffic congestion.

It's needed to introduce a new-concept metropolitan traffic mode for the environment-friendly, energy-efficient metropolitan traffic in order to promote the sustainable development and green growth. In terms of traffic, the concept means the introduction of high-speed public traffic mode for common persons' metropolitan passage and the introduction of high-speed public traffic mode to absorb cars' traffic.

In terms of social economy, it's needed to introduce the environment-friendly, energy-efficient transportation mode. In the domestic environment and energy sector, the transportation accounts for around 21% of the total energy consumption. Furthermore, Korea ranks the world-7th in the consumption of energy (imported by 97%). It's found that it's critical to secure an eco-friendly, energy-efficient traffic mode under the condition of the increased environment pollution and energy crisis.

Especially, the increased car traffic leads to the severe air pollution. As for the traffic mode-specific energy consumption, the road accounts for about 79% as the most proportion, and the marine transportation, airline and rail, 11, 9 and 1%, respectively. As for the traffic mode-specific CO₂ emissions, cars account for about 8.4 times more than rail and subway and vans about 3.5 times more (Figure 2).



(a) Energy consumption in traffic sector (b) Transportation mode-specific CO₂ emissions

Figure 2. Traffic sector-specific energy consumption and CO₂ emissions

3. CONSTRUCTION PLAN

This project sets the Seoul-linking metropolitan traffic axis as a key influential zone and the whole Seoul areas, including Seoul, Incheon-si and Gyeonggi-do, as the indirect influential zones. As for the project period, the year of 2016 was set as the short-term target year and the year of 30 years after opening was set as the final target year.

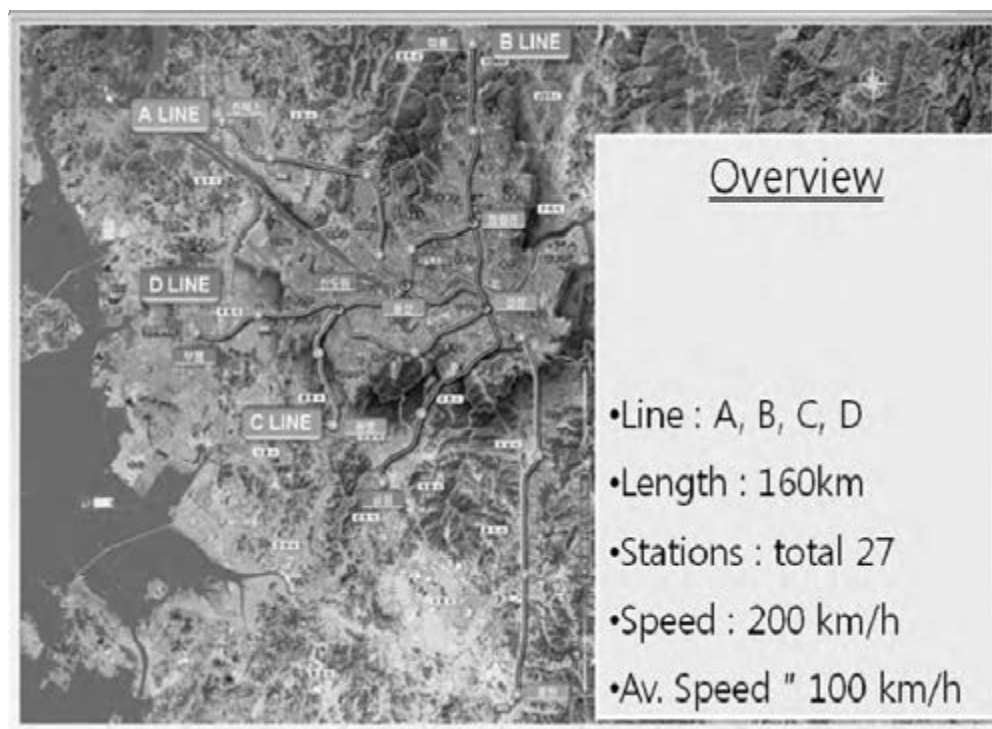


Figure 3. Expected GTX route

The number of routes is 4 (A, B, C and D) as seen at Figure 3, the total length 160km and the operation length including KTX common sections about 188km. The number of stations is scheduled to be totally 25 including 4 transfer stations of metropolitan express rail and the common 3 stations with KTX. The train base stations are scheduled to be 5. According to the planned standard, the design speed is expected to be about 200km/h and the minimum curve radius about 1,200m (R=600m in unavoidable circumstances). The average distance between stations is designed to be about 9km at Seoul areas and about 6km at Seoul.

As for the funding, 7 trillion 200 billion won, about 60% of the total project cost of 12 trillion won, is planned to be raised through private capital and the other 4 trillion 800 billion won, about 40% of the total project cost, through public financial support. The public financial support is composed of the development charge of 50% and the government support of 50%.

As seen at Figure 4, as for the station construction plan, the general stations are planned to apply the excavation + tunnel type and the tunnel type. The excavation + tunnel type is expected to be applied to 12 stations including Daegok Station, only to the excavation-possible sections. The tunnel-type general stations are applied to the GTX sections, namely 3 ones including Singal Station, to minimize the complaints during construction.

The transfer stations are divided into “+” shape and “T” one. “+” shape transfer station is applied to Samsung Station and Cheongyangri Station available for direct intersect and “T” shape station to Sindorim

Station and Yongsan Station transferred separately due to the difference of vertical alignment.



(a) Common station
(excavation + tunnel type)

(b) Common station (tunnel type)



(c) Transfer station (“+” shape)





(d) Transfer station (“T” shape)

Figure 4. Representative Station plan

The plan for preventing disasters was largely divided into main line section and station section. In case of main line section, the interval of ventilation devices was designed to be 2.5km through the safety analysis and a quick-exhaust ventilation-linking system is expected to be applied depending on the fire-occurring location and a pressure differential system is expected to be installed to a refuge room. The fire control section is planned to be installed to a quick escape-possible location from a fire-occurring point, a special step will be made for a direct escape to outside from the fire-occurring point and it is expected to control the inflow of smoke into platform through changing air supply into exhaust gas.

As seen at Table 2, the vehicle system is composed of the design speed of 200km/h and the highest speed of 180km/h and the vehicles to be able to run from Seoul surrounding areas to Seoul downtown in 20-30 minutes are expected to be selected. The domestically developed vehicles are preferred to be applied but the foreign vehicles in case of unavoidable situation.

Table 2. Suggested High Speed Train Type

Section	Korea Railroad Research Institute	Hitachi (Class 395)
		
Vehicle organization	One train with 6 vehicles	One train with 6 vehicles
Maximum speed	Design: 200km/h, operation: 180km/h	Design: 225km/h, operation: 200km/h
Number of seats	278 seats / 6 vehicles	348 seats / 6 vehicles

4. EFFECTS

GTX can create the expected effect on the increased transportation sector's efficiency, green growth and economic viewpoint and the solution of Seoul areas' problems. It can annually save 584.6 billion won through reducing the energy consumption of road sector by about 450 thousand tons and reduce 1,490 thousand tons of CO₂ emissions. In addition, the cost to treat CO₂ can be annually reduced by 59.5 billion won.

In terms of economy, the construction projects are expected to created jobs by about 260 thousand and the production inducement effect in local economy is expected to be about 30 trillion won. In addition, it is judged to contribute to solving the housing problems through the real expansion of daily living zone boundary within Seoul areas and to reinforce the competitiveness in the Seoul areas through expanding the economic activities basis.

5. CONCLUSIONS

Including Incheon, Ilsan, Bundang, and the neighboring satellite towns are very much present, and the population of these satellite cities is booming, traffic on handling the problem is most urgent problems. Public transportation is in the midst of this proposal is very encouraging phenomenon of GTX, and the future of this area is thought to be positioned as an alternative to transportation.

In particular, the deep tunnel constructions using TBM machine are thought to be still in the future, with plans to Seoul's U-SMARTWAY.

Urban transportation in the future increasingly will go down to deep

underground. Tunneling technology advances and demand for public transport will take place this.

The first evidence, GTX is the first construction worldwide success of the deep underground tunnel, and a lot of technical back-up and technical assistance is considered to be needed near the future.

REFERENCES

Korea Railway Research Institute, 2010, *The Master Plan of the GTX in Mega-City in Gyeonggi Province*, Reports of KRRI.

C. Y. Kim, 2010, *A Study on Present Status of Deep Underground Tunnel and Future Technologies*, the 21st KICT-JICE Joint Workshop

Geospatial technologies in wetland dynamics of Deepor Beel, India

Chitrini MOZUMDER¹, Taravudh TIPDECHO² and Nitin K TRIPATHI³

¹PhD Student

chitrini.mozumder@ait.asia

²Adjunct Faculty

taravudh@ait.asia

³Associate Professor and Coordinator

nitinkt@ait.asia

Remote Sensing and GIS

Asian Institute of Technology Thailand

ABSTRACT

Geospatial technologies offer cost effective methods for identifying and monitoring wetlands and their uplands. However due to mixed pixel problems it is difficult to directly delineate the wetland from its surroundings. In this study, topographic maps, Landsat (MSS, TM and ETM) and SRTM DEM have been used for identification and detection of spatio-temporal changes in the Deepor Beel, a Ramsar convention wetland in North East India. A water index (Normalized Difference Water Index, NDWI) derived from the LANDSAT was found effective in differentiating the wetland boundary from its upland. A multilayer classification technique for the wetland and its upland was adopted for the preparation of the LULC (Land Use Land Cover) maps. Deepor Beel is mainly rain fed and one or two narrow direct links exist between the wetland and the major river Brahmaputra in North East India. A few possible underground links between the Deepor beel and the river Brahmaputra were identified in this study. Approximately 57% downfall in the wetland water area was estimated over the last 38 years (from 1972 to 2010). However, in contrast to the wetland water area downfall, the area of marshy land increment up to 150% was observed beyond the wetland during the same time frame. This study is an initiative for assessing different issues associated with changes in the wetland and its upland for several factors like anthropogenic, climate change or many more.

Keywords: Remote Sensing, NDWI, Wetland, Flow accumulation, LULC change

1. INTRODUCTION

Wetlands, which are considered as the world's most productive environments are endangered and degraded by anthropogenic influences (urban, industrial and agricultural activities, increasing consumption of water resources) as well as natural processes (changes in precipitation inputs,

erosion and weathering of crustal materials). Deepor beel is a Ramsar convention wetland, which is the largest storm water basin in North East India. The entire beel was highly contaminated due to the inflow of enormous quantity (50%) of the untreated Guwahati city sewage and other inorganic/industrial effluents, and agriculture wastes (O'Hara, 2002; Bera et al, 2008; Planning, 2008). Also, there are number of dwelling units and concrete structures inside the beel which are increasing with a due pace of time. The wetland, once spread with 41 sq km of area, is now barely covers 5 sq km (Planning, 2008).

This study aims in accounting the change in extent and areal dimension of Deepor Beel and its upland areas in last 50 years or more. This demanded the use of multi temporal remote sensing data and techniques suitable for wetlands. There have been a number of satellite images which have been used in wetland studies such as Landsat (TM, ETM), IRS (LISS), Envisat, Radar, Lidar etc (De Roeck et al., 2008; O'Hara, 2002; Ozesmi and Bauer, 2002). But, it is really difficult to identify and map wetlands from satellite imageries since their reflectance confuse with other land areas. Hence there are several innovative approaches for identification, delineation and classification of the wetland systems (Grenier et al., 2008, Baker et al., 2006, DeAlwis et al., 2007).

Deepor Beel, located about 10 km southwest of Guwahati city, Assam, India is considered as one of the large and important riverine wetlands in the Brahmaputra valley of lower Assam (figure 1). It is surrounded by the Bharalu basin in the east, the Kalamani in the west, Jalukbari in the north and Rani and Garbhanga reserve forests in the south. It lies between 91°35' to 91 ° 43' E longitudes and 26°05' to 26°11'N latitude. It is recognized as one of the most significant wetland systems (10,000 acres) in the world under the Ramsar International Convention on Wetlands.

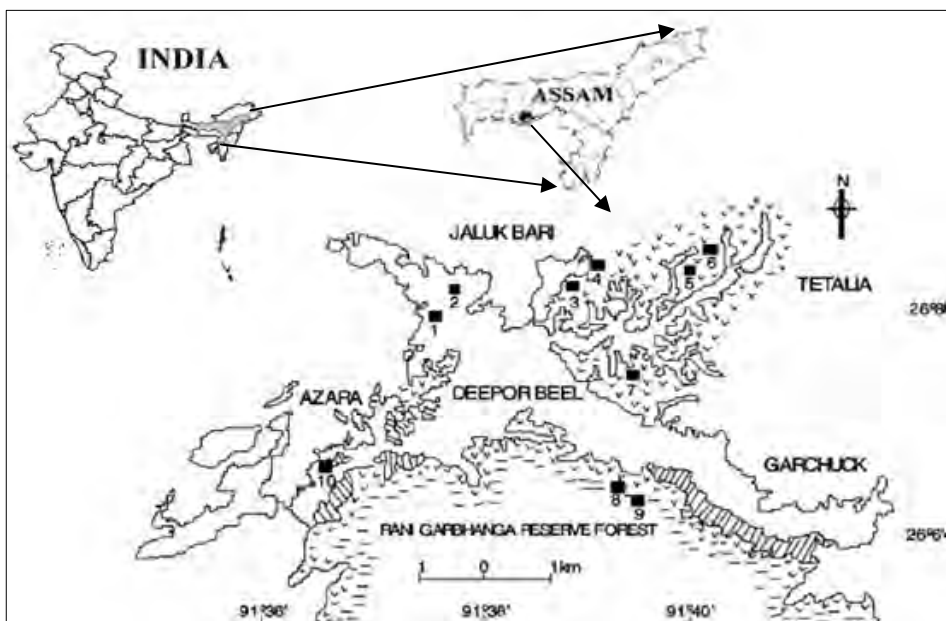


Figure 1: Overview Deepor Beel, India with its surrounding locations

2. DATA AND METHODS

2.1 Data

The Landsat (MSS, TM, ETM+) multi temporal data from 1972 to 2010 were the spectral data sources used for the study. Landsat MSS (Multi Spectral Scanner) sensor records spectral data in 5 bands of visible, infrared and Thermal wavelengths of Electromagnetic spectrum with a spatial resolution of 79 m (240 m for thermal). The Landsat TM (Thermal Mapper) and ETM+ (Enhanced Thermal Mapper) senses earth observation data in 7 bands of visible, infra red and thermal regions. The spatial resolution of these two sensors is 30 m (120 m in Thermal band in TM and 60 m in ETM+) resulting in a 900 m² minimum mapping unit. In addition to 7 bands, ETM+ also carries a panchromatic band with 15 m resolution which can be used to prepare 15 m resolution images from ETM+ sensor. Multi seasonal imageries were used for easy identification of the extent of the wetland.

Other data used for this study includes the 90 m SRTM DEM (Digital Elevation Model) for topographic information delineation. Also, topographical map from Texas Library (1940's) are used as the base maps.

2.2 Image Pre processing

The topographical maps and images are georeferenced to the same coordinate system and projection (UTM). This was done by image to image rectification method to avoid mismatching of features. The DEM which was initially in geographic projection is transformed to UTM. The satellite images are processed digitally to prepare them for visual and digital interpretation. The extent of image enhancement depends on the quality of the images. However, emphasis was given to enhance the water and moist lands to detect the wetland boundary. For this purpose, Normalised Difference Vegetation Index (NDVI) images and Normalised Difference Water Index (NDWI) images were prepared (figure 2). These can be obtained by a simple band ratioing as follows:

$$NDVI = \frac{NIR-R}{NIR+R} \quad (1)$$

$$NDWI = \frac{NIR-SWIR}{NIR+SWIR} \quad (2)$$

The next step was to classify the wetland as well as its upland using a hybrid classification technique which is a combination of supervised and unsupervised classification technique. The principal component analysis (PCA) was applied to the images prior to classification. However it was difficult to differentiate between the wetland and grasslands of the upland due to thick vegetation cover of the wetland (figure 3). Hence, a layerwise classification technique was adopted where the wetland was digitized from using the NDWI image and subset. This subset was separately classified and superimposed on the previous layer for the final classification map.

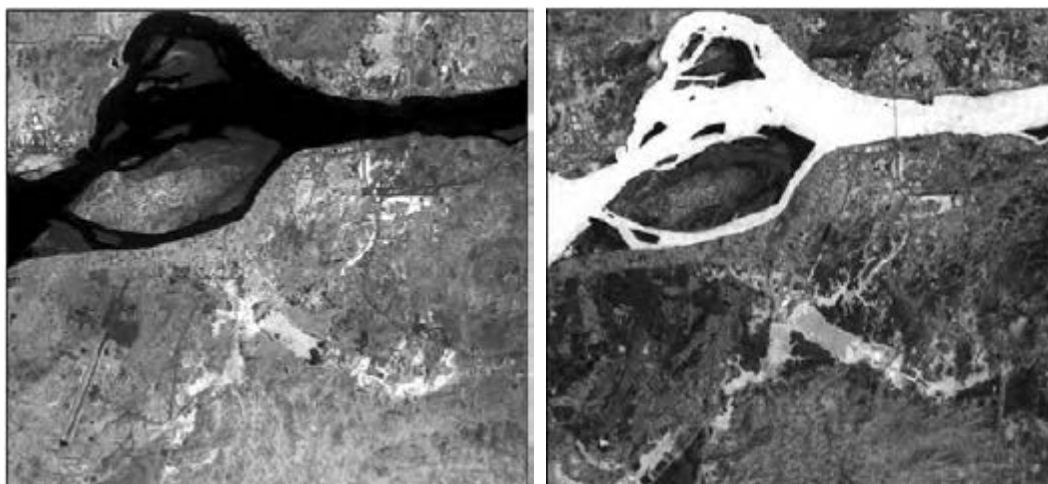


Figure 2: NDVI (left) and NDWI images of the study area

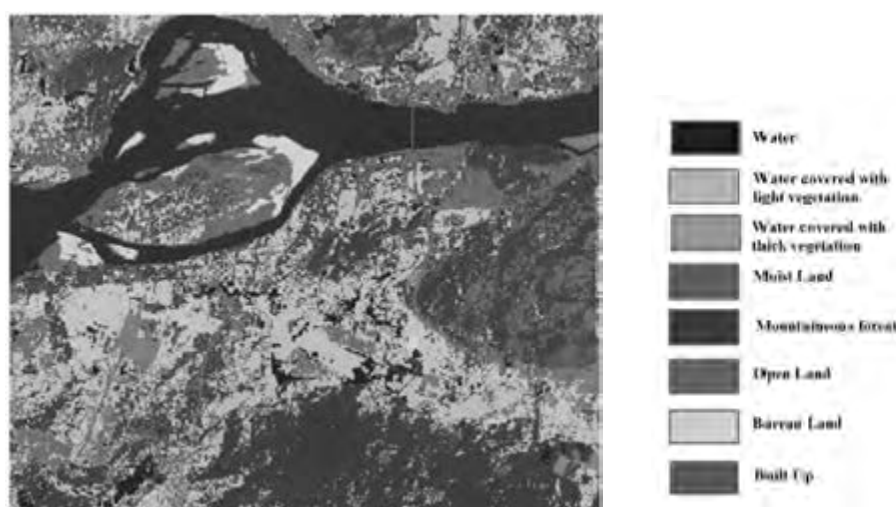


Figure 3: Classified image of the study area

Flow accumulation layer was prepared from the SRTM DEM to know the low elevated paths which are possible passage of water connecting different areas of the study area. The output of Flow Accumulation would then represent the amount of rain that would flow through each cell, assuming that all rain became runoff and there was no interception, evapo transpiration, or loss to groundwater. The results can be used to create a stream network by applying a threshold value to select cells with a high accumulated flow.

2.3 Change Detection Procedure

The change detection has been done in both qualitative and quantitative manner. For quantitative analysis, a model has been prepared in ERDAS which was used to detect the changes in the NDWI images of the input images. The thresholds of NDWI for each image are determined on a trial and error basis. For example, if in the NDWI image, the DN values greater than 0.1 are observed to be water, then in the model, the water areas are separated. Similar has been done for the second time series data, and

finally in the output layer, only 3 values are kept where (a) there is no change, (b) water changed to land and (c) land changed to water in the wetland area. The stepwise algorithms are as follows:

```
[1] EITHER 255 IF ( $n1_deepor_ndwi01 >= 0.1 ) OR 0 OTHERWISE
[2] EITHER 255 IF ( $n4_deepor_ndwi10 >= 0.1 ) OR 0 OTHERWISE
[3] CONDITIONAL { ( $n3_memory == $n6_memory ) 0 ,
    ( $n3_memory > $n6_memory ) 70 , ( $n3_memory < $n6_memory )
    255 }
```

Another way of quantifying the change was to use GIS techniques to obtain the areal extents of the wetland classes from the time series classified images. These were then compared and analyzed in tabular and graphical form.

3. RESULTS AND DISCUSSION

3.1 Historical Trends

Figure 4 (a) to (d) shows the toposheet and the NDWI images of 4 different years from 1940 to 2010 with the digitized wetland boundary. All the images are of pre-monsoon season. It has been observed from the scenario in 1940's that there were two separate wetlands (lakes) (figure 4(a)). The bigger one was Deepor beel with adjacent Berhala beel in its right side. The NDWI images show the water in a bright tone than the other features of the image. Hence, as observed from figure 4 (b), in 1972 the Berhala beel was shrinking and continued to move towards Deepor beel. Also, as observed from the toposheet, there was a well defined linkage between the Brahmaputra river and Deepor Beel which was not much visible from the image. Since, the 1972 image (figure 4(b)) is of 60 m resolution, this linkage may have been nullified by the sensor. Now, in 2001 (figure 4 (c)), the scenario was completely different where the extent of the moist land obtained in NDWI image was spread out and Berhala beel has been connected to the Deepor beel. As observed in figure 4 (d), the wetland has not much changed from 2001 except in the tail portion in the right hand bottom corner of the image. These all areas have been captured by agricultural fields due to the fertile land. A field photograph of some agricultural fields in the tail of the Deepor beel taken in January 2011 has been shown in figure 5. However, the linkage between the river and the Deepor beel has not been observed also in these two images of 2001 and 2010 of 30 m resolution.

Figure 5 shows the graphical representation of the change observed in the wetland from 1972 to 2010. Using the threshold of NDWI, the total area of the wetland in 1972 was found to be 5.2 sq km (2.4 % of the whole study area) changed to 12.4 sq km (5.5% of study area). This makes an increase of 138% in the wetland. However, if individual classes are noticed, the area of water has tremendously decreased from 1972 to 2010 (figure 5(a)). In 1972, the area of water was 3.4 sq km which decreased to 1.4 sq km in 2010 by decreasing an amount of approximately 57%. In 1972 the wetland with

vegetation was very less as compare to 2001 and 2010. This vegetation is supposed to be mostly the agricultural fields which are the activities of the local people due to fertile nature of the wetland. Hence, it is critical to say whether the wetland has expanded or due to anthropogenic activities the real wetland is shrinking.

Twenty one random locations were selected within the wetland boundary of 2010 to see the changes of NDVI from 1972 (figure 5 (b)). These points fall in both water and vegetated areas. Although there is no definite trend in the NDVI values, for different years, same season NDVI data shows drastic difference in their values. The pre monsoon (Feb-Apr) plot infers a gradual increase in NDVI from 2001 to 2003. However, there is no much difference in the average NDVI of 2003 and 2010 for all points, although there are some changes in each location. For post monsoon plot (Oct-Nov), there are few locations (1 to 8), where the NDVI was less in 1972 which increased in 2009, however in June 2000 the NDVI of these 8 locations are observed to be the highest. For the rest of the locations of the plot in this season, the pattern is random. But, in June 2000 the average of all the points can be assumed to be a constant horizontal line.

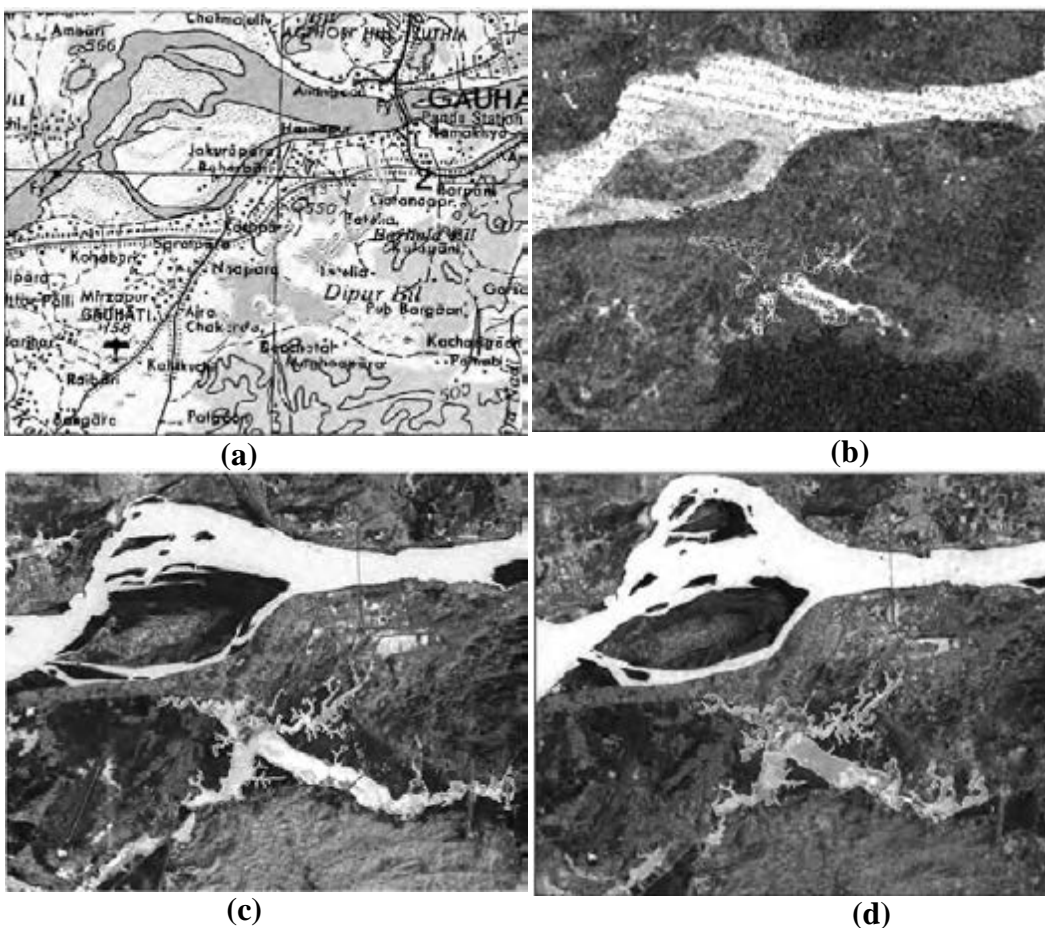


Figure 4: (a) Topographic map (1946) (b) NDWI image of Landsat (1972) (c) NDWI image of Landsat (2001) (d) NDWI image of Landsat (2010) of the study area

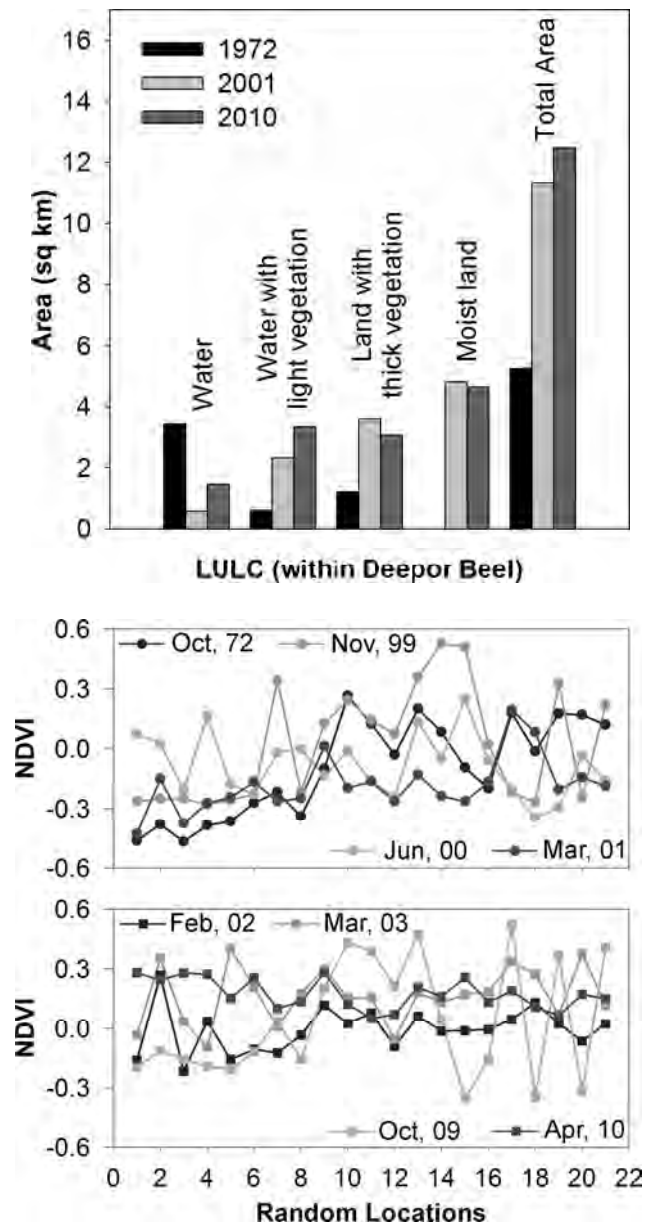


Figure 5: (a) Change in the area of the LULC classes (b) NDVI variation at 21 random locations within the Deepor Beel

a. Linkages between Deepor beel and river Brahmaputra

To determine the existence of the linkage between the Brahmaputra river and the Deepor beel, the SRTM DEM has been used to find the difference in elevations around the area (figure 6). Originally the Deepor beel had its natural linkage with the river Brahmaputra through the Borhola beel and the swampy areas of Pandu, lying to the Northeast. But owing to the construction of NH-37 and civil works like residential buildings the earlier link has already been severed (Saikia, 2005). The flow accumulation map derived from the DEM shows a number of possible linkages between the river and the wetland. However, the linkage observed in the toposheet of 1940's still exists with some disconnections in the middle. The disconnected portion of the linkage may have occurred due to some true elevated area in

the topography or due to existence of bridge. This was confirmed with the high resolution images of Google Earth (2005). The Google Earth image showed the continuous linkage with a small bridge over it.

Two more linkage between the river and the wetland was discovered which was not visible from the google earth imageries. These are the underground channels which feed the wetland from the river Brahmaputra.

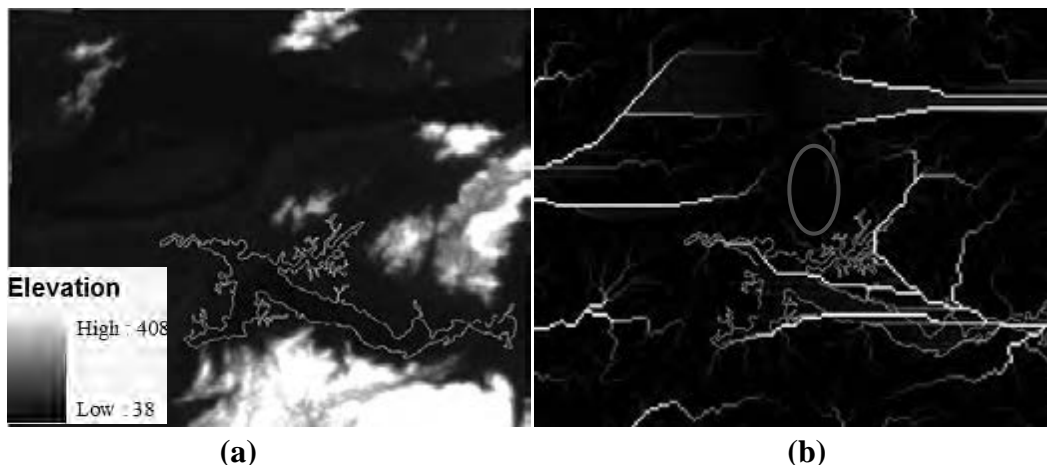


Figure 6: (a) SRTM DEM (b) Flow Accumulation map derived from the DEM

Table 1 shows the areas around the Deepor beel which have changed from water to land or vice versa. These have been obtained from NDWI images by running a model in ERDAS. Hence, four scenarios were obtained on pixel to pixel basis where the changes from water to water and land to land have been considered as no change. The other two scenarios are change from water to land and vice versa.

Table 1: Changes in land and water obtained from NDWI images

Change	count		area (sq km)	
	1972-2001	2001-2010	1972-2001	2001-2010
Water to water/Land to land	48854	49723	1.46562	1.49169
Water to land	1831	1993	0.05493	0.05979
Land to water	2529	1645	0.07587	0.04935

4. CONCLUSION

The present study is an attempt to use the techniques of remote sensing and GIS to delineate the changes in a wetland of Ramsar convention in North East India in last 7 decades. The NDWI image was found effective in deciding the boundary of the wetland. A layer wise classification technique on principal component images of Landsat was adopted to improve the classification of the wetland.

The wetland “Deepor Beel” has shrank in its water covered area as found in the study but, interestingly, the coverage of the moist land has been increased. The wetland has been spread out in its surrounding areas and most of these lands have been used for agricultural purpose due to their fertility. There is a narrow linkage between the river and the wetland and several other possible linkages around the wetland. The flow accumulation map shows some definite surface or underground linkages between the wetland and the surrounding areas which improves the fertility of the land.

The area covered by water in the Deepor beel has decreased by 57% whereas, the moist land has increased by almost 150% from 1972 to 2010. Most of the wetland is covered by water hyacinth and other aquatic plants. Interestingly, area changed from land to water is more than the area changed from land to water from 1972 to 2001. However this was calculated on a pixel to pixel basis from NDWI image by considering a threshold value different for each image by considering the actual conditions from the images.

REFERENCES

Baker, C., Lawrence, R., Montagne, C. and Patten, D., 2006. *Mapping Wetlands and Riparian using Landsat ETM+ Imagery and Decision Tree Based Models*. Wetlands 26(2), 465-474.

Bera, S. K., Dixit, S., Basumatary, S. K. and Gogoi, R., 2008. *Evidence of biological degradation in sediments of Deepor Beel Ramsar Site, Assam as inferred by degraded palynomorphs and fungal remains*. Current Science 95(2), 3.

De Roeck, E., Verhoest, N., Miya, M., Lievens, H., Batelaan, O., Thomas, A. and Brendonck, L., 2008. *Remote Sensing and Wetland Ecology: a South African Case Study*. Sensors 8(5), 3542-3556.

DeAlwis, Da., Easton, Z. M., Dahlke, H. E., Philpot, W. D. and Steenhuis, T. S., 2007. *Unsupervised classification of saturated areas using a time series of remotely sensed images*. Hydrology and Earth System Sciences Discussions 4(3):1663-1696.

Grenier, M., Labrecque, S., Benoit, M. and Allard, M., *Accuracy Assessment Method for Wetland Object Based Classification*. In: Geoffrey J. Hay TBaDM, editor; 2008; Calgary, Alberta, Canada. University of Calgary.

O'Hara, C. G., 2002. *Remote Sensing and Geospatial Application for Wetland Mapping Assessment and Mitigation*. Integrating Remote Sensing at the Global, Regional and Local Scale Pecora 15/Land Satellite Information IV Conference. Denver, Colorado.

Ozesmi, S. L. and Bauer M. E., 2002. *Satellite remote sensing of wetlands*. Wetlands Ecology and Management 10(5):381-402.

Planning CGoI. 2008. *Report on Visit to Deepor Beel in Assam - a wetland included under National Wetland Conservation and Management Programme of the Ministry of Environment & Forests*. Guwahati, Assam, 13-14 Aug, 2008.

Saikia PK. Qualitative and Quantitative Study Of Lower And Higher Guwahati; 2005. Available at:

<http://www.ndsu.edu/pubweb/~bezbarua/em/Documents/DeeporReport-PrasantaSaikia.pdf>.

Estimation of building stories for HAZUS using light detection and ranging (LiDAR)

Chomchanok LIANGWANNAPHORN and Kiyoshi HONDA
Remote Sensing and GIS, School of Engineering and Technology
Asian Institute of Technology (AIT), Thailand
Chomchanok.L@gmail.com

ABSTRACT

In this decade, Thailand was affected by a lot of disaster especially in Tsunami disaster triggered by an earthquake. HAZUS Loss Estimation methodology involves many parameters for damage estimation. One of the most critical parameter in estimating Hazard Loss is floor area. Floor area refers to the total of floor area of building which can be derived from building stories multiplied by footprint area. Therefore building stories is important. LiDAR provides high resolution spatial point data used in the numbers of applications especially in urban mapping. The capability of LiDAR, rapid data acquisition, eliminates the time consuming and costly problem which is the main problem from traditional survey. The point cloud LiDAR can be determined to be ground point data and non-ground point data. LiDAR is generated to digital surface model (DSM), the ground point from LiDAR is used to create a digital terrain model (DTM), afterwards normalize digital surface model (nDSM) which is a technique for eliminating the terrain affect in data set, created by subtracting DTM from DSM. Building's height is extracted by building footprint database, As the result, the numbers of building stories will be extracted using the relationship between building height and number of story of building.

Keywords: *LiDAR, HAZUS, earthquake loss estimation, building stories extraction*

1. INTRODUCTION

In this decade, Thailand was affected by a lot of disaster especially in Tsunami disaster triggered by an earthquake. Therefore, disaster management became the top priority concerned by the Thailand government and private sectors. Since 2006, Thai Meteorological Department (TMD) is developing a database for disaster management named as Thailand National Database for Earthquake and Tsunami Relief and Prevention. The mentioned database is based on HAZUS-MH program requirements. HAZUS-MH program was selected as the loss estimation methodology for Thailand.

HAZUS methodology, an inventory database contains various data which affected by hazard. The database consists of various databases such

as hazard database, boundary and infrastructure database and building database. During, hazard database initiation of the hazard scenario in loss estimation, building damage estimation is calculated by building database which provides the main calculating parameters, for instance; building location, structure type, footprint area, age of building, building occupancy type, numbers of building stories, etc.

1.1 Statement of the Problem

Thailand National Database is collecting from various sources, which results in different accuracy, scaling and reliability. The number of building stories in existing database is not much accurate when comparing with the updating data from surveying, which found in 25 percentages of non-matching in databases. Cross checking and modification of the existing dataset will take time and costly. Moreover the accuracy of building stories is directly contributing to floor area in building damage estimation using HAZUS-MH. The capability of LiDAR in automatic three dimension reconstruction is play an important role in extracting building stories. The result of LiDAR associated with building footprint is precise accuracy and reliability in building stories extraction.

1.2 Objective

The main priority of this research is extracting building stories from LiDAR image using building footprint from existing database.

- Overlay building's height from LiDAR and building footprint.
- Analyze Relationship between building height and building stories.
- Estimate building stories and validate the result.

2. BACKGROUND

2.1 HAZUS Method

HAZUS stands for HAZard United States which is a nationally applicable methodology and software program for estimation of loss from earthquake, floods and hurricane. HAZUS is being developed by the Federal Emergency Management Agency (FEMA) which uses geographic information system software to calculate, map, and display earthquake hazards and damage and loss estimation. The earthquake model provided by HAZUS was released in early 2003 as part of a multi-hazard version of HAZUS. The model allows users to forecast damage and loss to buildings, infrastructure and population that may result from potential earthquakes. Loss estimates produced by HAZUS are based on current scientific and engineering knowledge of the effects of earthquakes. (FEMA, 2008)

2.2 Building Dataset

Thai Meteorological Department (TMD) is developing a database for disaster management known as "Thailand National Database for Earthquake

and Tsunami Relief and Prevention”. The database is combined from existing database and data from ongoing surveys. Existing database in Bangkok area is provided by the Department of city planning, Bangkok Metropolitan Administration (BMA) which consists of building data sets such as building location, structure type, footprint area, age of building, building occupancy type, numbers of building stories, etc. Existing data is based on the data in 2003, therefore, is out of date and unorganized regarding existing building database. It may be caused by missing records, not-matching data, missing information and human error. Existing data modification is time consuming and accuracy improvement is not guaranteed because improvement depends on surveyor quality, time limitation of project, budget, etc. Furthermore, existing database is not compatible with HAZUS requirement. Existing database needs re-coding in building occupancy type according to HAZUS methodology.

2.3 Related work

There have been several related works on building detection using LiDAR data. Guoqing Zhou, C.Song, J. Simmers and P.Cheng used LiDAR and digital aerial images for generating urban 3D GIS. For ground point extraction; M.A. Brovelli and M. Cannata (2004) proposed filtering method for LiDAR data, called region growing algorithm and also mentioned in Claus Brenner’s research (2005). Another filter is the morphological filter that was used by Wolfgang Schickler in 2001, used for application of surface estimation based on LiDAR. Moreover, LiDAR data have the capability of acquisition of 3D features models for virtual reality application. Numerous application of LiDAR for 3D modeling, building extraction and 3D city modeling has been introduced by many researchers. Norbert Haala and Claus Brenner introduced two methods for data collection in urban environment in 1999. The first method combined multi-spectral imagery and laser altimeter data for the extraction of buildings in urban area. The second method used laser data and 2D ground plan information to obtain 3D reconstruction of buildings. In addition, building footprint extraction from aerial LiDAR data has been done by Oliver Wang, Suresh K. Lodha and David P. Helmbold. They presented a novel Bayesian technique for automatically constructing building footprint form a pre-classified LiDAR point cloud. Scott Orford and Jonathan Radcliffe presented a method for deriving living space estimated by using LiDAR associated with OS Mastermap for Cardiff which provides topographic and address layers to extracts the number of stories. Building heights were then calculated for each polygon within a building outline using a weighted average of the LiDAR data and then this was converted into a measure of the number of stories.

3. METHODOLOGY

The general methodology of the research and the procedures that relevant to analysis dataset for number of building stories is consists of three main procedures; (1) Derived Digital Terrain Model (DTM) for LiDAR data ; (2)

Normalized Digital Surface Model, also called nDSM. This technique reduces topographical affect from the objects on terrain in other words; the absolute height value of protruding objects is extracted; (3) Building data and number of building stories are extraction.

3.1 Ground point selection

Elevation derived from LiDAR dataset is normally stand on earth's surface, height is based on the sphere which is still having the terrain affect. The terrain affect is terminated by subtracting Digital Terrain Model (DTM) from Digital Surface Model (DSM). A digital surface model (DSM) on the other hand includes buildings, vegetation, and roads, as well as natural terrain features. Hence, features on surface have to eliminate the terrain affect before calculate net height. Points represented as ground point is generated a digital terrain model (DTM). Digital terrain model, also called DTM, is derives from ground point using interpolation technique. Bilinear interpolation is selected in this research because this interpolation is appropriate to for continuous data.

Bilinear interpolation is a one extension of linear interpolation which functions of interpolating two variables on a regular grid. The interpolation starting with interpolate in one direction, then again in another direction. Suppose, interpolate in x – direction first, and then interpolate in y – direction as equation 1 , equation 2 and equation 3 respectively. First, do linear interpolation in the x-direction with following equation.

$$f(R_1) \approx \frac{x_2 - x}{x_2 - x_1} f(Q_{11}) + \frac{x - x_1}{x_2 - x_1} f(Q_{21}) \quad \text{where } R_1 = (x, y_1), \quad (1)$$

$$f(R_2) \approx \frac{x_2 - x}{x_2 - x_1} f(Q_{12}) + \frac{x - x_1}{x_2 - x_1} f(Q_{22}) \quad \text{where } R_2 = (x, y_2). \quad (2)$$

Then again, do interpolating in the y-direction.

$$f(P) \approx \frac{y_2 - y}{y_2 - y_1} f(R_1) + \frac{y - y_1}{y_2 - y_1} f(R_2). \quad (3)$$

3.2 Normalize Digital Surface Model (nDSM)

The concept of Normalize DSM is calculates the difference between DSM and DTM as demonstrate in Figure1.

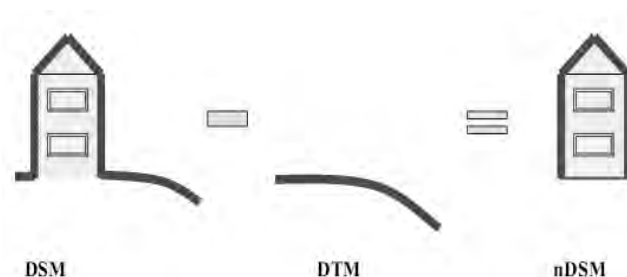


Figure 1. Normalized Digital Surface Model Concept

DTM is derived from DSM afterwards; simply subtracted DSM by DTM data which results in all objects stands on elevation height zero.

3.3 Building and Building Stories Extraction

The aim of this work is extract number of building stories using light detection and ranging (LiDAR) and building footprint dataset. Additional, the result form this research can contribute on increasing accuracy of building database in case of earthquake loss estimation using HAZUS program. The requesting dataset to finish this research are building footprint and height of building which derived from building database and LiDAR dataset respectively.

Data combination between building footprint and nDSM dataset, zonal analyst technique was chosen. Zonal analyst calculated nDSM for each cell using the value for each belonging the zone which defined by building footprint in another word, a statistic is calculated for each zone defined by a building dataset, based on values from nDSM dataset

Result of combined dataset between building information and nDSM, building occupancy type and building's height can reach for building stories extraction. Aforementioned, floor's height of building is limited by building occupancy type. Standard floor's height of building base on Bangkok Legislation act 2001: Building control regulation which defined floor height as Table 1

Table 1: Standard of Floor height
(Bangkok Legislation act 2001: Building control regulation)

Occupancy Type	Vertical High (Standard Height)
1. Residential, Town house	3.00 m.
2. Commercial and School	3.25 m.
3. Warehouse, Hall	3.50 m.

Building data from nDSM is firstly extracted, afterwards; zonal analysis is applied for average-height calculation in each building according to footprint data, result of calculated value which appeared in the tabular data. The tabular data from zonal analyst is joined with tabular data in building database. Finalize, all information both from LiDAR data and building information became unique dataset.

3.4 Error Assessment

Examined data should be reliability and up to date, so survey data is acquired in this research. Survey data is separated in two levels, first level is existing database verification and second level is building stories extraction validation.

Sampling data is differencing in existing database verification and building stories by LiDAR verification. For existing database verification is focusing on building stories and building occupancy type. Because building occupancy type is directly affects the standard of building floor's height. Therefore, error assessment is beginning with verify building occupancy type and building stories in existing database.

Since existing database verification is collected by visual survey, massive sampling is allowance. On the contrary, building stories by LiDAR verification is required more than visual survey. Building's height is measured using laser measurement which one set of measurement had to measured three time in each building; then average for the height of one building. Because laser instrument and building is not on the same elevation, triangle measurement technique is required in this section (1) measure the top of building (2) measure on middle in height and (3) measure the lowest of the building, mentioned steps is counted in one set of measurement.

An error over existing database found error data varies increasingly base on number of building stories. Major error is found in number of building stories is three and four as show in Table 2

Table 2: Error in Existing Building Database

Number of Building Stories	Error
	Percentage (%)
1 Story	-0.75
2 Stories	0.60
3 Stories	6.51
4 Stories	6.08
5 Stories	0.70
Total Error	6.90

In contrast, a total error of building stories which derived from LiDAR dataset is decreasing seven times comparing with existing building database. Most decreasing of error founds in building with three stories and four stories as Table 3

Table3: Error in Number Stories derived from LiDAR

Number of Building Stories	Error
	Percentage (%)
1 Story	-0.23
2 Stories	0.09
3 Stories	0.33
4 Stories	0.05
5 Stories	0.14
Total Error	0.37

4. CONCLUSION

The aim of this work is extract number of building stories using light detection and ranging (LiDAR) and building footprint dataset. Additional, the result form this research can contribute on increasing accuracy of building database in case of earthquake loss estimation using HAZUS program. The requesting dataset to finish this research are building footprint and height of building which derived from building database and LiDAR dataset respectively.

LiDAR dataset providing efficient result in number of building stories extraction which derived seven times increasing of accuracy. As mentioned reason, number of building stories is key factor in floor area calculation which directly affects to loss estimation by HAZUS program. Number of building stories is extracted and contributed in building database. The result from LiDAR is more accuracy than existing database which directly contributes more accuracy in loss estimation. Consequently, number of building stories derived from LiDAR is more efficiency in term of more accuracy, time-consuming and reliability data than traditional processes.

In conclusion, LiDAR is effective in number of building stories extraction which shows in correction of data is increasing approximated 75.54%.

REFERENCES

Claus Brenner., 2005, Building reconstruction from images and laser scanning. *International Journal of Applied Earth Observation and Geoinformation*,6, p 187-198.

Derek McNamara. Extracting Building Footprints from LiDAR and Aerial Imagery in the Wildland Urban Interface (WUI). available online <http://gis.cdatribe-nsn.gov/projects/images/BuildingExtractionFin.ppt>

F.Rottensteiner, J.Trinder, S.Clode and K.Kubik., 2005, Automatic Delineation of roof planes from LiDAR data. ISPRS Workshop "Laser scanning 2005", Enschede, the Netherlands

F.Rottensteiner, J.Trinder, S.Clode and K.Kubik. Detecting building and roof segments by combining LiDAR data and Multispectral images. available online http://espace.library.uq.edu.au/eserv/UQ:9764/ICVNZ_submitted.pdf

Friedrich Ackermann., 1999, Airborne laser scanning—present status and future expectations. *Journal of Photogrammetry & Remote Sensing*, 54, p.64–67.

G.Priestnall, J.Jaafar and A.Duncan., 2000, Extracting Urban Features from LiDAR digital Surface Models. *Computers. Environment and Urban Systems*, 24, p.65-78

George Miliareisis and Nikolaos Kokkas., 2007, Segmantation and object-based classification for the extraction of the building class from LiDAR DEMs. *Computers& Geosciences*, 33, p. 1076-1087.

Gunho Sohn and Ian Dowman., 2007, Data Fusion of High-resolution Satellite Imagery and LiDAR Data for Automatic Building Extraction. *ISPRS Journal of*

Photogrammetry&Remote Sensing, 62 , p.43-63

M.A.Brovelli and M.Cannata., 2004, Digital terrain model reconstruction in urban areas from airborne laser scanning data: the method and example for Pavia (northern Italy). *Computers& Geosciences*, 30, 325-331

Norbert Haala and Claus Brenner., 1999, Extraction of buildings and trees in urban environments. *ISPRS Journal of Photogrammetry&Remote Sensing*, 54, p. 130-137

Phisan Santitamnont. , 2007, Feasibility study of LiDAR Technology for Engineering Surveys. Lecture note online of Chulalongkorn University available online www.subweb2.dpt.go.th/orw/udti/data/training_online/TrainingProgram_Chula.pdf.

Phisan Santitamnont., 2008, Introduction of LiDAR. Lecture note of LiDAR Training at GISTDA on 2nd June 2008.

Ronald A. Bauer and Craig M. dePolo., 2006, Loss-Estimation Modeling of Earthquake Scenarios for Each County in Nevada Using HAZUS-MH. NEVADA BUREAU OF MINES AND GEOLOGY, Nevada, United State.

Scott Orford and Jonathan Radcliffe. Modelling residential living space for individual properties using digital infrastructure and remote sensing data: a Cardiff case study. School of City and Regional Planning, University of Cardiff

Wolfgang Schickler and Anthony Thorpe., 2001, Surface estimation based on LIDAR. ASPRS Annual Conference. St. Louis, Missouri.

Long and deep underground road tunnel projects of the mega-city in Korea

Chang-Yong KIM¹, Seong-Won LEE¹, Xiu-Mei ZHENG¹,
Ho-Keun KIM¹ and Kyung-Ho PARK²

¹Korea Institute of Construction Technology, Daehwa-dong, Goyangdae-ro,
Ilsanseo-gu, Goyang-si, Gyeonggi-do, Korea,
cykim@kict.re.kr

²Asian Institute of Technology, P.O. Box 4, Klong Luang,
Pathumthani 12120, Thailand

ABSTRACT

Recently, the developed countries such as Europe and USA are promoting to construct traffic facilities using the underground spaces of downtown area to develop the new sustainable space for Green Growth, securing green zone on the ground and solving traffic congestion. Expanding ground traffic facilities in a metropolis has gone as high as it can go due to land compensation and civil appeals during construction and especially, a traffic tie-up and concentration in Seoul and the Metropolitan area cause severe social/economical loss so it is necessary to construct deeply underground traffic facilities to solve traffic congestion fundamentally. Accordingly, the city of Seoul announced the U-Smartway project based on 6 underground roads and 4 circular road networks that extend to 149km. This project is the first challenge of urban deep road and longest tunnels in Mega City such as Seoul and Busan etc. Already, there are several lanes of Subway line number 1-9. But, this kind of the huge project in road tunnel in urban area is first in Korea.

However, compared with the developed countries experiences, Korea has been inexperienced in constructing underground roads of the downtown area with insufficient consideration on the related core technologies and accumulated knowledge. Then, if the project is promoted, we cannot help depending on overseas technologies. Accordingly, in this study, the concept of underground transportation infrastructures specially in road tunnels that is suitable for Korean circumstances was established and the core base technologies to construct economical and safe underground space was deduced to consider practical use in the future.

In this paper, we emphasis on the needs of consideration of the technical requirements of this kind of projects in long and deep urban road and railway tunnels

Keywords: *Urban Road Tunnel, Deep and Long Tunnel, U-Smartway*

1. INTRODUCTION

Approximately 70% of Korean peninsula consists of mountainous area and Seoul, in the capital of Korea also located in very hard rock condition (Figure 1). As shown in Figure1, Gneiss, Granite and Schist are the main formations of Korean peninsula. The percentage of these kinds of hard rock formation is almost over 64%. So, there are very good conditions for the development of underground infrastructures in Seoul, namely Mega-City of Korea.

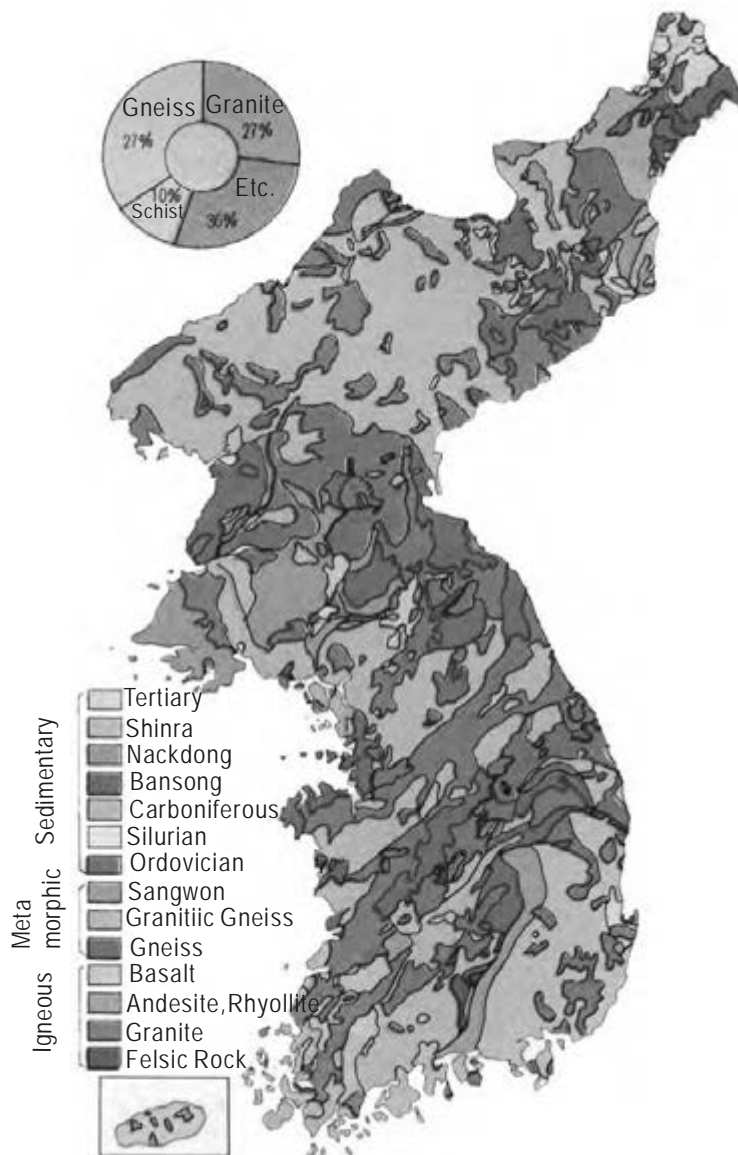


Figure 1: Geological Formations in Korean Peninsula

At present, the construction of transportation facilities utilizing urban deep underground to promote sustainable development, secure green zone above the ground and relieve traffic congestion has been briskly proceed in advanced nations. Even in Korea, the need for construction of urban deep underground transportation infrastructure came to the fore as a way of

relieving traffic congestion as economic loss of 21.5 trillion won a year was estimated as a result of traffic jam and traffic concentration on Seoul metropolitan area, and the expansion of traffic facilities above the ground was no longer available due to various problems related to civil affairs during construction and compensation for land required.

On this, Seoul metropolitan government presented its plan of U-SMARTWAY, which is designed to construct 2 belt highway and 6 underground road(total of 149km), and the Ministry of Land, Transport and Maritime Affairs and Gyeonggi provincial government presented the project of deep tunnel express line for metropolitan area (GTX). Currently, the need for underground expressway project of partial section in Gyeongbu[Seoul-Busan] Expressway and Gyeongin[Seoul-Incheon] Expressway is under the study, which is suggested by Seoul Policy Development Institute. Government is performing a study on the utilization, maintenance and development of underground space to activate construction of urban deep underground transportation infrastructure, and based on this, the Ministry of Land, Transport and Maritime Affairs is making systematic basis like enactment of 'Basic Regulations on underground space'.

However, since Korea doesn't have many construction experiences of urban deep underground transportation infrastructure, compared to advanced nations, and the review on core technologies and accumulation of technologies are lacked, we have no choice but to depend on foreign technologies in case the projects proceed. In addition, most projects which are suggested and reviewed until now are designed to cut and cover tunnel and NATM tunnel by blasting in spite the fact that tunnels pass through the lower part of existing road or crowded downtown area. Above all, in-depth reviews as well as technological and political alternatives are required since many people are concerned about the safety and disaster prevention of urban deep underground transportation infrastructure, and the specialists concerned have conflicting ideas on this kind of issue. Accordingly, it is said that now is the time that we have to establish the technologies of design/engineering for construction of safe and economical underground transportation infrastructure, and correct concept of underground transportation facilities suitable for domestic environment.

In this study, the direction of technology development is presented by deducing core technology items for construction of urban deep underground transportation infrastructure, reviewing the present status of major projects related to transportation facilities utilizing urban deep underground of Korea.

2. URBAN DEEP INFRASTRUCTURE

Urban deep underground infrastructure is defined as underground road designed to pass through the lower part of downtown areas for the purpose of controlling traffic volume and reorganizing the overcrowded city, and currently there is increasing demand for this because of awareness on importance of beautiful urban landscape and environment, alternative of

civil affairs during construction and compensation for land required, and problem of overcrowded downtown area.

Deep underground is defined as the point which is more than 40m, where there is no construction of subway in general, or more than 10m from the upper part of the support ground, where there is no use for foundation installation for structure.

For the underground transportation facilities in downtown area which is planning in Korea, the method utilizing urban deep underground which is more than 40m in depth is being reviewed. Table 1. shows that the general advantages of utilizing urban deep underground as transportation infrastructure and requirements precedent for construction of underground transportation facilities.

Table 1: The advantages of urban deep underground transportation infrastructure and technical requirements.

<p>The advantages of urban deep underground transportation infrastructure</p>	<ul style="list-style-type: none"> • Possible to reduce construction expenses of urban deep underground • Reducing construction period • Curtailing expenses by rational tunnel alignment • Cutting down noise and quake and preserving urban environment • Avoiding large-scaled civil engineering work above the ground in crowded downtown area • Little damage from earthquake
<p>Technical requirements</p>	<ul style="list-style-type: none"> • Environmental countermeasures of tunnel(ventilation tower, underground water) • Countermeasure for disaster prevention of tunnel • Ventilation method of tunnel • Structure of tunnel and method of construction • Increase of management and construction cost • Restriction of the entrance and difficulty of expansion in the future

3. U-SMARTWAY PROJECT

Seoul metropolitan government established the basic plan for underground road in 2006 and last year, the government came to present the plan for U-SMARTWAY underground road, which is total of 149km and has 9 lines in south/north and east/west axes to solve serious traffic problems through review for several years. U-SMARTWAY is new conceptual underground road, which is safer and more pleasant than space above the ground since not only driver but also system can control the vehicle, sending and receiving information through the cutting-edge communication system in urban deep underground of 40 to 60m. Estimated working expense amounts to 11.2 trillion won.

3.1 ROUTE

The composition in lines of U-SMARTWAY is designed to improve accessibility between Seoul and Incheon by reflecting regional characteristics like harbours and airports, which shows in Figure 2. In

addition, the traffic which passes through downtown area can be made to take a roundabout by connecting metropolitan area with subcenter of metropolis. In particular, the traffic volume which passes through downtown area can be effectively reduced by connecting 2 recurring lines which is to be constructed underground with internal circulating line and Gangnam circulating line above the ground. For additional method of restricting vehicles incoming downtown area, 4 access roads are to be installed in downtown area so that the vehicles can go into outskirts of the city rapidly.



Figure 2: Scheme Drawing of U-SMARTWAY

3.2 DESIGN CONCEPTS

The disaster prevention plan which is considered as the most important factor in U-SMARTWAY is designed and operated, connecting with the entire systems constructing underground road such as transportation management plan, ventilation plan and central control centers, including the prevention and extinction of fires. By all transportation measures, emergency road of 2.0m is installed in entire section of U-SMARTWAY to secure safety zone each, and water atomizing facilities and automatic fire sensing devices are installed to prevent from fire spreading. In addition, the 24-hour management on entire section is expected to be made through radio, VMS and CCTV in the central control center.

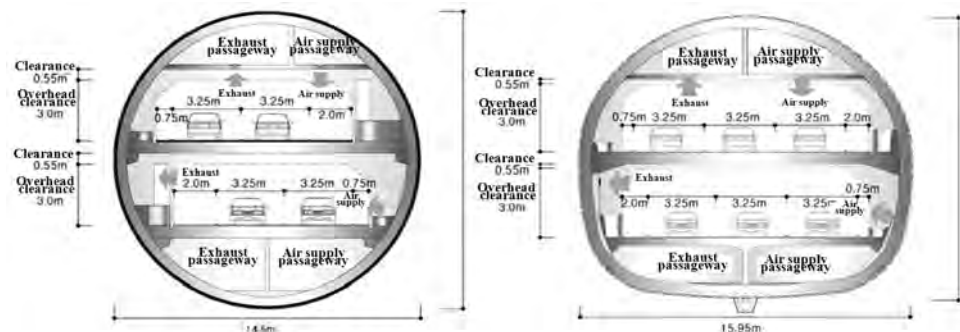


Figure 3 Cross Sectional Diagram for Main Tunnels

Looking at the sectional diagram of underground road, the rest 5 axes except for south/north 3 axes are planned as duplex structure for compact car exclusive like Figure 3, considering economical efficiency and easiness in construction of circulating lines. In addition, JCT is installed in the section at which south/north axis and east/west axis intersect so that vehicles can change direction without entering into the road above the ground in the center of the city and the secondary center of the city sections (Figure 4).

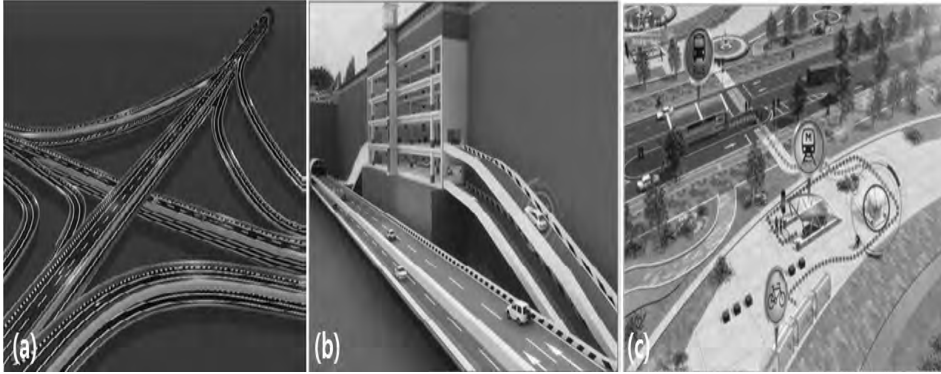


Figure 4 Connecting System with the Road above the Ground of U-SMARTWAY (a) JCT, (b) Underground Parking rot, (c) Connection with Transportation above the Ground

3.3 EMERGENCY EVACUATION SYSTEM

For ventilation plan, overflow-typed ventilation plan by exhaust duct is reviewed, targeting entire sections to realize stable evacuation efficiency after careful consideration of the fact that it is ultra long tunnel in which one axis is more than 20km, and the plan is connected with disaster prevention plan in coordinated way(Figure 5). In addition, the introduction of such purifying systems as electric precipitator and ventilation facilities will make it possible to filter out pollutant from vehicles in underground road and discharge clean air into the atmosphere.

Considering transportation aspect, the construction of underground road makes it possible to move the entire area of Seoul metropolitan city within 30 minutes, and promote space for environment-friendly public transportation since cycletrack(more than 492km) and green tract of land(615,000m²) can be secured in city spatial aspect. In addition, reduction in social expenditure of 2.4 trillion won a year is expected through reduction cost of traffic congestion and environmental pollution in economic aspect



Figure 5 Ventilation method and emergency evacuation facility

4. TECHNICAL REQUIREMENTS

Looking into such cases of transportation facilities utilizing urban deep underground as A86 underground road in France, central underground road in Tokyo, Japan, M30 project in Madrid, Spain, SMART project in Malaysia and Alaska Way project in Seattle, the United States, those projects commonly adopted Shield TBM method, environment-friendly tunnel method of construction to prevent obstruction of traffic flows and damage of surrounding environment during construction work, and construct duplex tunnel for compact car exclusive to achieve efficiency of sectional diagram. In addition to point of sameness in the technological method, those projects had powerful driving force for operation of the projects in common, while promoting harmonious communication with local residents.

The technological realization of urban deep underground transportation infrastructure is said to be completed in 2005 worldwide. However, 2016 is estimated for completion of the technological achievement in case of Korea since core technology related isn't prepared for the project, not to mention research on marketability and economical efficiency. Since the construction of urban deep underground transportation infrastructure in downtown area is aimed at solution of traffic problem in a metropolis, the core technologies required are ultra large sectioned Shield TBM technology, designing and engineering technology of ultra large sectioned duplex tunnel and safety management technology of underground passage. For this, research and development must be made. Considering foreign cases of commercialization, it seems that the technology connecting with existing transportation network is not systematically defined, so it is estimated that the technology connecting with existing transportation network can be utilized as major technology item as core technology development item.

It is said that Korea has large cross sectional and urban deep underground shaft technology for connection of underground tunnel with road above the ground and construction technology of excavation tunnel at present, but as interest and demand for protection of surrounding environment, minimization in obstruction of traffic flows during construction work and maintenance of pleasant city life increases, economical and environment-friendly shaft construction technology and technological development of excavation tunnel construction will be constantly required. In addition, securing ventilation and disaster prevention technology to guarantee safety in urban deep underground passage has to be put the first, and the cutting-edge technology to minimize damage of existing structures and surrounding environment has to be developed as well. Above all, to cope with the era of environment-friendly green growth, the study on technology of green space development and Net-zero energy tunnel technology producing energy on its own required for operation of tunnel has to be put the first, and space utilization technology for sustainable development of new space have to be also developed. Table 2 shows the summary of core technology development items for construction of urban deep underground infrastructure in downtown area.

Table 2: Core Technologies for Construction of Urban Deep Underground Transportation Infrastructure in Downtown Area

<p>Green Strategy Technology</p>	<ul style="list-style-type: none"> • Construction technology of green underground passage <ul style="list-style-type: none"> - Net-Zero Energy, tunnel technology - IT-based environment-friendly ventilation/disaster prevention technology - Environmental impact reduction design/construction technology • Human-centered space utilization technology <ul style="list-style-type: none"> - Human sensibility ergonomic green design technology - Underground road-downtown area connection utilizing technology - Environment-friendly green zone development technology
<p>Cutting-edge Application Technology</p>	<ul style="list-style-type: none"> • IT-based traffic control technology <ul style="list-style-type: none"> - Underground road traffic control and management system development technology - Intelligent traffic system(ITS) construction technology • K-SMART tunnel technology <ul style="list-style-type: none"> - Urban deep underground tunnel water circulating system technology - Underground road multipurpose utilization technology • The next generation metropolis environment-friendly express/safety tunneling technology <ul style="list-style-type: none"> - Drilling equipment developing and manufacturing technology - Complex ground corresponding TBM design/operation technology - The next generation metropolis drilling technology
<p>Core Base Technology</p>	<ul style="list-style-type: none"> • Underground road integrated design/construction technology <ul style="list-style-type: none"> - Underground road standardization technology - Urban deep underground passage survey/exploration technology - Underground road solid facility safety design/construction technology • Large cross-sectional duplex tunnel design/construction technology <ul style="list-style-type: none"> - Duplex tunnel design/construction technology - Duplex tunnel construction and maintenance equipment development technology

5. CONCLUSIONS

It is said that the utilization of urban deep underground is unavoidable to expand underground transportation network in Seoul metropolitan area and change the space above the ground into green zone. Since the project on construction of urban deep underground road network and great train express in metropolitan area is huge project which is unprecedented worldwide, new conceptual definition in all related areas like law, system, tunnel, construction technology, ventilation and disaster prevention technology is required. Until now, many debates on law, system and disaster prevention have been made rather than tunnel construction technologies, but from now on, the establishment of research and development strategy after figuring out various problems in the course of constructing urban deep underground transportation infrastructure in downtown area is urgently needed.

REFERENCES

C.Y. Kim, S.B. Yim, et al., 2011, *Urban Deep Underground Transportation Infrastructure Project in Korea and Technical Requirements*, Proceedings of the ITA-WTC 2011 in Helsinki , Finland, 295 pp.

C.Y. Kim, S.B. Yim, et al., 2011, *Urban Deep Road Tunnel Construction Project in Korea and Technical Requirements*, Proceedings of Twelveth East Asia-Pacific Conference on Structural Engineering and Construction(EASEC-12) in HongKong, 325 pp.

Seoul Metropolitan, 2009, *The Master Plan of the U-SMARTWAY in Seoul Metropolitan Area*, Reports of Seoul Metropolitan

Development of early warning system in Maldives

Mahmood RIYAZ^{1,5}, Dugkeun PARK², Chang-Yong KIM³,
Sung-Wook KIM⁴ and Kyung-Ho PARK⁵

¹Environment Research Centre,
Ministry Environment Energy and Water, Maldives,
mahmood.riyaz@gmail.com

²National Emergency Management Agency, 253-42, Gongdeok 2-dong,
Mapo-gu, Seoul, Korea

³Korea Institute of Construction Technology, Daehwa-dong, Goyangdae-ro,
Ilsanseo-gu, Goyang-si, Gyeonggi-do, Korea

⁴Geo-Information Research Group Co., Ltd., 1489-4, Geoje1-dong,
Yeonje-gu, Busan, Korea

⁵Asian Institute of Technology, P.O. Box 4, Klong Luang,
Pathumthani 12120, Thailand

ABSTRACT

The Early Warning System (EWS) has been developed to address the natural disaster risks in Maldives. Prior to 2004 Indian Ocean Tsunami, disaster the people of Maldives were not sentient about the disaster risks and so there was no consideration of EWS for the country. Soon after the disaster, a risk profile of the Maldives was developed and emergency response measures for various sectors, such as tourism, communication, education and defense etc. were considered. This study deals with the development of the EWS for the various sectors in Maldives. The National Early Warning System in the Maldives (NEWSM) has been developed in three main phases: (1) Phase I, establishment of the monitoring system of the surface meteorological conditions and seismic event occurrence; (2) Phase II, strengthening the monitoring system established in phase I by making it automated metrological monitoring system; (3) Phase III, confirmation of the information flow, establishment of backup and alternative electric power and telecommunication systems and linkages with international organization. Disaster warning messages from the NEWSM is transmitted to the national, regional, atoll and island offices through a commercial communication system, mainly computer network and hotline (leased lines). The only means of dissemination of disaster advisories and warning to general public is broadcasting through radio and television. Radio Trunking Network that uses TETRA technology is used as backup network.

While Maldives is exposed to various hazards, such as climate change (the risk from rising sea-level), gale force winds, storm surge, torrential rain, earthquake and tsunami, the established EWS seems to be focused only on the distant tsunami risk. The current EWS seems not very effective in communication and message dissemination. The establishment of proper

mechanism to outreach to the general public, remote communities and islands is needed by using more user friendly mechanisms.

Keywords: *Early Warning System, Disasters, Maldives*

1. INTRODUCTION

Maldives is an 800 km long archipelago, precariously located in the center of the Indian Ocean, and consists of more than 1200 low-lying coral reef islands with flat topography and grouped into 26 atolls (Figure 1). These low-lying islands are formed of accumulations of biogenic material provided exclusively by the local reef platform. The height of islands varies between 1~2 m with a maximum spring tide range of 1.2 m and the mean high water spring tide level is approximately 0.6 m above mean sea level.

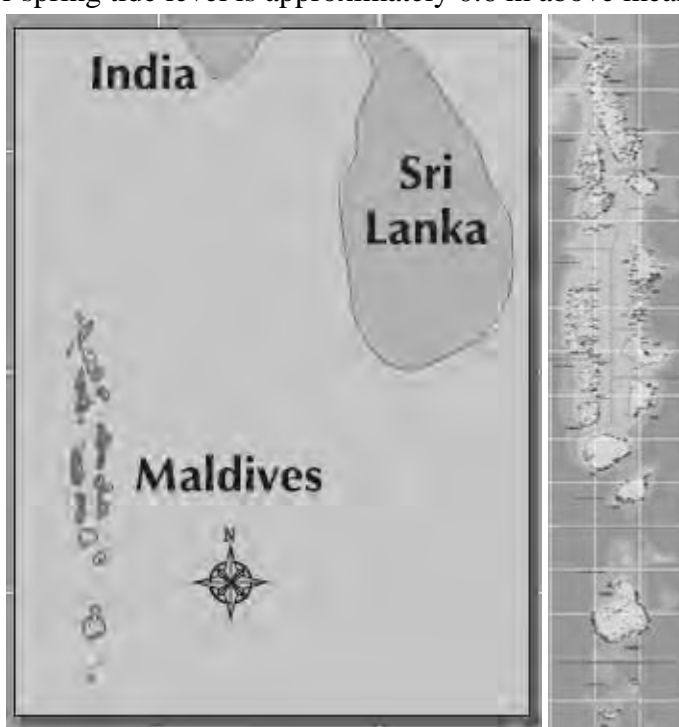


Figure 1: Location map of Maldives

Prior to the 2004 Indian Ocean Tsunami, the disaster management in the Maldives was merely focused on the impact of global warming and sea level rise. However, the disaster risk profile of Maldives, developed by UNDP (2006), indicated that disaster risk scenario of Maldives can generally be described as moderate due to low probability of hazard occurrence and high vulnerability from exposure due to geographical, topographical and socio-economic factors. Apart from the exposure to the obvious risks of sea level rise associated with the global climate change, Maldives is also occasionally prone to various natural hazards such as droughts, high waves caused by cyclones, gale force winds, storm surge, torrential rain, earthquake and tsunami. Like many countries in Asia, the 2004 Indian Ocean Tsunami was a wakeup call for the people of Maldives who were not sentient about the impending threats of natural disaster risks.

The devastating impacts of the disaster was also a test of resilience for the country and made people discern about the importance of adopting measures to pragmatically integrate disaster knowledge, disaster risk reduction measures and management perspectives into the government's planning and policy agenda.

Aftermath of the 2004 Indian Ocean Tsunami and following the UN Flash Appeal for the Maldives, many UN Agencies, NGOs and bilateral countries provided assistance and initiated development of disaster risk management programmes. The focus of the programmes is to develop multi hazard Early Warning System (EWS), preparedness planning, institutional and policy development needed for disaster management, emergency response capacity enhancement safe area development, vulnerability and natural hazard risk assessments. Those initiatives resulted in development of a national plan on disaster management and emergency response measures for various sectors, such as tourism, communication, education and defense etc. were established (MNDF, 2008).

This study focuses on the multi hazard EWS developed in the Maldives since the occurrence of 2004 Indian Ocean Tsunami. The study evaluates the effectiveness and functionality of the existing EWS. Particularly the ability to disseminate and coordinate the disaster warning messages to the national, regional, atoll and island is considered by taking into account recently established decentralized local government system in the Maldives.

2. METHODS

The qualitative and quantitative information were collected by combining the secondary sources (written reports, evaluations, media) and primary information (collected through Maldives Meteorological Center).

The existing reports on disaster risk management, hazard early warning system, preparedness planning, institutional and policy development on disaster management, emergency response capacity enhancement, safer island program, socio-economic and Environmental vulnerability assessments, detailed national and island specific risk assessments, training and capacity building workshops and the emergency telecommunication plan were reviewed. Because almost of the above mentioned reports were developed after the 2004 Indian Ocean Tsunami, they are mainly focused on the tsunami early warning system.

3. RESULTS

In 2008, Maldivians embraced a new constitution that introduced democratic reform and decentralized administrative system. Instead of 19 Atoll-based administrative system in the past, now the country is divided into 7 provinces governed by elected autonomous province councils. With

these changes, the disaster management structure of the country and the established EWS need to incorporate the new institutional and governance related developments in the Maldives. Recently developed Strategic National Action Plan (SNAP) on Disaster Risk Reduction and Climate Change Adaptation is designed to address disaster risk reduction and climate change adaptation and integrate the existing EWS into the new governance structure of the country.

3.1 Existing National Early Warning System in the Maldives (NEWSM)

National Meteorological Centre (NMC) of Maldives has the national mandate to monitor meteorological, oceanographic and seismological activities, as well as analyze and predict extreme hydrometeorological and seismic events, which may affect the country and to issue early warnings of natural disasters as per the EWS established. The NEWSM has been developed in three main phases (ADRC, 2005):

3.1.1 Phase I (2005-2006)

Prior to the 2004 Indian Ocean Tsunami, there was no seismic and wave monitoring network in the Maldives. The surface meteorological observations were conducted in five islands, Hulhulè, Hanimaadhoo, Kadhoo, Kaadedhdhoo and Gan Islands. Equipment used for observations in these stations were outdated, 12~30 years old. So they were not capable of providing continuous monitoring and online real-time displays and could not be synchronized with modern equipment. Most data readings and measurements were performed manually by the local staff in 1~3 hour frequency. The observation results were collected at the NMC in Hulhulè Island by using a modem system connected to the commercial telephone lines. Daily weather forecast as well as weather warning information was disseminated to the public from NMC.

As part of strengthening the existing monitoring system of the surface meteorological conditions, tide and wave variations, and seismic event occurrence, automated data processing functions and continuous monitoring systems of the output of exiting tide gauges were established. A new wave gauge, a short-period seismometer and a weather radar system were installed in Hulhulè Island. Observation data from these equipments were automatically transmitted to the NMC. The data, processed at the regional meteorological offices across the Maldives, was linked with NMC and, via the Regional Telecommunication Hub (RTH), transmitted to New Delhi and other regional offices.

3.1.2 Phase II (2006-2008)

As part of the NEWSM development, 17 automated weather stations across the Maldives were installed. Two broadband seismometers, two wave gauges and two tsunami GPS buoy were installed. Real time observation data from the equipment was transmitted to the NMC and the meteorological offices across the country. A system for acquiring meteorological satellite imagery directly from the METEO-SAT was installed. The seismic data from the stations were sent to IOTWS and

transmitted to the GFZ receiving station at Jakarta, Indonesia to monitor earthquakes across the region. The NEWSM's Global Telecommunication System (GTS) was equipped with a new function to allow automated input of observation data.

3.1.3 Phase III (2008-2010)

The most important aspect in natural disaster situation is to ensure that early warning information is transmitted throughout the nation in a timely and effective manner. The priority would be given to disseminate warning to national level and mass media then to regional provinces, Atoll and island communities. Figure 2 shows the flow of early warning information issued by the NEWSM across Maldives.

As part of the disaster preparedness, efforts were made to use alternative electric power particularly for the operation of equipment used for meteorological observations in the NMC (Anon, 2006). All the automated weather stations were solar powered and fully functional 24 hours, while some equipments in the regional meteorology offices were solar powered. National plan on emergency telecommunication incorporated dissemination of emergency alert via broadcasting (EAB), bulk SMS on mobile network, Radio Trunk Network that uses TETRA technology, priority calling and national roaming and use of existing equipment (HF, VHF, CB) for communication remote communities and vessels in the ocean (Anon, 2006). Also the NMC has established hotline between itself and main focal points, National Disaster Management Centre (NDMC), Maldives Police Service (MPS), Maldives National Defense Force (MNDF) and mass media.

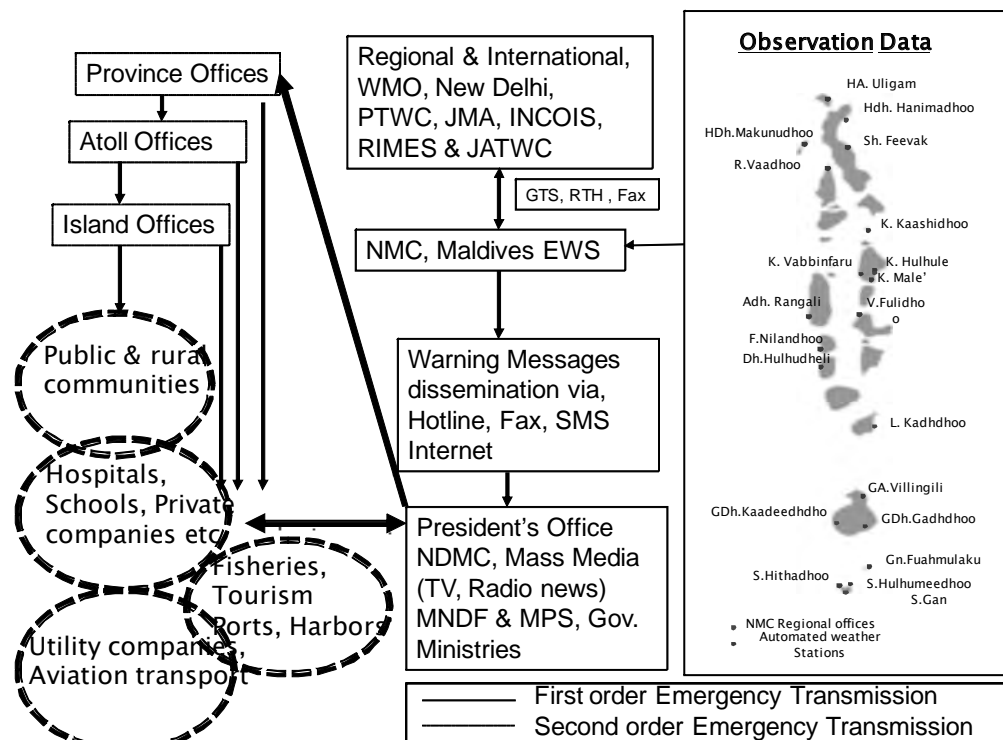


Figure 2: Flow of early warning information

The NMC established criteria for NEWSM for multi hazards generated from hydrometeorological and seismic condition. Figure 3 shows the warning alert levels, description and the mean of information disseminating to the public.

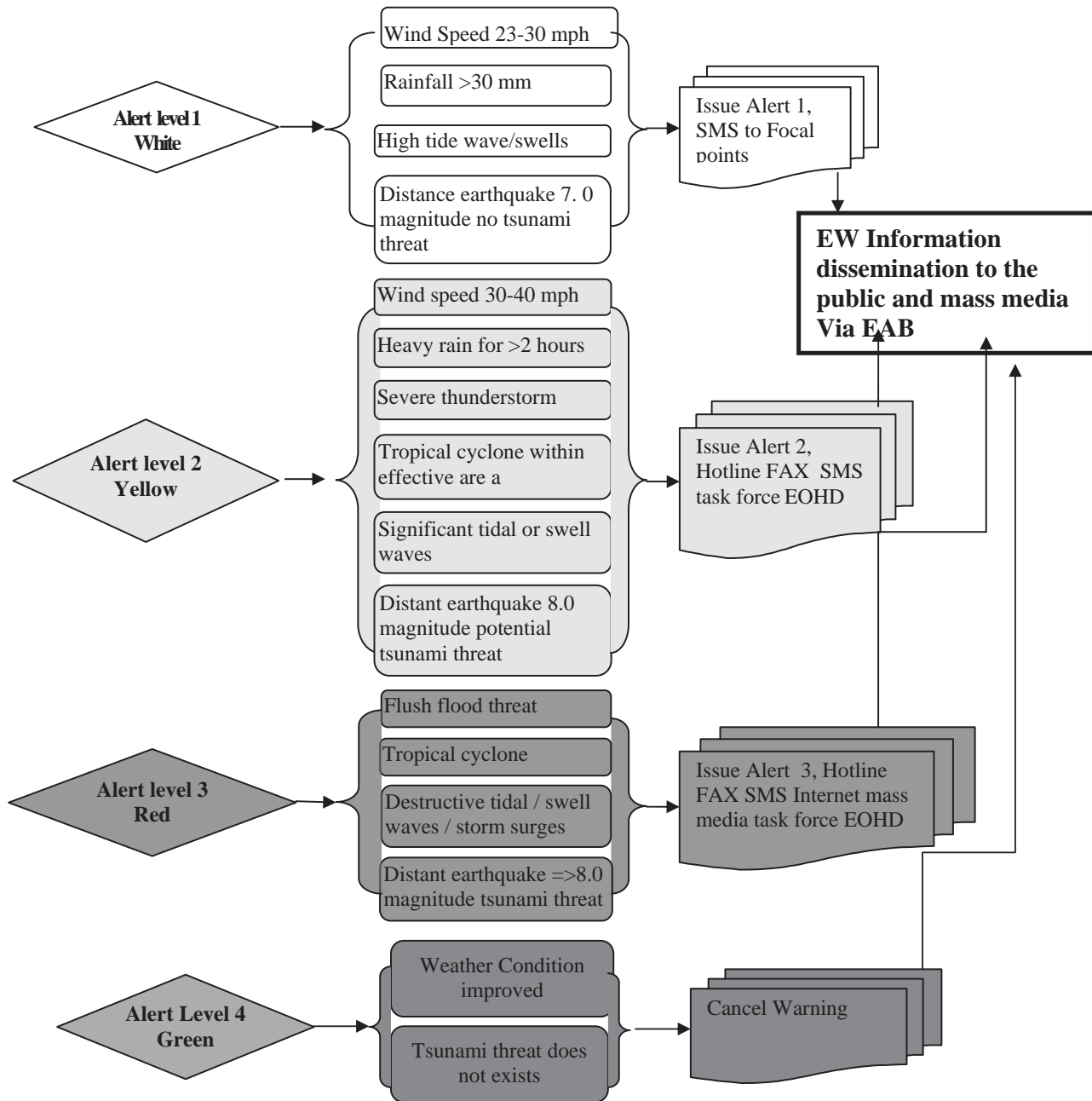


Figure 3: Multi hazard alert levels, description and meaning of information dissemination to the public

4. DISCUSSIONS

The NEWSM was developed by using fairly good three approaches. The development of the NEWSM initiated soon after the 2004 Indian Ocean Tsunami. Thus, greater emphasis was given in the NEWSM on tsunami early warning rather than addressing multi hazards. This aspects is clearly visible in the emergency response plans and standard operational procedures, developed to address disaster risks in various sectors such as tourism (UNDP, 2005a), fisheries (FAO, 2005), telecommunication (Anon, 2006), schools (MoE, 2009), housing development (UNDP, 2005b) and disaster risk profiling of various islands (UNDP, 2006, 2008).

In 2006, UN International Strategy for Disaster Reduction (ISDR) emphasized that sustainable EWS requires community based or people centered, and gender sensitive approaches in the establishment of EWS. Critical areas for establishing EWS are (UN/ISDR, 2004): (a) governance and institutional arrangements, (b) risk knowledge, (c) monitoring and warning systems, (d) dissemination and communication, (e) response capacity, and (f) gender aspect. The following section will discuss these critical areas in the context of the NEWSM.

4.1 Governance and Institutional Arrangements

The Government of Maldives altered its approach to disaster management since 2004 and shifted from more emphasis on relief and rehabilitation to a more proactive integration of mitigation and preparedness. The institutional arrangement for disaster management has been formulated in the Disaster Management Act of Maldives. The Act is under discussion at the Parliament. The Act sets the necessary legal and institutional arrangements with appropriate provisions on integrating decentralization, providing fast relief measures and gives the NDMC legal powers to conduct risk management activities. The Sector Specific National Disaster Management Policy and Plan have been formulated with establishment of EWS and clearly spelled out Standard Operation Procedures (SOP) in various sectors. The NMC has the national mandate for issuing early warning. However, roles of other individual agencies, institutions and the coordination mechanism with relevant Government authorities to operate and integrated EWS is still very vague. Linkages with the different administrative levels and the functional way for various committees in an emergency situation are not very clear. Figure 4 provides an overview of the main EWS functions, distributed across main institutional actor in Maldives.

4.2 Risk Knowledge

In the existing disaster management structure of Maldives, risk warning assurance falls under the mandate of the NMC. The meteorological center only has the capacity for collection and analysis of weather and seismological data. Instead of heavily relying on a single institution, the NMC needs to be changed and efforts should be made to strengthen the

systematic collection, sharing and analysis of the data on multiple hazards and vulnerabilities by different sources, and disseminate knowledge through training and education. The existing information on hazards is in varying data formats and within multiple sources and institutions. To gain further knowledge on disasters, there is a need to use modern tools to analyze historical data for the prediction of future disasters. Risk assessment, conducted after the 2004 Indian Ocean Tsunami to understand the socio-economic and environmental vulnerabilities, is far from complete. The process of translation of assessment suffers from weak enforcements and lack of political willingness to integrate them into the development strategies and plans.

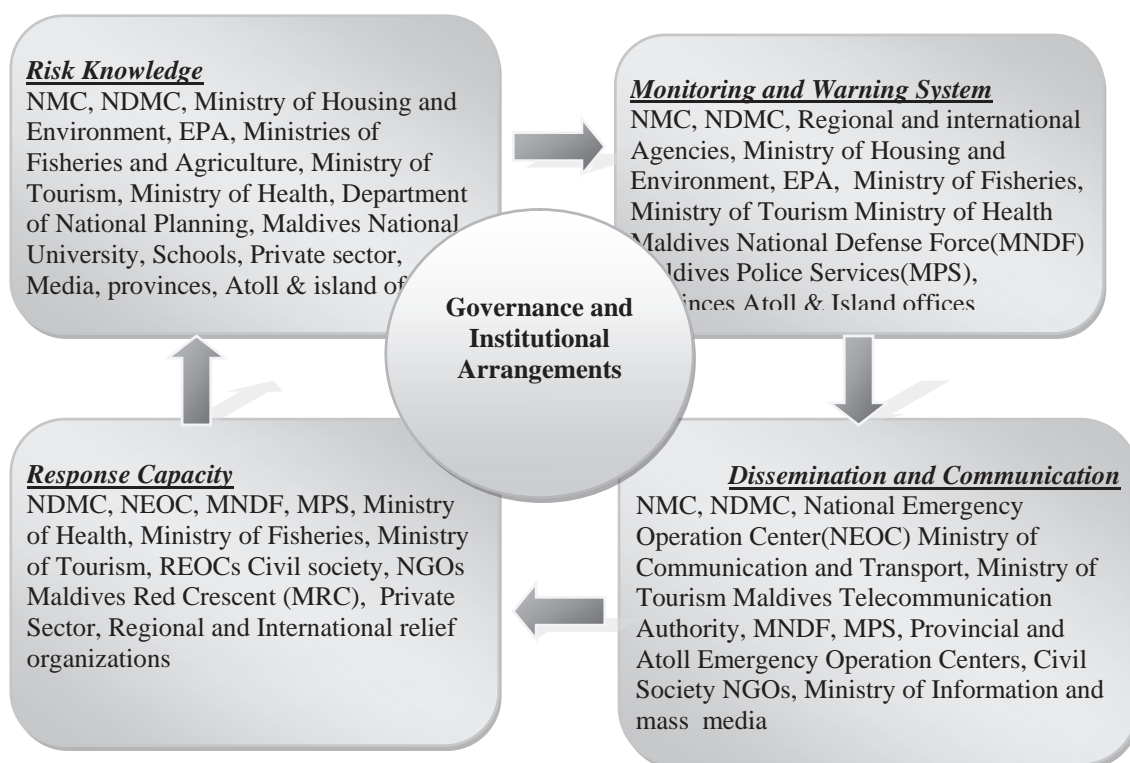


Figure 4: Institutional roles and responsibilities in the Maldives EWS

4.3 Monitoring and Warning System

Maldives has made remarkable progress towards strengthening hazard monitoring and EWS. The NMC has established two main networks to monitor meteorological and seismic hazards. National meteorological network is equipped with 5 synoptic stations, 3 tide gauge stations and 20 automatic weather stations. Seismic network is linked with global seismic network to monitor earthquakes across the region. The NMC continuously monitors sea level data from local and regional tide gauges as well as DART buoys deployed in the region. Also the NMC has the capability to receive high resolution satellite image, Doppler weather Radar data, and has established redundant communication links with local, regional and international centers by using 256 kbps VSAT, 10 mbps internet connection and satellite phone. Combined impact of climate change and environmental degradation will result in hydrometeorological disasters of unprecedented

scales in intensity frequency and extent. Therefore monitoring and early warning capabilities needs to move closer to the communities to prepare them to deal with these challenges.

4.4 Dissemination and Communication

As shown in Figure 2, the NEWSM has two stage warning message transmission process. The main weakness of the system is the limited capacity of provincial government, Atoll council and Island communities to receive interpret and further broadcast the warning messages. This is because clear responsibilities with standard operating procedures (SOP) have not been properly laid out for information exchange across government, civil society, media and the general public. In order to improve the existing EWS dissemination and communication to verify that the warning have reached the communities at risk, a feedback mechanism needs to be established.

4.5 Response Capacity

A warning system is ineffective if people do not know what to do next. EWS should continuously seek to improve the ability of people to respond disaster at regional, Atoll and Island level, incident command systems and SOPs. Disaster preparedness and response plans need to be developed utilizing hazard and vulnerability maps. Maldives is in the process of developing island vulnerability GIS for the country. Frequency of evacuation drills are still very low more work is needed to reach remote island communities.

4.6 Gender Aspects

Neither the draft disaster management act nor the national disaster management plans and policies address gender explicitly. The existing institutions can ensure woman participation in EWS and employ a gender sensitive approach by considering specific concerns such as physical strength, security and protection.

5. CONCLUSIONS

The EWS of Maldives, developed in three phase approach, has been described in this study. The existing EWS of Maldives is focused on tsunami early warning rather than multi hazards. The study found that following issues needs to be addressed to ameliorate the existing EWS:

(1) Enactment of Disaster Management Act of Maldives, development of a disaster management plan and schema addressing end-to-end multi hazard EWS, identification of all institutional actors and their roles, coordination mechanism with relevant Government authorities to operate and integrated EWS. Strengthen the disaster planning capacity of provincial

councils, atolls and island and integrated assessment to fill the capacity gaps in the existing Early Warning System.

(2) Systematic collection, sharing and analysis of data on multiple hazards and vulnerabilities by different sources and disseminate knowledge through training and education. Develop a reliable database on hazards in the Maldives and consolidate the existing information on hazards from multiple sources and institutions to agreeable formats. Convert risk assessment findings into standards codes and regulations and integrate them into the development strategies and plans.

(3) Strengthen the capacity of MNC to be able to analyze and provide timely disaster warnings. Monitoring and early warning capabilities needs to move closer to the communities to prepare them to deal with the challenges and impending threats of climate change.

(4) Develop the capacity of provincial government, Atoll council and Island communities to receive interpret and further broadcast the early warning messages. Upgrade the existing communication infrastructure to the international standards for efficient data exchange. Develop a feedback mechanism to improve the existing EWS dissemination and communication of the warning to ensure that EW message reaches islands at risk.

(5) Establish Emergency Operation Center (EOCs) at regional, Atoll and Island level, incident command systems and SOPs to improve the response capacity and ability of people to respond disasters. Conduct more frequent evacuation drills, build and maintain people's risk awareness coping capacities.

(6) Ensure that participation in the EWS employs a gender sensitive approach considering specific concerns such as physical strength, security and protection.

REFERENCES

Anon, 2006. *National plan on early warning dissemination and emergency telecommunications*, Technical Committee on Early Warning and Emergency Telecommunications, Unpublished report, 24 pp.

ADRC, 2005. *Report on the early assessment of early warning systems in the Maldives*, Asian Disaster Reduction Centre, 125 pp.

FAO, 2005. *Fisheries tsunami emergency programme, Maldives*, Fisheries sector rehabilitation mission report, Project: OSRO/MDV/502/JPN, 18 pp.

Ministry of Education (MoE), 2009. *Guide for school emergency operations plan Maldives*. School Health and Safety Section, Ministry of Education, 93 pp.

MNDF, 2008. *National plan on disaster management*, Maldives National Defense Force, Unpublished report, 104 pp.

UNDP, 2008. *Detailed island risk assessment Maldives*, United

Nations Development Programme Volume I and II, www.undp.org.

UNDP, 2006. *Developing a disaster risk profile for Maldives*, United Nations Development Programme, Volume I, www.undp.org.

UNDP, 2005a. *Disaster management plan, tourism sector, Republic of Maldives*, Unpublished report, 66 pp.

UNDP, 2005b. *Design of safe shelters in Maldives*, Disaster Risk Management Unit, United National Development Programme, 79 pp.

UN/ISDR, 2004. *Living with risk: a global review of disaster reduction initiatives*, Volume II, Annexes, New York and Geneva

Disaster information gathering behavior after the Tohoku earthquake part 2: Results of foreign respondents

Michael HENRY¹, Akiyuki KAWASAKI², and Kimiro MEGURO³

¹Project researcher, International Center for Urban Safety Engineering,
Institute of Industrial Science, the University of Tokyo, Japan
mwheny@iis.u-tokyo.ac.jp

²Project associate professor,

International Center for Urban Safety Engineering,
Institute of Industrial Science, the University of Tokyo, Japan

³Professor and Director, International Center for Urban Safety Engineering,
Institute of Industrial Science, the University of Tokyo, Japan

ABSTRACT

After the March 11 Tohoku earthquake, people living in Japan were faced with confusing and conflicting messages from differing information sources which created an atmosphere of uncertainty and led many people, particularly foreigners, to relocate to western Japan or leave the country entirely. In order to improve the dissemination of information after future disasters, a survey was conducted to understand how people in the Kanto region – the most populous area of Japan and bordering the Tohoku region – received their disaster-related information and how it affected their decisions in the aftermath of the disaster. This paper focuses specifically on the responses of foreigners, as the Kanto region has the highest number of foreigners in Japan and their response in the aftermath of the earthquake – particularly those who returned to their countries – caused various difficulties for their companies and universities. Responses were received from more than 850 foreigners. This paper presents a summary of their responses, compares it to the response of Japanese nationals, and discusses some initial impressions of the disaster information gathering behavior of foreigners in Japan.

Keywords: *Tohoku earthquake, disaster information, foreigners, social media, traditional media*

1. INTRODUCTION

As introduced in the preceding paper (part one of two), disaster information is important for providing people with the resources necessary to make informed decisions and take actions. However, after the Tohoku Earthquake there emerged a growing disparity between the information given by domestic Japanese information sources and overseas sources (Sanchanta, 2011). The conflicting information and differing approaches may have

contributed greatly to the response of the foreign community in Japan. A large number of foreigners, primarily those located in regions surrounding the Fukushima Daiichi nuclear power plant, relocated to other areas of Japan or left the country entirely. This perceived mass exodus spawned the term “fly-jin,” which is a play on the Japanese word for foreigner, “gaijin.”

The difference between domestic sources and overseas sources may be explained by the objectives and target audiences of these sources. Domestic (local) coverage of a disaster is primarily concerned with response and recovery, and in the case of the Tohoku Earthquake and subsequent tsunami and nuclear disaster, Japanese sources were focused on disseminating information to people in Japan for reducing panic; the domestic sources can also help build social connections and provide emotional support (Perez-Lugo, 2004). While foreigners residing in Japan are included in this target audience, information from domestic sources is provided almost exclusively in Japanese language and those foreigners with insufficient language ability are unable to directly receive such information. As a result, they turn to information sources provided in languages which they understand – English or their native language – to gather disaster information and understand the current situation. Unfortunately, however, the target audience of overseas sources is not people residing in Japan, but those people in the region of the overseas sources. Furthermore, the objective of overseas sources is not response and recovery but focused more on mitigation – lessons learned – or the effect of the disaster on other areas. Therefore, foreigners in Japan who were looking for disaster information from overseas sources instead found a perspective which greatly differed from the actual situation around them, which may have been a contributing factor in their post-disaster actions. In addition, foreigners residing in Japan may also have been under pressure to leave Japan from their overseas families, who could only receive information from overseas sources which may not have reflected the actual situation in Japan.

To resolve these problems with differing information, it is assumed that people sought out different sources of information or accessed different forms of media. Online information seeking and social media have been growing as access to the internet becomes more widely available, and literature has found that these tools have been effective for people seeking information (Lu et al., 2007). In particular, social media provides a forum for people to disseminate and discuss disaster issues and information and to connect to one another (Palen, 2008).

Although there may be a variety of reasons for foreigners’ post-disaster actions, information-related problems may have played a large role and thus it is important to understand what these problems were and how they were resolved. The objective of this investigation, as explained in part one, is to examine and clarify people’s information gathering behavior after the Tohoku Earthquake, to understand the relationship between information and people’s actions, and to contribute to improving information dissemination in the future, particularly for reducing miscommunication and misunderstanding for foreign nationals residing in Japan. This paper – part

two of two – presents the survey results of foreigners residing in Japan at the time of the earthquake and compares them with the results of the Japanese respondents given in part one.

2. SURVEY METHODOLOGY

The survey focused on the behavior of people living in the Kanto region of Japan. Not only does this region contain Tokyo, the largest metropolitan area in Japan, but it also has the largest concentration of foreigners residing in Japan. Figure 1 shows the number of foreigners residing in Tokyo and the surrounding seven prefectures and the distribution of foreigners in the Kanto region by nationality.

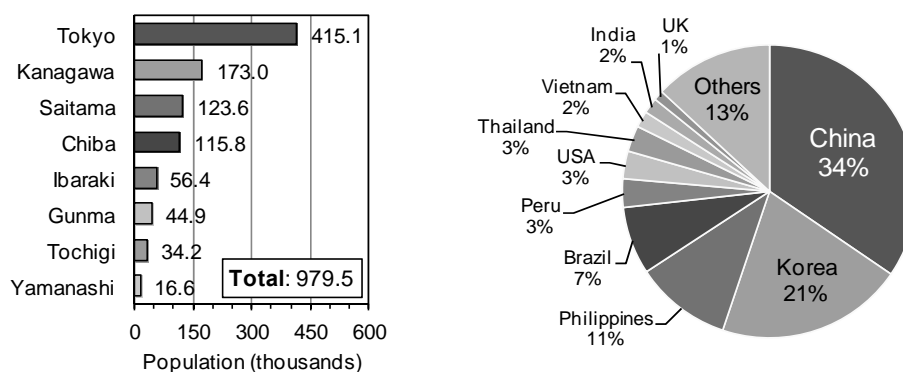


Figure 1: Number of foreigners in Kanto region by prefecture (left) and distribution by nationality (right) as of 2009
Data source: Ministry of Justice, 2009

Data on disaster information gathering behavior were collected using an online survey prepared in nine languages (Japanese, English, Chinese, Korean, Portuguese, Nepalese, French, Thai, Vietnamese). The survey contents and distribution methodology are described in full in the preceding paper (part one).

3. SAMPLE CHARACTERISTICS

The survey received 860 responses from foreigners representing 73 different countries. The distribution of the top ten countries is shown in Figure 2, where it can be seen that respondents from China made up the largest percentage. The remaining 63 countries made up 33% of the total number of respondents.

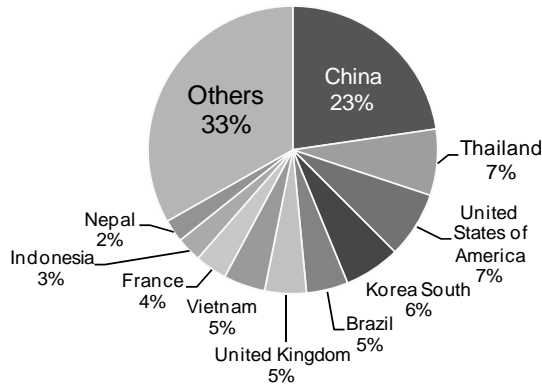


Figure 2: Distribution of respondents by country of origin

The distribution of foreign respondents by their location and occupation is shown in Figure 3. The majority were from Tokyo, followed by Kanagawa and Ibaraki Prefectures. Students made up the majority of the respondents, followed by employees at overseas and Japanese companies and Japanese educational institutions.

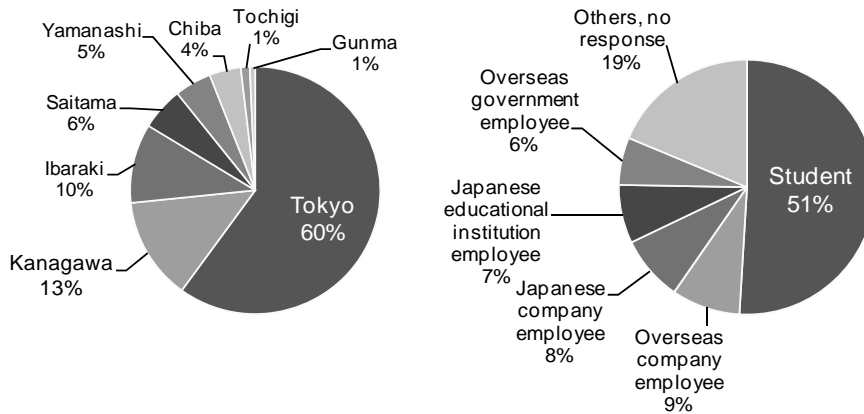


Figure 3: Distribution of respondents by location (left) and top occupations (right)

The age and income distribution of respondents are shown in Figure 4. The most responses were received from people in the 20-29 years old range, with the number of responses decreasing as age increases. The annual income of respondents fell mostly in the less than 1.95 million yen (approx. US\$24,900) range. These age and income distributions are understandable in the context of the large number of students which responded to the survey.

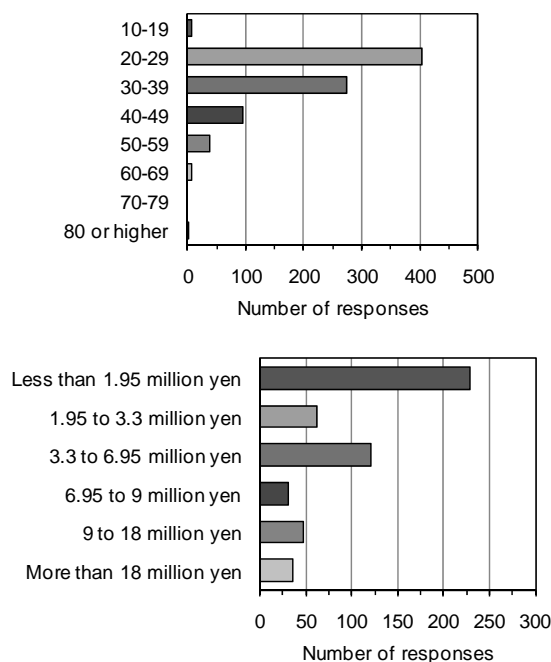


Figure 4: Distribution of respondents by age (left) and annual income (right)

Note: responses may not add up to the total as these responses were voluntary

4. SURVEY RESULTS & DISCUSSION

4.1 Information sources

Figure 5 shows the top five most-trusted information sources for foreign respondents. Japanese news sources were the most-trusted source of information, followed closely by international organizations such as the IAEA, Red Cross, and so forth. Japanese research/academic institutions, the Japanese national government, and overseas news sources rounded out the top five. For both foreigners and Japanese, Japanese news sources were the most-trusted source; in the case of the Japanese, however, there was a much larger disparity between the top most-trusted sources. Although four of the top five were the same (albeit in a slightly different order) for both Japanese and foreigners, foreigners trusted international organizations very highly whereas Japanese respondents trusted their family, friends, and colleagues very highly.

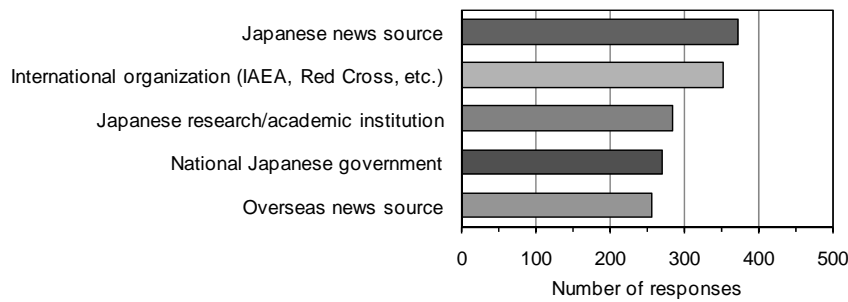


Figure 5: Top five most-trusted information sources

Figure 6 shows the top five least-trusted information sources. TEPCO topped the list, followed by overseas news sources and the national Japanese government. Similar to the case of Japanese respondents, sources which were ranked in the top five most-trusted sources also ranked in the top five least-trusted sources, such as overseas news sources, the national Japanese government, and Japanese news sources. The top five least-trusted information sources were the same for both foreigners and Japanese respondents.

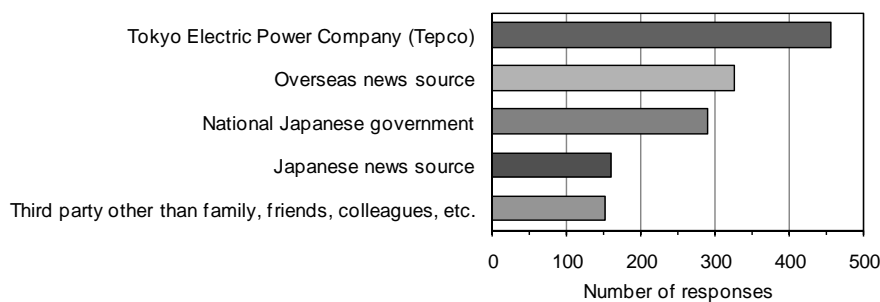


Figure 6: Top five least-trusted information sources

4.2 Media & language for information acquisition

Figure 7 shows the media and language which people used for acquiring disaster information. Japanese television and English traditional internet media were the most-utilized sources, followed by Japanese traditional internet media, English television, English social media, and other language traditional internet media. English-language was utilized more than Japanese or other languages for most types of media except television, radio, and inter-personal. For the case of inter-personal communication, other language was the most-utilized means, which can be understood in the context of the large number of non-native English speakers in the survey sample. While both Japanese and foreign respondents primarily utilized television and traditional internet media, Japanese respondents relied more highly on printed matter compared to foreigners.

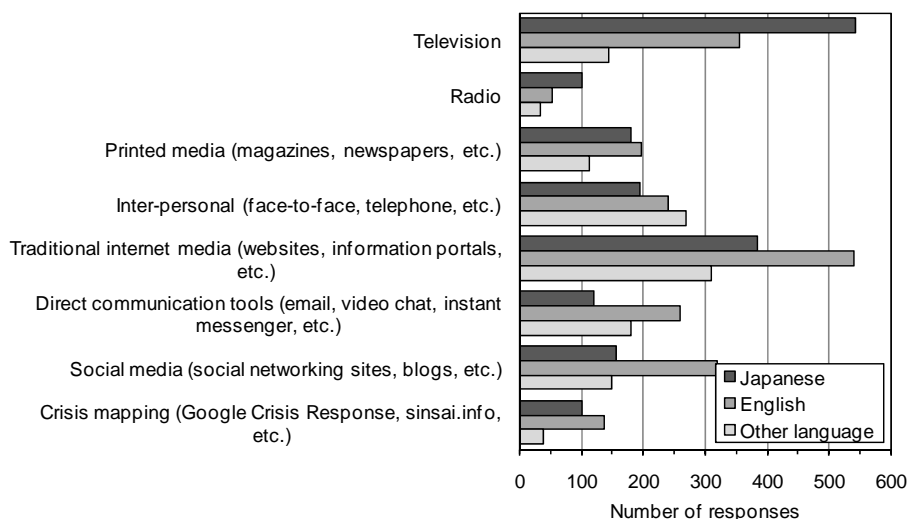


Figure 7: Utilized media and language for disaster information acquisition

Figure 8 shows by what media and language foreigner respondents would prefer to receive disaster information. English traditional internet media is the most-preferred media, followed closely by Japanese and English television. In contrast to Japanese respondents, foreigners had little preference for radio or printed media, understandable as these media are primarily only widely available in Japanese. Except in the case of television, English was the preferred language for acquiring disaster information.

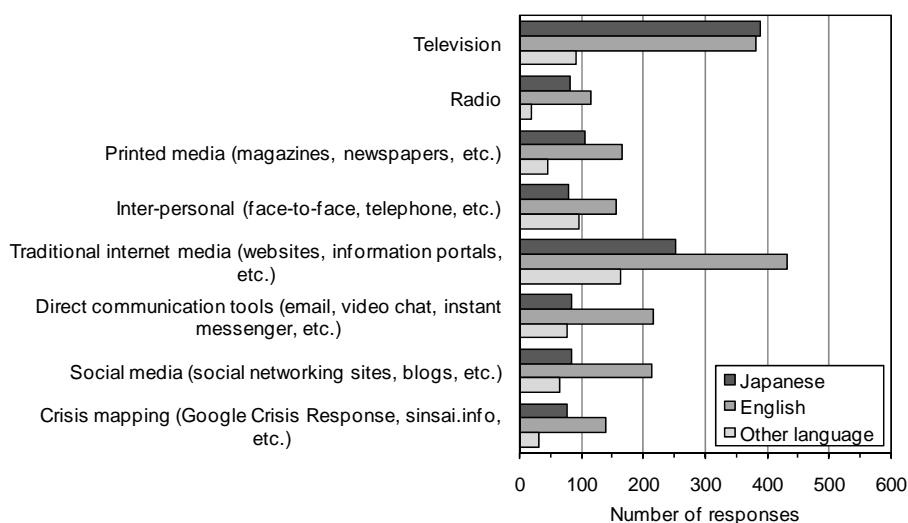


Figure 8: Preferred media and language for disaster information acquisition

4.3 Importance of information

Figure 9 shows the importance of information types for foreigners as it changed over time. On the first day, the safety of family and friends was by far the most important information. Although foreigners were also concerned about the earthquake and tsunami damage and transportation systems, they were much less concerned about these two types of

information, relative to their concern about safety of family and friends, than Japanese respondents were. By the first week, there was a large jump in the importance of information related to radiation level and risk, food and water supply, government response, electricity and other utilities, and school and business continuity. Except for radiation level and risk and government response, this change in importance for foreigners was much different than the change for Japanese nationals, for whom the importance of most information increased only slightly or decreased. By the second week, however, the importance of all the information types had decreased from the first week, with radiation level and risk remaining the most important information type.

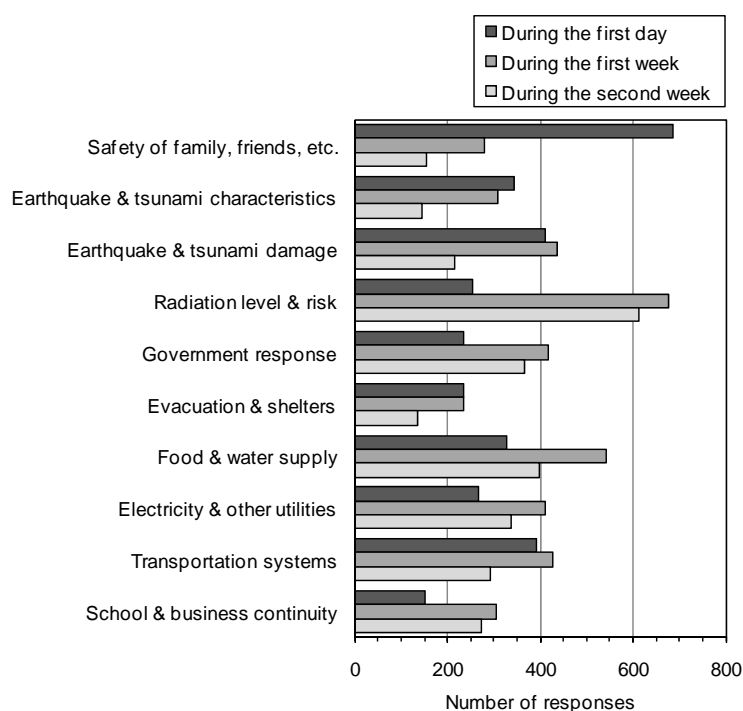


Figure 9: Importance of information types over time

4.4 Problems related to information

Figure 10 shows what information foreigners found to be unavailable, unclear, or hard to understand over the same time period. For the first day, information related to radiation level and risk was the hardest to find or understand, followed by the safety of family and friends and government response. In contrast, Japanese respondents had a harder time finding or understanding information related to transportation systems, perhaps because it had higher importance to Japanese respondents on the first day. By the first week, the difficulty in finding or understanding information related to radiation level and risk, government response, food and water supply, and electricity and other utilities had increased from the first day, following the increase in importance in these types of information over the same time period. From the first to second weeks, the difficulty in finding or understanding information decreased for all information types, similar to the Japanese respondents.

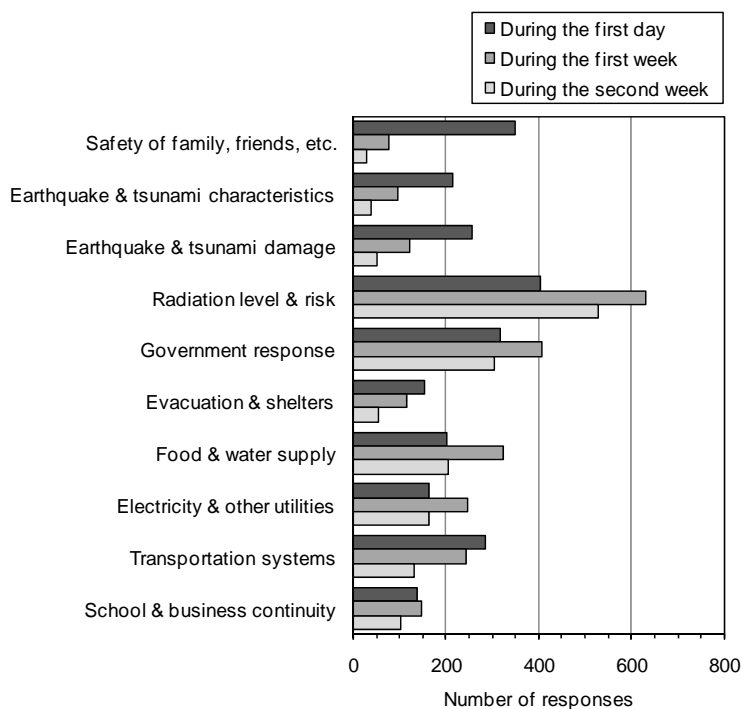


Figure 10: Unavailable, unclear, or hard to understand information over time

Figure 11 shows the reasons why the previously-discussed information was unclear or hard to understand. Similar to the Japanese case, the primary reason was that people were confused by conflicting or differing information, followed by the inability to access information due to mobile congestion, power outage, etc. However, for foreigners the inability to understand information due to a lack of language comprehension was the third-highest reason, whereas this reason was barely observed for Japanese respondents.

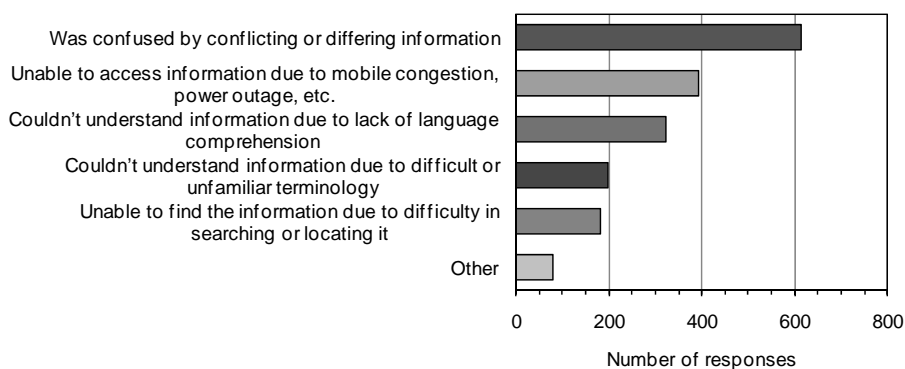


Figure 11: Reasons information was unclear or hard to understand

Figure 12 shows what media and language foreigners turned to in order to clarify problems they had with information. English traditional internet media was the most preferred method, followed by Japanese television, English social media, and Japanese and other language traditional internet media. The media type for foreigners was similar to that of Japanese

respondents, but the primary language was generally English except for television. Interpersonal communication in other languages was also highly rated.

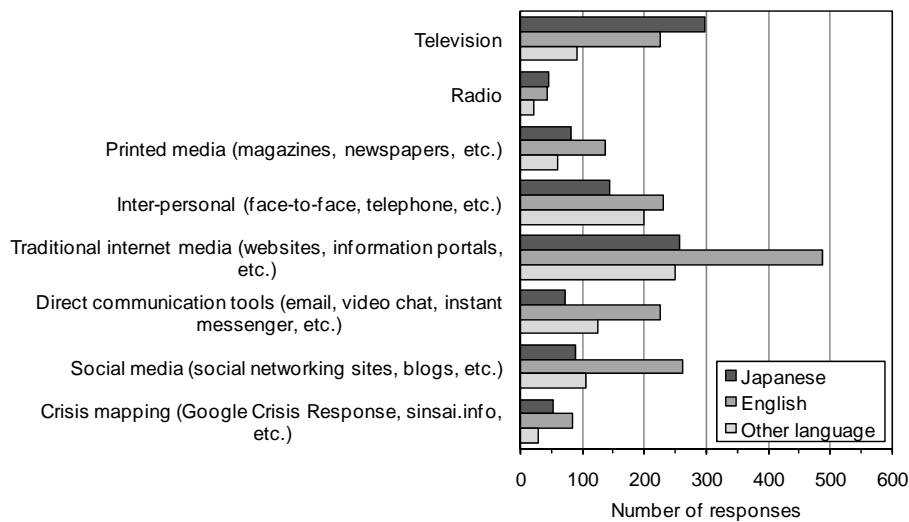


Figure 12: Media and language for clarifying information problems

4.5 Early warning system and rotating blackouts

The distribution of foreigners who were familiar with the Japanese Earthquake Early Warning System and whether respondents could properly receive information on the rotating blackouts is shown in Figure 13. In contrast to the Japanese respondents, slightly more than half of the foreign respondents were unfamiliar with the early warning system. The distribution of whether people could receive blackout information was, however, similar to Japanese respondents.

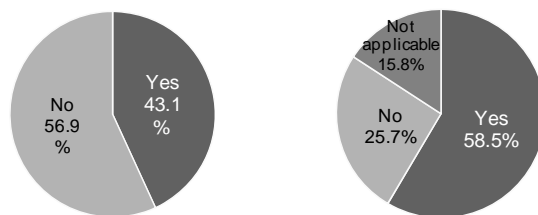


Figure 13: Distributions of whether respondents were familiar with the early warning system before the earthquake (left) and whether they could receive information on the rotating blackouts (right)

4.6 Post-disaster relocation & usefulness of information

The survey also asked people whether they remained in the Kanto area, relocated to another area of Japan, or left Japan within two weeks after the earthquake. In Figure 14, it can be seen that, among foreigners, most people chose to remain in the Kanto area, but a large number also chose to leave Japan. It can be seen in Figure 15 that, of those who left or relocated, the number increased from within 1 day to within 1 week, then decreased again.

Although the number of foreigners who left or relocated was much greater than the number of Japanese in this survey, the timing of leaving or relocating followed a similar pattern.

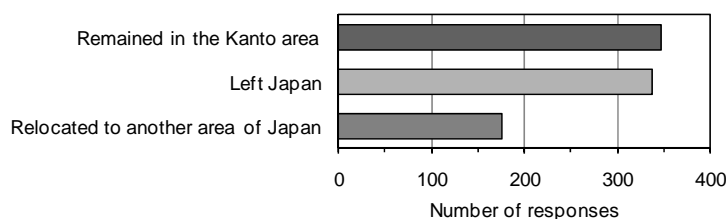


Figure 14: Distribution of whether respondents stayed, relocated, or left

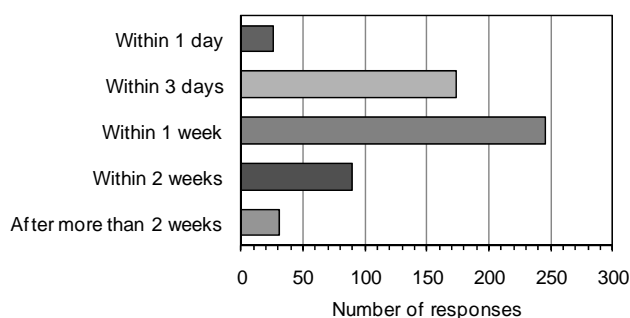


Figure 15: Timing of relocation or leaving

Figure 16 shows that the main reason for whether foreigners stayed, relocated or left was that it was a personal decision. Unlike the case of the Japanese respondents, where personal decision was by far the primary reason, a relatively large number of responses for family request and job obligation were also received. Overall, disaster-related information appeared to be somewhat useful for foreigners as well as Japanese respondents, as shown in Figure 17.

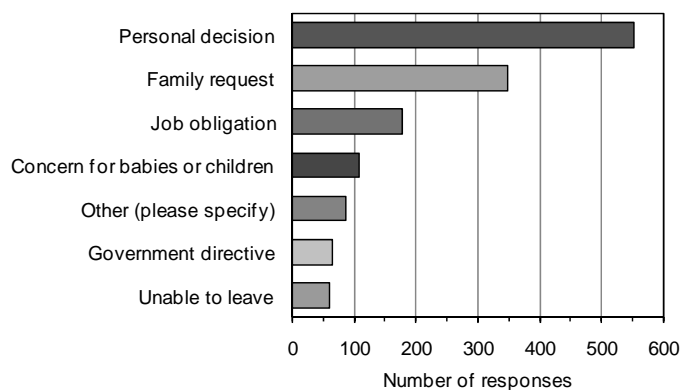


Figure 16: Reasons for staying in Kanto, relocating, or leaving Japan

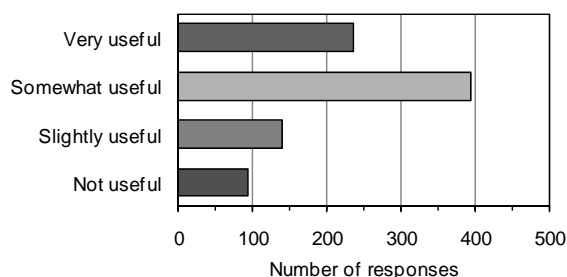


Figure 17: Usefulness of disaster-related information for decision making

5. INITIAL IMPRESSIONS AND FURTHER ANALYSIS

One of the goals of this investigation is to improve the dissemination of disaster-related information after future disasters, particularly considering the needs of foreigners residing in Japan. In order to make recommendations towards such improvement, it is necessary to consider from which sources information should be disseminated and by what media, as well as what information is important and how the importance of that information changes over time.

Similar to the case of the Japanese respondents, several sources which were in the top five most-trusted information sources were also in the top-five least-trusted sources. For foreigners, the most-trusted sources which were not in the top five least-trusted sources were international organizations and Japanese research/academic institutions. Foreigners may have turned to international organizations as these are experienced in providing support for people in various countries around the world, and thus are better at disseminating information for a varied audience. Japanese research/academic institutions were also one of the most-trusted sources for Japanese respondents, suggesting that these institutions may be able to play a strong role in disseminating disaster information targeted not only at Japanese people but also at foreigners as well.

The media foreigners used for gathering information were primarily in English, except for Japanese television and other language for interpersonal communication. Television is useful for disseminating disaster information as it can provide frequent updates with accompanying visuals and discussions, but the majority of domestic television is provided in Japanese only; this may have driven foreigners to internet-based resources or to their friends, family, or colleagues. As English language was preferred for internet-based media, this may be a possible method for improving information dissemination. However, as mentioned in part one, these results may be biased towards people who tend to use the internet regularly, as the survey was distributed online.

Similar to the case of the Japanese respondents, the trends of information importance and the unavailability or difficulty in understanding information were fairly similar over time for foreign respondents. The results verified that conflicting or differing information was the primary

reason causing information difficulties, but understanding whether this caused foreigners to relocate or leave Japan will require further analysis. However, compared to the Japanese sample a much larger number of foreigners relocated or left Japan. While the top reason for their action (remaining, relocating, or leaving) was personal decision, the second-highest reason was family request. This possibly supports the theory that overseas families who received information from overseas sources placed pressure on their relatives in Japan to take some action, but these results are going to require deeper analysis to determine which reasons corresponded with which actions.

The next step in analyzing these results will be to more deeply examine the relationship between demographic factors, such as nationality, occupation, age, language ability, and so forth, and the information gathering behavior, as well as the correlation with post-disaster actions. The results of the deeper analyses should form the basis for the recommendations for improving the dissemination of disaster information.

REFERENCES

Lu, H.Y., Case, D.O., Lustria, M.L.A., Kwon, N., Andrews, J.E., Cavendish, M.A., Floyd, B.R., 2007. Predictors of online information seeking by international students when disaster strikes their countries. *CyberPsychology and Behavior* 10(5), 709-712.

Ministry of Justice, 2009. Statistics of registered foreigners. Available from:

<http://www.stat.go.jp/data/jinsui/2008np/index.htm> (27 September 2011)

Palen, L., 2008. Online social media in crisis events. *Educause Quarterly* 3, 76-78.

Perez-Lugo, M., 2004. Media uses in disaster situations: a new focus on the impact phase. *Sociological Inquiry* 74(2), 210-225.

Sanchanta, M., 2011. Japanese, foreign media diverge. *The Wall Street Journal*. Available from:

<http://online.wsj.com/article/SB10001424052748703512404576209043550725356.html> (27 September 2011).

Survey on people's awareness of Earthquake Early Warning before and after the 2011 off the Pacific Coast of Tohoku earthquake

Miho OHARA¹, Kimiro MEGURO² and Atsushi TANAKA

¹ Associate Professor, Interfaculty Initiative in Information Studies
/ Institute of Industrial Science,
The University of Tokyo, Japan
ohara@iis.u-tokyo.ac.jp

² Professor, Interfaculty Initiative in Information Studies
/ Institute of Industrial Science,
The University of Tokyo, Japan

³ Professor, Interfaculty Initiative in Information Studies,
The University of Tokyo, Japan

ABSTRACT

Japan Meteorological Agency started the service of Earthquake Early Warning (EEW) to the public since October 1, 2007. The warning is widely broadcasted by TV, radio and mobile phone in the area whose JMA intensity is expected to be more than 4. In order to make the best use of the lead time before the arrival of strong tremors for reducing casualties, enhancing people's knowledge and capacity to take proper actions after the warning is essential.

There was a small earthquake in Fukushima Prefecture on September 29, 2010. The expected intensity in the Tokyo metropolitan area exceeded 4 and EEW was provided although observed intensity was less than 4. Recently, the percentage of the people who can get EEW by mobile phones is increasing. At this earthquake, a lot of people received the warning by mobile phone in the Tokyo metropolitan area and it became a good opportunity for making people familiar with EEW. After this, the off the Pacific coast of Tohoku Earthquake occurred on March 11, 2011 and numerous aftershocks continued. EEW was successfully provided in Tohoku area at the main shocks. On the other hand, in the Tokyo metropolitan area, EEW failed at the main shock but frequently announced at aftershocks. However, some of the warning at aftershocks failed to estimate intensity properly due to technical limitation.

In this paper, two questionnaire surveys were conducted to understand people's awareness of EEW. The first one was done after the earthquake in September 2010 for the people who received the warning by mobile phone. The second one was done after the earthquake in Tohoku region in March 2011. The change of their awareness was analyzed comparing both results. Their behavior after receiving the warning was also analyzed and

suggestions for enhancing their capacity to take proper actions after EEW were obtained.

Keywords: early warning, capacity building, questionnaire survey

1. INTRODUCTION

The Japan Meteorological Agency (JMA) began to provide the service of earthquake early warning (EEW) to the public on October 1, 2007. This is a new system that quickly analyses seismic wave data observed by seismographs near the epicenter and provides prompt alerts before the arrival of strong tremors (S-waves) as shown in figure 1. For public use, EEW is provided to the regions where the intensity of shaking was expected to be greater than JMA 4 in case the maximum estimated intensity is 5 lower. This system aims to mitigate earthquake-related damage by enabling individuals to protect themselves quickly in various environments such as houses, offices and factories. A warning is widely broadcasted by television, radio, mobile phone and loudspeakers.

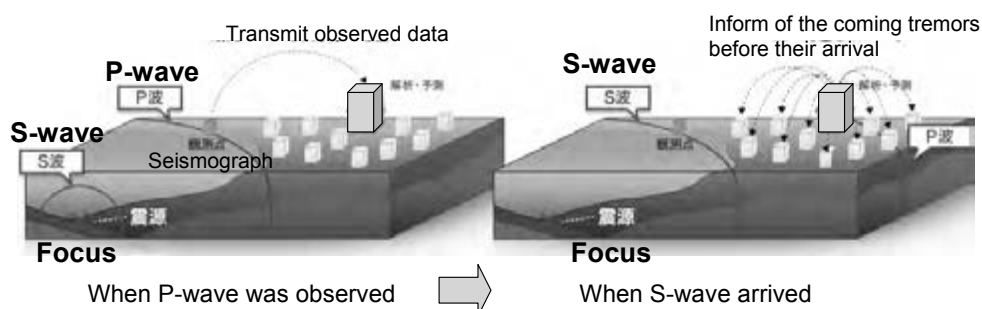


Figure 1: Concept of Earthquake Early Warning

The Iwate-Miyagi Inland Earthquake occurred in the southern inland region of Iwate Prefecture, Japan at 8:43 JST, June 14, 2008. It was the first earthquake since October 2007 for which EEW could be successfully broadcasted before the arrival of strong tremors. The lead time between the warning and the arrival of strong tremors was around 10-25 seconds in the area surrounding its epicenter. After this, a small earthquake occurred in Fukushima Prefecture at 16:59 JST on September 29, 2010. EEW was broadcasted in the eastern area of Japan as the expected intensity exceeded 4. It was broadcasted also in the Tokyo metropolitan area although observed intensity was less than 4. Recently, the percentage of the people who can get EEW by mobile phones is increasing. At this earthquake, a lot of people received the warning by mobile phone in the Tokyo metropolitan area for the first time and it became a good opportunity for making people familiar with EEW.

The 2011 off the Pacific coast of Tohoku Earthquake occurred at 14:46 JST on March 11, 2011 and numerous aftershocks continued. EEW was successfully provided in Tohoku area at the main shocks. On the other hand, in the Tokyo metropolitan area, EEW failed at the main shock but was

frequently announced at aftershocks. The number of broadcasted EEW from March 2011 to August 2011(6 months) was 87 although that number from October 2007 to February 2011(41 months) was 17. However, some of the numerous warning at aftershocks failed to estimate intensity properly because several earthquakes occurred at the same time could not be identified separately or some seismometers were unusable due to long-time power outage after the earthquake. These problems were due to technical limitation of EEW and some of them were solved by program modification after March 2011.

In this paper, two questionnaire surveys were conducted to understand people's awareness of EEW. The first one was done after the earthquake in September 2010 for the people who received the warning by mobile phone. The second one was done after the earthquake in Tohoku region in March 2011. The change of their awareness was analyzed comparing both results. Their behavior after receiving the warning was also analyzed and suggestions for enhancing their capacity to take proper actions after EEW were obtained.

2. OUTLINE OF TWO QUESTIONNAIRE SURVEYS

The first questionnaire survey was done after the earthquake in Fukushima Prefecture on September 29, 2010. Main target of the survey was the people living in the Tokyo Metropolitan area (Tokyo, Saitama, Chiba, Kanagawa Prefectures) who received the warning by their own mobile phone or neighbor's mobile phones. The number of respondents in each group was shown in table 1. The second survey was done after the earthquake in Tohoku region in March 2011. A questionnaire sheet was sent to the same respondent as the first survey. The ratio of the respondents who answered the second survey was 76.6%(613 people among 800). The number of the group A respondents who answered the survey in 2011 was 153. Among them, 11 people changed their mobile phones and could not receive EEW as of March 2011. The number of the respondents in each group who answered the survey in 2011 and could receive EEW as of March 2011 was shown in table 1.

Table 1: Number of respondents for surveys in 2010 and 2011

	2010 Survey		2011 Survey				Ratio of the respondents who answered the second survey	
			Could receive EEW by mobile phone as of March 2011			Could not receive EEW by mobile phone as of March 2011		total
				Received at home after march 2011	Received outside home after march 2011			
A	Received EEW by their own mobile phones	200	142	118	91	11	153	76.5
B	Received EEW by their neighbors' mobile phones	200	70	48	42	81	151	75.5
C	Received EEW by their own mobile phones and experienced the stop of train	200	119	65	52	31	150	75
D	Didn't receive or listen EEW	200	71	49	36	88	159	79.5

3. RESPONDENTS' KNOWLEDGE OF EARTHQUAKE EARLY WARNING

At first, change of respondents' knowledge of EEW was analyzed comparing the results of two surveys. All the groups had the same tendency between 2010 and 2011. Figure 1 shows the result of group A for example. After the earthquake in September 2010, 50.3% knew both the name of EEW and that it forecast a strong tremor just before its arrival. After the experience of the main shock and aftershocks of Tohoku earthquake in 2011, the ratio increased to be 89.5%. At the survey in 2011, the respondents who knew neither its name nor its meaning were drastically decreased to be 2.0%.

Figure 8 shows the respondents' knowledge of methods or conditions of EEW broadcasting. It is a result of group A for example as all the groups had the same tendency between 2010 and 2011. The ratio of the respondents who knew that EEW is broadcasted on TV or by mobile phone increased after 2010 and exceeded 90% in 2011. On TV, the name of the area where strong tremors are expected and the warning message are shown. On the other hand, neither expected intensity nor lead time before the arrival of strong tremors is explained. The knowledge on expected intensity or lead time was low in 2010 but increased especially in 2011. However, knowledge of criteria on intensity at which EEW is broadcasted was still low. In addition, change in the knowledge of special receiving devices was very small although the special receiving devices are important tools for receiving expected intensity or lead time at home. Enhancing these knowledges is necessary.

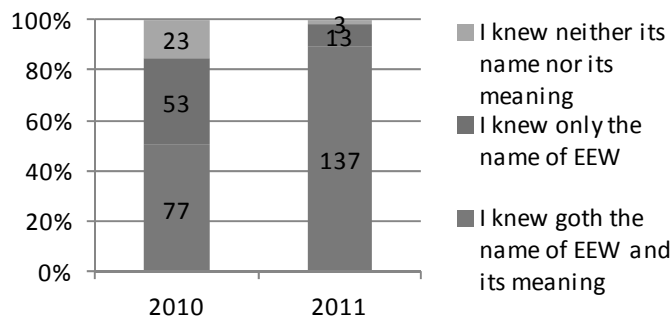


Figure 2: Respondents' knowledge of EEW

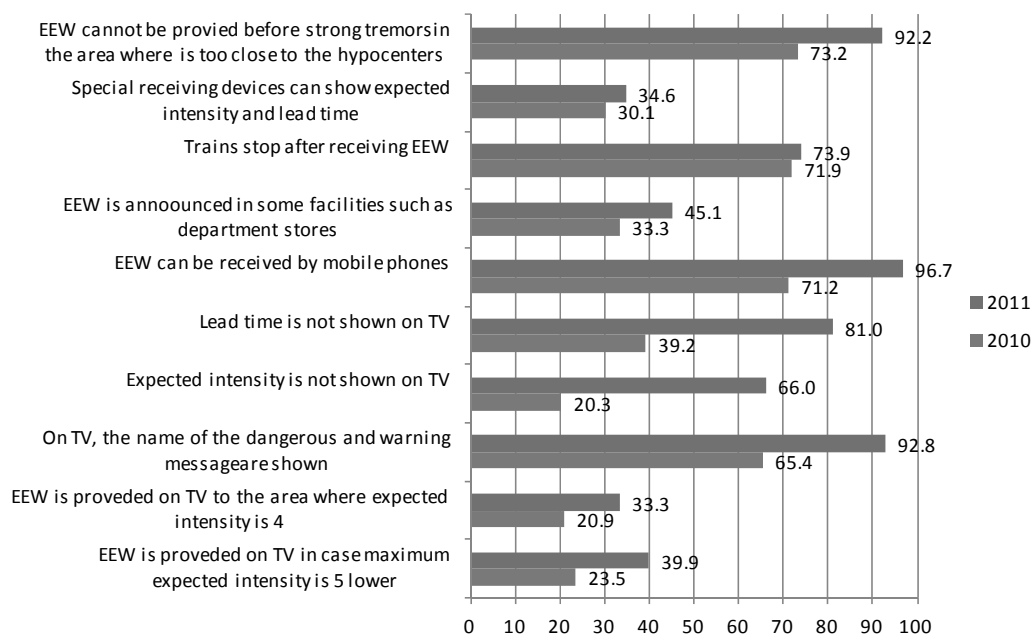


Figure 3: Respondents' knowledge of methods or conditions of EEW broadcasting

4. RESPONDENTS' ATTITUDE TOWARD FAILURE OF EARTHQUAKE EARLY WARNING

After the earthquake on March 11, 2011, numerous EEW was provided to the public due to continuous aftershocks. However, some of them failed to estimate intensity properly because several earthquakes at the same time could not be identified separately or some seismometers were unusable due to long-time power outage after the earthquake. These problems were due to technical limitation of EEW and were announced beforehand by Japan Meteorological Agency. Here, the knowledge of technical limitation before the earthquake and their attitude toward the failure of EEW were analyzed. 36.5% of the respondents among all knew the technical limitation before March 2011 that actual intensity can be more or less than the expected intensity within the range of intensity 1. About 90% of the respondents wished to use EEW even if it has a risk of failure regardless of whether they knew technical limitation before the earthquake or not. 55.4% of the respondents with the knowledge of technical limitation answered that they would like to use EEW aggressively even if they have a risk of failure. The ratio decreased to be 35.0% without the knowledge. It was verified that familiarization with technical limitation before the event is important in order to increase positive attitude in case that EEW fails.

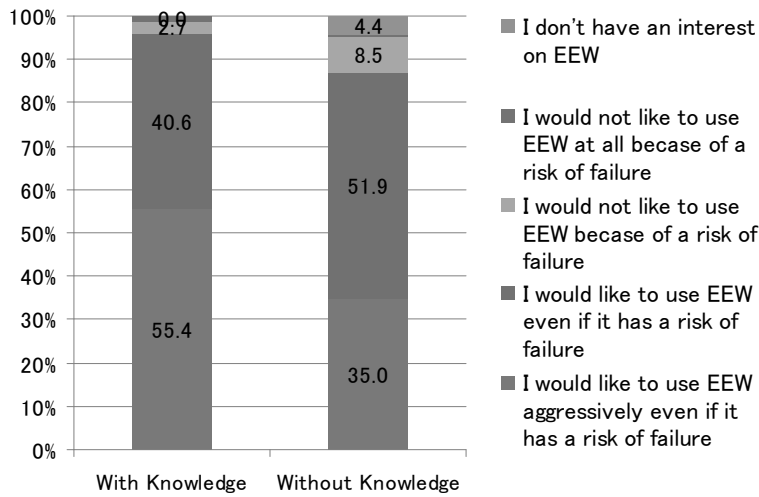


Figure 4: Respondents' attitude toward failure of EEW

5. RESPONDENTS' RESPONSE TO EARTHQUAKE EARLY WARNING

Next, respondents' response to EEW after EEW was investigated. More than 80% of each group watched EEW on TV at home after March 2011. The ratio of the respondents who received EEW at home was highest in group A. 88.4% of group A watched EEW on TV and 80.3% received by mobile phone at home. 59.4% received by mobile phone outside home. The feeling of respondents in group A after receiving EEW at home was investigated. Figure 5 is the comparison of their feeling after earthquakes in 2010 and 2011. The ratio of the respondents who thought that strong tremor would come soon drastically increased from 34% to 86.7%. It shows that experience of receiving many EEW after March 2011 led to high awareness of warning message.

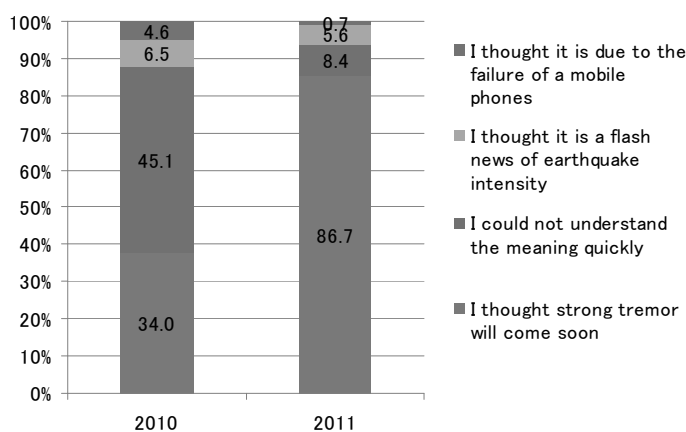


Figure 5: Respondents' feeling after receiving EEW

Figure 6 shows what respondents in group A did immediately after receiving EEW at home at the both earthquakes. Most frequent response after both earthquakes was to get earthquake information from television or

radio. The second one was to wait and the third one was to inform their children or people near them of the EEW. The ratio of the response for informing their children or people near them, protect their bodies, protect their children or elderly family members increased in 2011. The aim of EEW service is to enable residents to quickly protect themselves before the arrival of strong tremors. Considering this aim, it is said the experiences of receiving many EEW after March 2011 enhanced their capacity to take actions for protecting themselves or family members.

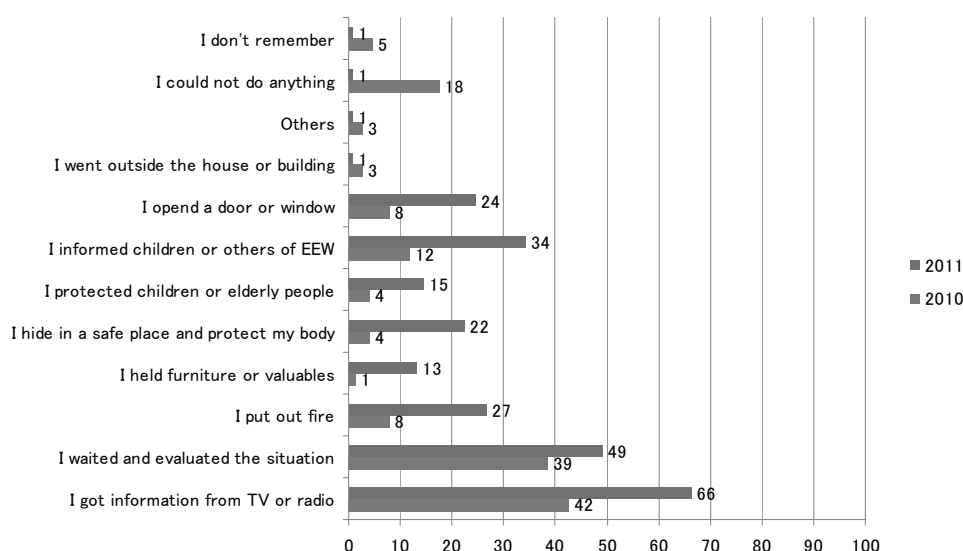


Figure 6: Respondent's action after receiving EEW

6. RESPONDENTS' OPINION ON EFFECTIVENESS OF EARTHQUAKE EARLY WARNING

Finally, their opinion on effectiveness of EEW was investigated. The ratio of the respondents who thought EEW was very effective for mitigating seismic damage was about 40% at the both survey in 2010 and 2011. Including the respondents who thought it is effective, the total ratio of positive respondents amounted to be about 90%. When we focused on the relationship between their opinion and the experience of receiving EEW after March 2011, the ratio of the respondents who thought to be very effective was 38.5% as shown in figure 7. It was verified that real experience of receiving EEW enhanced the understanding of effectiveness of EEW. Figure 8 is the relationship between their opinion and the knowledge on technical limitation before the earthquakes. In the chapter four, we found that familiarization with technical limitation before the event increased positive attitude toward the failure of EEW. In figure 8, the ratio of the respondents who thought to be very effective was 54.5% in case they had knowledge on technical limitation before the earthquake. This value was almost twice of the ratio in case of respondents without the knowledge. It is concluded that making people familiar with technical limitation led to their positive attitude toward EEW and it can increase high evaluation on the effectiveness of EEW

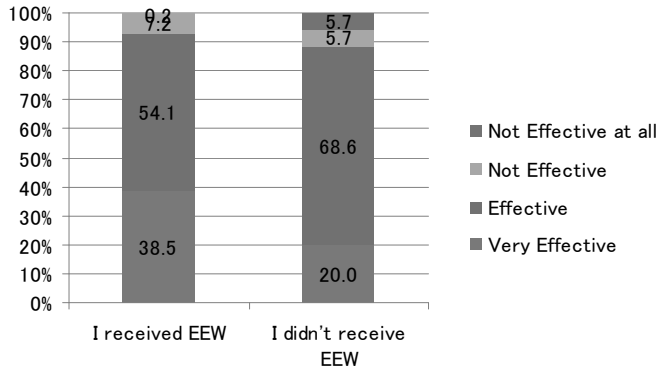


Figure 7: Relationship between understanding of effectiveness and the experience of receiving EEW

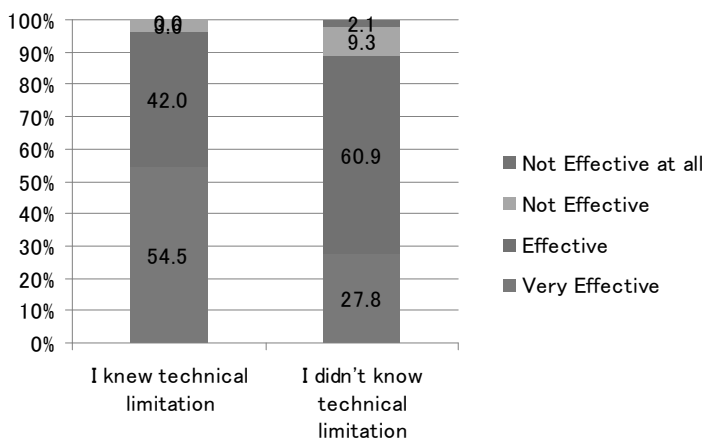


Figure 8: Relationship between understanding of effectiveness and the knowledge on technical limitation

7. CONCLUSIONS

In this paper, two questionnaire surveys were conducted to understand people’s awareness of EEW. The first one was done after the earthquake in September 2010 for the people who received the warning by mobile phone. The second one was done after the earthquake in Tohoku in March 2011. The change of their awareness was analyzed comparing both results.

After the experience of the main shock and aftershocks of Tohoku earthquake in 2011, knowledge of EEW among residents drastically increased. Some of the knowledges were low still in 2011 and required to be enhanced. Their behavior after receiving the warning was also analyzed. The ratio of the respondents who thought that strong tremor would come soon drastically increased from 34% in 2010 to 86.7% in 2011. It shows that experience of receiving many EEW after March 2011 led to high awareness of warning message. In 2011, the ratio of the response for informing their children or people near them, protect their bodies, protect their children or elderly family members increased, compared with the answers in 2010. The experiences of receiving many EEW after March 2011 enhanced their

capacity to take actions for protecting themselves or family members. People's awareness level and capacity can decrease easily as time passes after the disaster. It is very important to keep their awareness level by education or training in the future.

After the earthquake on March 11, 2011, numerous EEW was provided to the public due to continuous aftershocks. However, some of them failed to estimate intensity properly due to technical limitation. From the survey, familiarization with technical limitation before the earthquakes increased positive attitude in case that EEW failed. It also increased high evaluation of the effectiveness of EEW. Continuous information dissemination on technical limitation is important for positive attitude for taking action after receiving EEW,

REFERENCE

The Japan Meteorological Agency: *A List of Past Earthquake Early Warning*,

Website:

<http://www.seisvol.kishou.go.jp/eq/EEW/kaisetsu/joho/joho.html>

The Japan Meteorological Agency: *Earthquake Early Warning provided after the 2011 off the Pacific coast of Tohoku Earthquake*, JMA News Release, 2011.3.29.

The Japan Meteorological Agency: *Improvement of Earthquake Early Warning*, JMA News Release, 2011.8.10

Seismic risk evaluation on existing RC frame buildings for northern part of Sylhet city, Bangladesh

Ram Krishna MAZUMDER¹, Mushtaq AHMED²
and Mehedi Ahmed ANSARY³

¹Research Engineer, SHMRBBP, BUET, Bangladesh

²Associate Professor, Department of CEE, SUST, Bangladesh

³Professor, Department of Civil Engineering, BUET, Dhaka, Bangladesh
ansary@ce.buet.ac.bd

ABSTRACT

Bangladesh is one of the most earthquake prone countries in South Asia where Sylhet City is located. To evaluate the existing condition of Reinforced Concrete Frame Buildings, a multiple level assessment of the seismic vulnerability of 194 Buildings in northern part of Sylhet City, is presented. From the Tier1 assessment, 26% of the buildings performance score was low and 74% of buildings performance score was comparatively good. In Tier 2, it was revealed from the study that about 11% of the buildings fall under high risk group, 20% of the buildings fall under moderate risk group and 70% of the buildings in low risk group.

Keywords: *Immediate Occupancy, Life Safety, RC Buildings, Seismic Risk and Sylhet City*

1. INTRODUCTION

Bangladesh is running a high risk of Earthquake. The recent earthquake in India, Pakistan and Tsunami in Asia are the warning for Bangladesh. Specialists are expecting a severe earthquake in this area in near future, which will cause a serious human casualty, damages of infrastructure and other losses. One of them is the Dauki fault at the bordering area of Sylhet – Meghalaya about 70 km from Sylhet City. There are many seismic faults in the plains around Dhaka and Chittagong Hill Tracts, which can cause earthquakes. No earthquake occurred in these faults for many years, which means huge strength has gathered underground that could cause serious earthquakes in Bangladesh and its neighboring areas any time.

A recent study by OYO International Corporation (OIC), proposed five earthquake scenarios, where each scenario was set as a maximum possible earthquake (Mw) occurring within a fault zone, there are five major fault zones in Figure 1, i.e. Madhupur fault, Dauki Fault, Plate Boundary Fault -1, Plate Boundary Fault -2 and Plate Boundary Fault -3. In addition

to five scenarios, a special earthquake scenario where a magnitude-6 earthquake is occurring beneath Sylhet City was recommended, (OIC, 2009).

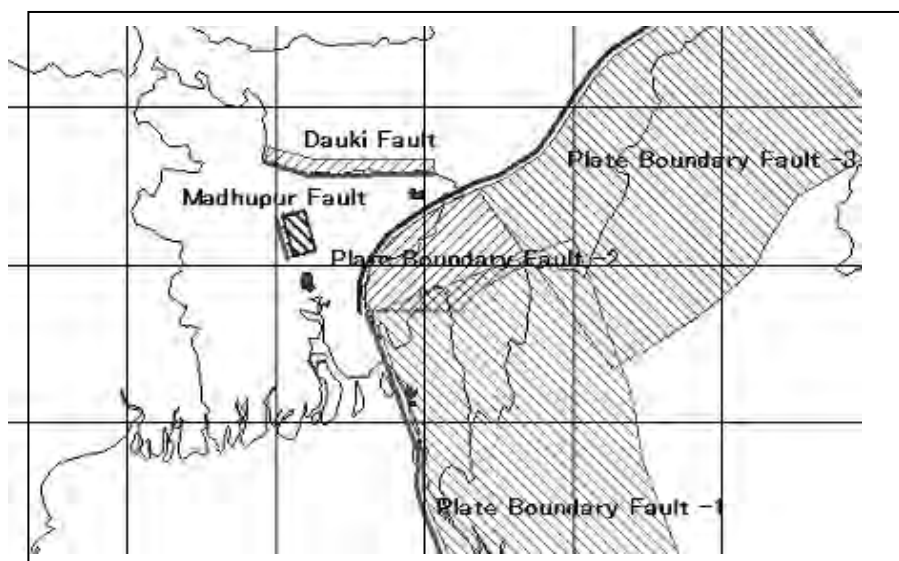


Figure 1: Earthquake Fault Model in Bangladesh, (OIC, 2009)

Table 1: Earthquake Scenario Parameters for Sylhet City, (OIC, 2009)

Case	M _w	Depth to fault (km)	Dip Angle	Fault type	Name of fault	Distance to Fault (km)
1	8	3	60°	Reverse	Dauki Fault	> 70
2	8.3	3	30°	Reverse	Plate Boundary Fault -3	> 90
3	6	15	90°	Reverse	M _w 6.0 beneath city	-

For determination of the addresses of seismically vulnerable buildings within the existing building stock of ward no. 9 of Sylhet City Corporation (SCC), a multiple level assessment technique (Ozcebe et al., 2006) is applied. Only RC frame buildings are considered in this study. This seismic vulnerability evaluation method can be classified in three main groups depending on their level of complexity. The first, most simple level is known as “Walkdown Evaluation”. In this first level, does not require any analysis and its goal is to determine the priority levels of buildings that require immediate intervention.

Preliminary assessment methodologies are applied when more in-depth evaluation of building stocks is required. In this stage, simplified analysis of the building under investigation is performed based on a variety of methods. These analyses require data on the dimensions of the structural and non-structural elements in the most critical storey.

The procedures in third tier employ linear or nonlinear analyses of the building under consideration and require the as-built dimensions and the reinforcement details of all structural elements.

This paper represents the first two level methodology used for assessing seismic vulnerability and a summary of the assessment being done for ward no. 9 of SCC area.

2. STUDY AREA

Ward no. 9 of the SCC is mainly consists of madina market, bagbari, akhalia, kanishail, surma and tapaban zones. Figure 2 represents the ward number 9 in the SCC map. It has the area of 247 acres with approximately 12000 populations with 2789 structures (Population Census, 2006). Different types of occupancy under the ward no. 9 were surveyed. In first tier, 194 RC frame buildings out of 1373 were surveyed. In second tier, 19 buildings resulted from first tier were analyzed.

Table 2: Different Type of Buildings in ward no. 9
(Population Census, 2006)

Structure (No. of buildings)					
Concrete		Masonry		Tin Shed + Bamboo + Other	Total
RC Frame	Lightly RC Frame	Brick in Cement Mortar Masonry with Concrete Floor	Brick in Cement Mortar Masonry with Flexible Roof		
1,373	60	77	1,124	155	2,789

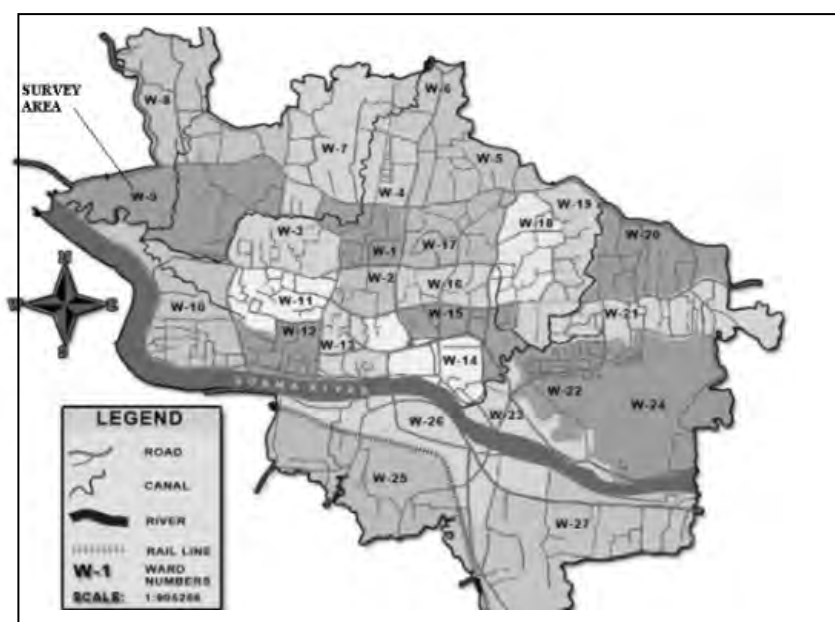


Figure 2: Location of the ward no. 9 of Sylhet City Corporation

3. METHODOLOGY

3.1 Tier 1: The Walk down Evaluation

The Walkdown evaluation procedure consists of taking notes of different external feature of the buildings. Buildings are described as belonging to high risk, moderate risk or low risk. The building features considered are described below:

(a) Number of Stories: This is the total number of floors above the ground level.

(b) Existence of a soft Storey: A soft storey usually exists in a building when one particular storey, usually employed as a commercial space, has less stiffness and strength compared to the other stories.

(c) Existence of heavy Overhangs: Heavy balconies and overhanging floors in multi-storey reinforced concrete buildings shift the mass center upwards; accordingly give rise to increased seismic lateral forces and overturning moments during earthquakes.

(d) Apparent Building Quality: A close relationship has been observed between apparent quality and experienced damage during recent earthquakes in Turkey.

(e) Existence of short Columns: Frames with partial infill lead to the formation of short columns which sustain heavy damage since they are not designed for the high shear forces due to shortened heights that will result from a strong earthquake.

(f) Pounding Effect: When there is no sufficient clearance between adjacent buildings, they pound each other during an earthquake as a result of different vibration periods. Uneven floor levels aggravate the effect of pounding.

(g) Topographic Effects: Buildings on slopes steeper than 30 degrees have stepped foundations, which cannot distribute ground distortions evenly to structural members above.

(h) Local Soil Conditions: The intensity of ground motion at a particular site predominantly depends on the distance the causative fault and local soil conditions. As there exists a strong correlation between Peak Ground Velocity and the shear wave velocities of local soils, in this study the PGV is selected as to represent the ground motion intensity. The intensity zones are expressed accordingly, in terms of the associated PGV ranges.

Zone I: $60 < \text{PGV} < 80 \text{ cm/s}^2$
Zone II: $40 < \text{PGV} < 60 \text{ cm/s}^2$
Zone III: $20 < \text{PGV} < 40 \text{ cm/s}^2$

Based on their number of stories and the seismic hazard level at the site buildings are assigned different base scores as shown in Table 3.

Table 3: Base Scores and Vulnerability Scores for Concrete Buildings, (Sucuoglu et al., 2003)

No. of Stories	Base Scores (BS)			Vulnerability Scores (VS)					
	Zone I	Zone II	Zone III	Soft Storey	Heavy Overhang	Apparent Quality	Short Column	Pounding	Topo. Effects
1 or 2	100	130	150	0	-5	-5	-5	0	0
3	90	120	140	-15	-10	-10	-5	-2	0
4	75	100	120	-20	-10	-10	-5	-3	-2
5	65	85	100	-25	-15	-15	-5	-3	-2
6 or 7	60	80	90	-30	-15	-15	-5	-3	-2

Once the vulnerability parameters of a building are obtained from walk down surveys and its location is determined, the seismic performance score, PS, can be calculated by using Eq. 1. The base scores, BS, the vulnerability scores, VS, and the vulnerability score multipliers, VSM, to be used in Eq. 1 are defined in Tables 3 and 4, respectively.

$$PS = (BS) - \sum (VSM) \times (VS) \quad (1)$$

Table 4: Vulnerability Parameters, (VSM)

Soft storey	Does not exist = 0; Exists = 1
Heavy overhangs	Does not exist = 0; Exists = 1
Apparent quality	Good = 0; Moderate = 1; Poor = 2
Short columns	Does not exist = 0; Exists = 1
Pounding effect	Does not exist = 0; Exists = 1
Topographic effects	Does not exist = 0; Exists = 1

3.2 Tier 2: Preliminary Assessment

In many instances statistical analysis based on the observed damage and significant building attributes would provide reliable and accurate results for regional assessments. Yucemen et al. (2004), Ozcebe et al. (2003) and Yakut et al. (2003) employed the discriminate analysis technique to develop a preliminary evaluation methodology for assessing seismic vulnerability of existing low- to medium-rise RC buildings in Turkey. The main objective of the procedure is to identify the buildings that are highly vulnerable to damage. The procedure is applicable to RC frames and frame-wall structures, having up to seven stories.

Definition of Parameters

The following parameters were chosen as the basic estimation parameters:

(a) Number of stories (n): This is the total number of individual floor systems above the ground level.

(b) Minimum normalized lateral stiffness index (mnlstfi): This index represents the lateral rigidity of the ground storey, which is usually the most critical storey. It is calculated by considering the columns and the structural walls at the ground storey. The mnlstfi parameter computed based on the following relationship:

$$\text{mnlstfi} = \min (I_x, I_y) \quad (2)$$

Where;

$$I_{nx} = \frac{\sum (I_{col})_x + \sum (I_{sw})_x}{\sum A_f} \times 1000, \\ I_{ny} = \frac{\sum (I_{col})_y + \sum (I_{sw})_y}{\sum A_f} \times 1000 \quad (3)$$

Where, $\sum (I_{col})_x$ and $\sum (I_{col})_y$ are the summation of the moment of inertias of all columns about their centroidal x and y axes, respectively. $\sum (I_{sw})_x$ and $\sum (I_{sw})_y$ are the summation of the moment of inertias of all structural walls about their centroidal x and y axes, respectively. I_{nx} and I_{ny} are the total normalized moment of inertia of all members about x and y axes, respectively. $\sum A_f$ is the total floor area above ground level.

(c) Minimum normalized lateral strength index (mnlssi): It indicates the base shear capacity of the critical storey. In the calculation of this index, unreinforced masonry filler walls are assumed to carry 10 percent of the shear force that can be carried by a structural wall having the same cross-sectional area. As in mnlstfi calculation, the vertical reinforced members with a cross-sectional aspect ratio of 7 or more are classified as structural walls. The mnlssi parameter calculated by using the following equation:

$$\text{mnlssi} = \min (A_{nx}, A_{ny}) \quad (4)$$

Where:

$$A_{nx} = \frac{\sum (A_{col})_x + \sum (A_{sw})_x + 0.1 \sum (A_{mw})_x}{\sum A_f} \times 1000, \\ A_{ny} = \frac{\sum (A_{col})_y + \sum (A_{sw})_y + 0.1 \sum (A_{mw})_y}{\sum A_f} \times 1000 \quad (5)$$

For each column with a cross-sectional area denoted by A_{col} :

$$(A_{col})_x = k_x \cdot A_{col}, (A_{col})_y = k_y \cdot A_{col} \quad (5)$$

Where; $k_x=1/2$ for square and circular columns; $k_x=2/3$ for rectangular columns with $b_x > b_y$; $k_x=1/3$ for rectangular columns with $b_x < b_y$; and $k_y=1-k_x$
For each shear wall with cross-sectional area denoted by A_{sw} :

$$(A_{sw})_x = k_x \cdot A_{sw}, (A_{sw})_y = k_y \cdot A_{sw} \quad (6)$$

Where; $k_x=1$ for structural walls in the direction of x-axis; $k_x=0$ for structural walls in the direction of y-axis; and $k_y=1-k_x$.
For each unreinforced masonry filler wall with no window or door opening and having a cross-sectional area denoted by A_{mw} :

$$(A_{mw})_x=k_x \cdot A_{mw}, (A_{mw})_y=k_y \cdot A_{mw} \quad (7)$$

Where; $k_x=1.0$ for masonry walls in the direction of x-axis; $k_x=0$ for masonry walls in the direction of y-axis; and $k_y=1-k_x$.

(d) Normalized redundancy score (nrs): Redundancy is the indication of the degree of the continuity of multiple frame lines which distribute lateral forces throughout the structural system. The normalized redundancy ratio (nrr) of a frame structure is calculated by using the following expression:

$$nrr = \frac{A_{tr}(nf_x - 1)(nf_y - 1)}{A_{gf}} \quad (8)$$

Where; A_{tr} is the tributary area for a typical column. A_{tr} is taken as 25 m² if nf_x and nf_y are both greater than and equal to 3. In all other cases, A_{tr} is taken as 12.5 m². nf_x , nf_y are the number of continuous frame lines in the critical storey (usually the ground storey) in x and y directions, respectively. A_{gf} is the area of the ground storey, i.e. the footprint area of the building. Depending on the value of nrr computed from Eq. 8, the following discrete values are assigned to the normalized redundancy score (nrs):

$$\begin{aligned} nrs &= 1 \text{ for } 0 < nrr \leq 0.5 \\ nrs &= 2 \text{ for } 0.5 < nrr \leq 1.0 \\ nrs &= 3 \text{ for } 1.0 < nrr \end{aligned}$$

(e) Soft Storey Index (ssi): On the ground storey, there are usually fewer partition walls than in the upper stories. This situation is one of the main reasons for the soft storey formations. Since the effects of masonry walls are included in the calculation of mnlsi, soft storey index is defined as the ratio of the height of first storey (i.e. the ground storey), H_1 , to the height of the second storey, H_2 .

$$ssi = \frac{H_1}{H_2} \quad (9)$$

(f) Overhang ratio (or): In a typical floor plan, the area beyond the outermost frame lines on all sides is defined as the overhang area. The summation of the overhang area of each storey, $A_{overhang}$, divided by the area of the ground storey, A_{gf} , is defined as the overhang ratio.

$$or = \frac{A_{overhang}}{A_{gf}} \quad (10)$$

The damage index or the damage score corresponding to the Life Safety Performance Classification (LSPC) computed from the discriminant function given in Eq. 11.

$$\begin{aligned} \text{Damage index for life safety (DI}_{LS}) \\ = 0.620n - 0.246mnlstfi - 0.182mnlsi - 0.699nrs + 3.269ssi + 2.728or - 4.905 \end{aligned} \quad (11)$$

In the case of Immediate Occupancy Performance Classification (IOPC), the discriminant function, where DI_{IO} is the damage score corresponding to IOPC, based on these variables is:

$$\begin{aligned}
 &\text{Damage index for Immediate Occupancy (DI}_{IO}) \\
 &=0.808n-0.334mnlstfi-0.107mnlisi-0.687nrs+0.508ssi+3.884or-2.86
 \end{aligned}
 \tag{12}$$

In the proposed classification methodology, buildings are evaluated according to both Performance levels. The steps followed are listed below.

- (1) DI_{LS} and DI_{IO} scores by using Eq. 11 and Eq. 12, respectively.
- (2) Determine the cutoff values for life safety (CV_{LS}) and cutoff value for immediate occupancy (CV_{IO}) by using Eq. 13.

The cutoff value ratio for life safety (LS_{CVR}) and cutoff value ratio for immediate occupancy (IO_{CVR}) are obtained from Table 5 based on the number of stories above the ground level. The cutoff modification coefficients (CMC) values are adjustment factors, which introduce the spatial variation of the ground motion in the evaluation process. These values taken from Table 6 based on the building location relative to the fault and the soil type at the site.

$$\begin{aligned}
 CV_{LS} &= LS_{CVR} + |LS_{CVR}| \times (CMC - 1); \\
 CV_{IO} &= IO_{CVR} + |IO_{CVR}| \times (CMC - 1)
 \end{aligned}
 \tag{13}$$

Table 5: Variation of LS_{CVR} and IO_{CVR} values with number of stories

n	LS_{CVR}	IO_{CVR}
3 or less	0.383	-0.425
4	0.430	-0.609
5	0.495	-0.001
6	1.265	0.889
7	1.791	1.551

Table 6: Variation of CMC Values with Soil Type and Distance to Fault

Soil Type	Shear Wave Velocity (m/s)	Distance to Fault (km)				
		0-4	5-8	9-15	16-25	>26
B	>760	0.778	0.824	0.928	1.128	1.538
C	360-760	0.864	1.000	1.240	1.642	2.414
D	180-360	0.970	1.180	1.530	2.099	3.177
E	<180	1.082	1.360	1.810	2.534	3.900

(3) By comparing the CV values with associated DI value calculate performance grouping of the building for life safety performance classification (LSPC) and immediate occupancy performance classification (IOPC) as follows:

- If $DI_{LS} > CV_{LS}$ take $PG_{LS}=1$
- If $DI_{LS} < CV_{LS}$ take $PG_{LS}=0$

If $DI_{IO} > CV_{IO}$ take $PG_{IO}=1$
 If $DI_{IO} < CV_{IO}$ take $PG_{IO}=0$

(4) To decide the probable expected performance level of the building the damage scores obtained from Eqs. 11 and 12 should be compared with the storey dependent cutoff values obtained from Eq. 13. In each case, the building under evaluation is assigned an indicator variable of “0” or “1”. The indicator variable “0” corresponds to “none, light or moderate damage” in the case of LSPC and “none or light damage” in the case of IOPC. Similarly, the indicator variable “1” corresponds to “severe damage or collapse” in the case of LSPC and “moderate or severe damage or collapse” in the case of IOPC. In the final stage, the building is rated in the “low risk group” if both indicator values are zero or in the “high risk group” when both indicator values are equal to unity. In all other cases buildings are classified as the cases “requiring further study.” Further investigations have indicated that these buildings generally lie in the “moderate risk group,” (Ozcebe et al., 2006).

4. SUMMARY OF ASSESSMENT RESULTS

The selected buildings were mainly low-rise buildings with two to six five stories above ground. Randomly selected 194 buildings were analyzed for scoring. According to current zoning map of seismic code, for Sylhet City (Zone I) the peak ground acceleration is around 0.25g on very firm soil, considering site effects it can be taken as 0.30g or more. Corresponding PGV can be taken as between 60 cm/s to 70 cm/s (Wu et al., 2003). Hence for calculating performance score Zone I ($60 < PGV < 80$) is considered.

The walk down survey yielded the complete inventory of the building stock. At the end of this survey the buildings were identified in terms of their structural systems, their number of stories and their type of use. Walkdown survey results showed that Table 7 catalogues the RC buildings with number of stories which are taken under investigation. Figure 3 and Figure 4 represent the existing vulnerability parameters and apparent condition of the buildings respectively.

Table 7: Tabulation of RC Buildings according to the number of Stories

Number of Stories	≤ 2	3	4	5	6	7	7+	Total
No. of Buildings	108	49	25	9	2	1	0	194

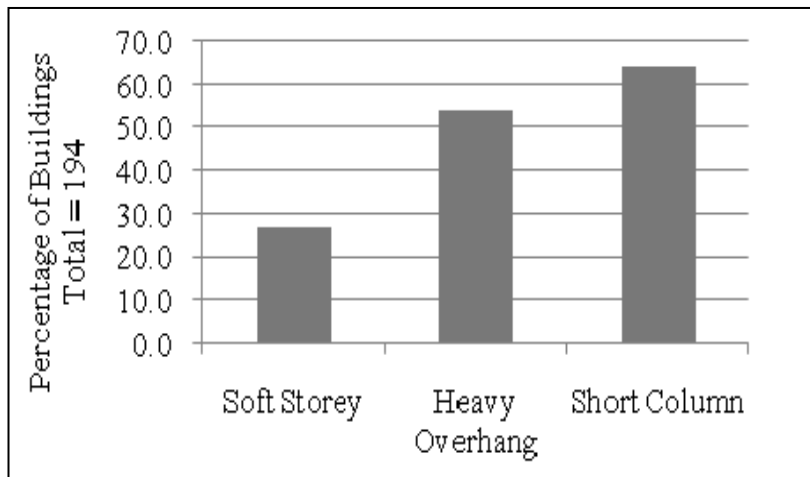


Figure 3: Presences of vulnerability parameters

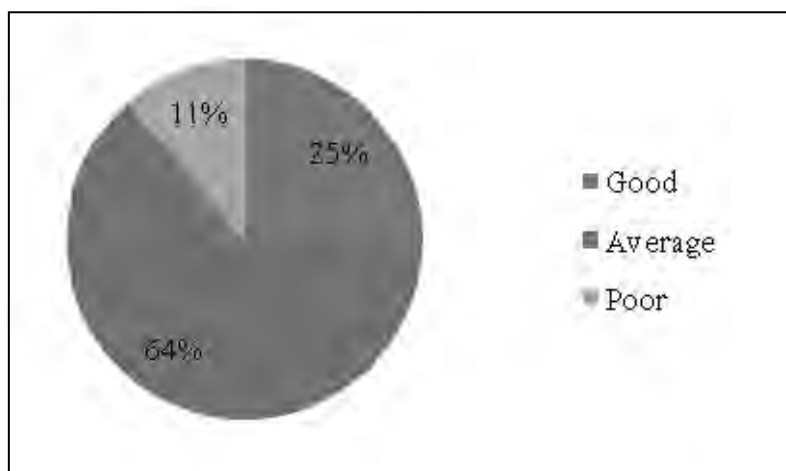


Figure 4: Apparent qualities of buildings

The walk down survey yielded a preliminary seismic performance grading of the existing RC buildings relative to each other. The calculated performance scores of the RC buildings with 7 stories or less are given in Table 8. This table shows that the performance scores of the buildings are inversely proportional with the number of stories. Entries in parenthesis indicate the expected risk distribution in percentages.

Table 8 Calculated performance scores of RC buildings having 7 stories or less.

No. of Stories	Performance Scores				Total
	PS≤30	30<PS≤60	60<PS≤100	100<PS	
1&2	0(0)	0(0)	108(100)	0(0)	108(100)
3	0(0)	15(30.6)	34(69.4)	0(0)	49(100)
4	3(12.0)	19(76.0)	3(12.0)	0(0)	25(100)
5	5(55.6)	4(44.4)	0(0)	0(0)	9(100)
6	2(100)	0(0)	0(0)	0(0)	2(100)
7	1(100)	0(0)	0(0)	0(0)	1(100)
Total	11(5.7)	38(19.6)	145(74.7)	0(0)	194(100)

From the spatial distribution of existing RC buildings in Ward No. 9 of SCC, With respect to the calculated performance scores, it is indicates

that the proposed methodology is capable of reflecting the adverse effects of the seismic hazard and building attributes on the seismic performance classification of buildings.

In second tier, buildings with a seismic performance score of 30 or less were given priority but due to the not allowance by the owner, all of the building PS below 30 could not surveyed. There were 7 buildings in this group of which a representative sample of 11 buildings has been studied. In addition, 12 buildings with performance scores greater than 30 were also included in the analyses. The main reason of this inclusion was to assess the correlation between the methods used in the first and the second tier analysis.

A total of 19 buildings were analyzed in second level of assessment. Field teams gathered specific information about the structural system of each building including all dimensions of structural and non-structural elements. This information was later tabulated in a spreadsheet format and the Preliminary Assessment Methodology was applied. Table 9 represents the analysis results in tier 2.

Table 9: Surveyed building data for Tier 2 (Contd.)

Building ID	n	mnlstfi	mnlisi	nrs	ssi	or
L2-01	5	0.01	0.90	2	1.05	0.09
L2-02	2	0.03	2.38	1	1.00	0.17
L2-03	4	0.01	1.44	1	1.18	0.17
L2-04	4	0.01	1.02	1	1.11	0.18
L2-05	3	0.02	1.28	1	1.10	0.26
L2-06	4	0.01	1.50	1	1.05	0.09
L2-07	4	0.01	1.21	2	1.05	0.17
L2-08	5	0.02	1.02	1	1.18	0.15
L2-09	5	0.01	0.80	1	1.05	0.15
L2-10	2	0.02	2.86	1	1.00	0.05
L2-11	2	0.02	2.93	1	1.00	0.00
L2-12	3	0.03	3.07	3	1.00	0.00
L2-13	2	0.02	3.26	3	1.05	0.11
L2-14	5	0.05	1.00	1	1.17	0.15
L2-15	6	0.02	1.56	1	1.11	0.13
L2-16	2	0.02	1.70	2	1.00	0.17
L2-17	3	0.02	2.01	3	1.00	0.00
L2-18	3	0.02	1.54	1	1.00	0.14
L2-19	3	0.01	1.60	1	1.11	0.06

Table 9: Surveyed building data for Tier 2

Building ID	Frame Line (X-dir.)	Frame Line (Y-dir.)	DI _{LS}	DI _{IO}	CV _{LS}	CV _{IO}
L2-01	4	4	0.31	0.57	1.573	0.001
L2-02	2	2	-1.06	-1.02	1.217	0.500
L2-03	3	2	0.93	0.78	1.366	0.717
L2-04	2	2	0.81	0.83	1.366	0.717
L2-05	2	2	0.32	0.29	1.217	0.500
L2-06	2	3	0.30	0.41	1.366	0.717

L2-07	3	3	-0.14	0.05	1.366	0.717
L2-08	2	4	1.57	1.55	1.573	0.001
L2-09	3	2	1.20	1.51	1.573	0.001
L2-10	2	2	-1.47	-1.53	1.217	0.500
L2-11	2	4	-1.63	-1.75	1.217	0.500
L2-12	4	4	-2.44	-2.34	1.217	0.500
L2-13	4	3	-2.63	-2.73	1.217	0.500
L2-14	2	4	1.57	1.55	1.573	0.001
L2-15	4	2	1.80	2.19	4.019	2.824
L2-16	4	4	-1.64	-1.64	1.217	0.500
L2-17	3	4	-2.24	-2.22	1.217	0.500
L2-18	2	2	-0.39	-0.26	1.217	0.500
L2-19	2	4	-0.25	-0.51	1.217	0.500

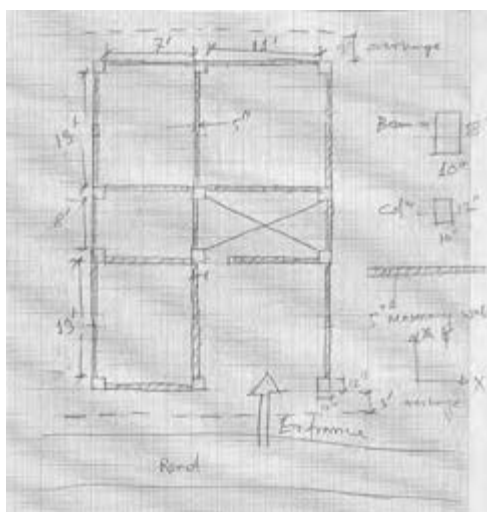


Figure 5: A sketch of ground floor plan in tier 2 survey

Figure 6 shows that number of buildings was classified in the seismic risk group. The spatial distribution of those buildings which were classified in the high seismic risk group indicated that those buildings were among the most vulnerable ones. This is mainly because of the high seismic hazard of the region and poor building quality.

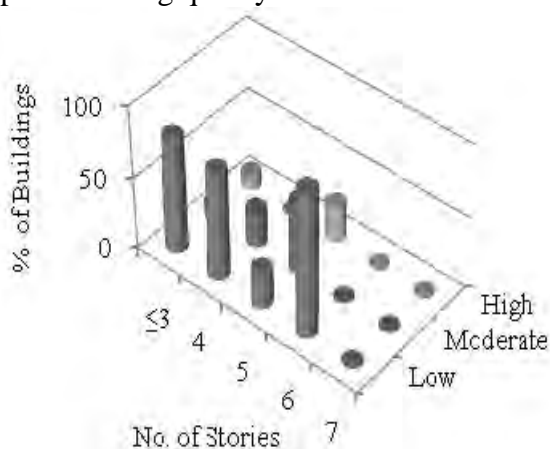


Figure 6: Results of the Preliminary Assessment Method when distance to fault > 26.km.

5. CONCLUSIONS

This paper presents a seismic vulnerability assessment application on a limited scale of Sylhet City. Some buildings, which were assigned very high performance scores at the end of first tier, may be ranked in the high seismic risk group buildings by the second tier survey. From the assessment, it was evident that many of the buildings in ward no. 9 area fall under low & moderate risk category. Among the surveyed buildings, about 70% were found to be in low risk group, 20% of buildings were found to be in moderate risk group and 11% percent of the buildings were found to be in high risk category. Field observations reveal that the number of stories, presence of soft storey and heavy overhang in a building are important parameters regarding seismic safety. Apparent qualities of building, pounding effect are also other important parameters. This survey procedure is not applicable for unreinforced masonry buildings which are also common in the ward no. 9 in the Sylhet City Corporation. Results of the rapid survey need to be followed up by other detailed seismic evaluation techniques for taking necessary action.

REFERENCES

- Ozcebe, G., Yucemen, M. S., Aydogan, V., and A. Yakut, (2003), Preliminary Seismic Vulnerability Assessment of Existing Reinforced Concrete Buildings in Turkey- Part I: Statistical Model Based on Structural Characteristics, Seismic Assessment and Rehabilitation of Existing Buildings, *NATO Science Series IV/29*, pp. 29-42.
- Ozcebe, G., Sucuoglu, H., Yucemen, S.M., Yakut, A. and Kubin, J. (2006), Seismic Risk Assessment of Existing Building Stock In Istanbul a Pilot Application in Zeytinburnu District, *8th National Conference on Earthquake Engineering*, Paper No. 1737, San Francisco.
- OYO International Corporation (OIC), (2009), Research Work, *CDMP-UNDP Fault Map Delineation for Bangladesh*.
- Population Census (2006), *Community Series*, Zila: Sylhet.
- Sucuoglu, H., and Yazgan, U. (2003), Simple Survey Procedures for Seismic Risk Assessment in: Urban Building Stocks, Seismic Assessment and Rehabilitation of Existing Buildings, *NATO Science Series IV/29*, pp. 97-118.
- Wu, Y. M., Teng, T. L., Shin, T. C., and Hsiao, N. C. (2003), Relationship between Peak Ground Acceleration, Peak Ground Velocity, and Intensity in Taiwan, *Bulletin of the Seismological Society of America*, Vol. 93, No. 1, pp. 386–396.
- Yakut, A., Aydogan, V., Ozcebe, G., and Yucemen, M. S. (2003), Preliminary Seismic Vulnerability Assessment of Existing Reinforced Concrete Buildings in Turkey -Part II: Inclusion of Site Characteristics, Seismic Assessment and Rehabilitation of Existing Buildings, *NATO Science Series IV/29*, pp. 43-58.
- Yucemen, M. S., Ozcebe, G., and A. C. Pay, (2004), Prediction of Potential Damage due to Severe Earthquakes, *Structural Safety*, 26(3), 349-366

Geospatial analysis of groundwater quality using Geographical Information System: A case study from Maharashtra State of India

Parmeshwar UDMALE¹ and Sangam SHRESTHA²

¹Master's student, Water Engineering and Management, School of Engineering and Technology, Asian Institute of Technology, Thailand
pd.udmale@gmail.com

²Assistant Professor, Water Engineering and Management, School of Engineering and Technology, Asian Institute of Technology, Thailand

ABSTRACT

Groundwater is one of the most important natural resources for human beings and surrounding environment. In semi arid region of Maharashtra State which receives an average annual rainfall 400 -700 mm, the availability of groundwater is extremely uneven both in space and time. This is due to the uneven distribution of rainfall and variations in basic characteristics and physiography of underlying hard rocks. This limited availability of groundwater resources in arid region further affected by quality deterioration restricting use of groundwater. An attempt is made to assess the degree of groundwater quality and suitability of groundwater for drinking purpose in combination with application of GIS tools for the drought prone study area 'the Dhubhdhubhi watershed' of Maharashtra State.

The groundwater quality index (GWQI) has been derived for five parameters namely Total Dissolved Solids (TDS), Chloride (Cl^-), Nitrate (NO_3^-), Fluoride (F^-) and Iron (Fe) based on water quality standards for drinking purpose as recommended by Indian standard specification of drinking water (ISO: 10500, 1993). The high value of GWQI relate with higher concentration of parameter in groundwater. The inverse distance weighted method to power interpolation technique is used to obtain spatial distribution of parameters in ArcGIS 9.3.

The study concludes that the 100% population in study area is dependent on groundwater for drinking purpose. Out of 45 villages, about 21 villages show the deteriorated groundwater quality. About 33.06 % of population is using groundwater which is unsuitable for drinking purpose and needs treatment prior to use. The groundwater quality deterioration can result in critical situation if adequate management practices are not implemented in relation to sustainable development of the resource.

Keywords: *Groundwater Quality Index, Geographical Information System, Maharashtra State*

1. INTRODUCTION

Groundwater is one of the most important natural resources for human beings and surrounding environment. Globally groundwater is estimated to provide at least 50% of drinking water needs, 40% of the demand of those industries that do not use urban mains water, and 20% of water-use in irrigated agriculture (Zektser and Everett, 2004). As compared to surface water, groundwater is generally of good quality, reduced susceptibility to contamination, less subject to seasonal and perennial fluctuations, and much more uniformly spread over large region. The problems of groundwater depletion, along with the problems of water logging and groundwater quality deterioration due to natural hazardous substances and anthropogenic activities poses constraint on use of groundwater. The problems of high arsenic, fluoride, nitrate and total dissolved solids (TDS) are major concerns in many countries, exceeding permissible limits of drinking water quality set up by United Nation's World Health Organization (Appelo, 2006). The present study attempts to assess the degree of groundwater quality and suitability of groundwater for drinking purpose in combination with application of GIS tools for the drought prone area 'the Dhubdhubhi watershed' of Solapur district in Maharashtra State.

2. STUDY AREA

The Dhubdhubhi watershed (Figure 1) with geographical area of 483.63 km² lies in Southeast part of Solapur district in Maharashtra State of India which is bounded between latitudes 17° 21' N to 17° 41' N and longitudes 76° 00' E to 76° 11' E. The Groundwater Survey and Development Agency of Maharashtra State has delineated the study area as a watershed of sub-catchment of 'Lower Bhima up to conflict with Sina River'. It is further divided into sub-watersheds as BM-138 with 4 miniwatersheds and BM-139 with 3 miniwatersheds.



Figure 1: Location map of the Dhubdhubhi watershed

3. METHODOLOGY

The thematic maps of study area are obtained from Maharashtra Remote Sensing Application Center, Nagpur and the groundwater quality data for village wells in the study area is obtained from database of Water Supply and Sanitation Department, Government of Maharashtra for the year 2006. The Water Quality Index (WQI) is generated (a mathematical instrument to convert large quantities of water quality data into a composite number which represents the level of water quality). In this study, groundwater quality index (GWQI) has been derived for five parameters namely Total Dissolved Solids (TDS), Chloride (Cl^-), Nitrate (NO_3^-), Fluoride (F^-), Iron (Fe) based on water quality standards for drinking purpose as recommended by Indian Standard Specification of Drinking Water (ISO: 10500, 1993). It is assumed that the weightage for various groundwater quality parameters are inversely proportional to the standards for drinking purpose as recommended by Indian standard specification of drinking water (ISO: 10500, 1993) (Mishra et al. 2001, Naik et al. 2001 and Reza et al. 2010).

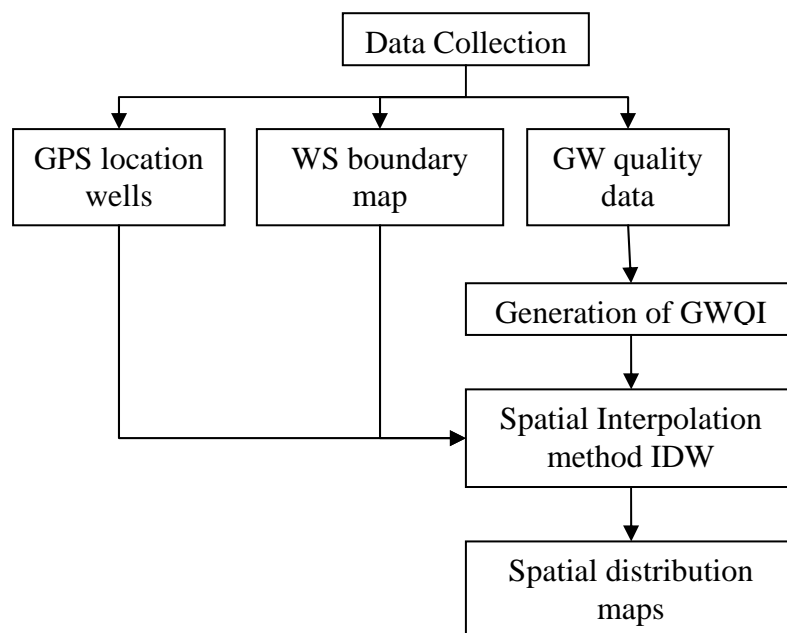


Figure 2: Flowchart of methodology for generating groundwater quality index map

The obtained GWQI is used as input data for well locations. The ‘inverse distance weighted (IDW) method to power’ interpolation technique is used to obtain spatial distribution of GWQI in ArcGIS 9.3. The spatial distribution of individual parameters for visual understanding is also obtained using IDW interpolation method in ArcGIS 9.3. Following are the steps for calculation of GWQI.

Step 1 Calculation of weightage of i^{th} parameter

The weightage for i^{th} parameter is calculated as,

$$W_i = k / S_i$$

Where, W_i is the unit weightage for i^{th} parameter,

S_i is the standard for i^{th} parameter recommended by Indian standard specification of drinking water (ISO: 10500, 1993) and k is the constant of proportionality.

The proportionality constant assuming five parameters mentioned above are obtained as 0.0009171 and calculated unit weightage is shown in Table 1.

Table 1: Unit weightage of five parameters based on BIS (ISO: 10500, 1993)

Sl. no.	Parameter	Highest permitted value (S_i)	Unit weightage (W_i)
1	TDS	500.00	0.000458552
2	Chloride	250.00	0.000917104
3	Nitrate	45.00	0.005095022
4	Fluoride	1.00	0.229275997
5	Iron	0.30	0.764253325

Step 2 Calculation of quality rating for each of the water quality parameter

Further individual quality rating scale Q_i for each parameter is given by,

$$Q_i = C_i / S_i$$

Where, Q_i is quality rating based on concentration of each parameter,
 S_i is the standard for i^{th} parameter recommended by Indian standard specification of drinking water (ISO: 10500, 1993) and
 C_i is concentration of chemical parameter in each water sample (mg/liter)

Then sub index for each parameter has been determined as,

$$SI = W_i * Q_i$$

Where, SI is sub index of i^{th} parameter.

Step 3 Summing of these sub- indices in the overall index.

Groundwater quality index is then calculated as,

$$GWQI = \sum SI$$

The obtained values of groundwater quality index (GWQI) for wells are divided into four classes as very good (0-25), good (25-50), poor (50-75) and very poor (75-100).

4. RESULTS AND DISCUSSIONS

The Figure 3, 4, 5, 6, 7, 8 shows the spatial distribution of various groundwater quality parameters in terms of concentration. The groundwater samples exceed the Indian standards of drinking water quality for dissolved solids and iron concentration in most part the study area. The TDS beyond 500 mg/liter causes decrease in palatability of drinking water and it may result in gastro intentional irritation. Excess concentration of iron affects the taste and appearance, has adverse effect on domestic uses and water supply structures and promotes iron bacteria. The concentration of other chemical

parameters such as fluoride, nitrate and chloride is within the limit of Indian standards of drinking water quality.

The 45.83 % area exceeds the permissible limit of TDS. In most of the part of study area, the concentration of iron is at upper concentration limit set by BSI. The chloride concentration over the study area is less than 100 mg/liter which is within the permissible limit of 250 mg/liter. Most of the area shows nitrate concentration in groundwater far below the permissible limit. The fluoride concentration in groundwater is found 0.2-0.3 mg/liter at most of the locations.

The suitability of groundwater for drinking purpose is decided based on the classification of GWQI as very good (0-25), good (25-50), poor (50-75) and very poor (75-100). The interpolation map of GWQI is shown in Figure 9, which concludes that about 25.20 % area is unsuitable or are of poor to very poor quality for drinking purpose. Out of 45 villages, about 21 villages show the deteriorated groundwater quality (Figure 10) and about 33.06 % of population in the study area is using groundwater which is unsuitable for drinking purpose.

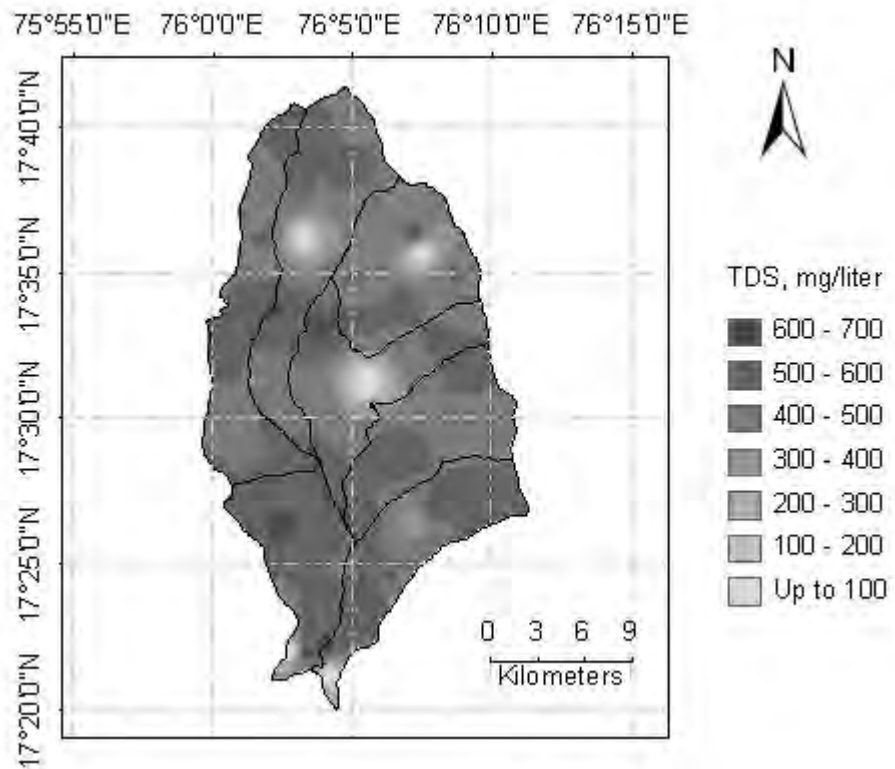


Figure 3: Spatial distribution of total dissolved solids (TDS) in the Dhubdhubhi watershed

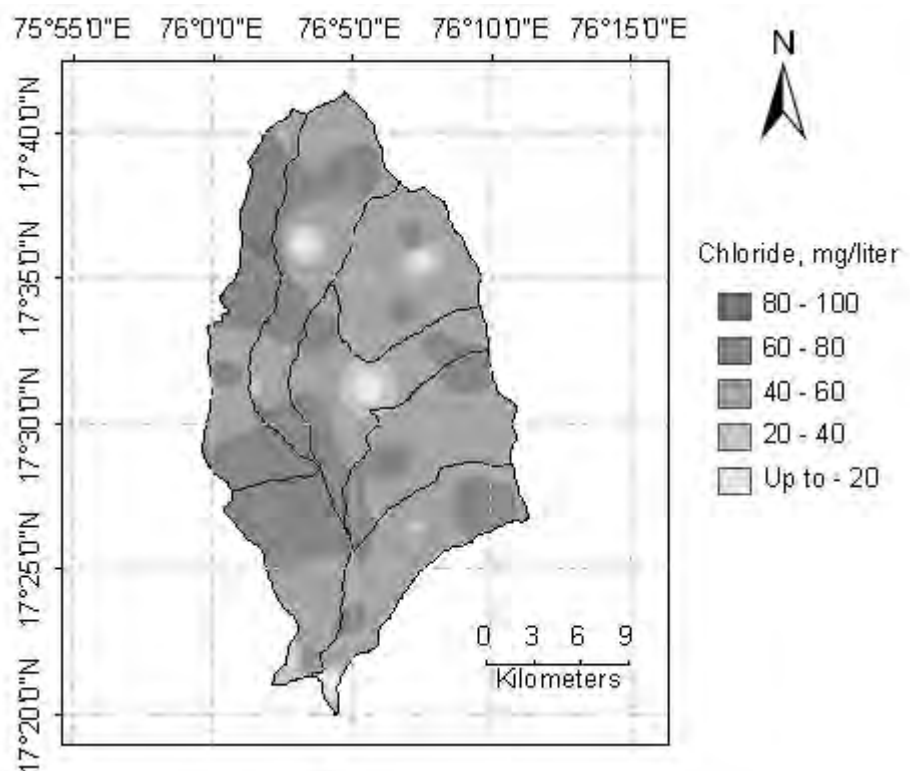


Figure 4: Spatial distribution of Chloride(Cl^-) in the Dhubdhubhi watershed

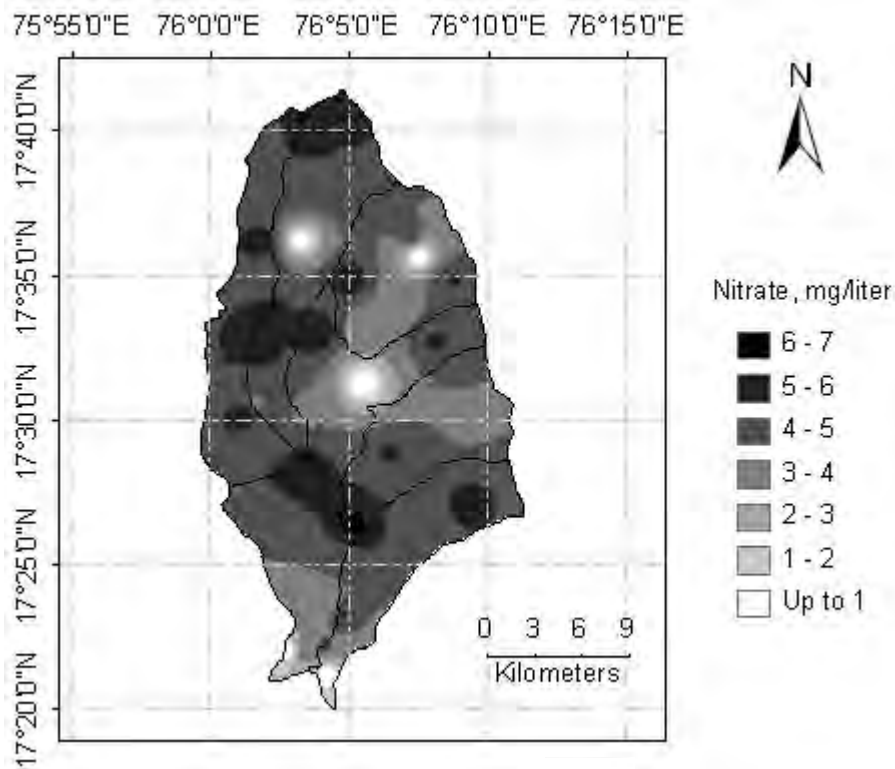


Figure 5: Spatial distribution of Nitrate (NO_3^-) in the Dhubdhubhi watershed

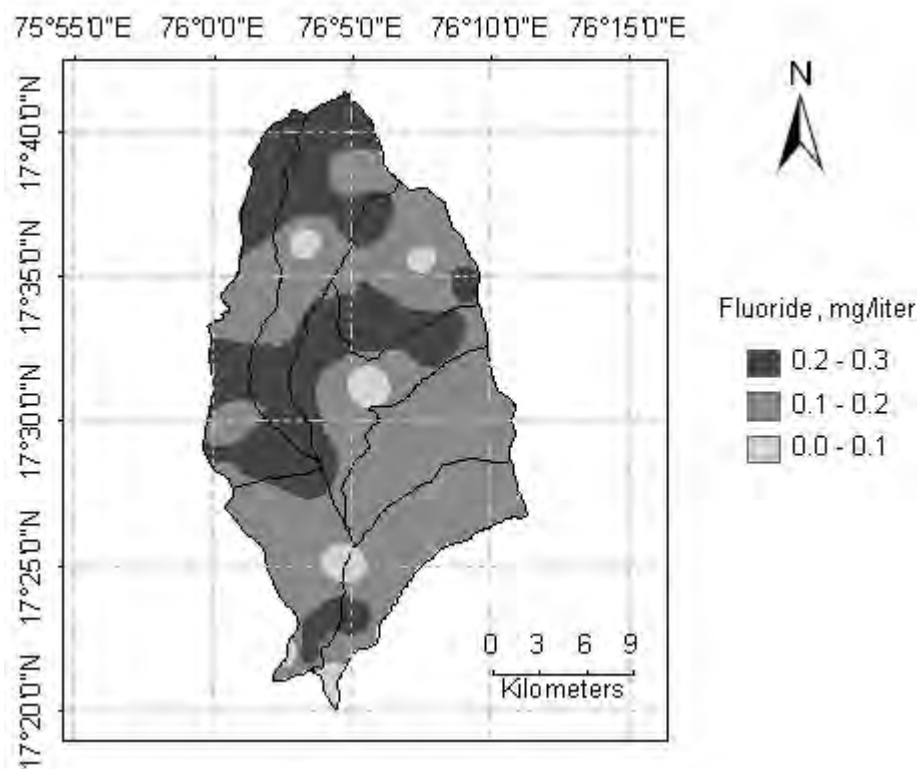


Figure 6: Spatial distribution of Fluoride (F^-) in the Dhubdhubhi watershed

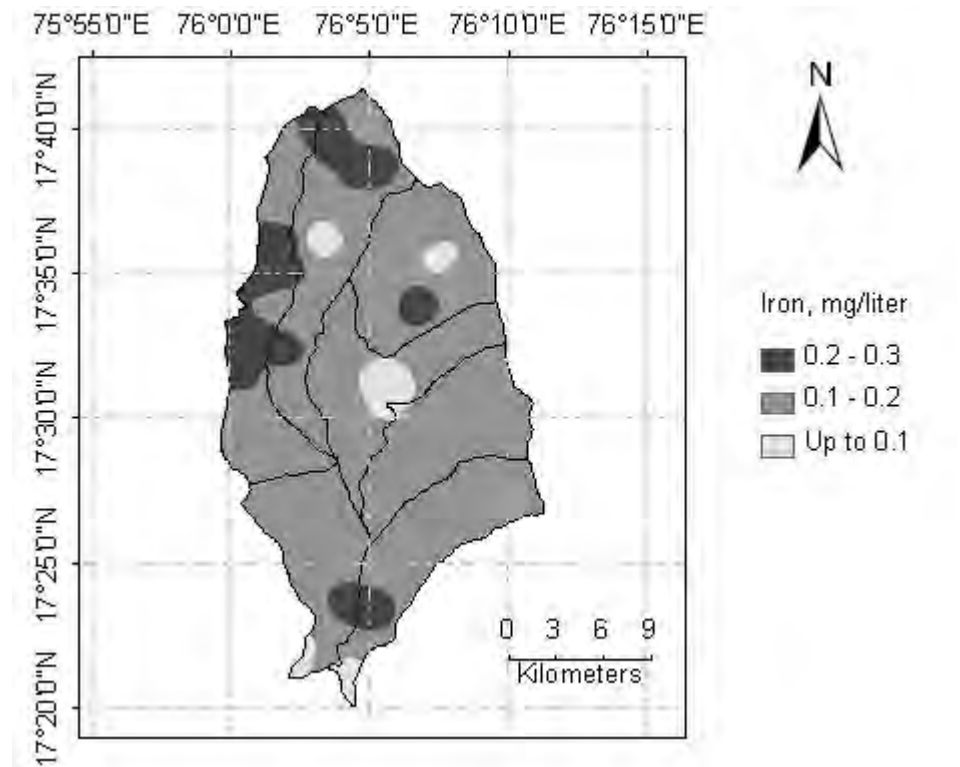


Figure 7: Spatial distribution of Iron (Fe) in the Dhubdhubhi watershed

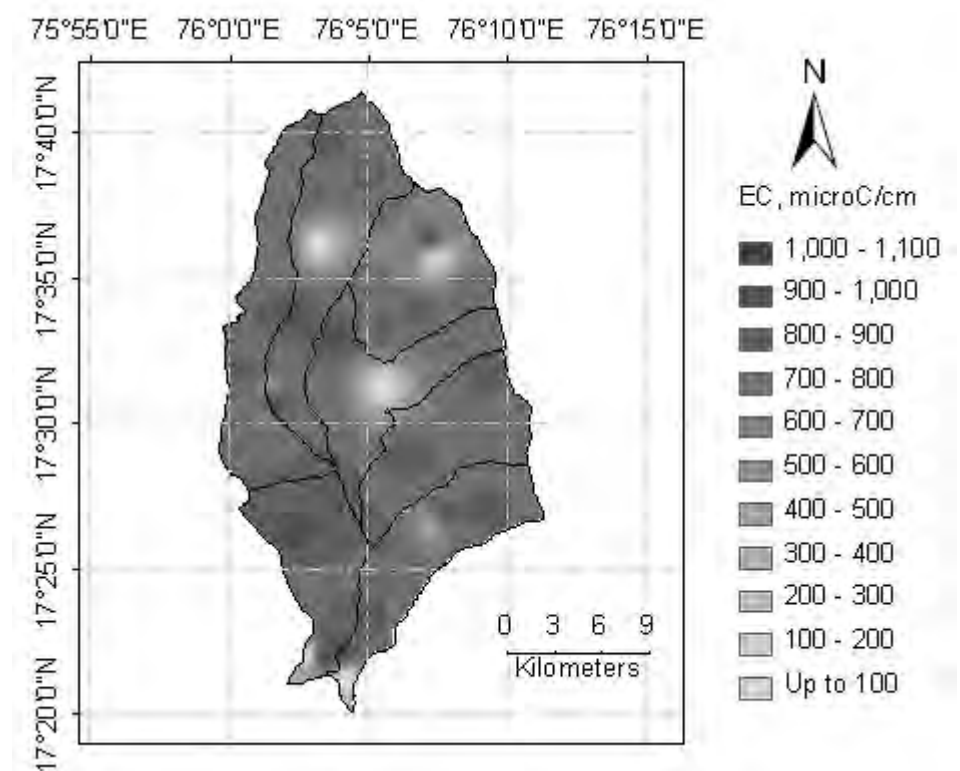


Figure 8: Spatial distribution of Electric Conductivity in Dhubdhubhi watershed

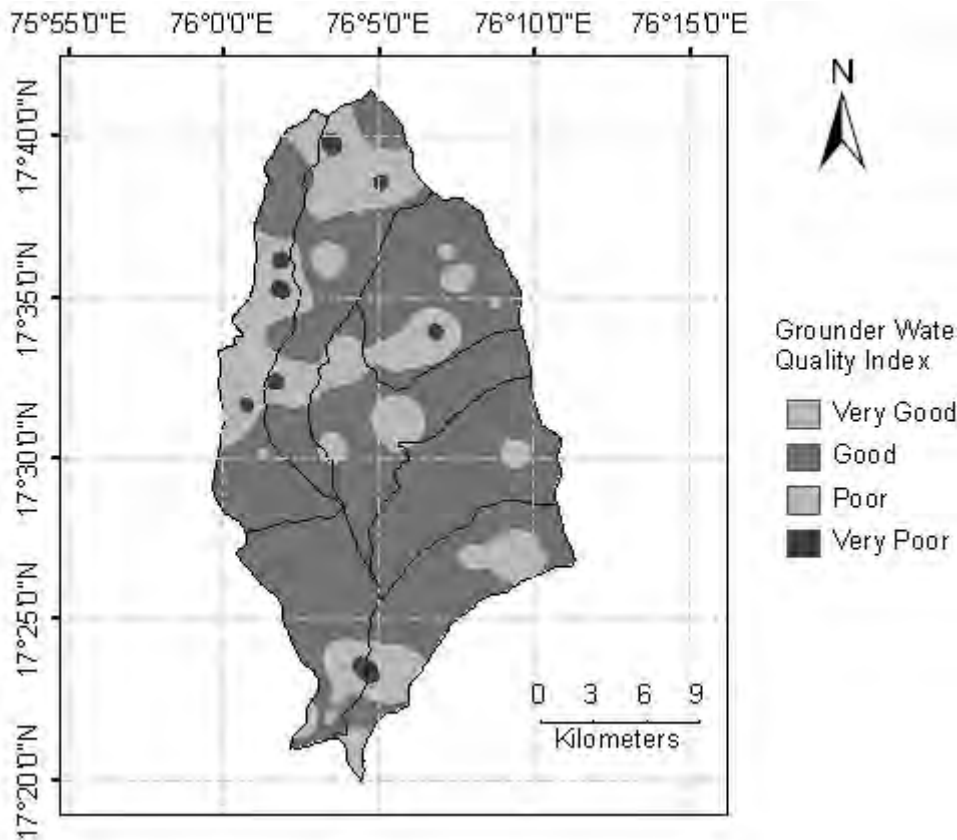


Figure 9: Spatial distribution of Ground Water Quality Index in the Dhubdhubhi watershed

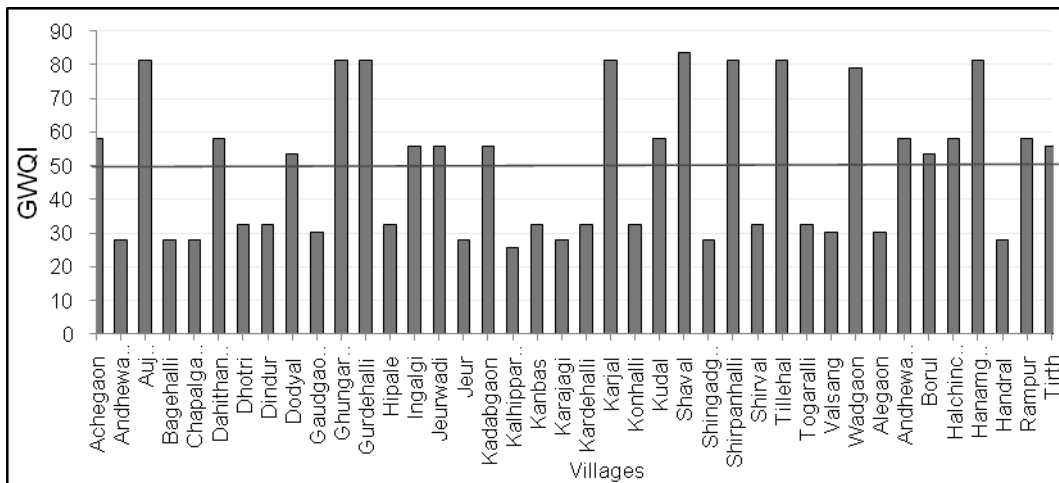


Figure 10: GWQI for various groundwater locations of the study area, above red line indicates groundwater is unsuitable for drinking purpose in the Dhubdhubhi watershed

5. CONCLUSIONS

The study concludes that the 100% population in study area is dependent on groundwater for drinking purpose. Out of 45 villages, about 21 villages show the deteriorated groundwater quality. About 33.06 % of population is using groundwater which is unsuitable for drinking purpose and needs treatment prior to use. The groundwater quality deterioration can result in critical situation if adequate management practices are not implemented in relation to sustainable development of the resource.

ACKNOWLEDGEMENT

Authors are thankful to Maharashtra Remotes Sensing Application Centre, Nagpur and Water Supply and Sanitation Department, Government of Maharashtra.

REFERENCES

- Appelo, T., 2006. *Arsenic contamination in groundwater: a global perspective*. National Chapter of IAH. The Netherlands.
- BIS (Bureau of Indian Standards) 10500, 1993 (reaffirmed). *Indian Standard of Drinking Water Specification*.
- Mishra, P.C. and R.K. Patel, 2001. Study of the pollution load in the drinking water of Rairangpur, a small tribal dominated town of North Orissa. *Indian Journal of Environment and Ecoplanning*, 5(2): 293-298.
- Naik, S. and K.M. Purohit, 2001. Studies on water quality of river Brahmani in Sundargarh district, Orissa. *Indian Journal of Environment and Ecoplanning*, 5(2): 397-402.
- Reza, R. and Singh, G., 2010. Assessment of Ground Water Quality Status by Using Water Quality Index Method in Orissa, India. *World Applied Sciences Journal* 9 (12): 1392-1397.
- Zektser, I.S. and Everett, L.G., 2004. *Groundwater resources of the world and their use*. UNESCO- IHP-VI, Series on Groundwater no.6, Paris, France.

Flood risk modeling in Bangkok Province, Thailand

Phalke APARNA¹, Tripathi NITIN² and Bharambe KHAGENDRA³

¹Master Student School of Eng., RSGIS FoS,
Asian Institute of Technology, Thailand
aparnapm16@gmail.com

²Coordinator, RSGIS FoS,
Asian Institute of Technology, Thailand

³Research Associate, RSGIS FoS,
Asian Institute of Technology, Thailand

ABSTRACT

Natural disasters like flood, drought, cyclone, forest fire, volcanic eruption, and landslide are occurring frequently all over the world. Natural disasters happening on earth always cause loss of life, property damage as well as social and economic disruption. Bangkok is developed on the delta of the Chao Phraya River Basin at a distance 25-56 km from its mouth and its average land level is about 0-1.5m above mean sea level so frequent floods have been a big obstruction in its development.

Due to climate change and its impact the risk of flooding has increased. Over the past few years the impact of flooding has become an important issue for Bangkok. The rapid urbanization and heavy soil settlement have adversely affected the flooding situation in Bangkok. Study of hazards and vulnerabilities from natural disaster is always important for risk analysis so that we can contribute somewhat in reducing damages will happen in future. This study models flood risk for Bangkok Province of Thailand using the Analytical Hierarchy Process (AHP). GIS is potential tool to assess the risk of flooding using parameters like rainfall, elevation, land use etc and indentified the flood risk areas in Bangkok by producing flood risk map. The study reveals that Bangkok is too much susceptible to flood where Nong Kok had the safe area with respect to hazard and Taling Chan amphoe had shown maximum area with high hazard. Overlay raster analysis had been used to predict the flood inundation area which showed that areas near Chao Phraya River or areas having high rainfall intensities consisting amphoe such as Taling Chan and Phasi Charoen had high flood risk.

Keywords: *Natural disasters, Flood risk mapping, Arc GIS and AHP*

1. INTRODUCTION

Natural disasters occurring on earth always cause loss of life, property damage as well as social and economic disruption such as earth quake, windstorms, tsunamis, floods, landslides, volcanic eruptions, wildfires,

grasshopper and locust infestations, drought and desertification and other calamities of natural origin. So study of hazards and vulnerabilities from natural disaster is always important for risk analysis so that we can contribute somewhat in reducing damages if same disaster will happen in future.

Here we are going to predict flood risk in Bangkok using some GIS spatial analysis technique as well as ArcGIS software tools. Bangkok is located on low lying alluvial deposit and most reports say that it always flooded every year by tide, river flow and also by direct precipitation. As Bangkok being capital of Thailand, It must be always protected from such type of natural disasters as it has 10% of total population in Thailand in this area and also it contributes much in Thailand economy. It is situated on low flat plain of the Chao Phraya River at a distance 25-56 km from its mouth and its average land level is about 0-1.5m above mean sea level (Wikipedia). So it holds greater risk of flooding Bangkok is within the monsoon region which has frequent and heavy rainfall. Over the past few years the impact of flooding has become an important issue for Bangkok. Although the Royal Thai Government has been undertaking various measures, it has not yet become possible to mitigate the flood disasters in this capital city and economic hub of Thailand. In the Bangkok Metropolitan and its vicinity, urban and built-up lands have increased by 115% from 1,058 km to 2,280 in the last 15 years. The rapid urbanization and heavy soil settlement have adversely affected the flooding situation in Bangkok. Climatic change is likely to worsen the situation. With changes to weather patterns (effects of climate change) and the impact that development has on water movement to streams and rivers, the risk of flash flooding and floods has increased.

Actually there is no technique like which can interpret accurate actual risk about natural disaster but here we have tried to work on these efforts little bit. We cannot say it can be completely accurate analysis. Here we have used ArcGIS software and some spatial analysis techniques for criteria weighting. The objectives of this study are such as, 1. To create hazard map for Bangkok 2. To create vulnerability map Bangkok 3. To create flood risk map Bangkok 4. . To create model for flood risk mapping

2. STUDY AREA

Bangkok is the capital city of Thailand characterized by a high population density. The city is located between 100°18'39.837" to 100°56'53.703" east longitude and 13°28'47.57" to 14°0'31.249" north latitude (Figure 1). It is bounded by the province of Pathumthani in the north, Chacheongsao in the east, Nakorn Pathom in the west and Samuth Prakam in the south. As of 2008, the province has an approximate population of 18 million competing for a limited surface area of 1,500 square kilometers. The Chao Phraya River cuts the city in the center from the north and drains towards the Gulf of Thailand. This river causes periodical flooding in the city resulting to major economic and social loss to its inhabitants.

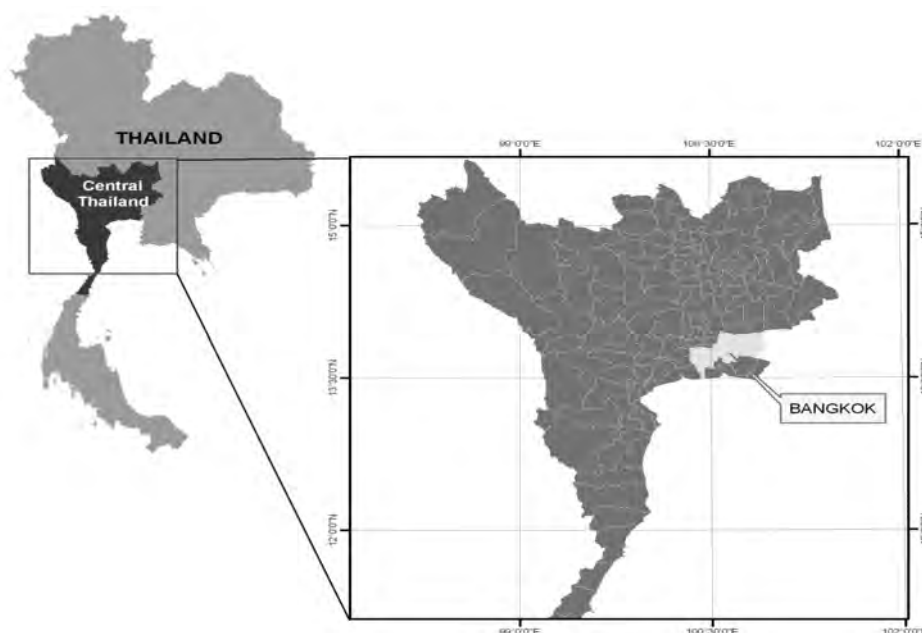


Figure 1: Location map of Bangkok province

3. METHODOLOGY

Flood risk is a function of flood hazard and flood vulnerability that involves several physical and socio-economic contributory factors. One of the problems associated with flood risk analysis is the handling of large amount of data as inputs for flood hazard and vulnerability models. Using GIS, data inputs can be stored in a standardized manner and analysis can be repeatedly performed if the desired outcome is not reached. For this project, raster analysis was used to derived flood hazard map, flood vulnerability map and flood risk map. Weights are applied to the identified factors which were derived using the Analytical Hierarchy Process and Rank Sum. The general methodology that was followed to create the flood risk map of Bangkok is shown in Figure 2.

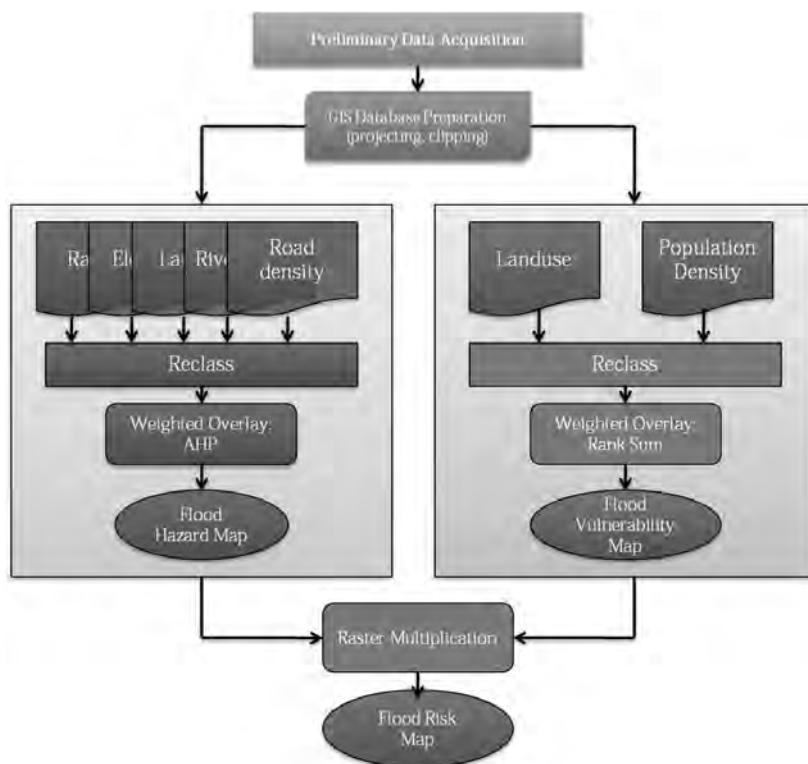


Figure 2. General methodology of flood urban flood risk mapping of Bangkok Province

Preliminary data acquisition involves gathering of digital map and demographic data of the province of Bangkok. The data used in this project was several thematic layers acquired from archived Thai GIS database and downloaded from the internet (<http://www.rsgis.ait.ac.th/~souris/thailand.htm>). Recent (2004) population data of Bangkok was also downloaded from the internet so that an updated population density can be derived. As a summary, the following are some of the raster and vector layers used for this study to derive other variables for the hazard and vulnerability mapping.

Table 1: Data used in the study

Data Layer	Data Type	Source
Bangkok political boundary	Vector (Amphoe and Tambon level)	Thai GIS Data (RSGIS Dept. AIT)
Bangkok DEM	Raster (90 m) [Tile 57,10]	http://srtm.csi.cgiar.org/
Landuse map	vector	http://www.star.ait.ac.th/~souris/thailand.htm
Rainfall map	Vector (point)	http://www.star.ait.ac.th/~souris/thailand.htm
Stream networks	Vector (line)	http://www.star.ait.ac.th/~souris/thailand.htm
Road networks	Vector (line)	Thai GIS Data (RSGIS Dept., AIT)
2004 population (amphoe level)	Statistical data	http://en.wikipedia.org/wiki/Bangkok
Elevation map	Raster	Derived from DEM

Database preparation is required for further processing of data layers. Flood hazard mapping was done using raster analysis specifically using the raster calculator of Spatial Analyst extension of ArcGIS. Weights derived from Analytical Hierarchy Process were applied for each factor or criteria that contribute to flood hazard susceptibility of Bangkok province. Several research studies have identified various factors for flood hazard analysis. In this study, the factors used in the study conducted by Tanavud et.al were followed these are: rainfall, elevation, landuse based on its infiltration capacity, distance to river (river buffer), and road density.

Table 2: Identified factors for flood hazard mapping

Factors/Criteria	AHP Weight	Subfactors	Hazard Ranking
Rainfall	0.395	< 900 mm	1
		900 – 1200 mm	2
		1200 – 1600 mm	3
		1600 – 2000 mm	4
		> 2000 mm	5
Elevation	0.075	< 1.5 meters	4
		1.5 – 3 meters	3
		3 – 6 meters	2
		> 6 meters	1
Landuse (infiltration capacity)	0.224	Water	4
		Airport/Bare/Urban	3
		Grass/Agriculture	2
		Mangrove Forest	1
River buffer (Chao Praya River)	0.109	0 – 5000 meters	4
		5000 – 10000 meters	3
		10000 – 20000 meters	2
		> 20000 meters	1
Road density	0.142	< 0.5 km/km ²	1
		0.5 – 1 km/km ²	2
		1 – 1.5 km/km ²	3
		1.5 – 2 km/km ²	4
		> 2 km/km ²	5

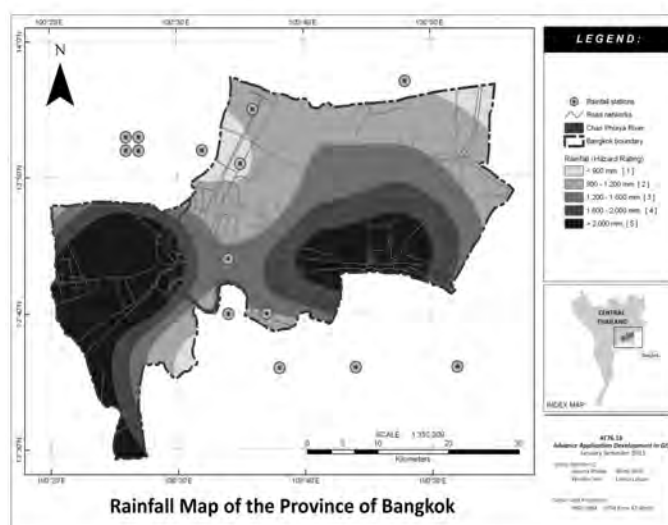


Figure 3: Rainfall map of Bangkok

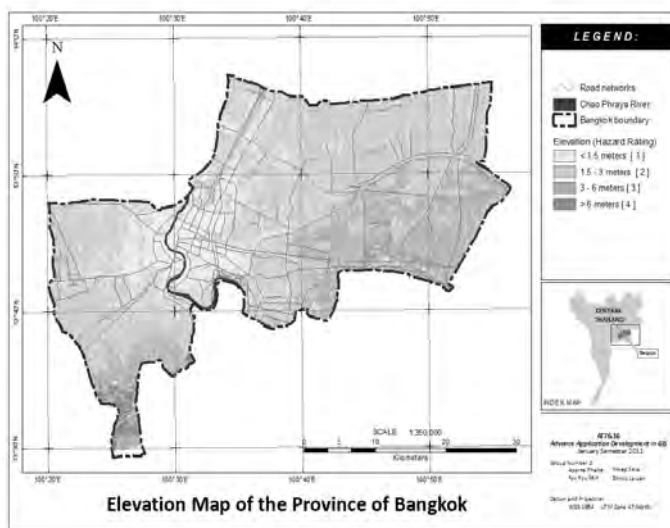


Figure 4: Elevation map of Bangkok

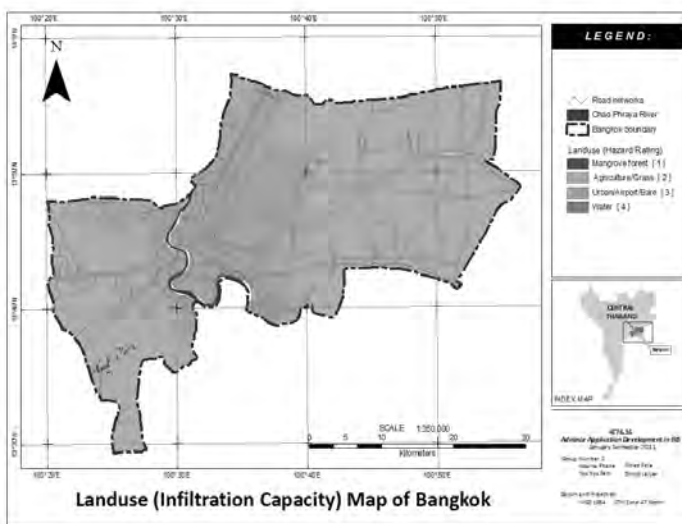


Figure 5: Landuse map of Bangkok

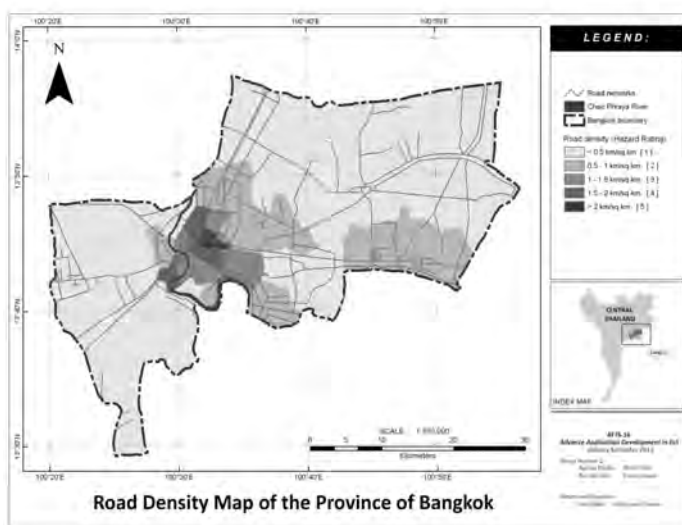


Figure 6: Road density map of Bangkok

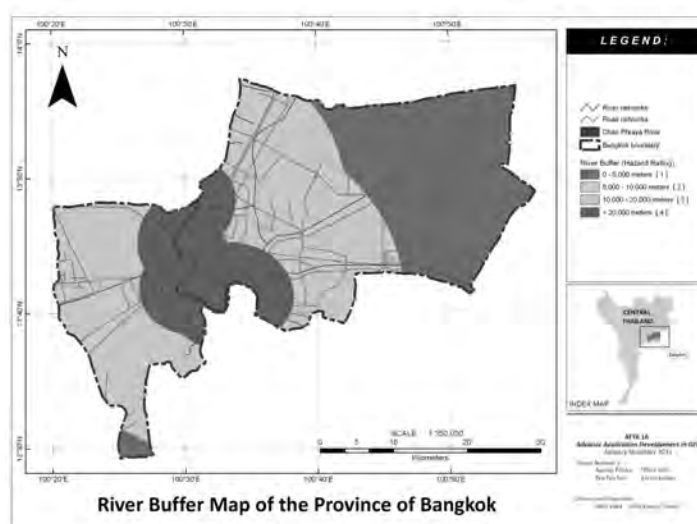


Figure 7: River buffer map of Bangkok

3.1.1 Flood Hazard Weighing by AHP

Designation of weights for each flood hazard factors was done using Analytical Hierarchy Process (AHP). The AHP developed by Saaty in 1980 was used to construct a matrix that weighs each criterion against each other based on a scale of 1 to 9, 1 being of equal importance and 9 of extreme importance. Table 4 shows the results of the Relative Importance Weights (RIW) using AHP derived for each factor.

Table 3: Table showing the weight matrix of relative importance for each factor

	Factors				
	Rainfall	Landuse	Road Density	River Buffer	Elevation
Rainfall	1	2	4	3	5
Landuse	0.5	1	2	3	2
Road Density	0.25	0.5	1	2	2
River Buffer	0.333333	0.333333	0.5	1	2
Elevation	0.2	0.5	0.5	0.5	1
Total	2.283333	4.333333	8	9.5	12

Table 4: Consistency matrix and the derived weights.

	Factors					Row Total	RIW	Lambda	Consistency Vector
	Rainfall	Landuse	Road Density	River Buffer	Elevation				
Rainfall	0.387102	0.418119	0.363636	0.352941	0.454545	1.976344	0.395269	10.56863	5.3475682
Landuse	0.193551	0.209059	0.181818	0.352941	0.181818	1.119188	0.223838	5.911208	5.281694023
Road Density	0.096775	0.10453	0.090909	0.235294	0.181818	0.709327	0.141865	3.604561	5.081666831
River Buffer	0.129034	0.069686	0.045455	0.117647	0.181818	0.54364	0.108728	2.684422	4.937864745
Elevation	0.07742	0.10453	0.045455	0.058824	0.090909	0.377137	0.075427	1.958483	5.193025545

The consistency ratio (CR) was calculated to check if the estimated weights are good or needs to be changed. The ideal value of CR must be less than 0.10; otherwise, the some values in Table X must be changed and recomputed again. CR is derived by taking the ratio of Consistency Index (CI) and the Random Index (RI). CI is calculated using the following equation:

$$CI = \frac{(\lambda - n)}{(n - 1)}$$

Where λ is the average value of the consistency vector and n is the number of factors. The following table gives the RI values for each given order of matrix:

Table 5: Random index values

No. of Factors	1	2	3	4	5	6	7	8	9
RI	0	0	0.58	0.90	1.12	1.24	.32	1.41	1.45

For this study, the calculated CI and CR were 0.042 and 0.037, respectively. Since the CR value is less than 0.10, the derived RIW are good enough to be used for the flood hazard model.

3.1.2 Flood Hazard Overlay

The weighted linear combination was applied to compute for the flood hazard index map of Bangkok.

$$FHI_i = \sum_{j=1}^n (RIW_j * X_{ij})$$

Where FHI_i is the flood hazard index for area I, RIW_j is the calculated weight for factor j, and X_{ij} is the hazard rating of sub-factor i.

The above equation was used to derive the following raster calculator expression in ArcGIS Spatial Analyst:

$$Hazard\ Map = [0.395 * rainfall] + [0.224 * landuse] + [0.075 * elevation] + [0.109 * rivbuffer] + [0.142 * roadden]$$

3.2 Flood Vulnerability Mapping

According to UNESCO-IHE (2011), flood vulnerability is the degree of loss (i.e. property and lives) for a given flood hazard at a given severity level. In this study two vulnerability factors was used; population density and landuse. Flood vulnerability mapping was also done using raster analysis using the raster calculator of Spatial Analyst extension of ArcGIS. But, since there were only two factors for vulnerability were identified, the weights were derived using rank sum instead of AHP.

3.2.1 Flood Vulnerability Factors

The ranking of the sub-factors for flood vulnerability are tabulated on the succeeding table:

Table 6: Factors for flood vulnerability mapping

Factors/Criteria	Rank Sum Weight	Subfactors	Vulnerability Ranking
Population Density	0.333	< 6000 6000 – 10000 10000 – 15000 15000 – 25000 > 25000	1 2 3 4 5
Landuse (Infrastructure)	0.667	Water Bare/Urban/Airport Agriculture Mangrove Forest/Grass	2 4 3 1

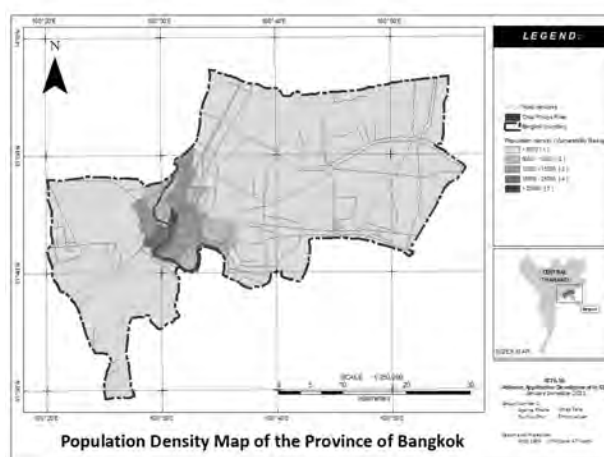


Figure 8: Population density map of Bangkok

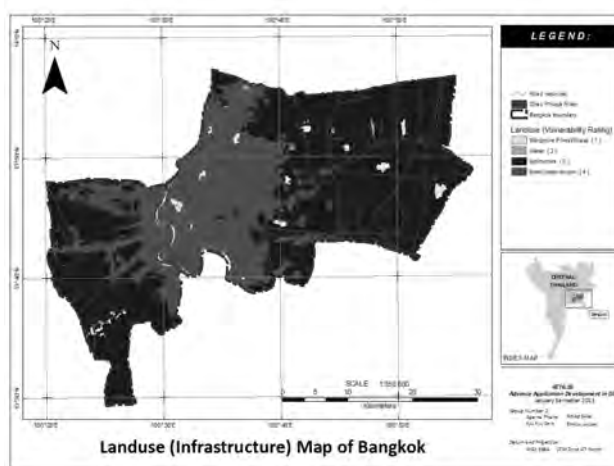


Figure 9: Landuse map of Bangkok

3.2.2 Flood Vulnerability Weights Using Rank Sum

Due to the limited number of factors identified for flood vulnerability, the Rank Sum method of obtaining weights was used instead of the Analytical Hierarchy Process. In rank sum method, an arbitrary rank was first specified for each of the identified factors. A weight for each factor was then computed using the following formula:

$$Weight = n - r + 1$$

Where n is the number of factors, and r is the arbitrary rank of each factor. The derived weights are then normalized to derive the final weights that will be used for the flood vulnerability model (Table 7).

Table 7: Derived weights for each vulnerability factors using the Rank Sum method.

Factors	Criterion	Rank	Weight (n-r+1)	Normalized Weights
Landuse	1	2	1	0.333
Population density	2	1	2	0.667
TOTAL			3	1

3.2.3 Flood Vulnerability Overlay

Following raster calculator expression in ArcGIS Spatial Analyst:
 Vulnerability Map = [0.333 * popden] + [0.667 * landuse]

3.3 Flood Risk Mapping

Flood risk is a function of flood hazard and flood vulnerability. To derived the flood risk map of Bangkok, the two derived layers from the previous steps where overlaid using raster multiplication.

Below is the raster calculator expression that was used to derive the flood risk map of Bangkok.

$$Risk\ Map = hazard\ map * vulnerability\ map$$

3.4 Model for Flood Risk Mapping

Aside from the conventional way of flood risk mapping using the raster calculator, a model to perform all the raster overlay tasks can be created using the Model Builder. The model has two main processes: weighed sum, and reclassification tool

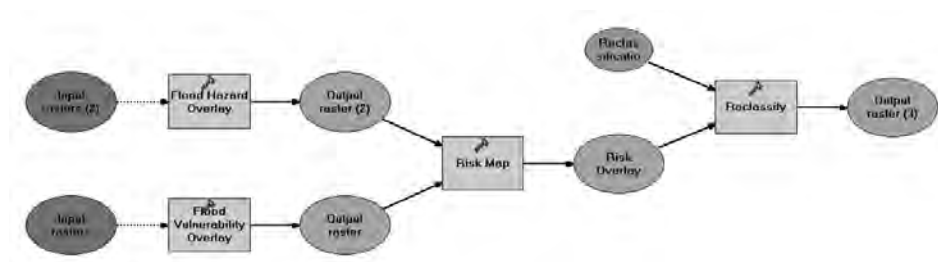


Figure 10: Flood risk model

4. RESULTS AND DISCUSSIONS

In this study we want to know the risk of flood in Bangkok. For this purpose we have first found hazard and vulnerability in the study area as we explained in methodology. The respective results on amphoe level for hazard, vulnerability and risk are explained as follows:

4.1 Distribution of Areas Based on the Level/Classes of Flood Hazard:

Figure 12 shows the distribution of hazard in Bangkok. According to Table 8, amount of area which has very high hazard is 13,762.03 ha but we can see that maximum total area for high hazard is more compared to other hazard level. So, Bangkok is too much susceptible to flood. Nong kok has more area with very low hazard. So, Nong kok is the safe area with respect to hazard but on other side Taling chan amphoe shows maximum area with high hazard

Following figure 11 shown graphical distribution of hazard in study area

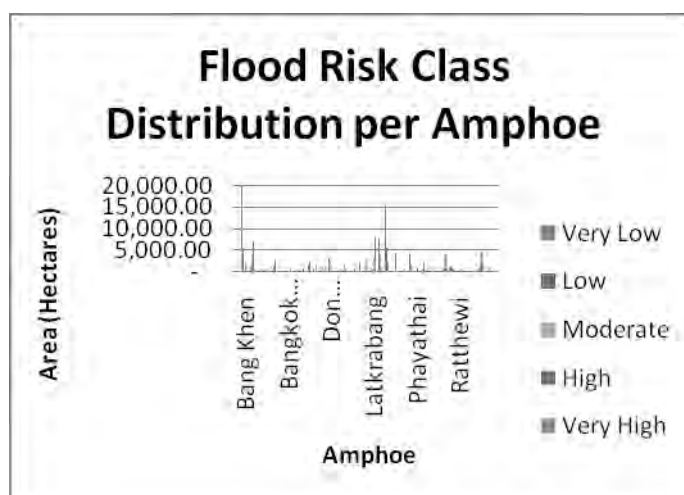


Figure 11: Area distribution of flood hazard class

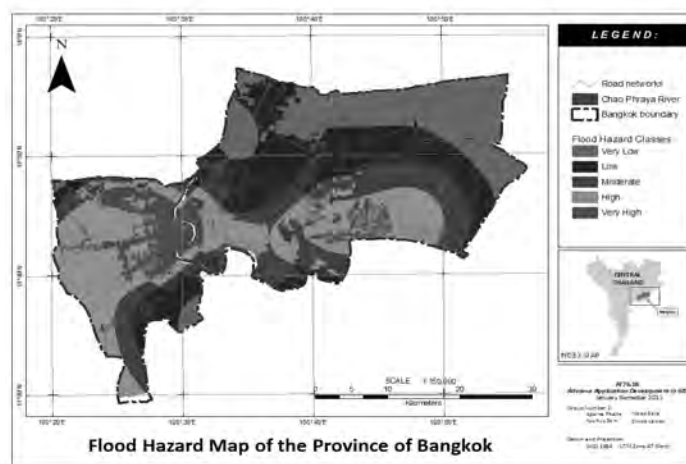


Figure 12: Flood hazard map of Bangkok

4.2 Distribution of Areas Based on the Level of Flood Vulnerability

Figure 13 shows the vulnerability distribution in Bangkok. Majority of Bangkok falls under the moderate vulnerability level with an approximate area of 100,613.34 hectares. Amphoe Bang Su which is located in the north central portion of Bangkok just which is just adjacent to Chao Phraya river has a very high flood vulnerability compared to other amphoe.

Unsurprisingly, amphoes which are far from Chao Phraya river have very low flood vulnerability. Some of these amphoes are Bang Khen, Bang Khun Tian, Minburi, Nong Chok, and Bankapi (Table 9)

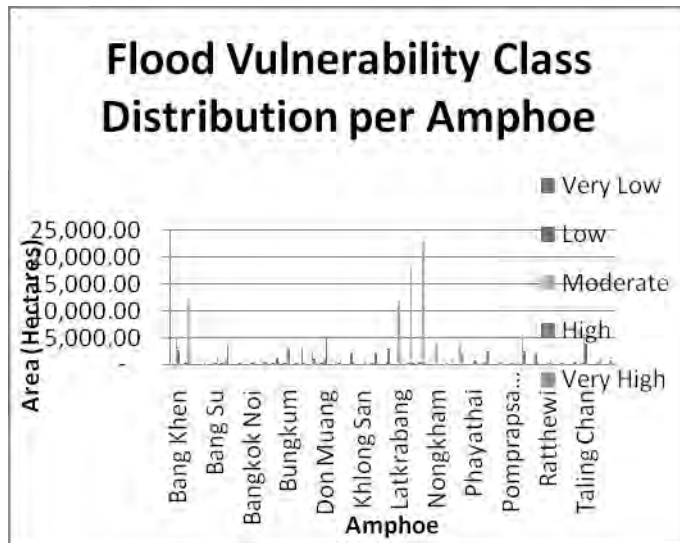


Figure 13: Area distribution of flood vulnerability classes

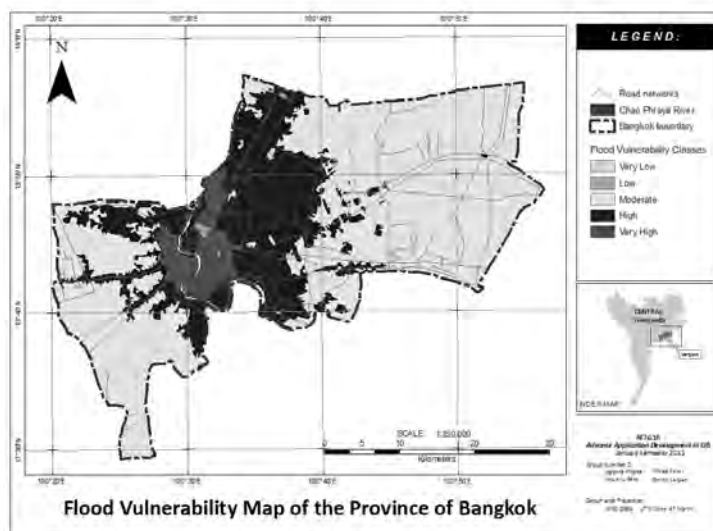


Figure 14: Flood vulnerability map of Bangkok

4.3 Distribution of Areas Based on the Level of Flood Risk

Using the flood hazard and flood vulnerability layers, the flood risk map for the entire Bangkok was derived using raster overlay analysis by employing raster multiplication. Figure 15 and Table 10 summarizes the distribution of flood risk in Bangkok at the Amphoe level. Majority of Bangkok province falls under the high risk category at 48, 977.43 hectares or 31% of the province’s total land area. As expected, areas that fall under the high risk category are either near Chao Phraya river or areas characterized by relatively high rainfall occurrence. Such Amphoe are Taling Chan and Phasi Charoen. In contrast, amphoe that are far from Chao

Phraya river like Nong Chok, Bang Khen, and Don Muang were very low risk to flooding

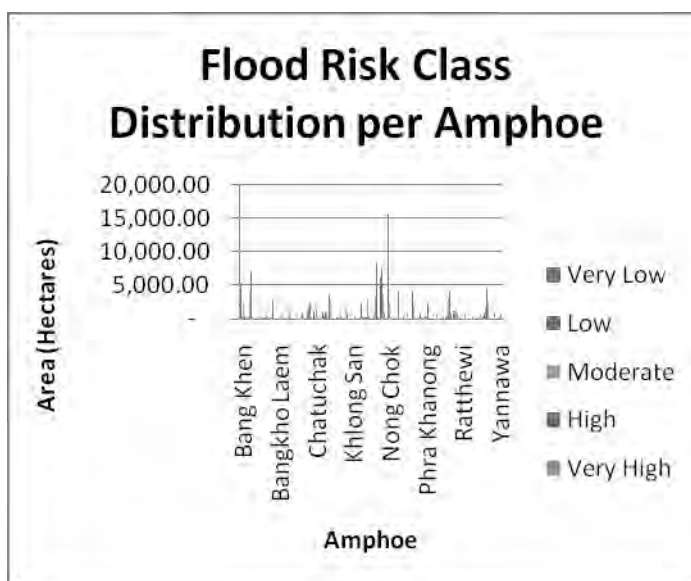


Figure 15: Area distribution of flood risk classes

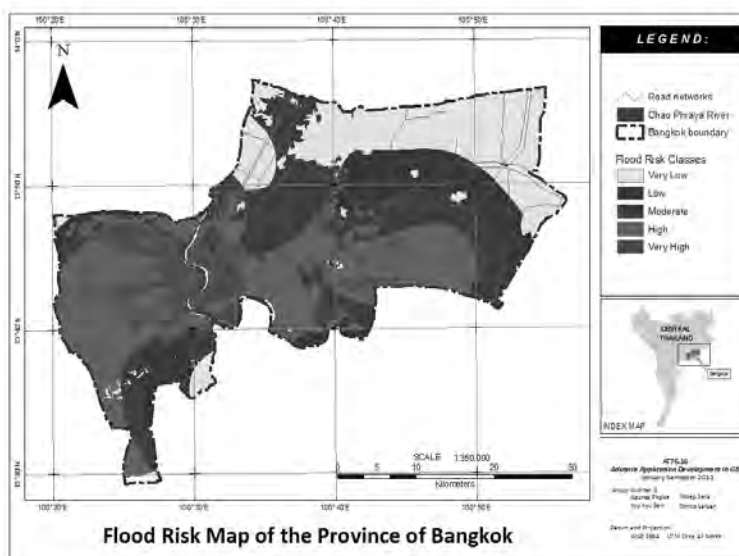


Figure 16: Flood risk map of Bangkok

5. CONCLUSIONS

For calculation of flood risk we used analytical hierarchical method for weighting different factors affecting flood risk which gives very efficient results as most of high flood risk along the river named chao phraya as it can be acceptable practically and also consistency ratio was 0.037 which was less than 0.1 so acceptable. On other hand we used Rank reciprocal method for calculating weights for factors affecting vulnerability which is also found to be efficient. We used ArcGIS package which gave high capability of utility tools in our project Flood risk analysis study is most

important because if we have idea about risk before disaster we can make some protective measures and can creat capability to fight against the disaster . As this risk is highest in such capital cities or main cities of country then it can affect the economy of that country at its most.This study results can help to government of respective countries for getting idea before disaster or upcoming future assessment .

There is limitation in AHP method we found that we cannot use this for less than three parameters.We can consider more factors like runoff, drainage density etc. for increasing accuracy of result and also field survey is important as a validation procedure.Outdated and limited data causes the results of the analysis to be less accurate.We can use artificial neural network for calculating weights and after comparing both AHP and ANN we can get more correct result.And also other interpolation methods can be used for rainfall and comparative results can be used for correction.

REFERENCES

Evans Sun Yan, Gunn Neil and Daniel Williams *undated*. Use of GIS in Flood Risk Modelling. Environment Agency: Kent, ME 19 5SH.

Sengtianthr Virany 2007. Flood Risk Map using RS and GIS: A Case Study of Champone District Savannakhet Province , Lao PDR. A paper presented during the 3rd JPTM held on 13-15 March 2007 at Le Meridien, Singapore.

Shoastal Cristy 2007. Combining GIS with a Hydraulic Food Prediction Model: Developing a Custom GIS Tool for Near Real-Time Flood Inundation Mapping in the Fargo-Moorhead Portion of the Re River Basin. Volume 9, Papers in Resource Analysis, 17 pp. Saint Mary's University of Minnessota University Central Services Press. Wirona, MN.

Tanavud, Charlchai et al. 2004. Assessment of flood risk in Hat Yai municipality, Southern Thailand using GIS.

UNESCO-IHE Homepage (2011). < <http://www.unesco-ihe-fvi.org/>>
Wikipedia Online Encyclopedia 2011.
<<http://en.wikipedia.org/wiki/Bangkok>

Geophysical investigation at Meghna Dhonagoda Irrigation Project (MDIP) using ground penetrating radar method

Ram Krishna MAZUMDER¹
and Mehedi Ahmed ANSARY²

¹Research Engineer, SHMRBBP, BUET, Bangladesh

²Professor, Department of Civil Engineering, BUET, Dhaka, Bangladesh
ansary@ce.buet.ac.bd

ABSTRACT

Meghna Dhonagoda Irrigation Project (MDIP) is located at northern part of Chandpur district and 40 km south east of Dhaka near the confluence of the Padma and the Meghna River. MDIP is a 60 km long embankment. Recently, severe seepage and boiling were observed in the countryside of MDIP. To find the reason behind these problems, various laboratory and field tests at different locations of the embankment were carried out. After collected geotechnical data, cement stabilization at 11 points were suggested as remedial measures. To assess the strengthening work of MDIP at different points, geophysical investigation was carried out using Ground Penetrating Radar (GPR). A 100 megahertz (MHz) frequency antenna has been used to determine the layer profile of the embankment. Common Depth Point (CDP) and bi-static high range reflection profiling has been used for data collection.

Keywords: *Geophysical, Ground Penetrating Radar and Common Depth Point*

1. INTRODUCTION

The project is located at 19 km North of Chandpur Town and 40 km South East of Dhaka near the confluence of the Padma & the Meghna River. MDIP comprises the gross area of 17584 ha in Matlab Upazilla of Chandpur district is bounded on the North and the West by the mighty Meghna and on the East and the South by the Dhonagoda River.

The Project is encircled by a 60.7 km of flood embankment completed in 1987. After completion of the embankment, severe seepage and boiling were observed along the countryside of the embankment during floods. The embankment was breached during 1987 and 1988 floods causing severe damages. During the flood of 2004, a breach at Nandalalpur occurred but no damage could be caused as the Bangladesh Water Development Board (BWDB) authorities repaired the breach quickly with the help of local

people. Furthermore, sliding of the slope of embankments occurred on the countryside at about 60 places, seepage problems developed at about 25 km length and boiling occurred at about 120 locations. Figure 1 shows the embankment location and the affected points. The damages were severe and it remained as a threat to future performance of the embankment during floods (Ansary et al., 2009).

To strengthening the embankment, currently BWDB authorities are injecting cement grouting up to 5 m to 12 m below the surface. This paper presents the geophysical study which was carried out to evaluate the performance of the embankment after the cement grouting was completed.



Figure 1: Location of Meghna Dhonagoda Irrigation Project (MDIP) and erosion points (right)

2. SUBSOIL INVESTIGATION

The field investigation at the embankment site consisted of drilling of boreholes, recording density or stiffness characteristics of soil layers by carrying out Standard Penetration Tests (SPT), collection of sufficient numbers of disturbed and undisturbed tube samples. Also portable seismograph was used to support the result obtained from SPT-N values. A total of fifty six boreholes at eleven sites were drilled vertically at this site using wash boring technique. The depth of boreholes below the ground surface varied from 10 m to 17 m. In general five boreholes were drilled at each site across an embankment section.

2.1 Soil Sampling

Disturbed and undisturbed samples were collected from the boreholes. A split-spoon sampler was used to obtain the disturbed samples in conjunction with the Standard Penetration Test. Undisturbed samples were also retrieved from cohesive layers of the boreholes by pushing conventional 76 mm external diameter thin-walled Shelby tubes following the procedure outlined in ASTM D1587. The locations of disturbed and undisturbed samples obtained from the boreholes are shown in the bore logs. The drilling of the fifty six boreholes at the project site, including collection of disturbed and undisturbed tube samples and performance of Standard Penetration Test (SPT) were carried out by the Groundwater Hydrology Division of BWDB.

2.2 Soil Profile and Parameters across Embankment Alignment

A typical soil profile across the embankment is shown in Figure 2.

Particle size distribution was obtained following procedures mentioned in ASTM D422, ASTM C136 and ASTM D1140 on samples from different boreholes and from different depths. Particle size characteristics (d_{10} , d_{15} , d_{30} , d_{50} , d_{60} , d_{85} , percentage of non plastic fines, C_u , C_c) are also presented tabular form. A summary of the amount of fine material (% finer than #200 sieves i.e. 0.074 mm) in soils at different depths and in different locations tested (Ansary et al., 2009).

As has been mentioned earlier the subsoil consisted mostly of cohesionless soil and undisturbed samples could not be retrieved from the boreholes. It therefore became apparent that shear strength parameters for this layer has to be interpreted from the field-N values based on appropriate corrections and available empirical relations. Since the soil mineralogy and grain characteristics could be different from those for which correlations is available, it was decided to perform laboratory shear strength tests on samples reconstituted from disturbed samples at different densities in order to achieve possible highest and lowest range of strength parameter (Ansary et al., 2009)..

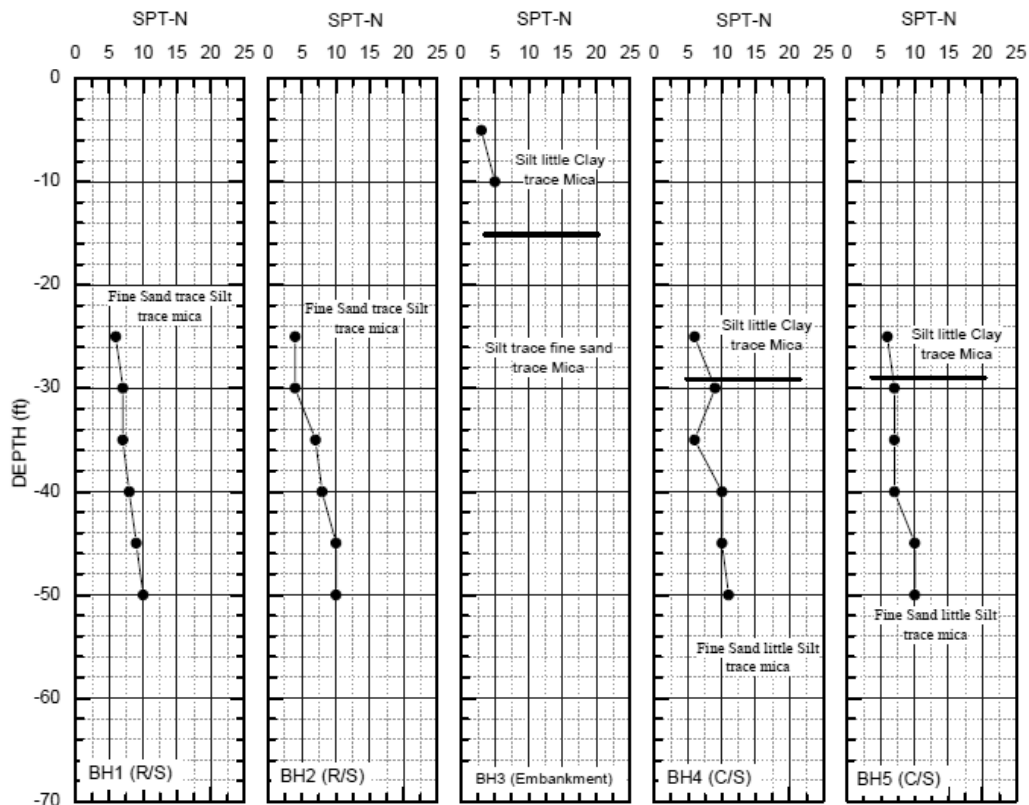


Figure 2: Typical Soil Profile across MDIP embankment (after Ansary et al., 2009)

Direct shear tests were performed on reconstituted (near to field density as depicted from SPT) disturbed soil samples from several location and depth to obtain the angle of internal friction, and cohesion intercept, *c* of the sub-soil. The tests were performed on air dry soil. Specimens were tested under three different normal stresses (45 kPa, 90 kPa, and 180 kPa) and the strength parameters were determined from the failure envelope with various physical properties of the soil encountered. For the soils tested apparent cohesion, *c* was found to be negligible and in the range of 0-16 kN/m. The angle of internal friction, the soils is in the range of 26.7 to 35.8. It can be seen that the range of void ratio (*e*) of the soil is 0.81 to 1.13 corresponding to porosities (*n*) of 0.45 to 0.53 respectively. The experimental results indicate that the soils of the site are predominantly fine sand existing in a loose to medium dense state.

Constant head permeability test was carried out on specimen prepared by mixing soils from different boreholes and depths. For better representation of field conditions the flow of water was allowed upward through the specimen by using a special constant head permeameter. The boiling phenomenon was simulated for the field conditions using this apparatus. The gradient was found to be lower than the theoretical value of 1.0. The permeability of the soil was also estimated using Allen Hazens well known empirical formula of $k=Cd^{2}_{10}$ using the range of *C* values of 100 to 150 (Lees and Chuaqui, 2004).

3. GPR PRINCIPLE

Geophysical exploration is a non-destructive, cost effective way to help locate and characterize features beneath the ground at many sites; GPR is one of the better techniques for this search in the shallow subsurface. GPR is a near-surface geophysical technique that can provide high resolution images of the dielectric properties about 20 meters of the earth. It is a very useful technique which employ the radio waves typically 16 to 2000 MHz frequency range, to study structure and features buried in the ground, groundwater, subsurface faulting, and underground cavities (natural or man).

A trigger pulse is generated in the control unit at a normal repetition rate of about 100 kHz. The trigger pulse is sent through the control cable to the transmitter electronics in the antenna. In the transducer, each trigger pulse is transformed into a bipolar pulse with higher amplitude than the trigger pulse. The pulse shape varies with the electronics and the antenna. The transmit pulse then propagates along the antenna and is radiated into the subsurface. The size of the antenna and electrical properties of the subsurface determine the frequency of the propagating energy. In the subsurface, reflections occur at boundaries where there is a dielectric contrast. The reflected portion of the signal travels back to the antenna. The receiver in the antenna detects the returning signal and sends it back to the control unit. In the control unit the signal is processed and displayed. The output of the graphic recorder or the display on the video is a representation of the analog signal. Horizontal axis is distance along the surface and vertical axis is two-way travel time of the radar pulse in nanoseconds (ns). The signal amplitude determines the shade of grey on the paper or the color on the video display.

The penetration depth is controlled by the GPR centre frequency, the electrical conductivity and the attenuation of the subsurface deposits. In low-loss (i.e., resistive) deposits a low centre frequency achieves a large penetration depth whereas a high centre frequency results in a lower penetration depth. Figure 3 shows the fundamental principal of GPR.

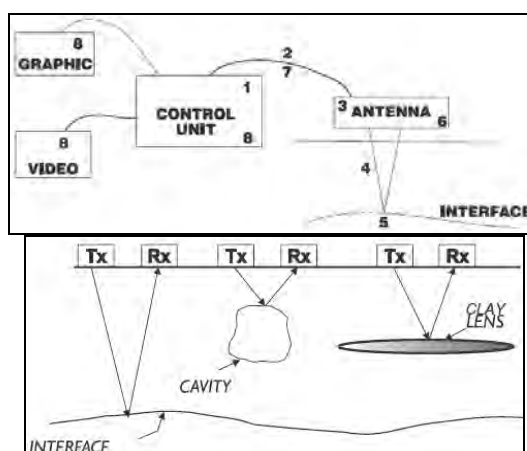


Figure 3: Fundamental principal of GPR

3.1 Modal propagation Theory

Modal propagation within a layer waveguide (of permittivity ϵ_2) refers to lossless propagation and is especially dispersive when the layer thickness is close to or less than an in-situ wavelength λ , (Arcone et al., 1998). In a two layer dielectric ground, lossless (nonleaky) modes occur when the confining layers (e.g. air above, for which $\epsilon_1=1$ and dry sand ϵ_3 below) have lower permittivities than the waveguide. In this case, a refraction will occur in the lower layer at the critical angle, and dispersive modes will develop in the upper layer (Figure 2). Depending on waveguide thickness d and ϵ_2 , higher order modes will develop which have phase fronts that propagate at speeds determined by discrete angles (measured from vertical) greater than the critical angle. The lowest order mode is always the strongest and most important. The modes are determined by the modal equation (Budden, 1961) for either transverse electric (TE) or transverse magnetic (TM) waves, such that

$$R_{01}R_{12} \exp (i2k_2d \cos\theta) = 1$$

Where R_{01} and R_{12} are the TE or TM reflection coefficients for the upper and lower layer interfaces, respectively; $k_2=k_0\sqrt{\epsilon_2}$ is the propagation function for the refracting layer; and θ is the modal angle of a particular frequency with respect to vertical. The quantity $k_0=2\pi f/c$, where f is frequency in Hz and $c=30$ cm/ns. The phase velocity of any particular frequency is

$$v_{ph}=c/\sqrt{\epsilon_2} \sin \theta$$

For our case of parallel and facing antennas, we consider only TE waves. In this case all modes have a minimal cutoff frequency where phase and group velocities equal the velocity within an adjacent, refracting layer and a higher frequency at which minimum group velocity occurs and energy is theoretically maximized. This latter phenomenon is known as the Airy phase (Grant and West, 1965). For given values of d and the permittivities of each layer, several modes might exist, each of which can support all frequencies above their own particular cutoff frequency.

Modal propagation losses are caused by transmission through the waveguide interfaces, intrinsic attenuation within the medium itself, and geometric wavefront spreading. Interface transmission losses and intrinsic attenuation, such as caused by conduction currents or scattering, may be expressed through a complex, equivalent propagation angle $\theta + i\gamma$, for which the phase velocity then becomes

$$v_{ph}=c/\sqrt{\epsilon_2} \sin\theta \cosh\gamma$$

If $\epsilon_1 > \epsilon_2$, then transmission leakage into the lower layer can produce values of γ near unity and attenuation rates can approach several tens of decibels per meter. For the case of our refractive waveguide, however, real energy loss occurs strictly through medium attenuation mechanisms. Apparent energy loss at any particular frequency occurs from the dispersive process itself.

For geometric spreading losses we consider that the amplitudes of modes, refractions, and any kind of lateral surface wave decay in proportion to r^2 , where r is the range separation between transmitter and receiver antennas. The range is both several wavelengths from the source and much greater than the surface layer depth. We assume this range dependency because very thin layers (in terms of γ) support nearly interfacial waves; interfacial waves along homogeneous ground follow this behavior (Annan, 1973), and so do seismic refractions (O'Brien, 1967). Furthermore, the low-frequency wave velocity that developed in our surface waveguide emulates refraction along the lower interface (Steven et. al., 2003)

4. FIELD TECHNICS

We used the Geophysical Survey Systems, Inc. (GSSI) model SIR-3000 control unit to set radar parameters and record data to hard disk. We used separate transmitter and receiver resistively loaded antennas with bandwidths nominally centered near dominant frequencies of 100 MHz (GSSI model 3207).

4.1 Reflection profiling

In reflection profiling mode the antennas are kept at constant separation, while they are moved along a profile (Figure 4). The electromagnetic pulses are transmitted at fixed time or distance interval. The signal is recorded and displayed immediately on a computer screen as GPR profiles, in which the vertical axis is two-way travel time in nanoseconds (ns) and the horizontal axis is distance along the measured profile. The GPR data are either collected along a single profile or in a grid of profiles to obtain 2D or pseudo 3D information on structures in the ground. The GPR data can also be acquired along lines so densely spaced that the line spacing equals the stepwise along the line. This leads to a 3D data cube, where data also can be displayed as time or depth slices. Study was conducted using bi-static high range profiling mode at distance interval according to Figure 4.

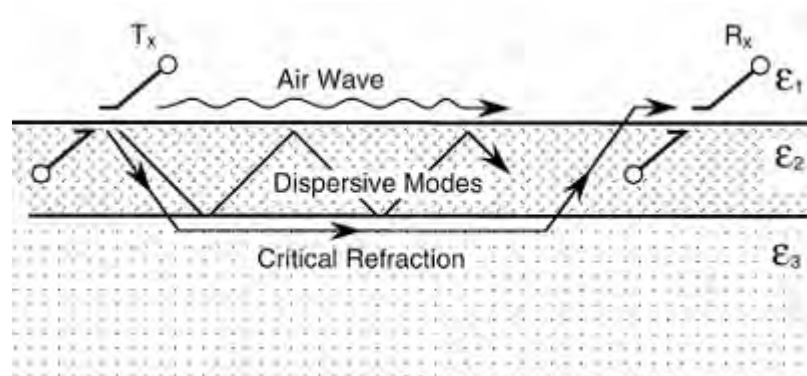




Figure 4: Diagram of the transmit (Tx) and receive (Rx) antennas, airwave, waveguide dispersive modes, and refraction (Top). 100-MHz antennas with fiber optic circuitry to trigger the receiver and antennas on the study line (bottom).

4.2 Common Depth Point

A common depth point dataset, CDP, is also called a velocity sounding, since the technique is commonly used for signal velocity establishment. In CDP mode the antennae separation is increased for each recording, while they are kept over a common midpoint (Figure 5a). A CDP plot contains the direct wave transmitted in the air above the ground, the direct wave transmitted in the ground and waves reflected from interfaces in the ground, where the dielectric properties change (Figure 5b). Refracted waves are seldom present in CDP soundings. This is related to the fact that the electromagnetic wave velocity decreases with depth together with increasing water content with depth.

5. RESULT ANALYSIS AND DISCUSSION

The test area of this study consisted of 75m along embankment foot and formed a 2-D section of underground stratum structure. Figure 6 displays the GPR section for distance on ground surface, at 0 m~40m. From the Figures, a clear surface of reflection can be observed along ground surface at underground depth of 6m, which shows different electrical properties of stratum above and below the reflection interface. This reflection interface is almost parallel to the ground level.

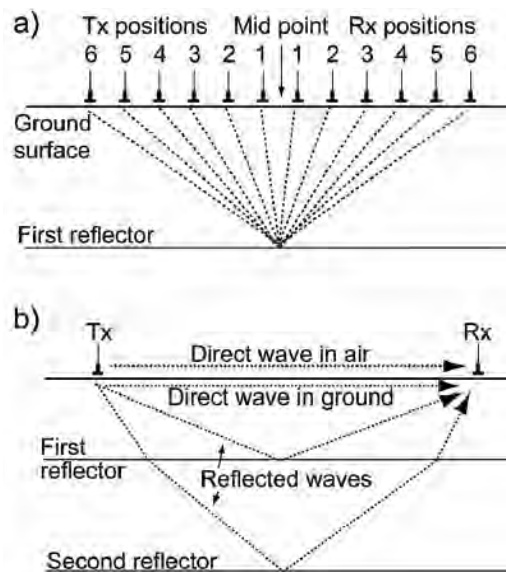


Figure 5: Principles of GPR in CDP mode. a) In CDP mode a set of a transmitting antenna (Tx) and a receiving antenna (Rx) are moved away from each other. The six first antenna positions are shown with the path of the reflected wave from the first reflector. b) Sketch of the path of the most common waves that is present in a CDP.

Groundwater table is present just below the 3m. Figure 6 implies that cement grouting has been successfully injected about 6m below the surface. The reflection signal is also very strong at 13m depth, which shows that the property of this layer differs a lot from the layers above and below it. Figure 7 shows the wiggly shape. This figure indicates that the strong signal of reflection below 6m depth is caused by rich content of underground water. Figure 8 shows the data collection in CDP mode. This data is used to estimate velocity of the soil with respect to depth profile.

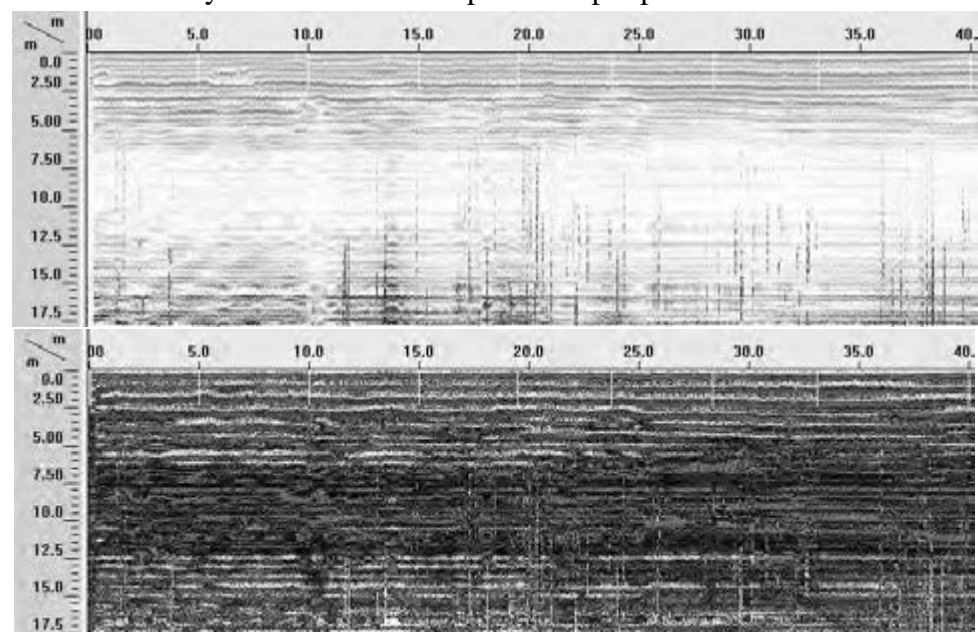


Figure 6: GPR Section at a distance of 0m~40m from ground surface (different color)

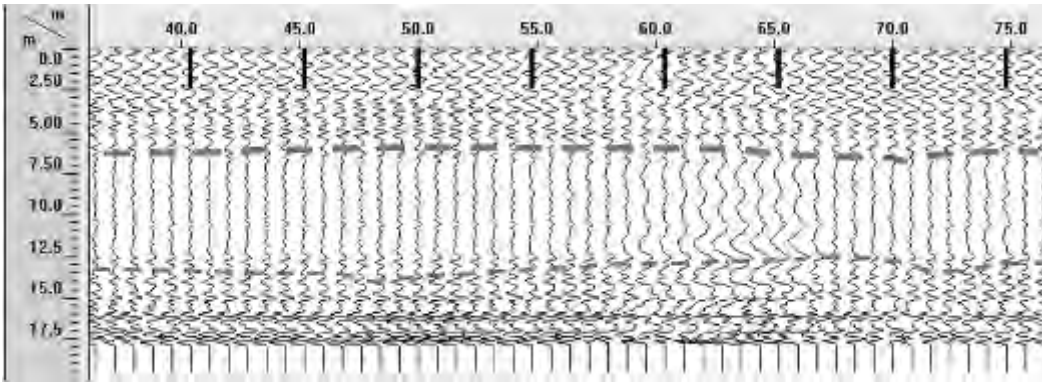


Figure 7: GPR Section in wiggle mode at a distance of 0m~75m from ground surface

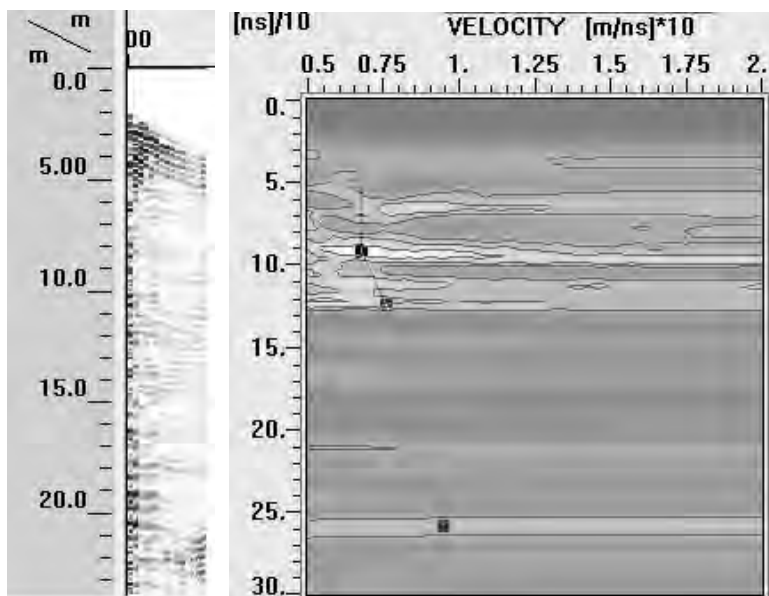


Figure 8: Multifold data are normally acquired or sorted in CDP gathers as represents in ray path form (left). An optimum stacking velocity versus travel time can be extracted which permits coherent summation of multifold survey data as well as a velocity depth function such as shown (right).

4. CONCLUSIONS

In this study, a 100 MHz frequency GPR antenna was used at Meghna Dhonagoda Irrigation Project (MDIP) site to evaluate the remedial measures undertaken using cement grouting technique at the river side in two affected embankment points. Common Depth Point (CDP) and bi-static high range reflection profiling was used for data collection. The collected data indicated that a water table did exist at a depth of 3m which was substantiated by the piezometer located at the investigated points. Also the collected GPR data indicated that the soil up to a depth of 6m might have improved by cement grouting technique.

REFERENCES

- Ansary, M. A., Yasin, S. J. M., Siddque, A., Abedin, M.Z. and Safiullah, A. M. M., (2009), Soil Investigation of Meghna Dhonagoda Irrigation Project (MDIP) Embankment, Proceedings of the Bangladesh Geotechnical Society's Conference in 2009 in Dhaka, Bangladesh.
- Annan, A. P., (1973), Radio interferometry depth sounding: Part I-Theoretical discussion, *Geophysics*, Vol. 38, pp. 557–580.
- Arcone, S. A., Lawson, D. E., Delaney, A. J., Strasser, J.C., and Strasser, J. D., (1998), Ground-penetrating radar reflection profiling of ground water and bedrock in an area of discontinuous permafrost. *Geophysics*, Vol 63, pp. 558-669.
- ASTM (2006), *American Society for Testing and Materials Standards*, Vol. 04.08.
- Budden, K. G., (1961), The wave-guide mode theory of wave propagation, *Prentice-Hall, Inc.*
- BWDB (2007), Cross Section of Flood Embankment at Boring Points of MDIP, Memo. No.PMO-JMREMP/ S-83/ 632, Project Director, JMREMP, *Bangladesh Water Development Board*, July 2007.
- Grant, F. S., and West, G. F., (1965), Interpretation theory in applied geophysics, *McGraw-Hill Book Co.*
- Lees, D. & Chuqui, M. (2004), Soil Grouting: Means, Methods and Design, *Grouting 2003*, pp. 1347-1359.
- O'Brien, P. N. S., (1967), The use of amplitudes in seismic refraction survey, in Musgrave, A. W., Ed., *Seismic refraction prospecting: Soc. Expl. Geophys*, pp. 85-118.
- Steven, A. A., Paige, R. P. and Lanbo, L., (2003), Propagation of a ground penetrating radar (GPR) pulse in a thin-surface waveguide, *Geophysics*, Vol. 68, No. 6 P. 1922–1933.

Review of nuclear energy demand in urban areas of India; VIS-À-VIS seismic disturbances

T.Sai Sumanth REDDY¹ and Ramancharla Pradeep Kumar²

¹B.Tech Student, Pandit Deendayal Petroleum University,
Ahmedabad, India

sumanth.bunty@gmail.com

²Associate Professor, Earthquake Engineering Research Centre,
IIIT Hyderabad, Hyderabad, India.

ramancharla@iiit.ac.in

ABSTRACT

Disaster Demand for electricity in urban areas is increasing world over, because electricity is the prime lifeline support. Due to increase in fossil fuel prices coupled with concerns related to global warming, demand for nuclear energy is increasing. Around 30 countries are now using nuclear energy for production of electricity. However, its share in electricity production is varying from country to country. In some countries it is only 3% and in some countries it is around 50%. In light of March 2011 nuclear energy are reviewing the safety of their reactors against natural disasters. In this regard, authors proposed to study the current and projected nuclear energy demand for electricity supply in urban areas of India on one hand and scenario of seismic hazard and risk on the other hand.

Keywords: Nuclear accident, active faults, seismic risk, safe energy

1. INTRODUCTION

Electricity is one of the world's fastest-growing form of end-use energy consumption. Net electricity generation worldwide will rise by 2.3 percent per year on average from 2007 to 2035 as compared to 1.4 percent per year growth for total world energy demand. The growth in electricity generation for non-Organization for economic Co-operation and development countries increase by an average annual rate of 3.3 percent, as rising standards of living increases the demand. Figure 1 shows the distribution of electricity generation from different sources till 2035.

The rise of global warming concerns throughout the world over the last ten years has led to an interest in what once considered a dead market-nuclear energy. After the Cold War, nuclear energy development was largely forgotten for many years until this renewed desire among developed nations for alternative energy sources once again thrust the idea of nuclear power into mainstream consciousness. As the price of oil and global

warming concerns both continue to raise steadily, a renewed interest in the clean-burning properties of nuclear power are becoming much more attractive.

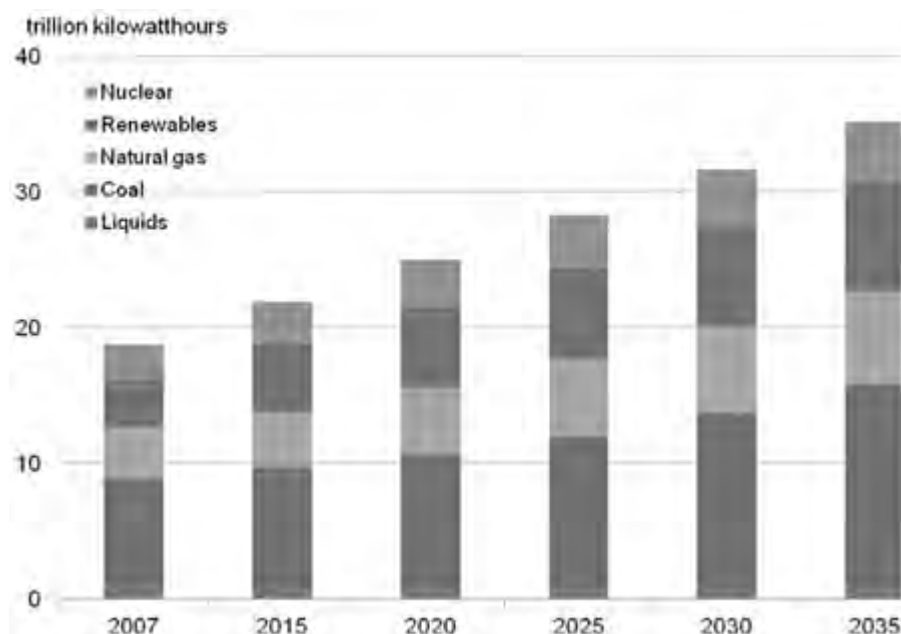


Figure 1: Electricity Consumption Bar Graph

Nuclear power is energy which is produced with the use of a controlled nuclear reaction. The process of generation of nuclear power starts with the mining and processing of uranium and other radioactive elements. These elements are used to feed the reactor of a nuclear power plant, generating a reaction known as fission which creates intense heat, turning water in the plant into steam. The steam powers steam turbines, which generate electricity and feed the electricity into electrical grid. When nuclear power is used to power something like a submarine, the reactor runs the engines, with the steam directly powering the engines. In both cases, the reactor requires careful supervision, because runaway nuclear reactions must be stopped as quickly as possible to prevent serious problems. Many nuclear power plants have extensive automated systems which help to identify potential trouble spots, and these systems can also re-route power, turn off parts of the plant, and perform other tasks which make the plant safer and cleaner.

2. NUCLEAR POWER SCENARIO AROUND THE WORLD

The world's first nuclear power station became operational in 1956 at Calder Hall in Sellafield, US with an initial capacity of 50 MW (later 200 MW). A year later in 1957 the United States got its first commercial nuclear generator, the Shipping port Reactor, in Pennsylvania. The worldwide capacity rose quickly to 100 GW by late 1970's and then to 300 GW by late 1980s. However, thereafter the growth slowed down reached only by 366 GW in 2005. It was largely due to rising economic costs, coming from extended construction time and the lower oil prices.

Nuclear power provides about 6% energy and 14% electricity requirement of the world. About 40% of electricity requirement is met by coal, followed by gas (21%) and hydro (16%). France, Japan and US account for about 50% of the nuclear generated electricity. Currently, there are 443 commercial nuclear reactors operating in 31 countries with about 378 GW total capacity. Over 60 power reactors are under construction in 15 countries, notably China, South Korea, India and Russia. The International Atomic Energy Agency (IAEA) anticipates addition of 73 GW in new capacity by 2020 taking the total to 463GW, and then to 546-800 GW by 2030.

Table 1: Top ten countries in 2010 with largest contribution from nuclear power

S.no	Country	Percentage
1	France	76.2
2	Lithuania	72.9
3	Slovakia	56.4
4	Belgium	53.8
5	Ukraine	47.4
6	Sweden	42
7	Slovenia	41.7
8	Amenia	39.4
9	Switzerland	39.2
10	Hungary	37.2

Table 2: Top10 countries by number of nuclear reactors in 2010 and nuclear energy as percentage of total energy

S.no	Country	Number of Reactors	Percentage
1	US	104	19.7
2	France	58	76.2
3	Japan	54	24.9
4	Russia	31	16.9
5	South Korea	20	35.6
6	UK	19	17.4
7	Canada	18	14.9
8	India	18	2.9
9	Germany	17	28.3
10	Ukraine	15	47.4

Table 3: The top ten countries planning for new nuclear reactor and MW planned

S.no	Country	New Reactors Planned	Number of MW Planned
1	China	37	38,360
2	France	23	21,500
3	Japan	13	17,915
4	US	11	13,800
5	Russia	7	8,000
6	South Korea	6	8,190
7	UK	4	6,600
8	UAE	4	5,600
9	Canada	4	4,400
10	South Africa	3	3,565

3. NUCLEAR POWER SCENARIO IN INDIA

India's electricity sector is struggling to cope with current demand, which has been mushrooming as a consequence of high population growth levels and continued economic expansion. This presents a major obstacle to the country's business environment and economic development, and cements existing regional wealth discrepancies. In response to the problem, utilities all over the country are busy growing their generation capacities.

Electricity demand in India is increasing rapidly the 830 billion kilowatt hours produced in 2008 was triple the 1990 output, though still represented in some 700 kWh per capita for the year. With huge transmission losses, this resulted in only 591 billion KWh consumption. Coal provides 68% of electricity at present, but reserves are limited. Gas provides 8% whereas hydro provides 14% of electricity.

Currently India produces about 4,780 MW power from its 20 operational nuclear power plants, which is only 3 percent of total power generated in the country. Indian stand on nuclear energy is clear, it sees it as an important clean source of energy along with other renewable sources that will reduce dependence on import of crude oil as well as help mitigate global warming.

India's energy requirement is growing at about 6 percent annually, fueled mostly by a growing population and a robust economy, the third largest in Asia. Besides, still nearly 40 percent of households have no access to electricity. Hence, it wants to expand the nuclear power program to cover its future energy need. It plans to add 20 GW of nuclear power capacity by 2020 and aims to meet 25% of its needs through nuclear power by 2050. This expansion became possible after the nuclear ban on India was lifted in 2008 after 34 years.

Table 4: New nuclear reactors on the anvil in India

S.no	Reactor type	Location	Capacity (MWe)
1	Indigenous PHWRs	Kumharia, Haryana	4 x 700
2	Indigenous PHWRs	Bargi, MP	2 x 700
3	LWR(Russian VVER)	Koodankulam, TN	4 x 1000*
4	LWR(French EPR)	Jaitapur, Maharashtra	6 x 1650
5	LWR(US, GE-Hitachi)	Chhanyamithi Viridi, Gujrat	6 x 1000**
6	LWR(US, GE-Hitachi)	Kovvada, AP	6 x 1000**
7	LWR(Russian VVER)	Haripur, WB	6 x 1000**
*Additional Potential 2 x 1000 Mwe already under construction			
**Final capacity will depend on the actual rating of reactors selected			
PHWR-Pressurised Heavy Water Reactors, LWR-Light Water Reactors			

4. MAJOR NUCLEAR DISASTER IN THE WORLD

4.1 The Three Mile Island Accident

This accident pertains to pressurized water reactor (PWR). A malfunctioning in the secondary water supply caused the pumps to stop working. Although the Emergency Core Cooling System started as it was designed to do, human error led to mistaken decision to shut it down. Large amounts of coolant escaped leading to heat buildup in the reactor. It resulted in severe core meltdown.

Some of the radioactive material from the fuel rods leaked into the primary coolant system, and was released into the atmosphere. However, since the reactor building and the structures remained intact, most of the radioactivity remained safely contained within the reactor building. The impact on the outside world was minimal.

4.2 The Chernobyl Disaster

The design of the Chernobyl was totally different from the Three Mile Island reactor in US. It was moderated by graphite and cooled by water. The accident occurred during a design test when safety interlocks were bypassed and the reactor was never actually shut down, thus the fission process continued uncontrollably, and the sudden surge in output shattered the reactor, opening up a gaping hole in the upper part of the building. The combustible graphite moderator then caught fire, sending out vast clouds of radioactive material over a huge area.

Despite several irregularities during tests on the reactor's power supply, including an unexpected drop in reactor output, operators continued the test, repeatedly violating operating procedures. Structural flaws in the reactor also exacerbated this situation.

Table 5: Comparison of Major Disasters in the world

	Fukushima(Japan)	Chernobyl(Former USSR)	Three Mile Island (USA)
Date of incident	March 11,2011	April 26,1986	March 28,1979
Rating on the nuclear events scale(1-7)	Level 7	Level 7	Level 5
Type of reactor	Light water reactor(BWR)	RBMK-type reactor graphite-moderated water cooled	Light water reactor(pressurized water reactor)
Reactor(s) affected	UNITS 1-4(total of 6 reactors)	Units 4(total of 4 reactors)	Units 2 (total of 3 reactors)
Output capacity at the time of accident	1244mw	1000mw	960mw
Date of Commencing	1971-1978	1984,march	1978,december
Causes and nature of accident	Loss of cooling due to damage caused by earthquake and tsunami	Power surge during testing causes fire and explosion.release of large amount of radioactive material	Equipment failure and human error causes leakage of reactor coolant.The reactor core undergoes 45% meltdown

4.3 The Fukushima Nuclear Disaster

The Fukushima disaster was triggered by earthquake and aggravated by the tsunami. The plant comprises of six separate boiling water reactors (BWRs). Experts consider this accident to be the second largest nuclear accident after the Chernobyl disaster, but more complex as multiple reactors were involved. At the time of the quake, reactor 4 had been de-fueled while 5 and 6 were in cold shutdown for planned maintenance. The remaining reactors shutdown automatically after the earthquake, the electricity grid was knocked out and generators started operating the cooling water supply. The plant was protected by a seawall designed to withstand a 5.7 m tsunami but not the 14m maximum wave which arrived 40-60 minutes after the earthquake.

The entire plant was flooded and the diesel generators got damaged. All power for cooling was lost and reactors started to overheat, due to natural decay of the fission products. Three reactors experienced complete melt down and hydrogen explosions led to release of radioactivity into the environment.

5. NUCLEAR ACCIDENTS IN INDIA

Nuclear establishment in India is known for its secrecy and the public, by and large, knows little about how the functioning of nuclear activities. In absence of an independent safety regulation body, people fear the safety standards are actually not very high in India. Following is a list of accidents that is known in the public domain.

April 2010: In a bizarre radiological accident in Delhi, the improper disposal of a derelict gamma-ray research device at the university of Delhi found its way to a scrap market in west Delhi and resulted in the death of a scrap-metal worker. It was owned by the university since 1968, but unused since 1985, and was sold to a scrap dealer in Feb 2010. Scrap workers dismantled and cut it into pieces unaware of the hazardous nature to the device. Eight were hospitalized where later, one died of exposure.

November 2009: Fifty-five employees consume radioactive material after tritiated water finds its way into the drinking water cooled in kaiga generating station. The NPCIL attributes the incident to “an insider’s mischief”

April 2003: Six tones leak of heavy water at reactor 2 of the narrow atomic power station (NAPS) in Uttar Pradesh, indicating safety measures have not been improved from the leak at the same reactor three years previously.

January 2003: Failure of a valve in the kalpakkam atomic reprocessing plant in Tamil nadu results in the release of high level waste, exposing six workers to high doses of radiation. The leaking area of the plant had no radiation monitors or mechanisms to detect valve failure, which may have prevented the employees’ exposure. A safety committee had previously recommended that the plant be shut down. The management blames the “over enthusiasm” of the workers.

May 2002: Titrated water leaks from a downgraded heavy water storage tank at the tank farm of Rajasthan atomic power station (RAPS) 1 & 2 into a common dyke area. Substantial amount of radioactivity was released into the environment.

November 2001: A leak of 1.4 tons of heavy water from the moderator system at NAPS unit 2. Various workers involved in the clean-up received ‘significant uptakes of tritium’, although only one had a radiation dose over the recommended annual limit.

March 1999: Somewhere near four and fourteen tonnes of water leaks from the pipes at madras atomic power station (MAPS) at kalpakkam, Tamil nadu, during a test process. The pipes have a history of cracks and vibration problems. Forty-two people were reportedly involved in mopping up the radioactive liquid.

February 1994: Helium gas and heavy water leak in unit 1 of RAPS. The plant was shut down until March 1997.

March 1993: Two blades of the turbine in NAPS unit 1 break off, slicing through other blades and indirectly causing a raging fire, which catches onto leaked oil and spreads through the turbine building. The smoke sensor fail to detect the fire, which is only noticed once workers see the flames. It causes a blackout in the plant, including the shutdown of the secondary cooling systems, and power is not restored for seventeen hours. In the meantime, operators have to manually activate the primary shutdown system. They also climb onto the roof to open valves to slow the reactions in the core by hand. The incident was rated as level 3 on the international nuclear event scale, INÉS.

May 1992: Tube leak causes a radioactive release of 12 curies of radioactivity from tarapur atomic power station.

January 1992: Four tons of heavy water split at RAPS.

December 1991: A leak from pipelines in a vicinity of CIRUS and Dhruva research reactors at the Bhabha atomic research center (BARC) in Trombay, Maharashtra, results in Cs-137 soil combination of thousands of times the acceptable limit. Local vegetation was also found to be contaminated, through contract workers digging of the leaking pipeline were reportedly not tested for radiation exposure, despite the evidence of their high dose.

July 1991: A contracted laborer mistakenly paints the walls of RAPS with heavy water before applying a coat of whitewash. He also washed his paintbrush, face and hands in the deuterated and titrated water, and has not been traced since.

March 1991: Heavy water leaks at MAPS take four days to clean up.

6. SEISMIC HAZARDS IN INDIA

The massive earthquake in Japan and the subsequent nuclear crisis has triggered fears of nuclear security across the world, including India.

Most of India falls in the moderate risk to very high risk seismic zones and so do majority of India's nuclear reactors. While there are no nuclear projects in zone 5 (seismic intensity of 8 and above), the proposed Jaitapur nuclear power plant falls in zone 4 on the earthquake hazard zoning map. The map below plots India's nuclear power plants on a seismic map.

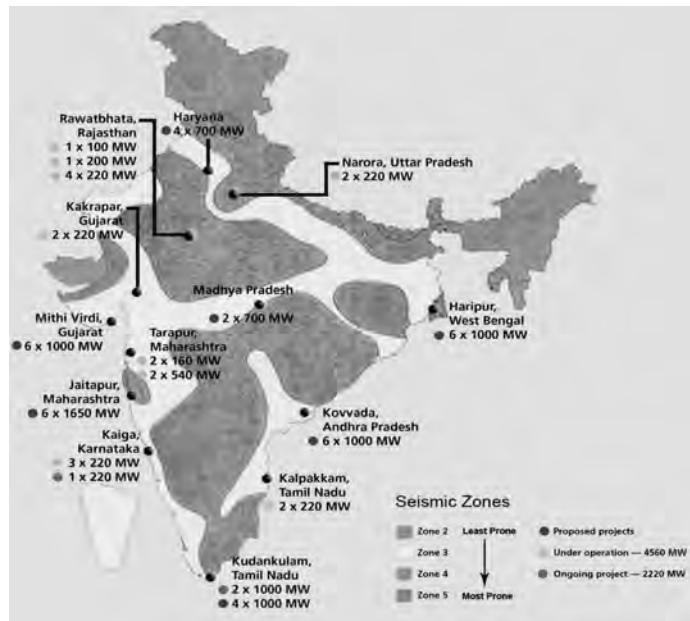


Figure 2: India map showing location of NPP and seismic zonation.



Figure 3: Seismic Faults in India [Based on GSI, 2003]

CONCLUSIONS

Energy has been crucial to the survival of mankind and every major step in our evolution has seen a manifold increase in energy consumption. Current perception is that nuclear energy holds the key to survival and growth of mankind for this century and beyond. Nuclear energy is proven to be the energy that the man will rely on in the future as alternative energy due to availability of the nuclear fuels and the low running cost and its long life.

In this paper it is clearly shown that world over there is a great demand for producing nuclear energy and India too is trying to increase its production. On the other hand, accidents world over have caused a great concern. Looking at the prevalent seismic hazard in the country India needs to cautiously decide whether to go for nuclear energy or other non-harmful energy sources.

REFERENCES

- <http://www.world-nuclear.org/education/wast.htm>
- <http://timeforchange.org/pros-and-cons-of-nuclear-power-and-sustainability>
- http://www.upi.com/Business_News/EnergyResources/2011/06/01/India_stands_firm_on_nuclear_power/UPI-29561306941789/
- <http://www.npcil.nic.in/main/Maps.aspx>
- <http://www.world-nuclear.org>
- <http://www.energyquest.ca.gov>
- <http://www.globalsecurity.org/wmd/world/india/reactor.htm>

Basic study on restoration capability of bio-cemented sandy soil

Reiko KUWANO¹, Makoto HOSOO²

¹ ICUS, IIS, The University of Tokyo, Japan

kuwano@iis.u-tokyo.ac.jp

² Kajima Corporation, Japan

ABSTRACT

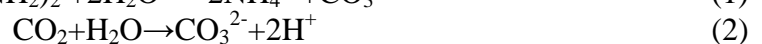
A new technique of ground improvement by microbial function has been recently proposed, as more eco-friendly technique than conventional one. Metabolic function of microbes produces carbon dioxide, which helps to generate calcium carbonate when sufficient amount of calcium ion is supplied in pore fluid of soil. Such a cementation process may be operated repeatedly as long as microbes' function is active.

In this study, a series of triaxial test was conducted in order to evaluate the recovery of shear-damaged cementation generated by those function in Toyoura sand specimens. The ureolytic bacterium, Bacillus pasteurii, was used to accelerate the precipitation of calcium carbonate (CaCO₃). It was found that stiffness of the bio-cemented specimen degraded by shear but it recovered when the microbes in the specimen were activated by grouting. The strength of the damaged specimen can be also recovered to some extent as long as the damage given by shear was not too large.

Keywords: *microbe, bio-cementation, sand, triaxial test, stiffness and strength recovery*

1. INTRODUCTION

It was reported that urease enzyme from “Bacillus Pasteurii” could be used to add cementation in sand (Dejong et al., 2006; Whiffin et al., 2007). Bacillus Pasteurii helps to precipitate calcium carbonate through the chemical process as shown in Equations (1), (2) and (3). Precipitated calcium carbonate on a soil grain and/or between soil particles seem to contribute to stiffen and strengthen the ground.



Hosoo and Kuwano (2010) and Hosoo (2011) conducted a series of trial test in order to evaluate the degree of soil cementation generated by those microbial function in Toyoura sand, and reported that the degree of cementation in soil can be monitored by the change of calcium ion in pore

liquid. In this study, a series of triaxial test was carried out in order to evaluate the recovery of shear-damaged cementation generated by microbes in Toyoura sand specimens.

2. TEST PROCEDURE

A cylindrical specimen of diameter of 5cm and height of 10.5cm was prepared by air pluviation method, using Toyoura sand. The specimen was initially water-saturated and isotropic stress of 50kPa was applied, before *Pasteurii* (2×10^6 cells/ml) of 100ml was penetrated into the specimen. Grout was then percolated into the microbe mixed specimen to accelerate the function of microbes. Composition of the grout is shown in Table 1. The bio-cemented specimen was sheared to some extent by triaxial compression, then axial force was unloaded to bring isotropic stress state. Grout was percolated again into the shear damaged specimen to restore the mechanical properties of the specimen. Shearing, grouting, and curing cycle was then repeated to examine the recovery of stiffness and strength of the specimen. In all process of the test, the density of calcium ion in the grout out-flown from the specimen was monitored. Small cyclic loading of 0.001% axial strain level was also applied to evaluate small strain stiffness of the specimen. Test procedure and condition are summarized in Table 2.

Table 1: Composition of the grout

Component	Amount (g/L)
Bacto nutrient broth	3
Urea	30
CaCl ₂ · 2H ₂ O	70
NH ₄ Cl	10
NaHCO ₃	2

Table 2: Test procedure and test condition

Initial state and cementation	Shearing and restoration
density : Dr=90% Grouting was applied to the microbe mixed specimen 5 times at every 24 hours.	Curing for 24hours, Shearing (1)→Curing for 24hours, Shearing (2)→Shearing (3)→grouting→Curing for 24hours, Shearing (4)→repeating cycle of grouting, curing and shearing, until shearing (13)

3. TEST RESULTS

The evolution of Young's modulus in the process of the cementation under isotropic stress of 50kPa is shown in Figure 1. The value of Young's modulus was increased with grouting and elapsed time. Relationship between Young's modulus and the content of calcium carbonate in the specimen is plotted in Figure 2. It is indicated that the stiffness notably increased with the precipitation of calcium carbonate in the range of 1 to 4%.

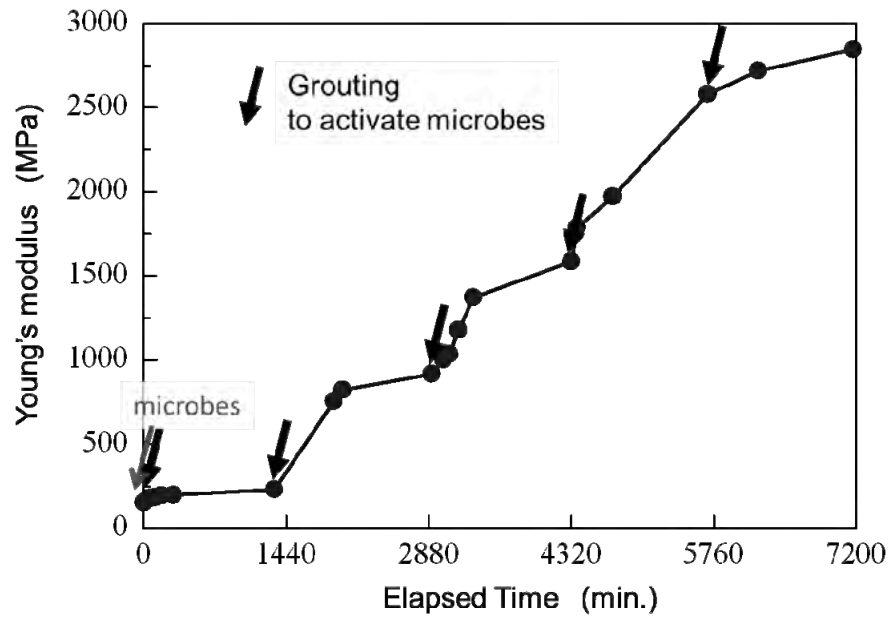


Figure 1: Young's modulus evolution during cementation process under isotropic stress of 50kPa

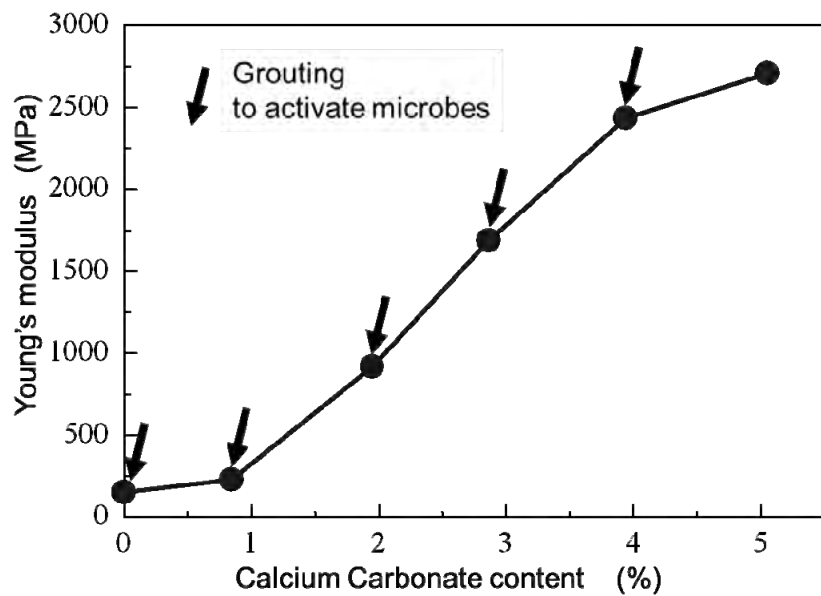


Figure 2: Relationship between small strain stiffness and calcium carbonate content during cementation process

Stress strain relationships until the 8th shearing and until the end are shown in Figure 3 and 4 respectively. At the 1st shearing, the maximum deviator stress, q_{max} , was about 1100kPa. Shearing was continued until the deviator stress dropped to 600kPa. Then axial unloading was made to the isotropic stress state. After 24 hours, the 2nd and 3rd shearing were given to confirm no further development of cementation, grouting was applied to the specimen and was cured for 24 hours. At the 4th shearing, the maximum deviator stress, q_{max} , was recovered to 750kPa. Such a process, shearing until q exceeding its peak and dropping to 600kPa, grouting and 24-hour-

curing, was repeated. As shearing steps progressed, q_{max} recovery became smaller. From 10th shearing, q_{max} recovery could not be recognized.

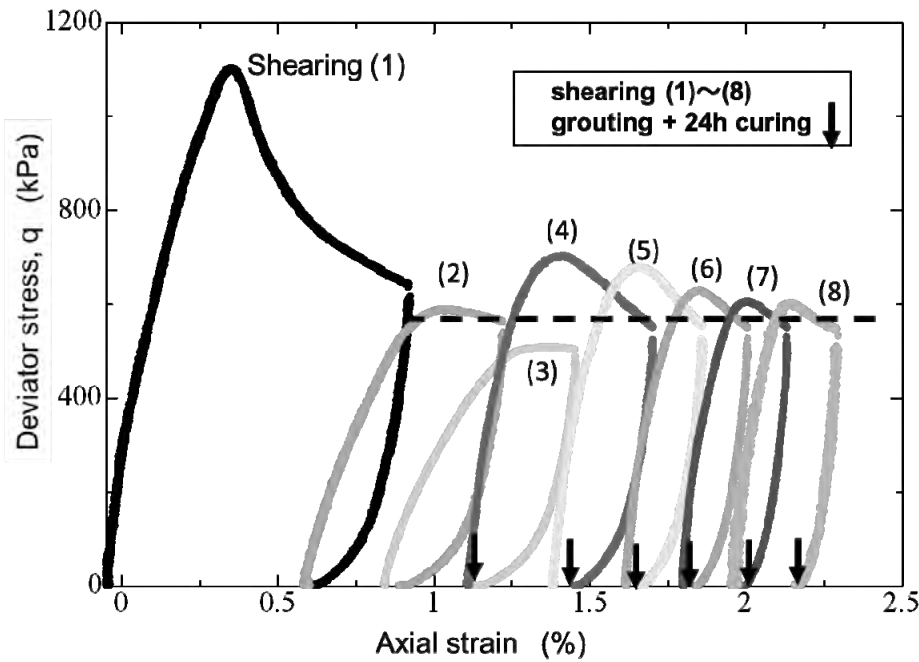


Figure 3: Stress strain relationship up to 8th shearing cycle

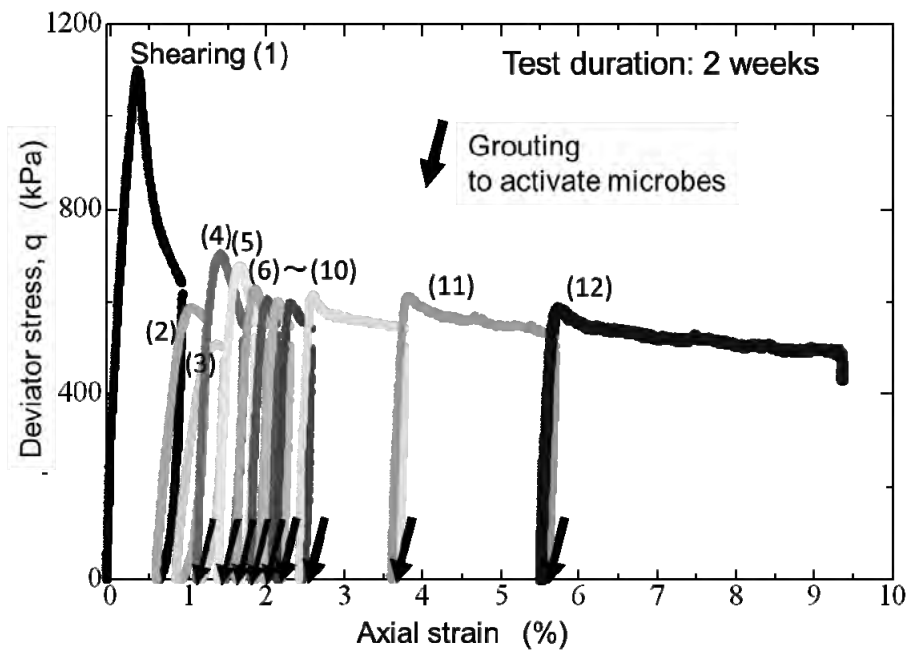


Figure 4: Stress strain relationship

Figure 5 shows the relationship between q_{max} and calcium carbonate content. When the shearing damage was accumulated, recovery of the strength could not be expected. Young's moduli are plotted against calcium carbonate content in Figure 6. (1) to (9) indicates the stiffness value just before the shearing process. After the 10th shearing, small strain stiffness could not be obtained because strain level exceeded the working range of

LDT. Young's moduli increase and decrease according to grouting and shearing. It seems that even though the specimen was severely damaged, stiffness increased to some extent as the grout tended to penetrate into the damaged location. The specimen after the test was found to be separated into several blocks, and the surface of the blocks was hardened. The grout appeared to penetrate along clacks and particular water pathway in the specimen.

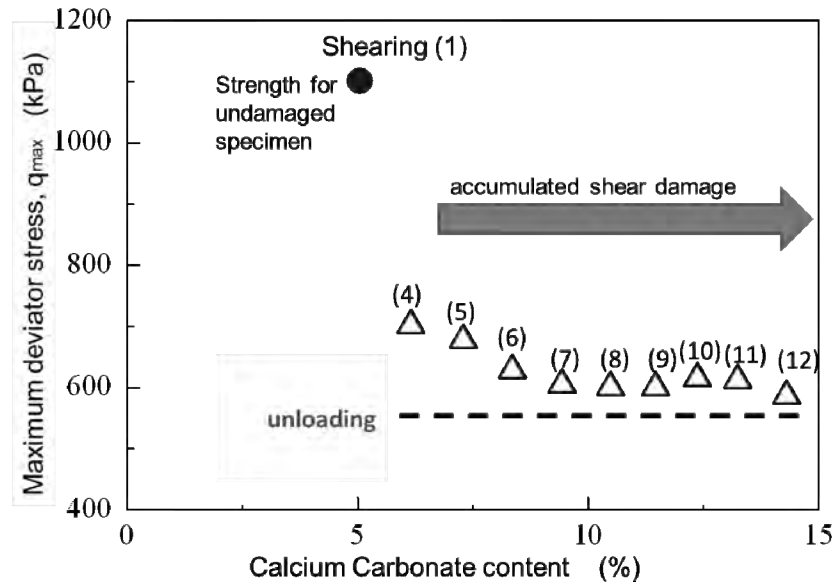


Figure 5: Maximum deviator stress and calcium carbonate content

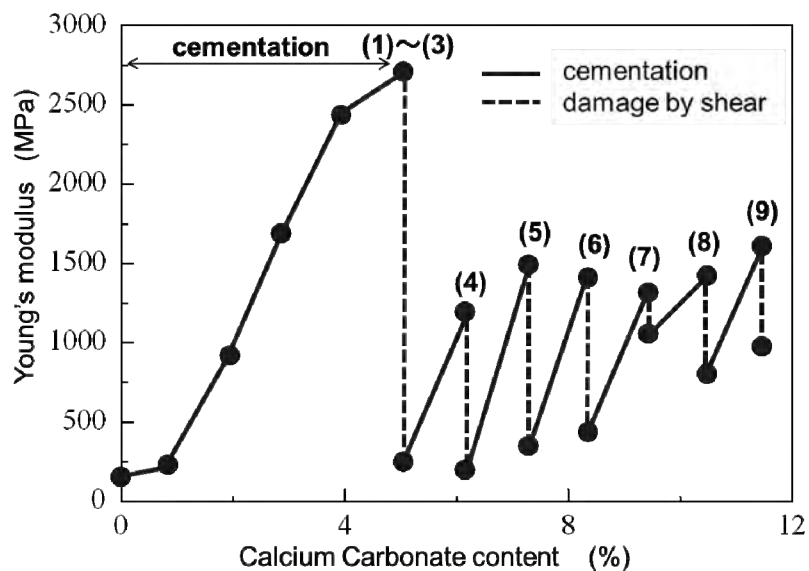


Figure 6: Small strain stiffness and calcium carbonate content

4. SUMMARY

In the bio-cemented sand specimen using the function of *Bacillus Pasteurii*, degree of cementation was monitored by the measurement of small strain

stiffness. It was found that the increase in stiffness had good agreement with the amount of calcium carbonate precipitation. The stiffness of the specimen significantly reduced when it was damaged by shear, but notably recovered by re-grouting to activate the function of microbes. The strength of the specimen was also recovered to some extent as long as the damage given by shear was not too large. Such restoration of mechanical property of bio-cemented soil by re-activating the function of microbes was continued for about two weeks.

REFERENCES

Jason T. DeJong, Fritzsche, M.B. and Nüsslein, K., 2006. *Microbially induced cementation to control sand response to undrained shear*. Journal of Geotechnical and Geoenvironmental Engineering, Vol.132, No.11, 381-1392.

Marien P. Harkes, Van Paassen L.A., Booster J.L., Whiffin V.S., Van Loosdrecht M.C.M., 2010. *Fixation and distribution of bacterial activity in sand to induce carbonate precipitation for ground reinforcement*. Ecological Engineering, Vol.36, Issue2, 112-117.

Hosoo, M. and Kuwano, R., 2010. *Effects of nutrient concentration on microbial cementation in Toyoura sand*, Proc. 9th International symposium on new technologies for urban safety of mega cities in Asia, USMCA, Kobe, October 2010, CD-ROM.

Hosoo, M., 2011. *Study on Healing Capability of Bio-Cemented Sandy Soil*. Master thesis, faculty of Engineering, the University of Tokyo (in Japanese).

Transformation of hybrid color space for road extraction using high resolution image

Sanit ARUNPOLD
Remote Sensing and Geographic Information System,
Asian Institute of Technology, Thailand
sanit.arunpold@ait.asia

ABSTRACT

This paper presents a methodology for the extraction of roads in urban area by using multi-color spaces rather than the convention RGB color space. The color spaces include HSI, YCbCr and $I_1I_2I_3$. The model was thoroughly investigated for accuracy using a high resolution Quick bird image for Dhaka City. The results showed that the hybrid color spaces are a better option for feature extraction as compared to RGB as they were able to show an accuracy of 75.42% by extracting 1317 m. of road from an actual 1746 m. of road

Keywords: Feature extraction, color space transformation, urban mapping

1. INTRODUCTION

Road network is changed at a rapid rate in recent years because of urban development. Therefore, it is difficult to maintain the accuracy and precision of the road network for some applications such as city planning, drainage system, and urban expansion management system. Semi-automatic and automatic extraction of roads for updating city map has recently come to research area.

Road extraction strategies can be divided into two categories as, semi-automatic extraction and automatic extraction. In terms of semi-automatic road extraction, all the initial points or road seeds need to be provided. However, in fully automatic extraction, the road seeds can be detected automatically and linked to complete the road network (X. Y. Jin and C. H. Davis, 2003). In generally, automatic way is more preferable than the manual operations that acquire lots of manpower and time in mapping the road network (A. Chang S. K. Kyu and B. R. Sang, 1997)

There are alternative ways suggested was based on “simply the best concept.” In this project, to study new algorithm based on hybrid simple color spaces segmentation is proposed for the road extraction. Moreover, hybrid color spaces segmentation can be extracted more information about road network categories separated into highway road network (asphalt road)

and rural road network (non-asphalt road).

Classification was based on different color spaces model, including HSI (Hue, Saturate, Intensity), $I_1I_2I_3$, YCbCr, RGBNIR and Intensity emphasis. All of models may obtain advantages to separate vegetation, build, highway and rural road network. Because each object characteristic affected an image scene with systematic reduction of reflectance caused by sun angle and light intensity, every area in the same scene are affected by the same condition. There are different reflectances in each characteristic of each object. Therefore, the color space segmentation can be seen by enhancing some color spaces in different ways.

1.1 Color Space Components

The satellite images in used were captured in full color forms. Thus, the basic RGB color model can be utilized to study the characteristics of the satellite image. In this study with more color models namely YCbCr, HIS, $I_1I_2I_3$ and intensity emphasis were selected for investigations. A meaning of each color space model as below:-

YCbCr model, which is commonly used as digital video formats, consists of below:-

- Y (represents luminance or a measurement unit of the energy amount that an observer perceives from a light source)
- Cb (represents the difference between the blue component and a reference value)
- Cr (represents the difference between the red component and a reference value)

HSI model meanings of below:-

- Hue (a color attribute that describes a pure color like yellow, orange, or red)
- Saturation (a measurement of the degree to which a pure color is diluted by white light)
- Intensity (intensity or average value of R, G and B at specific location).

$I_1I_2I_3$ model is performed systematic experiments of region segmentation derive a set of effective color features. Intensity emphasis is modification formula from $I_1I_2I_3$ and calculated into six different channels such as average all bands, find range and emphasis each band.

1.1.1. RGB

(Cheng, 2001) The RGB color space can be geometrically represented in a 3-dimensional cube. The coordinates of each point inside the cube represent the values of red, green and blue components, respectively. The laws of colorimetry are: (1) any color can be created by these three colors and the combination of the three colors is unique; (2) if two colors are equivalent, they will be again equivalent after multiplying or dividing the

three components by the same number; (3) the luminance of a mixture of colors is equal to the sum of the luminance of each color. The tristimulus values that served as the color basis are: 425.8 nm for blue, 546.1 nm for green, and 700.0 nm for red. Any color can be expressed by these three color bases.

1.1.2 HSI Color Space

The color space is established in 3 dimensions including hue, saturation and intensity. Hue is what most of us think of when we think of "color." It is the generic name used to describe a color, e.g., red, green, yellow, orange, etc. (Sara Agee, 2006) Saturation is how pure the color is. A fully saturated color is the truest version of that color. Primary colors (red, yellow, and blue) are "true", so they are also fully saturated. (Sara Agee, 2006). Intensity is brightness or dullness of a color. A pure color is a high-intensity color. A dulled hue (a color mixed with its complement is called a low-intensity color.) (Johannes Itten, 1916)

1.1.3 YCbCr

(David B.L. Bong, 2009) is a family of color spaces used as a part of the Color image pipeline in video and digital photography systems. Y is the luma component and Cb and Cr are the blue-difference and red-difference chroma components.

1.1.4 $I_1I_2I_3$

(Cheng, 2001) Performed systematic experiments of region segmentation derive a set of effective color features. At each step of the recursive region splitting, new color features are calculated by Karhunen-Loeve transformation of R, G, and B. It applied eight kinds of color pictures, analyzed over 100 color features, and found a set of effective color features as follows:

I_1 presents the average of DN in three bands same as I axis in HSI color space.

I_2 presents the different of DN between longest and shortest wavelength.

I_3 present the different of DN emphasis to the shortest wavelength.

1.1.5 Intensity Emphasis is modification formula from $I_1I_2I_3$ by emphasis each band so that in Intensity emphasis in this project will have six parameter as below:-

I_1 presents the average of DN in four bands.

I_2 presents the different of DN between longest and shortest wavelength.

I_3 present the different of DN emphasis to the NIR.

I_4 present the different of DN emphasis to the red.

I_5 present the different of DN emphasis to the green.

I_6 present the different of DN emphasis to the blue.

2. METHODOLOGY

2.1 Software and data uses

The processing in this paper was processed on raster and vector data. Thus there is necessary to use these software including

- ERDAS Imagine 9.1 was used for image processing, color spaces transformation, and model maker.
- ArcView GIS 3.2a was used for check accuracy assessment.

This paper works on the process to solve the problems on high resolution images. A scene of high resolution images was induced for processing including:-

- Image : RGBNIR, Multi-spectral Satellite Image from Quickbird
- Resolution : 0.6 meter
- Captured date:22 November, 2007
- Study Area : Dhaka Cooperation City
- Area for experiment : 467,500 sq.m.

2.2. Model

The methodology of this paper tries to extract/identification road network from high-resolution remote sensing image by using different color spaces then to select suitable color model for them. Moreover, create modeler to semi-automatic to classify road network by setup threshold of highway and local road.

2.3 Color space transformation

The color space which are using in this project as:-

- HSI (Hue, Saturate and Intensity)
- $I_1I_2I_3$
- YCbCr
- Intensity emphasis or $I_1I_2I_3I_4I_5I_6$

In this research, this study concentrates on color spaces, which is suitable for extracting road feature network and classifying road type as asphalt and non-asphalt. The color space transformation is the process of transform data(RGB) to differentiate types for enhancing color of each object. In this study, hypothesis of color space which classified and extracted road network are HIS, $I_1I_2I_3$, YCbCr and Intensity emphasis. Thus, the research tried many different band for extracting the meaningful of image, checking the spectral signature by selection on Area of Interest (AOI), and comparing together.

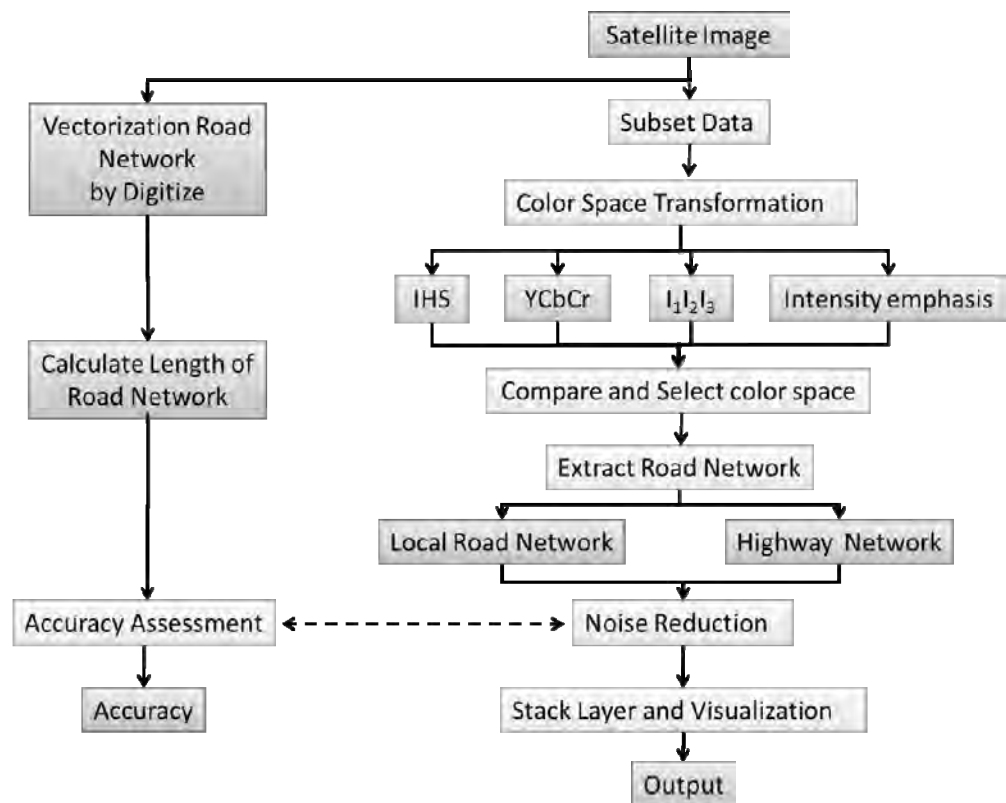


Figure 2.1: Flowchart for hybrid color space for road extraction

Since all colors can be matched by proper amounts of three primary colors, three numerical components are necessary and sufficient to define a color. It is then natural to represent colors as points in a three-dimensional vector space, called color space or color model. A color space is thus a mathematical representation of spectral colors in a finite dimensional vector space. It allows analyzes and manipulates color. By defining different primary colors, that is basis elements of the vector space, different color models can be devised. Moreover, additional representation systems can be developed according to physical, physiological or psychological properties. (Salvador, 2004)

2.5 Extract and Identification Road Network

In this process start from create reference AOI for comparing between each color different module. And then, setup comparing spectral profile in each object. Moreover, create statistics to analysis and setup threshold. In finally, create ERDAS modeler module to extract road network and process noise reduction. The flow of work after selected color model are suitable for extract road is extraction and identification as below:-

3. RESULT AND DISCUSSION

3.1 Color spaces transformation experiment for road network extract

RGBNIR

R, G, B, NIR are the spectral available of Quickbird image. Combination of grey value of each band presented in RGB color space can make true color and false color image.

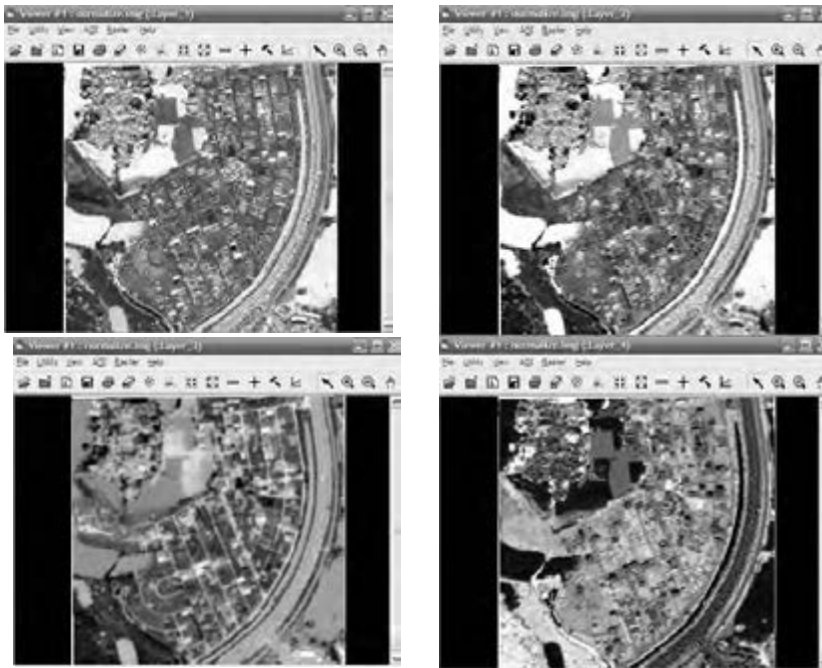


Figure 3.1 : RGBNIR images in separated bands



Figure 3.2 Normalize image in Band

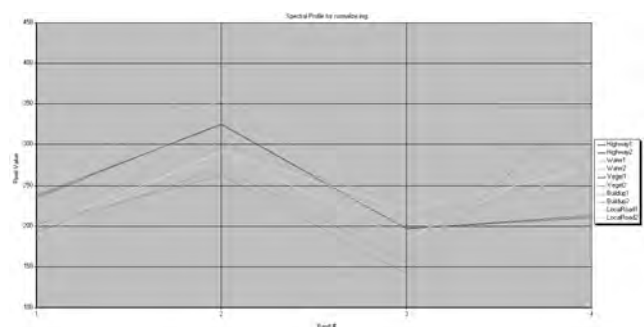


Figure 3.3: Spectral chart of RGBNIR image

As figure 3.2, show output of normalized image and visualization in 3 band of NIR-Red-Green. The spectral chart, Vegetable is easy to extract out from this image by using band 4 and 3 (NIR-Red) which is related to NDVI equation.

3.1.2 HSI (Hue, Saturate and Intensity)

Regarding refer to previous chapter, this project want to find the suitable color space for identify road type and extraction road network. In this part, HSI is testing to enhance in different band as below:-



Figure 3.4: Spectral chart of HSI combination from blue green red bands
(Band 1-2-3 = Intensity-Hue-Saturated)

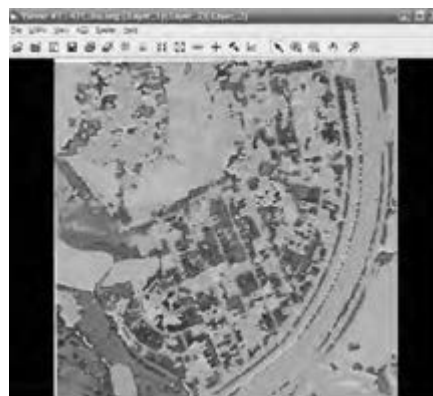


Figure 3.5: Spectral chart of HSI combination from blue red NIR bands
(Band 1-2-3 = Intensity-Hue-Saturated)

Comparing HSI from RGB with NIRBR, the range of local road in RGB->HSI is easier to classify than NIRBR->HSI. Both of them are mixed up with high intensity building but it separated from another objects.

3.1.3 YCbCr

From YCbCr color model above, All of layer is mixed up and cannot separated any object from imagery. So It mean this color model is not suitable for extraction.

3.1.4 $I_1I_2I_3$

Another color space which is using to extract in this project is $I_1I_2I_3$ or Intensity for each meaning following below:-

I_1 presents the average of DN in three bands same as I axis in HIS color space.

I_2 presents the different of DN between longest and shortest wavelength.

I_3 present the different of DN emphasis to the shortest wavelength.

Comparing both of spectral chart of $I_1I_2I_3$ from RGB and NIRBR, the figure of

RGB-> $I_1I_2I_3$ cannot classify and separated each object from image. By the way, another module NIRBR-> $I_1I_2I_3$ have some different from previous one, if we identify the trend of slope between I_3-I_2 , So we can separate group of object into 2 groups as:- 1.highway and water 2. Local road, building and Vegetation. In case want to using this model, it can generate model to separated highway and local road by mask out water and vegetation area before using this model.

3.1.5 Intensity Emphasis

This model is modification equation from $I_1I_2I_3$ for enhancing every bands, average band and find different rang of (short-long wavelength) as below meaning:-

- I_1 presents the average of DN in four bands.
- I_2 presents the difference of DN between longest and shortest wavelength.
- I_3 present the difference of DN emphasis to the NIR.
- I_4 present the difference of DN emphasis to the red.
- I_5 present the difference of DN emphasis to the green.
- I_6 present the difference of DN emphasis to the blue.

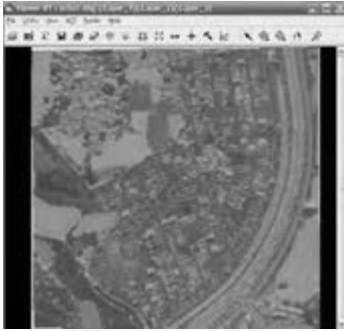


Figure 3.6: Spectral chart of YCbCr combination from red green blue bands (Band 1-2-3 = Y-Cb-Cr)



Figure 3.7 : Spectral chart of $I_1I_2I_3$ combination from blue green red bands



Figure 3.8: Spectral chart of $I_1I_2I_3$ combination from blue red NIR bands

3.2 Selection hybrid color space

As a result above from the spectral chart and satellite image, The result of each color space which is related in this project in brief a result as below:-

- HSI-RGB : Good
- HSI-NIRBR : Fair
- YCbCr: Bad
- Intensity emphasis : Good

In finally, in this project decided to use HSI-RGB and intensity emphasis color model for hybrid road network extraction.

3.3 Mark AOI and Set threshold from signature profile

Another step is to classify road network to mark AOI for viewing spectral profile of highway and rural road network. This project created about the point of AOI by random sampling to get signature the objects in different features.



Figure 3.9: Spectral chart of $I_1I_2I_3I_4I_5I_6$ combination from blue green red NIR bands



Figure 3.10: Mark AOI for highway and rural in HIS color space (Left hand side) and Spectral chart of IHS combination from blue green red in highway and rural (Right hand side)

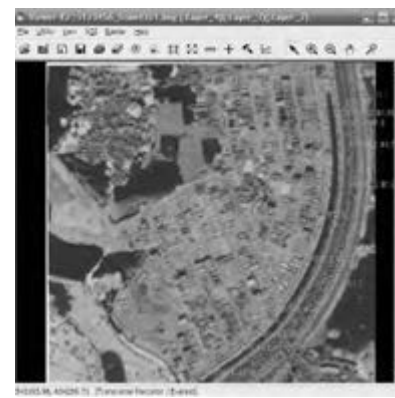


Figure 3.11: Mark AOI for highway and rural in intensity emphasis color space (Left hand side) and Spectral chart of emphasis combination from blue green red NIR in highway and rural (Right hand side)

3.4.1 Mark AOI

Following this figure show the range class is can separate highway and local network type by limited upper and lower bound in Hue channel, in different trend of highway and local road network, in this case have to make modeler to use if statement for limit upper and lower bound for each band to extract highway from local road.

Table 3.1: Show threshold for limit upper and lower bound for road extraction

	RGB->HIS	Intensity emphasis			
	Hue	I2	I3	I5	I6
Upper Bound	200	30	-25	100	10
Lower Bound	100	-5	-55	80	-10

3.4.2 Set threshold from signature profile

The next step is model maker using IF Logical Statement to limit upper and lower bound for each band to extract local road and highway in output file. Moreover, before stack layer have to remove noise from image by using low pass filtering with 7x7 windows size.

3.5 Output

The output product came up with separated band. Modeler will classify every highway network pixel value which is limited upper and lower bound and it will turn to 255 (See from figure 4.12 on left side modeler) Then pixel value which is classify by limit upper and lower bound to local road network it will turn to 128.

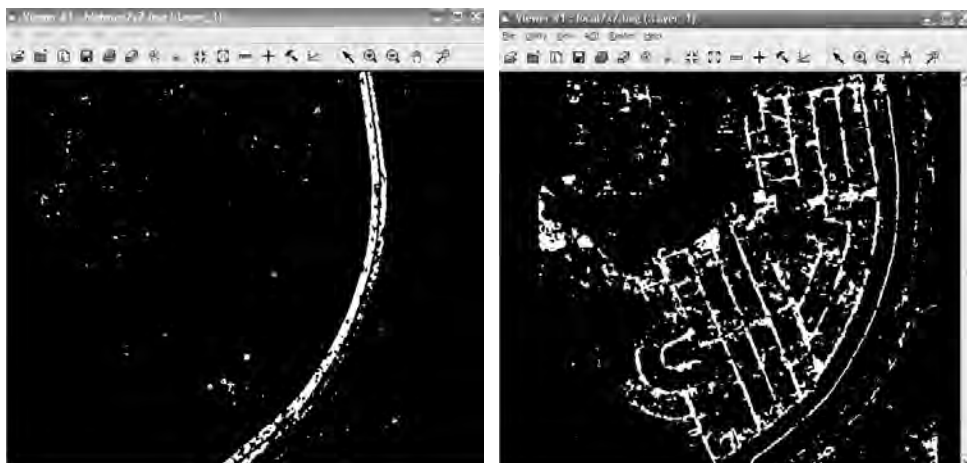


Figure 3.13: Show Output of Road extraction on highway(Left hand side) and rural (Right hand side) road network by using hybrid color space component



Figure 4.16: Overlay Raster and vector of rural road extraction for calculate length

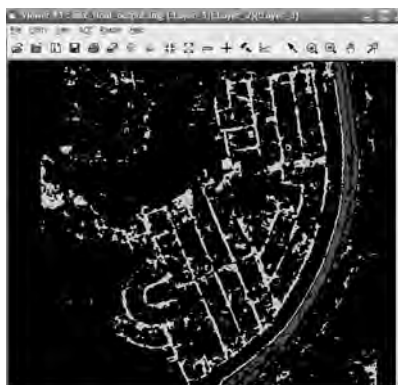


Figure 3.14: Show Overlay layer output of Road extraction and identification road type by using Hybrid color space component

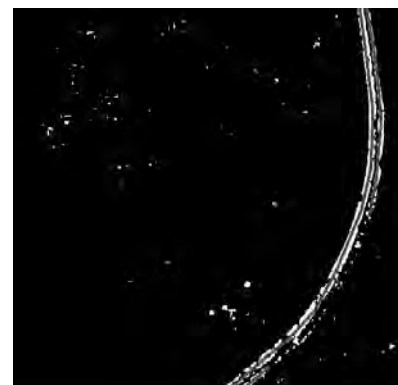


Figure 3.15: Overlay Raster and vector of highway extraction for calculate length

3.6 Accuracy Assessment

The last process is an accuracy assessment to measurement performance of this hybrid color model to extract and classify road network. It was done by digitizing original road network into vector file and calculating total length of each road type. After getting output of extract road network from satellite image and classifying each types, it has digitized into vector file and calculated total length of each road type.

Highway Accuracy assessment:

Actual highway road network length = 1,746 m.

Highway extraction using hybrid color space component = 1317 m.

Accuracy assessment = $1317 * 100 / 1746 = 75.42 \%$

Local road accuracy assessment :

Actual rural road network length = 4,378 m.

Rural road extraction using hybrid color space component = 2846 m.

Accuracy assessment = $2846 * 100 / 4378 = 65.00\%$

4. CONCLUSION

This study propose the simply method to extracted road network, also the benefit of this method is not only classify road network but it can be extracted road type information as highway and local road. By the way, the accuracy extracted of road network in some of area not good enough because there are high density traffic vehicle on the road that is effect into the classification method. And local road classification type not so accurate because it effect from the shade and shadow of satellite image, when it transform into color space model, some parts of the object are mix up into the same categories.

REFERENCES

- A. Chang S. K. Kyu and B. R. Sang. (1997). *A Road Extraction Method from Topographical Map Images*. IEEE Communications, Computers and Signal Processing, Vol 2. pp.839-842,.
- A.J. Spink, M.O.S. Buma and R.A.J. Tegelenbosch. (2000). *EthoVision color identification: A new method for color tracking using both hue and saturation*, 3rd International Conference on Methods and Techniques in Behavioral Research, 15-18 August 2000, Nijmegen, The Netherlands
- Cheng. (2001). *Color image segmentation: advance and prospect*, Available at www.elsevier.com/locate/patcog. Access on: 17 July 2009.
- C. L. Jia, K. F. Ji, Y. M. Jiang and G. Y. Kuang, (2005). *Road Extraction from High-Resolution SAR Imagery Using Hough Transform*. Proceedings of IEEE International Geoscience and Remote Sensing Symposium, Vol 1. pp. 1-4, 2005.
- David B.L. Bong, Koon Chun Lai, and Annie Joseph. (2009). *Automatic Road Network Recognition and Extraction for Urban Planning* ,International Journal of Applied Science, Engineering and Technology 5:1 2009
- Elena Salvador. (2004). *Shadow segmentation and tracking in real-world conditions*, Available at: ieeexplore.ieee.org/iel5/9455/30012/01374677.pdf. Access on 8 July 2009.
- J. Amini, M.R. Saradjian, J.A.R. Blais, C. Lucas, A. Azizi. (2002). *Automatic road-side extraction from large scale imagemaps*, International Journal of Applied Earth Observation and Geoinformation 4 (2002) 95–107
- J.B. Mena *, J.A. Malpica. (2005). *An automatic method for road extraction in rural and semi-urban areas starting from high resolution satellite imagery*, Pattern Recognition Letters 26 (2005) 1201–1220
- M. Mokhtarzade *, M.J. Valadan Zoej. (2007). *Road detection from high-resolution satellite images using artificial neural networks*, International Journal of Applied Earth Observation and Geoinformation 9 (2007) 32–40
- Taejung Kim. (2001). *Semi-Automatic Road Extraction from IKONOS Images Using Template Matching*, Asian conference on Remote Sensing,2001 Singapore

Future plan for the world longest undersea tunnel projects in Korea

Chang-Yong Kim¹, Seong-Won Lee¹, Ho-Geun Kim¹
¹Korea Institute of Construction Technology,
Daehwa-dong 283, Goyangdae-ro, Ilsanseo-gu,
Goyang-si, Gyeonggi-do, 411-712, Korea
cykim@kict.re.kr

ABSTRACT

Korea has several big islands. The largest island in Korea is Jeju. In Jeju island, almost 570,000 persons are accommodated, and Jeju island is about 73km wide and 41km long with a total area of 1,848 km². To go to Jeju, normally using airplane and the others are transported by ship. Jeju international airport has a total of 16 direct airlines within 12 local and 6 international airlines. But, air flight services heavily depend upon weather conditions, for example, 707 flights are canceled and 222 flights are delayed every year in average. The provision of secure and safe new transport mode might be needed. Already the construction of Honam high-speed rail line was started, so the extension of this Honam rail link to Jeju by subsea tunnel was suggested and staged in feasibility study. In this project, the route from Mokpo to Jeju(167km) consist of three part, the first is Mokpo-Haenam(66km) on Surface, and the second is Haenam-Bogildo(28km) by oversea bridge and finally Bogildo-Chujado-Jeju(73km) by undersea tunnel

Service and technical of the system will take the same standard as Honam High-speed Rail in order to prevent service disruption. The design speed of the train will be almost 350km/h and the operating speed about 300km/h. If this project will be launched, Seoul station to Jeju island will take 2 hours and 26 minutes

The challenge is the great depth of undersea level (maximum 120m) and overcoming the various geological conditions. Also, artificial islands are needed for the ventilation of the long and deep tunnels

In this paper, we will present the detailed plan of this project and the technical weakness and challenging factors are also discussed.

Keywords: Longest undersea tunnel, Artificial islands, Ventilation system

1. INTRODUCTION

Korea has several big islands; the largest island in Korea is Jeju. In Jeju Island, almost 570,000 persons are residing and it is about 73km wide and 41km long; the total area of 1,848 km². To go to Jeju, airplane and ship are

usually used. Jeju international airport has the total of 16 direct airlines; linked with 6 nations and 12 regions (Figure 1). But, air flight services heavily depend upon weather conditions; for example, 707 flights are canceled and 222 flights delayed every year in average. In case of the transportation by ship, it takes 3 hours or more between Wando and Jeju and 10 hours or more between Incheon City and Jeju. In 2007, 8,288,967 persons, ten times more than ones who traveled the island by ships, entered Jeju by airplane, so the travelers have been under the increased fare burden. Accordingly, the Honam-Jeju undersea high-speed rail can be an alternative through linking the high-speed rails under the situation to need a new transportation mode for overcoming the limitation of existing transportation modes and it's possible to link and develop the services and green industry promoted by both economic zones through linking the transportation between Honam and Jeju.



Figure 1: Jeju's flight routes

2. ROUTE

The Honam-Jeju route refers to a 176km line to link from Mokpo to Jeju, which is connected to Seoul through KTX and expressways. The Honam-Jeju route is divided into 3 parts: a ground section of about 66km from Mokpo to Haenam; a bridge (marine transportation) of about 28km from Haenam to Bogildo; and a undersea tunnel section of about 73km from Bogildo to Jeju via Chujado (Figure 2).



Figure 2: Honam-Jeju route

3. TECHNICAL REVIEW

The western coast and southern coast show a very complicated coastline unlike the eastern coast; especially, the southwestern coast, an archipelago region, consists of many islands and peninsulas and shows a world-renowned ria shoreline. The average water depth at the tunnel section is about 66.7m and the maximum depth around 130m (Figure 3).

Given the ventilation and environment problems, including the route length and waste gas treatment, it's recommended that the route would be operated centering on the passenger transportation through high-speed rails and the freight traffic through high-speed freight rails. As for the undersea tunnel structure, the two methods can be reviewed: the excavation of main line after excavating a service tunnel beforehand; and the direct excavation (Table 1).

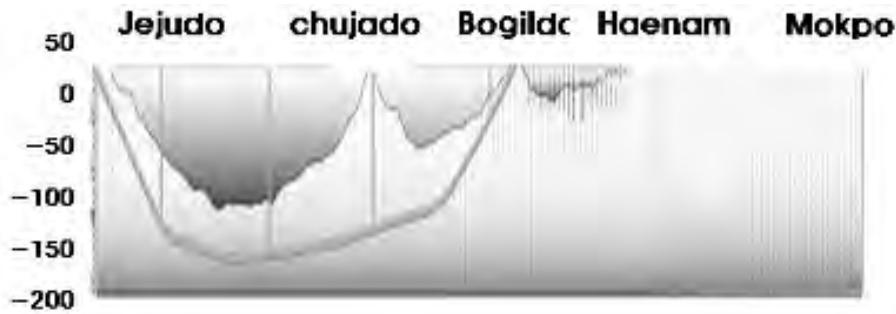


Figure 3: Water depth of the applied section

Table 1: Undersea tunnel structure

<p>Lines paralleled + service tunnel</p>	<p>A plan to operate the high-speed rails through excavating the paralleled tunnels after taking the necessary actions beforehand through excavating a service tunnel and grasping the undersea ground situation. It's judged that the service tunnel can be used not only for a vehicle to handle disaster, but also for a side track in time of operating the freight rails.</p>
<p>Line-paralleled tunnel</p>	<p>A plan to use the excavated medium-sized paralleled tunnels as the rails for high-speed rails and freight rails. It can be complementarily used for disaster prevention and maintenance through constructing a connecting gallery by each section.</p>

4. FUTURE PLAN

The Honam-Jeju project is planned to be operated with a design speed of 350km/h and an operation speed of 300km/h like the existing high-speed rails. Accordingly, it is anticipated to take less than about two hours and 30 minutes from Seoul to Jeju, about one hour and 40 minutes from Osong, the Honam intersection, about 40 minutes from Mokpo and two hours and 30 minutes from Daegu to Jeju (Figure 4).

The project is expected to take about 11 years: One year for a feasibility study and a master plan; one for a basic plan; one for a detailed design; and eight years for the construction of bridges and tunnels.

The construction is anticipated to cost about 14 trillion and 600 billion won: about 2 trillion and 800 billion won for ground section; 3 trillion won for the construction of sea bridges; and 8 trillion and 800 billion won for undersea tunnel (Table 2).

Table 2: Project overview

Construction period	Contents	costs	Contents
1st year	Feasibility study and master plan	2 trillion and 800 billion won	Ground section
2nd year	Basic design	2조 8천억	지상부분
2차년도	기본 설계	3 trillion won	Bridges on sea
3rd year	Detailed design	3조	해상 교량
3차년도	실시 설계	8 trillion and 800 billion won	Undersea tunnel
4th-11th year	Bridge and tunnel construction	8조 8천억	해저터널

5. EFFECTS

The Honam-Jeju high-speed rail makes the national development and the acquisition of new growth engine possible through lining with the existing high-speed rails and makes the linkage of service and green industry promoted both economic zones possible through linking the ground traffic between Honam and Jeju.

In addition, the route can become an alternative transportation mode to overcome the limitation (high cost, severer climate, security etc.) of the existing transportation modes (ship and airplane).

Furthermore, the foreign undersea tunnel projects are under the planning stage for the super long tunnel linking continents and islands, so the establishment of global transportation-network can lead to a huge geographical, economic change at the relevant region and give an opportunity to expand the business boundary for Korea's construction companies.



Figure 4. Living zone around Honam-Jeju high-speed rail

5. CONCLUSIONS

Undersea tunnels around the world are very active in construction or planned. In particular, over 80km super longest undersea tunnel there are not many examples around the world. Korea has very large tunnel construction experiences in urban area, mountain area and under river. Recently, immersed tunnel in Busan area are constructed. Many tunnels on the occasion of immersed tunnel construction will be built and planned in Korea. Especially, long and deep undersea tunnel projects as shown above are still planned.

In order to overcome technical weakness, many research projects also will be launched for the world subsea tunnel market. South Korea's government also recognizes the need for technical assistance in these undersea tunnel projects, and related areas will be continued support. Near the future, the plan of the Korea-China and Korea-Japan undersea tunnel construction will be realized.

REFERENCES

Ministry of Construction and Maritime, 2011, *The Feasibility Study on the Connection between Honam and Jeju with High Speed Rail Link*, Reports on MOCT .

C. Y. Kim, 2010, *A Study on Present Status of Deep Underground Tunnel and Future Technologies*, the 21st KICT-JICE Joint Workshop.

C.Y. Kim, S.B. Yim, et al., 2011, *Urban Deep Underground Transportation Infrastructure Project in Korea and Technical Requirements*, Proceedings of the ITA-WTC 2011 in Helsinki , Finland, 295 pp

Assessment of community fire hazard vulnerability: A case study of ward 65 in Dhaka city

Sharmin ARA
Research Planner, BNUS, Dhaka, Bangladesh
sharmin.ara14@gmail.com

Mehedi Ahmed ANSARY
Professor, Department of Civil Engineering, BUET, Dhaka, Bangladesh
ansary@ce.buet.ac.bd

ABSTRACT

Fires cause the greatest loss of life and property in urban areas. Urban fires have devastating impact on communities. Unplanned urbanization has intensified the problem further. The number of fire incidents in Dhaka was 1,686 in 2009, 1902 in 2010, and 605 up to March 2011 (Fire Service and Civil Defense, 2011). To mitigate such disasters at community level, community participation is important. To strengthen the resiliency of a community to natural and man-made hazards, before they become a disaster, a comprehensive risk and vulnerability assessment is must. Community Vulnerability Assessment Tool (CVAT) is a useful method to assess vulnerability of a community to any hazard. In this study, a traditional community of ward 65 of Dhaka has been selected. CVAT method will be applied here in three steps. At first, a hazard map has been created by land use in the study area. Then different vulnerability analyses have been conducted namely social vulnerability, critical facilities vulnerability, and economic vulnerability. To accomplish these vulnerability analyses different field surveys are required getting complete scenario of the community. Each of the vulnerability analysis includes certain specific steps which ultimately lead to a vulnerability map. After the preparation of hazard map, it is required to overlay the maps with each other. By using some parameters and attributes, community vulnerability has been evaluated with respect to fire hazard. Finally the overall vulnerability of the community has been assessed. This study might provide a baseline to prioritize mitigation measures and to evaluate the effectiveness of those measures over time in the community.

Keywords: *Fire hazard, community vulnerability, hazard map, vulnerability map, mitigation.*

1. INTRODUCTION

Fire hazard is something that increases the risk of fire. It causes immense loss of life and properties. In the urban area with haphazard development fire event occurs frequently and it has devastating impact on communities as well as the whole country. Social and economic effects are most conspicuous than the other impacts to the country. In Dhaka city unplanned urbanization and rapid industrialization are the major causes of large number of fire related accidents and increasing the vulnerability of the country's major population and its economy. Not only in Dhaka but also other major cities in Bangladesh which are unplanned and densely populated, suffering the rage of fire for many years. Congested building orientation, mixed type of use in a same building, flammable building materials, electrical system and lack of awareness regarding fire event are increasing the risk of fire in the residential area of Dhaka city especially in the older portion of Dhaka. Statistics shows that most of the residential fire events occurred in 2009 than the other statistical year (see figure 1). But the economic loss of fire is in decreasing trend. From table-1 it is evident that the economic loss due to fire incidents is very high. As Bangladesh is a developing country cannot afford the huge amount of loss due to fire accidents every year. Especially in most of the cases the victims are the low income group of the society.

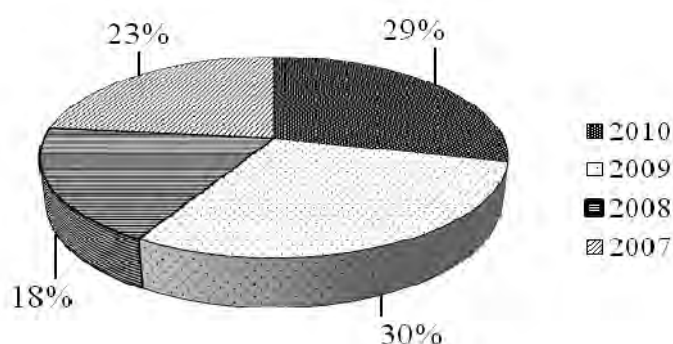


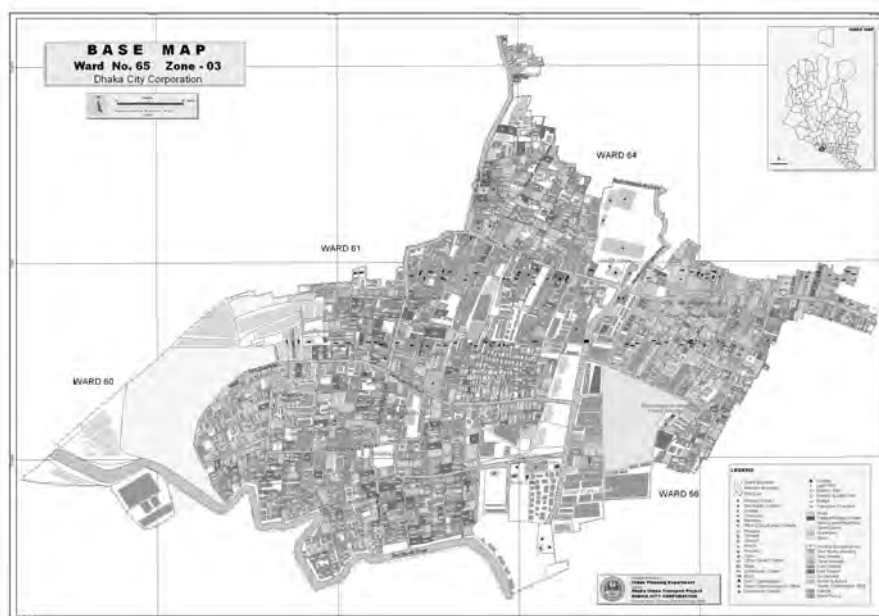
Figure 1: No of residential fire event in Dhaka city
(Source: Bangladesh Fire Service and Civil Defense)

Table 1: Extent of losses due to fire hazards in recent years
(1 Million USD = Taka 7 crore)

Year	Amount of loss due to residential fire (in Taka crores)
2010	107.42
2009	92.90
2008	56.45
2007	172.78
2006	238.7
2005	272.64
2004	213.78
2003	110.59
2002	112.21

(Source: Bangladesh Fire Service and Civil Defense)

Dhaka metropolitan area is divided into ninety wards for administrative purpose. Among these wards of Dhaka city, Ward 65 is most vulnerable to fire hazard than other because of its traditional land use and population density. Fire incidents are very common phenomenon in this portion. That's why a portion of this ward is selected as study area. Ward 65 of Old Dhaka is one of the oldest areas of Dhaka city. This area is mainly used as manufacturing area in Dhaka city. There is also other use exists here like go down, commercial use, chemical shop, clamber storage and processing shops are also prominent. Land use of this area makes it unique than the other area of Dhaka city which can be responsible for severe fire hazard. So that a fire hazard vulnerability of the community has done to examine the existing severity of the area and prepare the residents to face this sort of manmade disaster.



Map1: Study Area (ward 65 of Dhaka city)
Source: Dhaka City Corporation

2. EXISTING STATUS AND TRENDS OF FIRE INCIDENTS IN DHAKA CITY

The current trend of fire incidents in the mega city Dhaka shows increasing in number. Fire incidents are categorized into different causes. This categorization has done according to the building use, electrical system in the building. The figure 2 and 3 describes the number of recent fire events in Dhaka city with different reasons from 2005 to April 2011.

Residential fire events are increasing in every year tremendously and it causes loss of property and injures many people badly. Industrial fire is also in increasing trend. In between 2007 to 2010 fire caused by electric short circuit is higher in 2008 (40.26%) and for cooking appliance most of

the fire incidents occurred in 2010 (24.5%) and chemical reaction causes most fire accidents in 2009.

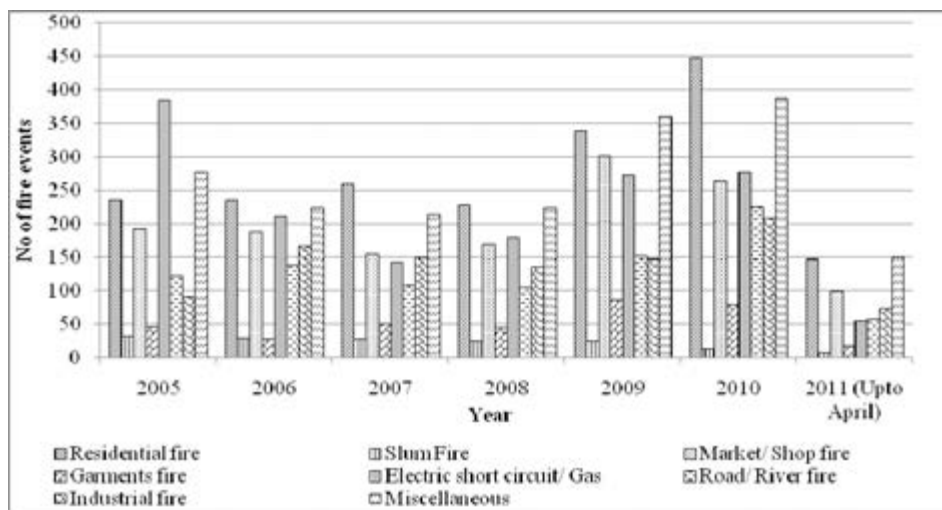


Figure 2: Trends in fire accidents in Bangladesh (2005 to April 2011) (Source: Bangladesh Fire Service and Civil Defense)

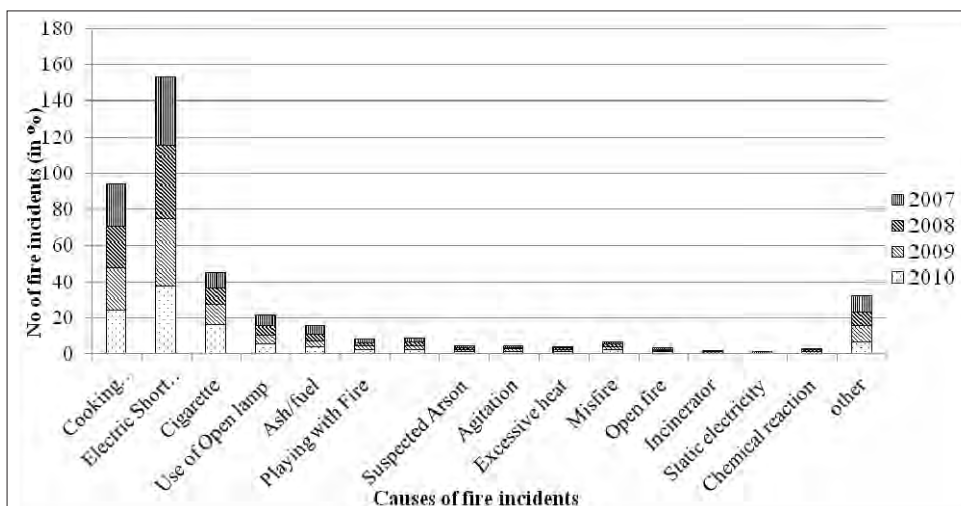


Figure 3: Causes of fire accidents in Dhaka city (Source: Bangladesh Fire Service and Civil Defense)

3. FIRE HAZARD VULNERABILITY ANALYSIS

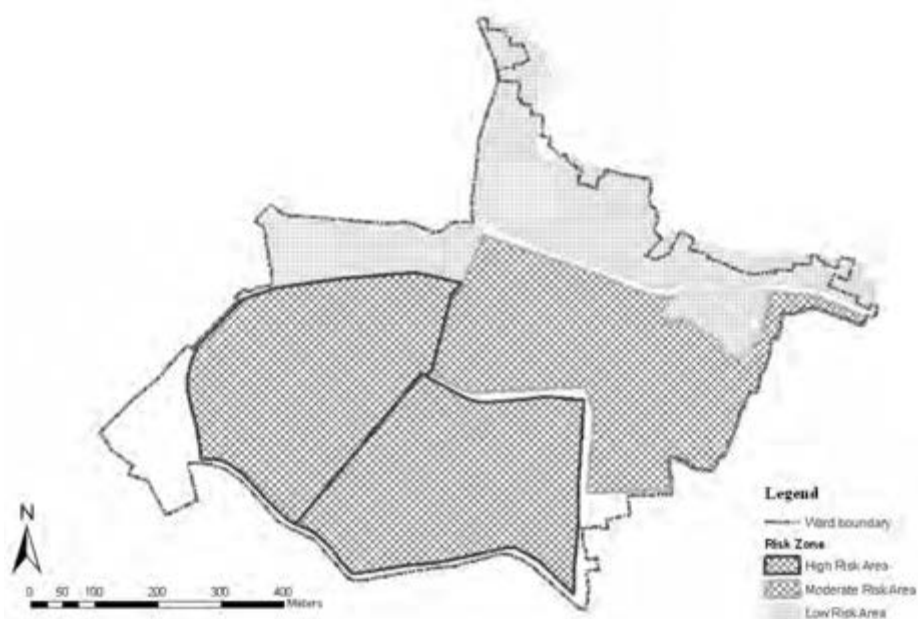
To assess the community vulnerability in old Dhaka, Community Vulnerability Assessment Tool (CVAT) is used to find out the existing scenario of the area. This tool has **step-by-step process** and it includes 7 steps with methods and tools for analysis within the steps. These 7 steps are:

- Hazard identification
- Hazard analysis
- Critical facilities analysis
- Social analysis
- Economic analysis

- Environmental analysis
- Mitigation opportunities analysis

The tools and methodologies used in this analysis consist of GIS and spatial mapping analysis. In this paper only critical facilities analysis, social analysis and economic analysis has done to assess the vulnerability of the community.

For analysis the study area is divided into three risk zones according to their land use from expert opinion. In this different risk zone land use is different than other (see map 2). The livelihoods of its inhabitants are primarily based on plastic processing industries. Here plastic manufacturing, recycling and processing factory exists with residential use is considered as high risk area. The name of this portion is Islambag. It displays a high building density with multi-storey buildings and very few urban public spaces left. In the moderate risk area clamber store and processing factory and different go down (plastic go down, cattle food storage) are dominant. In the low risk area residential use with commercial (retail shop, office, bank, and clamber storage) are found.



Map 2: Fire risk zone in the study area

3.1 Critical facilities analysis

Critical facilities analysis mainly focuses on determining the vulnerabilities of lifelines, health care facilities, and special community facility like religious centre, club, cultural center and educational institutions within the community. Main steps includes in this analysis are:

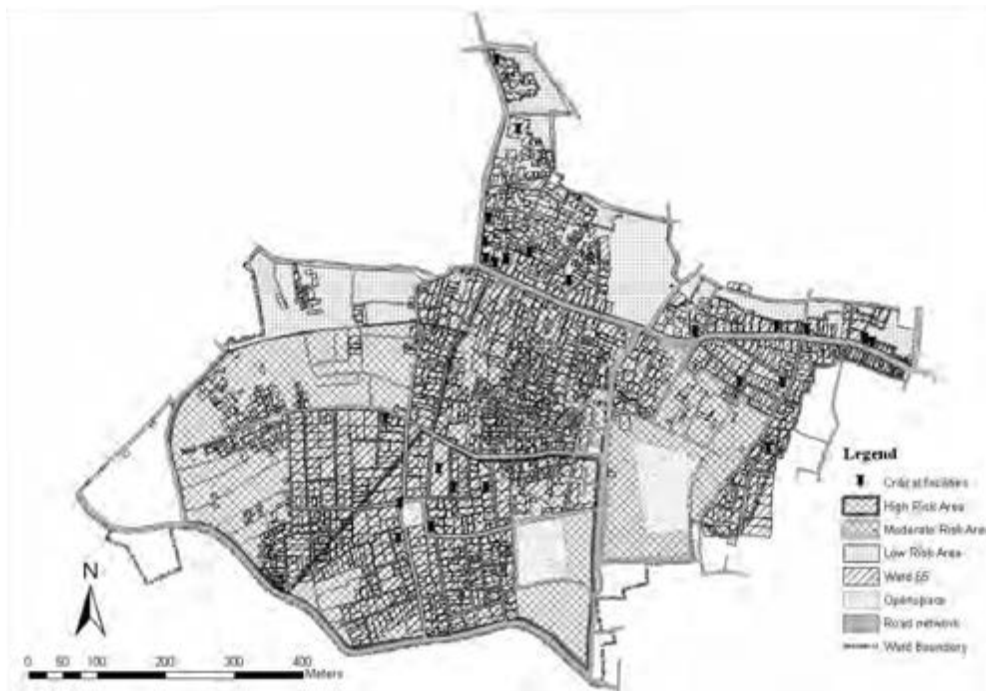
- Prepare a critical facility inventory and categorize the results
- Intersect critical facilities with different risk areas

- Conduct a vulnerability assessment on highest risk critical facilities

To do this at first all the critical facilities in ward 65 were identified and a complete inventory of these facilities was prepared. Then critical facilities that are in and within close proximity to high risk areas were identified by overlying the critical facilities location over the map of fire vulnerable areas. The most common critical facilities in an area are as following:

- Educational institutions
- Religious centers (Mosque)
- Government organizations/ NGO offices
- Healthcare facilities
- Bank/other office
- Community facilities
- Police stations
- Water pump house/ electrical sub station

Map-3 shows that 26% critical facilities are located in the high risk area and Islambag area is more vulnerable other part of the ward. The critical facilities in this portion are educational institution and religious center. Plastic industries are located in very close proximity to these facilities. On the other hand most of the critical facilities are located in the Lalbagh area. Because land use is completely different in these two risk zones. In the low risk area main land use is residential and in some case mixed (residential, retail shop, commercial) and the people in this area are less vulnerable to fire hazard.



Map 3: Critical facilities in the study area

So it can be said that the critical facilities of the study area are not at high risk from fire. It has a significant impact on the later stages of disaster management. If the service is interrupted during any fire disaster it may cause another grievous situation to the locality. Because these facilities always play an important role in post disaster management stage.

3.2 Social vulnerability analysis

In terms of preparedness, identification of the community's vulnerability gives a clear picture of risky and susceptible groups. By identifying these vulnerable groups, a better disaster preparedness plan can be undertaken and better public awareness studies can be developed in the pre-disaster phase. Social vulnerability analysis is very essential for any kind of vulnerability assessment. Because people lives in the society are most vulnerable to any sort of natural and manmade disaster. So to know the existing status of the society with respect to disaster, social vulnerability assessment is mandatory. For social vulnerability analysis two steps has been followed.

- Social indicators were identified
- Intersect special consideration areas with different risk areas

Social indicators include education level, population composition and number of total population in one holding. In the study area most of the people are not educated. Among them maximum people are working as employer in a plastic processing and manufacturing factory, shoe making factory etc. here proportion of male and female residents are almost same. From field survey it has found that population density is very high here. Because the working place and living place of the worker is in same area. In the plastic recycling and processing factory mainly women are working. With respect to these conditions of the area it can be said that the area is vulnerable to fire hazard.



Map 4: Population density in individual building of the study area

3.3 Economic vulnerability analysis

To identify the economic vulnerability to fire hazard this analysis has done. Because in this area various economic activities are going on the same building and which leads to severe fire hazard in the area. To analyze this vulnerability two steps are followed. They are:

- Economic sectors and its inventories were selected from the study area by land use survey and located in the map
- The economic activity maps were overlaid with the fire risk consideration areas analyzed its vulnerability

Four types of economic activities are distinctly dominant here. These are plastic manufacturing and processing industry, different type of factory, go down, clamber storage and processing shops, chemical shops (see figure 4). Location of these economic activities was determined by land use survey. Some economic activities makes the study are vulnerable to fire hazard. Among them plastic manufacturing industry is totally based on chemical materials which promote fire to spread within few seconds to the locality. So it is important to know how many hazardous economic activities are located in the study area.

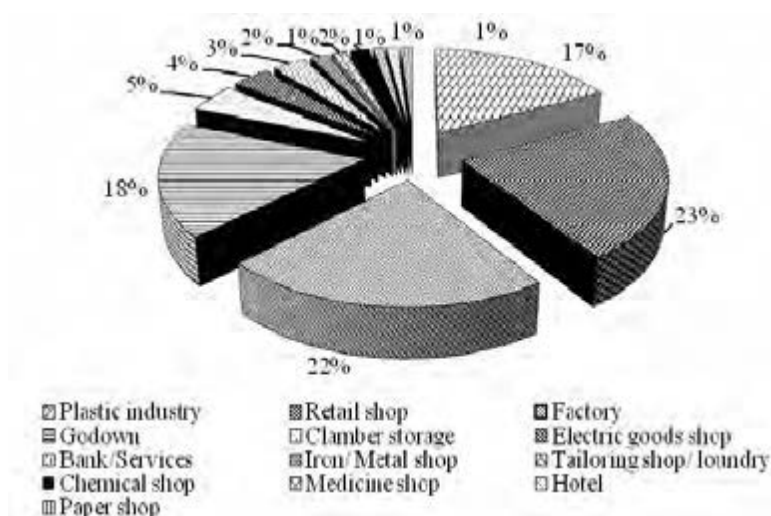


Figure 4: Land use in the Ward 65
(Source: Field survey, 2011)

3.4 Structural Vulnerability Analysis

There are other factors in the area which makes it vulnerable to fire hazard. These factors are width of staircase, road width of the area and accessibility to the building, position of transformer and electricity pole. If the roads are not accessible to fire service vehicle to douse/ put off the fire it may cause a loss to the community. For the emergency evacuation process

staircase width is also a vital issue to the resident of a building. That's why these factors get importance to the vulnerability assessment.

3.4.1 Staircase width

From field survey it has observed that in the study area most of the buildings (289 out of 781 surveyed buildings) are one storied and most of them are not RCC or masonry building. They are constructed by tin. These buildings are mainly used as clamber storage and processing activity and plastic manufacturing and processing. In this structure fire can propagate very swiftly. 164 buildings are two storied and mainly used as residential and plastic processing activity. The staircase width of these buildings varies from 2-3 ft. but some recently constructed buildings the width may vary from 3-4ft.in the older portion of Dhaka city it is a tradition that the width of staircase is very low than the new part of Dhaka. So that from the field survey it has observed that most of the elevated buildings staircase width varies from 2-3.5 ft. In case of some newly constructed buildings the width is 4 feet. Wider staircase is essential for any building during the evacuation process for any disaster. For fire hazard it get special priority because fire propagate very quickly in a building. So people need to protect themselves from the rage of fire in a very short time. In this respect the study area is vulnerable to fire hazard.

3.4.2. Road width/ Accessibility to building

For emergency response during any disaster road width is an important factor. If the road is not sufficiently wide to move fire service's vehicle it may cause another disaster to the people and it may extend the loss very much than the expected. In case of fire accidents in a building it can spread very quickly and can engulf lots of properties and life. This kind of event is very common in Bangladesh especially in old Dhaka. In the study area accessibility to each household is not found. The main roads are wide and accessible to the fire service vehicle but the local roads and connecting roads to the buildings are not accessible to the vehicle (see map-5). Road width varies from 5-2 feet. In most of the case from the main road the narrow connecting roads extends to the end of the block. These narrow roads are totally impossible for evacuation and recue process. In this respect this community is also vulnerable to fire hazard. They are not aware about widening the road.

3.4.3 Transformer and electricity pole

Position of transformer and electricity pole to a building is also assessed in this study because these may cause serious fire hazard to the locality. Recently in old Dhaka a fire incident occurred due to the blast of transformer. The death toll is around 150 due to this blast/ burst. It is examined with highly importance because the buildings in this area are constructed very closely to each other. So that fire can spread out to another building very ghastly. Among the surveyed buildings transformer is located in front of the building is 6%.



Map 5: Road network in the study area

4. CONCLUSIONS

From the above study it is obvious that the community is vulnerable to fire hazard. The land use pattern of ward 65 indicates the possibility of this kind of hazard. There are many plastic manufacturing and processing factory in the area. Mainly chemical materials will induce fire. Since ward 65 is a residential area, the loss due to fire will be catastrophic. To minimize the economic loss a coordinated planning is required and need to change the present land use pattern. A wider road network is also required to evacuate the community people.

REFERENCES

<http://www.spaenvis.nic.in/pdfs/monographs/fire-hazard.pdf>; accessed on 24th August, 2011

<http://etd.lib.metu.edu.tr/upload/1252196/index.pdf>; accessed on 24th August, 2011

A study on the preferable urban structure of provincial small town in the depopulation age

Shimpei IWAMOTO¹, Takahiro TANAKA², Daisaku NISHINA³

¹Graduate Student, Graduate School of Engineering,
Hiroshima University, Japan
m105912@hiroshima-u.ac.jp

² Associate Professor, Hiroshima University, Japan

³ Professor, Hiroshima University, Japan

ABSTRACT

Recently, the population is decreasing in Japan. If urban area keeps expanding to the suburbs, various problems will be caused. For example, daily lives without cars become difficult, efficient development and maintenance of urban structure will be also difficult, and energy consumption will be higher. To solve them, compact urban structure is requested corresponding to the population decrease especially in provincial small town. However, it is not clear where dense urban area should be located and how much population should be located there. Therefore, it is necessary to examine the appropriate future urban structure from several viewpoints. This is because the preferable urban structure from one viewpoint may not be good from other viewpoints.

Consequently, this study aims at examining the preferable future urban structure from several viewpoints, such as energy consumption, urban infrastructure development and maintenance cost, resident's livability. In this paper, authors examine the future urban structure from the viewpoint of urban infrastructure development and maintenance cost and energy consumption. Actually, this research is performed in Fuchu city, Hiroshima that is a provincial small town. Concretely, authors make 43 kinds of urban structure scenarios in 2035 such as "Complete compact type", "Partly compact type" and "Not compact type". Then, authors calculate the energy consumption for each scenario. As a result, it can be said that compact urban structure will lead to reducing energy consumption, and the effects are different from each other widely depending on scenarios.

Keywords: *urban structure, urban infrastructure cost, energy consumption, compact city*

1. INTRODUCTION

After the World War II, Japanese city has expanded to the suburbs because of rapid economic growth, population increase, and motorization.

Consequently, various urban problems, such as decline of downtown areas, urban sprawl, air pollution by car use, and increase of urban infrastructure development/ maintenance cost, have been caused. On the other, in Japan, population begun to decrease is rapidly increasing in recent years. Therefore, if urban area keeps expanding to suburbs, it is expected that urban area will become lower dense. In this case, it is though that daily lives without cars become difficult because keeping public transportation will not be easy. And, efficiency of urban infrastructure development and maintenance also decrease. From such background, compact urban structure is proposed corresponding to the population decrease. The followings are expected by making the urban structure compact: Revitalizing downtown, cutting urban infrastructure development and maintenance cost, decreasing environment load, and making daily lives without cars possible. Therefore, some local governments make the plan of compact city. However, such plan do not shows proper compactness quantitatively from the view of the issues above. Therefore, this study aims at making some scenarios for the target city quantitatively and evaluating the scenarios from the view of cutting urban infrastructure development and maintenance cost, decreasing energy consumption, and resident's livability, quantitatively. And, authors pursue better future urban structure. As a first step, this paper shows the results of making future scenarios and evaluating the scenarios from the view of cutting urban infrastructure development and maintenance cost and energy consumption.

This study considers about compact urban structure of provincial small town. Because, population is decreasing and aging rapidly, in provincial small towns. In addition, the number of provincial small town is many and the number of cities that have population of fifty thousand or less city is half or more in Japan. Therefore, this study focuses on provincial small town. It is one of the reasons that lots of past studies are case study of large population city.

As existing related studies, relationship between population distribution structures and energy consumption by car use were examined in Utsunomiya^[1], cost benefit of compact city was analyzed in Fukuoka^[2], traffic action change of people by making compact city was examined in Matsue^[3]. These existing studies consider urban structure from one viewpoint such as energy consumption of car, maintenance cost, and traffic action of people. But, it is necessary to examine comprehensively from some viewpoints in case of considering future urban structure. Because, the preferable urban structure from one viewpoint may not be good from other viewpoints. Therefore, urban structure should be appreciated from several viewpoints and examined most well-balanced from each viewpoints.

Therefore, this study aims at examining the preferable future urban structure from several viewpoints such as urban infrastructure development and maintenance cost, environmental load, resident's livability in Fuchu City, Hiroshima. Fuchu City is a town where the population is 39,345 and the area is 110.2km². As mentioned above, this paper, urban structure

(1) Complete compact scenario

In this scenario, urban area is compacted. And, population is distributed in only Compact district.

(2) Partly compact scenario

In this scenario, urban area is compacted. And, population is distributed also besides Compact district.

(3) Not compact scenario

In this scenario, urban area is not compacted. And, Compact district don't exist.

Besides, Complete compact scenario and Partly compact scenario are classified into the following two kinds.

(a) Single core model

In this scenario, urban area is compacted to one district. Consequently, there is a Compact district. Fuchu station that is pivot of transportation in Fuchu City is centered on Compact district.

(b) Multi-core model

In this scenario, urban area is compacted to plural districts. Consequently, there are plural Compact district. Stations, elementary schools, junior high schools, and main intersections are centered on Compact district. And, authors also two kinds of scenarios. One is that Compact districts are located in only urban planning area, the other is that Compact districts are located in the entire city.

In Complete compact scenarios, population density of Compact district is set to 150 per hectare, 100 per hectare, and 50 per hectare. In Partly compact scenarios, population density of Compact district is set to 90 per hectare, 80 per hectare, 70 per hectare, 60 per hectare and 50 per hectare. Besides, in Partly compact scenario in which population density of Compact district is 90 per hectare, 90% of population is located in Compact district and 10% of population is located in outside. And, in Partly compact scenario in which population density of Compact district is 80 per hectare, 80% of population is located in Compact district and 20% of population is located in outside.

3.3 Method of making scenario

First, authors forecast the population of each district in 2035^[7]. Next, authors step the following procedures.

(1) In case of Complete compact scenario

[1] Setting of population and center of Compact district

The population was set as shown in Table 2. The center was set in consideration of location such as station, bus stop, shop, school, community center and assembly halls based on hearing to local government officials.

[2] Setting of area that satisfy condition of Compact district

The criteria of Compact district were set as shown in Table 3. Because, Compact district should not be located in the area that is urbanization-restricted area, slope ground and high disaster risk area.

[3] Setting of Compact district boundary

Compact district boundary was set near distance from the center and satisfies all conditions of Table 3. And, the boundary was set so that

population density become 150 per hectare, 100 per hectare and 50 per hectare.

(2) In case of Partly compact scenario

[1] Setting of population and boundary of Compact district

Compact district boundary is Compact district boundary of Complete compact scenario with population density 100 per hectare. The population was calculated by multiplying Compact district area by population density.

[2] Setting of outside Compact district population

The population was calculated by subtracting Compact district population from all population. And, this population was apportioned each district.

(3) In Case of Not compact scenario

The population is forecast population of each district.

Table 2: Setting of population

Table 3: Condition of Compact district

Kinds of scenarios		Setting population	Condition of Compact district	
Single core model		all population	Urban planing area	Out of urban planing area
Multi-core model	station surround	$\frac{\text{each station ridership}}{\text{all stations ridership}} \times \text{all population}$	urbanization-designated area	-
	elementary school district	each district population	out of restricted industrial zone	-
	old elementary school district		slope angle is 8 degree or less	
	junior high school district		out of sediment disaster damage supposition district	
			outside river and lakes	

3.4. Examples of made scenario

Examples of scenarios are shown in Figure 1 and Figure 2. Figure 1 shows examples of Complete compact scenarios. Figure 2 shows examples of Partly compact scenarios and Not compact scenario. In addition, Compact district is surrounded area by broken line.

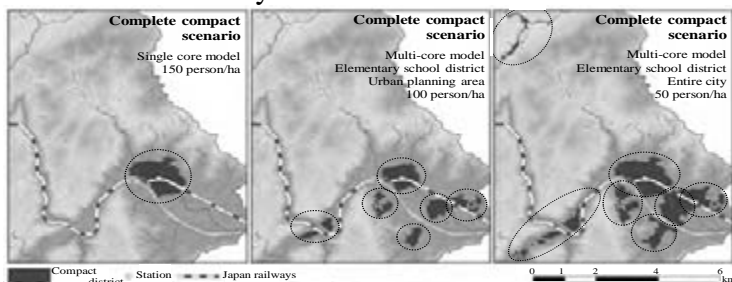


Figure 1: Examples of Complete compact scenarios

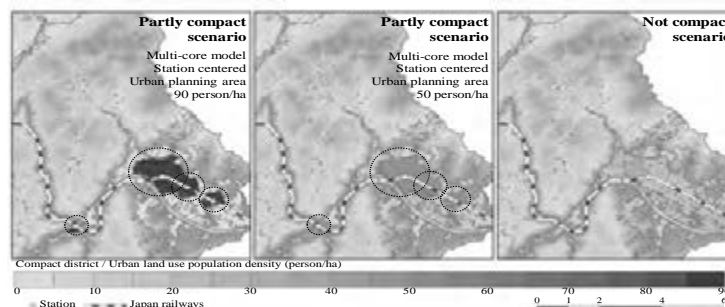


Figure 2: Examples of Partly compact scenarios / Not compact scenario

4. EVALUATION FROM THE VIEWPOINT OF URBAN STRUCTURE DEVELOPMENT AND MAINTENANCE COST

4.1 Calculation of urban structure development and maintenance cost

The necessary costs for development and maintenance of road, waterworks, sewer, elementary school, junior high school, preschool and community center are calculated for all scenarios. And, they are compared. The following formulas (Table 4) were used for calculating the costs. These formulas are made based on actual track record in the local government. In addition, X is development cost, Y is maintenance cost, and unit is JPY. The development cost is cost until 2035 and the maintenance cost is yearly cost.

Table 4: Formulas of urban infrastructure cost

Urban infrastructure	Formulas
Road	$Y_R = A * 684,362$ (JPY/projects) (1)
Waterworks	$X_W = 10,853,346$ (JPY/ha) *B (2)
	$Y_W = C+D+E+F$ (3)
Sewer	$X_S = 264,250,463$ (JPY/year) * G (4)
	$Y_S = 113,060$ (JPY/ha) * H+I (5)
Elementary school, Junior high school, Preschool, Community center	$X_B = J*K$ (6)
	$Y_{EJP} = \Sigma (L+M)$ (7)
	$Y_C = \Sigma (1,047,189$ (JPY/ m ²) *N) (8)

A: number of maintenance services (projects) F: water pipe maintenance cost (JPY) K: development cost per square meter (JPY/m²)
 B: development area (ha) G: development period (year) L: administrative cost for each facility (JPY)
 C: filtration plant maintenance cost (JPY) H: disposal area (ha) M: personnel cost for each facility (JPY)
 D: distribution reservoir maintenance cost (JPY) I: renewal cost (JPY) N: floor area for each community center (m²)
 E: pump station maintenance cost (JPY) J: development floor area (m²)

4.2. Result of calculation

Result of calculation is shown Figure 3 and Figure 4. Figure 3 is development cost. Figure 4 is maintenance cost. The major findings are followings.

1) Development and maintenance cost become lower in the following order.

- scenario type [1] Complete compact scenario [2] Partly compact scenario [3] Not compact scenario
- population density [1]150person/ha [2]100person/ha [3]50person/ha
- model of scenarios [1] Single core model [2] Multi-core model
- Compact district layout type [1] urban planning area [2] entire city [1] station centered [2] junior high school district [3] elementary school district [4]old elementary school district.

2) In case of Complete compact scenario, the effect of changing 100person/ha from 50person/ha is smaller than the effect of changing 150person/ha from 100person/ha.

3) Among the cases of Complete compact scenario with same population densities, the costs are different from each other by layout of Compact district. And the difference is larger in the case of 50person/ha scenario than others.

4) Among the cases of Complete compact scenario with same numbers of Compact districts, densities, the costs are different from each other by

layout of Compact district., The scenarios in which some Compact districts are near from each other and they can share the facilities make the cost lower.

- 5) In case of Partly compact scenario, cost difference by Compact district layout type is small.
 - 6) In development cost, the proportion of cost for sewer is higher.
 - 7) In maintenance cost, the proportion of cost for building facilities is higher.
- From the above, In order to reduce urban infrastructure development and maintenance cost, it is thought most effective to make clear the inhabited area and the non-inhabited area.

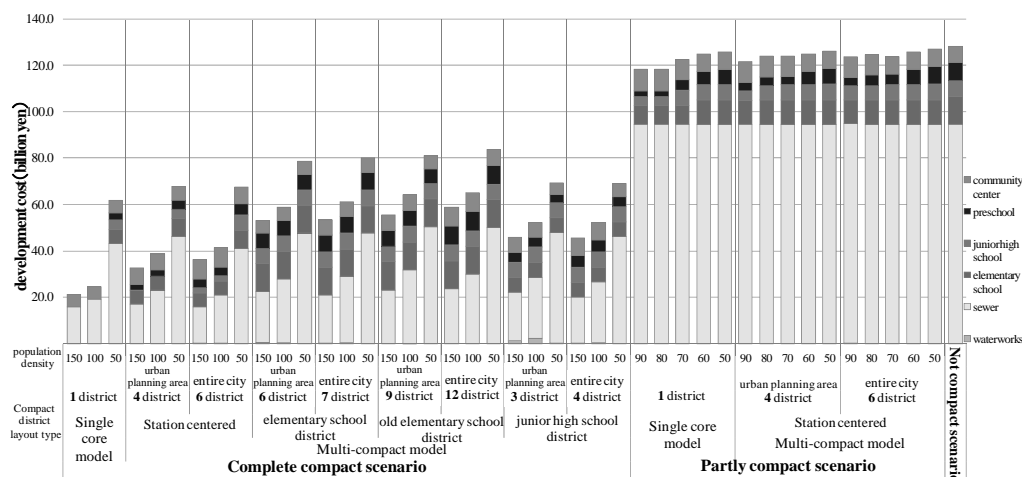


Figure 3: Calculation result of development cost

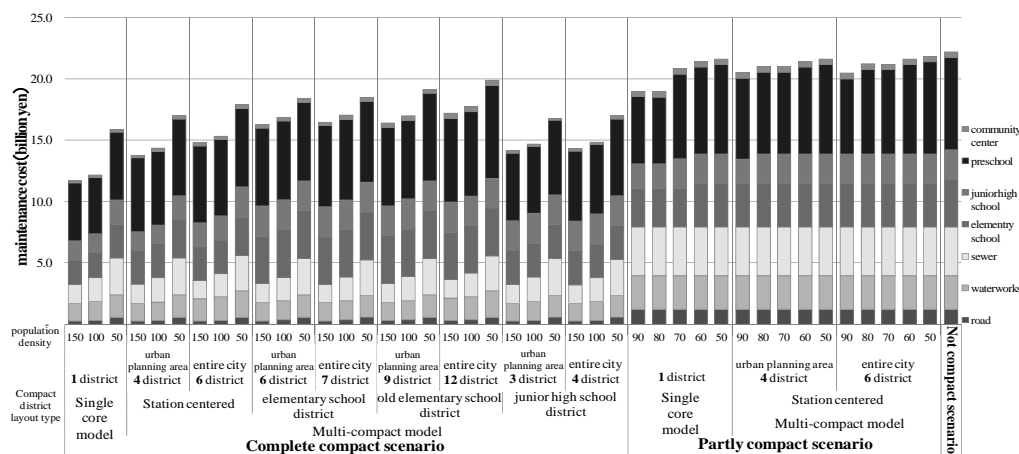


Figure 4: Calculation result of maintenance cost

5. EVALUATION FROM THE VIEWPOINT OF ENERGY CONSUMPTION

The cooling and heating energy consumption in houses and the urban infrastructure development energy consumption are calculated for all scenarios.

5.1.1. Calculation of cooling and heating energy consumption in houses

The following formulas (Table 5) were used for calculating the energy consumption.

In addition, R and T were set by thermal load calculation program LESCOM^[8], as shown in Table 6. And, detached house is wooden structure. Collective housing is reinforced concrete structure.

5.1.2. Result of calculation

Result of calculation is shown Figure 5. The major findings are followings.

- 1) The more the rate of household of collective housing is, the smaller annual cooling and heating energy consumption in houses in entire city is.
- 2) Annual cooling and heating energy consumption in houses in entire city of every scenario is smaller than that of Not compact scenario. But, the reduction effect has a big difference by scenarios.
- 3) In same compact district layout type scenario, the higher population density in compact district is, the smaller annual cooling and heating energy consumption of house in entire city is. However, annual cooling and heating energy consumption in houses in entire city is not proportional to population density. Therefore, the higher population density in compact district is, the smaller reduction effect of annual cooling and heating energy consumption of house in entire city is.
- 4) In same population density of compact district scenario, annual cooling and heating energy consumption in houses in entire city is different by compact district layout type. In general, it becomes small in order of the following.
[1] old elementary school district [2] elementary school district
[3] junior high school district [4] single core [5] station centered.
But, the difference before and behind order is small.
- 5) The annual cooling and heating energy consumption in houses in entire city of Partly compact scenario is bigger than that of Complete compact scenario. But, this difference is small.

From the above, in order to reduce annual cooling and heating energy consumption in houses in entire city, it turns out that it is most effective to make high population density urban structure. Only by raising the DID population density of Fuchu city (34.1[person/ha] to 50 [person/ha] , the difference of annual cooling and heating energy consumption in entire city with Not compact scenario is small, and it can seldom expect the big reduction effect.

Table 5: Formulas of cooling and heating energy consumption in houses

	$Z_H=O+P$	$O=Q*R$	$P=S*T$	(9)
Z_H : annual cooling and heating energy consumption in house in entire city (MJ) O : annual cooling and heating energy consumption in detached house (MJ) P : annual cooling and heating energy consumption in collective housing (MJ) Q : the number of detached house (building) R : basic unit of annual cooling and heating energy consumption in detached house (MJ/year*building) S : the number of collective housing (building) T : basic unit of annual cooling and heating energy consumption in collective housing (MJ/year*building)				
In Compact district	$Q+aS=b$		$cQ+dS=e$	
	a : the number of household per one collective housing (Table 6) b : the number of household of entire city in 2035 (9,384 households ^[4]) c : site area of detached house (Table 6) d : site area of collective housing (Table 6) e : area of housing site of entire city in 2035 (ha)			
	$Q=f*g$		$S=f*h$	
	f : the number of household by district in 2035 (household) g : rate of detached house by district in 2005 (%) h : rate of collective housing by district in 2005 (%)			
Out of Compact district	$Q=f*g$		$S=f*h$	
	$Q=f*g$		$S=f*h$	
	f : the number of household by district in 2035 (household) g : rate of detached house by district in 2005 (%) h : rate of collective housing by district in 2005 (%)			

Table 6: Setting of house and basic unit of annual energy consumption

Kind of house		Number of stories (story)	Number of household (households)	Basic unit of annual cooling and heating energy consumption per one building (MJ/year · building)	Basic unit of annual cooling and heating energy consumption per one household (MJ/year · household)
Detached house		2	1	51,227	51,227
Collective housing	150 [person/ha]	20	120	3,831,743	31,931
	100 [person/ha]	10	60	1,936,073	32,268
	90 [person/ha]	9	54	1,746,506	32,343
	80 [person/ha]	8	48	1,556,939	32,436
	70 [person/ha]	7	42	1,367,372	32,556
	60 [person/ha]	6	36	1,177,805	32,717
	50 [person/ha]	5	30	988,238	32,941
Out of Compact district Not compact scenario		3	18	609,104	33,839

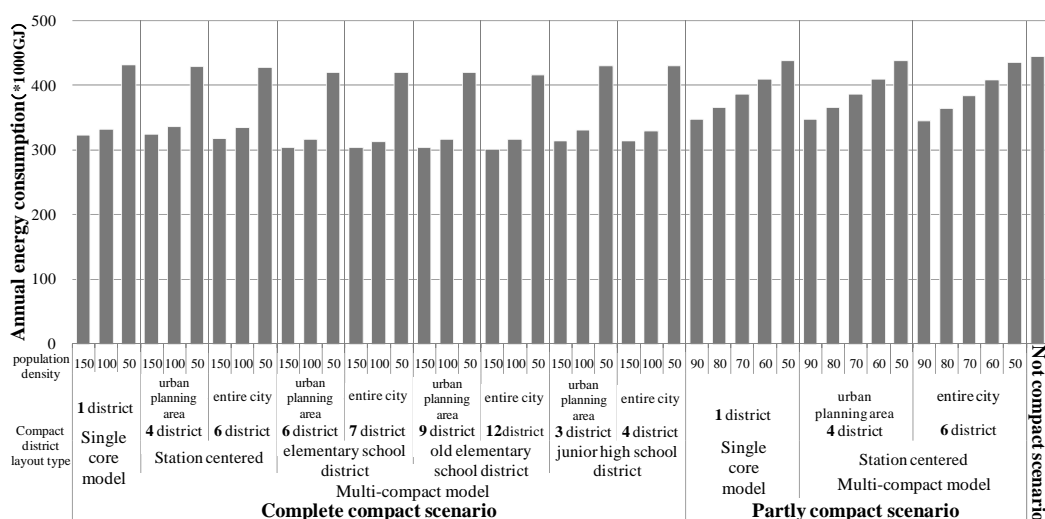


Figure 5: Calculation result of cooling and heating energy consumption in house

5.2.1. Calculation of urban infrastructure development energy consumption

Urban infrastructure development energy consumption is the energy consumption which will occur by 2035. The following formulas (table 7) were used for calculating the energy consumption.

Table 7: Formulas of urban infrastructure of development energy consumption

Urban infrastructure	Formulas
Waterworks	$Z_W = U * 74.312 (\text{MJ}/1000\text{JPY})^{[6]}$ (12)
Sewer	$Z_S = U * 45.331 (\text{MJ}/1000\text{JPY})^{[6]}$ (13)
Elementary school, Junior high school, Preschool	$Z_{EJP} = V * 15.759 (\text{MJ}/\text{m}^2)^{[6]}$ (14)
Community center	$Z_C = V * 12.105 (\text{MJ}/\text{m}^2)^{[6]}$ (15)

Z: urban infrastructure development energy consumption (MJ) U: development cost (1000JPY) V: development floor area (m²)

5.2.2. Result of calculation

Result of calculation is shown Figure 6. The same tendency as 1) ~ 6) result of urban infrastructure development and maintenance cost can be read from this figure 6. From the above, In order to reduce urban infrastructure development energy consumption, it is thought most effective to make clear the inhabited area and the non-inhabited area and to reduce the amount of sewer development.

6. CONCLUSION

In this study, several urban structure scenarios were made in order to examine proper future urban structure of provincial small town. And, quantitative urban infrastructure development and maintenance costs, cooling and heating energy consumption of house and urban infrastructure development energy consumption were calculated for all scenarios. And, these scenarios are compared and examined.

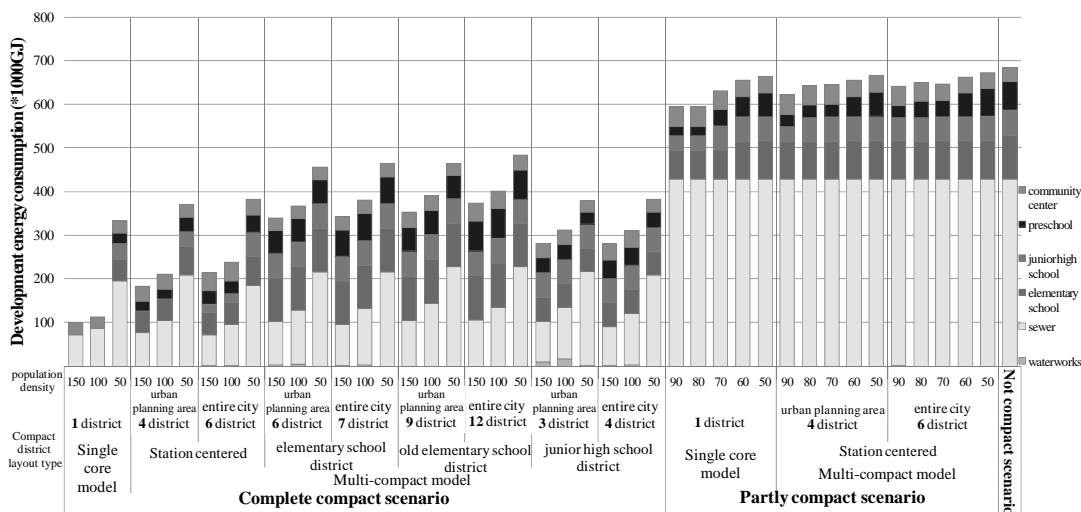


Figure 6: Calculation result of development energy consumption

In evaluation of urban infrastructure development and maintenance cost and development energy consumption, it was the conclusion that there was a big difference between Complete compact scenario and Partly compact scenario, and a big reduction effect to making clear the inhabited area and the non-inhabited area. However, in the viewpoint of the cooling and heating energy consumption in houses, there is almost no effect of making clear the inhabited area and the non-inhabited area.

As a next step, it is necessary to evaluate the future urban structure from several viewpoints such as traffic energy consumption and resident's livability.

REFERENCES

Hori, Y., Hosomi, A. and Kurokawa, T. 1999. Study on the Effects on Energy Consumption by Vehicle Trips in a Compact City. Papers on the City Planning Institute of Japan, No.34, pp.241-246, Japan.

Takahashi, M and Deguchi, A. 2007. Method for Cost-Benefit Evaluation System of Impact by Forming Compact City. Papers on the City Planning Institute of Japan, No.42-3, pp.487-492, Japan.

Yamane, K., Zhang, J. and Fujiwara, A. 2007. Influences of city compactness on travel behavior patterns in a local city. Papers on the City Planning Institute of Japan, No.42-3, pp.595-600, Japan.

National Institute of Population and Social Security Research, 2008. Future estimated population by municipality of Japan, National Institute of Population and Social Security Research, Japan.

Takeda, H., Inanuma, T., Yoshizawa, N., Isozaki, K., 2005. Standard meteorological data and a thermal-load-calculation program LESCOM, Inoue Shoin, Japan.

Architectural Institute of Japan, 2006. The LCA indicator of a building- The evaluation tool for warming, resource consumption, and provision for waste, Architectural Institute of Japan, Japan.

Microscopic risk analysis of rear-end collisions on Tokyo Metropolitan Expressway

Shinji TANAKA¹ and Hisashi MIURA²

¹Assistant professor, IIS, The University of Tokyo, Japan
stanaka@iis.u-tokyo.ac.jp

²Graduate student, IIS, The University of Tokyo, Japan

ABSTRACT

This paper analyzed the potential risk of traffic accidents on Metropolitan Expressway in Tokyo in a detailed way.

Tokyo Metropolitan Expressway (MEX) is the busiest urban motorway in Japan. It carries approx. one million vehicles every day and it also holds approx. 11,000 traffic accidents in a year. Rear-end collision is the most typical type of traffic accidents in MEX, which occupies about half of the causes of the total traffic accidents. Therefore it is very important to analyze accident risk in a microscopic way in order to make effective countermeasures for rear-end collisions.

This study analyzed traffic flows immediately before an accident in detail using pulse data from traffic detectors, and identified conditions which may lead to an accident. This condition is verified using pulse data from different time period, and a significant correlation between the number of accidents and this condition was found. Then a method to forecast this situation from observed data in advance was proposed. Applying this method to an actual dataset, it was confirmed that this method can forecast the situation of serious speed drop which can cause an accident with relatively high accuracy.

Keywords: *traffic accidents, rear-end collision, risk analysis*

1. INTRODUCTION

Traffic accident is one of the major risks in mega cities all over the world. The number of fatalities by traffic accidents in Japan is decreasing recently, but still a lot of accidents occur every year. Tokyo Metropolitan Expressway (MEX) is the busiest urban motorway in Japan, which carries approx. one million vehicles every day. It also holds approx. 11,000 traffic accidents in a year, and about half of them are rear-end collisions. Moreover, it causes approx. 12 % of traffic congestion. Therefore, effective countermeasures are needed not only to reduce traffic accidents but also to realize smooth traffic

flow. For this purpose it is important to analyze influential factors on traffic accidents in detail.

There are some existing researches which tried to analyze rear-end accidents in MEX in a macroscopic way. They used traffic flow data such as 1 minute or 5 minutes aggregated data, but they did not analyze it in an individual vehicle's movement.

This study aims at identifying the microscopic traffic states of high risk of accidents by analyzing raw data (pulse data) from traffic detectors at a sag section which holds a lot of rear-end collisions. And, an anticipation method of such high risk traffic states is also considered.

2. OUTLINE OF THE STUDY SECTION AND THE METHODOLOGY

2.1 Study section

A sag section which holds the highest accident rate of rear-end collisions in MEX is selected for the study section. Figure 1 shows the longitudinal sectional view of the section with the grade of the slope. This section has two lanes carriageway and lane change is prohibited at the downstream section from the 0.39kp.

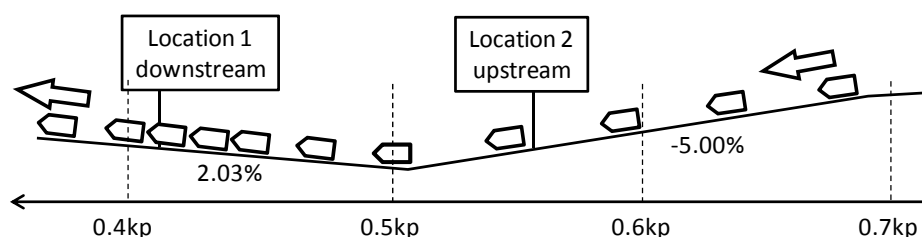


Figure 1: Longitudinal sectional view of the study section

2.2 Situation in the study section

The number of rear-end accidents in this section is extracted. As a new by-pass route opened during the period of this analysis, the results are shown in the separate figures. Figure 2 shows the number of the accidents by location during 3 months before the opening and Figure 3 shows the occurrence time of rear-end collisions out of them. Figure 4 and 5 shows the ones after the opening of the by-pass route.

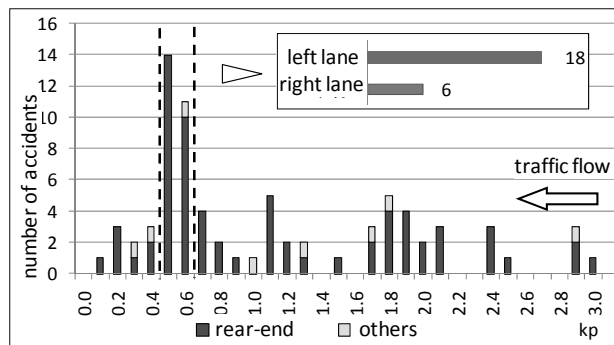


Figure 2: Number of accidents by location (Jan-Mar, 2010)

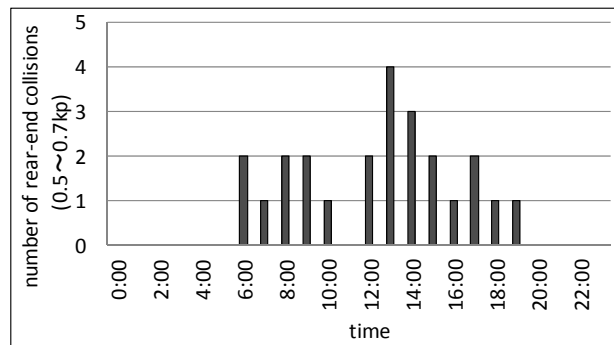


Figure 3: Number of rear-end collisions by time of day (Jan-Mar, 2010)

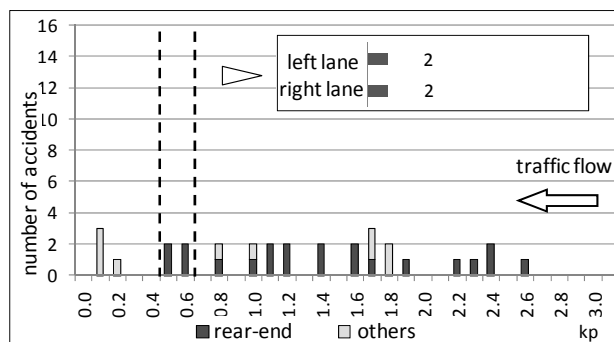


Figure 4: Number of accidents by location (Apr-Jun, 2010)

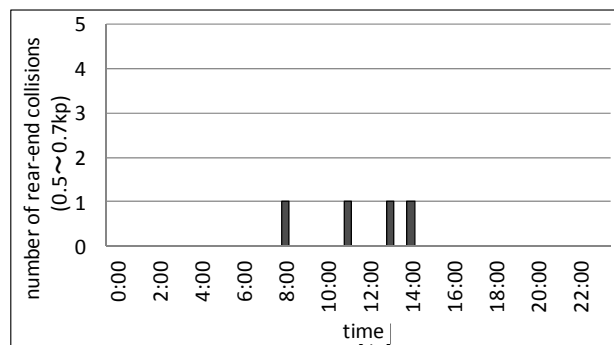


Figure 5: Number of rear-end collisions by time of day (Apr-Jun, 2010)

Figure 2 indicates many of the accidents occur in the down slope section (0.5-0.7kp) which is just upstream of the sag, and most of them are rear-end collisions. They occur much more on the left lane than the right lane, and most of them occur in the daytime (Figure 3). However after

opening of the by-pass route, the number of accidents in the same section decreased drastically, which means traffic situation change by new route influenced on the accident risk.

2.2 Analyzed data

In order to analyze the traffic flow around the sag section, pulse data from traffic detectors at two locations shown in Figure 1 was used.

Location 1: 0.41kp (downstream)

Location 2: 0.56kp (upstream)

Term: Feb 1 – 15, Mar 1 – Apr 30, 2010

We can tell the passing time, the speed and the length of the individual vehicles by analyzing the pulse data. Here, we assume all vehicles run in the same speed without lane change between two detector heads.

3. ANALYSIS ON TRAFFIC FLOW BEFORE ACCIDENTS

3.1 Extraction of target accidents

11 rear-end collision accidents were extracted from the accident record for detailed accident analysis. They were 5 cases on the left lane and 3 cases on the right lane before the opening of the by-pass route, and 1 case on the left lane and 2 cases on the right lane after the opening.

3.2 Analysis on traffic flow just before accidents

Analysis results of 5 cases are shown in Figure 6. It shows the transition of each passing vehicle's speed at the location 1 and 2 during 5 minutes just before the accident. The right end of the x-axis shows the accident occurrence time. Here, the accident occurrence time was estimated from the disturbance of the pulse data.

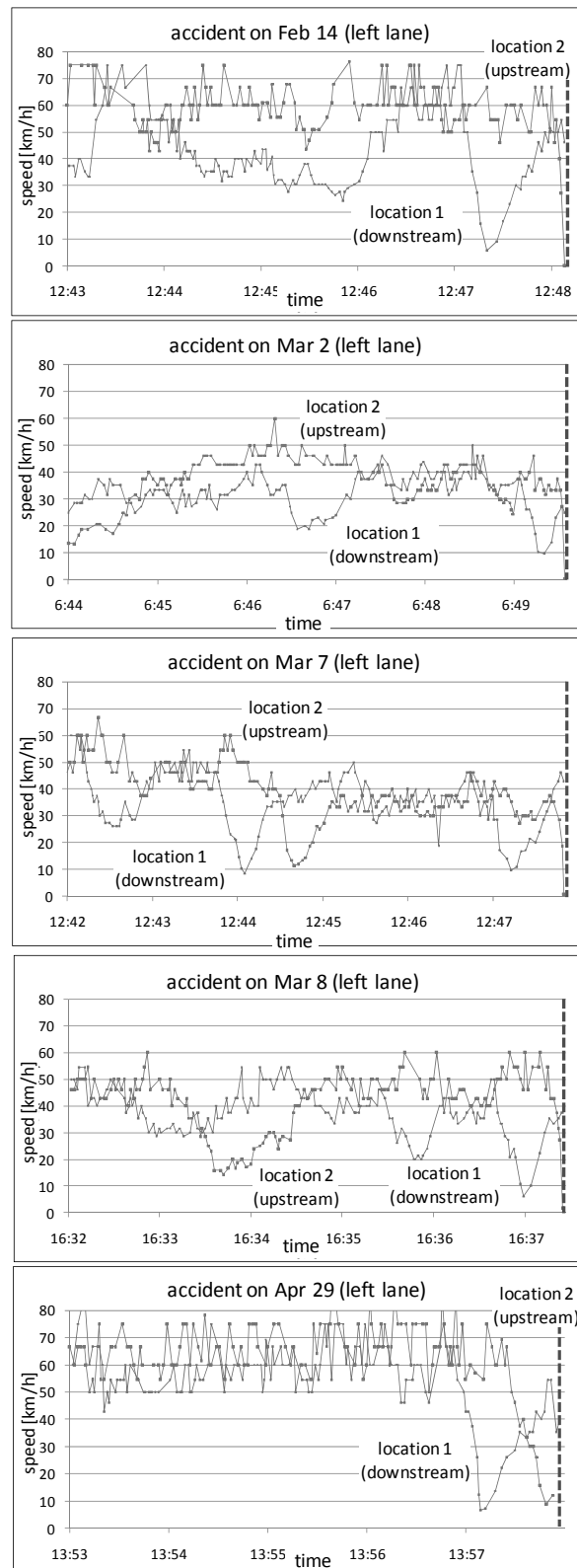


Figure 6: Speed transition before a rear-end collision accident

The common feature of these graphs is a sharp speed drop at the location 1 before 1 minutes of the accident. The speed at the location 1 gets less than 20 km/h temporarily while that at the location 2 is relatively high,

that is 30 – 60 km/h. This fact implies that the rear-end collision might be caused by a vehicle which could not react to a decelerating shockwave by the speed drop propagated upward from the location 1.

The cause of the speed drop at the location 1 cannot be identified from the range of the analyzed data. However, looking at the fact that most of the accidents occurred at the downhill section, the propagated shockwave from the uphill section to the downhill section may have increased the risk of rear-end collision accidents.

3.3 Conditions of high-risk traffic flow state

From the analysis mentioned in the previous section, we extracted the conditions of the high-risk traffic flow state as follows.

- I) Sharp speed drop less than 20 km/h at the downstream uphill section and generation of decelerating shockwave
- II) Propagation of the shockwave toward the upstream downhill section of 30 km/h or higher speed

These conditions are commonly seen in 7 cases out of 11 analyzed accidents. They were verified in the next section.

4. VERIFICATION OF HIGH-RISK TRAFFIC FLOW CONDITION

For the verification the conditions proposed above, the correlation between the number of accidents and the frequency of assumed high-risk traffic flow state by the proposed conditions were analyzed. The process of the analysis is shown as follows.

- i) extract detector pulse data of 1 week without accidents
- ii) count the cases when the speed at the location 1 dropped to below 20 km/h
- iii) extract the cases when the speed at the location 2 dropped from above 30 km/h to below 20 km/h within 60 seconds from the speed drop at the location 1
- iv) count the number of cases in iii) and compare it with the number of accidents

The following dataset is used for this verification.

Term: Feb 3 – 9, Apr 10 – 16, 2010

Time: daytime: 7am – 5pm, nighttime: 8pm – 6am

Lane: both left and right lanes

Table 1 shows the result of this analysis by lane, by time of day and by time before/after the opening of the by-pass route. The number of accidents in the right column shows the number of rear-end collision accidents during 3 months in the corresponding categories. Table 2 shows

the correlation coefficient of these 2 variables X and Y. The value shows a significant correlation between them, therefore we consider the conditions proposed in the previous section as valid to identify the high-risk traffic flow state.

Table 1: Comparison of traffic flow states and accidents

		Number of traffic flow states by proposed conditions (X)	Number of accidents (Y)
before opening	left	154	16
	right	85	2
	daytime	235	18
	nighttime	4	0
after opening	left	15	2
	right	81	2
	daytime	96	4
	nighttime	0	0

Table 2: Correlation between traffic flow states and accidents

correlation coefficient	0.914
number of observation	8
level of significance (1%)	0.834

Figure 7 shows the flow-speed relationship diagram by 1 minute traffic detector data using the proposed high-risk traffic flow condition. The high-risk traffic flow states occur more around 25 – 30 veh/min traffic flow region on the left lane, while there are fewer cases of that on the right lane. That means the occurrence of high-risk traffic flow state highly depends on the lanes because they are affected from the different routes in the downstream, and sometimes congestion propagates from there.

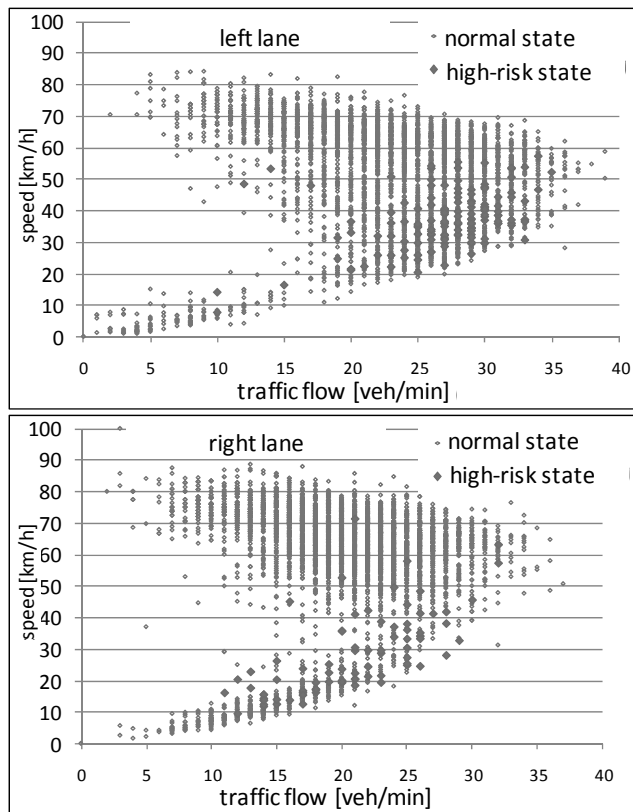


Figure 7: 1 minute flow-speed diagram during high-risk traffic states (Feb 3-9, 2010, daytime)

5. ANTICIPATION OF HIGH-RISK TRAFFIC FLOW STATE

The next challenge is to anticipate the occurrence of the high-risk traffic flow state in advance. However, it is difficult to tell a speed drop at the location 1 from the data of this time as mentioned before. Then this study focuses on anticipating an occurrence of speed drop propagation to the location 2 after the speed drop at the location 1 has been observed.

The speed at the location 1 after the speed drop and the traffic density at the location 2 were used as variables for the discriminant analysis. Here, we used 10 seconds for the aggregation duration considering the propagation time of the shockwave. The results of the discriminant analysis using 1 week daytime data are shown in Figure 8 and Table 3, that show about 80% of the occurrence of the shockwave propagation can be anticipated using this method.

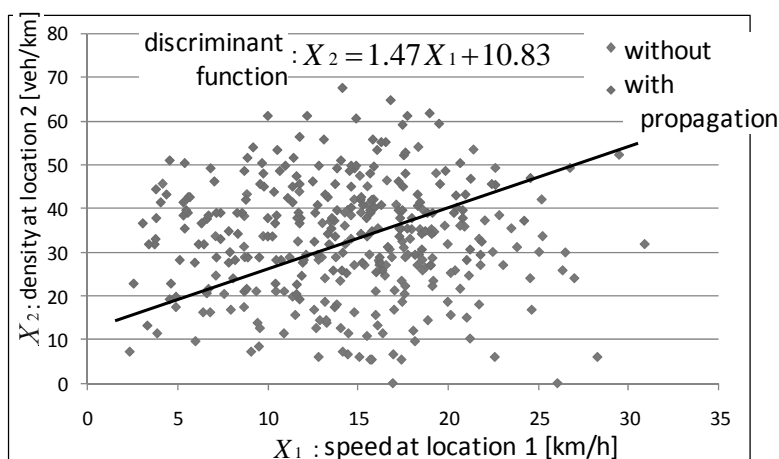


Figure 8: Distribution of speed at location 1 and density at location 2

Table 3: Hit ratio by discriminant analysis

		actual data	
		with propagation	without propagation
discriminant result	with propagation	151	32
	without propagation	42	120
hit ratio		0.78	0.79

6. SUMMARY

This study analyzed the pulse data from traffic detectors before an accident in a microscopic way and identified the conditions of the high-risk traffic flow state of rear-end collision accidents. The conditions are summarized as a sharp speed drop at the uphill of the sag section and its propagation to the upstream downhill section. They were verified using different period data without accidents and an anticipation method of the speed drop shockwave propagation was also proposed.

We could not anticipate the occurrence of the high-risk traffic flow state from the normal condition due to the limitation of the data. However, it is still useful because if we can detect a sharp speed drop at the downstream of the sag section we can provide an alert according to our proposed method for upstream drivers so that they can prepare for an expected risk. This kind of microscopic risk analysis methods should be explored more and should be incorporated with effective countermeasures to reduce the total risk of traffic accidents and to enhance the urban safety.

Development of Geospatial Disaster Management Information Service (GDMS) as a Social System

Takaaki KATO¹, Mitsuaki KOBAYASHI², Katsuyuki Yoshida³
and Jin NAKAMURA⁴

¹Associate Professor, ICUS, IIS, The University of Tokyo, Japan
kato-t@iis.u-tokyo.ac.jp

²Director, ICT Business Dept. JR East Consultants Company

³Deputy Director, ICT Business Dept. JR East Consultants Company

⁴Project Researcher, ICUS, IIS, The University of Tokyo, Japan

ABSTRACT

The information-collecting in disaster stricken region is essential to implement contingency response and recovery smoothly. According to Basic Act on Disaster Countermeasures in Japan, the disaster countermeasures headquarter established of a local government has responsibility to do, however, the limitation of ability of the headquarter makes each organization concerned gather and analyze information independently. A scheme to share such information with all the organizations concerned such as lifeline companies and public agencies will contribute to quick response for a disaster. This research proposes “Geospatial Disaster Management Mash-up Service” as a social system and develops supporting systems to the service. The service is based on two platforms: Google earth as a GIS technology, and a collaborative organization with concerned companies such as data vendors, GIS system vendor, and lifeline companies. The social system, “Geospatial Disaster Management Mash-up Service” will have participants from public and private sectors. This paper introduces the outline of the system and the trial use in the East-Japan Earthquake Disaster.

Keywords: GIS, disaster prevention, disaster information, recovery support

1. INTRODUCTION

Scheme for handling large-scale disasters is defined in Basic Act on Disaster Countermeasures in Japan. According to the act, local governments, public agencies, and public service companies in the disaster-stricken region are responsible for taking actions. Such bodies outside the region also devise effective support schemes and take measures based on agreements or from a humanitarian standpoint. The act stipulates that when a disaster happens, the disaster headquarter will be set up in the local government and all related organizations in the area should share all kinds of information needed to disaster response. However, the actual situations in the past indicate that each organization gathered information separately and took measures individually.

Our goal of this study is to eliminate waste of time and energy in collecting information and to support efficient use of information by mashing-up those which each organization can gather or already has. This study would enable smooth disclosure of information regarding disaster situations and progress in recovery works.

According to Wikipedia, “mash-up” is “a Web page or application that uses and combines data, presentation or functionality from two or more sources to create new services. The term implies easy, fast integration, frequently using open APIs and data sources to produce enriched results that were not necessarily the original reason for producing the raw source data.” An example of mash-up is to integrate CRM applications on the Web with open API services such as Google Map.

In this study, we redefine “mash-up” as “gathering various kinds of information or services scattered on the Web or in-house systems of each company, and integrating those information by putting them easily on one platform to achieve better result than just piling them up.”

We focused on two platforms. One is an organizational platform to operate this service on a commercial basis and the other is a systematic platform to store information. As an organizational platform, we plan to set-up “GDMS Consociation (tentative name)”. As a systematic platform, we adopted Google Earth, 3D GIS provided by Google Inc. In this paper, we call disaster countermeasures service that utilizes these two platforms as GDMS (Geospatial Disaster prevention information Mash-up Service.)

2. OUTLINES OF GDMS

2.1. Basic Concept

Basic concepts of GDMS are 1) independence 2) self-sustaining expansion 3) practicality and feasibility 4) private leading.

1) Independence: GDMS should be beneficial for participant companies' primary business and every relevant participant should cooperate voluntarily.

2) Self-sustaining expansion: Anyone who joins in this scheme can mash-up everything. This is based on the shared sense that what is helpful for someone is also helpful for others. As we do not venture to seek a perfect system from the starting point, we plan to put feasible functions into practice at the beginning. In addition, we plan to create a basis where those involved can offer data voluntarily.

3) Practicality and feasibility: Our top priority is to make this service useful at business. This will encourage companies to participate positively, which will lead to improving practicality and feasibility. We will secure feasibility by setting up a structure where every participant can establish give-and-take relationship.

4) Private leading: Core members of GDMS Consociation will be companies that provide infrastructure, which will facilitate to meet demands of companies in the same field.

The service will be provided for concerning major users of information, collectable information, and service operation. We supposes that major users of

this service at the first stage will be public service companies such as railway companies, electric power companies, gas companies, telecommunications companies. These companies are responsible for recovery of life-support services in case of natural disaster. If their information is mashed-up, it will be practical for local governments, companies, volunteer organizations, and citizens.

As for collectable information, we plan to collect data required for disaster drills, for post-disaster emergency recovery and for full-scale recovery. In addition, we plan to mash-up data possessed by local governments which is related to disaster prevention and preparedness. We also look forward to mash-up satellite images and aerial photos which are commercially available, and other useful data and application provided by private companies.

We finally plan to establish GDMS Consociation to coordinate the participants: public service companies, academic experts and contents providers. It will take an initiative role in operational management.

2.2. Constitution of GDMS

Those who will be involved in GDMS are public service companies, which are responsible for recovery work, service providers (contents venders and software-sellers), local governments, government agencies and government institutions (Fig. 1). Core members of GDMS among these organizations will be public service companies.

Core members will provide disaster information which they used to collect and store individually upon GDMS, the common platform. On the other hand, they will be able to collect information through GDMS. This structure simply has the advantage that those companies will be able to share data with other companies, which will contribute to cost reduction in data gathering and its management. It will streamline recovery efforts.

Service providers will be able to sell information or software to public service companies. Government institutions can open information to citizens. We anticipate that universities and research institutes will also provide information or software. These information and software will be provided through GDMS platform.

Users of mashed-up information on GDMS will be the core members of GDMS, government institutions, and the public. GDMS will be opened for anyone who would like to utilize the data upon its platform. The paid and free services would be controlled separately on GDMS. We will collect fee when users require paid services. However, we consider that it is essential for GDMS that free services are valuable enough.

If this plan is put to practical use, the data could be distributed to everyone who needs them. What is important for suppliers of data or services is that who pays for their data or services, or whether is more convenient for them to supply their services through GDMS compared to their conventional methods. From users' standpoint, the most important key to establish GDMS is that the data or services on GDMS are worth the cost.

2.3. SIGNIFICANCE OF GDMS

Public service companies will be able to obtain necessary information promptly on GDMS. They will be able to streamline their recovery work; in other words, they will be able to focus on what is most important. Moreover, it would be rather inexpensive to gather information through GDMS than to gather it on their own. Advantage for contents and software providers will be that their data or services will be more valuable by mashed-up, and that their data or services will spread even faster in society. Even if they provide their services at a lower price, it will benefit them on their business activity as they could possibly acquire more customers.

Governmental agencies will be able to acquire more channels to release information. It will be an efficient method to educate citizens about disaster prevention.

For citizens, GDMS will be helpful not only because it will increase their method to collect information, but also it will help them to obtain all necessary information at once. Universities and research institutes will be able to make use of GDMS to apply their research outcome to practical business.

To sum up, GDMS will be profitable to every organization or people concerned, and it will be beneficial socially and commercially if we could manage it properly.

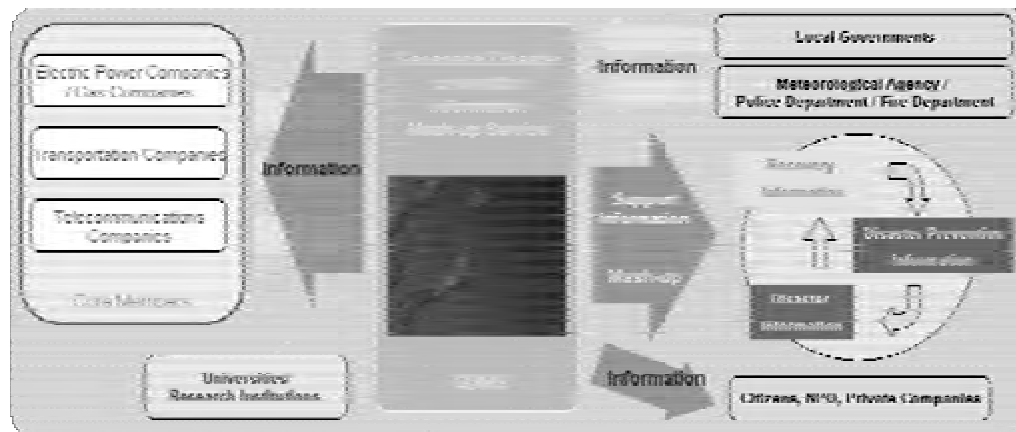


Fig. 1: Constitution of GDMS

2.4. QUALITY AND IMMEDIACY OF INFORMATION

When we discuss information gathering and sharing system, we must note that generally there are problems about quality and immediacy of information. However, it does not seem to fit in case of GDMS. Quality of information should be guaranteed as each organization would mash-up information they use in their ordinary activities. In other words, useless information will be cleared out in each organization. As for the immediacy, it should not be a problem, as organizations offering information are on the front line to cope with disaster. Market mechanism will also ensure immediacy. Paid services cannot attract customers if they are outdated, that is, it would be pointless if contents providers mash-up services without immediacy.

3. GEOSPATIAL DISASTER PREVENTION INFORMATION MASH-UP SYSTEM (GDMS SYSTEM)

3.1. System Configuration

GDMS system is consists of 4 components (Fig. 2).

- 1) Application for client computers to mash-up disaster information (GDMS Application);
- 2) Server which delivers data uploaded by GDMS Application (GDMS Server);
- 3) Server which compiles information (KML or KMZ files) from associated service providers or companies and delivers these files to GDMS Application (KML Server);
- 4) Google Earth Enterprise Server which delivers satellite images as base maps.

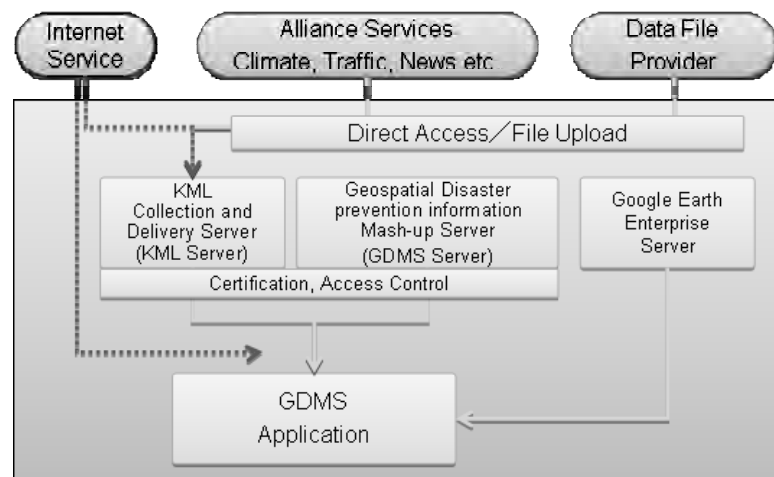


Fig. 2: GDMS System configuration diagram

GDMS Application is an add-on function for Google Earth, which transfers data and program commands interactively between external applications and Google Earth. KML file collection and delivery server is the site where KML files are uploaded or downloaded, and it collects updated KML files and adds them to the database automatically. And then it include search engine for users to find out the data needed.

4. UTILIZATION OF GDMS

4.1. INFORMATION CLASSIFICATION ACCORDING TO PHASES

We had workshop discussions to define information which would be necessary in case of disaster. We adopted simulation approach. Participants included public service companies and academic experts.

The information is categorized in three phases:

- 1) The first phase to grasp outline of the damage in the area (Phase 1);

- 2) The second phase to grasp the detail of the damage in the area (Phase 2);
- 3) The third phase to grasp information to assist recovery work (Phase 3).

In addition, there should be another phase to prepare in advance for Phase 1, 2 and 3.

In the pre-disaster phase, we plan to prepare basic information such as satellite images, statistics (population distribution, etc.), spatial information (condition of urban areas and roads), and hazard information (active fault zone and ground condition, etc.) (Fig. 3.)

In phase 1, the Meteorological Agency announces the seismic center and intensity of an earthquake. We will convert the information and mash-up them onto GDMS. We will also show damages estimated by damage-model (Fig. 4.)

In phase 2, we will provide photos shot in the area or shot by aerial photographs, and field survey results such as traffic conditions (Fig. 5.)

In phase 3, users will be able to collect and share necessary information to draw up a maneuver for recovery work. Assumed information is newest field survey results, conditions around the area, traffic report, and weather information (Fig. 6.)

We anticipate that other useful data will be accumulated on GDMS as it develops in the future.

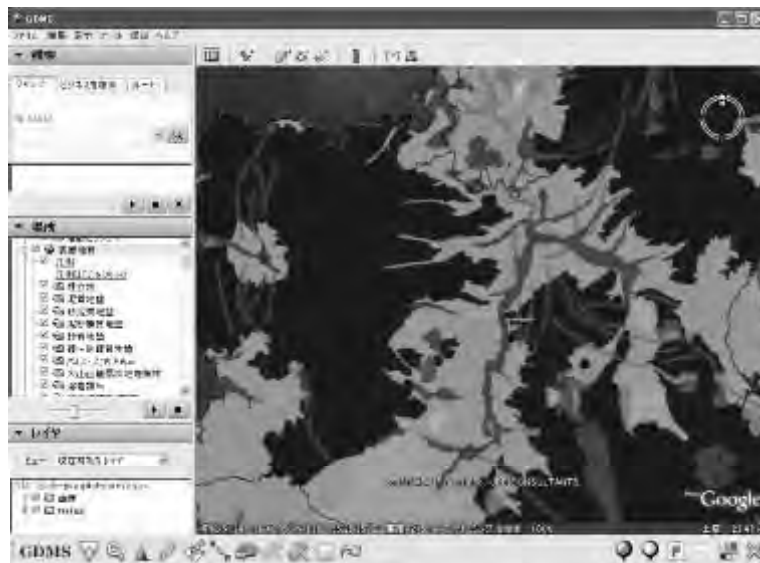


Fig. 3: Subsurface geological map and Active fault zone



Fig. 4: Estimation of seismic shaking (CRIERI, Japan)

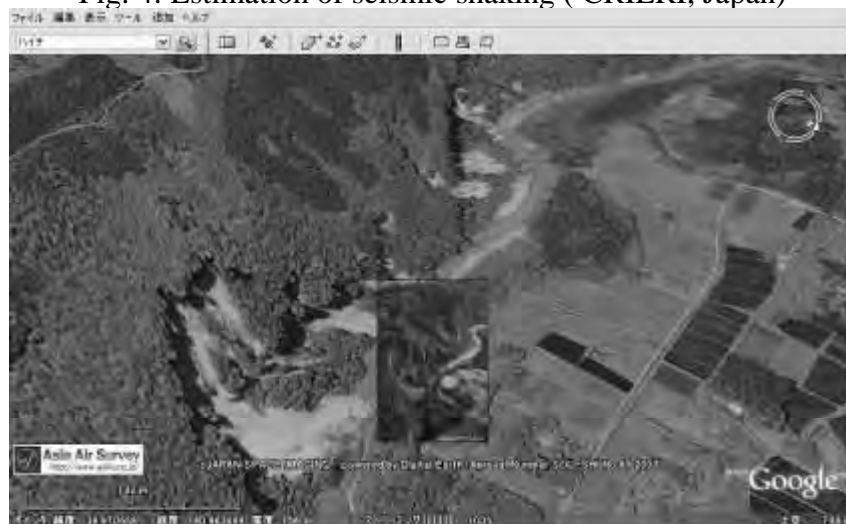


Fig. 5: Aerial photo after an earthquake and satellite image before the earthquake

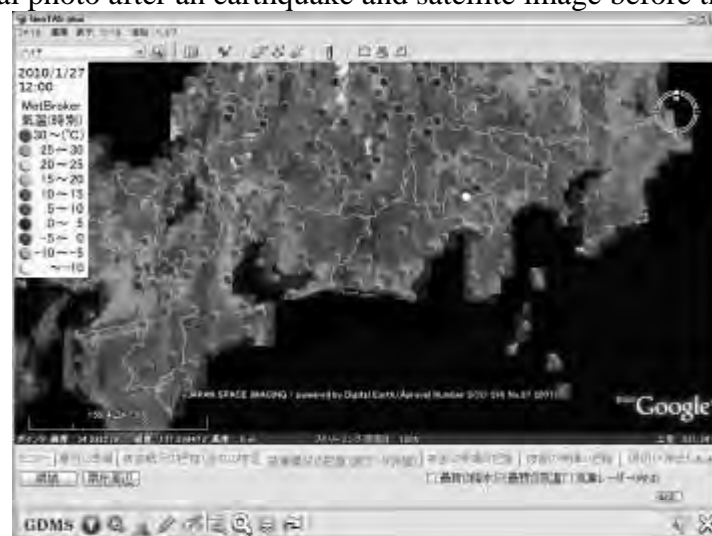


Fig. 6: Weather information in a disaster-stricken region (Weathernews Co.)

4.3. COLLECTING BASIC DATA

We have listed up necessary data from interviews with local governments and public service companies. Our business targets are railway companies, gas companies, electric power companies, water and sewerage departments, telecom companies, and local governments. Information is categorized by the phases mentioned above. We classified demands according to business categories and information categories.

Although we have collected necessary data, we acknowledge that we need to verify consistency between the data list and the requirements of users. We plan to interview with users again, and to update the data list based on the result of the previous interview. At the same time, we plan to estimate the costs required to meet the demands and define minimum contents which we should prepare at the startup of service operation.

In 2010 FY, we had a demonstration experiment in corporation with Shizuoka Prefecture to clarify the gap between our supply and demands of local government or public service companies.

5. GDMS in the Post-Disaster Phase in East-Japan Earthquake

East-Japan earthquake occurred on March 11 2011. GDMS had not been completed yet. We tried to support the contingency response and recovery works for the related organization inside and outside the affected region. We have provided KML files on Web since two weeks later. In addition, we expanded the object of support to reconstruction planning phase from the original.

The activities has continued, therefore evaluation of the outcome achieved by the activity will need more time. However, at present, it can be said that it performed a certain role at some points related to the fact that this disaster was super large-scale. Because of hugeness of the affected region, the whole image of the disaster was incomprehensive during the initial phase and, the strategy was essential because the needs for recovery exceeded to the supply. The accumulation of the information on GIS platform promoted the understanding and support to develop strategy and to make decision.



Fig. 7 the area damaged by tsunami and population distribution (GDMS)

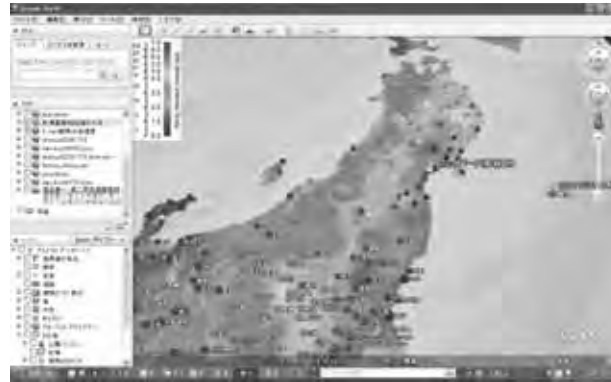


Fig 8 estimation of seismic intensity (AIST, Japan)

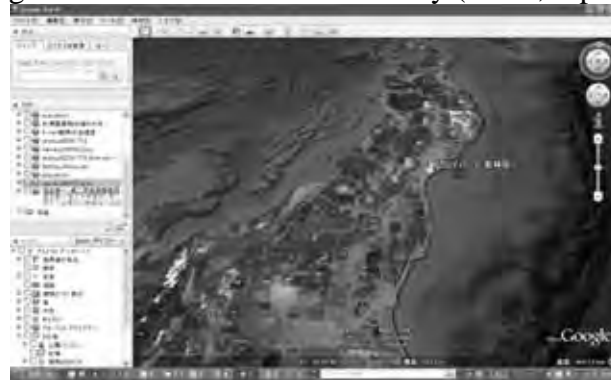


Fig. 9 the vehicle probe data (Honda Motor Co.)



Fig 10 pre-disaster scenery in the tsunami afflicted city (Kato.T lab. ICUS, IIS)

6. CONCLUSION AND FUTURE WORK

There are many challenges and difficulties left. There are some technical difficulties to be solved such as improvement of user interface and searching function. Moreover, we need to demonstrate whether this service makes good business sense. The important point is that we must demonstrate the efficiency and usefulness of GDMS for the related organization through the real experience in the disaster. It will be clarified in the feasibility survey.

Acknowledgment

This project has been supported by Ministry of Education, Culture, Sports, Science and Technology of Japan.

REFERENCES

Takaaki Kato, Mitsuaki Kobayashi, Teruyoshi Yotsuyanagi (2010). A report on the present situation of GDMS and discussion on requirement for success, Institute of Electrical Engineers of Japan

Takaaki Kato, Mitsuaki Kobayashi, Naohide Sato, Teruyoshi Yotsuyanagi (2009). Prototype Development of “Geospatial Disaster Control Mash-up System”, Institute of Electrical Engineers of Japan

Comparison of neural network learning algorithms; BR and LM for flood forecasting, upper ping catchment

Tawee CHAIPIMONPLIN¹, Linda SEE^{2,3} and Pauline KNEALE⁴

¹ Department of Geography, Faculty of Social Sciences,
Chiang Mai University, Thailand
tawee.c@cmu.ac.th

² Senior lecturer, International Institute of Applied Systems Analysis,
Schlossplatz 1, A-2361 Laxenburg, Austria

³ Senior lecturer, School of Geography, University of Leeds,
Woodhouse Lane, Leeds, LS2 9 JT, UK

⁴ Professor, Faculty of Science and Technology, University of Plymouth,
Plymouth, PL4 8AA, UK

ABSTRACT

The flood issue for forecasters at Chiang Mai derives from the monsoon rainfall, which leads to serious out-of-bank flooding two to four times a year. Data for stage and rainfall of hourly in Upper Ping catchment is limited as the historical flood record is limited in length. Neural Network forecasting models are potentially very powerful forecasters where the data are limited. However, insufficient data for Neural Network training reduces the model performance. All data for Neural Network is divided into three datasets: training, validation and testing. In addition most of learning algorithms require data for validation but Bayesian Regularization (BR) algorithm does not need validation data, as a result, the training dataset size is increased. The powerful of BR to forecast effectively where data set are limited. Therefore, this algorithm is worth exploring for the Upper Ping catchment. The Neural Network model is used to predict water stage at PI station at lead times of 6 and 12 hours with two different learning algorithms. The results have found that Neural Network performance training with BR algorithm is better than Levenberg-Marquardt (LM) algorithms by improving the peak stage.

Keywords: *neural network, flood forecasting, Bayesian Regularization, Levenberg-Marquardt, Upper Ping Catchment*

1. INTRODUCTION

Monsoon rainfall leads to serious flooding in Thailand almost every years. Particularly this year 2011, the tropical storm NOCK-TEN hit Thailand and caused flood over northern, upper northeastern and central of Thailand, approximately 30 provinces (Nan, Phrae, Lampang, Mae Hong Sorn, Lamphun, Chiang Mai, Sukhothai, Nakhon Sawan, Phra Nakhon Si

Ayutthaya, Nakhon Nayok, Phitsanulok, Ang Thong, Prachin Buri, Phichit, Utharadit, Tak, Prachuap Khiri Khan, Kamphaeng Phet, Nong Khai, Ubon Ratchathani, Mukdahan, Nakhon Phanom, Sakon Nakhon, Phetchabun, Roi Et, Kalasin, Loei and Udon Thani) were suffered by flood and 46 death (Department of Disaster Prevention and Mitigation, 2011).

There are many types of flood modeling such as physical based model or conceptual model or black box model. The disadvantage of physical and conceptual model is required lots of physical data. In contrast, neural network is one of the black box models and the big advantage is the ability to generalize to unseen data and does not concern the physical relationships. The Upper River Ping, which is the focus for this study, is a large catchment with very limited long-term data records. Calibrating a physical or conceptual model for a catchment of this size is inherently very difficult; many parameters would have to be estimated rather than known quantities within such a model. There are limited data available for hour stage at stations on the River Ping that can be used to drive a neural network model. The city of Chang Mai in the lower part of the catchment is subject to flooding, and would benefit from effective real-time flood warning. The black box neural network model approach offers the opportunity to create models that can be run in real-time, and which can be updated relatively easily as new data become available each year.

2. METHODOLOGY

The use of neural networks can be found throughout different areas of hydrology and water resource management. The ASCE (2000) review into the use of neural networks in hydrology considered applications across a range of areas including rainfall-runoff modeling, modeling streamflows, water quality modeling, ground water applications, estimation of precipitation and miscellaneous areas such as reservoir operation and flood wave propagation.

The most common neural network arrangement is three layers: the input layer, where data are supplied to the model, a hidden layer, necessary for processing, and an output layer, where the forecast or prediction is produced. In addition there are bias nodes necessary for the calculations to work. The number of hidden layers and hidden layer nodes is determined by the operator. Some neural networks have more than one hidden layer although it has been shown that any continuous function can be approximated with this neural network structure using only one hidden layer (Hornik, 1993). There are many types of backpropagation algorithm, which can be classified into two main groups. The first group is described as slow learning and uses batch gradient descent or simple gradient descent with momentum. The second, fast learning, group may employ conjugate gradient descent (CGD), quasi-Newtonian algorithms (which require more storage and computation for each iteration) and the Levenberg-Marquardt numerical optimization technique. The fast learning techniques can perform at 10 to 100 times the speed of the slow learning processes. The difference

between CGD and simple gradient descent is that it does not proceed along the direction of the error gradient but in a direction orthogonal to the one in the previous time step. The advantage for the modeler is a relatively fast training time. It has been used in hydrology for short and longer term stream flow forecasts (Kisi, 2007). Where the model has a very large number of hidden layer nodes, this process can be very efficient. However, where the input nodes and weights are small, there does not appear to be any advantage in using CGD over first order backpropagation methods. Levenberg-Marquardt (LM) is probably the most commonly employed algorithm (Beale et al., 2011). Fun and Hagan (1996) compared the performance of three different algorithms including Levenberg-Marquardt and found that it produced the best performing result. Bayesian regularization (BR) is another type of training procedure that can be applied to Levenberg-Marquardt (Mackay, 1992; Forsee and Hagan, 1997) and essentially reduces the impact of the network weights. It simultaneously minimizes the overall error function and the sum of the squared weights. A big advantage of the BR algorithm is that it does not require a validation data set, unlike in early stopping and therefore makes BR a potentially suitable algorithm where data are limited (Beale et al., 2011). This means that more data are available for the training process. The BR algorithm has been used in a few recent hydrological modeling applications (Anctil and Lauzon, 2004; Anctil et al., 2004a, b; Anctil et al., 2006; Chaipimonplin et al., 2010, 2011; Zhang and Govindaraju, 2000). To compare the most common used and fast learning algorithm (LM) with algorithm for limited data (BR) thus in this paper the neural network models are trained with LM and BR.

3. STUDY AREA

3.1 Upper Ping catchment

The Ping catchment is located in the Northern part of Thailand and is divided into two parts: the Upper and the Lower Ping. The entire Ping catchment covers approximately 33,898 km². The Upper Ping is a large complex river basin covering two provinces (17° 14' 30" – 19° 47' 52" N, 98° 4' 30" – 99° 22' 30" E); Chiang Mai and Lam Phun (Mapiam and Sriwongsitanon, 2009). It has an area of approximately 23,600 km² (Figure 1) with 15 sub-catchments.



Figure 1: The 15 sub-catchments of the Upper Ping basin.
 Source: Regional Centre of Geo-Informatics and Space Technology (2006)

The main concern of this paper is to forecast the water stage at P1 station which is located at Chiang Mai city. The available data are hour data at P1 (Second Part of the Mae Nam Ping sub catchment), P67 (Second Part of Mae Nam Ping) and P75 (Upper Part of Mae Nam Ping) (Figure 2). Chiang Mai is in a catchment with a relatively steep terrain (approximately 80%) with elevation higher than 500 meter (m) above sea level (Rodratana and Piamsa-nga, 2008). The elevation of the Ping River basin ranges from 380 m to 2,275 m above sea level

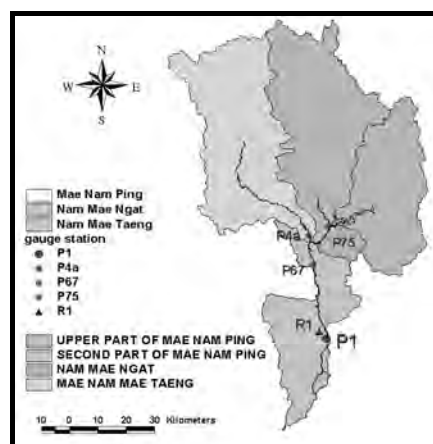


Figure 2: Study area sub catchments
 Source: Regional Center of Geo-Informatics and Space Technology (2006)

3.1 Flooding at Chiang Mai

All water gauge stations along Ping River are recorded by the Hydrology and Water Management Centre for the Upper Northern Region. At P1 station will be flood when the water discharge more than 440 m³/s and water stage levels in the main channel exceeding 3.70 m above local datum (304.2 msl) (Hydrology and Water Management Centre for Upper Northern Region, 2011). According to the flood records for the past 50 years in the Chiang Mai city area, the four highest monsoon flood events occurred in 1987, 1994, 1995 and 2005 (x axis) with water levels (y axis) of

4.53, 4.43, 4.27 and 4.93 m, respectively. Since 2004 the flood level at P1 has been changed from 3.40 m to 3.70 m due to, construction the extra flood defense wall along the river (Figure 3).

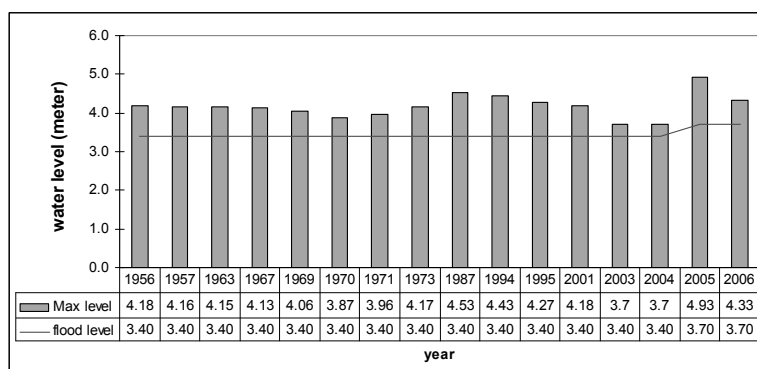


Figure 3: Record of maximum flooding at P1 station from 1956-2007.
Source: Chatchawan (2005)

4. DEVELOPMENT MODEL

As the Levenberg-Marquardt (LM) algorithm is fast training and common used and the power of Bayesian techniques to forecast effectively where data sets are limited therefore, both techniques were used to forecast water stage at the Upper Ping. Water stage from three water gauge stations at time lag: t , $t-3$, $t-6$, ..., $t-24$ and moving average 6, 12 and 24 hr were input variables, then all input variables were selected with Stepwise regression and the Bayesian Regularization (BR) and LM algorithm were run 50 times, taking the average of the 50 runs as the model forecast after Anctil and Lauzon (2004). The models were designed to forecast water stage lead time at 6 and 12 hour.

Data from only the main monsoon season were then used to develop and test the neural network models, in particular August to October between 2001 and 2005. The neural network trained with the Levenberg-Marquardt (LM) algorithm requires the dataset for validation but the Bayesian Regularization (BR) algorithm does not require a validation dataset. Therefore the longer 2001-2004 dataset was used for training with BR and training with LM was dataset 2001 - 2003 and 2004 was used for validation. For these tests **the number of hidden nodes was set to 10 after Chaipimonplin et al. (2008a, b)**. Data for the year 2005 was used for testing because it contains the biggest event in the record

Since the water stage changed from 3.40 to 3.70 meter in year 2004, it would has the effect to the flow behavior, then the training dataset was selected only storm 2005 (September to October) and testing the first storm in 2005 (August). Due to few training dataset, BR algorithm will take an action to perform this experiment. In addition, the lead time to forecast water stage at P1 is 12 hour to compare the results with Chidthong et al. (2009).

5. RESULTS

5.1. 6 hour lead time

Figure 4 contains the plots of actual and predicted stage for all storms in 2005 with x axis is time (day/month/year) and y axis is water stage (meter) and Table 1 provides the evaluation measures. These results clearly show that the overall performance of the BR algorithm is better than trained with LM as the MAE, RMSE and CE are all better.

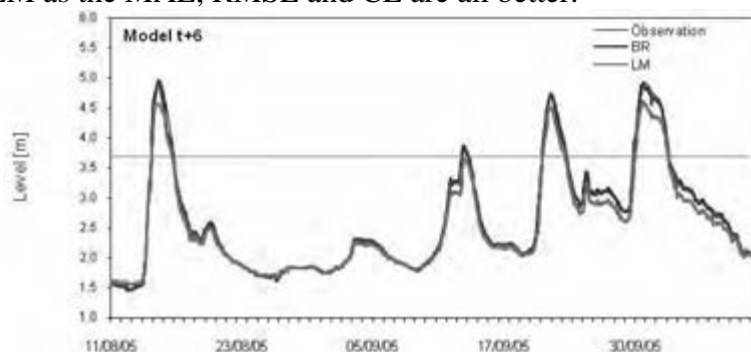


Figure 4: Results of forecasting 6 hour lead time with BR and LM algorithms, 2005 storms.

Table 1: Goodness of fit statistics for LM and BR models at lead time of 6 and 12 hour

Statistics	6 hour lead time		12 hour lead time	
	LM	BR	LM	BR
MAE	0.086	0.035	0.176	0.071
RMSE	0.139	0.072	0.142	0.140
CE	0.974	0.993	0.972	0.973

Visual inspection of the hydrographs shows that models developed with the BR algorithm all have more accurate peak stage and rising time results particularly the storm in October (Figure 5).

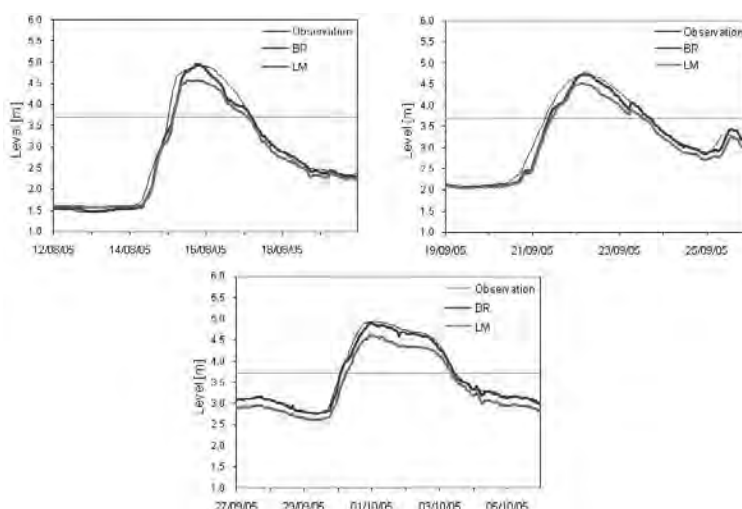


Figure 5: Comparison of the BR and LM algorithms, three big storms in 2005, t+6

5.2. 12 hour lead time

The evaluation measures are listed in Table 1 and the hydrographs are displayed in Figure 6. Visual inspection shows that the BR algorithm performs better than the LM algorithm as with the 6 hour lead time, and the statistical measures once again demonstrate the superiority of the BR algorithm over LM.

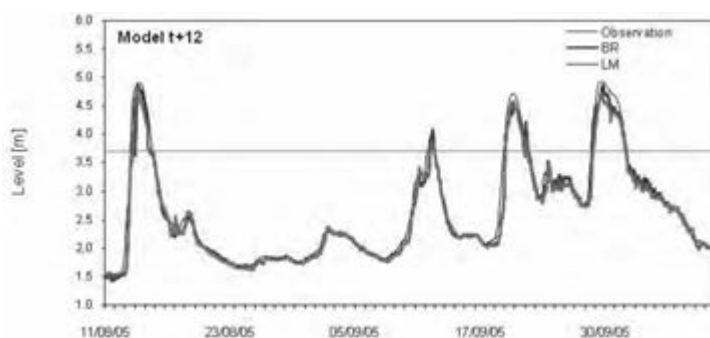


Figure 6: Results of forecasting 12 hour lead time with BR and LM algorithms, 2005 storms

To forecast water stage using upper water stage station has the limited to predict lead time at 12 hour as both models predicted delay at rising time and underestimate at the peak. However, when look at the peak closer the hydrographs shows that BR models have more accurate peak stage at storm in August and October but not all BR models perform better results of rising time (Figure 7).

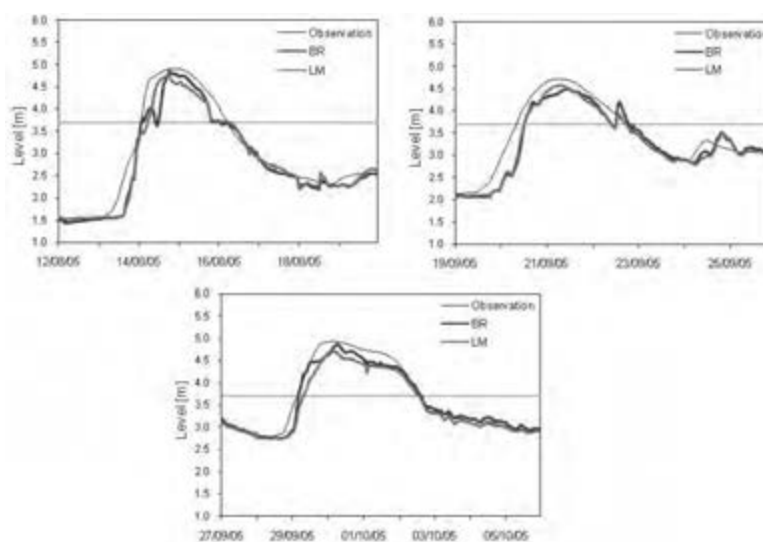


Figure 7: Comparison of the BR and LM algorithms all three big storms in 2005, $t+12$

5.2. An extra experiment of forecasting 12 hour lead time

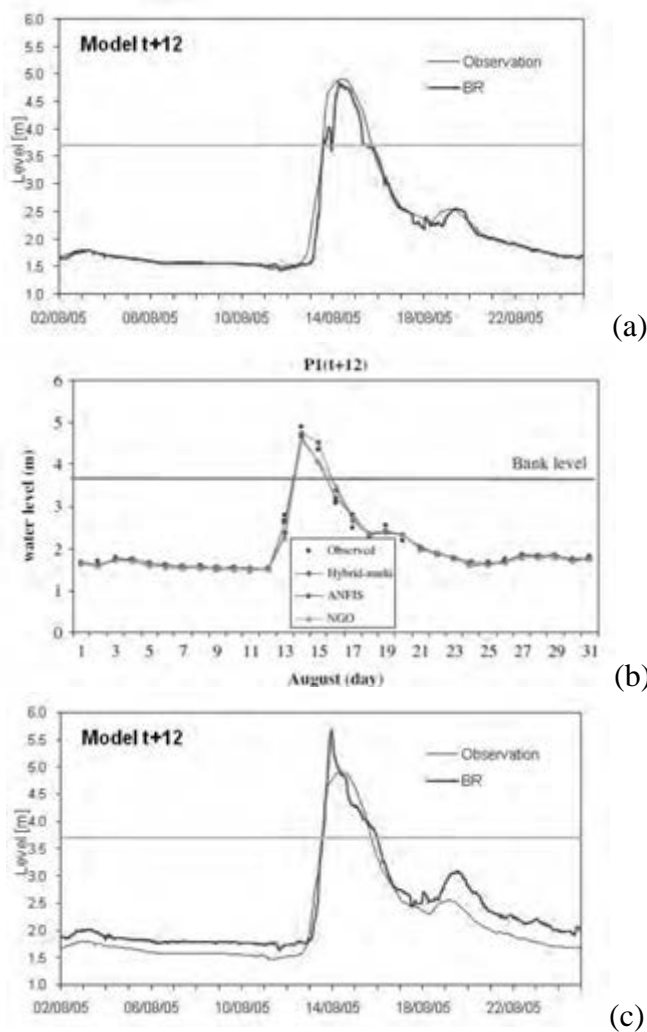


Figure 8: Comparison of three results at $t+12$ hours, first storm 2005

Figure 8 shows the results of BR model training with 2001-2004 dataset (hydrograph ‘a’), while both hydrograph ‘b’ (result of Chidthong et al., 2009) and ‘c’ (BR model) are trained with only 2005 dataset. It is obviously that the model’s performance increases when training models with only 2005 dataset as the lead time increase from 6 hour to 12 hour.

6. CONCLUSIONS

The Bayesian regularization (BR) algorithm clearly proved to have an overall advantage over the Levenberg-Marquardt (LM) algorithm on its own in terms of forecasting accuracy. However, model performance was improved by training neural network model with only 2005 data because the increasing flood level along Ping River at P1 then it has changed the water flow behavior. It also can draw the recommendation that for forecast water stage at P1 in the future, water stage recorded (P1, P67 and P75) before 2005 are not longer needed.

ACKNOWLEDGEMENTS

Thank you to the Hydrology and Water Management Center for the Upper Northern Region for the water stage data, also Faculty of Social Sciences, Chiang Mai University, Thailand for the funding of this research.

REFERENCES

- ASCE, 2000. Artificial neural networks in hydrology. II: Hydrologic applications. *Journal of Hydrologic Engineering*, 5, 124-137.
- Anctil, F. and Lauzon, N., 2004. Generalisation for neural networks through data sampling and training procedures, with applications to streamflow predictions. *Hydrology and Earth System Sciences*, 8, 940-958.
- Anctil, F., Lauzon, N., Andreassian, V., Oudin, L. and Perrin, C., 2006. Improvement of rainfall-runoff forecasts through mean areal rainfall optimization. *Journal of Hydrology*, 328, 717-725.
- Anctil, F., Michel, C., Perrin, C. and Andreassian, V., 2004a. A soil moisture index as an auxiliary ANN input for stream flow forecasting. *Journal of Hydrology*, 286, 155-167.
- Anctil, F., Perrin, C. and Andreassian, V., 2004b. Impact of the length of observed records on the performance of ANN and of conceptual parsimonious rainfall-runoff forecasting models. *Environmental Modeling & Software*, 19, 357-368.
- Chaipimonplin, T., See, L.M. and Kneale, P.E., 2011. Improving neural network for flood forecasting using radar data on the Upper Ping River, *International Congress on Modelling and Simulation*, Perth, Australia, Dec 2011, (In Press).
- Chaipimonplin, T., See, L.M. and Kneale, P.E., 2010. Using radar data to extend the lead time of neural network forecasting on the River Ping. *Disaster Advances*, 3(3), 35-43.
- Chaipimonplin, T., See, L.M. and Kneale, P.E., 2008a. Neural network prediction of flooding in Chiang Mai, Thailand: comparison of input determination techniques. EGU, Vienna, Austria, 13-18 April 2008.
- Chaipimonplin, T., See, L.M. and Kneale, P.E., 2008b. Use of neural network to predict flooding in Chiang Mai, Thailand: comparison of input determination techniques. AOGS, Pusan, South Korea, 13-18 June 2008.
- Chatchawan, S., 2005. The report of flood's situation and resolving at Chiang Mai City 2005 (published in Thai). *2005 Annual Conference*. Chonburi.
- Chidthong, Y., Tanaka, H. and Supharatid, S., 2009. Developing a hybrid multi-model for peak flood for forecasting. *Hydrological Processes*, 23, 1725-1738.
- Beale, M.H., Hagan M.T. and Demuth, H.B., 2011. *Neural Network Toolbox TM 7: User's Guide*. [Online], [Accessed 26 August 2011], Available at <http://www.mathworks.com>.
- Department of Disaster Prevention and Mitigation, 2011. *Flood Situation Report*. [Online] [Accessed 26 August 2011], Available at <http://disaster.go.th/dpm/flood/flood.html>.

Foresee, F.D. and Hagan, M.T., 1997. Gauss-Newton approximation to Bayesian learning, *Proceedings of the 1997 International Joint Conference on Neural Network*, 1930-1935.

Fun, M.-H. and Hagan, M.T., 1996. Levenberg-marquardt training for modular networks, *Proceedings of the 1996 International Conference on Neural Network*, 1, 468-473.

Hornik, K., 1993. Some new results on neural network approximation, *Neural Networks*, 6, 1069-1072.

Hydrology and Water Management Centre for Upper Northern Region, 2011. *Flood warning posters* [Online], [Accessed 26 August 2011], Available at <http://www.hydro-1.net>

Kisi, O., 2007. Streamflow Forecasting Using Different Artificial Neural Network Algorithms, *Journal of Hydrologic Engineering*, 12, 5, 532-539.

Mackay, D.J.C., 1992. Bayesian interpolation. *Neural Computation*, 4, 415-447.

Mapiam, P.P. and Sriwongsitanon, N., 2009. Estimation of the URBS model parameters for flood estimation of ungauged catchments in the upper Ping river basin, Thailand. *SciencesAsia*, 35, 49-56.

Regional Centre of Geo-Informatics and Space Technology, 2006. Faculty of Social Sciences, Chiang Mai University, Thailand.

Rodratana, P. and Piamsa-Nga, N., 2008. 'The study of flood alleviation of Chiang Mai city area', *The 13th National Convention on Civil Engineering (published in Thai)* Phataya, Thailand.

Zhang, B. and Govindaraju, R. S., 2000. Prediction of watershed runoff using Bayesian concepts and modular neural networks. *Water Resources Research*, 36, 753-762

Building back right learning from Tohoku

Tomoko MATSUSHITA¹⁾ and Kimiro MEGURO²⁾

¹⁾Graduate Student, Department of Civil Engineering,
The University of Tokyo, Japan
matsushita-t@risk-mg.iis.u-tokyo.ac.jp

²⁾Director/Professor, ICUS, IIS, The University of Tokyo, Japan
meguro@iis.u-tokyo.ac.jp

ABSTRACT

In the process of reconstruction after mass destruction from the Great East Japan Earthquake, speed and quality is required to respond to the immediate needs of people. The authors assert the importance of regenerating human activity as a vital part of reconstruction process and introduce the process of making architecture as a means to promote people's participation and revitalization of local industry. As a part of relief effort by the Japan Committee for UNICEF to reconstruct destroyed kindergartens, specific methods were introduced in the process and the result after six months is evaluated in this paper.

Keywords: *disaster response, reconstruction, community building*

1. INTRODUCTION

A common problem in the Tsunami-affected area after the Great East Japan Earthquake is that there are not enough suitable sites for rebuilding. All types of buildings including housing and public institutions such as hospitals and schools have suffered severe damage due to the Tsunami. Many of them cannot be rebuilt on the same location since there is a possibility of them being flooded again. Some locations have experienced a significant drop in the grade elevation due to the earthquake. Specifically the severely damaged coastal areas have a limited amount of flat surface area and some towns have entirely lost their ability to function because most buildings were built on flat areas. These towns are having difficulty in the reconstruction phase because they must first decide where to relocate their municipality which involves massive earthwork as well as surveys and drafting new town maps.

After conducting a number of hearings and visits to the affected sites a month and a half after 3.11, the condition of the evacuees proved to be quite stressful due to the lack of adequate space and privacy at provisional shelters. Many evacuees had no immediate hope of returning to a normal life at home, going to work or school as they used to. Children had no place to play which adds to the stress of the parents.

Local governments were making great efforts to restart schools so that children would not fall behind with their coursework. Most schools were built at higher elevations so they mostly survived the damage and were able to start classes as soon as the necessary infrastructure was restored. On the other hand, facilities for preschool children such as kindergartens and nurseries were typically built in the downtown area and many of them were washed away by the Tsunami. Therefore in order to restart the kindergartens, local government had to start by locating a suitable building site.

It was evident from the interviews with local government officials and principals of kindergartens that they were in desperate need to restart daily operations as soon as possible not only for the children's sake, but also for parents and teachers. Since it was not realistic to wait until the completion of a new town map, the local government prepared temporary sites to build temporary kindergartens to be used for 3 to 5 years.

2. ACHIEVING SPEED AND QUALITY

The given task was to achieve both speed and quality and we propose two possible alternatives to answer the needs: First, is to provide light-steel prefabricated structures and second is to make architecture.

The prefabrication technology in Japan is highly developed with a stable supply system able to produce safe and high quality habitable space in a short period of time. Compared to wood, steel is easier to control and it is suitable for factory production, its production system has reached maturity due to the competitive market in the Japanese housing industry after the housing shortage during the post WWII era. It does not matter where to source the production, from south to north within the Japanese Islands there is a robust, efficient and stable supply chain. As far as construction duration, it takes only a few months including the preparatory infrastructure, to restore all the facility needs as they were provided before, which is astonishingly fast. It is true that it sacrifices flexibility for the sake of efficiency, which is to say that size and shape are confined within limited parameters. However it is possible to customize to some degree, by using different materials such as natural wood, planning the arrangement of units to maximize the use of land, or by creating rich exterior space that is connected to the interior space.

2.1 Recovering Lost Human Activity

Another alternative we propose here is the main focus of this paper and it is the making of architecture. To respond to the required speed and quality, prefabricated structures seem to be the answer, then why make architecture? To make architecture means to facilitate human involvement and activity. Human in this case refers to both the creator and the recipient, who are both victims of the disaster. The creators are local craftsmen who know the local climate, materials and construction methods with

the network of craftsmen. Making architecture with the local craftsmen necessitates the revitalization of the damaged local industry.

The recipients in this case are the beneficiaries who will be the end-users of donated facilities. Typically when a disaster transpires, the beneficiaries are treated as a helpless mass. At first they need to recover from the shock and painful experience but after a while, they need to move on and a first step is to start human involvement and activity. In the process of making architecture, the beneficiaries will be able to participate by expressing their opinions which will foster a sense of responsibility and attachment to the end product that is not possible to obtain if the beneficiaries are excluded and given a completed result. In other words, this is an empowerment process where the victims themselves are proactively working to improve their own situation and gain strength through the experience. By making an effort to take control of their own future as a stakeholder in the process, it provides a sense of ownership.

What is lost after the mass destruction of natural disasters is not only physical buildings and infrastructure but also human activity itself. Rebuilding human activity is a vital part of the reconstruction process and there are several ways to achieve it. We believe that making architecture can contribute to both physical reconstruction as well as the facilitation of human involvement and activity.

We are not proposing which method is better, be it providing prefabricated structures or making architecture. Both methods satisfy the needs respectively and it is most important to understand what is really needed by carefully listening to the voices of people from the disaster-affected area and to choose the best alternative. When the situation is absolutely urgent and allows no time to spare, speed is prioritized and prefabricated structures will be the right choice. However, if the users can afford some time to wait, two alternatives may be suggested for them to choose.

After suggesting these two options and carefully listening to people, it became evident that most people did not consider making architecture as an option for it typically costs more and takes a longer time. However they preferred making architecture to prefabricated structures if they had the option of choosing and they were willing to wait for better quality. There seem to be two reasons for this choice. If it is only for a few more extra months of waiting, they were willing to accept less favorable conditions. The other reason is the uncertainty for the future. Nobody knows for certain how long the reconstruction process may take and the use of the temporary facility may be longer than initially promised, thus people preferred more permanent structure.

3. METHODS

Total of nine kindergartens and nurseries in Miyagi prefecture were selected for reconstruction after careful hearings. In order to smoothly execute the mission at the time of emergency, we introduced three methods; 1) making with local craftsmen's initiative; 2) making with people's participation; and 3) formation of an experts advisory group to supervise quality for mass production.

3.1 Making with Local Craftsmen's Initiative

To proceed with a project during the time of confusion, we propose to take a phased approach. At the disaster-affected area, unusual conditions such as the lack of certain building materials, craftsmen, or difficulty in the construction management are expected. In order to assess the actual situation, it is necessary to start with a 'trial & error' approach and recognize the importance of making the first step to move forward.

A pilot project will be initiated as Phase I. Its main objective is to grasp the situation as much as possible by running an actual project with a locally organized team of craftsmen to discover any potential issues. By running a pilot project, the limits of locally based activity becomes clear and it will provide important information as to what is missing at the local level and what kind of support is necessary from outside. It is vital to locate a key local coordinator who is well acquainted with the local craftsmen and construction industry to coordinate the first phase.

Based on findings from the pilot project, during Phase II, the team will be reorganized and supplemented by outside support. It will explore the possibility of the locally initiated activities that can further strengthen the overall idea.

3.1.1 Examples of Locally Initiated Activity

One example is a proposal to design a wooden structure that will revive the traditional carpenters' skill of a particular region – Kesen Daiku. The regional carpenters should be able to give hope and strength to the local people by performing their work and in return they will receive a sense of pride and contribution to the declining carpenters' world.

Another example is the effective use of a massive stock of knocked down trees of shelterbelt. A large amount of old trees that were planted along the coast became debris after being knocked down by the power of Tsunami, washed away and soaked in the salt water. It is possible to use such wood for new construction as flooring materials or finish materials but coordination is required between the fabricators and local government in order to handle the public property in a proper manner.

3.2 Making with People's Participation

People's participation helps to promote empowerment and ownership as discussed earlier. It is also an important process to understand the true needs of the people. Two ways to participate in the process are via: 1) design meetings and 2) workshops. These are nothing new and generally conducted as a part of typical development process. However, we find it important to promote these processes at the time of emergency during the recovery process.

3.3 Formation of Advisory Group

There are many stakeholders with different interests such as architects, craftsmen and beneficiaries that are involved in the making of architecture. Sometimes the discussion may be biased or one-sided due to diverse backgrounds or level of knowledge and it needs to be brought to a conclusion by a third party. A group of experts with relevant specialties will form an advisory group to play this role.

To take into account the fact that there will be more than a single facility to be constructed, the quality must be controlled to maintain a common standard. Although individual facilities will have uniqueness based on site conditions and specific needs of its users, it is advisable to share a common goal in the larger picture. The advisory group is responsible for creating a basic principle that represents a big concept with actual suggestions to be shared.

4. RESULT

To evaluate each of the alternatives taken for the reconstruction project of kindergartens, it can be said that the prefabricated structures were able to respond fully to the needs at the time by providing a building quickly. The making architecture approach is still ongoing and too soon to be evaluated but the following observations were made;

1) The pilot project was effective in identifying strong local networks and the availability of the local players with strong commitment to contribute to their own region. This was contrary to the expectations of some people who did not believe it was possible for local actors to take initiative due to the confusion.

2) Active participation by the beneficiaries was observed during the meeting and workshops and the design process was invigorated due to the involvement by many actors.

3) Basic principles worked effectively to provide guidelines to the designers while allowing room for creativity. In a process of designing a nursery on a difficult site condition, an expert from an advisory group joined the meetings to provide opinions and helped resolve the issue to everyone's consent.

The awareness of people has changed once they became active participants in the process of making architecture. Designing actual space and function of their future building, people started to speak freely to express concerns for their future and making a difference by taking ownership.

5. CONCLUSION

After mass destruction from a natural disaster, a municipality and its people face the long and phased process towards restoration of their lost entities, starting from emergency response through recovery phase to final reconstruction. It is important to start with the correct action in the earlier process for it influences the subsequent activities. In the case of the kindergarten reconstruction project, the decision to make architecture generated positive influences by revitalizing the local network of craftsmen and cultivating the people's consciousness, and by doing so, we believe it provided an important foundation for the regeneration of the region as a whole. Furthermore, this method allows for relief funds to stay within the affected community, providing employment and income directly to victims, thereby kick starting the local economy, rather than paying factories in distant regions unaffected by the disaster.

It is the people that hold the key to the success in the reconstruction process. Without the local people taking initiative, there is no recovery in the true sense. Locally based experts and craftsmen should be recognized as a valuable resource and key players. To learn from this experience in Tohoku, we suggest the establishment of a people's common ground joined by residents, community architects and craftsmen to discuss the future of their town and environment.

ACKNOWLEDGEMENT

We would like to express special thanks to the hard working people of local governments and the kindergartens / nurseries in Miyagi prefecture, mighty collaborators including local coordinators, advisors, architects, contractors and subcontractors, and the colleagues of Japan Committee for UNICEF for their cooperation throughout the project.

Note

The views and ideas discussed in this paper do not necessarily represent those of Japan Committee for UNICEF or UNICEF in any way

Oral Sessions

Importance of engineering judgment against unexpected hazards

Taketo UOMOTO
Chief Executive, Public Works Research Institute, Japan
uomoto@pwri.go.jp

ABSTRACT

The disasters caused by the Great East Japan Earthquake taught us the importance of engineering judgment against unexpected hazards, such as Tsunami, and nuclear plant accident. This paper shows how the engineers have to decide what to do in case of unexpected hazards.

Keywords: engineering judgment, hazards, engineers

1. INTRODUCTION

On March 11, 14:46, 2011, the massive “Great East Japan Earthquake” hit the country of Japan just off the Pacific coast. The magnitude of the earthquake was reported as 9.0, and shook Japan from Hokkaido to Nagoya City.

The disaster was tremendous compared to the Hanshin-Awaji Great Earthquake which took place in Hyogo prefecture in January 17, 1995. Table 1 summarizes a comparison of the two earthquakes. A large difference can be seen in not only the vibration of the ground caused by the earthquake, but also the tsunami and nuclear power plant accident.

Table 1: Comparison of the Great East Japan Earthquake and Hanshin-Awaji Earthquake

	East Japan	Hanshin-Awaji
Date	2011.03.11	1995.01.17
Time	14:46	5:46
Epicenter	N38.06.2	N34.35.9
Epicenter	E142.51.6	E135.02.1
Magnitude	M9.0	M7.3
Seismic Intensity	7	6
Depth	24km	16km
Tsunami	Large	None
No. of Dead (till June 6)	15405	6434
No. of Lost (till June 6)	8095	3
No. of Fishing Boat	22000>	40
No. of harbors suffered	300>	17
Area of Agriculture	23600ha>	213.6ha
Total Loss	¥16-25 trillion	¥9.9 trillion
Prefectures	Iwate, Miyagi, Fukushima	Hyogo
Gross product of the area	¥20.7 trillion	¥20.3 trillion
Percent/GNP	3.98%	4.18%

This paper is aimed to introduce the disasters caused by the Great East Japan Earthquake and explain the importance of engineering judgment against unexpected hazards

2. WHAT HAS HAPPENED DUE TO THE GREAT EAST JAPAN EARTHQUAKE

The epicenter of the Great East Japan Earthquake was about 130 km from the Sanriku area with a depth of 24 km. The maximum JMA (Japan Meteorological Agency) Seismic Intensity was 7.0, the maximum acceleration was more than 1000 cm/sec^2 , and the maximum value observed was 2933 cm/sec^2 . As shown in the Figure 1, more than one third of the whole Honshu Island and Hokkaido Island was above $\text{PGA } 5 \text{ cm/sec}^2$.

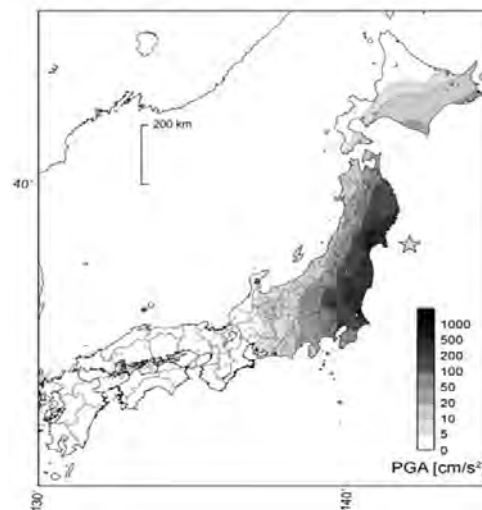


Figure 1: Maximum acceleration caused by the Great East Japan Earthquake (Earthquake Research Institute, University of Tokyo)

Furthermore, the aftershocks were also tremendous. As shown in Figure 2, the number of aftershocks above magnitude 5.0 within one month after the Great East Japan (up till April 10, 2011) was more than 440. As a result, some of the structures which were not damaged by the initial earthquake were severely damaged by the aftershocks.

After the earthquake a huge tsunami occurred. The total length of the tsunami was about 450 km from north to south, and it reached most of the coastal lines of Japan as shown in Figure 3. As shown in the figure, the coastal lines of the north-eastern part of Japan were attacked by a huge tsunami (more than 3 m in height) and the south-eastern part of Japan was also attacked by large tsunami. The figure is the tsunami warning issued by the Japan Meteorological Agency (JMA) just after the earthquake (March 11, 16:08). The estimated maximum height at the time of warning was more than 3 m, but the actual height was more than 10 m at some parts of the coast line.

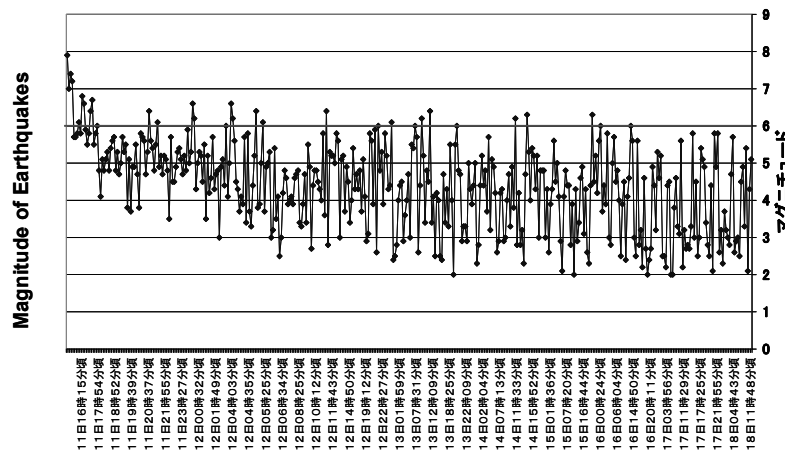


Figure 2: Number of aftershocks after the Great East Japan Earthquake



Figure 3: Tsunami warning issues by JMA just after the earthquake

Due to the huge tsunami, many structures located on the coast line were damaged and many houses were swept away. The newspapers reported that most of the houses located close to the coast line from Iwate Prefecture to Miyagi Prefecture were damaged and more than 15,000 people lost their lives and more than 8,000 people were missing (as of June 6, 2011). The damage was far larger than that caused by the earthquake. Most of the houses located near the coast were swept away and the houses located at hilltops could remain as shown in Figure 4.

Due to the tsunami, the Fukushima No.1 nuclear power plant was damaged. The tsunami attacked the plant by over-flooding the dikes and the sea water flooded the electric power facilities which shut down electric control of the plant. Due to the damage, the nuclear plants went out of control, causing hydraulic explosion and meltdown of the boiling water reactors (BWR).



Figure 4: Houses located on a hilltop which were spared tsunami damage

3. CAUSES OF THE DISASTER

Looking at the Great East Japan Earthquake, the main cause was quite simple. As shown in the Figure 5, the original cause was the earthquake with the magnitude of 9.0. In case of the Great Hanshin Awaji Earthquake which occurred in 1995, magnitude of the earthquake was 7.3, and the damages of the structures were mostly caused by the earthquake ①. However, the Great East Japan Earthquake was followed by a huge tsunami, damaging both the structures and the people ②. One of the structures was the nuclear electric power plant of Fukushima No.1 ③. The BWR of the power plant went out of control due to the loss of electricity (both normal and temporary electric supply were not available for some time) ④. As a result, meltdown of the BWR occurred ⑤.

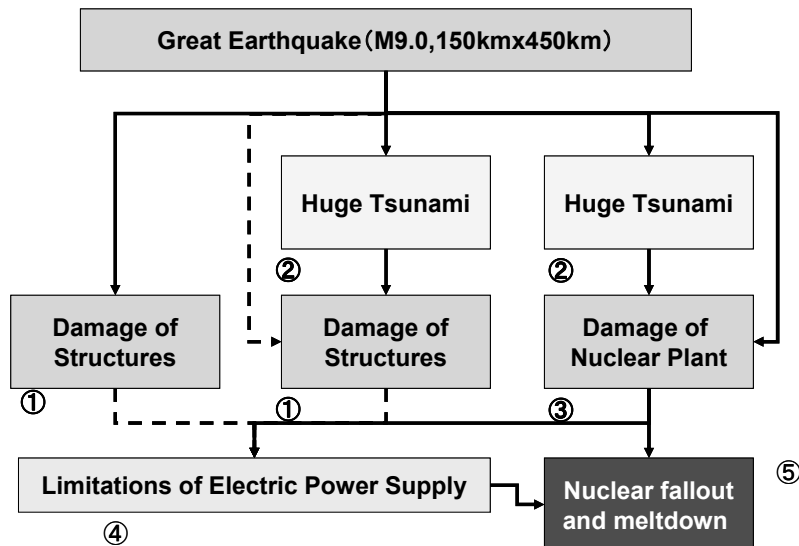


Figure 5: Causes of the disaster

After the hydrogen explosion, radioactive contamination spread around the surrounding area. This forced people to evacuate from the vicinity of the power plant, and citizens have been forced to live outside the evacuation area.

One of the main reasons why such a disaster occurred is that these situations were not expected even when the structures were designed. The expected conditions during the design of the structures were that a large earthquake may occur during their service lives, but the attack of tsunami was not strongly considered. Structures constructed after 1998 or strengthened using the modified standard specifications considering the damages of the Hanshin-Awaji Earthquake were not severely damaged by the Great East Japan Earthquake. But in the case of tsunamis, for structures such as houses and bridges the load was not considered. This is one of the reasons why so many houses and bridges were damaged.

After the earthquake, some engineers mentioned that “we did not expect to have such a large tsunami attacking the structures.” Although the available standard specifications did not mention the design considerations for when a tsunami attacks the structures, the engineers must think about the safety of the people who use the structures. It is important for the designer and construction engineers to realize how we should keep the structures safe enough or should give the information to what extent the structure can resist against any unexpected loads.

Nowadays, many engineers are conducting their work to meet the available standard specifications, but many engineers forget the fundamental works they should consider during designing and constructions. I hope engineers will reconsider the methodologies we are using now and check the most important concept “worst case scenario” during their works.

4. CONCLUSION

After the Great East Japan Earthquake, many investigations and research works have begun. We know that natural hazards may occur at any time and may exceed the expected situation and scale. Engineers must always be careful to conduct their works considering the “worst case scenario” and try to keep the users of the structures safe through any situation.

Seismic functional vulnerability of the road network of the metropolitan area of San Jose, Costa Rica

Grettel MOLINA¹, William VARGAS² and German VALVERDE³

¹Graduate Student School of Eng., University of Costa Rica
grettel.molina@gmail.com

² Associate Professor, School of Civil Engineering, University of Costa Rica.

³ Adjoin Professor, School of Civil Engineering, University of Costa Rica.

ABSTRACT

The seismic functional vulnerability of the road network of the San Jose's Metropolitan Area (SJMA) as a lifeline was assessed in terms of the impact of an earthquake upon the travel time between the Desamparados County, and the SJMA's most important public hospitals. According to a previous study, Desamparados is one of the counties of the SJMA with the highest density of population, physical vulnerability of residential buildings.

The analysis is based on a simplified model of the network of urban highways, roads and streets introduced into the computer software TSIS (Traffic Software Integrated System). A bi-proportional model, based on a travel survey conducted by a previous study, was used to generate the initial input origin-destination (OD) matrix. The number of vehicles for the target areas was projected to the year 2010 with an econometric model. The resulting OD matrix was then calibrated using the Single Path Matrix Estimation (SPME) method (Nielsen, 1994) and the traffic assignment tool of TSIS. Travel times were also measured in four different traffic conditions, ranging from the minimum expected traffic to the normal rush hour. The hourly traffic variation in the vicinity of the main hospital was also obtained by an automated counter.

Several different scenarios of events with epicentre in or near the study area were analyzed. An earthquake of magnitude 6.3 denominated Tablazo, originated in the Aguacaliente – Orosi fault was chosen, because of its vicinity to the Desamparados County. The earthquake effects upon the bridges of the SJMA were modelled by Campos and Marengo (2001) and, according to these authors, the Tablazo event has the largest probability of producing damage to bridges in the Desamparados – San Jose road network that would cause their temporary closure, even if they do not collapse. The SJMA's social seismic risk, in terms of the population exposed to suffer injuries or fatalities in a seismic event, as modeled by Salas (2003), was used to introduce changes in the OD matrix in the emergency scenario.

The impact of the earthquake on the functionality of the road network was analyzed using the service indicators in the output obtained from the TSIS simulation. Changes on the network and on the trip matrix were considered, as well as the social post-emergency behaviour. The most important functional seismic vulnerabilities of the network and its critical system components were

identified. Based on the results of the model recommendations are made to reduce the functional vulnerability, strategies and alternate routes for facilitating movement from Desamparados to the medical centres in case of an emergency.

Keywords: seismic functional vulnerability, road network

1. AREA OF STUDY

The San José's Metropolitan Area of (SJMA) delimits the study area of this project. It is shown in the figure below.

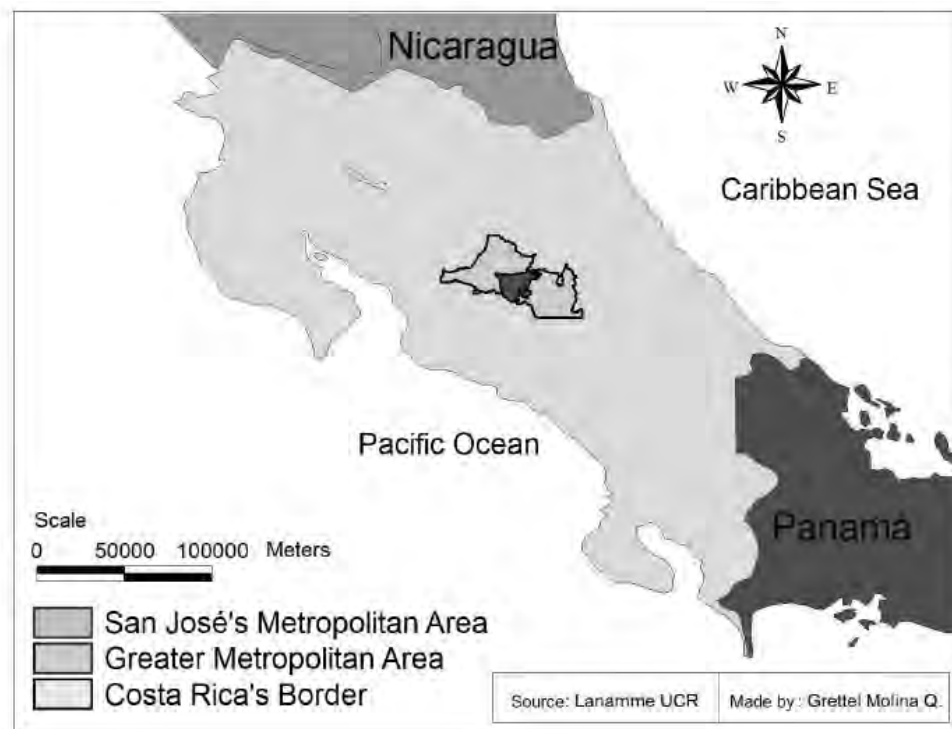


Figure 1: Location of the area of study

The project focuses on the urban zone of Desamparados County, on the zones and road network that connect the center of this county with the most important centers of medical attention in San José, the hospitals: Calderón Guardia, México and San Juan de Dios.

The network of the Metropolitan Area as a result of its complexity has important limitations in relation to accessing the central area from the surrounding urban zones. In addition to the complexity of the road network the central area of this study is bordered by the rivers Torres and Maria Aguilar; the roads over these rivers are reduced to a few bridges with just one lane in most cases.

Besides this physical limitation, the current volume of traffic on the access routes generates critical conditions and saturation during peak

periods of the day. It is predictable that in case of a seismic emergency the road system could collapse in a few minutes.

There are studies that supply valuable information to this project, the most relied upon studies are: Seismic Vulnerability of the Road Systems by William Vargas in 1985, the project about the impact of an earthquake on the road network of the San José's Metropolitan Area by Silvia Campos and Oscar Marengo completed in 2001 and the graduation project about Evaluation of the Seismic Risk in Residential Buildings of San José's Metropolitan Area of in regards to loss of human lives by Luis Salas in 2003.

The objective of this project is to analyze the seismic functional vulnerability of the road network in Desamparados and its connections with the major hospitals of San José.

1.1 Seismic Vulnerability of the bridge

The seismic model utilized in this project is derived from the worst case scenario of the Tablazo earthquake in Campos and Marengo 2001, depicting impassible bridges.

1.2 Social Seismic Vulnerability of the area of study

In 2003 Salas determined the map of social seismic risk as a result of combining the statistic distribution of social vulnerability and social threat.

2. METHODOLOGY

The following image contains the methodology used for the the development of this investigation.

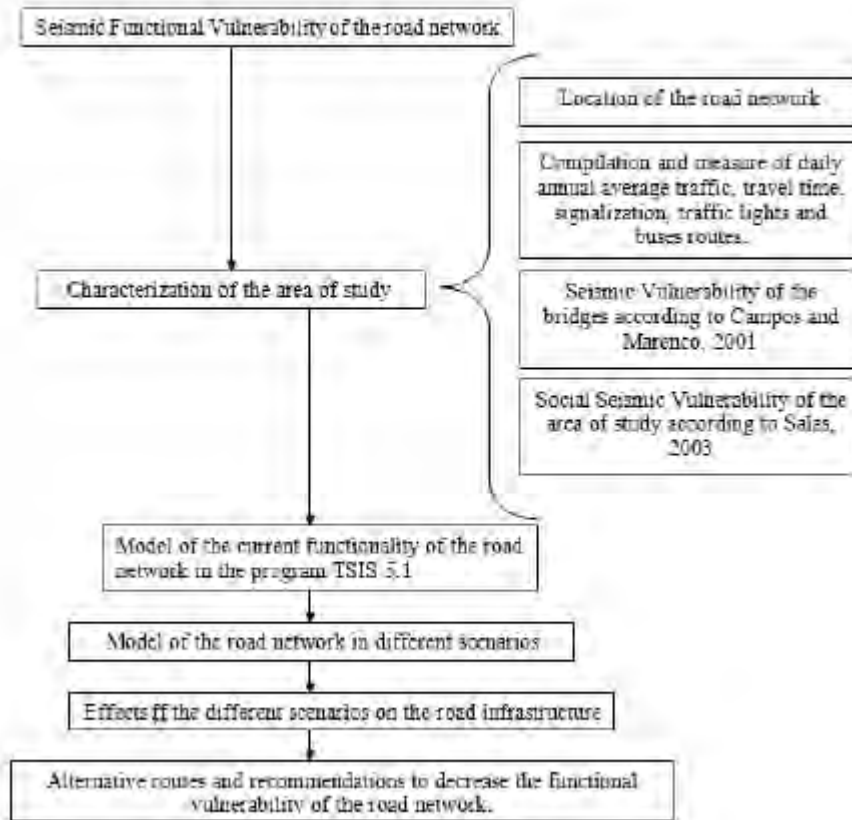


Figure 2: Methodology of the Investigation

The process of modeling the road network consists of the following steps:

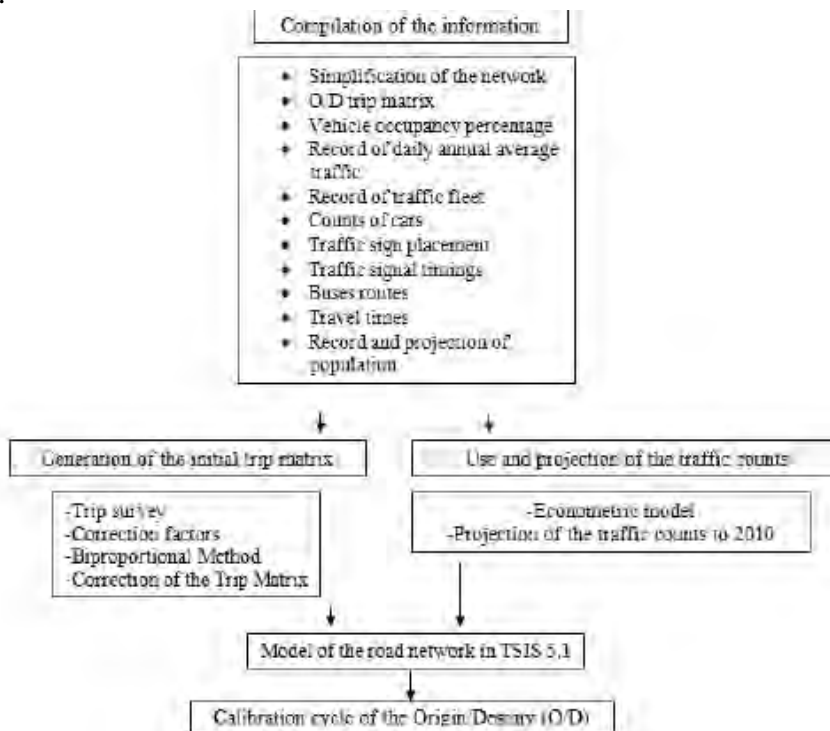


Figure 3: Methodology of the Model of the road network in TSIS 5.1

This is a screen capture of the model of the road network in the program TSIS 5.

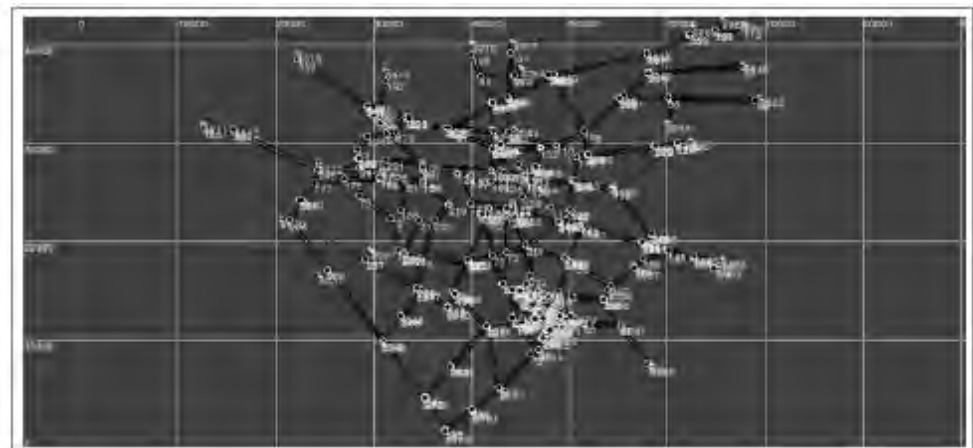


Figure 4: Model of the road network in TSIS 5.1

The calibration of the O/D matrix consists of the following stages:

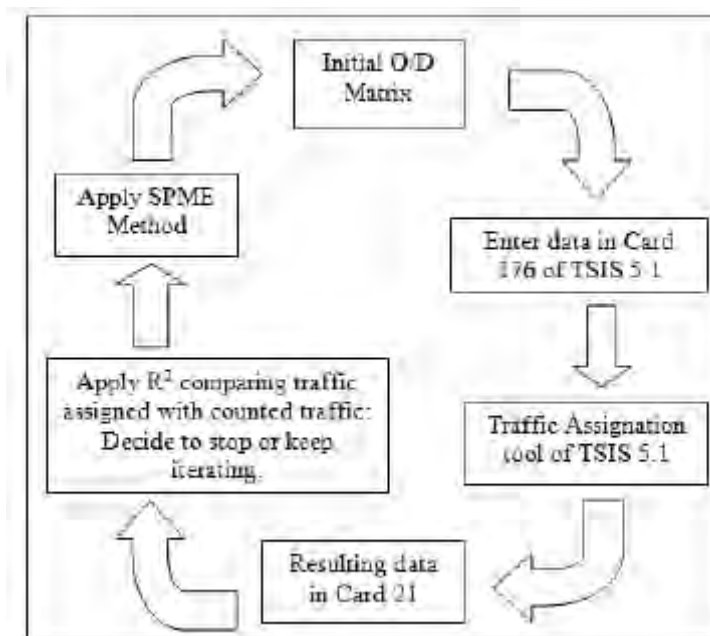


Figure 5: Methodology of the calibration of the O/D trip matrix

2.1 Model of the road network in different scenarios

The seismic scenario of the Tablazo earthquake is used for the model since that is the scenario that most directly affects the area of study. The Tablazo earthquake best embodies the worst consequences for Desamparados. The next image shows the four different scenarios that were simulated:

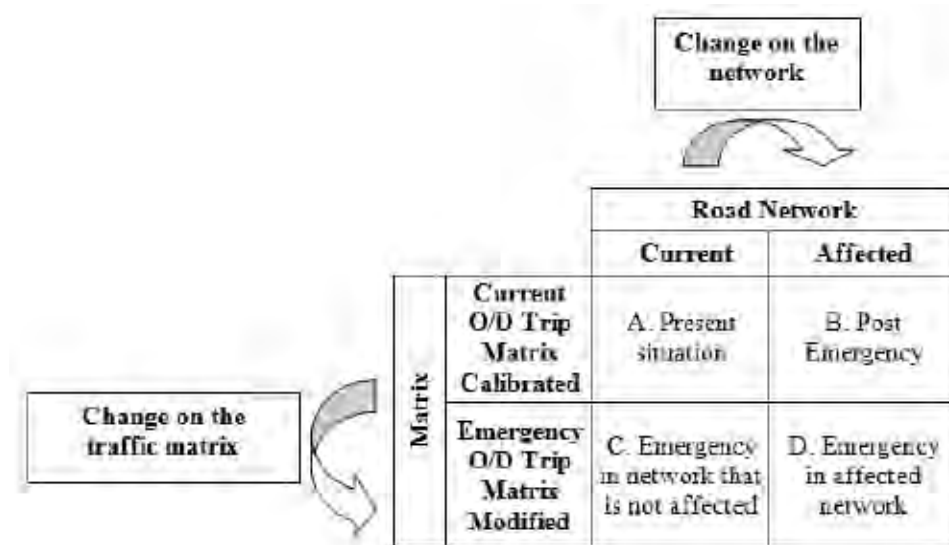


Figure 6: Modeled Scenarios

Scenario A represents the current geometry of the road network with the current trip matrix. In scenario D the network model is modified by marking the bridges indicated in Campos and Marengo, 2001 as impassable. Then using Salas 2003: the percentages of Social Risk Index are factored into the trip matrix.

Scenario B represents the conditions after the emergency in which the geometry of the network continues being affected due to the seismic emergency that happened but the event that caused the emergency has ended, so the trip matrix returns to its initial state.

Finally, in scenario C the emergency happens, using Salas 2003: the percentages of Social Risk Index are factored into the trip matrix. The geometry of the road network is not affected, because of the premise that the bridges are not critical elements of the network and they do not affect the functionality of the road network.

3. RESULTS

It is possible to quantify the functional seismic vulnerability of the road network analyzing the indicators of TSIS 5.1 and the travel time.

3.1 Analysis of Indicators of TSIS 5.1

A comparison of the indicators given by the program TSIS 5.1 for each scenario was made. The following table of comparison was obtained:

Table 1: Indicators of the road network

Indicators	A	B	C	D
	A. Present Situation	B. Post Emergency	C. Emergency in not affected network	D. Emergency in affected network
Total Vehicle-Mile	77017.47	83916.68	80928.66	88262.68
Average Speed (MPH)	11.71	11.72	12.26	10.73
Highest number of vehicles on the network	16365	25418	25774	27544
Maximum poured at X seconds	899	3581	3597	3599
Additional Indicators				
Vehicle hours of Move Time	3017.87	3288.23	3172.7	3376.76
Vehicle-hours of Delay Time	3666.45	3874.18	3429.59	4661.98
Total time	6574.31	7160.41	6602.3	8038.43
Move/Total	0.46	0.46	0.48	0.42
Minutes/Mile of Delay Time	2.77	2.77	2.54	3.24
Minutes/Mile of Total time	5.12	5.12	4.9	5.58

3.2 Analysis of the travel time

The travel time between Desamparados and the three major medical centers of San José was measured for the different scenarios, and the following table of comparison was obtained:

Table 2: Travel time in different scenarios

Origen	Destination Hospital	Scenarios			
		A. Present Situation	B. Post Emergency	C. Emergency in not affected network	D. Emergency in affected network
Desamparados	San Juan	854.8	1384.8	991.6	1581.4
Desamparados	Calderón	938.0	1416.4	1031.8	1594.6
Desamparados	México	1236.1	1767.6	1322.6	2039.6

Scenario A of present conditions is similar to scenario C of case of emergency where the network is not affected. This means that in case of an emergency the trip matrix will always get altered. If the road network does not get affected and it keeps being functional the scenario has better traffic indicators than the scenario B that represents the post emergency conditions with normal conditions of traffic and a still affected road network. This shows that the traffic system is more sensitive and it gets more altered by changes on the road network geometry than with changes on the trip matrix.

Scenario D indicates fewer vehicles per mile than scenario A because the cars cannot get into the system or move inside of it due to impassible spots that are impeding traffic flow. The indicators in the model show that after 899 seconds of scenario D, the network becomes saturated, the saturated state remains for the final 2700 seconds of the simulation.

The travel time of the different scenarios shows that in scenario D the average speed decreases by 44.5% compared to scenario A with the present conditions. After the emergency in scenario B, the speed stabilizes at 30% less than scenario A. In the ideal case C the travel time diminishes by just 10% compared to A.

4. RECOMMENDATIONS

This project is a pilot study, specific for the Metropolitan Area and the traffic circulation between Desamparados and the major medical centers of San José. The goal of this study is to provide a methodology for a new line of investigation in the planning and analysis of urban development and emergency response systems.

This methodology can be applied with infrastructure elements other than bridges; for example, hospitals, schools, electrical and water systems. Other natural disasters and threats which are more frequent and which can have similar effects on the functionality of the road network can also be modeled; such as, hurricanes, flooding, landslides, and tornadoes.

It is fundamental for investigations to use an actualized database with the volumes of traffic, traffic sign locations and traffic signal timings. In Costa Rica the most recent traffic volume information was taken in 1997 by the Ministry of Transportation and Public Works. There is no database of traffic sign locations and traffic signal timings. An incomplete and outdated database limits control of the road network's function, as well as planning and improvements of the road network.

It is very important and it should be a priority for Costa Rica to rebuild and maintain their bridges that in this moment represent the critical points of the road network. The functionality of the network depends on the bridges as components of the system.

Some of the specific possible solutions to decrease the seismic functional vulnerability of the road network are: The Ministry of Transportation and Public Works should retake the project to extend route 175 starting on route 213 because it would give a bigger redundancy and capacity to the road network of Desamparados.

It is recommended to model the seismic vulnerability of the road network with all bridges in the area in order to determine the priorities of its reconstruction, improvements and measure with greater accuracy the impact of each bridge on the functionality of the road network.

It is necessary to effectuate counts of the vehicle traffic in all the metropolitan area to increase precision of the initial O/D matrix.

Building a hospital in Desamparados would also alleviate stress on the road network in the case of an emergency. Desamparados has a very high population and this project demonstrated that its connection to the major medical centers in San José is seriously limited by the seismic functional vulnerability of the road network.

Another way to decrease the seismic functional vulnerability of the road network is to build public heliports, which can transport the population

of Desamparados to the closest medical centers in case of a major seismic event.

5. CONCLUSIONS

Through this investigation it was possible to model for the first time in Costa Rica, the functionality of a road network in case of an earthquake, different scenarios of damages were modeled. The on the zone between Desamparados and the most important health centers of San José demonstrated a need to decrease the seismic functional vulnerability of the road network of the metropolitan area.

This study concludes that it is extremely important to model and analyze the seismic risk of a vital system like road infrastructure to determine not only the damage that its seismic vulnerability can produce, but also to analyze the possible reduction of the functionality and capacity of the system or suspension of traffic circulation between different points.

This implies that the behavior model of the system as a vital system should be modeled as a network composed of components like structures, population and traffic behavior not as isolated road segments or infrastructure.

The methodology used in this study allows quantifying the seismic functional vulnerability with indicators of the situation before and after an emergency. The bridges stood out as the critical components of the system that impede the functionality of the network.

REFERENCES

- Araya, J., 1996. *Study of the validity of a model of simulation TRAF-NETSIM for the conditions in Costa Rica*. Graduation Project of the Civil Engineer School, University of Costa Rica, San José, Costa Rica.
- Campos, S., Marenco, O., 2001. *Evaluation of the impact of an earthquake on a road network on the San Jose's Metropolitan Area*. Graduation Project of the Civil Engineer School, University of Costa Rica, San José, Costa Rica.
- Climent, A., 2008. *Evaluation of the seismic thread of Costa Rica*. Resis Project II. NOR SAR, Costa Rica.
- De Solminihac, H., 2005. *Administration of road infrastructure*. Alfaomega, México.
- Federal Highway Administration, 2003. *TSIS User Reference Guide*. Office of Operations Research, Development and Technology. McLean, Virginia, USA.
- Figuerola, D., 2009. *Travel time of the public transportation system in San Jose's Metropolitan Area*. Graduation Project of the Civil Engineer School, University of Costa Rica, San José, Costa Rica.

National Institute of Statistics and Census, 2009. *Projected population for 2015*. San José, Costa Rica.

ITT Industries, Inc., Systems Division, 2003. *TSIS User's Guide version 5*. McLean, Virginia, USA.

Han, A., Dowling R., Sullivan, E., 1981. *Deriving Origin-Destination information from routinely collected traffic counts*. Institute of Transportation Studies. University of California, Berkeley.

Regional and Urban Planning of the Metropolitan Area, 2009. Proposal for the plan PRUGAM 2008-2030. San José, Costa Rica.

Salas, L., 2003. *Evaluation of the seismic risk of residential buildings of San Jose's Metropolitan Area in function of the human loss*. Graduation Project of the Civil Engineer School, University of Costa Rica, San José, Costa Rica.

Schmit, V., 1997. *Costa Rican Spectral Strong Motion Attenuation*. NORSAR, Laboratory of seismic engineering. University of Costa Rica.

Solórzano, S., 2010 *Road re-organization of the central area of Escazu, implementing pedestrian analysis*. Graduation Project of the Civil Engineer School, University of Costa Rica, San José, Costa Rica.

Valverde, G., 2004. *Calibration of a model of growth of travel demand using panel microeconomic data*. Graduation Project of the Civil Engineer School, University of Costa Rica, San José, Costa Rica.

Vargas, W., 1985. *Seismic vulnerability of the vital systems*. Project of the Civil Engineer School, University of Costa Rica, San José, Costa Rica.

Vargas, W., Garro, J., 2003. *Administration of natural risks of the road infrastructure*. National Laboratory of Materials and Structural Models of the University of Costa Rica.

Earthquake hazard in Ulaanbaatar city and its surrounding area

Ulziibat MUNKHUU¹, Yasuyoshi ICHIHASHI²,
and Demberel SODNOMSAMBUU³

¹Head Seismological Department, RCAG, MAS, Mongolia
ulzibat@rcag.ac.mn

²Visiting Professor, ICUS, IIS, University of Tokyo, Japan
Ysich555@iis.u-tokyo.ac.jp

³Scientific Secretary, RCAG, MAS, Mongolia
demberel@rcag.ac.mn

ABSTRACT

Mongolia is one of the most seismic active intra-continental regions in the Central Asia. In last century Mongolia suffered four great earthquakes of magnitude 8 and above in a period of 53 years (Tsesterleg 1905, Mw=7.9 - Bolnay 1905, Mw=8.3, Fu Yun 1931, Mw 8.0 and Gobi-Altay 1957, Mw=8.1). Beside that the large number of active faults capable of producing a devastating earthquake in Mongolia makes the prospect of strong events very concerning. About 70% of area of country belongs to with region intensity between VIII and XII (MSK).

Earthquake hazard has become one of the most important issues for Ulaanbaatar city because of the following reasons. First, since 2005 high seismic activity has been taking place near and within Ulaanbaatar area. Recent geological and seismological studies reveal strong clues about active structures around city that can dramatically increase the seismic hazard of the capital of Mongolia. Second, Ulaanbaatar is not only most populated city but also political and economic centre of the country. According to the economical growth and mechanical increase of the population of the Ulaanbaatar, intensive constructions are going on. These are translate into a significant level of seismic risk that needs to be realistically assessed and updated as new knowledge becomes available.

The seismicity recorded by local permanent and temporary networks reveals strong increase of seismic activity rate in region around U.B. For instance, 2 times as many earthquakes were recorded during the last five years (2005-2010) as between 1970 and 2004. Moreover, these swarms, consisting in more than 1600 events with a magnitude between 0.5 until 4.2, are mainly located close to 2 major active structures: NS Emeelt and EW Hustai striking faults. At the beginning (2005-2009), the swarm activity mainly concerns the Emeelt fault and was characterized by a strong time dependency consisting in a propagation of the activity toward North and South fault edges with an increase of the seismicity rate. In 2009, the seismic swarm extended his activity to the eastern edge of the Hustai fault which is the largest known structure near Ulaanbaatar able to produce large destructive earthquake on the city. Despite the relatively low

magnitude of these earthquakes, the lack of large magnitude earthquake in this area combined with the clear active fault morphology of the Hustai and Emeelt structure make the study of this recently triggered seismic swarm fundamental for the estimation of Ulaanbaatar seismic hazard. In this presentation, we will discuss some preliminary results of the analysis of this high seismic activity recorded by permanent and dedicated mobile networks, such as its spatial and time evolution or their relation with the regional seismo-tectonic context, as well as its impact on the seismic hazard assessment of Ulaanbaatar area.

Keywords: *seismic activity, swarm, seismic hazard*

1. INTRODUCTION

A seismic activity is taking place near and within Ulaanbaatar area since 2005 and it is still active up to now. The seismicity observed by local permanent and temporarily deployed networks has reveals significant increase of seismic activity in the Ulaanbaatar area. Twice high number of earthquakes were recorded during last 5 years than events recorded between 1970 and 2004 in the considering area. Such seismic activity might dramatically increase seismic hazard of the capital of Mongolia where 1/3 of the Mongolian population lives and the majority of industries of the country is concentrated. Moreover, these swarms consist of more than 1600 events within magnitude range of 0.5 to 4.2. Most of these events are located close to the 3 major active structures that are NS-Emeelt and EW-Hustai striking faults and Gunjiin active fault were located NE of city. Despite the relatively low magnitude events and lack of large magnitude earthquakes occurred in the area with combination of the clear active fault morphology of the Hustai and Emeelt structures shows that the recently triggered seismic swarms are fundamental factor for the estimation of Ulaanbaatar seismic hazard. On this paper we will discusses some preliminary results of the analysis of this high seismic activity recorded by permanent and dedicated mobile networks. The spatial and time evolution or their relation with the regional seismo-tectonic context as well as its impact on the seismic hazard assessment of Ulaanbaatar has been evaluated.

2. SEISMIC ACTIVITY AROUND ULAANBAATAR CITY

Since 2004, significant increase of occurrence of small to moderate earthquakes began to occur beneath a Hustai and Emeelt active fault area that are located about 10 to 40 km west of Ulaanbaatar (figure 1). The high seismic activity of Ulaanbaatar area starts from middle of 2005 and it is still continuing up to now. During this period, moderate size earthquake (M_L~4.2) occurred in the Hustai active fault area in May, 2008 and other two earthquakes with magnitude of ~4 occurred about 60 km south and north from Ulaanbaatar city in Oct, 2008 and Mar, 2009 respectively. These statistics showing seismic activity is increasing and migrating. Distribution of these swarms, with more than 2000 events, has interconnected the major

active structures in Ulaanbaatar area by a steeply dipping fault surface striking East-West Hustai and North to South Emeelt fault. The 2005/2010 swarms mostly occupied the Emeelt fault and its increasing number of events shows of extreme sites of this structure. It means fracturing is propagating two sites of fault and this process is happening caused by reactivation of paleoseismic active faults. The Hustai fault area activated by the 2009/2010 swarms and it shows probable main potential structure which may produce large earthquakes. Most activity is occurring east end of this active fault and shows somehow connection between these two active faults.

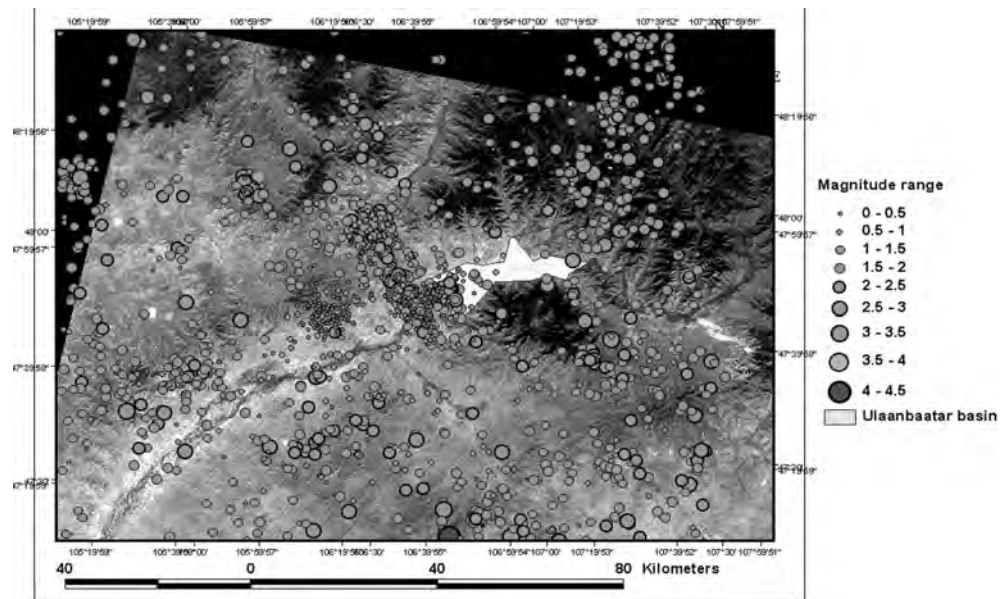


Figure 1: Seismic distribution map of Ulaanbaatar

The number of earthquakes occurred between 1970 and 2010 contains totally 3000 events, 900 events recorded during 1970 - 2003 and about 2100 events occurred from 2004 to 2010. There were 508 and 543 earthquakes correspond only for 2009 and 2010 respectively, and 210 events were already occurred in 2011 (Figure 2).

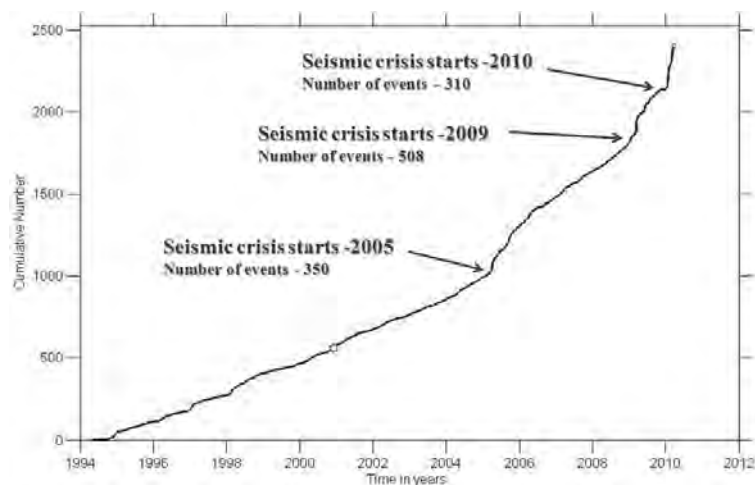


Figure 2: Statistic behavior of the seismic activation of the Ulaanbaatar area. Cumulative number of the events

3. SEISMIC NETWORK OF THE ULAANBAATAR AREA

The triangles denote the location of seismic stations around Ulaanbaatar and color of triangles shows time period of operation of those stations. First installations of the high sensitive seismic network within the area is started 1994. In 2000, this network expanded by ten elements of mini array that located 50 km apart from Ulaanbaatar to the west. Figure 3 shows location of seismic stations of Ulaanbaatar network.

Brief history of the network

- 1957: First installation of seismic station in Ulaanbaatar. (Three components, analogical low gain station SKM-3 with Galvanometric records)
- Since Nov. 1994: (2 stations with three components/long and short period station. 4 short period/vertical component)
- Since 2000: (1 station with three components long and short period sensors and 9 short period vertical component seismic array stations)
- Since Dec. 2008: (6 broad band + 3 short period three component mobile stations)

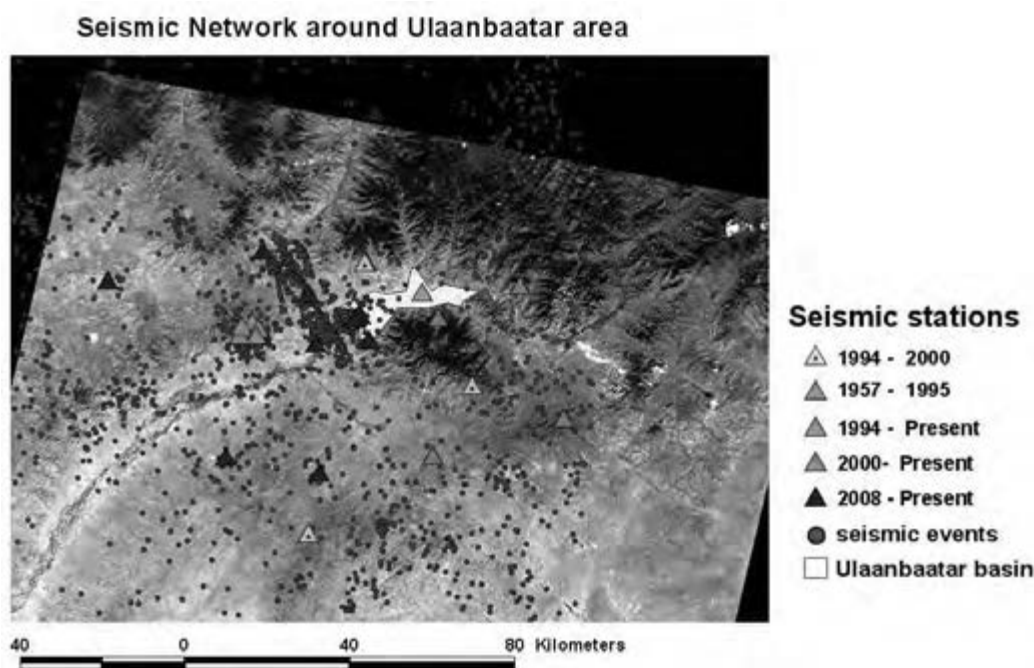


Figure 3: Seismic network around of Ulaanbaatar area

Figure 4 and 5 shows a sample seismograms of seismic events occurred near Ulaanbaatar city. All those events are felt well in Ulaanbaatar basin. Each signal traces are the vertical Z components recorded permanent and mobile seismic network of Ulaanbaatar.

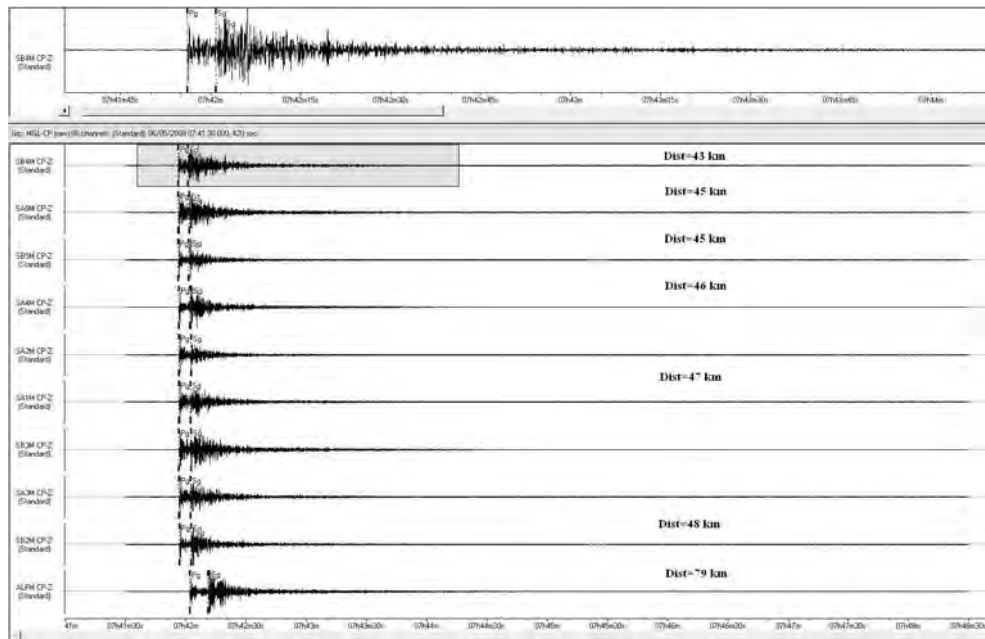


Figure 4: Sample record of shows an event on Oct 10, 2008 that was about 45 km from the Ulaanbaatar basin

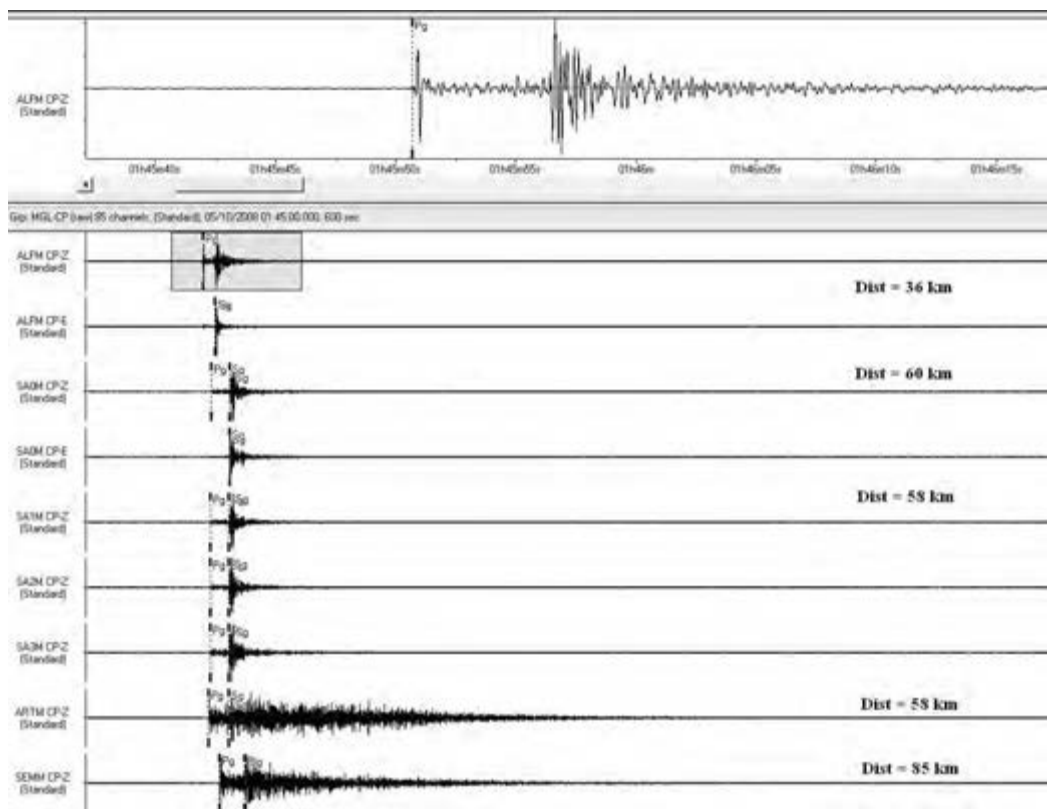


Figure 5: An seismogram shows an event on May 06, 2008 that was about 70 km West from the city, occurred in Hustai fault.

4. DEPTH DISTRIBUTION OF SEISMIC ACTIVITY

Depth distribution of seismic activity around Ulaanbaatar city, are shown in figure 6. Most of events are located shallow depth. However, majority of depth distribution are concentrated between 3 and 13km. According to the 2 cross-sections, all events are distributed 0-20km in depth. Concentrated events are corresponds to the Emeelt active structures where 2 volumes are crossing.

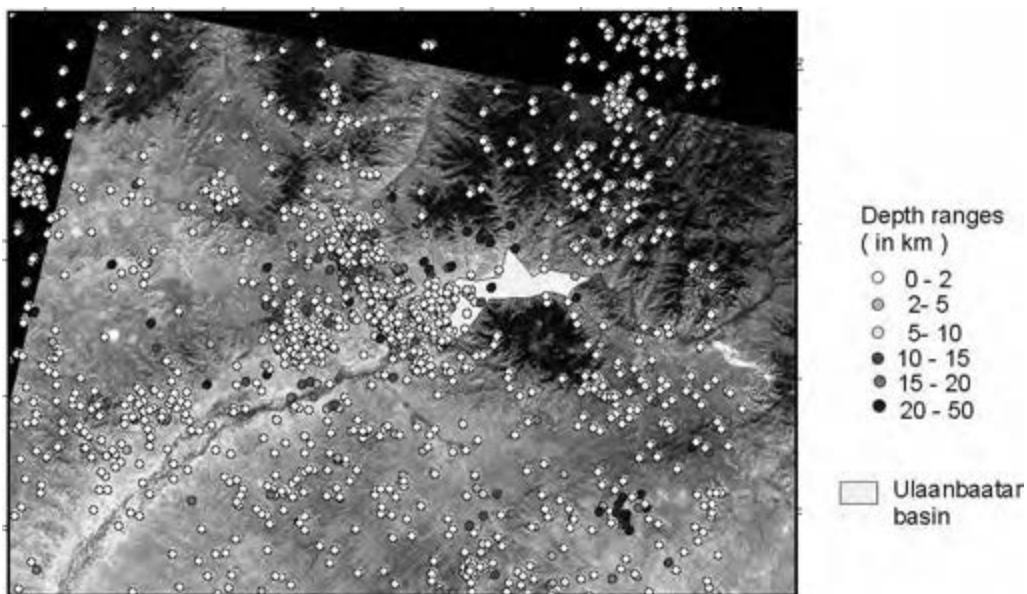


Figure 6: Depth distribution of seismic activity around Ulaanbaatar area. The colors are shows depth range.

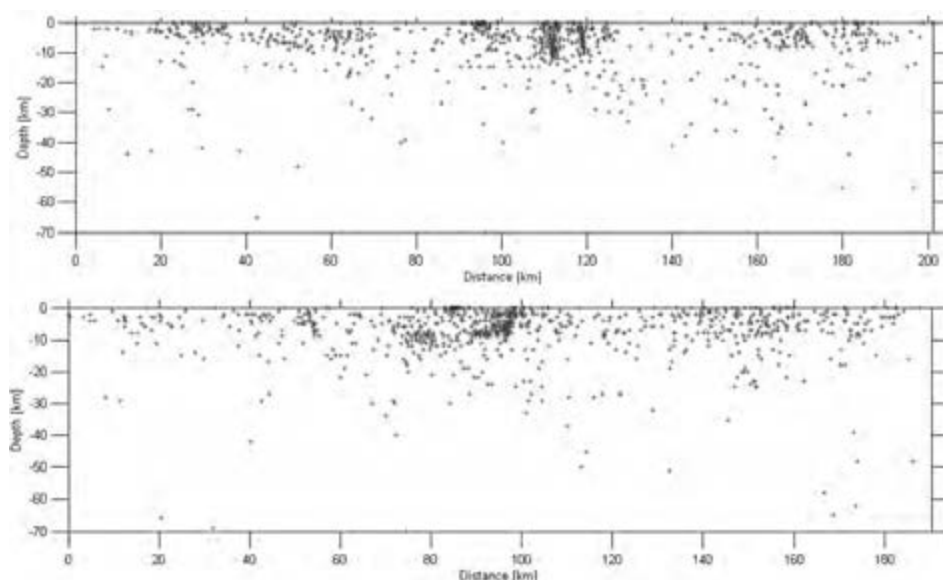


Figure 7: Cross-section of the depth distribution of seismic activity of the Ulaanbaatar area. Top picture is shows NS and down EW directed cross section along central activity.

5. DISCUSSION AND CONCLUSION

Preliminary observation and study on this area was a step which gives us important information about existence of active structures around Ulaanbaatar area. As following above information we discovered that Ulaanbaatar area is high seismic hazard region and one of important conclusion could be potential seismic source in this area starts to be reactivated. The potential seismic sources (active faults and seismicity) that could make very heavy damage in Ulaanbaatar area, is existing very short distance. Due to their impact on the hazard for Ulaanbaatar, it is absolutely necessary to upgrade or renew of seismic hazard assessments of Ulaanbaatar city.

REFERENCES

Baljinnyam, I., A. Bayasgalan, B.A. Borisov, A. Cisternas, M.G. Dem'yanovich, L. Ganbaatar, V.M. Kochetkov, R.A. Kurushin, P. Molnar, H. Philip, and Y.Y. Vashchilov (1993), Ruptures of Major Earthquakes and Active Deformation in Mongolia and its Surroundings. Vol. Memoir 181 of Boulder, Colorado: The Geological Society of America, Inc..

Khilko S.D., R.A. Kurushin, V.M. Kochetkov, L.A. Misharina, V.I. Melnikova, N.A. Gilyova, S.V. Lastochkin and D. Monhoo, (1985). Earthquakes and the base of the seismic zoning of Mongolia. Vol. 41 of The joint Soviet-Mongolian scientific - Research Geological Expedition. 225 p.

Natsag-yum, L., I. Balzhinnyam, and D. Monkho (1971). Earthquakes in Mongolia, in Seismic Regionalization of Ulan Bator,, S. V. Medvedev, Moscow, Nauk, 54-82

Antoine Schlupp, Dugarmaa T, Adiya M., Ankhtsetseg D., Baasanbat Ts., Battulga B., Batsaikhan Ts., Bayar G., Bayarsaikhan Ch., Demberel S., Dugarmaa T., Erdenezul D., Mungunsuren D., Munkhsaikhan A., Munkhuu D., Narantsetseg R., Odonbaatar Ch., Selenge L., Tsembel B., Ulziibat M., Urtnasan Kh., “ Seismic Hazard Assessment of Ulaanbaatar, capital of MONGOLIA. Seismic microzoning map” , 2006, Report of RCAG, MAS

Seismic risk analysis for intercity railway system in Tokyo metropolitan area

Yoshimasa MAEDA¹, Hisamichi HATTORI², Toshiro SHIZUMA³
and Hiromichi YOSHIKAWA⁴

¹ Assistant Manager, Civil Technology Dept, Tokyu Construction Co., Ltd, Japan
maeda.yoshimasa@tokyu-cnst.co.jp

² Chief Manager, Civil Technology Dept, Tokyu Construction Co., Ltd, Japan

³ Chief Manager, Shinozuka Research Institute, Japan

⁴ Professor, Advanced Research Laboratories, Tokyo City University, Japan

ABSTRACT

When railway structures are damaged by a large earthquake, the train service will be suspended for a long time. In such situation, passengers will want to know recovery time for their lines, and the owner will want to estimate how the number of passenger will recover.

In this paper, the railway system consists of three railway lines is simulated covering 40km² in Tokyo metropolitan area, assuming that the Great Kanto Earthquake occurred and railway viaducts are damaged. Seismic risk analysis is carried out by calculating recovery time expectancy, passenger recovery curve, and bottleneck index for the railway system.

Keywords: railway system, seismic risk analysis, recovery time expectancy, recovery curve, bottleneck index

1. INTRODUCTION

When railway lines are stopped by a large earthquake, passengers will want to know the information of recovery time for their lines, and the owner has the obligation to explain them. On the other hand, in order to formulate a business continuity plan (hereafter BCP) ¹⁾, the owner will want to estimate how the number of passenger will recover.

In this paper, the seismic risk for intercity railway system is estimated, assuming that the Great Kanto Earthquake²⁾ is occurred and railway viaducts are damaged. The railway system consists of three railway lines covering 40km² in Tokyo metropolitan area. Seismic risk analysis for the railway system is carried out by calculating recovery time expectancy, passenger recovery curve, and bottleneck index. On analyzing the damage of railway viaducts, it is considered that ground motion intensity in attenuation equation and site amplification factor at location ground.

2. SIMULATION MODEL

The simulation model is a railway system that consists of three lines connecting the suburbs and urban area as shown in Figure 1. It consists of radial A line in the inland, radial B line along the sea, and belt C line in the banks of a river. Every line in the system is a virtual line, the encircled number in Figure 1 shows the main stations made by reinforced concrete viaduct structure. Viaducts in C line constructed along the river bank on the soft ground, and the other viaducts are on normal ground.

In this paper, assuming that the Great Kanto Earthquake whose magnitude is 8.0 (JMA scale) occurred as the scenario earthquake and railway viaducts are damaged, seismic system risk are estimated. In addition, the region surrounded by solid line and dashed lines in the Figure 1 indicates fault plane of the plate boundary for the Great Kanto Earthquake. The system model is intended for one way route, stations in the suburbs (Excluding No.5, 11, and 13) are origin, stations in the central Tokyo metropolitan area (No.5, 11, and 13) are destination, where many companies locate.

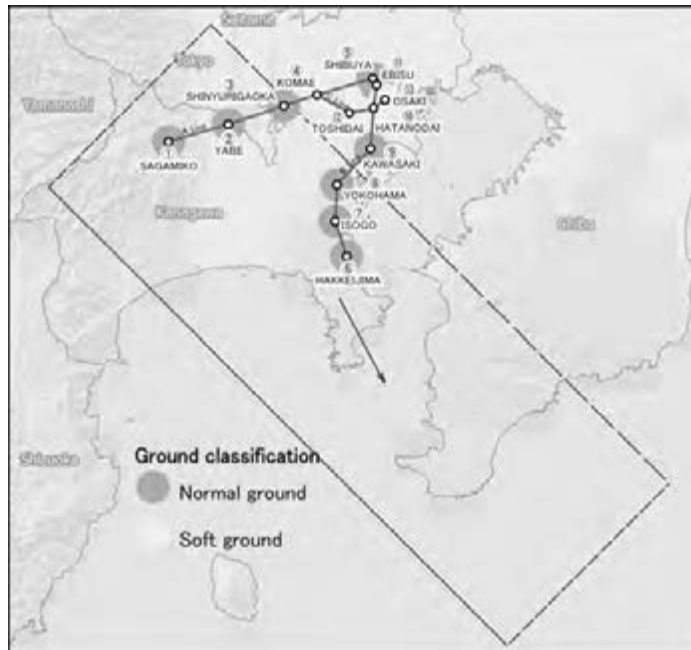


Figure 1 Railway system and scenario earthquake

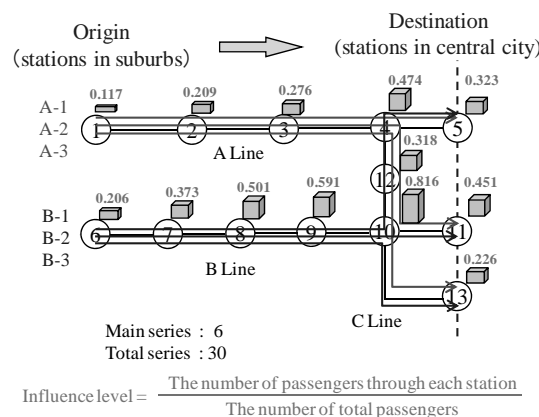


Figure 2 System model and influence level

This railway system can be modeled by the ladder system shown in Figure 2, and six main transport pathways (A1-A3, B1-B3) are shown in it. Considering the passengers who ride on along the way, six main lines can be divided into the 30 series. The ratio of the passenger's number in 30 series was added at each station, it shows by bar chart as an influence level to the entire railway system in Figure 2.

3. EVALUATION METHOD OF PROBABILITY FUNCTION FOR RECOVERY TIME

Since this model is intended for one way route, this system can be modeled as multiple serial systems. Recovery time in serial system, because it has been aimed at early recovery of facilities, shall be promoted to work on damaged facilities at the same time, recovery works shall be completed in the shortest time. According to this rule, the maximum time needed to recover in the system equals to that of the entire system.

When recovery time to N number of the facilities (hereafter component) shown in Figure 3 is represented by a random variable $T_1 \sim T_n$, recovery time can be expressed as Equation (1) under the condition that x is the seismic ground motion intensity.

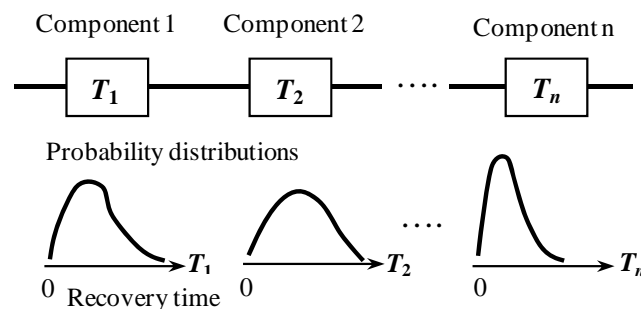


Figure 3 Recovery time in serial system

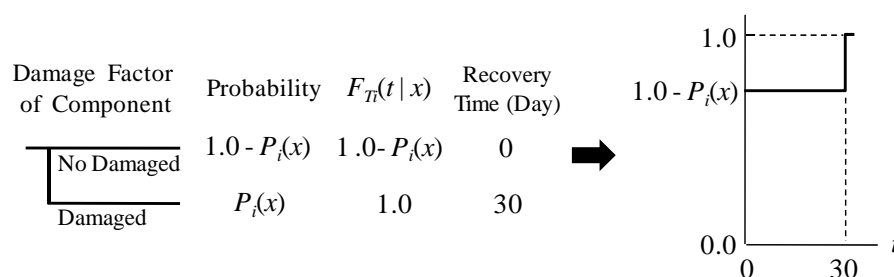


Figure 4 Cumulative distribution function of component i

$$T_{|x} = \max(T_1, T_2, \dots, T_n | x) \tag{1}$$

Assuming the independence of the component's damage, cumulative distribution function of the recovery time $F_T(t/x)$ in the serial system, is shown as follows.

$$F_T(t | x) = P(T_1 \leq t, T_2 \leq t, \dots, T_n \leq t | x) \tag{2}$$

$$F_T(t | x) = \prod_{i=1}^n F_{T_i}(t | x) \tag{3}$$

$$F_{Ti}(t | x) = 1.0 - P_{fi}(x), 0 \leq t < t_{max} \quad (4)$$

$$= 1.0, t = t_{max}$$

$F_{Ti}(t | x)$ represents cumulative distribution function of each component to the recovery time, it can be gotten by probability of damage to the components $P_{fi}(x)$ and recovery time t shown in Figure 4, and be given by Equation (4). Probability of damage $P_{fi}(x)$ is determined by the Fragility Curve based on structural reliability³⁾. Furthermore, Figure 4 is an example of two branches that the damage has occurred or not, if necessary, it can be changed at least three branches consisting no damage, moderate, and extensive etc.

4. EVALUATION METHOD OF SYSTEM RISK

4.1 Recovery curve

The recovery curve defined as the process to complete recovery, after the original function is reduced or stopped. The horizontal axis represents the time required for recovery, the vertical axis represents the recovery ratio, when the original function equals to 1.0. Figure 5 shows schematically the recovery curve, and the recovery curve is represented as equation (5)⁴⁾.

$$R(r_L) = \int_0^{\infty} (1 - F_T(t, r_k)) dt, k = 1 \sim L \quad (5)$$

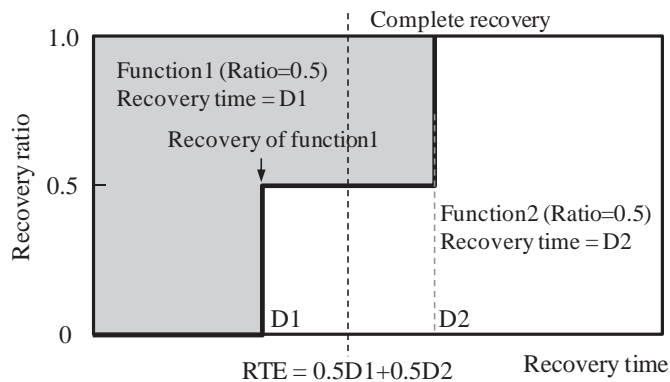


Figure 5 Recovery curve

Here, $F_T(t, rk)$ is the probability function of recovery time about function k , r_k is the recovery ratio, if the original state is defined 1.0.

In addition, RTE (Recovery time expectancy, hereafter RTE) in the Figure 5 are typical of the recovery time, it can be obtained by multiplying the recovery ratio of the component by the expected value of recovery time as shown in the Equation (6).

$$RTE = \sum_{k=1}^L R(r_k) \cdot r_k \quad (6)$$

4.2 Bottleneck index

In order to understand effectively the bottleneck component on the system which has many components, bottleneck index (hereafter, B.I.) has been proposed⁵⁾. B.I. is gotten by multiplying the influence (importance) level to the entire system by vulnerability (seismic performance), the Equation is as follows.

$$B_i = e_i \cdot E(T_i), \quad i = 1 \sim n \quad (7)$$

Here, i is component, e_i represents the influence level, and $E(T_i)$ is the expected value of recovery time to each component.

5. SIMULATION ANALYSIS

5.1 Vulnerability of viaducts

Three types of viaducts were adopted for analysis, referring to the history of railway design standards. TYPE 1 is shear failure type based on past design standard, TYPE 2 is flexural failure type of which seismic performance is comparatively middle, and TYPE 3 is flexural one whose seismic performance is comparatively high based on existing design standard. Damage level of the viaduct is classified to four states, non damage, minor, moderate, and extensive. Furthermore the mean value to each damage state is set on by elastic response acceleration basing on equal energy principle.

The mean value of seismic performance and recovery time to each damage level is indicated in Tables 1 to 3. In the case the viaduct TYPE 1 is retrofitted, it

Table 1 Vulnerability of viaduct TYPE 1

Damage state	Peak elastic response acceleration a_R (gal)	Recovery time (day)	Response spectrum ratio S	Normal ground (G3)		Soft ground (G5)	
				site amplification factor λ	peak bedrock acceleration $a_R/S/\lambda$ (gal)	site amplification factor λ	peak bedrock acceleration $a_R/S/\lambda$ (gal)
non damage	0	0	1.825	1.4	0	1.6	0
extensive	472	60	1.825	1.4	185	1.6	162

Table 2 Vulnerability of viaduct TYPE 2

Damage state	Peak elastic response acceleration a_R (gal)	Recovery time (day)	Response spectrum ratio S	Normal ground (G3)		Soft ground (G5)	
				site amplification factor λ	peak bedrock acceleration $a_R/S/\lambda$ (gal)	site amplification factor λ	peak bedrock acceleration $a_R/S/\lambda$ (gal)
non damage	0	0	1.825	1.4	0	1.6	0
minor	720	3	1.825	1.4	282	1.6	247
moderate	1188	10	1.825	1.4	465	1.6	407
extensive	1800	60	1.825	1.4	705	1.6	616

Table 3 Vulnerability of viaduct TYPE 3 (Post retrofitting TYPE 1)

Damage state	Peak elastic response acceleration a_R (gal)	Recovery time (day)	Response spectrum ratio S	Normal ground (G3)		Soft ground (G5)	
				site amplification factor λ	peak bedrock acceleration $a_R/S/\lambda$ (gal)	site amplification factor λ	peak bedrock acceleration $a_R/S/\lambda$ (gal)
non damage	0	0	1.825	1.4	0	1.6	0
minor	1296	3	1.825	1.4	507	1.6	444
moderate	2088	10	1.825	1.4	817	1.6	715
extensive	3060	60	1.825	1.4	1198	1.6	1048

assumed that the vulnerability becomes same as TYPE 3.

The mean value of peak bedrock acceleration (hereafter PBA) which is converted to seismic performance is shown on the right of Tables 1 to 3. This value can be derived by dividing site amplification factor and response spectrum ratio normalized by the PBA by peak elastic response acceleration. Here, characteristic periods of three kinds of viaduct are 0.7~0.75 second, response spectrum of ground surface and bedrock surface are referred to Level 1 Earthquake of reference 6). In the above conditions, response spectrum ratio is given 1.825, site amplification factor is given 1.4 on normal ground and 1.6 on soft ground. Thus the mean value converted by PBA is able to collectively manage the seismic performance of variety facilities that are designed in different ages.

Upon risk analysis, PBA to each site is simulated by attenuation equation of Annaka⁷⁾, a variation (logarithmic standard deviation) of the ground motion intensity is set to 0.5, and one of vulnerability of structure is set to 0.3.

5.2 Simulation case

Three simulation cases are carried out, Table 4 shows the combinations of the simulation cases and the viaduct types. Simulation Case 1 is the case before retrofitting, viaducts on A line are TYPE 2 (seismic performance are middle), and them on line B are TYPE 1 (seismic performance are small), and the other are TYPE 3 (seismic performance are big). Simulation Case 2 is the case that viaducts No.6 ~ 11 whose type is TYPE 1 are completed retrofitting and seismic performance becomes same as the viaduct TYPE 3. Moreover, simulation Case 3 is the case that all viaducts of TYPE 1 except viaduct No.9 are retrofitted.

Table 4 Simulation case

Station (Railway viaduct)	ground classification	Case 1	Case 2	Case 3
1 Sagamiko	Normal (G3)	Type 2	Type 2	Type 2
2 Yabe	Normal (G3)	Type 2	Type 2	Type 2
3 Shinyurigaoka	Normal (G3)	Type 2	Type 2	Type 2
4 Komae	Soft (G5)	Type 2	Type 2	Type 2
5 Shibuya	Normal (G3)	Type 2	Type 2	Type 2
6 Hakkejima	Normal (G3)	Type 1	Type 3	Type 3
7 Isoko	Normal (G3)	Type 1	Type 3	Type 3
8 Yokohama	Normal (G3)	Type 1	Type 3	Type 3
9 Kawasaki	Normal (G3)	Type 1	Type 3	Type 1
10 Hatanodai	Soft (G5)	Type 1	Type 3	Type 3
11 Ebisu	Normal (G3)	Type 1	Type 3	Type 3
12 Toshidai	Soft (G5)	Type 3	Type 3	Type 3
13 Osaki	Soft (G5)	Type 3	Type 3	Type 3

5.3 Result of simulation

Figure 6 shows the passenger recovery curves of each simulation case. Every curve has 30 stages equal to the number of combinations of series. Case 1 recovered about 20 percent from 10 days to 20 days, the remaining 80 percent has recovered in 49 days and 60 days. Since 80% of recovery is delayed, RTE of the entire system has become 47.65 days. In Case 2, recovery time was reduced significantly by retrofitting, RTE has become 8.44 days. On the other hand, since Case 3 is not completely retrofitted and one viaduct has not been retrofitted, RTE did not significantly improve, it has become 33.16 days.

Figure 7 shows the expected value of recovery time of each station (viaduct) with bar chart using GIS (Geographic Information Systems). It is obvious that expected value of recovery time can be expressed clearly and visually using the GIS.

Table 5 shows the results of expected value of recovery time from the departure stations to the destination stations, in case for example departure stations are No.2 and No.8. If the departure station is the same, expected value of recovery time is different depending on the destination stations. Thus, by using this model, it is possible to explain the recovery time for each pathway, and can meet the needs of the passenger.

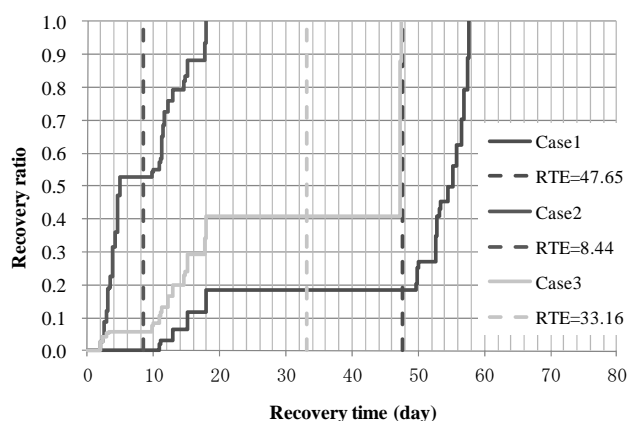


Figure 6 Comparison of passenger recovery curves

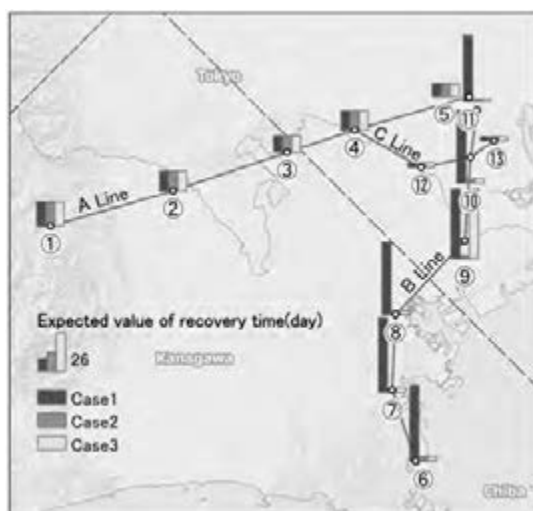


Figure 7 Comparison of expected value of recovery time

Table 5 Expected value of recovery time to destination stations
(For example No.2 and No.8 as departure stations)

Simulation Case1			Simulation Case2			Simulation Case3		
Departure	Destination	Recovery time (day)	Departure	Destination	Recovery time (day)	Departure	Destination	Recovery time (day)
2 Yabe	5 Shibuya	15.1	2 Yabe	5 Shibuya	15.1	2 Yabe	5 Shibuya	15.1
	11 Ebisu	52.7		11 Ebisu	14.7		11 Ebisu	14.7
	13 Osaki	49.9		13 Osaki	14.7		13 Osaki	14.7
8 Yokohama	5 Shibuya	55.3	8 Yokohama	5 Shibuya	11.3	8 Yokohama	5 Shibuya	47.4
	11 Ebisu	55.8		11 Ebisu	3.1		11 Ebisu	47.2
	13 Osaki	55.3		13 Osaki	3.4		13 Osaki	47.2

The results of influence level, vulnerability (recovery time), and B.I. are shown in Table 6. Focusing on the vulnerability in Case 2, by comparing No.3 on the normal ground to No.4 on the soft ground, in spite of the far distance from the epicenter, vulnerability of No.4 has become greater. In addition, comparing No.9 to No.10, the same matter can be said. It is considered that the result is affected by the site amplification. By taking in the site amplification factor, the vulnerability of the structures located in wide area is able to evaluate properly.

As mentioned previously, B.I. is represented by multiplication of influence level and vulnerability. In Case 1, B.I. of B Line are greater overall, the largest bottleneck has become No.10, because of both large influence and vulnerability. In Case 2, since TYPE 1 viaducts have been retrofitted, a significant bottleneck is not observed. The largest bottleneck was No.4, it is obvious that component of bottleneck was improved by retrofitting. In Case 3, B.I. of No.9 became greater, it is obvious that one component's damage impacts the entire system. Figure 8 shows the B.I. by using the GIS. The GIS makes the results of B.I. easier to understand.

Table 6 Bottleneck index
(1) Case1(Before retrofitting)

damage element	influence	vulnerability	B.I.
10 Hatanodai	0.816	49.66	40.53
9 Kawasaki	0.591	47.22	27.89
8 Yokohama	0.501	49.51	24.82
11 Ebisu	0.451	45.01	20.31
7 Isoko	0.373	50.78	18.96
6 Hakkeijima	0.206	51.56	10.63
4 Komae	0.474	13.16	6.23
3 Shinyurigaoka	0.276	11.18	3.08
2 Yabe	0.209	13.46	2.81
5 Shibuya	0.323	8.61	2.78
1 Sagamiko	0.117	16.54	1.93
12 Toshidai	0.318	3.30	1.05
13 Osaki	0.226	2.85	0.64

(2) Case2 (After retrofitting)

damage element	influence	vulnerability	B.I.
4 Komae	0.474	13.16	6.23
3 Shinyurigaoka	0.276	11.18	3.08
2 Yabe	0.209	13.46	2.81
5 Shibuya	0.323	8.61	2.78
10 Hatanodai	0.816	3.02	2.46
1 Sagamiko	0.117	16.54	1.93
8 Yokohama	0.501	2.96	1.49
9 Kawasaki	0.591	2.30	1.36
7 Isoko	0.373	3.44	1.28
12 Toshidai	0.318	3.30	1.05
11 Ebisu	0.451	1.83	0.83
6 Hakkeijima	0.206	3.78	0.78
13 Osaki	0.226	2.85	0.64

(3) Case3 (Ongoing retrofitting)

damage element	influence	vulnerability	B.I.
9 Kawasaki	0.591	47.22	27.89
4 Komae	0.474	13.16	6.23
3 Shinyurigaoka	0.276	11.18	3.08
2 Yabe	0.209	13.46	2.81
5 Shibuya	0.323	8.61	2.78
10 Hatanodai	0.816	3.02	2.46
1 Sagamiko	0.117	16.54	1.93
8 Yokohama	0.501	2.96	1.49
7 Isoko	0.373	3.44	1.28
12 Toshidai	0.318	3.30	1.05
11 Ebisu	0.451	1.83	0.83
6 Hakkeijima	0.206	3.78	0.78
13 Osaki	0.226	2.85	0.64

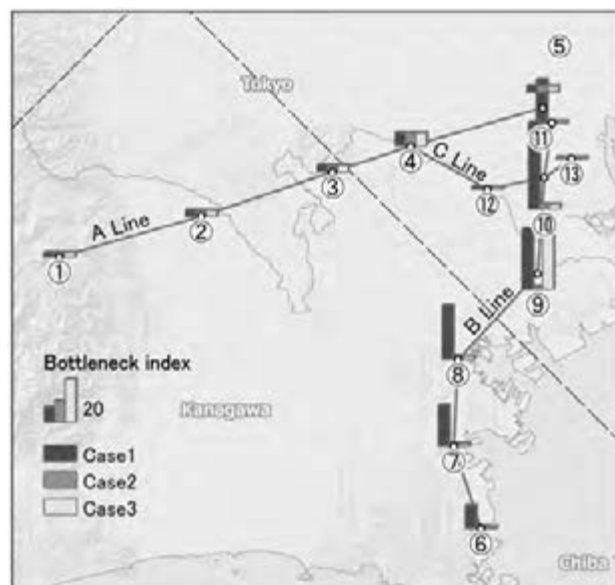


Figure 8 Comparison of Bottleneck index

6. CONCLUSION

This paper deals with seismic risk analysis for intercity railway system covering 40km² in Tokyo metropolitan area. The particular features in this paper are summarized as follows.

- By considering the site amplification factor and attenuation equation to the ground motion intensity, the vulnerability of facilities can be evaluated properly.
- Three cases of simulation were carried out, recovery curve, recovery time expectancy and bottleneck index were evaluated quantitatively.
- Expected value of recovery time to the destination stations which passengers will want to know is able to simulate by the proposed method.
- Due to simulate the bottleneck of the entire system, it was obvious that the recovery time expectancy of the entire system may be delayed because of one component's damage.
- By utilizing the GIS, the simulation results can be shown clearly and visually.
- The seismic risk analysis is considered to be effective for seismic management planning and formulation of BCP.

REFERENCES

- 1) Cabinet Office, 2007. Business Continuity central government guidelines first edition
- 2) Ryosuke Sato, 1989. the Japanese earthquake fault parameters handbook, Kajima Publishing
- 3) Takaaki Nakamura, 2007. Evaluation of earthquake probability of loss function for buildings considering the correlation, Proceedings of the Institute of Structural and Construction, No. 623, pp.49-56.
- 4) Toshiro Shizuma, 2009. Theoretical consideration of recovery curves and application to BCP, Business continuity Symposium on Seismic Risk Management Part 1 -Current Status and Issues SRM & BCP - Proceedings, pp.231-236.
- 5) Takaaki Nakamura, 2009. Studies on the function securement of the building with the aim to contribute to the BCP, Journal of the Society for General Construction, construction related to urban safety and security of the frontier No.7, pp.87-92.
- 6) Railway Technical Research Institute, 1999. Railway structure design standards, etc. (Seismic Design).
- 7) Tadashi Annaka, Fumio Yamazaki, Fuyuki Katahira, 1997. Proposal of the estimated maximum earthquake and response spectrum for strong-motion seismograph records JMA 87-type, Proceedings of the 24th Research Conference on Earthquake Engineering, pp.161-164.

SSI effect on seismic response of high-rise building in Jakarta, Indonesia

Kullachai TANTAYOPIN¹, James FRANK¹, Seong-Won Lee²
and Kyung-Ho PARK¹

¹School of Engineering & Technology, Asian Institute of Technology,
P.O. Box 4, Klong Luang, Pathumthani 12120, Thailand
E-mail: kullachai@gmail.com

²Korea Institute of Construction Technology, Daehwa-dong 283,
Goyangdae-ro, Ilsanseo-gu, Goyang-si, Gyeonggi-do, 411-712, Korea

ABSTRACT

High-rise buildings are conventionally analyzed under fixed base assumption without considering soil-structure interaction (SSI) because it provides a conservative design. However, recent studies show that conventional fixed base analysis may underestimate the seismic response and lead to unsafe design. This study deals with the effects of SSI for a typical high-rise building in Jakarta, Indonesia. Nonlinear time history analysis is performed and the inclusion of seismic SSI is modeled through dynamic beam on nonlinear Winkler foundation method. The results show that the peak story shear is reduced when considering SSI, while SSI analysis gives a larger interstory drift ratio than that of the non-SSI analysis. Especially the results show large different of the interstory drift ratio at the first floor and basement level, that might lead to be misconception in the design. Therefore, the effects of SSI for the typical example building are not always beneficial and may be detrimental in giving unsafe results in the deformation response.

Keywords: *soil-structure interaction, high-rise building, nonlinear seismic response*

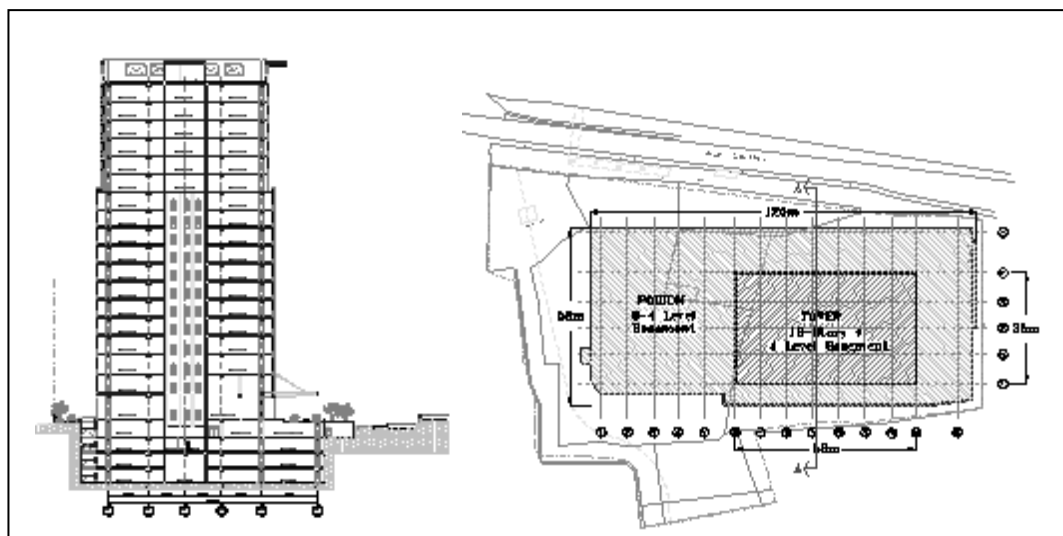
1. INTRODUCTION

High-rise buildings are conventionally analyzed under fixed base assumption without considering soil-structure interaction (SSI) because it provides a conservative design. However, recent studies show that conventional fixed base analysis may underestimate the seismic response and this may lead to unsafe design.

Mylonakis et al. (2000) investigated the role of SSI on the collapse of 18 piers of the Hanshin expressway during Kobe earthquake and found that the effects of SSI might cause collapse of Hanshin Expressway. Jeremic et al. (2004) studied the influence of SSI on seismic response of an elevated highway bridge (the I-880 viaduct) and found that the SSI can have both beneficial and detrimental effects. Yue and Wang (2009) studied the

influences of SSI on the high-rise frame shear wall structure in Fujian province of China. The results show that effects of SSI amplified dynamic response of structure in some stories which indicated that SSI cannot be neglected in analysis.

The previous studies indicate that fixed base analysis on seismic response can lead to unsafe design and the SSI effects shall be investigated for each different site. This study discusses the SSI effects on the seismic response for a typical high-rise building in Jakarta, Indonesia. As Indonesia has been well known with its high seismic activity (Irsyam et al., 2008), the seismic response of the high-rise building in Jakarta is important to be analyzed.



2. STUDY BUILDING

The selected typical building consists of 18-story floors and 4-level basements with central concrete core wall system. The basements are essentially larger in floor plate area comparing to the tower foot print area as shown in Figure 1. The gravity framing system at the tower is reinforced concrete post-tensioned beam with reinforced concrete slab. The gravity framing system at the ground floor and basement floor is reinforced concrete flat-slab with drop panel at the slab-column connection. The structure configurations are briefly described in Table 1.

Soil investigation and laboratory soil test were conducted to identify the subsoil condition at the site. The subsoil at the site can be divided into 3 major zones. The upper zone is occupied with recent deposits which are low in strength. The old deposits at the middle zone are competent as a bearing layer. The older deposits at the lower zone are also competent but less stiff than the middle zone. The generalized soil profile is presented in Figure 2 including shear wave velocity (V_s) obtained from field downhole seismic test. With the presence of relatively deep basements (4-level), the building is

originally designed with raft foundation which is able to sit directly on the middle zone. In order to study the effects of SSI for deep foundation, the building is also designed using pile foundation. Bored pile with the diameter of 800mm and the length of 24m is utilized to support the building. The 2D dynamic analysis is performed in transversal building cross section.

Table 1: Structure model configuration

Level	Vertical element				Horizontal element		
	Core wall thickness		Column size	fc'	Beam section	flat-slab thickness	fc'
	Outer	Inner					
	m	m	m ²	MPa	m ²	m	MPa
B4	0.45	0.25	0.90x0.90	50	-	0.250	32
B2-B3	0.45	0.25	0.90x0.90	50	-	0.175	32
B1	0.45	0.25	0.90x0.90	50	-	0.200	32
L1	0.45	0.25	0.90x0.90	50	0.45x0.65	0.200	32
L2	0.45	0.25	0.90x0.90	50	0.45x0.65	0.150	32
L3-L11	0.45	0.25	0.90x0.90	40	0.45x0.65	0.150	32
L12-L16	0.25	0.25	0.80x0.80	32	0.45x0.65	0.150	32
L17-L18	0.25	0.25	0.75x0.75	32	0.45x0.65	0.150	32

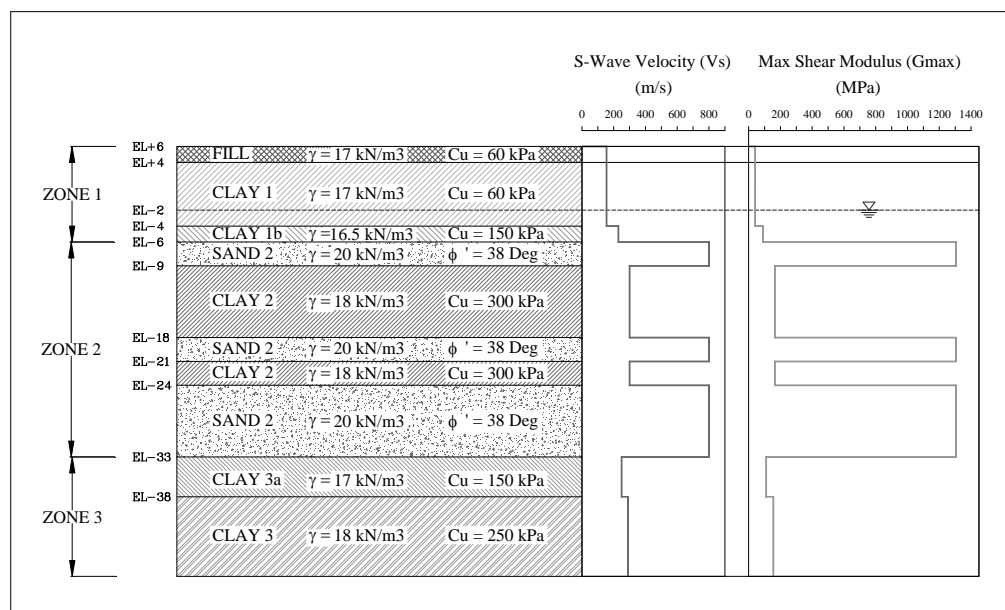


Figure 2: Generalized soil profile

3. NONLINEAR MODEL

The building is expected to exhibit the nonlinear behavior under severe earthquake level. In order to identify the actual response of the building, the

behavior of the SSI and structure elements need to be described using nonlinear model.

3.1 SSI Model

The nonlinear SSI is modeled based on the dynamic beam on nonlinear Winkler foundation (BNWF) method suggested by Boulanger et al. (1999) using the lateral load-displacement (p-y) element of the pile. The nonlinear (p-y) element conceptually consists of elastic, plastic and gap component in series. The gap and plastic components represent the near-field component while the elastic component represents the far-field component. Radiation damping is modeled using a dashpot in parallel with elastic component.

3.1.1 Pile Foundation

Boulanger (2000) originally implemented the nonlinear SSI model into OpenSees computer program platform for pile foundation case using three types of nonlinear SSI element: nonlinear (p-y); nonlinear (q-z); nonlinear (t-z) to represent the load-displacement behavior of lateral load capacity; bearing at pile tip; skin friction of the pile, respectively. In this study, only the PySimple1Gen command is used to generate nonlinear (p-y) elements along the pile in OpenSees developed by Brandenburg (2004). The influence of two other nonlinear elements is insignificant to the response of the pile.

3.1.2 Raft Foundation

Raychowdhury and Hutchinson (2008) modified the load-displacement relationship of the pile foundation to be applied for shallow foundation case. The nonlinear behavior of SSI for raft foundation is described using three nonlinear SSI elements: nonlinear (p-y); nonlinear (q-z); nonlinear (t-z) which represent the load-displacement behavior of lateral passive earth pressure at footing side; bearing capacity of footing; friction resistance along base of the footing, respectively. The nonlinear (p-y), (q-z), and (t-z) for shallow foundation case are implemented in OpenSees as PySimple2, QzSimple2, and TzSimple2 material models, respectively.

3.1.3 Structural Element

The nonlinear behavior of the structural element is described using lumped plasticity model which consists of elastic element and concentrated plastic hinge at each end. Concentrated plastic hinge is modeled using rotational spring where the monotonic backbone curve is calibrated from the experimental reinforced concrete test. The monotonic backbone curve of the concentrated plastic hinge is described by five parameters: yield moment (M_y), yield chord rotation (q_y), hardening stiffness (K_s), capping rotation (q_{cap}), and post-capping stiffness (K_c). These five parameters are determined based on the modeling parameter by Haselton et al. (2008) as recommended in PEER/ATC-72-1 (2010). The monotonic backbone curve of the concentrated plastic hinge is defined using Clough material model in OpenSees platform.

Table 2: Selected earthquake ground motions

No.	Earthquake Event	Year	Denotation	M_w	PGA (g)
1	Cape Mendocino	1992	CM-EUR-090	7.0	0.18
2	Hector Mine	1999	HM-H-000	7.1	0.27
3	Imperial Valley	1979	IMP-CH-012	6.5	0.27
4	Loma Prieta	1989	LP-HSP-000	6.9	0.37
5	Superstition Hills	1987	SH-PR-360	6.5	0.30
6	Mentawai Island	2007	MEN-ISL-HNN	7.9	0.13
7	South Sumatra	2007	SO-SUM-HNN	8.4	0.04

4. SEISMIC INPUT MOTIONS

The seismic input motions for the building are specified based on Indonesian Seismic Code SNI 03-1726-2003. The code determines the seismic design load based on design basis earthquake (DBE) corresponding to the uniform seismic hazard level of 10% probability of exceedance in 50 years. According to the code, Jakarta city is located in seismic Zone 4 with the peak base rock acceleration of 0.20g. Based on the subsoil condition at the site, the site can be categorized as medium soil site. The nonlinear time history analysis is required to be performed in maximum considered earthquake (MCE) level which is assumed to be 1.5 times the DBE level. The design response spectrum for MCE level is therefore defined for analysis.

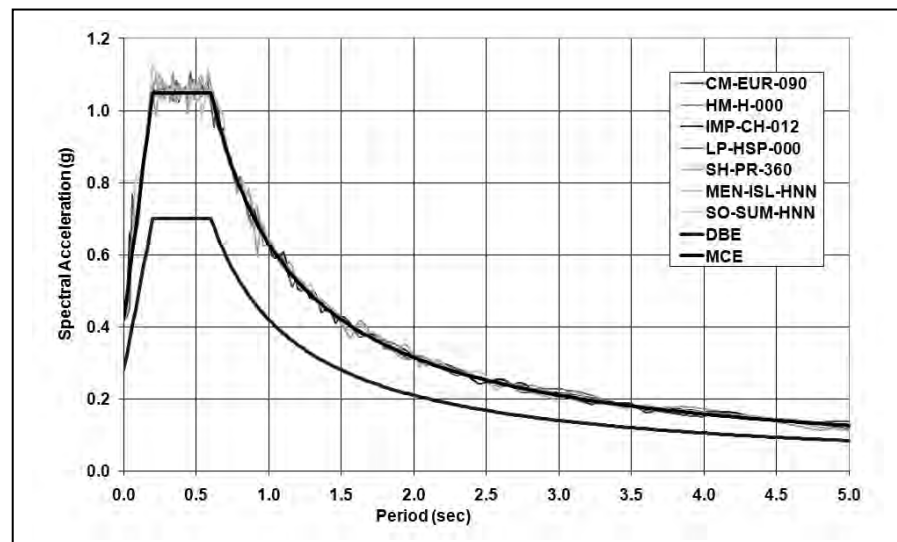


Figure 4: Response spectra of scaled ground motions

Seven earthquake records are used in this analysis to satisfy seismic design code requirement (UBC 1997, EURO8) for average response. Five strong earthquake records from worldwide database and two earthquake records from inside Indonesia area are selected to cover the wide range of

earthquake variation as shown in Table 2. The ground motions are scaled to match with the MCE response spectrum by using spectral matching software RspMatch2005 (Hancock et al., 2006) as shown in Figure 4. Free-field site response analysis is then performed using SHAKE91 software (Idriss and Sun, 1991) to provide the seismic input motions along the different depths considered.

5. ANALYSIS RESULTS

In order to identify the effects of SSI on seismic response of the buildings, the nonlinear time history analysis is performed for three foundation cases: fixed (Non-SSI), raft (SSI), and pile (SSI) foundation cases and the analysis models for three foundation cases are shown in Figure 5.

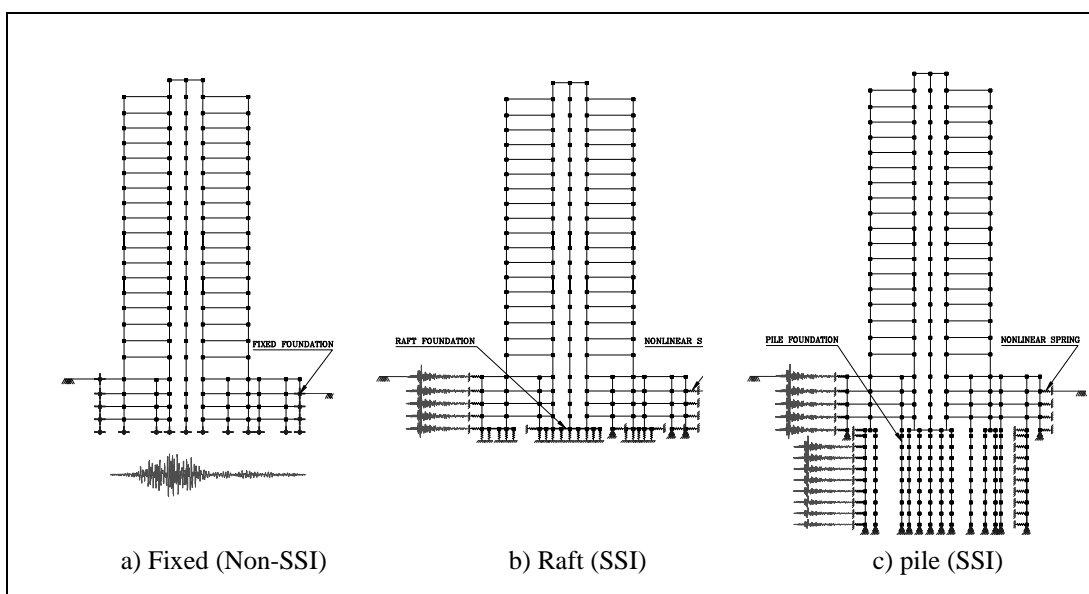


Figure 5: Fixed, raft and pile foundation models

The nonlinear time history analysis is performed to obtain the seismic response of the building. The seismic responses of the building are determined in term of force and deformation responses. The force response is described as shear force while the deformation response is described as interstory drift ratio.

5.1 Shear Force Response

The average response profiles of shear force from the seven earthquake ground motions are summarized in Figure 6. Non-SSI analysis shows the maximum response of shear force with the large reduction at the first floor. For SSI analysis, pile case shows lower shear force response than raft case excepting at the bottom basement which has high restrain of pile foundation.

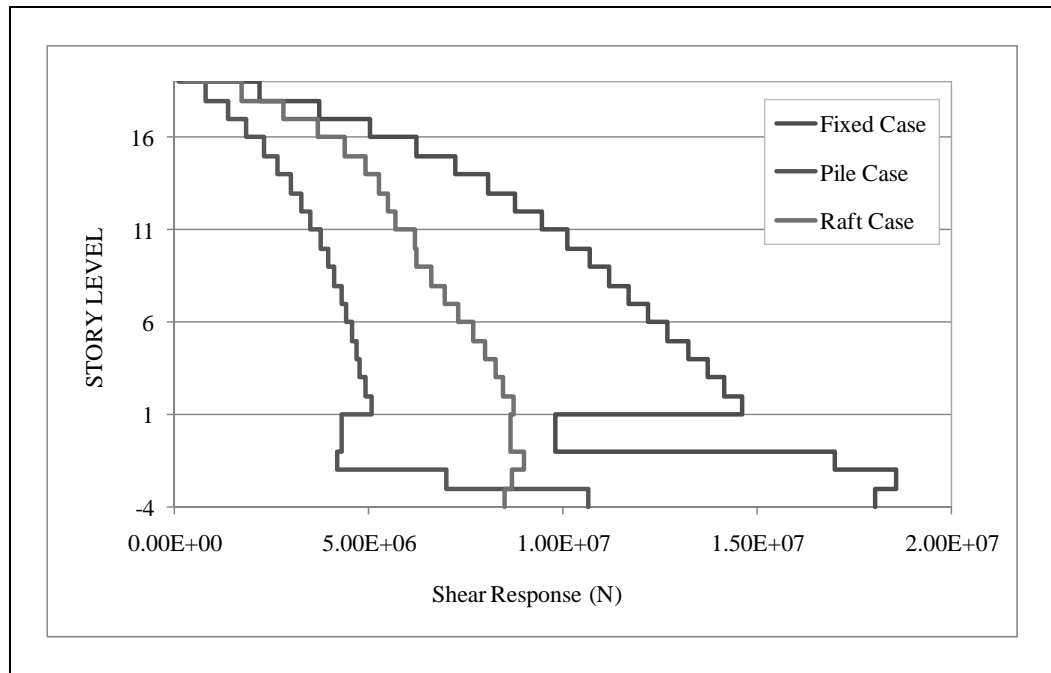


Figure 6: Average response profile of shear force

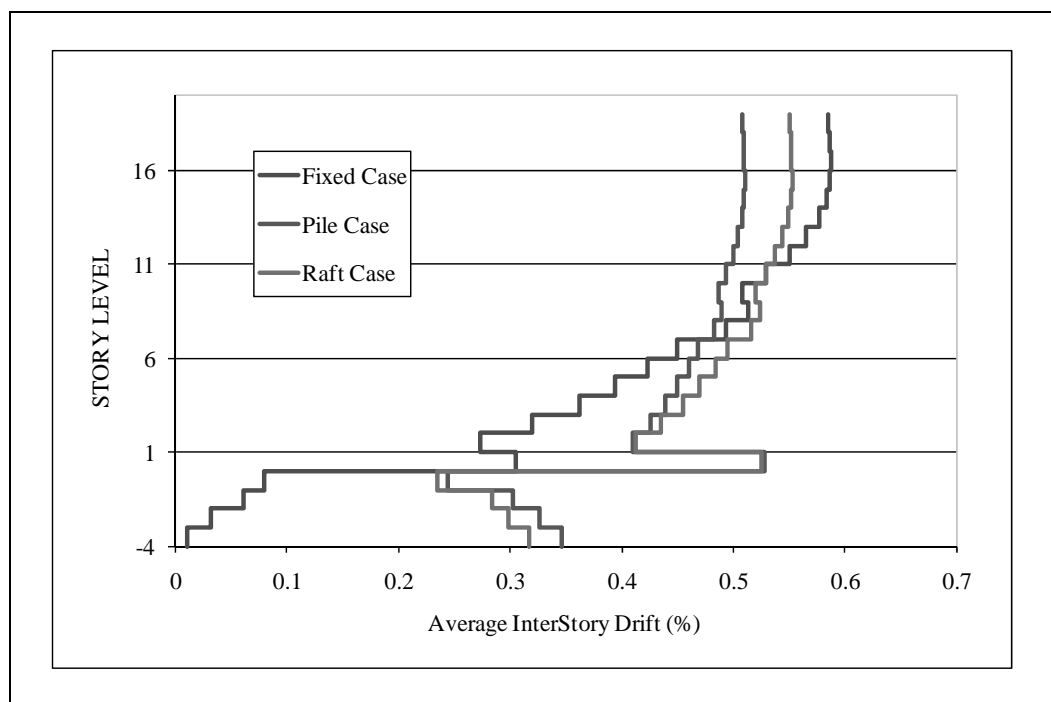


Figure 7: Average response profile of interstory drift ratio

5.2 Deformation Response

The average response profiles of the interstory drift ratio from the seven earthquake ground motions are summarized in Figure 7. The SSI analysis for pile and raft foundations show similar pattern of interstory drift ratio, while the large values of interstory drift ratio are found at the first floor. The non-SSI analysis shows very small results at basement level and first floor.

6. CONCLUSION

The effects of SSI have been considered for a typical high-rise building in Jakarta, Indonesia. The results show that the peak story shear is reduced when considering SSI, while the SSI analysis gives larger interstory drift ratio than that of the non-SSI analysis. Especially the results show large different of the interstory drift ratio at the first floor and basement level, that might lead to be misconception in the design. Therefore, the effects of SSI for the typical example building are not always beneficial and may be detrimental in giving unsafe results in the deformation response.

REFERENCES

- Boulanger, R. W., Curras, C. J., Kutter, B. L., Wilson, D. W., and Abghari, A., 1999. Seismic soil-pile-structure interaction experiments and analyses. *Journal of Geotechnical and Geoenvironmental Engineering*, Vol. 125, No. 9, pp.750-759.
- Boulanger, R. W., 2000. The PySimple1, QzSimple1, and TzSimple material documentation. Document for the OpenSees platform.
- Branderberg, S. J., 2004. PySimple1Gen OpenSees command. Document for OpenSees platform.
- FEMA, 2000. Prestandard and commentary for the seismic rehabilitation of buildings. *Report No. FEMA-356*, Federal Emergency Management Agency.
- Hancock, J., Lamprey, J. W., Abrahamson, N. A., Bommer, J. J., Markatis, A., McCoy, E., and Mendis, R., 2006. An improved method of matching response spectra of recorded earthquake ground motion using wavelets. *Journal of Earthquake Engineering*, Vol. 10, Special Issue 1, pp. 67-89.
- Haselton, C. B., Liel, A. B., Taylor Lange, S., and Deierlein, G. G., 2008. Beam-column element model calibrated for predicting flexural response leading to global collapse of RC frame buildings. *PEER Report 2007/03*, Pacific Earthquake Engineering Research Center, University of California, Berkeley, California.
- Idriss, I. M., and Sun, J., 1991. *User's Manual for SHAKE91*. Center for Geotechnical Modeling, Department of Civil and Environmental Engineering, University of California, Davis, CA.
- Irsyam, M., Dangkoa, D. T., Hendriyawan, Hoedajanto, D., Hutapea, B. M., Kertapati, E. K., Boen, T., and Petersen, M. D., 2008. Proposed seismic hazard maps of Sumatra and Java Island and microzonation study of Jakarta city, Indonesia. *Journal of Earth System Science*, Vol. 117, pp.865-878.
- Jeremic, B., Kunnath, S., and Xiong, F., 2004. Influence of soil-foundation-structure interaction on seismic response of the I-880 viaduct. *Journal of Engineering Structure*, Vol.26, Issue 3, pp.391-402.
- Mylonakis, G., Gazetas, G., Nikolaou, S., and Michaelides, O., 2000b. The role of soil on the collapse of 18 piers of the hanshin expressway in the Kobe earthquake. *Proceedings of 12th World Conference on Earthquake Engineering*, New Zealand, Paper No. 1074.

PEER, 2007. PEER Column Database. Pacific Earthquake Engineering Research Center, University of California, Berkeley, California.

PEER/ATC-72-1, 2010. Modeling and acceptance criteria for seismic design and analysis of tall buildings. Applied Technology Council, Redwood City, California.

Raychowdhury, P., and Hutchinson, T., 2008. Nonlinear material models for Winkler-based shallow foundation response evaluation. *Proceedings of GeoCongress 2008*, New Orleans, Louisiana, March, pp.686-693.

SNI, 2003. Indonesian Seismic Code for Buildings. SNI 03-1746-2003, Standard National Indonesia, Department of Public Work.

Yue, M., and Wang, Y., 2009. Soil-structure interaction of high-rise building resting on soft soil. *Electronic Journal of Geotechnical Engineering*, Vol.3, Bund. D, pp.1-20

A fundamental study on social vulnerability for public safety in China

Nan ZHANG¹ and Hong HUANG²

¹Institute of Public Safety Research (IPSR),
Tsinghua University, Beijing, China

²Professor, IPSR Tsinghua University, Beijing, China
hhong@tsinghua.edu.cn

ABSTRACT

It is greatly significant to analyze social vulnerability for taking measures of disaster prevention and emergency response for disaster relief. In this paper, taking Beijing as an example, the social vulnerability analysis index system was studied and an improved AHP (Analytic Hierarchy Process) method was developed. The social vulnerability evaluation index system including 27 influencing factors was established according to the data of social economy and demography of Beijing. Beijing is divided into 333 areas in detail according to the town and district distributions. The weight of each factor was evaluated through the improved AHP process which obviously decreases no-passing ratio of inconsistency of experts' questionnaire. At last, the following five kinds of distribution maps of Beijing: Social vulnerability, population vulnerability, career vulnerability, economy vulnerability and infrastructure vulnerability were obtained. The maps directly express the amount of different kind of vulnerability and the characteristic of distribution. Through the sensitivity analysis, the sensitive factors of each area were listed in the order of importance. The process and results are helpful for reducing social vulnerability and improving the capacity of public safety insurance.

Keywords: public safety, social vulnerability, analytic hierarchy process, parametric sensitivity analysis, Beijing

1. INTRODUCTION

All people put their attention on nature disasters because of the devastating destruction of 9.0-magnitude earthquake in Japan several months ago. If this disaster occurred in Beijing, what result it will be?

8.0 level earthquake occurred in Wenchuan caused 69,226 death, 17,923 missing, and direct economy loss was 8,451 hundred million RMB. The hurricane Katrina in USA in 2005 led to 973 people died and 400-thousand people unemployed. The 9.0 level earthquake in Japan in 2011 led to 15,534 people died and 7,092 people missed. Researchers recognize

gradually that the vulnerability of disaster's acceptor is an important reason of disaster occurring and loss difference for different areas. Analyzing the vulnerability of disaster's acceptor to provide the methods to reduce vulnerability is an effective measure of raising social disaster prevention ability and reducing emergency disaster's loss. It will be seen from this that the research of vulnerability is very important in public safety

In recent years, there are some researches on social vulnerability. Cutter et al. (2003) established the Social Vulnerability Index (SoVI) to examine the spatial patterns of social vulnerability to natural hazards at the county level in the United States. Christopher (2008) incorporated social vulnerability into numerical hurricane impact modeling to improve loss prediction; Jose (2010) constructed an index of social vulnerability to natural and technological hazards and to social risks in the Centre Region of Portugal, for all the municipalities of the region. The Portuguese center was divided into 78 areas. In China, the relevant research is little. As the capital of China, the research of Beijing's vulnerability should be given more attention. This research combines with the characteristic of Beijing to research the vulnerability of 333 areas of Beijing.

To analyze the vulnerability of all areas and to do relevant assessments focusing on Beijing's characteristic will contribute to implement responding action based on vulnerability situation of each areas and to act according to circumstances. When disaster is coming, we can make the emergency plan to rescue as soon as possible.

2. SOCIAL VULNERABILITY ANALYSIS

2.1 Area's Separation of Beijing

Because the newest 2010 census information will be published in 2012, the majority of these data published in 2000 was used in this study.

Beijing has 18 districts which including 16808 km² and 13,569,194 population. In this study, Beijing is divided into 333 areas according to the town and district distributions.

As a modern metropolis, Beijing has normal male-female ratio and age distribution. But the vulnerability of Beijing is increasing because of numerous transient population and migrant workers. Especially in urban areas, there is a big density of population, serious traffic jam and many narrow roads which are built before 1949 bring some negative influence in vulnerability. In rural areas, worse infrastructure, inconvenient traffic and high percentage of illiterate and ethnic minorities population also increase the vulnerability.

2.2 The brief instruction and distribution of influencing factor

In this study, social vulnerability divided into 4 primary indices: population vulnerability, career vulnerability, economy vulnerability and

infrastructure vulnerability. These four indices contain 27 secondary indices (Barry et al., 2001; Susan et al., 2003). The details are shown in Fig.1:

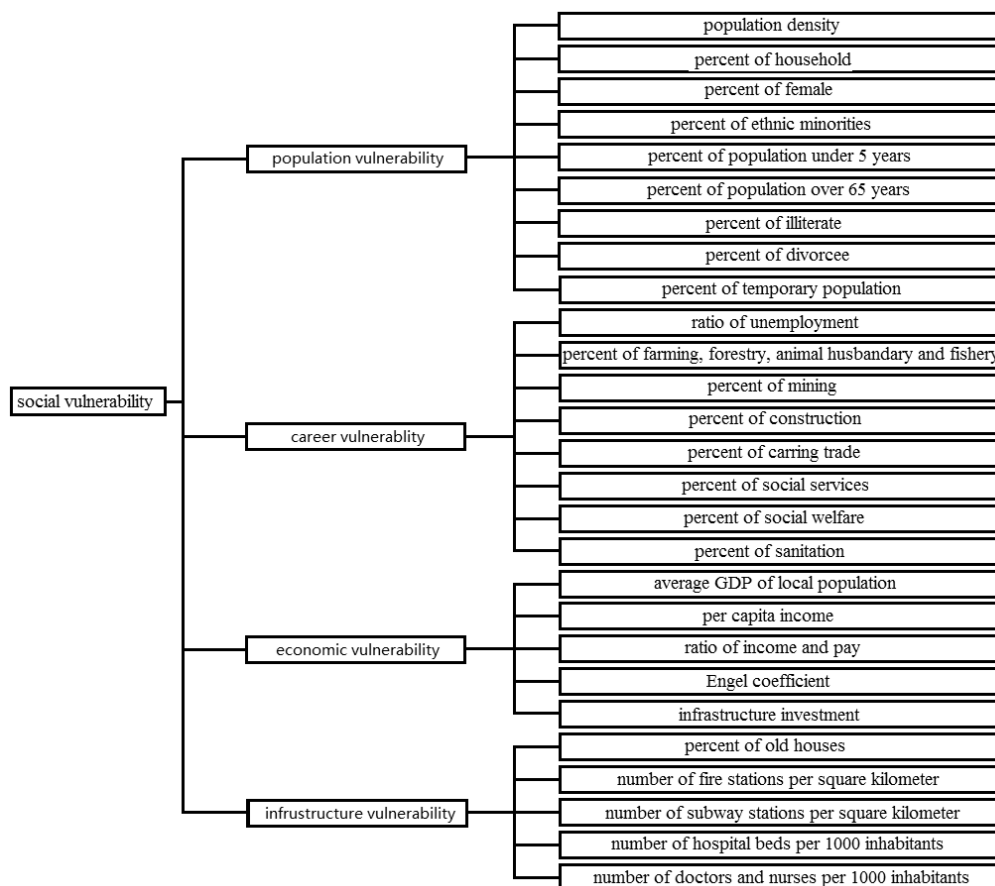


Figure 1: Indices metrics

For the “percent of old houses” (usage period over 40 years), the data of 18 districts of Beijing is used because of the limitation of data source. The data of smaller areas in the districts is regarded as the same with the districts.

3. METHOD

3.1 Data processing

The majority of these 27 influencing factors are from census information of Beijing, 2000 and census information of 18 districts, 2000, respectively. The number of subway stations and fire stations per square kilometer is acquired from metro route map of Beijing, 2010 and fire squadron several months ago respectively (Because these two factors have great changing in recent years, all data come from the information of 2010.)

SPSS is used to process the data in Z-score standardization in this study. Z-score standardization is a standard deviation standardization and the processed data conforms normal distribution. The invert function is:

$$x^* = \frac{x - \mu}{\sigma} \tag{1}$$

μ : the average of all sampled data

σ : the standard deviation of all sampled data

All data can be standardized according to this method.

3.2 Weight calculation

This study adopt AHP methods of subjective weighting methods (Wang et al., 2003) to calculate weight because there are many correlative spatial characteristics with each influencing factors which need to subjective judgement (Xueqiang Shan, 2010). AHP method has 4 steps:

- ① To analyze the relationship of each influencing factor and to build level structural model.
- ② To compare factors in the same level and to construct comparison matrix.
- ③ To calculate relative weight and to use coincidence indicator to make consistency check.
- ④ To calculate the weight of bottom influencing factor and make combined consistency check to general indices according to formulas.

(1) To build level structural model

Objective(top) level: social vulnerability

Primary indices level: population vulnerability, career vulnerability, economic vulnerability and infrastructure vulnerability.

Secondary indices level: 27 influencing factors

(2) To construct judgement matrix

In AHP method, scale is very important, and it can reflect the experts' evaluation to different factors. The following scale meaning table (Table 1) is suitable according to predecessor's experiment. Each factor can be compared using this table.

Table 1: Scale meaning table

scale	Meaning
1	Two factors have the same importance
3	One factor is a little important than other one
5	One factor is evident important than other one
7	One factor is intensive important than other one
9	One factor is extreme important than other one
2,4,6,8,	The average of above adjacent value
reciprocal	If the value of factor i compare to factor j is a_{ij} , the value of factor j compare to factor i is $a_{ji}=1/a_{ij}$

The shortcoming of this method is that expert's discretion easily goes wrong (The original judgement is different from later one.) when there are many indices. To consider this problem, there are two principles:

- ① Don't put 7-9 indices on one indices level otherwise expert easily makes inaccurate judgement.
- ② The different of indices classification shouldn't be too large, that is, every indices must be comparable.

(3) Consistency check

Level Sorting and consistency checking of result are very important when calculating weight. Level sorting is, according to judgement matrix, to calculate the factor's weight of importance sequence which is related to its own level against to factors from upper level. Calculating the consistent index CI is the first step when doing consistency check.

$$CI = \frac{\lambda_{\max} - n}{n - 1} \tag{2}$$

λ_{\max} : the max characteristic root of judgement matrix. n : the degree of the matrix

Second, to look up average random consistency index in Table 2.

Table 2 Average random consistency index R.I.

n	1	2	3	4	5	6	7	8	9
R.I.	0	0	0.58	0.90	1.12	1.24	1.32	1.41	1.45

Finally, to calculate the consistency ratio CR:

$$CR = \frac{CI}{RI} \tag{3}$$

Generally, when consistency ratio $CR < 0.1$, the inconsistent degree is in an acceptable range, which have gotten satisfied consistency and passed the test of consistency. Otherwise, we need to reconstruct compared matrix. The normalized characteristic vector can be treated as weight vector to adjust a_{ij} . The principle of weight calculating is shown below:

Given the matrix as A, the A is positive reciprocal matrix. First, we should calculating the product of per line and per column of A ($m_i = \prod_{j=1}^n A_{ij}$, $i=1,2,3\dots n$). Second, to calculate the n-th root of m ($\bar{w}_i = \sqrt[n]{m_i}$). Finally, to take normalized processing to vector \bar{w}_i .

$$w_i = \frac{\bar{w}_i}{\sum_{j=1}^n \bar{w}_j}$$

(4)

w_i : the weight of influencing factor.

(4) The particularity of this research

In this study, there are 84 judgements in the judgement table due to numerous influencing factors. The discretion of the people is influenced by numerous judgements. Considering the problem above, we change the methods in some point from judgement comparison to expert's direct marking. The specific method is that experts mark the influencing factors between 1 and 9 (1: the most unimportant factor; 9: the most important factor). Using this method, we can get the result through 35 judgements and the workload is two fifths compared with original method. The experts can keep awake to improve the efficiency and validity through this improved

method which turns qualitative comparison to quantitative comparison. Through the marking, the importance comparison of every influencing factor is easy to calculate.

In this study, there are 21 experts including 4 top experts and 17 normal experts participate the marking. We set the weight of 4 top experts 3 times to the weight of 17 normal experts in the weight calculating. The final statistical computing will be obtained by comparing the experts' judgement with experts' marking. This method reduces the consistency demand based on the expert serious marking.

(5) The weight calculating and integrated consistency check

The corresponding weight of each level's influencing factor can be calculated through this method. To calculate the weight through every experts' marking, the final result is obtained through the weighted mean of 21 experts. After that, every weight must be multiplied by a coefficient which is the number of secondary indices included by primary indices. Otherwise if the primary indices are more than secondary indices, the weight of every secondary indices will decrease. It will influence the weight of influencing factors. Finally, every final weight of influencing factor is obtained.

Table 3: Weights of influencing factors

Influencing factor	weight	Influencing factor	weight
population density	0.0536	percent of household	0.0196
percent of female	0.0322	percent of ethnic minorities	0.0223
percent of population under 5 years	0.0491	percent of population over 65 years	0.0523
percent of illiterate	0.0352	percent of divorcee	0.0275
percent of temporary population	0.0296	rate of unemployment	0.0161
percent of farming, forestry, animal husbandry and fishery	0.0073	percent of mining	0.0086
percent of construction	0.0105	percent of carrying trade	0.0078
percent of social services	0.0080	percent of social welfare	0.0076
percent of sanitation	0.0142	average GDP of local population	0.0537
per capita income	0.0756	ratio of income and pay	0.0465
engel coefficient	0.0525	infrastructure investment	0.0532
percent of old houses	0.0409	number of fire stations per square kilometer	0.0703
number of subway stations per square kilometer	0.0449	number of hospital beds per 1000 inhabitants	0.0785
number of doctors and nurses per 1000 inhabitants	0.0824		

Level sorting consistency index is CI_j and random consistency index is RI_j , the consistency ratio of integrated level sorting is:

$$CR = \frac{a_1CI_1 + a_2CI_2 + a_3CI_3 + \dots + a_mCI_m}{a_1RI_1 + a_2RI_2 + a_3RI_3 + \dots + a_mRI_m} \quad (5)$$

Integrated level sorting can be pass the consistency check when $CR < 0.1$. If $CR > 0.1$, we should readjust the factor's value of judgement matrix which consistency ratio is too high.

4. CALCULATION OF THE INTEGRATED SOCIAL VULNERABILITY SCORE

4.1 The classification of influencing factors

After the weight calculating, the population vulnerability, career vulnerability, economic vulnerability, infrastructure vulnerability and integrated social vulnerability will be calculated.

According to the function of influencing factors, 27 influencing factors are classified to two categories, one is negative, the other is positive (negative: the vulnerability will increase when the value of influencing factor increases. positive: the vulnerability will decrease when the value of influencing factor increases).

The influencing factors increasing the vulnerability includes: population density, percent of female, percent of ethnic minorities, percent of population under 5 years, percent of population over 65 years, percent of illiterate, percent of divorcee, percent of temporary population, rate of unemployment, percent of farming, forestry, animal husbandry and fishery, percent of mining, percent of construction, percent of carrying trade, Engel coefficient and percent of old houses. Other influencing factors decrease the vulnerability.

Due to the two functions play a contrary part in the vulnerability, the data's polarity must be transformed. Finally, all influencing factors have the positive correlation with vulnerability.

4.2 Calculating the vulnerability scores

After all data normalized by Z-score method, the data of influencing factor which decreases the vulnerability should multiply -1, then 27 final data which through normalization and polarity transformation will be obtained. Now, two methods can be used to calculate the social vulnerability index (SOVI), linear and nonlinear weighted integrated function method, respectively. The characteristic of later method adapts to condition which has intensive relationship of each indices and former method is contrary. Because every index is independent in this study, the linear weighted integrated function method is used to calculate the SOVI(Yi Ge, 2006). The equation is below:

$$SOVI = \sum_{i=1}^{27} (w_i \cdot x_i) \quad (6)$$

I(1-27): each 27 influencing factors.

w_i : the weight of each influencing factor.

x_i : the handled final data of every areas

The SOVI is a relative value through this method, and it can compare the vulnerability of 333 areas. As shown from the data, the SOVI of Beijing is between -0.5 and 0.5.

SOVI<-0.5: the vulnerability of the area is very low

-0.5<SOVI<0: the vulnerability of the area is lower, the ability to resist disaster is higher

0<SOVI<0.5: the vulnerability of the area is higher, the ability to resist disaster is lower

SOVI>0.5: the vulnerability of the area is very high

The SOVI of integrated social vulnerability equals the summation of the SOVI of population vulnerability, career vulnerability, economic vulnerability and infrastructure vulnerability.

5. RESULTS

5.1 Distribution of Beijing's vulnerability

The distribution of Beijing's social vulnerability is shown in Fig.2. Fig.3 shows the distribution of social vulnerability of central Beijing. Blue shows the lowest vulnerability and red shows the highest vulnerability and the intermediate stage is gradual changed from one color to another.

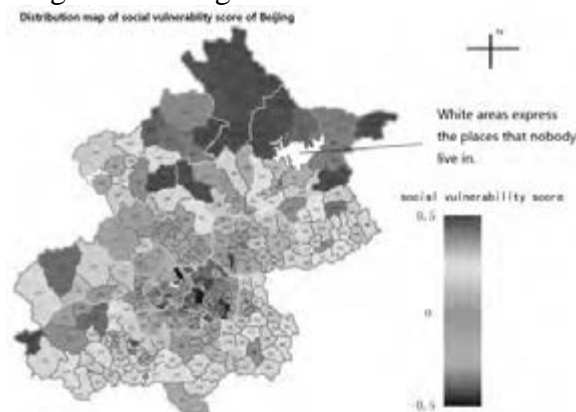


Figure 2: Distribution map of social vulnerability of Beijing



Figure 3: Distribution map of social vulnerability of central Beijing

The map (Schmidtlein et al., 2008) of Beijing's social vulnerability distribution is drawn according to the relationship of SOVI and colors. It can be seen that the social vulnerability in the center is lower than that in the suburban in spite of high population density in the center. This is because

that there are better personnel quality, economy and infrastructure in the center.

5.2 Sensitivity analysis

Analysis steps are below:

- (1) All processed data will be listed and each influencing factor must be multiplied by a coefficient (>1), the coefficient ($=5$) is set in this study (The value of coefficient doesn't influence the result, it only increases the diversity of each data. But we should attention that the coefficient must be smaller than 1.0. At first, the first influencing factor is multiplied by 5 in the case that other influencing factor's weights are maintained to be constant.
- (2) To assure that the proportion of other 26 influencing factor's weights are constant, we adjust other 26 influencing factor's weights and let the sum of these 27 influencing factor's weights equal 1. The method is as follow: Before the calculating, each influencing factor's weights are assumed to be $X_{m1} \dots X_{m2}$, and each new weights after the calculating are assumed to be $X_{n1} \dots X_{n27}$. The equation is :

$$X_{np} = \frac{X_{mp} \cdot (1 - C \cdot X_{mq})}{(1 - X_{mq})} \quad p, q \in [1, 27] ; p \text{ and } q \text{ are integer} \quad (7)$$

X_{np} : the new influencing factor's weights after calculating

X_{mp} : the original weights of soluted influencing factor

X_{mq} : the original weights of changed influencing factor

C: the coefficient. In this study, we define it to be 5.

The 27 new influencing factor's weights can be calculated, and a 27×27 data array can be obtained.

- (3) The new vulnerability scores are obtained through the 27-arrays data's calculating of each area. The sensitivity is defined to be the difference between the original normal vulnerability scores and the new vulnerability scores. The higher the value of sensitivity is, the bigger the influence of this influencing factor is. We can turn the value to a curve to reflecting the sensitivity of influencing factors of each area and it's easy to get the characteristics of sensitivity changing.
- (4) The most sensitive influencing factor can be found. The vulnerability level can be improved efficiently through improving the influencing factor.

The result of sensitivity analysis can be obtained through the above method. We can improve their vulnerability level through the sensitivity analysis, and it contributes to the urban plan and construction of Beijing.

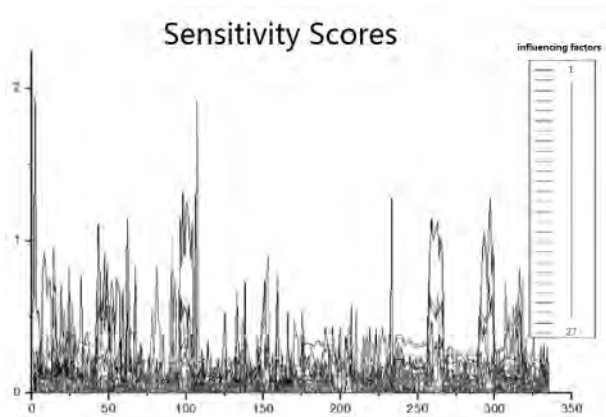


Figure 4: Sensitivity analysis result

ACKNOWLEDGEMENT

This work was supported by National Natural Science Foundation of China under Grant No. 71173128 and Ministry of Science and Technology of the People's Republic of China under Grant No. 2011BAK07B02.

REFERENCES

Barry E. Flanagan, Edward W. Gregory, Elaine J. Hallisey, Janet L. Heitgerd, Brian Lewis, 2001(8). *A Social Vulnerability Index for Disaster Management*. Journal of Homeland Security and Emergency Management 3,1-22

Christopher G. Burton, 2008(4). *Social Vulnerability and Hurricane Impact Modeling*. Risk Analysis, 58-68.

Jose Manuel de Oliveira Mendes, 2010(1). *Social vulnerability indexes as planning tools: beyond the preparedness paradigm*. Nature Hazards Review, 59-68.

Kun Wang, Haizhou Song, 2003(6). *The comparison and analysis of three objective weighted methods*. Technical economy and management research, 48-49

Susan L Cutter, Bryan J Boruff, W Lynn Shirley, 2003. *Social Vulnerability to Environmental Hazards*[J]. Social Science Quarterly, 84:242-261.

Xueqiang Shan, 2010(5). *System Research of Risk Evaluation on Primary and Secondary Schools' Emergent Events*, Department of Engineering Physics of Tsinghua university.

Yi Ge, 2006(4). *Research of social vulnerability committed by flood-taking -----Changsha, Hunan as example*. The research institution of disaster and public safety in school of resource, Beijing Normal university.

Flood and debris flow disaster management of Mae-Ngon basin Fang District Chiangmai Province

Januwat Leardsiljalearn¹ Chatchai Pedugsorn²

¹ Engineering Branch Director, ² Head of Dam Safety Management, Regional Royal Irrigation Office No.1, Royal Irrigation Department

ABSTRACT

Debris flow disaster occurred in Mae-Ngon basin 3 times in 40 years, recently 9 October 2006, there are 7 people death and 638 million bath loss. Flood and landslide sediment are studied by ground survey, soil survey, geological survey and laboratory testing for debris flow properties. Result shows that landslide sediment volume are about 343,148 m³ consisting of course particle (boulder, cobble, gravel) 47,548 m³, fine particle (sand) 236,480 m³ and soil particle (silt & Clay) 59,120 m³. Landslide sediment volume is 127.54 times of erosion sediment volume or erosion sediment is 0.78 percent of landslide sediment. Debris flow properties such as Density of debris flow 1.690 ton/m³, Sediment concentration 0.636. From X-ray diffractometer test, rock name is Carbonate alterate Meta – pelite. Clay mineral consists of Quartz, Magnesiumcalcite and Dolomite. Composition of clay mineral is Illite. A group name for non-expanding. Rock property is durable from swelling and expanding under water condition. Rock mechanic testing is accomplished in Hoek & Brown (2006) system. Basement rock has GSI about 30 – 35. Flood and debris flow disaster management of Mae-Ngon basin by non-measuring structure can reduce erosion sediment only 0.78 percent. Measuring structure can control 99.22 percent of basin sediment. Slit sabo dam of Japan are modified for Mae-Ngon basin which can reduce construction cost about 50 percent. Openings of slit structure are designed follow “Mizuyama (1995)” trapping sediment corresponding to its gradation which allows water and finer particle pass through its structure and dissipate flow energy. The flow passes to downstream to sediment-water storage dam. Modification of sabo dam to multipurpose as water storage and trapping fine sediment which can be flushed to maintain storage while original sabo dam functions as sediment trap structure. Research output is construction drawing of flood and debris flow prevention structures suitable to Thailand.

Keyword : *Flood and Debris flow disaster Management of Mae-Ngon Basin, Landslide Sediment, Erosion Sediment, Debris Flow, Slit Sabo Dam and Sabo dam*

1. PROBLEM OF FLOOD AND LANDSLIDE

Flood and Landslide in Thailand

After 1970, Thailand is increasingly susceptible to flood and debris flow (table1). Year after year the flood and debris flow disaster is more severely damage to property and lives because more people settle in flood and debris flow area, land use change, climate change from global warming. Example of damage from flood and landslide are in table1.

*Table1. Damage from flood and landslide (Varakorn, 2003)
(Chatchai, 2010)*

Month/Year	Area	Number of Death
November 1970	Tapsagae District, Prajunb Provincence	12
January 1975	Ronpiboon District , Nakornsritamarig Province	58
December 1982	Sribanphot District, Patalung Province	4
November 1988	Pipoon District, Nakornsritomaraj Province	>200
August 1998	Kichakood District , Juntaburi Province	1
June 2001	Vangchin District , Phrae Province	>30
August 2001	Lomsak District, Petchaboon Province	135
October 2006	Fang District, Chiangmai Province	7

Flood and Landslide in Mae-Ngon basin

During 6-9 October 2006, there are heavy rains in Mae-Ngon basin. Rain gauge stations at Ang – Khang, Fang District, collect the following rain fall data

- 6 October 2006, 3.80 millimeter
- 7 October 2006, 24.60 millimeter
- 8 October 2006, 138.60 millimeter
- 9 October 2006, 34.40 millimeter

After 4 successive days of rain fall, flash flood and landslide occurs. Debris flow which consists of lumber, boulder, cobble, gravel, sand and mud bring about 7 people death and damage 13 villages. There are effected to 3,520 families and 9,390 rai of agriculture area. Public infrastructures are widely destroyed. Evaluation of loss is totally 638,859,687 baths (Figure1)

Mae–Ngon basin is in Fang district north of Chiangmai city about 154 km. by road No.107 (Chiangmai – Fang) Mae–Ngon basin has boundary area by following direction

- North: Myanmar and Mae-eye district, Chiangmai Province
- East: Mae-suai district, Chiangrai Province
- South: Chaiprakan district, Chiangmai Province
- West: Myanmar

Research area is in Mae–Ngon Sub district, Fang District of Chiangmai Province at 47 QNC 173 – 060 (051729 mE,2206048 mN) 4848–IV Sheet, L7017 Series by military map

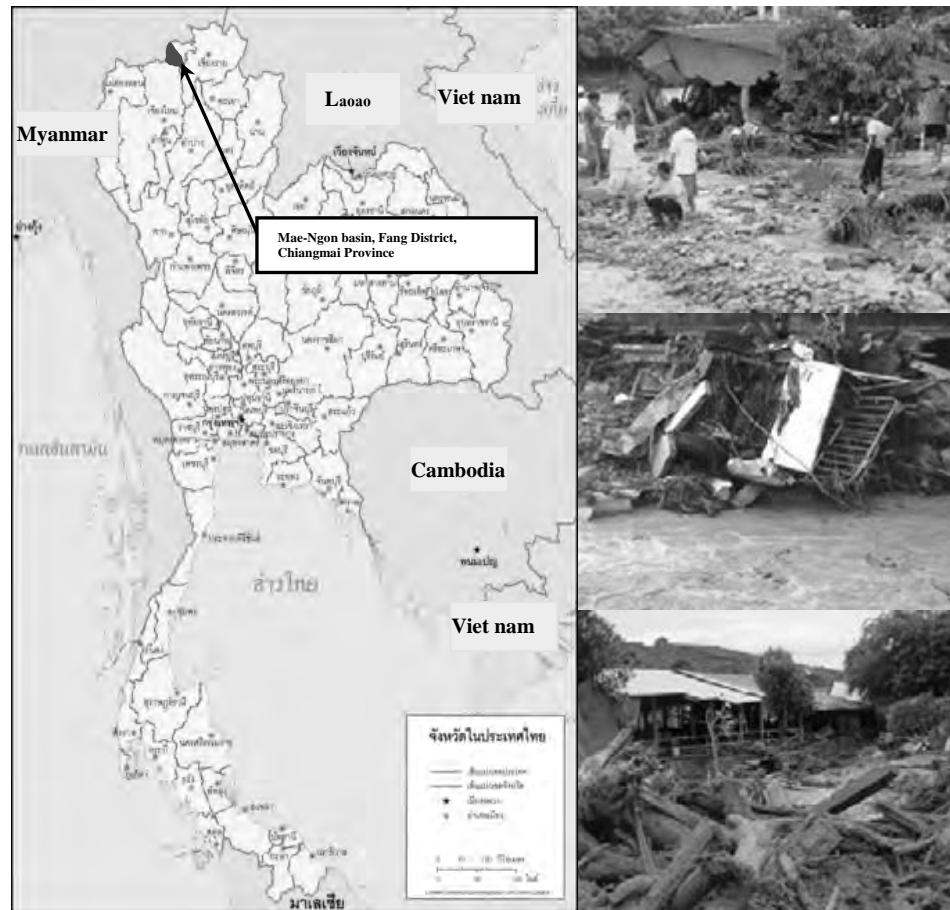


Figure: Location of Mae-Ngon basin in Mae-Ngon Sub district, Fang District Chiangmai Province and damages from Debris flow in 9 October 2006

Objective of study

The research objectives are to study about flood and landslide management of Mae-Ngon basin by measuring structure and non-measuring structure. Objective of measuring structure proposed on suitable of structure for Mae – Ngon basin while objective of non-measuring structure is participatory of community.

Methodology

The methodologies of this research are 4 steps

- 1) Study the properties of landslide sediment of Mae – Ngon basin, by ground survey, soil survey and geological survey.
1. Ground survey is investigated the depth and boundary of landslide sediment deposition (Figure2.)

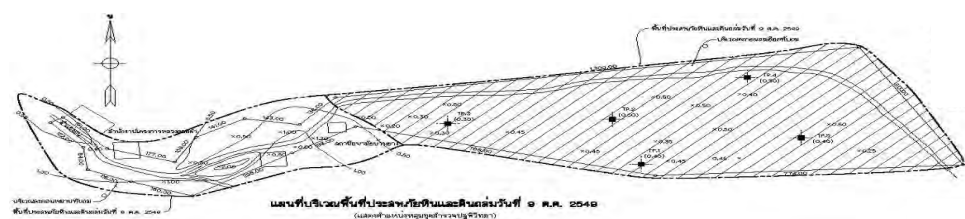


Figure 2: Boundary of land slide sediment deposit, by ground survey

2. Soil survey and geological survey

Landslide sediment deposition is investigated by hand auger drilled from deposition surface to original ground surface. Depth of landslide sediment deposition is the difference between deposition surface and original ground surface. Sample of landslide sediment are collected by test pit (Figure 3.). The objective of soil survey and geological survey are to investigate the boundary and depth of coarse sediment (boulder, cobble, gravel), fine sediment (sand, silt&clay) and to collect sediment sample.

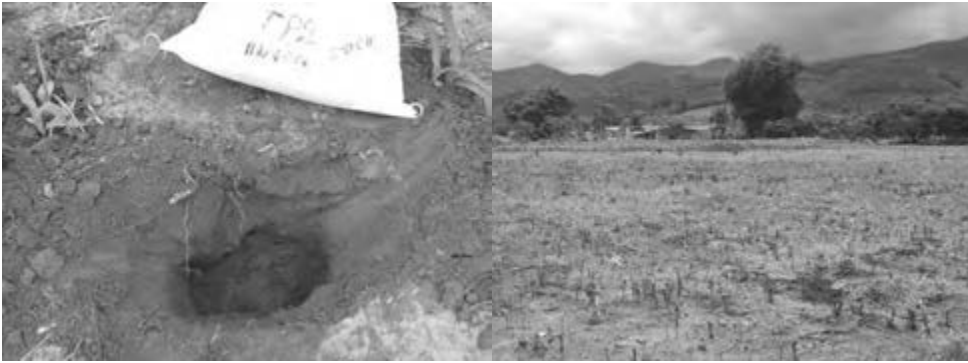


Figure 3: Sample of landslide sediment collected by soil survey in deposition area

2) Study the geological property of Mae-Ngon basin basement foundation

1. Geological survey at proposed sediment – water storage dam

Two proposed sediment – water storage dam site are bored totally 190 m. Location of bore hole are left abutment, river bed and right abutment as show in Figure 4.

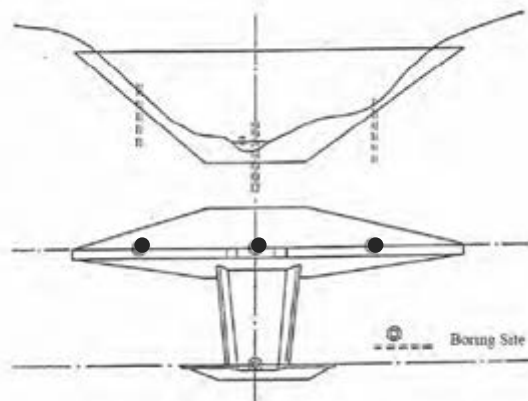


Figure 4: Location of bore hole along sediment – water storage dam axis

2. Rock testing

Rock sample from dam foundation are testing in both rock mechanic Laboratory and lithology and petrography Laboratory



Figure.5 Rock sample preparation for rock mechanic testing

Clay minerals are investigated by X – ray Diffractometer. Engineering properties of rock sample are tested by Hoek & Brown (2006) system to evaluate strength of rock mass from intact rock

3) Study measuring structure for flood and landslide sediment of Mae – Ngon basin

Detail designs are accomplish. Course sediment trap structure that suitable for flood and debris flow of Mae–Ngon basin is design following physical model of “Mizuyama at el (1995)” (Figure6.). Relation of sediment trap and dimensionless parameters are used equation 1.

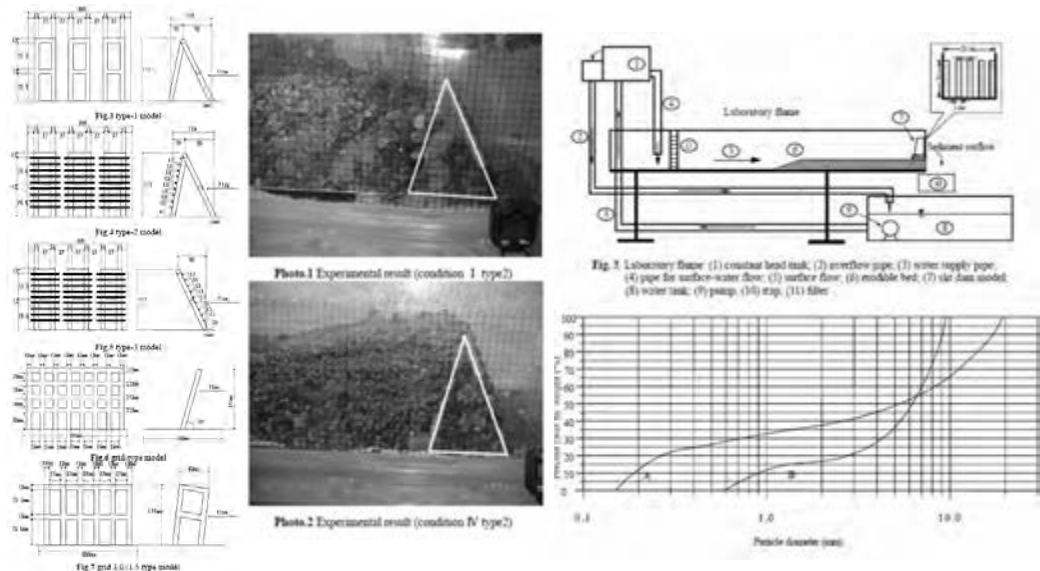


Figure 6: Physical Model study the relation of opening size and sediment trap “Mizuyama et al (1995)”

Mizuyama et al (1995)

$$eq.1 \quad S_T = \frac{4.39 (V_{sa}/V_m)^{0.506} (1-\sum b/B)^{1.0} C_a^{0.808}}{(b/D_{max})^{0.207}}$$

eq. 2
$$S_T = \frac{V_{sa} - V_{sb}}{V_m}$$

Where

S_T = Sediment storage rate ($0 \leq S_T \leq 1.0$)

V_m = Maximum sediment deposited volume at dam upstream

V_{sa} = Sediment volume in the debris flow before passing through a slit dam.

V_{sb} = Sediment volume in the debris flow after passing through a slit dam.

Σb = Total spacing of slit dam

B = Channel width

C_a = Sediment Concentration

D_{max} = Maximum diameter of sediment

- 4) Study of non-measuring structure and participatory of people in Mae–Ngon basin.

Participatory in Mae–Ngon basin are set by several government officer groups such as Royal Irrigation Department, Land Development Department and Huaihongkrai Royal Development Study Center. Meeting are at Mae – Ngon Sub district office, 1 April 2010, there are totally 42 people (35 male, 7 female) meeting (Figure7).



Figure 7: Non-measuring structure and participatory of Mae – Ngon basin

Research result

- 1) Damage areas of Mae – Ngon basin, 9 October 2006, (Figure.8) are caused by landslide sediment. Land slide sediment composes of boulder, cobble, gravel, sand and mud flowed under non-cohesive condition. As it flows with high velocity, it has high impact force. The debris flow has high potential of destruction. The result from laboratory test shows that landslide sediment has 127.54 times over erosion sediment volume. The result of this study corresponding to “Tera L. Curry (2007)” that conduct comparison study between land slide sediment and erosion sediment of Redwood Creek basin, north coastal California, USA, 244 square kilometers. Tera L. Curry (2007) analyzed recorded data from 1954 to 1981 and found that land slide sediment at fault zone of river basin has more than 100 times of erosion sediment volume.



Figure.8 Area of land slide and damage area by land slide sediment

- 2) Properties of landslide sediment of Mae – Ngon basin. From survey and laboratory testing, the significant debris flow properties are as following.
- 2.1 Volume of course sediment (Boulder, Cobble, Gravel) = 47,548 m³
 - 2.2 Volume of fine sediment (Sand, Silt & Clay) = 295,600 m³
 - 2.3 Area of course sediment deposit (Boulder, Cobble, Gravel) = 190,790 m²
 - 2.4 Area of fine sediment deposit (Sand, Silt & Clay) = 496,104 m²
 - 2.5 Fine sediment is consisting of sand 80 percent and silt & Clay 20 percent.
 - 2.6 Density of Debris Flow = 1.690 ton/ m³
- The result show that density of debris flow of Mae – Ngon basin is lower than density of debris flow in Japan river basin (Table 2)
- 2.7 Sediment Concentration, $C_d = 0.636$
 - 2.8 Peak Discharge of Debris Flow, $Q_s = 53.118 \text{ m}^3/\text{sec}$
 - 2.9 Erosion Sediment = 2,690 m³/year
 - 2.10 Ratio of landslide sediment to erosion sediment = 127.54:1
 - 2.11 Gradation of fine sediment (Sand, Silt & Clay) from laboratory test is show in Figure 9.

Table 2: Density of debris flow comparison between Mae – Ngon basin and Japan river basin

River	Maximum	Minimum	Average
Mt Yake	2.110	1.631	1.861
Nojiri River	2.039	1.121	1.784
Mae – Ngon River basin	-	-	1.690

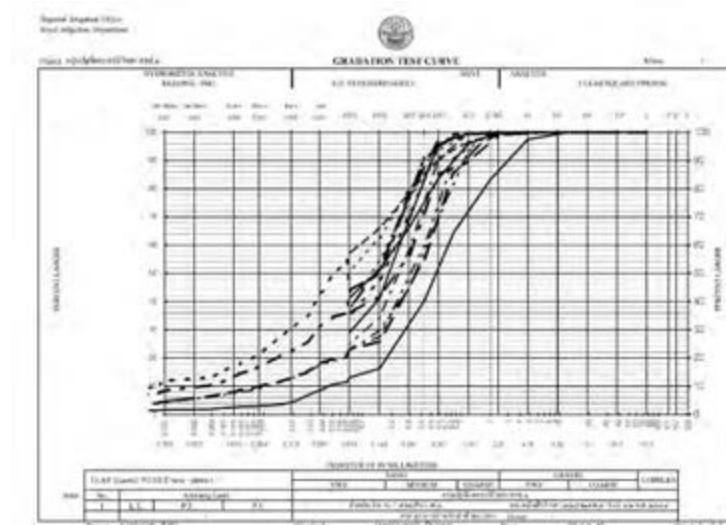


Figure 9: Gradation of fine sediment (Sand, Silt & Clay)

3) Geological and propertied foundation

3.1 Basement at sediment-water storage dam1 and dam2 are supported by sandstone shale and altered Cambrian siltstone, named Carbonate Alterate meta-pelite (meta-sandstone//Meta-mudstone) by testing for optical properties

3.2 Geological foundation along centerline of sediment-water storage dam1 and dam2 consist of shale and altered sandstone. Weathering condition is moderately to highly weathering. Shallow shale has high permeability while deeper have moderate to high permeability.

3.3. Stability of abutment is susceptible to sliding. Topography of steep slope appears the collapse of slope that characterize the rock fall and slide of soil and land mass. As a result of landslide hazard may induce some sliding around reservoir rim.

3.4 By analysis type of clay minerals using X – ray diffractrometer, basement rock consist of Quartz Magnesiumcalcite Dolomite. The composition of clay minerals is Illite, a group name for non – expanding so properties of rock is durable to swelling and decomposition.

3.5 Engineering and Physical properties of basement rock. The factors that affect rock mass and rock movement are discontinuities and weathering of rock. From lithology, basement rocks are meta-sandstone, meta-siltstone and meta-mudstone. Structure and discontinuities of rock are estimate by GSI value as follows

3.5.1 Sediment-water storage dam1, sandstone siltstone and mudstone are altered. Discontinuity is Blocky/Disturbed/Seamy – Blocky and surface is smooth to slickenside that related high altered minerals, estimate the GSI value about 30 -55

3.5.2 Sediment-water storage dam1, sandstone siltstone and mudstone are metamorphosed like phyllite. Discontinuity is Very Blocky – Blocky and surface is smooth to slickenside and both altered minerals occurs thus the GSI value is 30 -55 (Figure.10)



Figure 10: GSI of Sediment-water storage dam1 and Sediment-water storage dam2

4) Result of flood and landslide management of Mae–Ngon basin by measuring structure.

Sediment–water storage dam for Mae – Ngon basin should compatible to steep canyon. Sabo Dam of Japan is chosen as prototype due to similarity of dam site and objective. Modification of sabo dam to multi purpose dam that function as water storage and sediment trap structure can benefit both irrigation purpose and disaster management. As debris flow occurs 3 times in 40 years, the rest of critical time the dam are used as storage dam. The adjustment is installing of 4 gate valves at downstream opening and operating bridge. When basin is in critical API (Antecedent Precipitation Index), gate valves are automatically full open in that condition it function as original sabo dam. The gate valves are control by telemettering system. Sediment-water management due to relation of storage function and sediment concentration. Sediment deposit can be flushed out after debris flow stop. Due to similarity of dam site and river basin, sabo dam are chosen as prototype for modification. Both Japan river basin and Mae–Ngon river basin are similarity (Figure. 12) such as steep slope of river bed, stability of geological foundation, requirement of self cleansing. Comparisons are in table 3

Table 3 Comparison objective between original sabo dam and Modification for Mae – Ngon basin

Original sabo dam	Modification for Mae – Ngon Basin
<ul style="list-style-type: none"> • For flood protection • For debris flow protection 	<ul style="list-style-type: none"> • For flood protection • For debris flow protection • Storage water for Irrigation purpose • Storage water for water supply purpose • For recreation and tourism

General lay out of sediment trap structure and sediment – water storage dam are in Figureure 11

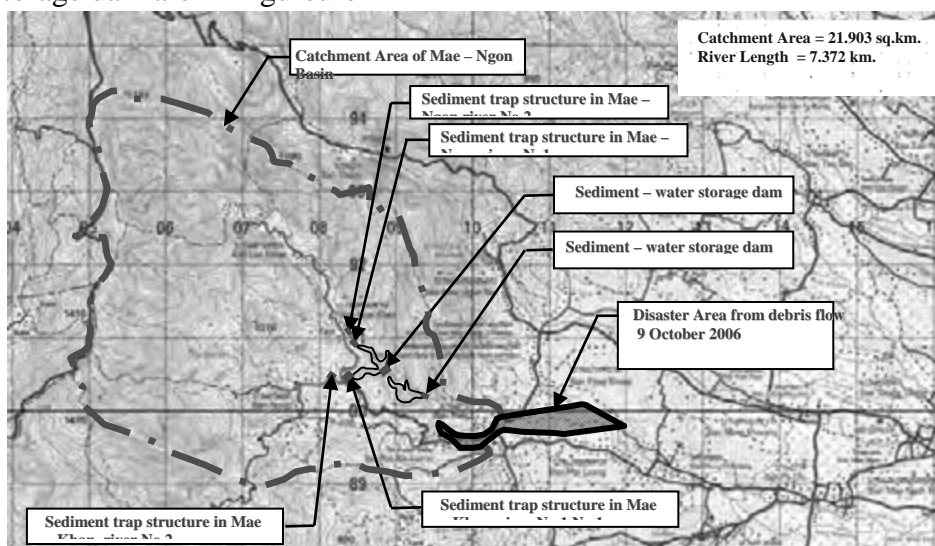


Figure 11: Location of sediment trap structure and sediment – water storage dam



Figure 12: Similarity of Sediment – water storage dam site No.1 (Left) and original sabo dam (Right)



Figure: 13 Original sabo dam of Japan for Nagano city protection

Original Sabo dam of Japan is single purpose of disaster protection structure (Figure. 13)



Figure 14: Sediment–water storage dam No.2 of Mae–Ngon basin

Design criteria for sediment trap structure of Mae – Ngon basin are follow “Mizoyama (1995)” to catch coarse particle. The sediment that gradation matches to opening size is deposit in front of structure. Original slit sabo dam of Japan (Figure. 15) are modified so that new pattern can save the construction cost more than 50 percent. The modification is necessary due to material should be easily to supply and to construct in steep area. Sediment trap structure of Mae – Ngon is show in Figure. 16 and Figure 17.



Figure 15: Original slit sabo dam of Japan

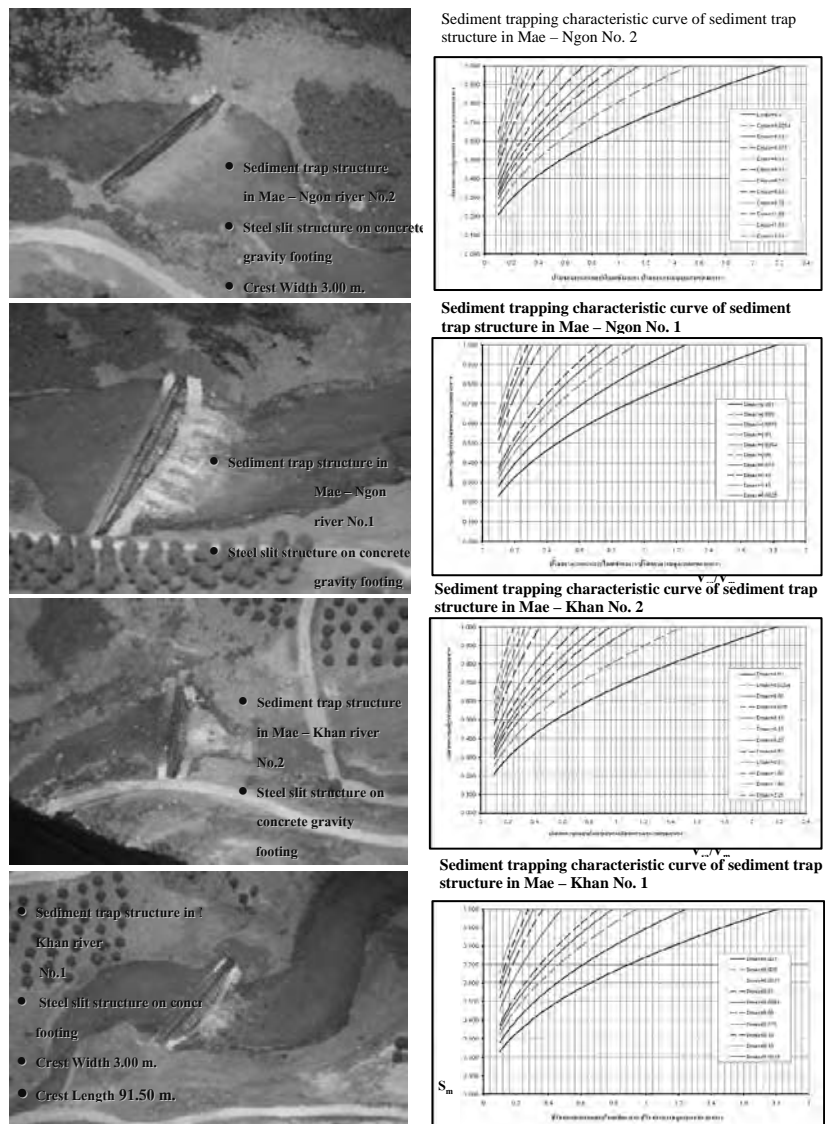
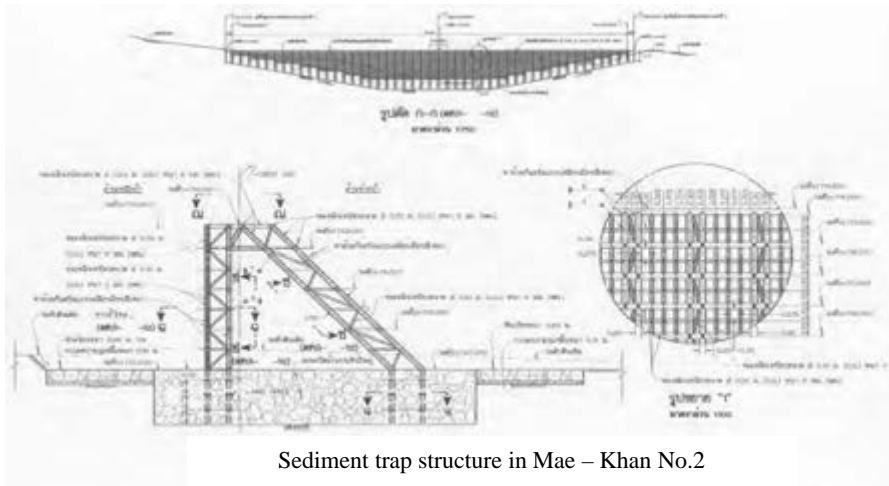
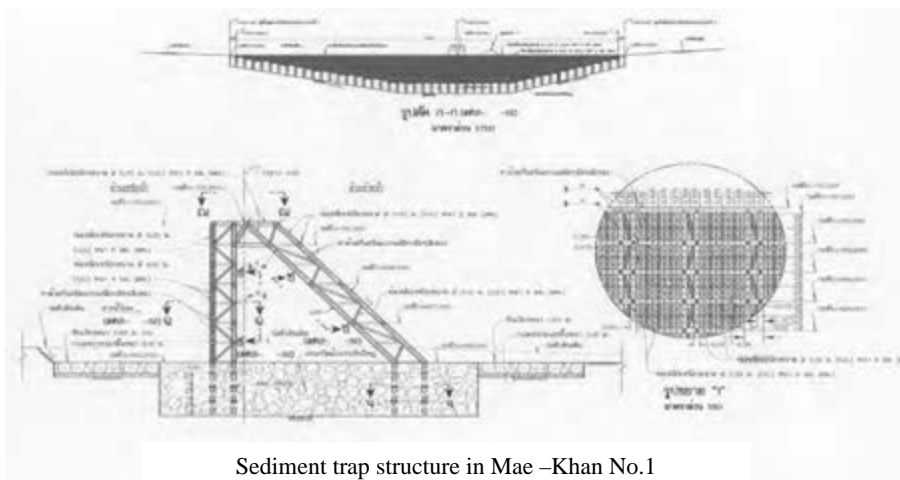


Figure 16: Sediment trap structure and sediment trap behavior



Sediment trap structure in Mae – Khan No.2



Sediment trap structure in Mae –Khan No.1

Figure 17: Sediment trap structure for Mae-Ngon basin

5) Result of flood and landslide management of Mae-Ngon basin by non-measuring structure by participatory and awareness of community.

5.1 People take part in this project can get all project information they express very good to excellent satisfied about 84.76 percent.

5.2 People participated this project can share idea and set plan to manage flood and debris flow of Mae-Ngon basin. People receive project information, fact so that they can set suitable non-measuring structure following their need. Participatory from community can reduce conflict to the project. By questionnaire evaluation they feel very good to excellent about 86.90 percent.

5.3 What people need from this research project during participatory meeting is they want to take part in making management plan about flood and landslide by non-measuring structure. The summaries of people need are as following :

1. People need reservoir in Mae – Ngon sub district to solve flood and debris flow and to storage the water for dry season.
2. People request for reservoir to prevent flash flood.
3. People want reservoir and irrigation system for high land agriculture activity.

4. People need social measuring to increase quality of life.
5. They want project that enhance occupation and agricultural which reduce the use of chemical substance.
6. They want retaining wall along Mae – Ngon river bank to protect erosion and increase efficiency of drainage
7. People want to know project information and to enhance the participation for every kind of project (Small medium and Large sole) and every process of project (Before during and after construction).
8. They need field trip to learn from other basin that success from flood and landslide management by non-measuring structure.

Conclusion of Research

1) Damage area from flood and debris flow is in Mae–Ngon basin. The disaster occurs on 9 October 2006. 13 Village and 3520 family effect from debris flow, 7 people death and 12 people wounded. Direct and indirect loss is totally 638,682,682 baths. The loss is cause by debris flow which composed of lumber, boulder, cobble, gravel, sand and mud. As debris flow with high velocity and no cohesion, it has high potential of devastation. Land slide sediment volume is 127.54 times over erosion sediment volume.

2.) To manage flood and land slide of Mae – Ngon basin, It need measuring structure together with non- measuring structure. Non-measuring structure can control only erosion sediment that limitation is 0.78 percent of total basin sediment. Non-measuring structure cannot control landslide sediment 99.22 percent of total basin sediment. Using only measuring structure is not sustainable, because. It lack of participatory and collaboration from community.

3.) Relocation by moving community out of risk area is not feasible and not possible, compare with measuring structure. Relocation has social effect moreover it shift the problem from Mae – Ngon basin to another basin. Flood and landslide management by relocation is not sustainable.

4.) In case of limitation of budget, construction should can accomplish in 2 phase

First phase construct sediment–water storage dam No.1 together with sediment trap structure in Mae –

Ngon No.1 and sediment trap structure in Mae–Khan No.1.

Second phase construct sediment–water storage dam No.2 together with sediment trap structure in Mae –

Ngon No.2 and sediment trap structure in Mae–Khan No.2.

Benefits of measuring structure are flood and debris flow protection and water usage. It is feasible if

Compare with investment cost.

5.) Management of sediment–water storage dam should use application of real time telemetering. Real time telemetering which monitoring soil moisture and rain fall forecast before critical condition of landslide. Operating gate of the dam can control by telemetering that can change purpose from storage dam to debris flow protection.

Mae–Ngon basin should have warning system. CCTV and movement sensor should be installed along the river to detect debris flow and warning to people living in risk area. By this mean people have enough time to excavate.

Recommendations

1. Physical Model of 4 sediment trap structure and 2 sediment–water storage dam should be study in laboratory. Physical model should focus of hydraulic properties and sediment trap behavior to recheck the design.
2. API and other Indicators of land slide and debris flow should be study that can apply with flood and land slide Management

ACKNOWLEDGEMENT

The author wishes to express most profound gratitude to National Research Council of Thailand (NRCT) and Royal Irrigation Department (RID) executives.

1. Mr.Chalit Damrongsak, Royal Irrigation Department Director
2. Mr.Suthep Noipairoi, Hydrology and Water Management Office Director
3. Mr.Venai Phongjinda , Regional Royal Irrigation Office No.1 Director

REFERENCE

Ashida, K. and Takahashi, T. 1980, Study on debris flow control-hydraulic function of grid type open dam, *Annuals. Disaster Prevention Res. Inst., Kyoto Univ., No. 23B-2, .pp. 1-9 (in Japanese).*

Fiebiger, G. 1997, Structures of debris flow countermeasures. *Proceedings, First International Conference on Debris-Flow Hazards Mitigation: Mechanics, Prediction, and Assessment: pp. 596-605, New York: ASCE.*

Food and Fertilizer Technology Center. 1995, *Soil conservation handbook. Food and Fertilizer Technology Center for the Asian and Pacific Region, II-41.*

Gregoretti, C. 2000, The initiation of debris flow at high slopes: experimental results. *Journal of Hydraulic Research, Vol. 38, No. 2, pp. 83-88.*

Heumader, J. 2000, Technical debris-flow countermeasures in Austria – a review. *Proceedings, Second International Conference on Debris-Flow Hazards Mitigation: Mechanics, Prediction, and Assessment: pp. 553-564, Taipei, Taiwan: ASCE.*

Ikeya, H. and Uehara, S. 1980, Experimental study about the sediment control of slit sabo dams. *J. of the Japan Erosion Control Engineering Society, Vol. 114,.pp. 37-44. (in Japanese)*

Innes, J. L. 1983, Lichenometric dating of debris-flow deposition in the Scottish highlands. *Earth Surface Processes and landforms, Vol. 8, pp. 579-588.*

Johnson, P. A., and Richard, H. M. 1989, Slit dam design for debris flow mitigation. *Journal of Hydraulic Engineering*, ASCE, Vol. 115, No. 9, pp. 1293-1296.

Lien, H. P. and Tsai, F. W. 1999, Volumetric sediment concentration in debris Flow. *International Journal of Sediment Research*. Vol.14, No.3, Sep., pp. 23-31.

Lien, H. P and Tsai, F. W. 2000, Debris flow control by using slit dams. *International Journal of Sediment Research*, Vol. 15, No.4, pp. 391-409.

Lin, P. S. and Lin, J.Y. 1999, The impact force and countermeasure structures of debris flow. *Sino-Geotechnics*, No.74, .pp. 67-80 (in Chinese).

Melis, T. S., Webb, R. H. and Griffiths, P. G. 1997, Debris flows in Grand Canyon national park: peak discharge, flow transformations, and hydrographs, *Proceedings, First International Conference on Debris-Flow Hazards Mitigation: Mechanics, Prediction, and Assessment*: pp. 5727-736, New York: ASCE.

Mizuyama, T., Suzuki, H., Oikawa, Y. and Morita, A. 1988, Experimental study on permeable sabo dam. *J. of the Japan Erosion Control Engineering Society*, Vol. 41, No. 2, pp. 21-25 (in Japanese).

Mizuyama, T., Kobashi, S. and Mizuno, H. 1995, Control of passing sediment with grid-type dams. *J. of the Japan Erosion Control Engineering Society*, Vol. 47, No. 5, pp. 8-13 (in Japanese).

Schilling, S. P. and Iverson, R. M. 1997, Automated, reproducible delineation of zones at risk from inundation by large volcanic debris flows. *Proceedings, First International Conference on Debris-Flow Hazards Mitigation: Mechanics, Prediction, and Assessment*: pp. 176-186, New York: ASCE.

Shih, B. J., Shieh, C. L. and Chen, L. J. 1997, The grading of risk for hazardous debris-flow zones. *Proceedings, First International Conference on Debris-Flow Hazards Mitigation: Mechanics, Prediction, and Assessment*: pp. 219-228, New York: ASCE.

Suwa, H., Yamakoshi, T. and Sato, K. 2000, Relationship between debris-flow discharge and ground vibration. *Proceedings, Second International Conference on Debris-Flow Hazards Mitigation: Mechanics, Prediction, and Assessment*: pp. 311-318, Taipei, Taiwan: ASCE.

International Journal of Sediment Research, Vol. 18, No. 1, 2003, pp. 74-87 - 85 -

Takahashi, T. 1991, Debris flow. *Monograph Series of IAHR*, A. A. Balkema, Rotterdam, The Netherlands, pp. 32-69.

Takahashi, T. 1997, Engineering problems in crossing potential debris flow ravines by bridges. *Workshop Series on Hazard Mitigation for Civil Infrastructures-Bridge Engineering*, Taiwan.

Tera L Curry 2007, A Landslide Study in Redwood Creek Basin, Northwestern California: Effect of the 1997 Storm, Master Thesis of Science in Environmental System: Geology, Humboldt State University: USA

Watanabe, M., Mizuyama, T, and Uehara, S. 1980, Review of debris flow countermeasure facilities. *J. of the Japan Erosion Control Engineering Society*, Vol. 115, pp. 40-45 (in Japanese)

Development of 3D viewer of flood disaster risk to enhance evacuation capacity of residents

Kohei MAKINODAN¹, Miho OHARA² and Kimiro MEGURO³

¹Master Student, Department of Civil Engineering,
The University of Tokyo, Japan
makinodan@risk-mg.iis.u-tokyo.ac.jp

² Associate Professor, Interfaculty Initiative in Information Studies
/ Institute of Industrial Science,
The University of Tokyo, Japan

³ Professor, Interfaculty Initiative in Information Studies,
/ Institute of Industrial Science,
The University of Tokyo, Japan

ABSTRACT

Eastern part of the Tokyo Metropolitan area has high risk of large-scale urban flood. Especially, Koto Delta Area whose elevation is lower than sea level is surrounded by rivers and expected to face severe problems of human evacuation in the future flood disaster. In order to reduce casualties due to the future flood disaster, it is important to encourage resident's awareness of the flood disaster risk and enhance their imagination capability of proper evacuation from their home to evacuation centers.

In this research, 3D viewer of flood disaster risk was developed as an educational tool for enhancing evacuation capacity of residents. This viewer can show 3 dimensional images of geography, building and estimated water level of the flood. Prototype system was developed using the data in Koto Delta Area. Residents can check the location of evacuation centers and difficulty in access to each evacuation center in the 3D view. In order to discuss the difficulty in evacuation, proper understanding of varying water level, its velocity and hydrodynamic force in the time-history is necessary. In this viewer, dynamic changing of flood water is shown in 3D spaces and it can contribute to the real imagination of difficulties during evacuation. Finally, the viewer aims that residents can image appropriate action of emergent evacuation during flood disaster.

Keywords: urban flood, risk analysis, evacuation, 3D viewer

1. INTRODUCTION

Eastern part of the Tokyo Metropolitan area has high risk of large-scale urban flood. Especially, Koto Delta Area whose elevation is lower than sea level is surrounded by rivers and expected to face the severe problems of

human evacuation in the future flood disaster. In case flood risk increases, local municipalities are usually responsible to issue evacuation counsel or evacuation order to the residents in the dangerous area. However, casualties due to inappropriate evacuation during flood are reported every year in Japan. In order to reduce casualties due to the future flood disaster, it is important to encourage resident's awareness of the flood disaster risk and enhance their imagination capability of proper evacuation from their home to evacuation centers. In this research, considering whole Koto Delta as a study area, 3D viewer of flood disaster risk was developed as an educational tool for enhancing evacuation capacity of residents.

2. IMPACT OF LARGE-SCALE FLOOD ON KOTO DELTA AREA

According to the Cabinet Office in Japan, the maximum predicted number of death is approximately 3,500 and that of isolated people is approximately 720,000 in case the bank of Arakawa river collapsed as a consequence of increase water due to extreme heavy rain. This is an estimation when drainage pump station, drainage pump vehicle and water gate are unavailable. Figure 1 shows location of Koto Delta Area and point of dike break in this simulation.



Figure 1: Location of Koto Delta Area

According to past research (makinodan,2010), detail flood risk analysis of the area was conducted using GIS in a 125m-mesh with flood data from Cabinet Office and additional information such as population

distribution and building inventory. Figure 2 shows inundation depth and inundated area. In most of Koto Delta Area, inundation depth comes up 2m and the number of buildings in this area is 49,449 among total 114,646 buildings.

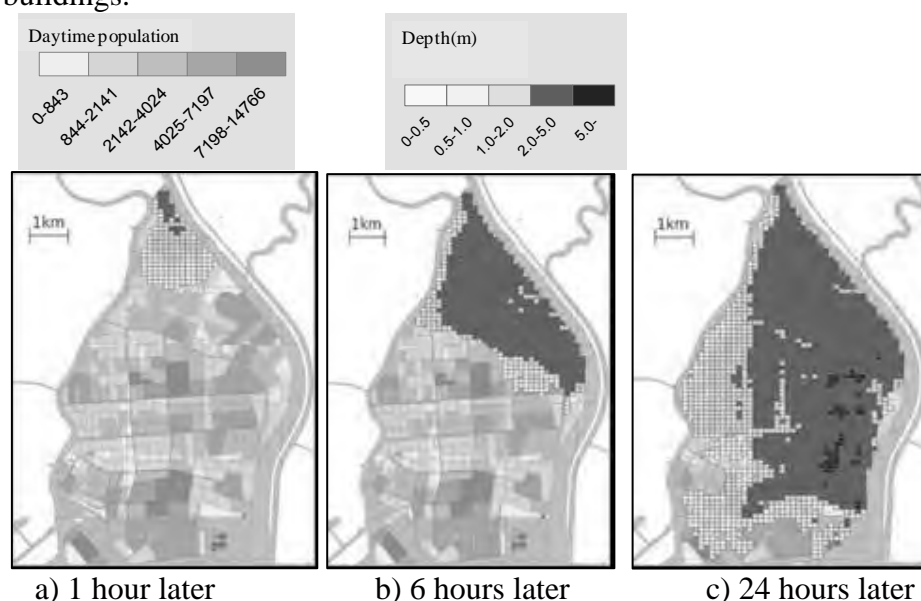


Figure 2: Alteration of inundated depth

3. CONCEPT OF A NEW EDUCATIONAL TOOL FOR ENHANCING IMAGINATION CAPABILITY

As an educational tool for flood disaster, a hazard map which shows inundation depth in each area is most popular in Japan. This map is prepared by municipalities and obligated to make under Flood Control Act. Also this map shows information about flood prevention and location of evacuation centers. Figure3 shows a hazard map in SUMIDA ward in Tokyo Prefecture, Japan.

However a hazard map has following problems.

- Alteration of flood with time history is not shown.
- It is difficult to understand real inundation depth.
- It is difficult to understand time to start evacuation and route to evacuation center.
- Suitable evacuation according to types of housing such as a single-family house or a collective housing is not properly instructed separately.

In order to solve these problems, 3D viewer of flood disaster risk was developed using VR space. Users can watch flooding condition varied with time-history from both bird's eye views and from views on ground level. Therefore, users can experience flood disaster with close realistic situation. Also, this system can help to understand difficulty in evacuation realistically. This function leads proper evacuation for residents. Figure 4 shows the proposed functions to be developed in the 3D viewer for solving current

problems of a hazard map.



Figure 3: Hazard map in SUMIDA ward

Problem of a hazard map	Proposed solution
<ul style="list-style-type: none"> Alteration of flood with time history is not shown. 	<ul style="list-style-type: none"> animation display (flood varied with time-history)
<ul style="list-style-type: none"> It is difficult to understand real inundation depth. 	<ul style="list-style-type: none"> 3D display, Display of difficulty in evacuation
<ul style="list-style-type: none"> It is difficult to understand timing to start evacuation and route to evacuation center. 	<ul style="list-style-type: none"> 3D display, walk-through, animation display, bird's eye views
<ul style="list-style-type: none"> Some types of evacuation is not shown depending on types of housing such as single-family house or collective housing. 	<ul style="list-style-type: none"> walk-through, animation display, 3D display

Figure 4: Proposed functions to be developed in the 3D viewer

4. DEVELOPMENT OF 3D VIEWER OF FLOOD DISASTER RISK

4.1 Used data in 3D viewer

As base data of system, 3D urban space data, digital cartographic data such as railway and park and flooding simulation data were used. As 3D urban space data, Map Cube (published by CAD CENTER CO.,Ltd), which was built up with high-accuracy laser ranging data constructed by PASCO Co.,Ltd and 2D map provided by INCREMENT P Co.,Ltd, was used.

Figure 5 shows formation of Map Cube and Figure 6 shows VRML data of railway, station and surface of water in Koto Delta.

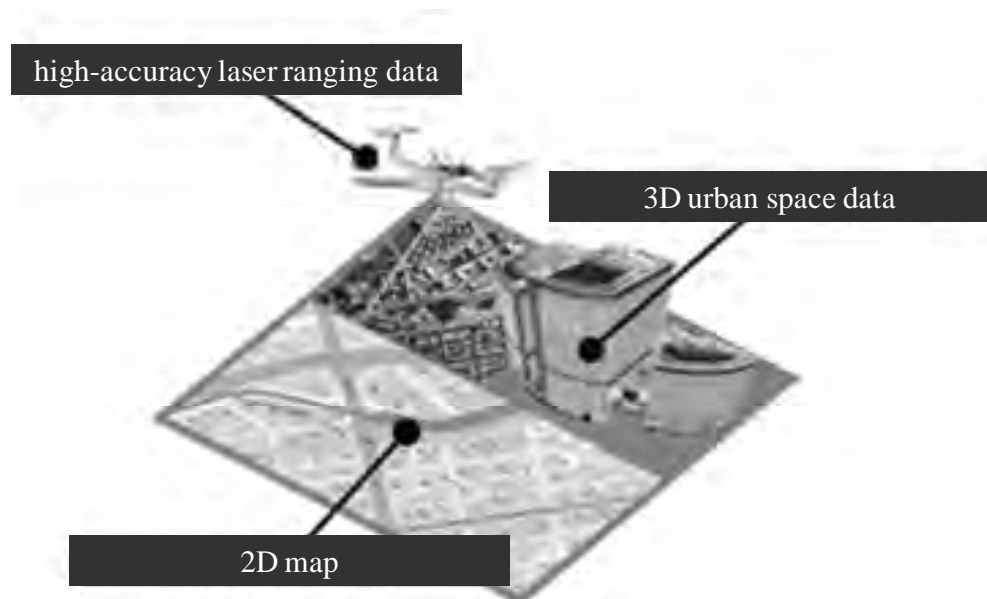


Figure 5: Formation of Map-Cube



Figure 6 : VRML data of railway, station and surface of water in Koto Delta

Ministry of land, Infrastructure, Transport and Tourism performed flood simulation in Arakawa-river. In this simulation, amount of rainfall which might occur once in 200 years was assumed. This simulation data consists of inundation depth, velocity and hydrodynamic power and mesh size is 125 meter. Although urban space data and digital cartographic data are static data, flood simulation data varied with time-history is a dynamic data.

4.2 Methodology

4.2.1 Difficulty in evacuation at the flood disaster

Although inundation depth, velocity and hydrodynamic power are important to understand flood risk, it is difficult to judge whether people can evacuate during inundation or not. In this research, difficulty in evacuation was determined by comparing inundation depth to maximum depth for walking calculated by equation (1). Figure 8 shows the area where adult male can't walk after flood occurs.

$$h_L = 0.7 \times (1 - u/2.5) \tag{1}$$

h_L : maximum depth for walking (m), u : velocity(m/s)

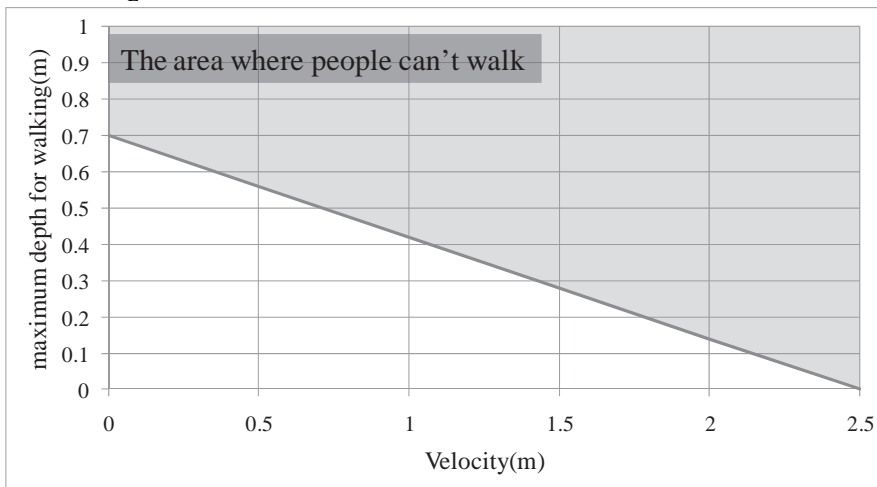


Figure 7: Relationship between maximum depth for walking and velocity (adult male)

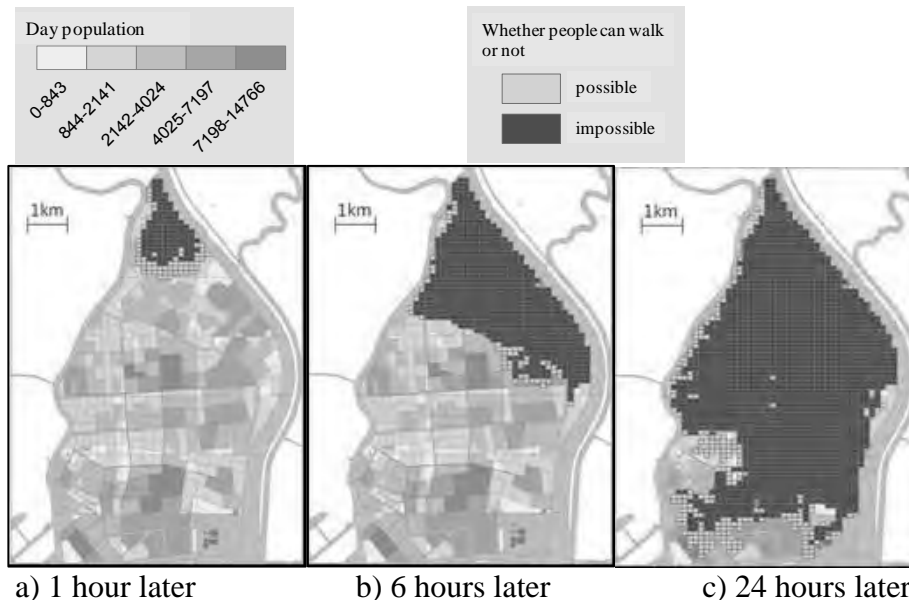


Figure 8: The area where it is impossible to walk (adult male)

4.2.2 Import of used data to 3D system

In order to combine all the data in 3D spaces, all data were needed to be converted to VRML (Virtual Reality Modeling Language) format and then imported to 3D spaces developed by “Omega Space” which is software by Solid Ray Corporation. VRML is a standard file format for representing 3D interactive vector graphics. Both dynamic and static data were layered in 3D spaces. 3D viewer system can show these VRML data according to time history. Figure 9 shows formation of system.

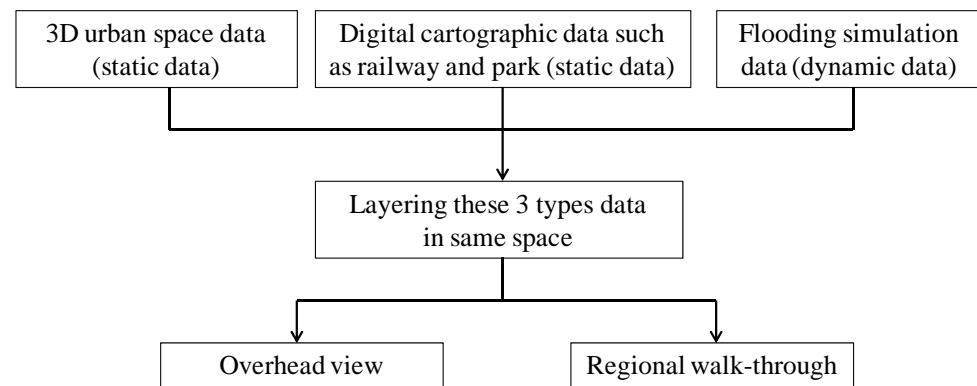


Figure 9: Formation of system

5. EXAMPLE OF SCREEN IMAGES BY 3D VIEWER

Figure 11 and Figure 12 show inundation depth on the 3D viewer. These 3D images can be projected on the screen. People can experience 3D simulation images with special glasses. In this research, compact 3D projector “Sight3D” (Figure 10) was used for projection. This projector has some merits that it can project 3D images without a special screen and it is portable as well. Figure 11 is a view without building images. Legend of inundation depth is shown on the lower right corner of screen and speed of playing and elapsed time are shown on the upper right corner. Part of aqua on the upper side of screen shows surface of river. As shown in figures 11 and 12, people can view the city from bird’s eye location and can watch flooded condition varied with time-history. By watching the flooding situation, user can know which buildings will be inundated. Figures 13 and 14 are views on the ground level. By using walk-through function on this screen, people can know inundation condition to the nearest evacuation center and change in inundation depth with time history.



Figure 10 : 3D projector and eyeglasses

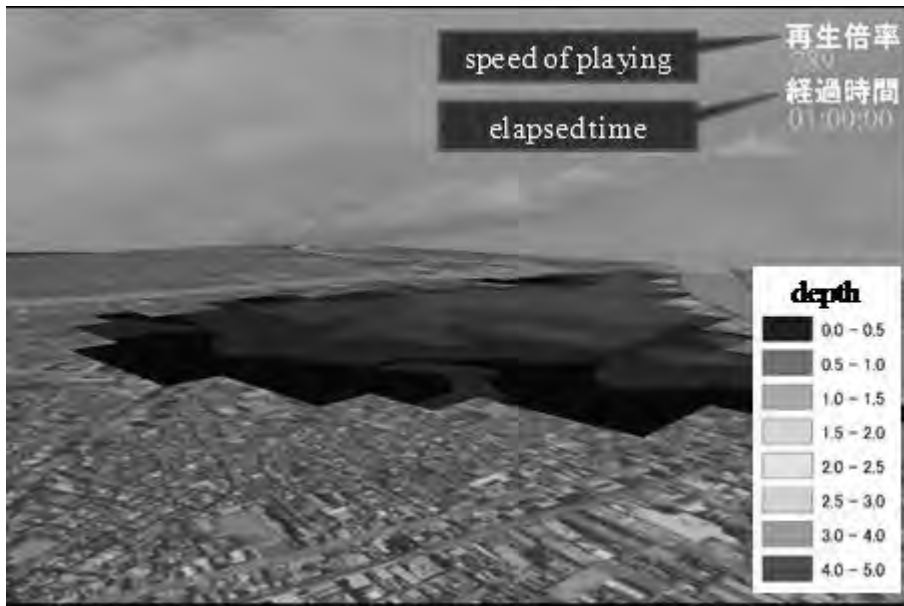


Figure 11: Inundation depth (without buildings)



Figure 12: Inundation depth (with buildings)

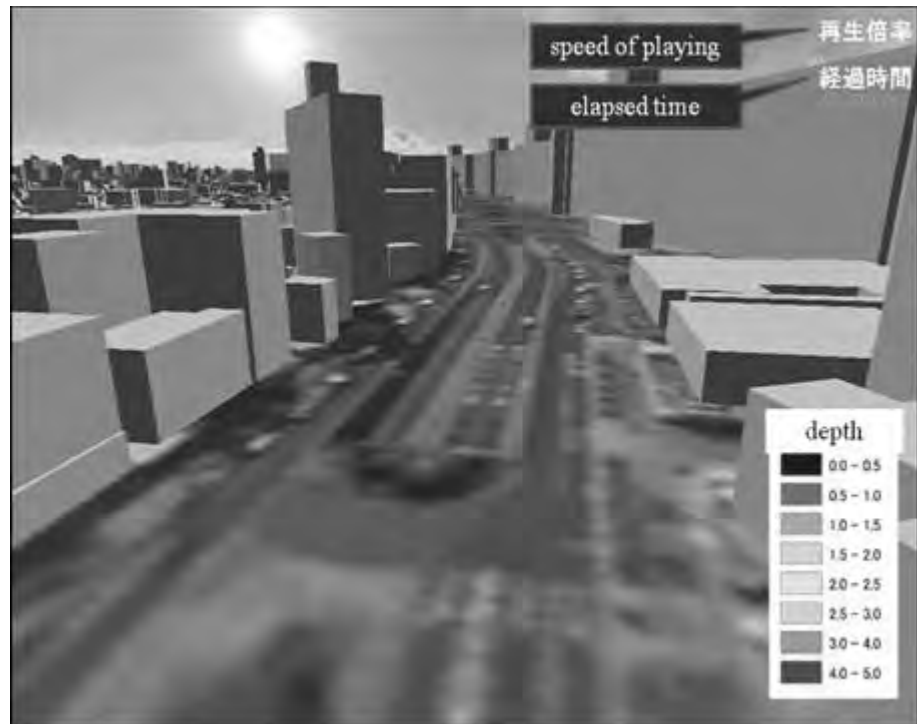


Figure 13: View from ground level (before flood)

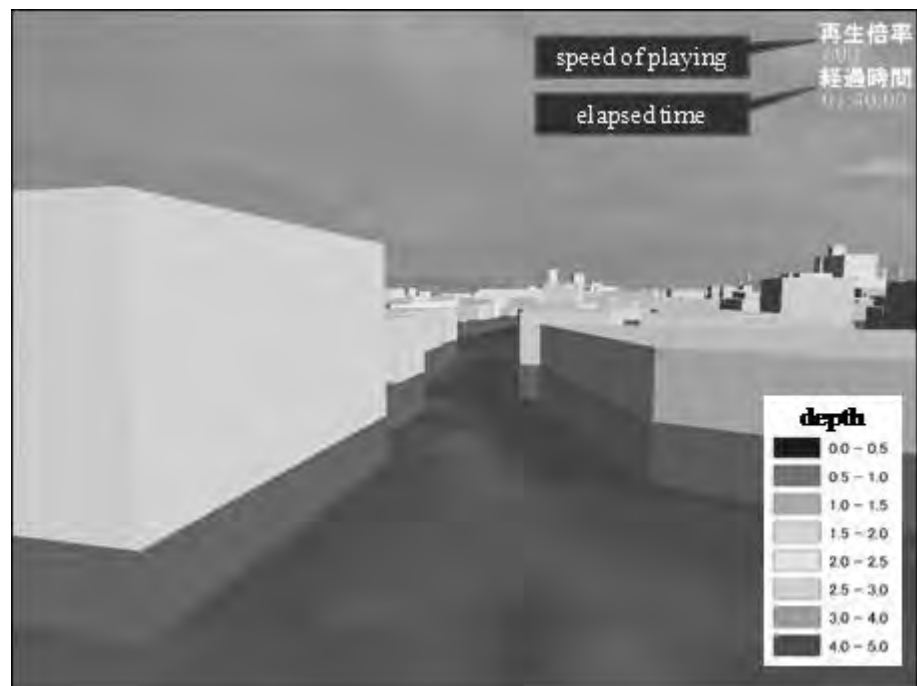


Figure 14: View from ground level (after flood)

6. CONCLUSIONS

In this research, 3D viewer of flood disaster risk was developed using VR space to fulfill deficiencies in current flood hazard maps. In addition to the current functions, several new functions which lead proper evacuation by resident are required to be imported in this system. In the future study, effect of the system should be evaluated through workshop with residents,.

REFERENCES

- Cabinet Office, Japan,
http://www.bousai.go.jp/jishin/chubou/suigai/100402/100402_shiryo_2.pdf,
2010, 4, 39-41.
- Bureau of Urban Development Tokyo Metropolitan Government,
Survey on Land Use in Tokyo Metropolitan Area.
- Kyozo SUGA, Preliminary Study on Feasible Safe Evacuation in
Flood Disaster, Annual Journal of Hydraulic Engineering, 1995, 2, 879-882

Sukhothai flood analysis and its response under climate changes

Patinya HANITTINAN¹, Anurak SRIARIYAWAT²,
and Sucharit KOONTANAKULVONG³

¹ Graduate Student, ² Instructor, ³ Associate Professor,
Department of Water Resources Engineering, Faculty of Engineering,
Chulalongkorn University, Thailand
Anurak.s@eng.chula.ac.th

ABSTRACT

Yom Basin is one of four main tributaries of Chao Phraya River where is a main rice bowl for Thailand food and export production. Besides, the Yom Basin is the only basin which has no large scale dam that can regulate the water flow during whole year. Therefore, flood and drought phenomena are common for this basin and cause regular damages to the farmers and communities. During year 2010, Sukhothai Province had suffered both drought and flooding events in the same year and caused the insecured situation for local authorities. Although, the authorities concerned had studied and set up flood mitigation schemes for the area, the impact of climate change may cause changes in flow patterns, quantities and intensities in the area. These proposed schemes may not be adequate to tackle the flooding.

In this study, the Sukhothai flood in Yom Basin is reviewed and simulated with calibration and verification from the past events. Future climate scenarios are setup using downscaled and bias corrected MRI-GCM, and then flooding phenomena in near and far future are simulated to see the impact of climate change towards runoff, water level and flooding duration. The present flood mitigation schemes will be assessed by simulation and flood damage in the past. Moreover, the field questionnaires are conducted to investigate the perception and adaptation opinions from farmers, municipal citizen, and concerned authorities. The information from field survey will be used for simulation to investigation the proper adaptation suggestions for future.

Keywords: *Sukhothai flood, climate change, adaptation, perception*

1. INTRODUCTION

Thailand is located in the southeastern region of Asia, where now is facing challenge from climate change including rising sea level, shifts of weather pattern and occurrence of extreme event such as floods and droughts. The range of temperature variation from climate model projected that mean temperature; precipitation and runoff in year 2100 for this part of the world

are found to be 1.0 to 4.5 °C, -20 to +20 %, and -10 to +30%, respectively (IPCC, 2007). This kind of change on climate characteristics will directly affect to hydrologic system, reservoir operation and water management in basin scale. The rainfall and runoff tend to increase and decrease in some areas. Changing rainfall pattern of upper watershed has so many effects; for instance, rules of reservoir operation must change in order to practically response to the climate change. Consequently, water demand for each activity in the downstream also faces considerable uncertainties in the future and availability of water supply, particularly in the irrigation system. Furthermore, flood management in wet season has to be changed. Obviously, reservoir operation in the future will be more difficult to manage due to the risk of natural disaster, climate uncertainty and complexity of social and economic benefits.

Sukhothai, a province in lower part of the northern Thailand, is also a flood-prone area due to the characteristics of Yom River and the floodplain area. Effects of climate change are anticipated to cause more loss and disaster in this area. Even though the existing flood mitigation system operated by the Thailand's Royal Irrigation Department (RID) is already in place, it might not has a sufficient capacity to response to extreme flood in the future. The alternative adaptation measures should be considered according to the changed magnitude of flood for the possible event.

This study aims to investigate the effect of climate change to flood situation and flood management in Sukhothai province. The guidelines of flood mitigation including both structural and non-structural measures under effects from climate change are suggested in this study in order to be the examples for adaptation.

2. STUDY AREA

The coverage area of Sukhothai province is about 6,596 square kilometers where 99.7% locates in the Lower Yom River Basin or 26.9% of the whole area of the Yom Basin. Sukhothai is located in the valley of the Yom River on the lower edge of the northern region as shown in Figure.1. Yom River Basin has the total catchment area of 23,616 km², and the main channel runs down a steep valley before passing through Song, Den Chai, and Sung Men districts, Phrae province. Then, the river flows westward through the valley passing Long and Wang Chin districts, and continues southward to a plain in Si Satchanalai district, Sukhothai province. The average annual income of people living in Sukhothai province is the lowest province in the northern region of Thailand. It was lower than the median income of USD 500 with 40.3% of 602,813 provincial populations.

3. FLOOD IN SUKHOTHAI

3.1 Cause of flood

The Royal Irrigation Department of Thailand (RID) reported that in 2006 the total flooding area was 1,189.55 km². More than 30 days inundation areas were found in Kong Krailat district, Muang Sukhothai district, and Sri Samrong district, and the total loss is more than 5 million Dollars (RID, 2006). In general, cause of flood in the Yom river basin comes from many reasons that are heavy rainfall in the basin and exacerbated by deforestation, inadequate water storage for flooding retention in the upper watershed, ineffective drainage capacity due to shallow river bed and small cross section, and land-use changes. Moreover, the shape of the river itself cause some flood problems, because the cross section of Yom river at the upstream of Sukhothai border with Phrae province in Srisatchanalai and Sawankhalok districts is larger than that at the main stream in Srisamrong and Muang Sukhothai districts and that at downstream border of Phitsanulok province in Kongkrailart district. This kind of “bottleneck” leads to drainage problem during the extreme flood. Flooding in the basin usually takes place in Sri Samrong, Sri Satchanalai, Muang Sukhothai and Kong Krailat districts during the South-western monsoon season, from July to September, leading to huge losses in agricultural and residential areas along the Yom River.

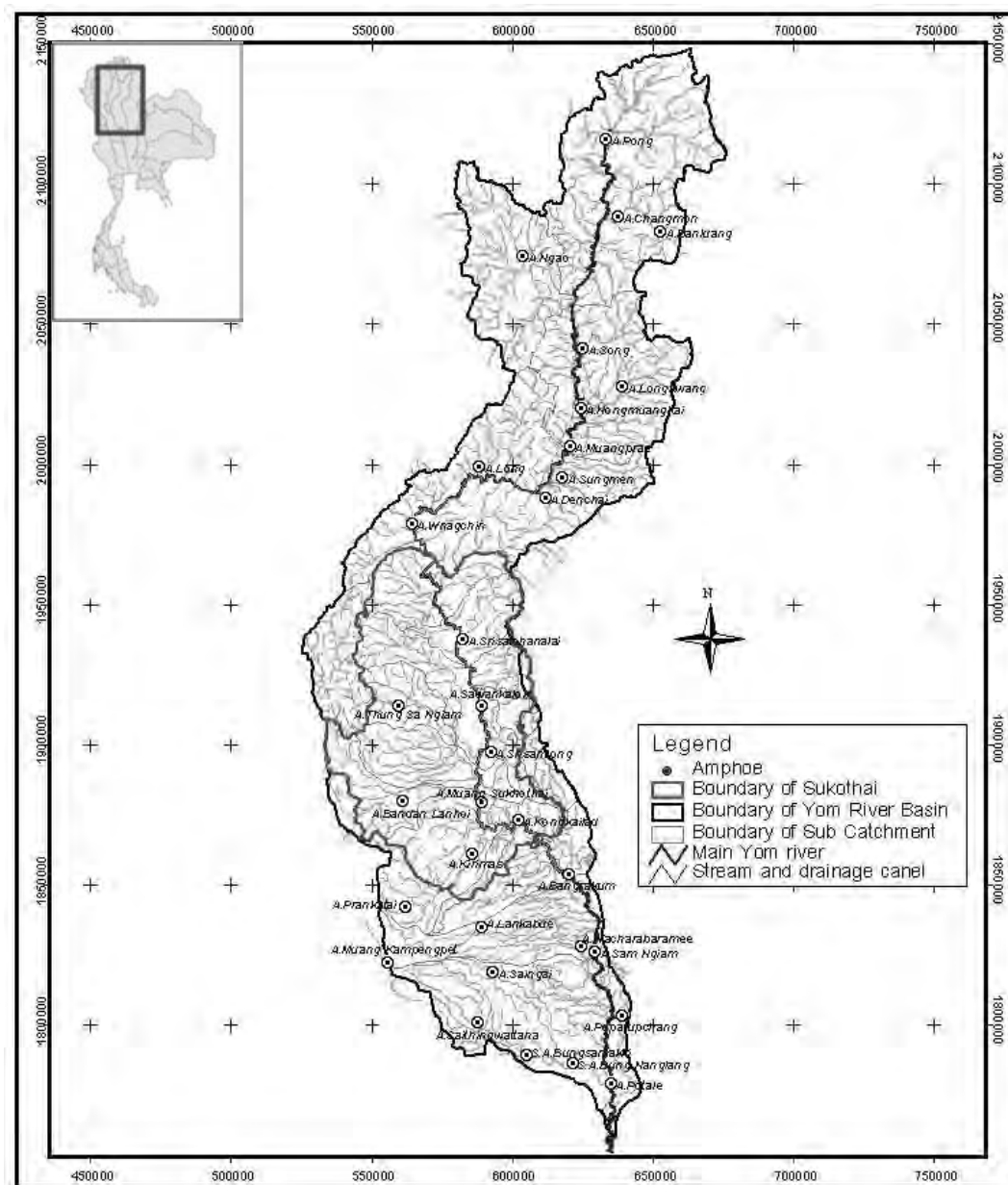


Figure 1: Sukhothai province and Yom river basin

3.2 Present flood mitigation in Sukhothai province

In the present day, RID plans and implement the flood mitigation measures based on recorded hydrological data. The components of these structural measures are Thung Taleluang and Bung Yai retention ponds, Yom-Nan diversion canal, Klong Hok Baht canal, and levees along Yom River. The core principle of these measures is mainly for protection of high-density business and residential area in Sukhothai municipality in order to reduce flood volume and level as much as possible before it reaches the city, by bypassing the flow of water to both sides of the Yom River as shown the schematic in Figure 2.

Current practice of flood management is largely considered in an emergency viewpoint and focus on structural measures, however it still

lacks of non-structural measures and does not taken the effect of flood volume to lower Chao Praya basin into account. Therefore, the important issue is an assessment of the mitigation capacity that could response to the climate change in the future.

Yom River is the only main river system in Thailand that still has no large reservoir in the upstream section. However many feasibility studies of the large dam, Kang Seu Ten dam, for mitigation flood had been conducted so many times since the 1970s by many organizations such as RID, Electricity Generating Authority of Thailand (EGAT), Howard Humphreys and Sons consultancy, the project is still put on hold because of the difficulty of negotiations between government and stakeholders.

RID (2001) focused on the response of Kang Seu Ten dam to 1995 flood (1st August – 31st October 1995) and found that Kang Seu Ten dam is able to reduce flood level and duration in upper Yom river basin, and the efficiency of dam is gradually decreased by the distance. The maximum discharge would be reduced by 1,452 CMS or 74.19%, and the maximum water level would be decreased by 5.7 m; whereas, the maximum discharge and water level at Y.17 station, Sam Ngam district at Phichit province, would not have any significant changes. Taesombat (2001) analyzed the flood mitigation potential of Kang Seu Ten reservoir and found that it would reduce the peak discharge on the downstream by 20.68 – 94.55% for recurrence interval range 2 – 10,000 years.

Thiramanus (2004) conducted a study about effectiveness on flood mitigation of Kang Seu Yen reservoir, using a river analysis simulation by HEC-RAS model from dam site to Pho Talae district at Phichit province. This study conducted in six different alternatives, no reservoir, reservoir capacity at 400, 800, 1,200, and 1600 MCM, and a very large reservoir (without releasing water). The results showed that, Kang Seu Ten reservoir has a capacity to decisively alleviate flooding from downstream of dam site to Muang Prae district and also quite effective for reducing flood at Sukhothai province, if very large reservoir scenario is implemented, it will help reduce a frequency of occurrence of flooding from 2 times in 3 years to 1 time in 6 years. At the downstream section, the effect of reservoir is disappeared. Moreover, this study found that the flood return period at Sawan Kalok district in Sukhothai will increase from 1.7 to 3.6 years and 10 to 12.5 years at Sam Ngam district in Phichit, when Kang Seu Ten reservoir had 1,200 MCM capacities (same size as RID study).

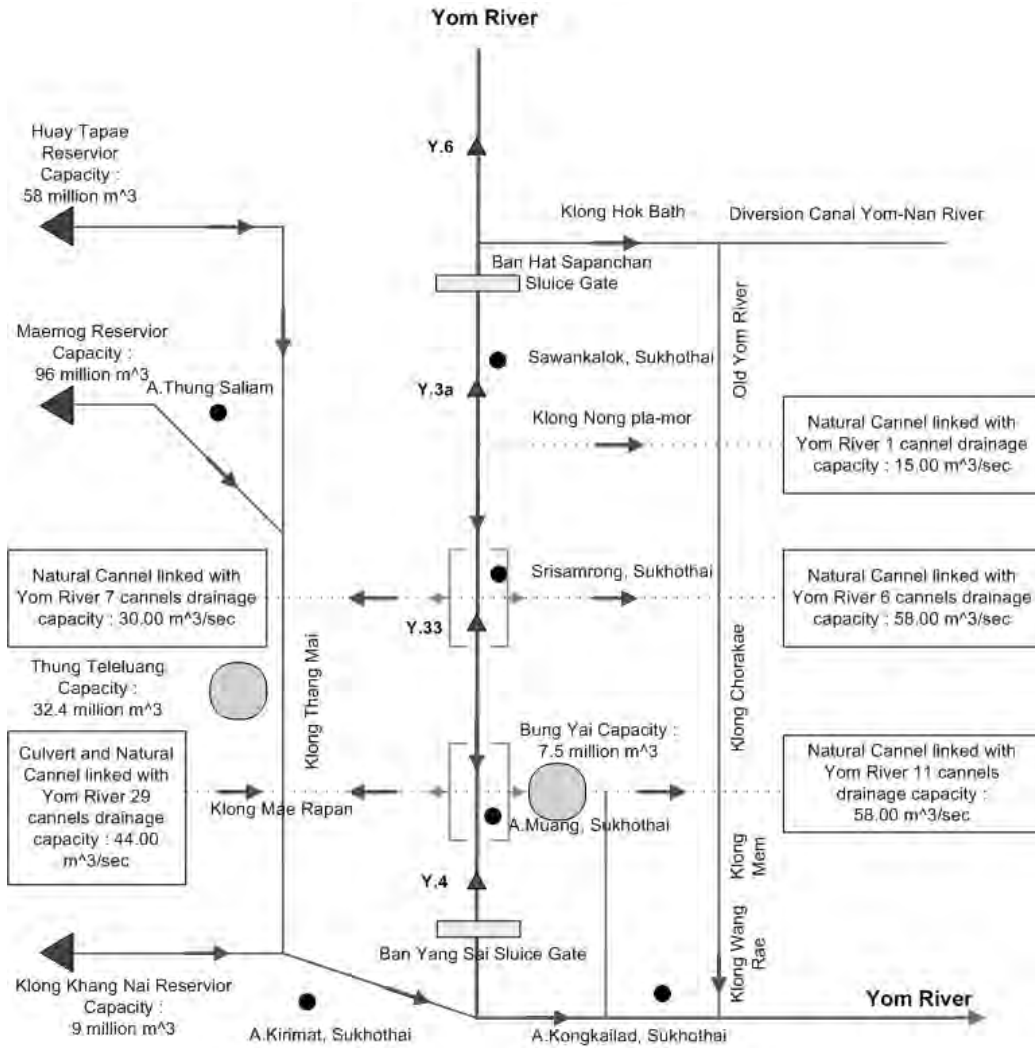


Figure 2: Schematic of existing flood mitigation measures in Sukhothai

4. METHODOLOGY

This study starts from the past investigation (year 2002 and 2006) by using river analysis model, HEC-RAS v4.1. The 2006 flood is chosen for model calibration and used as representation of a natural case of Yom River during wet period, while that of 2002 is used for validation. The daily streamflow data at Y.16 and Y.6 stations from 1st August to 31st October is used in simulations. Furthermore, this study also simulated 2011 flood from 26 June to 30 June 2011 by using hourly stream flow data provided by RID of Sukhothai province to investigate the effect of present structural measures. The second part of this study aimed to simulate future flood conditions in year 2019 and 2022 by using data from Japanese MRI rainfall model. At the same time, the field questionnaires are conducted to investigate the perception and adaptation opinions from farmers, municipal citizen and concerned authorities towards future flood adaptation. The present flood mitigation schemes are generated from the past flood simulation. The

information from field survey will be simulated to illustrate proper adaptations in the future.

5. MODEL SIMULATION

5.1 Calibration and Validation

In this study, Manning's n roughness coefficient is a main parameter for calibration. This parameter depended on many factors that are surface roughness of the river bed, effect of vegetation, channel irregularity, channel alignment, silting and scouring, obstruction, size and shape of channel, stage and discharge (Chow, 1958). It is a major parameter that determines discharge of flow in natural channel; therefore, trial and error method is chosen to perform this task.

The calibration and validation results are evaluated from two parameters; i.e. normalized root mean square error (NRMSE) and coefficient of determination (R^2). From the calibration case (2006 flood event) as shown in Figure 3, there are NRMSE = 0.096, 0.081 and R^2 = 0.887, 0.850 for Y.16 and Y.6 station respectively. For the validation case of year 2002, it shows the value of NRMSE = 0.062, 0.074 and R^2 = 0.860, 0.875 for Y.16 and Y.6 station respectively. These results are very good agreement with the observed data; therefore, it could be implied that the roughness coefficient in main channel, left overbank and right overbank, which are used in model (n varied between 0.032 – 0.041), could be represented the behavior of flood in this study area.

5.2 Recent flood cases without flood mitigation measures

In the past, Sukhothai province encountered extreme flood in 1995, 2002, and 2006. Since there are no flood control structures such as Ban Hatsapanchan gate, Thung Taleluang retention pond and Ban Yangsai sluice gate in the past, Sukhothai province faced with province-wide, month-long and devastating consequences on agricultural area in Sawan Kalok, Sri Samrong, Kong Krailat districts, and Muang Sukhothai Municipal area. Not only the overbank flow from the main Yom River, but the lateral flow from Mae Mok and Mae Rumpun subbasin also caused flood in Sukhothai province. Both sources of water generated flash floods from upstream, which is notoriously dangerous and hard to manage in an emergency situation.

Since 2007, RID has already implemented some structural measures as described in Figure 2. In order to investigate the effectiveness of these measures, the comparison between with and without measures is simulated by using 2011 flood events. As the results, these flood measures can actually reduce peak discharge at Y.6 and Y.3A station by 5.78% and 3.27%, respectively as shown in Figure 4.

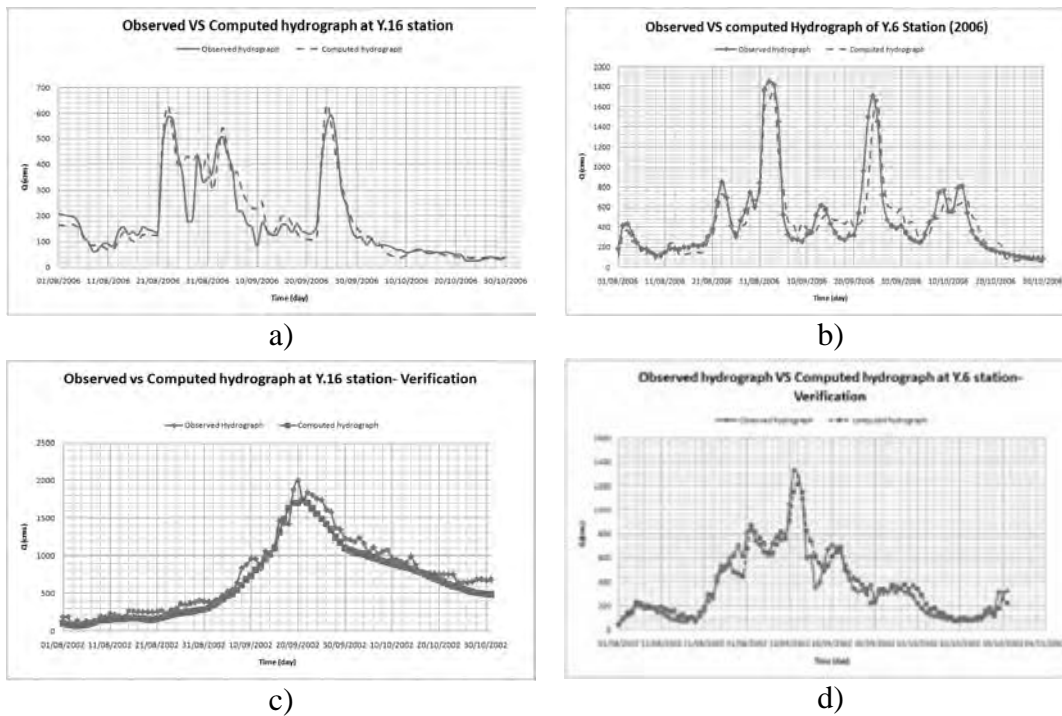


Figure 3: calibration and verification result from two river gauge stations.

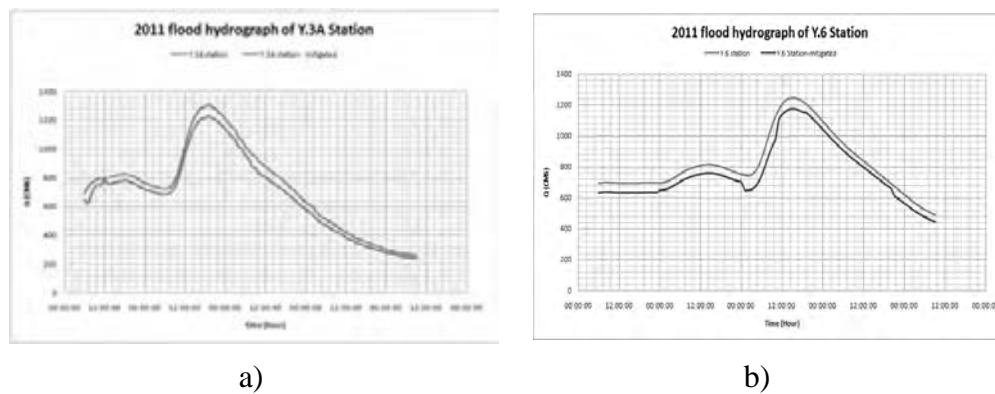


Figure 4: Effect of mitigation measures to flood hydrograph at Y.6 and Y.3A stations for 2011 flood case.

5.3 Future flood cases: concerning impact of climate change

For the future scenario, MRI-GCM rainfall model is used to forecast future rainfall. It showed that rainfall in Sukhothai area will increase around 20% and 39% in 2019 and 2022, respectively (Chaowiwat, 2010); then, the rainfall data is used to calculate the future flood runoff by rainfall-runoff model (HEC-HMS model). As the results, the flood volume at Y.14 and Y.33 stations in these two years will increase by 13% and 29.4% respectively as shown in Table 1; thus, this can be implied that flooding in Sukhothai province is having an upward trend and need more mitigation measures.

Table 1: Summary of future flood runoff in year 2019 and 2022

Station	Maximum discharge in 2006 (CMS)	Maximum discharge in 2019 (CMS)	Difference (%)	Maximum discharge in 2022 (CMS)	Difference (%)
Y.14	2,044	2,471	17.28	2,567	20.37
Y.6	2,171	2,592	16.24	2,648	18.01
Y.3A	1,568	1,908	17.82	1,974	20.62
Y.4	555	665	16.54	749	25.90

Although, RID has already implemented some structural measures as described in Figure 2, the whole project did not completed. In order to assess the future situation, this study does two types of simulation – no structural measures and completion of RID whole planned measures including with Ban Hat Sapanchan gate and Thung Taleluang 2 retention pond. From the simulation using river analysis model (HEC-RAS), the maximum discharge at Y.6 and Y.3A stations are projected to increase by 5.77% and 1.37%, respectively, for the 2022 flood case of only climate change effect (no structural measures). For another case of 2022 flood scenario, the whole system of structural measures can reduce the peak discharge by 4.67% and 4.32%, respectively as illustrate in Figure 5.

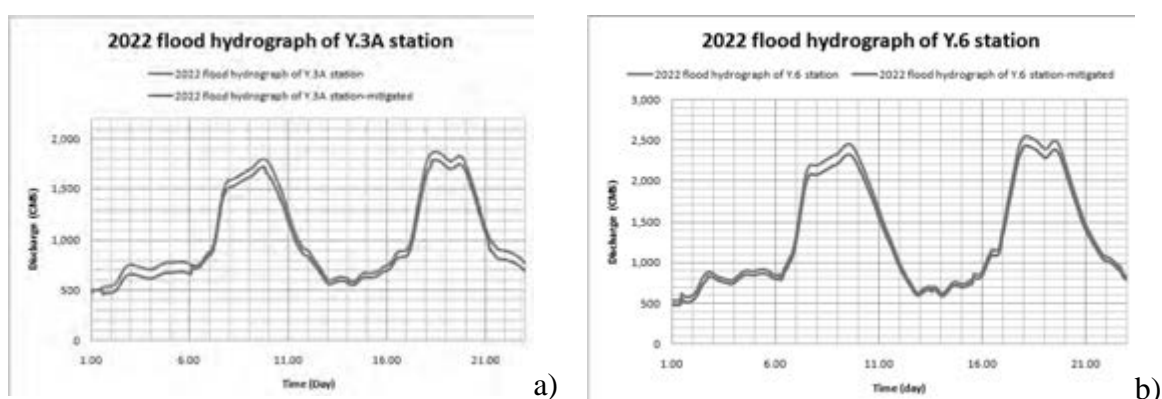


Figure 5: effect of mitigation measures to flood hydrograph at Y.6 and Y.3A stations for 2022 flood case

6. FIELD QUESTIONNAIRES

In this study, 120 field questionnaires were conducted at four places; i.e. Kong Krajong – Sawan Kalok district, Pakpra – Muang Sukhothai district, municipal area of Muang Sukhothai district and Krai Nai – Kong Krailat district. This helps the researchers to know about people's perceptions and their opinions of flood adaptation for future extreme event due to effect of climate change.

Results from questionnaires showed that the people request the government to tackle a problem of deforestation, to construct the Kang Seu Ten dam and small dam along the Yom River, and to perform channel dredging in terms of flood mitigation. For flood adaptation side, most people still embraces the idea of “top-down approach”, which relies mostly

from government projects, such as construction more levees, dikes, retention ponds, and new drainage canals (floodways). Nevertheless, the local people also adapt themselves to flood mitigation by using sandbags to heighten the levees, changing cropping pattern, and reducing an erosion of river bank by planting vegetation.

7. CONCLUSION

Climate change is going to increase an amount of flood volume in Yom River at Sukhothai province in the future. Results from simulation also carried out and showed that it can reduce maximum runoff at the Yom river gauge stations Y.3A and Y.6, when whole structural measures are already constructed. However only the structural measures are not completely sufficient for solving flood problems, non-structural measures are still required as recommended from the field survey results. Therefore, this study suggests the flood adaptation measures, both structural and non-structural measures, should be implemented as followed:

- 1) Fully construct and operate Thung Taleluang 1 & 2 retention ponds (with fully-functioned drainage canal and gate).
- 2) Construct new drainage facilities to accelerate flood inside Sukhothai municipal.
- 3) Assign the right side of Yom River as “flood-plain” area.
- 4) Construct and maintain levees, dikes and gabions, which protect the city from overbank flow.
- 5) Promote concept of “living with flood” to Sukhothai people – design a sensible system of flood compensation, such as flood insurance, if possible.
- 6) Reform land-use and flood zoning regulations.
- 7) Develop more sophisticate and responsive flood warning system, and strengthen cooperation between central and local government officers during crisis period.

ACKNOWLEDGEMENT

The study cannot be conducted without the data provided from various agencies, e.g., Royal Irrigation Department, Department of Disaster Prevention and Mitigation, etc. This project, CC522A, has been supported in part with National Research Universities fund from Office of Higher Education Commission (OHEC), Ministry of Education and the assistantship for researcher of the study was funded by UNU-ISP. The researchers would like to gratefully thank to Miss Mada Iaumsupanimit, Research Assistant at Water Resources System Research Unit (CU_WRSRU) for her tireless work that helps us so much.

REFERENCES

Chaowiwat, W. 2010. *The Adaptation Response for Flood Management, Case Study in Sukhothai Province in Thailand*, conference paper of UNU CSDS-IACC project.

Chow, V. T., 1958. *Open Channel Hydraulics*, McGraw-Hill College, Singapore

Hanittinan, P., 2011. *Flood Analysis and mitigation measures in Sukhothai province*, UNU seminar on National workshop: Comparative Studies on Strategies to adapt for the Natural Disasters Due to Climate Change in Thailand, Khon-Kaen University, Khon-Kaen.

IPCC, 2007. *Summary for Policymakers. In: Climate Change 2007: The Physical Science Basis. Contribution of Working Group I to the Fourth Assessment Report of the Intergovernmental Panel on Climate Change [Solomon, S., D. Qin, M. Manning, Z. Chen, M. Marquis, K.B. Averyt, M.Tignor and H.L. Miller (eds.)]*. Cambridge University Press, Cambridge, United Kingdom and New York, NY, USA

Kalonsri, P. 2011. *Research about Kang Seu ten project (That politician doesn't want to know)*, Bangkok

Koontanakulvong, S., 2010. *Thai Climate Change and its Impacts towards Water Sector*, Water Resources Research System Research Unit, Bangkok.

Koontanakulvong, S., et.al., 2010. *The corrected MRI-GCM data for Thailand*, Technical Report, Chulalongkorn University, December.

RID, 2001. *Feasibility study report of Kang Sei Ten project Prae Province*, Vol.2, Bangkok.

Sriariyawat, A., 2011. *Ensuring Flood Security in Sukhothai province*, UNU seminar on National workshop: Comparative Studies on Strategies to adapt for the Natural Disasters Due to Climate Change in Thailand, Chulalongkorn University, Bangkok.

Sriariyawat, A., 2011. *Social Responses and and Flood Adaptation in Sukhothai Province*, UNU seminar on National workshop: Comparative Studies on Strategies to adapt for the Natural Disasters Due to Climate Change in Thailand, Khon-Kaen University, Khon-Kaen

Taesombat, V., 2001. *Flood mitigation potential in upper Chaopraya river basin of large and medium-sized reservoir*. Final report, Bangkok.

Thiramanus, R. 2004. *Effectiveness on Flood Mitigation of Kaeng Sua Ten Reservoir*, Faculty of Engineering, Chulalongkorn University, Bangkok

Preparing water supply master plan for a newly declared city lacking land use guidelines and demographic information

Mustafa T. HASAN¹ and Mahmud R. AMIN²

¹ Junior Engineer, Institute of Water Modelling, Bangladesh
mth@iwmbd.org

² Junior Engineer, Institute of Water Modelling, Bangladesh

ABSTRACT

Urbanization proceeds gradually in developing countries with the commencement of industrialization, most likely without proper land use master plan. An adequate land use master plan provides required guidelines and specifications for the preparation of additional master plans regarding urban utilities. Preparing a water supply master plan for a growing city without proper land use master plan is a complex task for the engineers and planners. Particularly, assessment of water demand and computation of nodal demand is very difficult for a newly declared city enclosed by an administrative boundary different from the former judicial urban growth centre boundary because of insufficient primary & secondary data and unavailable land use guidelines. This paper presents a simple methodology to assess the demand for such an area where no primary demand data is available and thus demand has been assessed based on secondary data and consequently the nodal demand for the Water Distribution System (WDS) has been computed. Alamdanga Paurashava of Chuadanga district of Bangladesh has been taken as the case study area where no piped water supply exists currently. The demand assessment has been made analyzing the demographic data with the help of land use map using ArcGIS toolkit. For the population projection, census report data has been used. From the GIS land use map, build up area has been assessed and projected for future. By using these analysis results, demand with future projection has been determined. Thus this paper actually presents a methodology for preparing a WDS master plan of a newly declared city lacking sufficient land use plan and data support.

Keywords: *master plan, water supply, water demand, population projection, GIS*

1. INTRODUCTION

Being one of the most densely populated agriculture based rural dominating country; Bangladesh has vast scope of urban growth. Over the last 3 decades, due to the increment of population and increasing demand for improved life style, rural areas are being diminished rapidly and transferred to urban areas. This extensive urbanization is creating demand for various urban facilities.

Among those, safe water supply through pipe network is a priority issue in urban areas of Bangladesh. Presently about 28% of the urban population still do not have access to safe water.

Under the above circumstances, Dept. of Public Health Engineering (DPHE) has taken up the project in hand, titled “Groundwater Management and TPP for Survey, Investigation, and Feasibility Study in Upazila and Growth Center level Paurashavas having no Piped Water Supply System”. The project is very much relevant to The National Policy for Safe Water Supply & Sanitation 1998 of the Government of Bangladesh. Institute of Water Modelling (IWM) has been employed in the project for “Mathematical Modelling for Safe Drinking Water Source Identification”.

While performing the project activities, a unique method has been developed for preparation of a water supply master plan in a city or small town lacking adequate primary and secondary data such as proper land use policy and demographic information. Since, the traditional population based or modern land use based demand calculation approach is insufficient, a combined population and land use based demand calculation approach has been adopted. The authors are directly involved in the project and have illustrated a further modified computation technique in this paper.

2. STUDY AREA

Alamdanga Paurashava is the only municipal area of Alamdanga Upazila of Chuadanga District. It is located in 23°45' N latitude and 88°56' E longitude. The smallest administrative unit of a Paurashava is a ward and presently, Alamdanga Paurashava is divided into 9 wards. The Paurashava has good road connections to Dhaka (capital of Bangladesh) and other neighbor districts and regional centers. Activities related to trade and commerce are increasing day by day and now it is emerged as one of the few A class municipal areas of Bangladesh. Though Alamdanga is a Class A municipality, till the initiation of the aforesaid project, there was no piped water supply scheme in this Paurashava. According to the project requirements, the whole municipal area has been modeled for pipe water supply network coverage for the year 2040. The proposed master plan will be implemented in three phases commencing from the years 2010, 2020 and 2030, considering water demand for the years 2020, 2030 and 2040 respectively.

3. METHODOLOGY

3.1 Data collection

Two types of data are required for the preparation of a WDS master plan- spatial and non spatial data. Spatial data consists of the following GIS based maps of the Paurashava under consideration:

- i. Topographic map,
- ii. Physical map, and
- iii. Road network map.

Topographic survey was conducted in the baseline year 2010 by Institute of Water Modelling (IWM). All the survey data were processed and analyzed with the help of ArcGIS toolkit and corresponding maps stated above were produced. Digital format of the maps have been utilized in this assignment in the form of shape files (.shp extension).

Demographic data is the only non spatial data input here. Population data of the years 1981, 1991 and 2001 have been collected from the population census report of Bangladesh Bureau of Statistics (BBS). Population census data of 2011 is not published yet. Therefore, population for the baseline year 2010 has been collected from the Social Impact Assessment (SIA) Survey, 2010 conducted by Farhat Consultants to fulfill the project requirement.

3.2 Population projection

Conventional population projection methods require past population data for forecasting of future population. The administrative boundary of the Paurashava under interest needs to be constant throughout the census years under consideration. But for a newly established Paurashava it is very complex task to extract the previous year's population data while the town's administrative boundary didn't exist at all. In Bangladesh population census reports, the smallest unit of area for which the population data is available is "mouza". Therefore, the mouzas contributing to the whole Paurashava area have been identified at first. Then the population data of respective mouza is summed up to build up the Paurashava population for each census year. Thus the population data of the Paurashava for each census year are extracted.

Alamdanga Paurashava was established in 1985. So the population census data of 1981 is unavailable for the Paurashava area. The procedure stated above is applied to extract the population of Alamdanga in 1981. 'Geometric progression method' or 'compound rate of growth method', proposed by Hardenberg is adopted for population projection; since it is the most commonly used and efficient method for growing cities and areas which have vast scope for extension (Ahmed and Rahman, 2003).

$$P_f = P_p (1+r)^n \quad (1)$$

where P_f = future population; P_p = present population; r = rate of yearly population growth and n = number of years to be considered.

$$r = \sqrt[n]{\frac{P_2}{P_1}} - 1 \quad (2)$$

where P_1 and P_2 are the population data of two dates of n number of years apart.

Obviously the annual population growth rate r is not constant throughout the years under consideration. For computation purpose, the authors have assumed that the annual growth rate is constant over an individual census decade. Growth rates for census decade 1981-1991 and 1991-2001 are 2.72 and 2.63 respectively. Adopting SIA survey of 2010, growth rate for 2001-2010 has been calculated as 2.19. According to the assumption of constant annual growth rate in a census decade, growth rate of 2001-2011 can be adopted as the same as growth rate of 2001-2010 (Table 1).

Table 1: Growth rate calculation for census decades

Year	Population	GR
1971-1981	15,941	-
1981-1991	20,858	2.72
1991-2001	27,040	2.63
2001-2010	32,858	2.19
2001-2011	33577*	2.19

*projected population adopting same growth rate as of 2001-2010

Next step is to find out the projected growth rates for 2011-2021, 2021-2031 and 2031-2041. Various methods are available for growth rate projection such as Exponential ($Y = a e^{bX}$), Logarithmic ($Y = a + b \log X$), Semi-log ($\log Y = a + bX$), Reciprocal ($1/Y = a + bX$), Power ($Y = aX^b$) functions etc. The best equation can be identified on the basis of statistical criterion like mean square error, mean absolute error, coefficient of determination (R^2), standard error of the estimate and significance of the regression coefficients. Here, we shall restrict ourselves to the straight line method popularly known as 'method of least squares' or 'line of the best fit'. The method can be used independently when detailed information is not available (Mehta, 2004).

The general form of the equation of least square method is:

$$Y = a + bX \tag{3}$$

where Y = required variable to be projected (here, annual growth rate), X = no. of years, a = constant and b = slope of the regression line.

To compute the values of the constants of equation (3), the following equations are used:

$$\sum X = Na + b.\sum X \tag{4}$$

$$\sum XY = a.\sum X + b.\sum X^2 \tag{5}$$

where:

$\sum X$ = the sum of all observations of X ,

$\sum Y$ = the corresponding sum of all the Y observations,

ΣXY = the sum of all the products of X and Y,
 ΣX^2 = the sum of all the squares of X and
 N = total number of observations

Table 2: Growth rate projection based on 'method of least squares'

Year	Rate of Growth (%) (Y)	Sr. No. of Col. 1 (X)	Square of 'X'	X.Y
(1)	(2)	(3)	(4)	(5)
1981-1991	2.72	1	1	2.72
1991-2001	2.63	2	4	5.26
2001-2011	2.19	3	9	6.57
Total	(ΣY) 7.54	(ΣX) 6	(ΣX^2) 14	(ΣXY) 14.55

Replacing the above values in equation (4) and equation (5), and solving for a, b; we have got the required growth rate projection equation:

$$Y = 3.05 - 0.27X \quad (6)$$

Using equation (6), the projected annual growth rate for 2011-2021, 2021-2031 and 2031-2041 are found as 1.98, 1.71 and 1.44 respectively. These rates have been assumed constant for a decade; therefore can be adopted as the same for the years 2010-2020, 2020-2030 and 2030-2040 respectively with no considerable deviation in population projection. Projected population of the Paurashava for the years 2020, 2030 and 2040 are calculated using these growth rates and equation (1).

Paurashava has potential of future extension and it should be taken into account in population projection by considering the migration of populace from rural to extended urban areas. No government planning or policy is available on extension of Paurashava boundary. The authors have adopted the urbanization rates in Bangladesh from World Urbanization Prospects: The 2007 Revision by United Nations. The urbanization rates are provided in the report for every 5 years. For computation purpose, consecutive growth rates are averaged to find out the rates for every 10 years. Extension area is computed by applying these rates into the baseline year Paurashava area. Assuming the same population density in the extended area as of the Paurashava area, population in the extended area is calculated and added to the projected population of the Paurashava (Table 3).

For 2001-2010, ward wise population growth rate is calculated based on ward wise population for the years of 2001 and 2010. These ward wise growth rates are extended further for 2020, 2030 and 2040 by multiplying each with a factor so that summation of ward wise population equals with the projected Paurashava population of the years under consideration. The multiplying factors should be selected based on baseline population density in each ward, road network in baseline year, infrastructure development plan of the government, potential of improvement of living standard in an individual ward etc. The factored growth rates are then used in ward wise population projection (Table 4).

Table 3: Population augmentation for future urbanization

Rate of change of percentage urban (%)	2010-2020	2020-2030	2030-2040
	$(1.86+1.91)/2= 1.89$	1.92	1.71
Paurashava Area (km ²)	9.59	9.59	9.59
Paurashava Population	39,970	47,358	54,651
Population Density (person/km ²)	$(39,970/9.59)=4,168$	4,938	5,699
Extension area (km ²)	0.18	0.18	0.16
Cumulative Extension Area (km ²)	0.18	0.37	0.53
Population in extension area	$0.18*4168=755$	1,804	3,017
Total Population	$(39,970+755)= 40,725$	49,162	57,667

Table 4: Population projection

Locality	2010		2020		2030		2040	
	GR (%)	Population	GR (%)	Population	GR (%)	Population	GR (%)	Population
Paurashava	2.19	32,858	1.98	40,725	1.71	49,162	1.44	57,667
Ward No. 1	2.19	3,875	2.16	4,797	1.88	5,780	1.59	6,765
Ward No. 2	1.75	3,973	1.68	4,694	1.45	5,423	1.21	6,117
Ward No. 3	1.75	3,399	1.68	4,016	1.45	4,640	1.21	5,233
Ward No. 4	1.75	4,070	1.68	4,809	1.45	5,555	1.21	6,267
Ward No. 5	2.46	4,308	2.37	5,447	2.07	6,686	1.74	7,941
Ward No. 6	2.46	4,456	2.37	5,634	2.07	6,916	1.75	8,222
Ward No. 7	2.85	2,989	2.97	4,007	2.57	5,162	2.15	6,385
Ward No. 8	1.75	2,601	1.66	3,067	1.44	3,537	1.21	3,990
Ward No. 9	2.84	3,187	2.93	4,254	2.53	5,463	2.13	6,746

3.3 Land use classification

Five types of land use categories are considered (Figure 1) and corresponding per capita water demand are assigned (Table 5) as described by Ahmed and Rahman (2003).



Figure 1: Adopted land use category

Table 5: Land use category and corresponding per capita water demand

Land use Category	Area (km ²)				Average Consumption (lpcd)
	2010	2020	2030	2040	
Residential	2.43	2.43+6.64*20% =3.76	4.75	5.75	100
Commercial	0.24	0.24	0.24	0.24	40
Public/Institutional	0.25	0.25	0.25	0.25	25
Industrial	0.04	0.04	0.04	0.04	120
Agricultural	6.64	6.64-6.64*20% =5.31	4.32	3.32	0

It is more justified to include the agricultural water demand into irrigation scheme rather than piped water supply scheme. Therefore, per capita demand is nil under this category. However, for future land development, 20% 35% and 50% of the agricultural area are assumed to be transformed into residential area for effective area calculation of the years 2020, 2030 and 2040 respectively. This is a conservative assumption and yields more factor of safety in demand calculation as residential category has got considerable amount of per capita demand. The remaining agricultural area is not considered when computing population density. Figure 2 represents actual population density vs. population density in buildup area for design years.

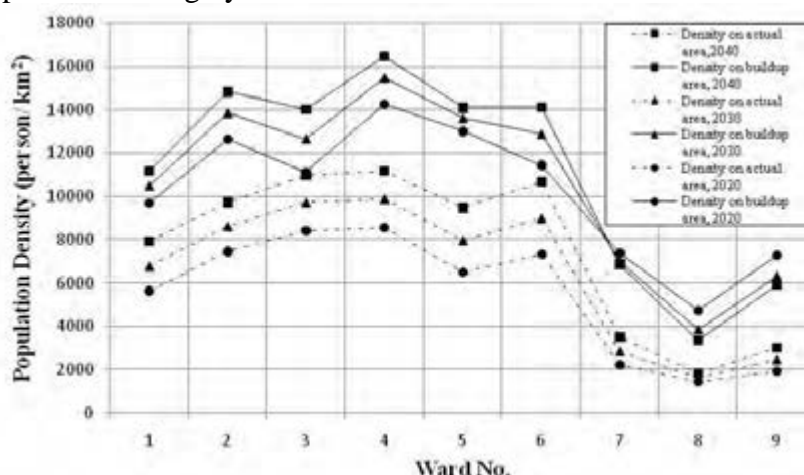


Figure 2: Actual population density vs. population density in buildup area.

3.4 Computation of nodal demand

Total 852 nodes are identified after digitization of the proposed pipe network. Commanding area of each node is demarcated by creating ‘Thiessen polygon’ using ArcGIS software. The approach of using Thiessen polygon for nodal area demarcation is similar to the approach given by Lancey and Mays (1989). Thereafter, union of ward boundary, Thiessen polygon and land use category is done. This assigns ward wise population density and per capita water demand of each land class into the Thiessen area. Thus a database is created in the form of shape file comprising of all necessary information for nodal demand computation.

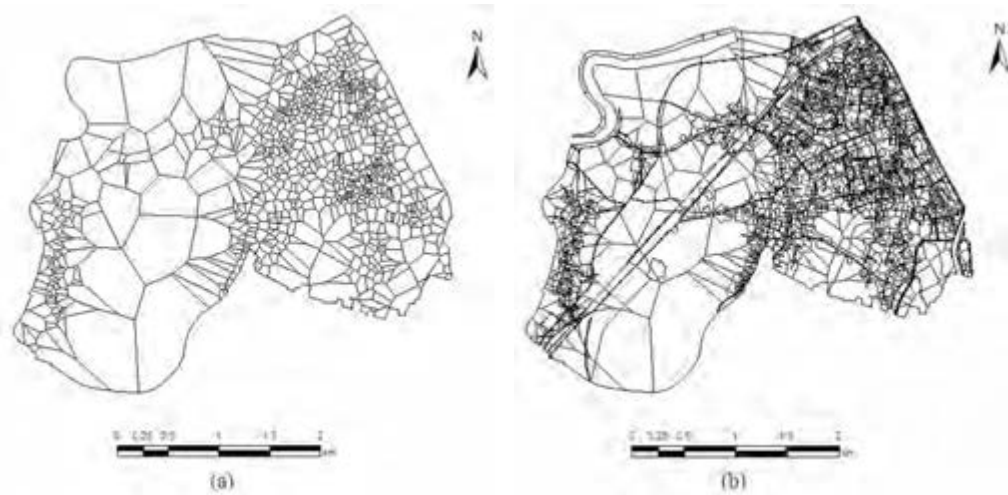


Figure 3: (a) Nodal area demarcation using Thiessen polygon and (b) Union of Thiessen polygon, ward boundary and land use classes

After union has been done, each Thiessen area segregates into several undividable segments. Each segment is a part of a distinct ward and denotes a specific land class. Water demand in such a segment is computed by the following equation:

$$ds_i = A_i \times PD_i \times LPCD_i \quad (7)$$

where:

ds_i = Water demand in segment i ,

A_i = Area of the segment i ,

PD_i = Population density of the corresponding ward in design year

and

$LPCD_i$ = Liter per capita water demand of the corresponding land

class

Nodal demand is calculated then using the following equation:

$$dn_j = \sum_{i=1}^n ds_i \quad (8)$$

where:

dn_j = Nodal demand of node j and

n = No. of segments in node j

For each node, percentage of unaccounted for water (UFW) is added. Since no metered data is available, the required UFW is assumed from trend of other existing water supply utilities in Bangladesh. According to *Bangladesh Water Utilities Data Book, 2008*, the minimum UFW is estimated at Chuadanga Paurashava (2.7%) and maximum is estimated at Gazipur Paurashava (52%). The average UFW in 11 water utilities is 22.5%. In addition, UFW is expected to increase with aging of pipe network due to

high water loss. Therefore, UFW for Alamdanga Paurashava is assumed 15%, 22% and 25% for design years 2020, 2030 and 2040 respectively.

3.5 Long range water supply facilities planning

The proposed pipe network master plan is to be implemented in 3 phases. For each phase, corresponding nodal demands are summed up to comprise the total water demand. During 1st two phases, water supply coverage is proposed to be limited in high density areas only. Water supply coverage is assumed 65%, 90% and 100% for 1st, 2nd and 3rd phase respectively. Figure 4 shows projected water demand and demand considering supply coverage vs. proposed water supply capability for the mentioned phases.

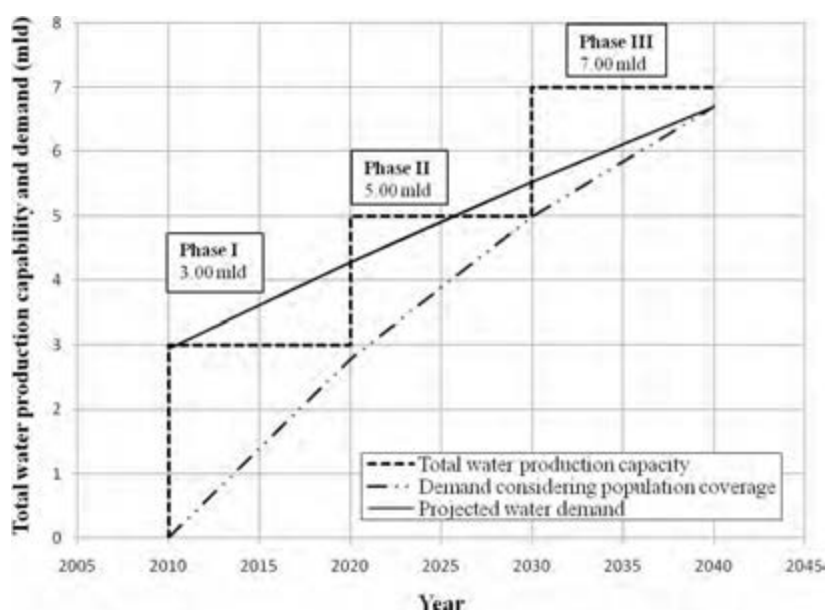


Figure 4: Projected water demand vs. water production capacity

Master plan of water supply facilities of Alamdanga Paurashava is done for the final phase using modeling software. Then the pipe network is truncated and tested for former two phases.

4. CONCLUSIONS

Computation of nodal and total water demand is the prerequisite for preparation of a long range water supply master plan. Combination of traditional population based and modern land use based approach is used for water demand projection. This method can predict population of a growing town despite the movement of the administrative boundary. Future urbanization prospect of the town is also considered and a feasible calculation approach is presented. Inclusion of factored growth rate in different portions of the town (wards, in case of Paurashava) yields more control over population density distribution.

GIS application for land use classification and nodal demand computation has made the calculation more accurate. Considering buildup area instead of actual area for population density distribution also accommodates the future land use transformation accurately.

The methodology described in this paper is very relevant to other growing small town or cities lacking land use guidelines and demographic information. The whole methodology can be programmed in MS Excel and ArcGIS interface and hence, easily can be updated based on the future development plan of the town or city.

ACKNOWLEDGEMENTS

The authors would like to particularly acknowledge the continuous guidance and assistance of Mr. A.K.M Abdus Satter, Senior Pipe Network Modeler, Comp-I, Mathematical Modelling for safe Drinking Water Source Identification, DPHE. Mr. Monowar Ali, Project Director, Ground Water Management Project, DPHE is also appreciated for his kind consent to the authors for this publication. The invaluable support of Mr. Emaduddin Ahmad, Team Leader, Comp-I, Mathematical Modelling for safe Drinking Water Source Identification, DPHE and Mr. S M Mahbubur Rahman, Director, Water Resources Planning Division, IWM will be remembered with gratitude. The authors are also thankful to Ms. Tanjia Akter Amy, Junior Engineer, IWM for her contribution in this particular assignment.

REFERENCES

- Ahmed, M. F., and Rahman, M. M., 2003. *Water Supply & Sanitation, Rural and Low Income Urban Communities*, ITN-Bangladesh, BUET, Dhaka.
- Mehta, A. C., 2003. *Projection of Population, Enrolment and Teachers with Focus on Elementary Education*, NIEPA, New Delhi.
- World Urbanization Prospects: The 2007 Revision*, United Nations, New York, 2008.
- Lansley, K., Mays, L., 1989. Optimization Model for Water Distribution System Design. *Journal of Hydraulic Engineering*, ASCE, 115(10), p. 1401-1419.
- Bangladesh Water Utilities Data Book*, Ministry of LGRD, GOB and World Bank Dhaka Office, 2008

The major research plan ‘study on unconventional emergency management’ in China

Wenguo WENG¹, Hong HUANG² and Weicheng FAN³

¹Associate Professor, Institute of Public Safety Research (IPSR),
Tsinghua University, Beijing, China
wgweng@tsinghua.edu.cn

²Professor, IPSR, Tsinghua University, Beijing, China

³Professor, Director, IPSR, Tsinghua University, Beijing, China

ABSTRACT

In recent years, more and more unconventional incidents were reported all over the world. Unconventional incident is the incident that has no precursor along with obvious complex characteristics, secondary disasters and great damages. It is difficult to respond the incident by the conventional management methods. In order to improve Chinese government’s emergency management ability, and promote the development of Chinese emergency management science, the National Natural Science Foundation of China (NSFC) launched the Major Research Plan ‘Study on Unconventional Emergency Management’ in 2008. The research plan aims to deeply understand the mechanism and provide the approach for the core parts in the emergency management - warning and response - by integrating the multidisciplinary observations, experiments and theories; establish the unconventional emergency management theory based on the ‘scenario-response’ approach; promote the scientificity of emergency plan and platform and establish the multidisciplinary education framework for emergency management. In this paper, the practical requirements and science backgrounds of the Major Research Plan are analyzed, the research targets and topics are introduced, and some important issues in the implementation are discussed. The Major Research Plan will provide more effective and scientific supports for Chinese emergency management.

Keywords: major research plan, unconventional incident, emergency management, scenario-response, emergency management platform

1. INTRODUCTION

The frequencies and scales of incidents are increasing and enlarging along with the development of the society and environmental change all over the world. Such as, 2011 Japan great earthquake, 2008 Wenchuan earthquake, 2005 Hurricane Katrina, 2004 Indian Ocean Tsunami, 2001 USA 911, etc. They all caused great damages to the society. Many incidents, which are called unconventional incidents here, have no precursor along with obvious

complex characteristics, secondary disasters and great damages. It is difficult to respond the incident by the conventional management methods. In order to improve Chinese government's emergency management ability, and promote the development of Chinese emergency management science, the National Natural Science Foundation of China (NSFC) launched the Major Research Plan 'Study On Unconventional Emergency Management' in 2008. In this paper, the practical requirements and science backgrounds of the Major Research Plan are analyzed, the research targets and topics are introduced, and some important issues in the implementation are discussed.

2. SOCIETY REQUIREMENTS

(1) The vulnerability of modern society needs emergency management

Modern society is a coupled system consisting of human and nature. It has typical characteristics of complex systems. In recent years, the vulnerability of actual society's system faces serious challenges because of frequent unconventional incidents. Such incidents are the most urgent problems of all nations, such as "9•11" in USA, the Tsunami in Indian Ocean, the massive earthquake in Wenchuan of China and in East-North of Japan. The enormous damages influenced social and economic development and even changed the regional political structure and strategy. To improve emergency management to those unconventional emergencies is a common demand of all nations including China (Cauchemez, 2008; Ferguson, 2006).

(2) It is necessary to improve the emergency management capability for increasing government's capability and building service-oriented government.

With the rapid development of the economy, Chinese government is improving economic regulation and market supervision levels, and reinforcing the capability of social management and public service. Improving the emergency management capability is an urgent demand and an important guarantee to enhance our country's governance capability and build service-oriented government.

Facing to the serious situation of the new type's incidents, Chinese government takes improving emergency management policy and responding various risks effectively as one of the most important tasks for building harmonious society. In March 2008, Prime Minister Wen Jiabao pointed out in governmental work report that we should improve the emergency management system, the capability of emergency prevention and response, the research of disaster's characteristics and mechanisms, and the capability of disaster prevention and reduction.

3. SCIENTIFIC BACKGROUND

(1) The development of emergency management science needs creative fundamental research

Emergency management science belongs to risk management science which has many study foundations. A “prediction-response” management mode and a “prediction-warning-response-recovery” process have been built. However, because the evolving mechanism of unconventional incidents is little known, and the incident situation, possibility and damage degree are little recognized, it is difficult to prevent ahead. Therefore, a new or creative emergency management approach is desired to solve the problem.

The scientific issues of unconventional emergencies management obviously show multidisciplinary characteristics including decision-making science, information science, psychology, etc. At the same time, these issues have the special study boundary conditions. The research of related disciplines must be built on the foundation of creative academic ideas (Britton, 2000; Gonzalex, 2008; Kossinets, 2006). Developing the fundamental research of unconventional emergency management will broaden the science thinking of emergency management and form the new emergency management theories and approaches.

(2) Emergency management science is very important for the development of Chinese management science.

- Research of emergency management has been paid extensive attention since 2003 “SARS” crisis in China.
- Public safety research is taken as one of the 11 most important areas of Chinese technology development in “Chinese mid-long-term scientific and technology development plan outline”(2006-2020).
- In “The 11th Five-Year Plan of the National Natural Science Foundation of China (NSFC)”, public safety is regarded as a priority development field.

Compared to the research in China, international emergency management research emphasizes more multidisciplinary intersection and derivation-coupling of incidents, especially the relevance between the incidents caused by nature and human (Gerstenberger, 2005; Harraid, 2007; Topper, 2005). It also emphasizes the influence of the national characteristics on emergency management.

In brief, to strengthen emergency management researches, innovating emergency management approaches and increasing the scientificness of emergency management works are urgent to all nations. The researches of unconventional emergencies management are necessary for creatively developing Chinese emergency management science.

4. KEY SCIENTIFIC ISSUES AND PURPOSES

4.1 The key scientific issues

“Study on Unconventional Emergencies Management” aims to study on the following three key scientific issues, the framework is shown in Figure 1.

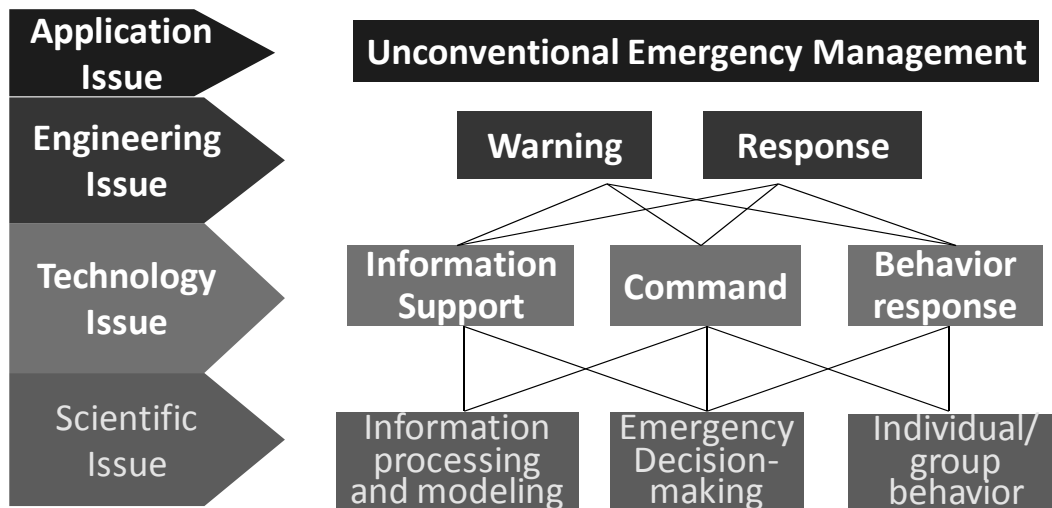


Figure 1: Framework of the key scientific issues

(1) Information processing and model development of evolutionary mechanism of unconventional incidents

Towards the massive, heterogeneous and real-time data of unconventional incidents during the event's possible precursors and evolvement, the following studies are needed:

- ① Studies on the scientific issues of the information processing of these data including collection, data analysis, transmission, visualization and sharing, etc,
- ② Studies on the theory and method on non-traditional (for example, data driven and computational experiments) complex modeling of unconventional incidents' evolution mechanisms.

The major research contents of this issue include:

- ① The information processing of unconventional incidents.
- ② Modeling of unconventional incidents' evolution mechanisms.

(2) The emergency decision-making theory of unconventional incidents

The studies include:

The whole-process dynamic assessment, decision-making theories and methods of the on-site decision-making of unconventional incidents; The theories and methods of emergency preparation system, decision-making command system, rescuing/administration system and the organization's

design, operation and evaluation of resource allocation system; The theoretical design of emergency platform, compilation and drilling methods of pre-plan system; The integrated decision-making theories and methods facing to multiple disasters and scenario-built, and the soft-hardware system integration.

The major research contents of this issue include:

- ①The theories and methods of emergency evaluation, analysis and decision-making;
- ②The organization design and operation optimization of emergency command system;
- ③Emergency decision-making support platform system.

(3) The behavior and psychological response mechanism of an individual and a group in emergency conditions.

It is necessary for us to study the mechanisms of cognition, mood, attitude, and requirement of the major participants including managers, rescuers and populaces when they face emergency and pressure. Also, the group’s behavior mechanisms and structural features should be studied.

The major research contents of this problem include:

- ① The mechanism of individual psychology under a pressured condition;
- The group’s action in emergency.

In this study plan, three key problems including seven major topics and their logical relations are shown in Figs.2 and 3, respectively.

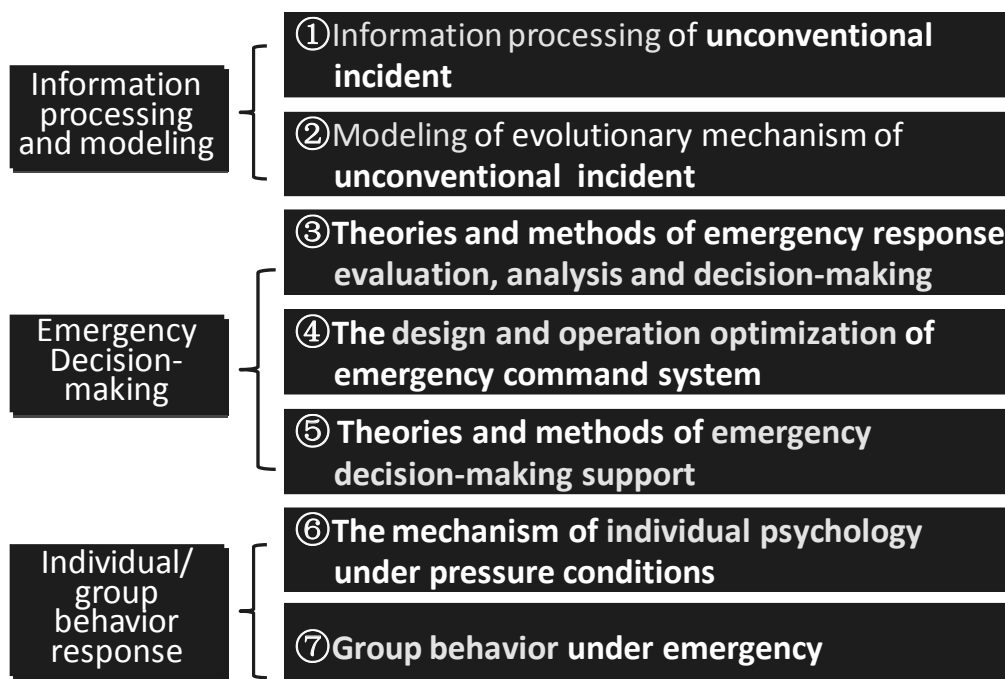


Figure 2: Main research contents

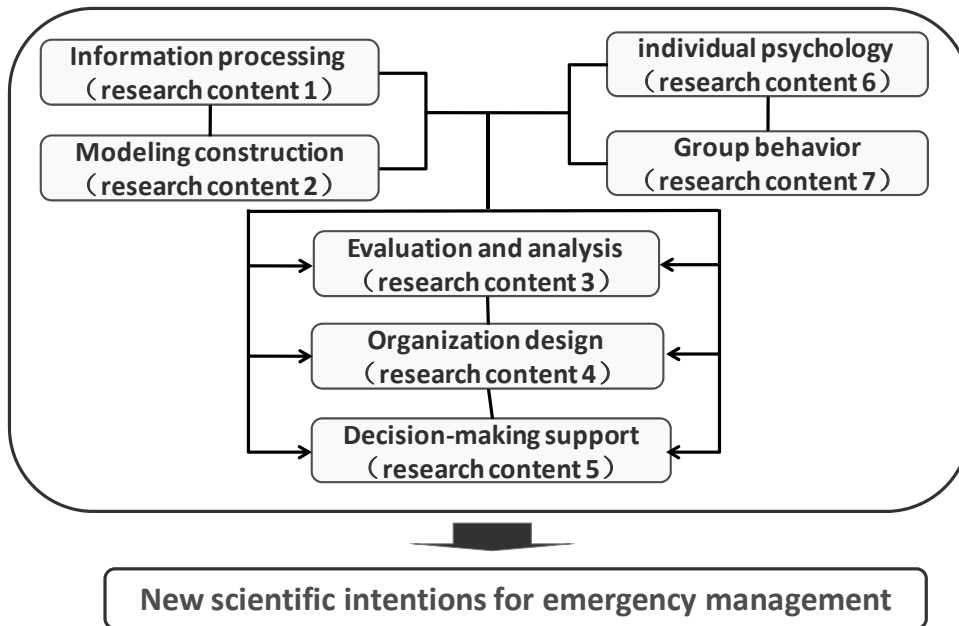


Figure 3: The logical relationship between the research contents

4.2 Research purposes

The main purposes of “Study on Unconventional Emergency Management” are as follows:

(1) To form a profound scientific cognition of objective laws in the core steps (warning and decision-making) of unconventional emergencies management through observation, experiment, innovation of theory and integration of the relating multiple disciplines in the specially restrictive condition of unconventional incidents.

(2) To build a “scenario-response” theoretical system of unconventional emergencies management and to improve innovation ability of emergency management science.

(3) To provide a scientific, efficient and ordered decision-making reference to respond unconventional incidents through improving the scientific level of nation’s emergency management system including emergency platform and pre-plan system.

(4) To develop emergency management interdiscipline and to train innovative emergency management experts.

The detailed purposes are as follows:

- To propose a series of key regulars and methods for unconventional emergencies management which include information processing methods and evolutionary mechanisms of unconventional incidents and the behavior and psychological

response regular of an individual and a group under emergency conditions.

- To integrate the key regulars and methods above and to get a general description of unconventional incidents; To form a profound scientific cognition of warning and response in emergency management combined with emergency decision-making theory of unconventional incidents, and provide scientific methods; To develop a “scenario-response” theoretical system of unconventional emergencies management.
- To provide a compilation and a revised manual of emergency pre-plan system; To apply scientific achievements into emergency platform system and to provide a platform of theory and experimental verification of emergency decision-making; To provide scientific measure and basis to improve emergency management level and to provide a scientific, efficient and ordered decision-making reference to respond unconventional incidents.
- To apply the achievements of the study plan to finally develop three integrated platforms which include simulation system of unconventional incidents, the fundamental platforms of emergency platform and emergency pre-plan system.
- To form a new interdisciplinary direction which jumps from separated to systematic and interdisciplinary researches for the purpose of “Emergency decision-making”. It also helps to lay the foundation of developing emergency management interdiscipline.

5. THE GENERAL ARRANGEMENT OF STUDY PLAN IMPLEMENTATION

According to the actual demand features of emergency works, the study periods of the study plan are set to be 6 years. The study plan will support a series of study projects. The executing periods of the supported projects are set to be 3-4 years. The series of study projects include 3 key scientific issues covering the 7 major study topics. Each topic contains 8-9 cultivated projects which will be 3 years and 3-4 key projects which will be 3-4 years. According to integrated purpose, the study plan has 3 integration projects in different scales which will be 3-4 years.

The settings of the projects are mainly proceeded in the first 3 years. The study plan will set up the fundamental exploration and the application research projects based on the objective demand as soon as possible. After the mid-term, the study plan will choose the research directions which can play key role to reach the overall objectives and launch “integration projects” to carry out the important integrated innovative researches on the basis of all types of project achievements in the first stage. In the last three years of the study plan, it will emphasize on the integration and innovation of the achievements in the relating projects. The first stage assessment intends to be arranged in the third year of the study plan implementation.

According to the results of the stage assessment, it will put forwards an adjusted scheme to the study plan and to establish the foundation of “integration projects” in the last stage.

6. EXPECTED OUTCOMES

The expected outcomes of this research plan include:

(1) Through the complex system model construction methods (such as, society calculations, complex network, etc.) and communication technology of computer and internet, the general description of unconventional incident will be obtained. In the academic aspect, this platform can be treated as a special “experimental” tool in study process. In the applied aspect, this platform combing with emergency decision-making of unconventional incidents can be treated as an important technology reference of emergency decision-making.

(2) After getting the support of the various relating directions, the emergency platform system will become a theoretical and validated-experiment platform for providing emergency decision-making and will form scientific and powerful national emergency platform and an emergency pre-plan system. Also, it can improve the service efficiency of national emergency management funding.

Through this research plan, great development on China’s emergency management science will be obtained in two aspects:

(1) To acquire the results with important international impact. Chinese scientists can contribute greatly and originally in this field and can develop Chinese emergency management fundamental theory with important international impact.

(2) To accelerate the formation of emergency management disciplinary direction.

7. CONCLUSIONS

In order to improve Chinese government’s emergency management ability, and promote the development of Chinese emergency management science, the National Natural Science Foundation of China (NSFC) launched the Major Research Plan ‘Study on Unconventional Emergency Management’ in 2008. The research plan aims to deeply understand the mechanism and provide the approach for the core parts in the emergency management - warning and response - by integrating the multidisciplinary observations, experiments and theories; establish the unconventional emergency management theory based on the ‘scenario-response’ approach; promote the scientificity of emergency plan and platform and establish the multidisciplinary education framework for emergency management. The Major Research Plan will provide more effective and scientific supports for Chinese emergency management.

ACKNOWLEDGEMENT

This work was supported by Ministry of Science and Technology of the People's Republic of China under Grant No. 2011BAK07B02 and No. 2011BAK07B03.

REFERENCES

Britton, N. R., Clark, G. J., 2000. From response to resilience; Emergency management reform in New Zealand. *Natural Hazard Rev.* 1(3), 145-150.

Cauchemez, S., et al., 2008. Estimating the impact of school closure on influenza transmission from sentinel data. *Nature* 452, 750-754.

Ferguson, N. M., et al., 2006. Strategies for mitigating an influenza pandemic. *Nature* 442, 448-452.

Gerstenberger, M. C., Wiemer, S., Jones, L. M., Reasenber, P. A., 2005. Real-time forecasts of tomorrow's earthquakes in California. *Nature* 435, 328-331.

Gonzalez, M. C., Hidalgo, C. A., Barabasi, A. L., 2008. Understanding individual human mobility patterns. *Nature* 453, 779-782.

Kossinets, G., Watts, D. J., 2006. Empirical analysis of an evolving social network. *Science* 311, 88-90.

Harraid, J., Jefferson, T., 2007. Shared situation awareness in emergency management mitigation and response. *System Sciences*, 23-23.

Topper, G. J., Worsley, P. M., 2000. The use of remote sensing and GIS technologies by New South Wales agriculture for emergency management. *Geosciences and remote sensing symposium* 4, 1489-1491

Effects of environmental condition on corrosion of structural steel in marine environment of Thailand

Prasong PERMSUWAN¹, Pakawat SANCHAROEN²,
Somnuk TANGTERMSIRIKUL³, Paiboon SREEARUNATHAI⁴,
Ekkarut VIYANIT⁵ and Wanida PONGSAKSAWAD⁵

- ¹ Graduate student, School of Civil Engineering and Technology, Sirindhorn International Institute of Technology, Thammasat University, Thailand
Prasong_civilnu@hotmail.com
- ² Researcher, Construction and Maintenance Technology Research Center, Sirindhorn International Institute of Technology, Thammasat University, Thailand
- ³ Professor, School of Civil Engineering and Technology, Sirindhorn International Institute of Technology, Thammasat University, Thailand
- ⁴ Lecturer, School of Bio-Chemical Engineering and Technology (BCET), Sirindhorn International Institute of Technology, Thammasat University, Thailand
- ⁵ Researcher, National Metal and Materials Technology Center (MTEC), 114 Thailand Science Park, Thailand

ABSTRACT

Structural steels which are hot-rolled steel grade SS400 according to JIS G3101, hot-rolled steel grade SM490YA according to JIS G3106 and hot-rolled atmospheric corrosion resisting steel grade SMA490A according to JIS G3114 were exposed from January 2010 until January 2011 to marine and industrial environment at Maptaphut industrial estate, Rayong, Thailand. The specimens were exposed in two conditions that were atmospheric and tidal zone. The corrosion behaviors of specimens were studied by means of weight loss measurement according to ISO8407, compositions of rust layers by XRD analysis and characteristic of rust layer by SEM analysis. Also, environmental conditions such as temperature, relative humidity, and deposition rate of chloride were monitored monthly. The corrosion rates of specimens were also measured by potentiodynamic polarization in laboratory. The results showed that corrosion rate at 12 months of carbon steel was higher than that of weathering steel. Furthermore, specimen in tidal zone showed higher corrosion rate than atmospheric zone obviously due to effects of biofouling and wet-dry condition. The result can be used for material selection and designing service life of steel structure in Thailand.

Keyword: *corrosion, marine, atmospheric, tidal, carbon steel, weathering steel, chloride*

1. INTRODUCTION

Structural design of both reinforced concrete and steel structures consider mainly the strength of members. But durability design or service life design, which also affects the safety of structure, is rarely concerned. Particularly, the steel can be deteriorated rapidly when it is subjected to corrosive environmental condition. Carbon steel and weathering steel are used in steel structure including high-rise building, bridge, offshore platform, sheet piling, steel pile and coastal facilities. Normally, steel structures in marine environment are deteriorated by atmospheric corrosion. Also, some part of those steel structures such as steel piles or sheet piles are immersed in the sea water. So the area between the lowest sea level and the highest sea level is influenced by tidal zone corrosion.

Atmospheric corrosion is an electrochemical reaction occurring on metal surface in a presence of thin film electrolyte. In case of atmospheric corrosion, structural steel in marine environment deteriorates primarily by climatic factors such as temperature, relative humidity, and the presence of chloride and SO_2 . Normally, rust formed on surface of carbon steel is porous with poor adherent, and cracked at the outer part (Castano et al., 2010). This phenomena causes oxygen, water, Cl^- and SO_2 from outside to penetrate to the steel substrate easily (Yuantai et al, 2009). For corrosion resisting steel, at the early stage, the rust is formed similarly to the carbon steel. But as the exposure time increased, the rust layer becomes more compact, denser, and tighter (Renato, et al., 2003). For this reason, the rust layer acts as the barrier to inhibit corrosive species and then the rate of corrosion is decreased.

The compositions of rust layer have been observed by several researchers. Mainly, the compositions of rust found in marine environment are composed of lepidocrocite ($\gamma\text{-FeOOH}$), goethite ($\alpha\text{-FeOOH}$), akaganeite ($\beta\text{-FeOOH}$) and magnetite (Fe_3O_4). The $\gamma\text{-FeOOH}$ is usually formed in the early stage and transformed to $\alpha\text{-FeOOH}$ and Fe_3O_4 . This $\alpha\text{-FeOOH}$ is important key to reduce corrosion because its compact and dense structure prevent penetration of water, oxygen and corrosive species from the environment. However, area with presence of chloride is often observed $\beta\text{-FeOOH}$ which has porous and loose structure.

In Thailand, environmental conditions are different from other countries. There is no sufficient data of atmospheric corrosion to model or predict steel corrosion in order to design service life of steel structures in Thailand. Also, there is limit information on atmospheric and tidal corrosion. In addition, the standard currently used to design steel structures in Thailand was adopted from other countries. It is essential to study the corrosion behavior of structural steel in Thailand. The aim of this paper was to investigate the corrosion behavior of SS400, SM490YA and SMA490A steels in the marine environment of Thailand.

2. EXPERIMENTAL PROGRAM

2.1 Specimen preparation

The materials tested in this study are three kinds of structural steel; 1) hot-rolled steels for general structure grade SS400 according to JIS G3101, 2) hot-rolled steels for welded structure grade SM490YA according to JIS G3106, and 3) hot-rolled atmospheric corrosion resisting steels for welded structure grade SMA490A according to JIS G3114. Their chemical compositions determined by spark emission spectrometer are shown in Table 1 together with the specified values in the standard. ISO 8565 standard specification suggests the following procedures for specimen preparation before exposure test. Specimens were cut from the steel plate to the size of 150×70×3 mm for SS400 and SM490YA steels, and 150×70×5 mm for SMA490A steel. The mill scale on the surface of the specimens was mechanically removed by sand blasting and then wet-polished by 600 grade sand paper on all surfaces. Finally, the specimens were rinsed with distilled water and ethyl alcohol, dried by blower, weighted and immediately placed in desiccators before the test.

Table 1: Chemical compositions of different types of steel

Steel types	Chemical composition (% by wt)									
	C	Si	Mn	P	S	Cr	Ni	Cu	Al	Mo
Standard JIS G3106	≤ 0.20	≤ 0.55	≤ 1.65	≤ 0.035	≤ 0.035	-	-	-	-	-
SM490YA	0.070	0.218	0.352	0.009	0.016	0.031	0.073	0.154	0.013	0.015
Standard JIS G3101	-	-	-	≤ 0.05	≤ 0.05	-	-	-	-	-
SS400	0.047	0.174	1.039	0.010	0.006	0.026	-	-	-	-
Standard JIS G3114	≤ 0.18	0.15-0.65	≤ 1.4	≤ 0.035	≤ 0.035	0.45-0.75	0.05-0.30	0.30-0.50	-	-
SMA490A	0.115	0.396	0.368	0.076	0.005	0.681	0.16	0.368	0.021	0.003

2.2 Exposure test

Exposure site is located at Maptaphut industrial estate, Rayong, Thailand as shown in Figure 1. The position coordinates of this location is 12° 39' northern latitude and 101° 10' eastern longitude. Even though, environment of exposure site is marine environment but this area is also an industrial estate with coal- power plant, oil refinery, chemical industry, etc. The experiment was conducted from January 2010 to January 2011. The exposure test was conducted in two conditions which were atmospheric and tidal zone exposure.

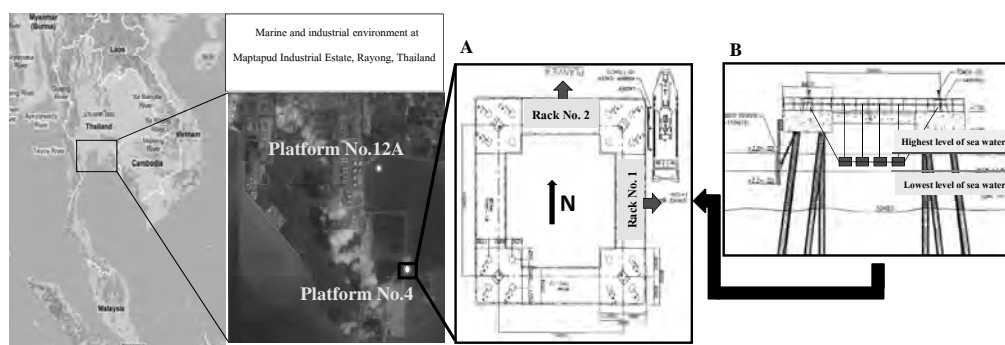


Figure 1: Details of the exposure site:
(A) atmospheric exposure and (B) tidal exposure

For atmospheric exposure, two exposure racks according to ISO 8565 were set on the high voltage transmission tower platform No. 4 only. Rack No.1 faced to the East and rack No.2 faced to the North directions with the rack slope of 45° to the horizontal as shown in Figures 1 and 2.

For tidal exposure, sample was placed in the plastic box and installed under the transmission tower platform number 4 and 12A of which water quality are different. The position of the boxes was set in the middle between the highest and the lowest sea water level in order to simulate wet-dry condition as shown in Figures 1 and 2. Environmental conditions such as temperature and relative humidity were monitored monthly by sensors connected to a data logger near the rack No.1. The results are shown in Table 2.



Figure 2: The exposure rack of atmospheric zone
(left) and tidal zone (right)

Chloride deposition rate was measured monthly by using the wet candle method according to ISO 9225, and surface of wet candle exposed to atmosphere is 100 cm². Also, the wet plate modified from standard wet candle method was installed in 4 directions in order to measure effect of wind directions on chloride deposition rate. The results are shown in Table 2. The sea water properties, mainly chloride and sulfate concentration, were measured by Ion-chromatography. The results are shown in Table 2.

The compositions of corrosion products were characterized by X-ray diffraction (XRD) method using X-ray diffractometer (Rigaku TTRAX III 50 kV 300mA) with Cu target. The scan is performed at a speed of 10°/min,

a scan step of 0.02 at 20 and range from 10° to 70° at 20. The characteristic of rust layer was observed by SEM analysis using JEOL model JSM-6301F.

After 1, 3, 6 and 12 months, exposed specimens and monitored data were collected for analysis. Corrosion products were removed chemically by HCl acid etching according to ISO 8407. After corrosion products had been removed completely, the specimens were rinsed with ethanol, dried with blower and weighted to measure weight loss.

Table 2: Atmospheric conditions and sea water properties

Atmospheric conditions			Sea water properties			
Monthly average	Monthly average	Monthly average	Chloride (ppm)		Sulfate (ppm)	
temperature (°C)	relative humidity (%)	Cl ⁻ deposition (mg/(m ² .day))	Tower4	Tower12A	Tower4	Tower12A
30.6	61.3	22.5	19586	18821	3147	3041

Table 3: Chloride deposition rate of each direction

Wet-plate Direction faced to	East	North	West	South
Chloride deposition rate (mg/(m ² .day))	27.75	27.39	27.94	39.43

3. RESULTS AND DISCUSSION

3.1 Environmental characteristics at exposure site

The environmental characteristics measured at the exposure sites are shown in Table 2. According to ISO 9223, environmental conditions are classified in term of chloride deposition rate (class S) and sulfur dioxide deposition rate (class P). Also, Time of wetness (TOW) (class τ), the period of time when relative humidity is greater than 80% and temperature is greater than 0°C, is also used for the classification. Environmental condition of exposure site is classified as S1 because chloride deposition rate is 22.47 mg/m².day which is between 3-60 mg/m².day. Environmental condition is classified as class τ 3 because TOW is 9.1% which is between $3 < \tau \leq 30$ %. Also, the corrosive categories of the exposure site can be classified as C2 (low) to C4 (high) class by S1 and τ 3 depending on classification of sulfur dioxide. As shown in Table 3, the result of the wet plate shows that chloride deposition of rack No. 2 facing north is higher than that of rack No. 1 facing east because of the wind direction.

3.2 Thickness loss

Figure 4 shows examples of the surface appearance of SS400 steel after 12 months exposure at atmospheric and tidal zone. In atmospheric zone, dark-brown rust product uniformly covered the entire surface while uneven surface was observed in specimens exposed to tidal zone and were covered with tightly attached biofouling. Other types of steel showed similar appearance after 12 months exposure.

Generally, the corrosion rate of steel exposed to real environment was calculated in term of thickness loss. The equation used to calculate thickness loss is shown in Eq.1

$$C = \frac{W}{\rho A} \times 10^4 \quad (1)$$

where C is the thickness loss (μm), w is the weight loss (g) of specimen after being exposed, ρ is the density of the steel (7.86 g/cm^3) and A is the exposed surface area of the specimen (both sides) (cm^2).

Figures 5a and 5b show thickness loss of SS400, SM490YA and SMA490A steels exposed to atmospheric zone for 12 months on rack No.1 and rack No.2, respectively. In both exposure racks, the thickness loss of SS400, SM490YA and SMA490A steels continuously increased from the beginning to 12 months but the rate of corrosion decreased with increasing time. Especially, corrosion rate of SMA490A steel obviously decreased at the long term because rust layer was more compact and denser.

The thickness loss of SS400, SM490YA and SMA490A steels exposed to tidal zone after 12 months under platform No.4 and 12A are shown in Figures 6a and 6b. In tidal zone, the thickness loss of specimens is very high (greater than- $200 \mu\text{m}$) after 12 months of exposure. Both platforms, thickness loss of SMA490A was the lowest because of its alloying composition. Particularly, rate of corrosion of specimens under platform No.4 shows almost constant increasing without effect of protective rust layer. As the results, the thickness loss of specimens under platform No.4 is significantly higher than those under platform No.12A. This is because different water quality such as higher O_2 and higher Cl^- concentration content which causes fast growing of biofouling as well as accelerates steel corrosion was observed under platform No.4.

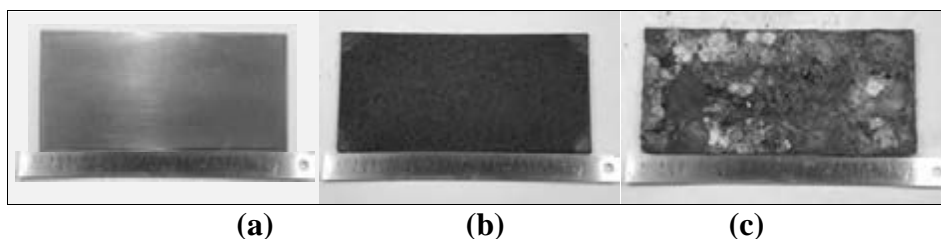


Figure 4: Appearance of SS400 steel: (a) before exposure, (b) after 12 months of exposure in atmospheric condition and (c) after 12 months of exposure in tidal condition

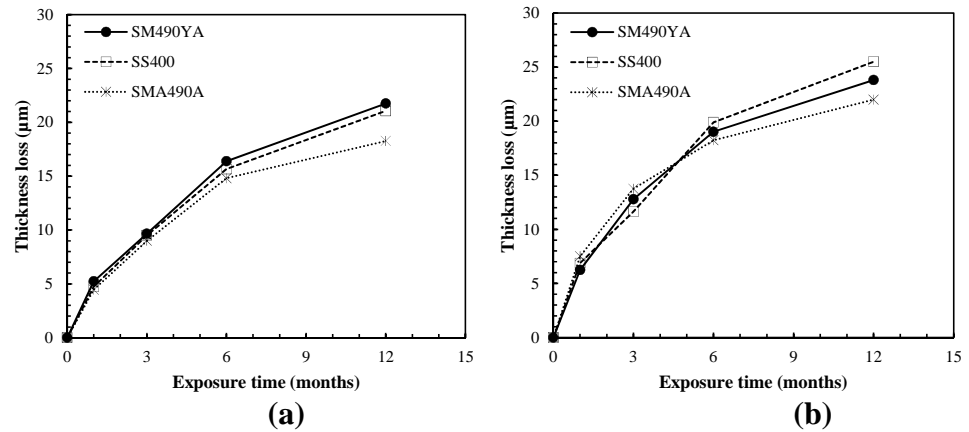


Figure 5: Thickness loss of specimens versus exposure time at atmospheric zone on; (a) rack No.1 and (b) rack No. 2

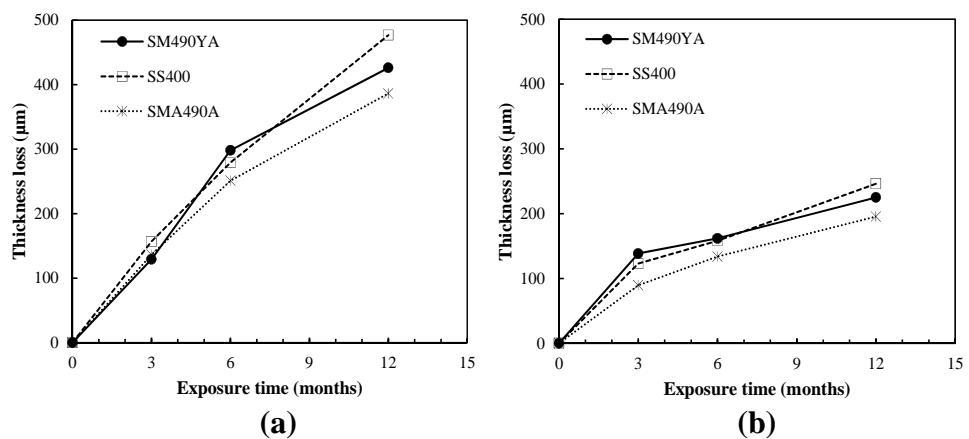


Figure 6: Thickness loss of specimens versus exposure time at tidal zone under; (a) platform No.4 and (b) platform No.12A

3.3 Corrosion product analysis

3.3.1 Cross section of rust layer

The cross section analysis of steel exposed to atmospheric zone for 12 months showed irregular layer of corrosion product with thickness about 25-70 µm. And rust layers were less compact as shown in Figure 7a. This layer showed some sites with localized corrosion, which probably act as anodes in the first steps of atmospheric corrosion (Castano et al., 2010). In tidal zone, the cross section showed thicker layer of corrosion products than that found in atmospheric zone as well as some site with deep localized corrosion as shown in Figure 7b. The thickness of the layer of corrosion products was approximately 25–200 µm. The deeper localized corrosion may be contributed by biofouling. It attached on part of steel surface and caused severe local corrosion. This can be the weak point of structures.

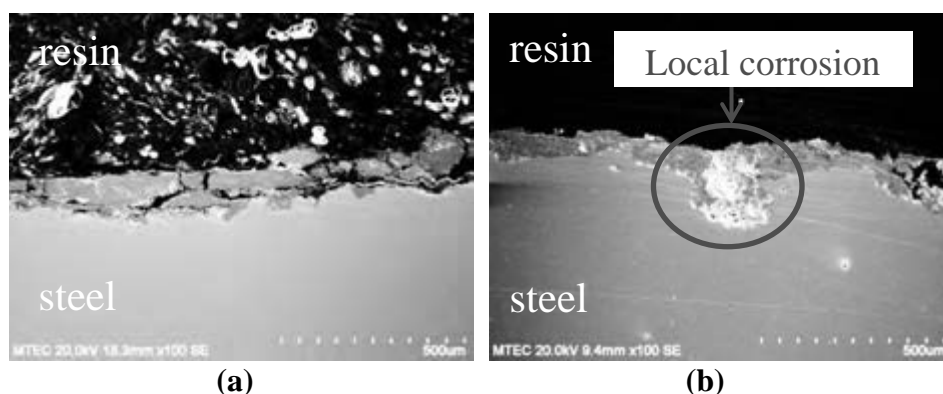


Figure 7: Rust layers on the SM490YA steel exposed for 12 months as; (a) atmospheric zone and (b) tidal zone

3.3.2 Composition of rust layer

The main phases of the rust layers formed on the steels exposed to atmospheric zone for 12 months were γ -FeOOH, followed by β -FeOOH and α -FeOOH as shown in Figure 8a. It can be seen that the main phase observed on SM490YA, SS400 and SMA490A was γ -FeOOH. It normally occurred at the beginning of corrosion. Then with the interaction of oxygen and water, γ -FeOOH partly or entirely transformed to more stable α -FeOOH (Zise et al., 2007). As the result, there was low amount of α -FeOOH that recently formed on the steels. Generally, β -FeOOH was only found in high chloride containing environment. As many researchers, investigated the effect of chloride ion on the transformation of rust formed on the carbon steel and observed that the content of β -FeOOH increased with the concentration of Cl ions in the environment. Kamimura et al. (2006) also reported that β -FeOOH was electrochemically active and the existence of β -FeOOH influenced the corrosion behavior of weathering steel exposed at marine site.

For tidal zone, the phases of rust layer formed on the steel exposed for 12 months in both locations was mainly Fe_3O_4 followed by γ -FeOOH, α -FeOOH and β -FeOOH, respectively as shown in Figure 8b. Peaks of Fe_3O_4 phases had high intensity with a small intensity of other phases. For occurring of Fe_3O_4 , many researchers reported that γ -FeOOH formed on the steel surface did not only reacts with the oxygen and water and become α -FeOOH, but also reacts with Fe^{2+} dissolved from the iron and forms Fe_3O_4 . As the results, there was Fe_3O_4 in rust layers only in tidal zone. There were many phases with high intensity because in severely corrosive sea water, rust layers formed very fast and rapidly transform to another phases. Anyway, rust layers in tidal zone did not act as efficiently protective rust layers like that of atmospheric zone because rust layers formed in this zone cannot inhibit corrosive species penetrated to surface of steel. For calcite phase, it was composition of biofouling shell attaching on the corrosion products.

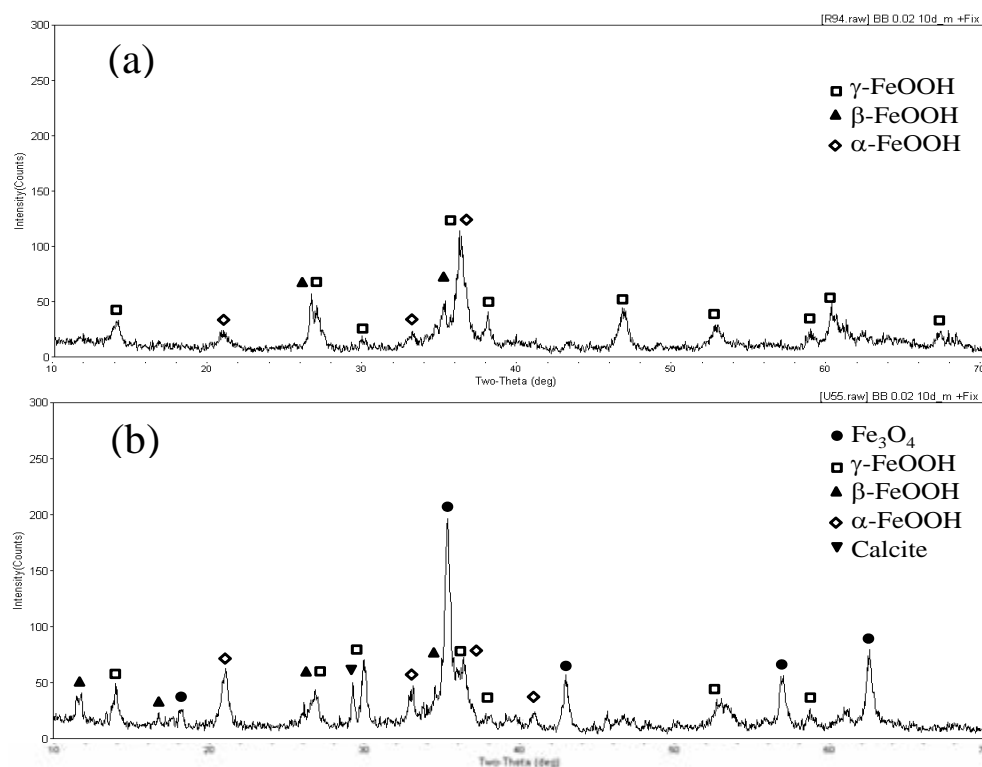


Figure 8: XRD spectra of corrosion products obtained from SM490YA for 12 months as; (a) atmospheric zone and (b) tidal zone

3.4 Corrosion rate

The prediction of corrosion rate of steel exposed to atmospheric condition was proposed by several researchers as a bi-logarithmic equation as shown in Eq.2. This equation usually fits well with corrosion behavior over time.

$$C = At^B \quad (2)$$

where C is the thickness loss (μm), t is the exposure time (month), and A , B are constants. The constants A and B can be determined by plot in log-log coordinate between steel thickness loss and exposure time. The regression analysis was conducted in log-log coordinate to determine values of constants A and B value.

For corrosion rate prediction equation, several researchers considered the B value as the growth law of corrosion product: parabolic or linear. If the B value is in the range of 0.5 to 1, the corrosion products do not significantly protect the steel surface from corrosion and is called a linear growth. On the other hand, if the B value is lower than 0.5, it indicates a parabolic growth by formation of protective rust layers to reduce rate of corrosion in the long term.

The corrosion rates per year and the values of A and B constant in all exposure zones of SS400, SM490YA and SMA490A steels were calculated from the bilogarithmic equation and shown in Table 4.

For atmospheric zone, the corrosion rate of rolled steel (SS400 and SM490YA) is higher than corrosion resisting steel (SMA490A) in both racks because B value of SS400 and SM490YA are higher than 0.5 which indicate high rate of corrosion. The key factor causing the difference of corrosion rate is the chemical composition of the steel. The corrosion rate of SMA490A is the lowest because the corrosion resisting steel contains some alloy elements such as Cu, Cr, and Ni that improve the corrosion resistance as shown in Table 1. Q.C. Zhang et al have studied the distribution of alloying elements during formation of rust layers. They reported that the presence of Cu restrains the supply of oxygen, retards the anodic dissolution and reduces the electronic conductivity of rust layers. For this reason, the corrosion rate of SMA490A steel is reduced. The corrosion rate of rack No.2 is higher than that of rack No.1 for all types of steel because rack No.2 is affected by the wind direction making higher Cl^- deposition rate on the specimen surface from the results of wet-plate. This shows the importance of the effect of local environmental conditions on steel corrosion. From the result, the corrosive category of environment at exposure site can be defined as class C3 (medium) based on ISO 9223.

In case of tidal zone corrosion, the corrosion rate of tidal zone is significantly more aggressive than atmospheric zone. The corrosion rates of tidal zone and atmospheric zone show the difference of more than 10 times. The high Cl^- concentration and wetting in tidal exposure accelerated corrosion process by formation of $\beta\text{-FeOOH}$. Although the $\alpha\text{-FeOOH}$ phase was formed on both carbon steel and weathering steel but the rust layers were not act as the protective barrier causing the high B value. Because, the $\alpha\text{-FeOOH}$ phase was not uniformly formed on the surface of steel and then rust layers cannot sufficiently protect the Cl^- penetration. Also, the effect of biofouling increased corrosion rate significantly. Biofouling is considered a major factor to control the corrosion behavior since the biofouling attached to the surface of steel tightly. Biofouling consumes oxygen, while supplies acid due to its excretion. As a result, steel subjects to extra corrosion due to acid (Coetser, 2005). Eventually, the corrosion affecting from biofouling is local corrosion which is more severe and difficult for predicting the rate. In term of location, corrosion of specimens under platform No.4 is more severe than that of the specimens under platform No.12A because the differences in Cl^- , sulfate and oxygen concentration. Moreover, specimens under platform No.12A is located in calm sea water and low water quality that has low oxygen concentration causing slow activity and slow growing of biofouling.

Table 4: Corrosion rate and constant values of steels

Steel type	Condition	Location	Corrosion rate ($\mu\text{m}/\text{year}$)	A	B
SM490YA	Atmospheric	Rack 1	22.68	5.25	0.59
		Rack 2	25.86	6.59	0.55
	Tidal	Under 4	461.42	54.45	0.86
		Under 12A	218.63	91.62	0.35
SS400	Atmospheric	Rack 1	22.21	4.83	0.61
		Rack 2	26.50	6.81	0.55
	Tidal	Under 4	480.29	65.46	0.80
		Under 12A	238.60	68.71	0.50
SMA490A	Atmospheric	Rack 1	19.93	4.63	0.59
		Rack 2	23.53	7.93	0.44
	Tidal	Under 4	398.53	61.66	0.75
		Under 12A	196.18	48.31	0.56

The typical rates of corrosion for structural steel suggested by BS 6349-1 standard are shown in Table 5. BS 6349-1 standard recommends the corrosion rate for steel structure design in various exposure zones. The results of this study show that average corrosion rate of the steels in atmospheric zone are approximately 23.45 $\mu\text{m}/\text{year}$. So the standard is acceptable to be used to design steel structures in atmospheric zone in Thailand. On the other hands, the results of average corrosion rates of the steels in tidal zone in this study are approximately 332.27 $\mu\text{m}/\text{year}$. The standard recommends maximum limit of 100 $\mu\text{m}/\text{year}$. Therefore, the standard is not suitable for steel structure design in tidal zone in Thailand.

Table 5: Typical rates of corrosion for structural steels temperate climates (BS 6349-1)

Exposure zone	Corrosion rate $\mu\text{m}/\text{year}$		Results of the study $\mu\text{m}/\text{year}$		
	Mean	Upper limit*	SM490YA	SS400	SMA490A
Atmospheric zone	40	100	25	26	23
Splash zone	80	170	-	-	-
Tidal zone	40	100	461	480	398
Seawater immersion zone	40	130	-	-	-

*The upper limit is the 95% probability values

4. CONCLUSIONS

1. Corrosion resistance of SMA490A steel is the highest in all conditions because its chemical compositions improve the characteristic of protective rust layers.
2. Corrosivity of sea water in tidal zone is significantly higher than atmospheric environment. This phenomenon is contributed by the effects of biofouling and high chloride concentration. Corroding mechanism of biofouling must be concerned in tidal zone corrosion and studied in the future.

3. Calculation of corrosion rate specified in the BS 6349-1 standard might not be suitable for structural steels exposed to Thailand environments especially for tidal zone corrosion.

ACKNOWLEDGEMENT

The research was funded by the Electricity Generating Authority of Thailand (EGAT).

REFERENCES

Castano J.G., et al, 2010, “*Atmospheric corrosion of carbon steel in Colombia*”, Corrosion science, 52, pp. 216-223.

Coetser S. E. and Cloete T. E., “*Biofouling and bio corrosion in industrial water systems*”, Critical reviews in microbiology, 31, 2005, pp. 213-232.

Kamimura, T. et al., 2006. “*Composition and protective ability of rust layer formed on weathering steel exposed to various environments*”. Corrosion Science, 48(9), pp.2799-2812.

Renato A.A., et al, 2003, “*Characterization of corrosion products formed on steels in the first months of atmospheric exposure*”, Materials research, 6, pp. 403-408.

Yuantai M., et al, 2009, “*Corrosion of low carbon steel in atmospheric environments of different chloride content*”, Corrosion science, 51, pp. 997-1006.

Zhang Q.C., et al, 2002, “*Corrosion behavior of weathering steel in marine atmosphere*”, Materials Chemistry and physics, 77, pp. 603-608.

Zise W. et al., 2007. “*The Morphology, Phase Composition and Effect of Corrosion Product on Simulated Archaeological Iron*”. Chin. J. Chrm. Eng, 15(3), pp.433-438

Influence of temperature on deterioration process due to chloride attack

Takahiro NISHIDA¹, Nobuaki OTSUKI² and Hiroshi MINAGAWA³

¹ Postdoctoral Fellow, Structural Mechanics Division,

Port and Airport Research Institute, Japan, nishida-t@pari.go.jp

² Professor, Graduate School of International Development Engineering,
Tokyo Institute of Technology, Japan

³ Associate Professor, Department of Civil Engineering,
Tohoku University, Japan

ABSTRACT

In recent years, maintenance of reinforced concrete has been considered as a major concern all over the world. One of the most serious deterioration issues is corrosion of reinforcing steel bars embedded in concrete due to chloride attack in marine environment.

On the other hand, it is generally said that the rates of ion diffusion and steel corrosion will increase with temperature elevation. Consequently, there is a possibility that the life time of reinforced concrete in warmer climates becomes comparatively shorter than colder regions. Therefore it is necessary to make the applicable methods for predicting the life time and maintenance management system responsive to the deterioration process in various temperature profiles.

From the backgrounds mentioned above, this paper presents influence of temperature on deterioration process of reinforced concrete members due to chloride attack. At first, the temperature dependency of deterioration phenomena in concrete is experimentally examined based on the Arrhenius theory. Secondly the life time of reinforced concrete are predicted and compared with the average temperature in each region. As a result of this paper, it is concluded that the influence of temperature on deterioration due to chloride attack is explained by the Arrhenius theory. In addition, the life time of the structures in south Asian cities are estimated relatively short.

Keywords: *deterioration process, activation energy, temperature dependency, life time, diffusion, steel corrosion*

1. INTRODUCTION

The maintenance of reinforced concrete is now becoming a major concern around the world due to the short supply of materials with the adequate qualities for construction and limited budget for construction. Chloride attack is one of the durability issues (Leeming, 1983), (Sørensen, 1982), (Popovics, 1983) especially in the coastal and marine areas. Since the deterioration of concrete is based on diffusion or chemical reactions, then

the deterioration progress has temperature dependency. It is generally known that, the rate of material diffusions or the chemical reactions rises up with the temperature elevation (Ohki, 1994).

The standards for construction materials or construction methods of reinforced concrete in the developed countries such as USA, EU or JAPAN have been established based from their studies and experiences under mild temperature condition (almost 20°C). These standards are now being used and followed by some developing countries without enough local investigations. When performing investigations using the standards established in another country, temperature becomes one of the most important parameters as well as the materials used.

In above viewpoints, it is necessary to determine the influence of temperature on the deterioration process of reinforced concrete due to chloride attack and discuss the appropriate predicting or maintenance method under several temperature conditions.

2. EXPERIMENTAL PROCEDURE

2.1 Materials used and Environmental Conditions

Ordinary Portland cement (density: 3.16 g/cm³, specific surface area: 3 270 cm²/g) was used as binder. River sand (density(SSD): 2.60 g/cm³, F.M.: 2.59) and crashed stones (density(SSD): 2.64 g/cm³, F.M.: 7.00) were used as fine and coarse aggregates respectively. Water-reducing and air-entraining agents were used as chemical admixtures. The type of steel embedded in the concrete specimen was SD 345 A (D16, deformed bar). Water cement ratio of concrete was set at 0.55.

The temperature during the experiments was controlled at 20°C, 30°C or 40°C in an environmental control chamber. Also the relative humidity was controlled and maintained at 60 %.

2.2 Investigated items

In order to evaluate the temperature effect on Cl⁻ diffusivity of minute region in concrete, the minute diffusion test (Otsuki, 2004) was conducted under three levels of fixed exposure temperatures (20°C, 30°C or 40°C). A small test piece (5x5x0.5mm) taken from concrete specimen (dia.100x200mm) was placed inside an acrylic cylinder cell as shown in Figure 1. One side of the cell was filled with NaCl solution (3.0 wt %) and the other side was filled with saturated Ca(OH)₂ solution. To measure the time-dependent changes of Cl⁻ concentrations in the Ca(OH)₂ solution side, the sample solution was taken every day. The concentration of Cl⁻ was then measured using ion chromatography. The diffusion coefficient was calculated using the Fick's law of diffusion as shown in Figure 1.

Also, in order to evaluate the temperature effect on the corrosion rate of steel bars in concrete, a corrosion monitoring test was conducted under the same three levels of fixed temperature (20°C, 30°C or 40°C). In this study, macrocell corrosion and microcell corrosion were separately evaluated using divided steel bars. In macrocell corrosion the anode and the cathode exist non-uniformly, while, in the case of microcell corrosion the anode and the cathode exist uniformly. The detail of reinforced concrete specimen is shown in Figure 2. The size of the specimen was 1500x 300 x 100 mm. This specimen was embedded with a divided steel bar, which was composed of divided steel elements as shown in Figure 2 for the purpose of making separate measurements for the rates of macrocell corrosion and microcell corrosion. The divided steel bars were electrically connected using lead wires soldered on each steel element. The measurement methods of microcell and macrocell corrosion rate are same with literature survey (Otsuki, 2000).

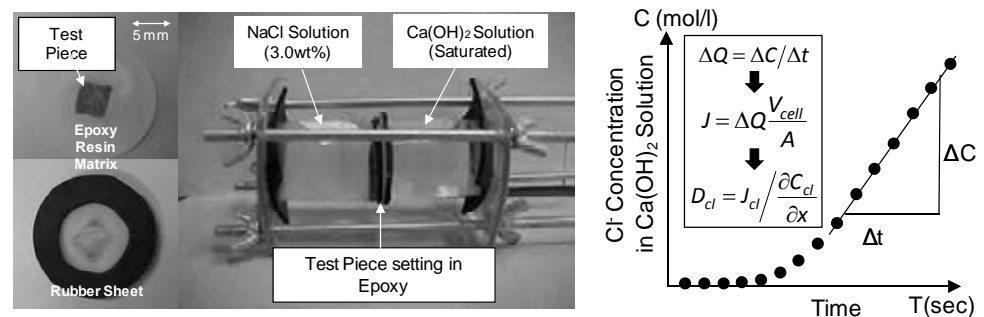


Figure 1: Outline of minute diffusion cell test

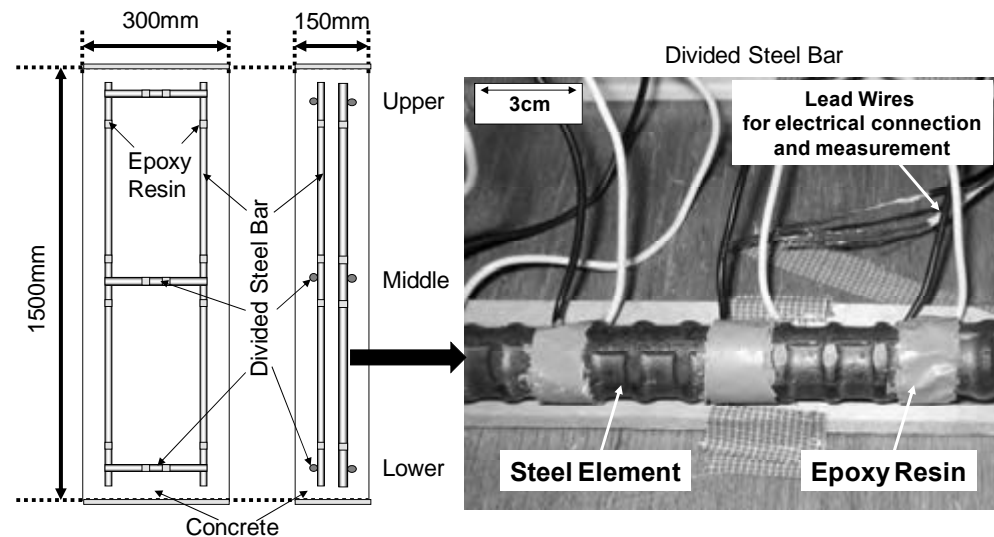


Figure 2: Outline of concrete specimen and divided steel bar

3. TEMPERATURE DEPENDENCY OF DIFFUSIVITY AND CORROSION IN CONCRETE

3.1 Theoretical background

Generally, the diffusion of substances and the chemical reactions rise up with the temperature elevation. Since diffusion and chemical reactions are the basis by which most cases of concrete deterioration occur, then the increase in concrete deterioration with the increase in temperature has to be considered.

When the influences of temperature on the diffusion of substance or the chemical reaction are discussed, the activation energy derived from the Arrhenius equation is the most important value. Therefore in this chapter, the deterioration progress of reinforced concrete is discussed based on the apparent activation energy calculated by Arrhenius equation. In general, the influences of temperature on diffusion or chemical reaction are theoretically illustrated using the Arrhenius equation as shown below.

$$k = a \exp\left(-\frac{\Delta E}{RT}\right) \quad (1)$$

here, k is Rate Constant, a is Frequency Factor (Constant), ΔE is Activation Energy (cal/mol), R is Ideal Gas Constant [1.99×10^{-3}] (cal/K/mol) and T is Absolute Temperature (K).

From equation (1), the increase in rate of the diffusion or chemical reaction with the temperature elevation can be theoretically confirmed. During the process of chemical reactions, the reactants seem to shift to the products side through an active state with high energy. The difference energy between the active state and the reactant is called as the activation energy (Ohki, 1994). In the process, where multiple chemical reactions are sequentially generated, the activation energy follows the reaction which determines the rate of reaction.

On the other hand, by taking the logarithm of the given equation, equation (1) will be transformed into the following equation.

$$\log k = \left(\frac{-\Delta E}{R} \cdot \log_{10} e\right) \left(\frac{1}{T}\right) + \log a \quad (2)$$

From experimental results, the relationship between logarithm of the rate constant and the reciprocal of absolute temperature is generally called the Arrhenius plot.

3.2 Temperature effect on Cl⁻ diffusivity in concrete

The influence of temperature on diffusivity of Cl⁻ in concrete is shown in Figure 3. From these graph, it can be seen that the rate of Cl⁻ diffusion in concrete rises up with the increase in temperature. Also the Arrhenius plots

of the Cl^- diffusivity in concrete are shown in Figure 4. From this, it can be seen that the relationship between logarithms of the diffusivity and the reciprocal of absolute temperature can be linearly distributed. Therefore it can be concluded that the diffusion of Cl^- in concrete follows Arrhenius theory. Moreover, the apparent activation energies of the Cl^- diffusivity in concrete obtained from Arrhenius plots are shown in Table 1. From this table, it can be seen that the apparent activation energies obtained in this study are a little high comparing with that obtained in literature survey (Page, 1981). This is because activation energies obtained in the literature survey are based on the data of cement paste. On the other hand, the Cl^- diffusivities of minute test pieces taken from concrete containing interfacial transition zone between aggregate and cement matrix are used in this study. That is, it is considered that the pore structure of cement matrix, especially the property of the interfacial transition zone, influences on the apparent activation energy and diffusion phenomenon.

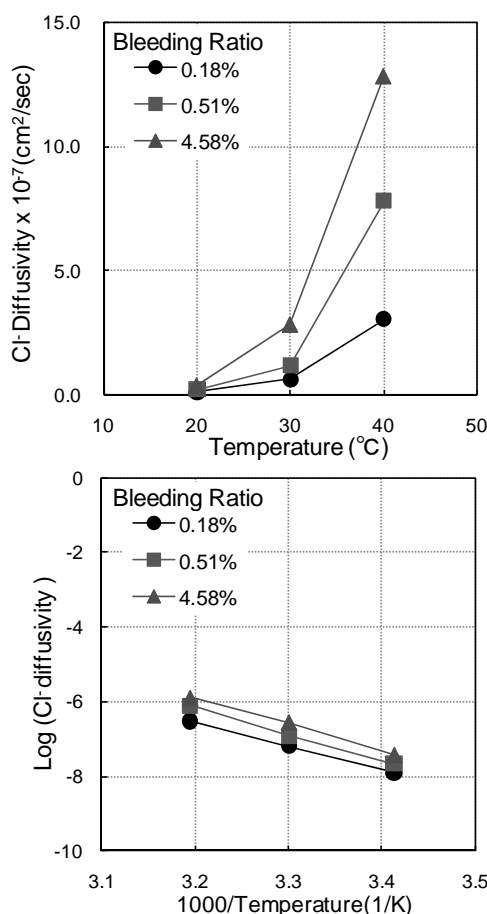


Figure 3: Influence of temperature on Cl^- diffusivity in concrete

Figure 4: Arrhenius plots of Cl^- diffusivity in concrete

Table 1: Apparent activation energies of Cl^- diffusivity in concrete obtained from Arrhenius plots

	Activation Energy (kcal/mol)
Present study: containing aggregate	16.8-32.2
Literature survey (Page, 1981): cement paste	7.7-10.0

Figure 5 shows the relationship between Cl⁻ diffusivity of concrete and water cement ratio proposed by JSCE standard specification (JSCE, 2001). And the broken lines in the graph show the Cl⁻ diffusivities considering with $\pm 10^{\circ}\text{C}$ difference against JSCE equation using obtained apparent activation energy. From this graph it is observed that the scattering of Cl⁻ diffusivity in the literature data seems to be explained by temperature effect. Therefore it can be concluded that the temperature profile is one of the most important factors when we check the diffusion coefficient of Cl⁻ in design stage.

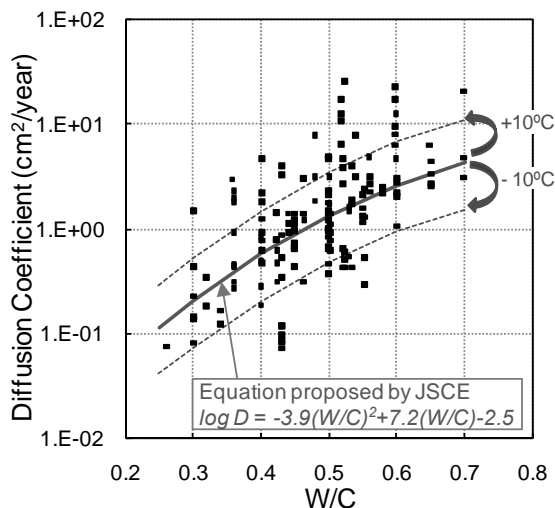
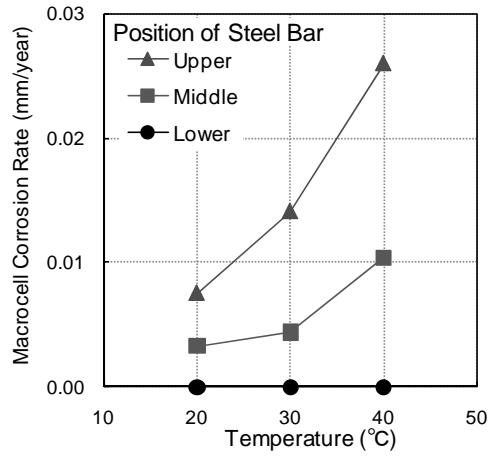


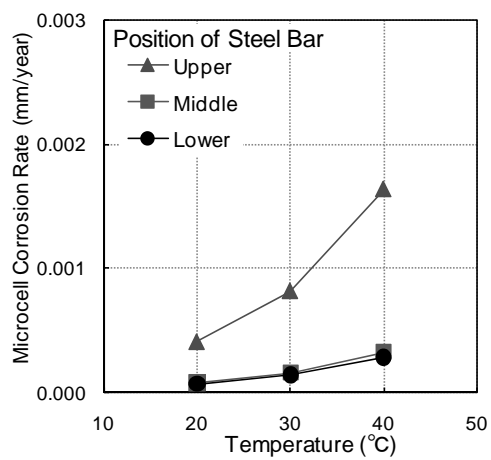
Figure 5: Relationship between Cl⁻ Diffusion Coefficient and W/C (JSCE, 2002) and temperature effect obtained in present study

3.3 Temperature effect on corrosion of steel bar in concrete

The influences of temperature on macrocell and microcell corrosion rate in concrete are shown in Figure 6. From these graphs, it can be seen that the macrocell and microcell corrosion rate in concrete rise up with temperature elevation. Also the Arrhenius plots of the corrosion rate in concrete are shown in Figure 7. From these figures, it can be seen that the relationship between the logarithms of corrosion rate and the reciprocal of absolute temperature can be linearly distributed. Therefore it can be concluded that the behavior of steel corrosion in concrete follows Arrhenius theory. Moreover, the apparent activation energies of macrocell and microcell corrosion in concrete obtained from Arrhenius plots are shown in Figure 8. From these figures, it can be seen that macrocell and microcell corrosion in concrete has different temperature dependency. That is to say, the apparent activation energy of macrocell corrosion increases with the increase in specific concrete resistance. On the other hand, the apparent activation energy of microcell corrosion is constant regardless of the specific concrete resistance.

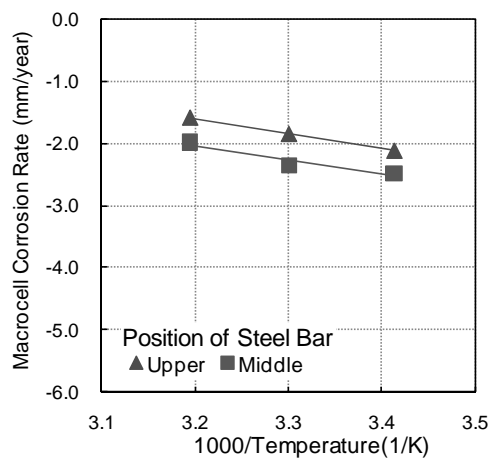


(a) Macrocell corrosion rate

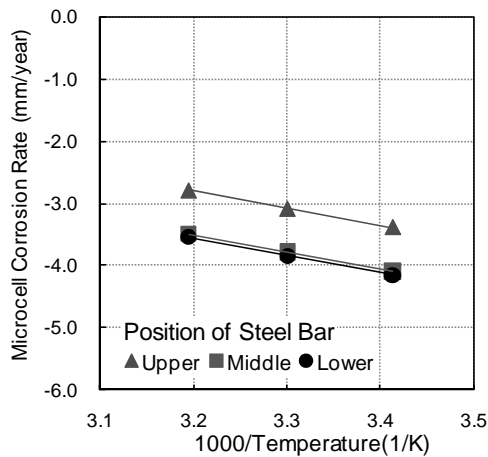


(b) Microcell corrosion rate

Figure 6: Influence of temperature on corrosion rate of steel bars in concrete



(a) Macrocell corrosion rate



(b) Microcell corrosion rate

Figure 7: Arrhenius plots of corrosion rate of steel bars in concrete

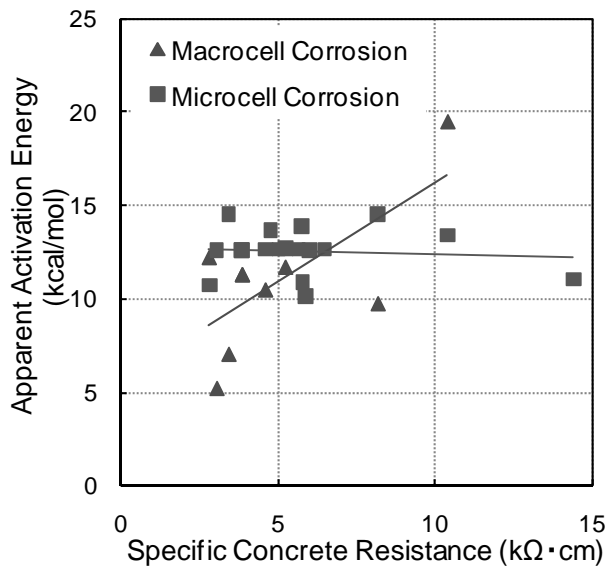


Figure 8: Apparent activation energy of corrosion rate of steel bar

4. PREDICTION OF DETERIORATION PROCESS CONSIDERING TEMPERATURE EFFECT

4.1 Life time of reinforced concrete due to steel corrosion

The determination of the life time of reinforced concrete is a difficult task because it includes many factors such as the importance of structures, part of the member or financial issue. However it is important to discuss the life time of structures based on several assumptions from the engineering point of view. In this study, the life time was defined as the sum of the terms of prediction results of the incubation, propagation and acceleration period, and the influence of temperature on the life time of reinforced concrete was discussed.

The water cement ratio, water content in mixture proportion and concrete cover were set at 0.55, 175kg/m³ and 7.0cm respectively. The

environmental condition considered in this prediction was tidal zone which is considered as the most severe environment that induces chloride attack. Also, in this prediction, the data of temperatures for 55 cities around the world was used.

4.2 Prediction of incubation periods

In order to predict the incubation periods, the rate of Cl⁻ diffusion in reinforced concrete considering the temperature was investigated using a numerical analysis. In this numerical analysis, Nernst-Planck equation considering with Debye-Hückel equation and electro-neutrality condition was used. By considering these equation and condition, the influence of co-existing ions in pore solution of concrete could be simulated. The effectiveness of this numerical analysis was already confirmed in the literature survey done by authors (Minagawa, 2002). In this study the above numerical analysis was modified as following equation in order to consider the effect of the temperature.

$$J_{Cl} = - \left(k \cdot T_1 \cdot B_{Cl} \cdot \left(1 - \ln 10 \times C_{Cl} \cdot \frac{0.51 \cdot Z_{Cl}^4}{4 \cdot \sqrt{I} \cdot (1 + \sqrt{I})^2} \right) - \frac{k \cdot T_1 \cdot \sum_n \left[Z_n \cdot \left(1 - \ln 10 \times C_n \cdot \frac{0.51 \cdot Z_n^4}{4 \cdot \sqrt{I} \cdot (1 + \sqrt{I})^2} \right) \cdot B_n \cdot \frac{\partial C_n}{\partial x} / \frac{\partial C_{Cl}}{\partial x} \right]}{\sum_n \left[Z_n^2 \cdot B_n \cdot C_n \right]} \right) \times \exp \left(\frac{\Delta E}{R} \left(\frac{1}{T_1} - \frac{1}{T_2} \right) \right) \cdot \frac{\partial C_{Cl}}{\partial x} \quad (3)$$

J is Flux of Ions (mol/cm²/sec), I is Ionic Species, k is Boltzman Number, $[=1.38 \times 10^{-23}]$ (J/K), T_1 is Basic Absolute Temperature $[=297]$ (K), T_2 is Absolute Temperature, B is Absolute Mobility (cm²/sec/V), C is Concentration of Ions (mol/cm³), x is Distance from Exposure Surface (cm), e is Elementary Electric Charge $[=1.60 \times 10^{-19}]$ (C), Z is Ionic Charge Number, ϕ is Electrostatic Potential (V).

The steel bar in concrete starts to corrode after the Cl⁻ concentration over the certain value (threshold concentration). “Technical Standards and Commentaries for Port and Harbour Facilities in Japan” (MLIT, 2009) describes that the threshold concentration of Cl⁻ can be set at around 2.0 kg/m³ in port and harbour port concrete facilities. In this study, the period until the Cl⁻ concentration around steel bar reaches to 2.0 kg/m³ is calculated by numerical analysis as incubation period.

4.3 Prediction of propagation and acceleration periods

In order to predict the propagation and acceleration periods, the rate of steel corrosion in concrete considering temperature effect was investigated. The total quantity of corrosion was calculated by taking the sum of the

quantity of corrosion in each period. The method of prediction for steel corrosion in concrete considering temperature effect is explained in the following.

Considering the influence of temperature on deterioration of reinforced concrete, the rate of corrosion of steel bar (macrocell and microcell) in concrete is different from each period. Especially it was confirmed that the influence of temperature on macrocell and microcell corrosion is different in previous chapters. Therefore, in case of predicting the propagation and acceleration period, it is necessary to consider the influence of temperature on macrocell and microcell corrosion rate separately. In this study the quantity of corrosion was calculated by integration of the rate of macrocell or microcell corrosion. The total quantity of corrosion was then calculated by the sum of the quantities of macrocell and microcell corrosion.

In the case of predicting the process of corrosion in concrete, it is necessary to know the basic rate of corrosion at a certain temperature. The data of corrosion rate at 20 °C as shown in Table 2 were used as a reference for the basic rate of steel corrosion in concrete. In the case of corrosion rate of steel bar in concrete before cracking, the experimental results obtained in the previous section were used. On the other hand in the case of the corrosion rate after cracking, the experimental results obtained by Otsuki (2000) were used.

Table 2: Data of corrosion rate at 20 °C

	Corrosion rate at 20 °C (mm/year)	
	Macrocell	Microcell
Before cracking	5.5×10^{-3}	2.6×10^{-4}
After cracking (Otsuki, 2000)	2.0×10^{-2}	6.0×10^{-2}

The total quantity of corrosion is calculated by taking the sum of the quantity of corrosion rates obtained in each period. Here it is reported that the total quantity of corrosion for crack propagation is equal to 10 mg/cm² (JSCE, 2001). Also it is reported that the bending property of reinforced concrete becomes 70% of the initial property when 15 % of the steel bar decreases due to corrosion (Miyagawa, 1998). According to this literature survey the quantity of corrosion at 15 % degradation of strength in case of steel bar with 16mm diameter is about 510 mg/cm². Therefore the quantities of corrosion at 10 mg/cm² and 510 mg/cm² were used in order to determine the periods of cracking (end of propagation period) and structural deterioration (end of acceleration period) respectively.

4.4 Predicted results

Figure 9 shows the relationship between the life time of reinforced concrete and the average temperature. From this figure it can be confirmed that the period of incubation, propagation and acceleration varied with the regional and seasonal temperature, and the life time of reinforced concrete exponentially decreased as the average temperature of the city. It is

therefore necessary to consider temperature effect on the design and maintenance of reinforced concrete, especially in the key cities of South-East Asian countries, where deterioration was most severe as indicated by reinforced concrete having only 70% of the life time compared to other countries with mild temperature environment (20°C). Also it can be considered that the life time of the reinforced concrete decreases 50% with 10 °C increase of temperature.

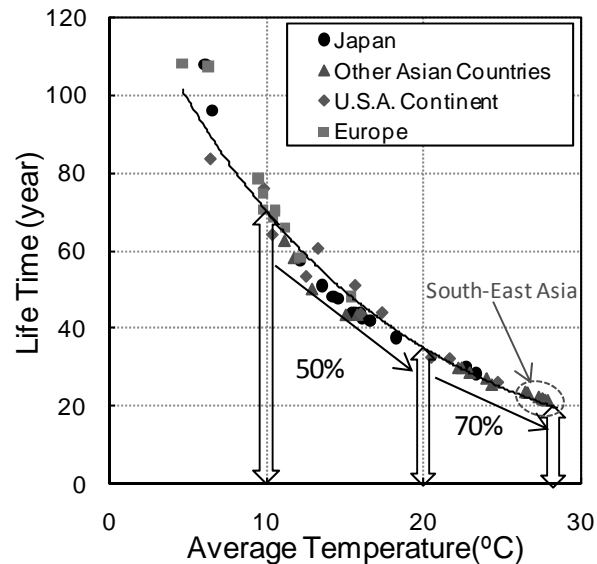


Figure 9: Predicted results of life time of reinforced concrete using the 55 cities of temperature profile

5. CONCLUSION

In present study, the influence of the temperature on the deterioration progress of RC due to chloride attack is theoretically and experimentally investigated. From the investigations the following conclusions are obtained;

- (1) The influence of temperature on deterioration due to chloride attack is explained by the Arrhenius theory from the view point of practice.
- (2) The life time of structures in several cities in severe marine environment are estimated. And the life time of the structures in south Asian cities are estimated relatively short.

REFERENCES

- Japan Society of Civil Engineers, 2001. Standard Specification for Concrete, Maintenance, 97-112.
- Japan Society of Civil Engineers, 2002. Complementary for Standard Specifications for Concrete Structures, Concrete Library 108, 55.
- Leeming, M. B., 1983. Corrosion of Steel Reinforcement in Off-shore Concrete Experience from the Concrete-in-the-Oceans Programme,

Corrosion of Reinforcement in Concrete Construction, Edited by. A.P. Crane. Ellis Horwood Ltd., Chichester, UK, 59-78.

Minagawa, H., Otsuki, N., Miyazato, S., and Nishida, T., 2002. Establishment of Numerical Analysis Method For the Prediction of Leaching of Calcium from Concrete Considering Migration of Multiple Ions, Concrete Library of JSCE, No.40, 253-268.

Miyagawa, T., Takewaka, K., Masuda, Y., and Moriwake, A., 1998. Report of Research Committee of Rehabilitation of Concrete Structures, Proceedings of the Japan Concrete Institute, V. 20, No. 1, 39-48.

Ohki, M., Ohsawa, T., Tanaka, M., and Tihara, H., 1994. Chemical Dictionary, 275.

Otsuki, N., Miyazato, S., Diola, N. B., and Suzuki, H., 2000. Influences of Bending Crack and Water-Cement Ratio on Chloride-Induced Corrosion of Main Reinforcing Bars and Stirrups, ACI Materials Journal, V. 97, No. 4, 454-464.

Otsuki, N., Yodsudjai, W., Nishida, T., and Yamane, H., 2004. New Test Methods for Measuring Strength and Chloride Ion Diffusion Coefficient of Minute Region in Concrete, ACI Materials Journal, V. 101, No. 2, 146-153.

Page, C. L., Short, N. R., and Tarras, A. El, "Diffusion of chloride ions in hardened cement pastes." Chemical and Concrete Research, 11, 1981, pp.395-406.

Popovics, S., Simeonov, Y., Boshinov, G., and Barovsky, N., 1983. Durability of Reinforced Concrete in Sea Water, Corrosion of Reinforcement in Concrete Construction, Edited by. A.P. Crane. Ellis Horwood Ltd., Chichester, UK, 19-38.

Ports and Harbours Bureau, Ministry of Land, Infrastructure, Transport and Tourism (MLIT), National Institute for Land and Infrastructure Management, MLIT, and Port and Airport Research Institute, 2009. Technical Standards and Commentaries for Port and Harbour Facilities in Japan, 370.

Sørensen, B., and Maahn, E., 1982. Penetration Rate of Chloride in Marine Concrete Structures, Nordic Concrete Research, Publication No.1, 24

Durability evaluation of marine structure based on continuous microstructure of concrete

Hitoshi AKIYAMA¹, Tomoya SAGAWA², Shafiqul Md. ISLAM¹
and Toshiharu KISHI³

¹ Graduate Student, School of Eng., The University of Tokyo, Japan
hito@iis.u-tokyo.ac.jp

² Toshiba Plant Systems & Services Corporation

³ Professor, Institute of Industrial Science, The University of Tokyo

ABSTRACT

This study discussed the relationship between chloride ion penetration and microstructure of concrete. The concrete cores were collected from the marine structures (the breakwater and launch slope) in the cold region of Japan. The blast furnace slag cement was used. This study applied the mercury step-by-step intrusion prosimetry (MSIP) to the measurement of porosity. The MSIP repeats the intrusion and extrusion of mercury several times while gradually increasing the maximum pressure in order to separately measure connective pores from ink-bottle pores and to detect the threshold pressure which starts to cause microstructure deformation. As a result, it turned out the chloride ion penetration was shallow in the case of horizontal cores. The apparent chloride ion diffusion coefficient of the horizontal cores tended to be lower than that of vertical ones. In addition, some cores showed high chloride ion density only near the surface. These cores had less connective pores near the surface. It suggested the less connective pores prevented the chloride ions from penetration into the deeper layer.

Keywords: *marine structure, chloride attack, blast furnace slag cement, mercury step-by-step intrusion prosimetry*

1. INTRODUCTION

Marine structures have the risk of deterioration by chloride attack. Surface concrete plays a role in protection of inside steel from the chloride attack. Chloride ion penetration into concrete is a phenomenon related to water ingress, ion diffusion or chemical adsorption. Blast furnace slag cement or fly-ash cement are effective to increase the resistance to the chloride ion penetration.

The objective of this study is to discuss the chloride ion penetration of blast furnace slag cement concrete. Especially, this study focused on the

relationship between the chloride ion penetration and microstructure properties of concrete.

2. FIELD WORK AND EXPERIMENTS

2.1 Investigated structure

This study investigated the some marine structures (the breakwater and launch slope) in the cold region of Japan. Figure 1 shows the length and construction period of the breakwater. It was constructed from 1993 to 1998 toward the sea, and the launch slope was built in 1970. The breakwater constructed in 1998 is located on the edge and its length is only 10m. Table 1 shows the material design of the breakwater. The blast furnace slag cement was used. The maximum water to cement ratio was 55%. The launch slope is located at the root of the breakwater. The material design of the launch slope is unknown.

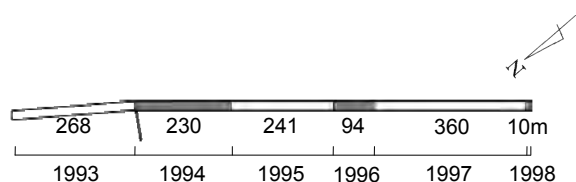


Figure 1: Length and construction period of the breakwater

Table 1: Material design of breakwater

Nominal strength at 28day(N/mm ²)	21
Slump(cm)	5
Air content(%)	4.5
Maximum aggregate size(mm)	40
Cement type	BB
Maximum water to cement ratio(%)	55
Maximum chloride ion content(kg/m ³)	0.30

Figure 2 shows the standard cross-section of the breakwater. The east side is offshore and wave-dissipating blocks are placed. The height of the east side is 6.7m above the sea level, and the west side is 5.0m. There was a slope 2.2m apart from the east side. Concrete cores were collected from the top, side or bottom shown in the figure. In addition, there were stripe patterns at the surface of the side of the breakwater constructed after 1995. They might be the marks where the water-permeable forms were used. In the case of the launch slope, the core was collected from the intertidal zone.

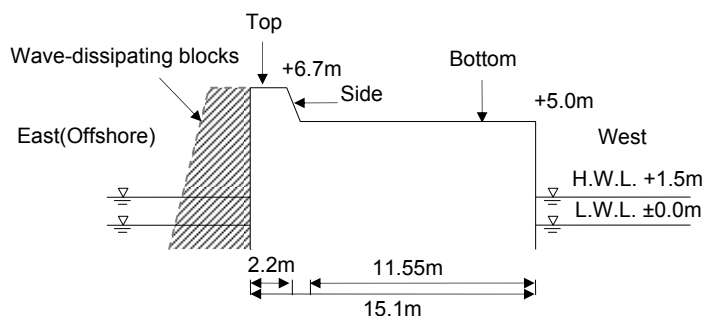


Figure 2: Standard cross-section of the breakwater

Table 2: Collected concrete cores

Construction Period		Surface		
		Top	Side	Bottom
Launch slope	1970		◇	
Breakwater	1993	○		
	1994		○	○
	1995		○	○
	1996	○	○	
	1997	○	○	
	1998	○	○	

◇: Intertidal zone ○: Splash zone

2.2 Measurement of chloride ion density

The collected cores were sliced 10mm intervals to the depth of 70mm by using the diamond cutter. The total chloride ion density was measured by the potentiometric titration. The apparent chloride ion diffusion coefficient (D_a in cm^2/year) and surface chloride ion density (C_0 in kg/m^3) were calculated by regression calculation based on the Fick's laws of diffusion (equation 1).

$$C(x,t) = C_0 \left(1 - \text{erf} \left(\frac{x}{2\sqrt{D_a \cdot t}} \right) \right) \tag{1}$$

where

C : chloride ion density (kg/m^3)

x : depth (cm)

t : material age (year)

C_0 : surface chloride ion density (kg/m^3)

D_a : apparent chloride ion diffusion coefficient (cm^2/year)

$\text{erf}(s)$: error function

2.3 Measurement of porosity

The microstructure at 0-10mm and 10-20mm from the surface was analyzed respectively by using the mercury intrusion porosimetry. However, the previous studies pointed out that the conventional mercury intrusion porosimetry has two problems: One is to overestimate the fine pore volume by the existence of ink-bottle pores. The other is to enlarge original

microstructure by the high intrusion pressure of the mercury. Then this study used the mercury step-by-step intrusion porosimetry(MSIP). The MSIP repeats the intrusion and extrusion of the mercury several times while gradually increasing the maximum pressure in order to separately measure connective pores from ink-bottle pores and to detect the threshold pressure which starts to cause microstructure deformation. The pore diameter is derived from the equation 2.

$$D = - \frac{4\gamma \cos \theta}{P} \tag{2}$$

where

D : pore diameter(m)

γ : surface tension of mercury(Pa/m)

P : intrusion pressure(Pa)

θ : contact angle($^{\circ}$)

Table 3: Pressure hysteresis of the mercury step-by-step intrusion porosimetry

Intrusion stage	Pressure(MPa)		Pore diameter(nm)	
	Start	End	Start	End
1	0.00365	1.25	342000	1000
2	0.312	4.16	4000	300
3	0.312	12.5	4000	100
4	0.312	15.6	4000	80
5	0.312	20.8	4000	60
6	0.312	31.2	4000	40
7	0.312	62.4	4000	20
8	0.312	125	4000	10
9	0.312	178	4000	7
10	0.312	250	4000	5
11	0.312	416	4000	3
12	0.312	416	4000	3

3. RESULTS AND DISCUSSIONS

3.1 Chloride ion density

Figure 3 shows the total chloride ion density. Firstly, the density in the horizontal direction tended to be lower. The density in 1970 was the highest among the horizontal cores. It might be because the concrete was located in the intertidal zone. The second highest was the density in 1995. The point to observe is that the density in 1994, 1997 and 1998 was high only near the surface and it sharply decreased at 1.5-2.5cm. Especially, the density at 1.5cm was zero in 1997.

In the case of the vertical concrete, the penetration in 1995 was largest. The second highest was the density in 1994. The density in 1997 and 1998 was relatively low.

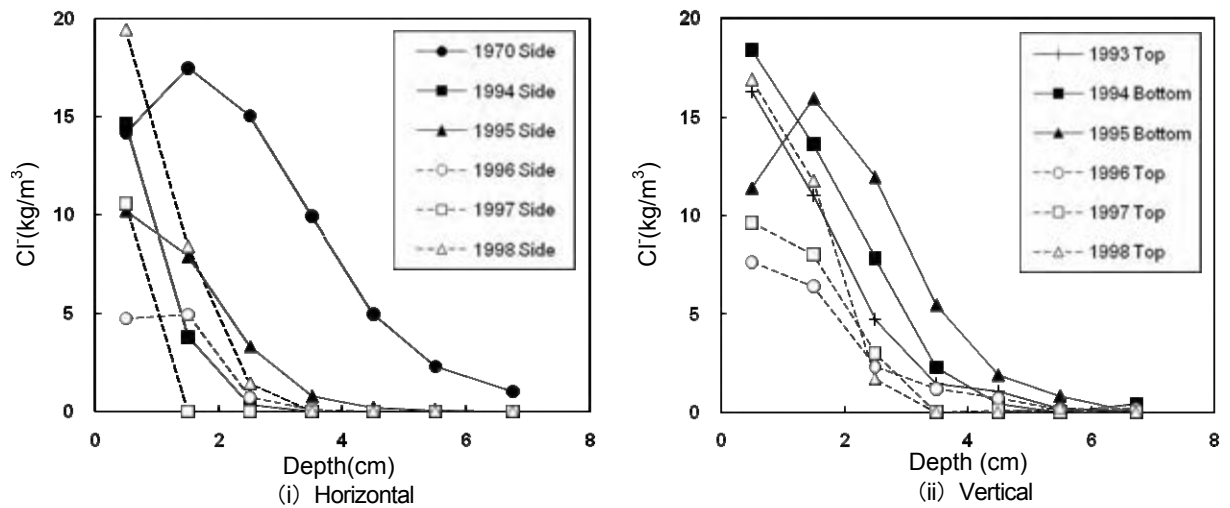


Figure 3: Chloride ion density

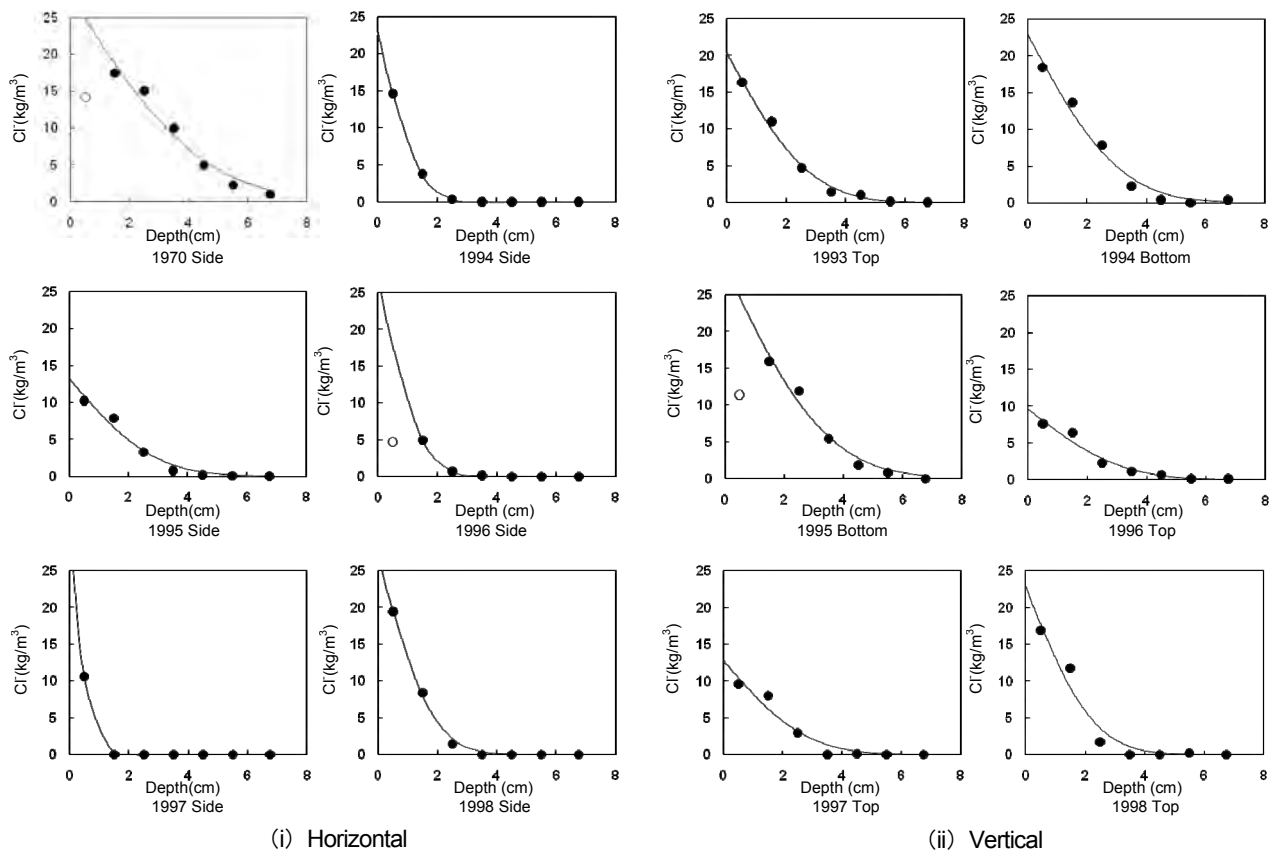


Figure 4: Approximate curves of the chloride ion density distributions (The white marks were ignored.)

3.2 Surface chloride ion density and apparent chloride ion diffusion coefficient

Figure 4 shows the approximate curves of the chloride ion density distributions when applying the Fick's laws of diffusion. The white marks represent the points which were not taken into account due to relatively low values as a consequence of washout by rainfall or something. Figure 5

shows the surface chloride ion density. According to this, the surface density was around 10 to 30 kg/m³. Figure 6 shows the apparent the chloride ion diffusion coefficient. The diffusion coefficient of “1995 Bottom” was highest. The diffusion coefficient of “1994 Side”, “1996 Side” and “1997 Side” was relatively low.

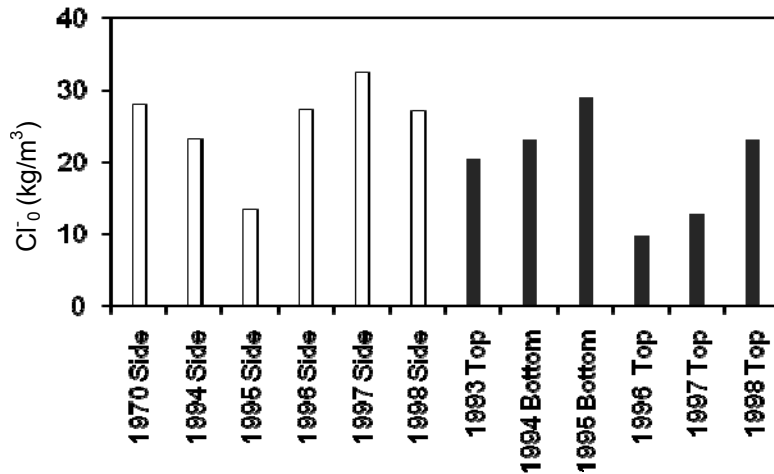


Figure 5: Surface chloride ion density

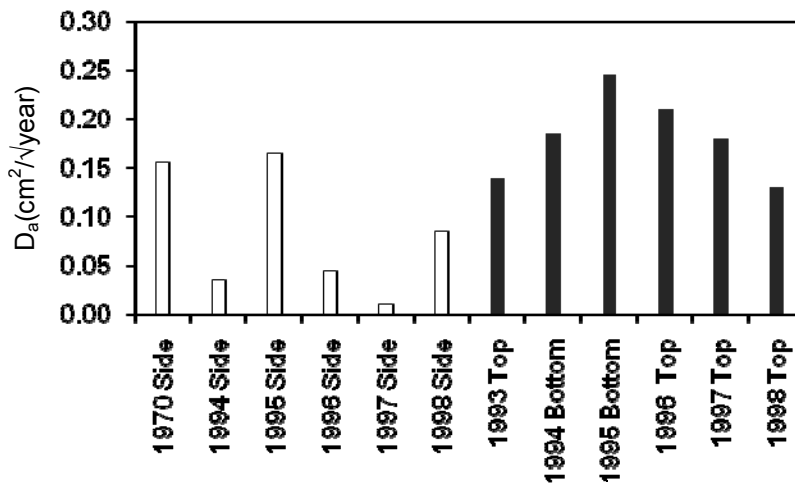


Figure 6: Apparent chloride ion diffusion coefficient

3.3 Porosity

Figure 7 shows the cumulative pore volume at 0-10mm and figure 8 shows that of 10-20mm. The total porosity and the connective porosity were shown respectively. The cumulative curves of the total porosity were described by the mercury volume which was totally intruded into the samples. The curves of the connective porosity were obtained by subtracting the volume of inkbottle pores from that of total porosity. The minimum diameter of the connective porosity was detected by overlapping each intrusion curve and observing their agreement. The measured minimum diameter was the 5 or 7nm.

In the case of 1994 and 1995, the total porosity and connective porosity were not so different while the chloride penetration in the vertical direction was higher. It seemed that the sea water was likely to remain at the horizontal surface and the gravity accelerated the sea water ingress. The total and connective porosity in the vertical direction in 1996 were less than horizontal direction, but the chloride ion penetration was higher. It also seemed the influence of the sea water ingress.

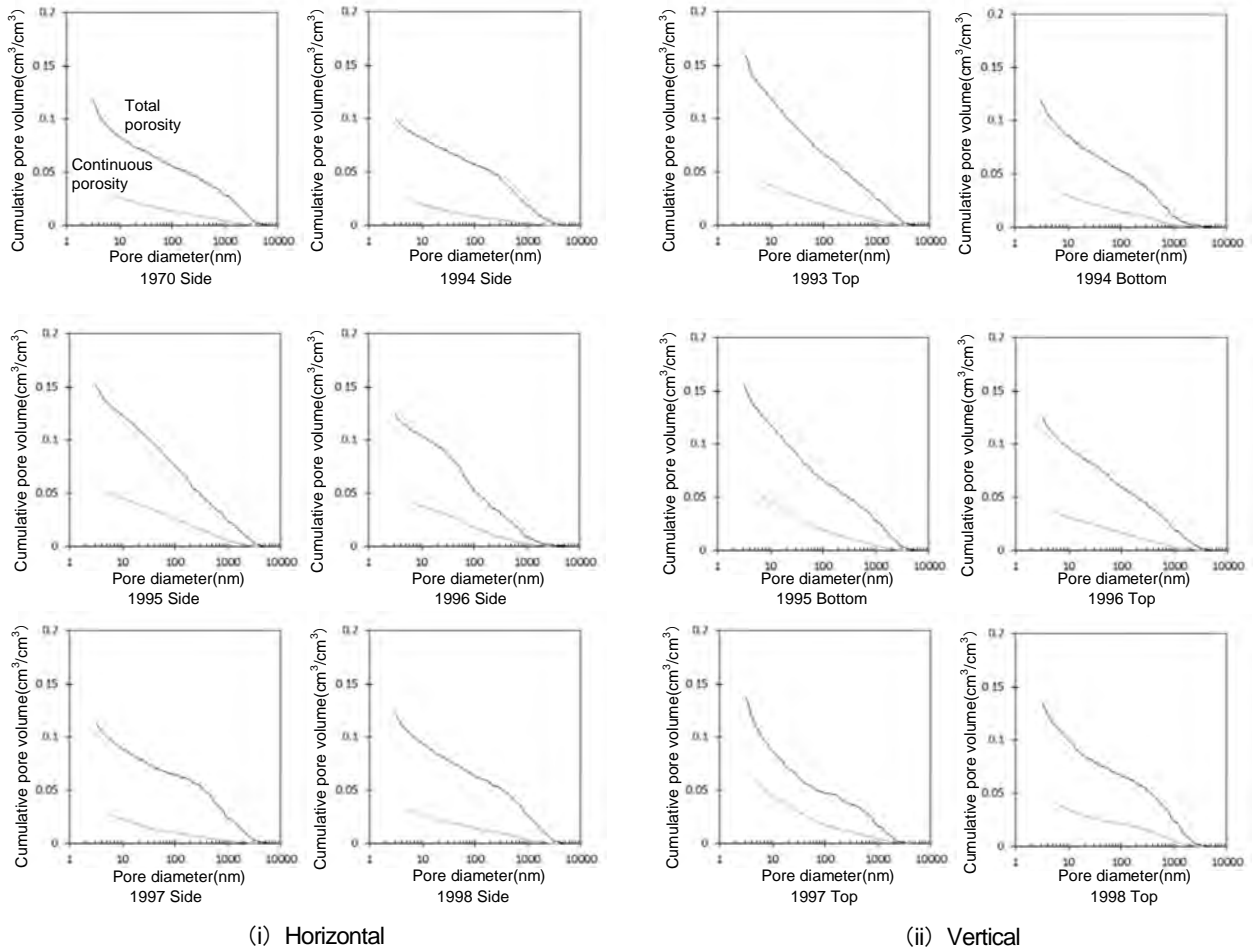


Figure 7: Cumulative pore volume (0-10mm)

The connective pore in 1997 was clearly less while its penetration was shallowest among all horizontal cores. It might reduce the chloride ion penetration.

In the case of 1998, the total and connective porosity in the horizontal direction were less than the vertical direction, while there was a slight difference in the chloride ion penetration. It could be explained by the location. The concrete in 1998 was on the edge of the breakwater where the sea water splashed severely. The supply of the sea water might be more than the other places.

By comparing all of the horizontal cores except for 1998, the connective porosity in 1997 and 1994 was least and the porosity in 1995 was most. Similarly, the apparent chloride ion diffusion coefficient in 1997 and 1994 was lowest and that in 1995 was highest. It is likely that there was a relationship between the chloride ion penetration and the connective porosity. If the direction is the same, the concrete with less connective porosity at the surface might prevent the chloride penetration. This type of concrete may show the high chloride ion density near the surface and shallow chloride ion penetration. This type of concrete may show the high chloride ion density near the surface and shallow chloride ion penetration.

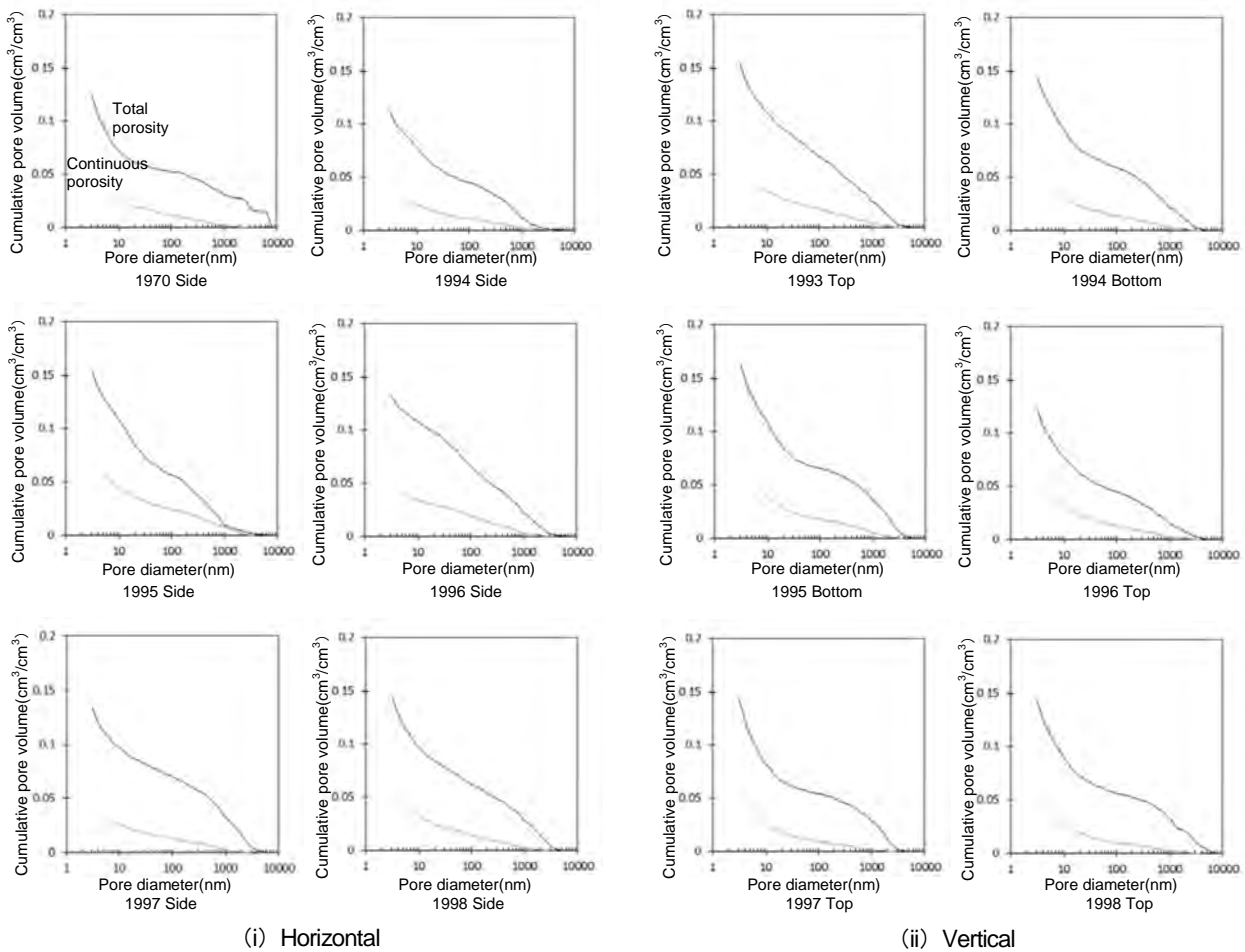


Figure 8: Cumulative pore volume (10-20mm)

4. CONCLUSIONS

The chloride ion penetration is likely to be affected by the continuous porosity. The less connective porosity can reduce the chloride ion penetration. The concrete with less connective porosity may show the high chloride ion density near the surface and shallow penetration. The direction of penetration should be also considered since the sea water ingress in the vertical direction can be higher than the horizontal direction.

ACKNOWLEDGEMENTS

We would like to thank the Hokkaido Development Agency for giving us the opportunity of the site investigation. Also thanks are due to Dr.Hiroshi UEDA(Railway Technical Research Institute) and Dr.Isao KURASHIGE (Central Research Institute of Electric Power Industry) for the cooperation on the site.

REFERENCES

Diamond, S., 2000. Mercury porosimetry: An inappropriate method for the measurement of pore size distributions in cement-based materials, *Cement and Concrete Research*, Vol.30, 1517-1525

Yoshida, R. and Kishi, T., 2007. A study on effect of air void and destruction of the pore structure at high pressure level based on hysteresis behavior on mercury Intrusion. *Cement Science and Concrete Technology*, No.60, 68-75

Yoshida, R. and Kishi, T., 2008. Proposal of a new approach for determination of pore continuity and suitable intrusion pressure based on step-by-step mercury intrusion porosimetry test. *1st International conference on Microstructure Related Durability of Cementitious Composites*, Vol.2, 1455-1464

Yoshida, R., Kishi, T., Nakarai, K., and Li, C., 2009. Effectiveness of connective porosity measured by mercury step-by-step intrusion porosimetry and proposal of its index. *Concrete technology series*, No.87, Japan Society of Civil Engineers

Takahashi, Y., Inoue, S., Akiyama, H., and Kishi, T., 2010. Study on chloride penetration into fly-ash concrete of existing structure and influence of material age. *Proceedings of Japan Concrete Institute*, Vol.32

Maruya, T., Tangtermsirikul, S., Matsuoka, Y., 1998. Modeling of chloride ion movement at the surface layer of hardened concrete. *Proceedings of Japan Society of Civil Engineers*, No.585

Ishida, T., Prince, O., and Ho, T.,2009. Modeling of chloride diffusivity coupled with non-linear binding capacity in sound and cracked concrete, *Cement and Concrete Research*, Vol.39, 913-923

Prince, O., and Ishida, T.,2009. Modeling of Chloride Transport Coupled with Enhanced Moisture Conductivity in Concrete Exposed to Marine Environment, *Cement and Concrete Research*, Vol.39, 329-339

Amino, T., Otsuki, N., Saito, T., and Hanebuchi, T., 2010. Proposal for estimation method of surface chloride content of RC deck in open-piled pier considering the structural types and the influence of wave action. *Concrete research and technology*, Vol.21, 1-11

Sugiyama, T., Sato, F., Ushijima, S., and Sakai, E., 2010. Relationship between microstructure and chloride ion penetration resistance of low water to powder ratio concrete with admixtures. *Proceedings of Japan Concrete Institute*, Vol.32

Defect detection and crack classification in cementitious materials by ultrasonic testing with ANN

Saowanee SAECHAI¹, Pansaran SARANROM²,
Raktipong SAHAMITMONGKOL³, Waree KONGPRAWECHNON⁴,
and Somnuk TANGTERMSIRIKUL⁵

¹ Graduate Student, School of Information, Computer,
and Communication Technology,
Sirindhorn International Institute of Technology,
Thammasat University, Thailand
saowanee.sae@hotmail.com

² Graduate Student, School of Civil Engineering and Technology,
Sirindhorn International Institute of Technology,
Thammasat University, Thailand

³ Researcher, Construction and Maintenance Technology Research Center
Sirindhorn International Institute of Technology,
Thammasat University, Thailand

⁴ Associate Professor, School of Information,
Computer, and Communication Technology,
Sirindhorn International Institute of Technology,
Thammasat University, Thailand

⁵ Professor, School of Civil Engineering and Technology,
Sirindhorn International Institute of Technology,
Thammasat University, Thailand

ABSTRACT

This paper introduces a newly developed testing system for the classification of defect and surface crack in the cement-based materials. With the system, the pattern of ultrasonic waves for each case of medium can be measured. The machine learning algorithm called back-propagation artificial neural network (ANN) classifier is employed for classification and verification of the wave patterns obtained from the different samples. By applying the system, the presence or absence of a defect in mortar can be identified. Moreover, the system is applied to determine whether crack depth reaches the reinforcing bar. The methodology is explained and the classification results are discussed. The effectiveness of the developed testing system is also performed. The comparison of the classification results between the time and frequency domain signals with the ANN classifier is also demonstrated. The system is proved to be beneficial to the structure inspection.

Keywords: *ultrasonic wave, defect detection, surface crack, artificial neural network, pattern recognition*

1. INTRODUCTION

In many constructions, the concrete structures can be degraded due to aging and, without an appropriate maintenance work, the failure of the deteriorated structure may occur in many different forms. There may be embedded defects or surface cracks in the structure. In the case of surface crack, if cracks penetrate through reinforcing bar, moisture and oxygen can easily reach rebar and drastically accelerate corrosion of rebar and causes the reduction rebar cross sectional area of rebar as well as spalling of cover concrete (Gebregziabhier, 2008). The information about cracks such as their locations, directions, widths, and depths are very important for condition assessment and structural evaluation of the cracked structures. While the locations, widths, and lengths of surface cracks can be measured and recorded by visual inspection with some basic instruments such as crack gages or digital camera, the information about depth of crack as well as the defect inside the material cannot be measured by visual inspection (Bungey, 1996). The inspection and evaluation can be done without any additional damage of concrete by non-destructive testing (NDT) techniques. One of the most extensively employed technique for defect detection and surface crack depth measurement is a well-known “ultrasonic pulse velocity (UPV)” which applies ultrasonic waves.

Ultrasonic waves are mechanical waves that have a frequency above approximately 20,000 Hz, which exceeds the limit of human hearing capacity and can be focused in narrow and straight beams (Schickert, 2002). Ultrasonic waves require a medium to propagate. If the ultrasonic waves travel from one medium to another different medium, with different acoustic impedances, they will partially refract if the angle of incidence is not 90 degree because of the change in propagation velocity, and the rest of energy will be reflected. For the interface between concrete and air, the ultrasonic waves almost completely reflect at this interface.

Ultrasonic waves are generally used to inspect structures by an apparatus called “Ultrasonic Pulse Velocity (UPV)”. The UPV only measures the traveling time that ultrasonic waves need to travel through the medium from transmitter to receiver. In other words, the apparatus does not provide useful data in some cases. According to the limitations of the original testing system (UPV’s system), the developed testing system is introduced to inspect concrete structures with higher capacity. By using the developed testing system, an ultrasonic wave pattern that travels through a medium can be obtained, instead of traveling time. The different wave patterns are classified by using machine learning called an “Artificial Neural Network (ANN)”.

The objectives of this study are to develop a new testing system and apply the artificial neural network classifier for detecting defects and determining whether crack depth reaches the reinforcing bar. The study is conducted under the conditions that the location, size, shape, and material of the defects as well as the location of the surface crack are predetermined.

2. EXPERIMENTAL PROGRAM

In the experimental program, the developed testing system with the ANN classifier was applied for detecting the defect and classifying the crack of the mortar. In the crack classification, the crack depths were varied into three cases. The direct and indirect measurements were used in the defect detection but only the indirect measurement was used in the crack classification.

2.1 Original testing system

The system configuration of the original testing system (or commercial UPV system) is illustrated in Figure 1(a). In this system, ultrasonic transducers with a mean frequency of 55 kHz (transmitter and receiver), were used to measure the traveling time of the medium. Only the traveling time of ultrasonic waves from transmitter to receiver is obtained. The traveling time can be used to determine the position that the defect may be present. More information about defects or cracks cannot be obtained. According to the limitations of original testing system, the developed testing system is developed to overcome this problem.

2.2 Developed testing system

The system configuration of the developed testing system is illustrated in Figure 1(b). In this system, an oscilloscope (TD2012B model) and computer are added to the original UPV system. The oscilloscope is used to measure and record the ultrasonic wave patterns which travel through the medium. The NI Signal Express program is used to collect the time and corresponding amplitude arrays. Both time and amplitudes are collected as the raw data. In addition, the ultrasonic responses in different patterns can be obtained and used for the further analysis.

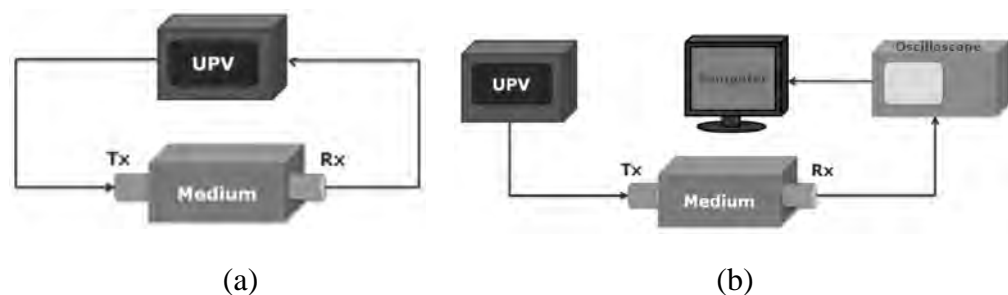


Figure 1: System configuration of (a) original testing system (b) developed testing system

The developed testing system is also composed of an artificial neural network (ANN) classifier. The pattern of normalized signals were classified and verified by the ANN classifier. An artificial neural network (ANN) is an information processing paradigm that is inspired by the biological nervous systems. It is composed of a large number of highly interconnected processing elements (neurons) working in unison to solve specific problems.

An ANN is configured for a specific application, such as pattern recognition or data classification, through a learning process (Aleksander, 1995).

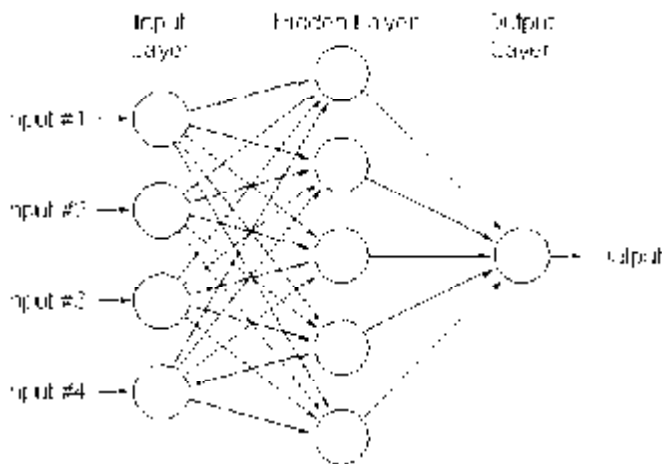


Figure 2: Back-propagated model with several input and hidden neurons and one output neuron

This study employs the back-propagated model (Figure 2) which is a feed-forward multi-layered ANNs that allow signals to travel one way only; from input to output. The feed-forward ANNs tend to be straight forward networks that associate inputs with outputs. The circles represent neurons. The neurons are arranged in a number of layers (called multi-layered), generally three. They are input, middle (hidden) and output layers, respectively (Masnata, 1996; Ni Hong-Guang, 2000).

2.3 Sample preparations

In this study, the mortar sample was used for the test. Ordinary Portland Cement type I, water, and sand were used to produce the mortar specimens in the proportion of 539, 269, and 1482 kg/m³, respectively.

2.3.1 Defect detection

For defect detection, the cube mortars, with size 150×150×150mm, were used as the sample for wave propagation. There were two cases of the mortar samples (Figure 3(a) and 3(b)) prepared for two classes of defect detection:

Case I (non-defective case): the pure mortar sample without defect

Case II (defective case): the mortar sample contains the two circle-shaped air voids in the diagonal location. Both air voids has the diameter of 25mm.

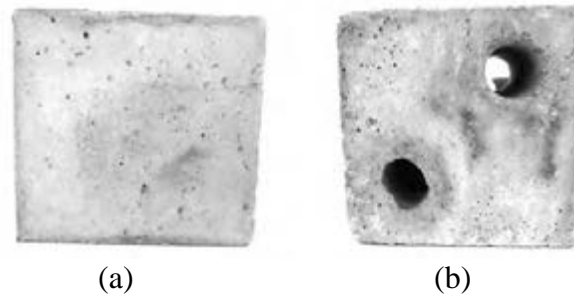


Figure 3: Samples for defect detection
 (a) non-defective specimen (b) defective specimen

2.3.2 Crack classification

For crack classification, the 100x100x500 mm mortar prism concentrically reinforced with 25 mm reinforcing steel bar were prepared with different crack configuration. The sample forming is shown in Figure 4(a). The cover thickness was thus approximately 37.5 mm. The creation of artificial crack was achieved by installing a 1.5-mm thick acrylic plate in each mold before the casting of the mortar. The plate was located at the middle of the specimen perpendicular direction to reinforcing bar. The width of the plates were 100 mm but the height of acrylic plates were varied so that the depth of the created artificial cracks could be varied at 25 mm, 50 mm, and 75 mm as shown in Figure 4(b). These acrylic plates were removed from the specimen at 24 hours after casting. In the case of the crack depth of 75 mm, the acrylic plates were split into two portions so that they can be removed from the specimen without any constraint from rebar. These three different crack depths represented different states of crack depths as follows:

Case I (crack depth = 25mm): Crack tip is above the reinforcing bar (shallow crack that does not reach the reinforcing bar)

Case II (crack depth = 50 mm): Crack tip is on the same level with the center of rebar

Case III (crack depth = 75 mm): Crack tip is below the rebar (crack propagates through the reinforcing bar).

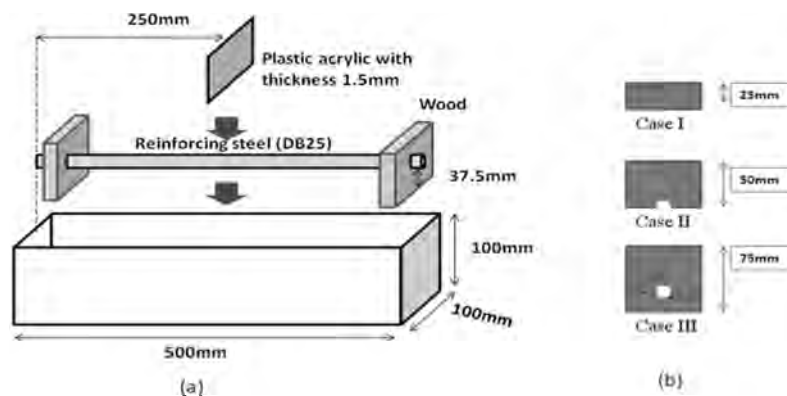


Figure 4: Samples for crack classification
 (a) Setting of formwork and instruments (b) Plastic acrylic with different depths

2.4 Test Methods

For different situations, the appropriate measurement setting must be chosen. There are three possible measurement settings in which the transducers of UPV equipment may be arranged on the medium. There are direct measurement, semi-direct measurement, and indirect (or surface) measurement (Figure 5(a) through 5(c), respectively).

For defect detection, the direct and indirect measurements were employed in this work while the positions of transmitter and receiver are varied. For crack depth estimation, in the real practical case, only the indirect measurement was used while the distance between transmitter and receiver were varied over the sample surface with different side of crack.

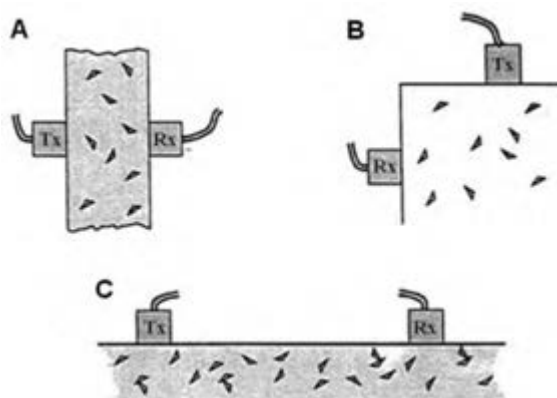


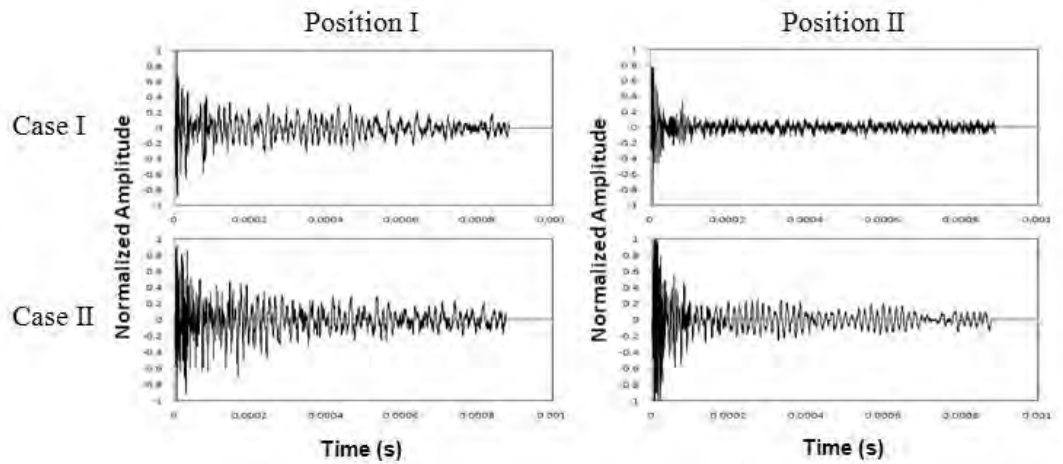
Figure 5: Pulse velocity measurement ways
(a) Direct (b) Semi-direct (c) Indirect measurement

3. ULTRASONIC SIGNALS

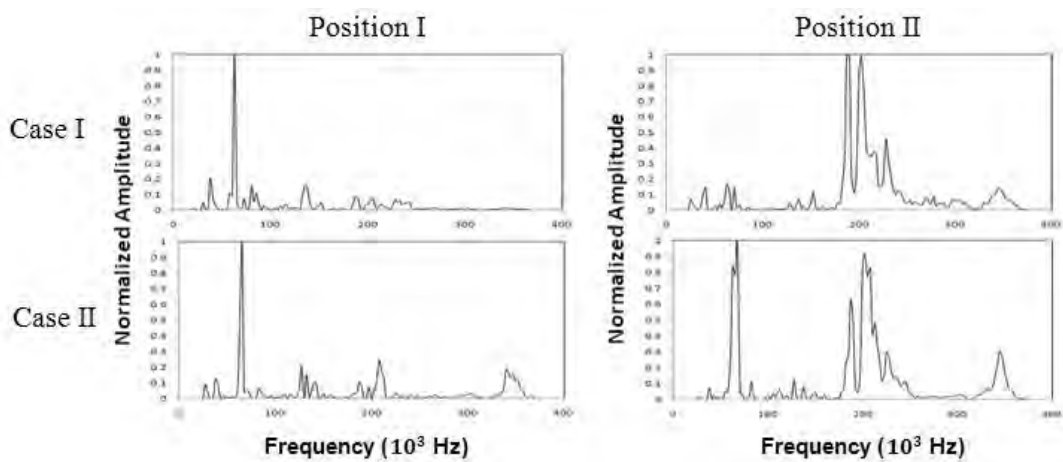
3.1 Defect detection

In time domain response, each ultrasonic wave contains 1,000 data points with sampling rate of 2,500 kHz for every case. To obtain the frequency domain response, the Power Spectral Density (PSD) of the signal is calculated from Fast Fourier Transform (FFT) calculation with the time domain response (Rao, 2010). To make adjustment for the effect of the pressure on probe during the measurement, the time domain response and the corresponding PSD signal are then normalized with its maximal magnitude to get the normalized signals.

By the direct measurement, the examples of normalized signals in time domain and frequency domain signals for the samples case I (non-defective case) and case II (defective case) are illustrated in Figure 6(a) and Figure 6(b), respectively. The figures show the examples of signals obtained from the transducer in different positions.



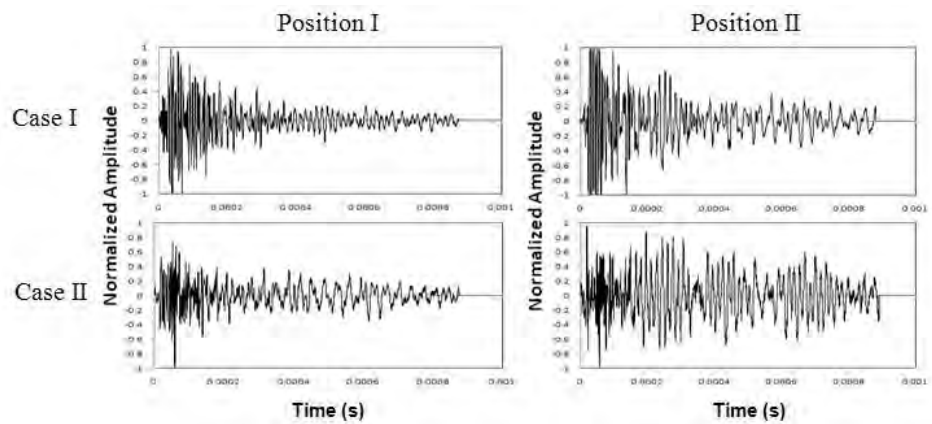
(a) time domain signals



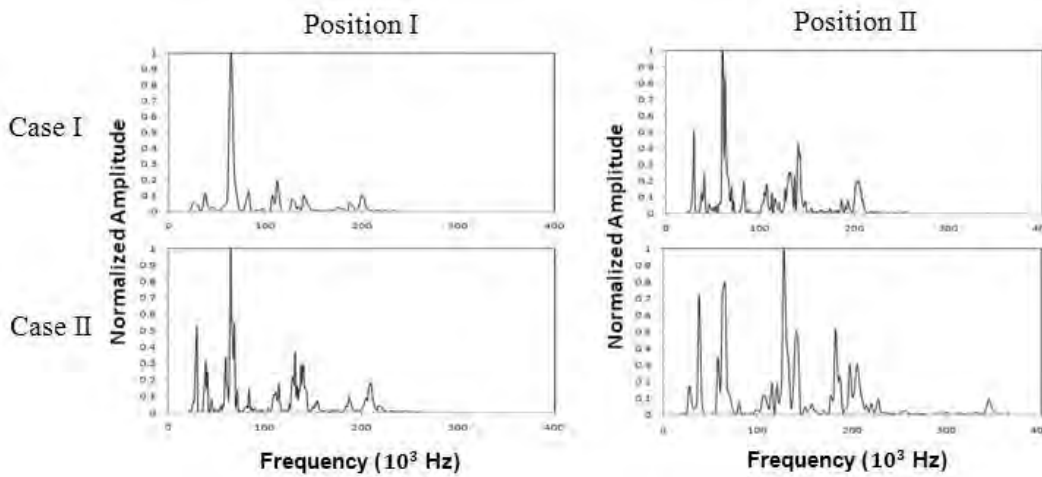
(b) frequency domain signals

Figure 6: Normalized signals from direct measurement for defect detection

By the indirect measurement, the examples of normalized signals in time domain and frequency domain signals for the samples case I and case II are illustrated in Figure 7(a) and Figure 7(b), respectively.



(a) time domain signals

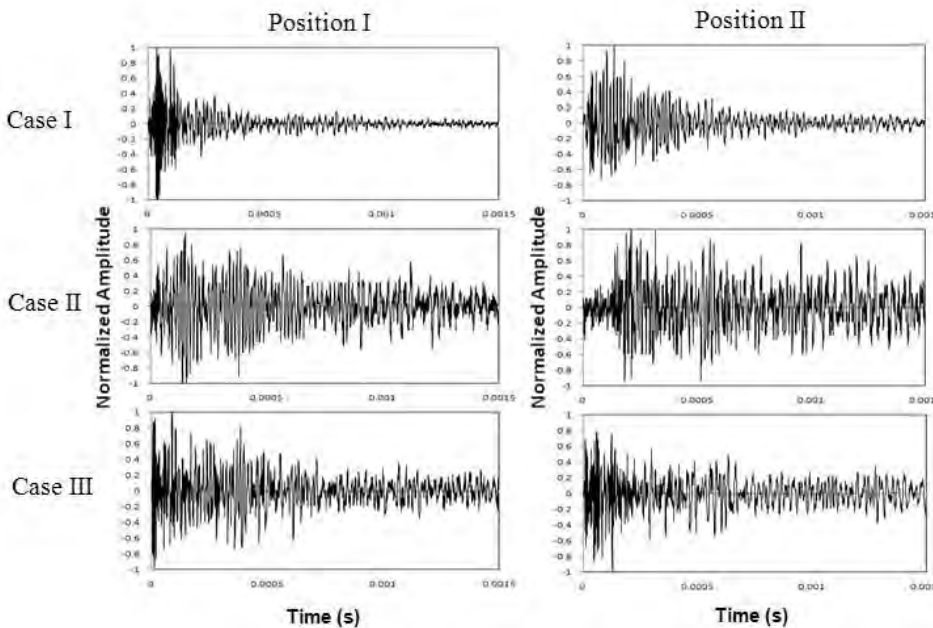


(b) frequency domain signals

Figure 7: Normalized signals from indirect measurement for defect detection

3.2 Crack classification

In time domain response, each ultrasonic wave contains 1,500 data points with sampling rate of 1,000 kHz for every case. The processes to obtain the normalized signals in time and frequency domain are similar to the case of defect detection. By using only indirect measurement, the examples of normalized signals in time domain and frequency domain signals for the samples case I (crack depth = 25mm), case II (crack depth = 50 mm), and case III (crack depth = 75 mm) are illustrated in Figure 8(a) and Figure 8(b), respectively. The figures also show the examples of signals obtained from the transducer in different positions.



(a) time domain signals

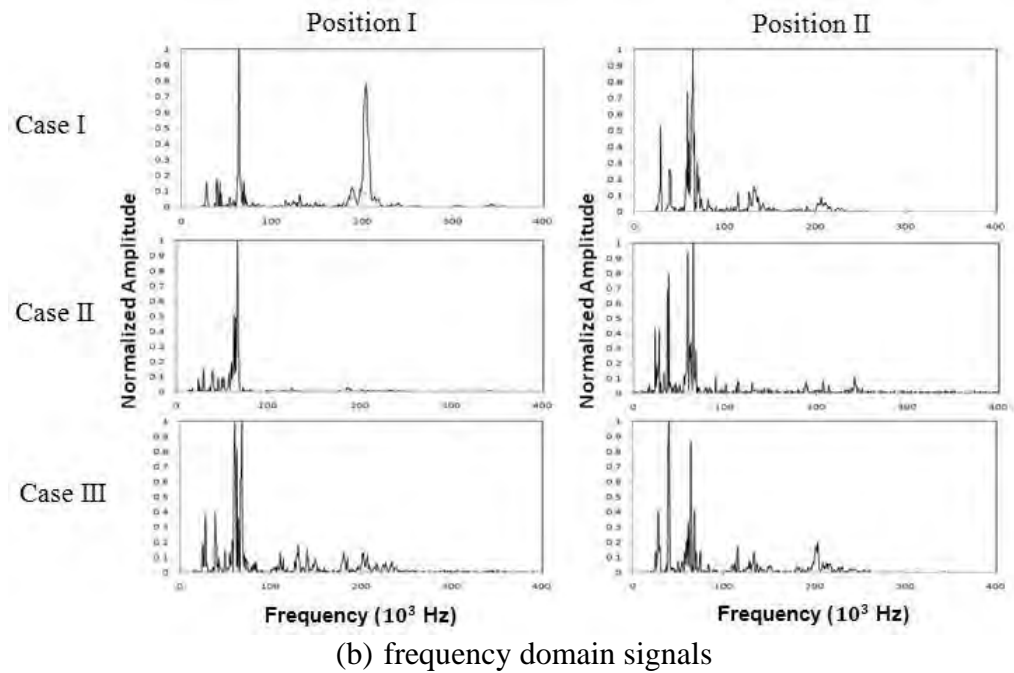


Figure 8: Normalized signals from indirect measurement for crack classification

4. INPUTS AND PARAMETERS FOR ANN CLASSIFIER

This section explains the selection of the ANN's input and parameter setting for the network training. For defect detection, there were totally 200 normalized amplitude arrays of the normalized signals with 1,000 data points used as the input of the network with 100 arrays for each sample cases. The ANN's output can be either 0 or 1 which are represented the non-defective and defective case, respectively. The 50 hidden neurons were used. For crack classification, there were totally 300 normalized amplitude arrays with 1,500 data points used as the input of the network with 100 arrays for each sample cases. The ANN's output which can be either $[1\ 0\ 0]^T$, $[0\ 1\ 0]^T$ or $[0\ 0\ 1]^T$ which represents the mortar with crack depth of 25mm, 50mm, and 75mm, respectively. The totally 50 layers of hidden neurons were also used.

The pattern recognition of the defect can be simulated and analyzed by the MATLAB Toolboxes. The training, validation, and testing parameters were set to be 70%, 15%, and 15% of the number of inputs, respectively. The normalized amplitude arrays in time and frequency domain were trained individually.

5. CLASSIFICATION RESULTS

After the training process, the confusion tables were obtained and used to analyze the accuracy of the network. The classification results obtained with

the ANN classifier are presented in the tables which are described below. The classification rate for each case is the mean classification rate of the four times network training.

5.1 Defect detection

For the defect detection, the 200 input samples were trained in the network according to two classes of the samples, so the training and testing samples are set to be 140 and 30 samples which are 70% and 30% of the input samples, respectively. Using direct measurement, the classification results of ANN classifier with the time domain and frequency inputs are presented in Table 1 and 2, respectively.

Table 1: Classification results using time domain signals from the direct measurement

Case	Training and testing samples	Mean classification rate (%)	
		Case I	Case II
Case I	140 training samples	96.75	3.25
Case II	30 testing samples	3.5	96.5

Table 2: Classification results using frequency domain signals from the direct measurement

Case	Training and testing samples	Mean classification rate (%)	
		Case I	Case II
Case I	140 training samples	100	0
Case II	30 testing samples	3	97

According to Table 1, with the time domain inputs, the accuracy rates are 96.75% and 96.5% for non-defective and defective cases, respectively. As shown in Table 2, the very high classification results were obtained using inputs in frequency domain with the accuracy rate of 100% and 97% for non-defective and defective cases, respectively.

For indirect measurement, the classification results of ANN classifier with the time domain and frequency inputs are presented in Table 3 and 4, respectively.

Table 3: Classification results using time domain signals from the indirect measurement

Case	Training and testing samples	Mean classification rate (%)	
		Case I	Case II
Case I	140 training samples	95	5
Case II	30 testing samples	5.5	94.5

Table 4: Classification results using frequency domain signals from the indirect measurement

Case	Training and testing samples	Mean classification rate (%)	
		Case I	Case II
Case I	140 training samples	100	0
Case II	30 testing samples	0	100

From Table 3, with the time domain inputs, the accuracy rates are 95% and 94.5% for non-defective and defective cases, respectively. From Table 4, the very satisfactory classification results were obtained using inputs in frequency domain with the accuracy rate of 100% for both cases.

5.2 Crack classification

For the crack classification, the 300 input samples were trained in the network according to three classes of the samples. The training and testing samples were set to be 210 and 45 samples which are 70% and 30% of the input samples, respectively. The indirect measurement was only employed in this work. The classification results of ANN classifier with the time domain and frequency inputs are presented in Table 5 and 6, respectively.

Table 5: Crack classification results using time domain signals (indirect measurement)

Case	Training and testing samples	Mean classification rate (%)		
		Case I	Case II	Case III
Case I	210 training samples	87	8	5
Case II	45 testing samples	18	75	7
Case III		13	8	79

Table 6: Crack classification results using frequency domain signals (indirect measurement)

Case	Training and testing samples	Mean classification rate (%)		
		Case I	Case II	Case III
Case I	210 training samples	96	1	3
Case II	45 testing samples	0	100	0
Case III		2	3	95

According to Table 5, with the time domain inputs, the accuracy rates are 87%, 75%, and 79% for the crack depth of 25, 50, and 75 mm, respectively. As shown in Table 6, the very high classification results were obtained using inputs in frequency domain with the accuracy rate of 96%, 100%, and 95% for crack depth of 25, 50, and 75 mm, respectively.

From the classification results, the accuracy obtained from the classification in frequency domain signals is, in all cases, better than those obtained from the classification with time domain signals. This may be because the reflection of ultrasonic wave in the structure can easily change in the frequency response by different configurations of specimens. The different patterns of the different specimens can thus be well classified. For defect detection, the results from using direct and indirect measurements are both highly satisfactory with a small difference in their accuracies.

6. CONCLUSION

The new developed testing system, implemented by the integration of UPV apparatus, oscilloscope, and ANN algorithm, can give the good recognition of defects and good evaluation of crack depths whether crack depth reaches

the reinforcing bar. According to the classification results of defect detection and crack classification, employing the frequency domain signals as the ANN's input gives higher accuracy and better reliability in classification.

For defect detection, using both direct and indirect measurement can give the very high accuracy. To use this system for defect detection, the selection of direct or indirect measurements depends on their suitability for each specific practical work while, for crack classification, the indirect measurement is generally used.

In summary, the developed system can be proved to be beneficial to the structure inspection and evaluation since more information of the ultrasonic signals is obtained instead of the traveling time. Furthermore, the developed testing system can also classify other types of damage in construction.

REFERENCES

Gebregziabhier, T. T., 2008. Durability problems of 20th century reinforced concrete heritage structures and their restorations, SAHC, pp. 19, 42, and 46.

Bungey, J. H. and Millard, S.G., 1996. Testing of concrete in structures (3rd ed), Blackie academic & Professional, 139-141.

Schickert, M., Krause, M. and Muller, W, 2002. Ultrasonic Imaging of Concrete Elements Using Reconstruction by Synthetic Aperture Focusing Technique. *Journal of Materials in Civil Engineering*. 15, 235-246.

Aleksander, I. and Morton, H, 1995. An introduction to Neural Computing (2nd ed), Chapman and Hall.

Masnata, A. and Sunseri, M., 1996. Neural network classification of flaws detected by ultrasonic means, Palermo, Italy, April, 87-93.

Ni, H. -G. and Wang, J. -Z, 2000. Prediction of compressive strength of concrete by neural networks, Hebei, People's Republic of China, August, 1245-1250.

Rao, K.R., Kim, D.N., and Hwang, J.-J., 2010. Fast Fourier Transform – Algorithms and Application, 1st Edition., XVIII, 340 p.

A study on the proper land use of the hillside urban area in depopulation tendency -evaluating future scenarios from the view of disaster mitigation and environmental conservation-

Iyo YONEMASU¹, Takahiro TANAKA² and Daisaku NISHINA³

¹Graduate Student, Graduate School of Engineering,
Hiroshima University, Japan
i.yonemasu@gmail.com

²Associate Professor, Hiroshima University, Japan

³Professor, Hiroshima University, Japan

ABSTRACT

In Japan, after the World War II, the population had been increased and urban areas were also formed on hillside areas because of the urban sprawl. In the hillside urban areas, there are many physical and social problems such as inadequate infrastructures, high disaster risks and so on. On the other hand, there are many places in which residents can enjoy some ecological services such as fresh air and recreation opportunity. Because the population decreasing and aging are severe there now, it is necessary to re-design such hillside urban areas. To figure out the ideal future vision, this study aims at making some future scenarios and evaluating them from the view of disaster risks and ecological services. Actually, we use scenario analysis method to figure out the future vision of urban land use distribution at the time of 2035. The site is Takatoriyama neighborhood, which is a typical hillside urban area and located in Kobe. Finally, evaluating 16 scenarios by using GIS, from the view of disaster risks such as the slope disaster, the seismic disaster, the flood disaster and the fire disaster, and the ecological services such as the cold air and biodiversity.

Keywords: *hillside urban area, GIS, scenario, disaster mitigation, environment*

1. INTRODUCTION

1.1 Background and aims

After World War II, the Japanese population increased in urban areas, creating urban sprawls that extended to surrounding hillside areas. In such areas, many problems arose, including inconvenience of life attributable to inadequate infrastructure, with tightly packed old houses, narrow roads, and paths with stairs. Moreover, such areas present high disaster risks such

as slope disasters and flood disasters. However, many places exist where residents can enjoy some ecological services such as fresh air and recreation opportunities. Now, populations are decreasing and aging rapidly, and that trend is expected to continue. Therefore, redesigning such hillside urban areas is necessary.

This study was undertaken to produce a future vision of hillside urban areas, including a view of disaster risks, ecological services, and the convenience of life in the Takatoriyama neighborhood, Nagata area, in Kobe city. Herein, to ascertain an ideal future vision, the authors produced some future scenarios and evaluated them from the perspective of disaster risks and ecological services.

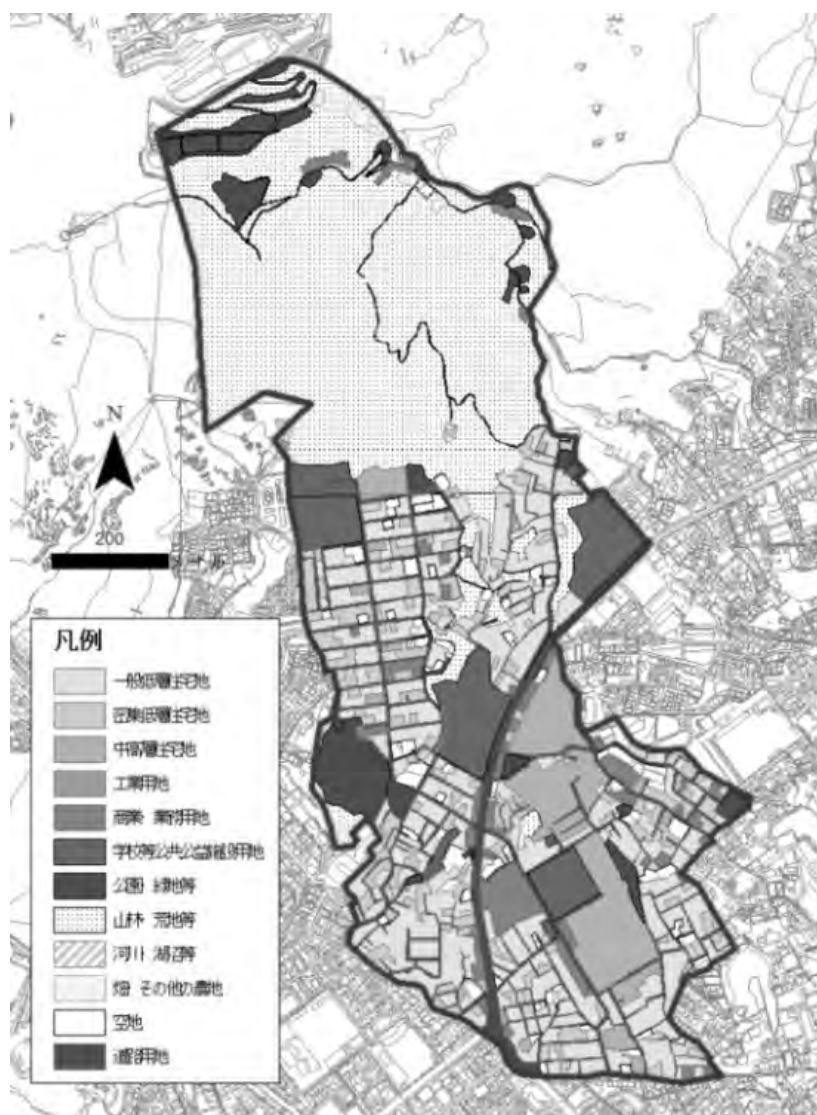


Figure 1 Takatoriyama neighborhood.

1.2 Previous researches

Some studies have examined the effects of decreasing population by producing urban future scenarios and evaluating compact cities.

These studies evaluate the future scenarios of the proper land use from the viewpoint of energy use of cars, costs for city facilities maintenances, in the urban level.

On the other, there are few researches using scenario analysis to examine depopulation tendency in the district level, which focus on mitigating heat environments²⁾. Such studies do not evaluate comprehensively.

2. OUTLINE

2.1 Site

This study examines the Takatoriyama neighborhood, Nagata area, in Kobe city. This is a typical hillside urban area formed on the outskirts of Takatoriyama as a result of urban sprawl. Although natural amenities are available there, steep slopes present high disaster risks from hazards such as slope disaster. Therefore, it is necessary to tackle these problems. In addition, most buildings were built before urban planning had adopted appropriate zoning and other regulatory measures. Therefore, the area has tightly packed old houses, narrow roads, and paths with stairs. It is not a comfortable environment for people, especially elderly people and those with disabilities.

2.2 Flow of this research

This study was assumed to advance according to the following.

- 1) Future scenarios targeting 2035 (16 types)
- 2) Evaluating scenarios from the view of disaster risks and ecological services and consideration

For 1), methods and the results are presented in Chapter 3. For 2), methods and results are explained in Chapters 4, 5 and 6.

3. MAKING FUTURE SCENARIOS

3.1 Composition of future scenarios

The authors produced 16 future scenarios (Table 1) based on site surveys and hearing research. They are roughly divisible into three patterns.

- 1) Designs with the compact concept

The scenario represents a collection of urban land use (residential area, industrial area, commercial area, public facility and road site) for the specific area (Scenario No. 1–10). There are two patterns: arterial highway area type and lower area type. The authors each produced five future scenarios incorporating changes of density type and building height type. In recent years, it is necessary that the urban structure be compact and that the master plan of this area proceed from that basis.

- 2) Designs with physical environment

Based on the present land use, authors considered physical elements such as the disaster danger and environmental amenities, what the land has potentially (Scenario No. 11–14). To produce each scenario, the authors examined the present land use and referred to relevant maps (slope disaster hazard map, seismic disaster hazard map, flood disaster hazard map, and fire disaster hazard map), and determined places that are likely to revert to a natural state. Four scenarios of this type entailed different degrees of physical environmental consideration. Moreover, as a target of comparison, one scenario in which urban area is located in the places where natural environmental resources are spoiled (Scenario No. 15).

3) Designs with present trends

This scenario includes decreased urban land use areas throughout the neighborhood while maintaining the present building density (Scenario No. 16).

Table 1: Future Scenarios

Scenario No	Concept	Type of Density	Type of building
1	"Design with Compact Concept" type	High	Low
2		Medium	Low
3		Low	Low
4		High	Medium
5		High	High
6		High	Low
7		Medium	Low
8		Low	Low
9		High	Medium
10		High	High
11	"Design with Physical Environment" type	High	Low
12		High	Low
13		High	Low
14		High	Low
15	Not Considering about Physical Environment	High	Low
16	"Design with Present trend" type	High	Low

The Present TAKATORIYAMA Area...Type of DENSITY is High and type of BUILDING is Low

3.2 Mode of making future scenarios

To produce future scenarios, the process is explained in the following 1), 2), and 3). The methods and the results are explained.

1) Predicted population

The predicted population of this site is taken using cohort data of the Nagata area population in Kobe city (77,389 people in 2035) and the present population of each area. Figure 2 shows the results. The Takatoriyama area population in 2010 was 9550, but the predicted population in 2035 is 7398, as shown in Table 1.

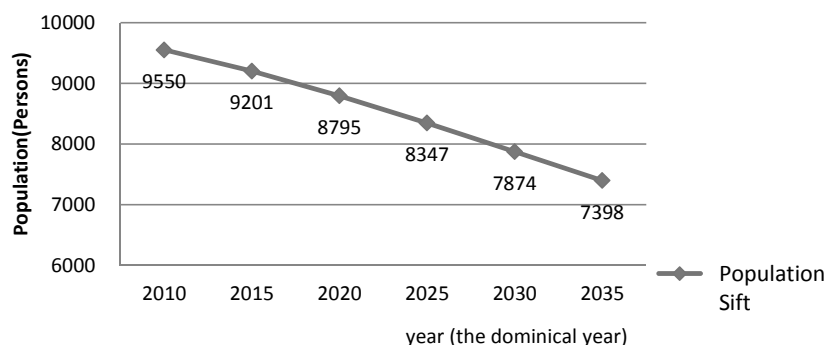


Figure 2: Population Shift in the site.

2) Area setting for each land use

The urban land use area of each scenario is shown in Table 2 by considering the reduction of urban areas and the expansion of green space with decreasing population.

The rate of population decrease was multiplied by the current population of each area, and the necessary area of land use was calculated (residential area, industrial area, commercial area, and road site). Areas of arterial highways were exempted from this calculation.

The present Takatoriyama neighborhood has high density and low raised building type. Therefore, the authors produced lower density type scenarios (Scenario Nos. 2, 3, 7, 8) and medium and high raised building type scenarios (Scenario Nos. 4, 5, 9, 10) for comparing (Table 1). The building arrangement concept Table is shown in Figure 3. The density of the premises is set by the type of density in Table 3. Scenario Nos. 2, 3, 7, and 8 differ according to the density comparison with the present is ascertained with the necessary area based on Table 3.

A design with the present trend type is made using the population of each administrative unit, and necessary areas were calculated from them.

Table 2: Area settings for land use (Scenarios 1, 6, 11, 16)

The kind of land use	Calculating Formula	Necessary Area(m ²)
Mountain forest, Agricultural land	Calculation of accession	494,125
Bare land		
Industrial area	Area of Present Condition × Population decreasing rate	207
Residential area		21,613
Commercial area		22,979
Road area		60,970
Park, Green space	Same as Present Condition	42,474
Public Facility (Ex.School)		58,936
River, Lake		1,592

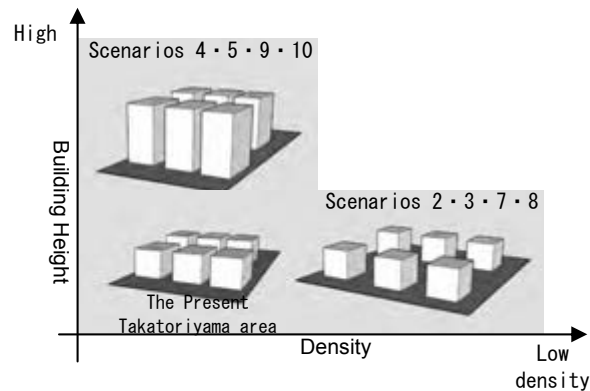


Figure 3: Conceptual diagram of layout buildings.

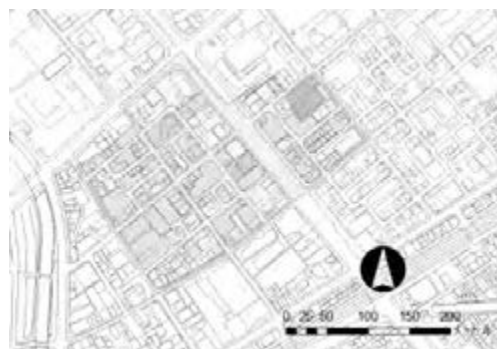


Figure 4: Mikuradori 5, 6, 7 Area

Table 3: Setting density

Type of Density	Reference Area	Building Area/Land Area
High Density	Takatoriyama Area	0.78
Medium Density		0.67
Low Density	Mikuradori 5·6·7Area	0.56

3) Zone setting

For this study, future scenarios are set up as the conformation of distribution of the proper urban land use. The area of the proper urban land use of each future scenario is set as the necessary area. Furthermore, the zone setting was referred from a survey based on the proper land use noted above.

3.3 Examples of future scenarios

Some examples are shown below. Figure 5 shows the Design with Compact Concept type. Figure 6 portrays the Design with Physical Environment type. Figure 7 depicts the Design with Present trend type. Figure 5 shows scenario No. 6: collecting urban land use in lower area with high-density type and low raised building type. Figure 6 presents scenario No. 11, which incorporates physical elements that the land already has. Figure 7 shows scenario No. 16: a design based on present trends.



Figure 5 Scenario 6
(Design with Compact Concept Type)



Figure 6 Scenario 11
(Design with Physical Environment Type)



Figure 7 Scenario 16
(Design with present trend type)

4. EVALUATING SCENARIOS: DISASTER RISKS

4.1 Mode of evaluation

The main disaster risks of the hillside urban area are slope disasters, seismic disasters, flood disasters, and fire disasters. Furthermore, from them, we evaluate future scenarios made in Chapter 3. Particularly to analyze the risk of slope disaster, the seismic disaster and the flood disaster, authors overlay the map showing each disaster risk (hazard map of the slope disaster, seismic disaster, and flood disaster made in reference 7) and each scenario on GIS, and calculated the risk area of the urban city area (Fig. 8).

Subsequently, we evaluated scenarios from calculated expectancy of the likely number of deaths (degree of risk) by multiplication of the area (m^2) by the expected population density (persons/ m^2). As for future scenario 16, authors used the value multiplication dimensions of the urban land use hazards of each administrative unit to estimated population density. Fire disaster was calculated by using the evaluation. Then, for that area, the forecast population density was multiplied to produce a forecast of likely deaths from a disaster (Table 4).

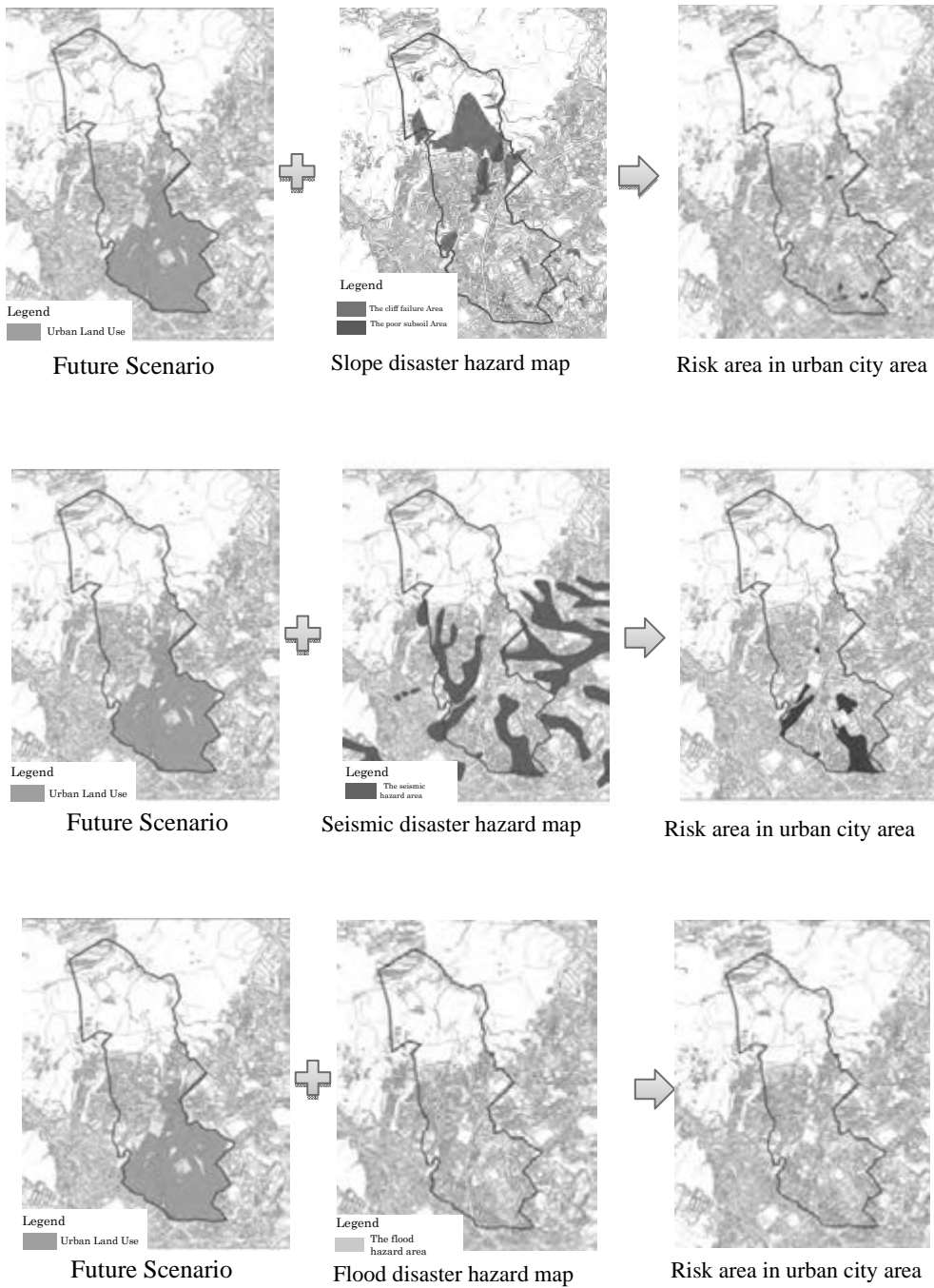


Figure 8: Way of evaluating disaster risks (Slope disaster, seismic disaster, flood disaster).

Table 4: Evaluation of a fire disaster

	Methodology	Content
1	Calculating unburnable area ratio	Unburnable area ratio(%)=open-space ratio+(1-open-space ratio/100) × fire-retardant ratio ※Open-space ratio(%)=(Open-space area/The site area) × 100 ※Fire-retardant ratio(%)=(Fire-retardant area/Building area) × 100
2	Calculating the wooden building-to-land ratio	Wooden building-to-land ratio(%)=(Wooden building-to-land area/Semigurosu district area) × 100 ※Semigurosu district area=The site area-(The road area more than 15m width, Waterway, Lakeside, big vacant area)
3	Calculating the ratio to hard fire-fighting operation	The ratio to hard fire-fighting operation(%)=(The hard area to fire-fighting operation/Semigurosu district area) × 100 ※The hard area to fire-fighting operation =Semigurosu district area-The easy area to fire-fighting operation ※The easy area to fire-fighting operation=The district area within 140m from the water area
4	Evaluating	Calculating arithmetic average from ①Unburnable area ratio, ②The wooden building-to-land ratio, ③The ratio to hard fire-fighting operation.

4.2 Results of evaluation

Evaluation results are presented in Figure 9. Risks of the design with the physical environment type are lower overall than those of city land use consolidation type when seen according to the pattern. Consequently, an urban land use zone will include disaster hazard areas if we design with a compact concept because such areas are dispersed complexly throughout the neighborhood.

The tradeoff between the disasters is regarded as the lowest risk in all scenarios when the scenario with the highest seismic risk is seen from the fire hazard rating.

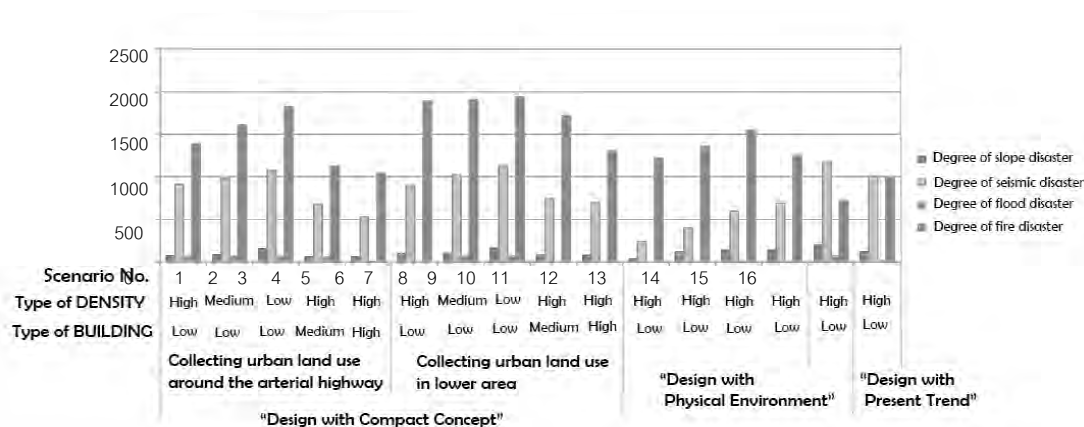


Figure 9: Result of evaluation in light of disaster risks.

5. EVALUATING SCENARIOS: ENVIRONMENTAL CONSERVATION

5.1 Mode of evaluation

The main environmental services of the hillside urban area to be conserved are cold air and biodiversity. Therefore, authors evaluated each future scenario from the view of them.

As for cold air, authors overlaid wind flow map with each future scenario for calculating overlapped area and evaluated scenarios by using the area. On the other, as for biodiversity, authors used ecological network map. The mode of the evaluation is shown in Figure 10.

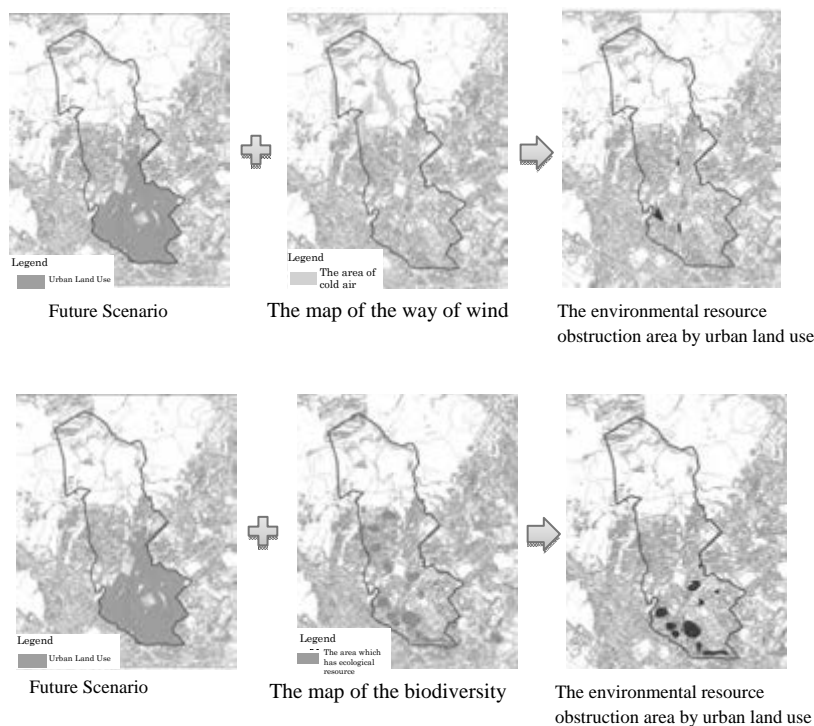


Figure10: Way of evaluating Environment conservation (cold air and biodiversity).

5.2 Result of evaluation

The evaluation result is presented in Figure 11. The area of the scenario with physical environment consideration is evaluated as good. Therefore it is said that even high density and low raised building type do not obstruct ecological services if physical environments are considered. Generally, because no mutual relation is apparent between ‘wind path’ and ‘biodiversity’, they must be considered individually.

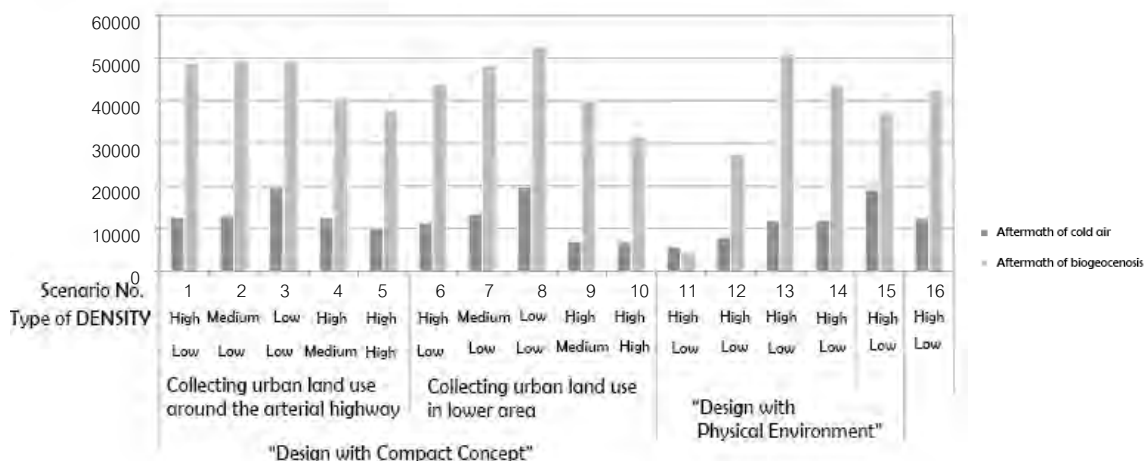


Figure 11: Results of evaluation related to environmental conservation

6. RESULTS OF THE PROSPECTIVE SCENARIOS

In Chapter 4 and Chapter 5, authors evaluated future scenarios from the perspective of disaster risks and the environmental conservation. To consider future scenarios comprehensively, it can be said that the disaster risks posed by ‘Design with physical environment’ type scenario are lower than those of ‘Design with compact concept’. Urban land use zones will include disaster hazard areas if we base the scenario design using the compact concept because such areas are dispersed complexly throughout the neighborhood. The tendencies among four disaster risks and ecological services mutually differ.

7. CONCLUSION

This study was undertaken to produce some future scenarios and evaluate them according to their attendant disaster risks and provision of ecological services. Results show that, for the hillside urban area, it is effectual to have land use like the type of design with the physical environment in view of both disaster mitigation and environmental conservation. However, as explained previously, to consider the future of hillside urban areas, one must consider the convenience of daily life according to the inhabitants’ evaluation. Subsequently, we will consider future scenarios including these elements.

REFERENCES

HORI Yuto, HOSOMI Akira, KUROKAWA Takashi, 1999. Study on the Effects on Energy Consumption by Vehicle Trips in a Compact City –

Using the 1975 and 1992 Person Trip Data of Utsunomiya City –, *Papers on city planning*, No. 34, pp. 241-246 (in Japanese)

IWAMOTO Shinpei, TANAKA Takahiro, NISHINA Daisaku, 2011. A study on the urban structure of small town in the depopulation age: Evaluation from the viewpoint of urban infrastructure development and maintenance cost, *AIJ Journal of Technology and Design*, Vol. 17, No. 36, pp. 661-666 (in Japanese)

HOYANO Akira, ASAWA Takashi, SATO Rihito, KAWAI Eitoku, NAKAMURA Ben, 2010. Evaluation of Environmental Impact of Vacant Lot in a Historical Urban District: Analysis of the impact of vacant lot on thermal environment and building heat load in summer using numerical simulation, *Journal of Environmental Engineering*, Vol. 75, No. 656, pp. 899-905 (in Japanese)

KANEKO Tadararu, MINOMOTO Toshitaro, 1985. A study on the Actual Condition of Existing Wooded Steep Slopes in Kawasaki-City, *Papers on City Planning*, No. 20, pp. 367-372 (in Japanese)

TANAKA Takahiro, TAKEDA Maiko, NISHINA Daisaku, 2010. Application of GIS to produce neighborhood design support system for hillside area: For design addressing environment, disaster mitigation and livability, *Architectural Institute of Japan*, D-1, pp. 941-942 (in Japanese)

Urban heat island creating a design tool for adaptation

Maria B. K. DEWI
Graduate Student, ICUS, IIS, The University of Tokyo, Japan
m.b.k.dewi@gmail.com

ABSTRACT

Urban heat island is a phenomenon of the cities which is indicated by higher temperature compared to the surroundings. As the Asian megacities growing, the prediction is in connection to the greater impact of urban heat island phenomenon. The urban heat comes from solar radiation, building, people, lack of vegetation, and machinery activities. Urban heat island brings impact in reducing human comfort, the health problems and the extra needs of energy to reach the thermal comfort. To combat heat island problems, there are some ways, such as providing green, water, the proper choice of materials, and configuration to arrange wind pattern.

Cities in Asia also have problem of urban heat. A design tool is made to adapt the urban heat in general, in the scale of building, street, and neighborhood. This design tool is made for designers, such as urban planners and architects. It contains words for explanations and pictures. Each scale contains of for category, which are: the green structure, water and humidity balance, heat and energy balance, and morphology. The tool explains sort of activities in the effective and less effective way based on the previous researches.

Keywords: *urban heat island; design tool; temperature; building; street; neighborhood; green; wind; water; configuration. the heat/energy balance, materials for outdoor urban space*

1. INTRODUCTION

Urban heat island is a phenomenon where cities accumulate heat and are consequently warmer than their surroundings (Oke, 1982). Urban heat island is a phenomenon of the warming atmosphere and surface in cities (urban areas) compared to the surroundings (Voogt, 2004). From the Fig. 1, there is different curve stated the difference of temperature in urban and rural or urbanized area. The city morphology, wind, density, shadow, various human activities cause the temperature rising, especially in urban area. The climate change brings impact to the urban heat island's temperature. The rising temperature by climate change can make the urban heat worse. But the urban heat island does not influence the global warming (Voogt, 2004). Temperature increase in the built environment has great impact on the cities living conditions (Kleerekoper, 2009). It results in the

less human comfort, health problems, and consumption of more energy and needs more air-conditioning.

City structures have important roles to tackle the urban heat. As the city is growing larger, the temperature difference between urban and rural becomes higher. The relation between temperature gap and city size is consistent that composition of buildings is taken into consideration in cooling both sun and wind orientation (Kleerekoper, 2009). Based on the United Nations report, in 2009 the world population reached 6.8 billion with over half live in the cities. By the 2050, the estimated population of the world will be 9 billion, with 70 per cent will live in urban (United Nations, 2009). As the cities growing, the challenge of urban heat island will increase.

2. URBAN HEAT ISLAND

2.1 Factors of urban heat island

There are lot of factors contribute to urban heat. The urban heat is caused by the heat of a city comes from building, people, lack of vegetation, and machinery activities (Kleerekoper, 2009). The heat is resulted from the trapped heat that buildings absorb during the day, is caused by the materials used rather than vegetation and soils in the countryside. That heat is radiated back by materials of buildings to the surrounding. Another contributor is the lack amount of trees and vegetation that support the evapotranspiration to cool the air. Machinery activities come from transportation, heating and cooling system, and industrial machinery. The sun has important role for urban heat, while the wind create cooling effect.

City form and city functions give effect for city's heating up. Urban heat islands will increase as the city grows and their effects affect the surface and ambient temperature in the city (EPA, 2008). Building and roads have significant role in increasing urban heat, this is regarding to the ability of heat absorbing and reflecting (Akbari, 2005).

There are four form of interaction between building and environment where the heat exchanges: the effective solar exposure of the glazed and opaque elements of the building envelope, the effective solar heat gain of the building, the rate of conductive and convective heat gain from and loss, the air, and the natural ventilation and building's passive cooling (Hien, et al.)

2.2 The impact of urban heat island

The urban heat islands impacts are: increased energy consumption, elevated emissions of air pollutants and greenhouse gases, and compromised human health and comfort (EPA, 2009). It also interfere the small water cycle.

Related with human health and comfort, the health problems occur, such as respiratory difficulties, heat cramps and exhaustion, heat stroke, and heat-related mortality (EPA, 2009). Another health problems also arises such as dehydration, concentration problems, skin problems, fatigue, sleep problems, and allergies happens as result of urban heat island (Kuypers, 2008). Those effects are higher on vulnerable population: children, old people, and sick people.

In addition, small water cycle will also affected by urban heat island (Kleerekoper, 2009). Urban areas tend to have less evaporation than surroundings, because buildings cover up the urban areas. The warmer and dry soil of urbanized area accelerates the water run-off (Kravcik et al., 2007; Kleerekoper, 2009).

The heating up temperature gives comfort in winter, but has negative side in summer, supports energy saving in winter but negative one in summer. By the study in the UK, in summer the urban heat island (UHI) will tend to results in an increased cooling load and an increased number of excess deaths due to overheating; but in winter, the UHI will tend to result in reduced heating loads and a reduced number of cold-related excess deaths (Davies, et al., 2008). It is important to adapt the urban heat, especially for summer, because of the impact that it creates.

2.3 Urban heat island adaptation

Addressing the urban heat problem, there are two effortst to do, which are mitigation and adaptation. The mitigation works with climate change and global warming, while it is not directly working with solution of urban heat island. And the second one is adaptation, which allows the city to adapt to the changing environment to minimize the effect of urban heat. While mitigation shows the solution in long term, adaptation can give the result in short and long term (PCCC, 2007 in Geerdink, 2009).

To adapt heat island problems, there are some ways, such as providing green, water, the proper choice of materials, and configuration to arrange wind pattern. This is based on Kleerekoper's study about the principles to reduce urban heat that can be achieved by arranging vegetation, water, built form, and albedo or reflectivity (Kleerekoper, 2009). There is another effort in her study, which is reducing anthropogenic heat. Since it is related to mitigation efforts, it is not included in this research about adaptation effort.

First of all, by evapotranspiration in active way and creating shadow, vegetation brings the effort of cooling down the environment. Green can be implemented in four ways, i.e. street trees, greens, and green roofs and facades, and urban park or forest. Vegetation can cool the temperature in 1 to 4.7° C (Comte, et al., 1981). Through evapotranspiration, the water vapours into the atmosphere so it provides cooling effect for the air temperature. Green provides shadow that can reduce the heat caused by solar radiation which is very high during summer.

Secondly, water provides cooling effect by absorbing heat, and it works when water is in the form of large mass of water, or moving on a river (Kleerekoper, 2009). Dispersed water gives cooling more than still water. Then, proper choice of materials related with albedo. Albedo is influenced by building materials' characteristics, colour, and roughness. In the study of Taha, an increasing city albedo from 25-40% results in 3° C temperature decreasing (Taha et al., 1988). Another result is by rising buildings' albedo from 9-70% can reduce the annual cooling demand in 19%. Reducing both buildings and city albedo resulted in 62% reduction of cooling energy demand (Taha et al., 1998).

The configuration or arrangement of buildings in the neighbourhood can influence urban heat. As the city is growing larger, the effect of urban heat island also increases. Directing wind by the H/W ratio is more effective than providing larger space around the building to direct the wind (Rafailidis, 1997).

The effort of urban heat island adaptation is divided into some parts, which are: the green structure, the water/humidity balance, the heat/energy balance, and the landscape morphology (Future Cities, 2010). The green structure has good effects for the city's temperature, air quality, and rainwater storage. Then, the water/humidity balance is related with water structures, such as ponds, water courses, rivers, and storage water on green roofs. They give the less temperature rising. The third one, heat/energy balance, gives the balance of heating up of city. Thus, landscape and morphology as the orientation and location of buildings give influence on temperature of an area.

2.4 Urban heat island in Asian Cities

The growing population and urbanization in Asia is rapidly increasing. Tran et al, (2006) explained that Asian cities are the most rapidly growing regions of the world nowadays and 16 of the world's 24 mega cities (cities with more than 10 million people) will be located in Asia by the year of 2015. The urban growth is followed by the increasing temperature of the city. Ichinose et al. (1999) in Tran et.al. (2006) found that in 135 years, urbanization has created a warm bias of 2.8° C in lowest air temperature in the climate record of Tokyo, while Boonjawat et al. (2000) in Tran et.al. (2006) found a increase of 1.23° C in lowest air temperature in the UHI of Bangkok for the last 50 years.

An increasing temperature in Seoul is 0.55° C, or 0.275 ° C per decade, compared to the rural area in Korea as 0.15° C or 0.075° C (Chung et al, 2004). While in Shanghai, China, the different of temperature between urban area of Longhua and suburban Songjiang is 1° C (Chen et al, 2003).

3. THE TOOL

3.1 The needed tool

Coming with the adaptive solution to urban heat island, the design tool will be used for urban planners, designers and architects. A tool containing pictures and explanation, preferably with dimensions will be practically used. The design tool is a design guidance, it should help the designers, as a guidance. The design guidance should give stimulation, option, and widen the view of designers towards a specific theme, in this case is about urban heat island.

All of the mentioned adaptation efforts in chapter 2.3 are used for making the tool, combined with the category, which are: the green structure, water/humidity balance, heat/energy balance, and urban morphology that will be explained in the following chapter.

3.2 The categorization of the tool

Measure to enhance and sustain an appreciated and attractive urban climate can be taken on building level, street level, neighbourhood level, and ultimately on regional level (Kuypers and de Vries, 2009). In the neighbourhood and regional level, urban morphology have important role in heat emission and cooling opportunities. The design tool in this research contains 3 scales, which are:

1. Building scale;
2. Street scale; and
3. Neighborhood scale.

Combining Kuypers's scale and the scale from Murakami, et al., (Murakami, et al., 2000; Murakami, 2004; Mochida, et al., 2008) the scale of area is defined as:

1. The building scale, is defined as each building, at the zone of approximately 30m-50m,
2. The street scale, is defined as one row of the street which might contains buildings or not.
3. The neighborhood scale, is defined as one neighborhood (up to 1 km x 1 km).

The categorization of each scale will be based on the solution that future cities has for adapting urban heat, which are: green structure, water/humidity balance, heat/energy balance, and urban morphology (Future Cities, 2010).

The effort which has been done by future cities is divided into some parts, which are:

1. The green structure, which has good effects for the city's temperature, air quality, and rainwater storage.

2. The water/humidity balance, which is related with water structures, such as ponds, water courses, rivers, and storage water on green roofs.
3. The heat/energy balance, which gives the balance of heating up of city; it can be consist of the choice of colour and materials.
4. The urban morphology, which is related with orientation and location of buildings give influence on temperature of an area (Future Cities, 2010).

3.3 Overview of the tool

The design tool as a guidance will be formed in 3 tables. Each table represents each scale, so there are 3 tables: in building scale, in street scale, and in neighbourhood scale. Each scale will be categorized into 4 categories: the green structure, water/humidity balance, heat/energy balance, and morphology. Each category includes some actions as written below. And the action will be defined in effective and less effective way. The actions from each category were got from researches. All of them were grouped in the suitable categories that are most related with.

1. Building scale, contains:

- a. The green structure : green roof and green façade/wall, garden for building
- b. The water/humidity balance : water close to green façade
- c. The heat/energy balance : roof and wall materials and colours
- d. The building morphology : building shape and its openings

2. Street scale, contains

- a. The green structure : street trees
- b. The water/humidity balance : none
- c. The heat/energy balance : materials for street, pavement materials for sidewalks, pavements, parking lots
- d. The street morphology : street dimension and direction, building shape which influence the street level

3. Neighbourhood scale, contains

- a. The green structure : urban forest/park
- b. The water/humidity balance : water, dispersed and flowing water
- c. The heat/energy balance : materials for outdoor urban space
- d. The urban morphology : size and density of neighbourhood, building configuration, square

3.4 The tool

Table 1: The urban heat island adaptation tool

No	SCALE AND CATEGORY	ACTIONS:
1	Building scale, includes:	
	A. The green structure (includes green roof, green façade/wall, garden for building)	1. Green roof 1a. Green roof should be use rather than roof without green 1b. Plant thick dark green vegetation on the green roof 1c. For the more than 15 cm substrate, it is better to full the surface of roof with combined plants Plant deciduous woody and conifers combined with other plants (mosses and ferns, bulbs, annual plants, herbaceous perennials, grasses and sedges) 2. Green façade/wall 2a. Green façade/wall should be use rather than wall without green 2b. Green wall and facades. Place the green wall towards the most solar radiation received, usually the west side. 2c. Percentage of green façade/wall Use large amount of covered wall with foliage. 2d. Based on the kinds of the green façade/wall Use of living wall - grid and modular, vertical interface with mixed substrate. The use of living wall – modular panel, vertical interface, with inorganic substrate. 3. Garden Provide garden in every building
	B. The water/humidity balance (includes water close to green façade)	Positioning water close to the green façade.
	C. The heat/energy balance (includes roof and wall materials and colours)	1. Roof 1a. Materials for roof based on the reflectivity Use clay tiles 1b. Material choice for sloped roofs Choose the white colour of: clay tile (1st best), concrete tile (2nd best), fiber-cement shingle (3rd best), white painted metal shingle (4th best), composite asphalt shingle, fiber-glass asphalt shingle, organic asphalt shingle (5th best) 1c. Materials for flat and low-sloped roofs Choose the white coloured of: White single-ply membrane (1 st best), smooth surface roof with white coating (2 nd best), white painted metal roof (3 rd best), built-up roof with white gravel and cementitious coating (4 th best), built-up roof with white gravel (5 th best) 1d. Use white coloured roof instead of others Use white coloured roof (1st best) Use gray coloured roof (2nd best) 1e. Use cool and reflective coating for roof made of concrete

		<p>2. Wall</p> <p>2a. The material colour choice for wall Material colour choice for building envelope, light coloured building than dark one, or white coloured than painted one.</p> <p>2b. The use of white or light coloured wall towards the sun exposed side. Place the wall with high albedo (light coloured) to face the solar radiation in the west and east.</p> <p>2c. The use of hollow block and concrete than brick. Choose the hollow block and concrete for wall.</p>
	D. The building morphology (includes building shape and its openings)	<p>Building shape: Openings on the building to allow wind blow. More openings on the buildings.</p>
2	Street scale, includes:	
	A. The green structure (includes street trees)	<p>1. Street trees</p> <p>1a. Placed the transpiring plants on the side of the street</p> <p>1b. Trees planted on both sides of the street</p> <p>1c. Related with the ability for evapotranspiration, deciduous trees is better than conifers</p> <p>1d. Related with the effectiveness for shading, the crown shape is really significant. Plant street trees which have large crown shape, create large shadow</p> <p>1e. Related with the shape and size of the leaves. Plant street trees:</p> <p>1. <i>Tilia tomentosa</i></p> <p>2. <i>Tilia platyphyllos</i></p> <p>3. <i>Tilia cordata</i></p>
	B. The heat/energy balance (includes materials for street, pavement materials for sidewalks, pavements, parking lots)	<p>1. Materials for street Combination between concrete and asphalt</p> <p>2. Paving materials for sidewalks, pavements, parking lots</p> <p>2a. The colour and material. The use of painted roads</p> <p>2b. Grass-covered pavement</p>
	D. The street morphology (includes street dimension and direction, building shape)	<p>1. Street</p> <p>1a. Dimension of the street. Street should have less than 0.25 ratio of H/W (widening the street or shortening the buildings' height)</p> <p>1b. Dimension of the street with the same amount of trees. Create a narrow street with the same amount of trees</p> <p>1c. Street direction. Direct the street to the main direction of the summer wind</p> <p>1d. H/W ratio to create mixed air from urban canopy layer and boundary layer. Create the ratio of H/W 0.5 as the best</p> <p>2. Buildings</p> <p>2a. Round shape building rather than angular shape for the entrance and end of street canyon</p> <p>2b. Tall buildings opposite tall buildings</p> <p>2c. Slanted roofs to increase the ventilation</p> <p>2d. Altering roofs shape arrangement is better than similar roof shape</p> <p>2e. Shading building by plants, materials, and buildings</p>
3	Neighborhood scale	

<p>A. The green structure (includes urban forest/park)</p>	<p>1. Urban forest/park 1a. Create urban forest/park and open grass field 1b. Larger urban forest/park gives greater impact than the small one 1c. Small and spread green. Create two small parks rather than one large park. 1d. Based on the size of the leaves to the cooling effect. Plants trees: <i>1.Aesculus hippocastanum</i> <i>2.Gleditsia triacanthos</i> <i>3.Platanus acerifolia</i></p>
<p>B. The water/humidity balance (includes water, dispersed and flowing water)</p>	<p>1. Create water square close to the green 2. Large surface of water 3. Dispersed water 4. Flowing water</p>
<p>C. The heat/energy balance (includes materials for outdoor urban space)</p>	<p>1. Material for outdoor urban space 1a. The use of cool materials rather than warm materials. Use light-coloured materials 1b. The use of smooth surface materials than rough surface materials</p>
<p>D. The urban morphology (includes size and density of neighborhood, building configuration, square)</p>	<p>1. Size and density of neighbourhood Adjust the neighbourhood becomes not too large. Develop a small and not crowded neighbourhood. 2. Building configuration 2a. More dynamic configuration of buildings. Diagonal configuration of buildings rather than grid configuration. 2b. Adjacent building placement 3. Square Dimension of the square which is surrounded by buildings Square should have less than 0.25 ratio of H/W</p>

4. CONCLUSION

The tool is guidance for design. It is made in 3 scales, which are: building scale, street scale, and neighborhood scale. Each scale contains 4 categories, which are: the green structure, water and humidity balance, heat and energy balance, and morphology. Regarding with the street and neighborhood scale, this tool also has possibility to be used by planners. Being performed in tables, the tool has 3 parts based on the scale: building scale table, street scale table, and neighbourhood scale table. In each table, there are 4 categories as mentioned on previous paragraph. Each of the categories contains some actions equipped with explanations. However, further research is needed in order to adapt this tool for specific location and condition.

REFERENCES

Akbari, Hashem. 2005. *Energy Saving Potentials and Air Quality Benefits of Urban Heat Island Mitigation*. Heat Island Group, Lawrence Berkeley National Laboratory.

Chen, L., et al. 2003. *Characteristics of the heat island effect in Shanghai and its possible mechanism*. *Advances in Atmospheric Sciences* 20: 991-1001.

Chung, U., et al. 2004. Urbanization effect on the observed change in mean monthly temperatures between 1951-1980 and 1971-2000. *Climatic Change* 66: 127-136.

Tran, H. et al. 2006. *Assessment with satellite data of the urban heat island effects in Asian mega cities*. *International Journal of Applied Earth Observation and Geoinformation* Volume: 8, Issue: 1, Pages: 34-48.

Comte, D.M. le, Waren, H.E. 1981. *Modelling the Impact of Summer Temperatures on National Electricity Consumption*. *Journal of Applied Meteorology* vol. 20, page 1415-1419.

Davies, Mike, Steadman, Philip, Tadj Oreszczyn. 2008. *Strategies for the modification of the urban climate and the consequent impact on building energy use*. *Energy Policy* 36: 4548-4551.

EPA, 2008 *Reducing Urban Heat Islands: Compendium of Strategies*. Environmental Protection Agency's Office of Atmospheric Programs. <http://www.epa.gov/heatisland/resources/pdf/BasicCompendium.pdf>
Retrieved in 14 May 2010

Environmental Protection Agency (EPA, United States). *Heat Island Impacts* (2009). <http://www.epa.gov/hiri/impacts/index.htm> Retrieved in March 2010

Future Cities website. <http://www.future-cities.eu>. Retrieved in February 2010

Geerdink, Tobias, et al. 2009. *Urban Heat Island: kwetsbare groepen in de stedelijke leefomgeving (vulnerable groups in urban environment)*. Saxion University of Applied Sciences.

Hien, Wong Nyuk, Eang, Lee Siew, Li Shuo, Ana nda Ram Bhaskar, Tan Kok Kwang. *Thermal Performance of Façade Materials and Design and the Impacts on Indoor and Outdoor Environment*.

Kleerekoper, Laura. 2009. *Urban Heat*. Graduation Thesis. Delft University of Technology.

Kuypers, Vincent, Vries, Barry de. 2008. *Groen voor Klimaat*.

Oke, T.R. 1982. *The energetic basis of the urban heat island*. The quarterly journal of the Royal Meteorological Society Vol 108, page 1-24.

Rafailidis, Stylianos. 1997. *Influence of Building Areal Density and Roof Shape on the Wind Characteristics above a Town*. *Boundary-Layer Meteorology* 85, page 255-271.

Taha, H. Rosenfeld, Akbari, A., J. Huang. 1988. *Residential Cooling loads and the urban heat islands-the effect of albedo*. *Building and Environment* 23, page 271-283.

United Nations. 2009. *Commission on population and development to focus on population growth in least developed nations, impact on development, 30 March-3 April*.

Voogt, James. A. 2004. *Urban Heat Islands: Hotter Cities*. <http://www.ActionBioscience.org>. (retrieved in March 2010)

Study on urban air quality risk using spatial technology and public perception: a case study of Vientiane Capital city, Laos

Southanome KEOLA¹, Edsel SAJOR²
and Vivarad PHONEKEO³

¹ PhD candidate, UEM, SERD,
Asian Institute of Technology, Thailand
st104504@ait.ac.th

² Associate Professor, UEM, SERD,
Asian Institute of Technology, Thailand

³ Senior Researcher, GIC, SET,
Asian Institute of Technology, Thailand

ABSTRACT

Vientiane Capital is one of the urbanized cities in Laos that has been continuously developed since the end of 90s after the Lao government has issued the open-door policies that introduced the marketing economy to develop the country. The critically change in the city is the number of variety vehicles which have been increasing yearly, traffic congested have been appeared in urban center where high density population located. This main objective of this study is whether this phenomenon could possible to be a source of air pollution that effects to metropolitan's health. However, Laos does not have baseline air quality data that is necessary for the study due to there is no systematic air quality measurement facilities yet. Therefore, it is necessary to carry a study for better understanding of the air quality scenario and regularly convey information to concerned stakeholder for making decision on health and environment prevention. To overcome this problem, the this study have proposed an alternative way to solve the problem, by introducing the application of spatial technology which includes 9 years MODIS aerosol optical thickness product from NASA as a tool for PM data acquisition. In the result of the study, the high and low concentration of PM areas was obtained which can refer to be the risk area for resident. Public risk perspective from the high risk area and upper respiratory symptoms from elderly people have obtained. These results could be informed for public health decision maker to improve and revise urban planning and regulations.

Keywords: aerosol optical thickness, MODIS, Particulate matter, public risk perspective

1. INTRODUCTION

Economic growth is linked to urbanization, and does not always positively contribute to improve the human well-being and living condition. If the economy grows rapidly, urban areas would expand without proper control and might lead to unexpected negative impacts such as increasing of urban environmental pollution. The increasing of economic activities, business and industries contribute to generate various environmental pollutions, one of them is urban air pollution which normally rises up silently during the building phase of urbanization (Fenger, 1999), (Wichitrakorn, 2002). Traditionally, capital city or urban areas is initial area of air pollution which results from rapid growth of population in urban center and peri-urban area (Sevilla *et al.*, 2004). Vientiane Capital is a capital city of Laos that faces of the initial urban air pollution and have certified by following facts: (i) the monitoring of air quality conducted in every three consecutive days per year in the period of 2002-2004 have found the particulate matter with aerodynamic diameter $10\ \mu\text{m}$ (PM_{10}) over WHO standard (ADB, 2006); (ii) derived Carbon Monoxide from SCIAMACHY imageries is in the high level (SCIAMACHY, 2008); (iii) the noise pollution have over the WHO standard (ADB, 2006); and the increasing of traffic congested area in the urban center.

Mobile source of air pollution is a critical source in Vientiane Capital that requires for proper information to support the air quality management. The increasing of annually road accident is an acute or visible impact of traffic that being rising up with number of selling vehicles (MCTPC, 2007), while chronic or silence impact of traffic is still unclear status. In addition, the important tools of air quality management such as air quality standard, emission standard and related regulations are limited.

Transportation is the most polluted factor for urban area, the level of air pollution depends on the physical construction and energy consumption with particular vehicles and it tends to be worst in cities that contain of high population density (Mage *et al.*, 1995). In this case of Vientiane Capital, there are many associated factors, (i) buying and selling tax is reduced; (ii) unclear quota for imported low cost vehicles or second hand car; (iii) the purchase capacity of population is increasing; and (iv) the rapid growth of population in the sub-urban with high demand on vehicle to travel to urban center. Recently, the growth of car passenger occupied about 17 % annually, the total number of motorcycles registered in 2009 is 272 thousand or 3.3 times more than number in year 2000 (Vientiane, 2010). Whilst the parking area is not properly designed in the urban center; some cars are parked on the roadsides, block the traffic flow which lead to traffic congestion and cause of car's emission to the urban atmosphere.

Maintaining and controlling in the initial stage of air pollution is possible to minimize its severities to harm human and environment (CIA-Asia and PAMA, 2004), and many countries could not conduct the air quality monitoring activities, due to unaffordable for instruments (CIA-

Asia, 2010). The efficient air pollution monitoring instruments are mainly produced by developed countries; one of them is Moderate Resolution Imaging Spectro Radiometer (MODIS). MODIS is an earth observation satellite which provides free Aerosol Optical thickness (AOT) for observing the air quality in the regional and global scale. However, the usage of MODIS AOT in the local scale have been recognized through the various studies on the relationship between MODIS AOT and particulate matter with aerodynamic diameter less than $2.5 \mu\text{m}$ ($\text{PM}_{2.5}$) and have resulted the reliable correlation, particularly in the urban areas (Mukai S. et al., 2007; Jeong E et al., 2006; and Hui Li et al., 2009). Thus MODIS AOT might be one of alternative solutions for air pollution monitoring in area where air monitoring station not available, but the ground measurement for validation is still needed (Gupta P et al., 2006).

This paper attempts to estimate the $\text{PM}_{2.5}$ derived from MODIS AOT and status public health in the area of high and low concentration of $\text{PM}_{2.5}$ of Vientiane Capital. The 9 year MODIS AOT data have been applied and the high concentration of $\text{PM}_{2.5}$ has occurred during February, March and April. The High and low risk area has been identified by visualized analysis with Google Earth application. Risk area found in the urban center and sub urban has great potential to become risk in the future. The extent through health survey in urban center and sub urban area, some health symptoms of upper respiratory diseases were found in elderly people who live in the high $\text{PM}_{2.5}$ concentrated area.

2. STUDY AREA

The study area locates in the Vientiane Capital which is situated in the southwestern part of Laos and on the banks of the Mekong River. It locates at $17^{\circ}58'$ North, $102^{\circ}36'$ East. The Vientiane Capital covers mostly plain and lowland area. The core urban area consists of 100 villages with belongs to Chanthabouly, Sisattanak and parts of Sikhottabong, Xaysetha and Hadxaifong districts where locate main offices, commercial centers, center of public services, banks, cultural resources, recreation places and educational centers.

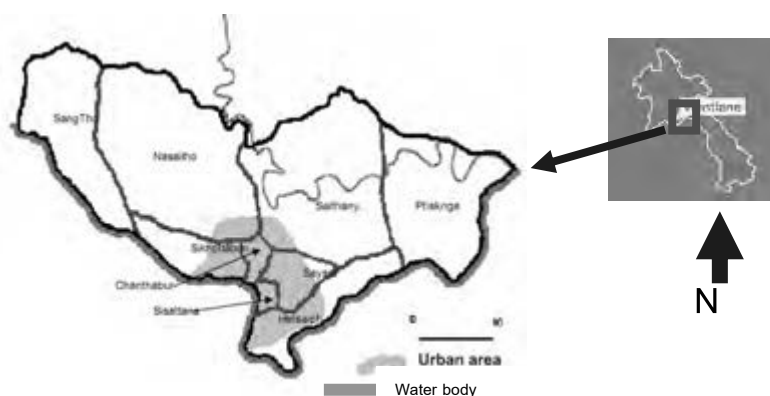


Figure 1: Map of study area

The built-up area doubled from approximately 3% of total area in 1995 to 6% in 2005. Vientiane Capital has the population of approximately 700 thousands persons in 2005. Approximately 350 thousand people or 50 % of the total population concentrates in the urban area and 50% in the sub urban area. The urban center has very limited population growth rate due to no more apace for development, while the suburban area has high population growth rate with plenty of apace for further urbanization. The population density of the urban center is 36.7 person/ha on an average, whilst some areas may be more densely inhabited with more than 80 persons/ha (MCTPC, 2007).

The urban center of Vientiane Capital consists of the whole areas of Chanthabouly, Sinathanak, Sikhottabong, Xaysetthan, Hatxayfong and Xaythany district and had divided in 36 traffic zones and 234 villages.

3. METHODOLOGY

According to lack of air monitoring station in Lao PDR, the air quality in the ground is not available for monitoring; this study have applied Aerosol Optical thickness (AOT) from the Moderate-Resolution Imaging Spectroradiometer or MODIS AOT to estimate the $PM_{2.5}$ mass concentration in Vientiane Capital. The process of methodology is explaining as follow: (i) the MODIS AOT data collection; a set of MODIS AOT in the dry season (February, March and April) for 9 years were downloaded and then the data were geometric corrected and stored as binary images; (ii) defined a reference table for the deterring the range of $PM_{2.5}$. Reviewing studies on relationship between MODIS AOT and $PM_{2.5}$; focused on the result from linear regression to determine its relationship. The reference table has obtained and this study applied this study to be a reference for estimate the range of $PM_{2.5}$ (Table 1); (iii) defining the risk area by applying the application of Google Earth to conduct the visualized analysis. Data on MODIS AOT, population density, travelling pattern, congested traffic points, urban infrastructures have used to identify risk area; and (vi) conduct health survey in high and low risk area. The questionnaires were also conducted by face to face interview individual households at high and low risk location. Respondent's age was between 18 and 65 years old. The flowchart of the methodology is shown in the Figure 2. All results of this study are described in the next section.

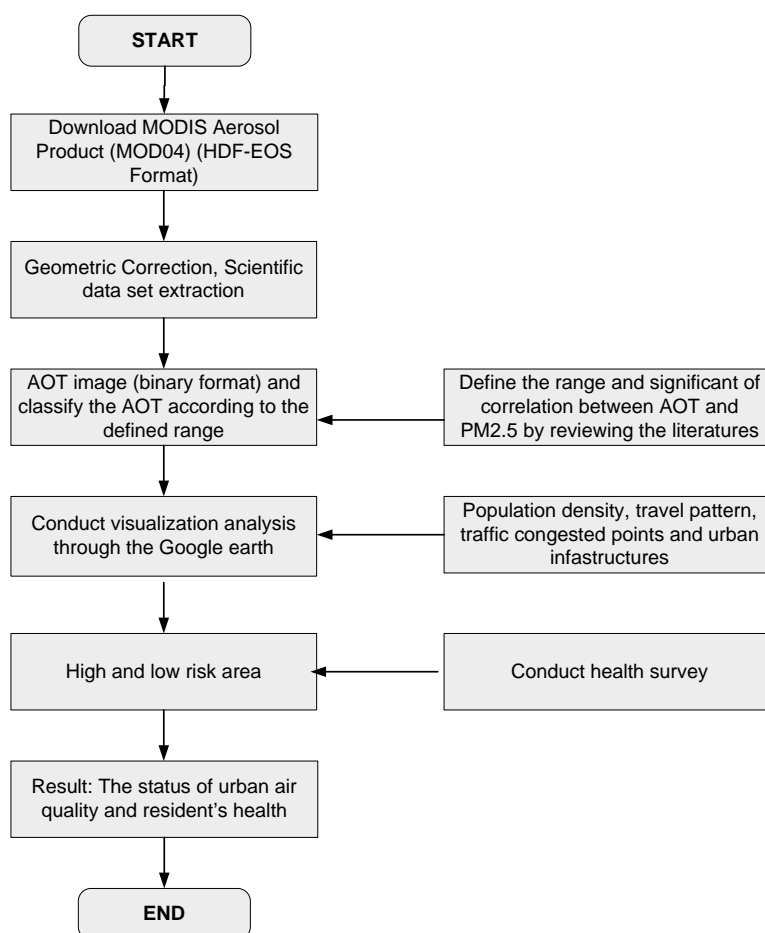


Figure 2: The process of methodology

Table 1: The reference range of MODIS AOT index and mass concentration of PM_{2.5}

Range of aerosol optical thickness (AOT) index	Range of PM _{2.5} (µg m ⁻³)	Range of correlation coefficient between PM _{2.5} and AOT
0-0.19	0-29	0.6, 0.96
0.2-0.49	30-69	0.77, 0.96
0.5-0.79	70-100	0.77, 0.96
0.8- more than 1	more than 110	0.87

Sources: (i) Keith D. Hutchison, Solar Smith and Shazia J. Faruqui , 2005; (ii) Nuno Grosso et al.,2008; (iii) Jeong E et al., 2006, Gupta P et al., 2008; Mukai S et al., 2007; R.B.A. Koelemeijer et al., 2006;

Note: the green, yellow, orange and red represent the value of written number in the table

4. AREA OF HIGH AND LOW PM_{2.5} CONCENTRATION

The MODerate resolution Imaging Spectrometer (MODIS) instrument is a sensor onboard Terra and Satellites which its mission is for Earth observation in global scale and multi-temporal time series for global environmental study. The application of MODIS data is widely used for land, ocean and atmospheric research and study because of the wide-range of spectral bands from red to thermal bands which is in total of 36

bands. With the launch of Terra and Aqua polar orbiting satellites, the usage of satellite to estimate the PM_{2.5} has been increased for alleviate some of the uncover ground measurements and several studies have shown that some information from satellite data could present for ground measurements. The studies on the comparison between satellite-derived aerosol optical thickness and PM_{2.5} mass found a good correlation between column AOT derived from the MODIS on the Terra/Aqua satellites and fine particulate mass (PM_{2.5}) (Engel Cox et al., 2006; Gupta et al., 2006, 2007, Wang and Christopher, 2004). Some studies have used local meteorological parameters along with satellite-derived products to form multiple regression equations that improve overall relationships.

Since the MODIS onboard EOS-Terra satellite was launched into a sun-synchronous polar orbit in December 1999 (R.B.A. Koelemeijer et al., 2005), the obtained MODIS AOT data is available from year 2001 onward. The free AOT MODIS data within 9 years (2001 and 2004-2010) for Vientiane Capital have downloaded from NASA website (<http://modis.gsfc.nasa.gov/>). The aerosol product or MOD04 is one of the MODIS products which is generated from MODIS data of Level 1B and contains the aerosol optical depth physical parameter. 13 grids (radius 10 x 10 Km) cover all of Vientiane Capital.

This study used data from 2001, 2004 to 2011 to estimate the potential of highest level of MODIS AOT. According the some limitation of MODIS, the cloud free day consists more in dry seasons. The received MODIS AOT data around 80% in each February and 60% in March and around 45-50% in April have downloaded, and these data were sufficient to identify the status of AOT. MODIS AOT data in each month have classified according to reference Table 1, the percentage of good air quality during dry season (Feb to April) is less than 23.2% of total MODIS AOT data, but the critical air quality also not more than 12.5 % and the 64.2% of air quality still in the level of consider for sensitive people. The details are listed in Table 2.

Table 2: The percentage of MODIS AOT by year and month

	February				March				April			
2001	10.0	20.0	50.0	20.0	17.5	30.2	12.0	40.3	30.4	26.2	30.4	13.0
2004	22.0	32.2	40.7	5.1	23.0	39.1	30.4	7.5	30.0	42.0	22.0	6.0
2005	12.1	32.8	36.0	19.1	17.5	12.0	40.7	29.8	34.5	32.1	26.0	7.4
2006	34.0	43.0	21.2	1.8	25.2	22.1	48.0	4.7	33.3	43.2	22.0	1.5
2007	24.4	15.7	42.1	17.8	12.9	29.1	49.3	8.7	17.0	33.5	28.8	20.7
2008	25.0	28.3	45.0	1.7	18.9	52.4	23.0	5.7	35.6	34.2	20.0	10.2
2009	24.3	41.1	33.3	1.3	13.5	22.4	45.1	19.0	23.7	43.1	30.0	3.2
2010	27.0	42.7	22.1	8.2	21.2	43.2	33.0	2.6	28.6	11.2	30.1	30.1
2011	22.0	35.4	27.2	15.4	16.4	34.1	32.0	17.5	27.2	45.2	7.5	20.1

The average of MODIS AOT within 9 years has displayed in the Figure 2, the green, yellow, orange and red represents the low, middle, high and very high range of PM_{2.5} respectively. The grid number 8 is the highest MODIS AOT. To discover more on this area, the map of population density, travelling pattern, congested traffic points, urban infrastructures have imported to the Google earth and high and low risk area have obtained.

The high risk area consists of 8 villages, and the low risk area consists of 25 villages which cover 1218 households (11189 people) and 3022 households (301156 people) respectively. From the study, it is obviously that MODIS AOT data can be used to apply for air quality monitoring in Vientiane Capital.

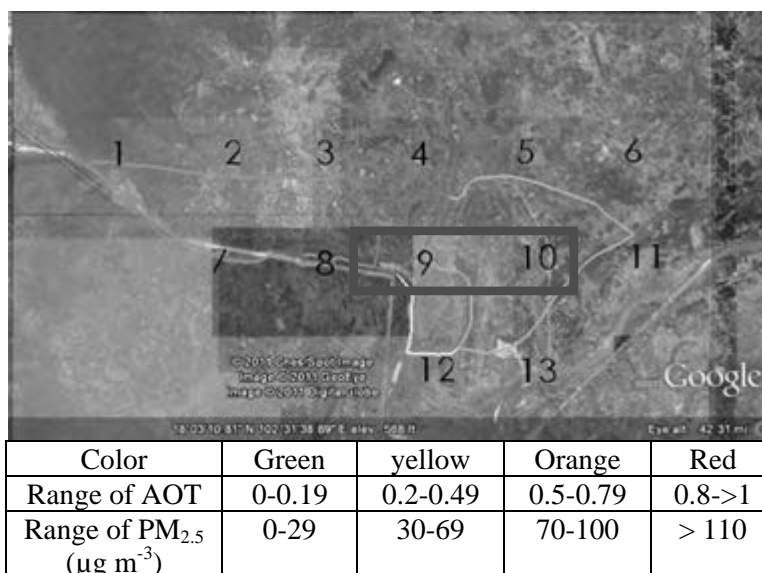


Figure 3: The average of MODIS AOT's Vientiane Capital

5. HALTH STATUS AND PUBLIC PERCEPTION

Air quality monitoring is the main source of information in assessing the exposure of the population to ambient air pollution. Exposure is determined by the concentrations people experience in their living environments. Thus, monitoring should measure the concentrations in places the people live. Human exposure to air pollutants may result in a variety of health effects depending on the type of pollutants: the magnitude, duration and frequency of exposure; and the associated toxicity of the specific pollutant. This study trends to estimate the population health status, but the measuring of air pollution is still not accurate yet. Therefore the dose exposure also will not reliable for predict the risk. Therefore the assessments on risk perception, annoyance of urban air pollution, and health-related quality of life have conducted during June to August 2011 to identify the health status of resident who live in area of high and low PM_{2.5} concentration derived from MODIS AOT. The designed population-based questionnaire has covered all of listed three aspects (risk perception, traffic annoyance, health-related quality of life).

The survey by questionnaires had conducted in 180 households, 100 households in high PM_{2.5} concentration area and 80 households in low PM_{2.5} concentration. 75% of responded household live in personal house and most of them are house owner and live in their own land more than 10 years.

Apart from the visible health impact from road traffic, the record of mortality and mobility in health center shows that the mitigation measure for road safety is need to revise and improve. The common reasons such as high speed, riding after alcohol and drugs consumption still have a dramatic impact on the frequency and severity of injuries and mortality from road accidents (S. Dhondt et al., 2010). The number of injuries from road accident keeps rising up annually (Figure 5). However, the invisible health impact still is silence and that is the one of the objective of this study.

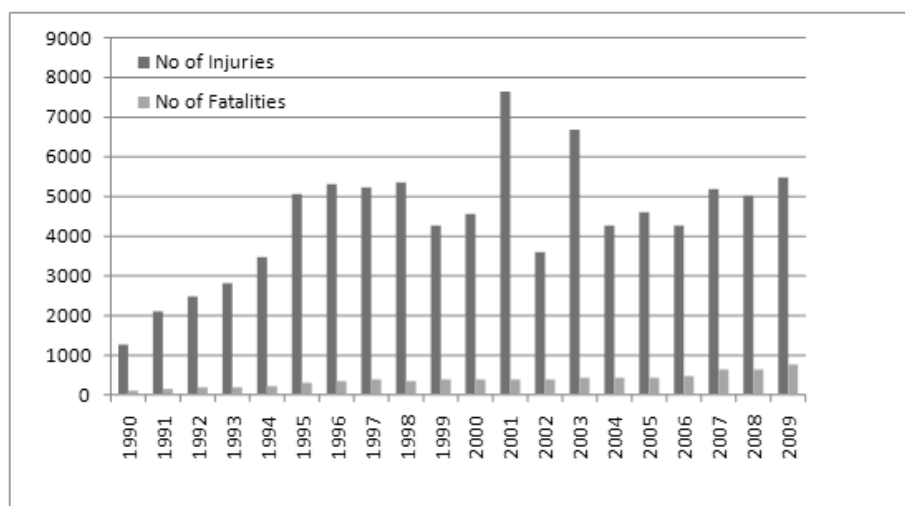


Figure 5: Number of injuries from road accident
Department of Transport, 2010

In this study find out a current picture of the way that residents think about the problem of urban air pollution. The most important source of air pollution is construction, vehicle emission, road dust and Garbage burning (Table 3). Direct, personal experience was clearly formative in each answer, the urban air quality is generally very good (the respondent have accepted 50%), and road traffic have to consider (only 30% of respondents who have personal car are strongly accepted, while respondent who drive the motorcycle have responded for neutral and poor) (Table 4). The visible indicators included physical depositional evidence (dust or dirt) at the household level help respondent to understand the level of urban air pollution easily (Karen Bickersta and Gordon Walker, 2001). The perception on the cognitive sources of urban air pollution and existing air quality in Vientiane Capital from residents have identified the critical source of urban air pollution and sense to the severity of air pollution.

Table 3: The perception on the cognitive sources of urban air pollution

Source of urban air pollution in Vientiane Capital	Percentage of respondents*			
	Agree	Not agree	Do not know	Void
Vehicle emission	93	-	7	-
Construction	100	-	-	-
Garbage burning	40	40	10	10
Industrial emissions	10	80	10	-

Slash and burn	-	90	10	-
Road dust	70	20	10	-

Note*: some respondents identified more than one source

Table 4: The percentage of cognitive perception on the existing air quality in Vientiane Capital

Air quality in Vientiane Capital	Very good	Good	Neutral	Poor	Very poor	Do not know	Void
General area	50	40	10	-	-	-	-
Road	30	30	20	10	10	-	-

55% percent of resident have agreed that they might have risk from exposure to urban air pollution while 45% still do not know urban air pollution. Since air pollution components may be odorless, people may react to the chemical substances as irritants, to bodily mediated reactions such as eye irritations, coughing and allergic responses (R. Klæboe et al., 2007). However, the risk perception on urban air pollution for resident is not big issue, but they are worrying the security risk such as robber, gangster or thief, drug and amphetamine (80% of respondent have emphasized on these risks). Moreover, respondent did not significantly emphasize on health problems, even most of them have experiences with listed health problems and symptoms in Table 5, particularly elderly. “*Health diseases or symptoms from exposure to air pollutant are possible to treat with medication, and it is not major problem here*” is the common expression from health perception survey. The discussed information has already been shown that the direct health impacts of air quality represent an important source of local air quality. However, respondents have confirmed the negative health impacts of air pollution on their own health with less significance. Table 5 shows the results of survey question which asked respondents whether they were aware of any particular health problems they or family members had experienced that they linked to poor air quality. Almost half of those surveyed (45%) identified some form of impact, mostly related to breathing, allergic and irritation problems.

Table 5: percentage of respondent reported on health impact

Diseases	% of total respondent have experience on these disease and symptoms*
Pneumonia	20
Allergic	70
Cardio-vascular disease	3
Chronic flu	50
Lung disease	37
Asthma	73
Health symptoms	
Difficult to breath (sometimes)	82
Chest pain	56
Chronic runny nose	37
Chronic sneezing	55
Cough without clear reason	23
Chronic cough without clear reason	11

*Some respondents identified more than one impact.

7. CONCLUSION AND DISCUSSION

The usage of MODIS AOT for estimate the air quality is not final answer, the ground monitoring is need to validate. However, this technique has illustrated a broad view of urban air pollution for the area that need preliminary assessment and air monitoring station is not available.

In case of Vientiane Capital, the main source of air pollution is line source. Vehicle fleet in the Vientiane Capital dominances by private vehicle, particularly motorcycle. In the year 2009, motorcycle cover 70 % of total vehicles and follows by pick up, light vehicle and others 14,6%, 5% and 10.5% respectively. Moreover, the standard of used car still not issued officially thus the various type of nonstandard car is imported. According to the EPA studies, 30% of five-year-old cars emit more than they were designed to emit. Fifty-five percent of seven-year-old cars will continue to pollute urban air quality. Base on facts above, the air pollution in Vientiane Capital exists but not reach to the critical status. Some of resident have health problem, but generally resident still happily lives in Vientiane Capital.

REFERENCES

Asian Development Bank (2006). *Country Synthesis Report on Urban Air Quality Management Lao PDR*. Asian Development Bank, 2006.

CIA-Asia and PAMA, 2004. *A Strategic Framework for Air Quality Management in Asia*. Stockholm Environment Institute, 2004

CIA-Asia (2010). *Air Quality in Asia: Status and Trends, 2010 Edition*. Clean Air Initiative for Asian Cities (CAI-Asia) Center, April 2010

Engel-Cox, J. A., Holloman, C. H., Coutant, B. W., & Hoff, R. M. (2004). *Qualitative and quantitative evaluation of MODIS satellite sensor data for regional and urban scale air quality*. *Atmospheric Environment*, 38, 2495–2509.

Fenger Jes (1999). Urban air quality. *Atmospheric Environment* 33 , 4877-4900

Gupta P, Sundar A, Christopher A., Wang J. G, Robert, Yc Lee, Kumar. (2006), Satellite remote sensing of particulate matter and air quality assessment over global cities. *Atmospheric Environment* (40). 5880–5892.

Gupta P, Sundar A, Christopher, Jun Wang, Robert Gehrig, Yc Lee and Naresh Kumar (2008).

Satellite remote sensing of particulate matter and air quality assessment over global cities.

Atmospheric Environment. (40), 5880-5892

Hui Li, Fazlay Faruq, Worth Williams, Mohammad Al-Hamdan, Jeffrey Luvall, William Crosson, Douglas Rickman and Ashutosh Linaye (2009). Optimal temporal scale for the correlation of AOD and ground measurements of PM_{2.5} in a real-time air quality estimation system. *Atmospheric Environment*. (43), 4303-4310

Jeong E. Kim, Seong Y. Ryu, Zhuanshi He and Young J. Kim (2006). Spectral aerosol optical depth variation with different types of Aerosol at

Gwangju, Korea . *Journal of Atmospheric and Solar-Terrestrial Physics* (68), 1609-1621

Karen Bickersta and Gordon Walker (2001). Public understandings of air pollution: the & localization of

environmental risk. *Global Environmental Change* 11 (2001) 133-145

Mage S., Ferraraccio F., Prati M.V., Annunziata S., A. Bianco, A. Mezzogiorno, G. Liguori, I.F. Angelillo and M. Cazzola. (1995). Urban air pollution in mega cities of the world. *Journal of Atmospheric Environment*, (30.) 5.

Ministry of Communication Transport Post and Construction (2007). *The study of master plan on comprehensive urban transport in Vientiane Capital in Lao PDR*. Progress report, Katahira & Engineers international July, 2007.

Matthias Schmidt and Ralf-Peter Schäfer (1988). An integrated simulation system for traffic induced air pollution. *Environmental Modelling & Software* 13 (1998) 295-303

R.B.A. Koelemeijer, C.D. Homan and J. Matthijsen (2005). Comparison of spatial and temporal variations of aerosol optical thickness and particulate matter over Europe. *Atmospheric Environment* (40) 5304-5315

R. Klæboe, A.H. Amundsen, A. Fyhri (2007). Annoyance from vehicular air pollution: A comparison of European exposure-response relationships. *Atmospheric Environment* 42 (2008) 7689-7694

Sevilla J., David C., Jaypee S. (2004). The Effect of Health on Economic Growth: A Production Function Approach. *The journal of World Development* 32 (1). 1121-1124.

SCIAMACHY (2008). The monthly concentration of CO from SCIAMACHY satellite data in Lao PDR.

SCIAMACHY website, http://www.iup.uni-bremen.de/sciamachy/NIR_NADIR_WFM_DOAS/, last updated on 2010.

Stijn Dhondt, Quynh Le Xuan, Hieu Vu Van and Luc Hens (2010). Environmental health impacts of mobility and transport in Hai Phong, Vietnam. *Stoch Environ Res Risk Assess*. DOI 10.1007/s00477-010-0374-3

S. Mukai, I. Sano, A. Nishimori, M. Sato, Y. Okada and B.N. Holben (2007). A comparison of aerosol properties with air pollutants. *Advances in Space Research* 39 (2007) 32-35

Vientiane (2010). Draft of Vientiane Master Plan. Vientiane Urban Development Administrative Authority 2010.

Wang Jun and Sundar A. Christopher (2004). Intercomparison between satellite-derived aerosol optical thickness and PM_{2.5} mass: Implications for air quality studies. *GEOPHYSICAL RESEARCH*. 30, doi:10.1029/2003GL018174, 2003

Wichitrakorn N. (2002). *The estimation of mortality and economic impact of urban air pollution in Bangkok*, College of Public Health, (Master Thesis No RA 576.6 T5) Chulalongkorn University

Potential greenhouse gas reduction in Samui towards becoming carbon neutral island

Poon THIENGBURANATHUM¹, Pongtip THIENGBURANATHUM², and Chaya VADDHANAPHUTI³

¹Associate Professor, Department of Civil Engineering, Faculty of Engineering, Chiang Mai University, Thailand
poon@eng.cmu.ac.th

²Research Assistant, Department of Civil Engineering, Faculty of Engineering, Chiang Mai University, Thailand

³Lecturer, Department of Geography, Faculty of Social Science, Chiang Mai University, Thailand

ABSTRACT

Worldwide is facing the impacts of climate change, in particular along coastal areas. Samui, one of the most popular tourist destination and business investment is encountering the risk of losing its precious natural resource due to human activities and climate change. This study explores the potential for Samui to reduce greenhouse gas (GHG) emission, towards becoming carbon neutral island by analysing the potential to reduce GHG emission based on historical and surveyed data and future activities from 4 sectors, namely: (1) solid waste management, (2) mass urban transportation, (3) energy efficiency, and (4) renewable energy. Calculations suggest that by changing technologies and infrastructures, Samui is able to reduce emission from solid waste sector, using landfill and methane capturing technology, between 2,414-21,633 tCO₂e/year. In transport sector, much reduction (up to 68,875 tCO₂e/year) comes from changing diesel motorcycle to electric motorcycle and switching from diesel cars to either electric and hybrid, or ethanol. In energy efficiency sector, the study finds switching to more efficient lighting and cooling technologies especially in hotels and residential area to help reducing GHG up to 11,894 tCO₂e/year. Lastly, a potential of at least 100 projects of photovoltaic installed in hotels are able to reduce 255-2,571 tCO₂e/year. In total, the entire island can reduce GHG by 5,990-9,490 tCO₂e/year.

Keywords: *Climate Change Mitigation, Samui Island, Clean Development Mechanism*

1. INTRODUCTION

Worldwide is facing the impact of Climate change, while it is important to recognize that the impact is greater along the coastline and especially on islands. These impacts includes for example: inundation of coastal areas where the majority of their inhabitants reside, loss of freshwater supplies, diminution of biodiversity, destruction of critical infrastructure, and possible increase in the incidence of serious diseases.

Historically Samui's economy has been based around subsistence agriculture and fishing, with coconuts as the main cash crop. From the 1980s onwards, tourism has become an economic factor and is now the dominant industry. The construction of a stable, high-speed Internet connection in recent years has also made the island a feasible location for IT-based enterprises, which are beginning to provide a certain degree of economic diversity. The island's climate and accessibility make it particularly attractive for international investors. Samui is attracting more and more investor and tourists to the island every year. However, with the economic shifted from agriculture to tourism, the island had to adapt itself to larger human footprint. Tourist brings income as well as increases pressure and requirement on natural resources consumption.

This study explores the potential for Samui to reduce greenhouse gas (GHG) emission, towards becoming carbon neutral island by analysing the potential to reduce GHG emission based on historical and surveyed data and future activities from 4 sectors, namely: (1) solid waste management, (2) mass urban transportation, (3) energy efficiency, and (4) renewable energy.

2. DEVELOPMENT OF TOURISM IN SAMUI

In 1980s East Asia and Southeast Asia experienced the most rapid growth in regional mass tourism in the world, with 9.2 % per annum increase in the number of tourists compared to the global average of 4.5% (Hitchcock et al 2008 p. 8). This was due to increasing affluence from the Far East, decreasing cost of travelling, increasing tourist availability and diversity, and most importantly, the 1992 "Visit ASEAN" campaign (Hitchcock et al 2008). After 2005, the region received \$ 43.2 billion as GDP, 7 million jobs created while tourist demand still increased by 6.2% per annum. Thailand has always and long been the top 20 in tourist destination.

The study of Green (2005) describes the establishment of tourism in Samui back in 1980s in a town called Chaweng as "no more than small beach bungalows and restaurants catering to backpackers owned and operated by locals as a means of providing additional income to that which they earned from other sources, such as coconut farming." Today, not only Chaweng is famous but also Tambon Angtong, Tambon Maret, Tambon Boput, Tambon Maenam, and Lamai community.

As the new millennium turns, massive and rapid growth of tourism

completely changed the socio-economic status of Samui. In 2002, the total number of tourist was 857,335 with 85.21% as foreigner mostly from Germany, United Kingdom and Australia, generating 10.4 billion Baht of cash flow. At the time, the island had 310 service accommodations with approximately 60% occupation rate. Although in 2003 alone the SARS situation decreased the growth rate by 6% (Department of Environmental Quality Promotion: DEQP, 2006), Samui received up to 10 million international tourists, which generated 10 billion US dollar income or 5.4% of the GDP (Green 2005) The figure for domestic and international tourist is 150,000 and 850,000 per year, respectively, or 2,903 persons per day ., generating between 12-14 million baht of cash flow per year (Samui Municipality 2010a). Chudintra and Pintukanok (1992, cited in Wong 1998) calculated that, for the whole island to maintain its identity, the maximum carrying capacity is put at the maximum 14,200 tourists/day. With such growth in the number of tourist, the population of local people of Samui in 2004 and 2010 was 45,493 (DEQP, 2006) and roughly 51000, respectively, and last updated on 30 April 2009, was 52,935 (Samui Municipality, 2010a). The unregistered population, mostly from Northeastern part of Thailand and Burma is roughly 200,000 (Samui Municipality 2010a).

In the past, the majority of local people engage in small-scale agricultural activity. Agricultural land is dominated by coconut plantation (84,310 rai), durian (11,037 rai), langsat (5,725 rai), mangosteen (430 rai), and rubber (1,185 rai), another sector includes fishing (Samui Municipality 2010a). Green (2005) observed that people from the Thai mainland and Westerns dominate ownership of the town's resorts, restaurants and bars. They tend to employ cheap workers, hence an influx of people from the mainland and illegal migrants (Burmese).

3. METHODOLOGY

The project boundary is Samui Island, Surrathani Province. The project analysed the potential to reduce Greenhouse Gas (GHG) emission from 4 sectors namely: (1) solid waste management, (2) mass urban transportation, (3) energy efficiency, and (4) renewable energy. The potential will analyse based on existing database as well as survey data. The project focused on historical activities and planned project activities. The methodologies used were base on the approved small-scale methodology for Clean Development Mechanism (CDM): AMS-III.G Landfill Methane Recovery, AMS-III.F. Avoidance of methane emissions through composting, AMS-III.T. Plant oil production and use for transportation applications, AMS-III.AK. Biodiesel production and use for transportation applications, AMS-III.C. Emission reductions by low- greenhouse gas emitting vehicles, AMS- III.S. Introduction of low-emission vehicles to commercial vehicle fleets, AMS-III.AA. Transportation Energy Efficiency Activities using Retrofit Technologies, AMS-I.A. Electricity generation by user, AMS- II.C. Demand-side energy efficiency activities for specific technologies, AMS.II.E Energy Efficient and fuel switching measures for buildings, and AMS -II.J Demand-side activities for efficient lighting technologies. The

formulas were used to calculate potential GHG emission reduction for each type of project for each sector.

4. CURRENT GREENHOUSE GAS EMISSION

4.1 Greenhouse Gas emission from waste

The estimation of the methane emission potential of a solid waste disposal site ($BE_{CH_4,SWDS,y}$ in tCO₂e) was undertaken using the “Tool to determine methane emissions avoided from dumping waste at a solid waste disposal site”. The assumption taken in this study was that the amount of waste entering the landfill site in 2009 was 45,267 tons, the amount of waste increase by 5% to 47,530 tons in 2010. The assumptions and detail calculations are shown in Annex 2. This is conservatively estimated based on the total amount of waste collected for disposal in 2008. The average baseline over the 10 years crediting period is 2,835 tCO₂e per year, if the landfill gas collection and destruction project starts in 2011-2020 (10 years crediting period). The result of the analysis is illustrated in Figure 11.

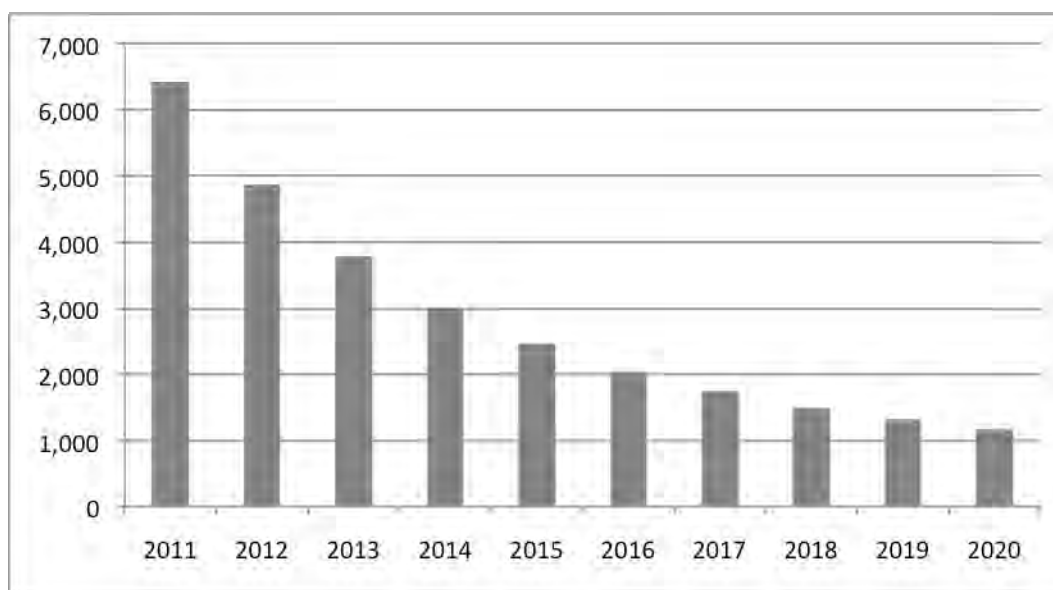


Figure 1: Baseline emission from waste collected and disposed at landfill site (tCO₂e/year) during 2009-2010 only (2 years of waste only).

4.2 Greenhouse Gas emission from transportation

Transportation sector in Samui is dominated by motorcycle. This is the most frequently used mode for both the residents and tourists. The total GHG emission from this sector was calculated as shown in table 15. However, the baseline for each project activity are different, depending on the design of each project. Therefore, the emission reduction will be calculated based on the different baseline. The detail calculation and assumptions are shown in Annex 3.

Table 1: GHG emission from transport sector in Samui Island.

Vehicle	No.	Fuel Consumption rate (l/km)	Fuel Consumption (l/year/vehicle)	Fuel Consumption (l/year)	Type of Fuel used	GHG emission (tCO ₂ e/year)
Motorcycle	40,616	5.7	1,087.56	44,172,336.96	Gasoline	106,014
Truck	4,314	12.26	2,339.208	10,091,343.31	Diesel	27,247
Sedan (<7 seats)	3,549	10.8	2,060.64	7,313,211.36	Gasoline	17,552
Sedan (>7 seats)	342	10.36	1,976.69	676,027.29	Gasoline	1,825
Van (> 7 seats)	416	7.55	1,440.54	599,264.64	Diesel	1,618
Total GHG emission estimated for Samui Island						154,255

Sources and Assumptions

- Number of Vehicles from Office of Transport, Samui Branch
- Average distance assume from each vehicle travel a distance of 19,080 km (53 km/day multiplied by 360 days). 53km is the distance of the road around Samui Island.
- Fuel consumption rate, calculated average from <http://www.environment.gov.au>, and <http://www.motorcyclefuelconsumption.com/>
- GHG Emission for petrol = 0.0024 tCO₂e/l. from <http://oee.nrcan.gc.ca/publications/transportation/fuel-guide/2009/index.cfm>
- GHG Emission for diesel = 0.0027 tCO₂e/l. from IPCC 2006

4.3 Greenhouse Gas emission from energy sector

Samui's electricity demand was met by transmitting electricity from the national grid electricity via underwater cables from Suratthani Province. Hence, GHG emission calculation is based on the national grid emission factor for Thailand, which is 0.5812 tCO₂e/MWh (TGO, 2010). In addition if the renewable energy is generated from solar or wind, the grid emission factor adopted for the calculation will be 0.598 tCO₂e/MWh (TGO, 2010), in accordance with "Tool to calculate the emission factor for an electricity system" Version 2.

5. POTENTIAL PROJECTS THAT WOULD REDUCE GREENHOUSE GAS EMISSION

The projects that are not feasible as CDM project activity, but are feasible as a CDM project may be develop without CDM but may consider other alternatives such as verified emission reduction (VERs) under the voluntary market instead.

Table 2: Potential emission reductions projects

Project	Feasibility with CDM		Feasibility without CDM	
	Yes	No	Yes	No
Waste Option 1: Landfill Recovery (flare/electricity generation)	✓*			✓
Waste Option 2: Methane Avoidance (compost)	✓*			✓
Transport Option 1: Replaced diesel fuel transportation vans with plant oil such as jatropa. By replacing diesel with 10% plant oil.	✓		✓	
Transport Option 2: Replaced diesel fuel transportation vans with plant oil such as jatropa. By replacing diesel with 100% plant oil.	✓		✓	
Transport Option 3: Replaced diesel fuel transportation vans with 20% waste oil.	✓		✓	
Transport Option 4: Replace transportation van with electric/hybrid		✓		✓
Transport Option 5: Replace petrol motorcycle with electric motorcycle.	✓		✓	
Transport Option 6: Replace commercial taxis with higher efficiency vehicles		✓		✓
Transport Option 7: Retrofit commercial taxis with energy efficient equipment		✓	✓	
Energy Option 1: Renewable energy power plant with less than 10 MW installed capacity	✓**		✓**	
Energy Option 2: The installation of photovoltaic at a group of hotels to replace electricity supply by the national grid.		✓		✓
Energy Option 3: The replacement of energy efficient air conditioners at group of hotels and resorts on Samui Island.		✓		✓
Energy Option 4: The replacement of energy efficient equipments at a large buildings on Samui Island. (assumed 15% saving)	✓		✓	
Energy Option 5: Adoption of self-ballasted compact fluorescent lamps (CFLs) to replace incandescent lamps (ICLs) in residential applications.	✓		✓	

* Without CDM project development cost

** Electricity generation from renewable biomass

6. POTENTIAL GREENHOUSE GAS EMISSION REDUCTION

The potential range of greenhouse gas emission reduction is as shown in table 2. The maximum greenhouse gas emission reduction is 104,973 tCO₂e/year if all the potential projects are carried out.

Table 3: Potential Greenhouse Gas emission reduction

Sector	GHG Reduction (tCO ₂ e/year)
Solid Waste	2,414-21,633
Transport	28-68,875
Renewable Energy	255-2,571
Energy Efficiency	23-11,894
Total	2,720-104,973

REFERENCES

Department Environmental Quality Promotion (DEQP) 2006, “Green Activity to promote environment, tourism and community involvement, Samui Island Municipality, Suratthani Province” prepared by TESCO Co., Ltd.

Hitchcock, M., King, V.T., Parnwell, M. 2008. *Tourism in Southeast Asia: challenges and new directions*. NIAS Press, Copenhagen.

Green, R. 2005. Community perceptions of environmental and social change and tourism development on the island of Koh Samui, Thailand. *Journal of Environmental Psychology* 25, 37–56

IPCC. 2007. *Climate Change 2007: The Physical Science Basis. Contribution of Working Group I to the Fourth Assessment Report of the Intergovernmental Panel on Climate Change* [Solomon, S., D. Qin, M. Manning, Z. Chen, M. Marquis, K.B. Averyt, M.Tignor and H.L. Miller (eds.)]. Cambridge University Press, Cambridge, United Kingdom and New York, NY, USA.

PEA Samui office. 2009. Energy database for national energy analysis and strategic planning, Suratthani province. Provincial Electricity Generation.

Office of Transport. 2010 Office of Transport, Samui branch, Ministry of Transport.

Provincial Electricity Authority. 2010. Provincial Electricity Authority, Samui Office.

Samui Municipality. 2010a. Samui Development Plan 2010-2012, <http://www.kohsamuicity.go.th/> [last accessed 24 November 2010]

Samui Municipality. 2010b. Waste data (primary data collection).
Samui Municipality, Suratthani province.

The Samui Green Island Project. 2010. The Green Island Project, Koh
Samui, Thailand

<http://www.thegreenislandproject.org/> [last accessed 24 November
2010]

Wong, P.P. 1998. Coastal tourism development in Southeast Asia:
relevance and lessons for coastal zone management. *Ocean & Coastal
Management* 38, 89-109

TGO, 2010. The Study of emission factor for an electricity system in
Thailand 2009, Summary Report

Using copper slag in cement concrete

Sudhir MISRA¹ and Kunwar Krishna BAJPAI²

¹ Professor, Department of Civil Engineering
sud@iitk.ac.in

² Senior Scientific Officer, Department of Civil Engineering
Indian Institute of Technology Kanpur, India

ABSTRACT

With growing scarcity of natural raw materials, use of industrial wastes and by-products as substitutes is being actively investigated to promote sustainable construction. In this study, utilization of copper slag as an alternative material for fine aggregates has been explored. Concrete mixes with a target compressive strength of about 30MPa and slump in the range of 50-60 mm were prepared at different levels of replacement of fine aggregates (by copper slag). Properties related to the mechanical behavior of concrete (compressive/flexural strength) and some others more related to long term durability in terms of water absorption, and resistance to chloride ion penetration, have been compared.

It was found that replacement of fine aggregates with copper slag to the extent of 50% does not result in any significant difference in the properties of the concrete. It was also found that given that the copper slag was about 40% heavier compared to the normally used fine aggregates, the density of concrete increases by about 6% at the level of 50% replacement, and about 15% at 100% replacement level. It was further found that even complete replacement of fine aggregates does not adversely affect the flexural strength and resistance to chloride ion penetration of the concrete, though a reduction in the compressive strength was found at replacement levels higher than 50%.

Keywords: *copper slag, density, concrete, compressive strength, flexural strength, durability, recycling*

1. INTRODUCTION

A number of industrial waste products are produced in huge quantities each year, and their accumulation causes environmental problems. Some of these products such as fly ash, ground granulated blast furnace slag, copper slag, etc. are now being used to produce value added products. On the other hand, with rapid depletion in natural aggregates, the construction industry worldwide is under pressure to explore the alternatives to the natural aggregates, river sand, etc. In India about 6-6.5 million tonnes copper slag is generated every year. Though there is not much evidence of pozzolonic activity of copper slag, it can be used as partial/full replacement of fine aggregates (FA) as its particle size distribution can be easily matched with

FA by suitable modification in the grinding process. In review articles (Bipra Gorai, R.K. Jana, and Premchand, 2003, Caijun Shia, et. al., 2008) on characteristics and utilization of copper slag, it has been reported that copper slag can be potential alternative to the admixtures used in concrete and mortars. An attempt has been made in this study to understand the effect of replacement of FA by copper slag on properties of fresh and hardened concrete.

2. MATERIALS USED IN THE STUDY

2.1 Cement, aggregates, coarse sand, and copper slag

Locally available Ordinary Portland Cement (OPC) was used along with coarse aggregates and sand. Physical properties of OPC were determined as per Indian Standard (IS) (IS 4031-1988 Reaffirmed 2005) and found to be conforming to IS 8112-1989. Similarly properties of aggregates used (sand and crushed granite aggregate) were found as per IS 2386-1963 Part I & III (Reaffirmed 2007) and found to be conforming to IS 383-1970 (Reaffirmed 2002). It may be noted that properties of the copper slag were determined in a manner similar to that used for fine aggregates, and the results are compared in Table 1. It can be seen that the copper slag is much heavier than the FA and has very little water absorption, whereas the fineness modulus is almost similar.

Table.1: Physical properties of fine aggregates and copper slag

Physical Property	Fine aggregates	Copper Slag
Fineness Modulus	2.95	2.87
Specific Gravity	2.61	3.68
Water Absorption (%)	0.42	0.06

2.2 Concrete mix proportions specimens used

Details of concrete mixes used having varying levels of copper slag replacements (of the FA) are given in Table 2. The mixes were designated as CS00, CS25, CS50, CS75 and CS100, respectively for 0%, 25%, 50%, 75% and 100% of the FA content replacement (by volume), the mix CS00 being a control mix (i.e. with no copper slag). For all mixes, the w/c ratio, and the unit water, cement and the coarse aggregate content, were kept at 0.45, 153 kg, and 340 kg, and 1202kgs, respectively. In all mixes a super-plasticizer was used to keep the slump in the required range of 40-65 mm (observed values also given in Table 2).

Table 2: Details of concrete mix proportions

Concrete Mix	Fine Aggregates	Copper Slag		Slump	Concrete mix density
	kg/m ³	kg/m ³	l/m ³ (~%)	mm	kg/m ³
CS 00	751	0	0	60	2452
CS 25	563	295	71.7 (25)	35	2562
CS 50	376	591	143.3 (50)	30	2646
CS 75	188	886	215.0 (75)	20	2707
CS 100	0	1181	286.6 (100)	45	2793

3. EXPERIMENTAL DETAILS AND TEST DATA

3.1 Compressive and flexural strength

Cube specimens (150mm side) for compressive strength tests and beam specimens (100 mm X 100 mm X 500 mm) for flexural strength tests were used as per IS 516-1959 (Reaffirmed 2008) and the test data (average of three specimens) are given in Table 3.

Table 3: Strength, density and water absorption of concrete at 28 days

Concrete Mix	Compressive strength (MPa)	Flexural strength (MPa)	Density (kg/m ³)	Water absorption (%)
CS 00	41.4	4.7	2305	3.6
CS 25	39.6	4.6	2379	3.2
CS 50	41.0	5.1	2436	3.7
CS 75	36.1	4.0	2566	3.4
CS 100	34.1	5.2	2603	3.0

3.2 Density and water absorption

Density and water absorption of hardened concrete have been measured using cylindrical specimens (diameter: 100 mm; length: 200 mm) as per ASTM C642-06 and the observed results have been given in Table 3.

3.4 Rapid chloride ion penetrability tests

The ASTM C1202-10 was used to measure the penetrability of chloride ions using concrete discs of diameter 95 mm and thickness 50 mm, at about 28 days and the average (of three specimens) values (Coulombs) are given in Table 4.

Table 4: Chloride Ion Penetrability Test Data (at 28 days)

Concrete Mix	Total Charge passed in 6 hours (Coulombs)	Chloride Ion Penetrability
CS 00	1571	Low
CS 25	1602	Low
CS 50	1111	Low
CS 75	1335	Low
CS 100	940	Very Low

4. RESULTS AND DISCUSSIONS

4.1 Density of copper slag based concrete mixes

From simply the mix proportions an increase in the mass per cubic meter of concrete mix was found to be about 17.5% with respect to control mix on account of the higher specific gravity of the copper slag (3.68 compared to 2.61 of fine aggregates). This data is compared with the density obtained in accordance with the ASTM C642-06 and plotted in Figure 1. It can be seen that the observed values also show the expected increase, and the increase is about 13% in CS 100.

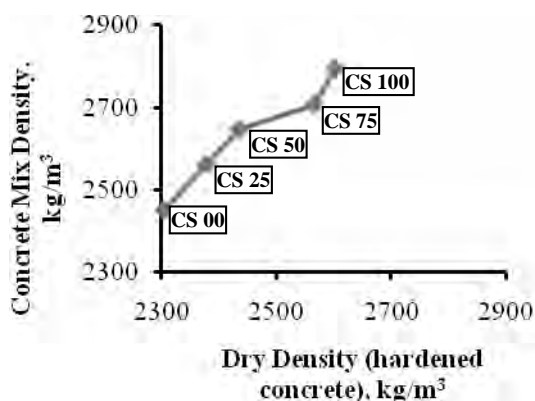


Figure 1: Density increase with copper slag content

4.2 Compressive and flexural strength

A diagrammatic representation of the variation of the compressive and flexural strengths (28 days) with respect to the replacement level of FA by copper slag is shown in Figures 2 and 3. As can be seen from Figure 2, the 28 days compressive strength of copper slag based concrete having up to 50% replacement is comparable with the control mix, at levels of 75% and 100% replacement, a significant decrease (12.8% to 17.6%) in compressive strength is observed. This suggests that whereas for up to 50% replacement

of fine aggregates with copper slag the concrete mixes may be prepared with ‘normal’ mix design considerations, higher levels of replacement, additional care should be taken.

As far as flexural strength is concerned, it was found that replacement of FA by copper slag even to the extent of full replacement does not adversely affect it. It may also be pointed out that for all concrete mixes, the measured values are higher than those estimated (3.8 MPa) in accordance with IS 456:2000. In fact, this level of the flexural strength is also marked in Figure 3 for reference.

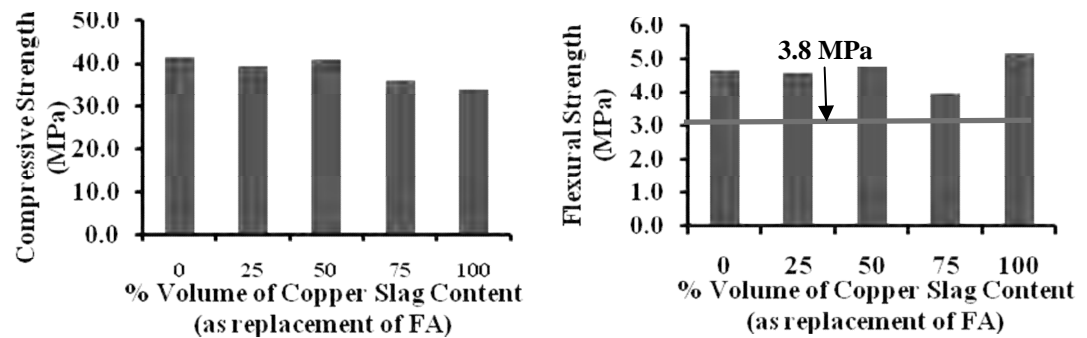


Figure 2: Compressive Strength (28 days) Figure 3: Flexural Strength (28 days)

4.3 Water absorption by hardened concrete

Water absorption by hardened concrete has often been suggested as simple measure of the porosity of the matrix and therefore the durability of the concrete. Measurement in accordance with ASTM C642-06, shows that the absorption for the control mix is 3.6% and that for the other concretes varies between 3.0 and 3.7% for the different levels of replacement. The data collected in this study is not sufficient to determine a definite trend with respect to the replacement levels, it can be stated that no increase in the water absorption was found upon replacing FA with copper slag.

4.4 Resistance to chloride ion penetration

The Rapid Chloride Ion Penetration Resistance Test (ASTM C1202-10) is another test for a quick evaluation of durability of concrete. A bar graph showing the results obtained is shown in Figure 4. It can be seen that the resistance to chloride ion penetration for most of the concrete mixes falls within the *Low* penetration zone.

A closer examination of the data collected reveals that though at 25% replacement level the RCPT value (Coulombs) is similar to that of control concrete, further replacement clearly lowers the chloride penetrability. More experiments are however, required to establish a more quantitative relationship between the level of replacement and the resistance to chloride penetration.

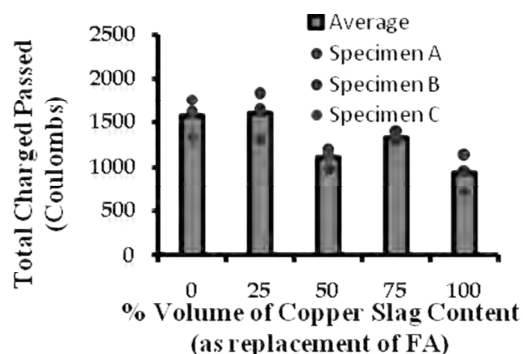


Figure 4: Resistance to chloride ion penetration (ASTM 1202)

5. CONCLUDING REMARKS

Based on tests carried out to better understand the effect of replacing naturally occurring sand (fine aggregates) to different extents by copper slag, which is by-product of the copper manufacturing process, the following can be stated as some of the salient findings.

- 1) Addition of copper slag does not make the concrete ‘unworkable’, and target values of slump can still be achieved with a suitable adjustment in the superplasticizer dosage.
- 2) The density of concrete is higher on account of the use of the heavier copper slag (replacing FA).
- 3) The compressive strength observed at 28days shows that the values are comparable with up to 50% replacement of FA, though some decrease is seen at higher replacement levels.
- 4) The flexural strength is not adversely affected by the replacement of FA by copper slag, and all values are found to be higher than the estimated by IS 456 (based on the actual compressive strength).
- 5) Water absorption of concrete with copper slag is comparable to that of control concrete and the values tend to be slightly lower at very high replacements. A similar trend is observed for resistance to chloride ions based on the results of the Rapid Chloride Penetration Test (where all concretes fall in the ‘LOW’ to ‘VERY LOW’ classification as per ASTM 1202).

ACKNOWLEDGEMENT

Funding for carrying out the work and the copper slag used in the present study was provided by M/s Sterlite Industries (India), Limited, Tuticorin. Special mention should be made of Mr. Lovish Ahuja, Manager & Head, Environment, Sterlite Industries (India), Limited for his participation in the work. Help from Mr. Pankaj K. Gupta (Jr. Technical Superintendent) of

Structural Engineering Laboratory, Department of Civil Engineering, IIT Kanpur, in terms of technical support, is also gratefully acknowledged.

REFERENCES

Bipra Gorai, R.K. Jana, and Premchand, 2003, "Characteristics and Utilisation of Copper Slag: A Review" Elsevier J. Resources, Conservation and Recycling, 39, 299-313.

Caijun Shia, Christian Meyer, and Ali Behnood, 2008, "Review: Utilization of Copper Slag in Cement and Concrete", Elsevier J. Resources, Conservation and Recycling, 52, 1115-1120.

Indian Standard IS 4031-1988 (Reaffirmed 2005), "Methods of physical tests for hydraulic cement"

Indian Standard IS 8112-1989, "Specification for 43 grade ordinary Portland cement"

Indian Standard IS 2386-1963 Part I & III (Reaffirmed 2007), "Methods of test for aggregates for concrete"

Indian Standard IS 383-1970 (Reaffirmed 2002). "Specification for coarse and fine aggregates from natural sources for concrete"

Indian Standard IS:516-1959 (Reaffirmed 2004), "Methods of tests for strength of concrete"

ASTM C-642-06, "Standard Test Methods for density, absorption, and voids in hardened concrete"

ASTM C-1202-10, "Standard test method for electrical indication of concrete's ability to resist chloride ion penetration"

Indian Standard IS:456-2000 (Reaffirmed 2005), "Plain and reinforced concrete - Code of practice (Fourth Revision)"

Role of coarse aggregate in a cement-based material with strain-hardening subjected to stress-field rotation

Kohei NAGAI¹, Benny SURYANTO², and Koichi MAEKAWA³

¹ Associate Professor, ICUS, IIS, The University of Tokyo, Japan
nagai325@iis.u-tokyo.ac.jp

² Postdoctoral Fellow, Department of Civil Eng.,
The University of Tokyo, Japan

³ Professor, Department of Civil Engineering,
The University of Tokyo, Japan

ABSTRACT

Strain Hardening Cementitious Composite (SHCC) is a cement-based composite that when pulled exhibits multiple-fine cracks and pseudo-strain hardening response. A new testing method was developed to reproduce possible rotation of principal stress axes during the material strain-hardening. Thus, not only tensile stresses, but also must shear stresses be transmitted across the cracks. Using this proposed testing method, twenty-three SHCC plates were tested. Of the twenty-three plates, four plates were made of plain PVA-ECC (a SHCC available in Japan), while the other 19 plates were constructed by adding coarse aggregate in the volume fractions of 5% to 20%. From the plates made of plain PVA-ECC, it was observed that rotation of principal stress lowered the strength and ductility, and always resulted in an orthogonal cracking pattern. From the plates containing aggregate, it was observed that, if no stress rotation took place, the plate load capacity decreased by 20% to 40%, while the plate ductility was reduced to approximately one half. If stress rotation occurred, the load capacity and ductility were within 80% to 120% of the plates experiencing no principal stress orientation change. The aggregate addition of 10% to 12.5% showed a better ability to control the orientation of secondary cracks.

Keywords: SHCC, principal stress rotation, shear transfer, multiple cracks, coarse aggregate

1. INTRODUCTION

In reinforced concrete highway bridge deck structures, wheel movement has been frequently observed to be the primary source of fatigue damage (Maeda and Matsui, 1984, Perdikaris and Beim, 1988). The wheel movement causes continual changes of concrete principal stress magnitude and continuous rotation of principal stress field at different locations on the deck (Maekawa *et al*, 2006 and Fujiyama *et al*, 2007). Due to the stress field rotation, in particular, cracks once formed at a certain orientation at various

locations on the deck will repeatedly open, slip, and close. It is essential to provide the necessary stress transfer ability to accommodate such repeated crack deformations for longer deck serviceability.

To apply SHCC for deck-type structures, it is essential to test the material performance to loading histories in which principal stress directions do rotate. It is, therefore, anticipated that the crack resistance to shear is as important as its resistance to tension. Nevertheless, cracked SHCC demonstrated strong anisotropic responses when subjected to principal stress rotation due to crack opening and slip (Suryanto *et al*, 2010). To limit this slip, extra load-carrying mechanism should be provided in addition to fiber bridging that is more effective for resisting crack from further opening.

This study investigates the effectiveness of coarse aggregate as a means of shear carrying mechanism in SHCC. Coarse aggregate is considered since it is widely available and comparatively cheap, although its addition would also elevate the toughness of the SHCC matrix and hence lower its ductility. Hence this study attempts to investigate the trade off between shear transfer improvement and tensile ductility loss. The effect of different coarse aggregate volume fractions is prompted.

2. EXPERIMENTAL PROGRAM

The experimental program involved the testing of 15 control plates (Plates PC) and 8 main plates (Plates PM). The dimension of the control plates was 400×250×20 mm, while that of the main plates was 550×420×20 mm. The main variable in the test program was the amount of coarse aggregate, ranging from 0% to 20% by volume.

The material properties of each aggregate volume fraction were determined from three 100×200 mm standard cylinders (Specimen MC), three 100×100×400 mm prisms (Specimen MP), and five dog-bone specimens (Specimen MT, but only applicable to the original mixture with no coarse aggregate). Specimen MT had a constant 80-mm long testing zone, with a width and thickness of 30 mm and 13 mm, respectively. Both MC cylinders and MT samples were tested at 28 days, while specimens MP were tested between 28 and 34 days. All tests were performed in accordance with the JSCE recommendations (JSCE, 2007).

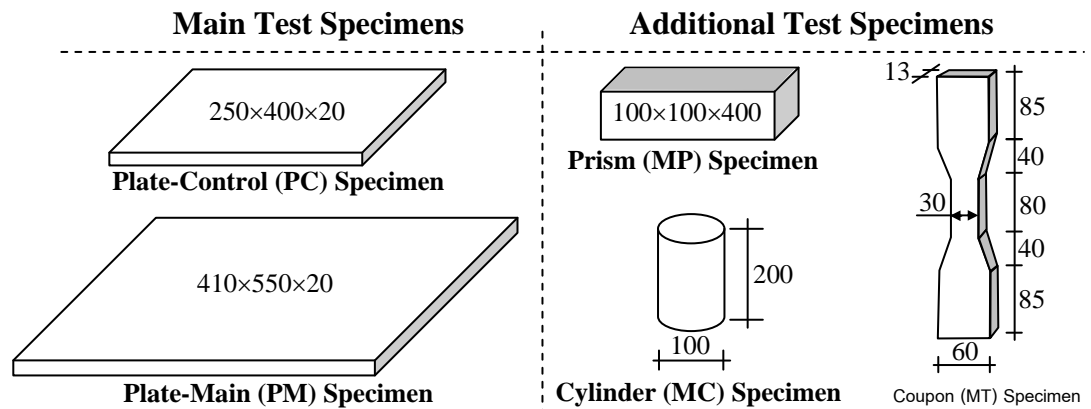


Figure 1: Details of test specimens

2.1 SHCCC Material: PVA-ECC

The material investigated is a mix of PVA-ECC and typical-crushed type, coarse aggregate available in Japanese market. Table 3 lists the mix proportion of the ECC and the original sieve analysis of the coarse aggregate. Considering the thickness of test plates, the aggregate size larger than 9.5 mm was omitted. Prior to casting, the aggregate was cleaned and kept in a saturated surface dry condition.

2.2 Preparation of Test Specimens

The mixing and casting of the specimens were all done at the Kajima Research Institute, Japan. The mixing of the ECC followed the JSCE guideline (JSCE, 2007). After the material being well mixed, coarse aggregate was added to the slurry and they were then remixed for about two minutes. Table 4 summarizes the fresh properties of the ECC before and after addition of coarse aggregate.

After casting, all plates were covered with a plastic sheet and demolded after one day. Afterwards, the plates were wrapped with wet burlap and plastic sheets. After a few days, they were delivered to the Concrete Laboratory, University of Tokyo, and stored in an ambient room with 60% relative humidity and a temperature of 20°C until the test date. The surface of the plates that had been at the bottom during casting was remarkably smooth and flat, while the upper finishing surface was uneven. As a result, the thickness of the plates varied in the order of 1 mm.

Table 1: Specimen numbers for each specimen type

Specimen		Aggregate Volume Content (%)						
Type	ID	0	5	7.5	10	12.5	15	20
Plate-Control	PC	3	2	2	2	2	2	2
Plate-Main-45deg	PM45	1	1	1	1	2	1	1
Material-Prism	MP	3	3	3	3	3	3	3
Material-Cylinder	MC	9	3	3	3	3	3	3
Material-Coupon	MT	15	-	-	-	-	-	-

Table 2: Mix proportion of ECC (JSCE, 2007) and sieve analysis of aggregate

PVA-ECC				Coarse Aggregate	
W / (C+FA) (%)	Water kg/m ³	S / (C+FA) (%)	PVA fibers (%), by Vol.	Sieve size (mm)	Cumulative Passing (%)
42.2	350	70	2.0	13.2	95
				4.75	5.7

Note: W: water, C: ordinary portland cement, FA: fly ash, and S: sand
 PVA fibers: diameter 0.04 mm, length 12 mm, tensile strength 1,600 MPa.

Table 3: Fresh property of PVA-ECC

Case	Aggregate volume (%)	Slump flow before adding aggregate (mm×mm)	Air Content (%)	Slump flow after adding Aggregate (mm×mm)	Density (kg/m ³)	Slump loss (mm)
1	0	510×495	12.5	–	1,804	–
2	5	495×485	11.5	455×440	1,822	–
3	7.5	500×500	12.0	430×420	1,851	–
4	10	515×505	11.1	405×390	1,881	–
5	12.5	505×505	11.7	380×380	1,879	–
6	15	485×470	10.6	340×330	1,914	16.5
7	20	480×480	9.5	320×310	1,966	16.0

2.3 Testing Procedure

Figure 2(a) shows the layout of test plates, while Figure 2(b) shows the testing procedure adopted in the experiment. For the control plates, a four-point bending test was performed. For the main plates, pre-cracks were first introduced by performing bending test (Step A). The plate was then unloaded when the strain at the plate soffit reached a value of 40% of ϵ_{tu} . After fully unloaded, the plate was reversed upside-down (Step B), further loaded in bending (Step C), and again unloaded (Step D). Steps B to D were carried out to flatten the plate. The plate was then cut (Step E) in order to alter the angle of the pre-cracks to a certain angle. Finally, the cut plate was re-tested in four-point bending (Step G).

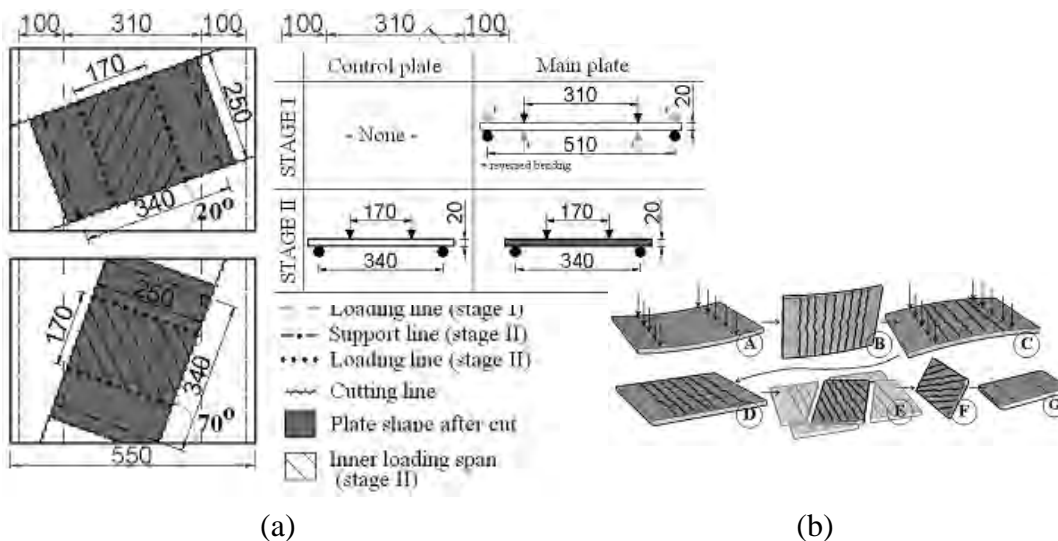


Figure 2: (a) Details of test plates, and (b) Testing Procedure

2.4 Material Test Results

Table 4 summarizes the average tensile properties from five dog-bone coupons, while Figure 3(a) and (b) compare the average flexural tensile strengths and compressive strength with different aggregate volume fractions obtained from three representative specimens. It appears that as the aggregate volume fraction is increased, the tensile strength decreases, while the compressive strength increases.

Table 4: Results of tensile tests

Specimen	Age (days)	Cracking Stress (MPa)	Tensile Yield Strength (JSCE 2007) (MPa)	Ultimate Tensile Strain (%)
MT-1-5	28	2.16(0.2)	2.99(0.3)	3.26(0.3)

Note: Values in the bracket are the COV in %

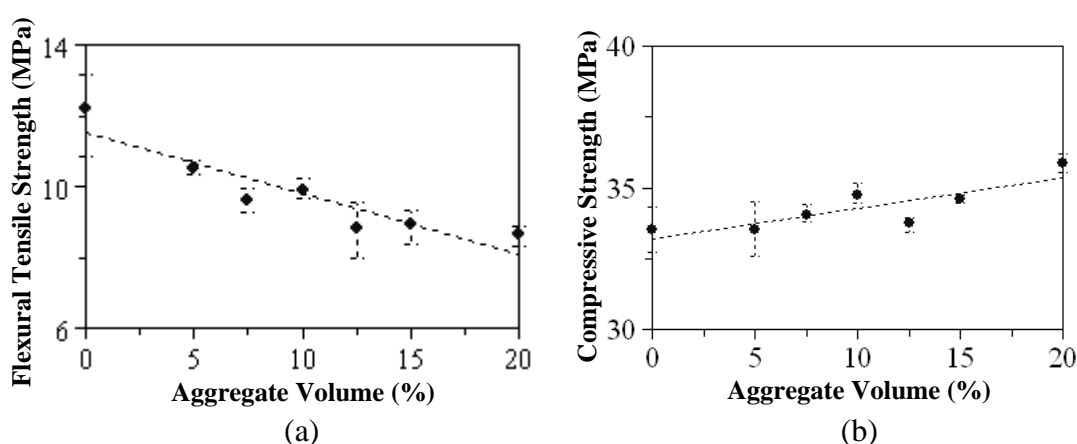


Figure 3: Results of bending and compression tests

3. EXPERIMENTAL RESULTS

Test history in terms of applied load versus midspan deflection of the control and main plates are shown in Figures 4 and 5, while Figure 6 shows the normalized plate load capacity and ductility experiencing principal stress rotation to the corresponding control plates experiencing no principal stress rotation for different aggregate volume fractions.

From Figures 4 and 6, it is clear that the addition of coarse aggregate always resulted in lower plate ductility. The ductility of control plates with coarse aggregate was of approximately one half of the plates made of the original mixture (no coarse aggregate) and appeared to vary more greatly, ranging from approximately 5 mm to 10 mm. There was no clear tendency how the plate ductility changed with increasing aggregate volume fractions. This reduced plate ductility was consistently observed when principal stress direction did not change. On the other hand, when rotation of principal stress occurred (see Figures 5 and 6), ductility of plates with no aggregates decreased by approximately 20%, while plates with aggregate exhibit comparable ductility values to the corresponding plates subjected to no stress rotation.

Regarding the plate load capacity, it is observed that the addition of coarse aggregate also always resulted in lower plate strength. As can be clearly seen in Fig. 6, the reduction in strength was approximately 20% to 40%. The reduction appears to increase as aggregate volume fraction also increases. These all phenomena occurred when no principal stress rotation took place. If rotation of principal stress direction occurred (such as in the main plates), the load capacity was within 80% to 125% of the corresponding control plates, indicating that the presence of coarse aggregate has a positive effect under such loading conditions. Figures 4 and 6(a) explain better this observed phenomenon.

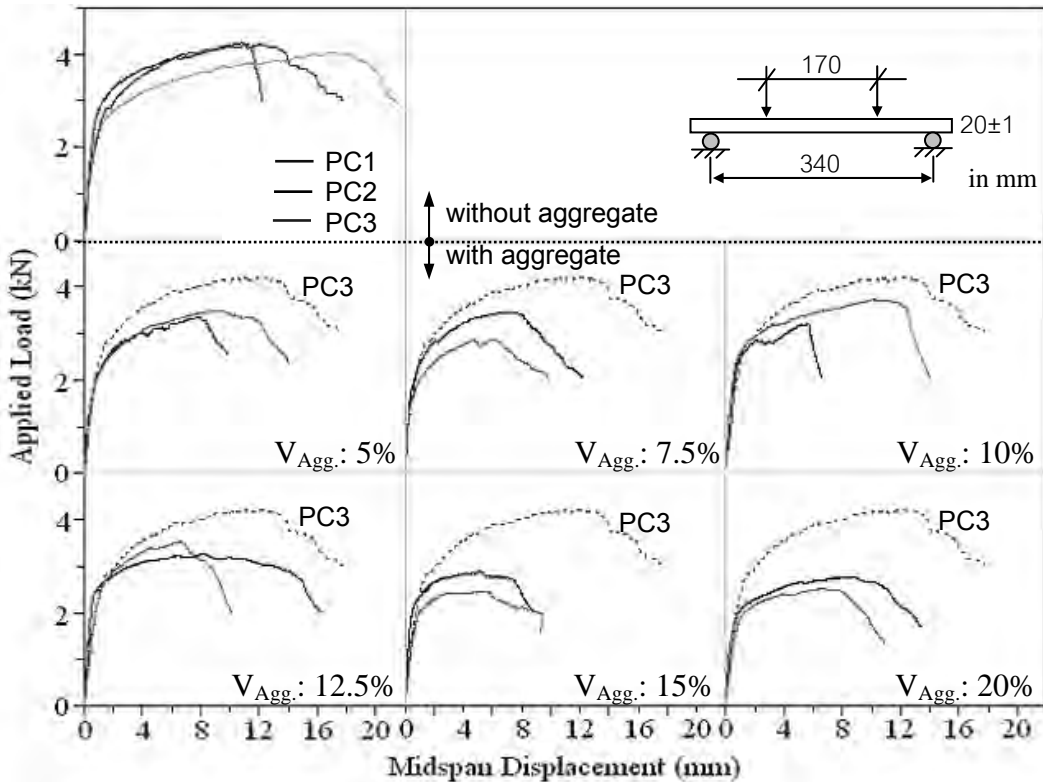


Figure 4: Response of control plates containing various amounts of coarse aggregate subjected to a fixed direction of principal stress field

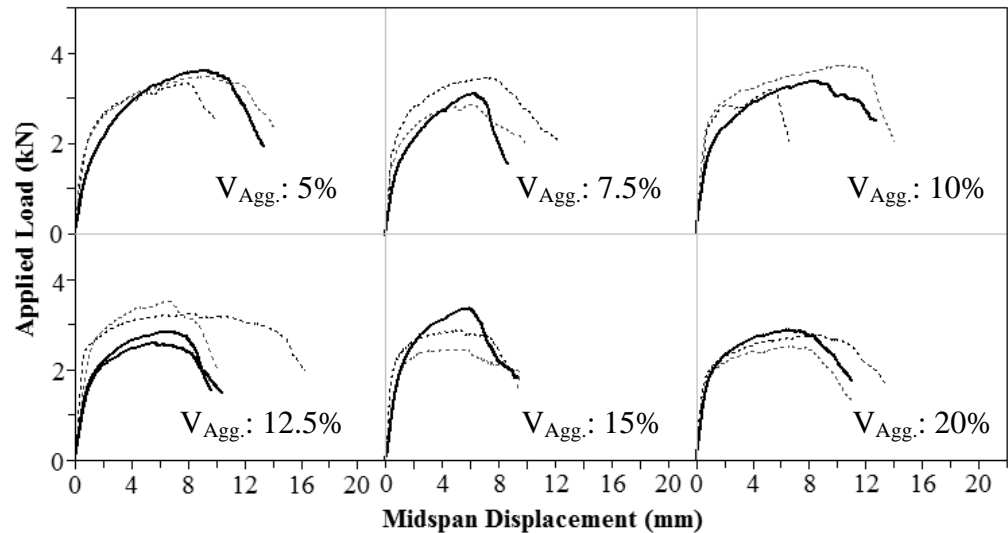


Figure 5: Comparison of responses of control plates (no stress rotation) and main plates (principal stress rotated) for PVA-ECC plates containing coarse aggregate

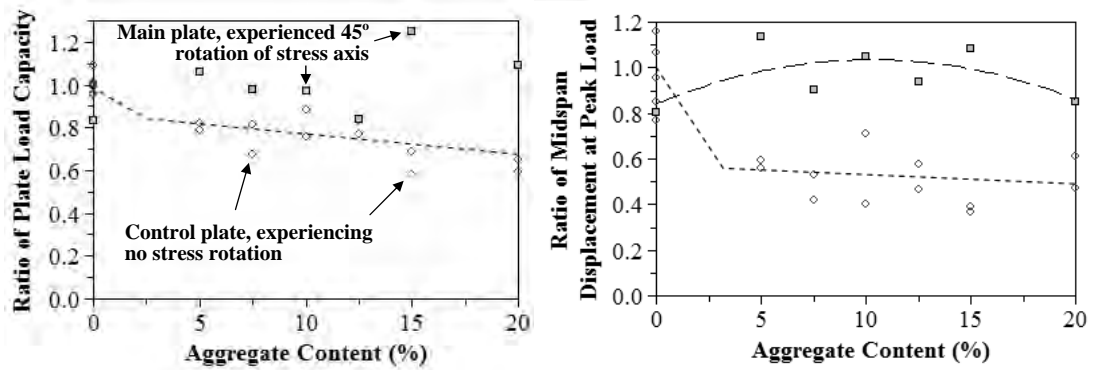


Figure 6: Normalized plate load capacity and ductility for plates with different volume fractions of coarse aggregate

Figure 7 shows the comparison of the observed cracking pattern of selected main plates. The cracking pattern shown was obtained from the 170-mm long bottom plate surface after testing. In all plates tested, a bi-directional cracking pattern was observed, consisting pre- and secondary cracks. The pre-cracks formed orthogonal to principal stress direction during pre-cracking, while the secondary cracks formed between Plane NP (orthogonal to the pre-cracks) and Plane P (orthogonal to principal stress direction during re-testing). Ideally, secondary cracks would form parallel to Plane P when the pre-cracks can transmit sufficient stresses across their planes and undergo limited crack opening and slip.

It appears from Figure 7 that the orientation of the secondary cracks can be related with the added amount of coarse aggregate. As the aggregate volume fraction increases, the inclination of the secondary cracks gradually changes from near orthogonal to the pre-crack plane (Plane NP) at aggregate volume fraction of 0% to the near ideal orientation (Plane P) at aggregate volume fractions of approximately 10% to 12.5%. This indicates the positive contribution of coarse aggregate to improve the resistance of crack

to transmit stresses across their planes. With increasing aggregate volume fractions, however, the orientation of secondary cracks gradually returns back again to Plane NP. This means that further improvement of stress transfer cannot be expected solely by more aggregate amounts, provided that sufficient tensile stress resistance must also exist across cracks.

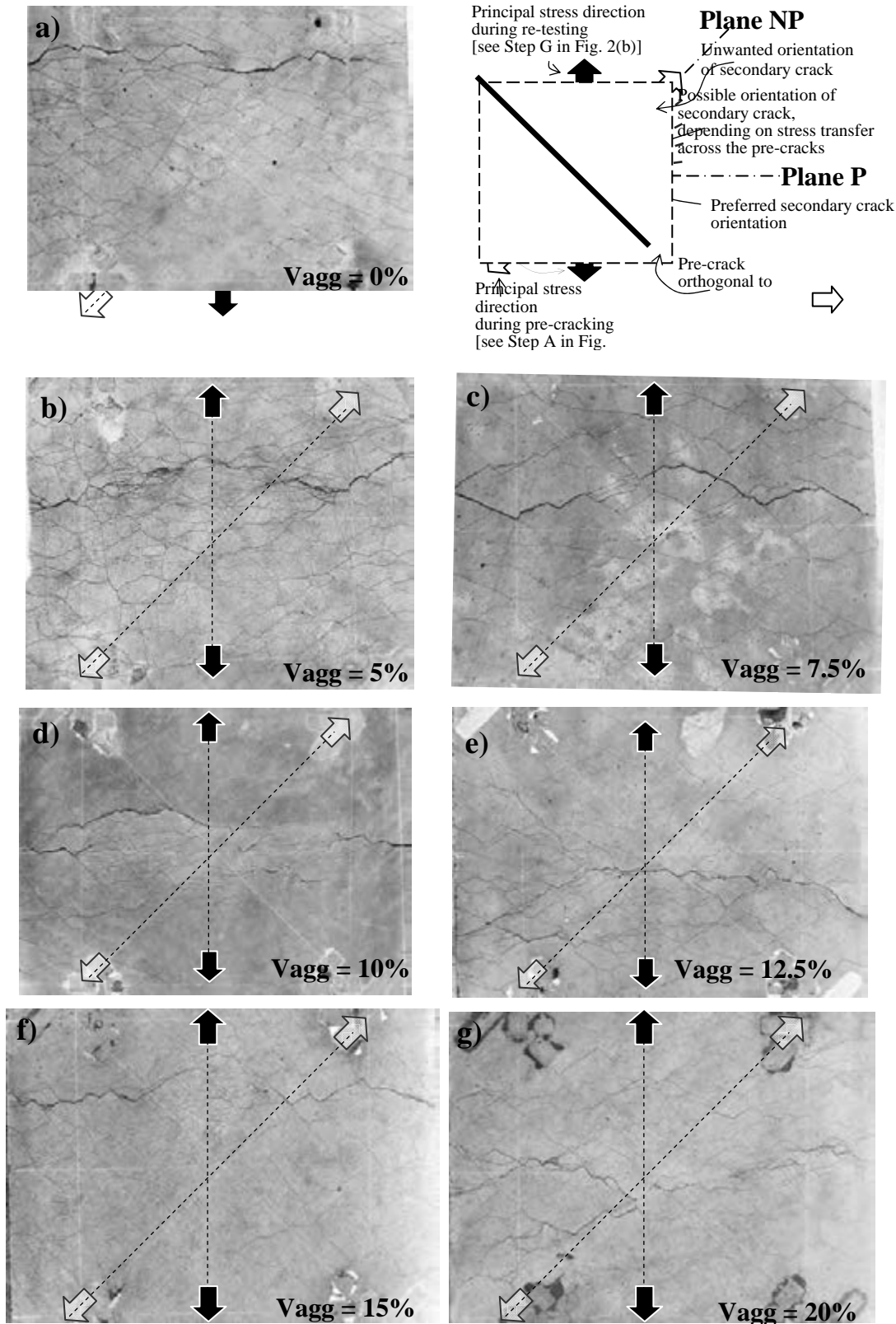


Figure 7: Cracking pattern of test plates

4. CONCLUSIONS

1. Cracked PVA-ECC exhibits degraded performance when subjected to a rotation of stress field as a result of shear that must develop at cracks in the ECC. The material exhibited limited shear transfer, as marked by a nearly orthogonal cracking pattern.
2. When there was no rotation of principal stress field, the addition of coarse aggregate always resulted in lower plate load capacity and ductility. When subjected to stress rotation, however, the aggregate addition resulted in comparable plate strength and ductility, indicating that the stabilizing effects of the aggregate on the post-cracking performance of the material.
3. The addition of coarse aggregate in the volume fraction of 10% to 12.5% is more viable to control the orientation of secondary cracks for following the latest principal tensile stress direction.

REFERENCES

- Fujiyama, C., Gebreyouhannes, E., Chijiwa, N., and Maekawa, K., 2007. Numerical analysis of various factors on fatigue life for slab under moving load. *Proceedings of the Japan Concrete Institute* 29(3), 727-732. (in Japanese)
- JSCE, 2007. *Recommendations for design and construction of HPFRCC with multiple fine cracks*. Concrete Library 127, 129-135. (in Japanese)
- Maekawa, K., Gebreyouhannes, E., Mishima, T., and An, X., 2006. Three-Dimensional Fatigue Simulation of RC Slabs under Traveling Wheel-Type Loads. *Journal of Advanced Concrete Technology* 4(3), 445-457.
- Maeda, Y., and Matsui, S., 1984. Fatigue of reinforced concrete slabs under trucking wheel load. *Proceeding of Japan Concrete Institute* 6, 221-224.
- Perdikaris, P. C., and Beim, S. R., 1988. RC bridge decks under pulsating and moving load. *Journal of Structural Engineering ASCE* 114(3), 591-607.
- Suryanto, B., Nagai, K., and Maekawa, K., 2010. Bidirectional multiple cracking tests on High Performance Cementitious Composite plates. *ACI Materials Journal* 107(5), 450-460.
- JSCE, 2007. *Recommendations for design and construction of HPFRCC with multiple fine cracks*. Concrete Library 127, 129-135. (in Japanese)

Effect of bottom ash and mineral admixtures on the curing sensitivity of concrete

**Kinaanath Hussain¹, Pongsak Choktaweekarn², Warangkana Saengsoy²
Somnuk Tangtermsirikul³**

¹Graduate student, School of Civil Engineering Technology, Sirindhorn International Institute of Technology, Thammasat University, Thailand

²Researcher, Construction and Maintenance Technology Research Center (CONTEC), Sirindhorn International Institute of Technology (SIIT), Thammasat University, Thailand

³Professor, School of Civil Engineering Technology, Sirindhorn International Institute of Technology (SIIT), Thammasat University, Thailand
Tel. 02-986-9009 ext 3002, Fax 02-986-9009 ext 3001, E-mail: kinaanath@gmail.com

ABSTRACT

In this paper, curing sensitivity of concrete with bottom ash and multiple binders was studied. Bottom ash was used as an internal curing agent and a partial substitution of fine aggregate. Curing sensitivity index was calculated by considering compressive strength as an indicator. Two series of concrete with water to binder ratios by weight (w/b) of 0.35 and 0.55 were produced for testing compressive strength. The specimens were subjected to two curing conditions which are continuously water-cured and continuously air-cured. The curing sensitivity of multiple binder concrete with fly ash and limestone powder (LP) as cement replacing materials, and with bottom ash as sand replacement was investigated. It was found that for the mixes without bottom ash, the use of fly ash increased curing sensitivity while LP reduced curing sensitivity of concrete. It was also found that the use of bottom ash in concrete reduced the curing sensitivity especially at low w/b ratio. Autogenous shrinkage, total shrinkage and crack width of cement-only and cement-limestone powder concrete without bottom ash and cement-only concrete with bottom ash were also investigated. It was found that bottom ash and LP mixtures reduced shrinkage of concrete. It was also found that bottom ash and LP mixtures reduced crack width of concrete. From the test results of compressive strength, curing sensitivity and shrinkage, bottom ash was proved to be one of the effective internal curing agents.

Key words: internal curing, bottom ash, fly ash, limestone powder, shrinkage

1. INTRODUCTION

In many cities, the development of durable infrastructure system is of great importance. Concrete is widely used in the construction of concrete structures. One of the important problems of concrete is curing. Appropriate curing gives good

strength development, low shrinkage, no crack and longer service life with a more durable structure.

In current practice, effective curing of concrete is a difficult task especially in a hot country like Thailand. Due to inefficient curing, concrete has low strength development and durability problems. Aitcin et al. (1997) found 17–22% reduction in compressive strengths of air-cured concrete when compared to the moist-cured one. Although engineers know the benefits of good curing, however, good curing practices are not always implemented. For structures having large exposed surfaces or mass concrete and for high elevation vertical concrete walls, curing process is a tremendous task. With poor curing conditions, the problems caused on mechanical and durability properties especially for shrinkage of concrete cannot be avoided. Recently, water-retaining materials or specific porous materials such as polymer and lightweight aggregate have been studied for being used in concrete for internal curing purpose. Internal curing is the curing of concrete from inside with the help of an internal curing agent. The water retained in these materials provides supplementary water in addition to the originally mixing water for the hydration reaction process. The extra water is gradually consumed in the hydration reaction so that it prolongs the hydration reaction progress and reduces shrinkage. It was reported that internal curing helped in avoiding internal micro cracking which might occur in low w/b concrete due to autogenous shrinkage (Lura et al. 2007).

Bottom ash is a porous material (see Figure 1) which has high water retainability so it is possible to be used in concrete as an internal curing material and has high potential in real practice.

Bottom ash is a waste material from coal power plants. A large amount of the produced bottom ash is dumped or used as a land-fill material. These practices cause some expense for disposing and may cause some environmental problems. As a result, a beneficial way in points of view of economic and environment is to utilize the bottom ash in concrete. Some previous researches have shown improvement on compressive strength with bottom ash replacement up to 10% of fine aggregate (Kasemchaisiri and Tangtermsirikul, 2007; Kuram and Kaya, 2008; Kasemchaisiri and Tangtermsirikul, 2008).

Concrete containing cement replacing materials such as fly ash and limestone powder is popular since the ready-mixed concrete producers can reduce the cost of the concrete, reduce environmental problem and enhance some performances of the concrete at the same time. These mineral admixtures require different curing periods. So to know the curing sensitivity of these mineral admixtures is of great interest. To respond to the problem of curing, it is useful to develop a concrete which is less sensitive to curing. Internal curing method and the use of multiple binders are some possible ways to develop a minimum curing concrete.

In this research, the curing sensitivity of concrete with multiple binders and with internal curing process by using bottom ash as an internal curing agent was studied.

2. EXPERIMENTAL PROGRAM

2.1 Materials

Ordinary Portland cement (OPC), fly ash and limestone powder (LP) were used as cementitious materials. The chemical compositions of the cement, fly ash and limestone powder are shown in Tables 1. The mean particle size of the LP used in

the test was 5 micron. The specific gravity of the cement, fly ash and LP are 3.15, 2.29 and 2.7, respectively. Natural river sand and crushed limestone were used as fine and coarse aggregates, respectively. The mix proportions of the tested concrete mixtures are shown in Table 3. In this research, mixtures were designed at two w/b; 0.35 and 0.55. Bottom ash passing ASTM sieve no. 4 was used to partially replace fine aggregate. The water retainability of bottom ash was determined according to the test method proposed by Kasemchaisiri and Tangtermsirikul (2006).

Table 1: Chemical composition of cement, fly ash and LP

Chemical composition	Cement	Fly ash	Limestone powder
SiO ₂ (%)	19.87	36.29	0.42
Al ₂ O ₃ (%)	4.87	21.26	0.11
Fe ₂ O ₃ (%)	3.55	13.77	0.08
CaO (%)	65.03	17.50	55.23
MgO (%)	0.73	2.89	0.48
SO ₃ (%)	2.52	3.67	0.01
Na ₂ O (%)	0.02	1.40	0.01
K ₂ O (%)	0.45	2.10	0.01
LOI (%)	2.26	0.09	44.16

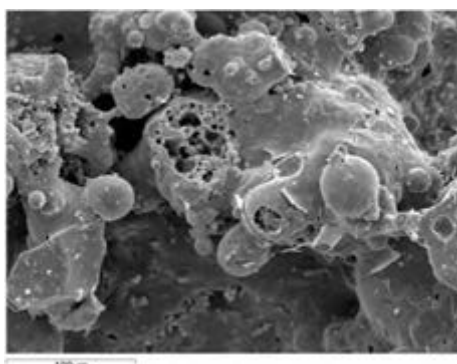


Figure 1: SEM micro graph of bottom ash

2.3 Method

2.3.1 Compressive strength

Mixtures were designed at two w/b ratios; 0.35 and 0.55. Natural river sand was partially replaced by bottom ash (BA) at 10% and 30% by volume. Details of all mix proportions are shown in Table 2. Cube specimens with size 100 × 100 × 100 mm were cast for the compressive strength tests. All mixes were exposed to two different curing conditions which are water-cured (WC) and air-cured (AC) until testing. Strength tests were carried out at the ages of 28 and 91 days. All air-cured specimens were kept in the room with temperature and RH of 28 ± 1°C and 68 ± 2%, respectively. To obtain one data, three specimens were tested for their average.

2.3.2 Autogenous and total shrinkage

For the autogenous and total shrinkage of concrete, the successful mixtures that showed outstanding performance in reducing curing sensitivity on compressive strength of concrete were selected. Two mixtures; BA10% (w35f0LP0BA10) and

LP10% (w35f0LP10BA0) were selected to compare with their respective control mixture (w35f0LP0BA0). Prism specimens of size 75x75x285mm were cast for shrinkage test. Mixtures were designed at w/b ratio of 0.35. Autogenous shrinkage specimens were wrapped with plastic and aluminum foil sheets to prevent moisture loss from the concrete.

Free shrinkage and restrained shrinkage tests were evaluated for the total shrinkage specimens. Two curing conditions were applied to the total shrinkage specimens; 7-days water-cured and air-cured. Crack widths were measured with a digital microscope in three areas of the restrained shrinkage specimens. All shrinkage specimens were kept in a controlled room temperature and RH of 23 ± 0.5 °C and $65 \pm 5\%$, respectively. Details of the mixture proportions are shown in Table 2.

Table 2: Mix proportions of the tested concrete.

Mixing code	Ingredients (kg/m ³)						
	c	f	LP	w	g	s	BA
w35f0LP0BA0	474	0	0	166	1055	737	0
w35f30LP0BA0	315	135	0	157	1055	737	0
w35f0LP10BA0	423	0	47	164	1055	737	0
w35f0LP0BA10	474	0	0	166	1055	663	58
w35f0LP0BA30	474	0	0	166	1055	516	174
w35f0LP10BA10	423	0	47	163	1055	663	58
w35f0LP10BA30	423	0	47	160	1055	516	174
w35f30LP0BA10	315	135	0	156	1055	663	58
w35f30LP0BA30	315	135	0	153	1055	516	174
w55f0LP0BA0	365	0	0	201	1055	737	0
w55f30LP0BA0	245	105	0	193	1055	737	0
w55f0LP10BA0	326	0	36	199	1055	737	0
w55f0LP0BA10	365	0	0	201	1055	663	58
w55f0LP0BA30	365	0	0	201	1055	516	174
w55f0LP10BA10	326	0	36	199	1055	663	58
w55f0LP10BA30	326	0	36	199	1055	516	174
w55f30LP0BA10	245	105	0	193	1055	663	58
w55f30LP0BA30	245	105	0	193	1055	516	174

Remarks: c: cement, f: fly ash, LP: limestone powder, w: water, s: fine aggregate, BA: bottom ash and g: coarse aggregate

3. RESULTS AND DISCUSSIONS

3.1 Compressive strength

The results of 28-day and 91-day compressive strengths of water-cured and air-cured concretes with w/b 0.35 and 0.55 are shown in Figures 2 and 3, respectively. As expected, air-cured concrete showed comparatively low strength when compared to water-cured concrete. When compared among the mixtures without BA, in case of water-cured specimens, at the age of 28 days, the highest compressive strength for w/b= 0.35 was given by w35f0LP0BA0 at 76 MPa, while w35f30LP0BA0 and w35f0LP10BA0 had compressive strength of 68 MPa and 74 MPa, respectively.

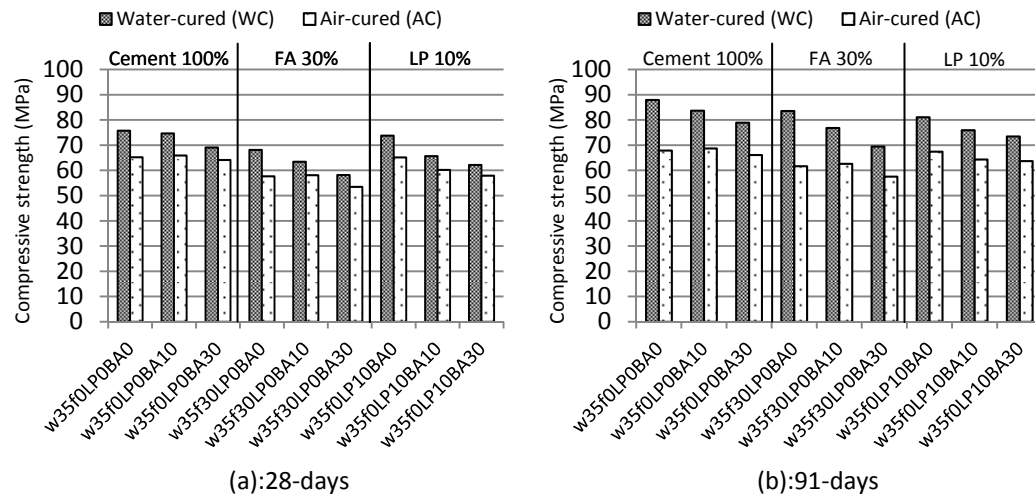


Figure 2: Compressive strength of water-cured and air-cured concrete with $w/b=0.35$.

For 91-day compressive strength, the highest compressive strength was observed with w35f0LP0BA0 at 88 MPa while w35f30LP0BA0 and w35f0LP10BA0 showed the values of 84 MPa and 81 MPa, respectively.

Interesting results are observed when air-cured concretes are analyzed. For 28-day compressive strength, w35f30LP0BA0, w35f0LP10BA0, showed the values of 58 MPa and 65 MPa, respectively, while w35f0LP0BA0 showed 65 MPa. With no proper curing the compressive strength of concrete with LP was the same as that of the control concrete at 28 days. For 91-day compressive strength of air-cured concretes, w35f30LP0BA0 and w35f0LP10BA0 showed the values of 62 MPa and 67 MPa, respectively, while w35f0LP0BA0 showed 68 MPa.

For water-cured specimens (see Figure 2) with $w/b=0.35$, it was found that the increase in BA content resulted in the reduction of compressive strength when compared to the mix without BA for all types of binder combination. The same tendency was also found in the case of $w/b = 0.55$.

For air-cured concrete with $w/b=0.35$, cement-only concrete with BA 10%, (w35f0LP0BA10), had compressive strength improvement of 1.1% and 1.3% at 28 days and 91 days when compared to the mixture without BA (w35f0LP0BA0). The mix with 10% BA and fly ash 30% (w35f30LP0BA10) showed 0.8% and 1.6% increase in compressive strength for 28 days and 91 days as compared to fly ash mix without BA (w35f30LP0BA0). For air-cured concrete specimens with $w/b=0.55$, the cement-only concrete with 10% BA (w55f0LP0BA10) had compressive strength of 35 MPa and 38 MPa at 28 days and 91 days, respectively, which are 2.8% and 1.83% below its respective control mix w55f0LP0BA0.

Fly ash improves long term strength with good curing condition. However, even for poor curing condition, when BA is present, fly ash can still improve long term strength because BA can supply the additional water required for the hydration and pozzolanic reaction with water.

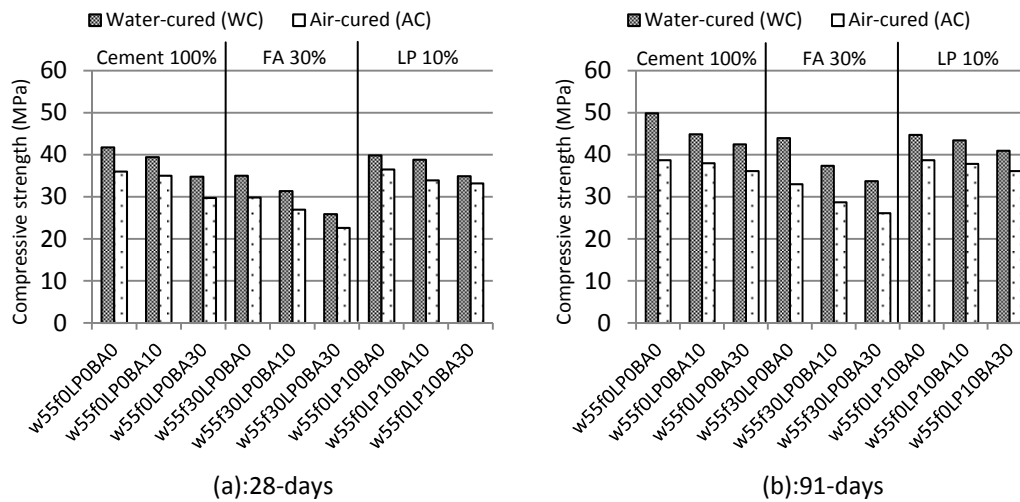


Figure 3: Compressive strength of water-cured and air-cured concrete with w/b 0.55.

So, in air-cured condition, the cement-only concrete with BA had almost the same compressive strength as the mix without BA, (see Figure 3). For binary binder mixtures, compressive strength continuously dropped with the increase in BA content. It can be concluded here that BA is more effective in low w/b concrete. This is because at high w/b, there is more water inside the concrete for hydration. The effect of internal curing is therefore not obvious.

In contrast, due to the low w/b, there is not enough water inside the concrete for hydration reaction, so internal curing becomes more effective. At low w/b, concrete is dense and external curing water cannot penetrate into the inner portion of concrete, so external curing is not effective. By adding BA, the additional internal curing is provided. As the relative humidity inside the concrete drops, BA releases water for subsequent hydration.

The similar behavior was also presented by other researches with other internal curing agents such as lightweight aggregate, super absorbent polymers, porous ceramic waste, etc (Cusson and Hooegeveen, 2008; Zhutovsky et al. 2004)

3.2 Curing sensitivity

The curing sensitivity of concrete on compressive strength was evaluated by using the curing sensitivity index (CSI_{f_c}) which is the percentage difference between compressive strength of concrete that is continuously water-cured and that of the continuously air-cured concrete as shown in Eq. (1). The higher curing sensitivity index means that the concrete is more sensitive to curing.

$$CSI_{f_c} = \left(\frac{f_c(WC) - f_c(AC)}{f_c(WC)} \right) \times 100 \quad (1)$$

where CSI_{f_c} is curing sensitivity index for compressive strength (%). $f_c(WC)$ and $f_c(AC)$ are compressive strength of water-cured and air-cured specimens, respectively (MPa).

Curing sensitivities of concrete with $w/b = 0.35$ and 0.55 are shown in Figure 4. For $w/b=0.35$, the mixtures having 30% fly ash replacement (w35f30LP10BA0) had the maximum CSI_{fc} . Concrete with 10% limestone powder replacement (w35f0LP10BA0) had the lowest curing sensitivity.

For both $w/b= 0.35$ and 0.55 , it was found that the use of BA reduced the CSI_{fc} of concrete significantly when compared to the mix without BA. LP accelerates the hydration of cement especially at early age (Bonavetti et al. 2000). As a result, a large portion of cement has reacted at early age and therefore, reduces CSI_{fc} of the concrete. The pozzolanic reaction of fly ash starts at later age, thus it requires a longer curing period. Another reason is that the rate of evaporation of fly ash concrete is higher than cement-only concrete (Tongaroonsri, 2009), so early water loss by evaporation in air-cured fly ash concrete results in less water inside the concrete for pozzolanic reaction. These make fly ash concrete more sensitive to curing.

Bottom ash reduces CSI_{fc} by its internal curing ability. In the air-cured condition BA supplies the additional water required for hydration making the concrete less sensitive to curing.

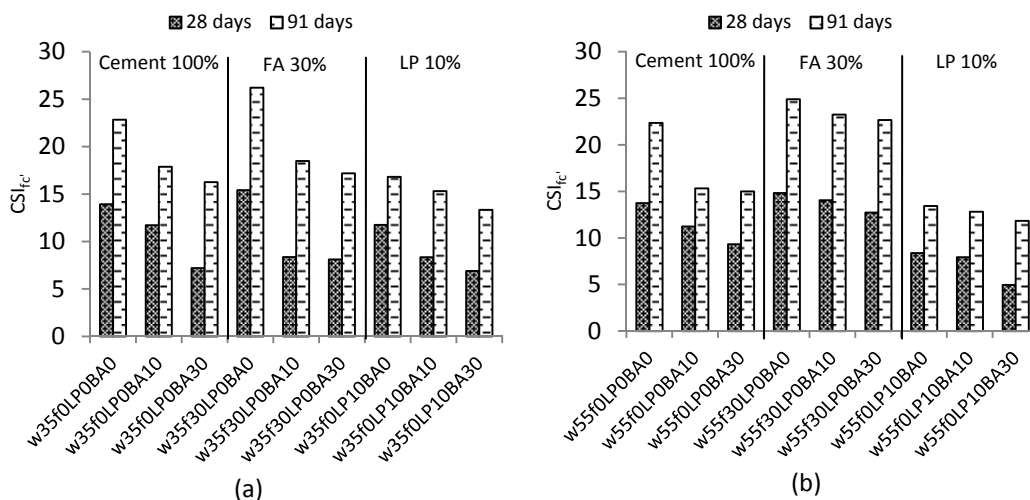


Figure 4: Curing sensitivity index (a): $w/b=0.35$ and (b): $w/b=0.55$.

3.3 Autogenous shrinkage

The autogenous shrinkage of mixtures with 10% replacement of limestone powder in binder and 10% bottom ash replacement in sand is shown in Figure 5. The mixture with 10% replacement of limestone powder had the least autogenous shrinkage among the three mixtures. Bottom ash reduced the autogenous shrinkage of concrete when compared to the mixture without bottom ash.

This phenomenon is similar to other types of internal curing materials (Lura et al. 2007; Cusson and Hoogeveen, 2008; Zhutovsky et al. 2004). Thus, it proves that BA can be used as an effective internal curing agent to reduce autogenous shrinkage.

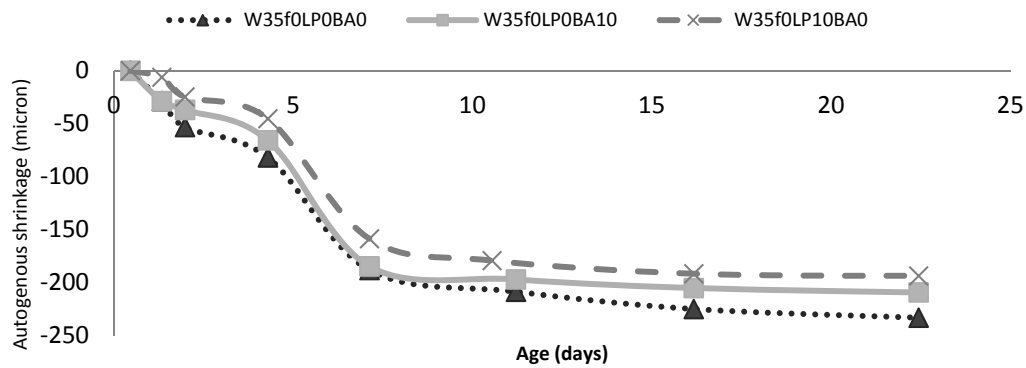


Figure 5: Autogenous shrinkage of concrete mixtures with LP and BA.

3.4 Total shrinkage

The results of total shrinkage for air-cured and 7-day water –cured conditions are shown in Figure 6, respectively. Bottom ash was effective in reducing total shrinkage for both water-cured and air-cured conditions. For the water-cured condition, bottom ash mixture had similar shrinkage values with that of the mixtures with limestone powder replacement. Mixtures that were water-cured for 7 days had significant reduction in total shrinkage as compared to the air-cured one. When the concrete is in water, there is no loss of moisture. In fact there is moisture gain which swells the concrete and no total shrinkage inside the concrete. For the air-cured condition, similar tendency as the autogenous shrinkage of concrete was observed. Concrete with limestone powder replacement had the least shrinkage and mixture with bottom ash reduced total shrinkage as compared to the cement-only mixture without bottom ash. In this study, although bottom ash replacement reduced total shrinkage, higher replacement of bottom ash would increase the total shrinkage due to the increased porosity and then increased amount of water evaporation from the concrete. However, adequate amount of bottom ash replacement can maintain the same level of total shrinkage or reduce the total shrinkage a little as compared to the control mixture.

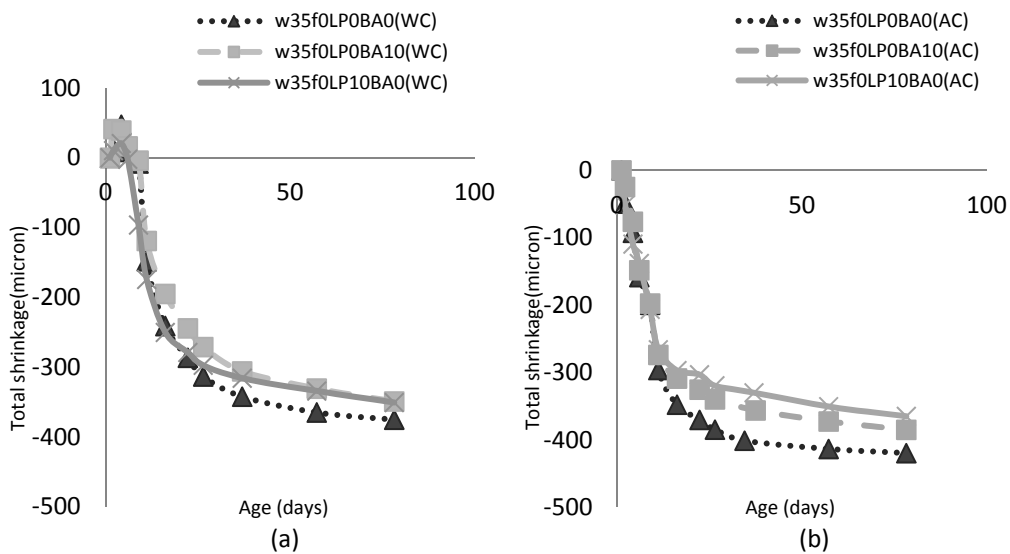


Figure 6: Total shrinkage of (a) 7 days water-cured and (b) air-cured concrete mixtures with LP and BA.

3.5 Crack width of concrete

The long term crack widths of concrete mixtures for water-cured and air-cured conditions are shown in Figure 7, respectively. In the air-cured condition, cement-only mixture had the largest crack widths and 10% limestone powder mixture had the smallest crack widths. The 10% bottom ash mixture had crack widths in-between the cement-only mixture and 10% limestone powder mixture. For the water-cured condition, bottom ash 10% had the smallest crack width. The reason for bottom ash mixtures to give such small crack widths were due to its porous nature and shrinkage reduction. With higher porosity, the concrete have lower internal stresses in the restrained shrinkage test specimen. As a result cracks occur slower with smaller crack widths. The similar explanation was mentioned in a previous research, Topçu and Bilir, (2010).

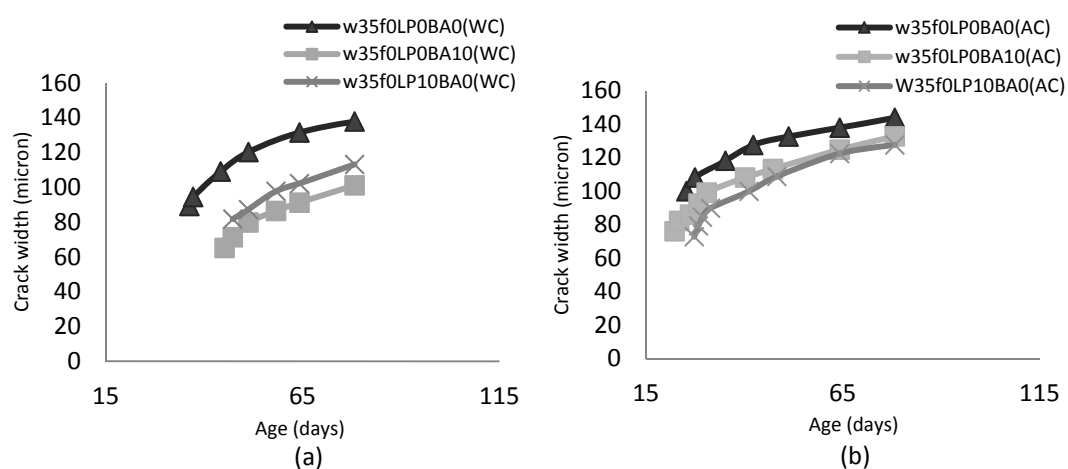


Figure 7: Crack width of concrete with (a) water-cured and (b) air-cured conditions

4. CONCLUSIONS

Based on the test results, the following conclusions are obtained.

1. For water-cured specimens, compressive strength of the mixes with BA were lower than the mixes without BA. However, for air-cured specimens, BA improved the compressive strength slightly for cement-only concrete and fly ash concrete at $w/b = 0.35$.
2. The use of 10% limestone powder reduced the curing sensitivity of the concrete.
3. Bottom ash reduced curing sensitivity of concrete significantly, especially at low w/b .
4. The use of 10% limestone powder in the binder together with 30% bottom ash in the fine aggregate was the most effective in reducing curing sensitivity.
5. The use of limestone powder and bottom ash reduced the crack width of concrete.
6. The use of limestone powder and bottom ash was effective in reducing autogenous and total shrinkage of concrete.
7. From results of compressive strength, curing sensitivity, shrinkage and crack width measurements, it was proved that BA could be used as an internal curing material.
8. From this study, it was found that limestone powder and bottom ash are useful materials for sloving the problem of curing and to develop a minimum curing concrete.

Acknowledgements

The authors wish to express their gratitude to BLCP power limited and Metal and Material Technology Center (MTEC), The National Science and Technology Development Agency (NSTDA), and Thailand's National Research universities, office of the higher Education commission, for their financial support and valuable assistance in carrying out this research

REFERENCE

- Aitcin, P.C., Neville, A.M., and Acker, P., 1997. Integrated View of Shrinkage Deformation, *Concrete International* 19: 35-41.
- Bonavetti, V., Donza, H., Rahhal V., and Irassar, E., 2000. Influence of initial curing on the properties of concrete containing limestone blended cement, *Cement and Concrete Research* 30: 703-708.
- Cusson, D., and Hoogeveen, T., 2008. Internal Curing of High-Performance Concrete with Pre-soaked Fine Lightweight Aggregate for Prevention of Autogenous Shrinkage Cracking. *Cement and Concrete Research* 38: 757-765
- Kasemchaisiri, R., and Tangtermsirikul, S., 2007. A Method to Determine Water Retainability of Porous Fine Aggregate for Design and Quality Control of Fresh Concrete. *Construction and Building Materials* 21: 1322-1334.
- Kasemchaisiri, R., and Tangtermsirikul, S., 2008. Properties of Self-Compacting Concrete in Incorporating Bottom Ash as a Partial Replacement of Fine Aggregate. *Science Asia* 34: 087-095.
- Lura, P., Jensen, O.M., and Igarashi, S.I., 2007. Experimental Observation of Internal Water Curing of Concrete. *Materials and Structures* 40: 211-220.
- Tongaroonsri, S., 2009. *Prediction of Autogenous Shrinkage, Drying Shrinkage and Shrinkage Cracking in Concrete*, PhD Thesis, Sirindhorn International Institute of Technology and Faculty of Engineering, Thammasat University, Thailand.
- Topçu, I.B., and Bilir, T., 2010. Effect of Bottom Ash as Fine Aggregate on Shrinkage Cracking of Mortars. *ACI Materials Journal* 107: 48-56.
- Zhutovsky, S., Kovler, K., and Bentur, A., 2004. Influence of Cement Paste Matrix Properties on the Autogenous Curing of High-Performance Concrete. *Cement & Concrete Composites* 26: 499-507

2nd dosage of superplasticizer and slump recovery of concrete using naphthalene based superplasticizer

Chalermchai WANICHLAMLERT¹ and Somnuk TANGTERMSIRIKUL²

¹Researcher, Construction and Maintenance Technology Research Center,
Sirindhorn International Institute of Technology,
Thammasat University, Thailand
chalermchai_w@siit.tu.ac.th

²Professor, School of Civil Engineering and Technology,
Sirindhorn International Institute of Technology,
Thammasat University, Thailand

ABSTRACT

This research is aimed to be a preliminary study for developing a concrete slump control method using additional superplasticizer (SP). Strength class C25/30 cement-only concrete with initial slumps of 7.5 cm and 10 cm were investigated. Naphthalene based SP is used for both concrete mixing and modifying. Volumetric paste to void ratio was designed at 1.1 and 1.2, while water to cement ratio and 1st SP dosage were fixed at 0.63 and 0.5% respectively. Slump before and after adding various 2nd SP dosages were observed until 2 hours. The relationship between the 2nd SP dosages needed for original slump returning and the slump loss before 2nd SP adding were found out. The setting times and compressive strength were also investigated. The higher the total SP dosage used, the longer the setting times were. With 2nd SP addition, the compressive strength reduced for all ages, while the percentage of strength reduction decreased for the longer age. The strength reduction might occur due to the effect of setting time extension and the existence of water in SP. According to this studied condition, it is recommended to adjust concrete by 2nd SP addition for original slump returning within 90 minutes after mixing.

Keywords: *compressive strength, concrete, setting time, slump, superplasticizer*

1. INTRODUCTION

Recently, ready-mixed concrete is ordered based on its slump and strength class in order to be ensured it has appropriate workability for the construction job and be able to achieve the required load-carrying capacity when it is mature. However, during fresh state the concrete always loses its workability with elapsed time. Therefore, occasionally the concrete batch does not meet the job requirement when it reaches the construction site and is discarded.

As slump loss of concrete mainly depends on the free water content in concrete and the surface of solid particles. After cementitious material come into contact with water in concrete, the free water content gradually reduces as a result of consumption in hydration reaction and evaporation, while the surface of solid particles increases with the hydration reaction [1, 2]. Hence, slump loss increases with elapsed time after mixing as the hydration reaction forming. In hot weather condition, the slump loss becomes more rapid due to increase in both hydration rate and water evaporation.

The relatively hot climate of Thailand coupled with the traffic congestion leading to the lower concrete slump than the requirement of ready-mixed concrete upon reaching delivery point.

There are generally four main methods used for slump control:

- (i) Use of high slump-retaining capability superplasticizers (at plant)
- (ii) Design of concrete mix which has excess slump initially (at plant)
- (iii) Adding of water (on site)
- (iv) Adding of chemical admixtures (on site)

The first 2 methods are needed to be done at concrete plant by using some means to estimate the slump loss behavior and to design the concrete with excessive initial slump. For (i), it might be a costly method due to the cost of superplasticizer (SP) and, however, the target slump may not be achieved at site because there are many uncontrollable factors which the designers would encounter, such as the time taken for concrete delivery or the fluctuation of ambient temperature. Similarly, for (ii), it may not easy to design a concrete mixture based on slump loss behavior to have excessive initial slump and exactly achieve a target slump when arrive the site. Most of the times, this excessive initial slump is achieved by overdosing of SP, because the range of water-cement ratio is already restricted by the required strength class. Sometimes, this lead to segregation of concrete at concrete plant which become more difficult for quality control staff to check whether the batching concrete is as design, mostly found in case of too much excessive slump for high slump class concrete.

The other 2 methods are needed to be done onsite, therefore instead of slump loss estimation the workability check before the mixture modification is necessary. For (iii), it may be an inappropriate practice way as this reduces the concrete strength as changing the mix proportion by increasing the water-cement ratio, which may be fatally harmful to the structure users. Whereas, (iv) the required amount of additional SP in order to return the concrete to its designed slump shall be much smaller than the required additional water in the previous method. This additional SP is still doubted whether it could meaningfully affect on the mechanical properties of concrete such as strength or not. The method to decide how much the additional SP or 2nd SP shall be used when concrete arrive the site is necessary.

Moreover, the behavior of concrete after re-dosing of SP needs to be investigated in order to clarify that the proposed method to control slump

loss does not have unacceptable adverse effect on concrete properties. The setting time of concrete after SP re-dosing has to be checked to ensure that there won't be excessive retarding effect on setting time. Compressive strength development of concrete was also investigated to ensure that the re-dosing of superplasticizer does not harmfully decrease the compressive strength of concrete.

2. METHODOLOGY

2.1 Materials

2.1.1 Cement

Ordinary Portland Cement Type 1, conforming to TIS 15 Part 1-2547, was used. Chemical compositions and physical properties of cement are shown in Tables 1.

Table 1: Chemical compositions and physical properties of cement

Chemical compositions (%)	
SiO ₂	20.29
Al ₂ O ₃	5.02
Fe ₂ O ₃	3.22
CaO	65.05
MgO	1.63
SO ₃	2.60
Na ₂ O	0.11
K ₂ O	0.44
Physical properties	
Specific gravity	3.15
Loss on ignition (%)	1.68

2.1.2 Aggregates

An aggregate mixture of natural river sand passing sieve no. 4 and crushed limestone with maximum size of 25mm conformed to ASTM C 33, were used as fine and coarse aggregates respectively.

2.1.2 Chemical admixtures

A type F admixture, naphthalene based superplasticizer (SP), was used for this study as it is economical and widely used in Thailand. A method for determining the water reducing efficiency of admixtures is described in Meyer and Perenchio (1979). The authors adapted the mini-slump technique developed by Kantro at the Portland Cement Association to test water reducing efficiency of admixtures [3].

From test results, the water reducing efficiency of naphthalene based SP used in this research was equal to 22% and 44% at dosage of 0.5% and 1% (sp/c), respectively.

2.2 Mix proportion

Details of concrete mix proportions used in this research are shown in Table 2. Two concrete mixtures designated as SL7.5 and SL10 represent concrete with initial slump of 7.5cm and 10cm respectively.

All concrete mixes were designed as follows: paste content (γ) of 1.1 and 1.2 for SL7.5 and SL10 respectively, water-cement ratio (w/c) of 0.63 and initial SP dosage of 0.5%. The design is based on the ready-mix proportions used in Thailand for strength class of C25/30.

Table 2: Mix proportions

Materials	Mix ID.	
	SL7.5	SL10
Cement [kg]	285	295
Water [kg]	175	185
Sand [kg]	865	865
Gravel [kg]	1095	1060
SP [kg]	1.425	1.475

2.3 Concrete mixing procedure

Concrete mixer used in this research was a drum type mixer which has a maximum volume of 50 liters. Concrete mixing procedure is described as follows:

Firstly, cementitious material, fine and coarse aggregate were weighted and put into mixer and mixed for about 20 seconds. Secondly, weighted water was poured into the mixer and mixed for about 2 minutes. Finally, weighted superplasticizer was put into the mixer and mixed together with aggregates and paste for 2 minutes 40 seconds. The total mixing time was around 5 minutes.

The mixing process and other subsequent tests were conducted in a temperature controlled environment at $28 \pm 2^\circ\text{C}$.

2.4 Slump loss testing procedure

The slump loss is determined by following steps. Firstly, concrete mixtures were measured for the slump values immediately after mixing and defined as initial slump. Then the concrete mixture is kept in a large tray and sealed with a plastic wrap to prevent loss of water due to evaporation. At stipulated time, a sample of the batch is tested for slump to determine slump loss. Slump is tested after the elapsed time of 30, 60, 90 and 120 minutes. Before every test, concrete is remixed for 3 minutes to ensure the homogeneity.

2.5 Re-dosing of superplasticizer procedure

For the SP re-dosing of concrete, the sample is similarly kept in a large tray and sealed with a plastic wrap. At the stipulated time, concrete is put into the mixer, and mixed for 3 minutes. A small sample is then use for test of slump. Meanwhile, concrete in the mixer is re-dosed with the specified amount of SP and mixed for another 3 minutes to ensure homogeneity. A sample is then tested for slump after re-dosing. The rest is then used for further testing for slump loss. In this study, re-dosing of superplasticizer at elapsed time of 30, 60 and 90 minutes were carried out. The amount of 2nd SP dosage used for re-dosing procedure is shown in Table 3.

Table 3: Variation of 2nd SP dosage

Elapsed time (min)	2 nd SP dosage (% by wt. of cement)
30	0.20
	0.40
	0.70
60	0.20
	0.50
	0.80
	1.00
90	0.30
	0.60
	0.90
	1.20

2.6 Setting time of cement and compressive strength development test

The initial and final setting time of cement with various dosages of superplasticizer was determined in accordance with ASTM C 191-08.

10x10x10 cm concrete cube specimens were used for testing of compressive strength development at the age of 1 day, 3 days, 7 days and 14 days. The specimens were sealed with a plastic wrap upon casting and demolded after 1 day. After demolding, they were cured in water at 25°C until the time of testing.

3. TEST RESULTS AND DISCUSSIONS

3.1 Effect of SP dosage on setting time of cement

As seen in Figure1, SPs cause the setting time for cement to increase, and this retarding effect was more pronounced with increase in dosage of SP.

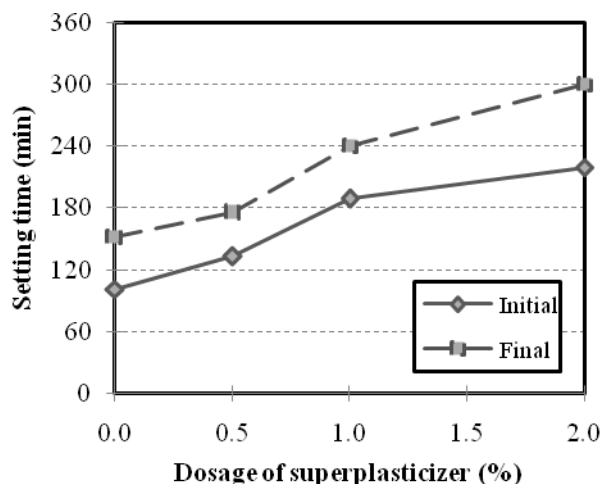


Figure 1: Setting time of cement with various dosages of superplasticizer

3.2 Re-dosing of superplasticizer and effect on slump regained

Upon re-dosing of concrete with SP, the slump of the concrete increased back to a certain percentage of the original slump. Figure 2 shows how slump was regained after re-dosing at various dosages at 60 minutes for SL10. Figure 3 shows the relationship between the percentage of slump regained with increase in 2nd dosage at 30, 60 and 90 minutes for SL10.

Interpolation was carried out to determine the required 2nd dosage in order to regain the original slump value for the two mixes at various times. It was found that the required 2nd dosage for two mixes with different initial slump were very close for their respective time of re-dosing, as shown in Fig 4. This probably suggests that mixes with similar w/c ratio but difference in amount of paste required roughly similar dosage for re-dosing in order to regain the original slump. However, future studies which vary various values of paste content (γ) and study the effect of w/c ratio needs to be carried out in order to confirm this behavior.

Moreover, Figure 4 also shows that the required 2nd dosage increases exponentially with increasing of elapsed time. This is due to the hardening of the cement paste with the elapsed time, hence, requiring a higher dosage of superplasticizer for it to effectively push the now larger and heavier hydration products apart to regain slump. Moreover, the amount of free water has also reduced and there is more friction between the particles.

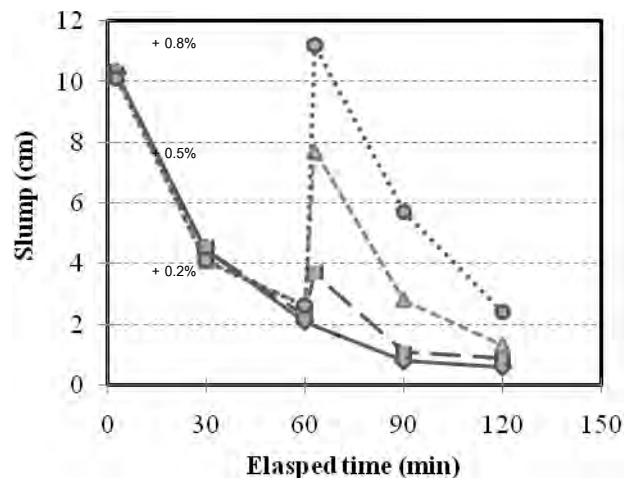


Figure 1: Slump for re-dosing at 60 min for SL10

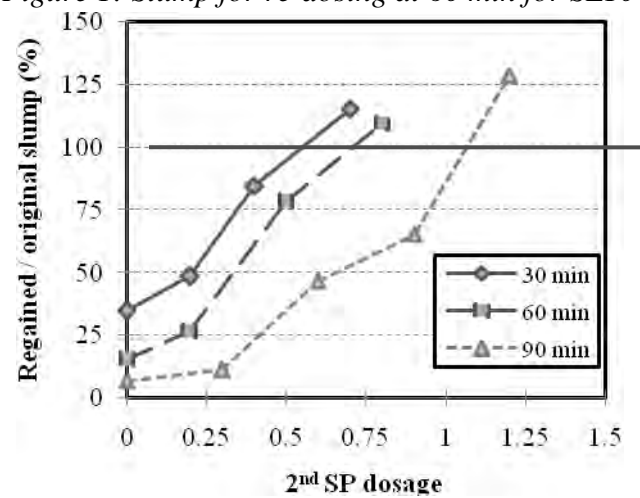


Figure 2: Effect of SP re-dosing on slump regained for SL10

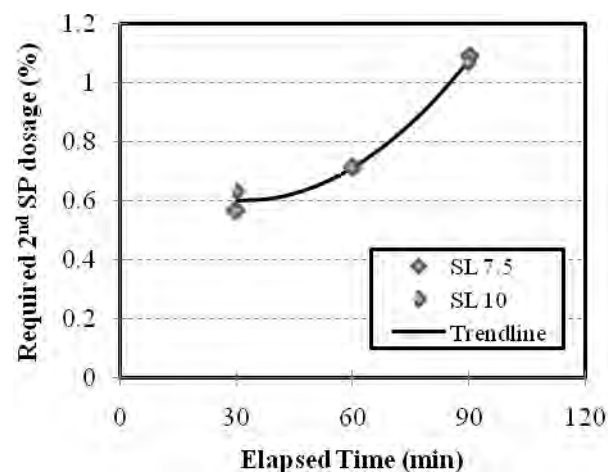


Figure 3: Required 2nd dosage to regain original slump and elapsed time

However, the re-dosing procedure shall not be based on elapsed time after mixing as the slump loss behavior may not be exactly the same due to various uncontrollable factors, such as variation in temperature or

movement when concrete is transported. It is suggested that the re-dosing procedure shall be based on the percentage of slump loss before re-dosing, as shown in Figure 5. From this test result, it shows that after concrete slump loss reaches about 80% of its original slump, the required 2nd SP dosage to regain its original slump increases dramatically.

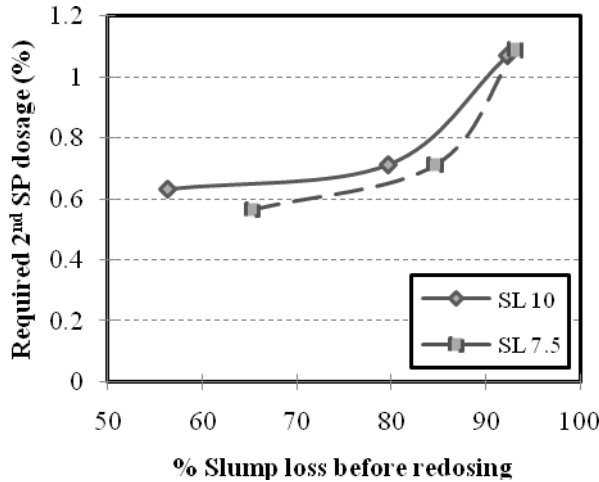


Figure 4: Required 2nd dosage to regain original slump and slump loss percentage before SP re-dosing

3.3 Re-dosing of superplasticizer and effect on compressive strength development of concrete

The simulated compressive strength values from FACOMP are compared to those from the real re-dosing test. By assuming that the 2nd SP dosage becomes the additional water content, then the w/c ratio of the mix in FACOMP is automatically increased.

FACOMP is computer software developed by Sirindhorn International Institute of Technology (SIIT), it is able to make accurate predictions for strength development, and some durability properties of concrete produced from Thai local materials.

As shown in Figure6, the actual strength of concrete reduces with the increasing of 2nd SP dosage for all concrete age. The FACOMP simulated strengths have the same order of strength reduction as those from the real re-dosing test, therefore it could be claimed that the existing water content in 2nd SP dosage leads to the increase in total water content of concrete then resulting as strength reduction. The difference between actual strength and FACOMP simulated strength becomes smaller as the concrete age is longer. This might be explained by the larger difference in early strength results from the retardation effect of SP, the higher the SP dosage is the longer the setting times are.

Moreover, the effect of decrease in strength due to re-dosing of superplasticizer was also found to be less pronounced as the concrete ages, as seen in Figure 7. It is obvious to find that the adjustment of concrete workability on site by using proposed SP re-dosing method could drop the

strength of mature concrete (usually referred to 28 days age concrete) only less than 5%.

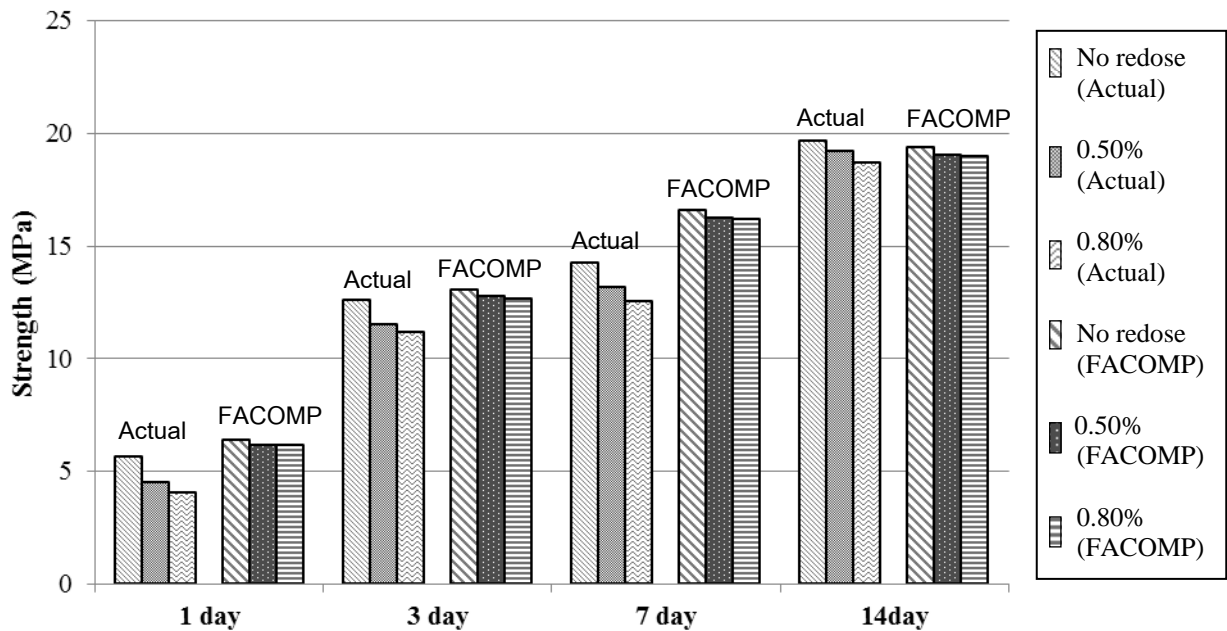


Figure 6: Comparison between FACOMP and actual results for 14-day compressive strength development

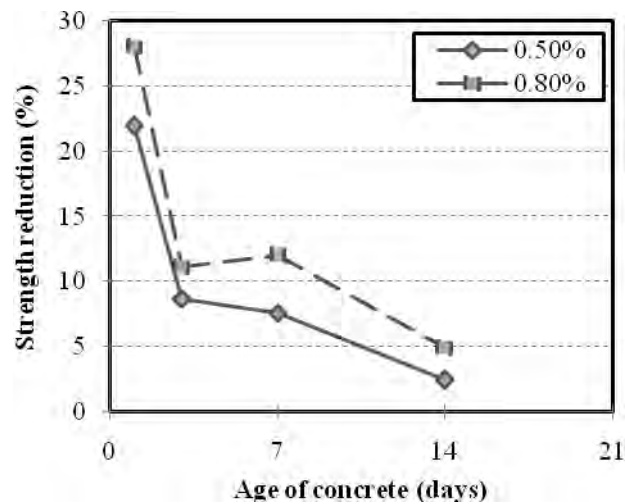


Figure 7: Strength reduction from original concrete for various dosages of 2nd SP

4. CONCLUSIONS

Based on the experimental results, the following conclusions can be drawn.

1. If superplasticizers are to be used for re-dosing to regain original slump at the construction site, one should take note that there would be an increase in the total amount of superplasticizer used, thus, a further increase in both initial and final setting times.

2. For re-dosing of superplasticizer in concrete, the higher the slump loss is, the higher the amount of 2nd dosage to regain the original slump required. The 2nd dosage increases exponentially as there is increase in slump loss, especially after slump loss reaches 80% of original slump.

3. For mixes with the same w/c ratio but different amount of paste, they seem to need the same required 2nd superplasticizer dosage to regain their original slumps regardless of their slump classes.

4. There is a slight decrease in compressive strength when a 2nd dosage is added. This decrease in strength is great in the early age of the concrete and become less pronounced as the concrete ages. The initial great drop in strength was probably due to the retardation effect of superplasticizer on concrete setting time, hence, slowing down initial strength development of concrete.

5. The concrete strength reduction induced by superplasticizer re-doing method decrease with the age of concrete, according to the referenced mixes the strength drop only less than 5% for mature concrete (28 days aged concrete) with strength class of C25/30

Future studies on more types of mix proportions should be studied on the effect of re-dosing, such as variation in w/c ratio, different types of cementitious materials in use, and other parameters affecting the slump of concrete. Effects of temperature on the slump loss and effectiveness of re-dosing of superplasticizer should also be studied as heightened temperature is regularly experienced in Thailand. Finally, the use of different types of superplasticizer for re-dosing on concrete, and the compatibility with other types of chemical admixtures present in concrete (i.e., retarders, accelerators) should also be studied.

REFERENCES

TANGTERMSIRIKUL S. and KITTICHAROENKIAT P., 1999. Water Retainability and Free Water in Fresh Concrete, *Research and Development Journal of the Engineering Institute of Thailand*, Vol. 10, No 1, 42-49.

TANGTERMSIRIKUL S., KHUNTHONGKEAW J. and KITTICHAROENKIAT P., 2001. A Workability Prediction Model for Concrete and Mortar, *JSCE Journal of Materials, Concrete Structures and Pavements*, No. 676, 149-157.

TANGTERMSIRIKUL S., and KHAYAT K.H., 2000. Fresh Concrete Properties, Self-Compacting Concrete, State-of-the-Art report of RILEM Technical Committee 174-SCC, 17-21

Evaluation of induced strain in concrete due to ASR expansion by digital image correlation

Yuichiro KAWABATA¹, Hiroki GODA², Ema KATO³
and Mitsuyasu IWANAMI⁴

¹ Researcher, Port and Airport Research Institute (PARI), Japan
kawabata-y@pari.go.jp

³ Assistant Professor, Kyushu Institute of Technology, Japan
³ Senior Researcher, PARI, Japan

(Researcher, ICUS, IIS, the University of Tokyo, Japan)

⁴Head of Structural Mechanics Division, PARI, Japan

ABSTRACT

In recent years, examples of deterioration of concrete structures due to alkali-silica reaction (ASR) have been reported, and methods used to diagnose such structures have become controversial issues. Regarding the diagnosis of ASR-affected structures, it is difficult to evaluate induced strain/stress of concrete due to ASR expansion. Therefore it is necessary to develop a method to evaluate the induced strain in reinforced concrete (RC) member. One of the conventional methods is to measure the strain with strain gauges before and after releasing induced stress by cutting and/or coring the surface of concrete. This requires, however, the attachment of many strain gauges in order to evaluate multidirectional strains since ASR expansion shows anisotropic behavior. Meanwhile, digital image correlation (DIC) analysis, a full-field optical measurement, gives strain distribution of concrete with high resolution. By using this technique, the authors developed a method to evaluate induced strain in RC member caused by ASR expansion.

This paper describes the new method to evaluate induced strain by using DIC analysis. After expansion, deformation of concrete before and after coring the concrete was measured. The results showed one possibility that the new method can evaluate the induced strain in RC member caused by ASR expansion.

Keywords: *alkali-silica reaction (ASR), digital image correlation (DIC), multi-rosette analysis, induced strain caused by ASR expansion*

1. INTRODUCTION

In recent years, examples of deterioration of concrete structures due to alkali-silica reaction (ASR) have been reported, and the rational repair and reinforcement to such structures has become a controversial issue (Japan

Society of Civil Engineers, 2005). In concrete structures damaged by ASR, reduction in concrete strength and Young's modulus and spalling of cover concrete are observed, resulting in degradation of structural performance of structural members, such as load carrying capacity and ductility. Moreover, cracks caused by ASR will make it easy for chloride ion, water and oxygen to penetrate into concrete. This may initiate corrosion of steel bars embedded in the concrete, degrading the durability of concrete structures. In severe cases, fracture of steel bars in structures has occurred, resulting in significant decrease of structural performance.

Regarding the diagnosis of ASR-affected structures, evaluation of the induced strain/stress in concrete is necessary in order to assess the damage in concrete structures because the induced strain may damage the steel bars. However, it is difficult to evaluate the induced strain/stress of concrete caused by ASR expansion. Therefore it is necessary to develop a method to evaluate the induced strain in reinforced concrete (RC) member. One of the conventional methods is to measure the strain with strain gauges before and after releasing induced strain by cutting and/or coring the surface of concrete. This requires, however, the attachment of many strain gauges in order to evaluate multidirectional strains since ASR expansion shows anisotropic behavior.

Meanwhile, digital image correlation (DIC), a full-field optical measurement, has been increasing in popularity in the fields of medical science and mechanics technology (Uchino, 2003). DIC can give multidirectional deformation of the object so that it is being applied to civil engineering field (Goda et al., 2011). By using this technique, the authors developed a method to evaluate strain distribution in RC member caused by ASR expansion.

This paper described a new method to evaluate induced strain in concrete caused by ASR expansion by using DIC. Applicability of the proposed method was discussed in this paper.

2. EVALUATION METHOD OF INDUCED STRAIN IN CONCRETE CAUSED BY ASR EXPANSION

2.1 Method and procedures

The method to evaluate the induced strain in concrete caused by ASR expansion is similar to conventional ones, while the measurement is different. Figure 1 shows the procedure for evaluation of induced strain in concrete caused by ASR expansion. Similar to the conventional method using strain gauges, concrete coring is carried out. Before coring concrete, some digital photographs are taken using a digital camera. Since a hole is formed by coring concrete, the strain of concrete around the hole is released. Consequently the concrete around the hole deforms according to restrained strain. After coring the surface of the concrete, several digital images are taken for multi-rosette analysis using DIC as explained in the next section.

By using this technique, the multidirectional strains around the hole can be evaluated.

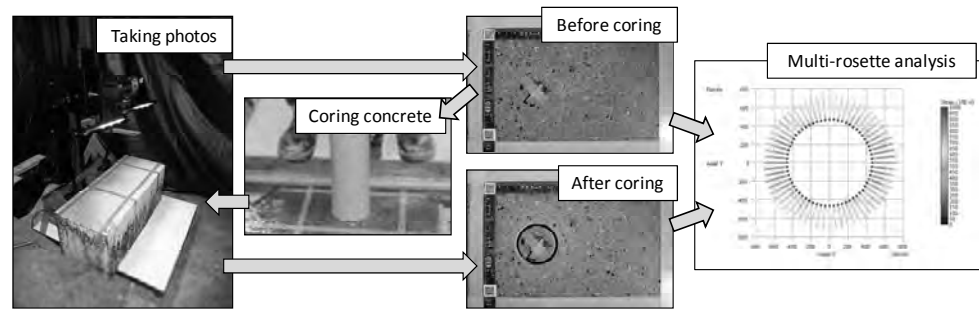


Figure 1: Procedures for evaluation of induced strain in concrete

2.2 Strain measurement of concrete

2.2.1 Digital image correlation (DIC)

DIC is a type of full-field strain measurement method. In DIC, digital photographs of a specimen at different stages of deformation are used. By tracking the subset, which is a block of pixels with 256 tones of monochrome digital image, DIC provides a full-field deformation vector field. The subset ($N \times N$) can be set to have any required size analyzed.

In order to correlate the subsets, two types of pattern matching: “rough search” and “detailed search” are conducted. Rough search can correlate the subsets to an accuracy of a pixel. In the rough search, the correlation function C_R for rough search can be determined by using the residual minimization method shown in the following Eq (1).

$$C_R(X+u, Y+v) = \sum_{i=-M}^M \sum_{j=-M}^M |I_d(X+u+i, Y+v+j) - I_u(X+i, Y+j)| \quad (1)$$

where, $I_u(X, Y)$ and $I_d(X+u, Y+v)$ are the light intensities before and after deformation, respectively; X and Y are the center coordinates of a subset; u and v are displacements in the x - and y -directions, respectively; and $N = 2M+1$. When the correlation function C_R shows the minimum value, the subset containing this position can be decided to be the nearest location where the center of the subset shifted.

On the other hand, due to the discrete form of the nature of digital image, it is necessary to decide deformation of the subset at sub-pixel level. Several kinds of interpolation formula are used in the previous work. In this study, the discrete brightness pattern of pixels is directly interpolated numerically to give the maximum correlation function. The correlation function C_D for detailed search at the sub-pixel level can be determined by using the following Eq (2).

$$(2) \quad C_D(X+u, Y+v) = \frac{\sum_{i=-M}^M \sum_{j=-M}^M I_d(X+u+i, Y+v+j) \times \sum_{i=-M}^M \sum_{j=-M}^M I_u(X+i, Y+j)}{\sqrt{\sum_{i=-M}^M \sum_{j=-M}^M \{I_d(X+u+i, Y+v+j)\}^2 \times \sum_{i=-M}^M \sum_{j=-M}^M \{I_u(X+i, Y+j)\}^2}}$$

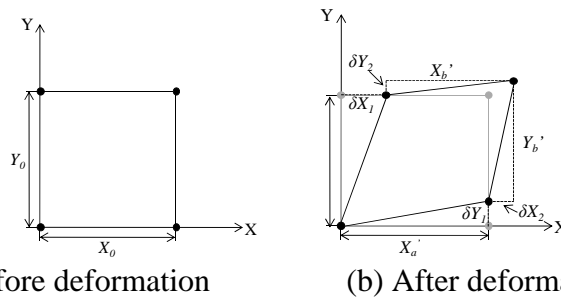


Figure 2: Schematic diagram of deformation of rectangular region

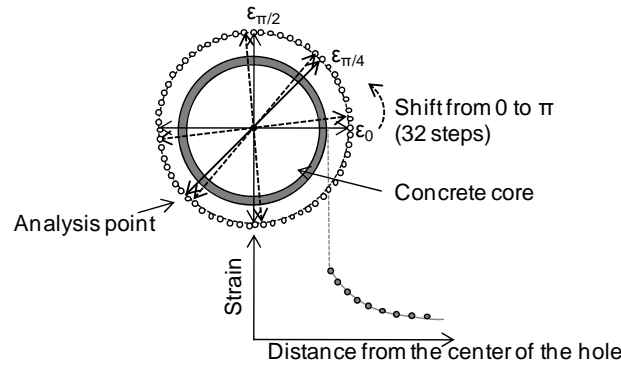


Figure 3: Schematic image of multi-rosette analysis

With analyzed data from DIC, the deformation vector field can be calculated. By comparing deformed rectangular regions to initial ones as shown in Figure 2, strains at each position can be calculated as shown in Eqs. (3)-(5). Major strains (ϵ_{max}), minor strains (ϵ_{min}) and maximum shear strains (γ_{max}) at arbitrary positions can be obtained by rosette analysis.

$$\epsilon_x = \frac{(X'_a - X_0)/X_0 + (X'_b - X_0)/X_0}{2} \tag{3}$$

$$\epsilon_y = \frac{(Y'_a - Y_0)/Y_0 + (Y'_b - Y_0)/Y_0}{2} \tag{4}$$

$$\epsilon_{xy} = \frac{(\delta X_1/Y'_a + \delta Y_1/X'_a) + (\delta X_2/Y'_b + \delta Y_2/X'_b)}{2} \tag{5}$$

2.2.2 Multi-rosette analysis

By using DIC, a new analytical method proposed by Uchino, multi-rosette analysis, is applied to evaluate stress distribution of concrete around the hole (Uchino et al., 2010). The principle of multi-rosette analysis is shown in Figure 3. At first, the calculation method on the change ratio of the hole diameter will be explained. As shown in Figure 1, analysis points will be arranged in a concentric pattern. In this case there are 64 analysis points. Two analyses points that are in symmetry with respect to the center point of the hole will be selected. The distance change between two points will be calculated using the images before and after deformation and 32 calculated data are obtained. In these calculated data, a combination 0, $\pi/4$, and $\pi/2$ rad along the x -axis will be selected and the maximum and minimum of the distance change ratios will be obtained using rosette analysis. Then multiple rosette analysis will be performed as the combination will be changed, and

the average maximum and minimum of the distance change ratios that reduced the error will be obtained. According to Uchino, the results of stress concentration around the hole under one dimensional tension corresponded

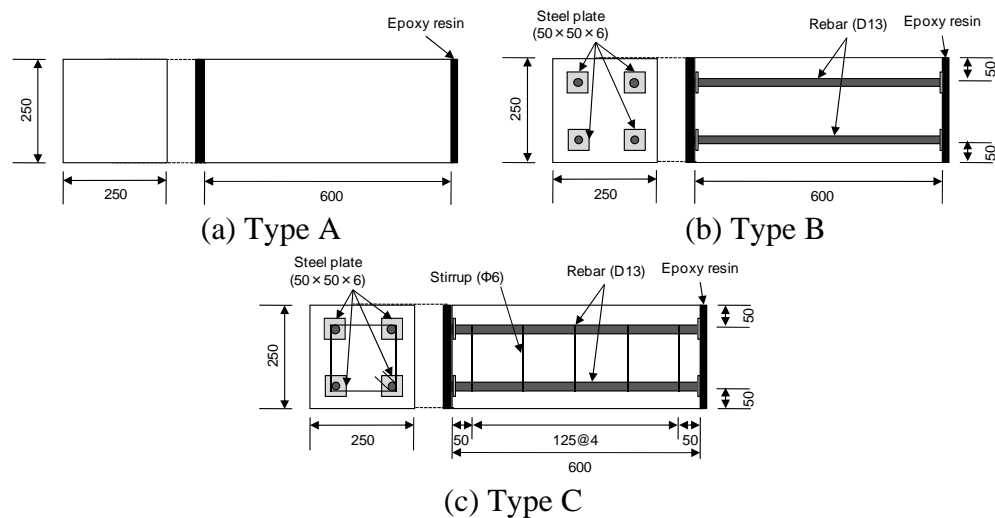


Figure 4: Shape and size of test specimens

Table 1 Expansion after exposure (unit: μ)

Exposure condition	Type A		Type B			Type C			
	Concrete		Concrete		Main rebars	Concrete		Main rebars	Stirrups
	Lo	La	Lo	La		Lo	La		
Ac	5922	5651	2938	9471	1520	2761	8469	1778	1676
Nt	3193	4040	1315	3171	1230	1557	3092	1359	1778

with the analytical results by the finite element method.

3. EXPERIMENTS

3.1 Test specimens

Figure 4 shows shape and size of the test specimens. Alkali-reactive coarse aggregate, and non-reactive limestone fine aggregate were used. Water-to-cement ratio was 47%. Sodium hydroxide solution was added into the water so as to control the total $\text{Na}_2\text{O}_{\text{eq}}$ amount in concrete to 6.0 kg/m^3 . Deformed steel bars with a diameter of 13mm 6mm were used.

The size of the test specimens were $250 \times 250 \times 600 \text{ mm}$. Type A has neither rebar nor stirrup so as not to restrict the concrete. Type B has 4 rebars to restrict the concrete along longitudinal direction only. Type C has both 4 rebars and 5 stirrups to restrict along longitudinal and latitude direction. Steel plates were welded to both sides of the rebars. Epoxy resin measuring 2mm in thickness was coated on the surface of the $250 \times 250 \text{ mm}$. Fifty-six days after the concrete was cast, the test specimens were exposed to two conditions; seawater wetting/drying test in the controlled outdoor (Nt) and accelerated seawater wetting/drying test at 60 deg C in the laboratory (Ac). The period of exposure was about 1.5 years. Strain gauges

were used to measure strain in the steel bars and stirrups. After 28 days of curing, the demec studs were attached over the concrete surface. The change in length between the demec studs was periodically measured by a digital extensometer. The measured data was treated as strain. The average of all measured longitudinal (Lo) strains is defined as Lo strain for each specimen. In the same way, the average of all lateral (La) strains is defined as La strain. After the exposure test, all of the surfaces of test specimens were washed to make the random patterns for DIC. Hereafter, the name of tested specimen was described as (Type of specimen)-(Exposure condition).

Table 1 shows the results of the expansion test. Regarding the exposure condition Ac, Type B and Type C show significant decrease in Lo strain compared to Type A whereas La strains of Type B and Type C were larger than that of Type A. This effect was attributed to the existence of rebars. Expansion of test specimens exposed to Nt was smaller than that exposed to Ac since the chemical reaction of ASR is strongly affected by exposed temperature.

3.2 Induced strain measurement

The proposed method described above was carried out. Outside diameter of the core for stress release was 52mm. At first, random pattern was distributed on the surface of the specimens using black, yellow and white sprays. Five images were taken with a digital CMOS camera. Pixel number of the camera was 14 million (4,800×2,800) pixels, and the area taken by the camera was 280×180mm. The diameter of the core was 890pixels. The length of a pixel shows 0.06mm. After taking the images, the core was drilled using a concrete coring machine. Depth of the core was 100mm, twice as deep as the diameter of the core. Then, some images of the surface around the core were taken using the same camera. Conditions for taking the image were the same before and after coring. Scale of the subset for DIC analysis was set to 30×30 pixels. In the multi-rosette analysis, the pitch along the normal vector was 5pixels.

4. RESULTS AND DISCUSSIONS

4.1 Strain distribution around the hole

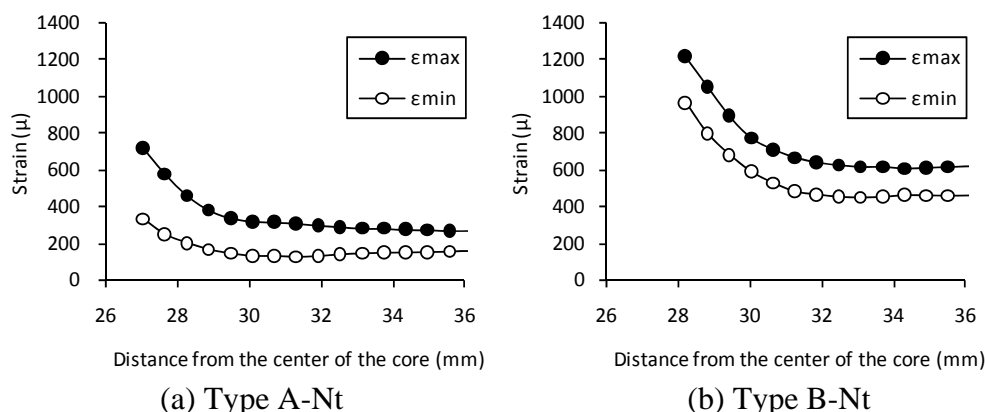
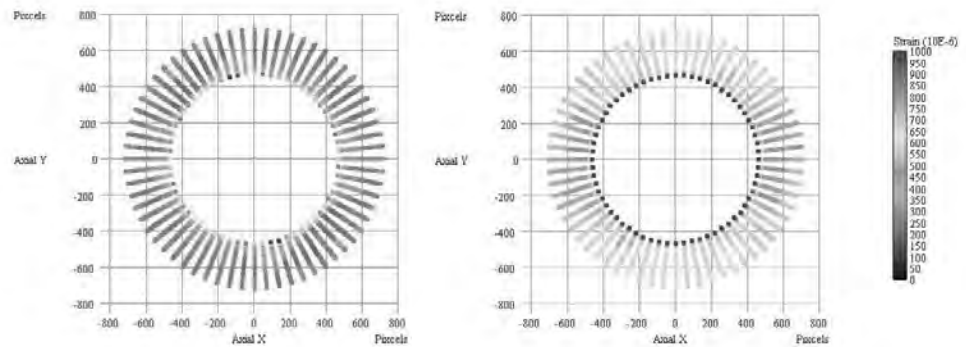


Figure 5: Relationship between distance from the center of the core and strain

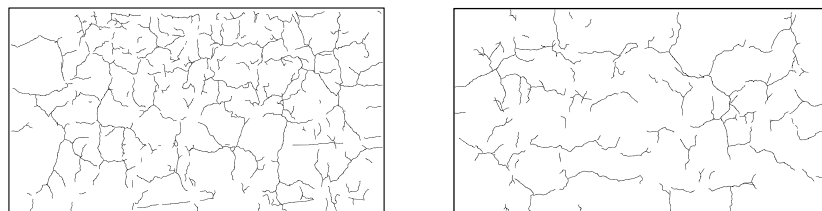
Figure 5 (a) shows the relationship between the distance from the center of the hole and strain evaluated by the proposed method in Type A-Nt. The major strain near the concrete core showed 700 μ . The strain tended to decrease significantly with the increase in the distance from the center of the core. At 36 mm from the center, major strain and minor strain showed approximately 200 μ . This tendency was attributed to the release of strain caused by coring the concrete. On the other hand, the test result of Type B-Nt shown in Figure 5 (b) showed similar tendency to Type A-Nt. The major strain near the concrete core showed 1200 μ while the strain at 36 mm from the center showed 500-650 μ . The difference between Type A-Nt and Type B-Nt is the existence of rebars embedded in concrete so that the expansion force due to ASR was accumulated in concrete due to the restraint of rebars. Consequently the released major strain in Type B-Nt was larger than that in Type A-Nt. From this result, it can be said that the released strain is affected by the restraint condition.



(a) Type A-Nt

(b) Type B-Nt

Figure 6: Major strain distribution around the concrete core



(a) Type A-Nt

(b) Type B-Nt

Figure 7: Crack pattern

Table 2 Released strain near the hole after coring (unit: μ)

Test specimen	Exposed condition	Released strain	
		Lo	La
Type A	Nt	370	640
Type B		1081	1177
Type C		1106	1274
Type A	Ac	654	864
Type B		1848	1935
Type C		747	1180

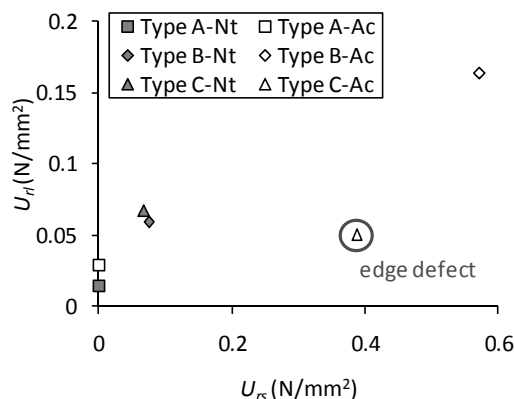


Figure 8: Relationship between U_{rs} and U_{rl}

Figure 6 shows the major strain distribution around the hole of the test specimens. Type A-Nt shows isotropic strain distribution. In Type B-Nt, the strain in the L_a -direction was larger than that in the L_o -direction. Figure 7 shows the crack pattern of the concrete surface after exposure. Type A-Nt shows multi-directional cracks. In Type B-Nt, cracks occurred in the L_o -direction so that strain in the L_o -direction was released. These tendencies are known as characteristics of ASR expansion of restrained concrete. The major strain distribution obtained from the proposed method agreed with the crack map of the test specimen. These results indicated that the major strain distribution around the hole can be evaluated by the proposed method.

4.2 Validity of the proposed method

Table 2 summarizes the results of the proposed method. The released strain near the hole formed after coring was smaller than the induced strain as shown in Table 1. This is attributed to the release of strain due to the cracking of the concrete. ASR expansion accompanies cracking of concrete so that the induced strain will decrease. Especially, most of the induced strain in covering concrete would be released due to cracking. On the other hand, concrete surrounded by rebars is restrained so that concrete will show larger strain after coring. The previous paper reports that the proposed method is more accurate than the conventional one using strain gauges (Goda et al., 2011).

Here, the relationship between the induced strain and released strain is discussed from the viewpoint of the conservation of energy. The energy derived from concrete expansion can be expressed using the following equation (6).

$$U_c = E\varepsilon_{L_o}\varepsilon_{L_a}^2 \quad (6)$$

where, ε_{L_o} and ε_{L_a} are longitudinal and lateral strain, respectively; E is Young's modulus ($= 33.2 \text{ kN/mm}^2$). The calculated energy of Type A can be assumed to be free-expansion energy (U_{free}). The difference between the energy of Type B or Type C and that of Type A is the energy stored in RC

member by rebars (U_{rs}). In addition, the released energy derived from coring concrete (U_{rl}) can be calculated by the strain obtained from the proposed method (Table 2). Figure 8 shows the relationship between U_{rs} and U_{rl} . There is a linear relationship between U_{rs} and U_{rl} except for Type B-Ac. In Type B-Ac, the edge defect was observed in the outside of the hole. It is considered that this defect affected the measured strain. The absolute value of U_{rs} was different from that of U_{rl} . This can be attributed to the lost energy derived from cracking, creep, and shrinkage of the concrete. From the test results, it can be said that the proposed method can evaluate the stored energy in RC member.

From these results, it is verified that the proposed method can evaluate the strain distribution around the hole and the stored energy in RC member derived from restraint of rebars. Though further research is necessary to evaluate the free-expansion energy of concrete, there is a possibility that the proposed method can evaluate the induced strain in concrete caused by ASR expansion.

5. CONCLUSIONS

This paper proposes a new method for evaluating the induced strain in concrete caused by ASR expansion, by using multi-rosette analysis based on DIC. The following conclusions can be drawn based on the test results:

- (1) The proposed method can evaluate the strain distribution around the hole.
- (2) Based on the conserved energy, the proposed method can evaluate the stored expansion energy in RC member due to restraint of rebars.

ACKNOWLEDGEMENT

A part of this work was financially supported by Grant-in-Aid for Young Scientist (B) (No.22760335) from the Japan Society for the Promotion of Science (JSPS).

REFERENCES

- Goda, H., Kawabata, Y., Uchino, M., Iwanami, M. and Hibino, M., 2011. Application of stress release method by digital image correlation method to concrete units deteriorated by alkali silica reaction, *Proceedings of JSEM 2011 Annual Conference on Experimental Mechanics*, Nara, Japan, 175-180 (in Japanese).
- Japan Society of Civil Engineers, 2005. State-of-the-art report on the countermeasures for the damage due to alkali-silica reaction, *Concrete Library 124* (in Japanese).
- Uchino, M., 2003. Sub-micron displacement measurement using a digital image correlation method, *Proceedings of ATEM'03*, CD_Paper No. OS01W0200.

Uchino, M., Okamoto, T., Hida, K., Ito, Y., Sumitomo, P. and Matsuda, H., 2010. Strain analysis method using multi-rosette analysis by digital image correlation method, *Proceeding of the International Conference on Bridge Maintenance, Safety and Management*, 2564-2569

Development of remote system for supporting building damage assessment during large-scale earthquake disaster

Makoto FUJIU¹, Miho OHARA² and Kimiro MEGURO³

¹ Ph.D. Candidate, Department of Interdisciplinary Information Studies,
The University of Tokyo, Japan
fujiau@iis.u-tokyo.ac.jp

² Associate Professor, Interfaculty Initiative in Information Studies
/ Institute of Industrial Science,
The University of Tokyo, Japan

³ Professor, Interfaculty Initiative in Information Studies,
/ Institute of Industrial Science,
The University of Tokyo, Japan

ABSTRACT

Building damage assessment is necessary for governments to issue the Victim Certificates for residents who suffered from housing damages. The process of assessment needs accuracy, quickness, objectivity and fairness because the results of assessment are used as criteria for providing public monetary supports for rebuilding of their livelihood. In Japan, several big earthquakes are expected to occur in the near future. A lot of structural damages due to these earthquakes will cause enormous needs for building damage assessment. However, there is a limit on the number of specialists with adequate assessment skills who can access the damaged area under bad traffic conditions. Delay in building damage assessment by local governments can disturb rapid reconstruction of the damaged area.

Considering these problems during large-scale earthquake disaster, this paper proposed the new system for building damage assessment using photos of damaged houses taken by residents or volunteer fire corps in damaged area. Specialists outside the damaged area confirm these photos on the website and assess their damage levels. All the data used for building damage assessment is managed with GIS database on the management server located outside the damaged area under cloud condition. This kind of digital management system can contribute to enhance the accuracy and efficiency of the procedures for issuing the Victim Certificates for residents. In this paper, the total system for supporting building damage assessment was designed and its prototype system was developed. The system for uploading the photos of damaged houses was developed as mobile communication service. The remote system for specialists to assess the damage level was developed as web service.

Keywords: earthquake disaster, building damage assessment, IT system

1. INTRODUCTION

In Japan, several big earthquakes are expected to occur in the near future. A lot of structural damages due to these earthquakes will cause enormous needs for building damage assessment. Building damage assessment is necessary for governments to issue the Victim Certificates for residents who suffered housing damages. However, current number of human recourses who are trained with the procedure of building damage assessment is not enough. It is necessary to develop the new system which can correspond to next large-scale earthquake disaster. The guidelines of general procedure for inspecting building damage and evaluating loss due to disasters were published by the Cabinet Office in 1968, 2001 and 2009. However, in past disasters, various problems of building damage assessment have been pointed out such as inaccurate inspection, difficulty in quick inspection and lack of human recourses with sufficient skill of assessment.

In this research, new remote system for building damage assessment using IT system was proposed and prototype system was developed. These systems have some features that can solve some problems pointed out by past building damage assessments and execute building damage assessment quickly after a large scale earthquake disaster. This proposed system has two sub-systems. First one is photo uploading system used in damaged area. Second one is assessment system for supporting experts such as registered architects and experienced workers outside the damaged area. Finally, we report that design and functions of developed system.

2. PROBLEMS OF PAST BUILDING DAMAGE ASSESSMENTS AND SOLUTIONS

There are 3 inspection stages in building damage assessment such as “Primary Inspection”, “Secondary Inspection” and “Issue of the Victim Certificates”. Through these stages, damage levels of buildings are decided by visual inspection. The primary inspection evaluates the damages appeared on the exterior of a building. The secondary one evaluates not only the exterior damage but also the interior damage. The purpose of the secondary inspection is to provide the second opinion for the evaluation when the owner or resident of a damaged house does not accept the result of the primary one. Therefore, the primary inspection is carried out for all the damaged buildings, while the secondary inspection is usually carried out by request. Finally, Victim Certificates for residents are issued from the local governments.

The process of assessment needs accuracy, quickness, objectivity and fairness because the results of the assessments are used as criteria for providing public monetary supports for rebuilding their livelihood. However, various problems have been pointed out for the building damage assessments after past earthquakes. We reviewed literatures regarding past several building damage assessments such as Shigekawa (2005) and classified reported problems as shown in Table 1. As a result, enormous

problems in each inspection stage were obtained. Our proposals to solve the problems at each stage were shown in table 1. For example, “primary inspection” stage has the problems with low inspection accuracy and insufficient inspectors’ knowledge. In order to solve these problems, we proposed double check procedures to enhance accuracy of assessments.

Table1: Problems and solutions of building damage assessment after earthquakes

Flow of Inspection		1995 Hyogoken-Nanbu Earthquake	2004 Niigata Chuetsu Earthquake	2007 Niigata Chuetsu-oki Earthquake	Solution of past problems in this research
I -Criteria	①Criteria	There is no standard to carry out the building damage assessment. (Murao,1999)	There is no standard to carry out the building damage assessment. Neither examination methods nor the inspection methods are clearly provided. Only guidelines were issued by the Cabinet Office. (Shigekawa, 2005)		-
II -Training of Inspector	②Summon of Inspection	Insufficient number of assistant staff (Murao,1999)	Insufficient number of assistant staff (Shigekawa,2005)	Difficulty in assemble of inspectors (Tanaka,2008)	Inspectors who goes in the damaged area becomes unnecessary.
	③Training	-	Because method of assessment is different in each local government, training is difficult. (Horie,2004)	-	Prior training to inspectors can be executed.
	④Organize	Inspector's knowledge was insufficient. (Murao,1999)	Difficulty in gathering enough number of Inspectors and keeping inspection quality (Shigekawa,2005)	-	<ul style="list-style-type: none"> •The owner of damaged house and the fire fighters can become an investigator. • Inspection quality can keep by doing prior training and taking a picture using instruction.
III-Screening	⑤Screening	-	Limit in on-site inspection for lack of inspectors (Shigekawa,2005)		Because of a lot of support workers exist outside of damaged area. So, a lot of investigations can be executed.
IV-Inspection	⑥Primary Inspection	-	-	Difference between structural engineer's aspect and the Cabinet Office guideline (Tanaka,2008)	-
		-	Inspector's knowledge was insufficient. (Shigekawa,2005)	-	The assessment result keeps accuracy by a double check.
		Problem concerning inspection accuracy (Murao,1999)	Problem concerning inspection accuracy (Shigekawa,2005)	Problem concerning inspection accuracy (Tanaka,2008)	The assessment result keeps accuracy by a double check.
	⑦Secondary Inspection	Difficulty in responding to residents who have dissatisfaction in inspection results (Murao,1999)	Difficulty in responding to residents who have dissatisfaction in inspection results (Shigekawa,2005)	-	-
		-	-	Difficulty in predicting number of application (Tanaka,2008)	Because of a lot of support workers exist outside of damaged area. So, a lot of investigations can be executed.
		-	-	Needs for assistant staff's for thirdly inspection (Tanaka,2008)	The assessment result keeps accuracy by a double check. So, number of execution of third inspection can be reduced.
⑧Victim Certificate	-	The efficiency of work was low, because the issue of enormous certificates was the first time for local governments. (Yoshitomi,2005)	-	Because of issue of the victims certificate was automated, the amount of work of administrative office can be greatly reduced.	
Use of electronics devices	①Use of GIS	Used by ex post analysis	Used by ex post analysis	Used by ex post analysis	Possible to use GIS by improving the Web environment.
	②Use of GPS	Not used because of technological development	Not used	Not used	Standard equipment in a smart phone.
	③Mobile phone		Used a little.	Used a little.	The usability has improved greatly with a smart phone.
	④Digital camera		Used a little.	<ul style="list-style-type: none"> • Only used for the record • Limit in data processing using PC for lack of capacity. 	Standard equipment in a smart phone.
	⑤Cloud computing		Not used because of technological development.	Not used because of technological development.	The Cloud computing can be used with a smart phone.

3. CONCEPT OF NEW REMOTE SYSTEM FOR BUILDING DAMAGE ASSESSMENT

As a new system for achieving all the solutions for the problems reported at the past building damage assessments as shown in table 1, we proposed a new remote system for supporting building damage assessments during large-scale earthquake disaster. The concept of the system is illustrated in figure 1. The total system consists of two sub-systems. The first one is photo upload system in damaged area. Photos of a damaged house are taken by residents or volunteer fire corps in damaged area and those data is uploaded to the server. The second one is remote assessment system for specialists. Specialists located outside the damaged area confirm these photos through the website, and assess their damage levels and area. All the data used for building damage assessment is managed with GIS database on the management server located outside the damaged area under cloud condition. This kind of digital management system can contribute to enhance the accuracy and efficiency of the procedures for issuing the Victim Certificates for residents.

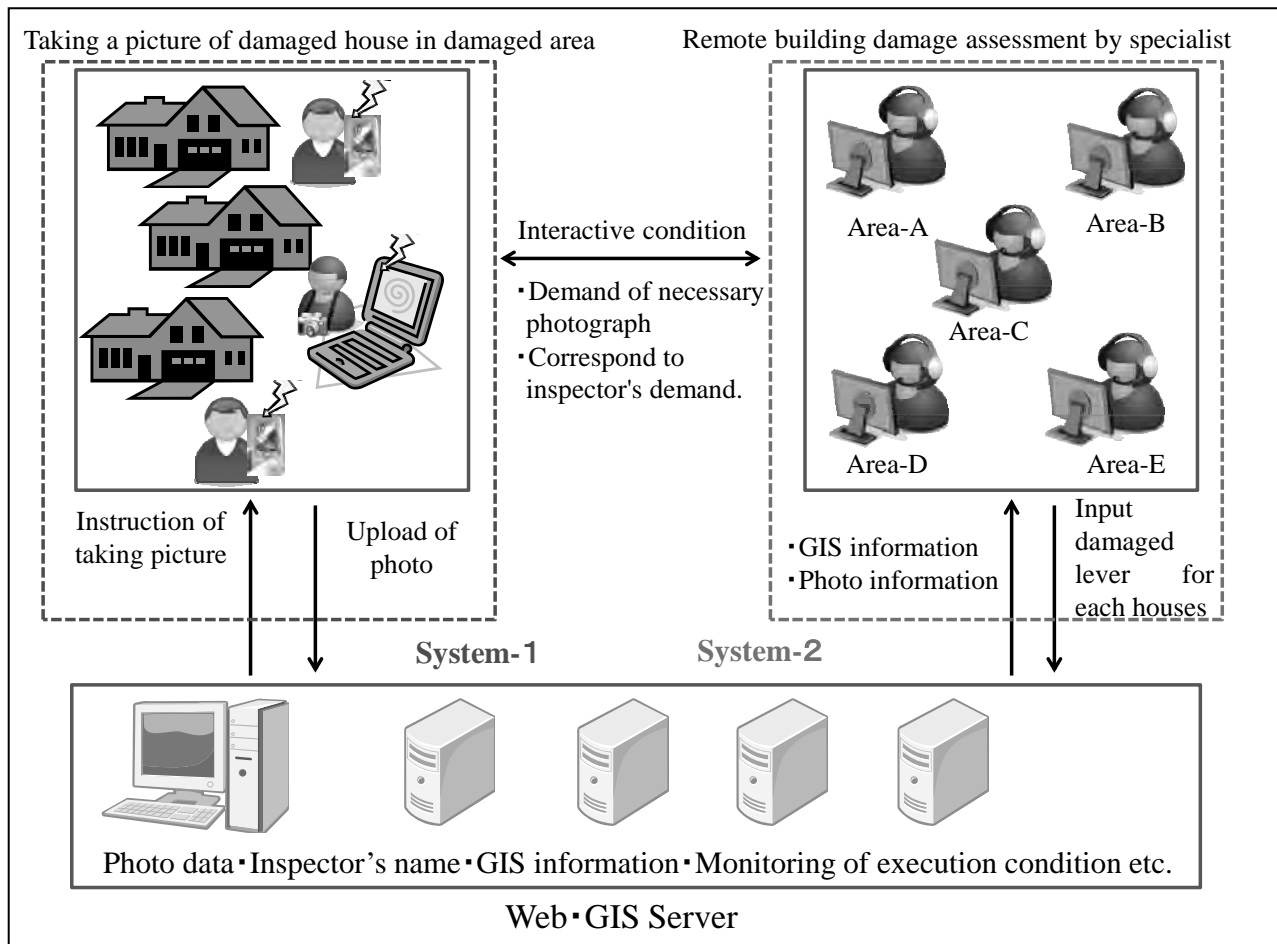


Figure 1: Concept of remote system for building damage assessment

4. DEVELOPMENT OF PROTOTYPE REMOTE SYSTEM FOR BUILDING DAMAGE ASSESSMENT

4.1 Development of photo upload system in damaged area

Here, prototype of “Photo upload system in damaged area” was developed. Photos of a damaged house are taken by residents or volunteer fire corps in damaged area and those data is uploaded to the server. This system was developed by Android as the mobile phone operating system which is installed in almost all the smart phones except iPhone. Photo upload application is installed to each Android smart phone by inspectors who are residents or volunteer fire corps in damaged area.

Flow of photo upload system is shown in figure 2. Firstly, residents or volunteer fire corps as inspectors input the basic information such as GPS information, address and owner name. Secondary, they upload some photos such as overview of damaged house, incline of damaged house and damaged point of roofs, walls and fundamentals. Finally, they confirm the input data and some photos.

Method of completing for photo upload in damaged area using upload application is as follows. Inspectors take some damaged house photos which are full views of a damaged house (north side, east side, south side and west side) and closeup views of damaged points.

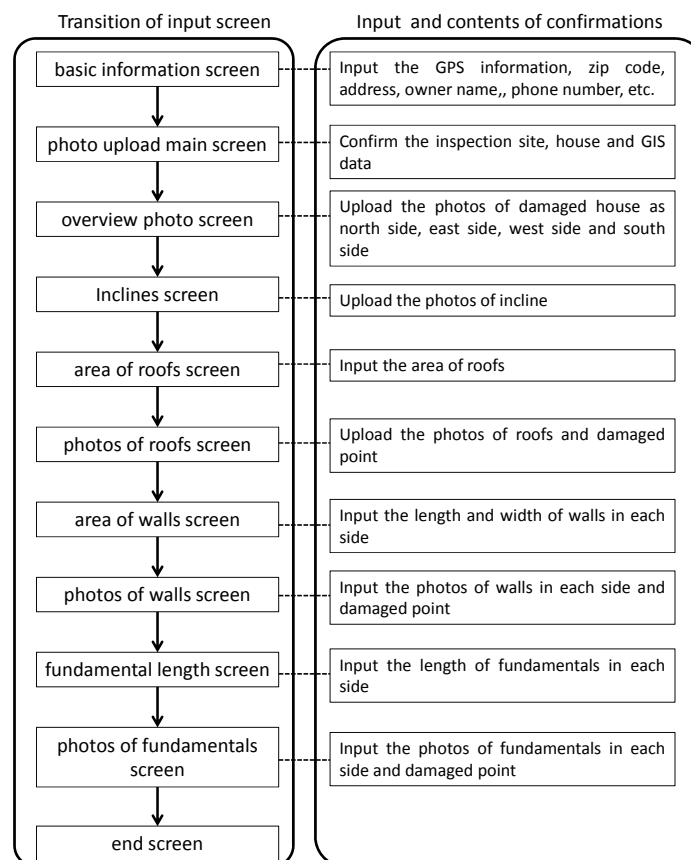


Figure 2: Flow of photo upload system in damaged area

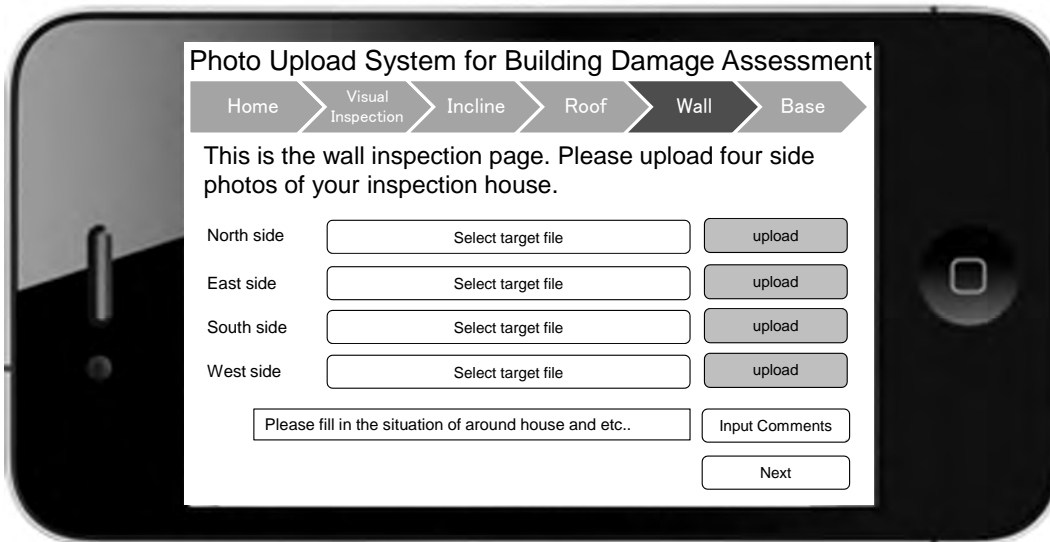


Figure 3: Photo upload system in damaged area (upload page)

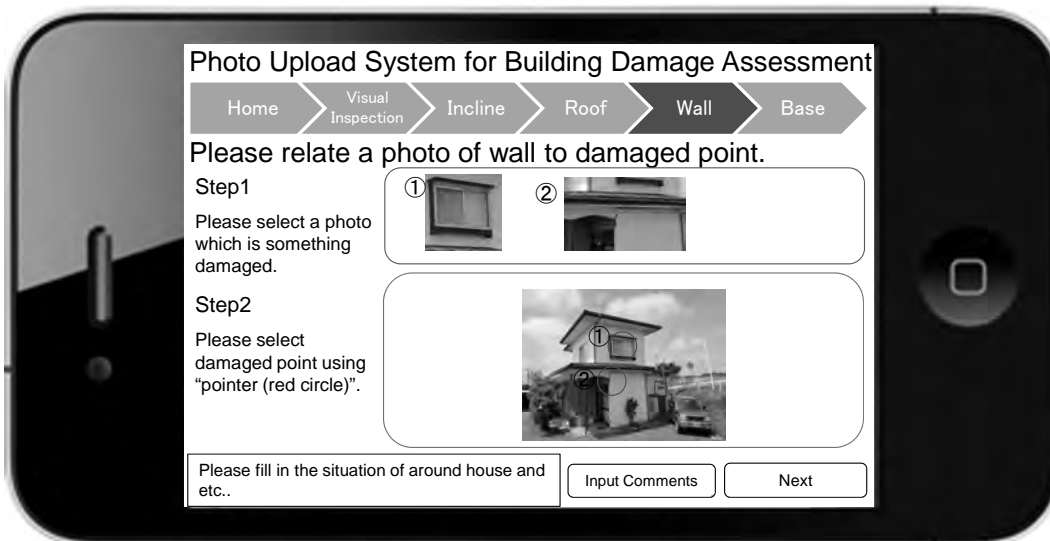


Figure 4: Photo upload system in damaged area (relationship page)

They select some photos for upload in each factors page, and fill in the comments about damage level and location of a house etc. as shown in figure 3. Inspectors should take pictures of damaged house concerning three factors: externals, inclination and building element (roof, exterior wall and foundation). Furthermore, they have to relate closeup views of damaged points to full views using touch screen functions as shown in figure 4. Figures 3 and 4 are the prototype images of the system for the primary inspection. The prototype images of photo upload system were developed based on the data of totally damaged houses due to the 2011 off the Pacific coast of Tohoku Earthquake. After taking some pictures, inspectors need to upload them to an exclusive server in cloud condition using upload application. Using this application makes it easier to select and upload

photos which are taken by inspector in damaged area. The reason is that smart phone has touch screen functions which are tap, drag, flick and pinch out/in operations.

4.2 Development of remote assessment system for specialists

Here, prototype of “remote assessment system of photos of damaged houses was developed. Specialists outside the damaged area confirm these photos on the website and assess their damage levels. All the data used for building damage assessment is managed with GIS database on the management server located outside the damaged area under cloud condition.

Flow of remote assessment system is shown in figure 5. Firstly, specialists who are registered architects and experienced workers outside the damaged area confirm the basic information such as shape of damaged house, location and seismic level on the web system and overview all the photos of a damaged house. Secondary, they assess the damage level and area using some photos such as overview of damaged house, incline of damaged house and damaged point of roofs, walls and fundamentals. Finally, specialists confirm the input data and some photos. Then result of first assessment is passed to the next specialist to carry out double check.

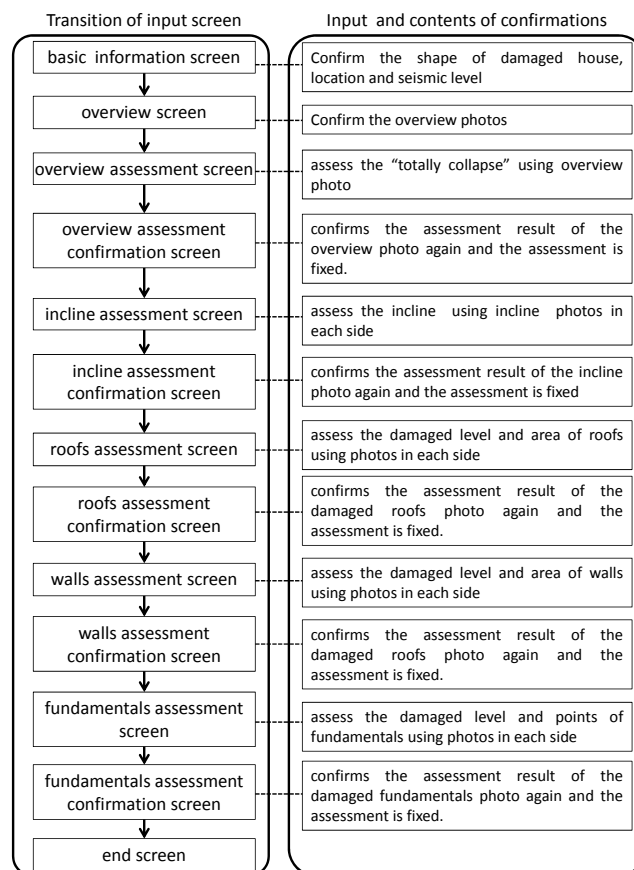


Figure 5 Flow of remote assessment system

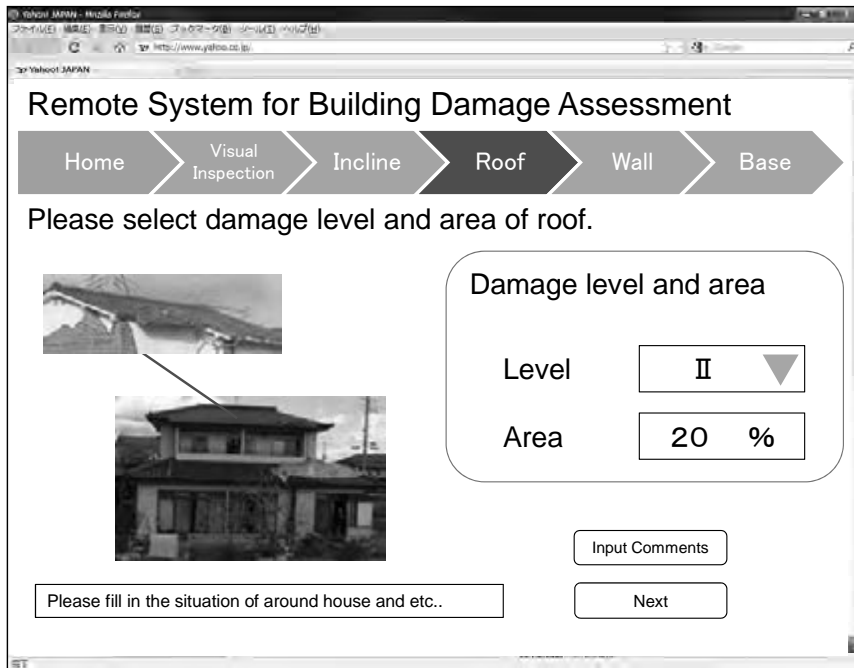


Figure 6: Remote assessment system (roof assessment page)

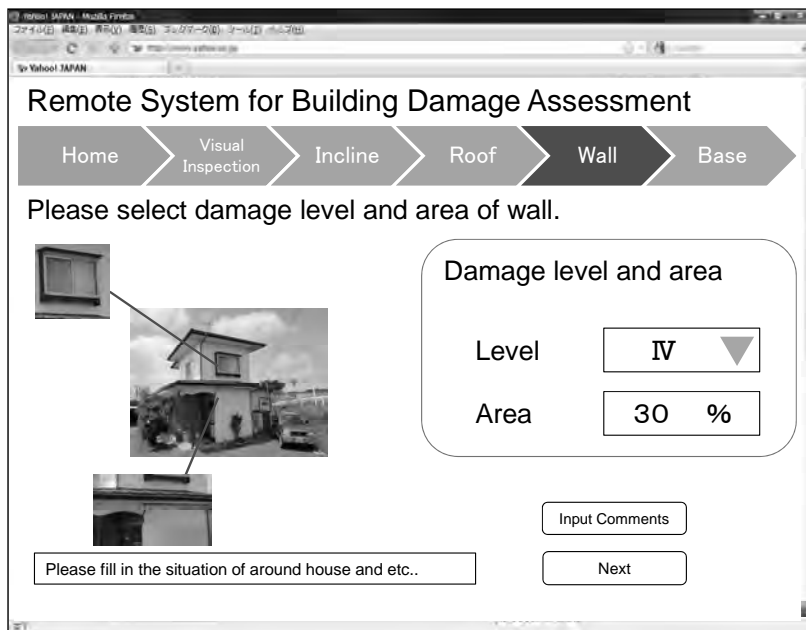


Figure 7: Remote assessment system (wall assessment page)

Figures 6 and 7 show the prototype images of the system for primary inspection. These images were developed based on the data of totally damaged houses due to the 2011 off the Pacific coast of Tohoku Earthquake. Total damage level of a house is decided based on damage levels of three factors: externals, inclination and building element. Assessment for one damaged house should be conducted by two or three specialists to double-check the result and keep accuracy, fairness and objectivity. They can see close-up photos if necessary. They evaluate the photos and decide its damage level as shown in figures 6 and 7. Specialists select the damage level and area from pull down choice set in each factor page. In addition, they can request additional photos for accurate assessment to inspectors in

damaged area through the each assessment page. In final page, fill in the special or caution comments of assessed damaged house and pass to the next specialist. When the assessment ends here, Victim Certificates for resident is issued from local government.

5. CONCLUSIONS

In Japan, several big earthquakes are expected to occur in the near future. It is necessary to develop the new system which can be corresponds to next large-scale earthquake disaster. In this research, new remote assessment system for building damage assessment was proposed.

Some problems of past building damage assessments were analyzed and applicability of new technologies including new electronics devices which are GPS, GIS, digital camera and mobile phone (smart phone) was discussed. Among these problems, this paper focused on “Inspection stage” and “Assessment stage”, and proposed new remote system for building damage assessment using both mobile communication service and web service.

The prototype images of remote building damage assessment system were developed based on the data of totally damaged houses due to the 2011 off the Pacific coast of Tohoku Earthquake. In the future, we plan to improve the functions of the system and examine its effectiveness through experiments for specialists.

REFERENCE

Murao, O., Yamazaki, F., 1999, Comparison of Building Damage Evaluation by Local Governments after the 1995 hyogoken-nanbu earthquake, *Journal of Architecture Planning and Environmental Engineering*, No.515, pp.187-194

Shigekawa, K., Tanaka, S., Horie, K., Hayashi, H., 2005, *Some Regulational Issues on Building Damage Assessment –A Case Study of Niigata-ken Chuetsu Earthquake-*, *Journal of social Safety Science* No.7, pp.133-140

Horie, K., Shigekawa, K., Maki, N., Tanaka, S., Hayashi, H., 2005, *Application of Damage Assessment Training (DATS) to Ojiya City following 2004 Niigata-ken Chuetsu Earthquake –Through a Disaster Response Support Activity for Issuing Victim Certificate-*, *Journal of social Safety Science* No.7, pp.123-132

Yoshitomi, N., Hayashi, H., Urakawa, G., Shigekawa, K., Tanaka, S., Horie, K., Matsuoka, K., 2005, *The Development of a Damage Certificate Issuing Support System –A new disaster response database schema created for the Niigata Chuetsu Earthquake-*, *Journal of social Safety Science* No.7, pp.141-150

Tanaka, S., 2008, *A Study on the Building Damage Assessment Processes for the 2007 Niigata Chuetsu Oki Earthquake Disaster :*

Kashiwazaki Case Study , Proceedings of social Safety Science No.22,
pp.35-38

Basin water management under land use and climate changes -Nan Basin as case study-

Sucharit KOONTANAKULVONG¹, Kwanchai PAKOKSUNG²

¹ Associate Professor, Chulalongkorn University, Thailand
Sucharit.K@chula.ac.th

² Researcher, Chulalongkorn University, Thailand
wrsru_kcp52@yahoo.com n

ABSTRACT

In the last two decades, land use in the upper watershed had changed drastically due to the rapid upland agricultural invasion. This affected the runoff pattern to the reservoir especially in the dry season and sometimes caused flash flood to the downstream area. The recent climate change trend causes additional impact to runoff pattern to the reservoir and make basin water management becomes more complicated.

Nan Basin is in the northern part of Thailand and provides about 25 % of the raw water source to the Central Plain of Thailand. The recent promotion for upland crop agriculture by price guarantee system from the government, i.e., maize, made the change in land use in the upper watershed area. The study on runoff change due to land use change had been conducted via runoff data at gauge stations in the main stream and precipitation data in the past 20 years. Besides, the climate change data derived from the bias corrected MRI-GCM were used to analyze the projected runoff in the basin and project the change. Both land use and climate changes will give impacts to the reservoir operation in the basin and there is a need for new tool to help manage water properly in this changing environment.

The study investigated the degree of change from the land use in the past and climate change for the future and a new tool were introduced to better water management for the basin which will secure water source for the country as well.

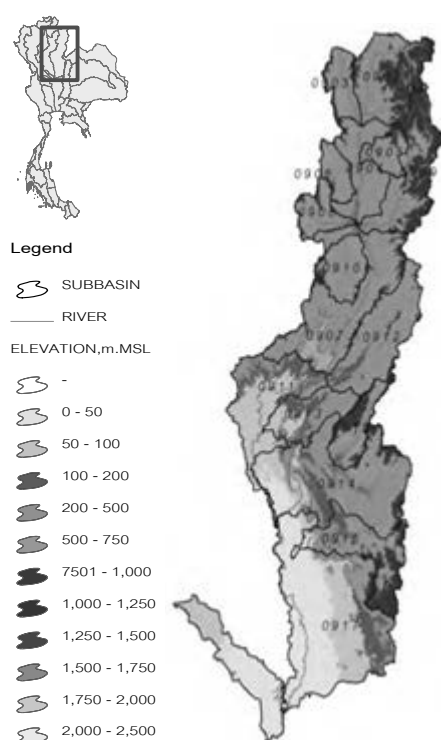
Keywords: *land use, climate change, basin water management, new tool*

1. INTRODUCTION

Land use in the upper watershed of Nan Basin had changed dramatically due to the increasing population and agricultural growth in the past decade. Forest area changed to agriculture and after that the agricultural area was transformed to industrial, residential or recreational areas. This change

affected the runoff and the use of natural resources which created the impact to the hydrologic and environmental conditions. The study aimed to investigate the degree of change from the land use in the past and climate change for the future and some new tools were introduced to better water management for the basin which will secure water source for the country as well.

The Nan river basin is located in the northern region of Thailand with the total catchment area of 34,682.04 sq.km. The basin originated from Bor Klua district, Nan Province and is situated between latitude 15° 42' 12" to latitude 19° 37' 48" N and longitude 99° 51' 30" to longitude 101° 21' 48" E, The basin covers the area of 6 provinces namely Nan, Uttaradit, Phitsanulok, Pichit, Phetchabun and Nakhonsawan Provinces and can be divided into 16 sub-river basin as shown in Figure 1 and Table 1.



Sources: Department of Water Resource

Figure 1 Topographic NAN Basin

Table 1: Catchment area of each sub basin in Nan Basin

COD E	SUB BASIN NAME	Area(km ²)
0902	UPPER PART OF MAE NAM NAN	2,222.34
0903	HUAI NAM YAO (1)	787.73
0904	SECOND PART OF MAE NAM NAN	2,200.39
0905	NAM YAO (2)	1,532.19
0906	NAM SAMUN	598.88

0907	THIRD PART OF MAE NAM NAN	589.57
0908	NAM SA	778.40
0909	NAM WA	3,375.80
0910	NAM HAENG	1,043.80
0911	FOURTH PART OF MAE NAM NAN	2,435.02
0912	NAM PAT	992.83
0913	KHLONG TRON	1,297.54
0914	MAE NAM KHWAE NOI	4,578.86
0915	NAM PHAK	2,008.04
0916	MAE NAM WANG THONG	2,470.50
0917	LOWER PART OF MAE NAM NAN	7,770.16
TOTAL		34,682.04

Sources: Department of Water Resources

Up to now, there were various studies on land use change and runoff coefficient changes in the NAN Basin. The land use change was mostly estimated from the satellite data and compared the change of area of each land use type, though the satellite images available were limited only for some years. The runoff coefficient indicated water release unit in each watershed which was calculated from the ratio of runoff, catchment area and rainfall. The runoff coefficient values in the year 2000 is greater than 2006's because the forest area in the year 2006 was less than 2000. In Nan basin, runoff coefficient changed at the rate of 2.1% per year (Kwanchai P. et. al., 2011). The impact of climate change towards water disaster in Thailand, i.e., drought, flood, landslides was also assessed by using the bias-corrected MRI-GCM data and there was an indication that Nan Basin will be one of the hot spot of change (Sucharit K. et.al., 2011).

1. OBJECTIVES AND METHODOLOGY

The study aimed to find the affect of land use change towards runoff pattern due to the economical growth in the upper basin. Future climate conditions are put into the consideration to investigate the water situation of both present and future.

The application of satellite data from TRMM is introduced as a new tool to see the opportunity to better water management from the main dam.

The collected data included rainfall, runoff, land use change (Forest area change) in each sub basin boundaries in the year 2000 and 2006. The analyzed runoff coefficients (Kwanchai P. et. al., 2011) were then illustrated spatially by using GIS technology.

The data used in the study in the main basin and each sub basin of Nan basin are the land use in the year 2000 and 2006, rainfall and runoff time series.

In the study procedure is as follows:

- 1) collect the economical data in the study area such as population, agricultural product/output etc.
- 2) prepare the land use map in the year 2000 and 2006,
- 3) classify land use type, i.e., forestry, agriculture, residential, irrigation, water
- 3) resource and other, in each subbasin,
- 4) simulate the runoff pattern using the previous analysed runoff coefficient,
- 5) analyze the runoff pattern with the changes in land use (forest area change),
- 6) analyze the flood and drought with new land use and climate conditions
- 7) simulate water condition and analyse water supply volume to central plain,
- 8) apply TRMM data for water control from dam.

2. RESULTS

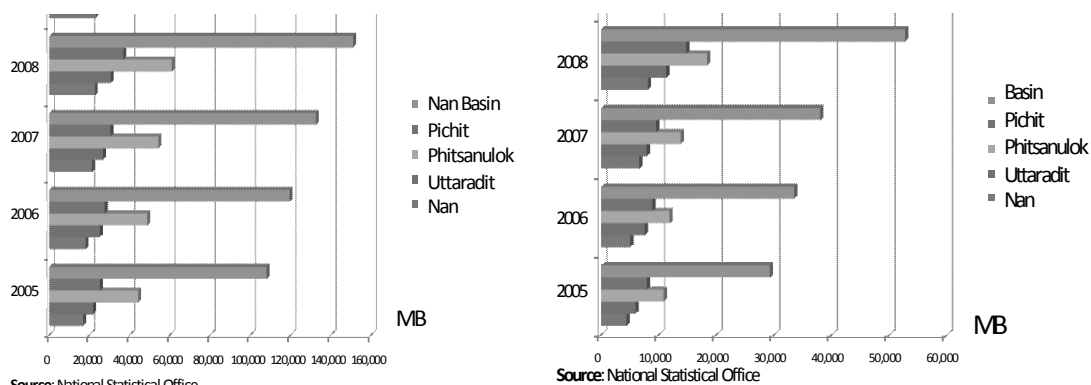
The difference of land use change and runoff in NAN basin in the year 2000 and 2006 was analyzed and the results are summarized as follows.

2.1 Economical growth

In 2009, the population in Nan Basin with a majority of the population lived in non municipality 85%, as shown in Figure 2. Phitsanulok Province had the highest population and Uttaradit Province had the lower. The socio-economical index for Nan Basin used in this study was the gross provincial product (GPP). In 2008, GPP in study area increased 39.76% from the year 1995 and with the value of 151,025 MB as shown in Figure 3. The GPP (including agriculture) increased 80.12% from the year 1995 with the value of 52,761 MB as shown in Figure 4. Agricultural statistics in the study area like maize grew at the highest about 73.8%. The summer rice, rainy rice and rubber grew about 47.3%, 7.4% and 7% respectively.



Figure 2: Population in Nan Basin in the year 2009



a) Gross Provincial Product b) GPP (Including Agriculture)
 Figure 3: Economical data in Nan Basin

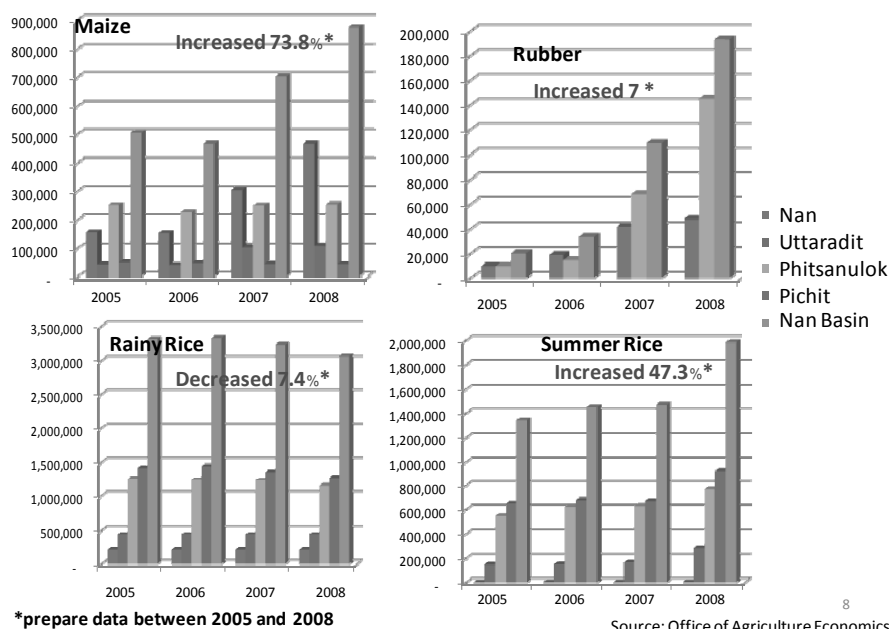


Figure 4 Cultivated area growth in Nan Basin

2.2 Land Use Change in NAN Basin

The land use in the study area, shown in Figure 4 and Table 2, can be classified into 6 major groups, i.e., forestry area, agriculture area, irrigation area, residential area, water resources area and other.

Table 2: Distribution of land use type in Nan Basin

Type of Land Use	2000		2006	
	Areas (sq.km)	%	Areas (sq.km)	%
Residential	781.11	2.26	872.32	2.65
Agriculture	14,991.73	43.33	16,299.58	49.60
Irrigation	2,480.72	7.17	2,695.00	8.20
Forestry	15,745.15	45.51	13,798.86	41.99
Unclassified	130.29	0.38	535.10	1.63
Water Resources	471.12	1.36	399.23	1.21
Total	34,600.10	100	34,600.10	100

Sources: Land Development Department

Forest area is the top of land use type in Nan basin while water resource area had the lowest in the year 2000 and 2006 because NAN basin was less developed but rich in natural resource.

The differential land uses (forest area) by sub basin were shown Figure 6 and Table 3. In the year 2006, the deforestation was greater than the 2000's because the economic in basin started to grow. The Khwae Noi sub basin had the highest deforestation rate of 115.7 sq.km/year or 6.2% per year out of 16 sub basin in NAN basin because Phitsanulok Province, where the Khae Noi sub basin is located, was highly developed. The Sa sub basin had lowest rate of 6.5 sq.km/year or 1% per year. In average, forest area in Nan basin decreased about 386 sq.km/year or 16% per year.

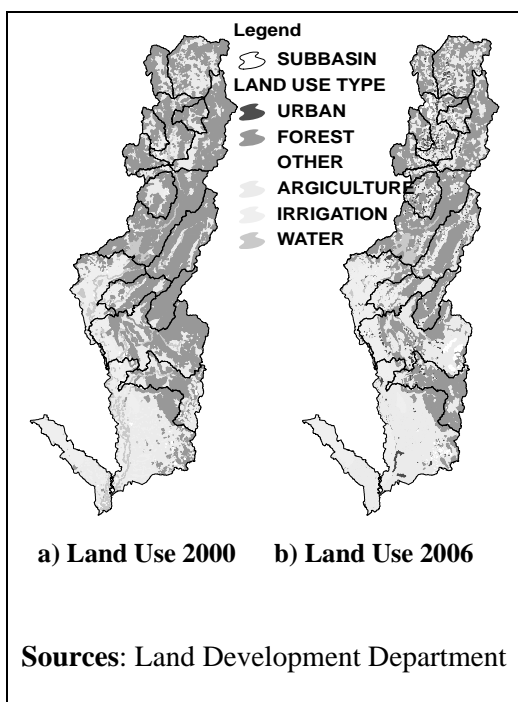


Figure 5 Land Use in NAN Basin

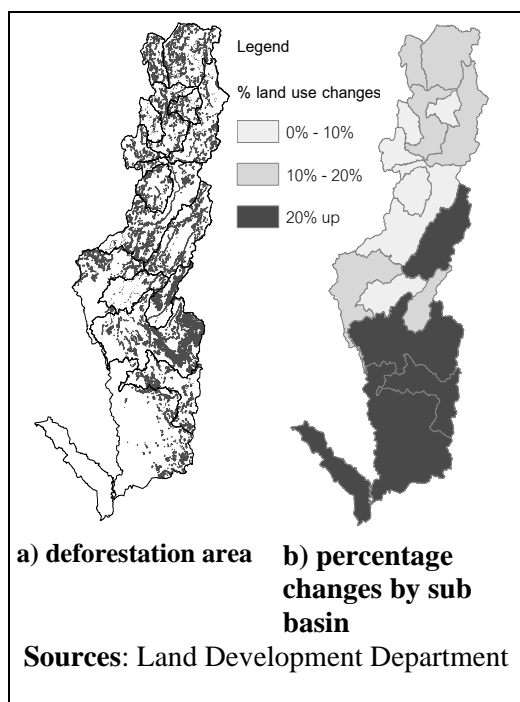


Figure 6 Land Use Change (forest area changes) in NAN Basin

2.3 Runoff and hydrograph change

The annual runoff volume in Nan basin will change with the rainfall change. The runoff in near future will decrease from the present but the runoff in far future will increase from the present as shown in Figure 7. The annual runoff volume of Nan basin in upper zone (U) and lower zone (L) in near future will decrease from the present but the runoff in far future will increase from the present. The middle zone (M)'s runoff will increase in both near future and far future as shown in Table 4.

Table3: Forest area change in NAN Basin.

Code	2000		2006		differential	
	A _F .km ²	%	A _F .km ²	%	A _F .km ²	%
0902	1,205.2	54.2	1,012.8	45.6	192.4	16.0
0903	420.1	53.3	353.2	44.8	66.8	15.9
0904	770.2	50.3	660.9	43.1	109.4	14.2
0905	329.3	55.0	291.9	48.7	37.4	11.4
0906	364.2	61.8	328.3	55.7	35.9	9.9
0907	2,789.2	78.6	2,571.8	72.5	217.4	7.8
0908	630.5	81.0	585.0	75.2	45.4	7.2
0909	1,557.2	70.8	1,424.8	64.8	132.5	8.5
0910	615.2	58.9	555.5	53.2	59.7	9.7
0911	549.2	22.2	431.2	17.5	118.0	21.5
0912	1,657.8	68.1	1,481.0	60.8	176.8	10.7
0913	1,151.5	88.7	1,059.0	81.6	92.5	8.0
0914	1,860.0	40.6	1,049.6	22.9	810.4	43.6
0915	838.6	84.5	634.5	63.9	204.1	24.3
0916	932.4	46.4	768.9	38.3	163.5	17.5
0917	823.4	10.6	590.6	7.6	232.9	28.3
Total	16,493.94	47.3	13,798.86	39.6	2,695.1	16.3

Remark: A_F is forest area

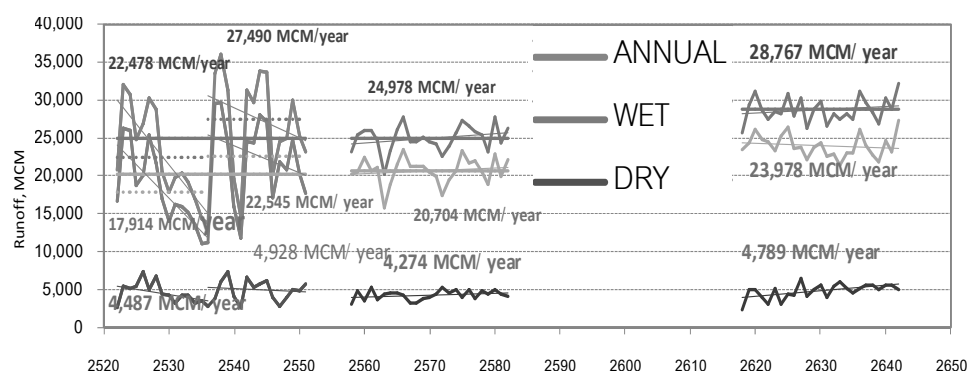


Figure 7: Runoff changes in the past and future

The hydrograph change was analyzed from the rainfall time series and the land use and recognized the change. The analysis in each zone, compared the average annual runoff between before 1993 and after 1993, showed the higher peak and one month shift due to the quicker rainfall and the land use change as shown in Figure 8.

Table 4 Runoff changes in each zone of present and future conditions

season	zone	Runoff, MCM				% different	
		past		Near	Far	Near	Far
		1979-1993	1994-2008	2015-2039	2075-2099	past	
Annual	U	12,498.9	15,438.1	12,467.7	14,430.0	-19.2	-6.5
	M	1,636.1	1,853.3	4,271.5	4,873.9	130.5	163.0
	L	8,343.2	9,981.8	8,239.2	9,463.2	-17.5	-5.2
	Basin	22,478.2	27,490.4	24,978.4	28,767.2	-9.1	4.6
dry	U	1,666.0	1,830.3	2,140.6	2,410.9	17.0	31.7

	M	510.7	522.1	712.1	793.6	36.4	52.0
	L	2,310.7	2,575.9	1,421.5	1,584.5	-44.8	-38.5
	Basin	4,487.4	4,928.3	4,274.3	4,789.1	-13.3	-2.8
Rainy	U	10,807.8	13,599.7	10,327.1	12,019.0	-24.1	-11.6
	M	1,119.2	1,548.8	3,559.4	4,080.3	129.8	163.4
	L	5,987.7	7,396.7	6,817.7	7,878.7	-7.8	6.5
	Basin	17,914.6	22,545.2	20,704.2	23,978.1	-8.2	6.4

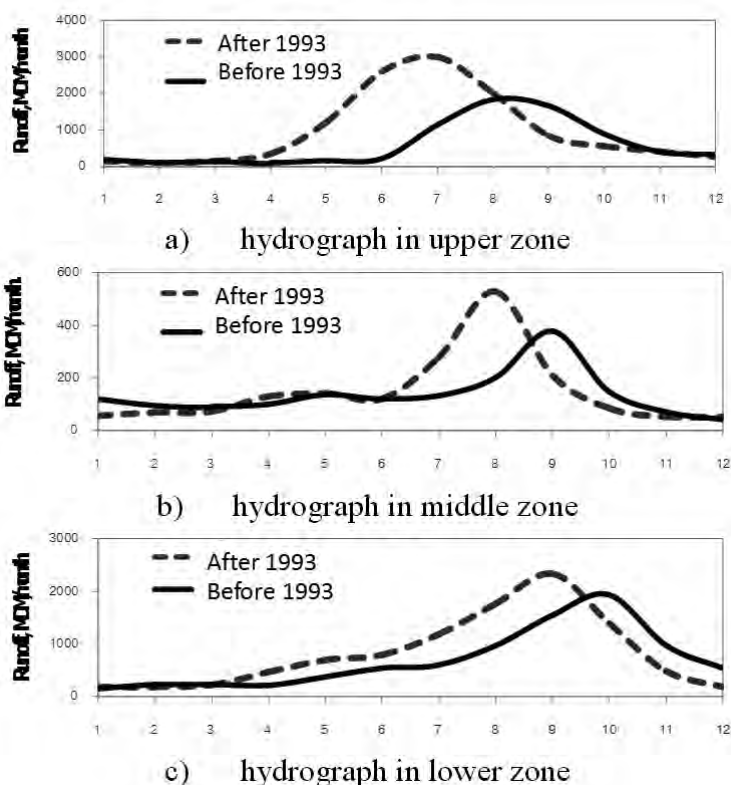
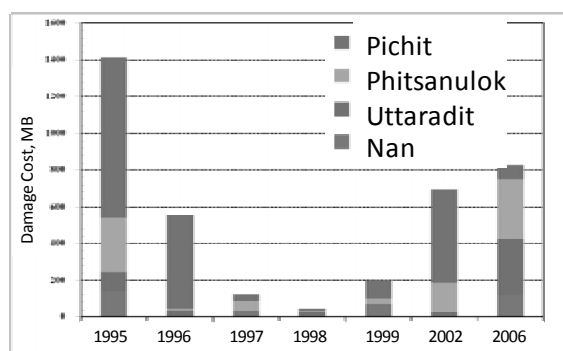


Figure 8: Hydrograph changes in each zone of Nan Basin



Source : DDPM, RID

Figure 9: Flood Damages in each province

2.4 Flood and drought

The effect of land use change and climate change on flood and drought issue in the study area were assessed by collecting past flood records and analyzing water balance in each zone to project the future possible drought

In the past, the damage caused by major flood of Nan basin that covered Nan, Uttaradit, Phitsanulok and Pichit Province were estimated in each province and shown in Figure 9. From the data, it can be seen that damage in the year 1995 was the worst, followed by the year 2006 and 2002. Damaged areas were mostly residential and agricultural areas.

The water deficit in the study area was analyzed to investigate drought situation from water balance analysis, i.e., water demand and water supply. The water deficit in each sub basin was shown in Table 5. The highest water deficit area of present, near future and far future is in the lower zone where the large irrigation areas are located.

Table 5 Water deficit in each sub basin and zone

Code	Past 1979-2008			Near 2015-2039			Far 2075-2099		
	use	deficit	conditio	use	deficit	conditio	use	deficit	conditio
	MCM/	MCM/	n	MCM/	MCM/	n	MCM/	MCM/	n
0902	95.31	1.6		80.68	0.66		93.32	0.29	
0903	8.79	0.15		7.36	0.07		9.86	0.02	
0904	70.77	1.04		64.37	5.68		62.79	6.35	
0905	14.18	0.15		19.36	0.09		11.33	0.05	
0906	24.66	6.29		19.56	0.29		29.18	0.05	
0907	10.53	0.05		7.29	0.06		7.17	0.04	
0908	22.37	0.81		14.42	0.17		13.83	0.04	
0909	18.3	0.46		15.28	0.01		10.92	0.02	
0910	26.97	4.1		20.24	0.87		18.06	0.95	
0911	795.46	50.73		713.16	30.23		801.28	30.77	
0912	94.68	7.41		83.22	3.53		87.03	2.67	
0913	48.65	7.88		44.03	3.95		47.23	3.41	
0914	450.61	36.56		466.04	41.99		461.82	39.73	
0915	24.54	0.01		22.56	0		22.3	0	
0916	5.69	0.05		5.56	0.03		5.07	0	
0917	1479.33	232.08		1634.83	279.24		1686.41	270.05	
upper	291.9	14.65		248.55	7.9		256.48	7.82	
middle	938.78	66.02		840.41	37.7		935.55	36.85	
lower	1960.16	268.7		2128.99	321.27		2175.59	309.79	
Basin	3190.84	349.36		3217.95	366.87		3367.62	354.46	

Remark:

high	middle	lower	none
------	--------	-------	------

4. TRMM APPLICATION

In order to better water operation in the Nan Basin, the flow estimate from ungauged sub basins is essential to help save water release from the dam. To analyze this side flow of sub basin in middle zone of Nan basin, data during Sep 30 to Oct 31, 2006 were used to test the application of TRMM data. The TRMM data, used Kalman filter, was estimated in each grid and compared with observed data distributed in each grid by the Thiessen method. Figure 10 showed the comparison of observed and filtered TRMM rainfall data with the correlation of 0.8 and RMSE of 3.6 which is acceptable to be used for further runoff analysis. The estimated runoff (side flow, Figure 11 b)) in the study area from TRMM filtered data was compared with the actual data

(Figure 11 a)) and found that the side flow volume from filtered TRMM gave acceptable side flow volume.

This method showed that the filtered TRMM rainfall pattern can be used to estimate runoff volume in ungage basin and help dam operator to save water release of both dry and wet **season**. Such tool can be applied for better water management and flood early warning in the future.

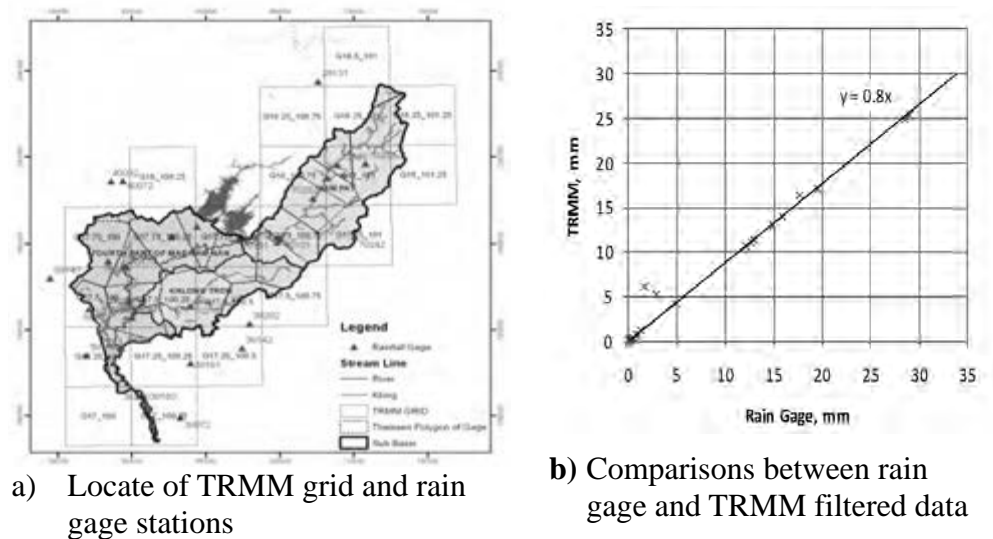


Figure 10: TRMM Grid and its correlation

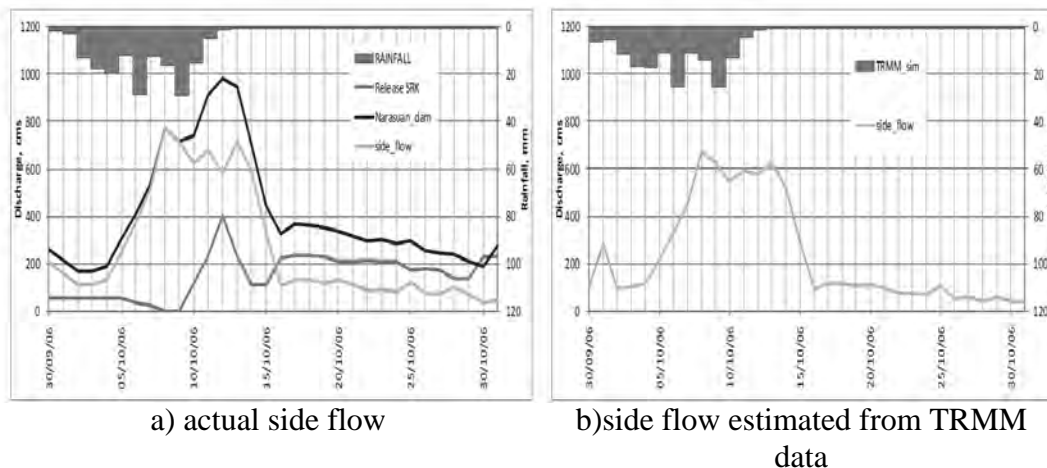


Figure 11 Side flow pattern estimated from TRMM data

5. CONCLUSIONS AND RECOMMENDATION

The study concluded that land use change affected runoff volume. The change in forests area influenced the runoff change. The deforestation was effected from the growth of the economic in basin which caused the increase in the agriculture area. The decreasing forest area in the basin affected the increase of runoff coefficient and decrease of total runoff as an impact chain. There is a need to find a balance between cultivated

area and forest area in the upper watershed. The study can be used as a data to determine the balance of natural resource utilization and socio-economical development in the more sustainable manner in the future for the study area.

Runoff had been changed in volume and hydrograph in near future will decrease while increase in the far future than present. Hydrograph peak, shifted about 1 month quicker when compared between before 1933 and after 1993, became higher due to the shift of rainfall pattern.

The TRMM data with the Kalman filter algorithm and GIS technique gave acceptable rainfall data compared with rain gage data and the runoff from ungauge sub basin using TRMM data gave also good correlation with the observed. The TRMM satellite data and technique gave future potential as a new tool for water management of both dry and wet season to alleviate drought and reduce flood.

The present study used monthly hydrological data of each sub basin for analysis with two year of land use data as available. In future if more land use data is available, the trend and rate of land use change can be determined more properly which will make the study more precised.

ACKNOWLEDGEMENT

We would like to thank to the agencies that provided important data and digital information, e.g., Land Development Department, RID, TMD, JAXA etc. and also to Thailand Research Fund as research funding and Chulalongkorn University for research unit funding.

REFERENCES

- Chow, V., D. Maidment, and L. Mays, 1988. *Applied Hydrology*, McGraw-Hill International Edition, Singapore, 572 p.
- Chulalongkorn, 2011, Strategic Water Management Planning in Nan Basin, Progress Report, submitted to Thailand Research Fund, August.
- Singh, V., 1992. *Elementary Hydrology*, Prentice Hall, New Jersey, 973 p.
- Singh, V., 1988. *Hydrologic Systems Volume I Rainfall-Runoff Modeling*, Prentice Hall, New Jersey, 480 p.
- Singh, V., 1988. *Hydrologic Systems Volume II Rainfall-Runoff Modeling*, Prentice Hall, New Jersey, 480 p.
- Sucharit K. and Chaiyuth S., 2011, GCM Data Comparison and Its Application to Floods/Droughts Adaptation, The Second International Conference on Sustainability Science in Asia' (ICSS-Asia2011), 2-4 March, Hanoi, Viet Nam
- Sucharit K. and Kwanchai P., 2011, *The Effect of Land Use Change on Runoff in The Nan Basin*, Proc. SSMS2011, Sri Lanka, Sep 14-15.

Tripathi, M., P. Shrivastava, and S. Dwivedi, 2003. Hydrological Modeling of A Small Watershed Using Satellite Data And GIS, *Journal of the Indian Society of Remote Sensing*, 32(1):313-329

Relationship among response, recovery and development from the view point of financial resource allocation

Yasuhito JIBIKI
Project Assistant Professor, CIDIR, III, the University of Tokyo, Japan
jibiki.yasuhito@iii.u-tokyo.ac.jp

ABSTRACT

Relationship between response, recovery and development is verified from the view point of financial resource allocation.

It has been emphasized that development is the highest priority for them and should not be undermined by response and recovery, thus it is important to provide sufficient resource to response and recovery activities against disasters. In addition, the concept of the disaster management circle is considered to implicitly assume or anticipate that good response leads good recovery, and good recovery contributes development. In other words, certain linkage can be found between response, recovery and development. Based on the relationship between these three phases, a hypothesis might be reasonable; amount of money disbursed for response, recovery and development to affected countries has correlation with each other. Affected countries receive financial assistance, depending on the extent of the loss, damages and their own vulnerability. A positive correlation could be observable; the more financial support is demanded for response, the more aid is required for recovery and development. In order to verify the hypothesis, financial data from three major funds is employed; the Central Emergency Response Fund (CERF), the Trust Fund for Human Security (TFHS), and Global Facility for Disaster Reduction and Recovery (GFDRR). CERF mainly provides its resource to response activities. TFHS and GFDRR distribute their resource to efforts for recovery and development.

As a result of empirical statistical analysis, only the linkage of response and recovery is significantly observed.

Keywords: *financial resource allocation, development*

1. INTRODUCTION: Backgrounds and Purpose

1.1 Backgrounds

This article examines relationship between response, recovery and development, from the view point of financial resource allocation.

In the field of global environment, the relationship between resource allocation and development has been argued for decades. Developing countries have been insisting that their first priority is development. Although these countries have shown their understandings to the importance of global environment, they have been repeatedly emphasizing that their “right to development” should be fully taken into consideration in the context of environmental protection (Williams, 1997; Kasa et. al, 2008).

Based on this preoccupation, developing countries have been demanding additional resource provision from developed countries (Miller, 1995b; Williams, 1997; Streck, 2001; Najam, 2002; Najam, 2004; Roberts et. al, 2007; Boyd et. Al, 2008). It has been claimed by developing countries that efforts for the environmental protection should not hamper actions and resource allocation for development. Developing countries have been concerning that their limited resource is divided and invested both to environment issues and development. Without any additional assistance, it is predictable that their limited resource becomes scarce in the end, and development as their first priority is not achieved.

Similar to the field of global environment, the relationship between resource allocation and development has also been discussed in the arena of humanitarian assistance. The United Nations General Assembly Resolution 64/251 in 2009 stressed the significance of “...*the timely provision of humanitarian assistance through all phases of a disaster, from relief and recovery to development, including the provision of adequate resources.*” Additionally, the linkage of response, recovery and development was stated in the United Nations General Assembly Resolution 48/192 in 1991, and the resolution reaffirmed that efforts to emergency are required to be recognized “*as a step towards long-term development.*”

Additionally, a concept of the disaster management circle is considered to implicitly assume or anticipate that good response leads good recovery, and good recovery contributes development. In other words, certain linkage can be found between response, recovery and development.

1.2 Purpose

Based on discourses of the relationship between resource allocation and development, and the linkage of these three phases, a hypothesis might be reasonable; amount of money disbursed for response, recovery and development to affected countries has correlation. It seems that affected countries receive financial assistance, depending on the extent of the loss, damages and their own vulnerability. A positive correlation could be observable and testified; the more financial support is demanded for response, the more aid is required for recovery and development.

In the following sections, a method for verification of hypothesis is noted in the section 2. The Section 3 demonstrates results of calculation in line with data described in the Section 2. The Section 4 concludes the results obtained at the Section 3 and discusses what these results mean.

Prior to start analyzing, definitions of terms are needed to be clarified. This inquiry employs a limited definition of the term “resource” and specifically uses the resource as financial resource. In this article, humanitarian assistance treats both natural and man-made disasters, since financial institutions do not separately distinguish these two types of disasters.

2. METHOD

2.1 Source of data

In order to examine the hypothesis stated in the Section 1.2, a data set of this paper is prepared. The data set contains eight variables compiled from sources mentioned below.

The data from financial resource is gathered from three major funds; the Central Emergency Response Fund (CERF), Global Facility for Disaster Reduction and Recovery (GFDRR), and the Trust Fund for Human Security (TFHS). CERF and TFHS were managed by the United Nations. GFDRR is operated and coordinated by World Bank and the United Nations.

CERF mainly provides its resource to response activities. Based on the United Nations Resolution 48/192 in 1991, the Central Emergency *Revolving* Fund (*old* CERF) was established. In 2006, the fund was reformed in the part of *Humanitarian Reform*, and the name and the types of provision of the fund were changed. The grants of *new* CERF consist both of Rapid Response and Under Funded Emergency. In this article, the data of Rapid Response and Under Funded Emergency from CERF is dealt as financial resource for response.

GFDRR allocates its financial resource both to recovery and development. GFDRR was established in 2006. GFDRR has several financial services, but in this article the data of its Track-II and Track-III is adopted. GFDRR Track-II mainstreams disaster risk reduction in development, and GFDRR Track-III provides standby recovery financing facility for accelerated disaster recovery (GFDRR, 2010). In this paper, the data of GFDRR Track-III is recognized as financial resource for development and GFDRR Track-II is coped as recovery resource.

TFHS was founded in 1999. Referring its “Key funding criteria” and the titles of projects, the fund is considered to tend to disburse its resource to projects relating with development (MOFA of Japan, 2009). Thus, in this article, the data of TFHS is regarded as financial resource for development. In comparison with these three funds, data of the number of affected people by disasters is added. From the data base of EM-DAT, the number of the affected population by natural disaster is organized. In addition, the data of internally displaced people (IDP) caused by conflicts and violence is also consolidated into the data set. The figure of IDP is taken from a data set managed by Internal Displacement Monitoring Centre and Norwegian

Refugee Council, since that data set is known as the most comprehensive data.

2.2 Procedure for developing the data set

A variable “Response” is an accumulated number of CERF grants from the year of 2006 to 2010. From 2006 to 2010, the provision of the grants has been reached 79 affected countries.

A variable “Recovery” is a summed number of GFDRR Track-III from the year of 2006 to 2010. If the resource is allocated to several countries or to regional level, such a data is not included, since it is not possible to specify that each country receives accurate amounts of money. From 2006 to 2010, the provision of the grants has been reached 22 affected countries.

Variables for “Development” have three types. The first variable is an accumulated number of GFDRR-II from the year of 2006 to 2010. As is in the case of GFDRR Track-II, if the resource is allocated to several countries or to regional level, such a data is not included, since it is not possible to specify that each country receives accurate amounts of money. 43 countries received assistance individually from GFDRR Track-II. The second variable is a summed number of TFHS from the year of 2006 to 2009. The TFHS data in 2010 is not available. As is in the case of GFDRR Track-II and Track-III, if the resource is allocated to several countries or to regional level, such a data is excluded, since it is not possible to specify that each country receives accurate amounts of money. 39 countries received assistance individually from TFHS. The number of recipient countries by funds is described in Table 1 below. Finally, the third variable is aggregated as the summed number of GFDRR Track-II and TFHS.

Table 1: The number of recipient countries by funds

	The number of recipient countries
Countries obtained CERF only	30
Countries obtained GFDRR Track-III only	1
Countries obtained GRDRR Track-II only	9
Countries obtained TFHS only	9
Countries obtained ALL 4 funds listed above	5
The total number of recipient countries	102

The data of the affected people by natural disasters and IDP by conflicts and violence are compiled from the year of 2006 to 2010. And, one variable is set as the accumulation of the data of the affected people by natural disasters and IDP by conflicts and violence.

All figures are organized by counties in the data set. If counties do not receive any resource from funds, or do not have the affected population by natural disasters or IDP by conflicts and violence, a cell of the data set is not filled by “zero (0),” but treated as a deficient value.

3. RESULTS

Table 2 in the next page provides summary statistics for eight variables used in the empirical analysis. The results of mean, median and standard deviation indicate that the figures in the data set are varied widely. Therefore, when correlation between variables is estimated, not only Pearson product-moment correlation coefficient as the parametric method, but also Spearman's correlation coefficients as the non-parametric method are calculated.

Table 3 illustrates the two types of the correlation analysis. The results of Pearson product-moment correlation analysis reveal that the relationship between the variable “Response” and “Recovery” has positive correlation and it is statistically significant. Also, the correlation between the variable “Recovery” and “Development 2” is statistically significant, but it is negative relationship.

Table 2: Summary statistics

Variable Name	Number of observation	Mean	Median	Standard deviation
1. Response (CERF)	79	23413201.00	9859577.00	33590169.89
2. Recovery (GFDRR Track-III)	22	432083.95	208807.00	629316.84
3. Development 1 (GFDRR Track-II)	43	1042211.19	730000.00	1154375.95
4. Development 2 (TFHS)	39	2682150.92	2399820.00	1507815.94
5. Development 3 (Sum of No.3 and No.4)	69	2165492.28	1504073.00	1739655.74
6. The affected people by natural disasters	98	10931646.51	546547.00	69111688.76
7. IDP by conflicts and violence	41	2719221.95	890000.00	5382081.61
8. Total affected number (Sum of No.6 and No.7)	100	11827894.58	806489.50	68487649.86

* The unit of figure for Response, Recovery, Development 1, Development 2 and Development 3 is US\$.

Table 3: Results of correlation analysis

Variables	Pearson product-moment correlation coefficient							
	1	2	3	4	5	6	7	8
1. Response	1.00	—	—	—	—	—	—	—
2. Recovery	.46 *	1.00	—	—	—	—	—	—
3. Development 1	.10	-.04	1.00	—	—	—	—	—
4. Development 2	.28	-.53 *	-.10	1.00	—	—	—	—
5. Development 3	.25	-.34	.64 ***	.91 ***	1.00	—	—	—
6. The affected people by natural disasters	-.01	.01	.04	-.04	-.07	1.00	—	—
7. IDP by conflicts and violence	.39 **	.07	-.08	.11	-.02	.03	1.00	—
8. Total affected number	.02	.01	.04	.07	-.07	1.00 ***	.41 ***	1.00

*** $p < .01$ ** $p < .05$ * $p < .10$

Variables	Spearman's correlation coefficients							
	1	2	3	4	5	6	7	8
1. Response	1.00	—	—	—	—	—	—	—
2. Recovery	.46 *	1.00	—	—	—	—	—	—
3. Development 1	.04	.14	1.00	—	—	—	—	—
4. Development 2	.10	-.48	-.09	1.00	—	—	—	—
5. Development 3	.03	-.31	.62 ***	.90 ***	1.00	—	—	—
6. The affected people by natural disasters	.35 ***	.05	.34 **	-.11	.02	1.00	—	—
7. IDP by conflicts and violence	.51 ***	-.20	.14	.06	-.04	.34 **	1.00	—
8. Total affected number	.54 ***	.04	.39 ***	.06	.10	.87 ***	.70 ***	1.00

*** $p < .01$ ** $p < .05$ * $p < .10$

The results of Spearman's correlation coefficients demonstrate that the relationship between the variable “Response” and “Recovery” has a positive correlation and it is statistically significant. On the contrary, the correlation between the variable “Recovery” and “Development 2” is not statistically significant.

In addition with these two types of the correlation analysis, partial correlation is calculated. In the partial correlation analysis, the variables “The affected people by natural disasters,” “IDP by conflicts and violence” and “Total affected number” are employed as control variables, since three variables have significant relationship with “Response.” The results of the partial correlation analysis shows that the significant and positive relationship between “Response” and “Recovery.” In the case between “Recovery” and “Development 2,” the relation is not observed statistically significant.

Table 4: Results of partial correlation analysis

Partial correlation coefficient	Control Variables		
	The affected people by natural disasters	IDP by conflicts and violence	Total affected number
by Response and Recovery	.46*	.53	.46*
by Recovery and Development 2	.12	-.99	-.54

*** $p < .01$ ** $p < .05$ * $p < .10$

4. CONCLUSION AND DISCUSSION

The relationship between resource allocation and development and the linkage of these three phases in humanitarian assistance is argued in this article. As the results of statistical analysis, only the linkage between response and recovery is verified. According to the results of Spearman's correlation coefficients, the variable "Response (CERF)" and "Development 1(GFDRR Track-III)" positively correlate with the number of the affected population by natural disasters, conflicts and violence. However, from the viewpoint of resource allocation, it is concluded that response and recovery do not significantly relate with development. Thus, it is considered that financial provision to each disaster phases are recognized as not a continuity process, but separated.

In order to verify the result of the paper, further inquiries are required to be done. This article presents a macroscopic trend at national level, but it is necessary to examine whether each projects or programs in specific sites have the linkage from response to development at field level.

Additionally, management of the funds is to be studied. In the field of global environment, transparency for management of Global Environmental Facility (GEF) has been severely discussed (Streck, 2001; Najam, 2005; Roberts et.al, 2007). Comparing with GEF, the total amount of funds for disaster is limited. However, it seems important particularly for recipient countries to investigate the transparency of the funds.

REFERENCES

- Boyd, E., Corbera, E., and Estrada, M., 2008, UNFCCC negotiations (pre-Kyoto to COP-9): what the process says about the politics of CDM-sinks, *International Environment Agreements*, Vol.8, 95-112.
- GFDRR, 2010, *Annual Report 2010*. http://www.gfdr.org/gfdr/sites/gfdr.org/files/publication/GFDRR_annual_report_2010.pdf [Accessed on 1st September 2011]
- Kasa, S., Gullberg, A.T., and Heggelund, G., 2008, The Group of 77 in the international climate negotiations: recent developments and future directions, *International Environment Agreements*, Vol.8, 113-127.
- Miller, Marian, A.L., 1995, *The Third World in Global Environmental Politics*. Buckingham: Open University Press.
- MOFA (Ministry of Foreign Affairs) of Japan, 2009, *The Trust Fund for Humanitarian Security: For the "Human-centered" in 21st century*. http://www.mofa.go.jp/policy/human_secu/t_fund21.pdf [Accessed on 1st September 2011]
- Najam, A., 2005, Developing Countries and Global Environmental Governance: From Contestation to Participation to Engagement, *International Environment Agreements*, Vol.5, 303-321.
- Najam, A., 2002. Unravelling of the Rio Bargain, *Politics and the Life Sciences*, Vol. 21, No.2, 46-50.
- Najam, A., 2004, Dynamics of the Southern Collective: Developing

Countries in Desertification Negotiations, *Global Environmental Politics*, Vol.4, No.3, 128-154.

Roberts, J. T., and Parks, B. C., 2007, *A climate of injustice global inequity, North-South politics, and climate policy*. Mass: MIT Press, Cambridge.

Streck, C., 2001, The Global Environmental Facility - a Role Model for International Governance?, *Global Environmental Politics*, Vol.1, No.2, 71-94.

Williams, M., 1997, The Group of 77 and Global Environmental Politics, *Global Environmental Change*, Vol.7, No.3, 295-298.

Development and application of triage system (TRACY)

Muneyoshi NUMADA¹, Yasunori HADA², Miho OHARA³
and Kimiro MEGURO⁴

¹ Research Associate, ICUS, IIS, The University of Tokyo, Japan
numa@iis.u-tokyo.ac.jp

² Associate Professor, Department of Education Interdisciplinary Graduate
School of Medicine and Engineering, University of Yamanashi, Japan

³ Associate Professor, ICUS, IIS, The University of Tokyo, Japan

⁴ Professor, ICUS, IIS, The University of Tokyo, Japan

ABSTRACT

This research developed an IT triage system for collecting disaster medical information in real time and sharing it among related institution in entire area. FeliCa card and card-reader are used to constitute of this system to obtain the number and condition of patients etc. in real time.

There are advantages by applying FeliCa on the daily basis to the triage. For example, the database of the personal information such as name, date of birth and address for the daily service can be applied for the triage to recognize the each patient in the disaster by using FeliCa ID. In this case, the hospital is not required to ask the patient for the personal information and can be understand the patient personal data who cannot speak due to heavy injury. As there are many people who have the FeliCa for daily service, therefore hospitals are not necessary to ready the FeliCa card in advance for all unpredictable large number of patients.

The unique serial number of FeliCa can be considered as the patient ID. Therefore the hospitals and other related institution can easily share and manage the patient transfer by using FeliCa ID for the entire region.

FeliCa reader and PC for pass-processing are set at triage zone and each zone such as Black (deceased), Red (immediate), Yellow (delayed) and Green (minor), and the department of medicine and radiation. PC and FeliCa reader at the each point for pass-processing can record the patient's zone pass time and location in the database server.

In the case for example, that the symptoms of patient is changed to the worse, the latest triage level can automatically be update in database server without special work or operation by conducting the usual pass processing in this system. This is same case, even if the symptoms improve.

A disaster drill was held at the Yamanashi University Hospital with 450 participants. TRACY was examined its availability and practicability by using in this drill. From the result of that, the present system can obtain the

number of patients for each triage level and the accepted number of patients in each diagnosis and treatment department in real time, including response for changing triage level and the people looking for their family in hospital. In the point of the information sharing in the entire area, the patient's information can be shared among hospitals, the administration, and residents in real time.

Keywords: *triage, disaster management in hospital, TRACY, real-time information, information sharing*

1. INTRODUCTION

Disaster medical care during accidents and disasters both large and small is carried out with less medical resources in normal situations.

Disaster medical care consists of triage, transport and treatment. In the case of a disaster or accident, it is necessary to exert maximum effect with limited medical resources, but to accomplish these hospitals need to estimate the expected number and condition of patients. The advancement of triage, including understanding and ensuring the capacity of beds, tracking the status of patients' visits and transport to other hospitals, managing the assignment of the appropriate medical staff and the distribution of medical materials is necessary. On the other hand, information sharing is important effective acceptance and transportation. These actions are required across the entire region outside the hospital for setting up the disaster headquarters, coordinating all tasks with the government and other hospitals, and supporting the patients' family and media.

To advance the triage, it is necessary to obtain patient information, such as the victim's status and number staying at hospital, discharging from hospital, and being transported to other hospital, in digital form and in real time.

Research using a digital pen with triage results can digitize patient information (Ashida et al. 2008). However, it is difficult to manage patient status when triage level is changed and to understand the number of patient in different triage levels. In addition, the usage of RFID tags and mobile RFID network equipment collection system can collect the patient information using mobile devices in real time (Sonoda et al. 2007, Kusuda et al. 2009), but it is necessary to overwrite data when the triage level is changed so the management is complicated. Furthermore, the flow line of patients cannot be confirmed when patients are moved between departments. For information sharing across an entire region, an information sharing system has been built to consolidate all kinds of information related to disaster conditions (The Ministry of Health and Welfare Health Policy Bureau 1996). With this system, staffs are necessary for entering the data in this system, but it is difficult to assign staff under the limited conditions during a disaster.

The purpose of this study is to develop a triage system which can collect and share the disaster medical information in real-time among hospitals including emergency medical institution both inside and outside the disaster area, with residents and with the government. In order to examine the feasibility and effectiveness of this system, it was applied to a large-scale disaster drill with 450 participants at the Yamanashi University Hospital.

Using this system, it is possible to estimate the number of patients in different triage levels in real time, to identify the number of patients visiting each department, to manage the triage level changes in real time and to share this information with related institutions across an entire region including people looking for their family in hospitals.

2. PROBLEM SETTING

Traditional triage problems are summarized from the result of the triage drill held at Yamanashi University Hospital.

2.1 Summary of triage

A triage team normally consists of the triage officer, nurse and support staff. The team conducts the triage in front of the hospital building. Patients taken to the triage are transferred to the treatment zones: the mild zone (green), the moderate zone (yellow), the severe zone (red) and death zone (black), depending on the level of injury. If the hospital cannot treat the patient with heavy injuries or due to lack of resources, the patient is transferred to another other hospital.

2.2 Triage problem

The following problems with the current triage method were obtained from the result of the triage drill at Yamanashi University Hospital.

2.2.1 Real-time information

It takes a certain amount of time for the disaster headquarters to know the latest patient information such as the number of accepted patients and the number of patients in the different triage levels because the copy of the current triage tag containing patient information such as name, age, etc. and triage level is carried by volunteer staff to the headquarters after a certain amount of information is collected in each zone. Furthermore, it takes time to copy the information to the patient's list handwriting one by one. In addition, patient information is written on a white board in front of the hospital near the triage zone to for people looking for their family in hospitals.

Therefore, it is difficult to grasp the number of patients in real time and assign the proper medical staff to the each zone in this triage method. When there is a change of triage level, the management of its change is very

difficult to update in real time. Also, some staff needs to work only for the management of patient's list. It can be wasted work under the limited resources of medical staff in the disaster.

2.2.2 Information sharing with other medical institutions

It is necessary to determine that; the patient needs to be transferred to other hospitals by such as the doctor helicopter, because of the heavy status of patient or the lack of hospital's resources. However, hospitals which need to transfer the patient cannot make a plan of transference of patient. Because hospitals don't know which other hospitals can accept the patient. On the other hand, the accepting hospital management also doesn't understand the status of coming patients.

The information sharing among related medical institutions is necessary for the effective transport in the entire region.

2.2.3 Information sharing with the family and government

The people look for the location of hospital in which their family is accepted due to the injury in the disaster. The hospital and the government asked by the people need to answer the location of hospital and the status of the family.

However, immediate response is difficult for the hospital in a situation of a huge number of patients. Because they cannot search the patient whom the family looking for in the paper-based patient's information and it takes a certain time to obtain the latest information.

In the point of the local government, even if the government needs to find the family where they are, the local government has to ask the possible hospitals one by one.

This situation is inefficient for all the relations, the family, the hospital and the government.

3. IT TRIAGE SYSTEM (TRACY)

TRACY has been developed as the triage system to solve the traditional problems observed in the result of triage drill and the things discuss as mentioned above. The structure and framework of this present system has been set after several interview and meetings with doctors and nurses in emergency department. This section describes the overview of this system.

3.1 System framework

We discussed the obtaining patient's information in real time and the sharing it in the whole area as main features. The obtained patient's information including the location, triage level and status of patient need to be updated in real time. It is effective and efficient to share the information for the patient transference to the other hospital. On the other hand, there are some advantages in traditional triage tag. When we need to know the

patient's information such as name, age and triage level, the current triage tag can show those by seeing it without special operation. Therefore, both present system and current paper based triage tag are used.

We discussed when the triage level change the information about triage level also should be changed without special operation of the system in real time. If there is a change of triage level of the patient such as patient moves to the new triage zone. When the patient arrive the entrance of the new zone, we proposed that the change can be recorded by the usual pass-processing used in present system. This method can update the triage level automatically without special and/or additional work. This method also can confirm the movement of the patient correctly.

To respond quickly to the people who are searching for their family member in the hospital, the staff can search the patient by using the search function of present system in the patient list. In addition, if the list can share in the whole area, it is beneficial for the government and the family living far from disaster area.

We discussed that it is important to conduct the effective transporting in the entire region. This could be done by understanding the condition of accepting patients in other hospital and then to decide whether the transporting is available. Therefore, the present system is required to show the condition of all related hospitals to decide the available transportation in the entire region.

3.2 Discussion of equipment

The following three points in selecting the equipment for this system were considered. 1) Using the equipment on a daily basis, because other than daily-life equipment does not work in a disaster. 2) Using low-cost equipment in order to spread to the lot of hospitals under the current economic condition for sharing information in entire area. 3) Using simple-operating equipment that is not required the special training for operation only for the disaster.

First, we discussed a handheld wireless UHF IC tag reader/writer that can write the patient information to the tag. But when the medical staff try to know the patient's information in the IC tag, the special operation is required. In addition to that, for the sharing information of patient in the entire area, same equipment is necessary to install in all related hospitals. In the consideration of cost, the writing function of the patient information to IC tags/cards is not the low-cost option.

Therefore, the concept of this system is to manage the patient's information in the server side. Then, the three method, IC tag, bar codes and FeliCa, were discussed how to recognize the patient ID. The IC tag is expensive, even for the models without the function of a tag writer. For bar codes, we have to consider the accuracy of reading the bar code, the preparation of bar codes in advance and the problem of cost. As the result of

these factors, the bar code is actually difficult to apply to the management of patient for triage. For FeliCa, USB-friendly FeliCa reader can be purchased at lower prices. It is available to use the PC, which is used on the daily treatment in hospitals, for connecting it. In addition, FeliCa cards are used by a lot of people for the train pass, student ID, and electronic money on a daily basis. Recently, there is also mobile phone with a FeliCa function. Therefore, FeliCa can be applied on a daily basis to conduct the triage in the disaster. The operation is simple "waving the card to the reader" and there is potential to be expanded further spread.

From the above discussions, FeliCa is used as the configuration of the equipment in this system.

3.3 Constitution of "TRACY"

There are advantages by applying FeliCa on the daily basis to the triage. For example, the database of the personal information such as name, date of birth and address for the daily service can be applied for the triage to recognize the each patient in the disaster by using FeliCa ID. In this case, the hospital is not required to ask the patient for the personal information and can be understand the patient personal data who cannot speak due to heavy injury. As there are many people who have the FeliCa for daily service, therefore hospitals are not necessary to ready the FeliCa card in advance for all unpredictable large number of patients.

The unique serial number of FeliCa can be considered as the patient ID. Therefore the hospitals and other related institution can easily share and manage the patient transfer by using FeliCa ID for the entire region.

Figure 1 shows an overview of this system. FeliCa reader and PC for pass processing are set at triage zone and each zone such as Black (deceased), Red (immediate), Yellow (delayed) and Green (minor), and the department of medicine and radiation. PC and FeliCa reader at the each point for pass processing can record the patient's zone pass time and location in the database server.

In the case for example, that the symptoms of patient is changed to the worse, the latest triage level can automatically be update in database server without special work or operation by conducting the usual pass processing in this system. This is same case, even if the symptoms improve.

3.4 Content of input item

We consider following kinds of information are necessary for triage in TRACY.

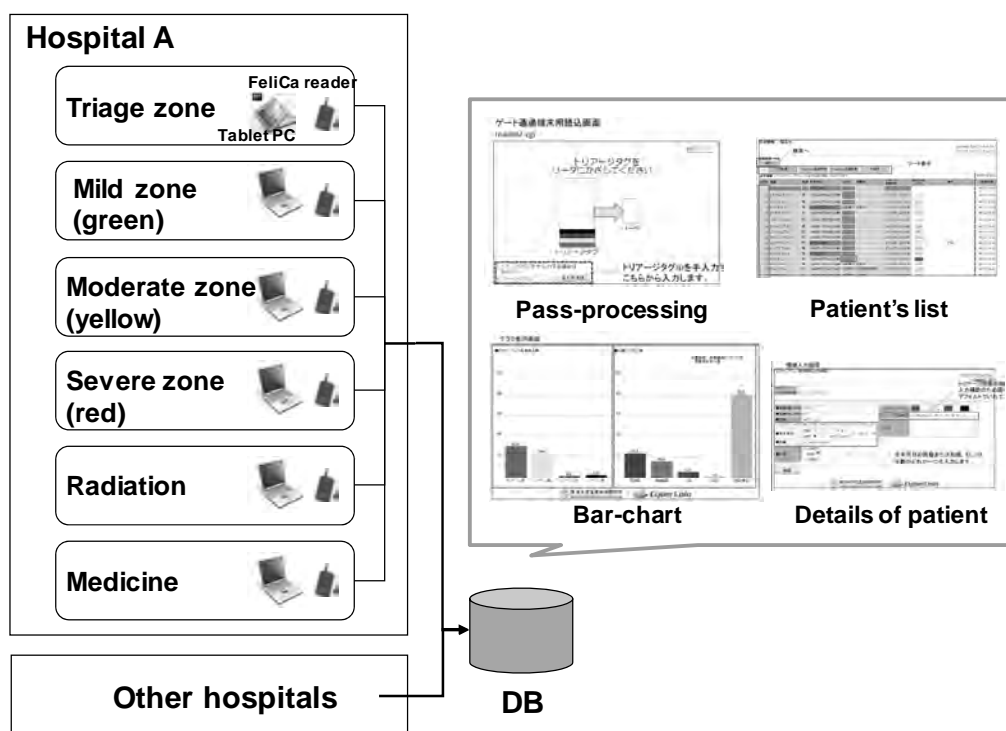


Figure 1: Overview of triage system “TRACY”

From the hospital point of view, patient personal information and medical information are taken in to account as patient detail. But this triage system only covers the personal information (name, gender, date of date, etc.) but not medical information. Because misunderstood medical information may lead to medical errors and troubles.

As the result, input items of personal information such as name, date of birth, age, address, and free entry for the remarks are read with the triage tag. One example of using remarks is to write the patient exterior features such as the color of shirts, jacket, glass etc. to identify an individual who cannot speak due to heavy injured.

There is high possibility to stay or transfer to other hospitals for the patient with the level of Red (immediate) and Yellow (delayed). In case of those, the room or building of staying and the hospital name of transferring can be entered in this system.

The interface of the personal information window was made considering easy to be used by hospital staffs.

3.5 Visualization of patient data at the headquarters

It is important for the forward-command-headquarters directing the assignment of medical staff and the emergency-response-headquarters to take a proper action to manage the triage work based on understanding the situation such as the number of current accepted patients in the hospital, the number in the different triage level for each treatment zone in real time.

We discuss how to show those data in present system. As the result, the bar-chart showing the patient number in different triage level and the all patient list are necessary to analyze the condition of hospital for the triage officer at the both headquarters. The chart and the list can be updated automatically every 5 seconds. When the patient's information is needed to edit, the details window of patient is available from the list of patient.

3.6 Preparation System

When a disaster occurs, the system must quickly starts with a minimum preparation of work as much as possible.

The present system is developed on the CGI (Common Gateway Interface). This system can work by the PC which can use WEB browser, is independent of PC type, and doesn't need any additional installation. The CGI program that runs on the WWW-server is independent of PC type/ OS and it can be work by the access form the browser of PC for pass-processing at the each zone. The result of the working of CGI returns to the browser of each PC at the zone.

As mentioned above, the digitize the patient information by FeliCa in real time can achieve not only the advancement of triage such as tracing of the patient treatment but also the sharing patient's information such as the transfer to the other hospitals, quick response to the person who asking of his/her family's location and coordination with the administration for the entire region.

4. VERIFICATION OF TRACY BY DEPARTMENT OF YAMANASHI UNIVERSITY HOSPITAL

The Yamanashi University Hospital in Yamanashi prefecture has experienced the triage drill since 2001. This triage drill becomes 10 times in total. The purpose of this drill is that the hospital staff makes accurate safety, accept the patient, implement triage and handle the treatment when the big earthquake occurs in Yamanashi prefecture.

The present triage system, TRACY, was examined its availability and practicality in the real disaster by applying the triage drill on this hospital with enough experience.

4.1 Triage drill of Yamanashi university hospital

In this triage drill, 48 doctors, 21 medical engineers, 48 nurses, 47 office staffs, 145 patients and support staff, totally approximately 450 people were attended. Participants were not only from this hospital, but also from the other hospital, the fire station, the government of Yamanashi Prefecture, the government of Kofu City, the government of Central City and residents.

The drill assumes the disaster level that, there is damage in the hospital building, but the lifeline and other medical equipment work normally. Therefore the triage and treatment are available even for a large number of visiting patients.

At 9:00 am a big earthquake with the epicenter of the west and southern area in Yamanashi prefecture caused a damage of houses, a fire and a traffic accident around the hospital. Then the staff in the hospital checks the status of the building damage and secures the safety of responsible department based on the disaster manuals and according to the instruction of the leaders of each department. All staff prepares to accept the number of patients as soon as possible. The team of triage set the necessary materials in the front of hospital building and to decide the triage level of each patient on the symptoms. After triage, the patient moves to the triage zone or is transferred to other hospital depending on the triage level.

4.2 Outline of installation of system

The PC set at Triage area in the front of hospital building, each triage zone, each treatment department and headquarters. Figure 2 shows the PC and FeliCa reader set at Department of Radiology. FeliCa cards is adhered to the back of triage tag, and managed to integrate triage tag and FeliCa cards together. As the reader of FeliCa card, the FeliCa port/ pasori (RC-S320) which is compatible with USB was used.

In this triage drill, FeliCa card has not been entered personal information such as name and date of birth, and assuming a situation in which these information was enter at the hospital. As for the timing and the person who enter the personal information, the patient information is input at the upstream process of triage to answer the person who asking from patient family as soon as possible. The special person who only input the patient data are assigned beside the doctors, nurses, clerks separately. By this way it can solve the problem that the patient cannot move during the entering their triage result or personal information in present system. In the case of a large number of patients compared with the number of staff for data input, even if all the data entering is not completed, the personal data can be registered on a temporary basis, and then all staff can modify or update the content of the personal data at the each triage zone or headquarter. All four triage teams consisted of triage officer (doctor), nurse and support staff (clerk) at the triage area.

The triage officer and nurse carry out usual triage work same as traditional triage way. On the other hand, the clerk read the FeliCa card to recognize its ID by Felica reader connected to the mobile PC by USB. Then clerks give the triage tag to triage officer, when just before triage officer begin to conduct triage. In this time, the only patient ID is input in the database.

After finishing triage, the clerk brings the first piece of triage tag (copy the paper written patient's information by triage officer) to the data-input-desk. Then the staff at the data-input-desk enters the patient's information such as the name, date of birth, age, address, remarks by reading the copy paper in the present system.

On the other hand, the patient who finished the triage moves to the each treatment zone. When the patient arrives at the zone entrance, the FeliCa card is read by the FeliCa reader to record the location and the time automatically as the pass-processing. This is same way for the other zone or department where the PC for the present system is set.

Thus, even if there is a change of triage level, it is possible to conduct the same pass-processing at the new place. The new triage level can be updated in the present system automatically in this way.

4.3 Result

Time history of the patient changes: Figure 3 shows the time history of each patient's triage level, taking the patient in the vertical axis and time in the horizontal axis. The staff in medical institute and the government can understand the triage level of all patients from the time when the patients are received in hospital to discharge from the hospital by following time history. The change of triage level also can be understood in this figure.



Figure 2: PC and FeliCa reader set at Department of Radiology

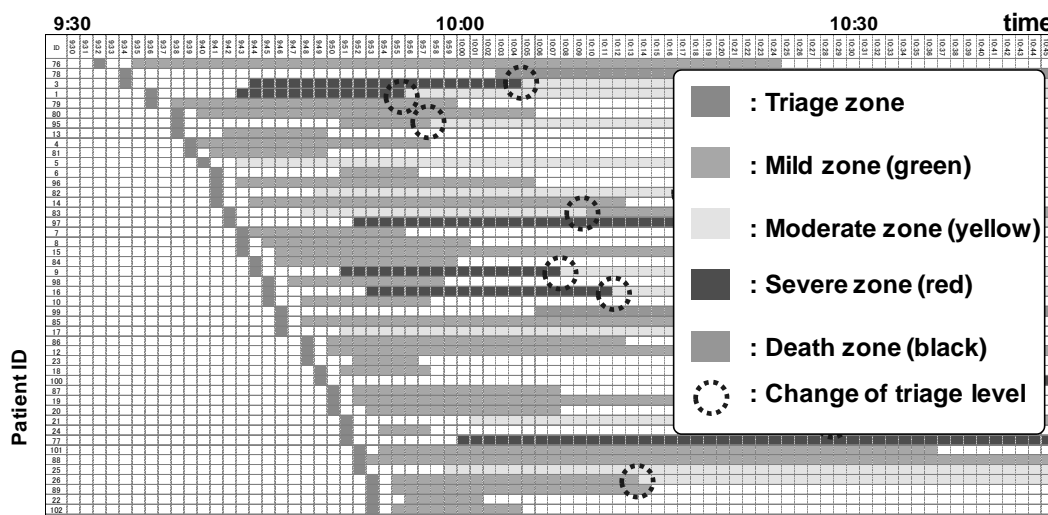


Figure 3: Time history of patient triage level

The forward-command-headquarters directing the assignment of medical staff could take a proper action to manage the triage work based on understanding the situation such as the number of current accepted patients in the hospital, the number in the different triage level at each treatment zone in real time provided by the present system.

The family of patient visits to the hospital, which can be considered as that the family stays to look for patient status and location. However, immediate response is difficult for the hospital in a situation of a huge number of patients. Because they cannot search the patient, for whom the family is looking for in the paper-based patient's information. By using the key-word search function in the present system in this drill, the all staff in hospital can search immediately the patient they are looking for.

5. CONCLUSION

This research developed an IT triage system for collecting disaster medical information in real time and sharing it among related institution in entire area. Felicia card and card-reader are used to constitute of this system to obtain the number and condition of patients etc. in real time.

A disaster drill was held at the Yamanashi University Hospital with 450 participants. TRACY was examined its availability and practicability by using in this drill. From the result of that, the present system can obtain the number of patients for each triage level and the accepted number of patients in each diagnosis and treatment department in real time, including response for changing triage level and the people looking for their family in hospital. In the point of the information sharing in the entire area, the patient's information can be shared among hospitals, the administration, and residents in real time.

The feedback and opinions were widely obtained from the entire evaluation meeting and the meeting with the mainly triage officer held after the triage drill.

These discussions are implementing to increase more practical level in the next drill. We will expand and examine TRACY according to the result obtained this triage drill.

ACKNOWLEDGEMENTS:

The authors acknowledge complete cooperation from the Department of Medicine at Yamanashi University hospital. This cooperation makes possible to develop and examine the present system. Especially, the authors got the valuable advice about system function and structures from Professor Kenichi Matsuda and Dr. Shoji Suzuki as a specialist of the emergency medicine. The authors also acknowledge support from the Japan Ministry of Education, Culture, Sport, Science, and Technology (MEXT) for development of present system.

REFERENCES:

Kusuda, J., Kiyama, N., Utiyama, A., Hiromori, A., Umedu, T., Yamaguchi, H. and Higashino, T. (2009), "Design and Development of Electronic Triage System Using Wireless Sensor Networks," The Institute of Image Information and Television Engineering Technical Report, Vol.33, No.36, 33-38.

Ashida, H., Takeshima, S., Wakisaka, H., Ueki, T., Yamamoto, T., Karasawa, K., Inaba, T., Tsuji, K., and Komura., T. (2008) , "A data input system for triage tag information using a digital pen: a training program for acceptance of a massive number of injured people at the Japan Self Defense Force Central Hospital," Japanese Journal of Disaster Medicine, 13(1), 56-60.

Sonoda, A., Inoue, S., Oka, K., and Fujisaki, S. (2007), "Experiment of Large Scale Triage with RFID Tags," Transactions of Information Processing Society of Japan, 48(2), 802-810.

The Ministry of Health and Welfare Health Policy Bureau (1996), "Disaster health care system of the 21st century - Ideal way of medical treatment offered to disaster," Herusu Shuppan, Co. inc., 25-48.

Shimora,H., Matsui, H., Noda, I. (2009), "Cooperation of Disaster Related Systems on Distributed System Architecture," Journal of JAEE, 9(2), pp.61-72.

The National Institute of Advanced Industrial Science and Technology (AIST) , "DaRuMa," <http://sourceforge.jp/projects/daruma/>

Yamanashi Prefecture HP : Base disaster Hospital , <http://www.pref.yamanashi.jp/ft-hokenf/60475114366.html>

Alkali-silica reaction in cement mortar with waste glass as fine aggregates

Kiang Hwee TAN¹ and Hongjian DU²

¹Professor, Department of Civil and Environmental Engineering,
National University of Singapore, Singapore
tankh@nus.edu.sg

²PhD Candidate, Department of Civil and Environmental Engineering,
National University of Singapore, Singapore

ABSTRACT

The alkali-silica reaction (ASR) in cement mortar containing waste glass was investigated using ASTM Standard C 1260. Mortar bars, consisting of cement, natural sand and waste glass in various proportions, were placed in a concentrated (1 N) sodium hydroxide solution at 80°C and removed for length measurements at intervals for up to 28 days. Green and brown glasses were studied together with two mitigating methods commonly used to control ASR in normal concrete. One method was to replace cement with pozzolans, that is, 30% by fly ash, 60% by ground granulated blast furnace slag (GGBS), or 10% by silica fume, while the other was to restrain the ASR expansion by the addition of 1.5% by volume of plain short steel fibers, or 1.0% by mass of lithium compounds. For each test parameter, the glass content was varied from 0 to 100% of the total aggregate content. Test results showed that ASR expansion decreased with increasing glass content, due to the non-swelling nature of the formed ASR gel. All glass mortar mixes showed ASR expansion less than 0.1% at 14 days, and are therefore considered as innocuous. Fly ash and GGBS were the most effective in further mitigating ASR expansion.

Keywords: *alkali-silica reaction; cement mortar; fine aggregates; mitigation methods; waste glass.*

1. INTRODUCTION

In recent years, there have been increasing global concerns on the sustainability of building materials, especially in view of the depleting natural resources and associated environmental issues. Concrete, a building material, is the second most consumed commodity after water. To ensure sustainable development, the concrete industry has continued to increase the use of recycled materials, including industrial byproducts, and explore the development of innovative cements and concrete mixtures.

At the same time, the reuse and recycle of urban waste has drawn increasing attention due to limited landfill for its disposal. Among the solid waste, glass is considered suitable for construction use, because of its

physical characteristics and chemical composition. Previous investigations have indicated that waste glass may be used in concrete provided that the potential deleterious expansion, caused by alkali-silica reaction (ASR) between silica in glass and alkali which is produced as a result of hydration of cement, could be mitigated (Jin *et al.* 2000; Park & Lee 2004; Park *et al.* 2004; Shi 2009; Taha & Nounu 2008; Taha & Nounu 2009; Topcu & Canbaz 2004; Topcu *et al.* 2008).

In this study, the effects of glass color and content on ASR in cement mortar were investigated and reported. Also, two ASR mitigation methods, that is: (1) by cement replacement by fly ash, GGBS, or silica fume; and (2) by adding discrete steel fibers or lithium compounds; were examined using both green and brown glass mortar with different sand to glass replacement ratios, and the results are discussed herein.

2. MATERIALS AND TEST METHODS

2.1 Materials

Type I ordinary Portland cement (OPC), with alkali content of 0.6% [that is, $(\text{Na}_2\text{O})_{\text{eq}} = \text{Na}_2\text{O} + 0.658\text{K}_2\text{O}$], was used. The chemical composition was analyzed according to ASTM C 150 and shown in Table 1. The waste glass used in this study was crushed from soda-lime glass bottles, that is, beer bottles, after they were washed with tap water. It was reduced into smaller particles complying with the requirement of fine aggregates as per ASTM C 33 using a jaw crusher. Both green and brown glasses were used. The chemical compositions of the waste glass and natural sand are summarized in Table 2. For the purpose of testing for ASR in accordance with ASTM C 1260, both the waste glass and natural sand were prepared with percentages of 10, 25, 25, 25 and 15% passing/retained on sieve sizes 4.75/2.36, 2.36/1.18, 1.18/0.6, 0.6/0.3 and 0.3/0.15 mm respectively.

Table 1: Chemical compositions of cement, fly ash, GGBS and silica fume

Composition, %	Cement	Fly ash	GGBS	Silica fume
SiO ₂	20.8	38.9	32.2	96.0
Al ₂ O ₃	4.6	29.2	12.9	0.28
Fe ₂ O ₃	2.8	19.6	0.36	0.32
CaO	65.4	2.5	40.7	0.16
MgO	1.3	2.1	6.05	0.37
SO ₃	2.2	0.19	4.95	0.18
Na ₂ O	0.31	0.26	0.28	0.05
K ₂ O	0.44	0.48	0.51	0.57

Class F fly ash, GGBS and silica fume were used as ASR suppressors, at 30%, 60% and 10% of cement by mass, respectively. The chemical compositions of these supplementary cementing materials are shown in Table 1. Plain, smooth steel fibers, with a diameter of 0.16 mm and length of 50 mm, was added at 1.5% by volume of mortar as an ASR mitigation

method. Also, solid lithium chloride and lithium carbonate was dissolved in water and added as chemical admixtures, at the dosage of 1% of cement content by mass, to act as ASR suppressors.

Table 2: Chemical compositions of waste glass and natural sand

Composition, %	Green Glass	Brown Glass	Sand
SiO ₂	71.2	72.1	88.5
Al ₂ O ₃	1.63	2.19	1.21
Fe ₂ O ₃	0.32	0.22	0.76
CaO	10.8	10.5	5.33
MgO	1.57	0.72	0.42
Na ₂ O	13.1	13.7	0.33
K ₂ O	0.64	0.16	0.31
TiO ₂	0.07	0.10	0.05
Cr ₂ O ₃	0.22	0.01	—

2.2 Mortar mixtures and test method

The reference mortar comprised cement, natural sand and water mixed in the ratio of 1: 2.25 : 0.47 by mass, as specified by ASTM C 1260. Other mixtures with natural sand replaced with green or brown waste glass sand at 0, 25, 50, 75, and 100% were prepared. For each glass mortar mixture, the ASR mitigation methods mentioned in section 2.1 were investigated. For each test parameter, three 25 mm × 25 mm × 285 mm mortar bars were prepared. They were demolded 24 hours after casting and placed in water at 80 °C for the next 24 hours. The initial lengths of the mortar bars were then recorded before they were immersed in 1N 80°C NaOH solution. The expanded lengths were subsequently measured after 2, 4, 7, 10, 14, 21 and 28 days. According to ASTM C 1260, expansion larger than 0.2% at 14 days is considered potentially deleterious while less than 0.1% is innocuous. However, for mortars with pozzolans such as fly ash, the ASTM C 1567, which states 0.1% as the threshold value for potentially deleterious expansion, should be followed.

3. TEST RESULTS AND DISCUSSION

3.1 Effect of glass color and content

Mortars with different glass sand contents showed larger ASR expansion with time, as shown in Figure 1. Both green and brown glass mortars exhibited smaller ASR expansion compared to natural sand mortar (i.e., mortars with 0% glass). According to Jin *et al.* (2000) and Park and Lee (2004), green color glass would be the least reactive in ASR due to its high content of Cr₂O₃, which is added to give the greenish color. Compared to green glass, brown glass exhibited similarly small ASR expansion although it has a smaller content of Cr₂O₃. The reason might be due to the Fe₂O₃ in brown glass which is added to produce the brownish color. Based on the double-layer theory (Prezzi *et al.*, 1997), the higher valence of Cr³⁺

ions in green glass and Fe^{3+} ions in brown glass could reduce the double-layer thickness and the repulsion forces, resulting in much lower ASR expansion.

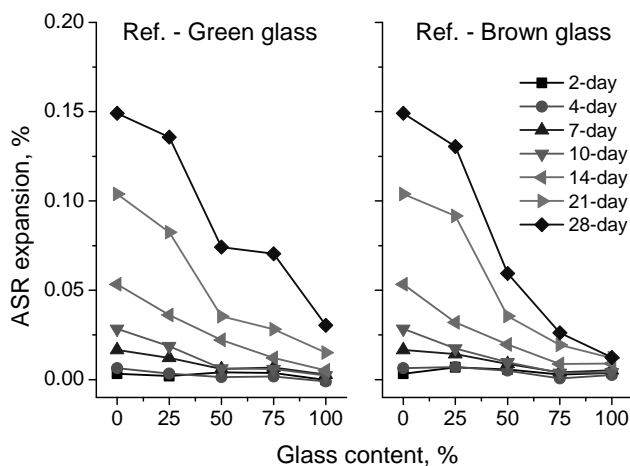


Figure 1: ASR expansions of glass sand mortars

The reduction in ASR expansion in mortar with higher glass sand content was quite apparent, for both green and brown glass. At 14 days, the natural sand mortar exhibited an expansion of 0.053%, indicative of non-reactive aggregates. The ASR expansions of green and brown glass mortar were 0.036, 0.022, 0.012, and 0.005%; and 0.032, 0.020, 0.009, and 0.009%, for glass replacement contents of 25, 50, 75, and 100%, respectively. All glass mortars showed ASR expansions less than 0.1% at 14 days, and less than 0.2% at 28 days. These results indicated that the glass sand may be not reactive in ASR, at least within 28 days, which is also supported by the findings of Zhu *et al.* (2009).

3.2 Effect of supplementary cementing materials

The effect of replacing cement with fly ash, GGBS or silica fume on ASR expansion is discussed.

3.2.1 Cement replacement by fly ash

The results of ASR expansions of glass sand mortars with 30% of cement content replaced by fly ash are shown in Figure 2. Fly ash could significantly reduce the ASR expansions at all sand replacement ratios, regardless of glass color. Moreover, the ASR expansion generally decreased with increasing glass sand content. All mixes showed expansion less than 0.015% at 14 days. For brown glass mortar in particular, the fly ash effectively reduced the expansion rate after 14 days. The ASR suppressing effect of fly ash could be explained by the pozzolanic reaction between fly ash and cement hydration product, $\text{Ca}(\text{OH})_2$. The fly ash would consume the OH^- ions and lower the pH value of the pore fluids in cement paste, thereby reducing the aggressive reaction with acidic aggregates and resulting in smaller negative charges on the surface of the glass particles [Prezzi *et al.* 1997]. Furthermore, due to the pozzolanic reaction, the

microstructure of cement paste, especially the interfacial transition zone (ITZ) could be enhanced. The ingress of OH ions, which is necessary for ASR gel to form and swell, could be reduced due to the decreased porosity and permeability of cement paste.

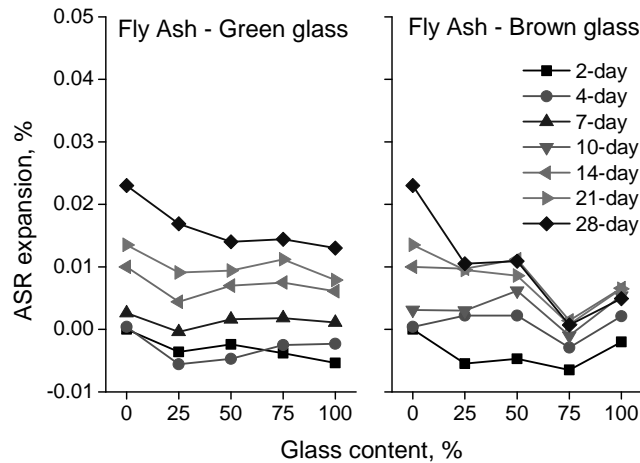


Figure 2: ASR expansions of glass sand mortars with 30% fly ash

3.2.2 Cement replacement by GGBS

As supplementary cementing materials, the ASR suppressing mechanism of GGBS is the same as fly ash. The ASR expansions of mortars with 60% of cement content replaced by GGBS are shown in Figure 3. All the mortar mixes showed ASR expansion less than 0.02% at 14 days and less than 0.05% at 28 days, indicative of the effectiveness of GGBS as a suppressor. The ASR expansion generally decreased with increasing glass content, regardless of the glass color.

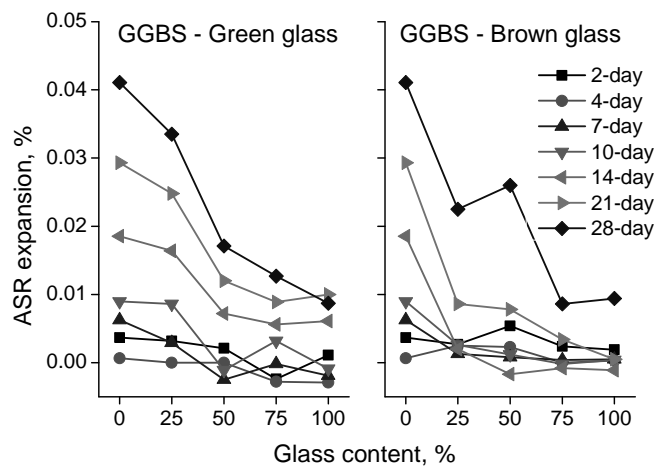


Figure 3: ASR expansions of glass sand mortars with 60% GGBS

3.2.3 Cement replacement by silica fume

The ASR expansion of glass sand mortar with 10% of cement content replaced by silica fume is shown in Figure 4. The purpose of silica fume in normal concrete is to obtain high strength, since the super fine particle size

of silica fume could substantially improve the microstructure of concrete at the ITZ. Due to the same reason, silica fume could be used as an ASR suppressor in glass mortar and proved to be effective in this study. Compared with fly ash and GGBS, silica fume showed slightly less effectiveness in restraining ASR expansion. All the mortars with silica fume showed expansions less than 0.04% at 14 days and less than 0.06% at 28 days.

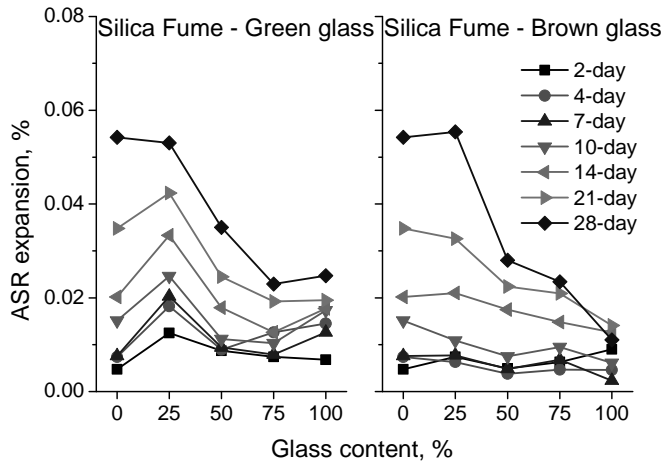


Figure 4: ASR expansions of glass sand mortars with 10% silica fume

3.3 Effect of additive materials

The effect of adding short, discrete steel fibers and lithium compounds on ASR expansion is discussed herein.

3.3.1 Addition of steel fibers

To prevent substantial loss in the flow of mortar, smooth steel fibers were used rather than deformed or hooked steel fibers. The test results for glass mortars with 1.5% of steel fibers are shown in Figure 5. All the mortar mixes showed expansion less than 0.03% at 14 days and less than 0.09% at 28 days. The steel fibers could prevent the ASR expansion by reducing the internal pressure caused by swelling ASR gel, and improving the tensile characteristics of the mortar. The ASR expansion also decreased with higher content of glass sand.

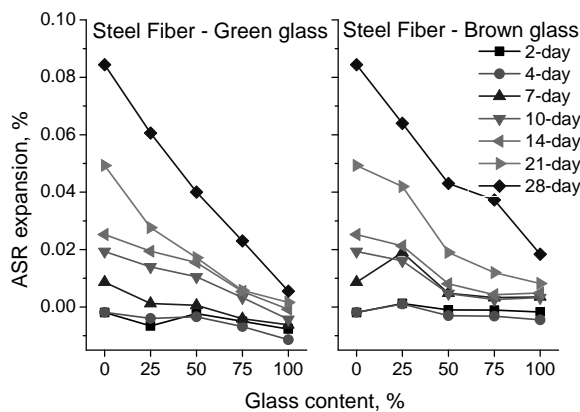


Figure 5: ASR expansions of glass mortars with 1.5% by volume of steel fibers

3.3.2 Addition of lithium chloride and lithium carbonate compounds

The ASR expansions of mortars with added LiCl and Li₂CO₃ compounds are shown in Figures 6 and 7, respectively. The amount of lithium compounds was 1% by mass of cement content. The restraining effect of LiCl compound was lesser than that of Li₂CO₃ compound due to the smaller ratio of [Li]/[Na], which has been found to be the key factor in restraining ASR expansion [Lumley 1997]. The [Li]/[Na] ratio for 1% LiCl and Li₂CO₃ compounds is 0.74 and 0.84, respectively.

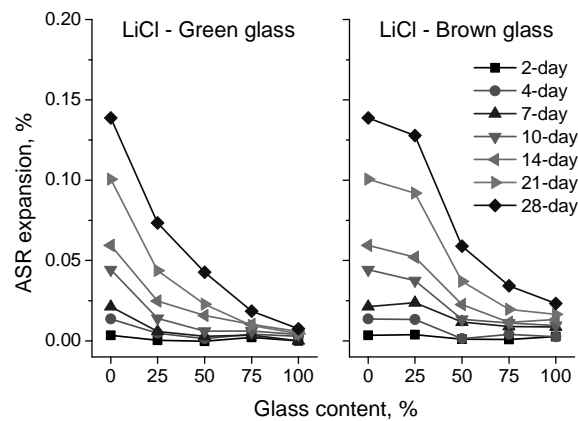


Figure 6: ASR expansions of glass sand mortars with 1% LiCl

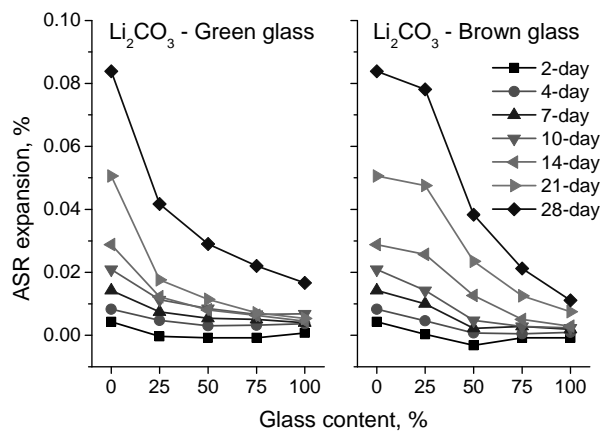


Figure 7: ASR expansions of glass sand mortars with 1% Li₂CO₃

At 14 days, brown glass mortars with 1% LiCl showed higher ASR expansions than the reference natural sand mortars regardless of the glass sand content, indicative of insufficient amount of lithium compound (also see next section). However, at 21 and 28 days, they exhibited slightly less expansion than the reference mortars, when the glass content was less than 50%. The ASR suppressing function of LiCl compound in green glass mortars as well as of Li₂CO₃ compound in both green and brown glass mortars was more obvious. The ASR mitigation mechanism of lithium compounds is not well established. It is expected that lithium compounds could change the natural and chemical compositions of the ASR gel and reduce the solubility of the reactive silica. The possibility of dissolved silica

to be repolymerised and the expansive ability of ASR gel would be subsequently reduced [Taha & Nounu 2009].

3.4 Comparison of different ASR mitigation methods

ASR expansions of glass mortars, with different mitigation methods, at 14, 21 and 28 days, are shown in Figures 8 and 9. For green glass mortar, all mitigation methods resulted in reduced expansion to a certain extent except with silica fume in 100% glass sand mortar at 14 and 21 days. For brown glass sand mortars, slightly larger expansions than the reference mortars were observed with LiCl compound at 14 days as discussed earlier and with steel fibers at 28 days for glass content of 75 and 100%.

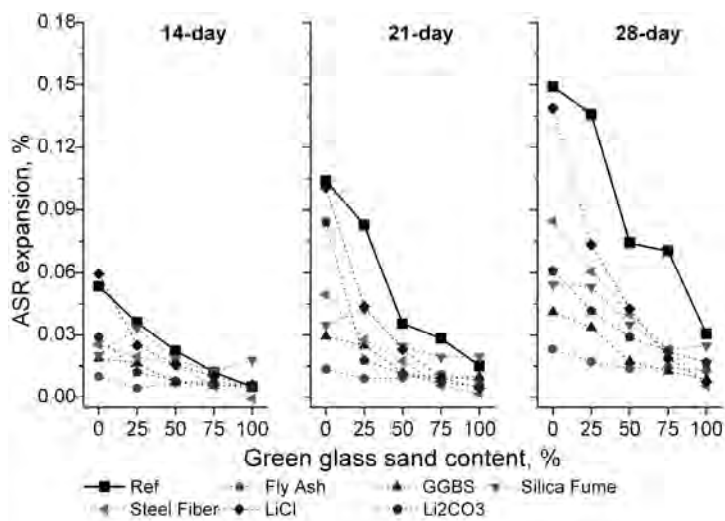


Figure 8: ASR expansion of green glass mortars with various mitigation methods

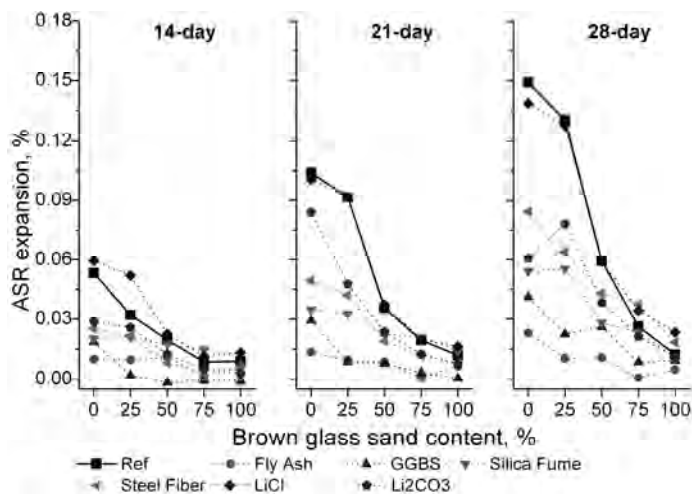


Figure 9: ASR expansion of brown glass mortars with various mitigation methods

The effectiveness of ASR mitigation methods investigated decreased in the order of fly ash, GGBS, Li_2CO_3 , silica fume, steel fibers and LiCl for

green sand mortars, and fly ash, GGBS, silica fume, steel fibers, Li_2CO_3 and LiCl for brown sand mortars.

4. CONCLUSIONS

Based on the study carried out on waste glass mortar, it is concluded that both green and brown glass sand mortars did not show potential deleterious ASR expansions according to the specifications of ASTM C 1260, regardless of the glass content. In general, use of supplementary cementing materials such as fly ash, GGBS, and silica fume, was shown to be more effective in mitigating ASR expansions, while additive materials such as steel fibers and lithium compounds were less effective. However, more work would be needed to determine the effect of different quantities of the above ASR suppressing materials.

REFERENCES

- ASTM C 33, 2004. *Standard specification for concrete aggregate*. ASTM International, Philadelphia.
- ASTM C 150, 2005. *Standard specification for portland cement*. ASTM International, Philadelphia.
- ASTM C 1260, 2007. *Standard test method for potential alkali reactivity of aggregates (mortar-bar method)*. ASTM International, Philadelphia.
- ASTM C 1567, 2008. *Standard test method for determining the potential alkali-silica reactivity of combinations of cementitious materials and aggregate (accelerated mortar-bar method)*. ASTM International, Philadelphia.
- Jin, W., Meyer, C., and Baxter, S., 2000. Glascrete-concrete with glass aggregate. *ACI Materials Journal* 2, 208-213.
- Lumley, J.S., 1997. ASR suppression by lithium compounds, *Cement and Concrete Research* 2, 235-244.
- Park, S., and Lee, B., 2004. Studies on expansion properties in mortar containing with waste glass and fibers. *Cement and Concrete Research* 7, 1145-1152.
- Park, S., Lee, B., and Kim, J. H., 2004. Studies on mechanical properties of concrete containing waste glass aggregate. *Cement and Concrete Research* 12, 2181-2189.
- Prezzi, M., Monteiro, P. J. M., and Sposito, G., 1997. The alkali-silica reaction, Part I: use of the double-layer theory to explain the behavior of reaction-products gels. *ACI Materials Journal* 1, 10-17.
- Shi, C., 2009. Corrosion of glasses and expansion mechanism of concrete containing waste glasses as aggregate. *Journal of Materials in Civil Engineering* 10, 529-534.
- Topcu, I. B., Boga, A. R., and Bilir, T., 2008. Alkali-silica reactions of mortars produced by using waste glass as fine aggregate and admixtures such as fly ash and Li_2CO_3 . *Waste Management* 5, 878-884.

Taha, B., and Nounu, G., 2008. Properties of concrete contains mixed colour waste recycled glass as sand and cement replacement. *Construction and Building Materials* 5, 713-720.

Taha, B., and Nounu, G., 2009. Utilizing waste glass as sand/cement replacement in concrete. *Journal of Materials in Civil Engineering* 2, 709-721.

Topcu, I. B., and Canbaz, M., 2004. Properties of concrete containing waste glass. *Cement and Concrete Research* 2, 267-274.

Zhu, H., Chen, W., and Zhou, W., 2009. Expansion behavior of glass aggregates in different testing for alkali-silica reactivity. *Materials and Structures* 4, 485-494.

Health survey of concrete in urban infrastructure by non-contact acoustic imaging method

Noriyuki UTAGAWA¹, Ryo AKAMATSU² and Tsuneyoshi SUGIMOTO³

¹ Project Researcher, Satokogyo Engineering Institute, Japan
utagawa@satokogyo.co.jp

² Under graduate student, Faculty of Engineering,
Toin Univ. of Yokohama, Japan

³ Professor, Faculty of Engineering, Toin Univ. of Yokohama, Japan

ABSTRACT

To automate the hammering test that can be measured remotely, “Non contact Acoustic Imaging Method” is developed. Advantage of this technology is a device that can move in a tunnel on the road. For example, the separation or flaking of the tunnel crown is able to be examined. By using this method, there is no danger in high places and agonizing effort, and examined possible high frequency. In this paper, both to demonstrate the principles of measurement, the result indicate a defect in the specimen was extracted distance 10m.

Keywords: *non contact acoustic imaging method, concrete structure, delamination, nondestructive inspection, long range acoustic device*

1. INTRODUCTION

To use the urban infrastructures continuously, the operation and maintenance of the structure becomes important. Up to now, a concrete structure has been thought for the performance to be maintained when almost permanent, but various performances actually has decreased because of the concrete deterioration and fatigue, etc. , and the influence has gone out to the performance of structure in a remarkable case. The deterioration of a concrete structure comes for the urban foundations such as the road, the railway, and the drainage built at the high-growth period of Japan to be shown after 50 years. Moreover, such an urban infrastructure can be updated if there is economical room. However, it is becoming direction of using it for a long term without updating the structure because there are neither economical room in recent years nor spatial room of the city. The impact to the structure is also large because there are a lot of natural damages such as earthquakes and typhoons in Japan. Then, the performance of the structure not only is maintained but also it is needed to improve the performance at the same time.

An efficient operation and maintenance including the cost of a concrete structure, is needed in such a situation. When the maintenance

management of the structure is done, the health survey of concrete structure is investigated first. Making to high accuracy and efficiency improvement of such an investigation technology are requested.

In the investigation diagnosis, the visual inspection from the distance, the visual inspection adjoining, and hammering test are executed. If it is necessary, a more detailed inspection is executed as a result. Big defects of surface are examined by watching from the distance. Distribution of cracks is examined by watching adjoining. Cavities and delaminations at surface of a concrete are examined by hammering test. Therefore, the visual inspection and hammering test are important inspections for examining the health survey of a concrete structure. The improvement to hasten the inspection speed of these techniques that man has executed up to now and to improve the inspection accuracy is done. Instead of the visual inspection adjoining, efficiency improvement and making to high accuracy are attempted by the use of the digital device such as CCD cameras and the crack extraction techniques (image processing technique). Instead of hammering test, Impact Acoustic method (IA method) have been developed to automatically determine the presence of defects. IA method is recording on the sound generated by a microphone with a hammer blow. The sound pressure is recorded and then analyzed to extract the internal defects of concrete. In addition to IA method, the infrared rays tomography method is used in the flaking off investigation of the tile of outward walls of a building and the radar method is used about a healthy investigation of the tunnel lining. However, the hammering test has been executed in the inspection of a general tunnel and the bridge.

The hammering test in a common road tunnel and the railway tunnel is executed by a dangerous, severe working environment. Moreover, there is a possibility that the defect is overlooked by the presence of the experience because it is a technology that is judged by the sound with a hammer blow, too.

In this development, it paid attention to “Non contact acoustic imaging method”. Non contact acoustic imaging method (NCAI method) is a technique to probe the defects of the concrete surface from a remote location. First, using sound waves generated from the speaker, vibrate the concrete surface. Next, the distribution of vibration is measured using remotely located vibrometer. The defects of concrete surface are probed from the measurement result. The authors have so far, using Non contact acoustic imaging method, has conducted research on technology to detect buried objects such as underground buried objects and landmines. These results are shown in the references. This method will be searchable of concrete health survey from a position away. For instance, concrete lining can be investigated from the road side by NCAI method in the tunnel. Moreover, the floor slab can be investigated from the road or the surface of the water under the bridge.

In this paper, it explains “Non contact acoustic imaging method”, first. Next, the result of measuring the test pieces that imitates the defect like as delamination and cavity is shown from a position 10m away by using NCAI

method. Finally, the possibility of NCAI method and the development in the future are described.

2. HEALTH SURVEY OF CONCRETE STRUCTURES BY NON CONTACT ACOUSTIC IMAGING METHOD (NCAI METHOD)

2.1 Technical summary

The NCAI method is a technique for vibrate the structure by the sound wave, and detecting the defect position from the distribution of the vibration. NCAI method and Hammering test are similar technologies. That is, it is a technology that vibrates the structure by some methods, and the internal situation of concrete can be presumed from the situation of the vibration. Hereafter, NCAI method and the hammering test are compared and it explains the principle.

About the vibratory source, shock with the hammer is used in the hammering test, and, on the other hand, a large sound that the speaker is generated is used in NCAI method. Therefore, it becomes the impulsive vibration of the point vibration about the generated vibration in hammering test, and it becomes a vibration of the periodicity of excitation on the side in NCAI method. In hammering test, the amplitude decreases while parting from source point though it depends on the range and the size of excitation in the point vibration. Therefore, the range of detection is limited. On the other hand, in NCAI method, because the certain scope is vibrated at the same time in excitation on the side, the range of detection can be widely taken. However, because the impact power cannot be given, it is difficult to generate only the vibration of normal mode such as the vibrations of a defective internally board.

For the measuring method of the vibration, the sound generated by the vibration is heard by the ear in hammering test. It is clear that the surface oscillation and the sound are equivalent from a past finding. Therefore, it is also possible to understand the vibration from the sound. On the other hand, vibration at each point is measured in NCAI method with a laser Doppler vibrometer. However, the vibration caught because of the sound heard by the ear is information on the expanded domain, and the vibration caught with a laser Doppler vibrometer is information on the point. Therefore, two-dimensional information of the vibration within the range of the area that is one time in hammering test can be obtained. On the other hand, the scanning is needed to obtain two-dimensional information in NCAI method.

In general, the presence of the defect is distinguished by "Sei-on" and "daku-on" in the hammering test. "Sei-on" shows the health part because of the shrill sound caused when the metal is beaten. "Daku-on" is bottom parts of the notes, and defective on the surface is shown. On the other hand, the defect position is detected from distribution of vibration (amplitude, frequency, and phase) in NCAI method. Either method also finds the defect

part by using the principle with a different vibration in the defect part and vibration in the health part.

2.2 Hardware of NCAI system

Figure 1 shows the composition of the equipment used in NCAI method. Long range acoustic device (LRAD : LRAD Corp, LRAD-300X) is a sound speaker for the distance, and the loud sound can be propagated far. Figure-2 shows the acoustic pressure distribution on the axis measured in outdoor. The measuring frequency is 2kHz. It was confirmed to obtain the maximum sound pressure of 143dB in the maximum because of the isolation of 0.5m, and to obtain the acoustic pressure of 110dB even at a position 20m away. Moreover, the sound was made with a function generator, amplified with the amplifier, and generated from the speaker by the microphone of LRAD.

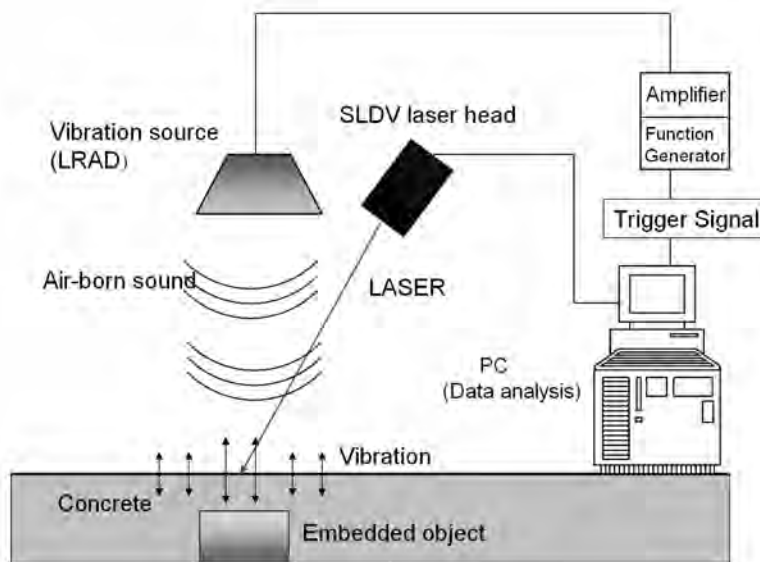


Figure1: Basic concept of NCAI method

Scanning laser Doppler vibrometer (SLDV : Polytec corp., PSV400-H4) is a device that measures the vibration velocity of the surface of the object by using the effect of Doppler of the laser beam. In this device, flat vibration distribution (It is a vertical direction in respect) can be measured by doing the multipoint in the scanning. In this measurement, the vibration of 195 points (15*13 points) is measured by taking the measurement time per point for 2.15 seconds, and doing the scanning. Moreover, the timing of the scanning beginning in the vibration measurement is corresponding to the generation time of the sound wave with a trigger signal from the function generator. In addition, the measurement is repeated until a good oscillation data in each point is obtained.

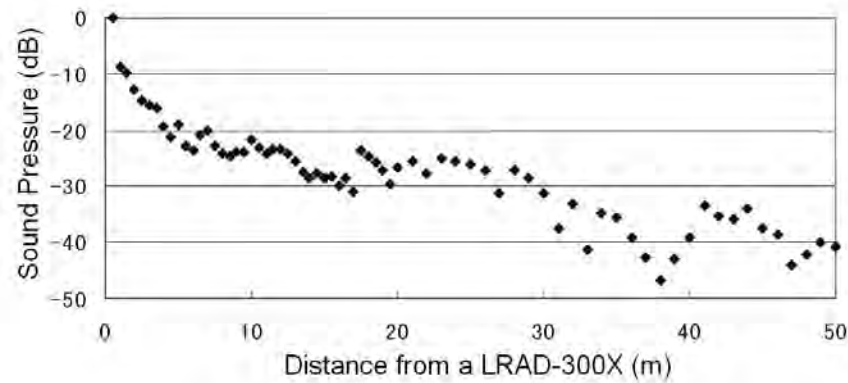


Figure 2: An example of the acoustic pressure distribution on the axis measured in outdoor.

2.3 Method of detecting defect area

The method of extracting the defect in the area is described by using the plane distribution data of the measured vibration velocity. Here, extract the range of the defect in the entire area on the assumption that information on one point in the health part and one point in the defect part in the area has already been obtained. The flow of the defect detection is shown as follows.

- White noise is entered to the test piece, and the vibration at some points are measured. The frequency analysis result of the already-known health part is compared with the frequency analysis result of the already known defect part. Some frequency domains where the vibration of the defect part grows compared with the vibration of the health part are extracted.
- The vibration measurement of all points in the attention area is done by entering the Chirp wave including the frequency domain extracted by an already-known measurement point.
- It pays attention to the frequency before and behind the extracted frequency by using the result of a measurement, and a flat vibration distribution chart is made. It is presumed that the area where the vibration is growing in the vibration distribution chart is a defect part.
- In this processing, when the defect part doesn't appear too much clearly, the defect position is presumed by the picture processing that pays attention to the optimum frequency range method and the phase difference method.

3. DEFECT DETECTION TO CONCRETE TEST PIECES THAT IMITATES DELAMINATION AND CAVITY

3.1 Outline of measurement

Figure-3 shows the setup of the experiment. SLDV and LRAD are arranged at a position 10m away from test piece. It is possible to enter into the test piece of the sound vibration energy of LRAD effectively by

arrangement in front of the test piece of LRAD. SLDV is arranged at a diagonal position in the LRAD back. The reason of this arrangement is to suppress the vibration of the laser head of SLDV by the generation sound of LRAD.

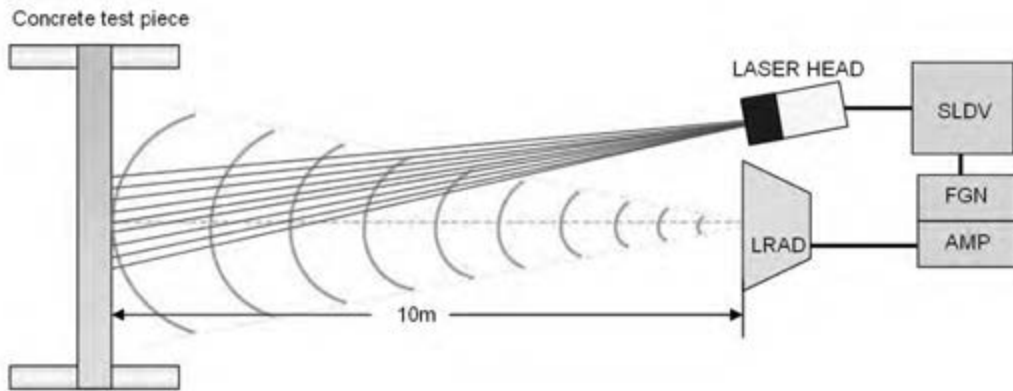


Figure 3: Experimental setup for non contact acoustic imaging method

3.2 Outline of test pieces

The test pieces are five reinforced concrete boards of 2m in width, 1.5m in height, and 0.3m in thickness. The defect of delamination and cavity are imitated by burying the board made of the styrene foam in concrete.

The size and the depth of laying underground of the board of the styrene foam have been changed. There are 32 kinds of the defect. Flat shape of the defect is a square. There is a size from the square whose length is a near 5cm to the square whose length is a near 70cm. The depth of the defect (distance from the styrene foam to the surface) is from 2.5 to 15cm. There is a case where the defect is arranged at the position of the reinforced bar. Figure 1 shows the examples of test pieces that arranged the styrene foam before concrete placing and the completed test pieces.

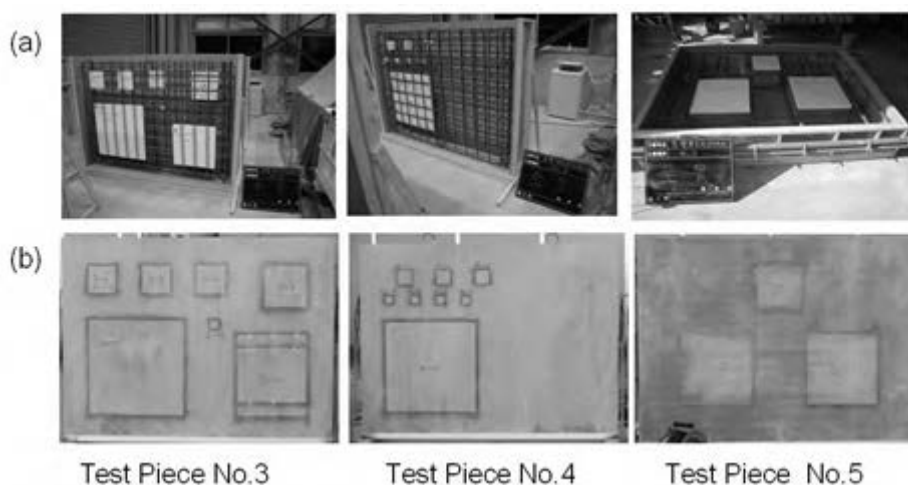


Figure 1: Examples of the concrete test pieces (No.3-No.5).
(a) Under construction, (b) after completion.

3.3 Result of detection

The defect from a position 10m away was detected. As a result, the defect of 2.5cm in depth was able to be detected about the case with a narrow plane scale (square of 10cm). Moreover, the defect that existed in 7.5cm in depth was able to be detected about the case with a wide plane scale (square of 50cm).

The result of a measurement of the defect of the plane scale 20cm and 2.1cm in depth is shown below as one example of the result. The thickness of the styrene foam board is 2.5cm. The frequency band of the entering chirp wave is 500-3000Hz, and 640 microseconds in the duration time.

First, measure the vibration of the center point of the defect, compared with the vibration of the surroundings. The results for the FFT analysis of vibration velocity are shown in Figure 4. In the range of 1400-1600Hz frequency, it is understood that the greater the vibration of the defective part. To ensure that the natural frequencies of plate vibrations were observed around the defective parts, another vibration measurement was performed by using impact acoustic method (IA method). Figure 5 shows the results of vibration measurement by IA method. The results of IA method, the natural frequency of defective parts are found to be around 1400Hz. In addition, the defect has arisen for a strong vibration, whereas it was found that the health of the surrounding almost no vibration occurs.

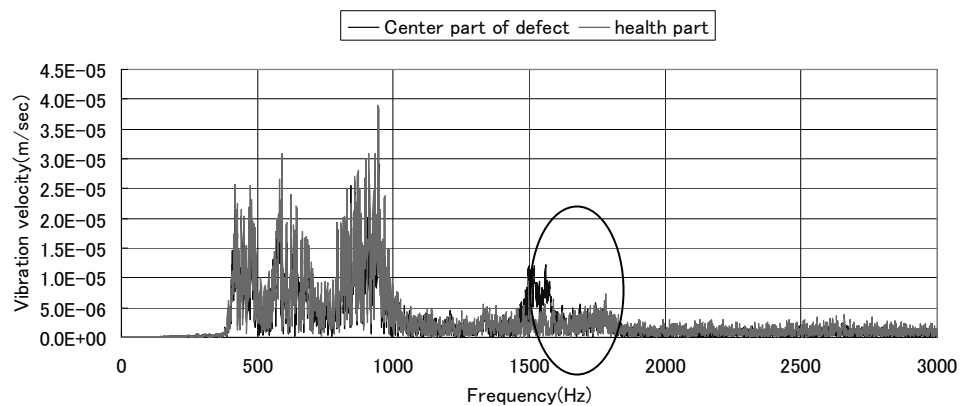


Figure 4: Vibration velocity vs. frequency. Blue line shows the velocity on the center point of defect, Pink line shows the velocity of health part

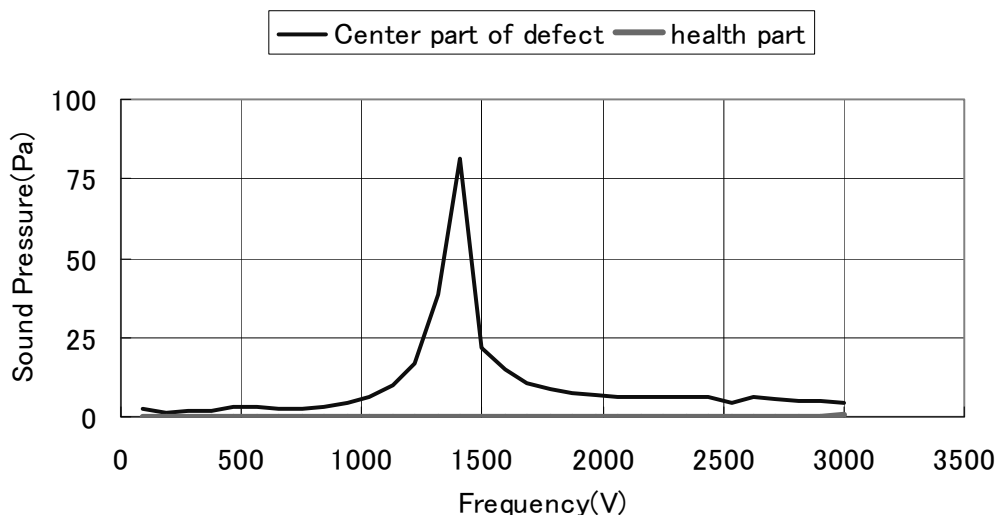


Figure 5: Sound pressure vs. frequency by IA method

Therefore, the peak position slightly different results though IA method, focusing on the vibration from 1400Hz to 1600Hz, the distribution of vibration are created. The distribution of vibration in 1495.5Hz is shown in Figure 6. It is clear that the large vibrations caused by the defective part. This result may be understood that defective parts can be extracted by NCAI method.

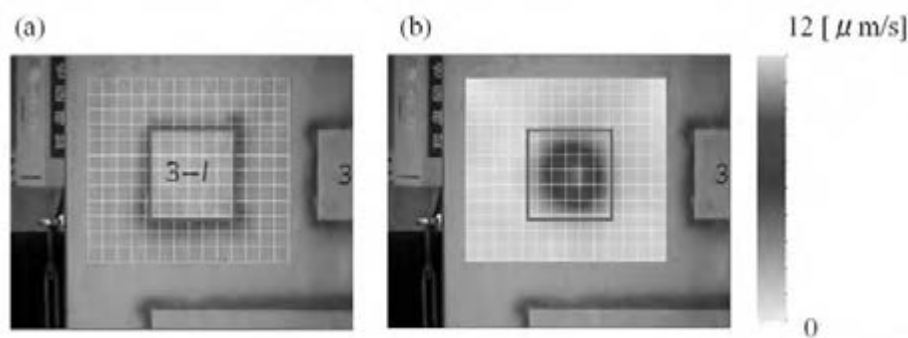


Figure 6: An example of the experimental result. Output wave is chirp (500 - 3000 Hz).

(a) Figuregraph of CCD camera, (b) Vibration velocity image at 1495.5 Hz.

4. CONCLUSIONS

It has been understood to be able to detect the defect in the surface part such as delamination and cavity of concrete from a position 10m away by NCAI method. As a result, the defect of 2.5cm in depth was able to be detected about the case with a narrow plane scale (square of 10cm). Moreover, the defect that existed in 7.5cm in depth was able to be detected about the case with a wide plane scale (square of 50cm). Moreover, the defect of the concrete at surface part can be vibrated from these results by the sound, and it has been understood to be able to measure the vibration from the remote

place. Therefore, the hammering test can be replaced by NCAI method in the near future.

Because it was assumption in this experiment that the defect position etc. understood beforehand, the vibration frequency that vibrated easily was able to be decided. Some improvements are necessary to make NCAI method available in the site. Whether the frequency of the vibration of normal mode is efficiently found (How does it vibrate the defect by using LRAD?) becomes an important problem because it understands neither depth nor the area of the defect in the site beforehand. Moreover, it is necessary not to use the vibration of normal mode, and to examine the probe algorithm that pays attention to the frequency band of the vibration for instance.

ACKNOWLEDGEMENT

This work was supported by the Ministry of Land, Infrastructure and Transport, technology of Japan, research development to contribute to improvement of the quality of the road policy (2010 Feasibility Study), “Research and development about the non-contact acoustic exploration method for non destructive Inspection”.

REFERENCES

- T.Abe and T.Sugimoto, 2009. *Extremely Shallow Underground Imaging Using Scanning Laser Doppler Vibrometer*, Jpn. J. Appl. Phys., 48, 07GC07
- T.Abe and T.Sugimoto, 2010. *Distinguishing Buried Objects in Extremely Shallow Underground by Frequency Response Using Scanning Laser Doppler Vibrometer*, Jpn. J. Appl. Phys., 49, 07HC15
- T.Sugimoto and T.Abe, 2011. *Buried object detection method using optimum frequency range in extremely shallow underground*, Jpn. J. Appl. Phys., 50, 07HC18

Service life cycle assessment of chloride attacked concrete structures with silane treatment considering environmental impacts

Aruz PETCHERDCHOO

Lecturer, Department of Civil Engineering, Faculty of Engineering,
King Mongkut's University of Technology North Bangkok, Thailand
aruz.rm@gmail.com

ABSTRACT

In this study, the service life cycle of chloride attacked concrete structures repaired with silane treatment considering environmental impacts is assessed by predicting the amount of penetrating chloride ions based on the Fick's second law of diffusion. The Crank-Nicolson based finite difference method is used as a tool, because it is suitable for the problem with space dependent diffusion coefficient due to applying silane treatment to concrete structures, and with considering time dependency of surface chloride and diffusion coefficient in computation. Moreover, the environmental impacts resulting from applying different strategies of silane treatment (the number of application, the application time, the effect, and the effective duration of silane treatment) are considered, and an optimum strategy is determined. From the study, it is found that the water to cement ratio of original concrete and the strategies of silane treatment all are related to the service life. Based on the parameters considered, the water to cement ratio affects more. And, the target time horizon also affects the optimum strategy to be selected.

Keywords: *service life cycle, assessment, chloride attack, concrete structures, silane treatment, environmental impacts.*

1. INTRODUCTION

The concern on how human activities affect the loss of biodiversity, the thinning of stratospheric ozone, the climate change, and the consumption of natural resources, has been increasing, hence the word "sustainable development" was introduced in the final report of the Brundtland Commission (World Commission on Environment and Development, WCED) of 1987 (Arskog et al., 2004).

In the present, sustainable construction is widely mentioned, because old-fashioned construction to support city expansion due to population increase was found to be the largest consumer of materials (Ho et al., 2000) leading to large environmental impacts, in particular, Greenhouse effect

gases, e.g., carbon dioxide (CO₂) from the process of cement production. This issue subsequently led to the Kyoto protocol (Sakai, 2005) which has been mentioned until now.

Uren et al. (2000) stated that the sustainable construction can be observed from the environmental criteria included in the project concept, and in the process of building, maintaining, and demolishing. Metha (2001) mentioned that the most efficient way for construction to approach the concept of sustainability is to reuse waste products from other industrial activities as well as improve the durability of the works to last. Therefore, a proper design for durability and long-term performance of concrete structures must be achieved, and the activities in life cycle should consequently be assessed.

The regulation in the ISO-EN-UNE-14.040 standard defines the word “Life Cycle Assessment (LCA)” as the collection and assessment of the inputs and outputs of any potential environmental impacts caused by the production system throughout its life cycle. From this, the activities, e.g., construction, reuse, and demolition, causing environmental impacts should be concerned in the life cycle assessment. For structures in operation, the assessment concerning life cycle can be defined as service life cycle assessment. The key aspects needed to consider are repair and maintenance (Peris Mora, 2007).

In this paper, the service life cycle of concrete structures under chloride attack by diffusion and under several repair strategies by silane treatment is studied using the finite difference method to predict the amount of penetrating chloride ions through concrete structures. Moreover, the environmental impacts resulting from applying silane treatment are determined, and an optimum strategy is considered.

2. SERVICE LIFE CYCLE ASSESSMENT

There are two main processes in assessing the service life; assessment of the service life of chloride attacked concrete structures without and with silane treatment as explained in the following.

2.1 Without silane treatment

Concrete structures under chloride attack by diffusion can be assessed based on the partial differential equation (PDE) of the Fick’s second law (Crank, 1975) as

$$\frac{\partial C}{\partial t} = \frac{\partial}{\partial x} D \frac{\partial C}{\partial x} \quad (1)$$

where C is the chloride content as a function of a position x and time t , and D is the chloride ion diffusion coefficient. With proper initial and boundary

conditions, equation 1 can analytically be solved and used in the assessing process which can be found elsewhere (e.g., Saetta et al., 1993).

2.2 With silane treatment

From NCHRP-558 (2006), silane treatment is categorized as one kind of penetrating sealers for hydrophobic treatment aiming to slow down the deterioration rate of concrete structures. There are two main steps in this process as follows:

2.2.1 Chloride ion penetration from the outer surface through the original concrete. For this, the Crank-Nicholson numerical scheme can be used. As the diffusion coefficient D is constant for the original concrete, the finite difference approximation for equation 1 (von Rosenberg, 1969) is written as

$$\frac{c_{i,j+1} - c_{i,j}}{\Delta t} = \frac{D}{2} \left[\frac{(c_{i+1,j+1} - 2c_{i,j+1} + c_{i-1,j+1}) + (c_{i+1,j} - 2c_{i,j} + c_{i-1,j})}{(\Delta x)^2} \right] \quad (2)$$

where $c_{x,t}$ is, in a general form, the chloride content at a mesh point x at time t . Δt and Δx are the incremental time step and the size of the mesh point, respectively.

2.2.2 Chloride ion penetration through silane treated concrete and original concrete (REHABCON, 2004). Let consider Figure 1. When the time passes by, the chloride ions penetrate through concrete structures, and the amount of chloride at concrete surface increases with time because of time dependent surface chloride.

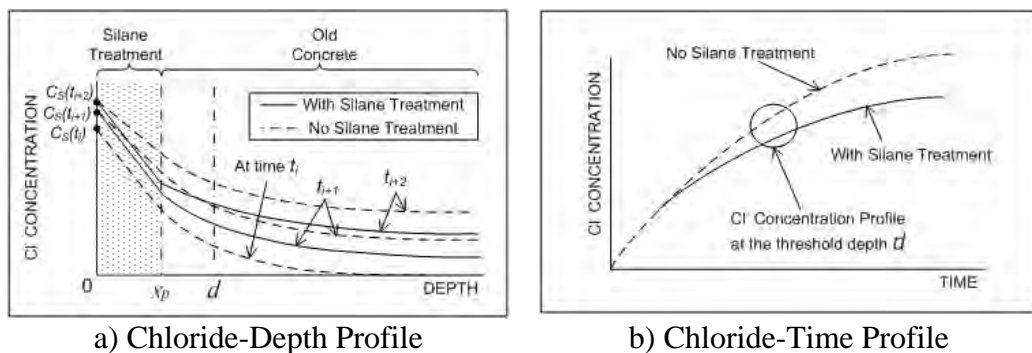


Figure 1: Chloride Profile: With and Without Silane Treatment

At the time t_i , silane treatment is applied at the surface of concrete, and then silanes will react with the pore structure within hardened concrete to create a nonwettable or hydrophobic surface as deep as the distance x_p (or repair depth). This will result in the problem involving space dependent diffusion coefficient, or $D(x)$, due to the difference of diffusion coefficients between the original concrete and the silane treated concrete. In addition, it is found that the diffusion coefficient is time dependent, or $D(t)$, because the continuous process of cement hydration results in connection and condensation of concrete pore structures. Mathematically, the PDE

concerning the space and time dependent diffusion coefficients can be written as

$$\frac{\partial C}{\partial t} = \frac{\partial}{\partial x} D(x,t) \frac{\partial C}{\partial x} \tag{3}$$

It is quite complicated to solve for a close-formed solution of equation 3, hence a Crank-Nicolson based numerical scheme is introduced as (Press et al., 1996)

$$\frac{c_{i,j+1} - c_{i,j}}{\Delta t} = \frac{1}{2} \left(\frac{[D_{i+1/2}(c_{i+1} - c_i) - D_{i-1/2}(c_i - c_{i-1})]_{j+1}}{(\Delta x)^2} + \frac{[D_{i+1/2}(c_{i+1} - c_i) - D_{i-1/2}(c_i - c_{i-1})]_j}{(\Delta x)^2} \right) \tag{4}$$

where $D_{i+1/2} = (D_i + D_{i+1})/2$ and $D_{i-1/2} = (D_{i-1} + D_i)/2$. If the diffusion coefficients in equations 3 and 4 are constant, these equations are reduced to equations 1 and 2, respectively. In computation, when the original concrete is treated with silanes, over the depth x_p , the diffusion coefficient of silane treated concrete will be updated as $(D_{0,t})_o = (D_{0,t})_{REP}$ at concrete surface, and $(D_{x_p,t})_o = (D_{x_p,t})_{REP}$ at repair depth x_p . $(D_{x_p,t})_o$ and $(D_{x_p,t})_{REP}$ are the diffusion coefficients of the original concrete and silane treated concrete, respectively, at the depth x_p and time t .

Figure 1b shows the chloride content at a threshold depth d (see also Figure 1a) plotted with time. With silane treatment, the increase of chloride content is retarded resulting in the reduction of penetrating chloride ions, and consequently the reduction of rebar corrosion and concrete structure deterioration.

2.3 Time dependant surface chloride and diffusion coefficient

The attack of chloride in this study is represented as the time dependent surface chloride proposed by Kassir and Ghosn (2002) as shown in equation 5 and plotted in Figure 2.

$$C_s(t) = 5.34(1 - e^{-0.25t}) \tag{5}$$

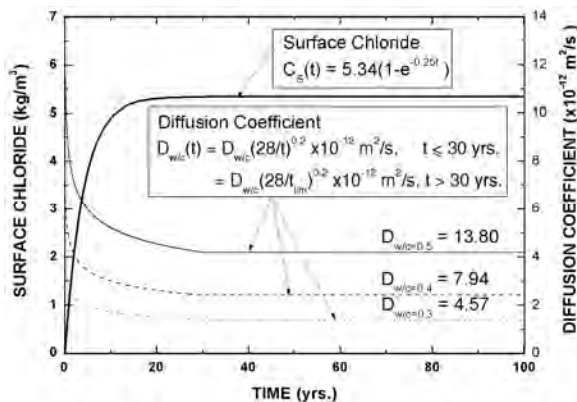


Figure 2 Time Dependent Surface Chloride and Diffusion Coefficient

The deterioration of concrete structures is related to their resistance or diffusion coefficient which is found to be time dependent, because the continuous process of cement hydration results in connection and condensation of concrete pore structures. The time dependent diffusion coefficient at time t can be represented as (Thomas and Bentz, 2000)

$$D_{w/c}(t) = D_{w/c} \left(\frac{28}{t} \right)^{0.2} \text{ if } t \leq 30 \text{ years; and } D_{w/c}(t) = D_{w/c} \left(\frac{28}{t_{lim}} \right)^{0.2} \text{ if } t > 30 \text{ years} \quad (6)$$

where $D_{w/c}$ is the diffusion coefficient of concrete structures at 28 days as equal to 13.8, 7.94, and 4.57 for the water to cement ratio (w/c) equal to 0.3, 0.4, and 0.5, respectively. The power of 0.2 represents the rate of diffusion coefficient decay, and t_{lim} is the limit time which is equal to 30 years (10950 days). The time dependent diffusion coefficient for w/c of 0.3, 0.4, and 0.5 are shown in Figure 2.

The diffusion coefficient of silane treated concrete structures $[D_{w/c}(t)]_{REP}$ can be related to that of the original concrete $[D_{w/c}(t)]_0$ as $[D_{w/c}(t)]_{REP} = n[D_{w/c}(t)]_0$ in which n is a number which represents the ratio between the diffusion coefficient of the silane treated concrete and that of the original concrete. In this study, n is selected to be 0.2 and 0.29 for four strategies (SL1 to SL4) as denoted in Table 1. These two values are chosen based on the test results of Medeiros and Helene (2009) and Shimomura (2005). In addition, Shimomura (2005) estimated the silane treated depth to be 30 mm as also used in this study (see Table 1). It is noted that concrete structures with lower diffusion coefficient are more resistant to chloride diffusion.

2.5 Application time and effective duration of silane treatment

In this study, the application time of silane treatment is cyclically time based, and adopted from the data of Denton (2002) as shown in Table 1. Carter and McGettigan (2001) referred to the paper of Weyers (1993) which stated that the effective duration or the service life of high-solid silanes fell between 5 and 10 years. In this study, the effective duration is chosen to be 7.5 or 10 years after previous application as shown in Table 1. It is observed that in SL4, when the effective duration is terminated, the silane treatment is immediately reapplied.

Table 1: Diffusion coefficient, application time and duration of SL1 to SL4

Silane Treatment Strategy	Diffusion Coefficient $[D_{w/c}(t)]_{REP}$	Silane Depth (X_P)	Application Time		Effective Duration (t_{DUR})
			First (t_{IST})	Subsequent (t_{SUB})	
SL1	$0.2[D_{w/c}(t)]_0$	30 mm	At year 7.5	Every 12.5 yrs.	7.5 yrs.
SL2	$0.2[D_{w/c}(t)]_0$				10 yrs.

SL3	$0.29 [D_{w/c}(t)]_0$			10 yrs.
SL4	$0.29 [D_{w/c}(t)]_0$		Every 10 yrs.	10 yrs.

2.6 Critical chloride content

The critical chloride content or the chloride threshold level Cl_{crit} can be used to indicate the current state of structures, e.g., start of corrosion, start of cracking etc. Schiessl and Raupach (1990) stated that the critical chloride content, Cl_{crit} , could be defined as the content of chloride ions that were necessary to sustain local passive film breakdown at the steel depth before the process of corrosion initiation. JSCE (2002) defined the critical value of 1.2 kg/m^3 as a value to initiate reinforcement corrosion. Moriwake (1996) defined the critical value of 2.0 kg/m^3 as a value to initiate concrete cracking. In this study, the critical chloride content is chosen as 1.2 kg/m^3 and 2.0 kg/m^3 to denote reinforcement corrosion free and concrete crack free control plans for concrete structures, respectively.

3. ENVIRONMENTAL IMPACTS OF SILANE TREATMENT

The environmental impacts of silane treatment were studied by Arskog et al. (2004), and can be classified into several categories. In this study, only Use of Energy and Global Warming are considered. The environmental impacts of these two categories are derived from four processes; production of silane agent, surface preparation for treatment, transportation and treatment process, and long-term degradation. The estimation of the environmental impacts per action for the four processes is shown in Table 2.

Table 2: Environmental Impacts of Silane Treatment (Per Action)

Processes	Impact category	
	Use of Energy (MJ/m ²)	Global Warming (g CO ₂ eq/m ²)
Production of silane agent	47	295
Surface preparation	17	10
Transportation and silane process	12	80
Long-term degradation	-	2171
Total	76	2559

These two categories will be considered in combination with the service life cycle assessment as shown in the numerical examples in the next section.

4. NUMERICAL EXAMPLES

Based on the aforementioned idea and data, a Crank-Nicolson based finite difference program was developed for computation, and called “SA2CR” (Service life Assessment of Concrete structures under Chloride attack with Repairs). In computation, the size of the mesh point, Δx , and the incremental time step, Δt , are selected as 1 mm and 1 week, respectively.

And, the threshold depth, d , is selected to be 80 mm as equal to the cover depth of concrete structures in the marine environment (MOCT, 2004).

The chloride profile for the original concrete structure having $w/c = 0.3$ without and with silane treatment of SL3 can be computed and plotted with respect to depth and time as shown in Figures 3a-c and Figure 3d, respectively. From Figure 3a, the chloride ions penetrate through the original concrete, when the time passes by (year 1 to year 7). At the surface, the chloride ion concentration increases with time because of the effect of time dependent chloride ion concentration. And, the rate of chloride ion diffusion is slower with increasing time, because of the effect of time dependent diffusion coefficient which decays with time.

From Figure 3b, silane treatment of SL3 is first applied to the original concrete at the year 7.5, hence the diffusion coefficient of the original concrete is updated to that of the silane treated concrete or $0.2[D_{w/c}(t)]_0$ as deep as 30 mm from concrete surface. At the year 17.5 (10 years after the first treatment), the effect of silanes vanishes due to the end of its lifetime. At the year 20 (12.5 years after the first treatment), silanes are reapplied, and its effect last for 10 years. After that, the same silane treatment is cyclically applied till the end of the target time horizon of 100 years as shown in Figure 3c. If the chloride profile at the year 100 for the case with silanes is compared to that without silanes, it shows that the diffusion of chloride ions though the depth of concrete with silane treatment is slower.

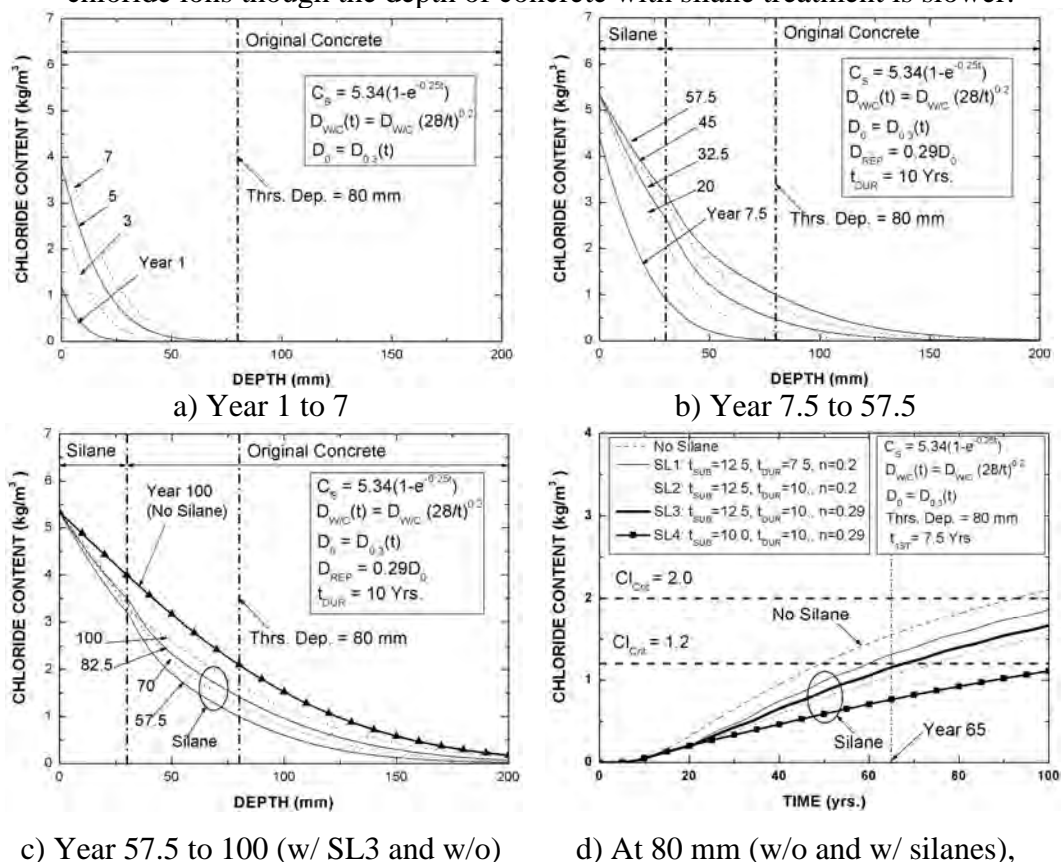


Figure 3 Chloride Profile Versus Depth and Time for the original concrete with $w/c=0.3$

Figure 3d represents the profiles of chloride diffusion through the original concrete having w/c of 0.3 without and with silane treatment (SL1 to SL4) at the threshold depth of 80 mm. Without silane treatment, the chloride content will increase causing continuous deterioration of the concrete structure. If the time that the chloride profile crosses the value of 1.2 and 2.0 kg/m^3 is defined as the service life of the structure for corrosion free and crack free control, its service life is about 50 and 93 years, respectively. However, if SL3 is applied, the service life of the structure will be extended to 68 years and larger than 100 years prior to the occurrence of corrosion and cracking, respectively. And, the service life of the structure with SL3 is longer than that with SL1 because of longer effective duration of SL3, but shorter than that with SL2 because of lower silane quality of SL3. It should also be observed that, for the target time horizon of 100 years, all the four strategies are effective only for crack free control, while only SL4 is effective for both corrosion and crack free control. And, the effect of silanes on the diffusion of chloride ions is obvious after the year 15 as shown by the profiles which start to deviate from the profile without silane treatment.

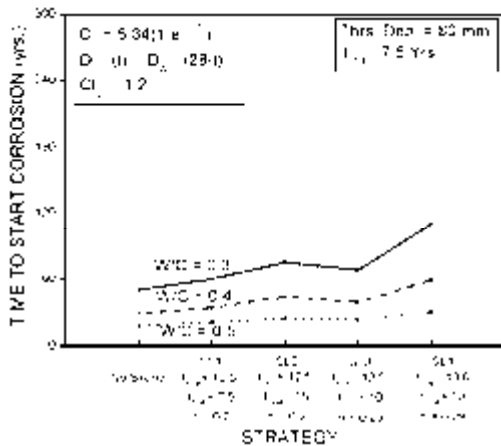


Figure 4 Time to start corrosion for $w/c = 0.3, 0.4,$ and 0.5 without and with silanes

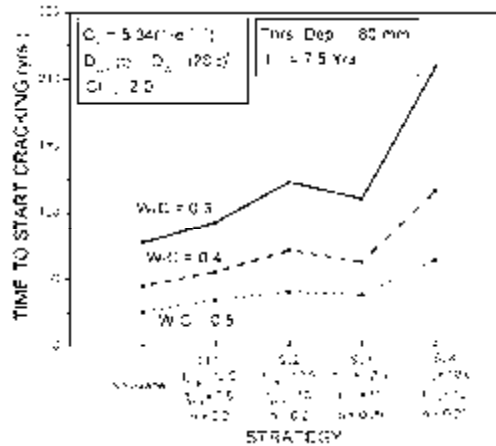


Figure 5 Time to start cracking for $w/c = 0.3, 0.4,$ and 0.5 without and with silanes

The service life of the original concrete structure having w/c of 0.3, 0.4, and 0.5 without and with silane treatment can be represented in terms of time to start corrosion and cracking (the time that the chloride profile to reach 1.2 and 2.0 kg/m^3 , respectively) as shown in Figures 4 and 5, respectively. It is found that the original concrete structure with lower w/c is better. And, the original concrete structure with w/c of 0.4 and 0.5 under SL1, SL2, and SL3 are not effective for controlling both corrosion and crack for the target time horizon of 100 years, because the time to start corrosion and cracking is less than the target time horizon.

The environmental impacts resulting from silane treatment for the target time horizon of 100 and 65 years are shown in Tables 3 and 4, respectively.

Table 3: Environmental Impacts of Silane Treatment for 100 year time horizon

Silane Treatment Strategy	Number of Actions in 100 Yrs.	Environmental Impacts			
		Use of Energy (MJ/m ²)		Global Warming (g CO ₂ eq/m ²)	
		Per Action	100 Yrs.	Per Action	100 Yrs.
1) SL1 to SL3	8	76	608	2559	20472
2) SL4	10	76	760	2559	25590
Ratio of 2) to 1)	1.25	1	1.25	1	1.25

Table 4: Environmental Impacts of Silane Treatment for 65 year time horizon

Strategy	Number of Actions in 75 Yrs.	Environmental Impacts			
		Use of Energy (MJ/m ²)		Global Warming (g CO ₂ eq/m ²)	
		Per Action	65 Yrs.	Per Action	65 Yrs.
1) SL1 to SL3	5	76	380	2559	12795
2) SL4	6	76	456	2559	15354
Ratio of 2) to 1)	1.20	1	1.20	1	1.20

Table 3 shows that the ratio of the number of actions between SL4 and the other strategies (SL1, SL2, SL3) is equal to 1.25, hence SL4 causes 25% higher environmental impacts. Although SL4 causes higher environmental impacts, it is more effective in controlling corrosion and crack than other strategies (see Figure 4 and 5). Considering both the service life upon corrosion and crack free control and the environmental impacts for the target time horizon of 100 years, SL4 is an optimum.

If the target is to control the structure to be only free of corrosion for the lowest environmental impacts for the target time horizon of 65 years, the original concrete structure with w/c of 0.3 under SL2 is an optimum (see Figures 3d and 4). But if the target is to control both corrosion and cracking without considering the environmental impacts, the original concrete structure with w/c of 0.3 under SL4 is an optimum instead because of its longest service life (see Figures. 4 and 5).

5. CONCLUSION

In this paper, the service life cycle of chloride attacked concrete structures with silane treatment considering the time dependency of surface chloride and diffusion coefficient is studied using the finite difference method. And, the environmental impacts are also considered, and an optimum strategy in applying silane treatment is determined. From the study, it can be concluded that

1. Not only the w/c is important for the service life, but also an appropriate plan of silane treatment is also required for minimum environmental impacts.
2. The target time horizon and control plan (corrosion and cracking) are important, because different targets lead to different optimum strategies.

3. The method in this study is useful for selecting suitable original concrete and silane treatment strategy for design service life upon corrosion and crack control.

4. The results in this paper are based on available data. It is necessary to collect more data for updated results. And, a probabilistic study should be conducted to see the sensitivity of each parameter in various groups of data.

ACKNOWLEDGEMENT

The financial support from the Faculty of Engineering, King Mongkut's University of Technology North Bangkok is gratefully acknowledged.

REFERENCES

- Arskog, V., Fossdal, S., and Gjørsv, O.E., 2004. *Life-Cycle Assessment of Repair and Maintenance Systems for Concrete Structures*. Int. Workshop on Sustainable Development and Concrete Tech. Beijing, China. May 20-21. 193-200.
- Ho, D.W.S., Mak, S.L., and Sagoe-Crentsil, K.K., 2000. *Clean Concrete Construction. An Australian Perspective*. Proc.of Concrete Tech. for a Sustainable Development in the 21st Century. E&FN Spon, London and New York, 236-245.
- Sakai, K., 2005. *Environmental Design for Concrete Structures*. Journal of Advanced Concrete Technology. 3:1. 17-28.
- Uren S., Brown A., and Gooch F., 2000. *Sustainable construction in practice*. Proceedings of International Conference on sustainable building. Ibid.
- Metha P.K., 2001. *Reducing the environmental impact of concrete*. Concrete can be durable and environmentally friendly. Concrete International. 23(10).
- Peris Mora, E., 2007. *Life Cycle, Sustainability and the Transcendent Quality of Building Material*, Building and Environment. 42. 1329-1334.
- Crank. J. 1975. *The mathematics of diffusion*. Oxford: The Clarendon Press (2).
- Saetta, V.A., Scotta, V.R., and Vitaliani, V.R. 1993. *Analysis of chloride diffusion into partially saturated concrete*. ACI Materials Journal, 90, 441-451.
- NCHRP-558, 2006. *Manual on Service life of corrosion-damaged reinforced concrete bridge superstructure elements*. Transportation Research Board.
- Von Rosenberg, 1969. *Methods for the numerical solution of partial differential equations*. Elsevier Publishing Co.
- REHABCON, 2004. *Final report on the evaluation of alternative repair and upgrading options: Strategy for maintenance and rehabilitation in concrete structures*. EC Innovation and SME programme project no. IPS-2000-0063, Department of Building Materials, LIT, Lund, Sweden.
- Press W.H., Teukolsky S.A., Vetterling W.T. and Flannery B.P., 1996. *Numerical recipes in C: the art of scientific computing*. Cambridge University Press. 2nd Ed.

Kassir M.K. and Ghosn M., 2002. *Chloride-induced corrosion of reinforced concrete bridge decks*. Cement and Concrete Research, pp. 139–43.

Thomas, M.D.A., and Bentz, E.C., 2000. *Life-365 manual*. Released with Program by Master Builders.

Medeiros MHF and Helene P., 2009. *Surface treatment of reinforced concrete in marine environment: Influence on chloride diffusion coefficient and capillary water absorption*. Construction and Building Materials, pp. 1476-1484.

Shimomura, T., 2005. *Evaluation of effectiveness of surface protecting materials for concrete by numerical analysis*. Proceeding of an international workshop on durability of reinforced concrete under combined mechanical and climatic loads, Qingdao Technological University, Qingdao, China.

Denton, S., 2002. *Data estimates for different maintenance options for reinforced concrete cross-heads*. Progress Meeting, Highways Agency, London, Parsons Brinckerhoff Ltd., Bristol, U.K.

Carter P., and McGettigan, E., 2001. *The fundamental of cleaning and coating concrete*. Chapter 8: Coating Materials: Sealer, pp. 149-166.

Weyers, R.E., 1993. *Concrete Bridge Protection, Repair, and Rehabilitation Relative to Reinforcement Corrosion: A Method Application Manual*. SHRP-S-360, Strategic Highway Research Program: Washington D.C., pp.59-61.

Schiessl, P. and Raupach, M., 1990. Influence of concrete composition and microclimate on the critical chloride content in concrete. *Corrosion of Reinforcement in Concrete*. Elsevier Applied Science, 49-58.

Japan Society of Civil Engineers (JSCE), 2003. *Standard specification for concrete structures – 2002*, Structural Performance, Guidelines for Concrete, 3.

Moriwake, A., 1996. *Study on durability and maintenance of reinforced concrete jetty deck against chloride induced deterioration*. PhD. thesis, Tokyo Institute of Technology, Tokyo, Japan.

Ministry of Construction and Transportation (MOCT), 2004. *Standard specification for concrete structures on durability*. Seoul, Korea (in Korean)

Development of probabilistic structural performance evaluation method for port RC structure

Ema KATO¹, Yuichiro KAWABATA², Mitsuyasu IWANAMI³
and Hiroshi YOKOTA⁴

¹ Senior Researcher, Port and Airport Research Institute (PARI), Japan
(Researcher, ICUS, IIS, the University of Tokyo, Japan)
kato-e@pari.go.jp

² Researcher, PARI, Japan

³ Head of Structural Mechanics Division, PARI, Japan

⁴ Professor, Faculty of Engineering, Hokkaido University, Japan
(Visiting Professor, ICUS, IIS, the University of Tokyo, Japan)

ABSTRACT

Port and harbor facilities often tend to suffer performance degradation during their service period due to various reasons including materials deterioration and damage of structural components. Therefore, the facilities need to be maintained appropriately so as to keep the performance over the required level throughout their service period. For this purpose, performance evaluation of the facilities becomes important to conduct suitable maintenance work.

The authors have tried to establish the simplified performance evaluation method for reinforced concrete (RC) members by focusing on the relationship between the deterioration grade and structural performance. In this paper, the total of 40 RC slabs extracted from existing port structures was tested in order to evaluate the relationship between visually judged deterioration grades and load carrying capacities. Wide variations were observed in the relationship in each deterioration grade, however, the load carrying capacity tended to be smaller than the design expectations when the symptom of deterioration appeared on the surface of concrete members. Based on the statistical analysis on the relationship between deterioration grades and load carrying capacities, the probabilistic evaluation method of the load carrying capacities of RC slabs was proposed as a quantitative evaluation method of residual structural performance of existing port RC structures.

Keywords: *reinforced concrete, performance evaluation, deterioration grade, load carrying capacity, Weibull distribution*

1. INTRODUCTION

Port facilities generally face severe environmental conditions compared to other infrastructure. They often tend to suffer performance degradation during their service period due to various reasons including materials deterioration and damage of structural components. Therefore, the facilities need to be maintained appropriately so as to keep the performance over the required level throughout their design service period. To achieve the effective maintenance of port facilities, the authors have tried to establish the life-cycle management system for a reinforced concrete (RC) deck of open-type wharf that is one of the most vulnerable structural types in port facilities, as shown in Figure 1 (Port and Airport Research Institute, 2007). The life-cycle management is a series of actions including judgment of the deterioration grade by periodic inspection, evaluation of the structural performance, prediction of the future progress of performance degradation, and proposal of alternatives of appropriate countermeasures based on lifecycle cost minimization or performance maximization under budget capping.

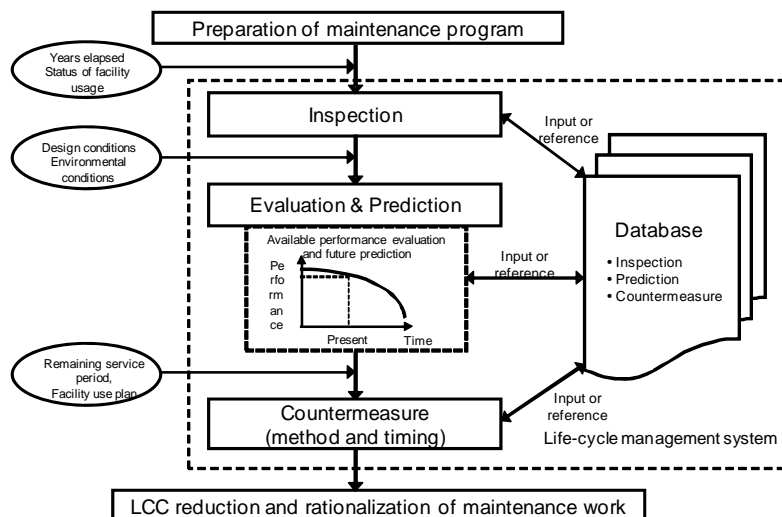


Figure 1: Life-cycle management system

During inspection of the present conditions of structural members and assessment of performance of structure, in general, appearances of RC members are visually observed and are more or less subjectively evaluated as the deterioration grade specified in the Maintenance Manual (Port and Airport Research Institute, 2007). However, it is not clear how the deterioration grade quantitatively represents the performance of RC members.

Aiming at the achievement of life-cycle management, the authors have tried to establish the simplified assessment procedure of performance of RC deck by focusing on the relationship between the deterioration grade and structural performance of RC members. Load carrying capacities of RC slabs extracted from various decks of existing open-type wharves showed large variations, even though those tested slabs indicated the same

deterioration state (Kato et al., 2008). The tested results implied that the probabilistic approach is required to appropriately evaluate the structural performance with considering the variations in the existing structure efficiently.

In this paper, the total of 40 RC slabs extracted from existing port structures was tested in order to make clear the relationship between visually judged deterioration grades and load carrying capacities. Then, based on the statistical analysis on the relationship between deterioration grades and load carrying capacities, the probabilistic evaluation method of the load carrying capacities of RC slabs was proposed as a quantitative evaluation method of residual structural performance of existing port RC structures.

2. DETERIORATION GRADE AND LOAD CARRYING CAPACITY OF TESTED RC SLABS

2.1 Procedure of test and measurement

To evaluate the relationship between visually judged deterioration grades and load carrying capacities, the total of 40 RC slabs extracted from the total of 7 existing port structures was visually inspected and experimentally load tested. Table 1 lists the configurations and deterioration grades of tested RC slabs. Slabs Nos. 1 to 33 were taken out from RC decks of open-type wharves that have been in service for more than 30 years, while Nos. 34 to 40 were taken out from RC superstructure of an access bridge used for 44 years. Figure 2 shows an example of sampling condition. The structural details of tested slabs are listed in Table 1. Unfortunately almost all the details of constituent materials and design calculations were not available to understand the designed conditions of the tested RC slabs.



Figure 2: Sampling of a slab

Those slabs were visually inspected on their surfaces at their loading spans as listed in Table 1. Visual inspection was carried out by focusing on cracks and their directions, spalling off of cover concrete, rust stain, and corrosion appearances. Deterioration grades of all the slabs given in Table 1

were judged by the grading system summarized in Table 2 (Port and Airport Research Institute, 2007). The total numbers of tested slabs are 2 for deterioration grade *d*, 17 for grade *c*, 11 for grade *b*, and 10 for grade *a*.

After the visual inspection and judgment, the slabs were experimentally load tested as a one-way slab. They were simply supported at their marginal regions having loading spans as listed in Table 1 and a monotonically-increased three-point (Slabs Nos.1~20) or four-point (Slabs Nos.21~40) bending load was applied. The supporting areas were repaired by mortar in case that the cover concrete had been already spalled off. During the test, the applied load and deflection at the supporting points and at the midspan were measured and recorded. Since no strain gauges were glued on the surface of reinforcement, the first yield load was determined when the midspan deflection showed a sharp increase.

Table 1: Configuration and deterioration grade of tested RC slabs

No.	Year	Grade	Min. width (mm)	Shear span (mm)	Tensile reinforcing bars (Type and diameter, number of reinforcing bar, ave. effective depth (mm))			P _{max} (kN)	Failure mode			
					Upper		Lower					
1	40	<i>b</i>	1490	400	D13	4	190	D13	8	290	869	F
2	40	<i>a</i>	1500	400	D13	4	190	D13	8	290	498	F
3	40	<i>b</i>	532	450	D13	3	93	D13	3	187	147	F
4	40	<i>c</i>	389	450	D13	2	91	D13	2	187	94	F
5	40	<i>d</i>	575	450	D13	3	82	D13	3	189	159	F
6	40	<i>a</i>	492	450	D13	3	89	D13	3	186	128	S
7	40	<i>a</i>	408	450	D13	2	77	D13	2	185	86	F
8	40	<i>a</i>	585	450	D13	3	67	D13	3	176	105	S
9	40	<i>b</i>	537	550	D13	2	94	D13	2	211	162	F
10	40	<i>b</i>	401	550	D13	3	92	D13	3	197	84	F
11	40	<i>b</i>	599	550	D13	3	98	D13	3	180	128	F
12	40	<i>c</i>	578	550	D13	3	122	D13	3	205	178	S
13	40	<i>c</i>	541	550	D13	3	97	D13	3	203	118	S
14	40	<i>c</i>	508	550	D13	3	97	D13	3	168	141	F
15	40	<i>d</i>	699	600	φ13	3	140	φ13	5	250	252	F
16	40	<i>b</i>	535	600	φ13	4	140	φ13	4	250	221	F
17	40	<i>c</i>	798	600	φ13	3	140	φ13	6	250	196	F
18	40	<i>c</i>	732	600	φ13	3	150	φ13	5	260	281	F
19	40	<i>b</i>	569	600	φ13	3	150	φ13	5	260	261	F
20	40	<i>c</i>	812	600	φ13	3	150	φ13	6	260	212	F
21	40	<i>b</i>	1940	750	D16	13	135	D16	5	242	384	F
22	40	<i>a</i>	1987	750	D16	13	135	D16	5	222	224	F
23	40	<i>a</i>	1984	750	D16	13	135	D16	5	241	267	F
24	40	<i>a</i>	1964	750	D16	13	135	D16	5	231	243	F
25	32	<i>c</i>	1560	1000	D16	8	86	D19	8	181	379	F
26	32	<i>c</i>	1500	1000	D16	7	81	D19	8	181	403	F
27	32	<i>c</i>	1370	1000	D16	7	84	D19	8	181	329	F
28	32	<i>c</i>	1540	1000	D16	7	75	D19	8	185	351	F
29	32	<i>c</i>	1385	1000	D16	7	67	D19	8	179	361	F
30	41	<i>c</i>	1518	1000	D13	14	80	D13	7	205	247	F
31	41	<i>c</i>	1508	1000	D13	14	73	D13	7	180	201	F
32	30	<i>c</i>	1010	1450	D16	2	225	D13	5	280	139	F
33	30	<i>b</i>	1010	1450	D16	2	220	D13	5	300	142	F
34	44	<i>b</i>	600	800	φ13	2	89	φ13	3	161	101	F

35	44	c	595	800	φ13	2	85	φ13	3	159	103	S
36	44	a	595	980	φ13	2	94	φ13	3	159	68	F
37	44	c	590	755	φ13	2	83	φ13	3	151	58	F
38	44	b	590	755	φ13	2	81	φ13	3	152	45	F
39	44	a	690	750	φ13	2	86	φ13	4	156	72	F
40	44	a	685	600	φ13	2	95	φ13	4	163	123	S

Note: Type D = deformed bar, Type φ = round bar, P_{max} = maximum bending load (P), F = flexural failure, S= shear failure after yielding

Table 2: Criterion for grading RC slab of open-type wharf from the viewpoint of steel bar corrosion

Deterioration grade	Criteria
a	Map cracking (> 50%) Spalling off of cover concrete Heavy rust stain
b	Map cracking (≤ 50%) Much rust stain
c	One directional crack or gel extraction Partial rust stain
d	No deformation and/or damage

To compare the load carrying capacities of tested slabs with various structural details, the loads were normalized by corresponding calculated results based on the beam theory by using designed values of strengths, dimensions, and the initial cross-sectional areas of reinforcing bars. The design values of compressive strength and Young’s modulus of concrete were assumed at 24N/mm² and 25kN/mm² respectively with considering the design standards for Japanese port and harbor facilities used more than 30 years ago. Based on the tensile tests of non-corroded reinforcing bars taken out from some test slabs, the design values of tensile strength and Young’s modulus of reinforcing bars were assumed at 345N/mm² and 200kN/mm² respectively.

2.2 Experimental result and discussion

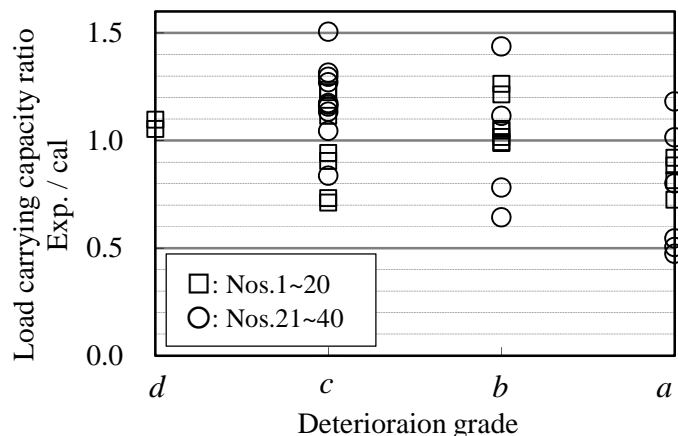


Figure 3: deterioration grades vs. normalized maximum loads

Figure 3 shows the relationships between the deterioration grades and normalized maximum loads of tested slabs. In slabs judged as deterioration

grades *c*, *b* and *a*, there were large variations in the load carrying capacities. There existed the cases of which maximum load ratios were smaller than 1.0 for deterioration grades *c*, *b*, and *a*. In case of deterioration grade *a*, in particular, the load carrying capacity dropped to approximately 50 percent of the design calculations. Some of the load carrying capacities of grade *c* slabs were reduced to the same level as that of deterioration grade *a*. From the safety evaluation point of view, when deterioration grade was judged as grades *c*, *b* and *a*, in other words, symptom of deterioration appeared on the surface of RC members, the load carrying capacity may become smaller than the design expectation.

Large variations in the load carrying capacities for deterioration grades *c*, *b* and *a* were considered to be influenced by two factors as follows: 1) mislead of judgment of the deterioration grades and 2) deteriorated portion in a tested slab.

1); Delamination of cover concrete was detected by hammering test at the midspan area of some tested slabs. However, the delamination was not directly related to the judgment of the deterioration grades as listed in Table 2. Furthermore, in some tested slabs, many small cracks and honeycomb existing on the surface layer of concrete disturbed the change in appearance due to corrosion, which may mislead the healthier deterioration grade. It was considered that the degree of corrosion of reinforcing bar was not always contribute to the surface appearance of slab; that is, judgment of the deterioration grade.

2); One deterioration grade is representatively judged for one slab. In some slabs, corrosion cracks and delamination of cover concrete were observed in a small part of their surface. According to Table 2, those slabs were judged as deterioration grade *c*. However, some of those slabs showed the different failure mode from the uniformly deteriorated slabs. In the range of this research, not uniformly deteriorated slabs showed a tendency of loss in load carrying capacity due to the shear crack progress. The concrete - reinforcing bars stress transmission changes according to the corrosion cracks, localized corrosion in reinforcing bars, and their parts and states. The change in stress transmission leads the change in failure mode and ultimate load consequently. As a result, load carrying capacities of RC slabs extracted from various decks of existing port structures showed large variations, though those tested slabs were in the same deterioration state.

The tested results implied that the probabilistic approach is required to appropriately evaluate the structural performance with considering the variation observed in the existing structure efficiently. In this research, based on the statistical analysis on the relationship between deterioration grades and load carrying capacities, the probabilistic evaluation method of load carrying capacities of RC slabs for each deterioration grade *a*, *b* and *c* was proposed as a quantitative evaluation method of residual structural performance of existing port RC structures.

3. PROBABILISTIC EVALUATION OF STRUCTURAL PERFORMANCE

3.1 Objective of probabilistic performance evaluation

The extreme value theory has been widely applied in reliability engineering and failure analysis, especially in the evaluation of localized corrosion of metallic materials, which has probabilistic features essentially. Tested slabs extracted from existing port structures were mainly deteriorated by corrosion of reinforcing bars due to chloride ion penetration into concrete. Hence, the load carrying capacities of the tested slabs can be considered to mainly depend on the corrosion state of reinforcing bars. Progress of corrosion of reinforcing bars in concrete shows large variation even if these are embedded in a structural member. This variation leads the various cross-sectional shapes of the reinforcing bars. As a result, it becomes a main cause of the large variation in the load carrying capacity of RC members. Based on the above discussion, it seemed possible that the extreme value theory was applied to evaluate the load carrying capacities of RC slabs probabilistically as well as the corrosion of metallic materials.

The actual load-bearing mechanism of port RC structures and the influences of corrosion of reinforcing bars on structural performance of RC members are not directly considered in the proposed probabilistic evaluation method of structural performance of RC slabs based on the deterioration grade judgment. The target of the probabilistic performance evaluation using the visually judged deterioration grades is to achieve the strategic and efficient maintenance of port RC structure based on the life-cycle management.

3.2 Probabilistic structural performance evaluation method

When data of the load carrying capacities of RC slabs are discussed with the extreme value theory, it is necessary to set the lower limit, 0.0, to the targeted extreme value. Hence, experimental load carrying capacity ratios for each deterioration grade were applied to Weibull distribution, Type III asymptotic distribution of extreme values, presented in Equation 1 (Ang, et al., 1984).

$$F_{-III}(x) = 1 - \exp \left[- \left(\frac{x - \gamma}{\eta} \right)^m \right] \quad (1)$$

Where $F_{-III}(x)$: cumulative distribution function, x : load carrying capacity ratio, η : scale parameter, and γ : location parameter, and m : shape parameter.

Experimental data of load carrying capacity ratios of RC slabs in each deterioration grade were assumed to be expressed as the cumulative

distribution function $F_{\text{exp}}(x_i)$ by the following equation based on the order statistics.

$$F_{\text{exp}}(x_i) = \frac{i}{N+1} \tag{2}$$

Where $F_{\text{exp}}(x_i)$: cumulative distribution function of the i^{th} statistics, x_i : experimental data in increasing order, and N : the total number of experimental data.

Load carrying capacity ratio x can be assumed to be $x \geq 0.0$, therefore, γ in Equation (1) can be set as 0.0. Parameters η and m were obtained by try-and-error calculation based on the least squares method to best fit to the cumulative distribution $F_{\text{exp}}(x_i)$.

3.3 Development of probabilistic performance evaluation method from deterioration grade judgment

Figure 4 shows the experimental and calculated cumulative distributions of load carrying capacity ratios for each deterioration grade. Parameters and characteristics values of the load carrying capacity ratio for each deterioration grade are listed in Table 3. Kolmogonov-Smirnov test reported the approximation of $F_{\text{III}}(x)$ and $F_{\text{exp}}(x_i)$ were performed at the 0.05 level of significance.

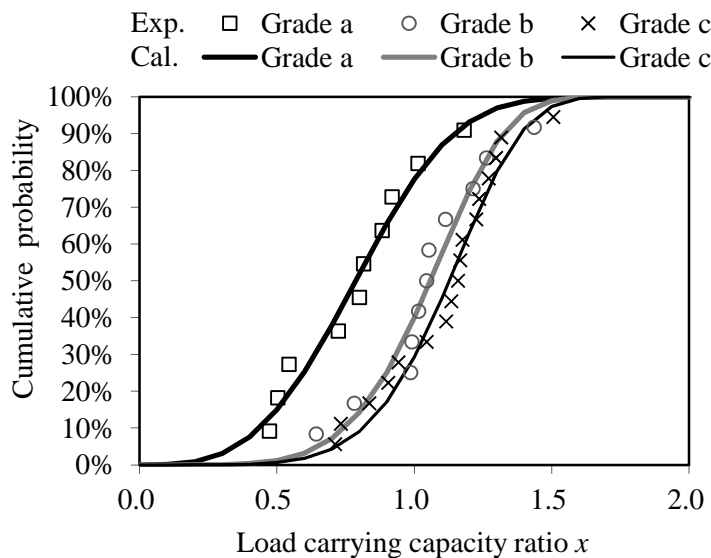


Figure 4: Cumulative distribution of load carrying capacity ratio

Table 3: Parameters and characteristics values

	Deterioration grade		
	<i>c</i>	<i>b</i>	<i>a</i>
η	5.80	5.39	3.21
m	1.20	1.13	0.88
Mean	1.11	1.04	0.79
Mode	1.16	1.09	0.78
Standard deviation	0.19	0.19	0.25

Mean and mode of the load carrying capacity ratio become small as the deterioration grade progresses. In deterioration grade *a*, mean and mode were less than 1.0, which indicates the experimental load carrying capacity is below the design expectation, in addition to the standard deviation of the load carrying capacity ratio was more than those in grades *b* and *c*.

By using obtained cumulative distributions of load carrying capacity ratio, the cumulative probability of the minimum load carrying capacity ratio x can be estimated; for example, the probability that the minimum load carrying capacity ratio x becomes 1.5 or less was 100%. The description, however, would not be suitable to the structural performance evaluation of RC structures, which should be maintained strategically. Therefore, in Figure 5, y-axis is shown as $1-F(x)$, which means the cumulative probability of the minimum load carrying capacity ratio becomes x or more. In this figure, the upper limit of load carrying capacity ratio was shown as 1.0 with the intention of applying it for the performance evaluation of actual port RC structures. According to these results, for example, the load carrying capacity ratio of RC slab becomes 1.0 or more with the probability of about 70 % for deterioration grade *c*, about 60 % for deterioration grade *b*, and about 20% for deterioration grade *a*, respectively. For another example, the minimum load carrying capacity ratio with the probability of 95% can be estimated as 0.72 for deterioration grade *c*, as 0.65 for deterioration grade *b*, and as 0.35 for deterioration grade *a*.

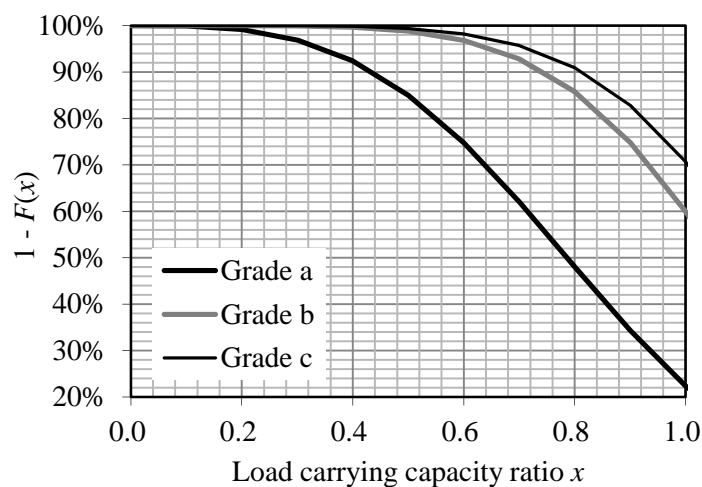


Figure 5: Cumulative distribution with which the minimum load carrying capacity ratio becomes x or more

In this research, the minimum experimental load carrying capacity ratio was 0.47 for deterioration grade *a*. Deterioration grade *a* describes the worst deterioration state; therefore, the extreme load carrying capacity ratio is considered to be 0.0 by accumulating further experimental data. The cumulative distribution of load carrying capacity ratio in deterioration grade *a* has a possibility of becoming a decentralized tendency.

The difference in the cumulative distribution of load carrying capacity ratios in deterioration grade *b* and *c* was not remarkable in this research. It

was considered to be largely influenced by the localization of deterioration and their state as discussed in 2.2. In addition, cross-sectional loss in reinforcing bars due to corrosion, that has a great influence on the load carrying capacity, was not apparently considered in the visually deterioration grading system. Moreover, the deterioration progress of RC member is greatly different associated with the exposed environmental condition, mixed material, construction condition, and service years of structures, etc.

The proposed structural performance evaluation method was developed by accumulating data of load carrying capacities and deterioration grades of RC slabs sampled from existing port RC structures located all over the country. However, the data used in this research would not cover the whole conditions related to service and maintenance of port RC structures in the whole domestic area. Therefore, it is necessary to accumulate further experimental data of load carrying capacity in each deterioration grade. Moreover, the accuracy of the load carrying capacity evaluation can be improved by considering the localization of deterioration as much as possible in judgment of the deterioration grades of b and c .

4. CONCLUDING REMARKS

The total of 40 RC slabs extracted from existing port structures was tested in order to evaluate the relationship between visually judged deterioration grades and load carrying capacities. Based on the statistical analysis on the relationship between deterioration grades and load carrying capacities, the probabilistic evaluation method of load carrying capacities of RC slabs was proposed as a quantitative evaluation method of residual structural performance of existing port RC structures. The performance index obtained by the proposed method is expected to become an effective evidence for decision of countermeasures for the strategic maintenance of large numbers of existing port structures. For this purpose, validities of the proposed structural performance index and optimization of cumulative distribution parameters for each deterioration grade, especially in deterioration grade d , have to be verified by accumulating further experimental data. In addition, the authors will examine the possibility of its application to the port structural member other than RC decks of open-type wharves and access bridges in the further research.

REFERENCES

- Ang, A. and Tang, W., 1984. *Probability Concepts in Engineering Planning and Design, Volume II Decision, Risk and Reliability*, John Wiley & Sons, Inc..
- Kato, E., Yokota, H., Iwanami, M., Akira, Y. and Kawabata, Y., 2008. Simplified Assessment for Structural Performance of Deteriorated RC Deck, *Proc. of Life Cycle Management of Coastal Concrete Structures 2*, Hangzhou, China, 75-80.

Port and Airport Research Institute, 2007. *Manual on Maintenance of Port and Harbour Facilities*, Coastal Development Institute of Technology (in Japanese)

Calibration of roughness prediction for asphalt pavement case study: Thailand's department of highways' roads

Siwarak UNSIWILAI¹ and Boonchai SANGPETNGAM²

¹Graduate Student, Department of Civil Engineering,
Faculty of Engineering

Chulalongkorn University, Thailand

²Lecturer, Department of Civil Engineering, Faculty of Engineering
Chulalongkorn University, Thailand

boonchai.sa@chula.ac.th

ABSTRACT

The Department of Highways of Thailand has implemented the Thailand Pavement Management System (TPMS) to serve as a maintenance management tool that assists the Bureau of Highways Maintenance Management and its district authorities to analyze their road network's condition, allocate their annual budget and schedule the maintenance works. The maintenance management process makes a decision based on the road condition which is represented by the International Roughness Index (IRI). The TPMS adopted the RNET equation for predicting IRI changes as a function of traffic, pavement strength, and pavement age. This paper presents the method for calibrating the IRI prediction model for flexible pavement in Thailand. The process is to adjust the factor called Kgp in the predicting equation so that the prediction resembles to the actual field condition. The IRI data obtained from the road condition survey throughout the country during 2008-2010 is selected to cover a wide range of related variables including geographic, traffic levels and pavement structures. The expected products of this study is to obtain the Kgp values that are apposite for each group of roads and help to improve the accuracy in roughness prediction of flexible pavement in the future.

Keywords: *HDM, Pavement Management System, IRI, calibration, flexible pavement*

1. INTRODUCTION

Pavement Management System (PMS) is a system tool for assisting the road authorities to efficiently plan and manage the maintenance tasks for their road network by ranking the priorities of maintenance works needed for those road sections based on the road conditions, budget allowance and effects to road users. The HDM (Highway Development and Management) is an example of the PMS software that is well known and has been implemented to the road authorities in many countries. The HDM version 3 was introduced to the Department of Highways (DOH) in Thailand in 1984.

After that, in 1987 DOH had developed its own PMS called TPMS (Thailand Pavement Management System) to suit its usage. Since then, the TPMS has been developing continually. The composition of program modules in the current TPMS is illustrated in Figure 1.

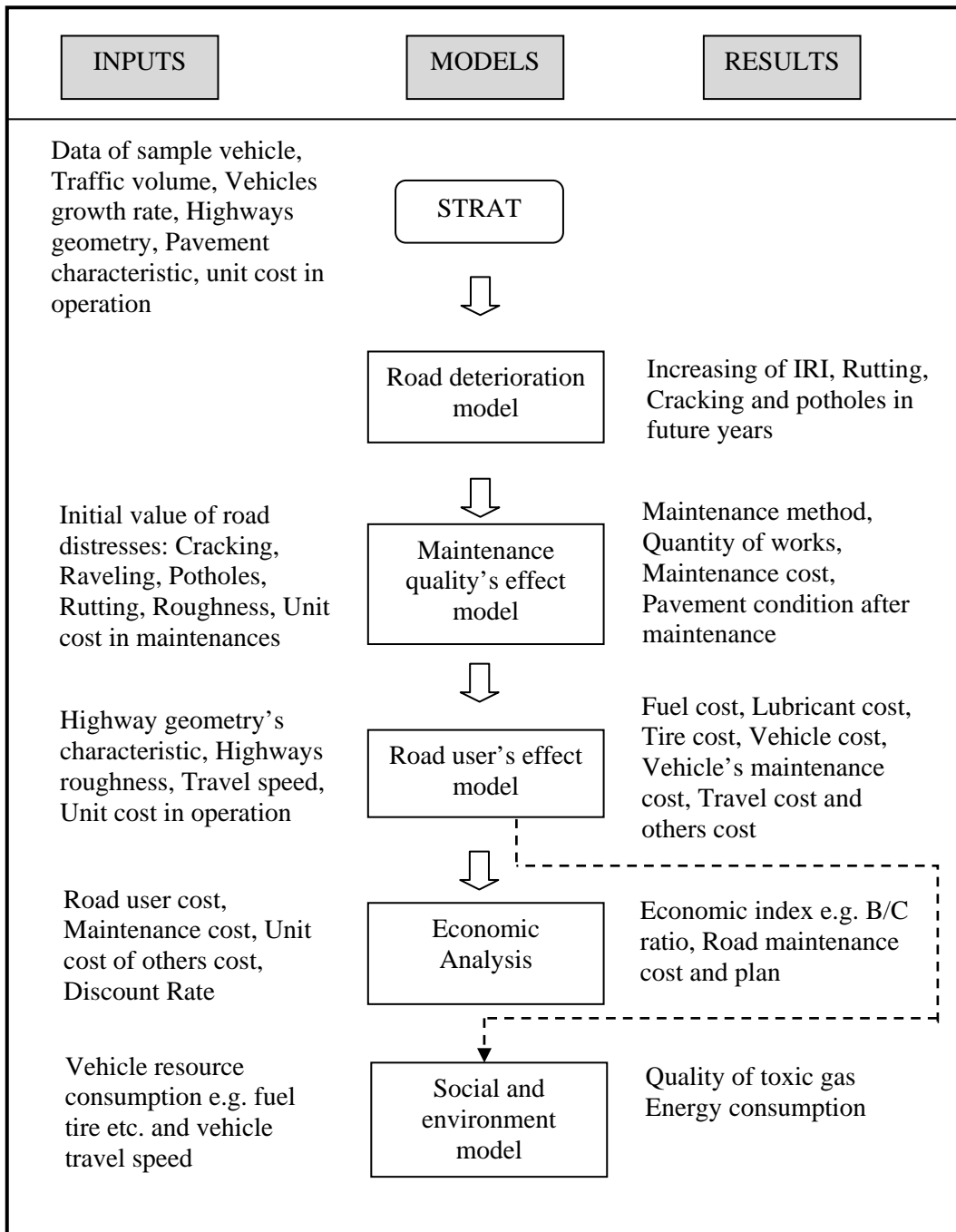


Figure 1: Composition and flow diagram of major modules in TPMS

International Roughness Index (IRI) is an indicator of the riding comfort of a standard vehicle traveling on the pavement surface. IRI is measured by recording the accumulative filtered suspension motion (in meters) of the standard vehicle and then divided by the distance traveled by the vehicle during the measurement (km), thus the unit of IRI is meters per kilometer (m/km) (Watanatada et al., 1987; WSDOT, 2005).

TPMS has adopted IRI as the principle indicator of the road surface condition and incorporated it into the road user effect module. As such, the users' vehicle operating costs are mainly dependent on the roads' IRI values. Additionally, the maintenance work type selection is based on the IRI criteria. Therefore, predicting the changes of IRI year by year is necessary for the authority to plan for the future (3-7 years) maintenance works. To predict the IRI changes, TPMS has adopted RNET's IRI progression model (Archondo-Callao, 2009) since its equation form is quite simple and is not tied to the road surface distresses such as rutting, cracking and potholes, etc. The RNET's IRI progression model is illustrated as follows.

$$dIRI = K_{gp} * (a_0 * \exp(K_{gm} * m * AGE_3) * [(1 + SNC * a_1)]^{-5} * YE_4 + a_2 * AGE_3) + (K_{gm} * m * RI_a) \quad (1)$$

where:

dIRI	=	change of IRI during one year
K _{gp}	=	calibration factor of roughness progression (1.0 for default)
K _{gm}	=	factor for environmental coefficient (1.0 for default)
m	=	environment coefficient (= 0.025 for Thailand)
AGE ₃	=	age of pavement since last reconstruction or last rehabilitation or last overlay (years)
SNC	=	modified AASHTO's structural number of pavement structure (Watanatada et al., 1987)
YE ₄	=	annual number of equivalent standard axles (million ESA/lane/year)
a ₀	=	coefficient = 134
a ₁	=	0.755, RNET study value to reflect the reduction of strength of pavement from pavement distress
a ₂	=	0.0121, RNET study value to reflect the increase in roughness from distress
RI _a	=	IRI at the start of interested year
RI _b	=	IRI at the end of interested year, = RI _a + dIRI

In the RNET equation (1), it provides the default values for the K_{gp} calibration factor of 1.0. However, Archondo-Callao (2009) suggests that the road authorities should perform calibration based on their annual IRI records from the road condition surveys to obtain a more realistic roughness prediction.

2. OBJECTIVE

The objective of this study is to perform the model calibration to obtain the new Kgp coefficient for better prediction of the IRI changes of DOH's road network.

3. METHODOLOGY

The DOH has routinely conducted IRI survey on its road network for more than 3,500 routes covering more than 59,000 kilometers using laser profiler vehicle since 2008. On a 1-kilometer length road section, the laser profiler measures a number of profile spots from the road surface, they are then averaged to obtain the representative IRI value of the road section. This valuable data along with the basic information related to the input variables in the equation (1) such as pavement structural characteristics for determining modified structural number, pavement age (years) after previous overlay/rehabilitation/reconstruction and traffic volume for estimating number of standard axles are obtained from DOH. The following processes are carried out to perform the calibration of Kgp factor based on the obtained data.

3.1 Selecting Road Sections

Since a lot of IRI data are surveyed by using laser profiler apparatus since 2008 – 2010. Our objective is to use this data to calibrate the pavement characteristic on the changes of IRI. Therefore, our interest in the data is focused on the road sections that are free of periodical maintenance and rehabilitation works. Furthermore, the select road sections must pass the following criteria:

- IRI of the selected road section increases every year
- There are at least 5 sections (5 kilometers) available on the same route vicinity.

Based on the explained criteria, IRI data from more than 40 routes covering 450 road sections is obtained and used in the calibration process.

3.2 Procedure for Calibrating Kgp value

The process of calibrating the Kgp factor is based on trial and error method to find the Kgp that produces minimum error between prediction and actual change of IRI. First, an initial Kgp is assumed for initial trial. In each step, the equation (1) is used to calculate dIRI between year 2008-2009 and 2009-2010 based on the trial Kgp, they are then compared with the actual dIRI based on the recorded data, the square of error between the prediction and actual dIRI within the two consecutive years is calculated as shown in equation (2). The square of errors of all road sections between year 2008-2009 and 2009-2010 are accumulated and is presented as the sum of error square value for the trial Kgp. In the next trials, the previous Kgp value is added by an incremental amount step by step. The calculation process is

repeated to obtain the new value of sum of error square. In the end, a relationship between Kgp and sum of error square can be plotted and the targeted Kgp that provides the minimum value of sum of error square is obtained.

The details of calibration steps are summarized as follows:

1. Calculate dIRI of selected road section from actual data by using IRI of each section between year 2008-2009 and 2009-2010, called IRI_{actual} .
2. Calculate dIRI from RNET equation (Equation 1) by using each road section properties and trial Kgp (begin with 0), called $dIRI_{\text{predict}}$
3. Calculate error^2 of each road section by the following equation:

$$\text{error}^2 = (dIRI_{\text{actual}} - dIRI_{\text{predict}})^2 \quad (2)$$

4. Calculate sum of error^2 by summing error^2 values of all road sections.
5. Add an incremental amount to the previously trialed Kgp and repeat step 2-3 using the new trial Kgp.
6. Calculate R^2 of relationship between IRI_{actual} and IRI_{predict}
7. Perform paired T-Test to verify that IRI_{actual} and IRI_{predict} are in the acceptable range of reliability of statistical meaning.

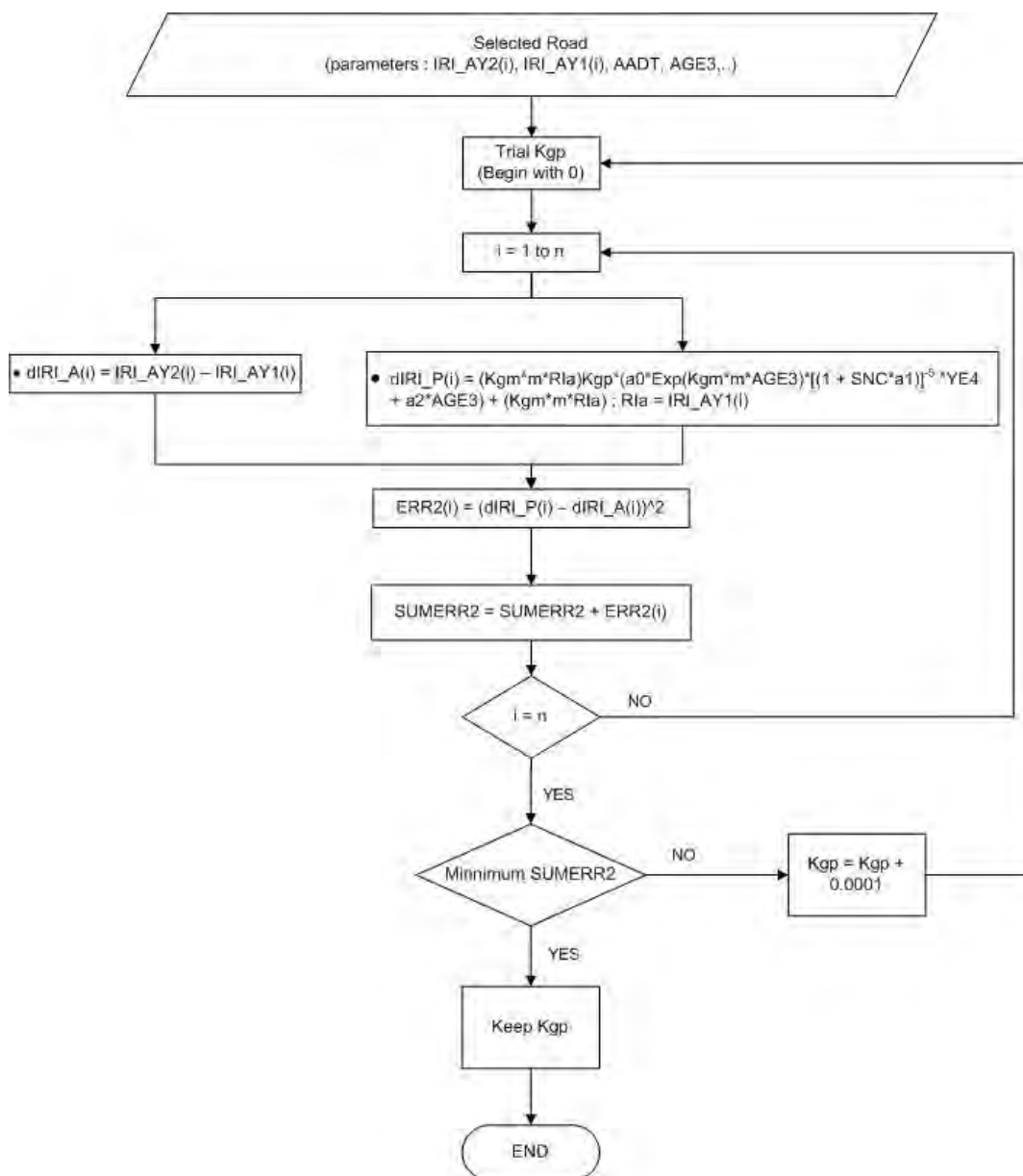


Figure 2: Flow chart shows calibration sequence

3.3 Grouping Data

The initial assumption is that the pattern of IRI change may vary by geographic location which may result in different calibration factor Kgp for each region. Additional data analysis is conducted by grouping the selected data by its geographic location into four regions of Thailand: northern, northeastern, central and southern.

Table 1: Summary of road sections allocated by region and traffic volume

-Regional	AADT (vehicles/day)	Number of sample
Northern	Less than 300	58
	300 – 1000	74
	1001 – 2500	70

-Regional	AADT (vehicles/day)	Number of sample
	2501 – 5000	70
	5001 – 10000	34
	10001 – 20000	NA*
	More than 20000	NA*
Central	Less than 300	NA*
	300 – 1000	NA*
	1001 – 2500	56
	2501 – 5000	60
	5001 – 10000	70
	10001 – 20000	NA*
	More than 20000	44
Northeastern	Less than 300	NA*
	300 – 1000	72
	1001 – 2500	54
	2501 – 5000	48
	5001 – 10000	56
	10001 – 20000	54
	More than 20000	NA*
Southern	Less than 300	NA*
	300 – 1000	NA*
	1001 – 2500	46
	2501 – 5000	42
	5001 – 10000	40
	10001 – 20000	NA*
	More than 20000	NA*

* There is no road section that fall into that particular category.

4. RESULTS AND DISCUSSION

From data of all selected road sections covering 450 kilometers throughout the country, Figure 3 illustrates the result of calibrating the Kgp factor under this data. It appears that Kgp value that yields the minimum sum of error square is 2.6077. Based on this calibrated Kgp, Figure 4 shows that the relationship between IRI_{actual} and $IRI_{predict}$ is very close to 1:1 with the corresponding R^2 value of 0.89. Finally, the result of testing paired T-Test at 95 percent confidential level in Table 2 confirms that IRI values from the prediction and from the recorded surveys of the sampled road sections are not different in statistic meaning.

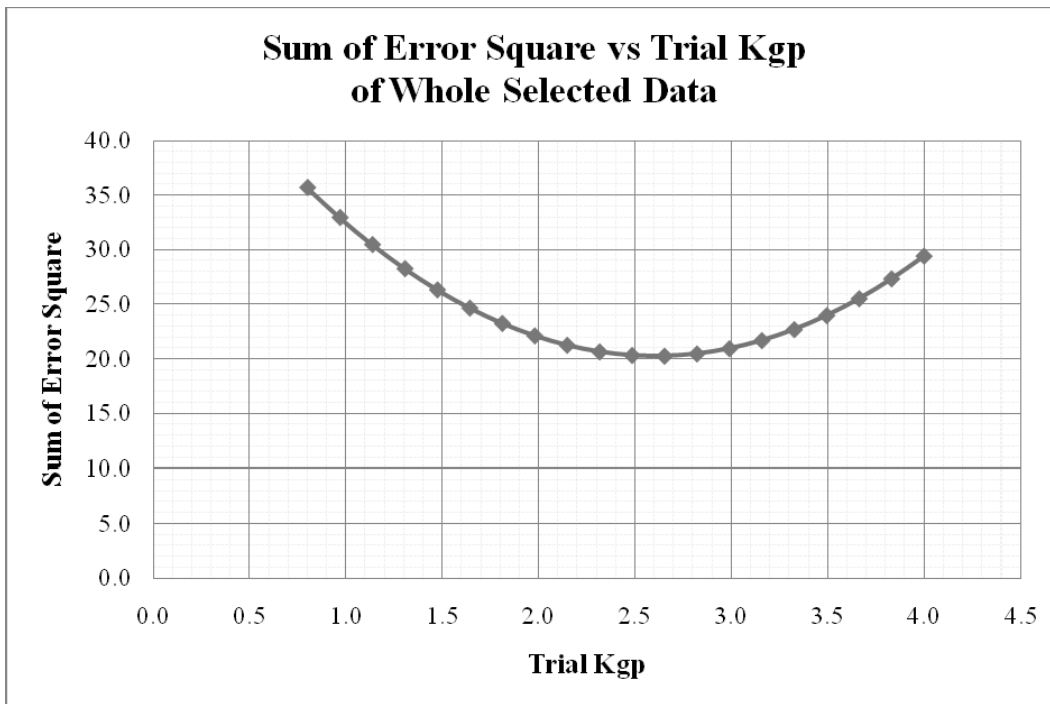


Figure 3: Result of Sum of error square and trial Kgp (throughout the country)

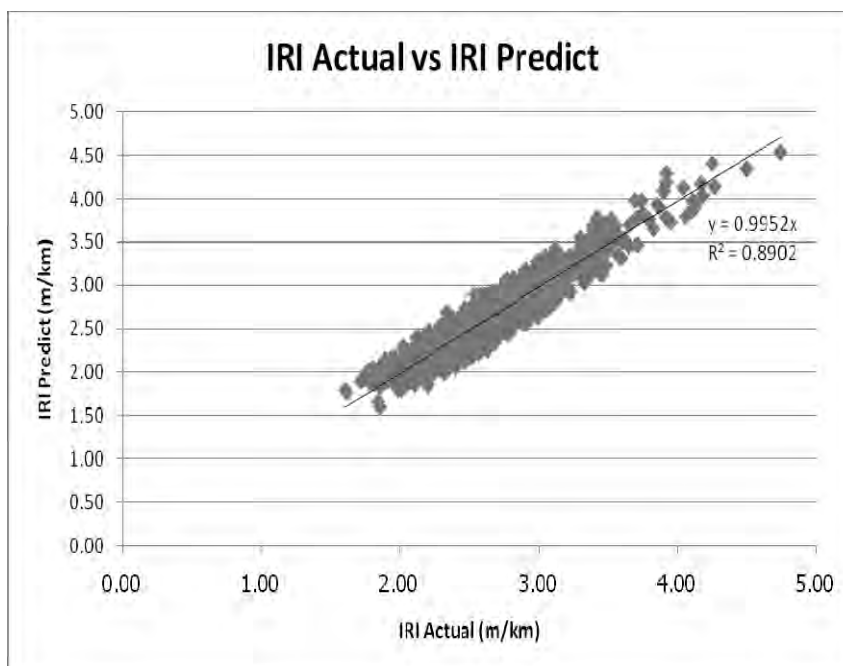


Figure 4: Predicted IRI and actual IRI (throughout the country)

Table 2: Result of paired T-Test (throughout the country)

	IRI Predict	IRI Actual
Mean	2.6738666	2.6822765
Variance	0.2524546	0.2506143
Observations	727	727
Pearson Correlation	0.9447249	

Hypothesized Mean Difference	0
df	726
t Stat	-1.3597386
P(T<=t) two-tail	0.1743348
t critical two-tail	1.9632369
95% confidential	pass

Table 3: Results from calibration based on road data of road sections throughout the country

Throughout the country	Number of sample	Kgp	R ²	Pair T-Test
	727	2.6077	0.890	Pass

For the case of calibrating Kgp factor based on grouping the road sections by 4 regions, the results of calibrated Kgp with the minimum sum of error square are presented in Table 4 along with the results of paired T-test at 95 percent confidential level. The results of calibrating the Kgp factor by region in northern, central and northeastern regions seem acceptable at R² values greater than 0.80. The result of calibration for southern region achieves R² of 0.743 considerably lower than the other regions. This might be due to the fact that the road sections of southern regions are absent of data from 4 traffic levels as illustrated in Table 1, and results in missing the complete range of IRI data.

Table 4: Results from calibration based on road data by allocated regions

Region	Number of sample	Kgp	R ²	Pair T-Test	Sampled sections
Northern	171	1.8066	0.952	Pass	see Table 1, some group of traffic levels are not available.
Central	203	2.3773	0.885	Pass	
Northeastern	226	2.9634	0.838	Pass	
Southern	128	3.8913	0.743	Pass	

4. CONCLUSIONS

The calibration of the Kgp factor in the IRI progression equation for TPMS is conducted in this paper. The results of calibration at the country level and regional level reveal that the calibrated Kgp factors are statistically acceptable based on the overall samples of 450 road sections.

For applying a proper Kgp factor into the TPMS, the Kgp factor of 2.61 is suggested. This means the rate of roughness progression in Thailand is 1.6 times faster than the default RNET prediction.

The results of calibrating Kgp factor by 4 regions indicate that the Kgp factor can vary by region: from 1.81 for northern region to 2.38 for central region, 2.96 for northeastern region and 3.89 for southern region. However, applying only one Kgp throughout the country should still predict

the IRI progression reasonably due to the statistically acceptable level of verification.

In the future, DOH should keep surveying the selected road sections to obtain the valuable data for a longer timeline. It will improve the quality of data for a better calibration.

ACKNOWLEDGEMENTS

The authors would like to acknowledge Bureau of Highways Maintenance Management, Department of Highways and the Stimulus Package 2 (SP2) of Ministry of Education under the theme of Green Engineering for Green Society for providing data, assistance and funding in this study.

REFERENCES

Archondo-Callao, R., 2009. *Road Network Evaluation Tools (RONET) Version 2.0 User's Guide*. SSATP Working Paper No. 89-A, Sub-Saharan Africa Transport Policy Program, available on (www.worldbank.org/afr/ssatp)

Center of Engineering Research and Technical Services, Faculty of Engineering Chulalongkorn University, 2009. *Department of Highways' Project: Central Road Database and Thailand Pavement Management*. Final Report. Bangkok, Thailand.

HDMGlobal., 2007. *Highway Development & Management (HDM-4) Version 2.0*. Volume 5 A Guide to Calibration and Adaptation.

HDMGlobal., 2007. *Highway Development & Management (HDM-4) Version 2.0*. Volume 6 Modelling Road Deterioration and Works Effects.

Watanatada, T., Harral, C.G., Paterson, W.D.O., Dhareshwar, A.M., Bhandari, A. and Tsunokawa, K., 1987. *The Highway Design and Maintenance Standards Model*, Volume 1 Description of the HDM-III Model. The International Bank for Reconstruction and Development/The World Bank.

Application on spatial information for the reaction of the huge earthquake -supporting recovering activities for the 2011 off the pacific coast of Tohoku earthquake-

Hirotoishi Kishi¹, Ryotaro Takeda¹, Dai Yamazaki¹, Kanya Tokunaga²,
Yoshito Sawada³, Shiro Ochi³, Takahiro Endo⁴ and Haruo Sawada⁵

¹Graduated Student, Department of Civil Engineering,
The University of Tokyo, Japan
kisshi@iis.u-tokyo.ac.jp

²Technical Assistant, Institute of Industrial Science,
The University of Tokyo, Japan

³Project Researcher, Institute of Industrial Science,
The University of Tokyo, Japan

⁴Assistant Professor, ICUS, Institute of Industrial Science,
The University of Tokyo, Japan

⁵Professor, ICUS, Institute of Industrial Science,
The University of Tokyo, Japan

ABSTRACT

Spatial information products for the response of the 2011 Tohoku earthquake were developed in this study. Firstly, reasonable information for the governmental sectors and field investigators in the hazarded area for the reaction of the earthquake were considered by our project members. We concluded the important points were the applicability and the accessibility for the spatial information. Secondly, remote sensing dataset such as aerial photos distributed by Geospatial information authority, Japan and GIS dataset were processed to share on the Google Earth (GE). In this process, Tsunami inundation line was interpreted and digitized comparing these aerial photos to satellite images taken before the earthquake on the GE. Finally, Tsunami line aerial photo map was published to understand the damaged area for the governmental sectors, field investigators, researchers and volunteers. This map is planned to keep publishing using new aerial photo taken after few months after the earthquake to support recovering activities. These all products were distributed through our project website.

Keywords: 2011 Tohoku earthquake, Tsunami, Disaster recovery, Aerial photo, GIS and Remote sensing.

1. INTRODUCTION

The 2011 off the pacific coast of Tohoku earthquake brought unprecedented damages not only for land shaken inland but also Tsunami inundated coast area. Over 20 thousand people are dead or missed because of this earthquake (MLIT, 2011) Disaster management cycle is a basic idea against natural hazards including earth quake, Typhoon, heavy rain. We humans can react in four stages against natural hazards; Mitigation and Preparedness in before disaster phase, and Response and Recovery in post disaster phase. In case of the earthquake, developing hazard maps and earthquake early warning system are classified as mitigation phase, and aseismic reinforcement and setting emergency bags are as preparedness phase. After the earthquake occurred, damage estimation and evacuation indication would be put on a importance firstly, then shifting to recovery planning in suffering area. Disaster management cycle helps local communities to prepare for the coming natural hazards (JICA, 2003).

Earth environment engineering research group, Institute of Industrial Science, The University of Tokyo has discussed what we can do at the response and recovery stage in this hazard driven by the 2011 off the pacific coast of Tohoku earthquake as spatial information engineers and discussed our activities considering situations of hazarded area and available resources. Quick damage estimation in response phase is one of the most important works for the rescue and activities for supporting the governments and regional people. Kishi et al., (2011) reported the activities focused on response stage.

Based on these backgrounds, the objective of this paper is to report the prepared spatial information and introduce application uses for the governmental sectors, volunteers and field investigators to support disaster response and recovery activities.

2. METHODOLOGY

2.1 Discussion for supporting disaster response and recovery activities

Firstly, our research group members discussed what we should do for supporting reaction and recovery activities for the governmental sectors, volunteers and field investigators. The most important information in reaction phase is to estimate the damaged area promptly. Although damaged area was extremely large in this earthquake, high resolution aerial photos or satellite images which could distinguish houses were regarded useful products for damage estimation. Secondly, finding Tsunami inundation line was regarded as important information for damage estimation because terrible damage was brought by Tsunami. Thirdly, GIS datasets including evacuation shelters, country borders, population and elevation information on the map would be useful for governmental sectors and field investigators to support recovery activities.

User friendly GIS system would be important for users because all spatial products should be accessed easily by all people who need them. Google Earth (GE) was employed as a basic GIS platform in this activity because it is one of the wide spread GIS systems all over the world, so that everyone can use it easily and free. It enables users to compare other spatial information prepared and being preparing by many contributors all over the world. For example, old information such as satellite and aerial photos, and near real time information such as traffic conditions, geo tagged pictures and GIS datasets could be modified and updated on the GE. In addition to web-based information, parpr-based products should be prepared for hazarded area use because internet connection and electric power supply are unstable or lost in some areas considering field activities. Based on these discussions, our research group concluded that 4 products should be prepared; 1) Fine resolution visible images which can distinguish buildings to understand damaged area, 2) Tsunami inundation line which clearly shows Tsunami damaged area, 3) GIS system which can refer and edit spatial information in city boundary to create recovery plans for local governments, 4) User friendly web and paper based products for delivering.

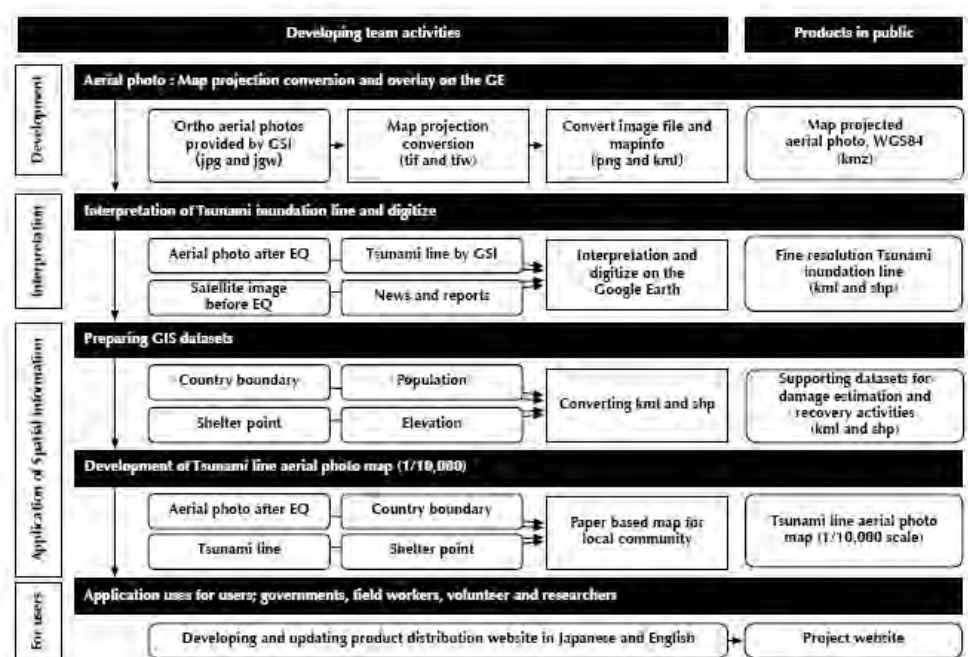


Figure 1 : Flowchart of this activity

2.2 Development of spatial products

Figure 1 shows flowchart of our activity. Firstly, Aerial photos taken over Tohoku coast area by Geospatial Information Authority, Japan (GSI) in 1 or 2 days after the Earthquake (About 80cm resolution and 2672 scenes in total) are employed. Map projection of this aerial photos is converted from zone 9 or 10 of the rectangular plane to latitude-longitude coordinate system (WGS84) to overlay on the GE. Secondly, Tsunami inundation line was interpreted by group members on the GE comparing converted aerial photos, old satellite and aerial photos, elevations and reports of governments.

Interpretation keys are defined to assure the quality of interpretations; 1) Interpreted inundation lines were basically following to the inundation line reported by GSI. 2) “Roads including Tsunami affected area” are interpreted as a clear inundation line to ensure project members share quality for interpretation and Tsunami inundation line quality is assured. Then, Tsunami inundation line another interpreter checked in heavy damaged area such as coast side urban area. Thirdly, statistical GIS datasets which would be useful for response and recovering activities were prepared to overlay on the GE. City boundary, population and area from Census in 2005, 5m digital elevation model from National land information, shelter point data from Google, DMSP night light image from NOAA/NGDC were collected. Finally, Tsunami line aerial photo map is developed in 1/10,000 scale in A1 print over heavy damaged area where many evacuated people are left. Shelters, country boundary, Tsunami inundation line are overlaid on the aerial photo. Maps are presented to local governmental sectors, field investigators and volunteer workers. Map contents such as shelter information, aerial photos and Tsunami line are updating to catch up actual situation to support recovering activities.

3 RESULTS AND DISCUSSIONS

3.1 Prepared products

Details of prepared products are shown below;

Map projected aerial photos. All projected aerial photos over Tohoku coast area distributed by GSI are converted to GE format (.kmz filetype). In this converting process, images are mosaicked before map projection conversion so that they can be divided into our intended size so that there are no space between each images; 0.05degree, 1:25,000 Japan standard map size and distributed size by GSI are prepared.

Fine resolution Tsunami inundation line. Interpreted Tsunami lines were in public soon after finishing interpretation as digital data formats for GIS users (.shp and .kml) through our project website shown in Figure 3. Immediacy is attached greater importance than accuracy to this disaster response stage. Interpreted Tsunami inundation area by our project group is about 10% larger than GSI estimation in Kesennuma city. Reasons of our overestimation are considered; (1) Road networks including Tsunami affected area are employed as Tsunami lines, (2) Coast side is regarded as inundation area, and (3) Run-up area is sometimes considered different from GSI. For the future work, cross checking is an important task because both interpretations have some missing inundation area.

GIS datasets for supporting damage estimation and recovery activities. Figure 2 shows Tsunami inundation line and 5m digital elevation model in Sendai area overlaid on the GE. It is found that elevation is one of the most important keys to avoiding Tsunami damage. We contributors all over the world can work together because not only our prepared products but also other GIS datasets can be overlaid on the GE.



Figure 2: Overlaid Tsunami inundation line and 5m DEM over Sendai area on the Google Earth.

Tsunami line aerial photo map (1/10,000 scale) Figure 5 shows the Tsunami line aerial photo map (1/10,000 scale) over Kesennuma area. Paper based map would be useful for local government, field investigators and volunteer workers.

These products are distributed through our project webpage shown in Figure 3 (http://stlab.iis.utokyo.ac.jp/eq_data/). Every products can be downloaded through this website, which is constructed in Japanese and English. There are still few websites of 3.11 constructed in English.

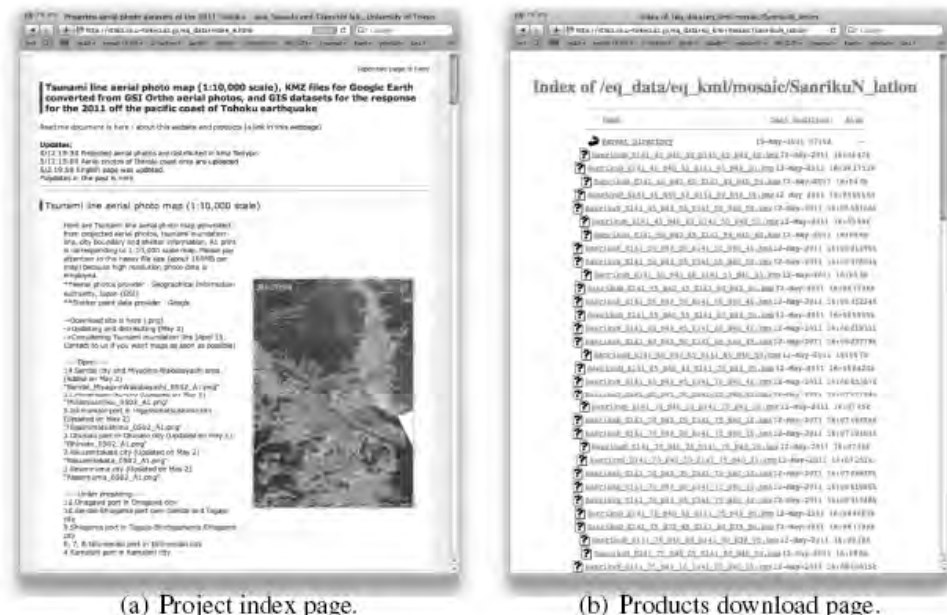


Figure 3 : Project webpage (http://stlab.iis.u-tokyo.ac.jp/eq_data/)

3.2 Application uses of products

Prepared products are widely used by governments, research institute and private company for damage estimation and recovery activities through our website as shown in Figure 3. Figure 4 shows examples of products application uses. Picture (a) is taken in Katsura-sima in Shiogama-city in April 2011. Tsunami line aerial photo maps were delivered by one of our project members to support volunteer works and local government activities. Katsura-shima had a huge damage because of earthquake and Tsunami so that many volunteer workers visited there. Paper based maps are useful information for understanding situations especially for volunteers at the site. (b) shows exhibition room in a school festival of University of Tokyo in May, 2011. Some students of Civil Engineering department in University of Tokyo who joined field survey in Tohoku area, employed the interpreted Tsunami Inundation line data as contents to make a large scale map for exhibiting their research results. Visitors could easily understand the Tsunami damages and geographical situations over Tohoku area. (c) shows land terrain elevation and inundation line in Sendai from Hokkaido-Chizu Inc. Predicted Tsunami inundation line shown by prepared hazard maps before 3.11 and actual tsunami line interpreted by this project after 3.11 are drawn in one map. It is found that Tsunami prediction didn't match for 3.11 earthquake. (d) shows iPhone/ipad application, "Chizu burari which is developed by ART-Promotion Inc. Tsunami line aerial photo maps shown by figure 5 and map projected aerial photos are employed as application contents. Maps can be checked even in under the offline conditions once they are downloaded and every user can download these prepared products in one's iPhone/iPad with GPS information.

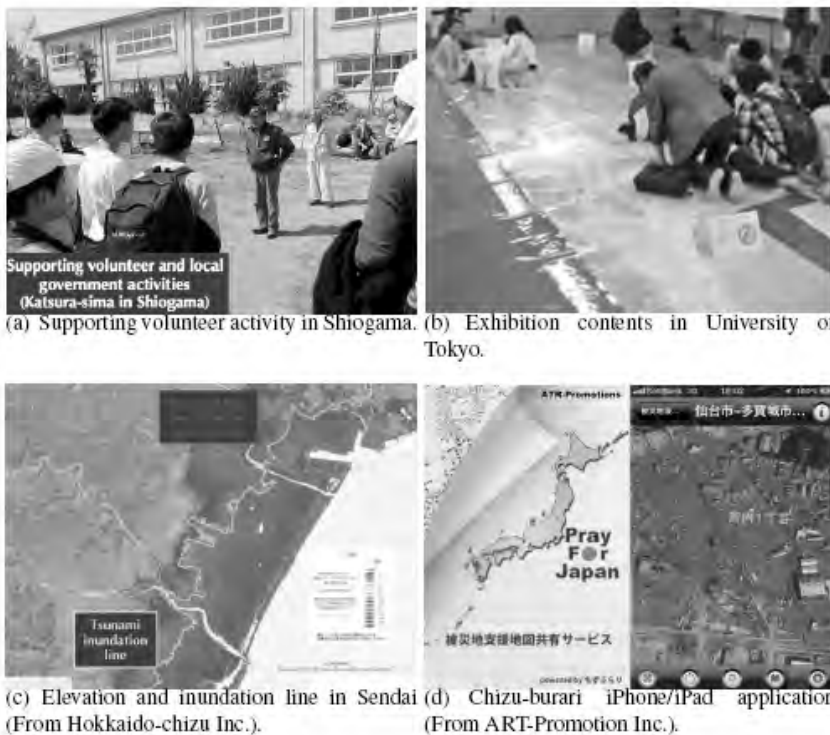
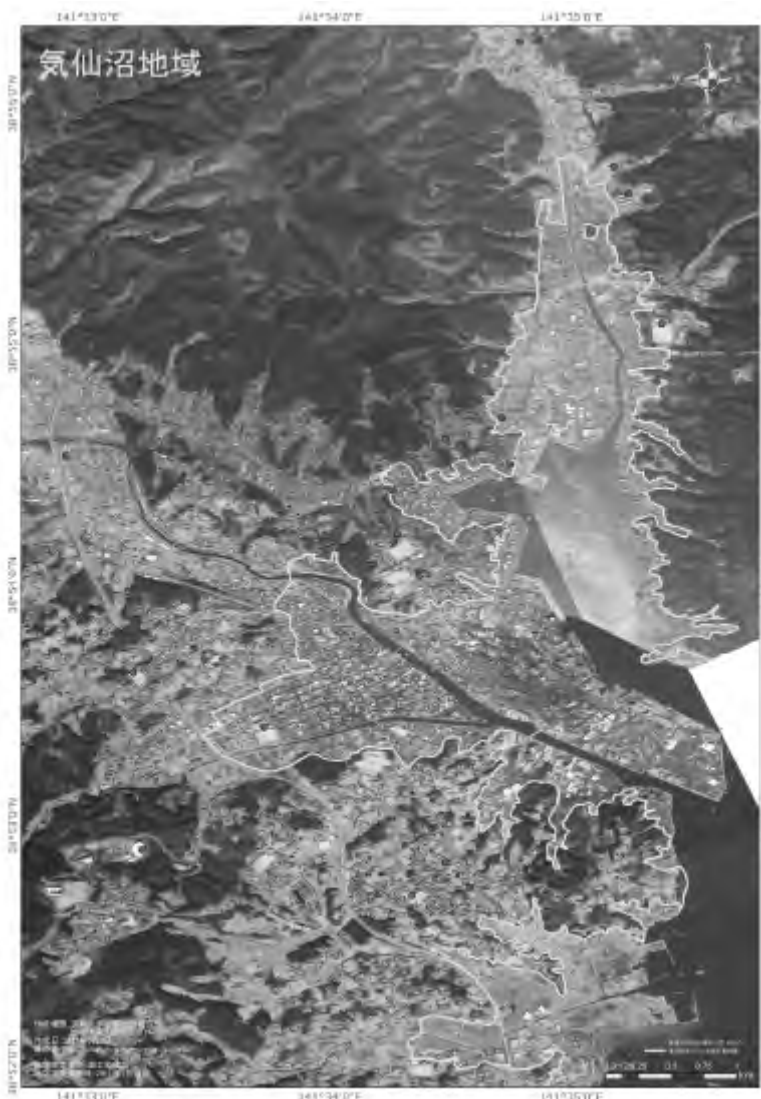


Figure 4 : Products application uses



*Figure 5 : Tsunami line aerial photo map
(Kesennuma, 1:10,000 scale original)*

3.3 Discussions and suggestions

Several difficulties are found through this project activities. Here shows the difficulties and suggested solutions for supporting disaster response and recovery activities. Firstly, establishing an agency that evaluates spatial information are highly recommended because much information were provided by many institutes, individuals and governments after the 3.11 EQ but it was not clear which information is suitable for users. The agency would introduce spatial information for users considering differences in spatial and temporal resolution, dataset level, accessibility of the spatial data. Secondly, satellite observation data application for large scale disaster should be discussed because aerial photos are of course very useful for disaster response but it took few weeks to deliver ortho images because large area were hazarded. Developing a framework of satellite image application is important for damage estimation soon after an earthquake happens automatically even in large area. If application method

of satellite images for disaster damage estimation were developed, we could understand damaged area more quickly. Thirdly, establishing co-contribution framework in spatial information engineers is urgent task because understanding other communities' activity was difficult in the disaster response activities. It was true that many efforts have done but we couldn't share ideas with other community contributors. Sharing information and constructing relationship among spatial information engineers or institutes are highly expected for the case of emergency.

4 . SUMMARY

Reasonable spatial information products are discussed and developed for the response to the 3.11 earthquake; aerial photo overlaid on the Google Earth, interpreted Tsunami inundation line, GIS datasets including country boundary and shelter points, and Tsunami line aerial photo map based on these products. These all products are distributed through our website and kept updating. Products are widely employed by field workers, researchers and private companies. For the future works, providing information are to be updated because conditions in suffering area are changing. 1/10,000 scale map are going to be updated using new aerial photos taken after few months from 3.11 EQ, which is planning to be distributed from GSI to support recovery activities.

REFERENCES

Japan International Cooperation Agency. 2003. Disaster prevention and development - Towards enforcement of social disaster prevention power-

Kishi. H., Takeda. R., Yamazaki. D., Tokunaga. K., Sawada. Y., Ochi. S., Endo. T.,

Sawada. 2011. Application of spatial information for the reaction of the huge earthquake -Response for the 2011 off the pacific coast of Tohoku earthquake- Proceeding of 50th Remote sensing society of Japan. pp83-86. 2011.

Ministry of Land, Infrastructure and Transport, Japan. 86th report for Tohoku earthquake released on August 15, 2011.

Challenges in preparedness, response and relief for people with special needs in times of disasters followings the great East Japan earthquake

Shigeo TATSUKI

Professor, Department of Sociology, Doshisha University, Japan
statsuki@mail.doshisha.ac.jp

ABSTRACT

Three major challenges were identified and their possible solutions were proposed in preparedness, response and relief measures for People with Special Needs in times of Disasters (PSND) following the 2011 Great East Japan Earthquake. First, recent developments in preparedness measures for PSND in Japan have been uncritically relying on the assumption that hazard maps represent “correct” estimates of future hazardous events, which are based on maximum probable event (MPrE) framework. In reality, however, maximum possible event (MPoE) has occurred in Tohoku regions. This has tremendous implications for fundamentally re-thinking entire hazard estimation process from MPrE to MPoE framework. Second, counter-disaster measures for PSND have focused mainly on warning and neighborhood-based evacuation assistance activities. Needs for shelters and temporary housing units that are specially designated for PSND arose following the earthquake. However, their provision was neither systematic nor universal due to the lack of pre-planning. More detailed guidelines for specially designated shelter and temporary housing operation need to be developed in order to address this issue. Third, people with disabilities (PWD) became invisible in shelters and communities or in eyes of local government administrators. This is due to the fact that majority of PWDs did not ask for help in evacuation shelters because they felt general shelters were not “barrier free” and unresponsive to their functional needs. Furthermore, many local government administrators felt hesitant to release PSND registry to NGOs and self-help organizations that were eager to check where-about and current situations of PWDs. This was due to the fear of breaking Personal Information Protection Bylaw despite the fact that the Bylaw provides exceptional conditions, where the onset of disaster is clearly one of these exceptional conditions. Further elaboration and education on the use of personal information of PSND during disaster period are needed among public and local government administrators.

Keywords: *people with special needs in times of disasters (PSND), the Great East Japan Earthquake, maximum probable event, maximum possible event, specially designated shelters and temporary housing for PSND, personal information protection bylaw*

1. INTRODUCTION

1.1 Counter-disaster measures for PSND in Japan

The issue of special needs population gained high attention after 2004 when a series of natural disasters hit the Japanese Archipelago. Those included July Niigata-Fukushima flood, October typhoon 23 and October Niigata Chuetsu earthquake disasters, wherein notably more than 60% of the victims were over the age of 65. As a response to these tragedies, Japan's Cabinet Office established a committee on "Communicating Disaster Information and Evacuation and Sheltering Assistance for the Elderly and Other Population during Heavy meteorological and Other Disasters." The committee published the first edition of the "Evacuation/Sheltering Assistance Guideline for People with Special Needs in Times of Disasters" in the following March 2005. After the guideline publication, the term *saigaiji-youengosha* or People with Special Needs in Times of Disasters (PSND) was popularized in place of *saigai-jakusha* or Disaster Vulnerable Population. PSND is defined as "a person who is able to function daily, whereby living independently given the proper resources and services when necessary".

Following another series of heavy rainfall, flood and land slide disasters in the year 2005, another Cabinet Office committee conducted field research of the 2005 meteorological disaster sites and revised the evacuation and sheltering assistance guideline in March 2006. The 2006 guideline emphasized 1) establishing a special team in each municipal government that was in charge of coordinating assistance to the target population, 2) encouraging the information sharing of special needs population within the local government and, if possible, with local community organizations such as neighborhood associations and community emergency and response team, and 3) planning individualized evacuation and sheltering procedures for each PSND.

In the following fiscal year 2006, the committee on PSND continued working on more detailed procedures and workflows in order to collect, to share information on PSND and to make individualized evacuation and sheltering assistance plans. In March 2007, the committee published the "Report on Preparedness Procedures for PSND." The 2007 report emphasized the establishment of a system to assist PSND by facilitating cooperation between the local/municipal government disaster management department and its health and welfare department. The role of the disaster management department is to provide local hazard information, while the health and welfare department provides information on potential vulnerabilities within the target population. The 2007 report encouraged the use of map where potential vulnerable individuals such as the frail elderly and people with disabilities (PWD) are projected onto multiple hazard layers such as flood, landslide and seismicity. The map can help identify who are at more risk because of their functional needs as well as of their geographic locations.

Since the publication of the 2006 guideline and the 2007 report, the Fire and Disaster Management Agency (FDMA) has requested every municipality in the country to formulate its own master plan that directs policy formation on PSND assistance, to identify potential target groups, to clarify ways to collect and share their personal information. Based on the master plan, municipalities have been further encouraged to start project planning to assign local resident helpers to each individual PSND in time of evacuation. According to the survey conducted by FDMA, as of April 1, 2011, 1,262 out of 1622 municipalities (76.8%) finished formulating PSND assistance master plan and additional 349 municipalities (21.2%) were expected to finish within one year. Similarly, 864 (52.6%) municipalities reported that they have finished creating and have been updating the PSND directory. 684 (41.5%) municipalities said that they were currently in the process of making the directories. Municipalities have been working hard even on assigning local residents/helpers to each PSND for evacuation, much more time consuming process. 361 (22.0%) reported that they have completed the assignment, 998 (60.7%) in the process, and 285 (17.3%) not yet initiated (FDMA, 2011).

1.2 Kobe PSND Mapping Project

Tatsuki and Comafay (2010) reported the 2008 Kobe PSND Mapping Project, which was characterized by a combined use of GIS and the social survey in order to assess overall hazard vulnerability of PSNDs. In response to the FDMA request as explained in the above, 1.5- million-resided Kobe city administration collated separate social service recipient databases, resulting in an integrated registry involving one hundred and twenty thousand individuals who were considered being potentially vulnerable in time of disaster. The registry database identified 4,329 people with physical disabilities in 107- thousand-resided Hyogo Ward. The 2008 project geocoded and mapped them on land slide, flood and tsunami hazard layers. 914 individuals were found residing in hazardous areas (see figure 1).

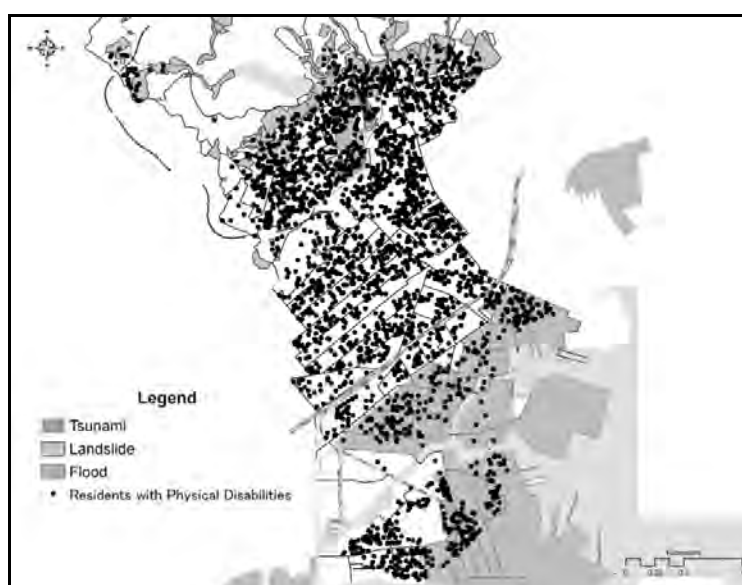


Figure 1: Persons with disabilities living in Kobe's Hyogo ward (N= 4,411)

These 914 individuals were then visited by interviewers and 612 or 67% responded to a structured questionnaire which measured demographics (i.e., age and gender), levels of disability, social isolation, housing fragility, and physical immobility. The 2008 project was based on the person-in-environment model of vulnerability, which defined hazard vulnerability (V) as a function of hazards (H), person (P), and environment (E) factors or $V = f(H, f(P, E))$ as illustrated by figure 2.

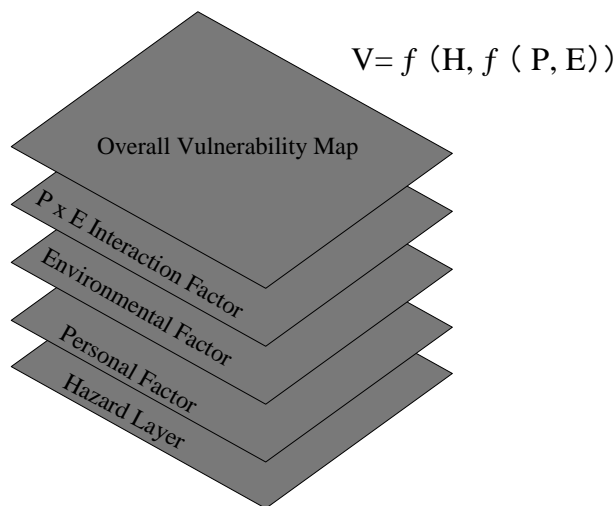


Figure 2: Person-in-Environment model of mapping hazard vulnerability

Based on the model, an overall vulnerability score was then calculated as a function of hazards and the five variables for each respondent. As a result, 17% of those who responded were found the most vulnerable and requiring priority assistance in time of disaster (see figure 3).

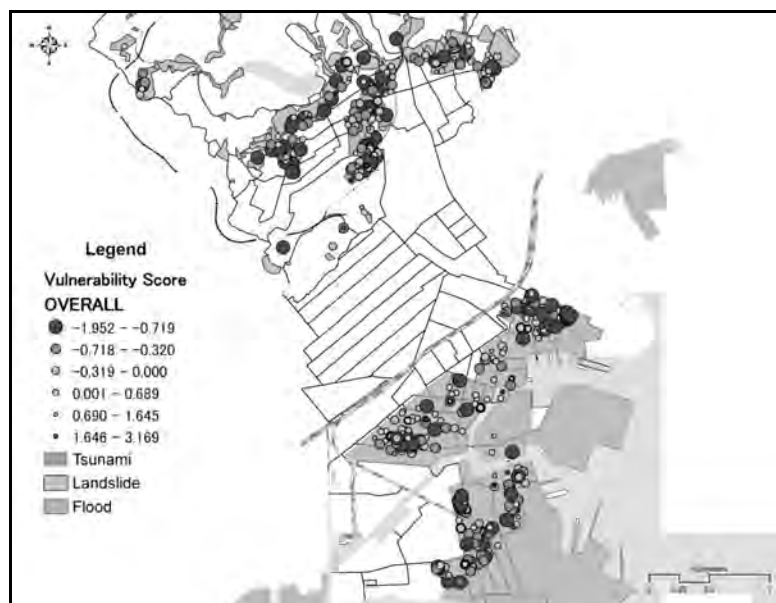


Figure 3: Overall vulnerability scores mapped on to hazard layers

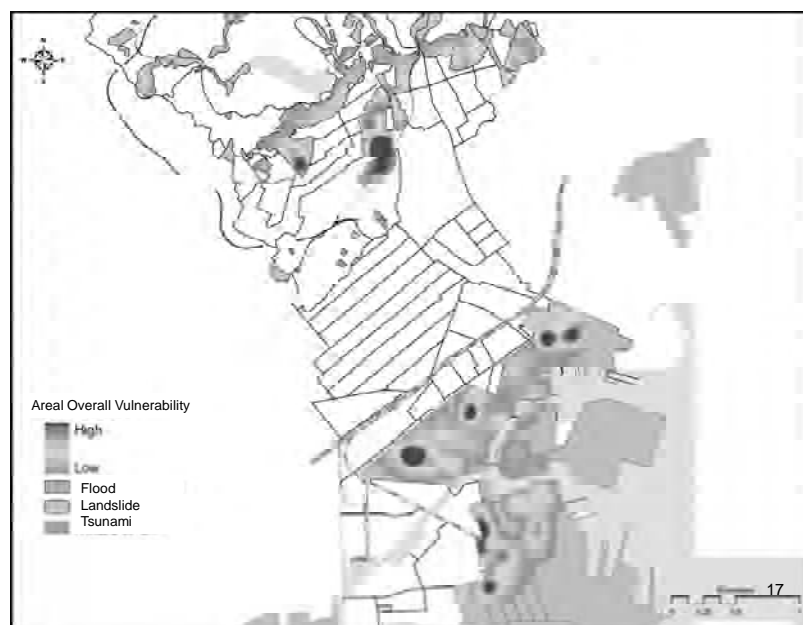


Figure 4: PSND kernel density estimation weighted by overall vulnerability index

Furthermore, a social vulnerability weighted kernel density map of people with special needs was created (see figure 4). This map indicated which particular areas require more human resources for assisting a special needs population for evacuation and sheltering. The project product maps helped representatives from special needs groups, community emergency response teams, community social services, and emergency management centers initiate evacuation and sheltering assistance planning in the project areas.

The 2008 Kobe PSND mapping project was an attempt that aimed to provide a standardized method using individual social vulnerability mapping as analysis tool to identify more comprehensively the risks that could affect a given community. This could help different stake holders, special needs groups, community emergency response teams, community social services, and emergency management centers initiate evacuation and sheltering assistance planning in high risk communities.

2. THREE CHALLENGES IN PSND COUNTER-DISASTER MEASURES AFTER MARCH 11, 2011

Despite the above mentioned nation-wide efforts on PSND counter-disaster measures in recent years, serious problems confronted municipalities, communities, PSNDs and their families at the onset of March 11 Great East Japan Earthquake Disaster. From three reconnaissance missions conducted by the author team in March and April, at least three major challenges were identified in preparedness, response and relief measures for PSND. Those were namely 1) challenges on identifying people at risk by re-thinking “correct” hazard estimates, 2) challenges on pre-planning specially

designated shelters for people with special needs, and 3) challenge on utilizing personal information on PSND. Each challenge is explained in the following sections.

2.1 Challenges on identifying people at risk: Re-think “correct” hazard estimates

Recent developments in preparedness measures for PSND in Japan have been uncritically relying on the assumption that hazard maps represent “correct” estimates of future hazardous events. As figure 5 in the below illustrates, this turned out to be a horribly wrong assumption. Hazard maps were created according to *maximum probable event* (MP_rE) framework. In reality, however, *maximum possible event* (MP_oE) has occurred in Tohoku regions. This has tremendous implications for fundamentally re-thinking entire hazard estimation process from MP_rE to MP_oE framework.

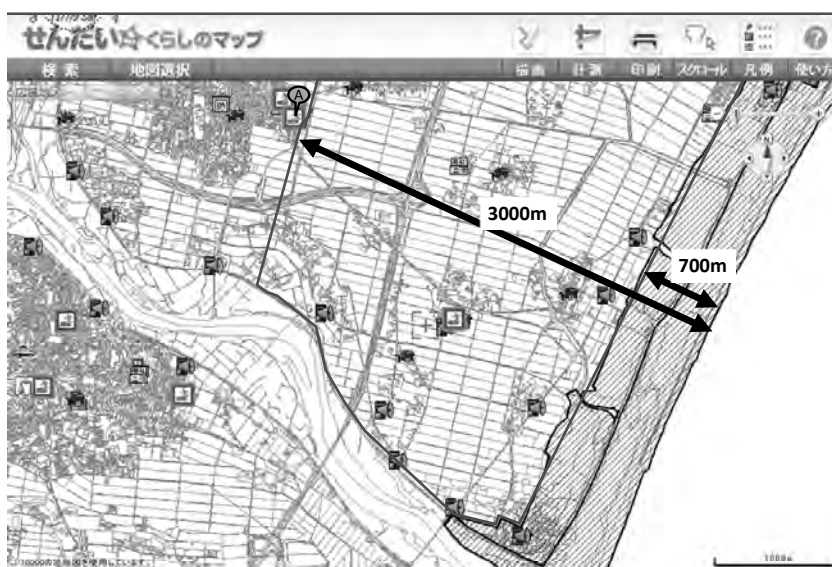


Figure 5: Tsunami hazard map and actual inundation east of Rokugo Junior high school, Wakabayashi ward, Sendai city

In the previous section, the person-in-environment model of hazard vulnerability (V) was introduced as a function of hazard (H), person (P) and environment (E) factors or $V = f(H, f(P, E))$. In practice, hazard factor was estimated by *maximum probable event* framework and therefore the model could be represented as $V = f(MP_rE, f(P, E))$. The challenge here is to replace *maximum probable event* hazard estimate with an alternative hazard estimate by incorporating *maximum possible event* framework. The modified person-in-environment model will therefore be represented as $V = f(MP_oE, f(P, E))$.

2.2 Challenges on pre-planning specially designated shelters for people with special needs

As was described in the introduction, counter-disaster measures for PSND have been focusing mainly on warning and neighborhood-based

evacuation assistance activities. Needs for shelters and temporary housing units that were specially designated for PSND arose following the March 11 earthquake. However, their provisions were neither systematic nor universal due to the lack of pre-planning. This is partly due to the fact that the 2006 guideline or the 2007 report has not provided detailed procedures on sheltering assistance planning for PSND. The concept of specially designated shelter for PSND or *fukushi-hinansho* emerged in 2004 from the discussions by the committee on “Communicating Disaster Information and Evacuation and Sheltering Assistance for the Elderly and Other Population during Heavy meteorological and Other Disasters.” It was recognized that general evacuation shelters as shown in figures 6 and 7 were not capable of responding to special or functional needs of PWD and the frail elderly. Functional needs include those in “communication, medical needs, maintaining functional independence, supervision, and transportation” (Kailes and Enders, 2007, p.234) that arise in times of disaster. The committees on PSND assistance, however, have not spent enough time to clarify requirements for, procedures or guidelines of specially designated shelters. Most hazards that the PSND committees have been studying since 2004 have mainly been meteorological and therefore sheltering needs were short-term and considered being less life-threatening than evacuation needs.



Figure 6: School Gym Shelter at Rokugo junior high school, Sendai City (April 6, 2011)



Figure 7: Arahama Residents on the 1st Floor Classroom at Hakken junior high school (April 6, 2011)

The March 11 earthquake disaster created a situation where a very large number of people rushed to general shelters and the length of stay was relatively long, creating high functional needs from PSND. This apparently required alternative shelters. Disaster hit municipalities responded to this situation in un-uniform manners. In the case of Sendai city, the city administration had already made pre-planned arrangements/compacts for alternative sheltering service with 52 local social service providers prior to the March event. Some of those compacted shelters conducted study seminars and practice drills in the previous year. Thanks to these preparations, some responded to the city administration request quickly and the other even voluntarily initiated sheltering operations. In total, 26 shelters operated and served about 260 individuals in Sendai city (see figure 8).



Figure 8: Specially Designated Shelter at Miyagino Day Service Center for PWD, Sendai City (April 5, 2011)



Figure 9: Specially Designated Shelter at Yugakukan Sport Center Gym, Ishinomaki City
(<http://road.nippon-foundation.or.jp/2011/04/007-fcd1.html>)

Downtown center of Ishinomaki city was badly damaged by March 11 tsunami forcing more than thirty thousand people or about one fifth of its population in general shelters at its peak. A medical doctor helping one of a large general shelters strongly demanded the city administration that an alternative shelter be provided for the frail elderly, PWDs and those out-patients that did not require intensive medical care from the tsunami unaffected Ishinomaki Red Cross hospital. The city temporally designated Inai junior high school gym and then later moved the 20 to 30 shelter occupants to Yugakukan sport center gym (see figure 9) on March 29. Yugakukan gym eventually accepted about 130 people including PSNDs and their family members. Yugakukan shelter was staffed initially by most of Ishinomaki Municipal hospital doctors, nurses and social workers who lost their work place due to the tsunami attacks. Volunteer doctors, nurses, social workers, nursing care workers and public administrators from other prefectures came to the Yugakukan shelter and assisted the operation from early April.

It should be noted that Ishinomaki city was renowned for its city wide community-based evacuation planning initiatives for PSNDs. The city was recognized as one of the ten model municipalities on PSND preparedness master planning as early as year 2004. By the end of year 2010, 401 out of 421 administrative districts in the city completed individualized evacuation planning for each PSND in the neighborhood. The city's master plan for PSND, however, did not include planning on specially designated shelters. Inai junior high school and later Yugakukan shelter operations were all improvised by city hospital doctors and nurses with the support from the city. The city, however, was not aware of special service provision clause in Disaster Relief Act that qualified additional financial compensations on top of general service provisions from the national government. It was not until almost the end of April that the city formally designated Yugakukan as the specially designated shelter for PSND. To sum up, specially designated shelters operated in Ishinomaki city but the operation remained lacking formal logistic support foundation for a prolonged period of time.



Figure 10: Specially Designated Shelters at Shunpo-en Special Nursing Home (Top) and Ochiai Nursery School (Bottom)

Like Ishinomaki, more than twelve thousand or one sixth of Kesenuma city population rushed to general shelters after the earthquake and tsunami in March. Until April, the frail elderly, PWDs and small children were all mixed with other evacuees who looked after those in needs at general shelters. In some shelters, partition cardboards were used to separate PSNDs from general evacuees in order to provide some privacy. On April 7, the city administration officially opened the first specially designated shelter for PSND on an unused nursery school site (see figure 10). In the following two weeks, additional four specially designated shelters were opened. Shunpo-en special nursing home for elderly (see figure 10) was one of those four new specially designated shelters. It was serving 60 elderly residents as well as more than one hundred general evacuees and some PSNDs from the neighborhood after the March disaster. Those PSNDs were taken care by the home staff workers. The director, however, was afraid of financial burden to run specially designated shelter for an extended period of time. Later in April, the city administrators learned that official designation would allow additional care service provision from Disaster Relief Act. This was on top of the provision of regular service hours as prescribed by long-term care insurance scheme. This alleviated tremendous financial burden which the city and/or the designated shelters like Shunpo-en home might have had to bear otherwise. In other words, Kesenuma city also lacked pre-planning on specially designated shelters and the administration was not aware of legal framework (i.e. Disaster Relief Act special service provision clause) to operate these shelters.

In conclusion, municipalities other than Sendai city did not have compacts on specially designated shelter operations with social service providers. It took nearly three weeks for Ishinomaki and Kesenuma to formally designate such shelters after the earthquake. It was learned that they were hesitant because they believed their facilities would not meet the standard for specially designated shelters, as outlined in pre-disaster planning manuals. Additionally, many local officials were unaware of the special service provision clause of the Disaster Relief Act covering shelters

for people with special needs. Nonetheless, these kinds of sheltering operations did emerge. Had the local municipalities officially declared that they were operating special-needs shelters, they would have been eligible for additional resources at the onset of the event from both the national and prefectural governments. More detailed guidelines for specially designated shelters and temporary housing operation for PSNDs need to be developed in order to address this issue.

2.3 Challenges on Utilizing Personal Information on People with Special Needs in Times of Disasters

Among different types of PSNDs, people with disabilities (PWD) were invisible in shelters and communities or in eyes of local government administrators. This was due to the fact that majority of PWDs did not ask for help in general shelters because they felt general shelters were not “barrier free” and unresponsive to their functional needs. Furthermore, many local government administrators felt hesitant to release PSND registry to NGOs and self-help organizations that were eager to check where-about and current situations of PWDs. This was due to the fear of breaking Personal Information Protection Bylaw despite the fact that the Bylaw provides exceptional conditions, where the onset of disaster is clearly one of these exceptional conditions. In fact, Minamisoma city officials did release that information to a local NGO, and in Higashimatsushima, members of groups who worked on behalf of disabled persons, such as the Japan Disability Forum, were allowed to accompany public health nurses on their home visits. Other cities might have been using similar approaches, but it appeared that in most affected areas officials were unaware of the needs of mentally ill and developmentally disabled persons and had not attempted to initiate outreach efforts for those populations. As of June 2011, Japan Disability Forum announced that they were able to meet 1,386 PWDs in person from their outreach project in Miyagi prefecture. This number (1,386) accounted for only 2.6 % of 53,511 persons who were registered to be PWD in the affected areas. Researchers and advocates for persons with disabilities were unable to determine what was happening with large numbers of survivors with disabilities. Further elaboration and education on the use of personal information of PSND during disaster period are needed among public and local government administrators.

CONCLUSION

This paper first introduced recent developments on counter-disaster measures for PSNDs in Japan. Based on three reconnaissance missions in March and April three major challenges and their possible solutions in preparedness, response and relief measures for PSND were presented. First, challenges on identifying people at risk were illustrated. This would require re-thinking from *maximum probable event* to *maximum possible event* framework. Second, challenges on operating specially designated shelters for people with special needs were identified. Further elaboration of the guideline on sheltering was suggested. Third, challenges on utilizing

personal information on PSND during disaster were presented. Further elaboration and education on this matter was recommended.

REFERENCES

Aoki, K. 2011. Report on supporting a specially designated shelter in Kesennuma city, Miyagi prefecture. West Tokyo City Elderly Center Kirara (<http://www.toshinkai.or.jp/image/C8EFBAD2C3CFC7C9B8AFCAF3B9F0.pdf>, October 1, 2011)

Fire and Disaster Management Agency, 2011. A research report on municipalities counter-disaster measures for people with special needs in times of disaster. (http://www.fdma.go.jp/neuter/topics/houdou/2307/230708_1houdou/02_houdoushiryuu.pdf, September 26, 2011)

Kailes, J. I. and Enders, A. 2007. Moving beyond “special needs”: a function-based framework for emergency management and planning, *Journal of Disability Policy Studies*, Vol.17, No.4, 230-237.

Tatsuki, S. and Comafay, N. 2010. Evacuation and sheltering assistance planning for special needs population: Kobe disadvantaged population mapping project, Presentation for International Sociological Association World Congress of Sociology, Gothenburg, Sweden, July 15, 2010.

Simple and inexpensive tsunami disaster mitigation system for Indian Ocean Rim Regions by combining multi-purpose ocean observation buoys and properly arranged evacuation centers using religious facilities

KIMIRO MEGURO¹⁾, Shiyunichi KOSHIMURA²⁾
and Muneyoshi NUMADA³⁾

^{1),3)} International Center for Urban Safety Engineering
Institute of Industrial Science, The University of Tokyo, Japan

²⁾ Tokoku University, Sendai, Japan

ABSTRACT

Triggered by a M9.0 earthquake that occurred along the Sunda Trench, Off-Sumatra, at 07:58 (local time), on December 26, 2004, a huge and devastating tsunami hit the Indian Ocean Rim countries, causing unprecedented disaster with over 300,000 dead and missing persons. The analysis of other potential tsunami scenarios in the region has revealed that 1.3 million dead and missing people may be expected, at worst. Therefore, an effective and sustainable framework against tsunami disaster is indispensable in this region.

Land use control, i.e. preventing people from residing next to the shore, is one way to mitigate tsunami disaster if people follow it. However, this is not always a proper option in the Indian Ocean Rim region where the economic activities, e.g. fishing, tourism, take place directly next to the seaside. For this case, a New Tsunami Disaster Mitigation System by combining a reliable warning system and proper evacuation facilities is proposed. Important characteristics of this system are its simplicity, economical efficiency and daily-usability.

This paper introduces the New Tsunami Disaster Mitigation System, highlighting. The New System for the Indian Ocean Rim region combines a reliable warning system and proper evacuation facilities. The warning system consists of multi-purpose observation buoys operated by local organizations such as hotels and beach associations. The system is not only used for tsunami warning but also to monitor temperature, current velocity, wave height, moisture, etc., information which can be used on a daily basis for the economic activities of the region.

The proposed evacuation facilities are designed taking into consideration: sheltering capacity, location, and structural strength. Location is especially important to prevent that the structures are washed away by the tsunami and to guaranty an easy access for the evacuees.

In order to verify the suitability of the proposed system, tsunami and evacuation simulations are carried out. The strong points of the proposed system are its simplicity, economy and daily usability, which makes it a sustainable option for the region.

1. INTRODUCTION

Triggered by the M9.0 Earthquake that occurred along the Sunda Trench, Off-Sumatra, at 07:58 (local time), on December 26, 2004, a huge and devastating tsunami hit the Indian Ocean Rim countries, causing unprecedented disaster with over 300,000 dead and missing persons. The tsunami was triggered by one of the possible earthquake scenarios along the Sunda Trench. Four other potential earthquake events along the trench have been identified and the expected number of casualties in case they occur has been estimated. As a result, it was revealed that 1.3 million dead and missing people are expected, at worst, as shown in Figure 1. This number is several times larger than the observed in the December 26, 2004 event, showing that an effective and sustainable framework against tsunami disaster is indispensable in this region.

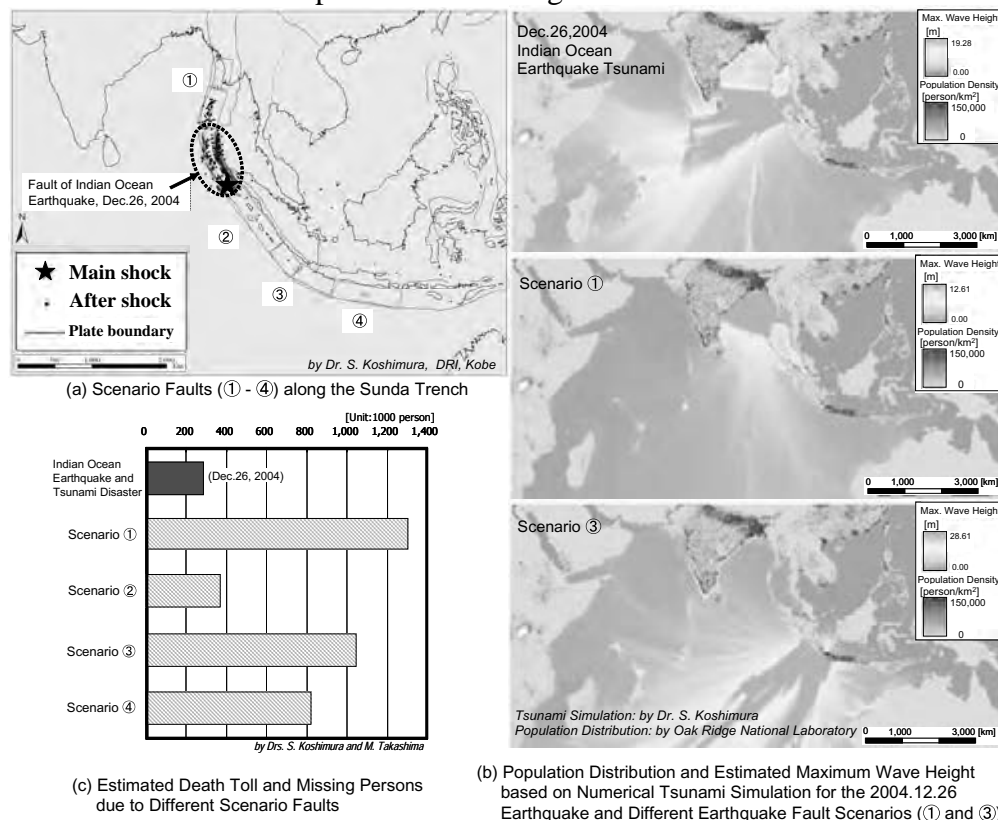


Figure 1: Estimated damage based on numerical tsunami simulation with possible fault scenarios along the Sunda Trench

Some countries along the Indian Ocean Rim have established a tsunami disaster mitigation system based on land use, i.e. prohibiting people inhabiting next to the seaside. Others are planning to adopt similar measures. Land use control is an efficient measure if people follow it. However, this is not always a proper option

in case activities such as fishing and tourism, which are the pillars of the region economy, take place directly next to the shore. Under these conditions, it is inapplicable to implement land use control policies.

In the Pacific Ocean Rim region, tsunami disaster mitigation relies on a sophisticated warning system, which is used not only for disaster mitigation but also for earth science research. This system is costly in terms of both installation and maintenance. Furthermore, it requires a great deal of knowledge to operate it. Although it is very useful and appropriate for this area, where countries with financial and technological resources such as US and Japan are located, it is not applicable for the Indian Ocean region (Figure 2).

Taking the above mentioned points into consideration, a New Tsunami Disaster Mitigation System which combines a warning system suitable for the Indian Ocean region and proper evacuation facilities in terms of location, strength and sheltering capacity is proposed. With this system there is no need to relocate the people living along the seashore; therefore, there is no impact on the local economies. The proposed system is simple, economically efficient and daily-usable.

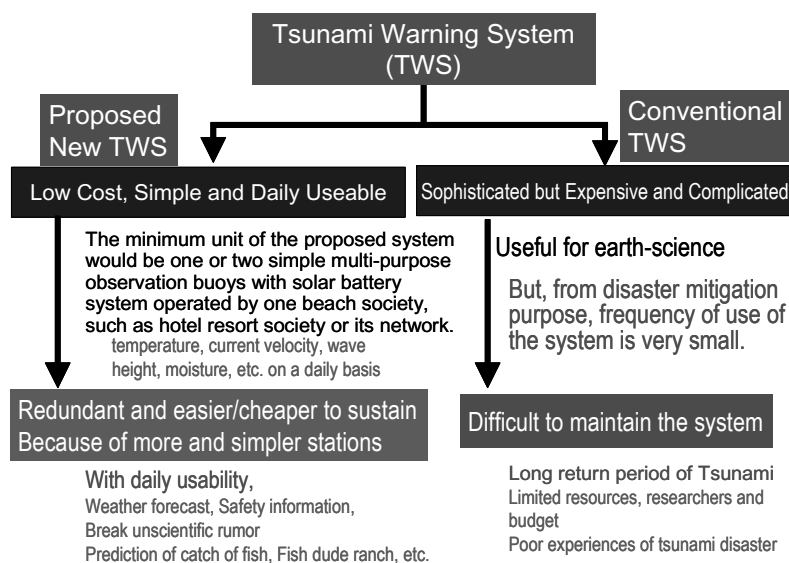


Figure 2: Comparison between conventional and newly proposed tsunami warning systems

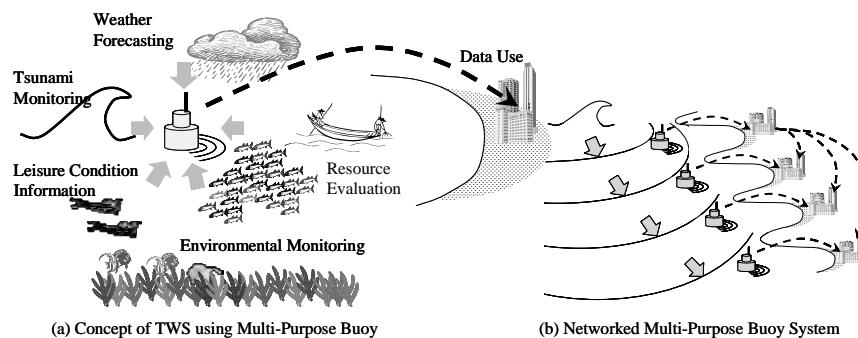


Figure 3: Concept of proposed tsunami warning system composed of networked simple multi-purposes observation buoys installed locally and internationally

2. PROPOSAL OF THE NEW TSUNAMI DISASTER MITIGATION SYSTEM

My proposed New Tsunami Disaster Mitigation System combines a reliable warning system and proper evacuation facilities. As mentioned earlier, a warning system such as the one available in the Pacific Ocean Rim region is not suitable for the Indian Ocean region which has fewer technological resources, researchers and experiences of tsunami disasters. For this reason, I am proposing to use simple multi-purpose observation buoys, which in addition to serve as a tsunami warning system, would record temperature, current velocity, wave height, moisture, etc. on a daily basis. This information can be used for weather forecasting, safety assessment, fish catch prediction, etc. which are useful for the local businesses (Figure 3(a)). My proposal is to use numerous and simple stations so that the system is redundant and easier/cheaper to sustain. The minimum unit of the proposed system would be one or two multi-purpose observation buoys operated and maintained by hotels/resorts or beach societies in the area. These businesses will benefit from the daily collected information.

It is expected that many beach societies install the system and join the multi-purpose observation buoy network beyond the administrative or international boundaries (Figure 3(b)). In this way, it may be possible to gather daily maritime information over a wider area and eventually forecast a transoceanic tsunami. A system for transferring this information between associations, domestic and foreign, already exists.

The installation of the proposed buoy system could have additional advantages. After the December 26, 2004 tsunami, the tourism industry has suffered greatly not only due to direct impact of the tsunami in the infrastructure but also due to the unscientific rumors. Visitors that used to come to resort facilities in the region started avoiding these destinations for fear that a new disaster may occur. In order to recover the tourists' trust, the information collected by the buoy system can be very useful. It is also known that buoys may become the center of marine ecosystems which could be an attraction for scuba divers.

Proper evacuation facilities in terms of location, strength and sheltering capacity are also part of the proposed system. In the region, it is common to observe temples, churches and shrines located along the coastal line. Therefore, I am proposing to use similar community centers as evacuation facilities. This scheme has two main advantages. Because worship centers are permanently used by the people, their location is well known so that in case an evacuation notice is released, everybody can easily access them. Additionally, because the people feel strong commitment with these facilities, they take active participation in their building and maintenance.

3. ESTABLISHMENT OF THE PROPOSED TSUNAMI DISASTER MITIGATION SYSTEM

In order to establish the proposed system, several works are needed as shown in Figure 4 and the reconnaissance team, which I headed, carried out them.

- 1) Structural damage survey
- 2) Tsunami numerical simulation
- 3) Topographical survey
- 4) Questionnaire/Interview survey
- 5) Evacuation numerical simulation

The first three activities are closely interrelated and their main objective is to design the configuration and location of evacuation centers. The structural damage survey is intended to evaluate the tsunami load and corresponding damage. With this information, the relationship between tsunami wave load and wave height/velocity can be obtained. With tsunami numerical simulations using potential earthquake scenarios, it is possible to estimate the wave height and velocity and the tsunami inundation area due to future tsunami hazards. These data enable us to properly determine location and structural design criteria for evacuation facilities.

In order to guaranty that the evacuation centers are fully functional, their location should be selected so that when the expected tsunami occurs they will not be washed away. For this purpose, it is indispensable to carry out a topographical survey. Real-time kinematic GPS and laser total stations are powerful tools for this purpose.

Questionnaire and interview surveys are useful to gather data necessary for the evacuation behavior simulation. Relationships between human evacuation velocity and water depth, which are needed for this study, have already been proposed. The simulation will confirm whether the escape routes and proposed evacuation centers are suitable. Because the proposed tsunami disaster mitigation system heavily relies on the participation of regional organizations, the interviews are also helpful to assess the level of acceptance of the system among the people involved.

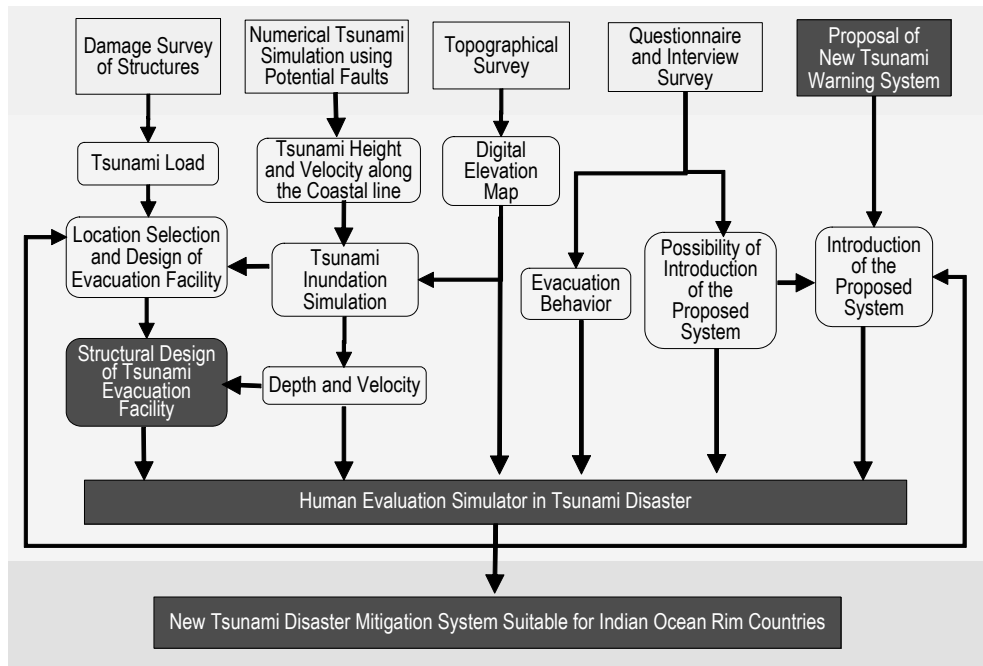


Figure 4: Establishment of the proposed tsunami disaster mitigation system

Figure 5 shows some samples of multi-purpose observation buoys that we have developed. With the solar panel system installed on the buoy, the system can continue observation permanently and users can get their favorite information with real-time basis. Initial cost of the system is about 10 to 20 million yen (changing with the equipments that the user wants to install the buoy). As we think that potential users of the system are resort hotel owners in beach resort as they can get the biggest benefit, when we calculate the additional cost (yen/room/day) to the normal room rate that is necessary for maintaining the system, we can get the numbers shown in Table 1. The numbers in Table 1 are obtained by assuming that life time of the system is 3 to 5 years, average number of rooms in each resort beach is 200 to 500 rooms, and average number days of use of the room is 100 to 200 days/year. From the numbers in Table 1, we can say that with reasonably low additional cost, our proposed system can be maintained.

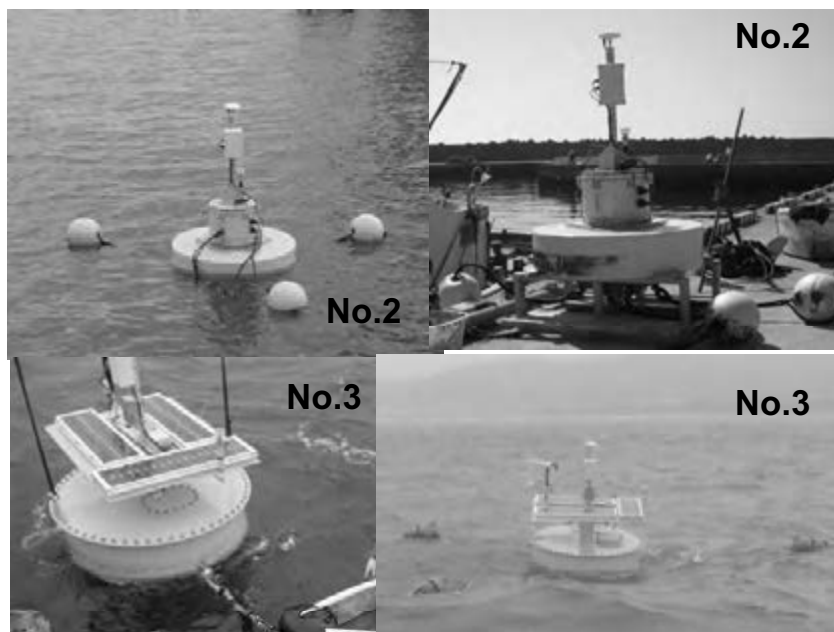


Figure 5: Samples of developed systems

Table 1: Cost needed to maintain the system (yen/room/day)

Cost (mill. yen)	Life time (years)	200 rooms/beach		500 rooms/beach	
		100 days	200 days	100 days	200 days
10	3	167	83	67	33
	5	100	50	40	20
20	3	333	167	133	67
	5	200	100	80	40

4. CONCLUDING REMARKS

This paper presents a New Tsunami Disaster Mitigation System for the Indian Ocean Rim region, which combines a reliable warning system and proper evacuation facilities. The warning system consists of multi-purpose observation buoys operated by local organizations such as hotels and beach associations. The system is not only used for tsunami warning but also to monitor temperature, current velocity, wave height, moisture, etc., information which can be used on a daily basis for the economic activities of the region.

The proposed evacuation facilities are designed taking into consideration: sheltering capacity, location, and structural strength. Location is especially important to prevent that the structures are washed away by the tsunami and to guaranty an easy access for the evacuees.

In order to verify the suitability of the proposed system, tsunami and evacuation simulations are recommended. Actually, the research team headed by the author

has already perform this type of study with some selected areas in Japan and Sri Lanka and proved the system effectiveness. The strong points of the proposed system are its simplicity, economy and daily usability, which makes it a sustainable option for the region.

Study on recovery curves for housing reconstruction in Sri Lanka, Thailand, and Indonesia after the 2004 Indian Ocean Tsunami Disaster

Osamu MURAO¹, Kazuya SUGIYASU², and Hideaki NAKAZATO³

¹ Assoc. Professor, The Graduate School of Systems and Information
Engineering, The University of Tsukuba, Japan
muraos@risk.tsukuba.ac.jp

² Doctoral Student, The Graduate School of Systems and Information
Engineering, The University of Tsukuba, Japan

³ The Okinawa Electric Power Company Inc., Japan

ABSTRACT

Each damaged country by the 2004 Indian Ocean Tsunami adopted proper recovery planning strategy respectively according to the situation for the resettlement of the victims after the event. It is generally important to clarify the relationship between the recovery process and the policy after disasters in discussions concerning future post-disaster recovery initiatives. The recovery curve proposed by the authors is a tool to solve the problems; in previous studies, recovery curves were developed to assess recovery from the Sumatra Tsunami using the rate of construction of both transitional and permanent houses in those three countries, Indonesia, Sri Lanka, and Thailand, from the viewpoint of urban physical environment. Following step should be comparison of the curves along with contexts of the recovery process, so this study aims to clarify differences of the recovery process. In this paper, differences of the constructed recovery curves of the three countries are discussed quantitatively. It clarified that the speediest recovery from the event is made in Sri Lanka and the slowest is in Indonesia. In order to consider the national recovery differences, it is necessary to follow the recovery timeline after the devastating event in the next stage.

Keywords: *the 2004 Indian Ocean Tsunami, recovery curve, permanent houses, urban recovery process, probability density functions*

1. INTRODUCTION

As of June 2011, six and half years have passed since the 2004 Indian Ocean Tsunami struck the coastal areas of several Indian Ocean rim countries. The authors had followed post-tsunami urban recovery processes in the most devastated three countries by the event for several years: Indonesia, Sri Lanka, and Thailand. Each country adopted proper recovery

planning strategy respectively according to its situation and background, and most victims settled themselves in permanent houses as a result.

It is generally considered important to clarify the relationship between the recovery process and policy, after disasters in discussions concerning future post-disaster recovery initiatives. For example, Haas et al. (1977) suggest a model of disaster recovery activity after the 1906 San Francisco Earthquake. However, it is not easy to clarify the relationship because of several complicated factors such as difficulty of collecting data, or diverse social background. Murao et al. (2007) propose a recovery curve construction method for Chi-Chi, one of the damaged areas due to the 1999 Taiwan Earthquake, as a tool to solve the problems. Actually there are many indicators to understand urban recovery conditions after disasters, but the authors chose the construction ratio of necessary buildings, such as transitional/temporary houses or permanent houses, in the damaged areas as an important physical indicator for the victims.

Following the research in Chi-Chi, recovery curves were developed for Thailand (Murao, Sugiyasu, and Nakazato, 2008), Sri Lanka (Murao and Nakazato, 2010), and Indonesia (Sugiyasu and Murao, 2010) to assess those recovery processes after the 2004 Sumatra Tsunami using the rate of construction of both transitional and permanent houses from the viewpoint of urban physical environment.

Following step should be comparison of the curves. This paper compares the recovery curves for the three countries in order to quantitatively clarify the national differences of the recovery process.

2. METHOD

The following procedure is employed to construct the post-tsunami recovery curves and to compare the curves for the three countries.

2.1 Construction of recovery curves

Recovery functions for the three countries were derived from the obtained building construction data of permanent houses given by the governments through authors' previous research. The factors of time (months) and completion ratio of building construction were used to construct the recovery functions. The time period starts in December 2004, with January 2005 being regarded as passing month "1". The time period extends fifteen to fifty months respectively in each country until the time that most planned houses are completed. The completion ratio of building construction for a given time period is calculated based on the total amount of completed buildings.

At the time T when the victims' lives have been sufficiently settled, for a time period of t (months), the cumulative completion ratio of building construction $R(t)$ is assumed to have the cumulative normal distribution, as follows:

$$R(t) = \Phi((t - \lambda)/\zeta) \quad (1)$$

where Φ represents the standard normal distribution, and λ and ζ are the mean and standard deviation of t , respectively. The two parameters for the distributions, λ and ζ , are determined using the least squares method on probability paper as shown in Figure 1, for the case of Thailand. Then recovery curves are drawn as shown in the following chapter.

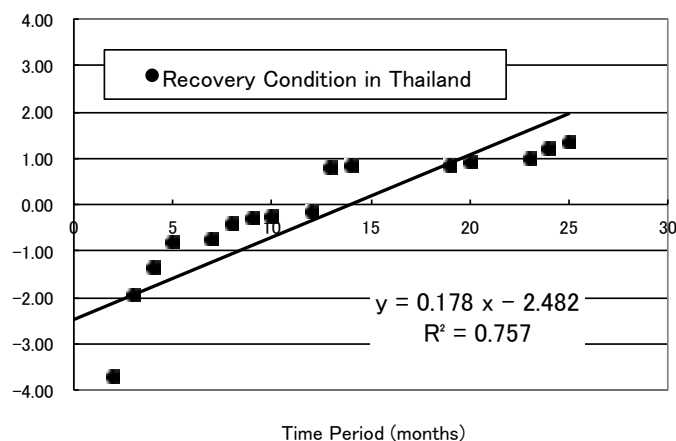


Figure 1: Relationship between time and completion ratio of permanent house construction in Thailand, as plotted on probability paper

2.2 Comparison of the recovery curves

The constructed recovery curves by the way of the above have two important parameters, mean (λ) and standard deviation (ζ). Those parameters suggest commencement time and average construction time period of the permanent houses built in each country. Then, those parameters are compared to quantitatively understand the national recovery tendency.

3. RECOVERY CURVES FOR PERMANENT HOUSES

This chapter presents the construction status of permanent houses in the three countries based on the acquired official data by the governments at first, and it is followed by the constructed recovery curves respectively.

3.1 Construction status of permanent houses and data source

The number of damaged buildings due to the tsunami rose to 629,316 in the world by the report of WHO (2005). Indonesia, Sri Lanka, and Thailand, the focused countries in the research, are the top three most devastated countries among the affected areas. Table 1 shows a damage outline by the tsunami in the countries.

Table 1: Damage outline by the 2004 Indian Ocean Tsunami in three countries

Affected countries	Sri Lanka	Thailand	Indonesia
Building damage	103,753	4,806	514,150
Displaced people	500,668	58,550	417,438
Deaths	30,959	5,392	114,573
Missing	5,644	3,062	127,749
Deaths and missing	36,603	8,454	242,322

Source: Research and International Cooperation Bureau (2006)
 Relief Web Map Center (2005)
 WHO (2005)

After the event, each government discussed strategy for urban recovery according to its damage situation and social context. Through arranging post-tsunami recovery plans, they estimated the number of necessary permanent houses for the victims before construction. Table 2 shows the number of planned permanent houses and the completion time of the first permanent housing site. The data sets of permanent house information from the governments shown in the table were used for the recovery curves.

Table 2: Construction status of permanent houses in three countries

	Sri Lanka ¹⁾	Thailand ²⁾	Indonesia ³⁾
Planned permanent houses	29,971	2,251	132,928
Completion time of the first permanent housing site	April 2005	March 2005	Dec. 2006

Source:

- 1) RADA (2006)
- 2) Provided by Provincial Social Department and Human Security in Feb. 2007
- 3) BRR (2005), BRR (2007), BRR (2009), and provided data by BRR in Feb. 2008

3.2 Recovery curves for permanent houses in Sri Lanka

Figure 2 shows the recovery curves for Sri Lanka along with observed recovery ratio constructed by Murao and Nakazato (2010). Although the curve for the permanent houses was fitted by the cumulative normal distribution described in 2.1, the curve for the transitional houses was based on the Gompertz distribution.

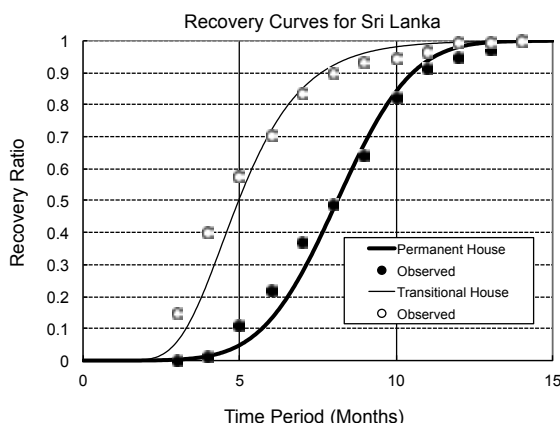


Figure 2: Recovery curves for permanent houses and transitional houses in Sri Lanka (Murao and Nakazato, 2010)

3.3 Recovery curve for permanent houses in Thailand

Figure 3 represents the recovery curve for the permanent houses in Thailand along with observed recovery ratio (Murao et al., 2008).

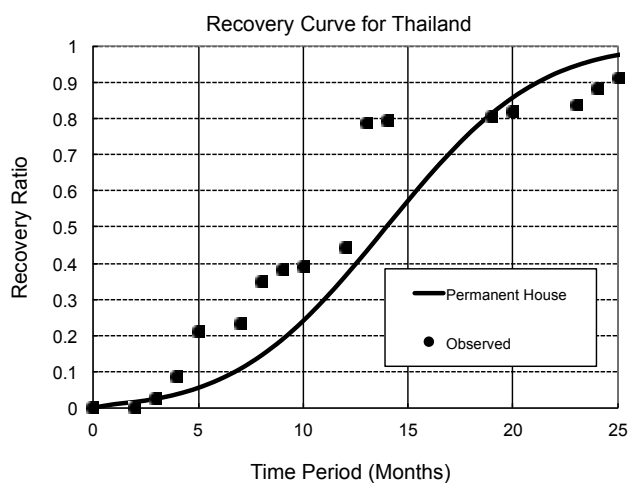


Figure 3: Recovery curve for permanent houses in Thailand (Murao et al., 2008)

3.4 Recovery curves for permanent houses in Indonesia

The recovery curves for permanent houses and transitional houses in Indonesia (Sugiyasu and Murao, 2010) are shown in Figure 4.

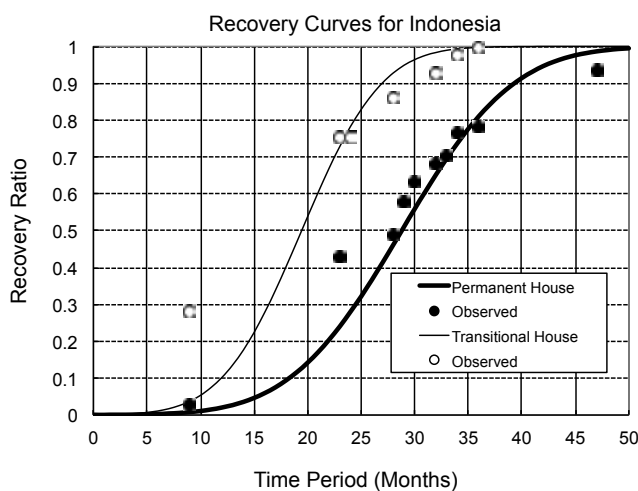


Figure 4: Recovery curves for permanent houses and transitional houses in Indonesia (Sugiyasu and Murao, 2010)

4. COMPARISON OF THE RECOVERY CURVES AMONG THE THREE COUNTRIES

4.1 Viewpoints of the comparative study

Showing the two parameters of the recovery curves, mean (λ) and standard deviation (ζ), the recovery curves for the permanent houses

indicate how each government dealt with resettlement for the victims. Table 3 shows the parameters of the curves for the three countries and some construction completion time obtained by the curves. Mean (λ) shows the number of months whose construction completion ratio of the permanent houses is 50%, and the value of standard deviation bring out the time period that 68.27% of the scheduled buildings are mostly constructed.

Table 3: Comparison of parameters for permanent house construction

	Sri Lanka	Thailand	Indonesia
Mean (λ)	8.2	14.0	28.8
Standard deviation (ζ)	1.9	5.6	8.2
Coefficient of determination (R^2)	0.96	0.76	0.92
Time period of most building construction (2ζ)	3.8	11.3	16.4
Completion time of the 1st permanent house site	April 2005	March 2005	Dec. 2006
50% completion time	Aug. 2005	Feb. 2006	April 2007
90% completion time	Oct. 2005	Sep. 2006	March 2008

4.2 Comparison of the construction processes in the three countries

The recovery curves for permanent houses in the three countries are demonstrated in Figure 5, and probability density functions are illustrated in Figure 6. These figures and the above table clarify quantitative differences of post-tsunami recovery process among the countries in terms of permanent house construction.

The speediest recovery from the event is made in Sri Lanka; the slowest is in Indonesia. The first permanent house site in Thailand was finished in March 2005, followed by Sri Lanka in April 2005. Compared with the two countries, the completion of those in Indonesia was too late, in December 2006, twenty-one months later from the month of Thailand.

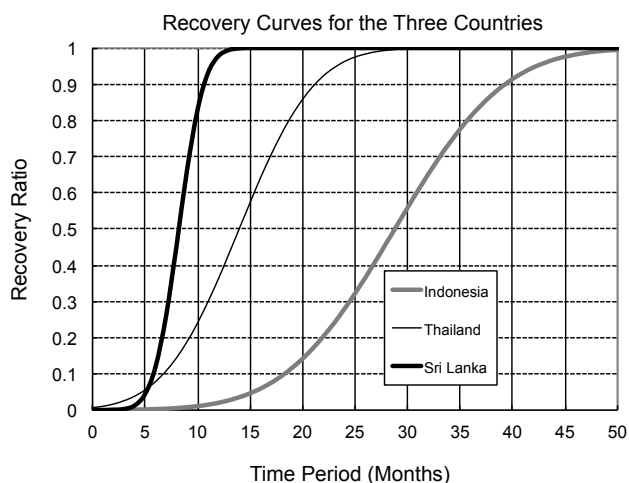


Figure 5: Recovery curves for Sri Lanka, Thailand, and Indonesia

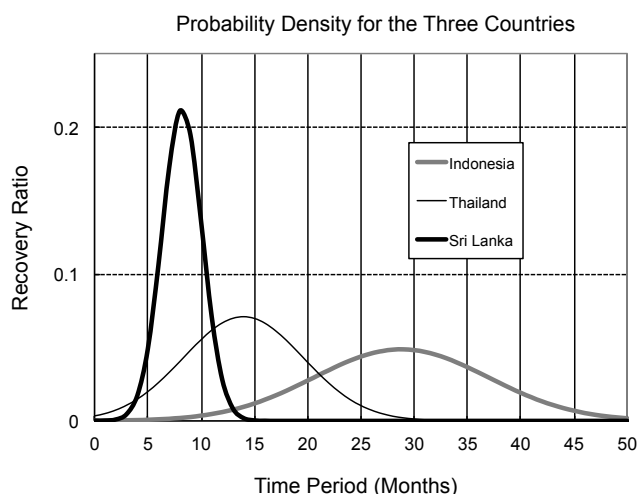


Figure 6: Probability density functions for Sri Lanka, Thailand, and Indonesia

Figure 5 and Figure 6 shows the time of the peak (λ : 50% completion time) for each country: 8.2 months (August 2005) in Sri Lanka, 14.0 months (February 2006) in Thailand, and 28.8 months (April 2007) in Indonesia. The gap between Sri Lanka and Indonesia is 20.6 months, more than one and half years. The 90% completion time is October 2005 in Sri Lanka, September 2006 in Thailand, and March 2008 in Indonesia. The difference between Sri Lanka and Indonesia is about thirty months.

Time period that 68.27% of the buildings are mostly constructed (2ζ) is 3.8 months in Sri Lanka, 11.3 months in Thailand, and 16.4 months in Indonesia. The slowest recovery of Indonesia spends four times of the speediest recovery of Sri Lanka. It means that Sri Lanka could concentrate the construction effort for shorter period than the others.

5. CONCLUSION

This paper presents the recovery curves for permanent houses constructed in Sri Lanka, Thailand, and Indonesia after the 2004 Indian Ocean Tsunami to quantitatively evaluate recovery processes. Constructed curves clarified differences of the recovery process among the three countries: (1) the speediest recovery from the event is made in Sri Lanka; (2) the slowest is in Indonesia; (3) time period of most building construction is 3.8 months in Sri Lanka, 11.3 months in Thailand, and 16.4 months in Indonesia. It means that Sri Lanka could concentrate the construction effort for shorter period than the others.

The differences of the recovery process among the countries were made by regional damage size, complexity of the society, governmental budget, political leadership, and so on. More discussions are required to clarify the relationship.

REFERENCES

Badan Rehabilitasi dan Rekonstruksi NAD-Nias (BRR), 2005. *Laying Down the Foundation for a Better Future, Six-monthly Report of the Executing Agency for the Rehabilitation and Reconstruction of Aceh and Nias*.

Badan Rehabilitasi dan Rekonstruksi NAD-Nias (BRR), 2007. *Tsunami Recovery Indicators Package for Aceh and Nias English Edition*.

Badan Rehabilitasi dan Rekonstruksi NAD-Nias (BRR), 2009. <http://e-aceh-nias.org/home/>, 2009.1.31.

Haas, J. E., Kates, R. W., and Bowden, M. J., 1977. *Reconstruction following disaster*.

Murao, O., Mitsuda, Y., Miyamoto, A., Sasaki, T., Nakazato, H., and Hayashi, T., 2007. Recovery curves and digital city of Chi-Chi as urban recovery digital archives, *Proceedings of the 2nd International Conference on Urban Disaster Reduction (CD-ROM)*, Taipei, Taiwan.

Murao, O., and Nakazato, H., 2010. Recovery curves for housing reconstruction in Sri Lanka after the 2004 Indian Ocean Tsunami. *Journal of earthquake and Tsunami, Vol.4, No.2*, 51-60.

Murao, O., Sugiyasu, K., and Nakazato, H., 2008. Consideration of recovery process and development of recovery curves for buildings in Thailand after the 2004 Indian Ocean Tsunami, *Journal of the City Planning Institute of Japan, No.43-3*, 745-750 (in Japanese).

Rebuilding and Development Agency in Sri Lanka (RADA), 2006. Progress Report.

Relief Web Map Center, 2005. South Asia Earthquake and Tsunami: Affected Population.

Research and International Cooperation Bureau, 2006. Thailand Country Report, Department of Disaster Prevention and Mitigation, Ministry of Interior.

Sugiyasu, K., and Murao, O., 2010. Comparative Analysis of the Reconstruction Process of Urban Facilities in Indonesia based on Recovery Curves after the 2004 Indian Ocean Tsunami, *Proceedings of the International Conference on Sustainable Built Environment 2010, Volume-02*, 363-370, Kandy, Sri Lanka.

World Health Organization (WHO), 2005. Situation Report 32

March 11, 2011, Tsunami Earthquake of Japan –Nine epistles to friends and colleagues

Tsuneo KATAYAMA
Professor, Tokyo Denki University, Japan
katayama@cck.dendai.ac.jp

ABSTRACT

Following the occurrence of the devastating tsunami earthquake which hit the Pacific Ocean side of the northern part of the main island of Japan on March 11, 2011, I wrote nine letters and sent them to my friends and colleagues in the field of earthquake engineering all over the world. By doing so, I tried to add some commentaries which, I did not think, were available on the world press in the wake of the disaster as well as to express my very personal views about the earthquake and its effects to the Japanese people. Although my comments are unduly weighted towards my personal impressions, they may be useful to understand how a Japanese person felt about the unprecedented calamity. In this paper, I would like to summarize the letters to share my impressions. It should be noted some of my comments could not be substantiated, partly because I have not so far visited the stricken areas, but this is what I would like to leave for my own memories.

Keywords: *2011 March earthquake of Japan, Tsunami disaster, personal impressions*

1. THE FIRST LETTER DATED MARCH 15, 2011

At the time of the earthquake occurrence, I was chairing a meeting held in the center of Tokyo. The shaking was the strongest and the longest I had ever experienced before. According to the record obtained by the Earthquake Research Institute, Uni. Tokyo, the duration of the motion in Tokyo was about 5 minutes with dominant period of 2 to 3 sec (This is my guess.). Buildings I saw from the windows of the meeting room were visibly swaying, and it was horrible to watch a tall construction crane just across the street moving back and forth. I felt that “THE ONE” had come. In spite of this, all the buildings were standing intact after the strong shaking, and I thought everything was OK in the end. We were in the second floor of a 7-story building. When the major shaking was over, we walked up, because elevators automatically stopped, to the 5th floor where I have my office. There are usually some 50 people on the 5th floor, but when we went there, the large office room was empty. All employees went down to the foyer on the ground floor according to the disaster preparedness program. Within probably an hour, it was decided that employees might go home. But soon after that, we learned all public transport was held up for inspection of possible damage. To tell

the truth, at that time I took the situations too easy. I just continued to watch TV, whereas I should have reserved a hotel or a cab as early as possible. Within 2, 3 hours time, there were no hotels or cabs available, and phones were disconnected because of heavy traffic. Many of the young employees went home on foot, some of them by walking for 2~3 hours. I learned later that getting a taxi did not mean getting home earlier, because expressways were held up for inspection and streets were completely jammed. The night of the earthquake, I was lucky that I could have a nap in the building of a sister organization of the one we were having a meeting at the wake of the earthquake. The room I stayed in is officially used by building guards.

On TV we saw Tsunamis swallow many towns and villages along the Pacific coast in the Tohoku area, i.e. the northeastern part of the Honshu Island. It was horrifying and hard to believe that such disasters were really taking place in front of us. Most of you must have seen on TV such scenes as Tsunami going over a breakwater as high as 10m. Many small cities and towns were completely destroyed. It is reported, or rather I expect, that the final death count will reach something between 15,000 and 20,000. In hard-hit isolated areas, water, food, and other daily stuff are short, because transport systems have been cut off. (Although some foreign media reported that things are scarce in Tokyo, it is not true. However, quite a few people rushed to convenience stores to get rice, canned food, and so on.)

Conditions of nuclear power stations are serious, and I am truly concerned about them. Information seems to be fragmentary, and some of the information released by the Company and the Government are difficult to understand. However, explosions did take place and radioactive levels are thousand times the ordinary values. Although they said until yesterday that radioactive effects had not reached the dangerous level, tones of media are changing today. We cannot stop feeling doubtful about what they say because they repeat "It is safe" too often. One of my daughters says: We all have enjoyed civilized, abundant, and bountiful life for a long time because of electricity. If something should happen to us this time, we would be paying heavy compensation to what we have enjoyed in the past.

I do think children outgrow their parents.

These are my personal observations and impressions on the 5th day of the Great Tsunami earthquake. I am rather a person with no religious belief, but now I find myself praying to God.

2. THE FOLLOWING WAS WRITTEN ON MARCH 17

This is the 6th day (March 17) after the earthquake. Life in Tokyo is coming back to normal. But, I see much less people and cars on the street, and public transport is much less crowded. Quite a few numbers of bus routes have been temporarily closed, because of oil shortage. This has taken place because several large-sized oil refineries were closed after the earthquake, people rushed to gas stations to fill tanks of their cars, and also because more oil is expected to be needed in the

stricken areas in future. Many companies are asking their employees to stay home and work there.

I am surprised that structures at least in Tokyo have survived the strong shaking of last Friday. The earthquake affected the Tokyo Bay shoreline areas of Chiba Pref., neighboring Tokyo, some 300~400 km from the epicenter. Liquefaction seems to be widespread there, forcing the Tokyo Disneyland to close.

In the Tsunami-hit areas, people are still in acute shortage of water, food, and basic daily stuff. If I am correct, the death count is over 13,000 and more than 400,000 people are still displaced from their homes most of which have been completely lost. Even undamaged hospitals have to move their patients because medicines are lacking. Damage to transport systems is causing a most difficult problem. Areas are not reachable from sea because of Tsunami damage.

People in the northern part of Japan are patient and hardworking. I cannot tell what might happen if a similar disaster hit one of larger cities in Japan.

Situations in the nuclear power stations in Fukushima are still bad, maybe getting worse and worse everyday. They have started to shoot the damaged containers and the surrounding facilities by pressurized water. We do not know how effective it is. Foreign students have left and are leaving Japan. Foreign companies have, I heard, begun moving their offices and employees to the western part of Japan.

After the 1995 Kobe earthquake, I talked and wrote: We the experts had been ignorant, too self-confident, and we did not tell people what we did not know. I like hard-boiled mysteries, especially those by Raymond Chandler. In one of his books, a woman says to the protagonist of the story, "You self-sufficient, self-satisfied, self-confident, untouchable bastard." I feel as if I were him. I think we have again been ignorant, self-confident, and we have not admitted that there are so many things we do not know. I still believe that Japan's earthquake engineering level is generally high. And it is true that we have done quite a few things to upgrade the strength of structures, including that of nuclear power stations. But, we stopped thinking any further.

Regarding the characteristics of ground motions, please refer to the following URL which unfortunately is available only in Japanese at the moment.

http://www.bosai.go.jp/news/oshirase/20110315_01.pdf

3. ACCOUNT OF MY WIFE ABOUT THE DAY OF THE EARTHQUAKE

My wife had been in Ginza, one of the busiest shopping areas in the center of Tokyo. She was in the subway going home, and the train jerked to stop between stations still in the general Ginza area. There was an announcement that the train stopped because the early earthquake warning had been received. My wife says that the shaking felt in the subway was not very violent. But, at the same time,

she says that she thought what she should do if destruction aboveground was serious. These are not contradictory, because, according to the announcement in the subway, very strong shaking was expected in Tokyo. After some 10 minutes, the subway began to move to the nearest station where all passengers were asked to leave. She walked up to the ground level to find all structures nearby sound. What she remembers most strongly was there were so many men in the dark business suit on the street where there usually are women (window) shopping. She started walking from Ginza to Shinbashi (Sorry for those who are not familiar with Tokyo.) I think it was at around 15:00~15:15 (The earthquake occurred at 14:46.). Streets were already becoming crowded with people walking home and cabs taking people from the central part of Tokyo to suburbs.

She took a cab, which was lucky because it must have become difficult or impossible to do so within a quarter of an hour. It took 2 hours to reach home, four to five times more than it does in the ordinary times. Our apartment house was undamaged except for some broken porcelain and glass ware. According to a cab driver I happened to meet later, there was some 5-6 seconds before strong shaking was felt in Tokyo after the issuance of the warning. He also said that he could decelerate his car to stop near the curb.

4. THIS IS MARCH 18 (FRIDAY)

A week has passed since the earthquake. People in the hard-hit areas are still struggling because of shortage of basic stuff. There are about 300,000 people displaced from their homes staying in refuges. It has been snowing and temperature at night went down below zero. We do not know what is taking place in the nuclear power plants in Fukushima. Unfortunately, there is news that gasoline was stolen in several but not many places in areas NOT affected by the earthquake.

Although I wrote yesterday that pressurized water would be aimed to the damaged nuclear power plants, it was not successful. In one case, water did not reach the aim. In another case carried out by the Self-Defense Force, they called it off at around 20:00 after having tried several times by changing workers as often as possible not to expose them to the radioactivity. I understand that, unless we cool down nuclear fuel rods, no farther step could be started.

On TV and in the other media, many so-called experts comment on and criticize what have been done in Fukushima. But, the laymen have never heard of millisieverts, microsieveverts, nor the radiation levels that cause health damage. Most of us are sick and tired of the comments by experts given on TV.

Every morning I have a cup of coffee in a café near my office. Customers there are denouncing the comments by experts. In the ordinary times, one usually stays in the shop reading newspapers or contemplating what may or may not be important to the others. But, this morning, we including a girl who serves us coffee had suddenly become friends. One of our conclusions was that those

experts should go near the power plants if they really believe they are safe, instead of smugly making useless comments on TV.

Last evening, it was extremely hard for most of us to go home from our working places. At around 16:00 yesterday, Minister of Economy, Trade and Industry at an urgent press conference said in person that large-scale blackout might take place in the TEPCO's service area, and that people should go home as early as possible. This caused extreme traffic jam of the public transport system in Tokyo. Blackout was fortunately evaded, but hundreds of thousands commuters were affected by the traffic jam.

Polat Gulkan, President of the International Association for Earthquake Engineering, responded to my e-mail as follows:

Dear Tsuneo,

I have read with much interest the description of the Sendai earthquake from your personal window where you and your immediate family happened to be on that day. Thank you for conveying to us your impressions for the events that occurred, but I think that you are too harshly critical of your fellow engineers in Japan. True, the nuclear plant proved to be a showcase for the principle that things can go wrong in horrible sequence, and that "outlier" events aren't necessarily to be ignored. But the performance of the building stock appears to have been good, and the discipline and self-sacrifice of your fellow countrymen and women are exemplary. You should feel proud for that. Our collective sympathies and prayers that Japan should soon begin to regain its balance are with you.

With best regards,
Polat Gulkan

Polat, I appreciate your kind words. But, what I wanted to do was not to be too harsh to my fellow engineers but to examine my conscience.

5. MARCH 19 (SATURDAY)

According to TV news, the confirmed death is over 7,000 and 11,000 are still missing. They say today is the age of telecommunications and the internet. But, in the aftermath of the earthquake of March 11, telephones including cell phones were disconnected and the internet did not function because of traffic congestion as well as power outage. In one of the hardest hit cities, the originals of family registers of all citizens are reported to have been lost. With respect to Tsunami warning, a city had a plan to use the internet, but it did not work because of the power outage soon after the earthquake, and because the emergency center were busy in dealing with inquiries from citizens.

For example, regarding to the severe accident in the atomic power plants, information on TV was probably more than enough because of so many channels available, but its quality was open to question. What commentators and experts talk on TV were inconsistent. Official announcement made at the same press conference from the government was often broadcast at different times on different TV channels without mentioning when the particular conference was held. There are basically four sources of information; the producer of the plant, the Tokyo Electric Power Company (TEPCO), the Ministry of Economy, Trade and Industry, and the Cabinet (i.e. the Government). Since the Self-Defense Force and several fire departments have begun to be engaged in cooling of destructed nuclear plants, the number of press conferences increased including that by Minister of Defense. We did not hear anything from the producer of the plant, but the remaining three organizations release almost the same information in the order shown above. It seems to be complete waste of time for most of viewers. It is much more efficient for the three (or more) organizations to get together to make one press conference. The worst and the most critical problem relating to so-called official press conference is, however, that we are feeling some important facts are concealed. My wife says, and I thoroughly agree with her, BBC and CNN are more direct in describing the state-of-the-art.

Access roads from the major north-south highway to hard-hit coastal areas have finally been secured. Isolated areas are becoming less and less in number. Food and potable water are still scarce. Representative of a volunteer organization said on TV this morning that there are about 400,000 displaced people and additional 300,000 people who need food in their homes. By assuming two meals a day per person, a total of 1,400,000 meals have to be prepared every day. It is a sheer impossibility in the disaster-stricken areas. Electricity is now back to service, but kerosene gas for stoves broadly used for heating in winter is running out in many places.

The scheduled power outage in the TEPCO's service area started on March 14 or 15 resulted in confusion, customers did not at the beginning know when the power outage of their homes would take place. The Daily Yomiuri (March 16) describes it as: TEPCO's poor publicity led to metropolitan mess.

I would like to quote from another Philip Marlowe mystery: The fear of to-day always overrides the fear of to-morrow.

6. MARCH 20, 2011 (SUNDAY)

As of noon today, the National Police Agency released the following numbers:

Confirmed death: 8,132
Missing (Officially filed): 12,272
Completely or partially damaged houses: 18,622
People in refuges: About 360,000

Death count will most probably exceed 20,000 which will be greater than my guess made in the first report, i.e. 15,000-20,000.

In the Fukushima No.1 Nuclear Power Plants, there are 6 reactors of which Nos. 4, 5 and 6 reactors were out of operation for regular checks at the time of the earthquake. Nos. 1, 2, and 3 reactors stopped automatically, but ECCS (Emergency Core Cooling System) did not work for all of them,

Hydrogen blast took place at No. 1 reactor on Saturday (March 12) followed by hydrogen blast at No. 3 reactor on Monday (March 14). Blast blew off reactors' external containment structures which are supposed to be the last barrier. And, at No. 2 reactor, reactor vessel was damaged on Tuesday (March 15). No. 4 reactor is now facing a critical moment. No. 4 reactor was out of operation for regular checks, but the earthquake knocked out electricity to the reactor needed to circulate cooling water in the pool that temporarily stores spent nuclear fuel.

The critical point is whether or not the damaged reactors could be cooled down. The Self-Defense Force and the Tokyo Fire Department are making their best, but the condition of the Fukushima No, 1 nuclear power plant still do admit of no presupposition. Whenever I hear Chief Cabinet Secretary say at press conference that a certain amount of result has been achieved, I cannot stop feeling how empty such an announcement is.

7. MARCH 21, 2011 (MONDAY)

This is the third day of three consecutive holidays. In Japan, Vernal Equinox Day is a national holiday. I am tired of writing in my poor English what are taking place here in Japan since the earthquake. So I decided on quoting headlines of English newspapers published in Japan. But, unfortunately, in a newsstand of the nearest local station, I was able to get only two, both dated March 21. One is The Japan Times (JT), and the other THE NIKKEI WEEKLY (NW).

- Death toll to exceed 15,000 in Miyagi alone: Police Chief (JT)
- Many children face trauma from disaster (JT)
- Pairs found in rubble in Ishinomaki (nine days after the earthquake) (JT)
- Evacuees want more water – to take baths (JT)
- Desperation tests crime taboo (JT)
 - Cases of looting emerge in areas hit by tsunami
 - Quake-hit stores in Miyagi hit by hundreds of thefts
- Old-style survival skills put local shop owners in disaster limelight – The panic buying will subside as people start to realize no real shortages exist and that it is their own panicky hoarding that is creating the problem (Noriko Hama, JT)
- Fight at Fukushima rages on – World watches as workers brave radiation in frantic attempt to cool crippled nuke plant (NW)
- Electricity restored at reactor No. 2 (JT)
- TEPCO faked Fukushima repairs – Revelation raises fresh questions over utility's state ties, tainted past (JT)

- Foreign citizens, workers being told to return home (NW)
- Foreign media take flak for fanning fears (JT)
- Short on gas, too close for comfort (although supplying gasoline for emergency vehicles are made a top priority.) (NW)
- Power precious in greater Tokyo (NW)
- Rain may force TEPCO to cut power (JT)

- Maximum radiation levels in eastern Japan (JT)
- Tokyo radiation levels said not harmful (NW)
- Latest threat: radiation-contaminated food (JT)
- Iodine from plant detected in Tokyo (JT)
- Radiation detected in U.S. Navy rescue crews (NW)

- Redirect budget outlays to quake relief measures (editorials, NW)
- Post-quake risk to the economy (editorials, JT)
- Quake shows how fear can choke stocks (NW)
- Promoting tourism (editorials, JT) : Promoting tourism constitutes a promising avenue for moving beyond manufacturing in a new borderless world. However, “*Man proposes, God disposes,*” and it remains to be seen how serious a blow the Tohoku-Kanto earthquake, tsunami and unfolding nuclear plant crisis have dealt to the new efforts.
- Effects of auto output suspension rippling through industry (NW)
- (Computer) Glitches at Mizuho (Bank) hold up wages (NW)

- In long run, horrific disaster may push Japan toward better future – Because the years of drift in Japan may be ending (because of the earthquake). If so, we will look back at the great quake as the moment when the nation truly seized its future (Japan Business Seminar by Michael Zielenziger, NW)
- “Ironmen of the North (Players from the Kamaishi Seawaves professional rugby team) use their mustles to help community (NW)
- Former quake victims, even toilet experts offer evacuee tips (NW)
- Twitter a good emergency response tool (NW)
- Helpful websites, and phone numbers (JT)
- Attention Steve Jobs: a few survival apps Japan needs (William Pesek, Bloomberg, JT)
- Mahathir (a former prime minister of Malaysia) expresses condolences to Japan (JT)

8. MARCH 23 (TUESDAY)

This is the twelfth day since the earthquake. Life in Tokyo is back to almost normal. Trains in commuting hours are as crowded as before. Bus routes temporarily suspended due to shortage of gas supply were reopened, because several of large oil refineries began operation. We do not have to queue up at gas stations. (My daughter went yesterday evening to a gas station. But, when she came home, she said that she filled only 20 liters, because she thought gas is more badly needed in the stricken areas.) But, some of necessary daily stuff is still difficult, not impossible, to get even in Tokyo, mainly because of the panic

buying. According to my wife, among others, rice, eggs, toilet rolls are short. My secretary's sister had to line up before going to work at a super market to buy rice. Prices of some food have gone up by 25%, 50%, or 100% in the worst case. Cabbages, onions, and lettuces became 25% to 50% more expensive, and price of milk at a super store almost doubled last weekend, according to my secretary. I think even after panic buying and shop-owners selfish behavior will have subsided, tendency for higher prices of food stuff will continue, because the hardest-hit Miyagi Pref. is one of the producers of a famous brand of rice, and Fukushima Pref. and Ibaragi Pref. are known as agricultural and dairy farming regions. In addition, most of the fishing ports in Iwate, Miyagi and Fukushima Prefectures are reported to have received deadly blow by the Tsunamis.

It may be too early to summarize what were the points of special concern for the March 11 Tsunami earthquake. I would like to do it at this moment in time, and, therefore, the following are not intended to be complete at all.

First of all, the earthquake accompanied Tsunamis which in some places exceeded 10m in height. They arrived at northeastern shores of Tohoku region much earlier than expected in disaster preparedness guidelines of municipal governments in the region. They washed away and devastated small to medium-sized cities and towns leaving thousands of casualties. Most of wooden Japanese houses could not resist Tsunami flow once they floated on the water. If there were ground motions alone, although they were quite strong, the death count must have been less than 10% of the presently reported number. I may be wrong, but Tsunami studies have so far focused on the simulation of propagation of Tsunamis over the oceans. Such studies are attractive to the laymen to look at, but academicians should have paid more down-to-earth issues related Tsunami disasters.

Secondly, the hardship of displaced and survived people with respect to food, water, medicine, gas, and so on, have dragged on, much longer than many municipalities assumed in their disaster preparedness plans. Hardly-hit areas were along the northeastern coast of Honshu island. Since the geographical features of the northern part of Honshu are small flat lands sandwiched between mountainous geography and the Pacific Ocean. The coastline is deeply indented, which magnified the Tsunami height, and small municipalities are scattered along the shoreline. After the devastation by the Tsunamis, areas became almost impossible to reach from the sea. The arterial highway runs north-south, and access roads running east-west from the highway were heavily damaged. Tens of patients died in hospitals because of lack of medicine, and several tens of elder people staying in refuges also died because of insufficient heating at night there.

Thirdly, urban life was found so fragile even for a disaster that did not hit the region. Of course, we should remember that many large companies stopped their operation because of power shortage and outage, and oil shortage. Buying panic, selfish shop owners, rise and fall of stocks, these are all expressions and signs of our sinfulness. When you encounter such a natural phenomena, you feel slightly to have become a philosopher.

Lastly, but very importantly, there are problems of reactor accidents. As to Nos. 1 – 4 reactors in the Fukushima No. 1 nuclear power plant, situations seem to be improving. External power supply was successfully obtained, and conditions of reactors will be more accurately monitored. (I then wonder how accurate the past information released at press conferences was!) This is only the first step. Most recent news tells us that iodine was detected in the water of Tokyo, and bottled water has already been sold out in super stores. On balance I think I am an optimist, but in the case of the present nuclear accident (?), I see calamity in every opportunity. Quoting from Robert Lowell, “If we see light at the end of the tunnel it is the light of an oncoming train.” I only hope that our train is running on the double track.

9. NINTH REPORT (MARCH 24, 2011)

This is my 9th report on my personal observations about the giant Tsunami earthquake of March 11. I am going to at least temporarily stop writing the report. “Nine” seems to be an appropriate number. A baseball game ends in the 9th innings, unless the game is a tie. It is difficult to tell whether or not we have suffered a complete defeat in this struggle against the Tsunamis. If I would find a special reason to restart my report, I promise to e-mail it to you. I have to start preparing for the lectures beginning in April.

Whenever I go home, I ask my wife, “Is there anything new at Fukushima?” In the past several days, she answers, “Nothing particular.” Both of us fully know that many things are being done there, some with successes and the others with failures. Information is too much intricate. It often is extremely hard to follow what is taking place in which particular reactor. As I wrote before, there are six reactors, i.e. from No. 1 to No. 6, in the Fukushima No.1 Nuclear Power Plant. Troubles are occurring in Nos. 1, 2, 3, and 4 reactors, but it is not easy to follow in what condition each of them is at the most recent moment. There may be many pieces of information available, but important pieces seem to be missing, or we just do not know how to put them into a picture of a jigsaw puzzle. We then become more and more indifferent to this critical problem, only sympathizing with the members of the Self-Defense Forces, and firefighters from Tokyo and Yokohama who are forced to be engaged in the most dangerous work.

The aftershock of the power shortage will be of extreme significance for everybody.

It is said that 2 to 3 years will be needed for TEPCO to recover to supply enough power. Although other companies will accommodate TEPCO, but the quantity will be very limited, because the Kansai Electric Power Company, the second biggest power company in Japan, supplies 60 Hz electricity whereas that in the eastern Japan is supplied with 50 Hz. TEPCO was badly affected, at least financially, by the 2007 earthquake in the Kashiwazaki-Kariwa Nuclear Power Plant facing the Japan Sea. Although the Nippon Bank has decided to make a big urgent financial support, TEPCO will be having hard times in the future.

Power shortage will have strong effects on Japan's industry. This does not simply mean that Japan's industrial output will be affected, but those of neighboring countries will be affected because there are many local subsidiary companies assembling final products by using key parts produced in Japan.

The country will be financially affected to a great extent. It requires a huge amount of money to recover and reconstruct the impacted areas. Japan's financial deficit which has already been evident in the global market will suffer a severe blow.

For ordinary people, some of the things for daily use will become more expensive and be hard to get. The scheduled blackout will continue, and public transport has to put up with partial services. Here, I remember what I wrote in my Report No.1.: We all have enjoyed civilized, abundant, and bountiful life for a long time because of electricity. If something should happen to us now, we would be paying heavy compensation to what we have enjoyed in the past.

But all that I wrote above is dependent on the outcome of what is taking place in Fukushima. Please keep your fingers crossed for us.

Thank you for having read my reports all the way to this "Thank you."

Seismic vulnerability of low-rise, single long span reinforced concrete buildings

Chayanon HANSAPINYO
chayanon@eng.cmu.ac.th

Assistant Professor, Department of Civil Engineering,
Chiang Mai University, Thailand

ABSTRACT

Low-rise, single long span reinforced concrete building is among the most typical building configurations adopted in governmental school building in Thailand. Without seismic consideration, the building configuration leads to sizing of high depth beams and slender columns. This paper describes seismic vulnerability of the buildings by considering earthquake performance of the existing buildings located near the Thai-Myanmar border which were recently hit by the M6.8 earthquake at Shan State, Myanmar. In addition, evaluation of seismic performance using nonlinear pushover analysis of a typical three story school building is presented. The analyzed building has 9.4 m. single span length with 3.4, 3.4 and 3.0 m. high for the first, second and third stories, respectively. Dimension of columns is 0.30 by 0.40 m. and beam spanning between the two columns is 0.25 by 0.80 m. From the earthquake event, severe cracks in columns and beam-column joints could be observed on the existing buildings. From the analysis, the maximum base shear coefficient is 8.67% which is less than the design value. In addition, the results show the weak column behavior of the typical school building. Collapse of the analyzed school building is initiated by yielding at two ends of the columns. The ultimate roof drift ratio is about 1.11% and the roof drift ductility ratio is 2.92. The ratios demonstrate the irreparable and non-ductile behavior. Hence, both evidences indicate seismic vulnerable and the need for strengthening of the building.

Keywords: *seismic evaluation, low-rise, single long span, Myanmar earthquake, pushover analysis*

1. INTRODUCTION

The demand of large open area at the first floor of school building leads to low-rise single long span reinforced concrete building configuration. The building model has long been accepted for a standard drawing utilized widely in construction of governmental school in Thailand. Without seismic consideration, before the enforcement of the seismic design law in the year of 1997, the long span beams are heavily loaded under gravity moment and then detailed with large depth. The depth of the beam is in the range of 0.8-1.0 m. for about 9-12 m. span length between two edge supporting columns. In contrary, the reinforced concrete columns may be subjected to a light

axial load. The dimension of the section can be only about 0.3 by 0.4 m. Hence, the column size is much smaller compared with that of the beams. This results to the weak column-strong beam behavior which is undesirable for earthquake resisting structural system.

It has long been considered that Thailand is a zone with no effect from the earthquake risk. However, many past earthquakes have shown a certain level of the attack in the Northern and Western regions. Many researches, for example Lukkunaprasit and Kuhatasanadeekul (1993) and Warnitchai and Lisantono (1996), have indicated the peak rock acceleration to be approximately 0.17g with a 10% probability of exceedance in 50 years. In this intensity of earthquake, seismic vulnerable buildings have high potential to be severely damaged.

This paper describes seismic vulnerability of the low-rise single long span reinforced concrete buildings by considering earthquake performance of the existing buildings located at Mae Sai near the Thai-Myanmar border which were recently hit by the 6.8 earthquake at Shan State, Myanmar. The distance from the epicenter to the area is about 35 km. In addition, evaluation of seismic performance using nonlinear pushover analysis of a typical three story school building is presented. Both evidences consistently indicate seismic vulnerable and the need for strengthening of the building.

2. EARTHQUAKE RESPONSE OF EXISTING LOW-RISE SINGLE LONG SPAN BUILDINGS

2.1 Myanmar-Thailand border M6.8 earthquake event

Although, geological structure has shown many active faults in the zone, there have not been large earthquake records since 1912. Until the evening of March 24, 2011, a violent earthquake was originated by the Nam Ma fault. USGS reported the magnitude of 6.8 while it was about 7.2 informed by local seismological agencies in China. The focal depth was estimated about 20 km. Figure 1 shows location and intensity of the earthquake event. The United Nations Office for the Coordination of Humanitarian Affairs (OCHA) reported number of casualties to 73 deaths and 125 injuries. 224 houses, 11 monasteries, 11 official buildings were damaged in Tarlay.

People living in the northern parts of Thailand, next to the Myanmar border, could feel nausea. Persons staying in high rise building in Bangkok which is 772 km southern away also got the shaking sense. Also, the tremor could be detected at the area close to the center e.g. Northern parts of Laos, Vietnam and Southern part of China. The most affected area in Thailand is Mae Sai in Chiang Rai province. From figure 1, the estimated potential damage is about light to moderate level with the peak ground acceleration about 0.18 g.

2.2 Damage of the existing low-rise single long span reinforced concrete buildings

Under the earthquake event, survey for damage information in Northern parts of Thailand was performed especially in Mae Sai, Chiang Rai Province. It is the most interesting zone not only because the area is very close to the epicenter, but also it is a major trading area crossing the Thailand-Myanmar border. The Mae Sai municipal covers an area of 5.13 km square. Most of the area is used for residential and commercial purposes. There are about 860 commercial building blocks and more than 13 hotels. The recent population is 19,443. Due to the earthquake, the survey found damages in both structural and nonstructural parts of buildings in the area. However, the present work focuses on the examination of school buildings which are the low rise-single long span reinforced concrete buildings.

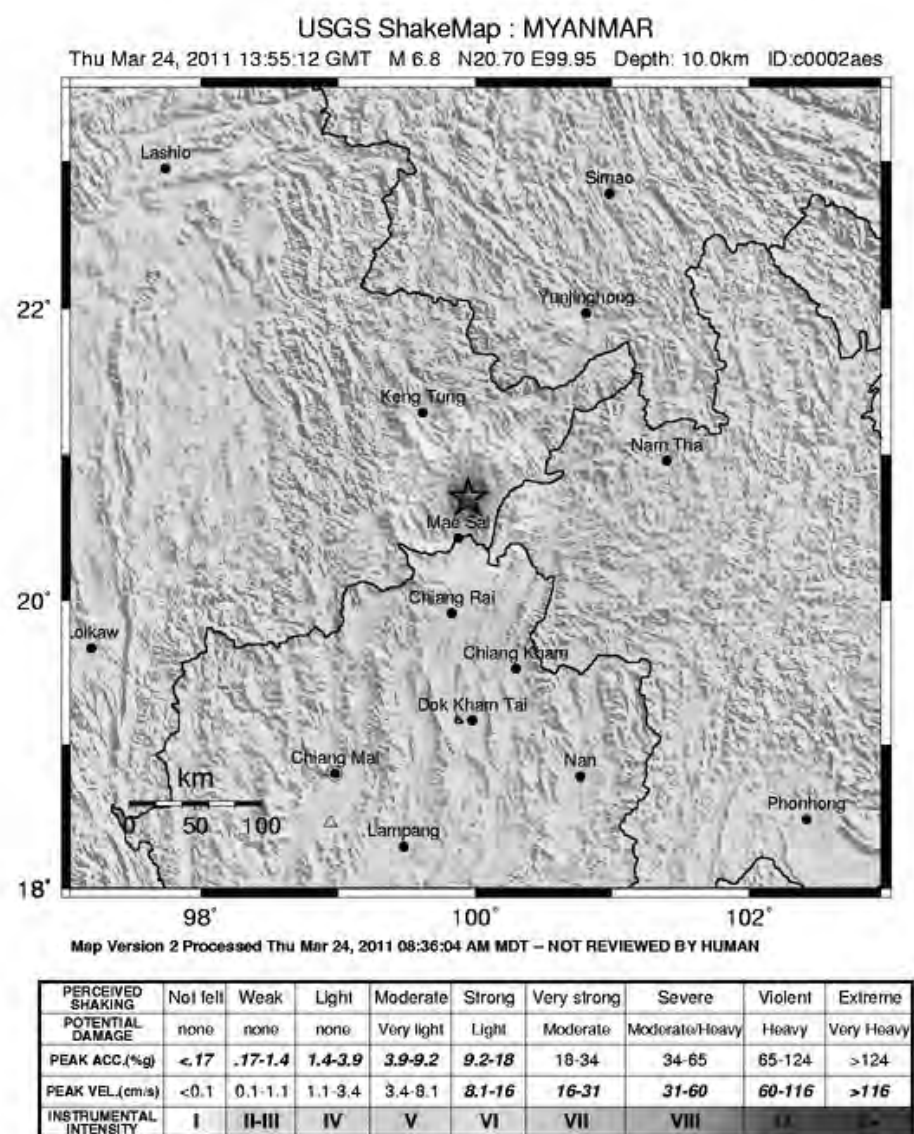


Figure 1: Location and intensity of the Myanmar March 24 M 6.8 earthquake (USGS)

Figures 2 and 3 show the low rise-single long span reinforced concrete school buildings in the area. The former shows a three-story building which was built more than 50 years ago. The latter is a four-story building which is about 10 years old. The buildings will be hereinafter called buildings “A” and “B”, respectively. The plan of the two buildings is rectangular shape. It is single span in one direction and multiple spans in the other perpendicular direction. The single span length is about 9-10 m. This large span length makes the spanned beam with about 0.8 m in depth. However, the two edge supporting columns are much smaller with the cross sectional dimension of 0.3 by 0.4 m. The height of the stories is about 3.5 m.

From the structural damage examination, severe upper end column cracks could be found in building “A”, especially at the first floor corner column. There were no cracks on other structural members. Only cracks on the beam plaster could also be observed. For nonstructural components, unreinforced masonry walls were cracked diagonally. In addition, roofing material which is cement based panel, was cracked and failed down. Substructure supporting the roof materials made of light gage steel truss was buckled.

For the building “B”, crack around the upper end of the first floor columns could be seen. However, the crack width was smaller compared to those of building “A”. This is due to the more recent of construction time with higher material quality and better standard of practice. Unreinforced masonry walls were also severely damaged in diagonal crack form showing highly distorted of the frame structure.



(a) Side View



(b) Front view



(c) Crack in first floor
(viewed from inside)

Figure 2: Damage investigation of the three-story school building



(a) Side view (b) Crack at upper end of the first floor column

Figure 3: Damage investigation of four-story school building

3. PUSHOVER ANALYSIS

To evaluate seismic capacity of existing buildings, nonlinear analysis is needed to trace cracking and yielding phenomena of reinforced concrete elements. Fibre-based finite element program called SeismoStruct (SeismoSoft, 2010) was employed in this study. The program contains computational scheme capable of predicting the large displacement behavior of frames under static or dynamic loading, taking into account both geometric nonlinearities and material inelasticity. The so called “Static pushover analysis” recommended by FEMA-356 (2000) and ATC-40 (1996) guidelines was adopted in the investigation. It is a method for estimating the strength capacity of building represented in form of lateral capacity and drift. This procedure applies a lateral load pattern that is distributed along the building height. The lateral forces are then incrementally increased to reach a displacement control at the top of the building representing the two figures as the Capacity curve.

3.1 A case study

The representative building used in this nonlinear pushover analysis is a typical school building model under the Ministry of Education of Thailand. The building model has been widely adopted in the country including schools in the seismic risk area and also Chiang Mai city. The building is a three-story concrete frame with unreinforced masonry infilled building which is classified as C3 type. As shown in Figure 4, the building floor plan is narrow rectangular shape with 9.4 m single span in x direction and 56 m with 14 equal spans in y direction. The story height is 3.4 m. The thickness of concrete slab is 0.1 m. The lateral resisting system is provided by general moment-resisting frame system with the contribution of brick infilled walls. However, in this study the effect of the infilled

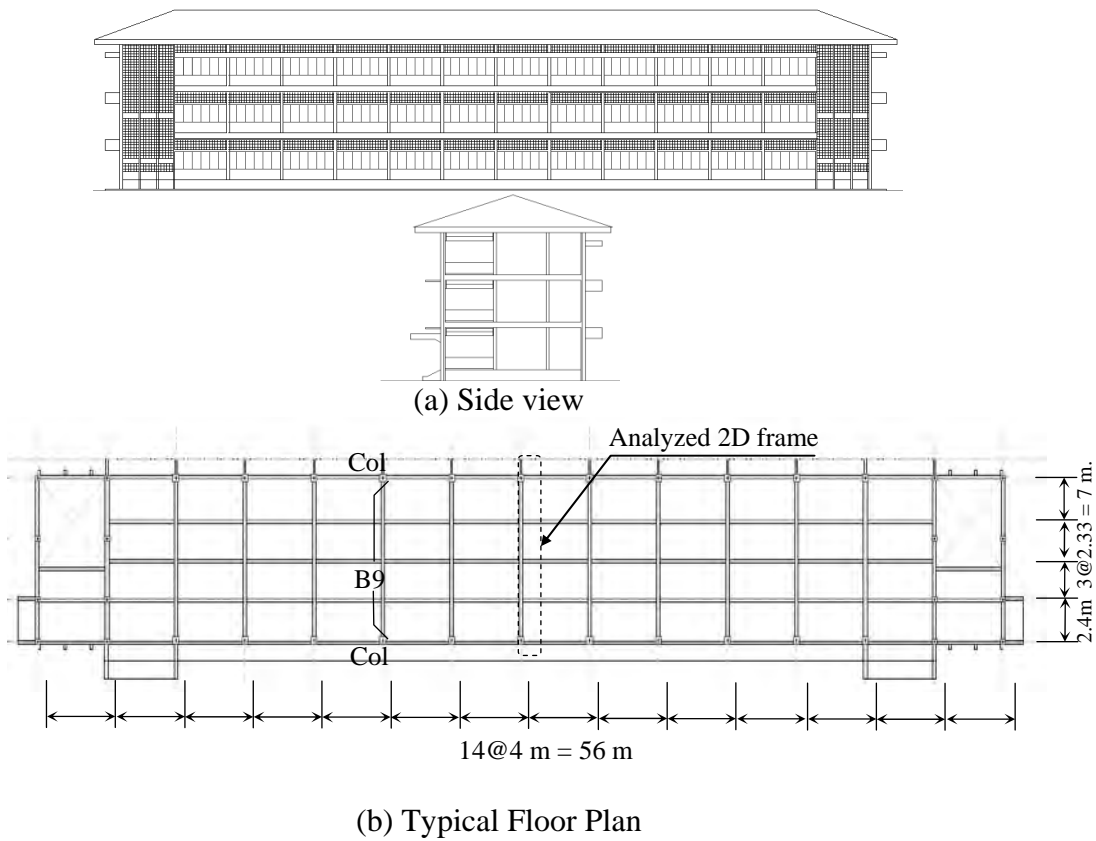


Figure 4: The representative school building

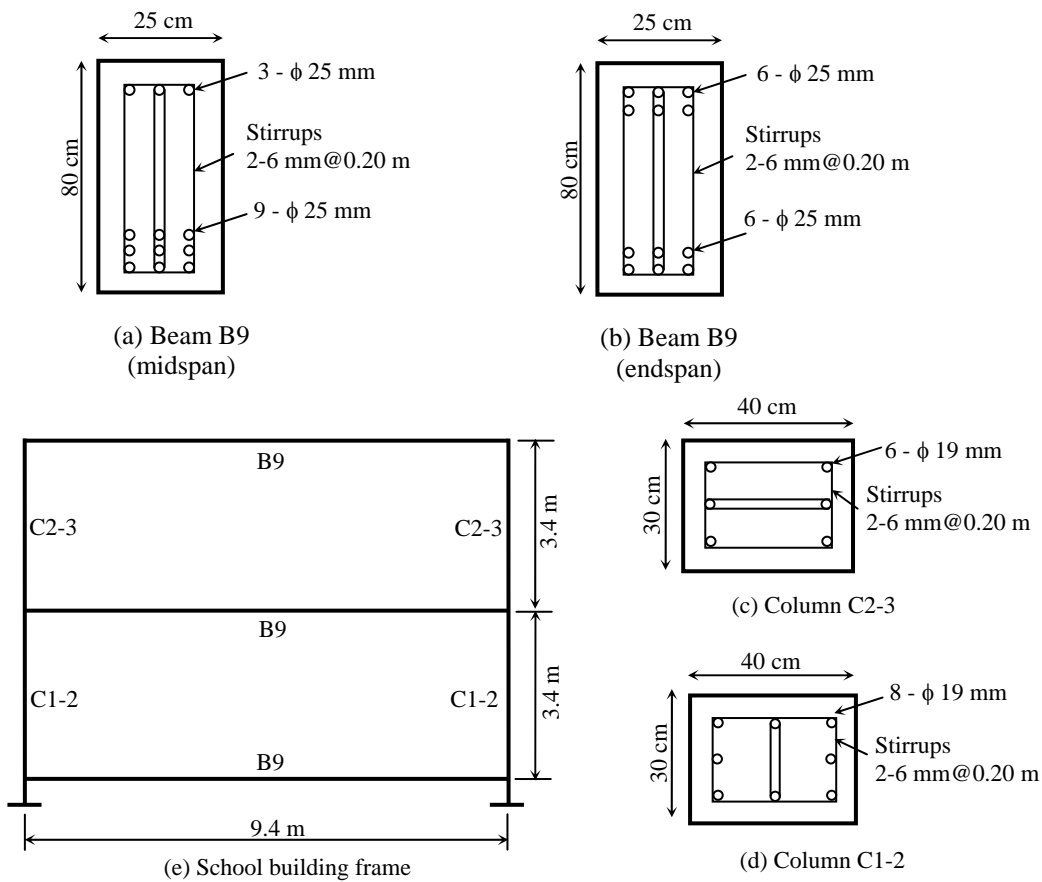


Figure 5: Analysed two dimensional frame

wall was neglected. Figure 5 shows the structural frame in the analysis. It is noted that the roof story was ignored in the study due to the less rigidity compared to other stories. From the figure, it can be obvious that the columns are quite small compared to the supported beams. The calculation for bending capacity of the beams and columns at joint interfaces are shown in Table 1 showing much lower columns bending capacity compared to those of the beams.

Table 1: Bending capacity of beams and columns at joint interfaces

Joint	Ultimate Bending capacity(kN-m)			$\Sigma M_C/\Sigma M_B$
	Column above joint (M_{C1})	Column above joint (M_{C2})	Beam (M_B)	
J1	84	84	690	0.24
J2	84	84	690	0.24
J3	84	-	690	0.12

3.2 Fibre Material models

The fibre-based approach discretizes cross-section of element into small fibre where each fibre is associated with a uniaxial stress-strain relationship for either unconfined concrete or confined concrete or steel reinforcement, as seen in Figure 6. Hence, material inelasticity can be easily implemented. Then, the sectional stress-strain state of beam-column elements is obtained through the integration of the uniaxial stress-strain response of the individual fibres. Based on the computational scheme, the fibre model has more advantages in relation to the simpler lumped-plasticity models that distributed inelasticity elements can be generally used without predefining concentrated-plasticity section. In addition, the spread of inelasticity along the member length and across the section depth is explicitly modelled.

Uniaxial compressive strengths of concrete is 24 MPa. The expected yield strength of steel bar graded SR24 is 348 MPa. which were used for both longitudinal reinforcement and stirrup. The constitutive models are shown in Figure 7.

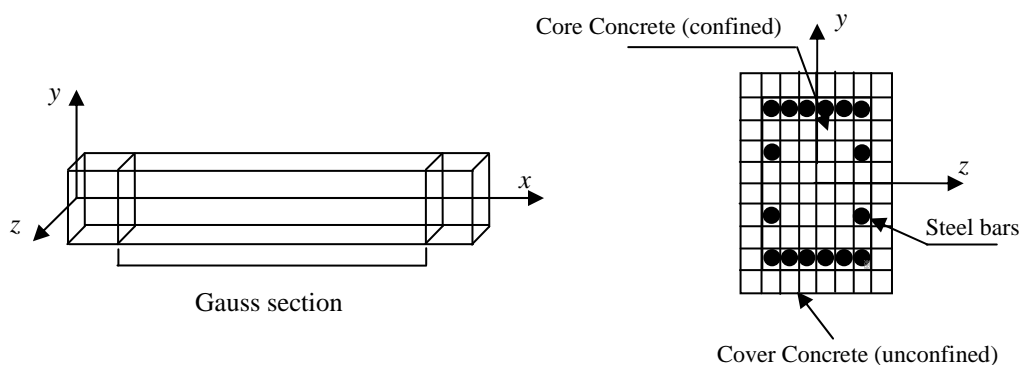


Figure 6: Discretization of cross section into small fibers

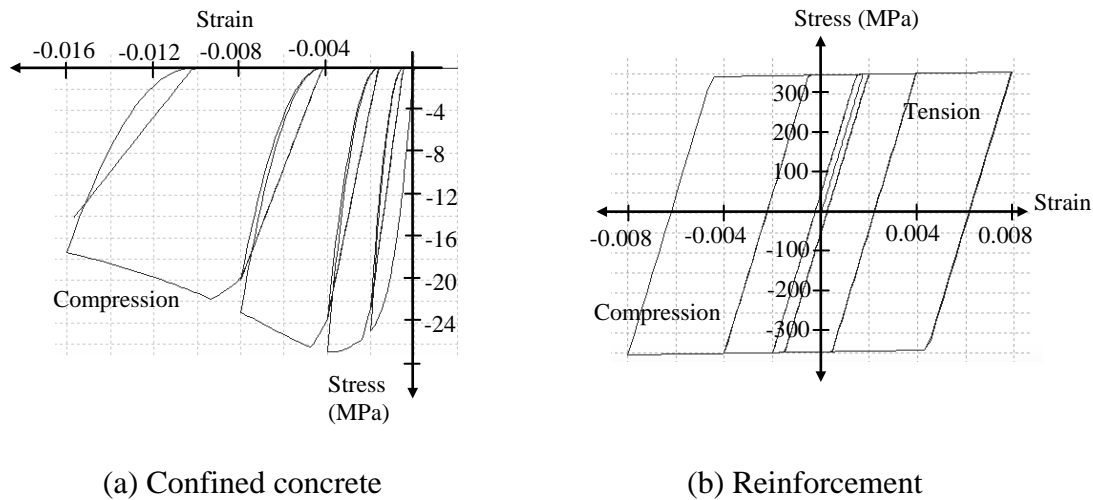


Figure 7: Uniaxial stress-strain relationships

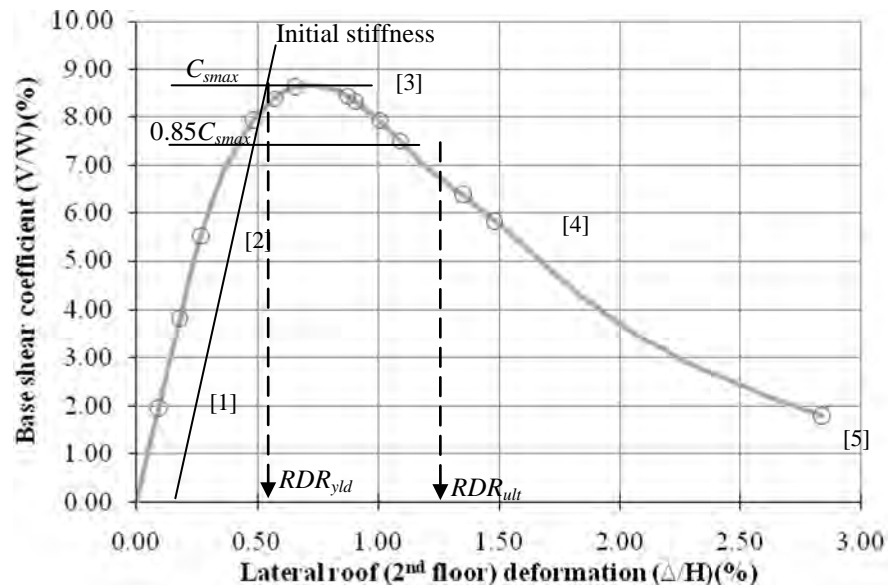
4. RESULTS

Figure 8(a) shows the capacity curve of the typical school building with maximum base shear coefficient (C_{smax}) of 8.67%. and the ultimate roof drift ratio (RDR_{ult}), defined by the drift ratio at 85% of the maximum base shear, of 1.11%. The roof drift ratio is defined as the ratio of lateral displacement at the third floor (Δ) to the height of the floor (H). The coefficient indicates the need for upgrading as compared with the calculated equivalent base shear coefficient of 13.07% according to the Thai Standard for earthquake design in the area (DPT, 2009). In addition, the RDR_{ult} is lower than 2% of ductile frame building. The roof drift ductility ratio (μ_{RDR}), expressed as the ratio RDR_{ult} -to- RDR_{yld} (see figure 8(a)), is 2.92. Figure 8(b) represents the damage level of the building corresponding to the level of the pushing force in which the damages are concentrated at building columns. The progressive of damages starts with yielding of all column ends and then further increase to severe failure of the first story columns.

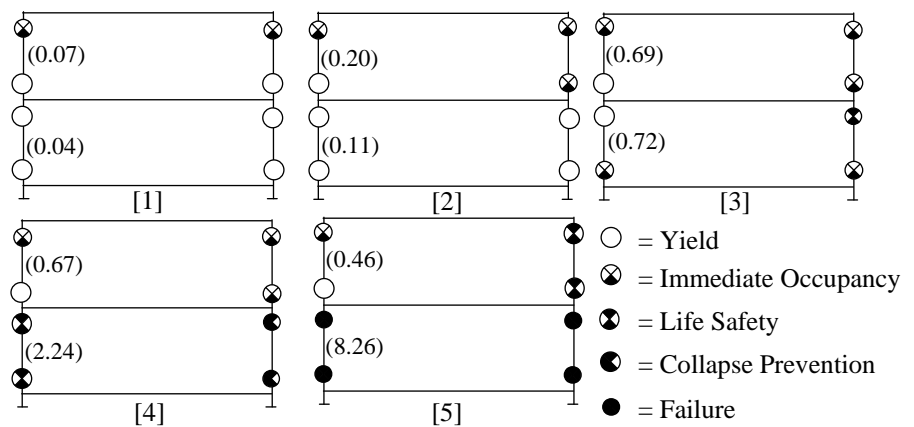
As seen in Figure 8(b), the story drift ratios are indicated by numbers in parenthesis. Referred to the FEMA 273 (1996), within load intensity [2] with the ratio less than 0.5%, the damage is in range of repairable. Between [2] to [3] stages, the damage level is too severe to be repaired. Eventually, after the [4] stage, complete collapse is identified when the ratio is more than 2.5%.

5. CONCLUSION

This paper presents the seismic vulnerability of Low-rise, single long span reinforced concrete buildings. The building model is among the most typical building configurations adopted in governmental school in Thailand. The study was performed by considering earthquake performance of the existing buildings



(a) Capacity curve



(b) Yield and failure mechanism with story drift ratio (in parenthesis)

Figure 8: Capacity curve and failure mechanism

located near the Thai-Myanmar border which were recently hit by the M6.8 earthquake at Shan State, Myanmar. In addition, evaluation of seismic performance using nonlinear pushover analysis of a typical three story school building is presented. The two results consistently indicate the weak column behavior. From the analysis, collapse of building can be observed with low ductility. Hence, both evidences indicate seismic vulnerable and the need for strengthening of the building.

ACKNOWLEDGMENT

The author wishes to acknowledge the Thailand's Office of the Higher Education Commission under the National Research University Project for financial support.

REFERENCES

Applied Technology Council-ATC., 1996. *Seismic Evaluation and Retrofit of Concrete Buildings (ATC-40)*, Redwood City, California, USA.

Department of Public Works and Town & Country Planning-DPT., 2009. *1302-Design Standard for Earthquake Resistant Buildings*, Bangkok, Thailand.

Federal Emergency Management Agency-FEMA. 1996, *NEHRP Guidelines for the Seismic Rehabilitation Buildings (FEMA 273)*, Washington, D.C., USA.

Federal Emergency Management Agency-FEMA., 2000. *Prestandard and Commentary for the Seismic Rehabilitation of Buildings (FEMA 356)*, Washington, D.C., USA.

Lukkunaprasit, P., and Kuhatanadeekul, N., 1993. Seismic zoning and seismic coefficients for Thailand. *1993 Annual Conference*, Engineering Institute of Thailand, pp. 268-287.

SeismoSoft, 2010. *SeismoStruct - A Computer Program for Static and Dynamic Nonlinear Analysis of Framed Structures [on line]*, available from URL: <http://www.seismosoft.com> (June 30, 2010).

Warnitchai, P., and Lisantono, A., 1996. Probabilistic seismic risk mapping for Thailand. *11th World Conference on Earthquake Engineering*, Acapulco, Mexico

A simple and effective seismic retrofit scheme for masonry-infilled non-ductile reinforced concrete frames

Panitan LUKKUNAPRASIT¹ and Jarun SRECHAI²

¹ Professor, Department of Civil Eng., Chulalongkorn University, Thailand
panitan.l@chula.ac.th

² Doctoral Student, Department of Civil Eng.,
Chulalongkorn University, Thailand

ABSTRACT

A simple and effective scheme has been developed for retrofitting masonry-infilled non ductile RC frames. Three $\frac{3}{4}$ scaled models of single bay, single story non-ductile RC frames with infilled un-reinforced masonry (URM) were tested under horizontal cyclic loading and a constant vertical load of 20% the ultimate capacity of the column based on the concrete gross section. The unretrofitted specimen suffered corner crushing and abrupt shear failure in the columns at a very small drift of 0.25%. The specimen was retrofitted by separating the masonry panel from the vertical columns so that no shear was transferred to them, eliminating totally shear failure caused by the strut forces from the masonry. Steel brackets were provided to transfer the interactive horizontal forces between the RC frame and the masonry panel. With the URM panel separated from the RC frame such that the panel width is reduced by 20%, the drift capacity is increased 6 fold, with desirable gradual drop in capacity. The last specimen with the wall aspect ratio of 1.0 could sustain a drift of 1.75% at 20% drop in strength.

Keywords: *masonry infill, retrofitting, reinforced concrete frame, cyclic load, non-ductile*

1. INTRODUCTION

Reinforced concrete (RC) frame buildings with un-reinforced masonry (URM) infill panels are prevalent in Thailand as well as developing countries. Earthquake reconnaissance in past earthquakes in high seismic prone countries has witnessed poor performance of such structural systems especially when the RC frames are detailed as non-ductile. Undesirable abrupt shear failure of the bounding columns or beam-column joints often follows due to transfer of the huge strut forces resisted by the infill to the columns. This is true not only in strong earthquakes, but also in moderate shaking such as that in Chiang-Rai caused by the March 24 2011 M6.8 Myanmar earthquake near Chiang-Rai border. Model tests as well as full scale tests on real buildings have also yielded similar results (Mehrabi et al. 1996, Korkmaz, et al. 2010, Corte et al. 2008). It is important to note that

such failure can occur at a relatively small drift ratio, in the order of 0.5%. On the other hand, there have been incidents of actual performance of such buildings in earthquakes (L'Aquila earthquake, Hassan and Sozen 1997) which demonstrate beneficial effect of un-reinforced infills. Laboratory tests with masonry reinforced with wire mesh or the like have also demonstrated the potential of transforming the brittle masonry panels to a more ductile one suitable for retrofitting. However, past attempts have accomplished limited success. Since infills are cheap building materials for constructing non-structural partitions, it would be economical and beneficial if they could be utilized to contribute to earthquake resistance, either in new construction or in retrofit work. To this end, it is necessary to invent a reliable means which can reduce the drawbacks of un-reinforced masonry infill in its interaction with RC frames.

2. RETROFIT SCHEME

In order to be able to effectively utilize the masonry walls for seismic resistance, one has to address and minimize the following major problems:

- a) shear failure of the (non-ductile) RC columns and /or beam-column joints;
- b) crushing of the corners of the infill;
- c) sliding of horizontal bed joints in the infill, including the masonry-beam interfaces.

All these modes of failure lead to relatively low ductility capacity of the structural system. Guided by failure mechanisms observed in the literature, the following innovative scheme (depicted in the diagram Figure 1) is adopted for resolving weaknesses in non-ductile infilled URM RC frame:

- a) The retrofitted masonry is separated from the vertical columns so that no shear is transferred to them, eliminating totally the shear failure caused by the strut forces from the masonry;
- b) Steel brackets are provided to transfer the interactive horizontal forces between the RC frame and the masonry panel;
- c) Small vertical steel members (or other equivalent components) are anchored to the vertical boundaries of masonry infill to prevent sliding joint failure. The steel members are not anchored to the surrounding beams to minimize tension that would otherwise be induced in the infill.
- d) The corners of the infill are reinforced with wire meshes and high strength mortar.

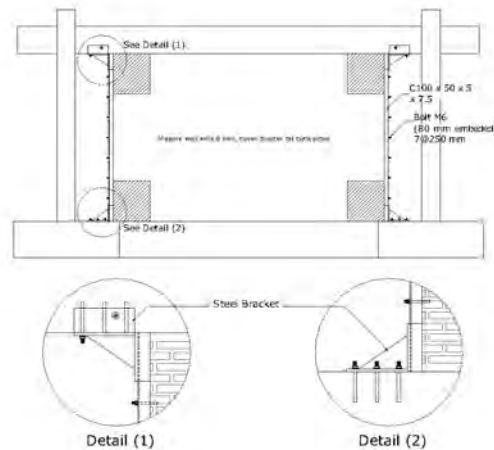


Figure 1: Retrofit scheme of URM infilled RC frame.

3. TEST SPECIMENS

In this study, three $\frac{3}{4}$ scaled models of single bay, single story non-ductile RC frames with infilled non-reinforced masonry (URM) were tested under horizontal cyclic loading and a constant vertical load of 20% the ultimate capacity of the columns based on the concrete gross section. Specimen MIRCFO1 was original unretrofitted that had panel aspect ratio (width/height) 2.0. Specimens MIRCFO2 and MIRCFO4 were retrofitted with the scheme proposed above.

4. EXPERIMENTAL RESULTS AND DISCUSSION

Figure 2 depicts Specimen MIRCFO1 with shear cracks in RC columns and beam-column joints, and corner crushing of the masonry infill. As mentioned earlier, the RC frame was non-ductile, and the clay tile panel was un-reinforced. This frame assembly attained peak load of around 30 tons at 0.25% drift, after which the load suddenly dropped to less than 40% at 0.5% drift only as illustrated in the hysteretic loop in Figure 3.

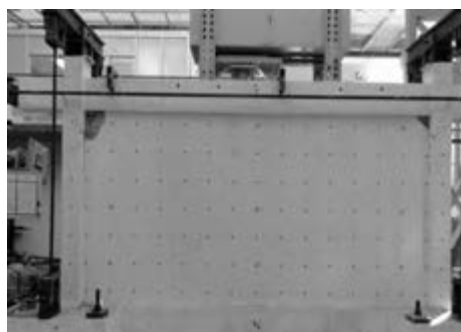


Figure 2: Un-reinforced masonry infilled non-ductile with column shear failure and corner panel crushing at 0.25% drift

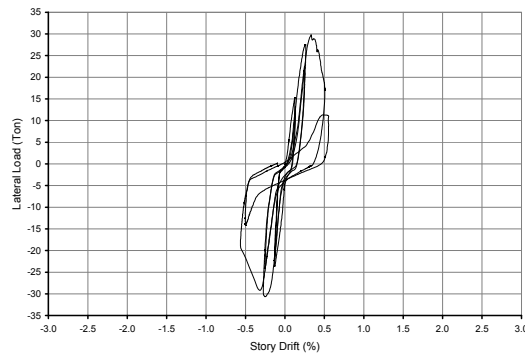


Figure 3: Hysteresis Loop of Specimen MIRCF01

Specimen MIRCF02 has demonstrated remarkable improvement in performance over the original system, with the drift capacity of 1.5% achieved at a sustainable lateral load of 80% the peak capacity and a gradual drop of load capacity (see Figure 5). It should be noted that at 2.0% story drift, although the URM panel suffered severe damage, only small shear- and flexural-cracks occurred in the RC columns (Figure 4).



Figure 4: Retrofitted masonry-infilled RC frame (MIRCF02) with the innovative scheme at 2% drift (test terminated for safety reason)

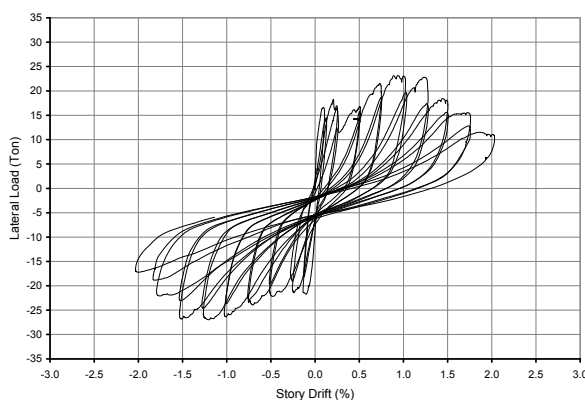


Figure 5: Hysteretic loop of specimen MIRCF02

Specimen MIRCF04 with the wall aspect ratio of 1.0 could sustain a drift of 1.75% at 20% drop in strength (see Figure 6-7). At a drift of 2.5%,

spalling of concrete and longitudinal steel buckling can be observed in the column near the beam-column joint. Significant rocking of the panel occurred and a major diagonal tension crack cut through the masonry infill (Figure 6).



Figure 6: Retrofitted masonry-infilled RC frame (MIRCF04) with the innovative scheme at 2.5% drift (test terminated for safety reason)

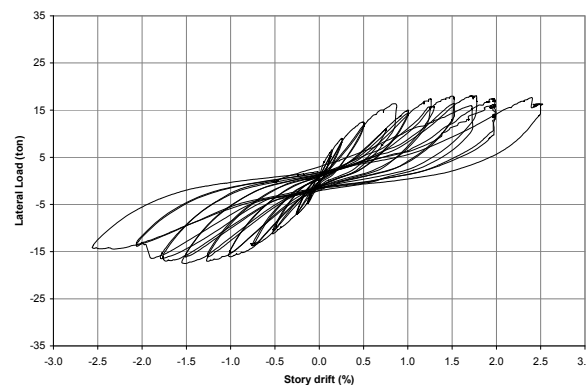


Figure 7: Hysteretic loop of specimen MIRCF04

It is interesting to compare the performance of the proposed retrofit scheme with others in the literature. As evident in Table 1, past retrofit schemes using heavy external mesh reinforcement with plaster composite achieved the best drift capacity of only 1.69 % at 20% drop in peak capacity (Korkmaz et al. 2010), while the best from carbon fiber reinforced polymer retrofit was 1.7% (Yuksel et al. 2010). The retrofit method presented is low cost and does not have any mesh or carbon fiber reinforcement, and yet it could attain a drift capacity of 1.5-1.75 % at 20% drop in peak capacity. With reinforcement applied to the masonry panel, better performance is anticipated.

Table 1: Comparison of different retrofit schemes

No.	Samples by	Masonry panel W/H	Drift @ 20% drop in capacity	Remark
1	Kyriakides et al. (2008) et al.	1.79	1.2%	sprayable ductile cement-based composites and welded wire fabric
2	Korkmaz et al. (2010)	1.63	1.19-1.69%	heavy external mesh reinforcement with plaster composite
3	Acun and Sucuoglu (2006)	1.72	0.75% to 1.1%	external mesh reinforcement
4	Altin et al. (2008)	1.73	1.0%	carbon fiber reinforced polymer; CFRP ruptured
5	Yuksel et al. (2010)	1.17	1.0% to 1.7%.	various configurations of CFRP
6	This research MIRCF01 (2011)	2.00	0.25%	Un-reinforced panel
7	This research MIRCF02 (2011)	1.60	1.50 %	Separated panel, load transfer bracket, corner strengthening
8	This research MIRCF04 (2011)	1.00	1.75%	Separated panel, load transfer bracket, corner strengthening

CONCLUDING REMARKS

The innovations presented seem to be promising judging from the satisfactory performance of the test specimens in the laboratory. Of course, the practicality and the effectiveness of the schemes over a wide range of applications are subject to further extensive investigations.

ACKNOWLEDGEMENTS

The authors are grateful for the funding from the Commission on Higher Education of Thailand, AUN/SEED-Net, and grant No. CA2/2553 from Faculty of Engineering, Burapha University, Thailand. The assistance of Building 33 Company Limited in casting the test specimens is greatly appreciated.

REFERENCES

Acun B., and Sucuoglu H., 2006. Strengthening of Masonry Infill Walls in Reinforced Concrete Frames with Wire Mesh Reinforcement. Proceedings of the 8th U.S. National Conference on Earthquake Engineering, San Francisco, California, USA, paper No. 1852.

Altin S., Anil OZR M., Emin Kara, and Mustafa Kaya, 2008. An experimental study on strengthening of masonry infilled RC frames using diagonal CFRP strips, *Composites: Part B* 39 680–693.

Kyriakides MA., and Billington SL., 2008. Seismic retrofit of masonry-infilled non-ductile reinforced concrete frames using sprayable

ductile fiber-reinforced cementitious composites. Proceedings 14th World Conf. on Earthquake Eng., Beijing. Paper Number 05-04-0063.

Yuksel E., Ozkaynak H., Buyukozturk O., Yalcin C., Dindar AA., Surmeli M., and Tastan D., 2010. Performance of alternative CFRP retrofitting schemes used in infilled RC frames. *Construction and Building Materials* 24 596-609.

Corte DC., Fiorino L., Mazzolani FM., 2008. Lateral-loading tests on a real RC building including masonry infill panels with and without FRP strengthening. *J Mater Civil Eng*, ASCE; 20(6):419_31.

Hassan AF., and Sozen MA., 1997. Seismic vulnerability assessment of low-rise buildings in regions with infrequent earthquakes. *ACI Struct J*; 94(1):31_9.

Korkmaz SZ., Kamanli M., Korkmaz HH., Donduren MS., and Cogurcu MT., 2010. Experimental study on the behavior of nonductile infilled RC frames strengthened with external mesh reinforcement and plaster composite, *Nat. Hazards Earth Syst. Sci.*; 10:2305-2316.

Mehrabi AB., Shing PB., Schuller MP., and Noland JL., 1996. Experimental evaluation of masonry-infilled RC frames. *J Struct Eng (ASCE)*; 122(3):228_37.

Evaluation model of the five story horizontally-mixed hybrid timber structure

Mengting TSAI¹ and Mikio KOSHIHARA²

¹Doctoral Student, Department of Architecture,
Faculty of Engineering, the University of Tokyo, Japan
tsai@iis.u-tokyo.ac.jp

²Associate Professor, ICUS, Institute of Industrial Science,
The University of Tokyo, Japan

ABSTRACT

The primary objective of this study is to understand the vibration behavior and the force distribution under seismic loading of the five storey horizontally-mixed hybrid timber structure, which has been constructed in a shrunk one third scale model and was tested in 2006, in order to find out a proper static evaluation model based on the building code in Japan. The proposed static evaluation model examined how the seismic loading suffered in timber part transmit to the core part, which is constructed by steel, through the floor system and connector. Furthermore, the displacement relationship between timber part and core part of each floor under seismic loading will also be calculated. In addition, the comparison of the analysis results between experimental study, static model and result from structural analysis program will also be discussed. This paper gives an overall view of the static evaluation of the horizontally-mixed hybrid timber structure, and with the confirming required knowledge of this kind of structural systems, the enhanced performance and improvement of the mid-rise hybrid timber structural system will also be expected.

Keywords: horizontally-mixed hybrid timber structure, force distribution, seismic loading, static evaluation model

1. INTRODUCTION

The mid-rise or high-rise timber buildings higher than 4 storey require at least two hours fire resistance ability based on the building code in Japan. Nowadays, the latest fire resistance technology of the timber structure can only last for one hour. In order to fit the requirement and study the feasibility of the mid-rise or high-rise timber buildings, the horizontally-mixed hybrid timber structure which were constructed by timber part and non-timber part (steel) was designed in a shrunk one third scale model (shown in figure 1) and was tested in 2006.

The primary objective of this study is to understand the vibration behavior and the force distribution under seismic loading of the five storey horizontally-mixed hybrid timber structure in order to create a proper

evaluation system including establish of the static and the dynamic analysis model based on the building code in Japan. In addition, the parameter studies of the stiffness of the timber floor are also studied in order to understand the efficient of the force transmit between timber part and steel part.

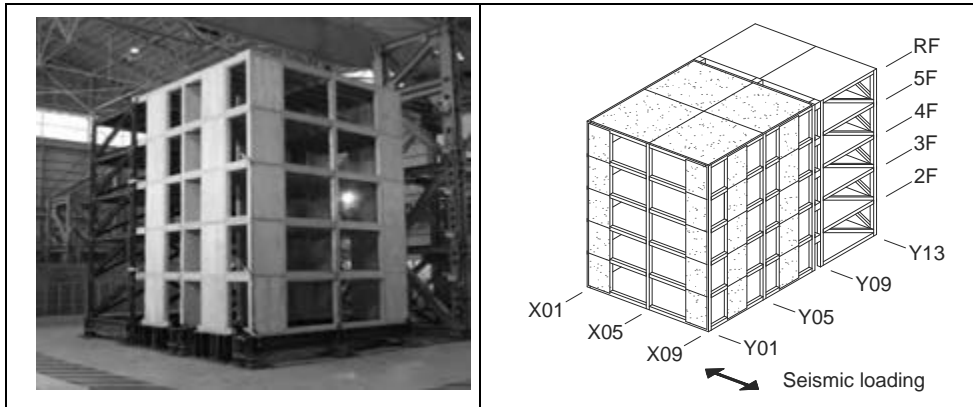


Figure 1: The experimental specimen (left) and the axis (right)

2. THE ESTABLISH OF THE STATIC EVALUATION MODEL

To establish the static evaluation model contains two steps. The first step is to find the value of the storey shear coefficient A_i , the distribution of the seismic force at each storey. After the value of A_i is obtained, the required seismic shear force Q_{ei} in each joint of each storey can be calculated as well. Figure 2 shows how A_i will distribute in the modified building model (Figure 2 left) and the distribution of the required seismic shear force Q_{ei} (Figure 2 right) after A_i is determined.

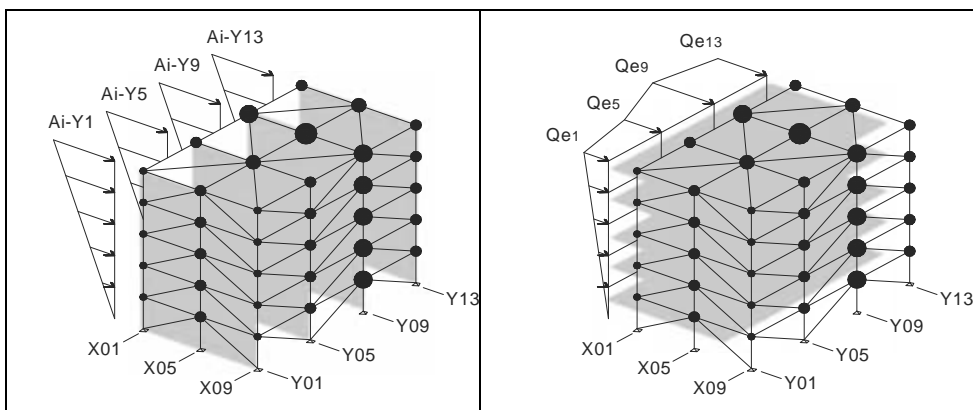


Figure 2: The model of A_i distribution (left) and required shear force Q_{ei} (right)

2.1 The A_i distribution

Based on the seismic design code in Japan, the A_i distribution is one of the factors used to generate the seismic force instead of inverted

triangular loading distribution that is used in North American. The equation (1) shows how the value of A_i can be calculated,

$$A_i = 1 + \left(\frac{1}{\sqrt{a_i}} - a_i \right) \times 2 \times \frac{T}{1 + 3T}$$

$$a_i = \frac{\sum_{n=i}^5 W_n}{\sum_{n=1}^5 W_n} \tag{1}$$

where i = storey number, W_n = weight of storey n , a_i = weight ratio at storey i ,

T = primary natural period according to $T=0.03h$.

2.2 The calculation of the required seismic shear force Q_{ei}

Once the storey shear coefficient A_i is determined, the seismic shear force Q_{ei} at each joint of each storey can also be calculated by following equation,

$$Q_{ei} = C_i \times \sum_{n=i}^5 W_n = Z \times R_i \times A_i \times C_o \times W_i \tag{2}$$

where Z = area modulus, R_i = vibration characteristic coefficient, C_o = standard shear coefficient, Q_{ei} = seismic shear force at storey i .

In the equation (2) the standard shear coefficient C_o represents the earthquake magnitude, for example $C_o=0.2$ can be described as the design of the building can resist 200gal loading in the earthquake. Usually, the value of C_o is from 0.2 to 1.0 depending on the demand or type of the building. In this study, it is considered $C_o = 0.2$ and 1.0 both, the area modulus $Z = 1.0$, vibration characteristic coefficient $R_i = 1.0$, which means the building is located on the ground type 2. The results of the shear force Q_{ei} in each storey along the Y axis are shown in the table 1.

Table 1(a): The calculation results of the Q_{ei} in Axis Y1

Storey	ai	$\sqrt{a_i}$	Ai	ΣW_i (KN)	Ci		Qei (KN)	
					Co=0.2	Co=1.0	Co=0.2	Co=1.0
5	0.19	0.436	1.384	4.75	0.277	1.384	1.31	6.57
4	0.39	0.624	1.202	9.79	0.240	1.202	2.35	11.77
3	0.6	0.775	1.107	14.77	0.221	1.107	3.27	16.35
2	0.8	0.894	1.046	19.78	0.209	1.046	4.14	20.69
1	1	1	1	24.78	0.2	1	4.96	24.78

Table 1(b): The calculation results of the Q_{ei} in Axis Y5

Storey	ai	$\sqrt{a_i}$	Ai	ΣW_i (KN)	Ci		Qei(KN)	
					Co=0.2	Co=1.0	Co=0.2	Co=1.0
5	0.19	0.436	1.384	9.15	0.277	1.384	2.53	12.66
4	0.39	0.624	1.202	18.73	0.240	1.202	4.5	22.51
3	0.6	0.775	1.107	28.3	0.221	1.107	6.27	31.33
2	0.8	0.894	1.046	37.88	0.209	1.046	7.92	39.62
1	1	1	1	47.45	0.2	1	9.49	47.45

Table 1(c): The calculation results of the Q_{ei} in Axis Y9

Storey	ai	$\sqrt{a_i}$	Ai	ΣW_i (KN)	Ci		Qei(KN)	
					Co=0.2	Co=1.0	Co=0.2	Co=1.0
5	0.19	0.436	1.384	13.48	0.277	1.384	3.73	18.66
4	0.39	0.624	1.202	27.57	0.240	1.202	6.63	33.14
3	0.6	0.775	1.107	41.66	0.221	1.107	9.22	46.12
2	0.8	0.894	1.046	55.75	0.209	1.046	11.66	58.31
1	1	1	1	69.84	0.2	1	13.97	69.84

Table 1(d): The calculation results of the Q_{ei} in Axis Y13

Storey	ai	$\sqrt{a_i}$	Ai	ΣW_i (KN)	Ci		Qei(KN)	
					Co=0.2	Co=1.0	Co=0.2	Co=1.0
5	0.19	0.436	1.384	8.78	0.277	1.384	2.43	12.15
4	0.39	0.624	1.202	18.38	0.240	1.202	4.42	22.09
3	0.59	0.768	1.111	27.97	0.222	1.111	6.21	31.07
2	0.8	0.894	1.046	37.56	0.209	1.046	7.86	39.29
1	1	1	1	47.16	0.2	1	9.43	47.16

2.3 The evaluation model and transmission of the force

After the seismic shear forces Q_{ei} at each storey are obtained, meanwhile the floor slab which resists the seismic shear force can be converted into the equivalent brace based on the stiffness of the floor which was generated from the results of the experiment, in order to simplify the analysis. Figure 3 illustrates the equivalent brace model of the floor and the transmission of the seismic shear force Q_{ei} . In this model, the transmission of the force is calculated span by span, and the supporting in point D, E and F are the connecting joints of each span in the building. The supporting located in axis Y09 is the connector connects the timber part and steel part. The spring supporting in point A, B and C shows the affection of the shear wall along the axis, and the stiffness is different because of the different numbers of the shear wall panels are applied in the experiment. The types and specifications of the shear walls and floor slabs are shown in the next chapter discussing the made of the dynamic analysis model.

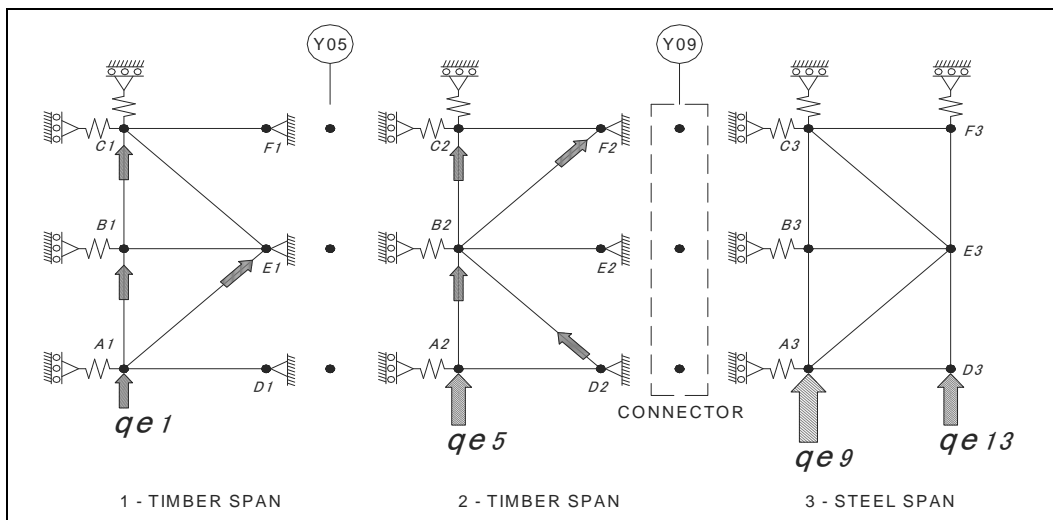


Figure 3: The equivalent brace model of the floor

2.4 The summary of the static evaluation

According to the analysis model show in figure 3, it is understood the maximum shear force occurs in the two side connectors (X01 and X09), which fits one of the force distribution pattern observed in the experiment (table 2). The value of the calculation shows the shear force calculated from the model is approximately 0.75 times the maximum value of the experimental result, which provides designers an estimating system to design the connector.

Also the results of the maximum deformations occur in axis Y01 shows in table 3 provide an outline of the deformation in each floor. The analysis results generally predicted the deformations. However, the evaluation model provided in this study assumes all the elements are elasticity, therefore the larger the seismic loading applied, with the deformations occurred in the experimental specimen coming in to the non-elastic area, and the deformations calculated from the static evaluation model will be smaller than the experimental results.

Table 2: The force (KN) in the connector

Storey	Results of the evaluation model			Experimental results					
				BCJ200			KOBE200		
	X01	X05	X09	X01	X05	X09	X01	X05	X09
1st	4.53	-	4.32	4.75	0.75	5.75	4.25	0.9	5.25
2nd	3.79	-	3.60						
3rd	2.99	-	2.85						
4th	2.16	-	2.04						
5th	1.23	-	1.13						

Table 3: The maximum displacement (mm) in Axis Y1

Storey	Evaluation model			Experimental results		
	Co=1	Co=0.5	Co=0.2	BCJ200	KOBE200	KOBE500
1st	5.19	3.22	1.31	1.45	1.1	4
2nd	4.33	2.69	1.09	-	-	-
3rd	3.42	2.13	0.86	2.55	2.1	5.95
4th	2.46	1.53	0.62	-	-	-
5th	1.38	0.85	0.35	0.85	1.05	2
Total	16.78	10.42	4.22	4.85	4.25	11.95

3. DYNAMIC EVALUATION

Structural elements and joints are modeled considering some idealizations. The idealizations and simplification make the results of the analysis different from the experimental results. In this chapter it is discussed that the basic specifications of the evaluation model that have been build in the computer analysis program MIDAS. With the confirmation of the basic specifications, the model can be used for the further analysis.

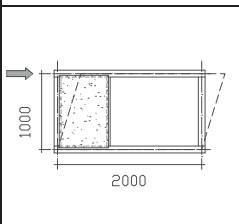
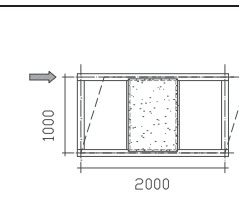
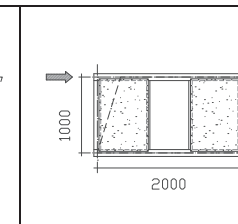
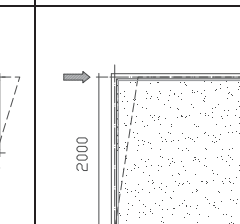
3.1 The made of the analysis model

To build an analysis model, the first step is to convert the wall panel and the floor slab, which are elements that resist seismic loading, into the equivalent brace. The types of these elements are shown in the table 4. And equation (3) shows how the equivalent brace can be converted,

$$P = K_w \cdot \delta_w = EA \cdot \frac{b^2}{(\sqrt{h^2 + b^2})^3} \cdot \delta_b \quad (3)$$

where P is the loading applied, K_w is the stiffness of the wall obtained from the specimen experiment, δ_w is the deformation of the specimen and δ_b is the deformation of the equivalent brace model, which is the same with δ_w . Based on the equation (3), it is expected to obtain the value EA of the equivalent brace.

Table 4: The types of the elements resisting seismic loading at timber part

Wall panel			Floor slab
			
2 panels (axis X1 to X9)	2 panels (axis Y1)	4 panels (axis Y5)	

The other specifications which are also required for the made of model are listed in table 5. And the final product that has been made in the computer program MIDAS is shown in the figure 5. The input of the seismic loading is alone the Y axis. The height of each storey is 1 meter and each span is 2 meters.

Table 5: The specifications of the model

Material	Size (mm)	Classification	Density (g/cm ³)	E (KN/mm ²)
Timber part				
Columns and Beams	100 × 100	E105-F300	0.5	10.5
Wall plate (4panels)	667 × 1000, t=9	Type1 Grade 2	0.5	1.54
Floor slab	2000 × 2000, t=9	Type1 Grade 2	0.5	2.55
Steel part				
Columns, Beams, braces	H-100*100*6*8	SN400	7.85	199.9
Floor slab	t=4.5	—	7.85	355.5

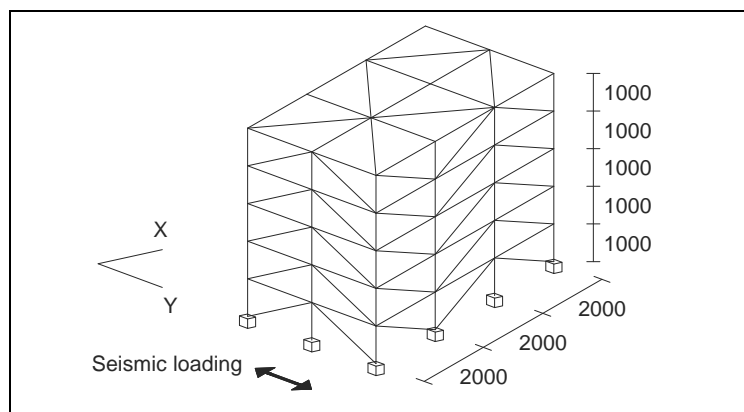


Figure 5: The analysis model with converted equivalent brace

4. PARAMETRIC STUDY OF THE FLOOR SLAB

From the previous study, it is understood that the floor is the key element to transmit the seismic force from the timber part to steel part through the connector. In this chapter, in order to realize the how the stiffness of the floor can influence the vibration behavior and the deformation of the building, the different parameters of the stiffness of the floors are studied.

4.1 The type of the floor stiffness

The types of the stiffness of the floors are shown in table 6. In the table 6, the stiffness of the analysis model Kf-4 is the standard one which the value was obtained from the experiment. Based on the model Kf-4, the other analysis models were made with the difference of the floor stiffness. The input of seismic loading in the analysis is Kobe 200 gal in order to simplify the analysis factor.

Table 6: The parameter of the floor slab

Model	Stiffness of the floor (KN/mm)		Converted EA (KN)
Kf-1	45	10 times Kf-4	255400
Kf-2	18	4 times Kf-4	102160
Kf-3	9	2 times Kf-4	51080
Kf-4	4.5	Experimental value	25540
Kf-5	2.25	0.5 times Kf-4	12770
Kf-6	0.45	0.1 times Kf-4	2554

4.2 The results of the analysis

The results of the analysis show that the improvement of the stiffness of the floor makes the stiffness of the building been improved. Furthermore, the deformation in each storey is also been reduced, figure 6 (left). In the other hand, it is observed that the stiffness of the floor been improved makes the deformation in the steel part increased, figure 6 (right). The reason can be explained that the floor is one of the most important elements to resist and to transmit the seismic force. Therefore when the building is suffering

the seismic loading, the seismic force occurred in the timber part can be transmitted through the floor span by span to the connector first and transmit to the steel part via connectors.

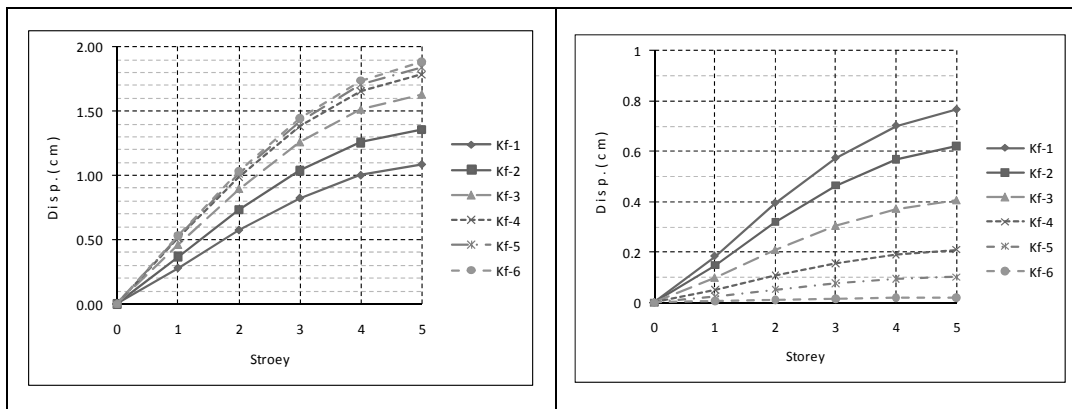


Figure 6: The storey displacement, left: timber part, right: steel part

According to the analysis results, it is believed that the stiffer the timber floor is, the more efficient the seismic force transmits from timber part to steel part through floors and connectors, and in the end the larger deformation is discovered in the steel part. In the figure 7, it is also noticed that the influence of the floor stiffness is much obvious in the lower floor than the higher floor.

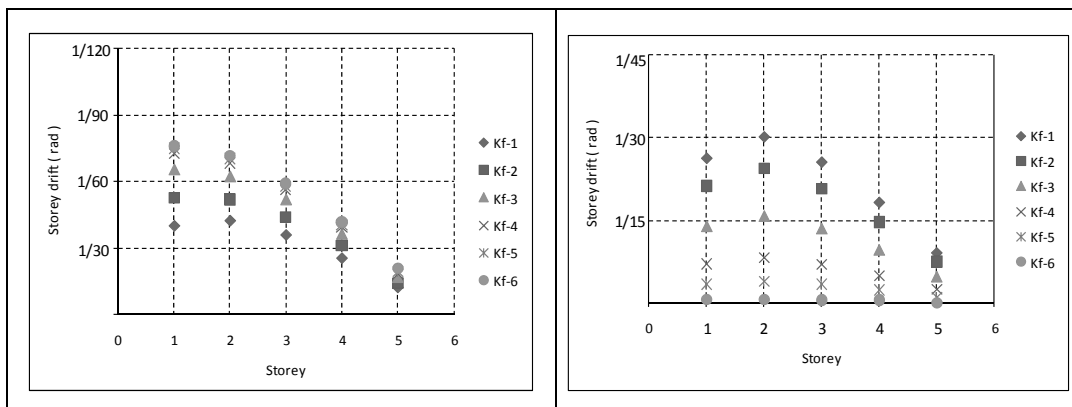


Figure 7: The storey draft angle, left: timber part, right: steel part

4.3 The summary

From the results of the analysis, it has been understood that the stiffness of the floor gives the great influence to the seismic force transmitting from timber part to the steel part. And the transmitting efficient can be simulated by the equation (4), which is called the force transmitting ratio,

$$D_{k-f-i} = \frac{D_{wood}}{D_{steel}} \quad (4)$$

where, D_{k-f-i} is the force transmitting ratio, D_{wood} is the largest deformation occurs at the timber part in model K_f-i , and D_{steel} is the largest deformation occurs at the steel part in model K_f-i . The smaller the

Dkf-i value is, the better the force transmitting efficient is, shown in figure 8 (left). And if each force transmitting ratio is compare to the Dkf-4(the standard stiffness), it is discovered that a trend line shows the same result as well, figure 8 (right).

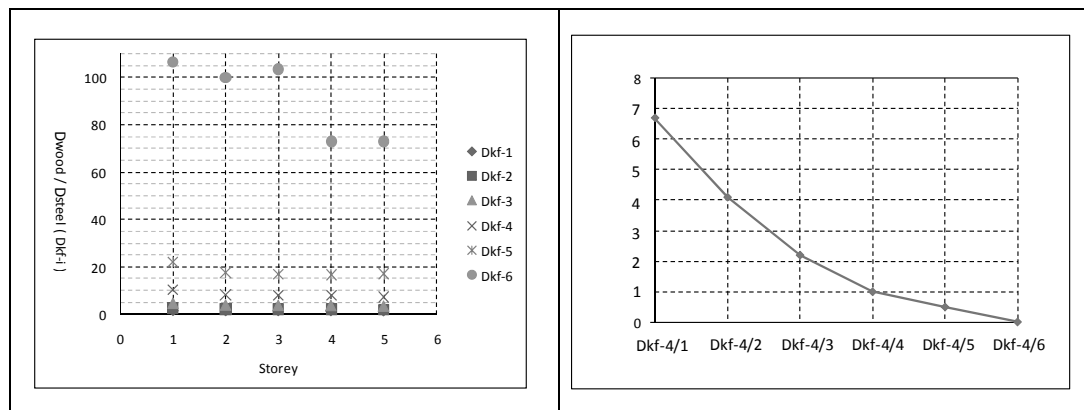


Figure 8: The force transmitting ratio $Dkf-i$ (left) and the trend line (right)

5. CONCLUSIONS

In this study, the general behavior of the five storey plane mixed hybrid timber structure under seismic loading becomes clarity, especially the transmitting of the force between timber part and steel part. The research results are concluded as follow:

1. As the final results which are obtained from the experiment examine the results that are calculated from the static evaluation model, the correction of the model is expected to be established. The results of the static evaluation model shows the shear force calculated from the model is approximately 0.75 times the maximum value in the experimental results, which provides designers an estimating system to design the connector. And the maximum deformation can be obtained according to the model as well.
2. According to the static analysis model, it is clear that the shear wall is the main element to resist the deformation of the building and the stiffness of the floor demonstrates the force transmission form the timber part to the steel part.
3. The additional study of the different parameters of the stiffness of the floor verifies the efficient system of the force transmitting from timber part to the steel part. The analysis result shows the stiffer the timber floor is, the more efficient the seismic force transmits from timber part to steel part through floors and connectors, and in the end the larger deformation is discovered in the steel part.

This study gives an overall view of the static evaluation of the horizontally-mixed hybrid timber structure, and with the confirming required knowledge of this kind of structural systems, the enhanced performance and improvement of the mid-rise hybrid timber structural system will also be expected.

REFERENCES

Koshihara Mikio, Isoda Hiroshi, Yusa Shuitsu, 2009, The design and installation of a five-story timber building in Japan, *The international symposium on timber structure*, Istanbul, Turkey.

Nakagawa Manabu , Kawai Naohito , Koshihara Mikio , Araki Yasuhiro , Isoda Hiroshi, 2007, Static tests of shear wall and structural floor to estimate behavior of scaled five story hybrid structure, *Summaries of technical papers of Annual Meeting Architectural Institute of Japan*, Vol.C-1, Structures III, 179-180.

Kawai Naohito and Okabe Minoru, 2002, Development of Technology for Hybrid Timber Building Structures: In-plane Shear Performance of Floor Systems, *Summaries of technical papers of Annual Meeting Architectural Institute of Japan*, Vol. C-1, 317-318

A study on seismic performance and reinforcement method of rammed earth wall, 'HANCHIKU'

Mikio KOSHIHARA¹ and Akiko TAKADACHI²

¹Associate professor, ICUS,
Institute of Industrial Science, the University of Tokyo, Japan
kos@iis.u-tokyo.ac.jp

²Structural engineer, Nikken Sekkei LTD

ABSTRACT

'HANCHIKU' wall is Japanese traditional rammed earth wall. They have been used as the wall around the old temple like 'HOURYU-JI'. But new 'HANCHIKU' wall could not be built because they have much damage due to large earthquake.

In this study a seismic performance of traditional 'HANCHIKU' is cleared using shaking table test and analysis. These walls are observed rocking phase and phase of resisting by bending moment depending on the scale of the input motion.

Some reinforcement methods are proposed and are verified the effect against earthquake. For stronger allowance shear force quicklime is mixed in soil. For rocking effect, a rammed earth wall is anchored by bamboos or plastics. For stronger allowance bending moment, they are reinforced using bamboo or plastics like reinforce concrete. Using bamboo has better seismic performance, but this method use the 1.6 times work forces than traditional method.

In this study the possibility for seismic designed rammed earth wall, 'HANCHIKU', is proposed.

Keywords: Cob, Rammed earth, Mud wall, shaking table test

1. INTRODUCTION

In Japan, from ancient time cob structured building such as cob storage or cob wall have been built. Not only in Japan but also all over the world there exists many cob structured building; for example, Great Wall in China. In Japan, the design and construction work are done by plasterer, various kinds of rule of thumb exists.

In this research, we define cob structured building, especially whose cob itself works as the structure as 'cob-structured-building'. This research works on especially 'Rammed Earth Wall', which is found in the ancient Houryuji-Temple or Nishinomiya-Shrine and still used in houses in the present. This Rammed Earth Wall is made by laminating cob layer, this cob

layer is made by stacking cobs which consists of bittern and lime in a mold until its volume become almost half.

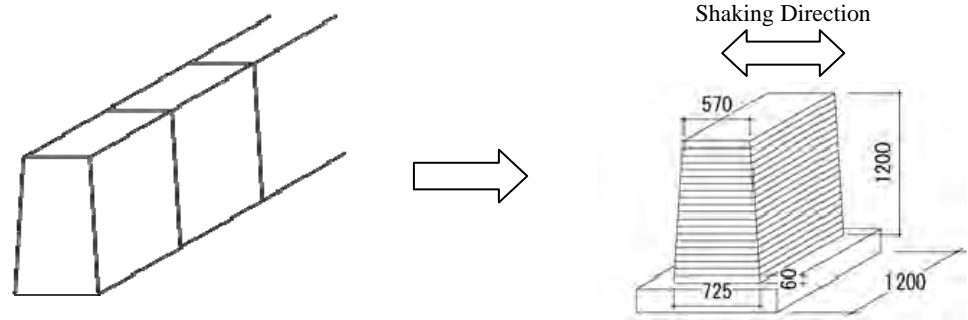
When this kind of cob structured building is designed and constructed, it is necessary to think over about the method scientifically, as well as taking rule of thumb into consideration. To clarify the seismic performance, shaking table tests of 1/2 scale models are conducted, this test focused on Rammed Earth Wall which don't have much resistance to the bending tension and tends to collapse to outplane direction in case of earthquake. Furthermore, we grasp the structural ability of Rammed Earth Wall when it's constructed in traditional way. We focused on the anchors between Rammed Earth Wall and basement, which is one of the problem in case of earthquake and we proposed reinforcement method and inspected the efficiency.

2. OUTLINE OF THE SHAKING TABLE TEST

2.1 Specimens

One part from the sequence of the Rammed Earth Wall was taken out as shown in Figure 1 and shaken in outplane direction. This research deals with 6 kinds of specimens, actually most of the Rammed Earth Wall constructed at the present time is classified in type HN1 or KN1, whose bottom is not anchored to basement.

The size of specimens is 1/2 scale model of Rammed Earth Wall from south-west side of Rammed Earth Wall in `Saiin in Houryuji-temple'. Each specimen is directly constructed on concrete basements. 2 kinds of cob were used to compare the performance between different kinds of cob. One cob (H) has sprinkling distribution of grading, is suitable for Rammed Earth Wall and is from Nara, the other (K) is from Chiba and contains much sand. The construction method of Rammed Earth Wall has its advantage in the point that, performance of any cob can be improved by handling grading distribution or adding admixture. The ratio of combination and admixture of each cob are shown in Table 1, cob H refers to the method in restoration of Horyuji-temple, cob K refers to the most suitable ratio of combination achieved from the result of room experiment by Lee(2009). In actual construction, because of the climate condition the ratio of the water was changed based on experience of the plasterer, thus the mixing ratio was measured during the construction work. Unconfined compressive strength obtained from test is shown in Figure 2. Compressive strength is proportional to its density.



‘Saiin in Houryuji-temple’

Specimen(unit : mm)

Figure 1: Specimen

Table 1: Mixing ratio

Cob H	Cob (H)	‘Nashimedo’	Water with Bittern (volume)
Target ratio	2	1	5-9%
Measured ratio	59	32	9

Cob K	Cob (K)	Sand	Quick Lime	Water
Target ratio	62	10	8	20
Measured ratio	58	10	8	24

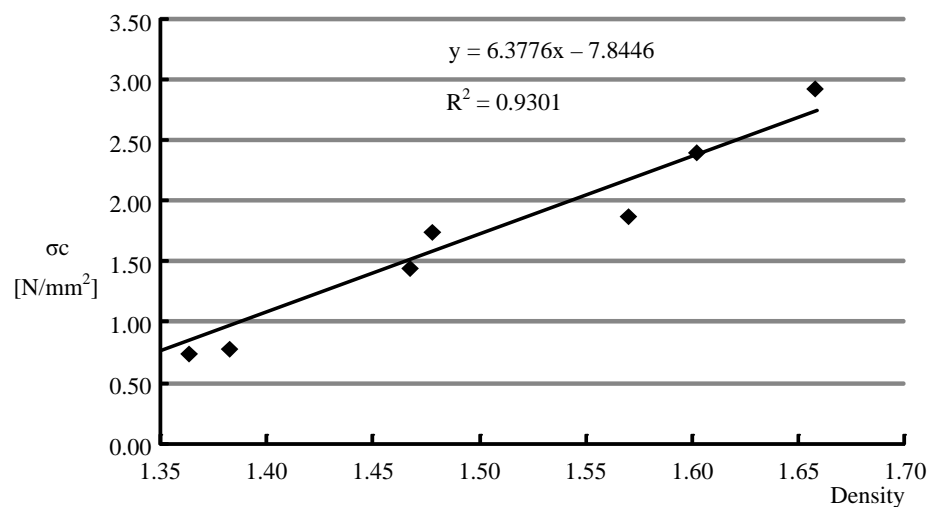


Figure 2: Compressive strength and density (Cob K)

2.2 Reinforcement method

This study proposes 2 sorts of reinforcement method for bending and overturning to the outplane direction, reinforcement by bamboo (KB) and mesh reinforce material of plastics (KM).

In KB natural material bamboo is used for tensile member, which is traditionally used for cob wall as reinforcement. Since direct anchor of bamboo to the basement leads rapid decay, steel reinforcement rod is used to anchor it and with grout reinforcement rod and bamboo are connected.

Takadachi [2009] has been reported about reinforcing bamboo of Specimens KB. This study made an experiment on tensile capacity of bamboo anchor in KB and indicated that the tensile capacity was determined by shearing strength of the node of bamboo. Moreover, shearing test of the node of bamboo was carried out, the shearing strength was evaluated. At the same time, adhesion test was put into practice, there the adhesion force between bamboo with a hemp rope(4,5φ mm) twisted around at intervals of 45mm and cob was examined. For the shape of the bamboo used for calculating the shearing strength of each node, the arithmetic mean of specimens at shearing test was used. With the value on table 3 and the tensile strength of cob 0.2N/mm², out of required capacity of reinforcement the specifications were determined. First of all, using ‘Standard for Structural Design of Reinforced Concrete Structures’, out of bending moment, the required amount of reinforcement rod was calculated, bamboo was designed to exceed the yield strength of the reinforcing rod. This experiment made use of such specimens with reinforcing bamboo as in Figure 3, D10 for reinforcement rod for anchor, ‘Madake’ bamboo from Chiba whose diameter is 50mm and for horizontal reinforcement split bamboo whose diameter is 60mm. For vertical reinforcement bamboo with a hemp rope (4,5φ mm) twisted around at intervals of 45mm was used so that it gets higher adhesion force.

Bamboo has demerit in construction method, that cob doesn’t get compacted well around the bamboo owing to the cylinder shape. Therefore a test on reinforced specimens KM with mesh reinforcement of plastic is carried out as well, which is often used for ground reinforcement as thin tensile reinforcement. The material capacity of reinforcement was referred to study [5]. Out of the result of calculation of required ability, reinforcement SS-35 with product standard strength 37.0 kN/m was arranged as in Figure 3.

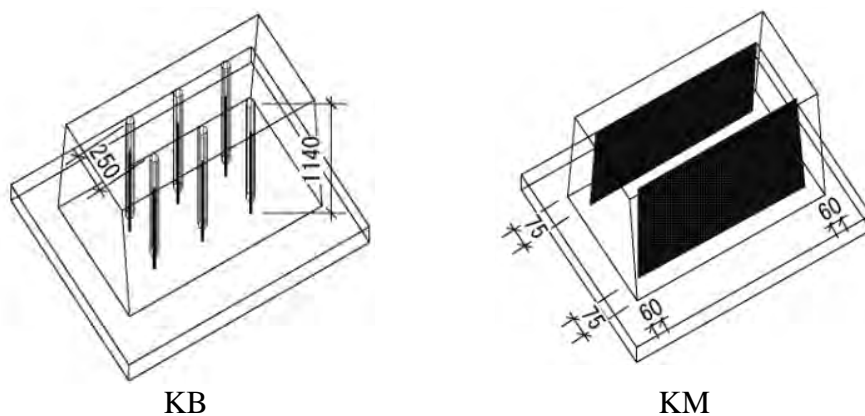


Figure 3: Specimen (Reinforced)

2.3 Input motion

This experiment made use of simulation wave of the building center of Japan (hereinafter BCJ-L2) and NS components of JMA Kobe recorded in Kobe earthquake in 1995 wave (hereinafter Kobe). As shown on table 2,

after shaking test No.4, because of the capacity of shaking table the time axis and the period of wave were shortened to half so that the maximum acceleration get bigger. The specimens were shaken until it collapsed, while the maximum acceleration increased.

Table 2: Input motion

No.	Wave name	Duration	Time axis	Max. Acc.
1	BCJ-L2	120 sec.	1	100
2	BCJ-L2	120 sec.	1	355
3	Kobe	80sec.	1	1049
4	Kobe	40sec.	1/2	1049
5	Kobe	40sec.	1/2	1200
6	Kobe	40sec.	1/2	1400
7	Kobe	40sec.	1/2	1600
8	Kobe	40sec.	1/2	1800
9	Kobe	40sec.	1/2	1950

2.4 Measuring plan

Measurement was done with total 31 channels of acceleration and deformation measuring instrument and image measuring system. The position of main acceleration and deformation measurement instrument is shown on figure 4. Each instrument has its positive direction like an arrow on figure 4.

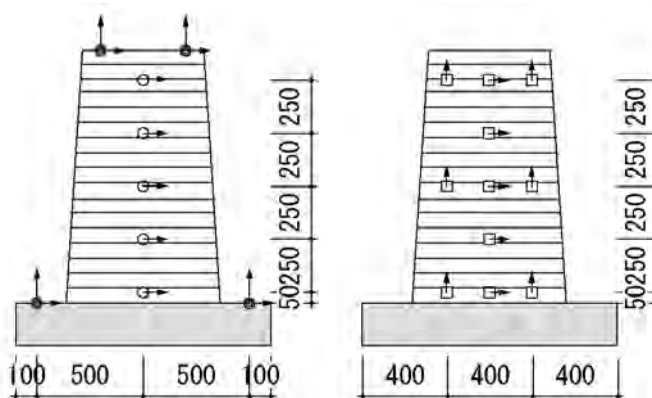


Figure 4: Measuring Plan

3. RESULT OF SHAKING TABLE TEST

3.1 Comparison of shaking level

The results of each specimen are shown in table.3. Table 3 shows maximum input acceleration of each shaking level on the concrete basement on which specimens are set up and the damage at each shaking level in round brackets.

Table 3: Result of Shaking Table Test

No.	HN1	KN1	HN2	KN2	KB	KM
1	148	179	182	139	150	173
2	449	444	472	477	463	491
3	(1050)	1060 Rocking	1069 Bending failure	955	952	1022 Crack at Pt.1
4	—	—	—	979	1029 Crack by bending moment	1191 Crack at Pt.2
5	—	—	—	1199 Bending failure	1232	1252
6	—	—	—	Collapse	1365	1401 Crack at Pt.3
7	—	—	—	—	1554 Crack by bending moment between 6 and 7 layer	1458 Crack at Pt.3
8	—	—	—	—	(1800)	(1800)
9	—	—	—	—	(1950)	(1950) Collapse

3.2 Damages

The damage was following; In KB, although a dry crack was expanded, that didn't result in collapse. Each specimen showed brittle fracture property.

During Shaking No.3 of specimens KN1, one side floated up because of overturning, however no large damage was observed except for that a part of the corner of bottom of the specimen was broken off (Figure 5).

Specimen HN2, KN2 didn't float up, however collapsed by bending tension collapse. In HN2, between 3rd and 4th layers a crack by bending tension was observed at first, afterwards the upper part floated up and fell, the impact caused interlayers between from 2nd to 5th layers peeled off. Figure 6 shows the frame by frame image from high speed camera. In KN2 a crack by bending tension was observed between 4th and 5th layers, while shaking No.5 was carried out. Furthermore, it stood by itself after bending tension collapse, thus shaking No.6 was done. The result was following; the upper part separated by bending tension collapse floated up, fell and gave an impact on the lower part, as a result the lower part collapsed. This result indicate that after bending tension collapse, unless it's reinforced between layers, Rammed Earth Wall doesn't possess resistance force.

In KM a dry crack on front of bottom of the specimen was expanded and penetrated to the sideways, while shaking No.3 was carried out. Next, during shaking No.4, 6 and 7, cracks by bending tension were observed on a side of bottom of the specimen. Afterwards during shaking No.8 there occur

a crack, because of these bending tension cracks, the shearing area become smaller and finally, shearing collapse was brought about during shaking No.9.

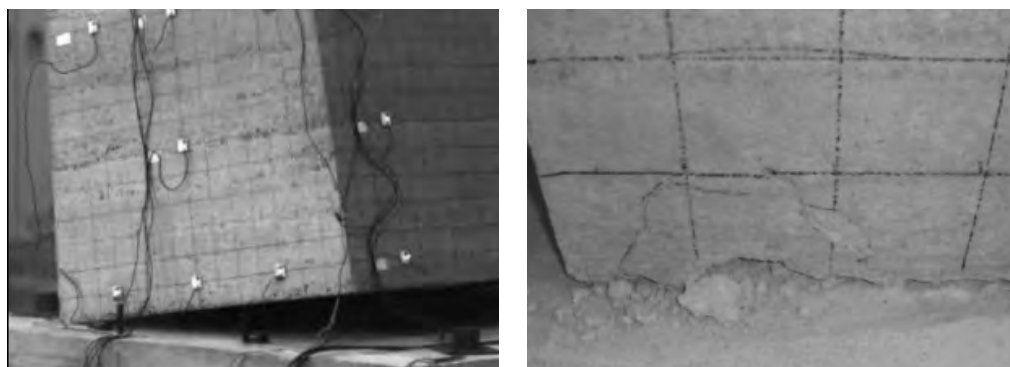


Figure 5: Overturning and Collapse of Bottom Layer (KN1 No.3)

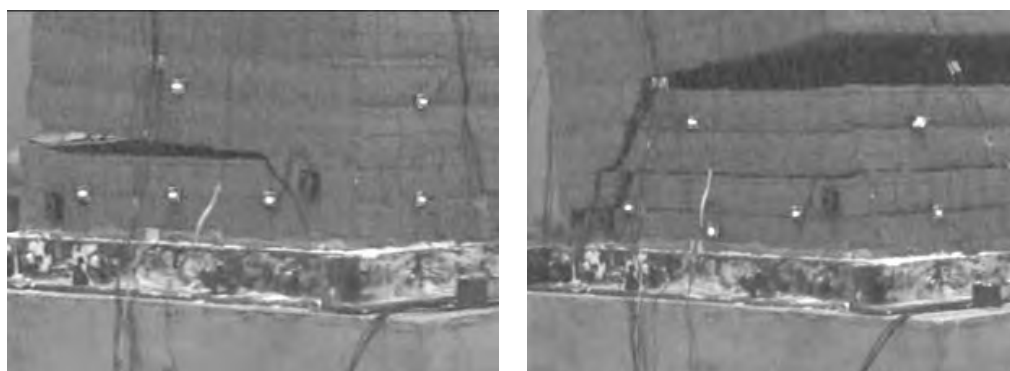


Figure 6: Process of Bending Failure (HN2 No.3)

4. Seismic performance and efficiency of reinforcement of Rammed Earth Wall

The properties of specimens are classified into 2 groups based on historical response acceleration and into 3 groups based on historical response deformation.

(1) Rigid body deformation

Before bending tension collapse, horizontal response acceleration was distributed in proportion to the height. From this one may say that Rammed Earth Wall behaves as one rigid body. Take No.5 of KB for example and look into the relationship between measured horizontal deformation on top of the specimen (δ [mm]) and rotation deformation calculated from rotation angle on bottom of the specimen. They are plotted along line $y=x$, which makes it clear that Rammed Earth Wall behaves as one rigid body. After shaking No.3 of specimen KM, a crack was found from front to side (between 1st and 2nd layer) of bottom of the specimens. This crack is thought to make the specimen behave divided into upper and lower part. Compare each horizontal deformation, rotation angle of bottom of the specimen (lower part) and rotation angle of the center of the specimen (upper part), the relationship between rotation deformation and measured

horizontal deformation on the center of the specimen are line up along line $y=x$, it behaved as 2 rigid bodies. However the horizontal response acceleration at each height on the center of the specimen are distributed in proportion to the height. The reason for it is thought that because deformation was restrained by reinforcement, response acceleration didn't differ each other so much. When shaken by No.8, the horizontal deformation was so big that the specimen behaved as 3 rigid bodies, in this case this principal was not applied.

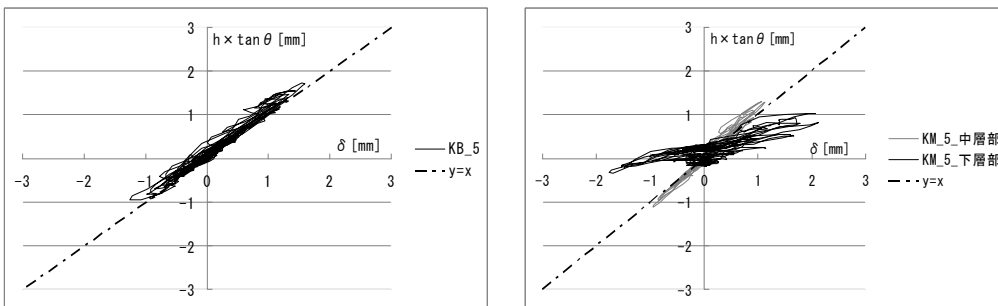


Figure 7: Horizontal deformation and rotation angle

(2) Relation of moment and rotation angle

When it behaves as a rigid body, the distribution of acceleration become a linear figure, the moment is calculated by following formula. $a(h)$ is approximation formula of the linear, each height of center of gravities hw become h through formula (2). Here $h+dh$ is approximated as h . In figure 8 of the relation between moment and rotation angle, the moment working on bottom of the specimen is used for Fig. 8. Rotation angle was calculated from vertical deformation obtained by the deformation measuring instrument on bottom of the specimen.

$$M(h) = \int_h^H \left\{ b1 + (b2 - b1) \times \frac{h}{H} \right\} \times L \times a(h) \div g \times hw \times \Delta h \tag{1}$$

$$h_w = \frac{\Delta h \times \left[\left\{ b1 + (b2 - b1) \times \frac{h}{H} \right\} + 2 \times \left\{ b1 + (b2 - b1) \times \frac{h + \Delta h}{H} \right\} \right]}{3 \times \left[\left\{ b1 + (b2 - b1) \times \frac{h}{H} \right\} + \left\{ b1 + (b2 - b1) \times \frac{h + \Delta h}{H} \right\} \right]} + h \tag{2}$$

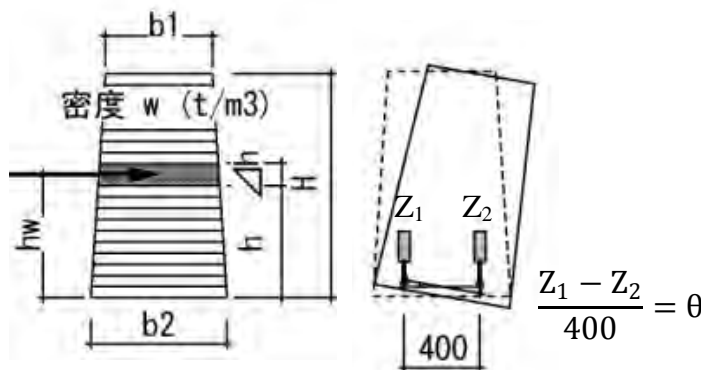


Figure 8: Moment and rotation angle

(3) Sliding

Seeing in the horizontal deformation on bottom of the specimen obtained from shaking No.1, No.2 of specimen HN1, KN1, no sliding was observed. This reveals that the friction modulus between cob and concrete is bigger than 0.51.

(4) Overturning

Given that specimen KN1 is rigid body, the theoretical value of moment M_f which cause uplift is 5.5kNm. Seeing in the time history of moment working on bottom of the specimen, floating occurred when the moment was bigger than theoretical value M_f (dotted line in figure 9).

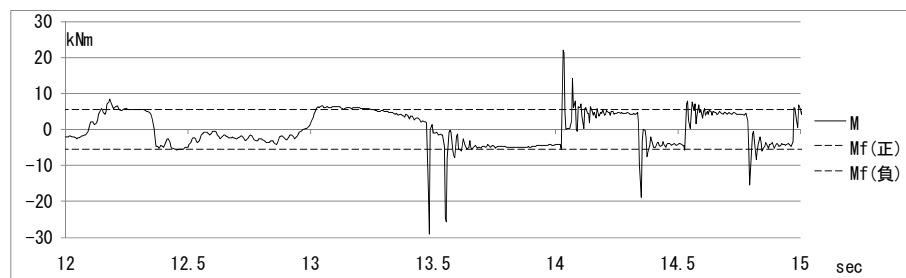


Figure 9: Moment of bottom of specimen and uplift

(5) Bending failure

As well as HN1, KN1, specimen HN2, KN2 deformed as rigid body. In case of KN2, maximum shearing stress caused by horizontal force working on each layers is 0.028 N/mm^2 , which is much smaller compared with the shearing strength calculated from the value obtained from 3 axial compression test of Lee[2009]. Also in case of HN2, compared with shearing strength in condition of $\phi = 0$, maximum shearing stress was far smaller. Therefore both specimens were thought to collapse by bending tension. Thus the stress caused by maximum moment M in the shaking level in which bending tension collapse happened (dotted line) and the stress working on each layers due to the dead load (solid line) were calculated and shown on figure 10. The maximum tensile stress at the edge is taken place in case of HN2 at height of 0.357m (0.075 N/mm^2) and in case of KN2 at height of 0.424m (0.140 N/mm^2). Material test shows tensile strength of the specimen is approx.5% of compression strength, 0.05 N/mm^2 (HN2), 0.11 N/mm^2 (KN2), each of maximum stress in figure 10 was over the tensile strength. The thick line on figure 10 shows interlayer, 2 layers on and under which weren't constructed in the same day. It collapsed in this interlayer, we can recognize that the interlayer had smaller tensile strength than the others.

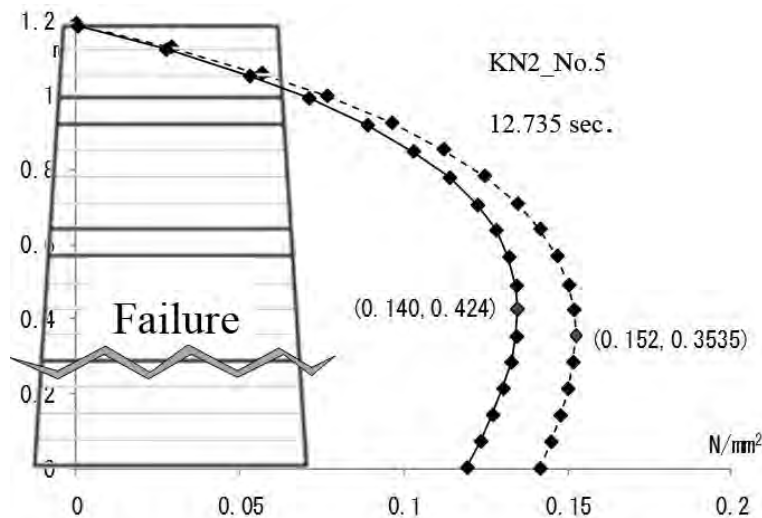


Figure 10: Bending moment distribution

(6) Efficiency of reinforcement

Let us evaluate the tensile force working on reinforcement. In specimen KB tensile force was measured by load cell set up with reinforcing rod in bamboo. From shaking No.4 it measured tensile force more than initial tensile force. At that time a bending tension crack was observed on side of the specimen. The theoretical value of tensile force whose center of rotation is calculated from the vertical deformation of bottom of the specimen is 29.8kN, which almost corresponds to the experimental value 28.6kN. The adhesion force of each bamboo ranges from 32.4kN to 35.9kN, the condition of the specimen after the test showed that it kept adhering. Thus bamboo reinforcement is thought to act effectively to bending tension.

(7) Result of test and comparative consideration

The theoretical value at which Rammed Earth Wall get damaged in earthquake was calculated and is shown on table 4 with experimental value, input acceleration at which the specimen get damaged is shown on table 5. Round brackets in the table means that phenomena weren't observed until the value in round brackets, that is, the specimen has superior property. The underline shows theoretical value.

Table 4: Bending moment and phenomena

	HN1	KN1	HN2	KN2	KB	KN
Sliding	(5.37)	(4.44)	/	/	/	/
Overturning M_f	(5.37) <u>6.82</u>	5.83 <u>5.50</u>	/	/	/	/
Bending Failure M_b	/	/	6.33	10.73	10.65	11.31
Allowable stress (Reinforced) M_a	/	/	/	/	17.08 <u>25.45</u>	14.42

Table 5: Input Max. Acceleration and phenomena

	HN1	KN1	HN2	KN2	KB	KN
Sliding	(449)	(444)				
Overturning	(449)	495				
Bending Failure			524	856	775	649
Shear Failure					1554	1458

(8) Reinforce efficiency

Table.4 and 5 make it clear that in the shape of this specimen, in case $M_b > M_f$, the resistance to earthquake is improved by anchoring to basement, and moreover, with reinforcement the resistance become even better. However in case $M_b < M_f$ it is possible to improve the resistance to earthquake by reinforcement with or without anchoring.

5. SUMMARY

Based on collapse property and test result of 6 kinds of specimens, this study indicated that in the shape of this specimen, up to the relationship between M_b and M_f , the method of anchoring to the basement and reinforcement can be decided. In this experiment specimen KB had the best performance to earthquake, however, in comparison to HN1 (HN2), KN1 (KN2), 1.6 times of labor is required to construct KB. Furthermore, during the drying period a lot of drying cracks are found on the surface of Rammed Earth Wall, further research on construction method and consideration of design are necessary.

REFERENCES

Lee Jina, 2009, Mechanical properties of lime-treated soil and its application to earthen walls, Doctoral thesis of the University of Tokyo, Japan

A.Takadachi and M.Koshihara, 2009, The Joint of using Bamboo's node, Summaries of technical papers of Annual Meeting Architectural Institute of Japan, pp.91-92, AIJ.

A study on the effect of wall stiffness on the vibration characteristics of traditional timber frames including Kumimono

Iuko TSUWA¹, Mikio KOSHIHARA²

¹ Graduate Student, Graduate School of Eng.,
the University of Tokyo, Japan
tsuwa@iis.u-tokyo.ac.jp

² Associate Professor, IIS, the University of Tokyo, Japan

ABSTRACT

In building or renovating traditional timber structures such as temples and shrines in Japan, earthquake resistant designed buildings are increasing. As the way of reinforcement for such traditional timber buildings, there are the change from mud wall to plywood wall and the insert of braces etc. These ways are same as conventional wooden houses. However the structural elements of traditional timber structures are different with conventional wooden houses. Additionally it is not clarified how each structural element of traditional timber structures behaves against earthquakes by using the present seismic reinforcement technique. In this study, we focused on Kumimono which is said that it is a structural seismic element in traditional timber structures. We conducted earthquake response analysis about traditional timber frames including Kumimono with the results of shaking table tests using two types of frames without walls and with a mud wall. Based on the model from the analysis, we analyzed the earthquake response of a frame including plywood walls in order to reveal how the vibration characteristics of traditional timber frames including Kumimono change by different wall stiffness. The vibration characteristics of Kumimono in each frame were compared.

Keywords: *traditional timber frame, Kumimono, shaking table test, earthquake response analysis,*

1. INTRODUCTION

In building or renovating traditional timber structures such as temples and shrines in Japan, earthquake resistant designed buildings are needed. Therefore the quantitative evaluation of their structural behaviors is indispensable. When we build temples and shrines, column, mud wall, *Nuki* which is a tie beam extending from one pillar to another, and bracket complexes called *Kumimono* in Japanese which is a structural component between a column and roof, etc, are considered as structural elements. Each element has been researched and modelled experimentally and analytically. However it is not clear how each element contributes to the whole structural

behavior. The aim of this research is to clarify the vibration characteristics of each element in a frame and how the vibration characteristics of traditional timber frame including *Kumimono* change by different wall stiffness. In this study, the shaking table tests were performed with specimens modeling the frame of the first story in fifth storied pagoda. We used two types of specimens. One is without walls. The other one is with mud wall. Based on the test results and existing theoretical model, we modeled restoring-force characteristics of each structural elements and we conducted earthquake response analysis. The analysis results were compared with experimental ones. Additionally, we analyzed with the model including plywood wall instead of mud wall.

2. EXPERIMENT

We conducted vibration tests as we presented at USMCA 2009. The details were shown in the paper. We explain the experimental outline and the results used in the analysis here.

2.1 Experimental method

Two types of specimens were used in the tests as shown in Figure 1. Specimen 1 consisted of columns, *Nuki*, bracket complexes. Specimen 2 was made by adding mud wall between the columns of the Specimen 1. The specimens were the 2/3 scale model of a frame in the *Asuka* style of the five-storied timber pagoda. A cornerstone was put under each column. They were connected with a dowel. Tree species were yellow cedar.

We carried out the shaking table tests as shown in Figure 2. Horizontal unidirectional shaking was conducted. The vertical load of 39.9kN made of steel frames and lead was put on the specimen. A load cell to measure axial force and shear force was placed under each column. The acceleration, displacement and the strain of specimens were measured using about 75 devices.

We put BCJ-L2, the level 2 of a simulated wave provided from the building center of Japan, as a large input motion. In the tests of Specimen 1, the maximum input acceleration was increased by 10% from 10% to 100%. In the tests of Specimen 2, one input with BCJ-L2 20% and two inputs with BCJ-L2 100% were carried out.

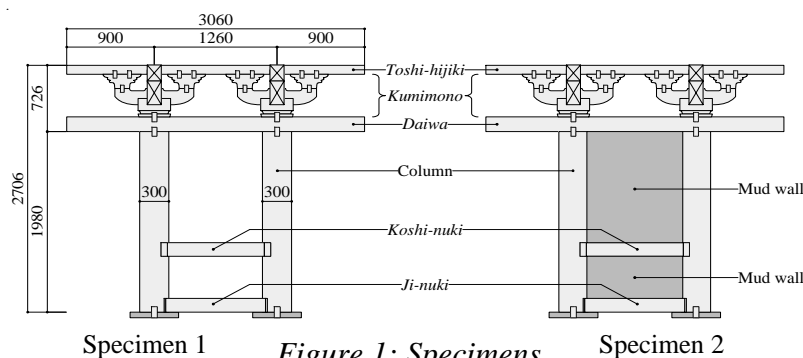


Figure 1: Specimens

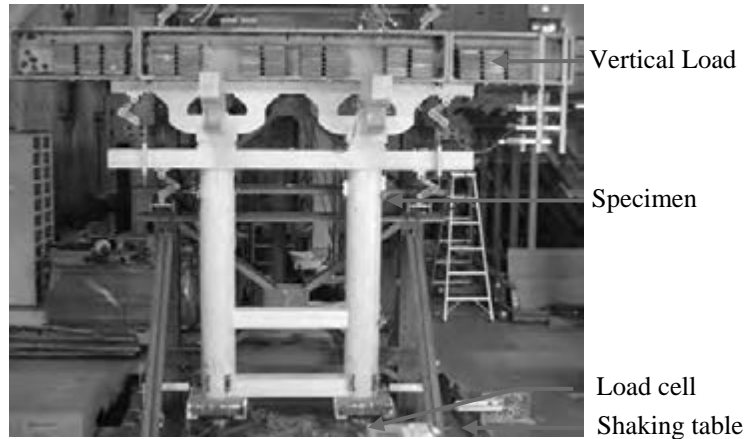


Figure 2: Experimental method

2.2 Experimental results

Figure 3 shows the relationship between load and displacement got by inputting BCJ-L2 100% of Specimen 1 and Specimen 2. The characteristics of every hysteresis curve were almost same after the collapse of the mud wall. However the load of Specimen 2 less than about 50 mm became higher than that of Specimen 1. It can be assumed to be due to the resistance force of mud wall. The deformation of bracket complexes in both specimens was very minute comparing with one of the whole structure as shown in Figure 4.

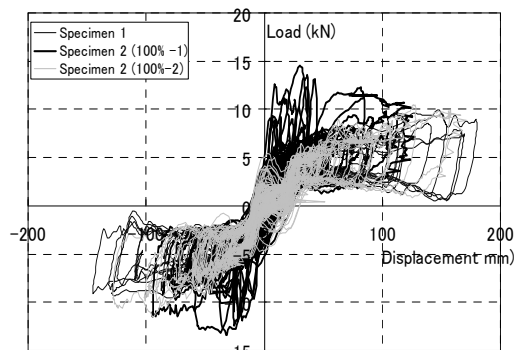


Figure 3: The relationship between load and displacement

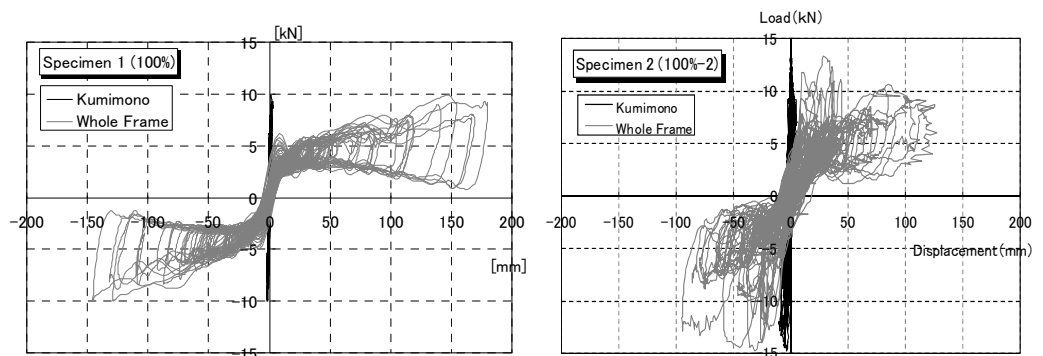


Figure 4: The relationship between load and displacement of bracket complexes

3. EARTHQUAKE RESPONSE ANALYSIS

3.1 Modeling of restoring-force characteristics

We conducted earthquake response analysis. Specimens were modeled as two-mass system with the springs of columns, *Koshinuki*, *Jinuki*, bracket complexes, and mud wall as shown in Figure 3. Restoring-force characteristics of each structural element were modeled as follows. Figure 5 shows each characteristic.

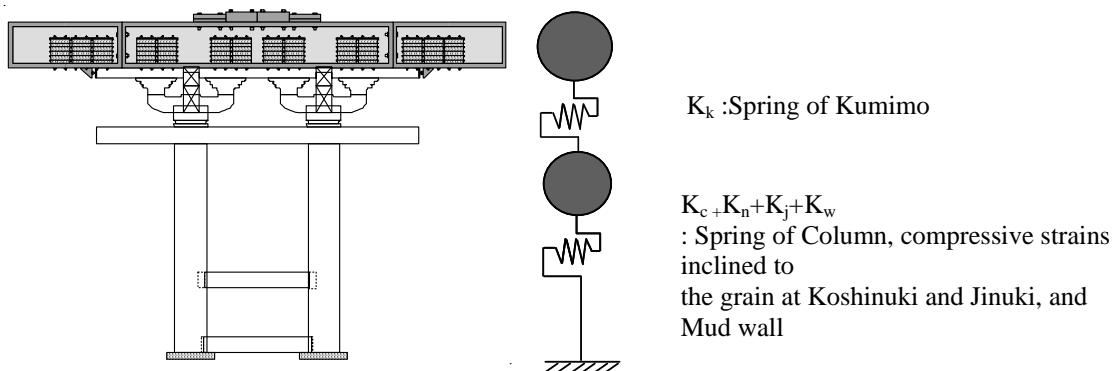


Figure 5: The model of a whole frame

Column:

Restoring force of columns was calculated by equation (1) with reference to previous experiments and researches of Ban, 1942 and Kawai, 1992.

$$y = H_0 \left\{ 1 - \frac{\delta}{b} + 0.99625e^{-7.5675 \frac{\delta}{b}} - 1.9963 / (25 \frac{\delta}{b} + 1) \right\} \quad (1)$$

y : Restoring force, δ : Horizontal displacement, b : Diameter of column, $H_0 = Pb/h$ Restoring force of rigid body, h : The length of column,

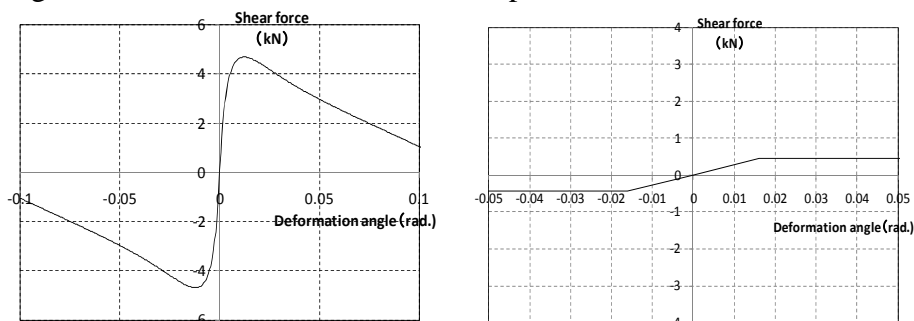
The maximum of restoring force was 80% of H_0 . The horizontal displacement of this force was 0.088 times of a column width. Assuming that two columns were connected with a parallel spring, the stiffness of both columns can be added.

In addition to the restoring force of columns, compressive strains inclined to the grain occurred at the bottom of the column were also calculated by the *Merikomi* theory (Inayama, 1992). The restoring-force characteristics were shown in Figure 6 (b).

Koshinuki:

Bending moment of column-*Koshinuki* joint was measured by strain gauges in experiments. We evaluated the rotational stiffness of *Koshinuki* in each specimen based on the experimental results. The stiffness was also

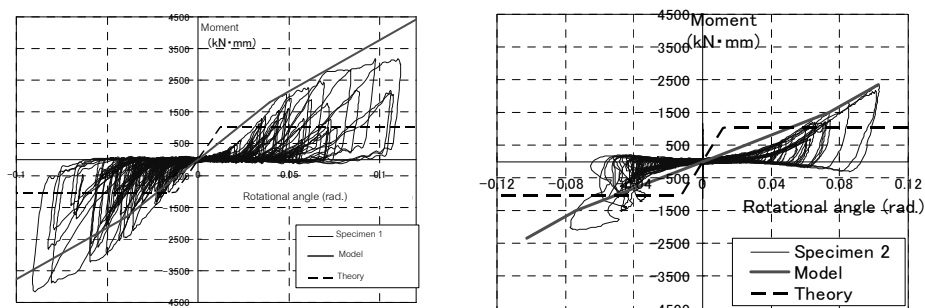
calculated by *Merikomi* theory (Inayama, 1992). However the second stiffness was smaller than experimental results. Thus we modeled the restoring-force characteristic based on the experimental results.



(a) Restoring-force of

(b) Restoring-force at the bottom of columns

Figure 6: The restoring force of columns



(a) Specimen 1

(b) Specimen 2

Figure 7: The restoring force of Koshinuki

Jinuki:

After experiments, compressive strains inclined to the grain occurred due to the joint of columns were observed on *Jinuki*. The restoring-force characteristic of *Jinuki* was given by *Merikomi* theory (Inayama, 1992).

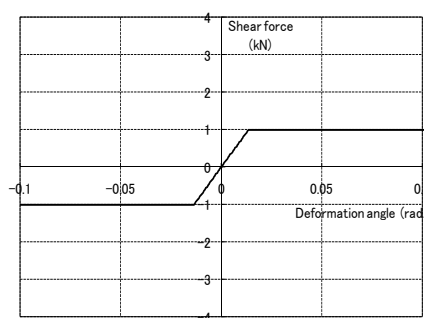


Figure 8: The restoring force of *Jinuki*

Kumimono:

Each relationship between load and displacement of *Kumimono* in specimen 1 and 2 was got as shown in Figure 9. The horizontal displacement of *Kumimono* was calculated by subtracting one of *Daiwa* from one of top. The results of *Kumimono* got by vibration tests were compared with ones of static horizontal loading tests (Tsuwa et al, 2010) as shown in Figure 10. From the comparison, both results were almost same

although the range of displacement was different. From the result, the restoring-force characteristic of *Kumimono* was given as bi-linear as shown in Figure 11.

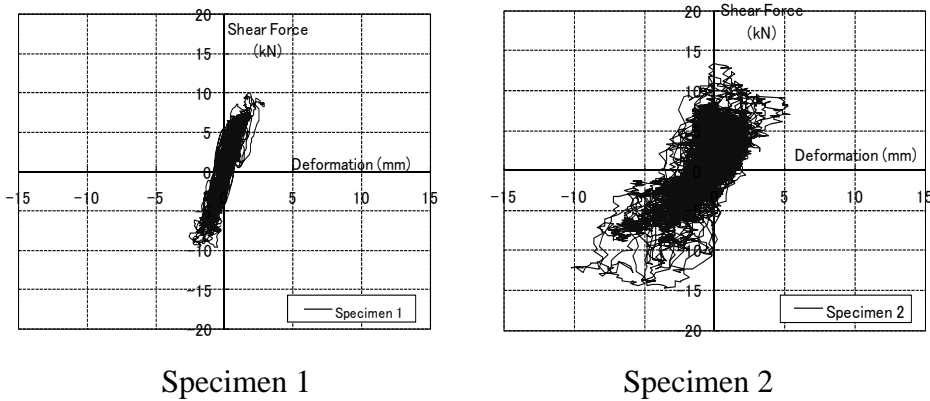


Figure 9: The relationship between load and displacement of *Kumimono*

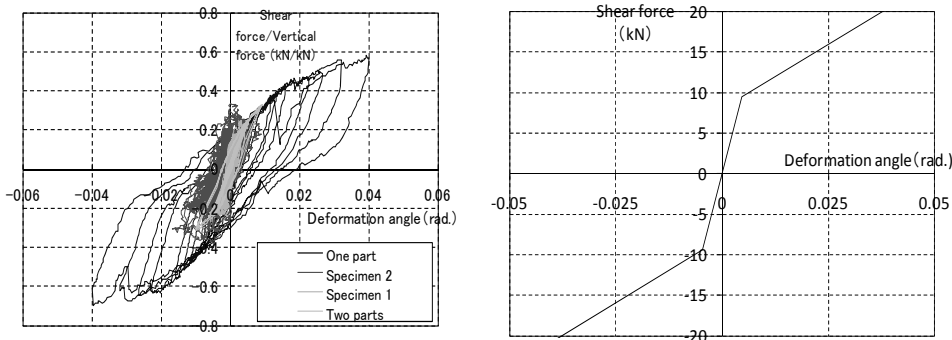


Figure 10: Comparison with static loading tests

Figure 11: The restoring-force of *Kumimono*

Mud wall:

We conducted the material tests of mud wall in order to figure the strength of mud wall out. From the results, the restoring-force characteristic of mud wall was modeled like a heavy line shown in Figure 12 (a). However the mud wall collapsed in vibration tests and the load decrease as much as 7kN in actual when the whole frame of specimen 2 deformed at about 50mm. Thus we modeled the restoring-force characteristic of mud wall based on both results of material and vibration tests as shown in Figure 12 (b).

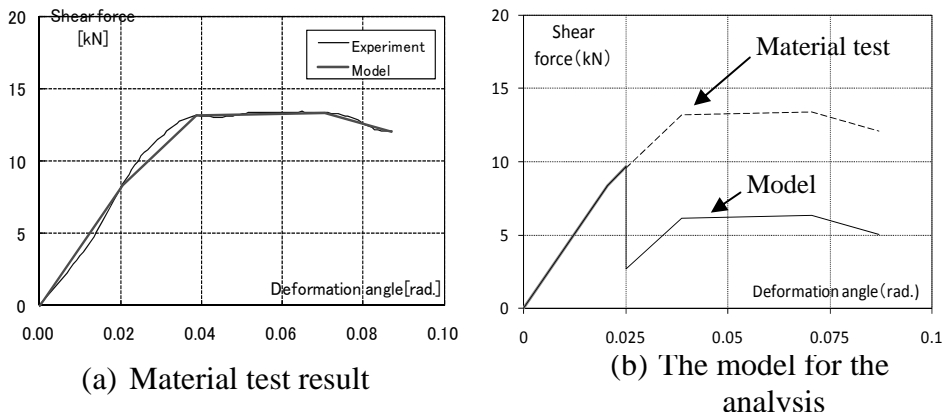


Figure 12: The restoring force of characteristic of *Mud wall*

3.2 Analysis results

Figure 13 shows earthquake response analysis results compared with experimental results of the relationship of load and displacement for whole frame in each specimen. The input wave was BCJ-L2 100%. Damping factor was 0.05. In both specimens, the analysis results almost corresponded to experimental ones. It is clarified that the restoring-force characteristics of columns, *Koshinuki*, *Jinuki*, and mud wall can be added.

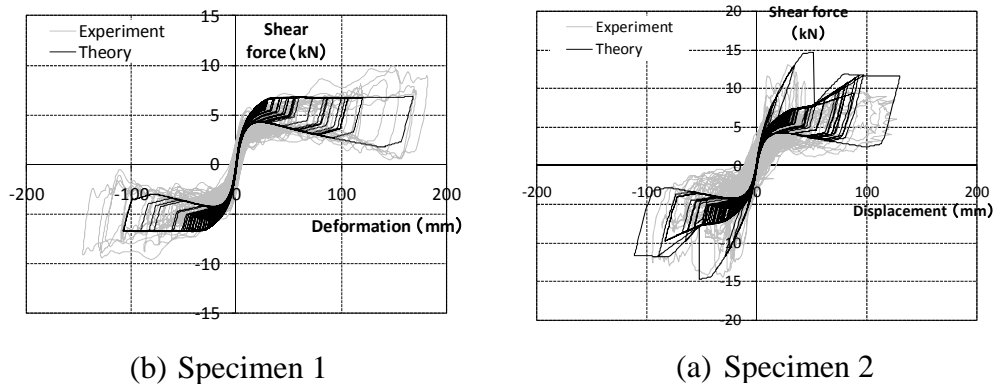


Figure 13: The relationship between load and displacement of Mud wall

3.3 Analysis of the frame including different wall

Based on the model of specimen 1 and 2, we simulated the model with plywood wall instead of mud wall and conducted the earthquake response analysis. Figure 14 shows the restoring-force characteristics of plywood wall. It was assumed that the wall input between the columns, that is to say that it did not cover the columns. Figure 15 shows the displacement of load and displacement of the whole frame from the analysis. Input wave was BCJ-L2 100%. We show the results of specimen 2 in the graphs for the comparison as well. The deformation of whole frame with plywood wall was smaller than one of specimen 2 as shown in Figure 15. Figure 16 shows the displacement of load and displacement for Kumimono in each specimen. The deformation of *Kumimono* in the frame with plywood wall was larger than one of specimen 1 and 2. It can be assumed that the higher the stiffness of wall is getting, the larger the deformation of *Kumimono* is.

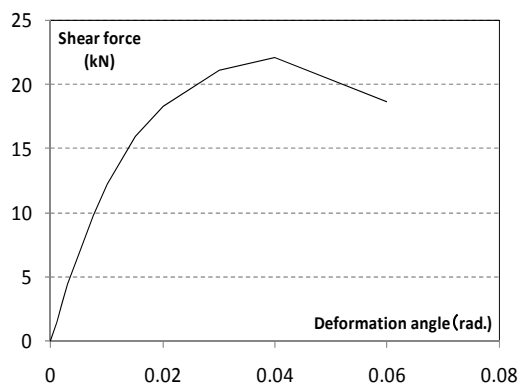


Figure 14: The restoring-force characteristics of plywood wall

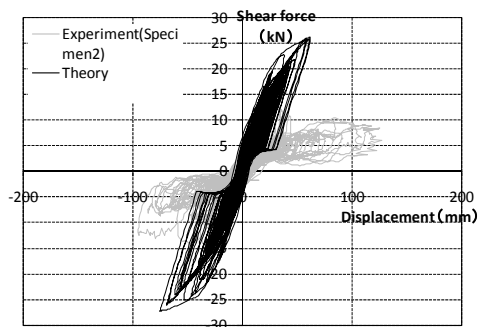


Figure 15: Analysis results of the frame including plywood wall

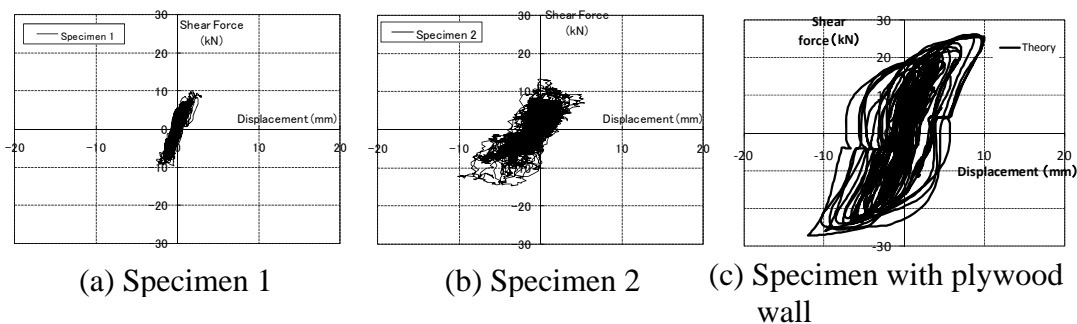


Figure 16: Load-displacement relationship for Kumimono in each specimen

4. CONCLUSIONS

Shaking table tests were performed using a traditional timber frame consisted of columns having large diameter, *Kumimono*, *Nuki*. Specimens were with mud wall and without one. The specimen was modeled on two-mass model with springs of columns, *Kumimono*, *Nuki* and mud wall based on the experimental tests and previous theory. We conducted the response earthquake analysis with the model. Additionally we simulated the model with plywood wall instead of mud wall. The results were compared with specimen 2 including mud wall. In the case of including plywood wall, the deformation of *Kumimono* became larger than specimen 2 with mud wall. It is clarified that the wall stiffness effect on the deformation of *Kumimono*.

REFERENCES

Ban, S., 1942. A study on the determination of the stability about main hall structures, Vol. 3: a mechanical study on the Japanese Traditional Frame, 1, the stability restoring force of a column. *Papers of annual meeting of Architectural Institute of Japan*, March, 252-258. (in Japanese).

Kawai, N., 1992. A study on the structural stability of traditional timber structures, *Report of the Building Center of Japan*, March. (in Japanese).

Inayama, M., 1991. The theory of compression perpendicular to the grain in wood and its application, Dissertation of the University of Tokyo. (in Japanese).

Kato, K., Tsuwa, I., and Koshihara, M., 2008. Shaking table tests of traditional timber frames including Kumimono Part 1 Experimental outline and results, *Summaries of technical papers of Annual Meeting Architectural Institute of Japan*, C-1, Structures III, pp.43-44 (in Japanese).

Tsuwa, I., Kato, K., and Koshihara, M., 2008. Shaking table tests of traditional timber frames including Kumimono Part 1 Experimental outline and results, *Summaries of technical papers of Annual Meeting Architectural Institute of Japan*, C-1, Structures III, pp.45-46 (in Japanese).

Tsuwa, I., Koshihara, M., 2009. Shaking table tests of traditional timber frames including Kumimono - Modeling of horizontal resistance force -, USMCA 2009

RYONO, S., TSUWA, I., et al, 2010. Static Lateral Loading Test of Bracket Complexes Used In Traditional Timber Five Storied Pagoda, *Summaries of technical papers of Annual Meeting Architectural Institute of Japan*, C-1, Structures III, pp.557-558, (in Japanese).

A new generation software for regulated river system operations

Dushmanta DUTTA^{1,2}, Wendy D. WELSH^{1,2}, David NICHOLLS^{2,3}
and Shaun KIM^{1,2}

¹ CSIRO Water for a Healthy Country National Research Flagship,
CSIRO Land and Water, Australia

² eWater Cooperative Research Centre, University of Canberra, Australia

³ DA Nicholls Pty Ltd, Nicholls, ACT, Australia

E-mail for correspondence: dushmanta.dutta@csiro.au

ABSTRACT

The eWater Cooperative Research Centre of Australia has recently developed a new generation software package called Source Integrated Modelling System (Source IMS), which allows a seamless integration of continuous rainfall-runoff and river system models for operational and planning purposes. The Source IMS provides tools for the prediction and quantification of water and associated constituents from catchments to the estuary. It has been designed and developed within Australia to provide a transparent, robust and repeatable approach to underpin a wide range of water planning and management purposes. It can be used to develop water sharing plans and underpin daily river operations, as well as be used for assessments on water quantity and quality due to changes in, i) land use & climate ii) the influence of demands (irrigation, urban, ecological) and iii) infrastructure types (weirs storages, reservoirs); iv) the influence of various management rules that may be associated with these, as well as v) the impacts of all of the above on various ecological indices. The model can be configured in either a spatial, or schematic layout, depending on the requirements of the modelling situation. Source IMS includes three modes for building project scenarios for various applications. One of those is the River Operations mode, which has been designed for improving daily and seasonal operations of regulated river systems. The paper introduces the Source IMS and discusses the key features and functionalities in River Operations mode.

Keywords: *Source IMS, river system modelling, river operation, Murray river system*

1. INTRODUCTION

Many of the large river systems around the world are highly regulated with numerous physical flow control and storage structures as well as a range of water sharing rules and regulations. Operation of a regulated river system involves directing releases from storages and controlling diversions of water from the river for irrigation, agricultural and environmental uses, and for

consumers in urban areas. River operators of large regulated systems are increasingly facing complex challenges in operations due to a range of issues including: rapid growth in urban and agricultural sectors, environmental mandates, recreational interests, hydropower generation, over-allocation, changes to land-use, climate change, and the fragmented nature of available information. The operational decisions take a range of technical considerations under different hydro-climatic conditions such as flow requirements, water level changes, estimated evaporation, forecast rainfall and the water-carrying capacity of the river at various locations for balancing competing objectives such as structural safety and maintenances, water orders, water security, water trade, environmental outcomes, navigation and recreation (MDBA 2011). River system modelling plays a key role in the operational decision making process.

In most of the countries around the world, river operations have historically utilized a diverse set of software tools in its decision-making and reporting processes (Carron *et al.* 2010). These tools require significant manual manipulation of data, are sometimes inconsistent, and do not always consider a priori all of the institutional constraints and policies in the decision-making process because such tools were not designed for planning purposes. For example, river operators in Australia have been using spreadsheet-based software for day-to-day river operations. Such tools are entirely dependent on input from an experienced user familiar with the nuances of the river system being modelled. Current operational tools in Australia model the river system in a manner that is distinctly different from the long-term planning tools used to develop water sharing plans. This creates a number of inconsistencies between the planning and operational management of river systems (Bridgart and Bethune 2009).

As demands on river systems have increased, and spurred on by a prolonged drought in southeastern Australia, the need to accurately account for policy and legal constraints in the decision-making process has grown. It has become increasingly important to operate the system more efficiently and to ensure that operational decisions appropriately reflect rules and policies. There is an increasing need for a new suite of river system operational models that have a more robust decision-making foundation for reservoir and river operations, which more accurately reflects water rights and operational policies in the decision-making process. Such tools should allow comparisons of water orders with actual diversions, forecast inflows with actual river gains, and environmental target operations with actual deliveries. A review of the user requirements for a river operational tool undertaken by Nicholls (2006) shows that no existing operational tools in Australia meet the key user requirements. End users of these models have also expressed a strong desire for a tighter link between operational and planning tools, based on river management models (Nicholls 2006).

There have been significant improvements in quantitative forecasts of precipitation by numerical weather prediction models in the recent years (BoM 2010). This brings an opportunity to improve short and medium term

streamflow forecasts for river operations by integrating rainfall-runoff models with the river system operational tools (Dutta *et al.* 2011).

The complexity and diversity of challenges faced by water management organizations highlight a need for new modelling tools to assist in decision making for operations of regulated river systems to not only meet today's needs, but tomorrow's as well. To meet these needs, a new software package called 'Source Integrated Modelling System (IMS)' is recently developed by the eWater Cooperative Research Centre (CRC) of Australia in collaboration with several of its research and industry partners.

River Operations is one of the three modes of the software, which can be used to underpin daily river operations to support the efficient management of water storage, flow and delivery in regulated river systems. The paper introduces the Source IMS and discusses the key features and functionalities of the River Operations mode of the Source IMS.

2. SOURCE INTEGRATED MODELLING SYSTEM

The Source IMS is designed as a transparent, robust and repeatable tool to underpin water planning and management in complex regulated and unregulated river systems. It provides tools for the prediction and quantification of water and associated constituents from catchments to the estuary. The components used to model regulated rivers within the Source IMS encompass (and enhance) the key functionalities of the three widely used river system modelling tools in Australia: IQQM, REALM and MSM-Bigmod, as well as new scientific research. The Source IMS is an evolution of the E2 catchment modelling framework (Argent *et al.* 2009), which itself is built upon the general purpose TIME framework (Rahman *et al.* 2003). TIME is an environmental software library designed to support environmental modelling applications. The physical and regulatory processes and management rules of a regulated river system are conceptualised in seven major components within the Source IMS simulation engine: i) Catchment runoff; ii) River system network; iii) Interactions between river and groundwater systems; iv) Water quality; v) River regulation and storages; vi) Demands (urban, irrigation and environmental) and vii) Complex river management rules. Each of these includes several subcomponents to comprehensively represent the underlying processes, rules and regulations. The various components and their functionalities are elaborated in Welsh *et al.* (2011).

The system as a whole is extensible through expression editor and plug-in (eWater 2011, Kim *et al.*, 2011) functionalities, which can modify either the simulation engine or the application user interface. A plug-in is a section of computer code compiled as a DLL (Dynamically Linked Library). Plug-ins can be used to add new modelling components to Source IMS that are not otherwise available in the system.

The Source IMS includes three scenario modes: catchment runoff (hereafter termed *Source catchment mode*), river management (hereafter termed *Source RM mode*) and river operations (hereafter termed *Source RO mode*). *Source Catchment mode* includes a conceptual rainfall runoff (RR) modelling framework for estimating catchment water yield and runoff characteristics. *Source RM mode*, which includes a conceptual river system modelling framework using a node and link concept, is designed primarily for use in the consideration of long-term water resources planning and management issues using historical data. *Source RO mode* is primarily designed for river system operators to forecast and route flow for daily river operations. *Source RO mode* uses same underlying node and link river network definitions and calculations as the *Source RM mode* to define and parameterise the river system being modeled. In the node-link system, a river network begins and ends with a node, and all nodes are interconnected by links. Runoff is fed into the network as an inflow at the relevant location in the network. Links represent a length of stream and are used to transfer flow and constituents between nodes, with or without routing and transformation. Lag time and storage routing concepts are used in links for routing. The length of a link can be zero for near coincident processes. Nodes represent a physical location along a river where flow and water quality constituents either enter the system or are stored, extracted, lost or measured, and can be used for the application of management rules. The details of links and nodes and their functionalities are elaborated in Welsh *et al.* (2011).

2.1 River Operations using Source IMS

There are many features and functions in the *RO mode* of Source IMS that allow the presentation of system behavior more realistically and accurately, leading to improvements in water resources management and water delivery. Some of the major features and functions are briefly explained here.

2.1.1 Graphical user interface

The *Source RO mode* has a robust graphical user interface (GUI) that allows river operators to interact with the underlying complex computer code and view and analyse model output. The GUI includes two views: schematic and tabular editors.

i) Schematic editor

The schematic editor is used to construct a river system network by selecting graphical icons representing system components (nodes and links and their attributes) and run the software for the user-defined scenarios. Figure 1 shows a schematic view of a river system operational model built using the schematic editor.

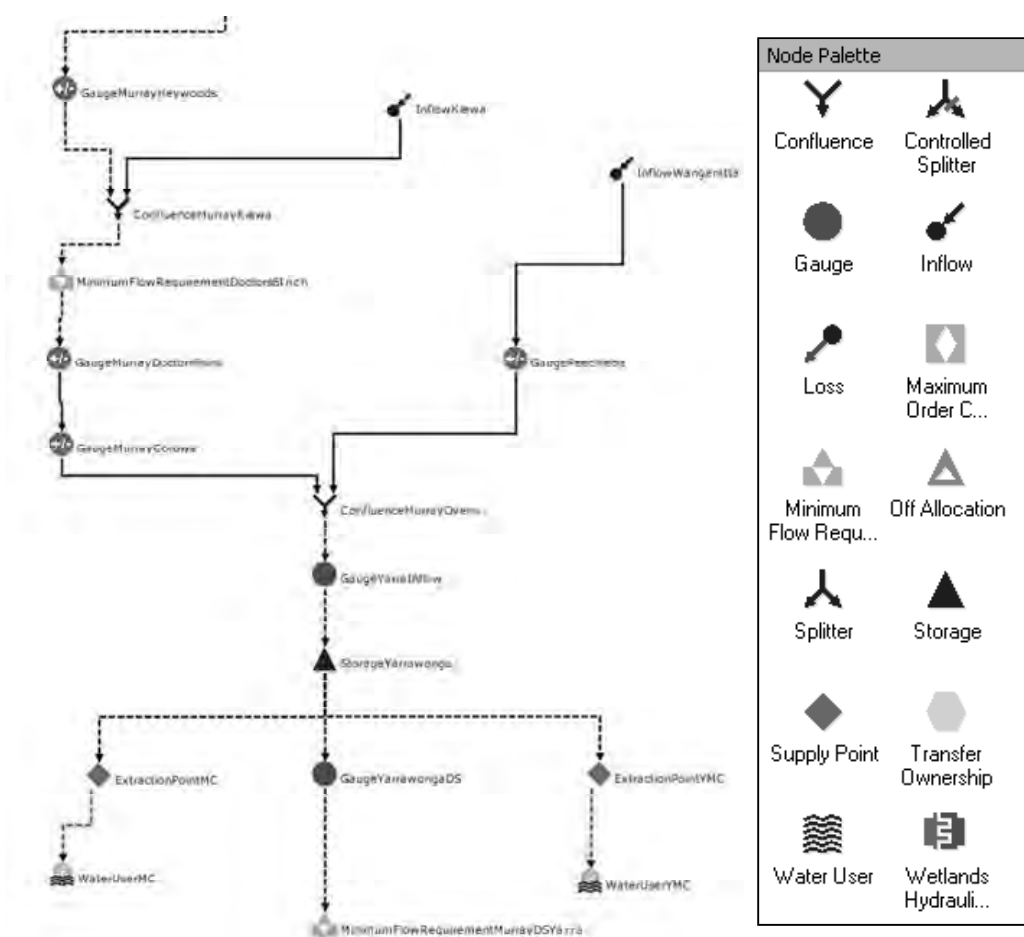


Figure 1: A snapshot of a river system operation model built in Source RO mode

ii) Tabular editor

The tabular editor presents a tabular view of temporal observed data and predicted results at every node. This allows an operator to simultaneously look at both temporal (y axis, columns) and spatial (x axis, rows) aspects of the river system. Time is represented with observed data at the top running down to the predicated future data below. The various network elements (nodes and links) are listed as a row from upstream (left side) and heading downstream (right end). Users are also given the ability to rearrange the columns. The view provides the individual data points, which are of interest to operators, in an easily accessible way. A snapshot of the tabular editor is shown in Figure 2. The tabular editor also allows the user to access and configure the underlying models for each of the network elements.

Time	Inflow @ Corone UD	Inflow @ Corone Flow	Divers @ Wangnata Flow	Inflow @ Pechi UD	Divers @ Pechi Flow	Storage @ Predicted Inflow (ML)	Yawongsi Weir Upstream Flow	Yawongsi Planned Extraction	Yawongsi Main Supplied	Subside Planned Extraction	Subside Canal Supplied	Yawongsi Weir Storage Level	Yawongsi Mainstem Storage Level	Yawongsi Weir Volume	Yawongsi Storage UD	Money @ Yawongsi Requested
23/04/2011 00:00	862	8954	3152	43	3160	4405	12114	0	254	0	2799	124.64	124.72	10686	2171	4930
24/04/2011 00:00	932	8826	2902	56	3110	4253	12048	0	254	0	2799	124.66	124.72	107118	1843	4930
25/04/2011 00:00	788	8641	2834	94	2990	42543	11847	0	254	0	2899	124.68	124.72	107851	227	4930
26/04/2011 00:00	749	8456	2743	80	2870	4126	11599	0	254	0	2899	124.69	124.72	108144	471	4930
27/04/2011 00:00	811	8394	2713	54	2780	39495	11303	0	441	0	2800	124.68	124.72	107595	863	2540
28/04/2011 00:00	694	8284	2594	77	2710	37880	11099	0	582	0	3100	124.61	124.72	104893	-1021	3890
29/04/2011 00:00	775	8141	2506	103	2640	37255	10901	0	690	0	3400	124.54	124.72	101735	-1293	3820
30/04/2011 00:00	885	7953	2529	41	2570	37255	10704	0	640	0	3700	124.46	124.72	98239	-1405	3760
01/05/2011 00:00	786	7478	2477	56	2560	37179	10440	0	673	0	4100	124.37	124.72	94358	-1793	3700
02/05/2011 00:00	696	7311	2295	174	2510	36173	10078	0	830	0	0	124.37	124.72	94161	-6295	3630
03/05/2011 00:00	580	7311	2229	168	2400	35415	9786	0	926	0	0	124.35	124.72	93562	-6848	3570
04/05/2011 00:00	1048	6930	2362	-3	2320	34288	9562	0	964	0	0	124.33	124.72	92981	-7165	3460
05/05/2011 00:00	436	6288	2743	-222	2400	33230	9225	0	1003	0	0	124.29	124.72	90775	-7885	3390
06/05/2011 00:00	-25	6488	2585	89	2710	31888	9074	0	985	0	0	124.24	124.72	88834	-8556	3320
07/05/2011 00:00	-1286	6488	2585	140	2710	30877	9115	0	959	0	0	124.2	124.72	86962	-8883	3260
08/05/2011 00:00	-491	8141	2362	197	2620	34449	9548	0	958	0	0	124.16	124.72	89582	-6871	3190
09/05/2011 00:00	934	9840	2276	94	2480	37253	10621	0	1188	0	0	124.15	124.72	89279	-6254	3140
10/05/2011 00:00	488	9152	2248	102	2380	40779	11623	0	1206	0	0	124.16	124.72	89467	-8444	3090
11/05/2011 00:00	784	8785	2362	18	2340	41513	11575	0	1222	0	0	124.17	124.72	89722	-9647	3030
12/05/2011 00:00	729	7953	2448	180	2320	43055	10985	0	1151	0	0	124.16	124.72	89527	-8729	2990
13/05/2011 00:00	-143	7281	2506	66	2420	41325	10361	0	658	0	0	124.11	124.72	83136	-10282	2940
14/05/2011 00:00	275	8517	2477	25	2510	37584	10199	0	304	0	0	124.05	124.72	80977	-12888	2890
15/05/2011 00:00	1128	10159	2506	8	2490	34189	11091	0	0	0	0	124.83	124.72	80635	-13059	2840
16/05/2011 00:00	1851	10253	2362	86	2490	3232	12288	0	0	0	0	124.84	124.72	80289	-13842	2800
17/05/2011 00:00	972	10330	2295	96	2400	36243	12000	0	8	0	0	124.85	124.72	80836	-14572	2760
18/05/2011 00:00	685	9264	2048	78	2188	38712	12168	0	62	0	0	124.28	124.72	80272	0	2710
19/05/2011 00:00	671	8543	1844	59	1956	43223	11280	0	71	0	0	124.48	124.72	80788	0	2710
20/05/2011 00:00	863	7713	1859	43	1740	40146	10218	0	79	0	0	124.62	124.72	105205	0	2660
21/05/2011 00:00	779	8906	1493	28	1552	38667	9329	0	87	0	0	124.88	124.72	107984	0	2610

Figure 2: A snapshot of tabular editor of a river system operation model

2.1.2 Daily Operation

The *Source RO mode* can be used for daily operations to model alternative storage release patterns and weir pool operations. It allows users to estimate an optimal operating scenario for a storage release while satisfying all the short-term system demands, and adhering to any operating rules in place for the system under the set of forecast conditions. Users can reconcile data collected from the field on a daily basis against the model predictions, and if necessary, reconfigure the inflow, demand or unaccounted difference forecasts to reflect the system behaviour that is currently being observed.

2.1.3 Seasonal Operation

The planning of seasonal operations is especially critical where a system has one or a combination of channel capacity constraints, en-route storages, parallel storages, compressed demand periods or large volumes of water to transfer. The *Source RO mode* can be used for seasonal operations to analyse system responses for a given level of resource allocation under a number of possible climate conditions and to investigate system behavior in terms of storage levels and flows, making sure the system has the ability to satisfy demands across the full delivery period. In general, users review extractions to date, storage levels and unaccounted differences on a monthly basis, and depending on these results, might increase allocation levels and modify operating plans for the remainder of the season.

2.1.4 Data Import Interface

For any river operation, river operators need to use input data from a range of different sources. Data sources could vary from industry databases such as Hydstra, to text files and web services. The *Source RO mode* includes a user interface capable of supporting interactions with some of the widely used databases, namely: Hydstra, MySQL and Oracle (Figure 3). Through this interface, the software allows users to import data from these databases and converts to a standard format for modelling.

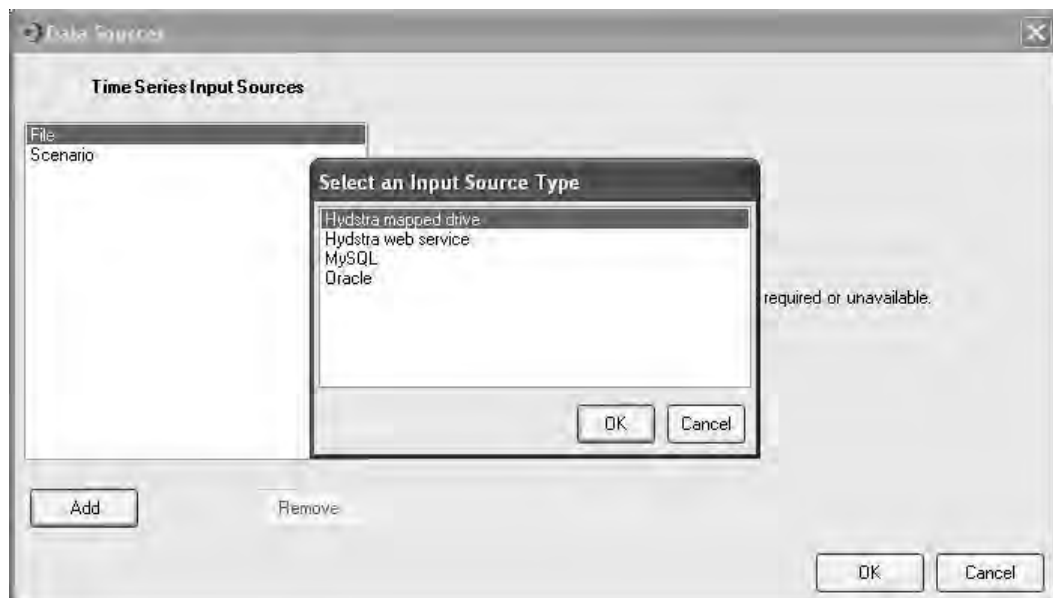


Figure 3: GUI for importing time series inputs from standard databases

2.1.5 Forecast models

Both observed and forecast data are required for a river system operation. Forecast data, which refers to the prediction of future occurrences for any variable (e.g., inflow and demand) in the system, can be generated using various mathematical forecast models. Forecast models range in complexity from simple regression models to more complex models that use data such as rainfall predictions to approximate future tributary inflows. The *Source RO mode* provides users with several options to incorporate forecast models.

For any given forecast variable, *Source RO mode* can include multiple forecast models. The first model can generate a forecast of the near future (typically one week out) and the second generates a forecast from the end of the first onwards. This enables the user to specify a suitable model for use in the immediate future, such as a simple regression model to predict stream flow, and to then revert to a model which might use historic, monthly or seasonal averages to produce its forecast. A snapshot of short-term water demand forecast using three different forecast options are shown in Figure 4.

Several demand forecast models are built into *Source RO mode* to forecast irrigation and environmental demands. *Source RO mode* also allows users to incorporate user-specific forecasting techniques through expression

editor and plug-in functionalities. Streamflow forecasts from unregulated catchments by RR models in the *Source Catchment mode* can also be linked to a *Source RO* project scenario.

Recently, Dutta *et al.* (2011) undertook a case study using the *Source RO mode* for a comparative evaluation of streamflow forecasting by three time series based linear models and a suite of RR models in two selected unregulated sub-basins in the upper Murray River system of the Murray-Darling Basin. The study showed that third party forecast models, such as linear time series models, can be efficiently plugged into the *Source RO mode* using the expression editor functionality of the software. The outcomes of the case study demonstrated that a well calibrated RR model can provide accurate forecasts when using high quality quantitative precipitation forecasts. With a suite of six RR models and a combination of objective functions and optimization methods for calibration of these models in the *Source catchment mode*, Source IMS can be effectively utilised for improved streamflow forecasts for river operations.

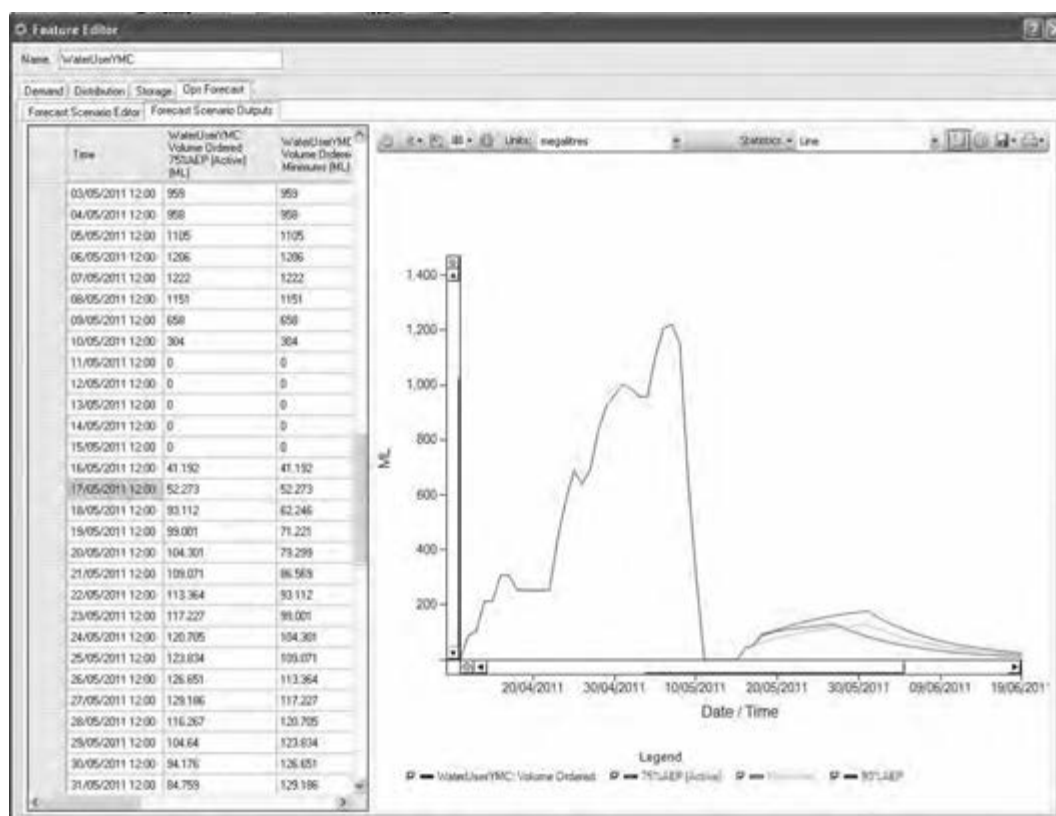


Figure 4: A snapshot of short-term water demand volume forecast using three different forecast options and actual volume of water ordered

3. DISCUSSION

The paper has introduced the new generation software package: Source IMS, and described the functionality and applicability of the *Source RO mode* for improving daily and seasonal operations of regulated river systems in the 21st Century.

The *RO mode* of Source IMS represents a significant and positive advance in daily and seasonal river system operations modelling through the integration of catchment flow simulation, river planning and operational tools into a single software platform. The software is a transparent, robust and repeatable tool to underpin water planning and management. It provides an opportunity to use new forecast tools based on recent advances in climate science and water engineering for improving the efficiency of river operations.

With the tailored interface of the *Source RO mode*, the ability to dynamically calibrate RR models and plug-in functionality to incorporate third party forecast techniques, the Source IMS fulfils the need of an integrated system to support river operational decisions. It is expected that this new generation package will contribute to improved decision-making in river operations, leading to increased economic benefits through more efficient water allocations.

REFERENCES

Argent, RM, J-M Perraud, JM Rahman, RB Grayson and GM Podger (2009). A new approach to water quality modelling and environmental decision support systems, *Environmental Modelling & Software*, 24(7):809-818.

BoM (2010). Operational implementation of the ACCESS Numerical Weather Prediction systems, NMOC Operations Bulletin No. 83, Bureau of Meteorology, Australian Government, 34p.

Bridgart, RJ and M Bethune (2009). Development of RiverOperator: a tool to support operational management of river systems, Proceedings of the 18th World IMACS/MODSIM Congress, Cairns, Australia 13-17 July 2009, 3782-3788.

Carron J, D Walker, K Wheeler, G Saunders, R Brown (2010). The Lower Colorado River Authority Daily River Operations Model, Proceedings of the 2nd Joint Federal Interagency Conference, Las Vegas, NV, June 27 - July 1, 2010.

Dutta D, W Welsh, J Vaze, S Kim, D Nicholls (2011). Improvement in short-term streamflow forecasting using an integrated modelling framework, International Congress on Modelling and Simulation, MODSIM 2011 (in press).

eWater (2011). How to write a Source plugin. eWater CRC, Canberra. 46p. Kim S, D Dutta, R Singh, J Chen and W Welsh (2011). Providing flexibility in GUI-based river modelling software - Using plug-ins to create Custom Functions in Source IMS, 2011 International Congress on Modelling and Simulation (MODSIM 2011) (in press).

MDBA (2011) River Murray System Annual Operating Plan 2011-12, Murray—Darling Basin Authority, Canberra, MDBA Publication No. 211/11, 55pages.

Nicholls, D (2006). River Operations and Management (ROM) Products, River operations tools and guidelines (P1). eWater CRC, Canberra, Australia.

Rahman, JM, SP Seaton, J-M Perraud, H Hotham, DI Verrelli and JR Coleman (2003). It's TIME for a new environmental modelling framework. *Proceedings of MODSIM 2003*, 4: 1727–1732.

Welsh, W, J Vaze, D Dutta, D Rassam, J Rahman, I Jolly, P Wallbrink, G Podger, M Bethune, MJ Hardy, J Teng, J Lerat (2011). An integrated modelling framework for regulated river systems, *Environmental Modelling & Software* (in review).

Environmental management in Cambodia case study: Community forest governance at local context

Ham KIMKONG

Senior lecturer and Researcher of the Royal University of Phnom Penh,
Department of Environmental Science
Cambodiakimkongham@yahoo.com

ABSTRACT

This paper discusses about environmental management in Cambodia, particularly a case study on community forestry governance at local context. In ecological perspective, forest plays very important role and help to protect the soil erosion, stabilize the watershed and regulate water flows and weather system. Cambodia is particularly dependent on its forest system due to the unique hydrological system of Mekong River and Tonle Sap Lake. From economic point of view, forest is considered as one of the country's most valuable economic assets that provide an important source of revenue. Both forest resource and institutional contexts are either enabling or constraining the construction of well-being of people in communities as well as urban residents. In particularly, this paper demonstrates that the Upper Mekong basin ecological systems provide fisheries and forestry resources on which a great number of people living in the along the Mekong area (O'svay village) have been sustaining their living. However, the forest resource is not only important for local people livelihoods, but also a source of income of the state and private logging firms. Competing for logging in which amongst different parties have been mounted, resulting the destruction of forest resources and environmental disasters. The erosion of forest resources, the growing scarcity of forest product will directly result on the livelihoods, especially lowering well-being of the poor which lead to migrate out to cities. Have seen issues, Royal Government of Cambodia (RGC) has taken action to reform forestry policies, established new forestry law, giving more rights to access forest resource, and more roles to protect forest resources to "Community Forestry Management". Albeit such policy reform and new forestry law received a national political supports, this policy and law has not yet materialized, especially at local forest governance level. This paper shows changes in exchange and mobility between two ecological regimes in which livelihoods of forest resources—communities are likely to be affected negatively. People from outside have migrated into the areas for over-exploit/harvest resources, grabbing lands. This has increase tension on the use, conflict interests and destruction of forest resources significantly. Livelihoods of people in community forestry are therefore at jeopardy.

Keywords: Governance, Conflict over Natural Resources, Migration

1. HISTORICAL BACKGROUND

Generally, Cambodia forest cover to have up to 73% of the total country lands in 1970s. However, according to Forestry Administration (FA) 2004 shows that this figure, has reduced down to about 58% to 60% of total land cover area corresponding to approximately 10.7 million hectares.

Referring to FA recently has conducted several studies and reported that the net annual rate of deforestation was estimated as 0.5 per cent during the period 2002-2005/06 representing a significant decrease compared to earlier estimates. According to the forestry outlook 2020 shows that Cambodian Millennium Goals aim to maintain forest cover at 60% by 2015. However, the forest outlook illustrates that there are some challenges and difficulties such as an insecure title over forested land and unclear rights to use *de facto* open access forest resources mitigate efforts to maintain the forest cover, to secure livelihoods or to contribute to rural economic growth in Cambodia(Forestry outlooks, 2008).

This situation reflects a lack of coherence in rural land management policies, weak capacities of sub-national sector line agency departments, poor service delivery mechanisms and the limited involvement of rural land and resource users in formalized natural resource management procedures. The key challenges in the sector are the need to ensure sustainable management and equitable use of forests, to improve rural livelihoods, and to promote a balanced socio-economic development in Cambodia. Past forest management systems have not contributed sufficiently to these broad policy objectives (Forest Outlook, 2008). The Forest Administration (FA) is the key government agency in the forestry sector in Cambodia. There are also a large number of other actors including forest-dependent rural communities, Development Partners (DPs), investors and international and national Non Governmental Organizations. In 1998 the Royal Government of Cambodia (RGC) initiated the forestry reform process by establishing a national committee on forest policy reform with support from DPs.

In 2002, the secretariat of the committee formulated a national forest policy statement. Subsequently, a new Forest Law was promulgated in 2002, and a new Forestry Administration was established in 2003 (replacing the former Department of Forestry & Wildlife). A temporary Joint Coordinating Committee, representing RGC and DPs, and chaired by the Minister of MAFF, commissioned an Independent Forest Sector Review in 2003, (available at <http://www.cambodia-forest-sector.net/index.htm>). In 2004, the RGC established a Technical Working Group on Forestry and Environment (TWG-F & E) to provide a mechanism for government-DP coordination to support and strengthen development activities within the sectors (www.twgfe.org). As a result, a four-year *Forestry and Environment Action Plan 2007-2010* and one-year *Framework Work Plans and Indicative Budgets* for 2007 and 2008 have specified 26 prioritised activities within six prioritized programmes of National Forestry Planning (NFP). The national forestry

planning aim at assisting FA's efforts to promote sustainable and equitable forest management in Cambodia in period of 2008-2020.

2. FOREST MANAGEMENT AND CONSERVATION

Brief of Forest Policy Formulation

Since the 1980s the forestry sector has been reformed and created under the Ministry of Agriculture and Forestry and Fisheries, such as Sub-decree, regulation and laws after Khmer Rouge regime. First, Sub-Decree (Kret-Chbap) No. 35 entered into force in 25 June 1988 and had been implemented up until 2002, to manage and control forestry sector activity. To Compliance with main regulations, following there has been a bunch of forest regulations issued and established (Forestry Outlook, 2008),

- In 2006, Royal Decree on the establishment of the National Authority for forestland
- conflict resolution was set up. The National Authority plays role in identifying illegal
- forestland encroachment of state forest.
- Sub-Decree on the Forestry Sector:

Table 1: Sub-Decree and regulations, Law on the Forestry Sector

Date	Institutional function	Key roles and responsibilities
In 2003	Re-structured of Department of Forestry and Wildlife entered officially recognition as Forestry Administration (FA)	Management of forest land covers. Protecting and controlling illegal forestry activities. National Forestry planning strategy.
Early, 2003	Establishment of Community Forestry Sub-Decree.	The community forestry Sub-decree plays a key roles and empower to deliver decentralization of forest governance and management from central to local communities, to manage and use forest resource sustainability and effectively. As a result, since 2006 reported that in whole county, there are 264 communities forestry has been established.
2004	Elephant corridor in southwestern Cardamom Mountain. It has been created by NGOs collaborated with FA.	The areas of the corridor used to be under forest concession. As the areas are important for local communities and wildlife conservation, elephant, the FA and its partners, WildAid, seeking approval of the Premier to have the areas for special protection and community development.
2006	Convention of International Trade in Endangered Species (CITES).	CITES was introduced to Cambodia in early 1990s and Cambodia became member of the CITES in 1997. It plays to conserve and protect endangered species in particular places such as Tonle Sap, Upper Mekong... etc.
2000	Forest Concession Management Sub-Decree	To manage and use forest resource in sustainability.
2004	Declaration (Prakas)	Mother Tree Seeds (2004)

		Endangered tree species banned classification (2005) NTFPs classification and rights of their use (2005)
1996.	Prohibition on Export of Round Logs and Sawn Wood from the Kingdom of Cambodia	Having seen that processing of round logs in the country could provide more jobs and save wood materials, the RGC declared that export wood could be permitted unless sawn. Export of all kinds of round logs from Cambodia had been prohibited.
No date	National Forest Statement	Take into consideration of sustainable development, good governance, poverty alleviation, environmental protection, and equity benefit sharing compliance with the 1992 Rio de Janeiro declaration of the United Nation Conference on Environment and Development (UNCED) in forest management and biodiversity conservation.

Source: Forestry Outlook, 2008

3. THE HISTORY OF FOREST GOVERNANCE

The Concept of Forest governance has been emerged through various regimes with different system aspects. Many studies shown that the forestry sector started its management systems in 1898 since of French protectorate ruling Indochina and Cambodia, however, at that time before the French management initiative forest and non-forest products uses were completely free of control. It is because of the use of forest resources as in community and domestic scale for substitute purpose only (FA, 2008). Then, the French strict forest management rules in Cambodia have applied, however, confronted with traditional uses. Since then, the forest governance system which set up by France, had been continuously implemented till the early 1970s by then the country entered into civil unrest and civil war. The French forest management system had considered as centralized governance because the center made all decisions in regard to forest exploitation, rehabilitation, and or plantation.

During the 1970s to 1980s forests, part of civil war, the country has difficult to control resources, particular, and natural resources, therefore, there was no proper and legal government control on forest sector. Even more, in Khmer Rouge, public sectors were under absolute decision of the leader of top ranking people (Angkar or Organization). It was hard to know clearly about how the top lead decision making on using and managing of natural resources due to very limited studies and document shown. It was seemed that the forest management system was even more top- down approach. People Republic of Kampuchea, and later on called State of Cambodia (1979-1993), was a communism management regime. During that time Cambodia forests were under central decision annual timber harvest plans. With technical recommendations of the Department of Forestry and Wildlife (DFW) and the MAFF, timbers and non-timber forest

products (usually timber only) were exploited according to the central government plans. Again, this system of forest management was central governance with annual or five-year plan (FA 2004).

Significantly, in 1990s, the system of forest governance was changed. New forest management approach was introduced into forest management system in 1993. In 2001 all forest concessionaires were required to develop Strategic Forest Management Plan (SFMP) for forest concession management and by the communities were involved in the process of forest management. In addition to the involvement of communities in forest management, communities have been given rights to establish their community forestry (CF) that located near communes or villages. Very recently, in 2003, CF Sub-Decree was ratified and entered into force through out the country. This is shown that some level of decentralized governance of forestry management system has been introduced into the Kingdom of Cambodia (FAO, 2006). According to Heng, (2007) study shows that forest management and governance have been noticeably improved. In 2006 the National Forest Programme was established under technical and financial support from Danida, DEFID, NZ, and FAO. It is developed under new model that is broadening as many stakeholders as possible including inter-ministerial, private, and civil society to participate in policy development and planning (Sokh Heng, 2007).

4. SUSTAINABLE FOREST MANAGEMENT

With the increase of both technical capacities, number of skilled staffs that supports from regional and international cooperation in forestry sector. Royal government of Cambodia, especially, Forestry Administration had put its efforts to improve sustainable forest management by establishing of most important guidelines, regulations and forestry laws such as:

1. *Forest management guidelines including Reduce Impact Logging and forest concession monitoring guidance;*
2. *Code of practice for forest harvesting (1999), officially bound;*
3. *National Forest Statement (2002);*
4. *Sub-Decree on the Request of Master management plans of all legitimacy forest concessions (till present);*
5. *Ministerial declaration (Prakas) on Seed Source Site establishment. (FA, 2008)*

But it is remarkable that to make sustainable forest management is a great challenge and difficulties which FA had faced, like in many other countries, due to a variety of influenced factors such as high population growth caused to forest degradation and deforestation, high timber market demand, and expansion of agricultural and settlement lands. In addition, currently, economic land concessions, forestland concessions to agro-industrial crops have been granted widely in the country. According to many studies recently shows that there is approximately 6 percent of country

forest-land has been allocated for economic land concessions throughout country. Nevertheless, MAFF permitted agro-industrial lands only on already degraded forestlands in order to develop country economics and contribute to rural poverty alleviation (Sokh Heng, 2007).

5. COMMUNITY FORESTRY ESTABLISHMENT

Background of Community forestry Set Up

Community forestry establishment in Cambodia had been introduced and initiated by international NGOs, as known Concern Worldwide and the Mennonite Central Committee, in the early 1990s at a few pilot sites in two provinces (Takeo and Kampong Chhnang) (Sokh & Iida 2001:116; Braeutigam 2003:8). Community forestry then grew rapidly as of 2002 there were approximately 83,000 ha under introduced community forestry management, representing 0.7% of Cambodia's total forest area suitable for community forestry. According to Fichtenau 2002 shows that area of community forestry encompassed 57 initiatives at 22 sites, and comprising 404 villages and 415,000 people (3.6% of Cambodia's population). These sites were situated in 18 of Cambodia's 24 provinces, although most of these sites are concentrated in agricultural areas, where most of Cambodia's population is found. In relation to this, the objectives of community forestry creation are to protect and rehabilitate sustainable uses of forestry resources. The use of these forests is limited to the collection of NTFPs and firewood, so income generation in the medium term is likely to be very limited, according to Braeutigam (2003:41).

McKenney & Tola (2002:97) shown that the Ministry of Agriculture, Forestry and Fisheries had the authority to allocate an area of Permanent Forest Reserve to a community or a group of people, and the cantonment chief of the Forest Administration had approved mandate for the period of 15 years for community forestry agreements. However, for the Community Forest Management Plan governing will be revised every five years (Braeutigam 2003:11). The FA plays very important roles and direct responsibility for sites on production forest lands, whereas the Ministry for the Environment has responsibility for sites in protection forests.

6. COMMUNITY FORESTRY CHALLENGE AND DIFFICULTIES

Many studies have shown that community forestry system faces several problems and challenges as the community forestry aims at improving the local livelihoods of villagers who depends on collecting non-timber forestry products for their survival condition only. Furthermore, the challenges are including a tendency toward conflict which are related in part to unclear and insecure tenure and lack of land use planning; a lack of benefit sharing arrangements; and weak government finances and capacity in support of the system (Forestry outlook, 2008). According to Fichtenau, et al, 2002, indicated there are key main of conflict occurred in community forestry are following such as, conflict among villagers and villagers of un-equality of

forest resource used, conflict between outsiders (military, commercial enterprise, agriculture and forestland concession) with communities of unclear boundary demarcation between forest concession and community forestry boundary, and conflict including distrust of forest authorities...etc.

Another difficulty for the community forestry is late of endorsement and approval from government agency because of some unclear condition such as unclear community forestry boundary, conflict over overlapping demarcation frontier between commercial forest land concession with allocation of community forestry areas, (Braeutigam, 2003:2 & 26). Financial resources and personal capacity are most difficulties and challenges for community forestry as most of community forestry set up is heavily dependent of external foreign assistances and local and international non-governmental organizations.

7. A CASE STUDY ON FORESTRY GOVERNANCE AT O'SVAY COMMUNITY FORESTRY INITIATIVE

The case study is a part of course field based teaching which implemented by the Department of Environmental Science, Royal University of Phnom Penh. The study explored and observed how local villagers formed and established their natural resource to be own common property through creation for community forestry management. In addition, the study emphasizes on teaching competition over natural resources in Mekong, in forestry resource at local level in particularly O'svay community, Thalaboriwat District, Stung Treng province. This case study is a complementary field base practice with courses in which regular teaching in the classroom. It also aims at bringing the students to learn and explore about what and why the conflict over natural resource have been occurred such as over-exploited fishing, illegal logging and land use grabbing, especially forestry resource competition between local community, private forest land company and powerful business.

8. BACKGROUND OF O'SVAY COMMUNITY FORESTRY MANAGEMENT

Historically, O'svay community is located along upper Mekong River, and adjacent to Cambodia-Laos border shared, within Thallaboriwat district, Stung Treng province. Most of populations have been migrated from different provinces, under the state policy to protect Cambodia border line. It reported that they are retired soldiers and government officers during Sang Kumreas Niyum since 1962. In meantime, individual household was divided a pieces of land for their cultivation and subsidy from the State. Currently, they have been living in O'svay community and formed up to village. Now there are 5 villages in O'svay commune, living with mixed Khmer, Kuy (ethnic minority) and Laos who are evacuated from neighbor area during Pol Pot regime.

In past decades, the area was rich in natural resource, especially forest and fish. Main occupation of villager is found that they totally depend on agricultural based practices, collecting of non timber forest products and fishing activities for their livelihoods. However, it shown that O'svay commune has rapidly changed and natural resources have been gradually declined due to many factors influenced such as forestland concession, rubber plantation investment and illegal logging and fishing activities in the last recent decade. As a result, a lot issue and problem that communities have challenged and coped with them and also faced difficulties such as huge amount of losing natural forest resources for livelihoods. Natural forest land conversion for commercial and cash crops and plantation, and individual greedy powerful land grabbing are being sensitively taken places. Obviously, the changes have however, increases of some families in the communities are vulnerable with losing more and more of natural resources in community. Fisheries resources provide such protein and food diet from majority of communities have been dramatically decreased and declined.

Increasing of tension and more difficulties with their daily lives, villagers sought out to find alternatives and helps therefore, in 2002, CEPA is a local non governmental organization, conducted studied and found that the area has potential to set up community based natural management, therefore, CEPA has offered technical assistances to enhance local people in O'svay commune, to start developing forestry community in some particular areas, in order that they would be able to maintain and protect, manage remained natural resources for their internal management, protection and sustainable uses.

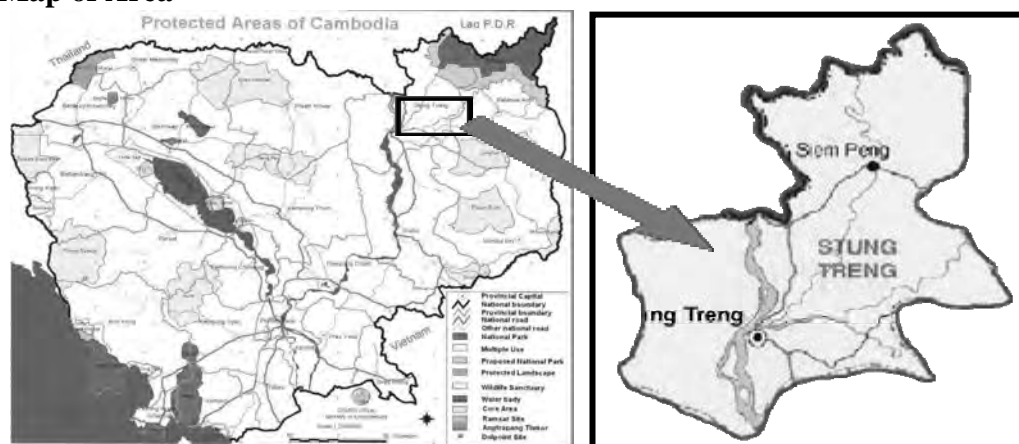


Students visited O'Svay CF,

O'svay commune encompasses five villages, namely O'svay, O'run, Koh Phnov, Veun Sien, Koh Heb. These villagers have strongly committed and agreed to set up community fisheries and forestry since 2002 with initially assisting technical support by a well-known local non government organization as CEPA. Until now these have been passed through some required steps principle to set up community establishment process such as, [1] dissemination of information and identify problems, [2] establish committee by voting by all people in the 5 villages, [3] establish the internal principle of the community, [4] map the boundary of the community. Even though some communities have been passed significant steps, but members

of committees are still concerns how to manage those communities in sustainable and achievable ways, when the CEPA has finished its mandate, how far is strongest commitment of local villagers in protection and preservation of natural resource, because of this area is currently and potentially under threatened and influenced from feasibility of new development paradigms (development corridors), commercial investments (natural forest land conversion) and border development special economic zone,... etc.

Map of Area



Source, CEPA, 2007

9. APPROACHES OF THIS STUDY

The case study is part field base teaching activities. There are simply methods have been applied to obtain data and or information. These applicable methods are literature review from different sources, field observation, and informal group discussion during over-night-home-stay.

- Information related to community forestry management and governance from different reports. Selecting particular case study in which written on the over natural resources and key actors who involved in the conflict and forestry management. This process of secondary data collection need to get involvement some of students in order that they would have learn and gain experiences in research capacity building skills.
- Secondly, field observation and informal group discussion were used to get information and data related to how they managed and controlled their resources and how to they share and allocate natural resources for sustainable uses and management.
- Key informants are chosen such as village head man, local authorities, staff from provincial department of water resources, and environment.
- Participatory consultations with villagers were also conducted during the field data collection. This approach used aims at exploring and recovering existing on conflict over natural resources uses and completion.

10. LESSON LEANT

O'Svay Community Forestry Governance Challenges

- **Local Villagers Challenge with Outsiders**

Traditionally, villagers harvest and practice slash and burn farming, collecting non-timber forest products for their income and subsistence. They have freely accessed to forest area without any interference and disturbance. Some villagers have their own plots of land for cultivation farm and rice within the forest areas.

Forests are an important source of food, medicine construction material and income for rural population. Usually, local people use forest products in their daily livelihood. However, some not timber forest products are in highly demanded in both local and international markets, (Hirsch & Ahmed, 2002). In addition, the villagers hold the Baddish religion and believe in spirits to protect forest “Prey Nakta--spiritual forest”. Therefore, the forests are highly respected and recognized, when those forests destroy, it results to harmful accident to local villagers get sick and or die. At that time, the villagers live with their harmony condition with nature.

In 1994, a Flour Manufacturing Company¹ has conducted feasibility study in O' Svay commune to seek for potential natural forest land to invest for teak and cassava plantation. By 2001, the company has given and approval by Ministry of Agriculture Forestry and Fisheries a forestland concession with amount of 4,700 hectares inside evergreen-dense forest in which located in O' Svay Commune, Thalabariwat district, Stung Treng province. Since then, the company has started cleared forest for exports and small proportion of land given to grow cassava plantation².

Within forestland concession, there were 75 families who have their small piece of farmlands. In early year that company came, those families allowed cultivate their rice-farm and access to forest for collecting non-timber forest products. But gradually, the families have threatened and violated by banning not planting and cultivating rice. The company has also expended their activities and forest area. In early stage, the company has promised to employ many local villagers to works with their company, but until now there are not many villagers who have been recruited yet.

The company has very strict to villagers who have their rice field to cultivate and others to access forest for collecting non timber forest products and other products within land concession boundary where areas that villagers used to collect. At the present, the conflict over natural resource is being increased gradually for example, state-land, forestland have been grabbed and taken away by powerful business and companies. According to

¹ This company is a jointed shared- investment with Khmer- Chinese-Malay. It name is Koe Vuthy flour Manufacturing Company, based in provincial town of Stung Treng province.

² Villagers at O' Svay reported and complained.

some concerns raised by villagers during informal group discussion, found that:

Concerns:

- Villagers are not confidential and they are so worry about the lost of natural resources as forest and fisheries in their commune as currently many illegal logging and fishing occurs.
- Rapid unclear planned investment and development might be impacts on villagers and their communities in sense of loss their livelihoods.
- Presently many migrants have come to villages and they try to change the traditional way of life of villagers.
- Regarding to community forestry management and establishment, local villagers still have limited their capacity building and supporting from laws, regulation and sub-degree is taking place very inappropriate way and low.
- Unclear demarcation of boundary of forest area of company on the ground which result causing to creating intention and conflict over natural resource.
- Most of villagers and committee needs more supports in order to enhance and strengthen legal committee structure, roles and tasks. Economic incentive is very crucial for effective resource management, but it is being challenging now in community forestry.
- More concerns about potential investment for economic growth rather than conservation perspectives.

- **Local Response on Scarcity Resource Competition**

The study shown that in 2002, the villages mentioned earlier have formed and organized a peaceful demonstration to show their concerns about their scarcity of resources that faced to villagers to make their living condition and livelihoods. According to village statistically record shows that 90% of population in village have depended on natural resources such as forest, fish and non timber forest products for generating income on their livelihoods.

However, since, some companies have come to make investment by converting natural forest to plantation, there were intention and conflict over resource use between company and villagers because, some villagers who have their own farm areas existed in company land boundary, did not allow to access into their farming for rice cultivation and also collecting non timber forest product. As a result, villagers have organized movement to show their demand and concerns against to the company. Since then, there have no better/appropriated resolutions yet, local people complained that they face suffers from a limited forest area and not allowing to cultivate their rice-farm in forest land concession.



Hand-drawing CF map of O'svay, 2002

Having seen problem, villagers have discussed among themselves with facilitated and technical assistance from different agencies. Early 2003, the villagers have proposed and requested land forest area within amount of 5,000 hectares, with good condition of forest covered area to establish community forestry. The reason to set up community forestry aim at protecting, preserving and sustainable use and management of existed forest resources. Until now that community forestry area has yet been recognized and approved from Forest Administration (AF), Ministry of Agriculture, Forestry and Fisheries (MAFF). Villagers have seriously concerns and worry as forest area still has valuable and commercial timber trees because the company has also attempted to get that area for their own forestland concession. Therefore, MAFF since now has not yet responded to their proposal since 2003 until 2006. Even though, their proposed community forestry area approval yet and in order to protect illegal cutting tree and hunting from outsiders, villagers have divided up their roles and tasks voluntarily to have patrol and guard regularly to curb-down an illegal logging, wildlife hunting and other activities in their own. Below are villagers having strong optimism on creating of Community forestry:

Optimism:

- They have very strongly commitment amongst villagers in social capital spirits by giving their hands-in-hands; value times and efforts to protect, conserve and manage the remaining of natural resources such as forest resources.
- Community Forestry now has gained a highly experience in managing and protecting and preserving value forest resources their livelihoods.
- Successful with supporting from local authorities and agencies, NGOs and compliance with the Forestry Law, Sub-degree and others... etc.

11. CONCLUSION

This paper illustrates about environmental management in Cambodia, particularly case study on Community forestry governance at local perspectives and context. Rural population in O'svay commune particularly depends on natural resources such as forestry and others for improving their livelihoods and quality of life. However, villagers have faced recently to destruction of forest resources and environment by many factors, as a result, the erosion of forest resources, the growing scarcity of forest product will directly result on the livelihoods, especially lowering well-being of the poor which lead to migrate out to cities.

To response this, Royal Government of Cambodia (RGC), especially Ministry of Agriculture, Forestry and Fisheries has taken action to reform forestry policies, established new forestry law, giving more rights to access forest resource, and more roles to protect forest resources to "*Community Forestry Management*". The policy reform and forestry law received a national political supports, this policy and law has not yet materialized, especially al local forest governance level.

For instance, unclear demarcation of boundary community forestry area is still remaining unsolved. As a result, there is creation some difficulties to recognize and solving with where is boundary of Community Forestry to manage and control. In addition, local and international non government organizations have supported technical advises on communities forestry establishment, training to local authorities to make their knowledge improvement and competency. The efforts and achievements and community forestry establishments are tools and strategies to poverty alleviation, sustainable use of resources and improve local livelihoods and well-being, but those needs to come along with reinforcement of policy reform, complied with laws and participation from all stockholders, especially local people in order to achieve its efforts and mutual achievement.

REFERENCES:

- Arnold, J. E. M. (1991). *Community Forestry: ten years in review*, FAO, Rome.
- Country Paper. (2008). *Country Paper on Forestry outlook 2002*, Forestry Administration, Ministry of Agriculture and Forestry, Cambodia.
- Independent forest sector Review. (2004). *Policy Choice, issues and options*, Forestry Sector in Cambodia, Forestry Administration, Cambodia.
- Sokh Heng and Iida Shigeru. (2000). *Community forestry guidelines, Sustainable forest management project*. Faculty of Agriculture, Graduate School, Kyushu Univ., Fukuoka 812-0053
- Tom Blomley. T, Tola. P, Mam Kosal. M, Dyna. E and Mark Dubois.K (2010). *Review of Community Forestry and Community Fisheries in Cambodia Report*, Fisheries Administration (FiA), Cambodia.
- William D. Sunderlin. (2004). *Community Forestry and Poverty Alleviation in Cambodia*,

Lao-PDR, and Vietnam: An Agenda for Research, Center for
International Forestry Research (CIFOR), Jakarta, Indonesia

Potential bioavailability of pops in lake sediment: A case study of Mae Thang reservoir, Northern Thailand

Pannawee MEKWICHAJ¹, Preeda PARKPIAN²
and Nguyen Thi KIM OANH³

¹Research associate, AIT-SINTEF cooperation, EEM, SERD,
Asian Institute of Technology, Thailand
pannawee@ait.ac.th

²Associate Professor, EEM, SERD, Asian Institute of Technology, Thailand

³Professor, EEM, SERD, Asian Institute of Technology, Thailand

ABSTRACT

As the population has significantly increased in various developing countries over the last few decades, and the great pressure is being placed on agricultural sector for high demand of food. The obsolete pesticides, especially those of Persistent Organic Pollutants (POPs) are still being used for agriculture and vector control of diseases in order to increase their productivity which ultimately contaminate the environment. This study investigated Organochlorine Pesticides (OCPs) contamination levels, which are well-known as POPs, as well as to predict potential ecological risk by using hazard quotient (HQ). Sediment core samples were collected from four locations along Mae Thang reservoir, Northern part of Thailand during dry season (November) in 2007. This reservoir supplies irrigation water for cultivation, fishery, consumption and recreation activities for people living arounding along downstream areas. The samples were measured for various OCPs residues using soxhlet extraction method and gas chromatography with electron capture detector (GC-ECD). Hexachlorocyclohexanes (HCHs) which average ranged 17.87-79.48 $\mu\text{g kg}^{-1}$ dry wt was the main residue compound that consist of α HCH (average ranged 12.11-50.47 $\mu\text{g kg}^{-1}$ dry wt) and γ HCH (average ranged 5.76-29.01 $\mu\text{g kg}^{-1}$ dry wt) following by endosulfans (average ranged 2.08-130.67 $\mu\text{g kg}^{-1}$ dry wt) and heptachlor (average ranged 1.27-51.65 $\mu\text{g kg}^{-1}$ dry wt). Whereas its bioavailable fraction from LDPE method were HCHs (ranged 0.01-0.23 $\mu\text{g kg}^{-1}$ dry), endosulfans (ranged 0.67-2.50 $\mu\text{g kg}^{-1}$ dry), and heptachlor (ranged 0.36-0.90 $\mu\text{g kg}^{-1}$ dry). This indicated that the eroded particles carry with the pesticides were deposited into the lake corresponding with runoff and sedimentation time. In addition, the environmental risk was assessed through HQ using bioavailable fraction extracted by LDPE to compare with Thailand, Canada and Netherlands standards. The results illustrated that based on the HQ values all were acceptable which mean that harmful effect on living species and ecological systems in the reservoir is unlikely to occur.

Keywords: *Persistent Organic Pollutants, Organochlorine pesticides, Hexachlorocyclohexane, Endosulfan, Mae Thang reservoir*

1. INTRODUCTION

Under the treaty of the Stockholm Convention in 2001, 92 countries agree to reduce or eliminate the production, use and release of 12 key POPs (U.S. EPA, 2006) which known as the Dirty Dozen. All of POPs are toxic and accumulate in living organisms and plants. They do not readily break down in the environment with half-lives in soil in the order of years, and they are transported across boundaries far from their sources, even to other regions where they have never been used or produced. The ecosystems and human populations are particularly at risk because of the long-range environmental transportation and biomagnifications of these substances (UROPA, 2006).

Organochlorine Pesticides (OCPs) is a major substance in the 10 intentionally produced chemicals of POPs. 80% of OCPs has been used in agriculture and moved in the environment through volatilization, runoff, infiltration, biomagnifications via the transmission process in the food chain (El-Shahawi et al., 2009). In Thailand, restrictions on use of organochlorine pesticides (OCPs) were imposed in the late 1980s (Ruangwises et al., 1994). Even though most OCPs have been phased out, their residues are still found in different environmental substrates, such as air, water, soil and sediment as well as accumulated in the living organism because of their lipophilic properties that can potentially harmful to human health (Leadprathom, 2009). One of the matrices that acts as a natural sink of these toxic chemicals is soil (Cupr et al., 2009), these compounds are strongly sorbed onto the surface of particles associated with the organic content of solid-phase matrix and can be deposited to the depth increments in the sediment (Doong et al., 2008). Furthermore, they are prone to further redistribution (erosion, percolation and re-emission) or can be recirculated in the aquatic environments via natural or anthropogenic processes and then back to the water bodies which becomes increasingly release to wildlife health and ecosystem (Fatoki and Matha batha, 2001).

Mae Thang reservoir is located in Rong Kwang district, Phare province in Northern part of Thailand. This reservoir is provided irrigation water for various functions for people in the surrounding areas. Therefore, there are many farmlands in the vicinity where agricultural chemical applications are commonly used to improve crop yields. These agrochemicals could be the major sources of contaminates by means of eroded particles with sloping land and runoff during the wet season which discharge directly into the reservoir. This study aims to determine the concentration distribution and toxicity of several OCPs in the sediment along the Mae Thang reservoir in order to develop the database of the pollution potential and predict ecological risk in aquatic environment in this region.

2. MATERIALS AND METHODS

2.1 Study area and sediment sampling

The landscape of Mae Thang reservoir is rolling to mountainous in northern of Thailand (Figure 1). The maximum water capacity of the reservoir is $35 \times 10^6 \text{ m}^3$ and the maximum depth is 43 meters (Thothong, 2005). In the region, The main land use pattern along the Mae Thang watershed is the agricultural activities included planting rice, corn, beans, vegetables and fruit trees on a very steep slope of the mountain which increasing pesticides use and enhances soil erosion (MSEC, 1999). According to the cultivation activities, the soil is splashed downhill which causes deterioration of soil and contaminants discharged into the terrestrial. Two sediment cores were collected randomly for each sampling point (totally 8 cores) from different zones of the reservoir based on the water depth (Figure 2) by using KC Kajak sediment core during dry season in November 2007. The samples were preserved at -20°C until analysis.

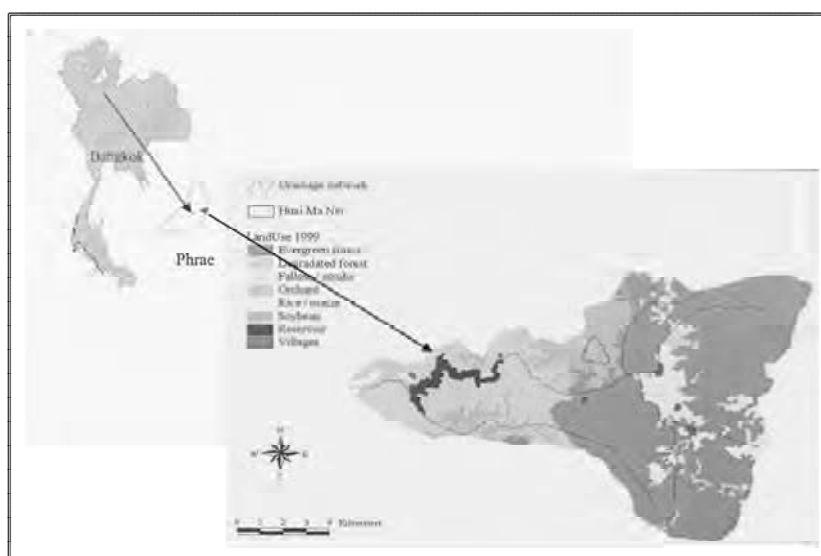


Figure 1: The Mae Thang reservoir located in Phrae, Northern Thailand

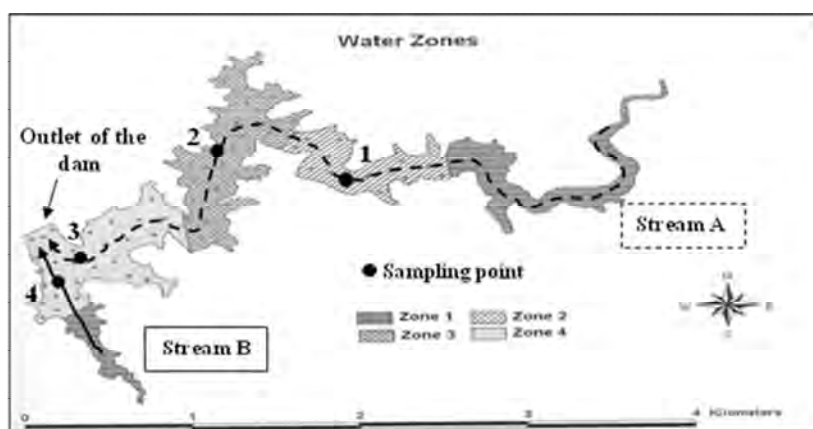


Figure 2: Sampling zones and points

2.2 Samples preparation and extraction

The sediment samples (0-35 cm) were homogenized and decanted from wet samples by centrifugation. After that the samples were passed through 0.2 mm sieve, and 4-gram sediment was mixed with Na₂SO₄ to reduce the moisture and water before extraction. OCPs residues in sediments were extracted for 16 h with a mixture of 200 ml of *n*-hexane and acetone (V:V = 1:1) in a Soxhlet apparatus and used the florisil column to cleanup the extracts (U. S. EPA., 1998; U.S. EPA., 2000). Bioavailable fraction extracted by low density polyethylene (LDPE) method were analyzed base on Leadprathom 2009, 10 gram of LDPE plastic pellets were mixed within 90 gram of wet sediment samples and placed into shaker machine for 7 days at 27 °C which the temperature in the water from Mae Thang reservoir, then separate LDPE plastic pellets to further soxhlet extraction following the sediment extraction method.

2.3 Samples analysis and analytical quality assurance

The OCPs residues were measured using HP 5890 series II gas chromatography system equipped with an electron capture detector (GC-ECD). The concentrations of OCPs were calculated against known concentration standard (pesticide standard mix) peak area. Recovery rate (%) was performed for each sample by adding of pesticide surrogate standard prior to extraction (U.S. EPA., 2000).

3. RESULTS AND DISCUSSION

3.1 Contamination level of OCPs in sediment

The concentration of OCPs levels in sediment for different locations along Mae Thang reservoir during November 2007 is summarized in Table 1. Despite OCPs have been official banned and restriction on the usage in Thailand, pesticide residues were detected in all sampling sites. The OCPs found in this study included α -HCH, γ -HCH (Lindane), α -endosulfan, β -endosulfan and heptachlor.

The results of the mean concentrations showed that HCH compounds were the predominant OCPs in sediment of Mae Thang reservoir following by endosulfan and heptachlor. This is due to the fact that the contamination of HCH isomers is a serious problem worldwide from usage for agricultural purpose (Fellin et al., 1996). Moreover, the chemicals properties such as solubility and vapor pressure of HCHs (vapor pressure, 3.26×10^{-5} mm Hg at 25°C and solubility, 7.3 mg/L at 25 °C) would have more tendency to be deposit into sediment or long range hydrological transport by river discharge and atmospheric fallouts from remote source as compared to endosulfans (vapor pressure, 1×10^{-5} mm Hg at 25 °C and solubility, 0.32 mg/L at 22°C) (UNEP Chemicals, 2002).

For the distribution of HCH isomers, the dominant isomer in this study was α -HCH which concentration is higher than γ -HCH in all locations (Table 1.) It could be noted that a high percentage of α isomer was reflecting the composition of technical mixture for industrials consist of 65-70% α -HCH, 14-15% γ -HCH, and 7-10 % β -HCH (Ramesh et al., 1989; Kim, et al., 2006) and α -HCH is more likely to partition to the air and transport for long distance (Doong et al., 2008).

From the comparison all of locations, Σ OCPs concentration in location 3 (261.80 $\mu\text{g kg}^{-1}\text{dw}$) was highest following by location 1 (83.99 $\mu\text{g kg}^{-1}\text{dw}$), 4 (65.91 $\mu\text{g kg}^{-1}\text{dw}$) and 2 (23.66 $\mu\text{g kg}^{-1}\text{dw}$). Regarding to HCHs, the main OCPs compounds was found in each locations except endosulfans detected with the high residue only at location 3, it is possible that water current from stream A, which come from upstream and flows into downstream at outlet of the dam (Fig 2.). Because of this, it has tendency to bring up resuspension process of endosulfans from water current (Maldonado and Bayona, 2002; Holvoet, et al., 2007) that cause of higher suspended particulate and deposit into the sediment.

Table 1: Organochlorine Pesticides concentrations ($\mu\text{g kg}^{-1}$ dry wt) in the sediment core across the 35 cm depth at Mae Thang reservoir

	Location			
	1	2	3	4
α -HCH	30.23 \pm 14.67	12.11 \pm 17.13	50.47 \pm 17.30	43.86 \pm 29.33
γ -HCH	11.88 \pm 5.73	5.76 \pm 3.05	29.01 \pm 30.08	16.20 \pm 9.88
HCHs ^a	42.11 \pm 20.40	17.87 \pm 14.07	79.48 \pm 12.78	60.10 \pm 39.21
Endosulfan I	16.31 \pm 9.52	1.54 \pm 2.18	67.69 \pm 67.39	0.44 \pm 0.48
Endosulfan II	14.29 \pm 3.69	2.98 \pm 4.21	62.70 \pm 60.61	1.64 \pm 2.31
Endosulfans ^b	30.60 \pm 13.22	4.52 \pm 6.39	130.67 \pm 128.00	2.08 \pm 2.79
Heptachlor	11.29 \pm 0.26	1.27 \pm 0.32	51.65 \pm 63.14	3.78 \pm 5.35
Σ OCPs ^c	83.99	23.66	261.8	65.91

Data show average concentration from duplicate samples (\pm Standard deviation)

^a Sum of α -HCH, γ -HCH

^b Sum of α -endosulfan and β -endosulfan

^c Sum of the average of α -HCH, γ -HCH, α -endosulfan, β -endosulfan and heptachlor.

3.2 Potential risk evaluation of OCPs compound

3.2.1 Determination of bioavailable fraction by low density polyethylene (LDPE) method

The study for bioavailable fraction from Belfroid et al., 1996 and Leadprathom 2008 were described that bioavailability is an important factor to determine the degree to which a chemical is able to move into organisms. It is also defined as the fraction of bulk amount of the chemical accumulates in soil/sediment, and by water taken up potentially by organisms during their lifespan into tissues. In order to determine bioavailability of contaminants, semipermeable membrane device (SPMDs) that is made with low density polyethylene (LDPE) was used. This is a tool which widely used to determine the potential of hydrophobic contaminants in the

environment such as OCPs adsorption through hydrophobic sorption from water and sediment (Takada, et al., 2005)

Bioavailable fraction concentrations from LDPE method at 0-35 depths sediment was presented in Table 2. These comprised of α -HCH, γ -HCH, α -endosulfan, β -endosulfan and heptachlor. Based on chemical analysis along the reservoir seemed to have endosulfans contamination, following by heptachlor whereas HCHs did not have much present in bioavailable fraction.

Table 2: Bioavailable fraction of OCPs ($\mu\text{g kg}^{-1}$ dry wt) by LDPE extraction method from combination of 4 locations along Mae Thang reservoir

	HCHs ^a	Endosulfans	Heptachlor
LDPE	0.01-0.23	0.67-2.50	0.36-0.90

^aHCHs = α -HCH, γ -HCH

^bEndosulfans = α -endosulfan, β -endosulfan

3.2.2 Ecological risk assessment

The hazard quotient (HQ) is widely used as a screening method for potential risk under an ERA (Driscoll et al., 2002). The HQ approach was applied in preliminary risk assessment by comparing concentrations of toxicity chemicals found in the environmental media with benchmark which calculated using the following equation:

$$\text{HQ} = \text{Exposure concentration} / \text{Screening Benchmark} \quad (1)$$

Final determination of risk from contaminants in question is made in the Baseline Ecological Risk Assessment. When the HQ is calculated to be greater than one for a particular contaminant, the assessed ecological system is assumed to be potential for adverse impact to ecological system (NEPC, 1999).

Environmental contaminant concentration in reservoir was represented by sediment media which was determined from the bioavailable fraction using LDPE extraction method. The HQ values of each compound are shown in Table 3. HCHs, endosulfans and heptachlor concentrations of LDPE method was 0.01-0.23 $\mu\text{g kg}^{-1}$ dry wt, 0.67-2.50 $\mu\text{g kg}^{-1}$ dry wt and 0.36-0.90 $\mu\text{g/kg}$, respectively. The HQ values by bioavailable fraction of HCHs, endosulfans and heptachlor on Thailand benchmark, Canada and Netherlands benchmark were not shown potential risk because the values obtain were lower than 1 indicating no potential risks of pesticides to aquatic life at the time cause of assessment. As a result, HQ value obtained from the LDPE method indicated acceptable risks when Thailand, Canada and Netherlands benchmark were applied.

Table 3: Hazard quotient (HQ) of OCPs in sediment from Mae Thang reservoir

Exposure Concentration		Screening Benchmark					
Pesticide contaminant	Maximum ($\mu\text{g kg}^{-1}$)	Thailand ^a (mg kg^{-1})	HQ	Canada ^b ($\mu\text{g kg}^{-1}$)	HQ	Netherlands ^c (g kg^{-1})	HQ
HCHs	0.23	< 4.4	0.00005	2.74	0.08	0.05	0.0000046
Endosulfans	2.50	-	-	-	-	0.01	0.00025
Heptachlor	0.90	< 1.1	0.00005	1.38	0.65	NV	NV

NV: No value

^a Pollution Control Department, 2004

^b Canadian Sediment Quality Guidelines for the Protection of Aquatic Life (CCMC), 2002

^c Netherlands Environmental Assessment Agency, 2005

3.3 Comparison of OCPs levels in sediment at different area

Comparison of OCPs concentrations in this reservoir sediment with other studies was shown in Table 4. From the result of this study, HCHs and heptachlor concentration were higher when compared to those reported from the other parts of Thailand. Except the result in agricultural areas, northern part of Thailand from Thapinta and Hudak, 2000 that were extremely high on endosulfans. Furthermore, when compared pesticide concentration of Thailand (including this study) with Asian locations they were much higher than other locations. The reason for this due to the fact that the fast development in agricultural sector during 1994-2003, Thailand mostly imported organic and inorganic chemical substances, which comprised chemical products and active ingredients (PCD, 2006) and mostly imported pesticide in ASEAN Member Countries in 1988 (FAO, undate). Consequently, a similar low concentration of all three pesticides monitored in sediments of selected Asian countries was observed.

Table 4: Comparison of OCPs concentration ($\mu\text{g kg}^{-1}$ dry wt) in the sediment from other Asian locations

Location	Σ HCH	Σ endosulfan	Heptachlor	Reference
- Agricultural areas, Northern part of Thailand	ND	1.22–634.90	ND	Thapinta et al., 2000
- Agricultural areas, Eastern part of Thailand	ND	0.011–8.818	0.005–0.297	
- Tributaries of Mae Klong river	0.64-6.92	<0.001-2.050	<0.001-1.920	Poolpak et al., 2007
- Rang Tub Tab Canal, MaeKlong river basin	0.34-24.10	<0.001-16.18	<0.001-5.95	
- Chanthaburi estuary Eastern part of Thailand	0.5-49.5	4.0-70.5	0.4-13.0	Leadprathom et al., 2008
- Mae Thang reservoir,	7.92-88.51	nd-221.18	nd-96.30	This study., 2008

Northern part of Thailand				
- Osaka Bay, Japan	0.073-6.20	ND	ND	Tanabe et al., 2002
- Ariake Bay, North Japan	0.78-1.5	ND	nd	Kim et al., 2006
- Kyeonggi Bay, Korea	<0.19-1.20	ND	ND	Lee et al., 2001
- Lake Shiwha, Korea	0.59-2.40	ND	ND	
- Bay of Bengal, India	0.17-1.56	ND	ND	Rajendran et al., 2001
- Hugli estuary, India	<1-130	<1-220	ND	Bhattacharya et al., 2003
- Da-han river, North Taiwan	<0.12-4.94	<0.08-3.78	<0.15-1.57	Doong et al., 2002
- Erh-jen river, South Taiwan	<0.12-6.90	<0.08-7.16	<0.15-5.61	Doong et al., 2002
- Daya Bay, China	0.32-4.16	ND	ND	Zhou et al., 2001
- Minjiang river estuary, China	2.99-16.21	0.57-8.84	0.88-2.77	Zhang et al., 2003
- Ha long Bay, Vietnam	nd-0.85	ND	ND	Hong et al., 2008
- Hai Phong Bay, Vietnam	0.15-1.00	ND	ND	

ND: no data
nd: non detectable

4. CONCLUSION

The results obtained in this study suggest that there still remained OCPs residues in the sediment of Mae Thang reservoir, although the use of POPs in Thailand had been prohibited for 30 years. The organochlorine pesticide compounds particularly α -HCH, γ -HCH among HCHs, α -endosulfan and β -endosulfan among endosulfans and heptachlor were detected along the reservoir. This might due to their previous extensive applications in agriculture activities, runoff from cultivation, and the hydrological characteristic such as water current, seasonal variation of flow and flood disasters. HCHs is a predominate compound showed as the highest concentration in each location, only in one location near the dam outlet showed high level of endosulfans which might be because of sediment resuspension influenced by water current. In addition, an ecological risk assessment from this study indicated that Mae Thang reservoir is not at risk since the hazard quotient from bioavailable fraction of LDPE method is lower than 1. However, all the OCPs concentration of this reservoir are generally higher than other Asian areas, thus monitoring program for POPs contamination in this reservoir is recommended in order to protect harmful effects on the ecosystem and living organisms especially on human health.

ACKNOWLEDGEMENTS

The authors wish to acknowledge Dr. Warinya Thothong for helping in sediment samples collected at Mae Thang reservoir. The authors also express their gratitude to Dr. Supat Ponza and Dr. Napaporn Leadprathom for their valuable suggestions and useful comments.

REFERENCES

- Bhattacharya, B., Sarkar, S. K., and Mukherjee, N., 2003. Organochlorine pesticide residues in sediments of a tropical mangrove estuary, India: implications for monitoring. *Journal of Elsevier* 29, 587-592.
- CCME, 2002. Canadian Sediment Quality Guidelines for the Protection of Aquatic Life. *Canadian Council of Ministers of the Environment*, Canada.
- Cupr, P., Bartos, T., Sanka, M., Klanova, J., Mikes, O., and Holoubek, I., 2009. Soil burdens of persistent organic pollutants-Their levels, fate and risks Part III. Quantification of the soil burdens and related health risks in the Czech Republic. *Science of the Total Environment* 408, 486-494.
- Doong, R. A., Sun, Y. C., Liao, P. L., Peng, C. K., and Wu S.C., 2002. Distribution and fate of organochlorine pesticide residues in sediments from the selected rivers in Taiwan. *Journal of Chemosphere* 48, 237-246.
- Doong, R., Lee, S., Lee, C., Sun, Y., and Wu, S., 2008. Characterization and composition of heavy metals and persistent organic pollutants in water and estuarine sediments from Gao-ping River, Taiwan. *Marine Pollution Bulletin* 57, 846-857.
- Driscoll, S. B. K., Wickwire, W.T., Cura, J. J., Vorchees, D. J., Butler, C. L., and Moore, D. W., 2002. A comparative screening-level ecological and human health risk assessment for dredged material management alternative in New York/ New Jersey harbor. *Human and Ecological Risk Assessment* 8(3), 603-626.
- El-Shahawi, M. S., Hamza, A., Bashammakh, A. S., and Al-Saggaf, W. T., 2009. An overview on the accumulation, distribution, transformations, toxicity and analytical methods for the monitoring of persistent organic pollutants. *Talanta* 80, 1587-1597.
- Fatoki, O. S., and Matha batha, S., 2001. An assessment of heavy metal pollution in the East London and Port Elizabeth harbours. *Water SA* 27, 233-240.
- FAO (Food and Agriculture Organization of the United Nations), undate. Value of Pesticide and Fertiliser Trade in ASEAN Member Countries, 1998. *Second ASEAN State of the Environment Report 2000*, Virginia, USA.
- Fellin, P., Barrie, L. A., Dougherty, D., Toom, D., Muir, D., Grift, N., Lockhart, L., and Billeck, B., 1996. Air monitoring in the Arctic: results for selected persistent organic pollutant for 1992. *Environmental Toxicology and Chemistry* 15, 253-261.
- Holvoet, K. M. A., Seuntjens, P., and Vanrolleghem, P. A., 2007. Monitoring and modeling pesticide fate in surface waters at the catchment scale. *Ecological Modelling* 209, 53-64.

Hong, S. H., Yim, U. H., Shim, W. J., Oh, J. R., Viet, P. H., and Park, P. S., 2008. Persistent organochlorine residues in estuarine and marine sediments from Ha Long Bay, Hai Phong Bay, and Ba Lat Estuary, Vietnam. *Journal of Chemosphere* 72, 1193–1202.

Kim, S. K., Eun, H., Katase, T., and Fugiwara, H., 2006. Vertical distributions of persistent organic pollutants (POPs) caused from organochlorine pesticides in a sediment core taken from Ariake bay, Japan. *Journal of Chemosphere* 67, 456–463.

Leadprathom, N., 2009. Ecological risk assessment of organochlorine pesticide in sediment: Case study on Chanthaburi river mouth area. *Dissertation No. EV-09-04 Asian Institute of Technology*, Bangkok, Thailand.

Lee, K. T., Tanabe, S., and Koh, C. H., 2000. Distribution of organochlorine pesticides in sediments from Kyeonggi Bay and nearby areas, Korea. *Journal of Elsevier* 114, 207-213.

Maldonado, C., and Bayona, J. M., 2002. Organochlorine compounds in the north-western black sea water: distribution and water column process. *Estuarine, Coastal and Shelf Science* 54, 527-540.

MSEC (the Management of Soil Erosion Consortium), 1999. Huai Ma Nai Catchment: The MSEC Benchmark Site in Thailand. International Water Management Institute- Southeast Asia Regional Office, Bangkok, Thailand. Available online <http://msec.iwmi.org/res/benchmark/benchmark/profiles/thailand.pdf>.

NEPC (National Environment Protection Council), 1999. *Guideline on ecological risk assessment*. Australia.

Netherlands Environmental Assessment Agency, 2005. Pesticide in the soil in the Netherlands. Available online <http://www.mnp.nl/mnc/i-en-0264.html>.

PCD. (Pollution Control Department), 2004. Soil Quality Standards for Habitat and Agricultural. Bangkok, Thailand. Available online http://www.pcd.go.th/info_serv/en_reg_std_soil01.html.

PCD. (Pollution Control Department), 2006. Thailand National Profile for Persistent Organic Pollutants (POPs) Management, *Enabling Activities for Development of National Plan for Implementation of the Stockholm Convention on POPs*. Bangkok: NIP/POPs coordination office, Thailand.

Poolpak, T., Pokethitiyook, P., Kruatrachue M., Arjarasirikoon, U., and Thanwaniwat, N., 2007. Residue analysis of organochlorine pesticides in the Mae Klong river of Central Thailand. *Journal of Hazardous Materials* 156, 230–239.

Rajendran, R. B., Imagawa, T., Tao, H., and Ramesh, R., 2004. Distribution of PCBs, HCHs and DDTs, and their ecotoxicological implications in Bay of Bengal, India. *Journal of Elsevier* xx, xxx-xxx.

Ramesh, A., Tanabe, S., Tatsukawa, R., and Subramanian, A. N., 1989. Seasonal variation of organochlorine insecticide residues in air from Porto Novo, South India. *Environmental Pollution* 62, 289-304.

Ruangwises, S., Ruangwises, N., and Tabucanon M. S., 1994. Persistent organochlorine pesticide residues in green mussels (*Perna viridis*) from the Gulf of Thailand. *Marine Pollution Bulletin*, Vol 28, No 6, 351-355.

Takada, H., Mato, Y., Endo, S., Yamashita, R., and Zakaria, M. P., 2005. Pellet Watch : Global Monitoring of Persistent Organic Pollutants (POPs) using Beached Plastic Resin Pellets. *Laboratory of Organic Geochemistry, Institute of Symbiotic Science and Technology*, University of Agriculture and Technology, Tokyo, Japan.

Tanabe, S., Lee, K. T., and Koh, C.H., 2002. Distribution of organochlorine pesticides in sediments from Kyeonggi Bay and nearby areas, Korea. *Journal of Chemosphere* 48, 237–246.

Thapinta, A., and Hudak, P. F., 2000. Pesticide use and residual occurrence in Thailand. *Environment Monitoring Assessment* 60, 103–114.

Thothong, W., 2005. GIS-aided spatial and temporal mapping of reservoir water quality in an agricultural watershed: A case study of Mae Thang reservoir, Northern Thailand. *Master Thesis No. NR-05-04 Asian Institute of Technology*, Bangkok, Thailand.

UNEP Chemicals, 2002. *Regional reports of the regionally based assessment of persistent toxic substance program*. Available online <http://www.chem.unep.ch/pts>.

UROPA (Uropean Commission Environment), 2006. POPs-Persistent Organic Pollutant. Available online <http://ec.europa.eu/environment/pops/indexen.htm>.

U.S. EPA., 1998. 8081B method organochlorine pesticide by gas chromatography, U.S. Environmental Protection Agency, USA. Available online <http://www.epa.gov/osw/hazard/testmethods/sw846/pdfs/8081b.pdf>.

U.S. EPA., 2000. 3620C method florasil cleanup, U.S. Environmental Protection Agency, USA. Available online <http://www.epa.gov/osw/hazard/testmethods/sw846/pdfs/3620c.pdf>.

U.S. EPA, 2006. Persistent Organic Pollutants: A Global Issue, A Global Response. Environmental Protection Agency, USA. Available online <http://www.epa.gov/oia/toxics/pop.htm>

Zhang, Z. L., Hong, H. S., Zhou, J. L., Huang, J., and Yu, G., 2003. Fate and assessment of persistent organic pollutants in water and sediment from Minjiang river estuary, Southeast China. *Journal of Chemosphere* 52, 1423–1430.

Zhou, J. L., Maskaoui, K., Qiu, Y. W., Hong, H. S., and Wang, Z. D. 2001. Polychlorinated biphenyl congeners and organochlorine insecticides in the water column and sediments of Daya Bay, China. *Environmental Pollutant* 113, 373– 84.

The effect of moisture on the ground surface for LiDAR DEM generation

Takahiro ENDO¹, Yoshito SAWADA² and Haruo SAWADA³

¹Assitant Professor, ICUS, IIS, The University of Tokyo, Japan

²Project Researcher, ICUS, IIS, The University of Tokyo, Japan

³Professor, ICUS, IIS, The University of Tokyo, Japan

ABSTRACT

Recently, LiDAR (Light Detection and Ranging) measurement is becoming useful tool to generate Digital Elevation Model (DEM) and Digital Surface Model (DSM) on national land surface. Especially in the forest area, LiDAR becomes a powerful tool for forest management, since LiDAR can directly measure the elevation under tree canopy which visible sensors can't measure. However, LiDAR sometime directly can't generate DEM due to a lack of points under tree canopy. Authors considered that the reason of this phenomenon mainly depends on an effect of soil moisture on the ground surface, since laser beam is a kind of microwave. An aim of this study is to quantitatively reveal relationship between moisture on the ground surface and the probability of DEM generation using a simulation. The relationship was analyzed by a LiDAR simulator which consists of computer graphic technology and a 3D plant growth model. Five conditions of moisture on the ground surface were simulated. As the results of analysis, the reflectance decreased in proportion to increment of moisture on the ground surface. The result indicated that DEM generation depends on three parameters which are the sensitivity of sensor, the moisture on the ground surface and the gap size. It was difficult to generate DEM in case of high moisture condition. LiDAR measurement should avoid wet condition on the ground surface in order to get DEM with high accuracy.

Keywords: *simulation, reflectance, forest, gap size, crown edge*

1. INTRODUCTION

LiDAR is one of remote sensing tools. The LiDAR consists of the transmitting and receiving apparatus of laser beam, the DGPS and the IMU. At present, the LiDAR is widely used for the survey of national land, the shape of urban area and forest management. The reasons why be used LiDAR in these work fields is that the LiDAR can directly measure three dimensional shape and position of a target. Principle of airborne LiDAR measurement is that firstly, laser beam is emitted from the position decided by the DGPS and the IMU and secondly, the receiver detects the echo from a target, and thirdly, CPU calculates the geographical position of a target using both the position of sensor and the traveling time of laser beam.

Wavelength used by LiDAR is usually 1064nm. Since laser beam is electromagnetic wave, an intensity of the echo from target depends on reflectance of a target at 1064 nm. Hence, DEM generation rate is expected to depend on moisture content on the ground surface. Especially, soil moisture on the ground surface is expected to affect DEM generation in forest.

This study aims to investigate that the moisture on the ground surface effect for DEM generation in forest using a LiDAR simulator.

2. MATERIALS AND METHODS

2.1 An over view of a LiDAR simulator

The LiDAR data is simulated using a three dimensional plant model and ray tracing method. The method consists of four steps; (1) modeling a target in virtual space, (2) calculating intersections between an object and laser beam by ray tracing method, (3) calculating intensity of an echo at the intersection, and (4) creating points in case of the echo over a specific threshold.

2.2 Modeling of forest and the ground

Trees are created in virtual space using 3DCG software and a plant growth model. In this study, natFX (commercial software) was used as a plant growth model. The natFx can create tree as full polygons using three parameters which are species, age of stand and season. The shape of created trees is similar to actual tree shape in the point view of crown, leaves and stems.

On the other hand, the ground data is used from actual DEM data or a virtual data. Table 1 shows software configurations of LiDAR simulator.

Table 1: The software configurations of LiDAR simulator.

3DCG software	Autodesk 3ds max 2011
Tree growth model	natFX
Programming language	max script and Matlab 2011a

2.3 Simulation of the discrete LiDAR measurement

To create LiDAR's point cloud, ray tracing is carried out against the modeled trees and the ground in 3DCG. This simulation calculates intersection points and reflectance of the echo. Specifically, point density of laser beam, scan angle, footprint size, reflectance of leaves and the ground and leaf size are used as initial values. Intersection points and its reflectance are calculated by the following steps; (1) origin of laser beam is calculated from point density, (2) sub rays are created in a main ray from footprint size and leaf size, (3) intersection points are calculated using sub rays and the target, (4) reflectance of each intersection points is calculated using

inclination of the target. In this study, each inclination was calculated as horizontal, since reflectance mechanism at intersection point define as lambertian.

Moreover, the discrete LiDAR can't record two strong intensities within 3m due to hardware limitation. Usually, the discrete LiDAR records four points per one laser beam. Therefore, point generation algorithm in this simulation was adapted to this procedure. The algorithm is the followings. Firstly, an intersection point with maximum Z value was selected as a start point for calculation of reflectance of the echo. Secondly, summation of reflectance of the echo by 15 cm interval was calculated. If the summation value is over threshold value, a point is created using average value of all intersection points within 15 cm interval. Next search position is skipped 3m from the created point. This procedure is repeated until the last intersection point.

2.4 Modeling condition for simulation of soil moisture effect

In this study, moisture on the ground surface defined as reflectance on the ground surface. To investigate moisture effect in forest in DEM generation, virtual forest and the ground were created in 3DCG. In this study, the ground was set as flat to investigate only soil moisture effect. *Japanese cedar* was selected as species of virtual forest, since this species was one of dominant plantation species. Figure 1 shows a vertical view of the created virtual forest and the ground. Nine trees were modeled using parameters which were 45 years age of stand and summer. Trees were distributed as closed or open canopy like Figure 1 to evaluate canopy condition. LiDAR simulation was carried out as the followings; footprint size was 20cm, scan angle was 90°, point density was 10 points/m², wavelength was 1064 nm, leaf reflectance was 50% at 1064 nm, the ground reflectance was 50%, 40%, 30%, 20% and 10% at 1064 nm, respectively, leaf size was 0.09 m² derived from virtual tree's leaves.

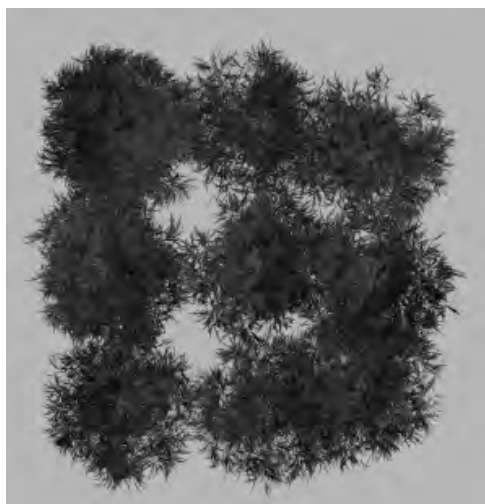


Figure 1: The created virtual forest.

3. RESULTS AND DISCUSSION

3.1 Effect of moisture on the ground surface for DEM generation

Figure 2 (a) shows a result of relationship between each reflectance of the ground surface and the number of reached laser beams on the ground. Also, Figure 2 (b) shows a result of relationship between each reflectance of the ground surface and the ratio of DEM generation. Since the reflectance of the ground that was 10% was less than the threshold, naturally, the number of reached laser beams on the ground and the ratio of DEM generation were zero, respectively. In case of the decrement of the reflectance of the ground, the number of reached laser beams on the ground was decreased (Figure 2 (a)), and also the ratio of DEM generation was decreased (Figure 2 (b)). The results indicate that the moisture on the ground surface affects DEM generation.

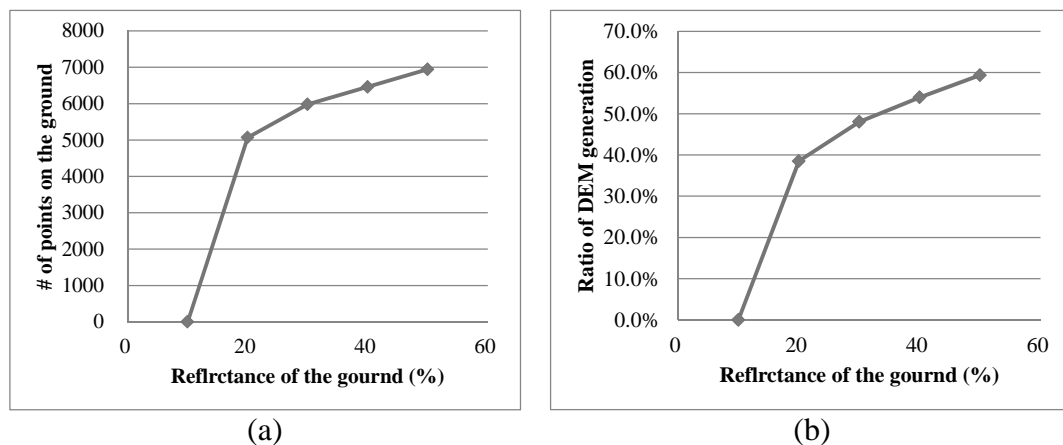


Figure 2: A result of relationship between each reflectance of the ground surface and the number of reached laser beams on the ground (a), and relationship between each reflectance of the ground surface and the ratio of DEM generation (b).

3.2 Relationship between the ratio of DEM generation and the size of gap areas

The ratio of the DEM generation in range of from 50% to 20% wasn't linear, but was exponential relation. Authors considered that the reason depended on relationship between the gap size and mesh size of rasterization. Therefore, a vertical 2D black and white image (BW image) was created from 3D virtual forest data (Figure 3) and investigated relationship between the gap size and its number using the rasterized BW image. Its mesh size was 10 cm for understanding the relation in detail. Figure 4 stands for the relationship between the gap size and its number of pixels.

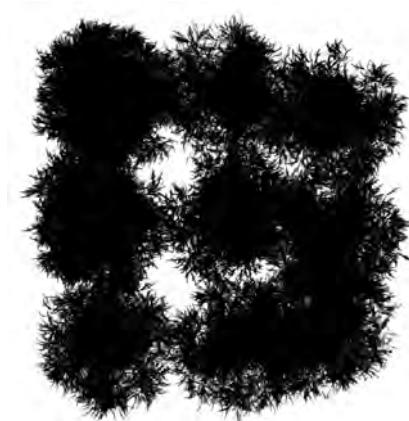


Figure 3: The 2D black and white image derived from the 3D virtual forest

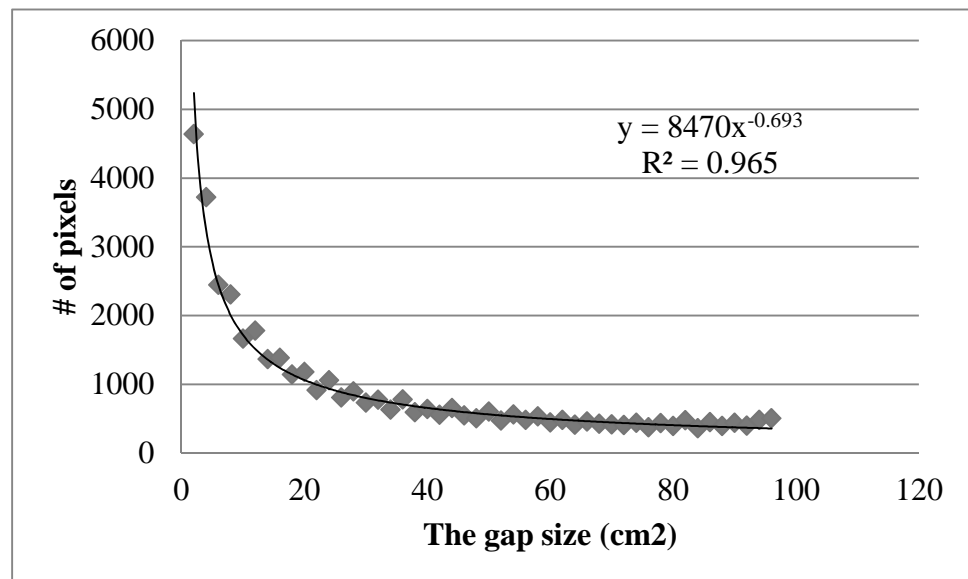


Figure 4: Relationship between the gap size and its number of pixels

As a result of the analysis of the relation, the relationship between the gap size and its number of pixels was exponential relation. Its multiple correlation coefficient (R^2) was 0.965. Both curves were quite similar. The result indicates that DEM generation depends on three parameters which are the sensitivity of sensor, the moisture on the ground surface and the gap size.

3.3 The affected area by moisture

Figure 5 (a) – (d) are results of 1 m grid DEM generation derived from the simulated data. Figure 4 (a)-(d) are 50%, 40%, 30% and 20% of reflectance of the ground surface, respectively. White pixels stand for success of DEM generation. On the other hand, black pixels stand for failure of DEM generation. Figure 5 (e) is the subtracted image. R:G:B corresponds with 50%: 40%: 20%. Gray pixel is the difference. The distribution of the different was around edge of tree crown. Hence, the results showed that it was difficult to create DEM around the edge of the crown, in case of the low value of the reflectance of the ground surface.

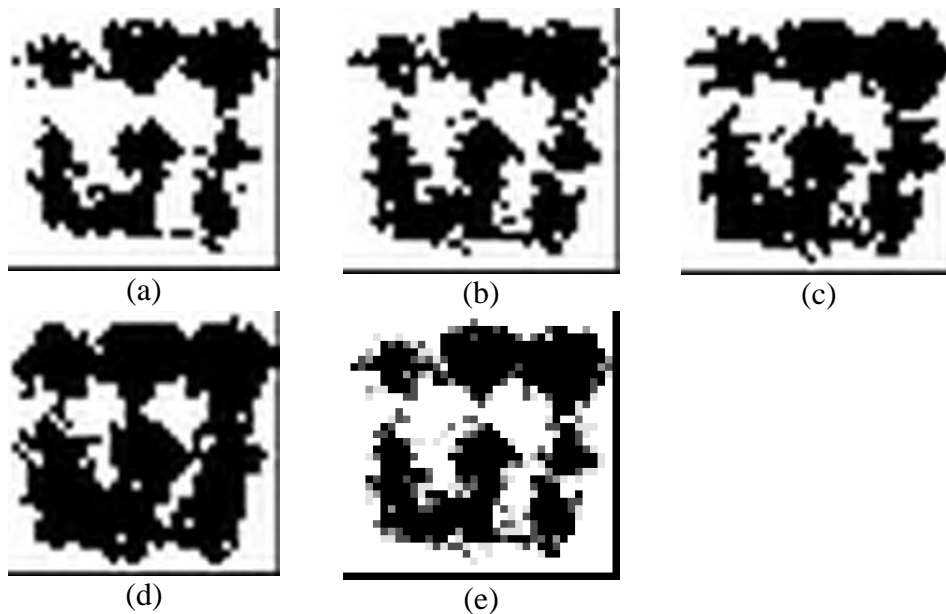


Figure 5: the results of 1 m grid DEM generation derived from the simulated data. (a) –(d) are 50%, 40%, 30% and 20%, respectively. (e) is the subtracted image (R:G:B=50%, 40%, 30%).

4. CONCLUSION

To investigate the effect of moisture on the ground surface for DEM generation, LiDAR simulation was carried out. As the results, DEM generation depended on three parameters which were the sensitivity of sensor, the moisture on the ground surface and the gap size. Moreover, in case of low reflectance on the ground surface, the affected area was edge of crown.

To make laser beam frequently be hit against the ground in forest, the only parameter we can control is measurement condition. In other words, LiDAR measurement should avoid wet condition on the ground in order to get the DEM with high accuracy.

REFERENCES

Endo,T. and Sawada,H. 2010. Development of a LiDAR simulation system for forest, SEISAN KENKYU, 62 (4), 445-448

Multi-temporal study on PM₁₀ distribution for urban air quality in upper Northern of Thailand using spatial technology

Nion SIRIMONGKALERKAL ¹, Vivarad PHONEKEO ²
and NGUYEN Luong Bach ³

¹ PhD candidate, NREM, Fahluang University, Thailand
nion_siri@hotmail.com

² Senior Researcher, GIC, SET, Asian Institute of Technology, Thailand

³ Assistant Professor, NREM, Mae Fahluang University, Thailand

ABSTRACT

Upper northern region of Thailand yearly faces with smoke and haze problem due to open-spaced biomass burning activities related to land use preparation for agriculture of the local people, in particularly in March – April 2007. It is direct negative impact to the health of the people in many cities in the region, as reported by the Ministry of Public Health of Thailand. In order to manage this smoke-and-haze problem, Pollution Control Department (PCD) is monitoring the air quality in the region continuously using the 5 measurement stations. However, these stations can provide the data only in limited area and it is not possible to cover large area. Therefore, to have better understanding the air quality scenario in the region, the authors have conducted air quality monitoring using spatial technology including remote sensing and GIS. In this paper, the authors used MODIS aerosol optical thickness (AOT) product from NASA and PM₁₀ concentration hourly data from PCD measurement stations during 2007 to 2010 for data analysis and generating estimated PM₁₀ concentration distribution maps. The obtained result could be useful guiding information for spatially understanding of the PM₁₀ concentration distribution which would support for public health decision making and urban planning.

Keywords: *urban air quality, aerosol optical thickness, PM₁₀ concentration, MODIS, remote sensing*

1. INTRODUCTION

Smoke haze related to biomass burning is a recurring environmental problem in Southeast Asia which affects air quality not only in the source regions, but also in the surrounding areas. Major episodes of fire and trans-boundary haze pollution occurred in the region during the 1980s and 1990s. The blaze of 1997-1998 which affected Brunei Darussalam, Indonesia, Malaysia, Philippines, Singapore and Thailand, was among the most damaging in recorded history. More than 9 million hectares of land were burnt, 6.5 million of which were forested areas. The damage was estimated

at more than 9 billion US dollar in terms of economic, social and environmental losses, including the release of an estimated 1-2 billion tons of carbon. More recently, trans-boundary haze pollution has also become a serious problem in Cambodia, Lao PDR, Myanmar and Thailand. In northern Thailand, land and forest fires caused the air quality to deteriorate to unhealthy levels during the dry season of 2006 and 2007 (Environment Division of ASEAN Secretariat Haze Online v.2008).

In Upper North Thailand (UNT), smoke haze problem recurs in dry season yearly (February-April) when the level of particulate matter or PM₁₀ in the ambient air is elevated typically by forest fires. Forest fires are found or increase during this season in this region due to dry weather conditions. Additional burnings of agricultural residues to prepare land for next-cycle plantation (in the rainy season) also worsens the problem. UNT borders on East Myanmar, North and East Laos, and is not too distant from South China. Its geography is generally mountainous with north-south-aligned hill ridges parallel from west to east, forming a number of valleys, e.g., Chiang Mai-Lamphun, Chiang Rai, Lampang, Mae Hong Son valleys. This geographical characteristic can also cause the ventilation of air pollutants out of a valley to be difficult. One of the worst air pollution episodes in UNT and Thailand took place in March 2007, during which elevated smoke haze pollution was prolonged for 2-3 consecutive weeks and the 24-hr average ambient PM₁₀ concentration exceeded the national ambient air quality standard for many days (Kasemsan et al, 2009). However the main causes that initiate haze/smoke crisis in the upper northern part of Thailand are forest fires and agricultural residue burning (Kasemsan, 2010). Furthermore, the hot spot occurrence found in the upper northern part of Thailand occurred in forest area 79%, agricultural area 20% and only 1% in urban area. (Ketsisri, 2009).

In term of the impact of smoke and haze distribution to the local people health, the Office of Disease Prevention & Control has reported that the haze/smoke occurred in Northern Thailand has affected a large number of local people health. According to the report in March 17, 2007, the respiratory syndrome patients were increased dramatically. In total, there were 34,769 patients with some patients with acute severe symptom such as 159 heart disease patients, 782 infected eye disease patients and 6 dermatitis patients. The average number of patients admitted for treatment was 1,500 patients a day. Based on these reasons, it is necessary to conduct research on the distribution of the smoke and haze in the study area. Only using the information gathering from the ground air quality measurement stations, sparsely distributed in the study area are not enough to understand the smoke and haze phenomenon, Therefore, it is necessary to apply space technology, in particularly remote sensing and GIS to the study of the distribution of PM₁₀ for better understanding of the phenomenon and to support air quality management in the study area.

2. OBJECTIVES OF THE STUDY

The objectives of the study are listed below

1. To analyze the trend of the aerosol optical thickness (AOT) acquired from Terra/Aqua MODIS and PM₁₀ concentration from 12 PCD air quality ground measurement station in the period of 2007 – 2010 and find out their relationship.
2. To generate estimated PM₁₀ Concentration maps for Upper Northern of Thailand during the period of 2007-2010 based on the obtained relationship.

3. SCOPE OF THE STUDY

The study focus on Upper Northern Thailand, which is our study area, that smoke and haze problem occurs in dry season each year, mainly from February to April, when the level of PM₁₀ concentration raise up due to forest fires and biomass burning related to agricultural activities. In this study, we use MODIS aerosol optical thickness product (MOD04/MYD04) which has spatial resolution of 10x10 km² and PM₁₀ concentration from 12 PCD air quality measurement stations located in many provinces of the study area (Figure 1). Since the main purpose of the study is to study the relationship between MODIS AOT and PCD PM₁₀ concentration distribution, other atmospheric or meteorological parameters such as air temperature, air humidity, wind speed and direction are not considered in this study.

4. STUDY AREA

The study focus on Upper Northern Thailand, covering 8 provinces which are Chiang Mai, Chiang Rai, Mae Hong Son, Nan, Prae, Phayao, Lampang and Lamphun, within the approximated geographic coverage of 20.47° N, 97.37° E and 17.18° N, 101.37° E with approximated area of 159,100 km². The study area also includes partly the area of the neighboring countries (Laos and Myanmar) along the borders with Thailand (Figure 1)

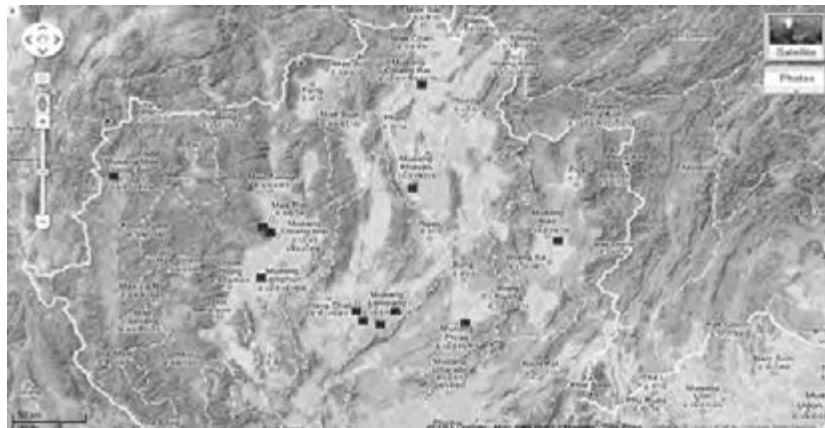


Figure 1: PCD air quality measurement stations in upper northern part of Thailand, marked by red squares.

5. METHODOLOGY

The study on the distribution of the PM_{10} in the Upper Northern Thailand is related to the understanding on the trend and relationship of two main parameters which are aerosol optical thickness acquired by MODIS on board Terra/Aqua and PM_{10} data recorded by 12 PCD air quality measurement stations, therefore, the methodology of this study has two main parts as the following:

5.1 Trends and relationship of MODIS AOT and PCD PM_{10} Concentration Distribution

MODIS AOT product for the duration of 2007 – 2011 was downloaded from NASA website, from which the AOT physical value was extracted at the selected pixels where the 12 PCD stations are located. The hourly PCD PM_{10} data also collected from 12 PCD stations for the same duration. AOT MODIS data which has the same acquiring date and time with the measurement date and time of PM_{10} stations were selected to make yearly and monthly groups of matching pairs. Using these matching pairs, we can generate graphs to observe the trend of the AOT and PM_{10} distribution available within the interested year and month. The relationship of these two datasets can be found by calculating the correlation coefficient and the linear regression equations. Figure 2 shows the dataset of matching pairs for year 2009 and 2010 and for the months of February, March and April of each year, and only February for 2011. The total matching pairs used in this step are 140. In this Figure, the total number of matching pairs available within year 2007-2011 were used to calculate the correlation coefficient and generated linear regression equation. Here the correlation is 0.32 which is not high, due to scattered points that are unusual observations, according to the statistical analysis which need to be investigated. Other

possible reasons related to meteorological and environmental conditions could be also the factors that cause unusual observations.

An additional study the trend of the two parameters is to use the AOT value extracted from the AOT product available within one month at the pixel where a interested measurement station is located to plot a graph to see the its monthly temporal distribution. Similarly, hourly PM_{10} concentration value recorded within a period of the same month at the same measurement station can be used to plot a graph to see observe the trend of its temporal distribution. Figure 3 shows an example of the monthly distribution of AOT concentration detected by MODIS (red graph) within the month of February 2007 at the location of measurement station 'ChiangMai1' in Chiang Mai province, and also the monthly distribution of PM_{10} concentration (blue graph) measured at the same station within the same period.

From visual analysis of these graphs, we found that most of the MODIS AOT and PCD PM_{10} matching pairs have very similar trend, for example, the graphs of February, March and April in year 2007, 2008, 2009 and 2010 for station ChiangMai1, March 2008 for ChiangMai2, March and April 2010 of ChiangMai2, April 2009 and March 2010 of ChiangRai1, February and March 2008 with February and April 2009 of Lampang1, March 2008, February 2009 and March 2010 of Lampang2, April 2010 of Lampang3, March 2010 of Lampang4, April 2010 of Lampoon1, March and April 200, February and March 2010 of Maehongson1 and February and April 2010 of Nan1. However, there are still many graphs of many stations that show different trend of the two parameters, which is possibly related to many environmental and geographical factors that are not taking to considerations in this research.

The correlation coefficients and linear regression equations which we have obtained for each yearly and monthly matching pairs of the AOT and PM_{10} can be also used to have more clear explanation for the trend of these graphs. One another possible reason, for the measurement of the PM_{10} concentration, we assume that the landscape, where the measurement stations are located has influence to the measurement of the PM_{10} , since the wind speed and direction including air humidity can be influent to the measurement. For the case of the MODIS AOT, a pixel with coarse spatial resolution of $10 \times 10 \text{ km}^2$ could give more deviation to the calculated AOT value within the large observed pixel. These factors will be taken to investigation in further study.

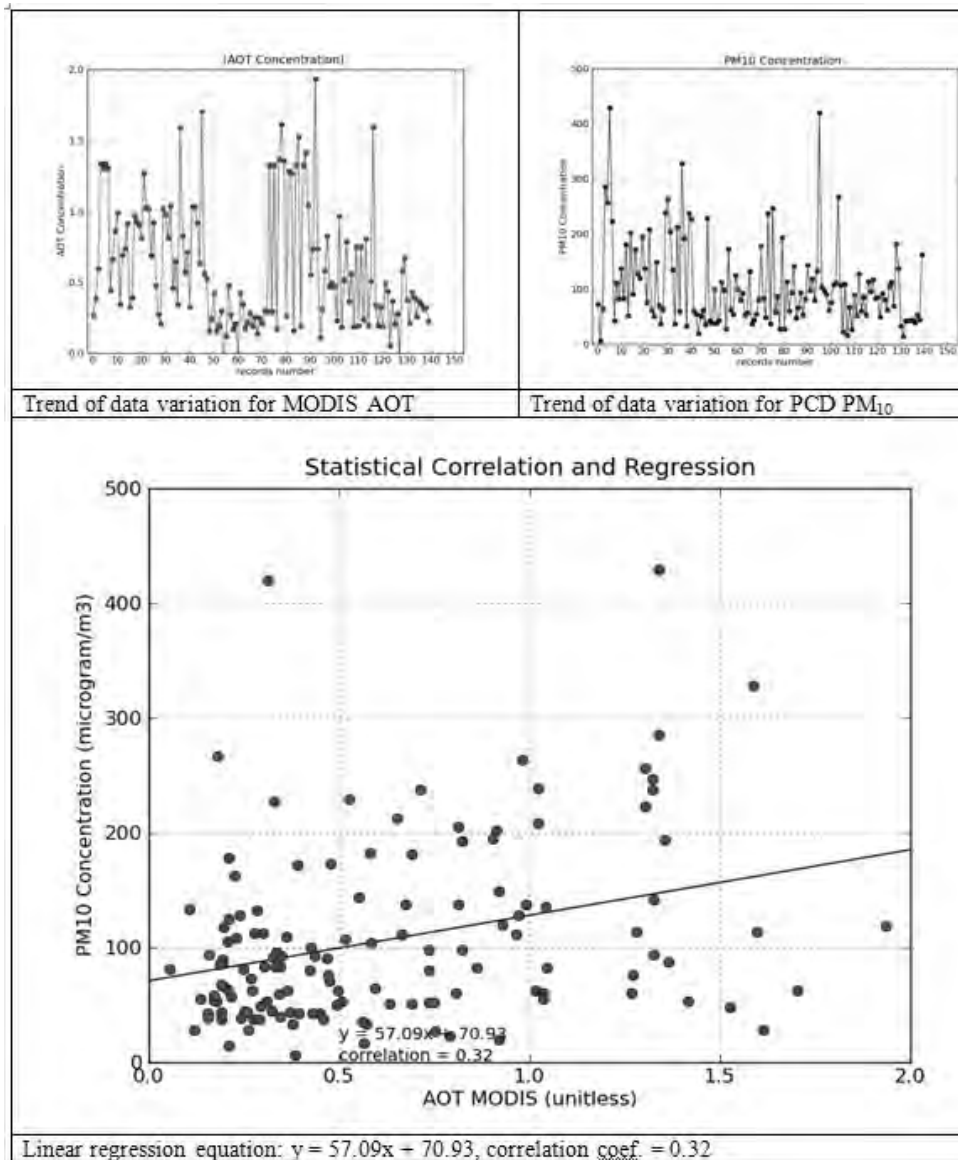


Figure 2: Temporal distribution of MODIS AOT and PM₁₀ concentration within the period years 2007-2011 of 140 matching pairs and its statistical relationship.

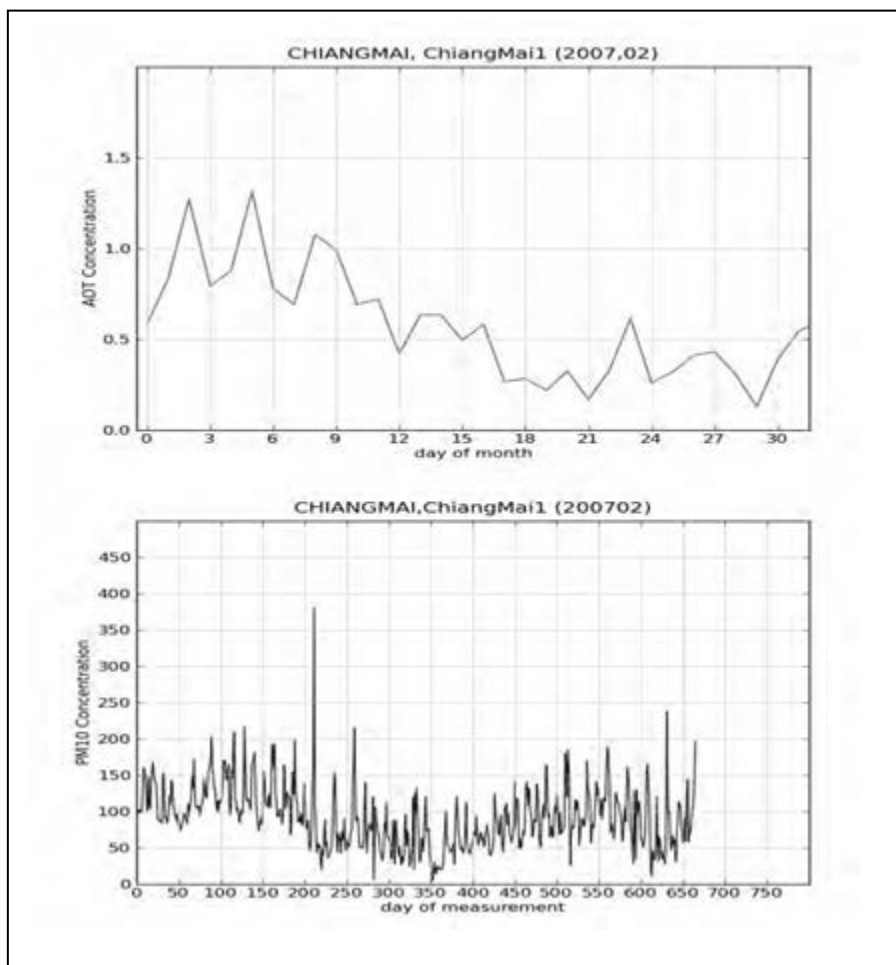


Figure 3: Trend of monthly distribution of MODIS AOT and PM_{10} concentration obtained at the geographic location of station 'ChiangMai' in Chiang Mai province in February 2007

5.2 Generation of Estimated PM_{10} Concentration Maps for Upper Northern of Thailand

In previous section, we have analyzed the trend of yearly and monthly distribution of MODIS AOT and PM_{10} concentration obtained for the location of 12 measurement stations in the study area in the period of 2007 to 2011, and obtained fairly relationship, as the correlation coefficient is 0.32, with the linear regression equation of $y = 57.09x + 70.93$, where, x is AOT value in digital number (DN), it should be multiplied by a scale factor of 0.001 to be AOT physical parameter, and then can be converted to PM_{10} value. We apply this equation to convert AOT to PM_{10} , even though the correlation is fairly small (correlation = 0.32), but since it was generated from the data collected from 12 stations located in the study area within the period of 4 years from 2007 to 2010. Figure 4 shows the quick look image of the MODIS AOT map (top) and the estimated PM_{10} concentration (bottom) generated from the MODIS AOT map for Southeast Asia region.

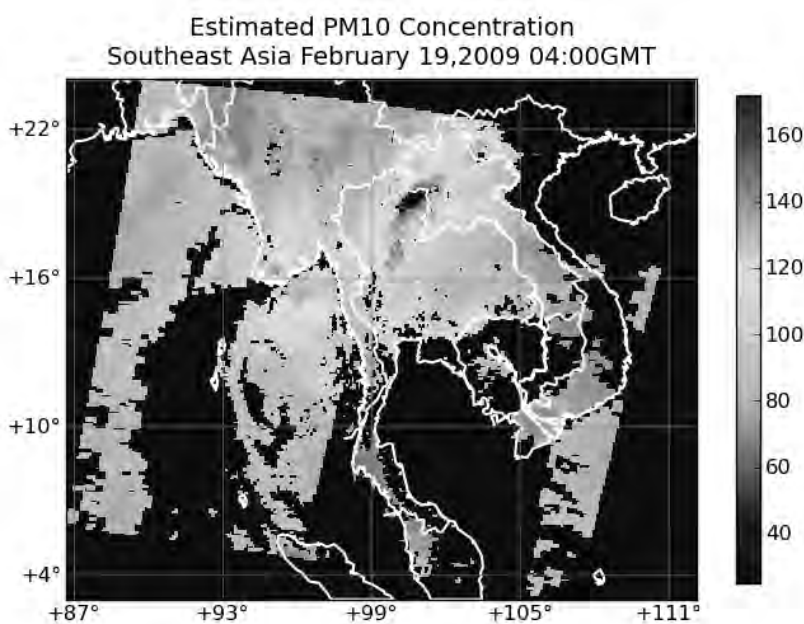
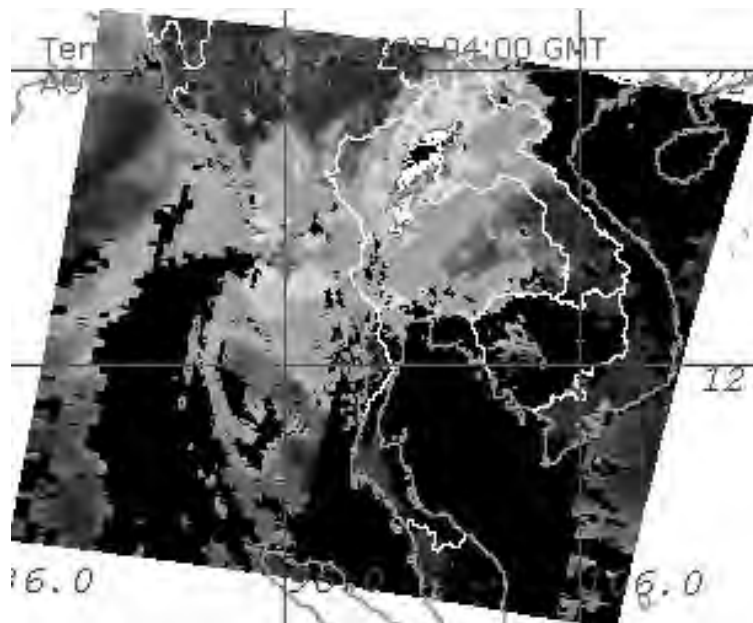


Figure 4: MODIS AOT map of February 19, 2009 04:00 GMT from (top) and the estimated PM₁₀ concentration (bottom) for Southeast Asia region.

6. RESULTS AND DISCUSSION

Figure 5 shows an example of the output of our study which is an estimated PM₁₀ concentration map for Upper Northern Thailand for the date of February 19, 2009 04:00 GMT, which is generated using MODIS AOT of the same date and time. The color bar on the right side show the maximum

(reddish color tone) and minimum (dark blue color tone) estimated PM_{10} value of the PM_{10} image, therefore, the area with reddish color tone has high value of PM_{10} concentration, while the area with dark blue tone is considered to be the area with low value of PM_{10} concentration. The area covered by clouds or out-of-scene area have value of $25 \mu\text{g}/\text{m}^3$ which is marked by the lowest part of the color bar. The white line on the map is the political boundaries. As the original input AOT image has spatial resolution of $10 \times 10\text{km}^2$, therefore, the output estimated PM_{10} also has same spatial resolution which is represented by coarse pixels on the output map. The PM_{10} value obtained by this conversion can be considered as ‘estimated value’ or an appearance of the actual PM_{10} value, which is need to be validated using ground truth data. As this AOT to PM_{10} conversion was done using linear regression equation with low correlation, we can improve it by investigating the unusual observed point in the scatter graph shown in Figure 2, and if it is reasonable to remove it, it would improve the relationship of the datasets and their correlation. In the another hand, the PM_{10} data provided from PCD in this study, do not cover all of the months within the time period and also not cover for all stations. Therefore, it is necessary to have hourly-data cover all months and stations in the year and for long period of many years, to ensure the best result of data statistical analysis. The cloud cover in AOT MODIS images, downloaded from NASA is also one reason that causes data unavailability of AOT value for the image pixel where the ground station is located, therefore, having multi-temporal MODIS AOT data can ensure the availability data within the study period.

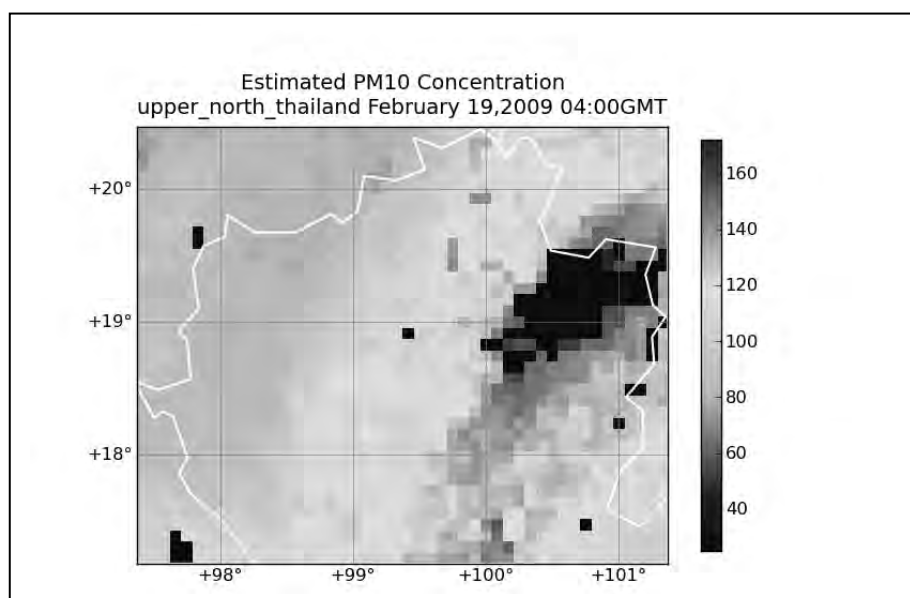


Figure 5: Estimated PM_{10} concentration map for Upper Northern Thailand for February 19, 2009 04:00 GMT

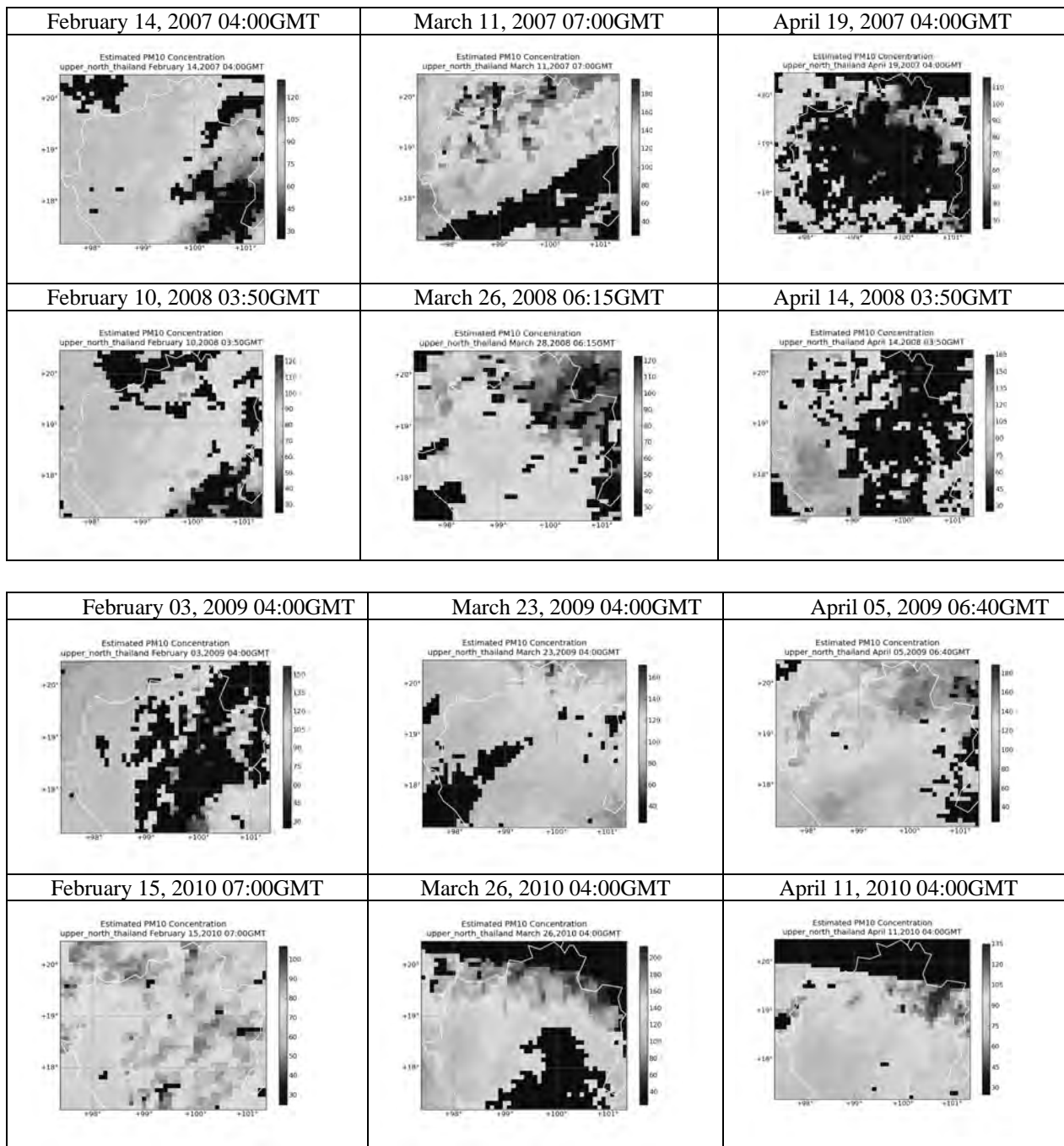


Figure 6: Estimated PM_{10} concentration maps for Upper Northern Thailand of selected dates in February, March and April of 2007 - 2010

6. CONCLUSIONS

Trend of MODIS AOT and PM_{10} concentration from 12 PCD ground measurement station in the period of 2007 – 2010 were studied and their statistical relationship is obtained and the estimated PM_{10} Concentration maps for Upper Northern of Thailand during the period of 2007-2010 based on the obtained relationship were generated.

REFERENCES

Environment Division of ASEAN Secretariat HazeOnline. (2008). Tenth Meeting of the Sub-Regional Ministerial Steering Committee (MSC) on Transboundary Haze Pollution. Retrieved ,<http://haze.asean.org/news/1280390969/>, Last access on April 9, 2010

Kasemsan Manomaiphiboon¹, Petch Pengchai, Vanisa Surapipith, Sarawut hepanondh, Rattapon Onchang, Nuwee Wiwatwattana, Veerachai Tanpipat, & Savitri Garivait. (2009, May). Smoke-Haze Forecast Modeling for Upper North Thailand during March-April 2008. Paper presented at The 3rd International Conference on “Sustainable Energy and Environmet, Bangkok, Thailand.

Ketsiri Leelasakutum. (2009). The Chiang Mai haze episode in march 2007: Cause investigation and exposure assessment. Master research study. Asian Institute of Technology, Bangkok.

Site characteristics estimation of BUET campus by microtremor H/V technique

Mehedi Ahmed Ansary¹ and Md. Saidur Rahman²

¹Professor, Department of Civil Engineering,
BUET, Dhaka, Bangladesh
ansary@ce.buet.ac.bd

²Research Engineer, BNUS, BUET, Bangladesh,
srahman.ce.71@gmail.com

ABSTRACT

Degree of damage during earthquakes strongly depends on dynamic characteristics of buildings as well as amplification of seismic waves. Among the other approaches, microtremor is the easiest and cheapest way to understand the dynamic characteristics of soil as well as structural element. The purpose of this research is to apply H/V Microtremor Technique for Site Response Analysis at Bangladesh University of Engineering and Technology (BUET) campus. Microtremor measurements have been carried out in one hundred and thirty two selected locations in free-field and forty five buildings within BUET campus. The amplitude ratio (H/V) of horizontal to vertical spectra has been used to estimate predominant frequency and amplification.

For spectral analysis three low noise to signal ratio segments of 20.48s of the recordings have been taken at 100 Hz instrumental sampling. Fast Fourier Transformation (FFT) has been applied on the time domain records. Then, spectral ratio (H/V) technique has been applied. The resultant of two horizontal components of H/V ratio have been digitally filtered using suitable average smoothing point. After calculating three sets of the H/V ratios at selected location, the mean H/V ratio has been plotted with half standard deviation in order to assess the deviation of microtremor data at different time instants.

From analysis of data it can be said that Horizontal to Vertical spectral (H/V) ratio provides stable data to estimate predominant frequency and amplification of soil without source effect. Fourier Spectrum along East-West and North-South provides better result to estimate predominant frequency at building. Out of 132 sites, the overall mean predominant frequency and mean peak H/V ratio are 1.39 Hz and 2.09. The predominant frequency for most of the locations lies between 1.0 Hz and 1.99 Hz. Four buildings have been identified as vulnerable due to resonance criteria within BUET campus. Most of the buildings predominant frequency is not close to the predominant frequency of site soil.

Keywords: *Fast Fourier Transformation, microtremor H/V ratio, predominant frequency, resonance criteria*

1. INTRODUCTION

In the recent past, Bangladesh has not suffered any damaging large earthquakes, but in the past few hundred years, several large catastrophic earthquakes struck this area. So far, all the major recent earthquakes have occurred away from major cities and have affected relatively sparsely populated areas. In 1897, an earthquake of magnitude 8.7 caused serious damages to buildings in the northeastern part of India (including Bangladesh) and 1542 people were killed. Recently, Bilham et al. (2001) pointed out that there is high possibility that a huge earthquake will occur around the Himalayan region based on the difference between energy accumulation in this region and historical earthquake occurrence. The population increase around this region is at least 50 times than the population of 1897 and city like Dhaka has population exceeding several millions. It is a cause for great concern that the next great earthquake may occur in this region at any time.

The use of microtremor, an idea pioneered by Kanai et al. (1954) turns into one of the most appealing approaches in the site effects studies, due to its relatively low economic cost and the possibility of recordings without strict spatial or time restrictions (Rodriguez and Midorikawa, 2002). The H/V spectral ratio technique of microtremors gained popularity in the early nineties, after the publication of several papers (Nakamura, 1989; Lermo and Chávez-García, 1994) claiming the ability of this technique to estimate the site response of soft sedimentary deposits satisfactorily. This method is rather attractive in developing countries characterized by a moderate seismicity, where only very limited resources are available for seismic hazard studies. The H/V spectral ratio determined from microtremors has shown a clear peak that is well correlated with the fundamental resonance frequency at “soft” soil sites (Bard, 2004; Horike et al., 2001; Field et al., 1995; Lachet and Bard, 1994; Lermo and Chávez-García, 1993). Comparison of microtremor and earthquake spectral ratios at strong-motion instrument sites across SW British Columbia showed similar fundamental periods and in greater Victoria remarkably similar amplitudes, validating the use of the method for linear earthquake site response Molnar et al. (2007).

Ohmachi et al. (1991) and Lermo and Chávez-García (1994) applied the H/V ratio method to analyze microtremor measurements. Lermo and Chávez-García (1993) used it to assess the empirical function of the S-wave, part of an earthquake record, obtained from three cities in Mexico. Their results clearly indicated that the H/V ratio could provide a robust estimate of frequency and amplitude of the first resonant mode, albeit not of the higher modes. In the meantime, Field et al. (1995) considered the response of sedimentary layers to ambient seismic noise and claimed that the H/V ratio method has been an effective and reliable tool to identify the fundamental resonance frequencies of all layered sedimentary basin. Further evidence

has been given by Suzuki et al. (1995) who used both microtremor and strong-motion data in Hokkaido, Japan and ascertained that the peak frequency determined by the H/V ratio seemed to correspond with the predominant frequency estimated from the thickness of an alluvial layer. Based on numerical calculations, many other researchers (Lermo and Chávez-García, 1993, 1994; Lachet and Bard, 1994; Dravinski et al., 1996) have shown that the H/V ratio method is obviously able to predict fundamental resonant frequency well. Huang et al. (2002) found that the ground vulnerability index (K_g) values in the liquefied areas have been higher than those in the neighboring areas without liquefaction at 42 points in central Taiwan. This study shows supporting evidence for the first time that the H/V ratios of microtremor can be a good alternative indicator for an area's potential for liquefaction. Site amplification characteristics can be evaluated by one-point two-component surface recordings of earthquake ground motion, in a similar manner as proposed by Nakamura for microtremor (Ansary et al., 1996).

For this research microtremor observation has been carried out at one hundred and thirty two selected locations in free-field and forty five buildings within BUET campus. Although it is not possible to prevent such calamities, it is however, possible to mitigate the impacts of earthquake. Specific roles and responsibilities relating to earthquake hazard should be emphasized in our disaster mitigation plan. The objective of this thesis is to analyze seismic hazard of BUET campus in terms of dynamic characteristics of soil (Predominant frequency and Amplification) and resonance criteria.

2. MICROTREMOR STUDY AND SITE SELECTION

Microtremor consists of different types of waves producing in soil from various sources. The common noise sources are vibrating machine, traffic, environment and human movement. Microtremor observation is carried out to record time history of noise data. Horizontal to Vertical (H/V) Fourier spectral ratio technique is applied to assess the vulnerability of soil and building. To check the stability of microtremor observation fourteen locations of West Palashi within BUET campus has been selected. After checking the stability of microtremor data, microtremor observation has been carried out at one hundred and eighteen additional locations in soils and 45 buildings within the BUET campus (See Figure 1).

3. OUTLINE OF METHODOLOGY

The amplitude ratio (H/V) of horizontal to vertical spectra of microtremor has become popular to determine predominant period and amplification of a site. It is well known that, degree of damage during earthquakes strongly depends on dynamic characteristics of buildings as well as amplification of seismic waves. Among the other time consuming and expensive approaches,

microtremor is the easiest and cheapest way to understand the dynamic characteristics of soil as well as structural element. In a short period of time it provides several information including natural frequency, amplification and vibration characteristics of soil and structure at different frequencies. Following steps have been followed in this research:

A. Microtremor Analysis:

Microtremor observation has been carried out in selected locations within BUET campus of Dhaka city. Each record comprises of three components, viz., EW, NS and UD. For spectral analysis three noise-free segments of 20.48s of the recordings have been taken at 100 Hz instrumental sampling. At each point of sensor location microtremor data recording have been carried out at different time of the day. Time domain data is not suitable for the clear identification of soil response due to ambient noise. This is why First Fourier Transformation (FFT) has been applied on the time domain records. After smoothing the corresponding spectra, spectral ratio (H/V) technique have been applied to derive transfer functions. The applied sequences are given below:

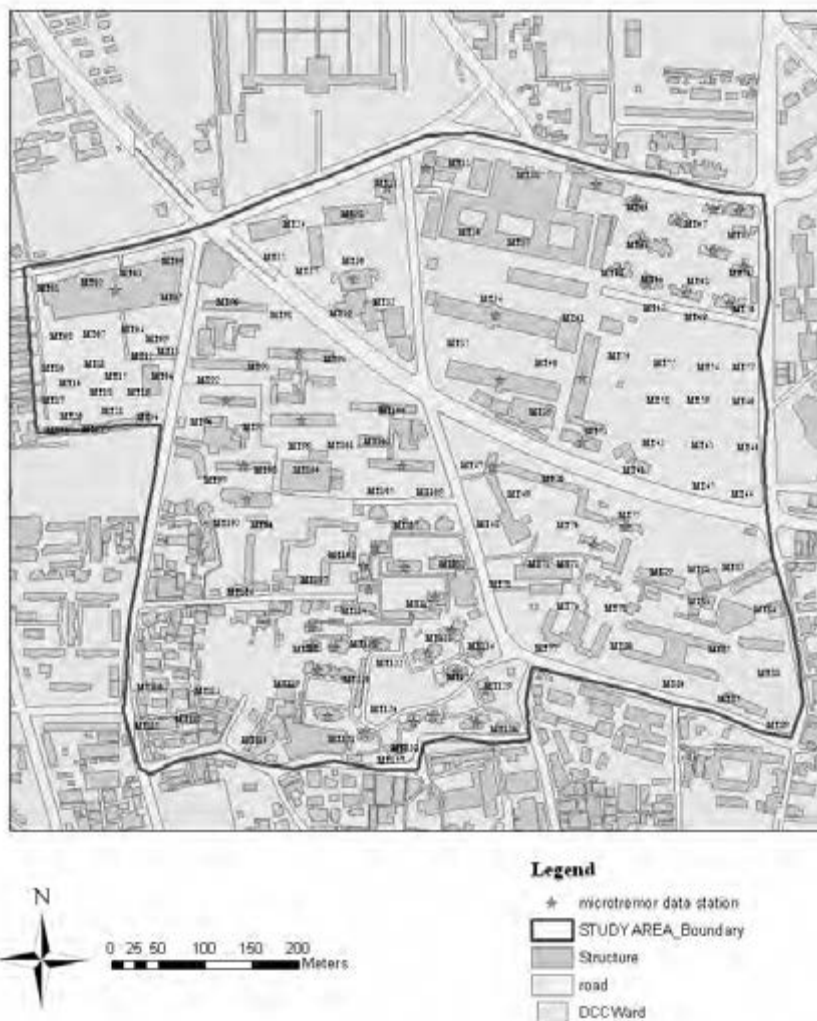


Figure 1: One hundred and thirty two microtremor observation points in site soil and forty five points in various building of BUET campus

I. FFT Transformation:

At first, Fourier spectra of the two horizontal directions (East-West and North-South) and the vertical component (Up-Down) have been calculated.

II. Smoothing of the Spectra:

After Fast Fourier transformation (FFT), the combined horizontal and vertical spectra have been digitally filtered applying a logarithmic window with a suitable bandwidth coefficient. These filtering techniques have been applied to reduce the distortion of peak amplitudes.

III. Calculation of the Soil Response functions:

The smoothed combined horizontal spectrum have been divided with the smoothed vertical component to plot Horizontal to vertical spectral ratio (H/V) which will provide the desired predominant frequency and corresponding amplification factor of the investigated portions (20.48 s) of records.

IV. Estimation of Predominant Frequency and Amplification:

After calculating three sets of the H/V ratios at selected grid, they have been normalized to obtain a relatively non-biased site specific H/V ratio. Then, Normalized H/V ratios at different time of the day have been plotted in Logarithmic window. From this normalized H/V ratio the predominant frequency and corresponding amplification factor of this site have been taken.

4. MICROTREMOR DATA COLLECTION AND ANALYSIS

Microtremor measurement was carried out in 132 selected locations (Figure 1) within BUET campus. In BUET campus, 240 second duration were recorded at different times in the specific locations. The measurements have been carried out from morning to midnight in order to minimize artificial noises due to traffic and human activities. The microtremor measurement apparatus for data recording includes Geodas 15-HS equipment (Data logger and Laptop), Sensor, Cable, Battery and GPS. Mtobs.exe software is used to record microtremor data. Sensors comprise three components, which can record the horizontal motion (in Latitude and Longitude directions) and the vertical motions (up and down). Microtremor sensor sensitivity was 295900 $\mu\text{m}/\text{sec}/\text{V}$. The converting speed was 50 kHz. The sampling frequency was 100 Hz. The amplification factor was used 20 db in observation system.

Figure 2 shows a typical time history field data recording of MT132 at 1:52 AM on 12 February, 2011. The content of all input data are 2 CR4.5-1S velocity type sensors, 24000 observation data length, 100Hz sampling frequency, 0.05 Hz Low-pass filter and 20db amplification ratio. Time history data is not suitable to estimate the dynamic properties (predominant frequency and amplification ratio). So, transformation of time domain data

to frequency domain data is required with Fourier Transformation. Therefore, Fast Fourier Transformation (FFT) has been used to transfer time domain data to frequency domain data.

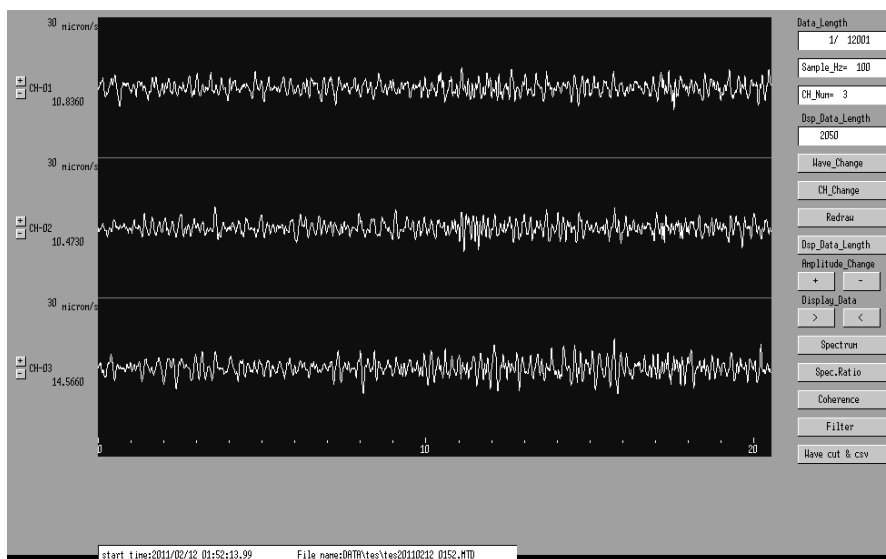


Figure 2: Time history free-field data recording at MT132 of BUET campus.

5. STABILITY OF MICROTREMOR DATA

Microtremor is the combination of shear wave, Rayleigh wave and Love wave. The effect of different waves on microtremor data is significant. Therefore, stability check of microtremor data is important to estimate dynamic properties of any site soil. To carry out this research velocity time history data have been recorded time ranging between morning to midnight at 14 locations in West Palashi, BUET. The observation microtremor data recording varies from 5 to 20 minutes. Ten minutes observation time has been taken in most of the observation points. Three segments of 20.48 s time domain data have been used to transform frequency domain spectrum. In order to get low noise data these Fourier spectra have been filtered using rectangular windows. The mean of these three segments of frequency domain data have been calculated using smoothing function with average smoothing point 5. From these observations, stability of time variation microtremor data has been compared from Fourier spectrum. The horizontal to vertical spectral ratio has also been calculated in these locations to analyze the stability of H/V ratio with Fourier spectrum.

Instead of using all the observed time records, three to four different times instants are selected from 24 hour observation for fourteen sites, for investigation. Figure 3 shows the vertical and horizontal Fourier spectra of microtremors observed at MT05. The mean peak value of Fourier spectra varies from 2.1 Hz to 3.1 Hz for both the horizontal and vertical motions. Figure 3 also illustrates three time instants (13:07 PM, 16:20 PM and 01:06 AM) and their mean value. From the Fourier spectra analysis of 14 sites, it can be said that the amplitude level of Fourier spectra vary at different time

instants of a day. It is not possible to estimate the dynamic characteristics (Predominant frequency and Amplification) of these sites on the basis of the amplitude level of Fourier spectra.

The Horizontal to Vertical spectral ratio along EW and NS directions are shown in Figure 4 for three different time instants (13:07 PM, 16:20 PM and 01:06 AM) at MTO5. The characteristics of the peak frequency of the amplitude ratios are different from those for Fourier spectra. The predominant frequency of two horizontal directions at MT05 is around 0.77. Although the Fourier spectra are not stable with time, the amplitude ratios at different time instants along three directions within a day are stable at these sites. From analysis of Fourier spectra ratio, it can be concluded that the change of amplitude ratio at different time instants of a day is comparatively small. In addition to this, the amplitude ratio is less influenced by the source of vibration than the Fourier spectrum of any direction and may reflect the particular characteristics of the site. Therefore, the Horizontal to Vertical spectra ratio has been found more reliable to estimate dynamic properties (Predominant frequency and Amplification) of any particular soil.

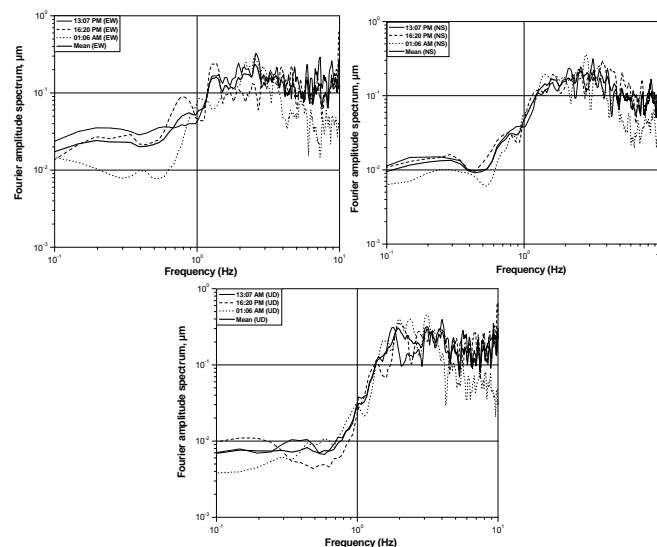


Figure 3: Stability of Fourier Spectrum at different times along EW, NS and UD directions at MTO5

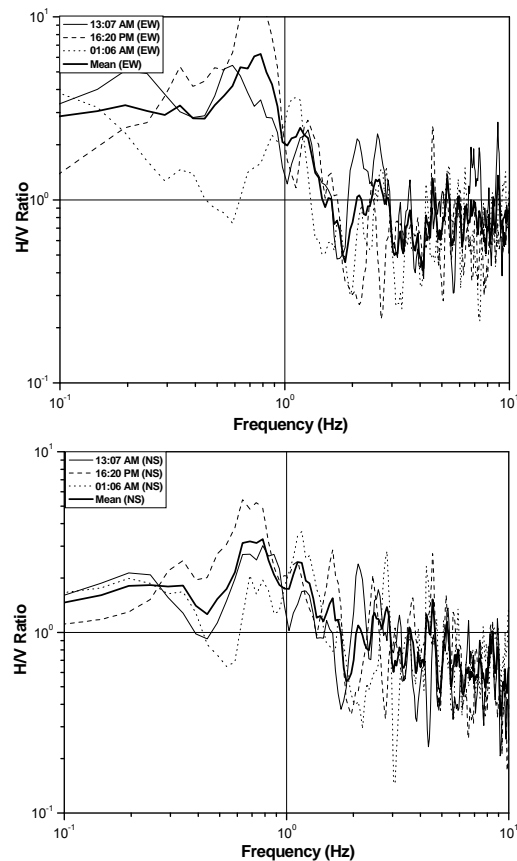


Figure 4: Stability of H/V ratio data at different times along EW and NS direction at MT05.

6. ANALYSIS RESULTS AND DISCUSSION

The BUET campus is situated in latitude ranging from 23°43'16.58" N to 23°43'59.44" N and longitude from 90°23'13.31"E to 90°23'43.56" E. Microtremor observation at 132 selected points in soils and 45 locations in building have been carried out in BUET campus. The analysis results of these points have been discussed in Section 6.1 and 6.2.

6.1 Soil sites

Figure 1 shows the observed microtremor locations at 132 selected locations. Out of 132 sites, the overall predominant frequency is 1.39 Hz where as standard deviation is 0.289. On the other hand, the overall peak H/V ratio is 2.09 where as standard deviation is 0.523.

Out of 132 microtremor observation locations, the maximum predominant frequency is around 9.62 Hz where as H/V ratio is 2.43 at MT82. Horizontal to Vertical spectral ratio (H/V) varies from 1.65 to 2.51. On the other hand, the minimum predominant frequency is around 0.25 Hz where as H/V ratio is 9.51 at MT72. This is the highest peak of H/V ratio in 132 selected locations in BUET campus.

The predominant frequency of 132 locations has also been classified into five types. Type I (0 – 0.49), Type II (0.50 – 0.99), Type III (1.0 – 1.99), Type IV (2.0 – 2.99) and Type V (> 3.00). From this classification of predominant frequency, it can be said that most of the locations predominant frequency lies between 1.0 Hz and 1.99 Hz. These predominant frequencies are classified as Type III. The second most common type of predominant frequency is Type II. The number of locations predominant frequency classified as Type V is 21. In addition to this, there are sixteen Type I locations.

On the other hand, Horizontal to Vertical spectral ratio (H/V) has been classified into four types. Type I (0 - 0.99), Type II (1.0 - 1.99), Type III (2.0 - 2.99) and Type IV (>3.0). According to classification of H/V ratio, most of the selected locations are classified as Type III. There are seventy five Type III locations. Type II is the second most predominant H/V ratio. There is no H/V ratio ranging between 0 and 0.99. The number of locations H/V ratio greater than 3 is 15.

6.2 Building sites

Microtremor observations at 45 residential and academic buildings of BUET campus are shown in Figure 1. The Horizontal to Vertical spectra ratio at building does not provide reliable dynamic characteristics. In that case Fourier Spectrum provides better result of predominant frequency at building. Out of 45 microtremor observation in buildings, the maximum predominant frequency is 5.56 Hz along both EW and NS directions in MTB10 at Controller of Examination Building. This is a four-storied frame structure building with 324sqm floor area. There are no lift and shear wall in this building. The foundation of the building is individual footing. There are no structural irregularities in building. But torsional irregularity, re-entrant corner and diaphragm discontinuity exist. The minimum predominant frequency is 2.00 Hz along EW and NS directions at MTB02 at the Eleven Story Tower Building. This is an eleven-storied frame structure with 673sqm floor area. There are three lift cores and a shear wall in the building. The foundation of the building is pile-raft system. No structural irregularity exists in this building. But torsional irregularity, re-entrant corner and diaphragm discontinuity exist.

7. DAMAGE ASSESSMENT

Earthquake vulnerability of the 45 buildings within BUET campus is carried out from predominant frequency obtained by the analysis of microtremor data. Microtremor observation has been carried out at 132 selected free-field locations within BUET campus. The Horizontal to Vertical spectra ratio (H/V) of these locations have been compared with the predominant frequency of building along EW and NS direction, respectively. The occurrence of resonance between building and soil has been discussed in section 7.1. The damage assessment of consolidated soil using Nakamura's Seismic Vulnerability Index (Kg) has been described in section 7.2.

7.1 Resonance between site soils and buildings

The resonance criteria of building and soil can be explained using the following simple relation:

$$\text{Resonance criteria, } \beta_R = \frac{f_B}{f_s} \quad (1)$$

Where, β_R = Coefficient for resonance occurrence, f_B = Predominant frequency of building and f_s = Predominant frequency of soil.

In equation (1), if β_R becomes close to 1 (1 ± 0.20), resonance may occur. The resonance between buildings and soil has been analyzed using this resonance criterion, β_R , in both EW and NS directions. Four buildings have been found as vulnerable due to resonance occurrence. These buildings are Eleven Story Tower Building, URP Building, Titumir Hall and Building # 1.

7.2 Seismic damage assessment of soils using Nakamura's technique

Seismic vulnerability index (Kg) is an index indicating the level of vulnerability of a layer of soil to deform. Therefore, this index is useful for the detection of areas that are weak zone (unconsolidated sediment) at the time of occurrence of earthquakes. Some studies like Daryono (2009) and Nakamura (2000) showed a good correlation between seismic vulnerability index (Kg) and the distribution of earthquake disaster damage. This index is obtained from the peak value of HVSR squared, divided by the value of the predominant frequency. From the analysis at 132 locations, the overall mean Vulnerability Index (Kg) is 1.77 whereas standard deviation is 3.51. The Vulnerability Index (Kg) value lies between 0.52 and 9.51. The maximum Kg value is 9.51 at MT-72. On the other hand, the minimum Kg value is 0.52 at MT-09.

8. CONCLUDING REMARKS

From the overall result and analysis of the study following findings may be summarized.

(a) Stability of microtremor data on ground:

Fourier spectra depend on the source of vibration. This data does not show significant site amplification. That's why horizontal to vertical spectral ratio (H/V) of both East-West and North-South have been calculated. Microtremor H/V ratio do not show the source vibration effect. Whatever the source is, the amplification result is similar for different time instants. From this research, it can be concluded that Horizontal to Vertical spectral (H/V) ratio of microtremor is effective for site response analysis. This technique is reliable for site soil response compared to Fourier spectra.

(b) Microtremor observation within BUET Campus:

Microtremor observation at 132 selected points in soil has been carried out in BUET campus. Out of 132 locations, the overall predominant frequency is 1.39 Hz. On the other hand, the overall peak H/V ratio is 2.09 where as standard deviation is 0.523. The maximum predominant frequency is around 9.62 Hz MT82. On the other hand, the minimum predominant frequency is around 0.25 Hz at MT-72. This lower predominant frequency and higher amplification ratio show that this location is highly susceptible due to any seismic hazard. The minimum Horizontal to Vertical spectral ratio (H/V) is 1.24 at MT 108. From this classification of predominant frequency, it can be said that most of the locations predominant frequency ranging between 1.0 Hz and 1.99 Hz. There is no H/V ratio ranging between 0 and 0.99. The number of location H/V ratio greater than 3 is 15.

Microtremor observation on 45 buildings has been carried out within BUET campus. Fourier Spectrum provides better result of predominant frequency for buildings. Out of 45 microtremor observation in buildings, the maximum predominant frequency is 5.56 Hz along both EW and NS directions at Controller of Examination Building. The minimum predominant frequency is 2.00 Hz along EW and NS directions at Eleven Story Tower Building.

(c) Resonance between site soil and building:

The resonance between the site soil and building has been analyzed using the H/V ratio of soil and Fourier spectra of building in both EW and NS direction. It has been found that resonance may occur at four BUET buildings. These buildings are Eleven Story Tower Building, URP Building, Titumir Hall and Building # 1. For most of the building predominant frequency is not close to the predominant frequency of soil. From the sub-soil characteristics within BUET campus, it can be concluded that stiff soil with higher SPT value exists in most of the investigated locations.

(d) Seismic Vulnerability Index (Kg) for soils:

From the analysis at 132 locations, the overall mean Vulnerability Index (Kg) is 1.77 whereas standard deviation is 3.51. The Vulnerability Index (Kg) value lies between 0.52 and 9.51. The maximum Kg value is 9.51 at MT-72. On the other hand, the minimum Kg value is 0.52 at MT-09.

REFERENCES

Ansary, M. A., Yamazaki, F. and Katayama, T., 1996. Application of microtremor measurements to the estimation of site amplification characteristics, Bulletin of Earthquake Resistant Structure Research Center, IIS, University of Tokyo, No. 29, PP. 95-113.

Bard, P. Y., 2004. Effects of surface geology on ground motion: Recent results and remaining issues, Proceedings of the 10th European Conference on Earthquake Engineering, Vienna, Austria, August 28 – September 2, 1994, 305-325.

Bilham, R., Gaur, V. K. and Molnar, P., 2001. Himalayan Seismic Hazard, SCIENCE, 293.

Daryono, 2009. Efek Tapek Lokal (Local site effect) di Graben Bantul Berdasarkan Pengukuran Mikrotremor. International Conference Earth Science and Technology. Yogyakarta.

Dravinski, M., Ding, G. and Wen, K. L., 1996. Analysis of spectral ratios for estimating ground motion in deep basins, Bull. Seism. Soc. Am., 86, 843-847.

Field, E. H., Clement, A. C., Jacob, K. H., Aharonian, V., Hough, S. E., Friberg, P. A., Babaian, T. O., Karapetian, S. S., Hovanessian, S. M. and Abramian, H. A., 1995. Earthquake site response study in Giumri (Formerly Leninakan), Armenian using ambient noise observation. Bull. Seism. Soc. Am., 85, 349-353.

Horike, M., Zhao, B. and Kawase, H., 2001. Comparison of site response characteristics inferred from microtremors and earthquake shear waves, Bulletin of the Seismological Society of America, 91, 1526-1536.

Huang, H. C. and Tseng, Y. S., 2002. *Characteristics of soil liquefaction using H/V of microtremors in Yuan-Lin area, Taiwan*, TAO, Vol.13, No.3, 325-338, September, 2002.

Kanai, K., Tanaka, T. and Osada, K., 1954. Measurements of Microtremors 1. Bulletin Earthquake Research Institute, Tokyo University, 32, 199-210.

Lachet, C. and Bard, P. Y., 1994. *Numerical and theoretical investigations on the possibilities and limitations of Nakamura's technique*, Journal of the Physics of the Earth, 42, 377-397.

Lermo, J. and Chavez-García, F. J., 1993. Site effect evaluation using spectral ratios with only one station, Bull. Seism. Soc. Am., 83, 1574-1594.

Lermo, J. and Chavez-Garcia, F. J. (1994). Are Microtremors Useful in Site Response Evaluation? Bulletin of Seismological Society of America, 84, 1350-1364.

Molnar, S., Cassidy, J. F. Monahan, P. A. and Dosso, S. E., 2007. Comparison of geophysical methods to determine shear-wave velocity, Proceedings of the Canadian Conference on Earthquake Engineering, June 24-27th 2007, Ottawa, ON, Paper 1173.

Nakamura, Y., 1989. A Method for Dynamic Characteristics of Sub-surface Using Microtremors on the Ground Surface, Quick Report of Railway Technical Research Institute, 30, No. 1, 25-33 (in Japanese).

Ohmachi, T., Nakamura, Y. and Toshinawa, T., 1991. Ground motion characteristics in the San Francisco Bay area detected by microtremor measurements, Proc. 2nd International Conference on Recent Advances in Geotech. Earth. Eng. & Soil Dyn. Saint Louis, Missouri, 11-15

Rahman, M. S., 2011. Applicability of H/V Microtremor Technique for Site Response Analysis in Dhaka city, Masters of Science Thesis, Department of Civil Engineering, Bangladesh University of Engineering and Technology.

Rodriguez, V. S. H. and Midorikawa, S., 2002. Applicability of the H/V Spectral Ratio of Microtremors in Assessing Site Effects on Seismic Motion, Earthquake Engineering and Structural Dynamics, 31, 261-279.

Suzuki, T., Adachi, Y. and Tanaka, M., 1995. Application of Microtremor measurements to the estimation of earthquake ground motions in the Kushiro city during the Kushiro-Oki earthquake of 15 January 1993, Earthquake Eng. Struc. Dyn. 24, 595-613

Passporting of buildings, its safety and quality in Ulaanbaatar city, Mongolia

Enebish NINJARAV¹, Mendbayar OYUNCHIMEG²,
Yasuoshi ICHIHASHI³ and Danzan DAMIRAN⁴

¹ Vice director, Associate professor,
School of Civil Engineering and Architecture,
Mongolian University of Science and Technology (MUST), Mongolia
ninjarave@gmail.com
ninj@must.edu.mn

² Associate professor, School of Civil Engineering and Architecture,
Mongolian University of Science and Technology (MUST), Mongolia

³ Visiting Professor, ICUS, University of Tokyo, Japan

⁴ Associate professor, School of Civil Engineering and Architecture,
Mongolian University of Science and Technology (MUST), Mongolia

ABSTRACT

Researching and preventing from sudden natural disasters and earthquakes is one of the most important issues, as half of the population lives in Ulaanbaatar, the capital city. In Mongolia, most of the buildings built before 1970 year was not checked for the stability, safety and rigidity during earthquake. Due to these, in 1998 year there was released a government decision to issue the buildings a passport or a special document that shows the quality and all of the related information about it. Furthermore, there was done a project, whose aim was to register and check the building quality, moreover prevent it from sudden destructions and damages; and renew or reconstruct buildings not satisfying the meeting requirements. In Ulaanbaatar, we need several additional projects to be fulfilled including to continue register all of the existing and newly constructed buildings and make some research on risk of how the earthquake will affect and what kind of damages it can cause on buildings.

Recently, most of the apartments in nine districts of Ulaanbaatar were checked and classified for the rigidity and stability during earthquake.

Keywords: *passporting of buildings, safety, earthquake, building quality, destruction, damage, register*

1. INTRODUCTION

Objective of the experiment and research:

As a result of industrialization, climate change and global warming, natural disaster occurs so often that we have to protect and take some prevention before irreversible damage of buildings, bridges and all of the

facilities people use. Earthquake is one of common types of disaster that can occur in Mongolia, therefore we have conducted a research on 20 buildings in Ulaanbaatar and in other provinces that were built in 1950-1960 years and are not resistive to earthquakes of more than 7 Richter scales. The objective of our research is to determine buildings not satisfying the Mongolian standards, and to take some reconstruction and preventions on these buildings.

According to their resisting properties to earthquake and its quality, the buildings were divided into 3 main categories including high risky, risky and low risky to the earthquake. The figure of the building, located in Songino-Khairhan district, belonging to the most risky category is shown below. As an example, all of the calculations and research result will be shown on Songino-Khairkan district building.



Figure 1: Map of Songino-Khairkhan district



Figure 2: Apartment-4 of Songino-Khairkhan district

2. THE GENERAL CHARACTERISTICS OF THE BUILDING

Songino-Khairkhan district building has 12 floors and it was built at the end of 1980s. After some years of use, cracks, deformations and some detrition appeared in the walls of the building and it was classified to high risk building, because of its location in the zone of earthquake of Richter scale 8. In this and in other 20 buildings, some of the main structures were modified or destroyed by the owners without consulting the specialists of construction and engineering, which may cause some difficulties and deteriorates the quality of the building.

2.1 The methods and equipments used in experiments and research

In order to research and determine the exact condition of Songino-Khairkhan district building, we analyzed and tested the properties such as vibrational resistivity, physical detrition, deformation, rigidity and

resistivity of construction materials and its mechanical and physical properties.

To test the properties above, the following equipments were used:

- “DIGI-SCHMIDT 2000”, concrete test hammer performing rapid non-destructive quality testing
- “SilverSchmidt”, the concrete test hammer
- “Profometer-5”, device indicating location and orientation of reinforcing bars
- “Canin”, corrosion analyzing instrument
- “Pundit Lab”, ultrasonic concrete test
- “GSR-24”, apparatus for measuring microvibration
- “SOUTH ML-421”, electronic device for measuring the deformation



Figure 3: GSR-24 is being placed outside of the building



Figure 4: Profometer-5 indicating reinforcing bars

3. RESEARCH PROCEDURES:

Vibration measurements and research

The center for Geophysics and Astronomy of Mongolia conducted a research on earthquake magnitude measurements that can occur in Ulaanbaatar city. According to their research work, the strongest possible earthquake in Ulaanbaatar city is about 6.5 magnitude and the degree of possible damage and destruction were determined. (Recent earthquakes and related measurements with it are shown in table3.) The nearest activation of earthquake to Ulaanbaatar city is in Gavjin shand and Songino-Sonsgolon, that are located in the west of Ulaanbaatar city. Although it is not known when the earthquake will occur, it is obvious that it has high occurrence possibility, so in order to prevent damages and destructions, we have to be prepared.

Table-3. Recent earthquakes that were near Ulaanbaatar city

Date	Occurred time	Geographic location		MS	Distance from UB, km	Place name
		Latitude	Longitude			
09.29.1987	10:04:18.8	47.96	106.93	3.5	6	Ulaanbaatar
11.17.1987	13:24:12.2	47.88	106.95	2.8	6	Ulaanbaatar
09.25.1989	01:55:45.9	49.33	104.47	4.1	236	Burengiin Nuruu, Khentii province
02.24.1991	10:22:17.1	47.70	108.92	4.2	154	Baganuur
02.27.1998	05:22:25.8	49.34	107.89	4.1	174	Selenge
09.24.1998	18:53:41.0	46.26	106.30	5.5	180	Deren sum, Dundgovi province
12.03.2005	00:50:05.3	47.97	105.36	5.0	113	Lun sum, Tuv province
02.18.2006	01:52:16.9	50.25	105.47	5.2	279	Selenge province

Building vibration measurements

The measurements were done in the 1st 8th and 12th floors of the building with GSR-24 device during 30th of May to 13th of June, 2011. The data we got from these measurements are given in the table 4, table 5 and table 6.

Table-4. 1st floor measurement result (Acceleration)

No	Year	Month	Day	Acceleration along z axis10 ³	Acceleration along y axis10 ³	Acceleration along x axis10 ³	average acceleration along z, y, x axis 10 ³
1	2011	06	2	0.0007	0.0011	0.0009	0.0009
2	2011	06	3	0.0005	0.0006	0.0005	0.0005
3	2011	06	4	0.0008	0.0005	0.0007	0.0006
4	2011	06	5	0.0007	0.0008	0.0006	0.0007
5	2011	06	6	0.0007	0.001	0.0008	0.0008
6	2011	06	7	0.0008	0.0009	0.0006	0.0007
7	2011	06	8	0.0007	0.0008	0.0008	0.0007
8	2011	06	9	0.0008	0.0009	0.0008	0.0008
9	2011	06	10	0.0006	0.0009	0.0007	0.0007
10	2011	06	11	0.0005	0.0003	0.00035	0.0003
11	2011	06	12	0.0006	0.0007	0.0006	0.0006
12	2011	06	13	0.0006	0.0007	0.0006	0.0006
Average value				0.0006 m/sec ²	0.0007 m/sec ²	0.0006 m/sec ²	0.00063 m/sec ²

Displacement

№	Year	Month	Day	Displacement along z axis 10 ⁶	Displacement along y axis 10 ⁶	Displacement along x axis 10 ⁶	Average displacement, 10 ⁶
1	2011	06	2	0.0000007	0.0000008	0.0000013	0.0000009
2	2011	06	3	0.0000012	0.0000013	0.0000013	0.000001
3	2011	06	4	0.0000006	0.000.001	0.0000006	0.0000022
4	2011	06	5	0.0000001	0.0000008	0.0000012	0.0000001
5	2011	06	6	0.0000012	0.0000007	0.0000008	0.0000009
6	2011	06	7	0.0000001	0.0000002	0.0000001	0.0000013
7	2011	06	8	0.0000006	0.0000001	0.0000008	0.0000005
8	2011	06	9	0.0000007	0.0000016	0.0000015	0.0000001
9	2011	06	10	0.0000001	0.0000006	0.0000001	0.0000005
10	2011	06	11	0.0000012	0.0000001	0.0000008	0.0000001
11	2011	06	12	0.0000013	0.0000013	0.0000001	0.0000012
12	2011	06	13	0.0000001	0.0000006	0.0000012	0.0000006
Average value				0.000001 m	0.0000009m	0.000001m	0.0000009m

Table 5: 8th floor measurement result (Acceleration)

№	Year	Month	Day	Acceleration along z axis 10 ³	Acceleration along y axis 10 ³	Acceleration along x axis 10 ³	average acceleration along z, y, x axis 10 ³
1	2011	06	6	0.0011	0.001	0.0013	0.001
2	2011	06	7	0.001	0.0002	0.0014	0.0008
3	2011	06	8	0.0009	0.0002	0.0012	0.0023
4	2011	06	9	0.0006	0.0002	0.0008	0.0007
5	2011	06	10	0.001	0.0002	0.0013	0.0008
6	2011	06	11	0.001	0.0003	0.0017	0.001
7	2011	06	12	0.0009	0.0003	0.0013	0.0008
8	2011	06	13	0.001	0.0002	0.0012	0.0008
Average value				0.0009 m/sec²	0.0003 m/sec²	0.001 m/sec²	0.0007 m/sec²

Displacement

	Year	Month	Day	Displacement along z axis 10 ⁶	Displacement along y axis 10 ⁶	Displacement along x axis 10 ⁶	Average displacement, 10 ⁶
1	2011	06	6	0.000005	0.000003	0.000004	0.000004
2	2011	06	7	0.000003	0.000002	0.000003	0.000008
3	2011	06	8	0.000005	0.000002	0.000005	0.000002
4	2011	06	9	0.000019	0.000014	0.000003	0.000012
5	2011	06	10	0.000005	0.000002	0.000007	0.000004
6	2011	06	11	0.000005	0.000002	0.000004	0.000003
7	2011	06	12	0.000006	0.000004	0.000006	0.000005
8	2011	06	13	0.000005	0.000003	0.000006	0.000004
Average value				0.000006 m	0.000004m	0.000004m	0.0000046m

Table 6: 12th floor measurement result (Acceleration)

No	Year	Month	Day	Acceleration along z axis 10^3	Acceleration along y axis 10^3	Acceleration along x axis 10^3	average acceleration along z, y, x axis 10^3
1	2011	06	2	0.06	0.06	0.007	0.04
2	2011	06	3	0.1	0.09	0.09	0.09
3	2011	06	4	0.12	0.11	0.11	0.1
4	2011	06	5	0.13	0.12	0.11	1.12
5	2011	06	6	0.14	0.14	0.15	1.14
6	2011	06	7	0.15	0.17	0.16	0.16
7	2011	06	8	0.11	0.11	0.1	0.1
8	2011	06	9	0.09	0.09	0.1	0.09
9	2011	06	10	0.12	0.14	0.12	0.12
10	2011	06	11	0.06	0.06	0.05	0.05
11	2011	06	12	0.05	0.05	0.05	0.05
12	2011	06	13	0.1	0.1	0.1	0.3
Average value				0.1 m/sec ²	0.1 m/sec ²	0.09 m/sec ²	0.096 m/sec ²

Displacement

No	Year	Month	Day	Displacement along z axis 10^6	Displacement along y axis 10^6	Displacement along x axis 10^6	Average displacement, 10^6
1	2011	06	2	0.0005	0.0007	0.0007	0.0006
2	2011	06	3	0.0005	0.0005	0.0005	0.0005
3	2011	06	4	0.0006	0.0005	0.0007	0.0006
4	2011	06	5	0.0006	0.0004	0.0006	0.0005
5	2011	06	6	0.0006	0.0005	0.0009	0.0006
6	2011	06	7	0.0005	0.0005	0.0006	0.0005
7	2011	06	8	0.0005	0.0005	0.0004	0.0004
8	2011	06	9	0.0004	0.0004	0.0005	0.0004
9	2011	06	10	0.0007	0.0007	0.0008	0.0007
10	2011	06	11	0.0003	0.0003	0.0003	0.0003
11	2011	06	12	0.0003	0.0003	0.0004	0.0003
12	2011	06	13	0.0004	0.0004	0.0004	0.0004
Average value				0.0004m	0.0004m	0.0005m	0.00048m

Table 7: Comparison of displacement values in each floor

Floor	Y axis	Z axis	X axis	Average Displacement
1	0.001mm	0.0009mm	0.001mm	0.0009mm
8	0.006mm	0.004mm	0.004mm	0.004mm
12	0.4mm	0.4mm	0.5mm	0.4mm

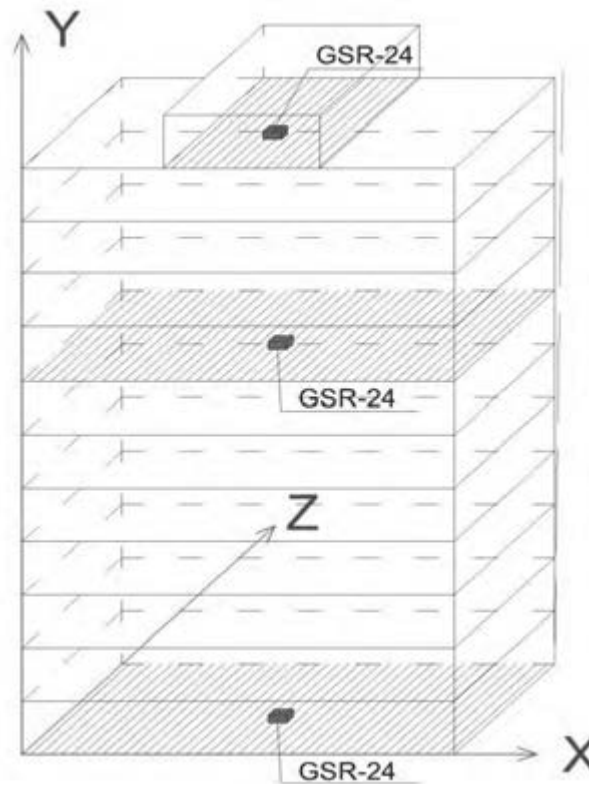
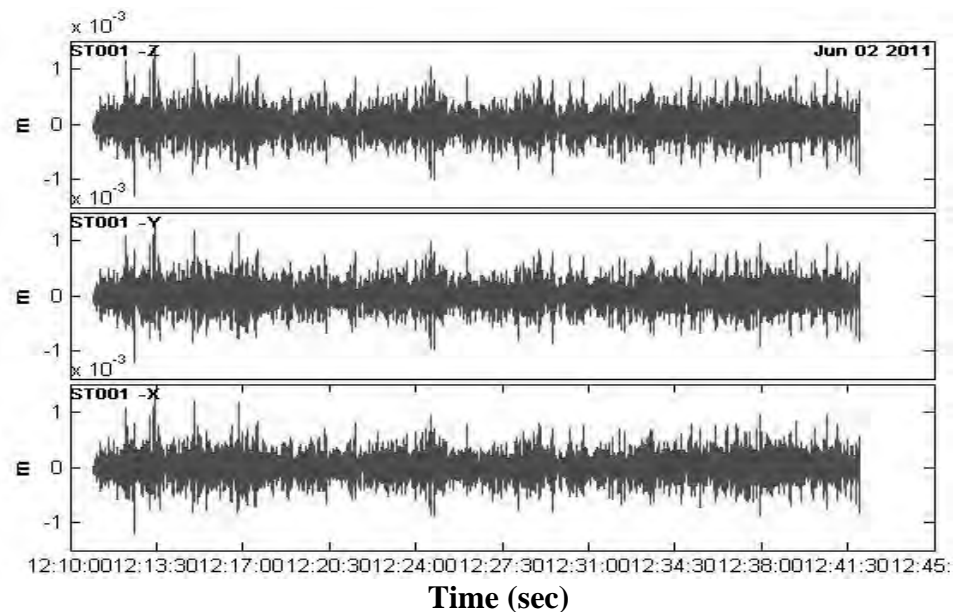


Figure 5: Vibration measurement X,Y,Z axis



According to the measurements shown in table 6,7,8 the most displacement

Figure 6: Device records of displacement measurement

was along y axis, which implies that this building is not resistive to earthquake of 8 Richter scale. Results of the engineering calculations were done on the program Lira. The building located in Songino-Khairkhan district is a reinforced concrete construction that is in earthquake region of 8 Richter scales. The soil was unstable soil type classified to degree of 2 according to the earthquake properties.

CONCLUSION

- Physical detrition of the building is 24 percents, which implies that a reconstruction is needed. If the rehabilitation is done as on the Mongolian standards of construction, it is possible to use the building.
- Concrete and reinforced concrete structures are sufficient enough and is resistive to earthquakes, however the reinforcing bars don't meet the technical requirements.
- According to the vibration experiment result, the most displacement was from right to left, from which we come to a conclusion that this building is not resistive to the earthquake of Richter scale of 8.
- In the result of this research, most of the buildings were classified and analyzed by their properties and passported depending on its stability and resistivity to earthquake.

REFERENCES

- Standards for construction of buildings on seismic zones "BNbD22.01.01*", 2006
Handbook for Analysing resistivity of old buildings to earthquakes
" BNbD 31-102-00, 2007
Program "Monomakh-SAPR 2011
Program "Lira-SAPR" 2011
Handbook for Passporting of buildings on seismic zones " BD31-103-00

Influence of underground structures on cavity formation due to repetition of water penetration

Mari SATO¹, Reiko KUWANO²

¹Ph.D Student, Dept. of Civil Engineering,
Faculty of Engineering, the University of Tokyo, Japan
msato@iis.u-tokyo.ac.jp

² Associate Professor, ICUS, IIS, the University of Tokyo, Japan

ABSTRACT

Many cave-in accidents happen nowadays in urban roads. Cave-in means sudden collapse of the ground like a pitfall. The accidents are serious problem because it sometimes injures people.

Recent research showed that expansion of underground cavities finally leads cave-in accidents. Underground cavities have expanded in the ground without being noticed. Then finally surface ground is crashed when cavities have reached near the surface ground. Many cavities were found close to underground structures. Some of those cavities were caused due to breakages of buried structures such as sewer pipes. Soil is flowed out from a crack of a pipes with water, and then a cavity is formed. However, in many cases, obvious breakages are not found in underground structures when a cavity is formed. It is not clear why cavities were generated around buried structures even if they didn't have clear damages, but is empirically suggested that water flows more easily around underground structures than in other part of the ground. Soil is carried with water flow around buried structures, which might cause a cavity around underground structures.

In order to study the influence of a buried structure on formation of a cavity due to water penetration, a series of model tests was conducted with a small soil chamber in various conditions. Specifically, the soil chamber has an opening, from which soil can be flowed out. A wooden block simulating the underground structure was placed into the soil chamber. Then small amount of water was flowed into the soil chamber repeatedly from a certain position and deformation of the model ground was observed. Position of the wooden block, relative density of soil and direction of water penetration were changed. From a series of model test, it was suggested that position of the block and direction of water penetration has large influence on cavity formation. In addition, the ground around the block has high water content.

Keywords: *underground cavity, model test, water penetration, underground structure, cave-in accident*

1. INTRODUCTION

Many ground cavities are found in the ground close to underground structures nowadays. It is a serious problem in urban cities because cavities sometimes lead to cave-in accidents which injure people. (Referring to Figure 1) One of main factor of expansion of cavities is a distinct spot of soil outflow like broken parts of sewer pipes, as shown in Figure 2. Kuwano et al. (2006) conducted model test simulating how a cavity is generated due to the broken parts of sewer pipes.1) However, specific spots of soil outflow are seldom found near to cavities. The reason why cavities and loosening are generated and expanded around the underground structures without visible spots of soil outflow is not clear. But existence of “water pathway” surrounding buried structures was empirically suggested. To reveal influence of underground structures on generation of cavities, model test simulating soil outflow around an underground structure due to repetition of water inflow was conducted with a small soil chamber.



Figure 1: Cave-in accident
(6th August, Tokyo Newspaper)

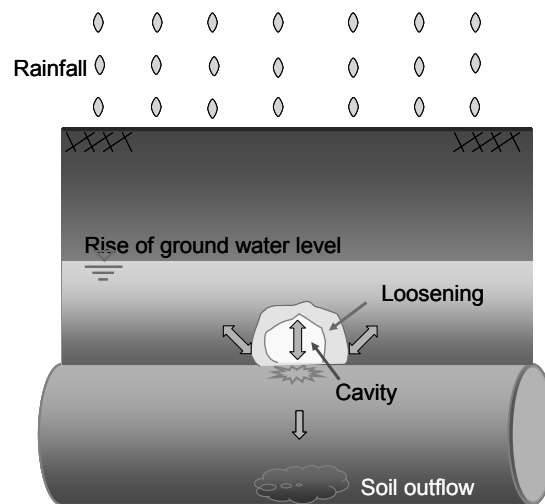


Figure 2: Process of cavity expansion
due to breakage of a sewer pipe

2. TEST APPRATUS AND PROCEDURE

2.1 Test apparatus and procedure

Model ground of 300mm long, 50mm wide and 200mm high was made by compaction in the small soil chamber having an opening of 5mm in a base plate. Water is flowed out from the opening when drainage valve was released. A wooden block of 21cm long, 50mm wide and 100mm high was place into the model ground. Width of the wooden block is same as that of soil chamber This wooden block is waterproof so that water doesn't pass inside the block. Overburden weight was put on the top of the model ground by a wooden stand.

Water is supplied from two different positions which are shown in Figure 3 and Figure 4. In this paper, test cases of supply position like Figure 3 is named as “Position (A)” and test cases like Figure 4 is named as “Position (B)”. In Position (A), water is supplied from the opening at the center of the bottom plate. After stopping water supply and waiting for 1 minute, drainage valve was released. The process of water inflow and outflow is repeated. In Position (B), water is supplied from light or left end of the ground and 150mm height from the bottom. During the test, drainage valve is kept released. Only water inflow was repeated. In both water supply positions, Water was supplied from a water tank, which has 100cm head difference from the soil chamber. The amount of water supply in one time was approximately 100cc. Details of experimental procedure of Position (A) and Position (B) is shown in Figure 5. This paper defined “a cycle” as water supply in one time. Cycles were repeated till a cavity expanded large enough. Photograph was taken in front of the chamber during the test and the weight of drained soil in dry condition was measured after the test.

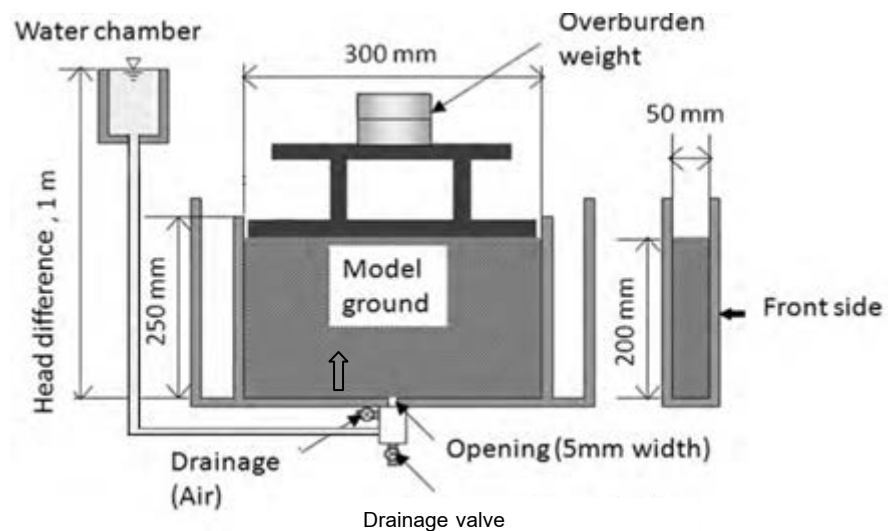


Figure 3: Test apparatus of Position (A)

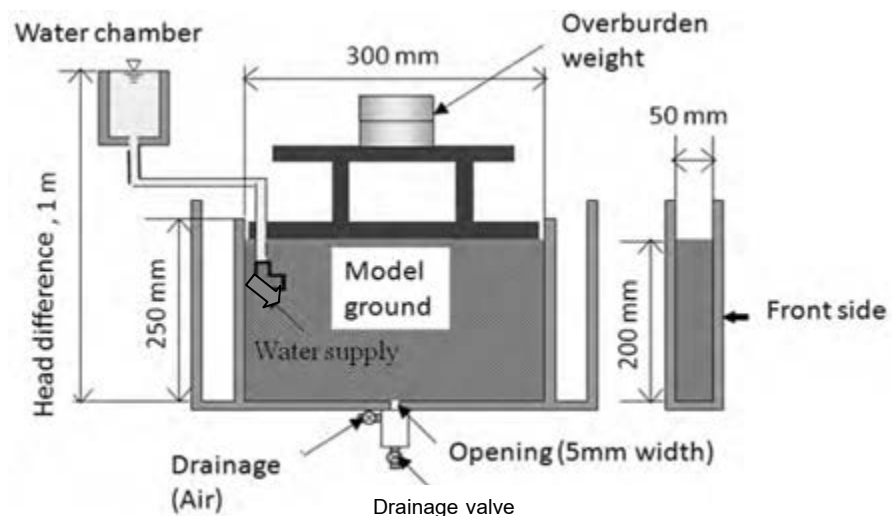


Figure 4: Test apparatus of Position (B)

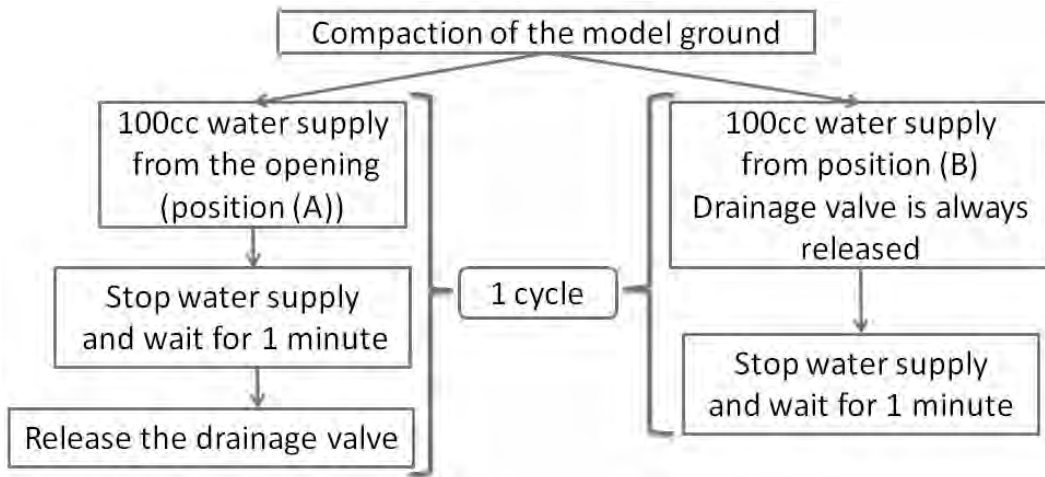


Figure 5: Flowchart of test procedure

3. TEST CONDITIONS

All experimental conditions are shown in Table 1. Relative density was 80%, initial water content was 10% and overburden weight was around the weight of 80cm depth of the ground in all the test case. Two different types of water supply position are prepared (Referring to chapter 2). An experimental code represents Position of the water supply,(Material, position of the block).Two kinds of materials are employed: Toyoura sand and Silica sand. Both of two materials are clean uniform sand but average particle size of silica sand no.5 is twice as that of Toyoura sand. Particle size distribution is shown in Figure 6. 4 patterns of position of the block were employed, as indicated in Figure 7. Data of A(T,N) is referred from Sato et al (2010)²⁾.

Table 1: Test conditions

Materials	Positon of water supply	Position of the block	Initial water content (%)	Relative Density (%)	Test code
Toyourea	A	Vfar	10%	80%	A(T, Vfar)
Toyourea	A	Vnear	10%	80%	A(T,Vnear)
Toyourea	A	H	10%	80%	A(T,H)
Toyourea	A	Vside	10%	80%	A(T,Vside)
Toyourea	A	No block	10%	80%	A(T,N))
Silica no.5	A	Vside	10%	80%	A(S,Vside)
Toyourea	B	Vfar	10%	80%	B(T,Vfar)
Toyourea	B	Vnear	10%	80%	B(T,Vnear)
Toyourea	B	H	10%	80%	B(T,H)
Toyourea	B	Vside	10%	80%	B(T,Vside)

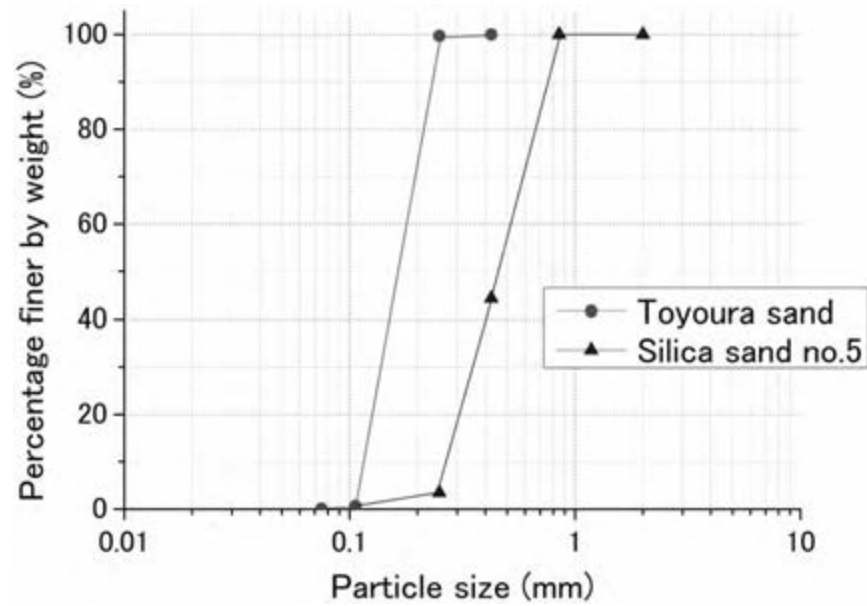


Figure 6: Particle size distribution

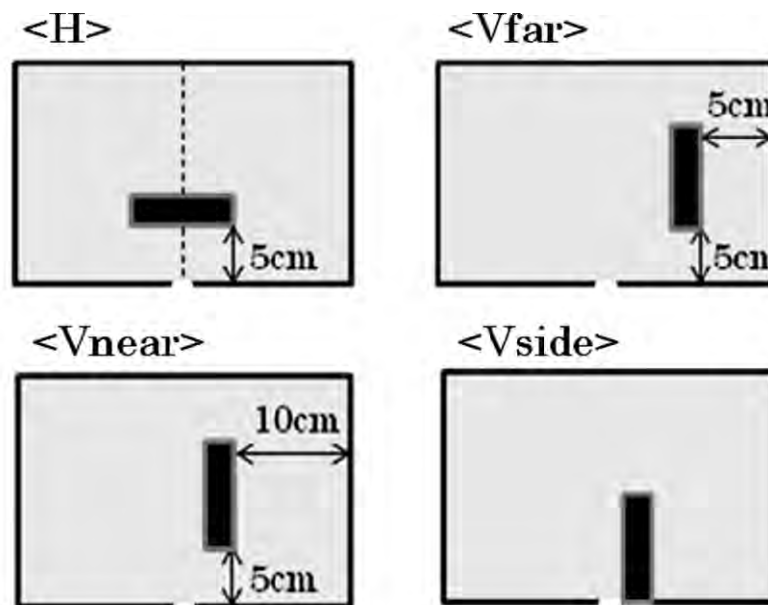


Figure 7: 4 patterns of position of the block

4. TEST RESULT

4.1 Cavity formation

4.1.1 Common formation without the block

Typical forms of a cavity created in the model ground are obtained from test A(T,N) as shown in Figure 8. A cavity of fan-like shape, having slope at both sides and arching ceiling, was generated above the opening. If

a cavity became large and 100cc water didn't reach to the top of the cavity, cavity didn't expand anymore.



Figure 8: Typical formation of Cavity

4.1.2 Cavity formation with the block of Position (A)

Cavity formations of Position (A) are shown in from Figure 9 to Figure 13. By comparing Figure 9 with Figure 10, distance of the block from the opening didn't much influence on generation of cavity. However, cavity and ground deformation expanded top or the ground even if the amount of supply water in one time is only 100cc. (Referring to 4.1.1)

Figure 11 suggested that the block which is above the opening prevents soil drainage and a cavity was expanded below the block. Boiling happened during water inflow in case the block was beside the opening, which cause rapid expansion of a cavity (Referring to Figure 12 and Figure 13).

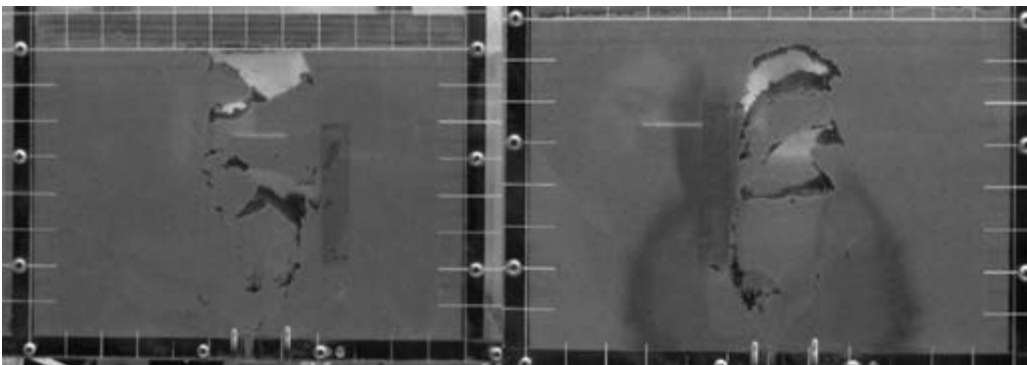


Figure 9: A(T,Vfar) at 14th cycle

Figure 10: A(T,Vnear) at 15th cycle

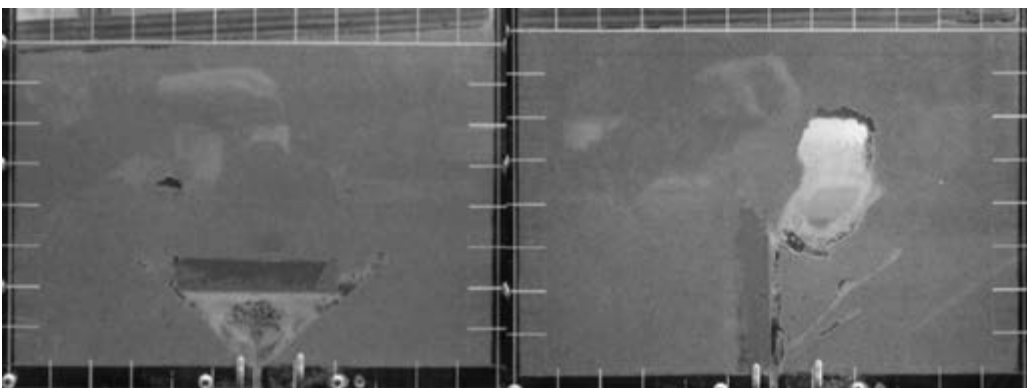


Figure 11: A(T,H) at 9th cycle

Figure 12: A(T,Vside) at 7th cycle

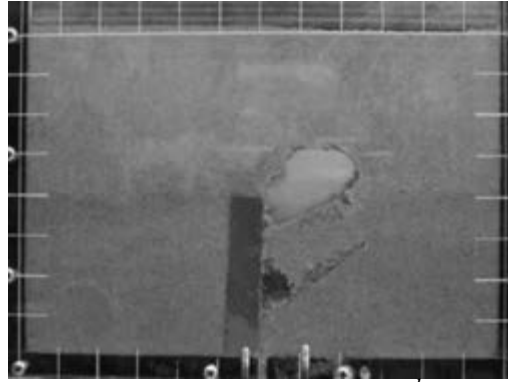


Figure 13: A(S, Vside) at 3rd cycle

4.1.3 Cavity formation with the block of Position (B)

Cavity formation of Position (B) is shown in from Figure 14 to Figure 18. White arrow line represents the water supply position. Figure 18 is a previous condition of Figure 14. In all test cases of Position (B), cavity was generated close to the block. Dot arrow line of Figure 15 and Figure 16 represents the direction of water flow. Therefore, direction of expansion of cavities was along the direction of water flow.

Colored sand layer was formed in every 3cm for observation of the ground deformation in B (T, Vfar) as Figure 14 and Figure 18. Figure 14 and Figure 18 suggested that the ground deformation happened before cavity was generated.

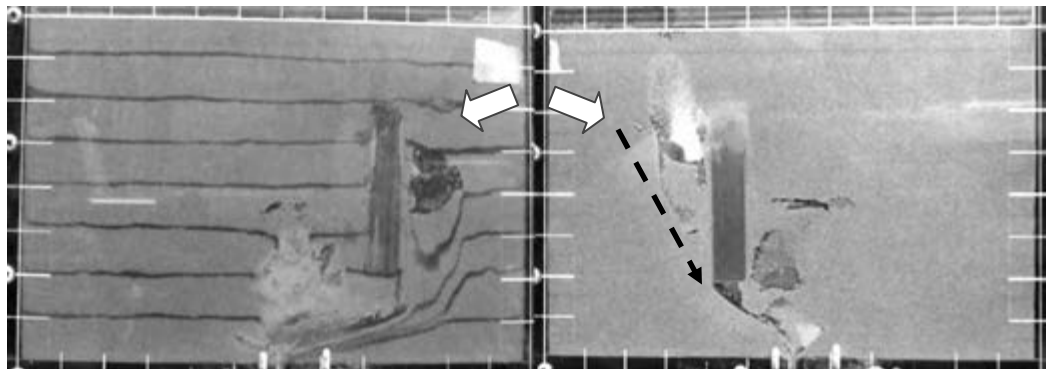


Figure 14: B(T, Vfar) at 12th cycle

Figure 15: B(T, Vnear) at 7th cycle



Figure 16: B(T, H) at 7th cycle

Figure 17: B(T, Vside) at 7th cycle

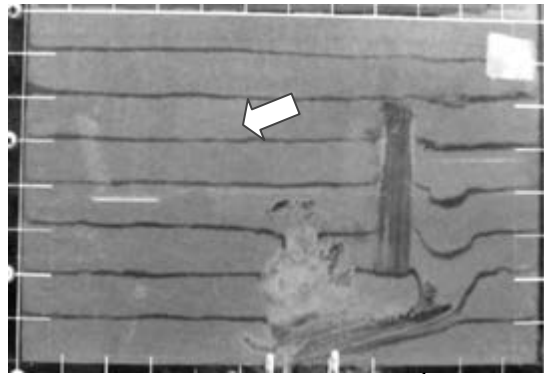


Figure 18: B (T,Vfar) at 10th cycle

4.2 Weight of soil loss

4.2.1 Soil loss of Position (A)

A relationship between cycles and cumulative weight of soil loss in Position (A) was shown in Figure 19. It was suggested that rapid soil drainage happened in A (S,Vside), A (T,Vside) and A(T,H). Silica sand no.5 caused more rapid soil outflow than Toyoura sand. On the other hand, in A (T,Vfar) and case A (T,Vnear), soil drainage didn't happen so much until 10th cycle. It is supposed because the block is not to close to the direction of water inflow/outflow from/to the opening. Then after 10th cycle, soil drainage happened very rapidly. In case A (T,N), soil outflow stopped at 8th cycle because cavity became too large to be filled by the water (Referring to 4.1.1). Consequently, it was supposed that existence of the block made cumulative weight of soil loss at final cycle larger than that without the block.

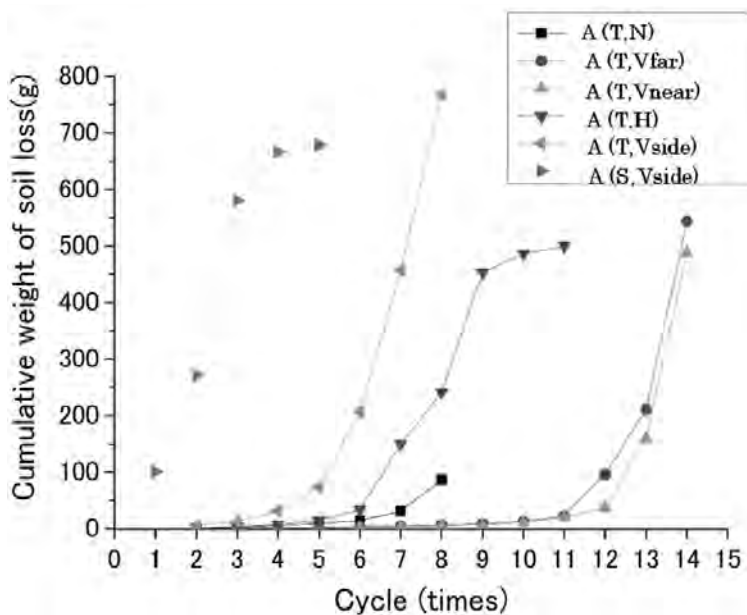


Figure 19: Cumulative weight of soil loss in Position (A)

4.2.1 Soil loss of Position (B)

A relationship between cycles and cumulative weight of soil loss in Position (B) was shown in Figure 20. From Figure 20, it is suggested that rapid soil outflow happens if the block is near to the opening like B (T,Vnear) and B (T,Vside). On the other hand, soil outflow was very gentle in the case the block is not near to the opening like B (T,Vfar) and B (T,Vfar). Influence of the block’s distance from the opening on soil outflow was suggested.

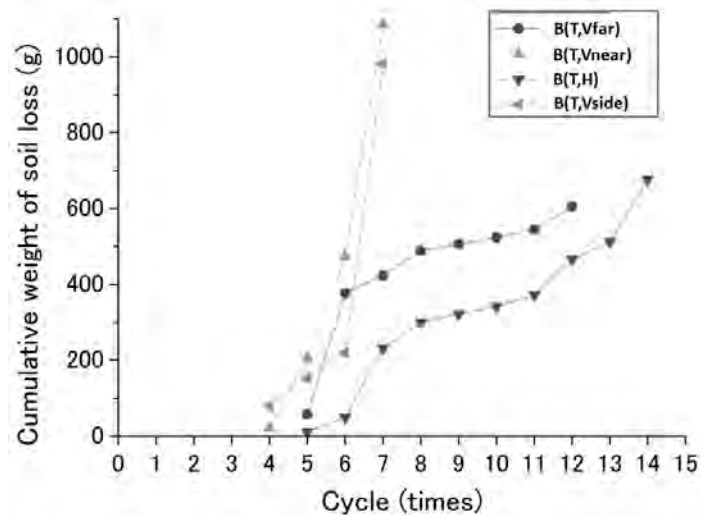


Figure 20: cumulative weight of soil loss in Position (B)

5. DISTRIBUTION OF WATER CONTENT IN THE MODEL GROUND

For examining of the distribution of high water content area in the model ground, water content ratio was measured at 9 spots in B (T,Vfar) after finishing the experiment. Result of water content ratio in each spot is shown as Table 2. From Figure 21 and Table 2, the high water content area existed right side of the block. This area especially extended from the water supply point to the opening. Therefore, it was proposed water pass through left side of the block to the opening and the water flow caused the cavity and ground deformation. On the other hand, at spot 6, water content ratio was very high but the cavity didn’t generated because direction of water flow didn’t set to the opening.

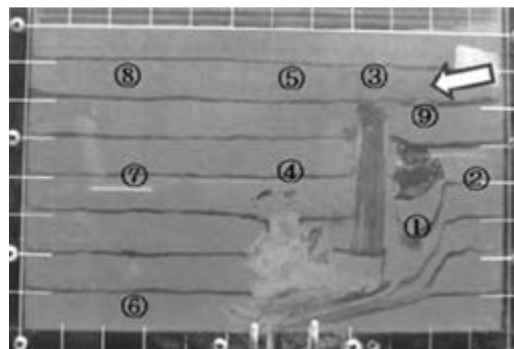


Figure 21: measurement spot of B (T,V far)

Table 2: water content ratio of each spot

Spot	Water content (%)	5	23
1	34	6	41
2	26	7	32
3	34	8	20
4	29	9	39

6. DISCUSSION AND CONCLUSION

Water flow to the opening causes soil drainage. The block has large influence on the generation of cavity when the block was placed as blocking the water flow to the opening. The wooden block caused rapid soil outflow in some conditions. Concentration of water flow surrounding the block caused cavity expansion and sometimes boiling happens. On the other hand, Water flow was prevented by the block in the other conditions, which makes soil outflow gently. However, if direction of water flow was changed, sudden expansion of cavity may happen. In the real ground, same process is supposed to occur around the underground structures. Process of generation of cavity around an underground structure is estimated in Figure 22.

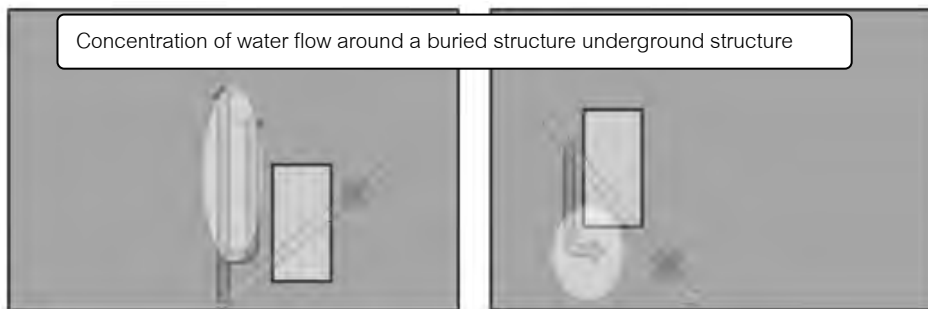


Figure 20: Schematically water flow surroundings a buried structure

REFERENCES

Sato, M. & Kuwano, R. *Model Tests for the Evaluation of Formation and Expansion of a Cavity in the ground*. Proc. of the 7th International Conference on Physical Modelling in Geotechnics 2010. Zurich, June 2010, pp.581-586

Kuwano, R, Yamauchi, K., Horii, T. and Kohashi, H. 2006. *Defects of sewer pipes causing cave-in's in the road*. Proc. of 6th International Symposium on New Technologies for Urban Safety of Mega Cities in Asia. Phuket: No.H63.

Application of elastic wave measurement to model tests using bender elements

Sho OH¹ and Reiko KUWANO²

¹ Graduate Student, School of Eng., The University of Tokyo, Japan
soh@iis.u-tokyo.ac.jp

² Associate Professor, ICUS, IIS, The University of Tokyo, Japan
kuwano@iis.u-tokyo.ac.jp

ABSTRACT

Elastic wave measurement using Bender Elements have been developed as a dynamic measurement method for element test in geotechnical field. Now this method is expected to apply also for model tests in order to obtain the pressure distribution inside soil chamber. This research aims to obtain the basic performance information of bender elements in model tests. First, in order to detect the wave arrival clearer, signal analysis is conducted. Low frequency noise is reduced by polynomial approximation, and high frequency noise is dealt with FFT filter. Next, the effect of attaching aluminum block to bender element is discussed. Some change in the received wave form is found, but wave velocity was almost same. Also, property of wave propagation is checked using plural receiver for one transmitter. Finally, shear modulus is calculated for obtained data for validation. Results showed good agreement with those of element test.

Keywords: *elastic wave measurement, bender elements, model test, aluminum block, increment of earth pressure*

1. INTRODUCTION

Box culvers are structures buried inside high embankment as tunnels for water, electric line, communicate line and so on. In designing of these box culverts, increase in vertical earth pressure must be considered, since differential settlement often occurs around a buried structure, as schematically shown in Figure 1. However, in practice, the increment of vertical earth pressures on underground structures is estimated in the empirical manner, mainly based on the information of past earth pressure measurements in limited of sites (General guidelines for road earthworks, 1999). In this method, degree of settlement and mechanical properties of backfill materials are not considered. Some research have been conducted to solve this problem. However, due to the limited performance of earth pressure transducers used in experiment, details of the earth pressure distribution were not clearly understood.

Recently, a sophisticated trap door apparatus is developed by Ebizuka and Kuwano (2010), in order to improve the problems in previous studies. A soil chamber for trap door testing is constructed, the inside of which is

shown in Figure 2. It can accommodate model ground of 700mm wide, 294mm long and 555mm high. The base of the chamber consists of five separated movable blocks whose size is 99.8mm wide, 293.6mm long and 105mm high, and fixed parts in both sides, in order to create uneven settlement in the model ground, as schematically shown in Figure 3.

The final goal of this research is to obtain pressure distribution inside model test using this soil chamber to quantitatively evaluate the vertical earth pressure acting on buried structures. For the method of measurement, elastic wave measurement using bender element is chosen.

Elastic wave measurement using bender elements have been developed as a dynamic measurement method for element test. Measuring propagation time of S wave inside soil gives shear modulus of soil. And by conducting shear wave tomography, distribution of pressure can be obtained. Although this is a useful method, no application for model test is conducted before. In this paper, basic performance information of bender elements is studied for model tests.

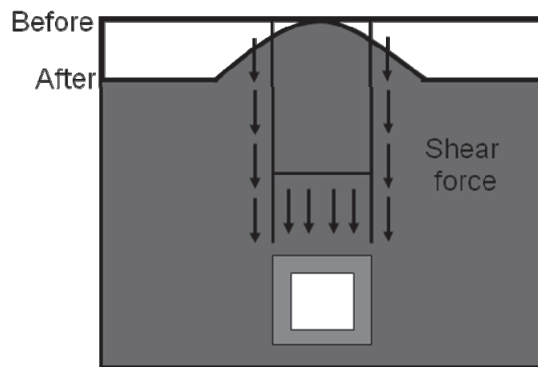


Figure 1: Increment of the earth pressure due to the uneven settlement

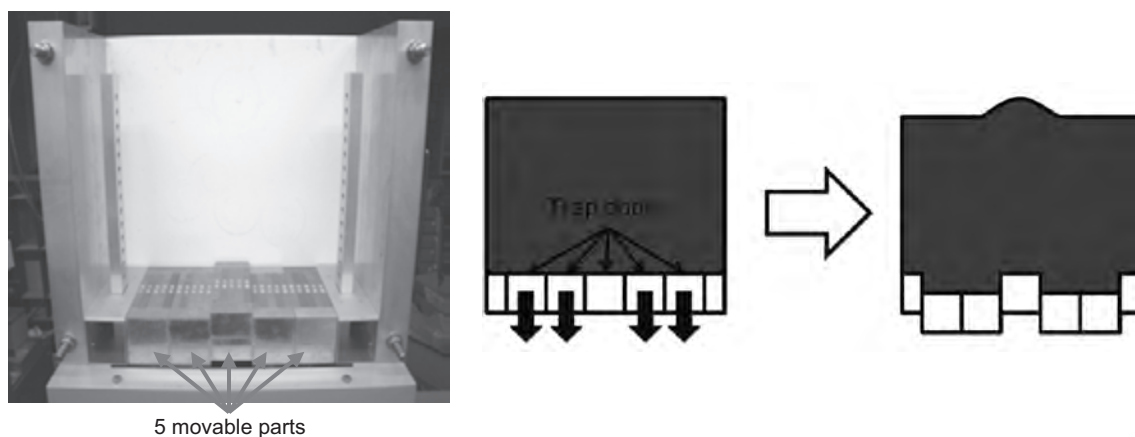


Figure 2: Detail of soil chamber

2. ELASTIC WAVE MEASUREMENT

2.1 Bender Elements

Bender elements are small measurement device that transfer electric voltage to physical deformation and vice versa. There are two types of elements as shown in Figure 3. Series type is more suitable for receiver and parallel type is better used as transmitter. Measurement is done by burying these two types of bender elements in soil.

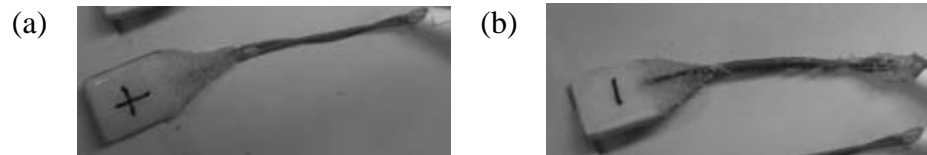


Figure 3: Bender Elements of (a) Series and (b) Parallel type

2.2 Measurement Apparatus

Measurement apparatus used in this study is shown in Figure 4, and the details of setting are shown in Table 1.

Table 1: Setting of Aparatus

Output Voltage of Function Generator	8Vpp
Trigger Interval	1s
Wave form	Sin wave
Amplifier rate	100 time
Averaging times by Oscilloscope	20

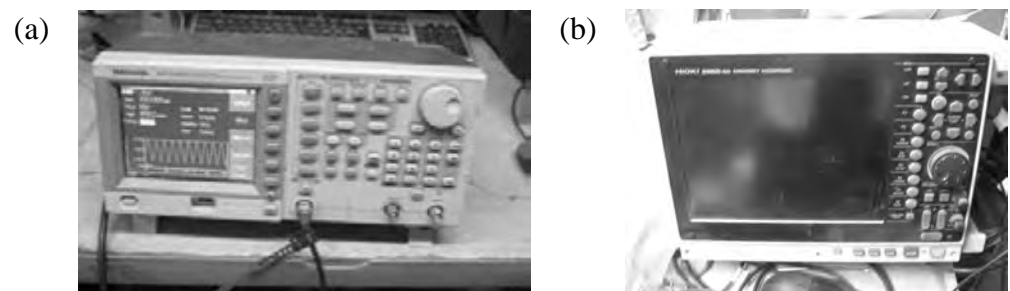


Figure 4: Aparatus used in this study. (a) Function Generator (b) Oscilloscope

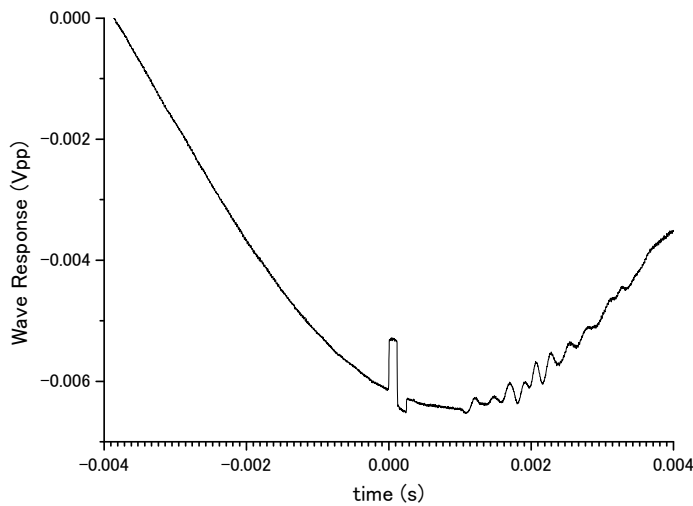
3. DETECTION OF WAVE ARRIVAL

The biggest problem of bender element application in model test so far is the difficulty of detection of wave arrival. In order to make the detection more accurate, two methods are taken. One is signal analysis and another is attaching an aluminum block on the top of bender element. The effect of each method is discussed in this chapter.

3.1 Signal Analysis

Figure 5 (a) shows original obtained wave signal. To reduce the large low noise in this signal, polynomial approximation using quadratic curve is conducted for 2000 points out of 5000. Subtracting the fitted curve from the original signal gives more clear view of response but still some high frequency noise as shown in Figure 5 (b).

(a)



(b)

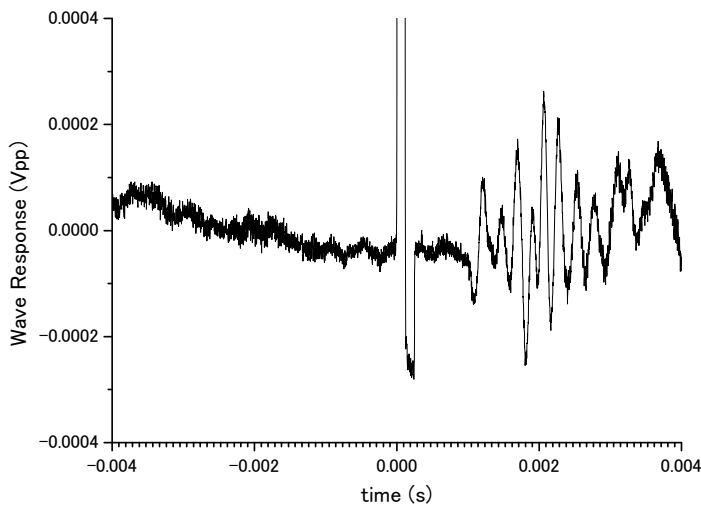


Figure 5: (a)Original obtained signal and (b) Low noise reduced signal

In order to reduce the high frequency noise, the spectrum intensity of signal at -0.003 to -0.001s (before wave arrival) and 0.001 to 0.002 (after wave arrival) is compared and shown in Figure 6. Three strong peaks seen before wave arrival (a) are reduced after wave arrival (b), therefore these frequency can be regarded as noise.

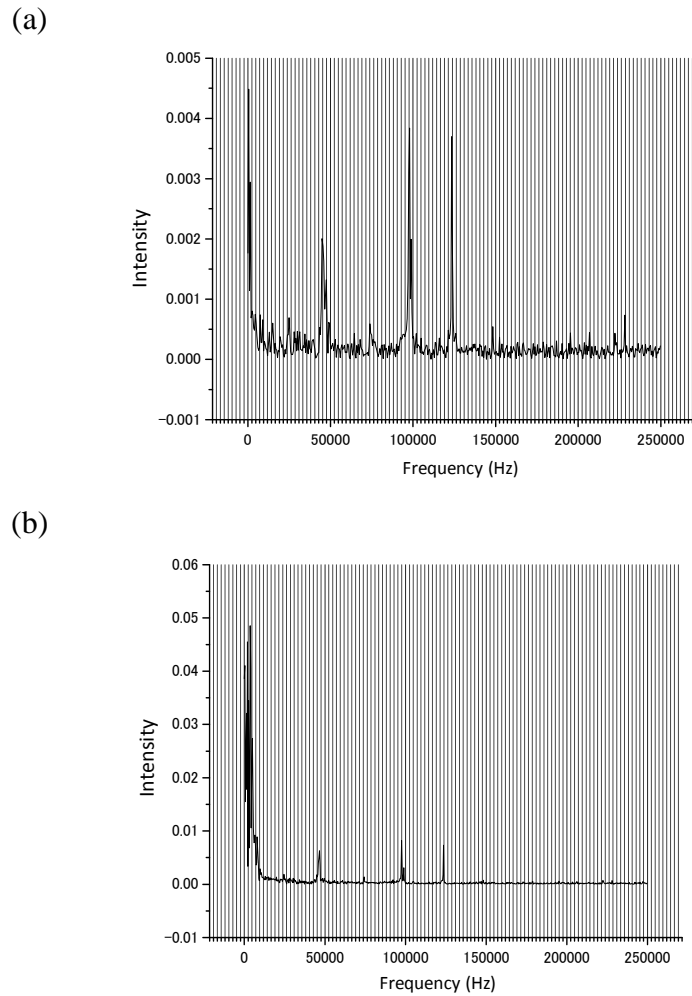


Figure 6: Spectrum intensity (a) before wave arrival and (b) after wave arrival

Removing high frequency noise by FFT filter gives final version of wave signal as shown in Figure 7. Method of wave detection is shown in Figure 8.

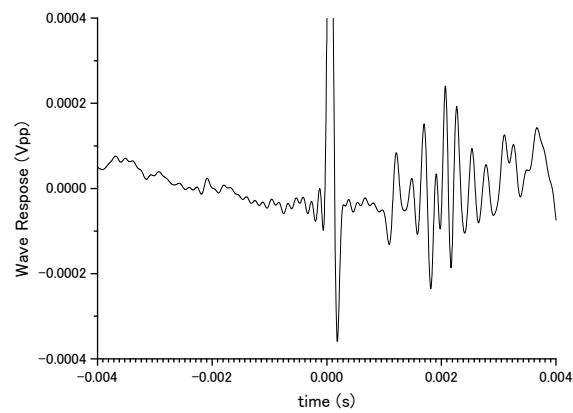


Figure 7: Wave signal after noise cutting

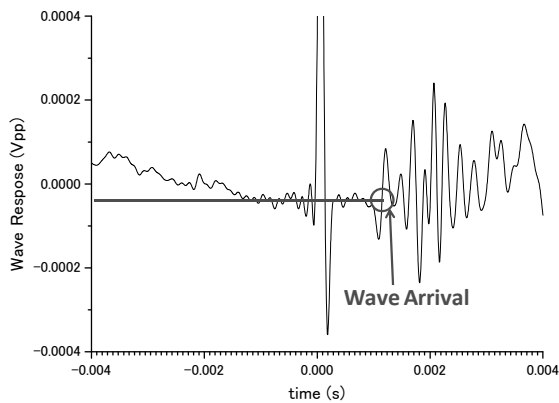


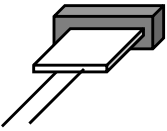
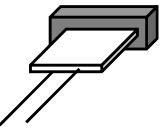
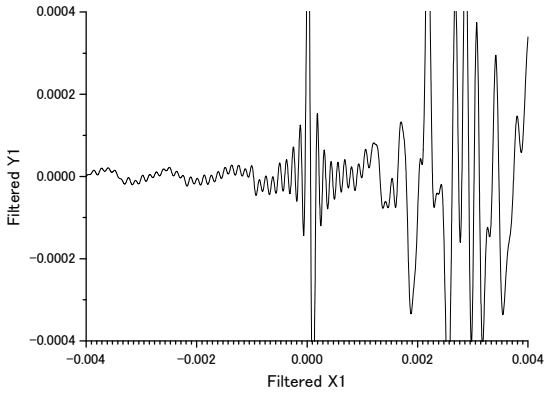
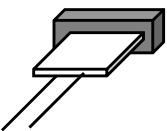
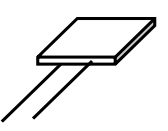
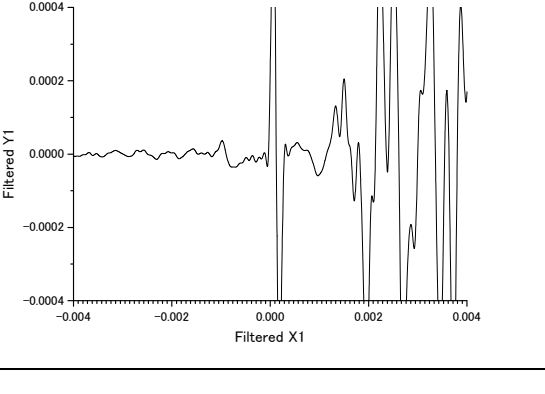
Figure 8: Wave arrival point

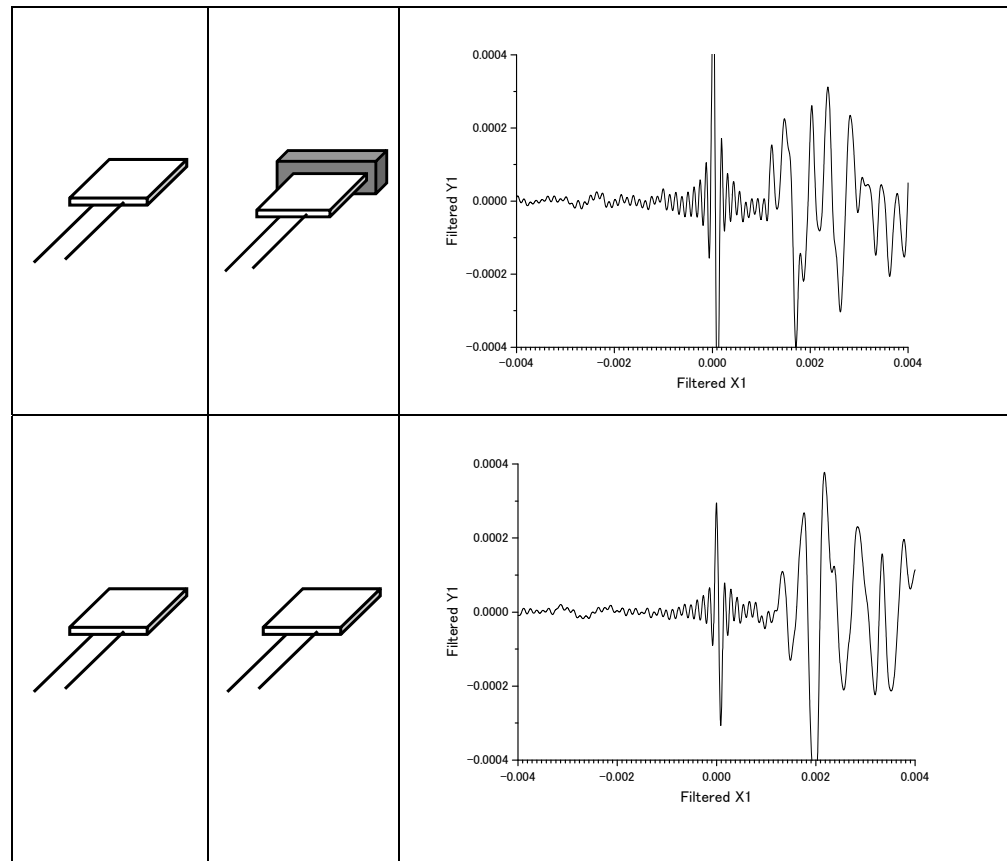
3.1.1 Effect of Aluminum Blocks

In element tests, attaching aluminum blocks on top of a bender element reduced much noise and gave clear wave. This method is applied also for model tests. Size of aluminum blocks used in this study is 5mm/5mm/10mm.

There are several ways of attaching. Results are shown in Table 2.

Table 2 Results of aluminum block

Transmitter	Receiver	Obtained Signal
		
		



Following facts can be said from this result. Attaching aluminum block to both transmitter and receiver make arrival of wave small. Transmitter with aluminum block cause different shape of arrival wave, but travel time is almost same as non-aluminum block. Attaching aluminum block to receiver gives almost same wave shape and arrival time with non-aluminum blocks. As a result, attaching aluminum blocks does not have effect to clear arrival wave in model test.

4. VALIDATION OF OBTAINED DATA

4.1 Simitenous Recieving

Property of shear wave propagation should be checked. Three receivers are set for one transmitter to see if wave is propagating in straight way as shown in Figure 9.

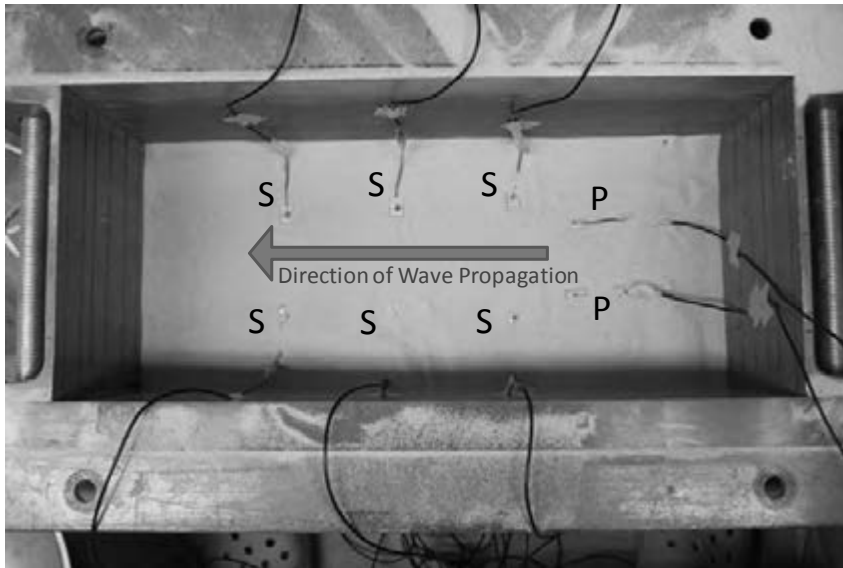


Figure 9: Experiment for wave propagation checking

Results are shown in Figure 9. Divergence of result for last receiver is rather large because of the long distance between bender elements. Wave velocities are almost same, which suggest wave is propagating in straight way.

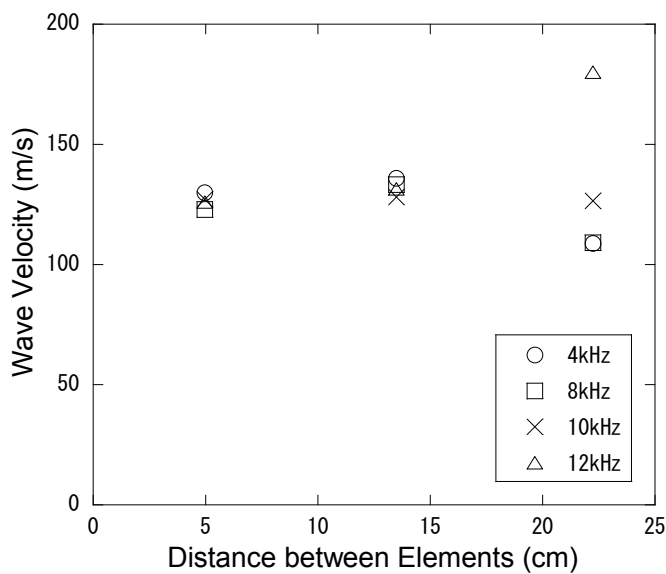


Figure 9: Results for wave propagation checking

4.2 Shear modulus

Shear modulus is calculated for obtained data using following formulas.

$$G = \rho V_s^2 \quad (1)$$

$$f(e) = \frac{(2.17 - e)^2}{1 + e} \quad (2)$$

where G is shear modulus, e is density, V_s is shear wave velocity and e is void ratio. Since model test is conducted under nearly uniform condition, next relationship is approximated for calculation. Results agreed favorably with element test as shown in Figure 10.

$$\sigma_h = \frac{1}{2} \sigma_v \quad (3)$$

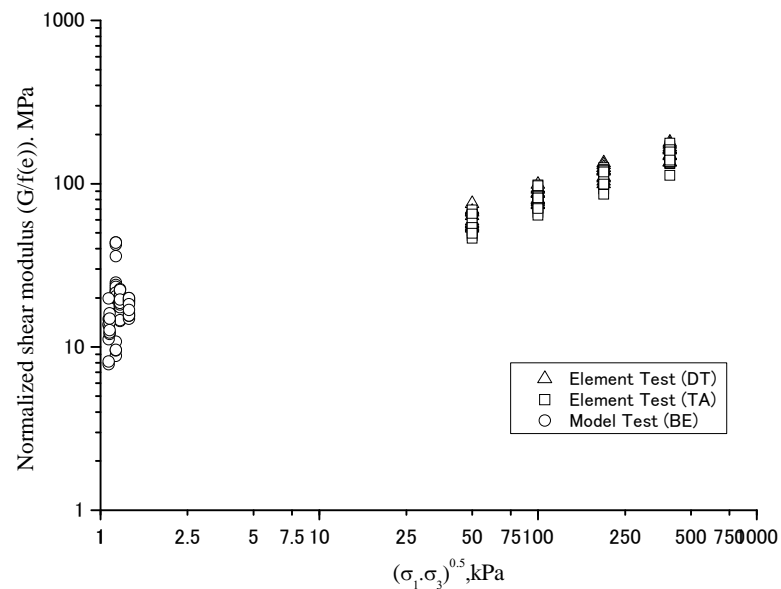


Figure 10: Normalized shear modulus versus earth pressure

5. CONCLUSION

1. In order to detect the wave arrival clearer, signal analysis is conducted. Low frequency noise is reduced by polynomial approximation, and high frequency noise is dealt with FFT filter.
2. Effect of attaching aluminum block to bender element is discussed. Some change in the received wave form is found, but wave velocity was almost same.
3. Property of wave propagation is checked using plural receiver for one transmitter and found to be in straight way.
4. Shear modulus is calculated for obtained data for validation. Results showed good agreement with those of element test.

REFERENCES

General guidelines for road earthworks - culvert work -, 1999. Japan road association, ISBN 978-4889504101, Maruzen Print Co. Ltd. (in Japanese).

Kuwano, R., Horii, T. and Kohashi, H., 2007, Increment of Earth Pressure Acting on a Buried Box Structure due to Differential Settlements, *New Frontiers in Chinese and Japanese Geotechniques, Proceedings of the Third Sino-Japan Geotechnical Symposium, 2007*, 309-314.

Suwal, L., Kuwano, R., Small strain stiffness measurement of sand and gravel using disk shaped piezo-electric transducer, 5th International Conference on Earthquake Geotechnical Engineering, 2011

City development safety and improvement of urban planning of Ulaanbaatar city

Yondonsuren JARGALSAIKHAN¹, Yasuoshi ICHIHASHI²

¹ Senior officer, National Security Council, Mongolia
jargalsaikhan@nsc.gov.mn

² Visiting Professor, ICUS, University of Tokyo, Japan
yo_jagaa@yahoo.com

ABSTRACT

Since its transition from socialist planned economy to market oriented in 1990, considerable changes occurred in all social and economic sectors of Mongolia. While before 1990, entire population has job, living standards were quite alike, today we have high rate of unemployment and poverty, particularly in rural areas. In this regard, people are constantly migrating to the capital and other cities where the industrial and business environment is segmenting.

As a result, population of Ulaanbaatar city increased from 600,000 in 1990 to 1,150.0 thousand today, in other words 2.1 times increase; where most of which migrated from rural areas. Following this increase, demand for social and economic sectors such as health, education and many others substantially increased, consequently with subsiding supply of these sectors.

Taking in consideration the future perspective of Ulaanbaatar City, a major planning challenge is how to address further growth of city and mainly continuation of migration. Current situation as well many social and economic parameters directly impact the urbanization level of Ulaanbaatar city. Expansion of economy, migration of population to the city, both have immediate connection to Ulaanbaatar's population diversion.

Given a scenario of "Do-Nothing" in terms of land-use management during urbanization, urban sprawl will continue to take place in any available areas in Ulaanbaatar City. Land occupation will be disorderly, hereby blighting the city and eroding its potentials for urban economic growth. Therefore, the management of urban growth will surely become crucial along with the growing urban economy.

Surrounding area of Ulaanbaatar City, as part of it, is becoming independently growing economic zone. With sensible planning of satellite cities and formation of Ulaanbaatar city, alleviate of population concentration will be manageable with provision of necessary security.

Mongolian Housing Program includes following strategies, namely:

- *New town development;*
- *Densification of housing in the center of the city;*

- “Ger” area improvement;
- Development of mortgage capital market; and
- Capacity building, promotion of the construction industry and construction materials’ production.

1. INTRODUCTION

During 20 years time, since its transition from central-planned economy to a market- oriented economy in 1990, considerable changes occurred in all social and economic sectors of Mongolia. Before 1990, all the working age people used to own jobs, living standards and level of the population were similar. However, today unemployment and poverty level is in high rate, particularly, in rural areas. Due to this challenge, people are constantly migrating to the capital and other cities where the industrial and business environment is segmenting.

As a result of it, population of Ulaanbaatar city increased 2.1 times from 550,000 in 1990 to 1,160.0 thousand today, where most of them migrated from rural areas. Following this increase, demand on social and economic sectors such as health, education and many others substantially increased. In other words, the existing capacities cannot cover the required demands.

Today Mongolia has 2.7 million populations. The biggest city is Ulaanbaatar, where 1161.8 thousand people are and next 2 cities /Darkhan, Erdenet/ have 50.0-100.0 thousand people respectively, 10 cities have 20.0-50.0 thousand people, 10 cities with 10.0-20.0 thousand people respectively. Ulaanbaatar, Darkhan, Erdenet cities have formed central region of the country, becoming more manufactured and agricultural cities with infrastructure. 48.6 percentage of the whole population live in these three cities.

The other cities are aimags centers which hold main administrative unit of the country. Comparing to the cities of another countries there are few populations in Mongolian aimag centers-cities. Mongolia has vast land but few populations. Therefore, slowing down the migration from countryside to the center, developing regions delivering social services and introducing urban culture to the rural area people are very important for Mongolia.

Table 1: Comparison of the cities population

	Urbanization level	City quantity	Name of the cities /population in thousand people/ by date 01/01/2011
1	More than 1.000.000	1	Ulaanbaatar (1,161.8)
	Between 100.000-1.000.000	-	-

2	Between 50.000-100.000	2	Darkhan (87.6), Erdenet (80.1)
3	Between 20.000-50.000	10	Choibalsan (39.1), Murun (33.1), Ulgii (30.0), Khovd (28.4), Undurkhaan (26.9), Bayankhongor (26.3), Arvaikheer (25.1), Zuunkharaa (22.9), Sainshand (22.6), Ulaangom (21.9),
4	Between 10.000-20.000	10	Tsetserleg (18.8), Altai (18.5), Uliastai (16.5), Bulgan (15.7), Dalanzadgad (14.8), Zuunmod (13.6), Mandalgovi (10.2), Sukhbaatar (12.4), Baruun –Urt (12.4), Choir (7.6)
	Total	23	Cities population in total 1,760.7 thousand, which means 63.9 % of the total population of Mongolia.

As seeing by the official census of population number of population in Ulaanbaatar was 1,500 in 1926, 10,500 in 1930, but 1,031.2 thousand people in 01/01/2008, and it became one of the world cities, which have over one million population. Population census shows that since 1990, our population has been increased twice, and if the mechanic increase continues as this way, the city population will estimated 1,563.7 thousand by 2015, and 1,965.1 thousand by 2020. Our calculation shows that if Ulaanbaatar city's population increases continuously this way, almost 59-63 percent of Mongolian population will live in the capital.

In recent years, the country's GDP per capita has been continuously increasing, and as a result of the government actions such as for improving social life of the rural people, giving livestock to herders (who's livestock died by harsh winter), supporting small and medium facilities and farmers, building road networks, creating industry & trading zones trend of the migration to the cities has been slowing down.

Ulaanbaatar city has totally 9 districts, including central districts namely Sukhbaatar, Chingeltei, Bayanzurkh, Bayangol, Khan-uul, Songinokhairkhan, and outskirt districts namely Baganuur and Nalaikh. It has 4,704 square km area. Whereas Bayanzurkh, Songinokhairkhan districts have 1200 square km area, the Bayangol district has only 29.5 square km area. In the last 3 years, the capital city's population has been increased by 110.0 thousand people.

Table 2: Ulaanbaatar city's population and number of households

	Districts	Population	Households	Average family members	Territory (km ²)	Density (person/km ²)
1	Sukhbaatar	136,917	34,503	4.0	208,40	657,0
2	Chingeltei	147,438	31,648	4.2	89,30	1,651,0
3	Bayanzurkh	265,997	63,483	4.2	1,244,12	213,8
4	Bayangol	185,104	43,545	4.3	29,49	6,276,8
5	Khan-Uul	112,055	27,808	4.0	484,66	231,2
6	Songinokhairkhan	252,264	55,600	4.5	1,200,63	210,1
	Central districts	1,099,775	256,587	4.3	3,256,60	337,7
7	Baganuur	26,905	7,092	3.8	620,20	43,4
8	Nalaikh	31,458	8,527	3.7	687,64	45,7
9	Bagakhangai	3,647	976	3.7	140,00	26,1
	Outskirt districts	1161785	273182	4.2	470444	2469

Eventually in Mongolia, population density is 1.7 people per 1 square km, while in most provinces 0.5-1.0, in Ulaanbaatar city 237.2, by the district such as: in Sukhbaatar district 657.0 in Chingeltei district 1651.0, in Bayangol district 6276.8.

Japan's density is 337 person per square km, which ranks 4th (Bangladesh -975, South Korea -477, Nederland – 386, this are top 3 countries) in the world, has 14 cities, which have over 1 million people, 6 of them has density of 6-13 thousand per square km. Now Ulaanbaatar city's population number is reaching to the level of the world biggest cities facing the same problems as in the big cities.

Ulaanbaatar which is in distinguished geological condition and location surrounded by Bogdkhan, Chingeltei, Bayanzurkh, Songinokhairkhan mountains and urban infrastructure has limited space. First urban planning was drafted during 1960 to 1980's and in this planning Ulaanbaatar city's population was predicted to be 500.0-600.0 thousand people. But in reality, the population has been doubled and facing some difficulties. Therefore, there is an urgent need to determine the right ways and rational policies to solve these problems:

- Current urban development implementation has not being complied with Ulaanbaatar city's urban development master plan, construction norms and standards for last 10 years. That's why urban development has not been carried systematically, green area, public space, road, parking space are small or not

built by the requirements of the related norms and standards and some of them even disappeared.

- City is located in seismic active area, but it might be that most of the existing buildings are not resistant enough to earthquake.
- 61.2 percent of the city's population lives in a traditional "ger" tent house, which doesn't have central heating, water supply, and sanitation system, proper roads, green zones, and the ger area is heavily polluted with smoke and dust.
- Now the air-pollution in the city is many times over the permitted level, since in winter time, ger area people use ordinary stove and coal for heating.
- Tuul river has been polluted because many leather processing factories, which use harmful chemicals, are located in the central area.
- Solid waste and other rubbish pollute the city's land, water and air.
- Traffic jam and crashes occur many times due to insufficient traffic network.
- The city, which has over 1 million people, uses big and small buses, cabs, for public transport and always lacks of transport service.
- Central heating, electric, water supply source are not sufficient with the public demand.

In last 8-9 years, our economy is stabilizing, manufactures, companies' capacities are strengthening, and there are many positive changes in the living conditions of the people.

However the problems occurred during the transition period, which influence to the development and safety of Ulaanbaatar city. In order to resolve the problems we are taking the following measures:

- We are drafting "Urban redevelopment law" to create a favorable legal framework in order improving urban planning of Ulaanbaatar city. The draft law includes matters such as neutralizing centralization, developing satellite towns, renewing old apartment buildings and districts, building new apartment areas in the existing ger areas or introducing land readjustment plans in ger areas.
- We are planning to develop the following satellite cities to reduce disaster risk, improve social and economic development:
 - Developing Zuunmod city as wholesaling and servicing, warehousing and transportation center;
 - Develop Baganuur area: as mining, coal- chemistry, electricity, construction material, processing livestock raw materials, developing export oriented production facilities and transportation;

- Developing Nalaikh area: as tourism, student campuses, advanced technology, developing export oriented small size production facilities;
 - Developing Bagakhangai area: as developing export oriented production facilities, wholesaling and trading service, warehousing and transportation;
 - Developing Emeelt-Songino-Tuul mini zone area: as breeding livestock, farming, agriculture and settlement area ;
 - Developing Gorkhi- Terelj area: as relaxing, tourism center.
 - Developing Jargalant mini zone area: as breeding livestock, advanced farming, agricultural, warehousing;
 - Developing Argalant area living area: as product processing, and warehousing.
- Also we are taking some actions such as enforcing to follow urban planning rules and standards, demolishing some non-standard constructions, building roads and creating green areas.
 - Have started checking quality of all apartment buildings using professional tools and devices within 2 years time since its operation. Using the results of this checking process we are going to have a detailed plan to renew the old buildings.
 - In June, the Mongolian Government has made a decision to establish earthquake early warning public system in the capital city and nationwide. To implement the Government's decision, we have started choosing equipments and looking for financial sources. Also "Technical council" with participants of the related organizations has been established.
 - "Law on reduction of the Capital city's air pollution" was approved in January, 2011 by the Parliament of Mongolia. In accordance with the law confinement zones are determined, and non-smoke or smokeless stoves are being introduced.
 - Removing leather processing factors from the central area to isolated area.
 - Research work and studies are under implementation to use metro, monorails and special roads for public bus services.
 - Working to build new 5th Power plant in Ulaanbaatar city.

We hope by implementing the above-mentioned measures, Ulaanbaatar city will become safest city and have clean air, non-polluted water and soil, and green environment, with good quality and modern buildings and infrastructure and the citizens will have good working and living conditions

Evaluation of tsunami strengths of houses subjected to a Tsunami wave load

Gaku SHOJI¹ and Hirofumi SHIMIZU²

¹ Associate Professor, University of Tsukuba, Japan
gshoji@kz.tsukuba.ac.jp

² Graduate Student, University of Tsukuba, Japan

ABSTRACT

The damage of confined-masonry-brick and concrete-block houses is assessed subjected to a tsunami wave load due to the recent three earthquakes and tsunamis at the 2001 Near Coast of Peru, the 2009 Samoa Islands, and the 2010 Maule, Chile. We analyze 13 data surveyed for affected houses, which are single-storey ones located along the coastlines, focusing on the evaluation of tsunami wave pressure distribution on a house inferred by various failure modes when subjected to an inundation depth. Based on the related formula by Asakura et al. (2000) hydraulic experimental results, we identify the required tsunami strength of a wall which is not suffered with an inundation depth.

Keywords: *tsunamis, damage assessment, confined-masonry-brick, concrete-block, tsunami wave pressure*

1. INTRODUCTION

Recent severe earthquakes and tsunamis in the world cause many fatalities and missing: the 2001 Near Coast of Peru, June 23 (UTC 20:33:14, $M_W=8.4$) (2001 Peru tsunami), the 2004 Sumatra, Indonesia, Dec.26 (UTC 00:58:53, $M_W=9.1$) (2004 Indian Ocean tsunami), the 2006 South of Java, Indonesia, July 17 (UTC 08:19:28, $M_W=7.7$) (2006 Java tsunami), the 2009 Samoa Islands, Sept. 29 (UTC 17:48:10, $M_W=8.1$) (2009 Samoa tsunami) and the 2010 Maule, Chile, Feb.27 (UTC 06:34:14, $M_W=8.8$) (2010 Chile tsunami) as well as the Great East Japan earthquake and tsunami occurred on March 11, 2011 in Japan (UTC 05:46:24, $M_W=9.0$) (2011 Japan Tohoku tsunami). The reason of the catastrophe is that houses located within few kilometers from a coastline are suffered severely by a tsunami wave. Therefore it is very essential to clarify the mechanism of a tsunami wave load acting on a house, based on the tsunami damage assessment for suffered houses.

Matsutomi and Izuka (1998) propose the simple formulation to derive the tsunami fluid velocity on a house, based on the results of hydraulic experiments. Matsutomi et al. (2004) clarify the dependence of tsunami fluid force on a house on hydraulic quantity such as a drag coefficient. Asakura et al. (2000) propose the formula (Asakura formula) to evaluate tsunami wave pressure distribution on a structure located at the land behind

on-shore structures and this formula is used for designing a tsunami evacuation building (Japanese Cabinet Office, 2005). Shoji et al. (2007) discuss validness of Asakura formula from damage assessment for suffered houses at the 2006 Java tsunami. Regarding the research on development of tsunami damage function of structures, Matsutomi and Shuto (1994) reveal relations between the inundation depths and velocities, and damage ranks of suffered houses. Koshimura et al. (2009) propose the methodology to develop the tsunami damage function by using tsunami damage data from remote sensing, field survey and numerical analysis.

From the reason above, we analyze the tsunami damage data of confined-masonry-brick and concrete-block houses affected by the 2001 Peru tsunami, the 2009 Samoa tsunami and the 2010 Chile tsunami. Based on the Asakura formula, we identify the required tsunami strength of a wall which is not suffered with an inundation depth.

2. SUBJECT EARTHQUAKE TSUNAMIS AND STRUCTURES

We use the investigation data for damage of concrete-block houses at the 2001 Peru tsunami (Tani et al., 2010) (Peru data), that for damage of lifeline systems and confined-masonry-brick houses at the 2009 Samoa tsunami (Miyajima et al., 2009) (Samoa data) and that for damage of confined-masonry-brick houses at the 2010 Chile tsunami (Shoji et al., 2010) (Chile data). Walls in suffered houses are analyzed. Among all survey data we select houses for analysis which are single-storey ones located along the coastlines and do not affected by floating debris as well as by seismic excitations. It means that houses for analysis have no crack at joint parts of beams and columns, and related structural components such as a beam, a column and a wall get damaged dominantly due to a tsunami wave load. Table 1 shows height H , width B and thickness w of subject wall. In addition Table 1 shows inundation depths h and the related references. Height H , width B and thickness w of subject wall are basically from Peru, Samoa and Chile survey data. When the related data are lacked, we detect those parameters by analyzing the digital pictures for subject walls.

Table 1: Height, width and thickness of subject wall and related observed inundation depth

House's number [※]	Wall's number	Latitude	Longitude	Wall's height <i>H</i> [m]	Wall's width <i>B</i> [m]	Wall's thickness <i>w</i> [m]	Inundation depth <i>h</i> [m]	References for inundation depths
p1	p1	S16°39'19.6"	W72°40'35.1"	2.35	3.50	0.16	2.60	Inundation depth measured 3.3km in the nearest direction (Tani et al., 2010)
p2	p21	S16°39'31.8"	W72°38'45.3"	2.60	3.20	0.16	2.60	Inundation depth measured in the house (Tani et al., 2010)
	p22			2.60	3.60	0.15	2.60	
p3	p3	S16°39'36.0"	W72°38'04.7"	0.65	4.95	0.16	2.13	Inundation depth obtained near the investigation spot(Koshimura, 2001)
p4	p4	S16°39'35.9"	W72°37'59.9"	2.20	3.30	0.16	2.13	Inundation depth obtained near the investigation spot(Koshimura, 2001)
p5	p5	S16°39'35.8"	W72°37'57.2"	2.50	2.80	0.16	2.28	Inundation depth measured in the house (Tani et al., 2010)
s1	s11	S14°15'06.7"	W170°33'53.5"	2.00	2.53	0.15	2.55	Inundation depth measured at the front wall in subject house(Miyajima et al., 2009)
	s12			2.03	3.96	0.15	2.55	
s2	s21	S14°15'15.5"	W170°33'51.9"	1.80	2.68	0.15	2.55	Inundation depth measured 0.3km in the nearest direction(Miyajima et al., 2009)
	s22			1.80	2.16	0.15	2.55	
c1	c1	S36°33'9.69"	W72°57'25.33"	2.33	3.82	0.15	0.97	Inundation depth measured at the side wall in subject house(Shoji et al., 2010)
c2	c2	S36°32'14.89"	W72°57'32.42"	2.07	1.35	0.15	0.81	Inundation depth measured at the side wall in subject house(Shoji et al., 2010)
c3	c3	S36°44'48.72"	W73°53'57"	2.67	2.90	0.15	1.00	Inundation depth measured at the side wall in subject house(Shoji et al., 2010)

※p denotes Peru, s denotes Samoa and c denotes Chile respectively.

3. COMPUTATION OF TSUNAMI STRENGTHS OF SUBJECT WALLS

3.1 Calculation of Tsunami Strengths

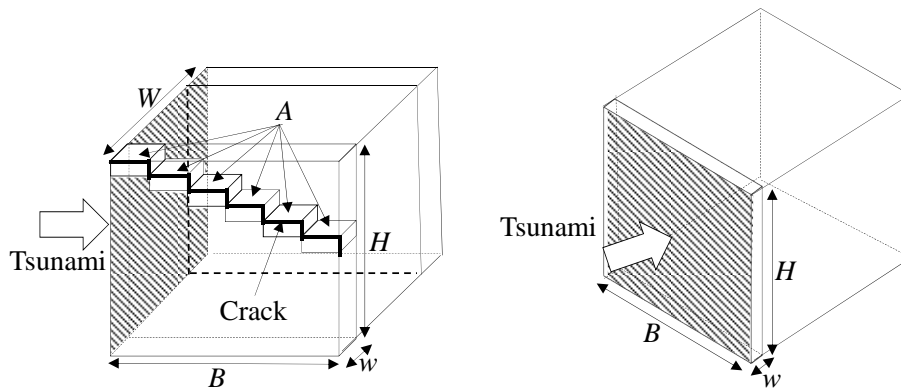
3.1.1 Type1 Failure Mode

As shown in Figure 1(a), when shear cracks occur in paired walls which are placed at right angles to a coastline, we classify the failure mode of a wall as type1 failure mode (hereinafter ty1). Shear strength of a wall with ty1 V_1 is calculated as the following equation, by setting $W=W/2$ when adapting Asakura formula,

$$V_1 = \tau_1 A \tag{1}$$

where A is cumulative surface areas of bricks and concrete-blocks, since a wall is made by bonding bricks and concrete-blocks with mortar. In Eq. (1) τ_1 is shear stress and we set the value of τ_1 based on the following procedure by referring the value of 0.4 N/mm² by previous research (Nakano, 2005, and Nakano and Park, 2005a, 2005b). For dealing with Peru data (concrete-blocks) τ_1 is assumed to be 0.2N/mm² which is 1/10 of compression strength of a concrete-block used for a non-proof-

strengthening wall (Ministerio de Vivienda, Republica del Peru, 2006). For dealing with Chile data (masonry-bricks) τ_1 is assumed to be 0.35N/mm^2 , which is conservative value, and which is 1/20 of compression



(a) Paired walls placed at right angles to a coastline
(b) A wall out of placed along a coastline

Figure 1: Relation between direction of a tsunami wave and longitudinal axis of subject wall strength of a brick used for a prism-type wall specimen (Yanez et al., 2004).

3.1.2 Type2 Failure Mode

As shown in Figure 1(b), when tensile and shear failures occur out of a wall placed along a coastline, we classify the failure mode of a wall as type 2 failure mode (hereinafter ty2). Ty2 is classified into two mechanisms: tensile failure between bricks and concrete-blocks bonded with a frame by mortar (mechanism 1; ty2-m1) and shear failure between those (mechanism 2; ty2-m2).

We calculate tensile strength T_2 and shear strength V_2 by the following equations, by setting $W = B$ when adapting Asakura formula,

$$T_2 = 2(B + H)w\sigma_2 \quad (2a)$$

$$V_2 = 2(B + H)w\tau_2 \quad (2b)$$

where σ_2 is tensile stress between bricks and concrete-blocks bonded with a frame by mortar, and we use the value of $\sigma_2 = 0.24\text{N/mm}^2$ by referring Architectural Institute of Japan Standard Specifications for Concrete-Block Structures (1997). τ_2 is shear stress between bricks and concrete-blocks bonded with a frame by mortar, which value is assumed to be 0.09N/mm^2 from the research by Sanada et al. (2006).

3.2 Results on Tsunami Strength

Table 2 shows results of ty1 shear strength V_1 , ty2 tensile strength T_2 and ty2 shear strength V_2 , and the parameters related with tsunami wave pressure on subject wall as we mention later.

Wall p1 failure mode is assumed to be ty2 since p1 failed out of the plane. Based on ty2-m1, $T_2=2\times(2350\text{mm}+3500\text{mm})\times 160\text{mm}\times 0.24\text{N}/\text{mm}^2=449.28\text{kN}$, while based on ty2-m2, $V_2=2\times(2350\text{mm}+3500\text{mm})\times 160\text{mm}\times 0.09\text{N}/\text{mm}^2=168.48\text{kN}$. As well wall p21 failure mode is assumed to be ty2 since most part of it was collapsed. Hence, for p21 T_2 and V_2 are computed respectively as shown in Table 2. In contrast, wall p22 is placed at right angles to the coastline in the same house as wall p21, then the failure mode is assumed to be ty1. Based on ty1 for wall p22 $V_1=0.2\text{N}/\text{mm}^2\times 3600\text{mm}\times 150\text{mm}=108.00\text{kN}$. On the other hand we can suppose wall p22 failed out of the plane after the tsunami flow attacked wall p21. Viewed in this light wall p22 failure mode is assumed to be ty2, and the related values of T_2 and V_2 are computed as shown in Table 2. Wall p3 failure mode is assumed to be ty2 since most part of it was collapsed as well as wall p1. By considering wall p3 boundary conditions as upper and one side boundaries are free, we compute T_2 and V_2 by modified Eq (2a) and (2b): $T_2 = (B + H)w\sigma_2$ and $V_2 = (B + H)w\tau_2$ as shown in Table 2. In the same way, for rest of Peru data (p4, p5), Samoa data (s11, s12, s21, s22) and Chile data (c1, c2, c3), the related wall failure mode is classified into ty1 and ty2, and we compute V_1 , T_2 and V_2 as shown in Table 2.

Table 2: Computed ty1 shear strength V_1 , ty2 tensile strength T_2 and ty2 shear strength V_2 , and the parameters related with tsunami wave pressure on subject wall

Wall's number	Failue mode number	Tensile stress [kN]	Shear stress [kN]	η'	a
p 1	p 1-ty2-m1	449.28	-	6.75	2.60
	p 1-ty2-m2	-	168.48	3.26	1.25
p21	p21-ty2-m1	445.44	-	6.76	2.60
	p21-ty2-m2	-	167.04	3.35	1.29
p22	p22-ty1	-	108.00	2.77	1.07
	p22-ty2-m1	446.40	-	6.16	2.37
	p22-ty2-m2	-	167.40	3.12	1.20
p3	p3-ty2-m1	215.04	-	7.14	3.35
	p3-ty2-m2	-	80.64	2.88	1.35
p4	p4-ty 1	-	105.60	2.66	1.25
p5	p5-ty2-m1	407.04	-	7.18	3.15
	p5-ty2-m2	-	152.64	3.47	1.52
s11	s11-ty2-m1	326.16	-	7.57	2.97
	s11-ty2-m2	-	122.31	3.46	1.36
s12	s12-ty2-m1	431.28	-	6.49	2.55
	s12-ty2-m2	-	161.73	3.06	1.20
s21	s21-ty2-m1	322.56	-	7.72	3.03
	s21-ty2-m2	-	120.96	3.46	1.36
s22	s22-ty2-m1	218.88	-	8.38	3.29
	s22-ty2-m2	-	82.08	3.70	1.45
c1	c1-ty2-m1	442.80	-	6.23	6.77
	c1-ty2-m2	-	166.05	3.07	3.34
c2	c2-ty 1	-	70.88	3.57	4.41
c3	c3-ty 1	-	152.25	5.12	5.12

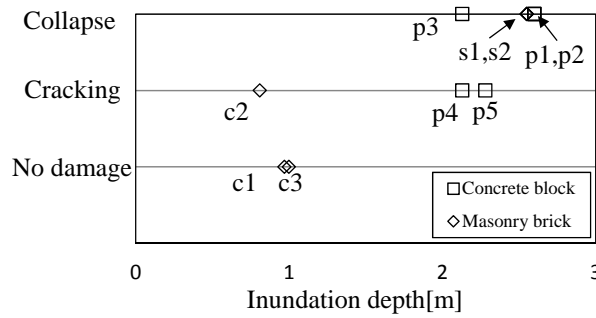


Figure 2: Relation between inundation depth and damage rank of subject wall

4. TSUNAMI WAVE PRESSURE DISTRIBUTION ON SUBJECT WALLS

4.1 Relation between Inundation Depth and Damage Rank

Figure 2 shows relation between observed inundation depth and damage rank of subject wall. We categorize wall damage into three damage ranks: completely and mostly collapse (collapse), partially collapse and occurrence of cracks (cracking), and no structural damage (no damage). Damage ranks of ‘collapse’ and ‘cracking’ for concrete-block houses (Peru data) show in the range of inundation depth from 2.13m to 2.60m. Damage ranks of ‘no damage’ and ‘cracking’ for masonry-brick houses (Samoa and Chile data) show with inundation depth from 0.81m to 1.00m, and damage rank of ‘collapse’ with inundation depth 2.55m.

4.2 Evaluation of Tsunami Wave Pressure Distribution based on Observed Inundation Depth

Tsunami wave pressure distribution on subject wall in horizontal direction is computed by the following Asakura formula (Asakura et al. 2000),

$$p_x(z) = \rho g (a\eta_{\max} - z) \tag{3}$$

where $p_x(z)$ is horizontal wave pressure, η_{\max} is maximum run-up height, ρ is density of mass of sea water in a unit volume and z is height from ground level. a is defined as horizontal wave pressure index which means magnification factor of hydrodynamic pressure on a rigid body due to a tsunami wave compared with hydrostatic pressure with η_{\max} . Asakura et al. indicate $a = 3.0$ for a non-breaking wave from their experimental results. Therefore it indicates that assumption of $a \geq 3.0$ is required theoretically to design a tsunami-proof structural component subjected to a non-breaking tsunami wave. To put it another way for a non-breaking tsunami wave, horizontal wave pressure distribution of $a = 3.0$ on a structural component is the border that a structural component becomes whether damaged or

undamaged. In this study firstly we suppose ty1, ty2-m1 and ty2-m2 failure modes defined in Section 3.1 for subject walls exposed to a tsunami wave and calculate the corresponding tsunami strength R (including ty1 shear strength V_1 , ty2 tensile strength T_2 and ty2 shear strength V_2). Second we compute inversely the value of a as the following equations by assuming η_{\max} equal to be observed inundation depth h . By comparing the value of a with tsunami damage of subject walls, we discuss validness of Asakura formula.

$$a = \frac{1}{h} \sqrt{\frac{2R}{\rho g W}} \quad (4a)$$

$$a = \frac{1}{2h} \left(\frac{2R}{\rho g W H} + H \right) \quad (4b)$$

where W is width of a wall subjected to a tsunami wave as shown in Figure 1. When the value of $\eta' = a\eta_{\max}$ is less than or equal to a wall height H , horizontal wave pressure distribution is the triangle one as shown and a is computed by Eq (4a). When the value of $\eta' = a\eta_{\max}$ is more than a wall height H , horizontal wave pressure distribution is the trapezoid one and a is computed by Eq (4b). Table 2 shows computed η' and a . Figure 3 shows relation of a with observed inundation depth h . Similarly, Figure 4 shows the results for Sri Lank and Thailand data at the 2004 Indian Ocean tsunami by Nakano et al. (2005) and Java data at the 2006 Java tsunami by Shoji et al. (2007) as well as in Figure 3, with showing the analytical results corresponding to ty1 and ty2 failure modes for subject walls.

From Figure 3(a) among Peru data 10 data with $a \leq 3.0$ are observed. a shows 1.07~2.60 for inundation depth h of 2.13m~2.60m, which indicates Asakura formula is valid in these cases because these walls are actually suffered with the damage rank of either 'collapse' or 'cracking'. On the other hand among Peru data 2 data with $a > 3.0$ are observed, showing the collapse: 3.35 with h of 2.13m and 3.15 with h of 2.28m. It is inferred from these data that when the value of a is slightly larger than 3.0, a wall has low possibility to actually collapse due to variation of strength of material properties and construction condition when fabricating a wall. For Samoa data (Figure 3(b)) 6 data with $a \leq 3.0$ are observed, showing 1.20~2.97 with h of 2.55m. These walls collapse actually, the reason is why Asakura formula is valid in these cases. In addition 2 data with $a > 3.0$ are observed as well as for Peru data: 3.03 and 3.29 with h of 2.55m. These walls also collapse although $a > 3.0$. From Figure 3(c) Chile data has 4 data with $a > 3.0$: they show 3.34~6.77 with h of 0.81m~1.00m. Among them we can say Asakura formula may be valid because 3 data have no damage although one data shows cracking.

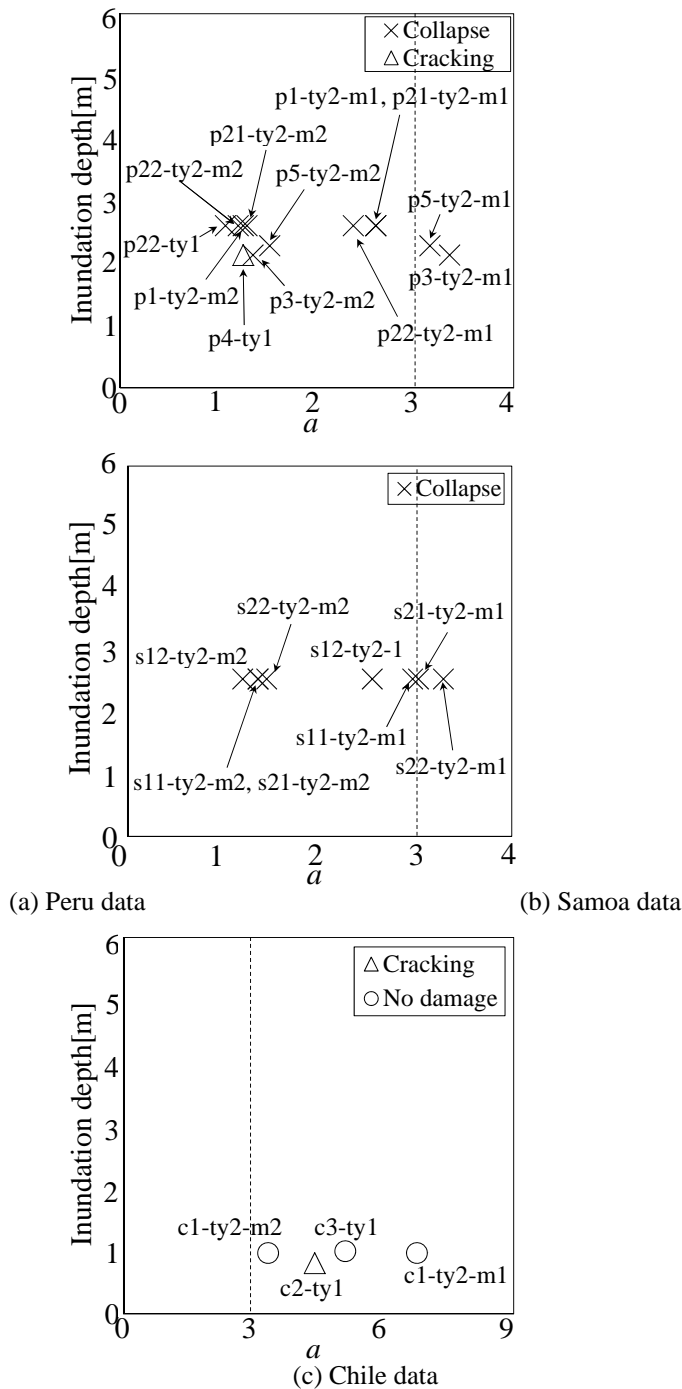
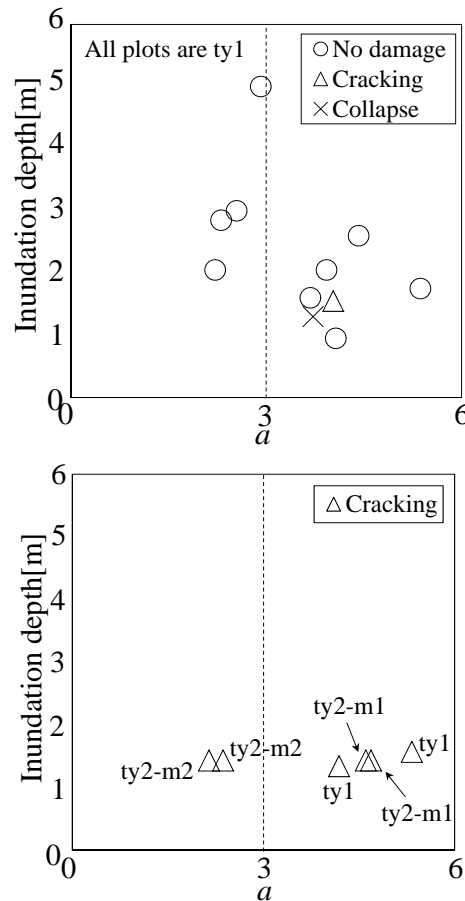


Figure 3: Relation between computed horizontal wave pressure index a and observed inundation depth h for Peru, Samoa and Chile data

When walls with a of slightly larger than 3.0 in Peru and Samoa data are assumed to be suffered by ty2-m2, a becomes less than or equal to be 3.0. It is quite likely that these walls actually collapsed with a failure mode by not ty2-m1 but ty2-m2.

By comparing Figure 3(a), (b) with Figure 4(a), no data with $a \leq 3.0$ showing no damage in Peru and Samoa data are observed while 4 data with $a \leq 3.0$ showing no damage in Sri Lanka and Thailand data are observed. In contrast, Sri Lanka and Thailand data have one data with collapse regardless

of $a > 3.0$ as well as Peru and Samoa data. By comparing Figure 3(c) with Figure 4(b), as we mentioned above, there are one data with $a > 3.0$ showing cracking with ty1 failure mode in Chile data as well as two data in Java data, which a especially show 4.19~5.33. Therefore it is possible that a wall with a of around 4~5 beyond $a = 3.0$, that has larger tsunami strength, suffers with cracking failure mode due to a tsunami wave.



(a) Sri Lanka and Thailand data

(b) Java data

Figure 4: Relation between computed horizontal wave pressure index a and observed inundation depth h for Sri Lanka and Thailand data (Nakano et al., 2005), and Java data (Shoji et al., 2007)

5. CONCLUSIONS

We analyzed the tsunami damage data of confined-masonry-brick and concrete-block houses affected by the 2001 Peru tsunami, the 2009 Samoa tsunami and the 2010 Chile tsunami. We classified them into three failure modes of a wall subjected to a tsunami wave: shear cracks induced in paired walls which are placed at right angles to a coastline (ty1), tensile failure induced out of a wall between bricks and concrete-blocks bonded with a frame by mortar (ty2 mechanism 1) and shear failure induced out of a wall between those (ty2 mechanism 2). Based on the formula proposed by Asakura et al. (2000) (Asakura formula) to evaluate tsunami wave pressure distribution on a structure located at the land behind on-shore structures,

used for designing a tsunami evacuation building (Japanese Cabinet Office, 2005), by assuming 24 failure modes for subject 13 walls, we identified the required tsunami strength of a wall which is not suffered with an inundation depth. Following conclusions were deduced.

(1) 16 data with $a \leq 3.0$ show collapse and cracking failure modes, and 3 data with $a > 3.0$ show no damage among 24 assumed failure modes. Hence from these results, Asakura formula is almost valid to evaluate tsunami strength of a wall subjected to a non-breaking tsunami wave.

(2) When subject walls with a of slightly larger than 3.0 (3.03~3.35) in Peru and Samoa data are assumed to be suffered by ty2 mechanism 2, a becomes less than or equal to be 3.0. It is quite likely that these walls actually collapsed with failure mode by not ty2 mechanism 1 but ty2 mechanism 2.

(3) One data with $a > 3.0$ showing cracking with ty1 failure mode in Chile data is observed as well as two data in Java data, which a especially show 4.19~5.33. Therefore it is possible that a wall with a of around 4~5 beyond $a = 3.0$, that has larger tsunami strength, suffers with cracking failure mode due to a tsunami wave.

ACKNOWLEDGEMENTS

This study was sponsored by the research project on earthquake and tsunami disaster mitigation in Peru under the framework of "Science and Technology Research Partnership for Sustainable Development (SATREPS)", by Japan Science and Technology Agency (JST) and Japan International Cooperation Agency (JICA) (leader, Professor F. Yamazaki at Chiba University and Professor S. Koshimura at Tohoku University). And the authors deeply appreciate research information and valuable assistance associated with the field survey provided by the related professors, researchers and officers of local government at Peru, American Samoa and Chile.

REFERENCES

- Architectural Institute of Japan, 1997. *Standard Specifications for Concrete-Block Structures*.
- Asakura, R., Iwase, K., Iketani, T., Takao, M., Kaneto, T., Fujii, N., and Ohmori, M., 2000. Experimental study on wave force acting on on-shore structures due to overflowing tsunamis. *Proceedings of Coastal Engineering* 47, JSCE, 911-915.
- Japanese Cabinet Office, 2005. *Guideline for Tsunami Evacuation Building*. <http://www.bousai.go.jp/oshirase/h17/050610/guideline.pdf>, 2011.2.13.
- Koshimura, S., Okal, E., Dengler, L., Araya, S., Borrero, J., Gomer, B., Laos, G., Olcese, D., Ortiz, M., Swensson, M., Titov, V., and Vegas, F., 2002. Field survey of the 2001 Peruvian Earthquake Tsunami. *Proceedings of Coastal Engineering* 49, JSCE, 1461-1465.

Koshimura, S., Namegaya, Y., and Yanagisawa, H., 2009. Fragility functions for tsunami damage estimation, *Doboku Gakkai Ronbunshuu B*, Vol.65, No. 4, 320-331.

Matsutomi, H., and Shuto, N., 1994. Tsunami inundation depth, tsunami velocity and the related damage of houses. *Proceedings of Coastal Engineering* 41, JSCE, 246-250.

Matsutomi, H., and Iizuka, H., 1998. Tsunami current velocity on land and its simple estimation method. *Proceedings of Coastal Engineering* 45, JSCE, 361-365.

Matsutomi, H., Ohmukai, T., and Imai, K., 2004. Fluid force on a structure due an inundated flow caused by a tsunami. *Proceedings of Hydraulic Engineering* 48, JSCE, 559-564.

Ministerio de Vivienda, Republica del Peru, 2006. *Reglamento Nacional de Edificaciones E.070* Albanileria.

Miyajima, M., Shoji, G., and Shigihara, Y., 2009. Reconnaissance of the damage caused by the September 29th, 2009, Samoa Islands Earthquake and Tsunami in American Samoa. *Proceedings of the symposium on disaster mitigation of lifelines considering system interactions*, JSCE, 40-45.

Nakano, Y., 2005. *Investigation Report for Damaged Structures due to the 2004 Indian Ocean Tsunami* Ver. 2.2. <http://sismo.iis.u-tokyo.ac.jp/Research.files/topic4.files/topic4-007.files/T4-7-1.pdf>.

Nakano, Y., and Park, J., 2005a. Studies on lateral resistance of structures and tsunami load caused by the 2004 Sumatra Earthquake Part 1 Outline of survey. *Proceedings of AIJ Annual Meeting*, 723-724.

Nakano, Y., and Park, J., 2005b. Studies on lateral resistance of structures and tsunami load caused by the 2004 Sumatra Earthquake Part 2 Comparison of tsunami load and lateral resistance. *Proceedings of AIJ Annual Meeting*, 725-726.

Sanada, Y., Nakamura, Y., Yamauchi, N., Ho, C., and Nakano, Y., 2006. A method to enhance seismic performances of unreinforced masonry structures derived from lateral force resisting mechanisms of masonry infilled frames. *Journal of Structural and Construction Engineering* 605, AIJ, 159-166.

Shoji, G., Moriyama, T., Kosa, K., Matsutomi, H., Shigihara, Y., and Murashima, Y., 2007. Damage assessment of structures due to the 2006 Java Tsunami. *Proceedings of Coastal Engineering* 54, JSCE, 861-865.

Shoji, G., Pulido, N., Sekiguchi, T., Alva, J., Lazares F., and Saito, T., 2010. Damage investigation of the 2010 Chile Earthquake and Tsunami - consideration to the damage of a structure subjected to a seismic excitation and a following tsunami wave load. *Proceedings of 13th Japan Earthquake Engineering Symposium*, 1146-1150.

Tani, Y., Shoji, G., Koshimura, S., and Estrada, M., 2010. Damage assessment of houses due to the 2001 Southern Peru Earthquake and Tsunami. *Proceedings of 13th Japan Earthquake Engineering Symposium*, 829-836.

USGS, http://neic.usgs.gov/neis/eq_depot/2001/eq_010623/, 2011.2.13.

USGS, <http://earthquake.usgs.gov/earthquakes/eqinthenews/2009/us2009mdbi/>,

2011.2.13.

USGS,<http://earthquake.usgs.gov/earthquakes/eqinthenews/2010/us2010tfan/>, 2011.2.13.

Yanez, F., Astroza, M., Holmberg, A., and Ogaz, O., 2004. Behavior of confined masonry shear walls with large openings, *Proceedings of 13th World Conference on Earthquake Engineering*, Paper No. 3438

Integrated climate adaptation and disaster resilience - a landscape cooperatives paradigm

Alfredo ANCENO¹, Nitin TRIPATHI², and Oleg SHIPIN³

¹ Research Scientist, EEM FoS, Asian Institute of Technology, Thailand

² Associate Professor, RS-GIS FoS, Asian Institute of Technology, Thailand

³ Associate Professor, EEM FoS, Asian Institute of Technology, Thailand
anceno@ait.ac.th, nitinkt@ait.ac.th, oshipin@ait.ac.th

ABSTRACT

Strategic approaches to climate change adaptation (CAA) and disaster risk reduction (DRR) have traditionally operated in isolation from each other, posing a challenge to integration into development planning processes. CAA deals exclusively with climate-related hazards of global and longer temporal scale, while DRR focuses mainly on national/local levels. Interactions and funding between these two approaches are often ad-hoc, while systematic efforts to sustain and institutionalize these interactions have been limited. Recently, however, developments in CAA and DRR approaches are converging. DRR approaches tend to coincide with a future-oriented perspective of CAA on vulnerabilities, while CAA emphasizes improved government capacity in addressing climaterelated disaster risks and vulnerabilities. Vulnerabilities and gaps nevertheless remain due to uncoordinated initiatives, particularly true of many Southeast Asian countries where disaster efforts are focused on relief and rehabilitation while existing CAA-DRR measures and policies remain uncoordinated. We hence expound a landscape cooperatives paradigm whereby the governance, technology, and policy support layers that rationally integrate climate adaptation (CA) and disaster resilience (DR) strategies are amply addressed.

Keywords: *climate adaptation, disaster resilience, landscape cooperatives, integrated approaches to sustainable development, web-based geospatial information, strategic environmental assessment*

1. CONTEXTS AND RATIONALE

Hazards are phenomena that may manifest with or without warning that threaten natural, economic, political, and social processes. A full range of hazards includes those of natural cause or induced by anthropogenic processes. Whereas *climaterelated* or *hydro-meteorological hazards* only represent one type of hazard, these actually constitute 90% of natural hazards. *Climate change* alters the average climatic conditions and climate variability, causing increased magnitude and frequency of climate-related hazards. *Disaster* results from a progression of vulnerability from

underlying causes and trigger events or hazards, while *adaptation* or *resilience* results from reduction of vulnerabilities and mitigation of hazards (Figure 1). Policies and measures aimed at addressing climate change and disaster management issues are referred to as *climate change adaptation* (CCA) and *disaster risk reduction* (DRR), respectively. CCA is defined as an adjustment in natural or human systems in response to actual or expected climate stimuli or their effects, which moderates harm or exploits beneficial opportunities (IPCC, 2007); whereas DRR the broad development and application of policies, strategies and practices to minimize vulnerabilities and disaster risks throughout society, through prevention, mitigation and preparedness (UNISDR, 2004).

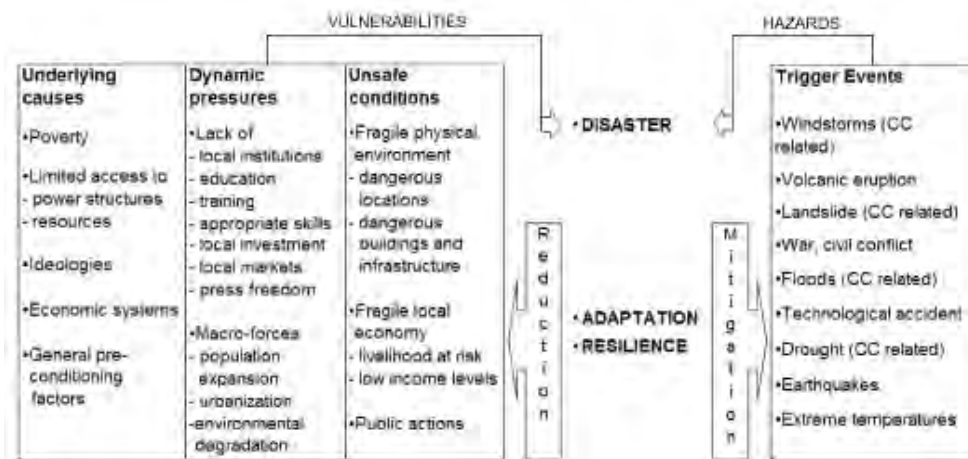


Figure 1: Contextualization of climate change (CC) related disasters and adaptation/resilience pressures, adapted and modified from IFRCRCS (2006).

Because the time frames for reactive adaptations to climate change (longer time scale) and disasters (immediate) are distinct, CCA deals exclusively with climaterelated hazards of global scope while DRR is focused on national/local levels (Table 1). In many Asian countries, DRR is the concern of national disaster management offices, while CCA is led by the departments/ministries of environment (USAID-OFDA, 2009). Interactions between these two and funding are often ad-hoc and systematic efforts made to sustain and institutionalize these interactions were limited (Ahmed, 2010). On the other hand, the aims of both CCA and DRR to reduce adverse effects of external impacts, natural hazard risk and climate change are increasingly converging (Schipper and Pelling, 2006; Thomalla et al., 2006). DRR adopts a more anticipatory approach on future vulnerabilities, typically a CCA disposition. CCA also increasingly emphasize on improving the capacity of governments and communities in addressing vulnerabilities and hazards, typically a DRR disposition. Despite efforts, Asia-Pacific governments still seem to have little capacity to systematically organize and prioritize CCA-DRR activities (SELA, 2010).

Table 1: Comparison of CCA and DRR contexts

	DRR	CCA
Objective pursued	Identify risk reduction measures; reduce probability of damage	How to face a progressive climate change: adaptation relevance and strategies
Kind of process	Natural hazards—"shock", relevant to all hazard types	Progressive and irreversible—"stress", relevant to climate-related hazards
Timescale	Event-scale (before/during/after), discrete events, static processes	Long-term and progressive viewpoint (e.g. 2100) discrete and continuous, dynamic processes
Spatial scale	From a local consideration to a global one	From a global awareness to a local need
Functional scale	Often lies within the responsibility of the Ministry of the Interior, Defense or Development	Mainly environment ministries and meteorological services
Simplified formulation	Risk = Hazard × Exposure × Vulnerability	Vulnerability = Impacts - Adaptation
Vulnerability assessment	Step within risk assessment	End in itself
Level of uncertainty	Low to medium: risk is associated with a notion of probability of occurrence at any time	Medium to very high; prospective scenarios until a given term
Origin and culture	Humanitarian assistance following a disaster event, stem from experience	Scientific theory, stem from policy agenda
Traditional or indigenous knowledge	Basis for resilience at community level	May be insufficient for resilience against types and scales of risk yet to be experienced
Structural measures per safety levels	Modeled on current and historical evidence	Modeled on current and historical evidence and predicted changes
Application	Practical application at local level	Theoretical application at local level
Tools	Full range of established and developing tools	Limited range of tools under development
Development and recognition	Incremental development, political and widespread recognition often quite weak	New and emerging agenda, political and widespread recognition increasingly strong
Funding streams	Ad hoc and insufficient	Sizeable and increasing

SOURCES: Schipper and Pelling (2006), Thomalla et al. (2006), Tearfund (2008), Romieu et al. (2010) and Mercer (2010).

Given that a variety of factors exacerbate vulnerability to the climate related disasters, often unrelated to physical environment but are rather societal in nature (USAID-RDMA, 2008), an integrated approach is needed to address this complex issue without compromising environmental sustainability. Here we address a major strategy and implementation gap characteristic of the entire planet but particularly relevant to the third countries, notoriously prone to climate change and disaster-related risks. The gap is an improper and insufficient integration of issues pertaining to CCA and DRR into development planning both in developed and developing worlds (Tearfund, 2008; USAID-RDMA, 2008; Wamsler, 2009). This calls for an approach that simultaneously addresses such adaptation/resiliency capacity aspects as (i) institutional framework, (ii) technological support, (iii) policy advocacy, and (iv) community-driven interventions, including appropriate spatial and temporal scales for planning and assessment.

2. INSTITUTIONAL FRAMEWORK

Mechanisms to address the short-comings of the nexus between climate change, development planning and the incomplete approaches to risk reduction and its mainstreaming require a governance framework to enhance cooperation. An inspirational example of such a knowledge sharing-coordination platform is the recent introduction of the Landscape Conservation Cooperatives (LCC) by the US Fish and Wildlife Service: 20 LCCs were introduced across the US. Essential features of LCCs include a steering committee that provides management direction, science and technology coordinators, geospatial information system capacity, and decision analysis expertise. LCCs are expected to provide a major boost to frequently failing community-based conservation of natural landscapes impacted by land use pressures and resource threats, amplified by a changing climate and related disasters (USFWS, 2009). The concept of conserving wildlife communities the LCC way may well be adapted for the “conservation” of human communities—*i.e.* saving them from the effects of climate change and disasters— a conceptually similar effort within identified landscapes. We hence envision *landscape climate adaptation and disaster resilience cooperatives* (LCADRCs) which are fundamental units of partnership in planning and science capacity, targeting the right scientific and technological approach for efficient and effective climate adaptation (CA) and disaster resilience (DR) in defined geographic areas or landscapes. We define *landscape* as the entire range of identified priority terrain or topography classified according to density of settlements (*e.g.* urban, peri-urban, rural), ecosystem quality (*e.g.* pristine, semi-pristine, exploited/degraded), elevation (*e.g.* high-altitude, low-lying), and relevant hazard and vulnerabilities.

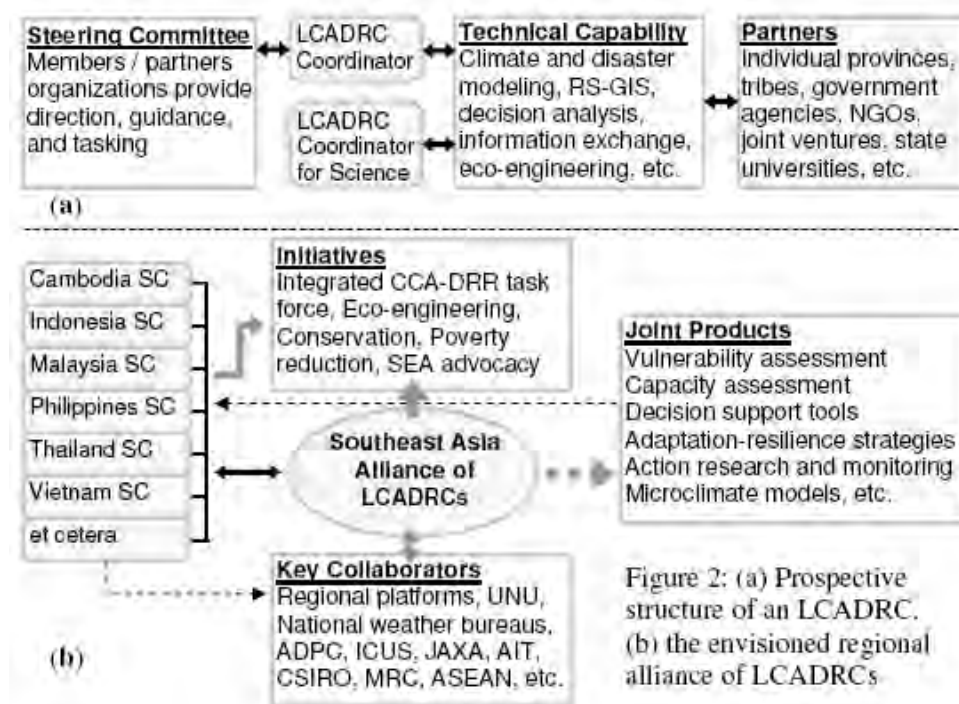


Figure 2: (a) Prospective structure of an LCADRC. (b) the envisioned regional alliance of LCADRCs

LCADRCs' core functions will be predicting climate and disaster impacts, mitigating them and, if not possible, adapting to them, thereby reducing vulnerability to risks and as a result creating optimal functional conditions for the communities. The LCADRC coordinator will facilitate the link between science, technology and management, and provide day-to-day leadership of the partnership. All staff positions, including the coordinator, may be supported through any participating organization, or shared between organizations. Core staff may be colocated within a partner facility while complementary staff may participate virtually from remote locations. Staff may be added in phases as the LCADRC matures and demand for LCADRC products and services change and grow. LCADRC technical personnel will share their expertise both within and across LCADRCs by participating in local, national, and international training programs. Not to overburden existing governance structures, these cooperatives are best integrated into national community empowerment national programs (CENPs) that are already operational. Since climate change and disasters contribute to poverty and hit hardest on the poor, CENPs can be value added by introducing LCADRC components and also represented in national LCADRC steering committee (SC). Appropriate examples of CENPs are Program Nasional Pemberdayaan Masyarakat of Indonesia, Gawad Kalinga of the Philippines, The Learning Institute of Cambodia, etc.

As a shared local platform, the cooperatives will deliver geospatial and decisionsupport tools and products to *coordinate* action of local communities, NGOs, government agencies, donors, and others. LCADRCs will also strengthen the capacity of local governments and communities to support implementation of the governments' national plan for disaster risk reduction and climate adaptation. At the national level, the LCADRC steering committee will form partnerships with local governments to form local LCADRC partnerships and to establish the core functions and services within the institutional framework of local governments and administrative structure of CENPs. Internationally, LCADRCs will collaborate with regional and international partners to obtain scientific and technical support for a wide range of CA-DR activities tailored to local priorities and needs.

3. TECHNOLOGICAL SUPPORT

Regional geospatial Earth observation capability is a powerful and essential tool to achieve CA-DR via environmental management. However, there exists a very limited Asian network of national geospatial centers and therefore no exchange of regional expertise takes place. A *geospatial information sharing tool* (GIST) is hence envisioned. GIST is a hardware-software and applications framework that facilitates geospatial information sharing and technical coordination/support issues in addressing regional climate adaptation, disaster resilience, and other environmental challenges. A motivating example of a model platform is SERVIR (www.servir.net), an earth observation, monitoring, and visualization system (NASA-USAID). Established in 2008, SERVIR integrates satellite and other geospatial data

for improved scientific knowledge and decision-making by managers, researchers, students, and the general public including local communities. SERVIR decision support tools and data are currently used to address issues related to climate change, disasters, ecosystems, biodiversity, health, and water in the Central America and Africa. In 2010, the first Asian SERVIR node was introduced in the Himalayas through the International Center for Integrated Mountain Development (ICIMOD).

Networking of National Spatial Data Infrastructures (NSDI) in Southeast Asia is encouraged as a testing ground for GIST, *conceptually modeled* after SERVIR. The NSDIs can provide a backbone for the regional cooperation with the creation of a regional geospatial hub, bringing together partners through collaborations among national and regional atmospheric, meteorological, and geophysical bureaus. There is also a necessity to explore and better understand mechanisms of strengthening specific policy, governance, and capabilities of national geospatial mapping centers (Philippine's PAGASA, Thailand's GISTDA, Indonesia's BAKUSORTANAL, etc.) to best support information sharing for planning and coordination of climate adaptation activities at the local and national levels through GIST in the LCADRC framework. Baseline needs assessment must be undertaken to address a multitude of relevant spheres for which GIST is critically important. The established GIST framework will (i) provide a common web-based platform for sharing geospatial information, maps, and satellite data among LCADRCs; (ii) provide a common web-based platform for sharing weather related data, including meteorological data gathered from sensors installed in target landscapes; (iii) tap state universities to serve as regional service centers for training and capacity building in geospatial applications for development; and (iv) provide decision support tools and data to address issues related to disasters, ecosystems, health, water, weather, and climate change.

4. POLICY ADVOCACY

Strategic environmental assessment (SEA) is an approach for mainstreaming and 'upstreaming' environmental sustainability in the decision-making hierarchy, addressing the issue of environmental sustainability as early as possible in the decision making process (OECD, 2006). SEA has emerged due to the shortcoming of conventional environmental assessment approaches (*e.g.* environmental assessment or EIA) to tackle increasingly complex environmental issues, including their integration with economic and social issues at the highest levels of planning and decision making (Partidário, 2004). A major advantage of an SEA framework is setting a strategic context for project environmental assessment, making the latter more efficient (Stinchcombe and Gibson, 2001). As Figure 3 shows, SEA for flood control is a tiered planning process.

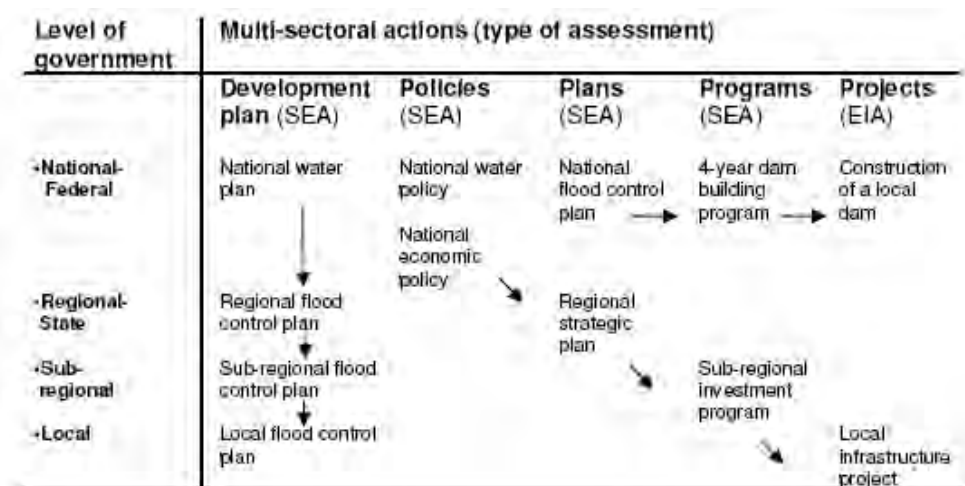


Figure 3: Tiered decision making for water and flood control development, adapted and modified from Jones et al. (2005).

Although some developing Asian countries very recently introduced SEA as a legal requirement for newly proposed development planning at the national and local levels, implementation is constrained by weaknesses in technical capacity to apply the SEA framework in policy, planning, and implementation at the local and national levels. Building capacity for SEA provides an opportunity for strategic planning to apply “CA-DR lens” to the development scenarios (OECD, 2008a, b). Mechanisms such as stakeholder seminars and participatory rural appraisals will be applied to help bridge macro-level (SEA-based) and micro-level (landscape/community-based) environmental management. With micro-level currently a neglected area, such mechanisms will provide a feedback loop for addressing local grassroots issues to better inform strategic planning at and national level. Actively engaging local communities in the strategic planning process will lead to an increased acceptance of the SEA concepts at district and local community levels. Introducing SEA into CA-DR, and, vice versa, will be viewed as a novel feature and good practice among LCADRCs.

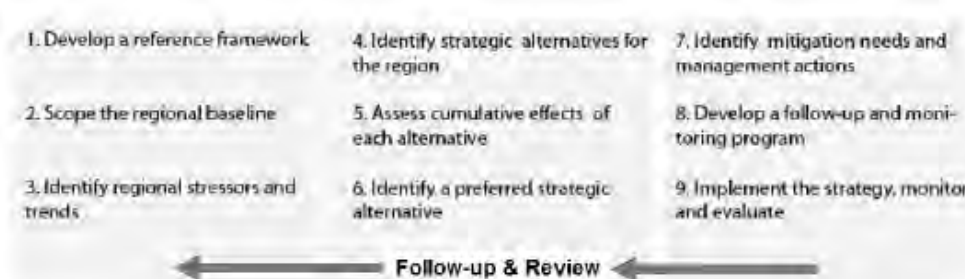


Figure 4: R-SEA framework, adapted and modified from Gunn and Noble (2009).

Also a recently explored “futures-oriented” approach in regional development planning, *regional SEA* (R-SEA, Figure 4), emphasizes alternative development scenarios and the means of achieving these (Gunn and Noble, 2009). In the RSEA approach, developed in Canada and endorsed by the Canadian Council of Ministers of Environment (2009),

emphasis is placed on ensuring the sustainability of a region and a desired level of environmental or socio-economic quality, rather than solely on impact mitigation. It facilitates a more proactive and integrated approach to SEA, and one that explicitly operates at the regional scale so as to facilitate the assessment of cumulative environmental effects of multiple initiatives within a relevant region (river basin, *etc.*). A major feature of R-SEA is *cumulative effects assessment* (CEA) to account for the complex nature and pace of interventions related to climate adaptation and water, rather than primarily focus on program/plan/policy approval. Of particular concern are *cumulative effects* of development on the environment which are critically important but problematic to integrate into environmental assessment. An illustrative example is water scarcity which, in the face of competing cumulative demands for food production, domestic, industrial, energy and environmental purposes, reduces community resilience to disasters. Fresh water is such a limited resource that scarcity leads to a potential for user conflicts (USAID-OFDA, 2009). The need to increase community resilience to droughts and water scarcity through programs that promote efficient water management practices (water harvesting, treatment and conservation) is thus prominent. Furthermore, small-scale disasters in aggregate frequently affect more people and cause greater economic damage than less frequent, large-scale disasters. Developing communities often fail to comprehend the significance of cumulative effects or see the long-term accumulation of impacts by drivers of change. This therefore calls for serious consideration in strategic development planning in the context of LCADRCs.

5. COMMUNITY-DRIVEN INTERVENTIONS

Ecological engineering (EE) offers a nature-based, robust and sustainable approach to deal with multiple cumulative effects of climate change, disasters and poverty reduction. In the case of wetland landscape for example, the *multifunctional wetlands approach* based on EE appears to be most appropriate (Wickramasinghe et al., 2009) way to tackle the challenges while generating cobenefits such as livelihoods, carbon sequestration, green energy, health, and wellbeing, *etc.* EE systems are becoming progressively more established, although due to various reasons some are still underused (many issues remain to be researched). These include (i) bio-geochemical and ecological mechanisms (that is where reverse engineering is helpful) underlying ecosystem processes and (ii) social mechanisms of acceptance by communities and political buy-in. An approach that looms large in addressing the issues is the one dealing with a bottom-up perspective in community-driven activities, which is particularly relevant for climate change-dependent scenarios.

Environmental management (EM) based on the “sufficiency economy philosophy”, originating from Thailand, is another ecologically friendly approach that assists communities to withstand, apart from climate change, disasters, other pressures such as economic insecurity caused by trade globalization and market price fluctuations. Capacity building centers serve as “learning by doing” hubs on

natural agriculture and local knowledge, *green* energy, surplus food storage for economic gain, household product and earth-house making, soil and water management, tree planting, charcoal making, bio-diesel production, *etc.* Interventions are desirably linked up with the envisioned Southeast Asian alliance of LCADRCs which relates with local communities in the region.

Climate change, moreover, is viewed by the local communities as only one contributory factor impacting their development (Mercer, 2010). It therefore appears inappropriate to solely address climate change without focusing on other underlying factors, such as poverty, social deprivation, gender imbalance, lack of resources and poor education with a view to reducing community vulnerabilities. Undertaking community-driven pilot projects based on EE and EM systems will require study by reverse eco-engineering and improved appropriate, locally preferred water, green energy, sanitation, health, food security-related interventions by participatory methodologies. Lessons learned and good practices of how the integrated CA-DR-EE-EM and poverty reduction approaches help the communities adapt to climate change and cope with disasters will be documented and made available to communities via a network of GIST-interlinked LCADRCs.

6. CONCLUDING REMARKS

Landscape climate adaptation and disaster resilience cooperatives (LCADRCs) are envisioned to contribute to the sustainability of ecosystem services for climate and disaster proofing of vulnerable communities in diverse Asian tropical conditions (*i.e.* landscapes). By mainstreaming the *integrated* climate adaptation, disaster resilience, ecological engineering, environmental management, and poverty reduction approaches in development planning, the socio-economic vulnerability to climate change and related disasters is appropriately addressed. To enhance capacity for integration, LCADRCs are proposed to be embedded into existing community empowerment alliances and to be studied and fine tuned with a view to regional replication. *Geospatial information sharing tool* (GIST) will provide technological support for decision-makers through the cooperatives. Policy advocacy for improved environmental management of risks and vulnerabilities will be carried out through a developed system based on *regional strategic environmental assessment* (R-SEA), including cumulative effects assessment. LCADRCs will promote a bottom-up, gender sensitive approach to ensure a buy-in and commitment by communities and administrations.

REFERENCES

Ahmed, A. K. 2010. Linking disaster risk reduction to climate change adaptation: Evolving regional perspectives in Asian countries. In ADPC and BDPC (organizers), *Climate Change and Extreme Cyclones*, Regional

Conference on Disaster Risk Reduction and Emergency Response in a Rapidly Changing World, Dhaka, Bangladesh, 17–18 February 2010.

Gunn, J., and Noble, B., 2009. A conceptual basis and methodological framework for regional strategic environmental assessment (R-SEA). *Impact Assessment and Project Appraisal* 27, 258–270.

IFRCRCS, 2006. *What is VCA: an introduction to vulnerability and capacity assessment*. International Federation of Red Cross and Red Crescent Societies, Geneva, Switzerland.

IPCC, 2007. *Climate Change 2007: Impacts, Adaptation, and Vulnerability*. In Parry, M. L., Canziani, O. F., Palutikof, J. P., van der Linden, P. L., and Hanson, C. E. (editors), *Contribution of Working Group II to the Fourth Assessment Report of the Intergovernmental Panel on Climate Change*.

Cambridge University Press, Cambridge. UNISDR, 2004. *Living With Risk: A Global Review of Disaster Reduction Initiatives*. United Nations International Strategy for Disaster Reduction Secretariat, Geneva, Switzerland.

Jones, C., Baker, M., Carter, J., Jay, S., Short, M., and Wood, C., (eds.), 2005. *Strategic Environmental Assessment and Land Use Planning: An International Evaluation*. Earthscan, London.

Mercer, J., 2010. Disaster risk reduction or climate change adaptation: are we reinventing the wheel? *Journal of International Development* 22, 247–264.

OECD, 2006. *Applying Strategic Environmental Assessment to Development Cooperation*. Organization for Economic Co-operation and Development

(OECD). Paper No. 12. World Bank, Washington DC.

OECD, 2008a. *Applying Strategic Environmental Assessment and Adaptation to Climate Change*. Organization for Economic Cooperation and Development, Paris, France.

OECD, 2008b. *Strategic Environmental Assessment and Disaster Risk Reduction*. Organization for Economic Cooperation and Development, Paris, France.

Partidário, M.R., 2004. *Strategic Environmental Assessment (SEA) – current practices, future demands and capacity building needs*. Course Manual, IAIA Training Courses, International Association for Impact Assessment (IAIA).

Romieu, E., Welle, T., Schneiderbauer, S., Pelling, M., and Vinchon, C., 2010. Vulnerability assessment within climate change and natural hazard contexts: revealing gaps and synergies through coastal applications. *Sustainability Science* 5, 159–170.

Schipper, L., and Pelling, M., 2006. Disaster risk, climate change and international development: scope for, and challenges to, integration. *Disasters* 30, 19–38.

SELA, 2010. *Climate Change Adaptation and Disaster Risk Reduction Institutional and Policy Landscape in Asia and Pacific*. Sistema Económico Latinoamericano y del Caribe, Caracas, Venezuela.

Stinchcombe, K., and Gibson, R.B., 2001. Strategic environmental assessment as a means of pursuing sustainability: ten advantages and ten

challenges. *Journal of Environmental Assessment Policy and Management* 3, 343–372.

Tearfund. 2008. *Linking Climate Change Adaptation and Disaster Risk Reduction*. Tearfund, London.

Thomalla, F., Downing, T., Spanger-Siegfried, E., Han, G., and Rockström J., 2006. Reducing hazard vulnerability: towards a common approach between disaster risk reduction and climate adaptation. *Disasters* 30, 39–48.

USAID-OFDA, 2009. *Asia Strategy Development, Exercise for the Period of 2009-2011*. USAID Office of Foreign Disaster Assistance (OFDA).

USAID-RDMA, 2008. *Global Climate Change in the Asia-Pacific Region*. An Analysis and road map for the USAID Regional Development Mission for Asia (RDMA). Bangkok, Thailand.

USFWS. 2009. *Conservation in Transition: Leading Change in the 21st Century*. US Fish and Wildlife Service.

Wamsler, S., 2009. *Urban Risk Reduction and Adaptation*. How to promote resilient communities and adapt to increasing disasters and changing climatic conditions? VDM Verlag, Saarbrücken.

Wickramasinghe, S., Borin, M., Kotagama, S., Cochard, R., Anceno, A., and Shipin, O., 2009. Multi-functional pollution mitigation in a rehabilitated mangrove conservation area. *Ecological Engineering* 35, 898–907.

‘Urban environment climate maps (UECM)’ for supporting ‘Urban planning with urban climate’: trial for mitigating urban heat island in Shanghai, China

Kaoru MATSUO¹, Takahiro TANAKA²

¹ Graduate Student, Graduate School of Engineering,
Hiroshima University, Japan
cafeaulait.2125@gmail.com

² Associate Professor, Hiroshima University, Dr. Eng., Japan

ABSTRACT

In Shanghai, they have an originally hot and humid climate. The inhabitants of the city are exposed to the more severe climate caused by urbanization, because Shanghai is growing and urban heat island is becoming severe. Therefore they must take countermeasures to urban heat island for comfortable life of inhabitants and reduction of energy consumption. Therefore, it is thought that urban planning that considers urban heat island mitigation is necessary in Shanghai.

Consequently, this study aims at analyzing urban heat island phenomenon in Shanghai by using meso-scale meteorological model and measurement data, and making Urban Environmental Climate Maps (UECM). UECM is made for urban planning with urban climate and environmental policy making. The role of this map is to provide some information and advices (hints) from the view of urban heat island mitigation to the place of decision making. Actually, UECM consists of a Climate Analysis Map (CAM) and a Hint Map for Urban Planning (HM). The role of CAM is representing actual climate conditions. That of HM is presenting some advices (hints) for urban planning.

Keywords: *Urban Environmental Climate Map, Shanghai, WRF, Urban Heat Island*

1. INTRODUCTION

1.1 Background

In recent years, Asian countries have continued their rapid economic growth. Urban development in large cities is especially remarkable. It is apparent that the urban heat island phenomenon is remarkable in those major cities because they have always had hot and humid climates. Especially in China, rapid population growth is thought to have worsened the urban heat island phenomenon. Reportedly, the severe urban heat island

phenomenon engenders temperatures in downtown area of Shanghai that are higher than in other large cities in China¹). Therefore, Shanghai needs urban planning incorporating mitigation of the urban heat island phenomenon. The authors intend to produce Urban Environmental Climate Maps of Shanghai as the ultimate objective of this study.

1.2 Previous Studies and Objective

Although the urban heat island phenomenon is regarded as a problem in Japan, few examples exist for which planners (or stakeholders) consider urban heat island phenomenon mitigation based on scientific knowledge in their planning processes. That is true apparently because the urban climate phenomenon is difficult to understand for stakeholders: residents, local government officials, designers, and planners. Urban Environmental Climate Maps (UECMs) are therefore proposed as a tool supporting urban planning. Trial UECMs incorporating urban heat island mitigation²), have been made for Tokyo³) and Osaka⁴). Those maps, which show the present climate conditions of the object area (e.g. wind patterns), are thought to be effective in elucidating present climate conditions. However, when trying to produce an urban plan that incorporates urban heat island phenomenon mitigation, practical countermeasures are difficult for many people to understand. Urban environmental climate maps should therefore include recommendations for urban planners⁵). Some maps presenting recommendations have been made at the district level, showing some proposals from a climatic environment perspective. However, such maps showing recommendations for entire city areas are needed. Because stakeholders must incorporate various elements in their process when they plan the whole city area, the map should show issues to be considered in planning processes and climatic resources, rather than only actual proposals. Therefore, indicating zones that are classified from a climatic perspective is thought to be effective. This study analyzes the urban heat island phenomenon in Shanghai using a meso-scale meteorological model and measurement data, yielding a climate zoning based on the analyses, with a map providing hints for planning.

2. RESEARCH OUTLINE

2.1 Overview of the Targeted Area

For this study, Shanghai in China is selected as a targeted area (Figure. 1). Shanghai is at north latitude $31^{\circ} 14'$, which is approximately the same latitude as Japan's Kagoshima Prefecture. Shanghai, which faces the East China Sea on the east, has an urban area extending along the lower Huangpu River, which runs north–south through central Shanghai. Basic information related to Shanghai is given below.

- Resident population: 19,213,200 (2009)
- Family registered population: 14,007,000 (2009)
- Area: 6,340.5 [km²]

- Population density: 29,030.49 [persons/ km²]

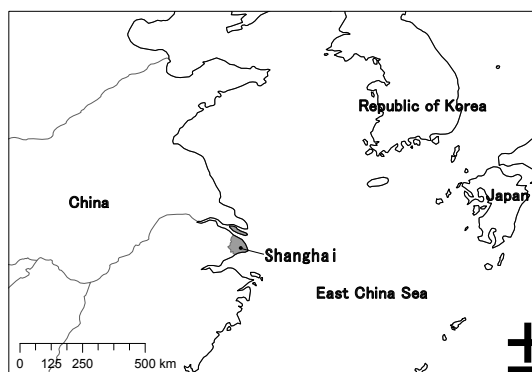


Figure 1: Position in Shanghai

2.2 Method

This study progressed by the following steps.

- 1) Analyzing the urban heat island phenomenon using measurement data
- 2) Simulating the urban heat island phenomenon for all of Shanghai using a meso-scale meteorological model, and analyzing the urban heat island phenomenon using simulation results.
- 3) Discussion based on results of analyses 1) and 2).
- 4) Climate zoning for all of Shanghai

3. ANALYSES USING MEASUREMENT DATA

3.1 Outline of Measurement Data

Measurement data of the National Climate Data Center (July 2008) were used. Two measurement stations (Hongqiao and Pudong) are shown in Figure. 2. Hongqiao is located in the urbanized city center; Pudong is located in a coastal area.

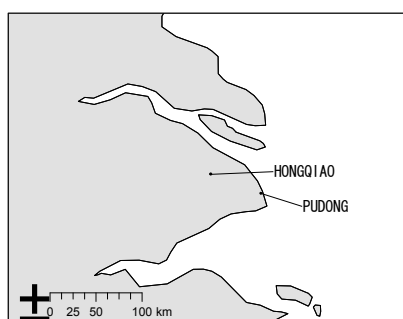


Figure 2: Measurement stations

3.2 Temperature

The average temperature for each hour (July 2008) is depicted in Figure 3, which clarifies that the temperature in Hongqiao is higher than that in Pudong throughout the day. Hourly differences in average temperatures of the two stations (July 2008) are portrayed in Figure 4, which shows that the difference is 2.0°C or more between the city center and suburb at around 13:00. Although it is necessary to analyze details to know the causes, the difference of temperatures is presumably influenced by wind because the daytime temperature is strongly influenced by wind in general¹⁰⁾. However, the difference between city center and suburban temperatures is 0.5–1.0°C at night. Presumably, that temperature difference is influenced by surrounding land cover because the nighttime temperature is strongly influenced by surrounding land cover¹⁰⁾.



Figure 3: Average Temperature for Each Hour (July 2008)



Figure 4: Hourly Differences in Average Temperatures (July 2008)

3.3 Wind Speed and Direction

Wind roses of the two stations are presented in Figure 5, showing that prevailing winds come from the south or south–southeast all day long during summer in Shanghai. Still, according to Figure 3, the temperature rise in Pudong stopped at about 12:00, but the rise in temperature in Hongqiao continued to about 14:00. Considering this tendency and Figure 5

together, Pudong, which is near from a sea and located windward, is probably influenced earlier by sea breezes.

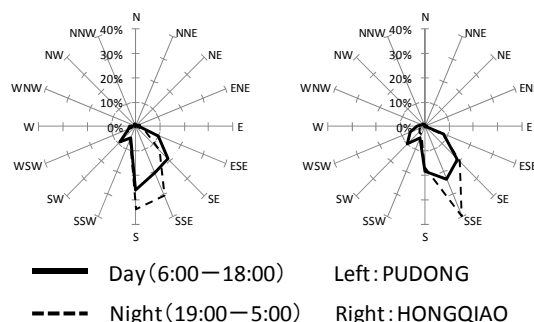


Figure 5: Wind Rose (July.2008)

4. CALCULATION CONDITIONS AND RESULTS

4.1 Outline of a Meso-scale Meteorological Model WRF

Weather Research & Forecasting (WRF), a meso-scale meteorological model developed by the National Center for Atmospheric Research (NCAR), is an advanced version of meteorological model MM5.

4.2 Calculation Conditions

The authors used WRF-ARW ver. 3.0 in this study. The calculation object domain on this study is depicted in Figure 6. A nesting technique is used: Domain 1 is a 120×120 grid with spatial resolution of 3 km. Domain 2 is a 103×103 grid with a spatial resolution of 1 km. Analyses of Domain 2 is conducted. Table 1 presents the conditions of calculations, which were done for three days (July 23–25, 2008).

Figure 7 shows the inputted land cover data. The land cover data are made from the Normalized Vegetation Index (NVI) map, which is derived from satellite remote sensing data and Land Cover data of International Steering Committee for Global Mapping. In addition, satellite remote sensing data were obtained: ALOS AVNIR-2 in 2009.

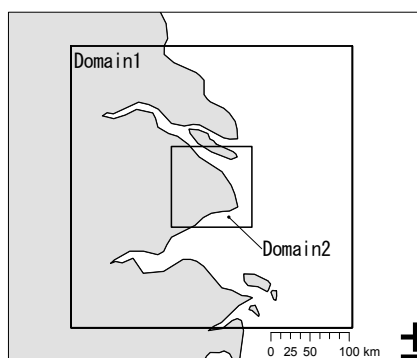


Figure 6: Calculation Object Domain

Table 1: Calculation Condition

Period		July 23-25, 2008
Vertical grid		28 layers (Surface ~ 100hPa)
Horizontal grid		Domain1 : 3 km (dimension 120×120) Domain2 : 1 km (dimension 103×103)
Meteorological data		NCEP Re-analysis global objective analysis data (every 6 hour, 1° Grid, 17 layers)
Land data	Elevation	GTOP030
	Land cover	International Steering Committee for Global Mapping Land Cover data, Satellite remote sensing data acquired by ALOS AVNIR-2 (2009)
Microphysics		Purdue Lin scheme
Radiation	Long wave	Rapid Radiative Transfer Model (RRTM) Longwave
	Short wave	MM5 (Dudhia) Shortwave
PBL scheme		Mellor-Yamada-Janjic PBL
Surface scheme	Urban area	Urban Canopy Model (UCM)
	Nonurban area	Noah LSM
Cumulus parameterization		none
FDDA		none

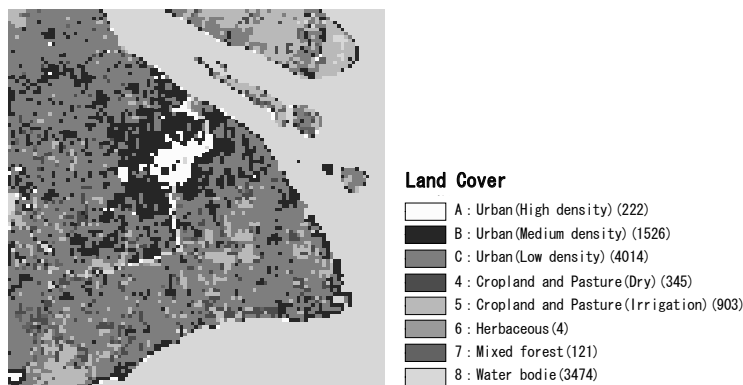


Figure 7: Land Cover Data (Mesh number in parentheses)

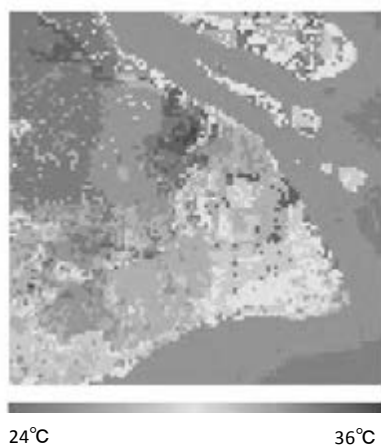


Figure 8(Left): Distribution of Daytime Temperature at 2.0 m Height (14:00, July 25, 2008)

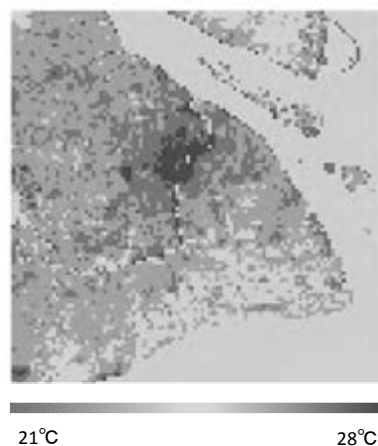


Figure 9(Right): Distribution of Night Temperature at 2.0 m Height (4:00, July 25, 2008)

4.3 Results and Discussion

Figure 8 shows some results: distribution of daytime temperatures at 2.0 m height (14:00; July 25, 2008). Furthermore, Figure 9 shows the distribution of nighttime temperature at 2.0 m height (4:00; July 25, 2008). The authors considered distributions of daytime and night temperatures as the following. 1) Distribution of daytime temperature First, it seems certain that the temperatures of the urbanized area and the surroundings are high. This is apparently true because the heat island phenomenon occurs in this urban area. Additionally, the temperature of the northwest zone in Shanghai is high, just as it is in the city. Apparently it takes much time for wind from the south or from the south–southeast to reach this zone in the daytime. The temperature of the southeast coastal zone tends to be low, probably because of the influence of a sea breeze blowing on this zone. 2) Distribution of nighttime temperatures First, temperatures of the urbanized areas and the surroundings are higher in the daytime, apparently because heat island phenomenon occurs (by heat storage on surfaces, etc.) in urban areas. Also, temperatures are lower according to distance from the urban area. The temperatures of the southeast coastal zone are lower still, probably because the south wind blows there at night, just as it does in the daytime. Results show that the temperature difference between the urbanized area and southeast coastal zone during the day and the daytime temperature difference are greater than the nighttime temperature difference. This tendency resembles the change of the temperature difference between Pudong in the southeast coastal zone and Hongqiao in the city center during the day, as reported in Section 3.

5. CLIMATE ZONING

Daytime and nighttime climate zoning was done using temperature and wind distribution results obtained during daytime and nighttime (Figures. 10, 11). For daytime, the whole Shanghai area was first classified according to temperature based on the temperature distribution. Concretely, the zone of 35°C or more, where the temperature is the highest, is a zone for which the highest necessity of the measure of heat island in daytime, a zone of less than 35°C is classified at intervals of 1°C, 34°C, 33°C, 32°C, 31°C, and every 30°C. The zone where the temperature is low does not require heat island measurements in the daytime relatively. Then the zone of less than 30°C is assumed to be a zone with little necessity of heat island measurements during the daytime. Next, the whole area of Shanghai is classified into zones that are affected and unaffected by the sea breeze by overlaying the wind distribution on this classification map. Then, the urban planning proposal that considers heat island measures is attempted for zones such as those affected and unaffected by the sea breeze.

For nighttime temperatures, as for the daytime, first, the whole area of Shanghai was classified according to temperatures based on the temperature distribution. Concretely, the zone of 28°C, where the temperature is highest, is made a zone where it was the highest necessity of the measure of heat

island in the night, the zone of less than 35°C is classified at intervals of 1°C, 27°C, 26°C, 25°C, and every 24°C. The zone in which the temperature is low has low necessity of the heat island measure in the night. The zone of less than 25°C is assumed to be a zone where the necessity of the heat island measures during the night is small. The subsequent procedure resembles that used for daytime.

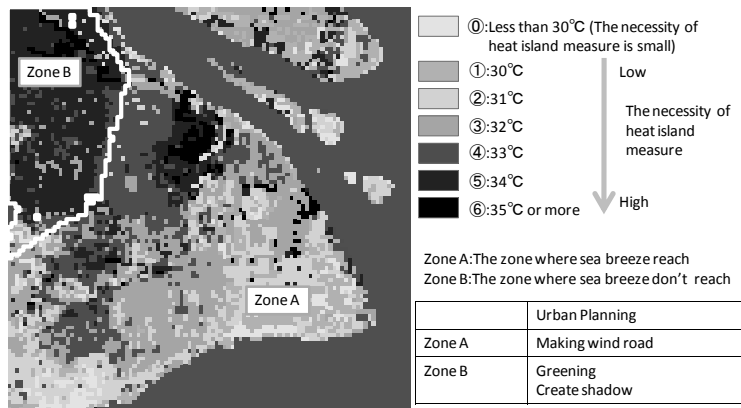


Figure 10: Recommendation Map (Daytime)

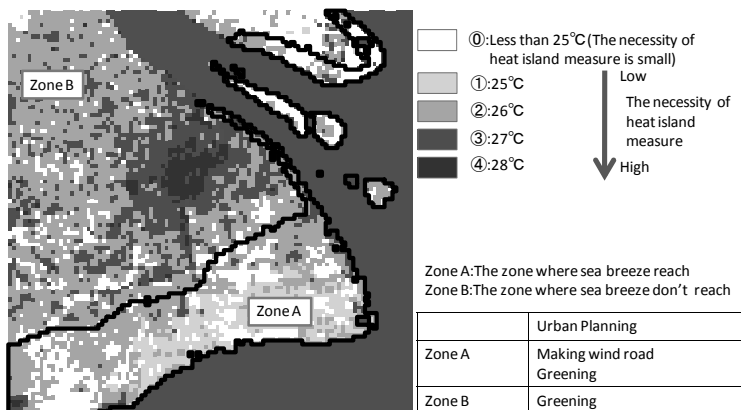


Figure 11: Recommendation Map (Night)

6. SUMMARY

This study was undertaken to analyze the urban heat island phenomenon in Shanghai using a meso-scale meteorological model and measurement data, producing a climate zoning with that analysis, and making a recommendation map. As the next step, the authors will advance analyses of measurement data and results to improve detailed climate zoning, ultimately producing Urban Environmental Climate Maps.

REFERENCES

Bai Y., and Mikami T., 2007. Measuring and Mitigating Urban Heat Island in Summer in Shanghai, China. *Environmental Information Science*,

No.21, 387-392.

AIJ. 2000. *Klima Atlas of Urban Environment: Urban planning with using the climate information*. Gyosei.

Chairman: Toshio OJIMA. Supervision (Learning Community for Promoting Coo-City Eco-City 2010). *THE COOL CITY strategy of heat island mitigation :Architecture and Urban planning utilizing green, water and wind, Building technology*.

Tanaka T., and Moriyama M., 2004. Making and Using of "Urban Environmental Climate Map" for Supporting Urban Planning which is Adapted for Climate. *Papers and Proceedings of the Geographic Information Systems Association*, Vol.13, 391-394.

Moriyama M., 2004. *Measures and technology of heat island*. Gakugei Shuppan.

Working Group for Practical Use of Klimaatlas, Environment Planning Sub-committee in Architectural Institute of Japan, Study Group of Klimaatlas. 2001. Study on Practical Use of Klimaatlas: A Trial to Make the Recommendation Map by Workshop. *AIJ Journal of Technology and Design*, No.14, 207-210.

Working Grope for Practical Use of Klimaatlas Environment Planning Sub-committee in Architectural Institute of Japan. 2003. Study on Practical Use of

Klimaatlas (Part2): A Trial to Make the Climate Analysis Map and the Recommendation Map by Kitakyushu workshop. *AIJ Journal of Technology and*

Design, No.18, 203-206.

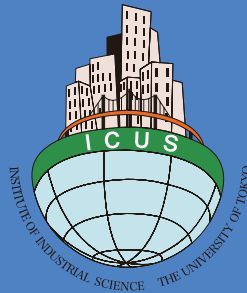
Working Group for Practical Use of Klimaatlas Sub-committee in Architectural Institute of Japan. 2004. A Trial to Make the Climate Analysis Map and the recommendation Map by Workshop for Sendai City Region: Study on Practical Use of Klimaatlas (Part 3). *AIJ Journal of Technology and Design*, No.20, 183-186.

Iwai K., Takagi N., Takizawa Y., and Yamada C., and Sub-Committee on Klimaatlas Steering Committee in Architectural Institute of Japan. 2006. A Study on Practical Use of Klimaatlas: Part4 Klimaatlas Workshop with Citizens in Nagano City. *AIJ Journal of Technology and Design*, No.24, 229-232.

Takeayashi H., and Moriyama M., 2005. Urban Heat Island Phenomena Influenced by Sea Breeze. *AIJ Journal of Technology and Design*, No.21, 199-202.

Skamarock, W.C., Klemp, J.B., Dudhia, J., Gill, D.O., Barker, D.M., Duda, M.G., Huang, X.-Y., Wang, W., Wang, W., Powers., J.G. 2008. *A description of Advanced Research WRF Version3, NCAR/TN-475+STR*.

Hirano Y., 2001. Estimation Method of Vegetation Cover Ratio Using NVI Based on Linear Combination Model. *Summaries of technical Papers of AIJ*, D-1, 571-572



International Center for Urban Safety Engineering
Institute of Industrial Science, The University of Tokyo

4-6-1 Komaba, Meguro-ku,

Tokyo 153-8505, Japan

Tel: +81-3-5452-6472

Fax: +81-3-5452-6476

<http://icus.iis.u-tokyo.ac.jp>

E-mail: icus@iis.u-tokyo.ac.jp